Computer Graphics Through OpenGL®

From Theory to Experiments

Third Edition

Sumanta Guha
Asian Institute of Technology, Thailand

CRC Press
Taylor & Francis Group
Boca Raton London New York

CRC Press is an imprint of the
Taylor & Francis Group, an informa business

Cover Designed by Sumanta Guha

CRC Press
Taylor & Francis Group
6000 Broken Sound Parkway NW, Suite 300
Boca Raton, FL 33487-2742

Printed on acid-free paper
Version Date: 20181022

International Standard Book Number-13: 978-1-138-61264-8 (Hardback)

Library of Congress Cataloging-in-Publication Data

Names: Guha, Sumanta,
author.
Title: Computer graphics through openGL / Sumanta Guha.
Description: Third edition. | Boca Raton : Taylor & Francis, a CRC title,
part of the Taylor & Francis imprint, a member of the Taylor & Francis
Group, the academic division of T&F Informa, plc, 2018. | Includes
bibliographical references and index.
Identifiers: LCCN 2018027365 | ISBN 9781138612648 (hardback : acid-free paper)
Subjects: LCSH: Computer graphics. | Microcomputers--Programming. | OpenGL. |
BISAC: COMPUTERS / Computer Graphics. | MATHEMATICS / General.
Classification: LCC T385 .G85 2018 | DDC 006.6/633--dc23
LC record available at https://lccn.loc.gov/2018027365

Visit the Taylor & Francis Web site at
http://www.taylorandfrancis.com

and the CRC Press Web site at
http://www.crcpress.com

Taylor & Francis

Taylor & Francis Group

http://taylorandfrancis.com

Contents

V Making Things Up 263

VI Lights, Camera, Equation 327

Taylor & Francis
Taylor & Francis Group
http://taylorandfrancis.com

Preface

Welcome to the third edition of *Computer Graphics Through OpenGL: From Theory to Experiments* ! The first edition appeared late 2010 and the second four years after in 2014. Now, it's been another four years in which I received a lot of thoughtful and, happily, mostly positive feedback. I heard from instructors, students, as well as individuals using the book for self-study. Their observations together with my own classroom experience started me off a year ago writing a new edition. It's been a fairly intense past several months, most of my waking hours spent sitting where I am now in front of the computer. But it's been fun too – being in communion with an imaginary reader who I am trying to enlighten and keep engaged at the same time – and I am pleased with the result. I hope you will be too. Let's get to the facts.

About the Book

This is an introductory textbook on computer graphics with equal emphasis on theory and practice. The programming language used is C++, with OpenGL as the graphics API, which means calls are made to the OpenGL library from C++ programs. OpenGL is taught from scratch.

The book has been written to be used as a textbook for a first college course, as well as for self-study.

After Chapters 1-16 – the undergraduate core of the book – the reader will have a good grasp of the concepts underpinning 3D computer graphics, as well as an ability to code sophisticated 3D scenes and animation, including games and movies. We begin with classical pre-shader OpenGL before proceeding to the latest OpenGL 4.x (more about our exposition style further on). Chapters 17-21, though advanced, but still mainstream, could be selected topics for an undergraduate course or part of a second course.

Specs

This book comprises 21 chapters, an extended appendix on a fundamental math topic, plus two more appendices containing a math self-test and its solutions. It comes with approximately 180 programs, 270 experiments based on these programs, 750 exercises, including theory and programming exercises, 110 worked examples, and 700 four-color illustrations, include drawings and screenshots. An instructor's manual containing solutions to selected exercises is available from the publisher. The book was typeset using LaTeX and figures drawn in Adobe Illustrator.

From the Second Edition to the Third

- Cover to cover revision and reorganization of topics.

New topics include:

- Timer queries and performance measurement.
- Importing externally created objects.
- Texturing spheres.
- Framebuffer objects.
- Rendering to texture.
- Texture matrices.
- Cube mapping a skybox.
- Shadow mapping curved surfaces.
- OpenGL 4.x:
    - Procedural textures.
    - Specular maps.
    - Normal maps.
    - Multiple program objects.
    - Particle systems with transform feedback.
- 10 new programs, 20 new experiments, 100 new exercises, 10 new examples, 50 new figures.
- Programming environment simplified, programs developed on Windows 10 and Microsoft Visual Studio (MSVS) 2015 and tested on MSVS 2017.

Target Audience

- Students in a first university CG course, typically offered by a CS department at a junior/senior level. This is the primary audience for which the book was written.
- Students in a second or advanced CG course, who may use the book as preparation or reference, depending on the goals. For example, the book would be a useful reference for a study of 3D design – particularly, Bézier, B-spline and NURBS theory – and of projective transformations and their applications in CG.
- Students in a non-traditional setting, e.g., studying alone or in a professional course or an on-line program. The author has tried to be especially considerate of the reader on her own.
- Professional programmers, to use the book as a reference.

Prerequisites

Zero knowledge of computer graphics is presumed. However, the student is expected to know the following:

- Basic C++ programming. There is no need to be an expert programmer. The C++ program serves mainly as an environment for the OpenGL calls, so there's rarely need for fancy footwork in the C++ part itself.
- Basic math. This includes coordinate geometry, trigonometry and linear algebra, all at college first-course level (or, even strong high school in some cases). For intended readers of the book who may be unsure of their math preparation, we have a self-test in Appendix B, with solutions in Appendix C. The test should tell exactly how ready you are and where the weaknesses are.

Resources

The following are available through the book's website www.sumantaguha.com:

- Sample chapters, table of contents, preface, subject and program index, math self-test and solutions at the Home page.
- Program source code, developed on a Windows 10 platform using the Microsoft Visual Studio Community 2015 IDE and subsequently tested to run with MSVS Community 2017, which should run on other versions of Windows/MSVS, as well as Mac OS and Linux platforms. The programs are arranged chapter-wise in the top-level folder ExperimenterSource at the Downloads page.
- Guide to installing OpenGL and running the programs on a Windows/MSVS platform at the Downloads page.
- Multiplatform *Experimenter* software to run the experiments at the Downloads page. *Experimenter*'s interface is Experimenter.pdf, a file containing all the experiments from the book; except for those in Chapter 1, each is clickable to bring up the related program and workspace. *Experimenter* is only an aid and not mandatory – each program is stand-alone. However, it is the most convenient way to run experiments in their book order.
- Book figures in jpg format arranged in sequence as one PowerPoint presentation per chapter at the Instructor page.
- Instructor's manual with solutions to 100 problems – instructors who have adopted the textbook can submit a request at the Instructor page.

Pedagogical Approach

Code and theory have been intertwined as far as possible in what may be called a theory-experiment-repeat loop: often, following a theoretical discussion, the reader is asked to perform validating experiments (run code, that is); sometimes, too, the other way around, an experiment is followed by an explanation of what is observed. It's kind of like discovering physics.

Why use an API?

Needless to say, I am not a fan of the API-agnostic approach to teaching CG, where focus is on principles only, with no programming practice.

Undergrads, typically, love to code and make things happen, so there is little justification to denying the new student the joy of creating scenes, movies and games, not to mention the pride of achievement. And, why not leverage the way code and theory reinforce one another when teaching the subject, or learning on one's own, when one can? Would you want Physics 101 without a lab section?

Moreover, OpenGL is very well-designed and the learning curve short enough to fully integrate into a first CG course. And, it is supported on every OS platform with drivers for almost every graphics card on the market; so, in fact, OpenGL is there to use for anyone who cares to.

Note to student : Our pedagogical style means that for most parts of the book you want a computer handy to run experiments. So, if you are going to snuggle up with it at night, make it a threesome with a notebook.

Note to instructor : Lectures on most topics – both of the theory and programming practice – are best based around the book's experiments, as well as those you develop yourself. The *Experimenter* resource makes this convenient. Slides other than the plentiful book figures, the latter all available on-line, are rarely necessary.

How to teach modern shader-based OpenGL?

Our point of view needs careful explanation as it is different from some of our peers'. Firstly, to push the physics analogy one more time, even though relativistic mechanics seems to rule the universe, in the classroom one might prefer doing classical physics before relativity theory.

Shaders, which are the programmable parts of the modern OpenGL pipeline, add great flexibility and power. But, so too, do they add a fair bit of complexity – even a cursory comparison of our very first program square.cpp from Chapter 2 with its equivalent in fourth-generation OpenGL, squareShaderized.cpp, complemented with a vertex and a fragment shader in Chapter 15, should convince the reader of this.

Consider more carefully, say, a vertex shader. It must compute the position coordinates of a vertex, taking into account all transformations, both modelview and projection. However, in the classical fixed-function pipeline the user can simply issue commands such as glTranslatef(), glFrustum(), etc., leaving to OpenGL actual computation of the transformed coordinates; not so for the programmable pipeline, where the reader must write herself all the needed matrix operations in the vertex shader. We firmly believe that the new student is best served learning first how to transform objects according to an understanding of simply how a scene comes together *physically* (e.g., a ball falls to the ground, a robot arm bends at the elbow, etc.) with the help of ready-to-use commands like glTranslatef(), and, only later, how to define these transforms mathematically.

Such consideration applies as well to other automatic services of the fixed-function pipeline which allow the student to focus on phenomena, disregarding *initially* implementation. For example, as an instructor, I would much prefer to teach first how diffuse light lends three-dimensionality, specular light highlights, and so on, gently motivating Phong's lighting equation, leaving OpenGL to grapple with its actual implementation, which is exactly what we do in Chapter 11.

In fact, we find an understanding of the fixed-function pipeline makes the subsequent learning of the programmable one significantly easier because it's then clear exactly what the shaders should try to accomplish. For example, following the fixed-function groundwork in Chapter 11, writing shaders to implement Phong lighting, as we do in Chapter 15, is near trivial.

We take a similarly laissez-faire attitude to classical OpenGL syntax. So long as it eases the learning curve we'll put up with it. Take for example the following snippet from our very first program square.cpp:

```
glBegin(GL_POLYGON);
   glVertex3f(20.0, 20.0, 0.0);
   glVertex3f(80.0, 20.0, 0.0);
   glVertex3f(80.0, 80.0, 0.0);
   glVertex3f(20.0, 80.0, 0.0);
glEnd();
```

Does it not scream square – even though it's immediate mode and uses the discarded polygon primitive? So, we prefer this for our first lesson, avoiding thereby the distraction of a vertex array and the call glDrawArrays(GL_TRIANGLE_STRIP, 0, 4), as in the equivalent 4.x program squareShaderized.cpp, our goal being a simple introduction of the synthetic-camera model.

With these thoughts in mind the book starts in Chapter 2 with classical pre-shader OpenGL, progressing gradually deeper into the API, developing CG ideas in parallel, in a so-called theory-experiment-repeat loop. So, what exactly is an experiment? An experiment consists either of running a book program – each usually simple for the purpose of elucidating a single idea – or attempting to modify one based on an understanding of the theory in order, typically, to achieve a particular visual result.

By the end of Chapter 14 the student will have acquired proficiency in pre-shader OpenGL, a perfectly good API in itself. As well, equally importantly, she will have an understanding of CG principles and those underlying the OpenGL pipeline, which will dramatically ease her way through the concepts and syntax of OpenGL 4.x, the newest generation of the API, covered in Chapters 15-16.

Does this kind of introduction to modern OpenGL, via the old and, possibly, obsolete, not ingrain bad habits? Not at all, from our experience. When push comes to shove, how hard is it to replace polygons with triangle strips? Or, use vertex buffer objects (VBOs) and vertex array objects (VAOs) to store data? Does our approach cost timewise? If the goal is OpenGL 4.x, then, yes, it does take somewhat longer, but there are various possible learning sequences through the book and 4.x certainly can be reached and covered in a semester.

In short, then, we believe the correct way to modern OpenGL is through the classical version of the API because this allows the learning process to begin at a high level, so that the student can concentrate on gaining an overall end-to-end understanding of the CG pipeline first, leaving the OpenGL system to manage low-level processes (i.e., those inside the pipeline like setting transformation and projection matrices, defining fragment colors, and such). Once she has a high-level mastery, subsequently "descending" into the pipeline to take charge of fixed-function parts in order to program them instead will, in fact, be far less arduous than if she tried to do both – learn the basics and program the pipeline – at the same time.

Another point to note in this context is that, as noted before, classical OpenGL is a complete API in itself which, in fact, can be more convenient for certain applications (e.g., it allows one access to the readymade GLUT objects like spheres and toruses). There are, as well, thousands of currently live applications written in classical OpenGL, which are not going go to be discarded or rewritten any time soon – the reason, in fact, for the Khronos Group to retain the compatibility version of the API – so familiarity with older syntax can be useful for the intending professional.

What about Vulkan?

We thought you might ask. Vulkan is the much-hyped "successor" to OpenGL. It is a highly explicit API, taking the programmer close to the hardware and asking her to specify almost all facets of the pipeline from end to end. Benefits of programming near the hardware include thin drivers, reduced run-time overhead and the ability to expose parallelism in the GPU. (Vulkan is not only a 3D graphics API, but used to program GPU-heavy compute applications as well.)

However, Vulkan's explicitness and consequent verbosity make it highly unsuitable as an introductory CG API. Here are some program sizes to begin with. The first OpenGL program in the book, square.cpp, which draws a black square on a white background, is about 90 lines of code in pre-shader 2nd generation OpenGL; a functionally equivalent program, squareShaderized.cpp, written in OpenGL 4.3 later on in the book is 190 lines plus 25 lines of shader code; a minimal equivalent Vulkan program, squareVulkanized.cpp, written separately by the author is 1,100 lines (no, that's no misprint – the reader will find the program at the Downloads page of the book's website) plus 30 lines of shader code. Figure 1 is a screenshot.

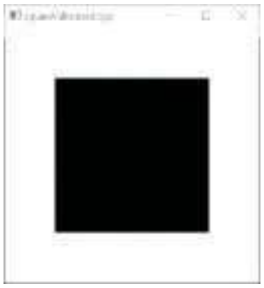

Figure 1: Screenshot of squareVulkanized.cpp, a 1000+ line Vulkan program.

Moreover, explicitness requires a Vulkan programmer to be familiar with the functioning of the graphics pipeline at a low level in order to specify it, which almost instantly disqualifies it from being a beginner's API. Further, delaying programming until after the pipeline has been covered goes utterly against our own pedagogical approach which is to engage students with code the first day.

So, is OpenGL, or for that matter, this book, of any use for someone intending to learn Vulkan? Well:

(a) The Vulkan graphics pipeline is essentially the same as OpenGL's. Therefore, learning OpenGL is progress toward Vulkan. Moreover, once a programmer has mastered OpenGL, she has most of what's needed to "take full charge" of the pipeline, which is what Vulkan is all about.

(b) The runtime gains of Vulkan don't begin to show up in any significant way until one gets to complex scenes with lots of textures, objects and animation. Less complicated applications - including, obviously, those in any introductory CG book - benefit little performance-wise from being written (or, rewritten) in Vulkan, not justifying the huge overhead in code.

This means that many OpenGL apps are going to stay that way and new ones continue to be written. It's a matter of knowing which tool to use: pre-shader

OpenGL, OpenGL 4.x, Vulkan,........(Hooking up a U-Haul trailer to the back of a Ferrari is never a good idea.)

Nevertheless, if you are of the Vulkan or bust frame of mind then the advice we would have is to study this book up to Chapter 16, when you will have a solid understanding of fourth-generation OpenGL, then pick up, say, the canonical Vulkan guide [131], through which you should then be able to make quick progress.

Capsule Chapter Descriptions

Part I: Hello World

Chapter 1: An Invitation to Computer Graphics
A non-technical introduction to the field of computer graphics.

Chapter 2: On to OpenGL and 3D Computer Graphics
Begins the technical part of the book. It introduces OpenGL and fundamental principles of 3D CG.

Part II: Tricks of the Trade

Chapter 3: An OpenGL Toolbox
Describes a collection of OpenGL programming devices, including vertex arrays, vertex buffer and array objects, mouse and key interaction, pop-up menus, and several more.

Part III: Movers and Shapers

Chapter 4: Transformation, Animation and Viewing
Introduces the theory and programming of animation and the virtual camera. Explains user interactivity via object selection. Foundational chapter for game and movie programming.

Chapter 5: Inside Animation: The Theory of Transformations
Presents the mathematical theory behind animation, particularly linear and affine transformations in 3D.

Chapter 6: Advanced Animation Techniques
Describes frustum culling, occlusion culling as well as orienting animation using both Euler angles and quaternions, techniques essential to programming games and busy scenes.

Part IV: Geometry for the Home Office

Chapter 7: Convexity and Interpolation
Explains the theory of convexity and the role it plays in interpolation, which is the procedure of spreading material properties from the vertices of a primitive to its interior.

Chapter 8: Triangulation
Describes how and why complex objects should be split into triangles for efficient rendering.

Chapter 9: Orientation
Describes how the orientation of a primitive is used to determine the side of it that the camera sees, and the importance of consistently orienting a collection of primitives making up a single object.

Part V: Making Things Up

Chapter 10: Modeling in 3D Space

Systematizes the principles of modeling both curves and surfaces, including Bézier and fractal. Shows how to import objects from external design environments. Foundational chapter for object design.

Part VI: Lights, Camera, Equation

Chapter 11: Color and Light

Explains the theory of light and material color, the interaction between the two, and describes how to program light and color in 3D scenes. Foundational chapter for scene design.

Chapter 12: Textures

Explains the theory of texturing and how to apply textures to objects and render to a texture.

Chapter 13: Special Visual Techniques

Describes a set of special techniques to enhance the visual quality of a scene, including, among others, blending, billboarding, stencil buffer methods, image and pixel manipulation, cube mapping a skybox, and shadow mapping.

Part VII: Pixels, Pixels, Everywhere

Chapter 14: Raster Algorithms

Describes low-level rendering algorithms to determine the set of pixels on the screen corresponding to a line or a polygon.

Part VIII: Programming Pipe Dreams

Chapter 15: OpenGL 4.3, Shaders and the Programmable Pipeline: Liftoff

Introduces 4th generation OpenGL and GLSL (OpenGL Shading Language) and how to vertex and fragments shaders to program the pipeline, particularly to animate, light and apply textures.

Chapter 16: OpenGL 4.3, Shaders and the Programmable Pipeline: Escape Velocity

Continuing onto advanced 4th generation OpenGL topics, including, among others, instanced rendering, shader subroutines, transform feedback, particle systems, as well as tessellation and geometry shaders.

Part IX: Anatomy of Curves and Surfaces

Chapter 17: Bézier

Describes the theory and programming of Bézier primitives, including curves and surfaces.

Chapter 18: B-Spline

Describes the theory and programming of (polynomial) B-spline primitives, including curves and surfaces.

Chapter 19: Hermite

Introduces the basics of Hermite curves and surfaces.

Part X: Well Projected

Chapter 20: Applications of Projective Spaces: Projection Transformations and Rational Curves

Applies the theory of projective spaces to deduce the projection transformation in the graphics pipeline. Introduces rational Bézier and B-spline, particularly NURBS, theory and practice.

Part XI: Time for a Pipe

Chapter 21: Pipeline Operation

Gives a detailed view of the synthetic-camera and ray-tracing pipelines and introduces radiosity.

Appendix A: Projective Spaces and Transformations

A CG-oriented introduction to the mathematics of projective spaces and transformations. Provides a complete theoretical background for Chapter 20 on applications of projective spaces.

Appendix B: Math Self-Test

A self-test to assess math readiness for intending readers.

Appendix C: Math Self-Test Solutions

Solutions for the math self-test.

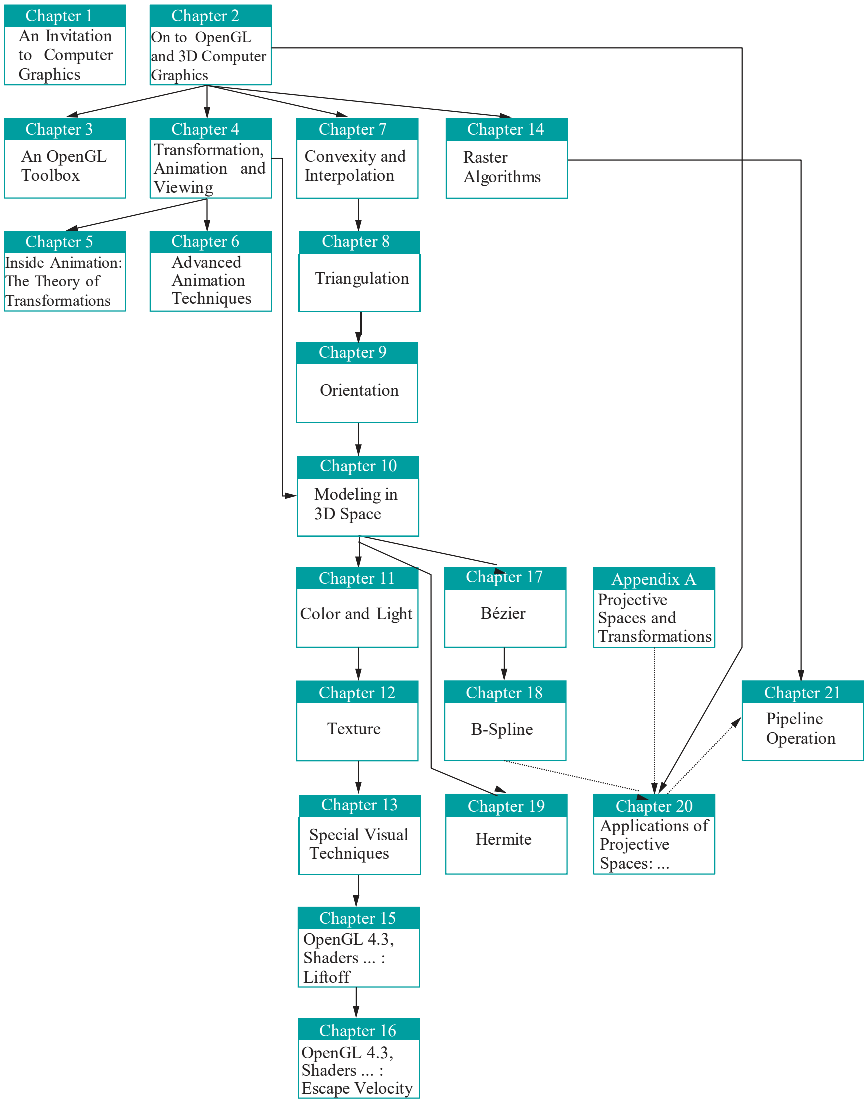
Chapter 1
An Invitation to Computer Graphics
Chapter 2
On to OpenGL and 3D Computer Graphics
Chapter 3
An OpenGL Toolbox
Chapter 4
Transformation, Animation and Viewing
Chapter 7
Convexity and Interpolation
Chapter 14
Raster Algorithms
Chapter 5
Inside Animation: The Theory of Transformations
Chapter 6
Advanced Animation Techniques
Chapter 8
Triangulation
Chapter 9
Orientation
Chapter 10
Modeling in 3D Space
Chapter 11
Color and Light
Chapter 17
Bézier
Appendix A
Projective Spaces and Transformations
Chapter 12
Texture
Chapter 18
B-Spline
Chapter 21
Pipeline Operation
Chapter 13
Special Visual Techniques
Chapter 19
Hermite
Chapter 20
Applications of Projective Spaces: ...
Chapter 15
OpenGL 4.3, Shaders ... : Liftoff
Chapter 16
OpenGL 4.3, Shaders ... : Escape Velocity

Figure 2: Chapter dependence chart: dashed arrows represent weak dependencies.

Suggested Course Outlines

See the chapter dependencies in Figure 2.

(1) Undergraduate one-semester first CG course:

This course should be based on Chapters 1-16, though full coverage might be ambitious for one semester. Instructors may pick topics to emphasize or skip, depending on their goals for the course and the chapter dependence chart.

For example, for more practice and less theory, a possible sequence would be 1 → 2 → 3 → 4 → 6 (only frustum culling) → 7 → 8 → 9 → 10 (skip curve/surface theory) → 11 → 12 → 13 → 15 → 16.
Even this abbreviated sequence may be hard to pack into one semester. Please keep in mind that when choosing what to write about the author preferred to err on the side of excess rather than less. So, almost always will the instructor find more material in a chapter than she cares to teach – we leave her to pick her way out.

The most effective teaching method with this book is to base discussion around experiments – both from the book and those the instructor develops herself. Our *Experimenter* software makes this especially convenient. Students should be involved in the experiments, running code simultaneously on their own machines in class. Use of slides should be minimized except, possibly, for the plentiful book figures, which are available to download, arranged as one PowerPoint presentation per chapter.

(2) Advanced CG courses:

This book could serve as a reference for a study of 3D design – particularly, Bézier (Chapter 17), B-spline (Chapter 18) and rational Bézier and NURBS theory (Chapter 20) – and of projective transformations and their applications (Appendix A and Chapter 20). From a practical point of view, Chapters 15-16 go fairly deep into the fourth generation of OpenGL and the GLSL, useful for students who may be familiar with only the classical pipeline.

(3) Self-study:

A recommended first pass would be 1 → 2 → 3 → 4 → 7 → 8 → 9 (go light on 7-9 if your math is rusty) → 10 (skip theory) → 11 → 12 → 13 → 15 → 16.
Following this the student should take up a fair-sized programming project, returning to the book as needed. For the theoretically-inclined there's a lot to keep her busy in Chapters 5 and 17-21.

Acknowledgments

I owe a lot to many people, most of all students whom I have had the privilege of teaching in my CG classes over the years at UW-Milwaukee and then the Asian Institute of Technology.

I thank KV, Ichiro Suzuki, Glenn Wardius, Mahesh Kumar, Le Phu Binh, Maria Sell and, especially, Paul McNally, for their support at UWM, where I began to teach CG and learn OpenGL.

I am grateful to my colleagues and the staff and students at AIT for such a pleasant environment, which allowed me to combine teaching and research commitments with the writing of a book.

Particular thanks at AIT to Vu Dinh Van, Nguyen Duc Cong Song, Ahmed Waliullah Kazi, Hameedullah Kazi, Long Hoang, Songphon Klabwong, Robin Chanda, Sutipong Kiatpanichgij, Samitha Kumara, Somchok Sakjiraphong, Pyae Phyo Myint Soe, Adbulrahman Otman, Sushanta Paudyal, Akila de Silva, Nitchanun Saksinchai, Thee Thet Zun, Suwanna Xanthavanij, Visutr Boonnateephisit, Matt Dailey, and our ever-helpful secretaries K. Siriporn and K. Tong.

I am grateful to Kumpee Teeravech, Kanit Tangkathach, Thanapoom Veeranitinun, Pongpon Nilaphruek, and Wuttinan Sereethavekul, students of my CG course at AIT, for allowing me to use programs they wrote.

I owe an enormous debt of gratitude to my former student Chansophea Chuon for hundreds of hours of help with the first edition, which got this book off the ground in the first place. I thank Somying Pongpimol for her brilliant Illustrator drawings. She drew several of the figures based on my rather amateurish original Xfig sketches. I would like to thank Olivier Nicole for help with the book's website.

I am especially grateful to Brian Barsky for encouraging me to persevere after seeing an early and awkward draft of the first edition, and subsequently inviting the finished product to the series he was then editing. Relatedly, I thank my neighbor Doug Cooper two floors down for putting me in touch with Brian at the time Brian was scouting prospective authors.

I want to acknowledge the production team at Taylor & Francis who went out of their way for this book. Particularly, I want to thank my editor Randi Cohen who is as professional and efficient as she is pleasant to deal with.

I am grateful to readers of the first and second editions, as well as reviewers who looked over drafts and proposals, whose comments led, hopefully, to significant improvements.

I have nothing but praise for the DJs and kindly staff of the Mixx nightclub in downtown Bangkok whose dance floor provided a much-needed sanctuary for me to blow off steam after long hours on the computer.

I acknowledge the many persons and businesses who were kind enough to allow me to include images to which they own copyrights.

On a personal note, I express my deep gratitude to Dr. Anupam De for keeping Kamaladi healthy enough that I could concentrate on the first edition through the few years that I spent writing it.

Finally, I must say that had I not had the opportunity to study computer science in the United States and teach there, I would never have reached a position where I could even contemplate writing a textbook. It's true, too, that had I not moved to Thailand, this book would never have begun to be written. This is an enchanting country with a strangely liberating and lightening effect – to which thousands of expats can attest – that encourages one to express oneself.

Website and Contact Information

The book's website is at www.sumantaguha.com. Users of the book will find there various resources including downloads. The author welcomes feedback, corrections and suggestions for improvement emailed to him at sg@sumantaguha.com.

About the Author

Sumanta Guha earned a Ph.D. in mathematics from the Indian Statistical Institute, Kolkata, in 1987. From 1984 to 1987 he taught mathematics at Jadavpur University in Kolkata. He left in 1987 to study computer science at the University of Michigan in Ann Arbor, where he earned a Ph.D. in 1991. On graduating from Michigan he joined the Electrical Engineering and Computer Science faculty of the University of Wisconsin-Milwaukee where he taught from 1991 to 2002. In 2002 he moved to the Computer Science and Information Management program of the Asian Institute of Technology in Thailand, where he is currently an adjunct professor. His research interests include computational geometry, computer graphics, computational topology, robotics and data mining.

Taylor & Francis
Taylor & Francis Group
http://taylorandfrancis.com

Part I

Hello World

Taylor & Francis

Taylor & Francis Group

http://taylorandfrancis.com

CHAPTER 1

An Invitation to Computer Graphics

Computer graphics, or CG as it is often simply called, is the use of computers to generate images. This is as opposed to the capture of images from the real-world with, say, a camera, or the realization by hand of an artist's imagination on a drawing medium.

Figure 1.1: A cell phone, news opening graphics, car dashboard.

To not see the end product of CG, that being computer-generated imagery (CGI), throughout your day, you would have to be on a deserted island. Images on the screen of the cell phone you probably check first thing on waking are digitally synthesized by a processor. Almost every frame on the TV showing the morning news has CGI in some part. If you commute, then the vehicle carrying you to school or work likely communicates with its operator through multiple computer-managed console panels, displaying information ranging from fuel level to geographical location.

Figure 1.2: A computer at work, handheld game player, part of AIT home page (thanks Asian Institute of Technology).

At work, if at all you use a computer, then, of course, there you are sitting right at a fountainhead of computer graphics. And, CGI probably plays an even more important role in your recreational life. Even the most casual video game amusing commuters headed home nowadays has sophisticated interactive 3D graphics. The web on which we spend so many hours a day is increasingly becoming a multimedia smorgasbord synthesizing animation, movie clips, CGI and sound.

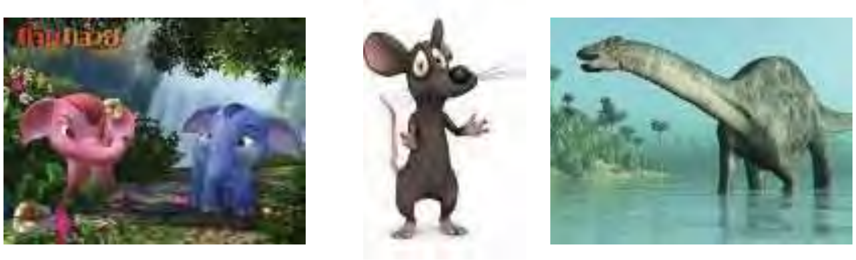

Figure 1.3: Khan Kluay, the first 3D animated Thai movie (courtesy Kantana Animation), an anthropomorphic mouse, a massive (fortunately herbivorous) dinosaur.

When you watch a movie you are seeing a product from an industry, which together with the gaming industry, has the biggest relationship with CG of any other, not only as a consumer of the latest and greatest in technique, but also as a multimillion-dollar promoter of cutting-edge research. A little blue elephant which grows into a mighty warrior, an eccentric mouse with a ribald sense of humor, and a massive dinosaur looking so hungrily for food that you would think its species had never really become extinct more than fifty million years ago – to contemplate such achievements is to be in awe of the human imagination, as well as the ingenuity of the engineers and programmers who materialize these fantastical conceptions as palpable and believable digital presences.

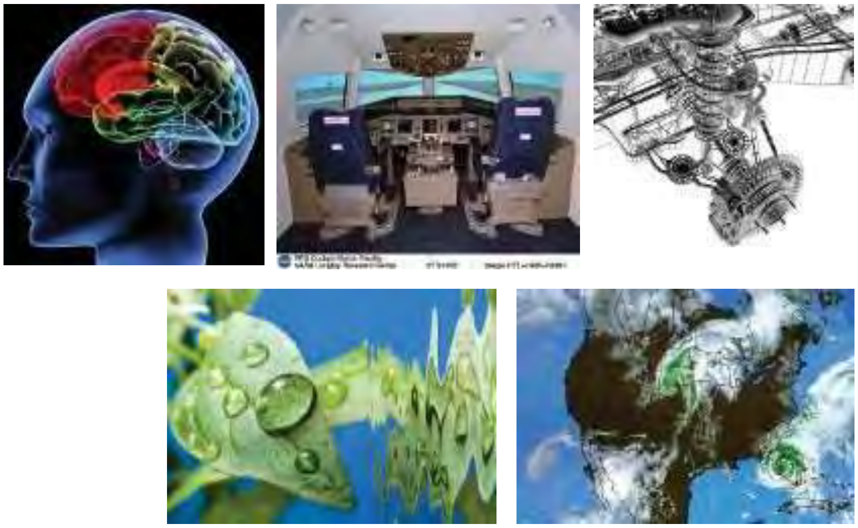

Figure 1.4: Clockwise from top left: Image of the human brain, flight simulator cockpit (from NASA), engine design, hurricane over Florida, water drop on a leaf.

Then there's the quiet CG impacting our lives some would say even more profoundly than its more flamboyant manifestations. Doctors and surgeons practice their craft in simulated environments detailed to the tiniest capillaries. Commercial pilots put in hundreds of hours on a flight simulator before entering a real cockpit. (Flight simulators are a sentimental favorite because they were the first killer CG app, drawing attention and investment dollars to the then nascent field in the sixties.)

Automobiles, airplanes and almost any fairly complex manufactured object we see around us are designed, fabricated and even put through regulatory tests as virtual entities – which exist entirely as a collection of bits perceptible only as an image on a monitor – gestating often for years before the first physical prototype is ever built.

Supercomputers implement extremely complex mathematical models of the weather, but their predictions have to be visualized – again CGI – in order to be meaningful to humans.

Because its business is the creation of pictures, computer graphics has an immediate allure. But, it is a science as well, with intellectual challenges ranging from the routine to about as deep and difficult as you please. Think of modeling a drop of water rolling off a leaf. There would be a fair amount of physics and, probably, a differential equation or two to solve on the way to getting just the mechanics of the rolling drop right, not to mention texturing the leaf, creating a translucent (and changing) shape for the drop, and determining illumination.

The field of computer graphics brings particular pleasure to students and practitioners alike because it's always about making something – just like sculpting or painting. Part by part you watch your creation come together, and alive even, if it is animated. Aside from the aesthetic, there are more tangible rewards to be had too. One would be hard pressed to name a sphere of social or scientific or industrial activity where CGI does not have a role. Wherever it is that ultimately you want to be, medicine or fashion, rocket science or banking, weapons development or disco dancing, CG skills not only can make a difference, but also make you a career.

1.1 Brief History of Computer Graphics

Although the term "computer graphics" itself was coined in 1960 by William Fetter, a designer at Boeing, to describe his own job, the field can be said to have first arrived with the publication in 1963 of Ivan Sutherland's Sketchpad program, as part of his Ph.D. thesis at MIT.

Sketchpad, as its name suggests, was a drawing program. Beyond the interactive drawing of primitives such as lines and circles and their manipulation – in particular, copying, moving and constraining – with use of the then recently invented light pen, Sketchpad had the first fully-functional graphical user interface (GUI) and the first algorithms for geometric operations such as clip and zoom. Interesting, as well, is that Sketchpad's innovation of an object-instance model to store data for geometric primitives foretold object-oriented programming. Coincidentally, on the hardware side, the year 1963 saw the invention by Douglas Engelbart at the Stanford Research Institute of the mouse, the humble device even today carrying so much of GUI on its thin shoulders.

Figure 1.5: Ivan Sutherland operating Sketchpad on a TX-2 (courtesy of Ivan Sutherland), Douglas Engelbart's original mouse (courtesy of John Chuang).

Although Sketchpad ran on a clunky Lincoln TX-2 computer with only 64KB in memory and a bulky monochrome CRT monitor as its front-end, nevertheless, it thrust CG to the attention of early researchers by showing what was possible. Subsequent advances through the sixties came thick and fast: raster algorithms, the implementation of parametric surfaces, hidden-surface algorithms and the representation of points by homogeneous coordinates, the latter crucially presaging the foundational role of projective geometry in 3D graphics, to name a few. Flight simulators were the killer app of the day and companies such as General Electric and Evans & Sutherland, co-founded by Douglas Evans and Ivan Sutherland, wrote simulators with real-time graphics.

Interestingly, the advent of flight simulators actually predated that of CG – at least Sutherland and his Sketchpad – by nearly two decades, when the US Navy began the funding of Project Whirlwind at MIT during the Second World War for the purpose of creating simulators to train bomber crews. Those early devices had actually little graphics and consisted essentially of a simulated instrument panel reacting in real-time to control input from the pilots, but Project Whirlwind helped fund the talent and research environment at MIT which enabled Sutherland, a student then at MIT, to create Sketchpad, launch computer graphics and, finally, complete the circle by establishing a company to make flight simulators.

The next decade, the seventies, brought the z-buffer for hidden surface removal, texture mapping, Phong's lighting model – all crucial components of the OpenGL API (Application Programming Interface) we'll be using soon – as well as keyframe-based animation. Photorealistic rendering of animated movie keyframes almost invariably deploys ray tracers, which were born in the seventies too. Emblematic of the advances in 3D design was Martin Newell's 1975 Utah teapot, composed entirely of bicubic Bézier patches, which became the testbed of choice for CG algorithms of that era. The latter half of the decade saw, too, the Apple I and II personal computers make their debut, bringing CG for the first time to the mass market.

Figure 1.6: Utah teapot (from Wikimedia), Apple II Plus (courtesy of Steven Stengel), SIGGRAPH 2006 expo floor in Boston (courtesy of Jason Della Rocca).

From the academic point of view, particularly important were the establishment in 1969 of the SIGGRAPH (Special Interest Group in Graphics) by the ACM (Association for Computing Machinery, the premier academic society for computers and computing) and, subsequently, the first annual SIGGRAPH conference in 1973. These two developments signaled the emergence of computer graphics as a major subdiscipline of computer science. The SIGGRAPH conference has since then become the foremost annual event in the CG world. In addition to being the most prestigious forum for research papers, it hosts a giant exhibition which attracts hundreds of companies, from software developers to book publishers, who set up booths to promote their wares and recruit talent.

Since the early eighties, CG, both software and hardware, began rapidly to assume the form we see today. The IBM PC, the Mac and the x86 chipsets all arrived, sparking off the race to become faster (processor), smaller (size), bigger (memory) and cheaper (particularly important if one has student loans to pay off). As computers became consumer goods, the market for software spilled over from academia to individuals and businesses.

Nintendo released Donkey Kong in 1981, the wildly successful arcade video game which revolutionized the genre, and soon after Wavefront Technologies released its Preview software, used then to create opening graphics for television programs. Now, of course, Nintendo is a star of the video games industry producing the Wii and it successors, while Wavefront has morphed into Alias (owned by Autodesk) whose 3D graphics modeling package Maya is ubiquitous in the design world.

3D graphics began to displace its plainer 2D sister through the nineties as hardware increasingly became capable of supporting the rendering needs of 3D models, even in real-time, thus allowing interaction and its myriad consequences (such as gaming).

The difference between 2D and 3D graphics is that models in the latter are created in a (virtual) 3D world, geometrically identical to real world, and then projected onto the viewing screen, while all drawings in 2D graphics are on a flat plane.

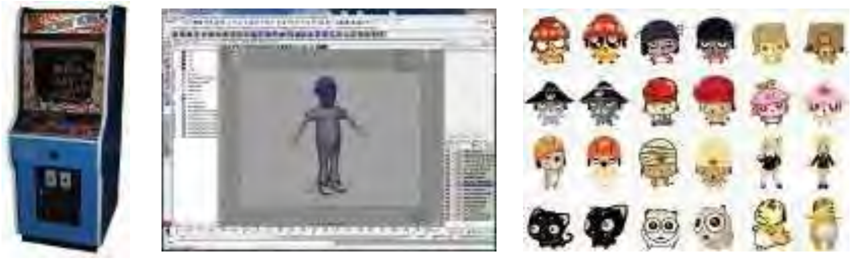

Figure 1.7: Donkey Kong arcade game (from Wikimedia), Maya screenshot of Scary Boris (courtesy of Sateesh Malla at www.sateeshmalla.com), 2D characters on the left of each column vs. 3D to their right (© Mediafreaks Cartoon Pte. Ltd., 2006. All rights reserved.).

Models drawn in 3D are more realistic because they belong to the space we actually live in, but they are more complex as well; moreover, the 3D-to-2D projection step, absent for 2D graphics, is computation-intensive too. Graphics cards, manufactured by companies such as ATI and Nvidia, which not only manage the image output to the display unit, but have, as well, additional hardware support for rendering of 3D primitives, are now inexpensive enough that desktops and even notebooks can run high-end 3D applications. How well they run 3D games often, in fact, is used to benchmark personal computers.

Figure 1.8: T. Rex: heartthrob of the Jurassic Park movies, Quake 1 game (courtesy of Quake ® © 1996 id Software LLC, a ZeniMax Media Company, All Rights Reserved).

Through the nineties, as well, the use of 3D effects in movies became pervasive. The Terminator and Star Wars series, and Jurassic Park, were among the early movies to set the standard for CGI. Toy Story from Pixar, released in 1995, has special importance in the history of 3D CGI as the first movie to be entirely computer-generated – no scene was ever pondered through a glass lens, nor any recorded on a photographic reel! It was cinema without film. Quake, released in 1996, the first of the hugely popular Quake series of games, was the first fully 3D game.

Another landmark from the nineties of particular relevance to us was the release in 1992 of OpenGL, the open-standard cross-platform and cross-language 3D graphics API, by Silicon Graphics. OpenGL is actually a library of calls to perform 3D tasks, which can be accessed from programs written in various languages and running over various operating systems. That OpenGL was high-level (in that it frees the applications programmer from having to care about such low-level tasks as representing primitives like lines and triangles in the raster, or rendering them to the window) and easy to use (much more so than its predecessor 3D graphics API, PHIGS, standing for Programmer's Hierarchical Interactive Graphics System) first brought 3D graphics programming to the "masses". What till then had been the realm of a specialist was now open to a casual programmer following a fairly amicable learning curve.

Figure 1.9: OpenGL and OpenGL ES logos (used with permission of Khronos).

Since its release OpenGL has been rapidly adopted throughout academia and industry. It's only among game developers that Microsoft's proprietary 3D API, Direct3D, which came soon after OpenGL and bearing an odd similarity to it but optimized for Windows, is more popular.

The story of the past decade has been one of steady progress, rather than spectacular innovations in CG. Hardware continues to get faster, better, smaller and cheaper, continually pushing erstwhile high-end software downmarket, and raising the bar for new products. The almost complete displacement of CRT monitors by LCD and the emergence of high-definition television are familiar consequences of recent hardware evolution.

Of likely even greater economic impact is the migration of sophisticated software applications – ranging from web browsers to 3D games – to handheld devices like smartphones, on the back of small yet powerful processors. CG has now been untethered from large immobile devices and placed into the hands and pockets of consumers. In fact, a lightweight subset of OpenGL called OpenGL ES – ES abbreviating Embedded Systems – released by the Khronos Group in 2003, is now the most popular API for programming 3D graphics on small devices.

Another important development is the advent of WebGL – OpenGL for the web as its name suggests. WebGL is based on OpenGL ES and is currently supported by almost all browsers, making possible real-time interactive CGI via the web.

1.2 Overview of a Graphics System

The operation of a typical graphics system can be split into a three-part sequence:

$$\text{Input} \dashrightarrow \text{Processing} \dashrightarrow \text{Output}$$

The simplest example of this is when you click on a thumbnail image in, say, YouTube, and a video clip pops up and begins to play. The click is the input. Your computer then reacts to this input by processing, which involves downloading the movie file and running it through the Adobe Flash Player, which in turn outputs video frames to your monitor.

Figure 1.10: YouTube and Adobe Illustrator screenshots.

Graphics systems can be of two types, non-interactive and interactive. The playing of a YouTube clip is an example of a non-interactive one: beyond the first click to get the movie started you have little further say over the output process, other than maybe to stop it or manipulate the window. On the other hand, if, say, you are using a package like Adobe Illustrator, then the output – what you have drawn – changes in real-time in response to input you provide by pressing keys and moving and clicking the mouse; e.g., you can change a shape by dragging an anchor point with the mouse. In an interactive system output continuously reacts to input via the processor.

Input/output devices (or I/O devices, or peripheral devices, as they are also called) are of particular importance in interactive systems because they determine the scope of the interaction. For example, an input device that functions like a steering wheel would be essential to a video game to race cars; simulating flight through a virtual 3D environment, on the other hand, needs something akin to a joystick used to maneuver an aircraft.

Because it is, in fact, interactive computer graphics – theory and programming – which we'll be studying the next twenty chapters, we'll survey in the next two sections the most common I/O devices found in graphics systems nowadays. As for the processor which comes between the I and the O, from the point of view of the CG programmer, this is just a box to do her bidding, particularly, run her apps. For the sake of completeness, though, here's a list of the important ones, all somewhat different one from the other in the context of CG (Figure 1.11 pictures them):

Computer : As far as we are concerned, this category includes PC's, workstations, servers and the like.

Portable computer : This, of course, is simply a small and light computer with a built-in display, keyboard and pointing device. Because of the size constraint, limited power supply and also the lack of space for a large cooling fan, CPU's and graphics cards in portables tend to underperform their desktop counterparts. Software writers need to take this into account, especially for graphics-intensive applications.

Figure 1.11: Processing devices clockwise from top: laptop, smartphone, game console (used with permission from Microsoft), computer box.

Handheld device: The size-weight constraint on this class of devices – of which the mobile phone is the most visible example – is even more severe than for portable computers. Handhelds are expected to travel in bags and pockets. Low-end handhelds often have no peripheral other than a limited keypad, while higher-end ones may come equipped with a high-res end-to-end touchscreen. In addition to the possibly small RAM and slower CPU, another consideration to keep in mind for graphics developers for handhelds is the limited real estate of the display: busy scenes tend to become chaotic on a handheld.

Game consoles: All stops are off for programming these devices. Running graphics-intensive applications at blinding speeds is what these machines were born to do.

1.2.1 Input Devices

The following is by no means a complete list of input devices, but it does cover the ones we are most likely to encounter in everyday use. The devices are all pictured in Figure 1.12, ringing the processing devices in the middle, and our list goes clockwise starting from the top rightmost.

Keyboard : This device is a mandatory peripheral for any computer. Its alphanumeric keys, evidently derived from the traditional typewriter, are used to enter text strings, while additional keys, such as the arrow and function keys, perform special actions.

Mouse: This is an example of a *pointing device* which inputs spatial data to the computer. As the mouse is moved by the user's hand on a flat surface, a mechanical ball or optical sensor at its base signals the amount of movement to the computer, which correspondingly moves a cursor on the screen. Effectively, then, the user determines the location of the cursor. Strictly speaking, a mouse is more than just a pointing device if it has buttons, as most do, each of which can be clicked to give binary input.

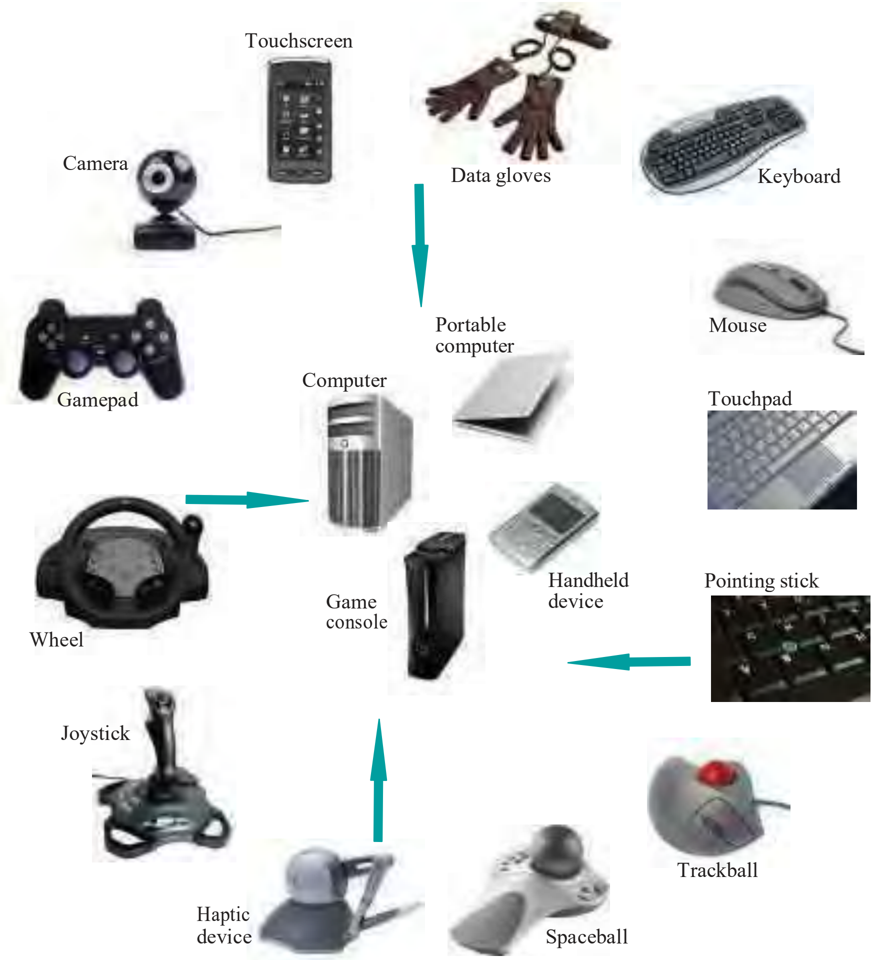

Figure 1.12: Input devices clockwise from top right (surrounding processing devices in the middle): keyboard, mouse, touchpad, pointing stick (courtesy of Long Zheng), trackball, spaceball (courtesy of Logitech), haptic device (© SensAble Technologies, Inc.), joystick, wheel, gamepad, webcam, touchscreen, data gloves (courtesy of www.5dt.com).

Touchpad : Another 2D pointing device, particularly common on portable computers, the touchpad is a small rectangular area embedded with electronic sensors to determine the position of a touching finger or stylus. Movement of the finger or stylus is echoed by movement of the cursor.

Pointing stick : Yet another 2D pointing device common on portable computers, the pointing stick is, typically, a rubber peg located between the 'G', 'H' and 'B' keys, which moves the cursor in response to pressure applied with a finger.

Trackball : This is essentially an upside-down mouse, with a socket containing a ball which the user manipulates with her hand to make the cursor move.

Spaceball : This is a pointing device with six degrees of freedom versus the two of an ordinary mouse. It is used in special applications such as manipulating a camera in a 3D scene, where the camera not only moves, but also rotates. The spaceball itself consists of a pressure-sensitive ball which can distinguish different kinds of forces – including forward and backward, lateral and twist – the applied force manipulating the selected object.

Haptic device: This is a pointing device which gives physical feedback to the user based on the location of the cursor or, possibly, that of an object being moved along with the cursor. The easiest way to understand the functioning of a haptic device, if you have never used one, is to imagine a mouse with a mechanical ball which is (somehow) programmed to lock and stop rolling when the cursor reaches the side of the screen. The reaction the user then has is of that of the cursor running into a physical obstacle at the edge of the screen, though evidently it is moving in virtual space. The device depicted in Figure 1.12 is not a haptic mouse, of course, but one commonly seen in HCI (human-computer interaction) labs. The three-link arm swiveling on a ball gives it six degrees of freedom.

Haptics has numerous applications, a couple of noteworthy ones being the tele-operation of robots (where the operator gets haptic feedback as she manipulates a robot in either a virtual or a remote real environment) and simulated surgery training in medicine (which is similar to training pilots on a flight simulator, except that surgery has the added component of tactile feedback, mostly absent in flying).

Joystick : This is an input device popular in video games and applications such as flight simulators. It originated from its namesake found in real aircraft cockpits. A joystick pivots around a fixed base, gaining thus two degrees of freedom, and usually has buttons which can be depressed to provide additional input. In a game or simulator setting a joystick is typically used to control an object traveling through space. Nowadays, high-end joysticks have embedded motors to provide haptic feedback to user motion, e.g., resistance as a plane is banked.

Wheel : This again is a specialized input device for games and simulators, obviously derived from the car steering wheel, and provides rotational input in an exactly similar manner, most often to a virtual automobile. Again, haptic feedback to give the user a sense of the vehicle's response, and even of the terrain over which it is traveling, is becoming increasingly popular.

Gamepad : This device is the standard controller for many modern game consoles. Usual features include action buttons operated usually with the right thumb and a cross-shaped directional controller with the left.

Camera: Although this input device needs no introduction, it's worth noting the increasingly sophisticated uses a peripheral camera is being put to with the help, e.g., of software to recognize faces, gestures and expressions.

Touchscreen: Increasingly popular as the interface of handheld devices such as smartphones, a touchscreen is a display which can accept input via touch. It is similar to touchpads and tablets in that it senses the location of a finger or stylus – one or the other is usually preferable based on the particular technology used to make the screen – on the display area. A common application of touchscreens is to eliminate the need for a physical keyboard by displaying a virtual one responding to taps on the screen.

Touchscreens often respond not only to the location of the touch, but also the motion of the touching object. For example, a flicking motion with a finger may cause a window to scroll. Multi-touch capability, now increasingly common, makes possible for the device to respond to gestures with more than one finger, e.g., pinching and spreading with two fingers.

Data gloves: This device is used particularly in virtual reality environments which are programmed to react to the position of the gloves, the direction in which fingers are pointing, as well as to hand motion and gestures. The gloves themselves are wired to transmit not only their location, but also their configuration and orientation to the processor, so that the latter can display the environment accordingly. For example, an index finger pointing at a particular atom in a virtual-reality display of a molecule may cause this atom to zoom up to the viewer.

1.2.2 Output Devices

Again, the following list is not meant to be comprehensive, but, rather, representative of the most common output devices. We go clockwise around the outer ring of devices pictured in Figure 1.14 beginning with the rightmost.

CRT (cathode-ray tube) monitor : Though now nearly obsolete CRT monitors are worth a review because they were the first visual output devices, for which reason their configuration greatly influenced the development of foundational graphics algorithms. A CRT monitor has phosphors of the three primary colors – R(ed), G(reen) and B(lue), the basis of CG color application – located at each one of a rectangular array of pixels, called the raster. Additionally, it has three electron guns inside, causing its infamous bulk, that each fires a beam at phosphors of one color. A mechanism to aim and control their intensities causes the beams to travel together, striking one pixel after another, row after row, exciting the RGB phosphors at each pixel to the values specified for it in the color buffer. Figure 1.13(a) shows the electron beams striking one pixel on a dog.

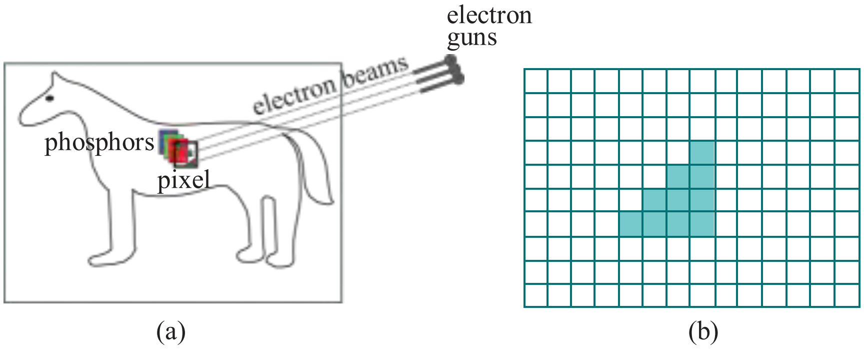

Figure 1.13: (a) Color CRT monitor with electron beams aimed at a pixel with phosphors of the 3 primaries (b) A raster of pixels showing a rasterized triangle.

From the point of view of OpenGL and most CG theory, what matters is that the pixels in a monitor are arranged in a rectangular raster (as depicted in Figure 1.13(b)). For, this layout is the basis of the lowest-level CG algorithms, the so-called raster algorithms, which actually select and color the pixels to represent user-specified shapes such as lines and triangles on the monitor. Figure 1.13(b), for example, shows the rasterization of a right-angled triangle (with terrible jaggies because of the low resolution).

The number of rows and columns of pixels in the raster determines the monitor's resolution. Typical for a CRT monitor is a resolution in the range of 1024 ×768 (which means 1024 columns and 768 rows). High-definition monitors (as needed, say, for high-definition TV, or HDTV as it's acronymed) have higher resolution, e.g., 1920 × 1080 is common.

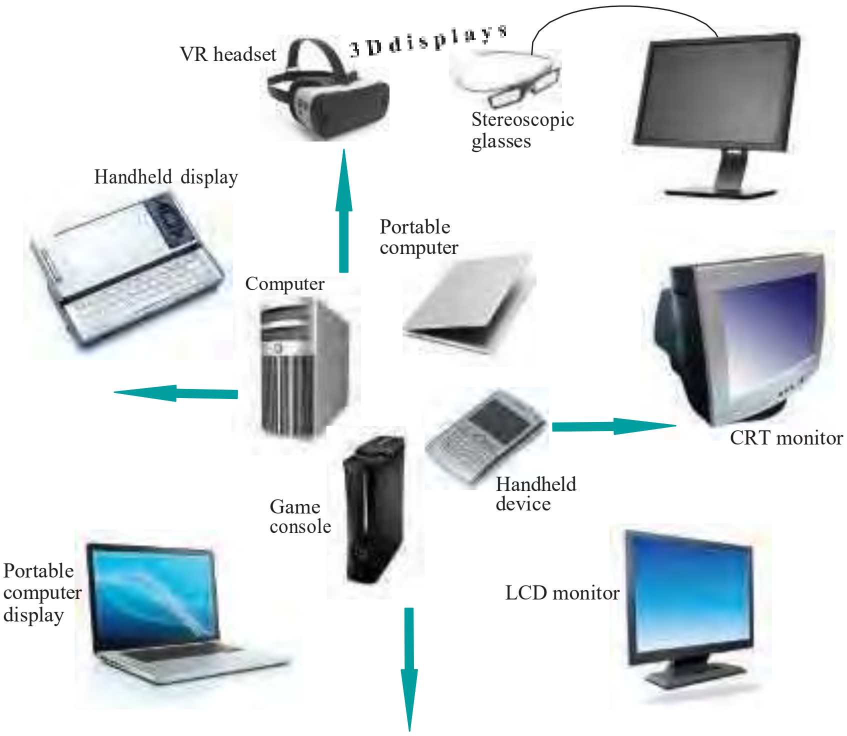

Figure 1.14: Output devices clockwise from the rightmost (surrounding processing devices in the middle): CRT monitor, LCD monitor, notebook, mobile phone, 3D displays including a VR headset and stereoscopic glasses tethered to a PC.

Moreover, a memory location called the color buffer, either in the CPU or graphics card, contains, typically, 32 bits of data per raster pixel – 8 bits for each of RGB, and 8 for the alpha value (used in blending). It is the RGB values in the color buffer which determine the corresponding raster pixel's color intensities. The values in the color buffer are read by the raster – in other words, the raster is refreshed – at a rate called the monitor's refresh rate. Beyond this, the technology underlying the particular display device, no matter how primitive or fancy, really matters little to the CG programmer.

For decades a bulky CRT monitor, or two, was a fixture atop work tables. Now, of course, they have been nearly totally supplanted by a sleeker successor which we discuss next.

LCD (liquid crystal display) monitor : Pixels in an LCD monitor each consist of three subpixels made of liquid crystal molecules, which separately filter lights of the primary colors. The amount of light, coming from a backlight source, emerging through a subpixel is controlled by an electric charge whose intensity is determined by subpixel's corresponding value in the color buffer. The absence of electron guns allows LCD monitors to be made flat and thin – unlike CRT monitors – so they are one of the class of flat panel displays.

Technologies other than LCD, e.g., plasma and OLED (organic light emitting diode), are used as well in flat panel displays, though LCD is by far the most common one found with computers. Keep in mind that what's called an LED monitor is simply a kind of LCD monitor where the backlighting comes from array of light-emitting diodes (LEDs) - in fact, almost all LCD monitors nowadays have this kind of backlighting, so would be classified as LED monitors.

Again, for a CG programmer the view to keep in mind of an LCD monitor, as of any other flat panel display, is as a rectangular raster of pixels whose RGB intensities are individually set by values in the computer's color buffer.

Portable computer display : This display is again a raster of pixels whose RGB values are read from a color buffer. The technology employed, typically, is TFT-LCD, a variant of LCD which uses thin film transistors to improve image quality.

Handheld display : Handheld displays, such as those on devices like mobile phones, commonly use the same TFT-LCD technology as portable computers. The resolution, though, is necessarily smaller, e.g., 480×640 would be in the ballpark for low-end mobiles.

3D display : Almost all 3D displays are based on the principle of stereoscopy, in which an illusion of depth is created by showing either eye of the viewer images of the scene captured by one of two cameras slightly offset from one another (just like a pair of eyes as in Figure 1.15). Once the scene has been recorded with two cameras, it is in ensuring that each eye of the viewer sees frames only from one of them, called stereoscopic viewing, that there are primarily two competing technologies.

Figure 1.15: An early model stereo camera filming a newish bike.

In the first, frames alternately from either camera are displayed on the monitor, a process called alternate frame sequencing. The viewer herself wears stereoscopic glasses, each lens embedded with a layer of liquid crystals which can be darkened with an electrical signal (such glasses are also called LC shutter glasses). The glasses are synchronized with the monitor's refresh rate, either lens being alternately darkened with successive frames. Consequently, each eye sees images from only one of the two cameras, resulting in a stereoscopic effect. Typically, the frame rate is increased to 48 per second as well, so that both eyes experience a smooth-seeming 24 frames each second. The great advantage of LC shutter glasses is that they can be used with any computer which has a monitor with a refresh rate fast enough to support alternate frame sequencing, as well as a graphics card with enough buffer space for two video streams. So with these glasses even a high-end home system would qualify to play 3D movies and games.

In the second, polarized 3D glasses are used to view two images, from either camera, projected simultaneously on the same screen through orthogonal polarizing filters. The lenses too contain orthogonal polarizing filters, each allowing through only light of like polarization. Consequently, either lens sees images from only one or other camera, engendering a stereoscopic view. Polarized 3D glasses are significantly less expensive than LC shutter glasses and, moreover, require no synchronization with the monitor. However, the projection system is complicated and expensive and primarily used to equip theaters for 3D viewing.

VR headsets, increasing popular nowadays for an immersive 3D experience, are each a two-stream projection system with twin-lens viewing all in one, which can use either of the above technologies.

OpenGL, the API we'll be using, is well-suited to making scenes and movies for 3D viewing because it allows multiple (virtual) cameras to be positioned arbitrarily.

1.3 Quick Preview of the Adventures Ahead

To round out this invitation to CG we want to show you four programs written by students in their first college 3D CG course, taught by the author at the Asian Institute of Technology using a draft of this book. They were written in C++ with calls to OpenGL.

But, first, what exactly is OpenGL? You may have been wondering this awhile. We said earlier in the section on CG history that OpenGL is a cross-platform 3D graphics API. It consists of a library of over 500 commands to perform 3D tasks, which can be accessed from programs written in various languages. Well, here's a glimpse of something concrete – an example snippet from a C++ environment to draw 10 red points:

```
glColor3f(1.0, 0.0, 0.0);
glBegin(GL_POINTS);
   for(int i = 0; i < 10; i++)
   {
      glVertex3i(i, 2*i, 0);
   }
glEnd();
```

The first function call glColor3f(1.0, 0.0, 0.0) declares the red drawing color, while the loop bracketed between the glBegin(GL_POINTS) and glEnd() calls draws a point at (i, 2i, 0) in each of ten iterations. There are calls in the OpenGL library to draw straight lines, triangles, create light sources, apply textures, move and rotate objects, maneuver the camera, and so on – in fact, not surprisingly, pretty much all one needs to create and animate 3D scenes.

In the early days, coding CG meant pretty much addressing individual pixels of the raster to turn on and off. Compared with using OpenGL today this is like programming in assembly compared with programming in a high-level language like C++. OpenGL gives an environment where we can focus on imagining and creating, leaving low-level work all to the underlying engine.

Isn't that old OpenGL, though, the code you show above? Yes, it is. Precisely, it's pre-shader OpenGL.

But, the fact you are asking this question probably means you are not familiar yet with our pedagogical approach, which is described in the book's preface. We explain there why we believe in setting the reader's foundations in the classical version of OpenGL before proceeding to the new (namely, fourth generation or 4.x) of which there is complete coverage later in the book. We urge you to read at least that part of the preface in order to be comfortable with how we plan on doing things.

Getting back to the student programs, code itself is not of importance and would actually be a distraction at this time. Instead, just running the programs and viewing the output will give an idea of what can be accomplished even in a fairly short time (ranging from 3 weeks to 3 months for the different programs) by persons coming to CG with little more than a good grasp of C++ and some basic math. Of course, we'll get a feel as well for what goes into making 3D scenes.

Experiment 1.1. Open ExperimenterSource/Chapter1/Ellipsoid and run the (Windows) executable there for the Ellipsoid program.* The program draws an ellipsoid (an egg shape). The left of Figure 1.16 shows the initial screen. There's plenty of interactivity to try as well. Press any of the four arrow keys, as well as the page up and down keys, to change the shape of the ellipsoid, and 'x', 'X', 'y', 'Y', 'z' and 'Z' to turn it.

It's a simple object, but the three-dimensionality of it comes across rather nicely does it not? As with almost all surfaces that we'll be drawing ourselves, the ellipsoid is made up of triangles. To see these press the space bar to enter wireframe mode. Pressing space again restores the filled mode. Wireframe reveals the ellipsoid to be a mesh of triangles decorated with large points. A color gradient has apparently been applied toward the poles as well.

Drawing an ellipsoid with many triangles may seem a hard way to do things. Interestingly, and often surprisingly for the beginner, OpenGL offers the programmer

*Experimenter.pdf does not have clickable links to run the executables for this chapter. Clickable links to bring up source code and project files start from the next chapter.

only a tiny set of low-level geometric primitives with which to make objects – in fact, points, lines and triangles are, basically, it. So, a curved 3D object like an ellipsoid has to be made, or, more accurately, *approximated* , using triangles. But, as we shall see as we go along, the process really is not difficult.

That’s it, there’s really not much more to this program. It’s just a bunch of colored triangles and points laid out in 3D space. The magic is in those last two words: *3D space*. 3D modeling is all about making things in 3D – not a flat plane – to create an illusion of depth, even when viewing on a flat plane (the screen). End

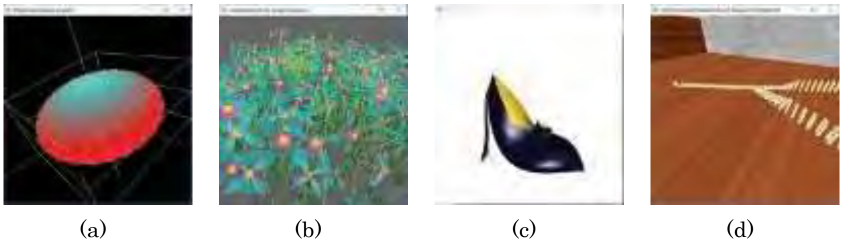
(a) (b) (c) (d)

Figure 1.16: Screenshots of (a) Ellipsoid (b) AnimatedGarden (c) BezierShoe (d) Dominos.

Experiment 1.2. Our next program is animated. It creates a garden which grows and grows and grows. You will find the executable in ExperimenterSource/-Chapter1/AnimatedGarden. Press enter to start the animation; enter again to stop it. The delete key restarts the animation, while the period key toggles between the camera rotating and not. Again, the space key toggles between wireframe and filled. The second image of Figure 1.16 is a screenshot a few seconds into the animation.

As you can see from the wireframe, there’s again a lot of triangles (in fact, the flowers might remind you of the ellipsoid from the previous program). The plant stems are thick lines and, if you look carefully, you’ll spot points as well. The one special effect this program has that Ellipsoid did not is blending, as is not hard to see. End

Experiment 1.3. The third program shows fairly fancy object modeling. It makes a lady’s shoe with the help of so-called Bézier patches. The executable is in ExperimenterSource/Chapter1/BezierShoe. Press ‘x’-‘Z’ to turn the shoe, ‘+’ and ‘-’ to zoom in and out, and the space bar to toggle between wireframe and filled. The third image of Figure 1.16 is a screenshot.

Keep in mind that, as far as CG goes, the *techniques* involved in designing a shoe are the same as for designing a spaceship! End

Experiment 1.4. Our final program is a movie which shows a Rube Goldberg domino effect with “real” dominos. The executable is in ExperimenterSource/-Chapter1/Dominos. Simply press enter to start and stop the movie. The screenshot on the right of Figure 1.16 is from part way through.

This program has a bit of everything – textures, lighting, camera movement and, of course, a nicely choreographed animation sequence. Neat, is it not? End

All fired up now and ready to rumble? Great! Let’s go.

Acknowledgments: Kumpee Teeravech wrote Ellipsoid and AnimatedGarden, Pongpon Nilaphruek wrote BezierShoe, while Kanit Tangkathach and Thanapoom Veeranitinunt wrote Dominos.

Chapter 2

On to OpenGL and 3D Computer Graphics

The primary goal for this chapter is to be acquainted with OpenGL and begin our journey into computer graphics using OpenGL as the API (Application Programming Interface) of choice. We shall apply an experiment-discuss-repeat approach where we run code and ask questions of what is seen, acquiring thereby an understanding not only of the way the API functions, but underlying CG concepts as well. Particularly, we want to gain insight into:

(a) The synthetic-camera model to record 3D scenes, which OpenGL implements.

(b) The approach of approximating curved objects, such as circles and spheres, with the help of straight and flat geometric primitives, such as line segments and triangles, which is fundamental to object design in computer graphics.

We begin in Section 2.1 with our first OpenGL program to draw a square, the computer graphics equivalent of "Hello World". Simple though it is, with a few careful experiments and their analysis, square.cpp yields a surprising amount of information through Sections 2.1-2.3 about orthographic projection, the fixed world coordinate system OpenGL sets up and how the so-called viewing box in which the programmer draws is specified in this system. We gain insight as well into the 3D-to-2D rendering process.

Adding code to square.cpp we see in Section 2.4 how parts of objects outside the viewing box are clipped off. Section 2.5 discusses OpenGL as a state machine. We have in this section as well our first glimpse of property values, such as color, initially specified at the vertices of a primitive, being interpolated throughout its interior.

Next is the very important Section 2.6 where all the drawing primitives of OpenGL are introduced. These are the parts at the application programmer's disposal with which to assemble objects from thumbtacks to spacecrafts.

The first use of straight primitives to approximate a curved object comes in Section 2.7: a curve (a circle) is drawn using straight line segments. To create more interesting and complex objects one must invoke OpenGL's famous three-dimensionality. This means learning first in Section 2.8 about perspective projection as also hidden surface removal using the depth buffer.

After a bunch of drawing exercises in Section 2.9 for the reader to practice her newly-acquired skills, the topic of approximating curved objects is broached again in Section 2.10, this time to approximate a surface with triangles, rather than a curve with straight segments as in Section 2.7. Section 2.11 is a review of all the syntax that goes into making a complete OpenGL program.

We conclude with a summary, brief notes and suggestions for further reading in Section 2.12.

2.1 First Program

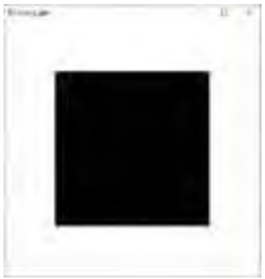

Figure 2.1: Screenshot of square.cpp, in particular, the OpenGL window.

Experiment 2.1. Run square.cpp.

Note: Visit the book's website www.sumantaguha.com for a guide how to install OpenGL and run our programs. *Importantly* , we have changed our development environment significantly for this edition so programs for the second edition will not run off the bat in the environment for this one and vice versa. The needed change in code itself is fairly trivial though. The install guide should make everything clear.

In the OpenGL window appears a black square over a white background. Figure 2.1 is an actual screenshot, but we'll draw it as in Figure 2.2, bluish green standing in for white in order to distinguish it from the paper. We are going to understand next how the square is drawn, and gain some insight as well into the workings behind the scene.

End

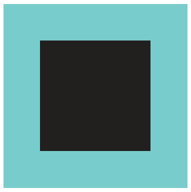

Figure 2.2: OpenGL window of square.cpp (bluish green pretending to be white).

The following six statements in square.cpp create the square:

```
glBegin(GL_POLYGON);
   glVertex3f(20.0,  20.0,  0.0);
   glVertex3f(80.0, 20.0, 0.0);
   glVertex3f(80.0, 80.0, 0.0);
   glVertex3f(20.0, 80.0, 0.0);
glEnd();
```

Remark 2.1. *Important* ! If, from what you may have read elsewhere, you have the notion that glBegin()-glEnd(), and even GL_POLYGON, specifications are classical and don't belong in the newest version of OpenGL, then you are right insofar as they are not in the core profile of the latter. They are, though, accessible via the compatibility profile which allows for backward compatibility. Moreover, we explain carefully in the book's preface why we don't subscribe to the *toss-everything-classical* school of thought as far as *teaching* OpenGL is concerned. Of course, we shall cover thoroughly the most modern – in fact, fourth generation – OpenGL later in the book. If you have not done so yet, we strongly urge you to read about our pedagogical approach in the preface in order to be comfortable with what follows.

The corners of the square evidently are specified by the four vertex declaration statements between glBegin(GL_POLYGON) and glEnd(). Let's determine how exactly these glVertex3f() statements correspond to the corners.

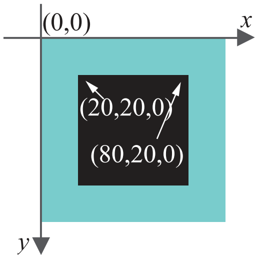

Figure 2.3: The coordinate axes on the OpenGL window of square.cpp? *No.*

If, suppose, the vertices are specified in some coordinate system that is embedded in the OpenGL window – which certainly is plausible – and if we knew the axes of this system, the matter would be simple. For example, *if* the x-axis increased horizontally rightwards and the y-axis vertically downwards, as in Figure 2.3, then glVertex3f(20.0, 20.0, 0.0) would correspond to the upper-left corner of the square, glVertex3f(80.0, 20.0, 0.0) to the upper-right corner, and so on.

However, even assuming that there do exist these invisible axes attached to the OpenGL window, how do we tell where they are or how they are oriented? One way is to "wiggle" the corners of the square! For example, change the first vertex declaration from glVertex3f(20.0, 20.0, 0.0) to glVertex3f(30.0, 20.0, 0.0) and observe which corner moves. Having determined in this way the correspondence of the corners with the vertex statements, we ask the reader to deduce the orientation of the hypothetical coordinate axes. Decide where the origin is located too.

Well, it seems then that square.cpp sets up coordinates in the OpenGL window so that the increasing direction of the x-axis is horizontally rightwards, that of the y-axis vertically upwards and, moreover, the origin seems to correspond to the lower-left corner of the window, as in Figure 2.4. We're making progress but there's more to the story, so read on.

The last of the three parameters of a glVertex3f(*, *, *) declaration is evidently the z coordinate. Vertices are specified in *3-dimensional* space (simply called 3-space or, mathematically, $\mathbb{R}^3$). Indeed, OpenGL allows us to draw in 3-space and create truly 3D scenes, which is its major claim to fame. However, we *perceive* the 3-dimensional scene as a picture *rendered* to a 2-dimensional part of the computer's screen, in particular, the rectangular OpenGL window. Shortly we'll see how OpenGL converts a 3D scene to its 2D rendering.

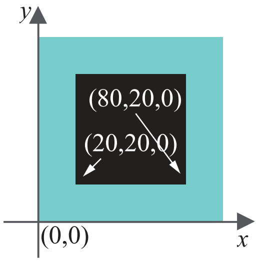

Figure 2.4: The coordinate axes on the OpenGL window of square.cpp? *Well, pretty much, but there's a bit more to it.*

2.2 Orthographic Projection, Viewing Box and World Coordinates

What exactly do the vertex coordinate values mean? For example, is the vertex at (20.0, 20.0, 0.0) of square.cpp 20 mm., 20 cm. or 20 pixels away from the origin along both the x-axis and y-axis, or is there some other absolute unit of distance native to OpenGL? Let's do the following experiment.[*]

Experiment 2.2. The main routine's glutInitWindowSize() parameter values determine the shape of the OpenGL window; in fact, generally, glutInitWindowSize(*w*, *h*) creates a window w pixels wide and h pixels high.

Change square.cpp's initial glutInitWindowSize(500, 500) to glutInitWindowSize(300, 300) and then glutInitWindowSize(500, 250) (Figure 2.5). The drawn square changes in size, and even shape, with the OpenGL window. Therefore, coordinate values of the square appear not to be in any kind of absolute units on the screen. End

Figure 2.5: Screenshot of square.cpp with window size 500 × 250.

Remark 2.2. Of course, you could have reshaped the OpenGL window directly by dragging one of its corners with the mouse, rather than resetting glutInitWindowSize() in the program.

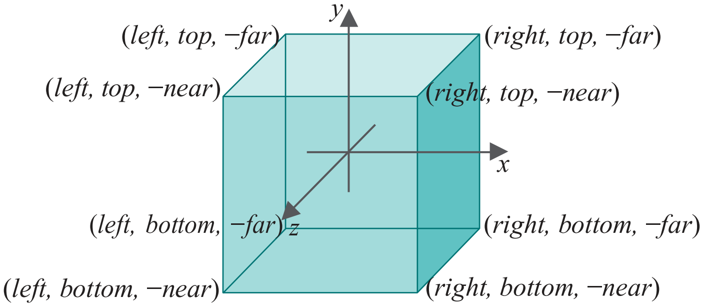

Figure 2.6: Viewing box defined by glOrtho(*left*, *right*, *bottom*, *top*, *near*, *far*).

Understanding what the coordinates actually represent involves understanding first OpenGL's rendering mechanism, which itself begins with the program's *projection statement*. In the case of square.cpp this statement is

```
glOrtho(0.0, 100.0, 0.0, 100.0, -1.0, 1.0)
```

in the resize() routine, which determines an imaginary (or, virtual, if you like) *viewing box* inside which the programmer draws scenes. Generally,

glOrtho(*left*, *right*, *bottom*, *top*, *near*, *far*)

[*] Experiments are an integral part of our teaching method so we urge you to run them as you read. The file *Experimenter.pdf* at the book's website makes this easy by allowing you to open the project file for successive experiments with a single click each. However, even if you don't run an experiment, make sure always to read its discussion in the text.

sets up a viewing box, as in Figure 2.6, with corners at the 8 points:

$(left,\ bottom,\ -near)$, $(right,\ bottom,\ -near)$, $(left,\ top,\ -near)$,
$(right,\ top,\ -near)$, $(left,\ bottom,\ -far)$, $(right,\ bottom,\ -far)$,
$(left,\ top,\ -far)$, $(right,\ top,\ -far)$

It's a box with sides aligned along the axes, whose span along the x-axis is from *left* to *right* , along the y-axis from *bottom* to *top*, and along the z-axis from −*far* to −*near* . Note the little quirk of OpenGL that the *near* and *far* values are flipped in sign. The viewing box corresponding to the projection statement glOrtho(0.0, 100.0 , 0.0, 100.0, -1.0, 1.0) of square.cpp is shown in Figure 2.7(a).

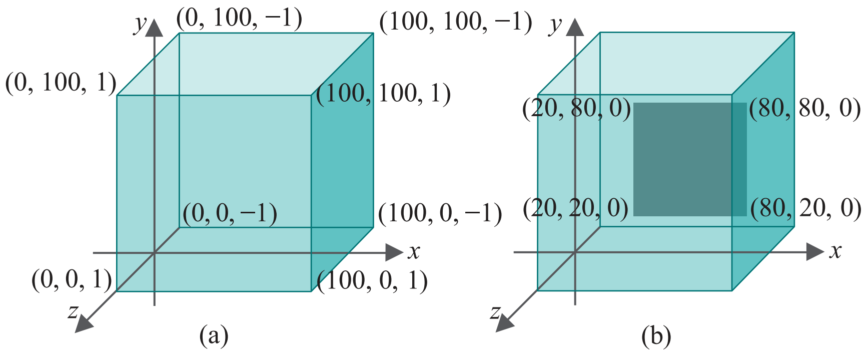

Figure 2.7: (a) Viewing box of square.cpp (b) With the square drawn inside.

The viewing box sits in a 3D space, also virtual, called *world space* because it is the space which will contain every object that we create. The reader certainly may wonder at this time how the coordinate axes of world space themselves are calibrated – e.g., is a unit along an axis one inch, one centimeter or something else – as the size of the viewing box depends on this. The answer will be evident once the rendering process is explained momentarily.

As for drawing now, the vertex declaration glVertex3f(x, y, z) corresponds to the point (x, y, z) in world space. For example, the corner of the square declared by glVertex3f(20.0, 20.0, 0.0) is at (20.0, 20.0, 0.0). The square of square.cpp then, as depicted in Figure 2.7(b), is located entirely inside the viewing box.

Once the programmer has drawn the entire scene, if the projection statement is glOrtho() as in square.cpp, then the rendering process is two-step:

1. *Shoot* : First, objects are *projected perpendicularly* onto the front face of the viewing box, i.e., the face on the $z = -near$ plane. For example, the square in Figure 2.8(a) (same as Figure 2.7(b)) is projected as in Figure 2.8(b). The front face of the viewing box is called the *viewing face* and the plane on which it lies the *viewing plane*.

   This step is like shooting the scene on film. In fact, one can think of the viewing box as a giant version of those archaic *box cameras* where the photographer ducks behind the film – the viewing face – and covers her head with a black cloth; so big, in fact, that the whole scene is actually inside the box. Moreover, mind that with this analogy there's *no* lens, only the film.

2. *Print* : Next, the viewing face is *proportionately scaled* to fit the rectangular OpenGL window. This step is like printing film on paper. In the case of square.cpp, printing takes us from Figure 2.8(b) to (c).

   If, say, the window size of square.cpp were changed to one of *aspect ratio* (= width/height) of 2, by replacing glutInitWindowSize(500, 500) with glutInitWindowSize(500, 250), printing would take us from Figure 2.8(b) to (d) (which actually distorts the square into a rectangle).

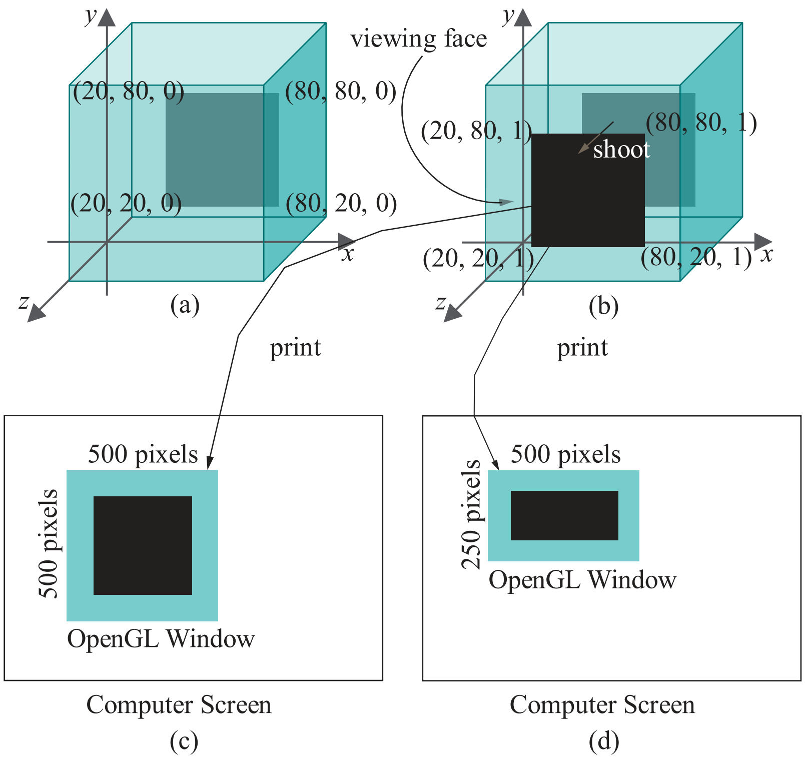

Figure 2.8: Rendering with glOrtho().

The answer to the earlier question of how to calibrate the coordinate axes of world space should be clear now: the 2D rendering finally displayed is the same *no matter* how they are calibrated, because of the proportionate scaling of the viewing face of the box to match the OpenGL window. So it does not matter what unit we use, be it an inch, millimeter, mile, . . .! And, of course, this is why OpenGL never prompts us for information about our world space and how it's coordinatized – it doesn't need to know for it to do its job. Here's a partly-solved exercise to drive home the point.

Exercise 2.1.

(a) Suppose the viewing box of square.cpp is set up in a world space where one unit along each axis is 1 cm. Assuming pixels to be 0.2 mm × 0.2 mm. squares, compute the size and location of the square rendered by shoot-and-print to a 500 pixel × 500 pixel OpenGL window.

(b) Suppose next that the coordinate system of the world space is re-calibrated so that a unit along each axis is 1 meter instead of 1 cm., everything else remaining same. What then are the size and location of the rendered square in the OpenGL window?

(c) What is rendered if, additionally, the size of the OpenGL window is changed to 500 pixel × 250 pixel?

Part answer:

(a) Figure 2.9 on the left shows the square projected to the viewing face, which is 100 cm. square. The viewing face is then scaled to the OpenGL window on the right, which is a square of sides 500 pixels = 500 × 0.2 mm. = 100 mm. Scaling from face to the window, therefore, is a factor of 1/10 in both dimensions. It follows that the rendered square is 60 mm. × 60 mm., with its lower-left corner located both 20 mm. above and to the right of the lower-left corner of the window.

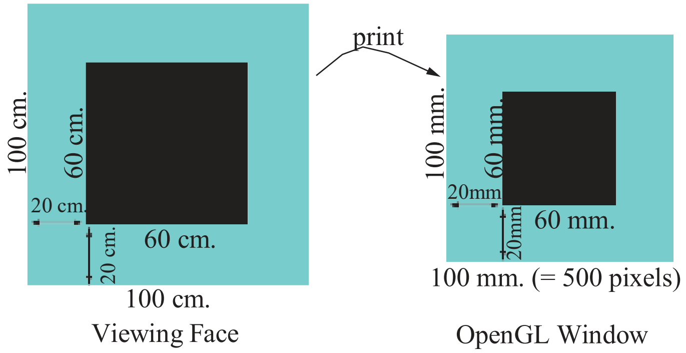

Figure 2.9: The viewing face for square.cpp, given that one unit along each coordinate axis is 1 cm., scaled to a 500 pixel × 500 pixel OpenGL window.

(b) Exactly the same as in part (a) because, while the viewing box and viewing face are now 100 times larger in both the x and y dimensions, the scaling from face to window is now a factor of 1/1000, rather than 1/10.

We conclude that the size and location of the rendering in each coordinate direction are independent of how the axes are calibrated, but determined rather by the *ratio* of the original object's size to that of the viewing box in that direction.

Although the calibration of the world space axes doesn't matter, nevertheless, we'll make the sensible assumption that all three are calibrated *identically*, i.e., one unit along each axis is of equal length (yes, oddly enough, we could make them different and still the rendering would not change, which you can verify yourself by re-doing Exercise 2.1(a), after assuming that one unit along the x-axis is 1 cm. and along the other two 1 meter). The only other assumptions about the initial coordinate system which we make are conventional ones:

(a) It is *rectangular*, i.e., the three axes are mutually perpendicular.

(b) The x-, y- and z-axes in that order form a *right-handed* system in the following sense: a rotation of the x-axis 90° about the origin so that its positive direction matches with that of the y-axis appears *counter-clockwise* to a viewer located on the positive side of the z-axis (Figure 2.10).

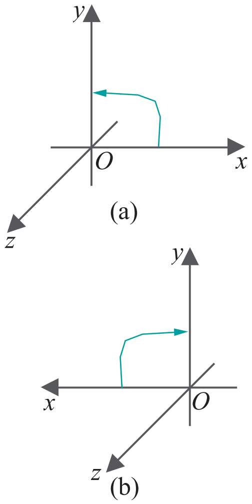

Figure 2.10: The x-, y- and z-axes are rectangular and form a (a) right-handed system (b) left-handed system.

Fixed World System

To summarize, set up an initial rectangular right-handed coordinate system with axes all calibrated identically. Call a unit along each axis just "a unit" as we know it doesn't matter what exactly this unit is, or, equivalently, treat each axis as just a unitless line of numbers. Imagine the system located wherever you like – on top of your desk maybe – and then leave it fixed.

See Figure 2.11 – it actually helps to imagine this system of axes as real and fixed forever. The system coordinatizes world space and, in fact, we shall refer to it as the *world coordinate system*. All subsequent objects, including the viewing box and those that we create ourselves, inhabit world space and are specified in world coordinates. These are all virtual objects, of course.

Remark 2.3. Even though the world coordinate system can be located wherever you like, it is most often helpful to imagine the x-axis running rightward along the bottom of your monitor, the y-axis climbing up the left side, and the z-axis coming at you.

Remark 2.4. Because it's occupied by user-defined objects, world space is sometimes called *object space*.

Figure 2.11: A dedicated 3D graphics programmer in a world all her own.

Incidentally, it's clear now that our working hypothesis after the first experiment in Section 2.1, that the OpenGL window comes with axes fixed to it, though not unreasonable, was not entirely accurate either. The OpenGL window it turns out is simply an empty target rectangle on which the front face of the viewing box is printed. This rectangle is called *screen space*.

So, there are two spaces we'll be working with: world and screen. The former is a virtual 3D space in which we create our scenes, while the latter is a real 2D space where scenes are rendered in a shoot-and-print process.

Experiment 2.3. Change only the viewing box of square.cpp by replacing glOrtho(0.0, 100.0, 0.0, 100.0, -1.0, 1.0) with glOrtho(-100, 100.0, -100.0, 100.0, -1.0, 1.0). The location of the square in the new viewing box is different and, so as well, the result of shoot-and-print. Figure 2.12 is a screenshot and Figure 2.13 explains how. End

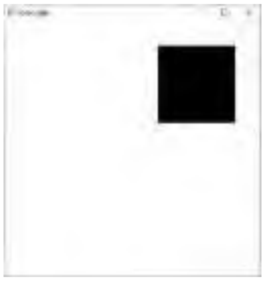

Figure 2.12: Screenshot of square.cpp with glOrtho(-100, 100.0, -100.0, 100.0, -1.0, 1.0).

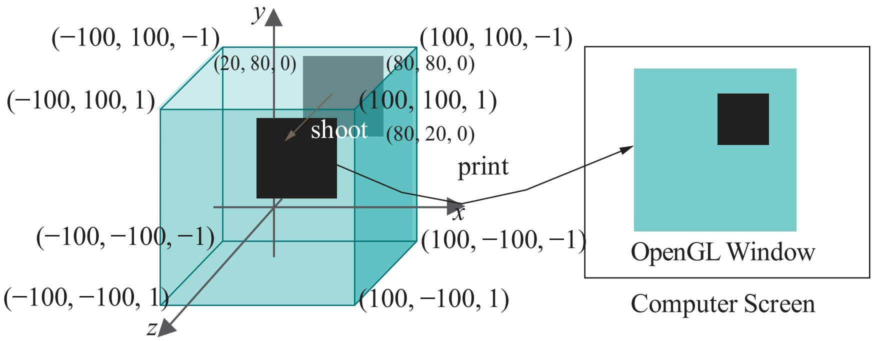

Figure 2.13: The viewing box of square.cpp defined by glOrtho(-100, 100.0, -100.0, 100.0, -1.0, 1.0).

Exercise 2.2. (Programming) Change the viewing box of square.cpp by replacing glOrtho(0.0, 100.0, 0.0, 100.0, -1.0, 1.0) successively with the following, in each case trying to predict the output before running:

(a) glOrtho(0.0, 200.0, 0.0, 200.0, -1.0, 1.0)

(b) glOrtho(20.0, 80.0, 20.0, 80.0, -1.0, 1.0)

(c) glOrtho(0.0, 100.0, 0.0, 100.0, -2.0, 5.0)

Exercise 2.3. If the viewing box of square.cpp is changed by replacing glOrtho(0.0, 100.0, 0.0, 100.0, -1.0, 1.0) with glOrtho(-100.0, 100.0, -100.0, 100.0, -1.0, 1.0), and the OpenGL window size changed replacing glutInitWindowSize(500, 500) with glutInitWindowSize(500, 250), then calculate the area (in *number of pixels*) of the image of the square.

Exercise 2.4. (Programming) We saw earlier that, as a result of the print step, replacing glutInitWindowSize(500, 500) with glutInitWindowSize(500, 250) in square.cpp causes the square to be distorted into a rectangle. By changing *only one* numerical parameter elsewhere in the program, eliminate the distortion to make it appear square again.

Exercise 2.5. (Programming) Alter the z coordinates of each vertex of the "square" – we should really call it a polygon if we do this – of square.cpp as follows:

```
glBegin(GL_POLYGON);
   glVertex3f(20.0, 20.0, 0.5);
   glVertex3f(80.0, 20.0, -0.5);
   glVertex3f(80.0, 80.0, 0.1);
   glVertex3f(20.0, 80.0, 0.2);
glEnd();
```

The rendering does not change. Why?

Remark 2.5. Always set the parameters of glOrtho(*left*, *right*, *bottom*, *top*, *near*, *far*) so that *left* < *right*, *bottom* < *top*, and *near* < *far* . However, we'll revisit this edict in Problem 2.11.

Remark 2.6. The aspect ratio (= width/height) of the viewing box should be set same as that of the OpenGL window or the scene will be distorted by the print step.

Remark 2.7. The perpendicular projection onto the viewing plane corresponding to a glOrtho() call is also called *orthographic projection* or *orthogonal projection* (hence the name of the call). Yet another term is *parallel projection* as the lines of projection from points in the viewing box to the viewing plane are all parallel.

2.3 The OpenGL Window and Screen Coordinates

We've already had occasion to use the glutInitWindowSize(*w*, *h*) command which sets the size of the OpenGL window to width w and height h measured in pixels. A companion command is glutInitWindowPosition(*x*, *y*) to specify the location (x, y) of the upper-left corner of the OpenGL window on the computer screen.

Experiment 2.4. Change the parameters of glutInitWindowPosition(*x*, *y*) in square.cpp from the current (100, 100) to a few different values to determine the location of the origin (0, 0) of the computer screen, as well as the orientation of the screen's own x-axis and y-axis. End

The origin (0, 0) of the screen it turns out is at its upper-left corner, while the increasing direction of its x-axis is horizontally rightwards and that of its y-axis vertically downwards; moreover, one unit along either axis is *absolute* and represents a pixel. See Figure 2.14, which shows as well the coordinates of the corners of the OpenGL window as initialized by square.cpp.

Note the inconsistency between the orientation of the screen's y-axis and the y-axis of the world coordinate system, the latter being directed *up* the OpenGL window (after being projected there). One needs to take this into account when reading data from the screen and using it in world space, or vice versa. We'll see this when programming the mouse in the next chapter.

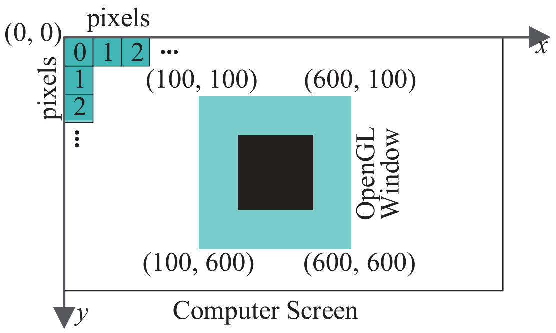

Figure 2.14: The screen's coordinate system: a unit along either axis is the pitch of a pixel.

2.4 Clipping

A question may have come to the reader's mind about objects which happen to be drawn outside the viewing box. Here are a few experiments to clarify how they are processed.

Experiment 2.5. Add another square by inserting the following right after the code for the original square in square.cpp:

```
glBegin(GL_POLYGON);
   glVertex3f(120.0, 120.0, 0.0);
   glVertex3f(180.0, 120.0, 0.0);
   glVertex3f(180.0, 180.0, 0.0);
   glVertex3f(120.0, 180.0, 0.0);
glEnd();
```

From the value of its vertex coordinates the second square evidently lies entirely outside the viewing box.

If you run now there's no sign of the second square in the OpenGL window. This is because OpenGL *clips* the scene to within the viewing box before rendering, so that objects or parts of objects drawn outside are not seem. Clipping is a stage in the graphics pipeline. We'll not worry about its implementation at this time, only the effect. End

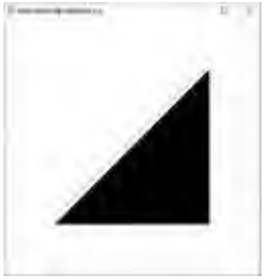

Figure 2.15: Screenshot of a triangle.

Exercise 2.6. (Programming) In the preceding experiment can you redefine the viewing box by changing the parameters of glOrtho() so that both squares are visible?

Experiment 2.6. For a more dramatic illustration of clipping, first replace the square of the original square.cpp with a triangle by deleting its last vertex; in particular, replace the polygon code with the following:

```
glBegin(GL_POLYGON);
   glVertex3f(20.0, 20.0, 0.0);
   glVertex3f(80.0, 20.0, 0.0);
   glVertex3f(80.0, 80.0, 0.0);
glEnd();
```

See Figure 2.15. Next, lift the first vertex up the z-axis by changing it to glVertex3f(20.0, 20.0, 0.5); lift it further by changing its z-value to 1.5 when Figure 2.16 is a screenshot, then 2.5 and, finally, 10.0. Make sure you believe that what you see in the last three cases is indeed a triangle clipped to within the viewing box – Figure 2.17 may be helpful. End

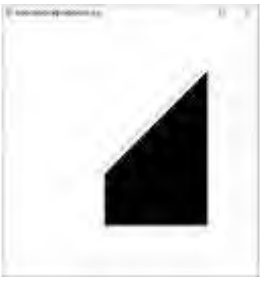

Figure 2.16: Screenshot of the triangle clipped to a quadrilateral.

The viewing box has six faces that each lie on a different plane and, effectively, OpenGL clips the scene off on one side of each of these six planes, accordingly called

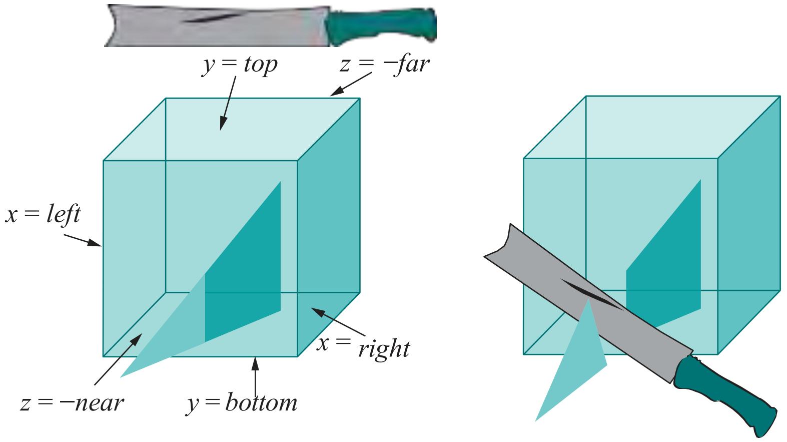

Figure 2.17: Six clipping planes of the glOrtho(*left*, *right*, *bottom*, *top*, *near*, *far*) viewing box and a "clipping knife".

clipping planes. One might imagine a knife slicing down each plane as in Figure 2.17. Specifically, in the case of the viewing box set up by glOrtho(*left*, *right*, *bottom*, *top*, *near*, *far*), clipped off is to the left of the plane $x = left$, to the right of the plane $x = right$, and so on.

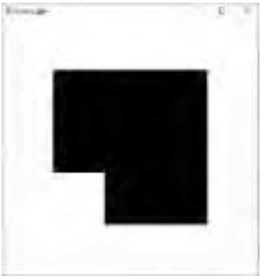

Figure 2.18: Screenshot of the first vertex of square.cpp raised.

Remark 2.8. As we shall see in Chapter 3, the programmer can define clipping planes in addition to the six that bound the viewing box.

Exercise 2.7. Use pencil and paper to guess the output if the polygon declaration part of square.cpp is replaced with the following:

```
glBegin(GL POLYGON);
   glVertex3f(-20.0, -20.0, 0.0);
   glVertex3f(80.0, 20.0, 0.0);
   glVertex3f(120.0, 120.0, 0.0);
   glVertex3f(20.0, 80.0, 0.0);
glEnd();
```

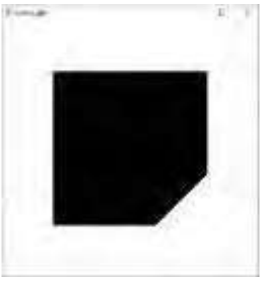

Figure 2.19: Screenshot of the second vertex of square.cpp raised.

Exercise 2.8. (Programming) Here's a bit of a "mathy" question. A triangle was clipped to a (4-sided) quadrilateral in the earlier experiment. Can you come up with a triangle which gets clipped to within the viewing box to a figure with more than 4 sides? What's the maximum number of sides you can make happen?

We'll leave this section with a rather curious phenomenon for the reader to resolve.

Exercise 2.9. (Programming) Raising the first vertex of (the original) square.cpp from glVertex3f(20.0, 20.0, 0.0) to glVertex3f(20.0, 20.0, 1.5) causes it to be clipped – see Figure 2.18.

If, instead, the second vertex is raised from glVertex3f(80.0, 20.0, 0.0) to glVertex3f(80.0, 20.0, 1.5), then the figure is clipped too, but very differently – see Figure 2.19. Why? Should not the results be similar by symmetry?
Hint: OpenGL draws a polygon after triangulating it as a so-called *triangle fan* with the first vertex of the polygon, in code order, the center of the fan. For example, the fan in Figure 2.20 consists of five triangles around vertex v_0.

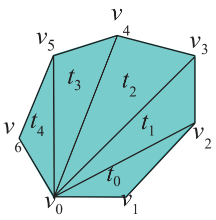

Figure 2.20: A triangle fan.

2.5 Color, OpenGL State Machine and Interpolation

Experiment 2.7. The color of the square in square.cpp is specified by the three parameters of the glColor3f(0.0, 0.0, 0.0) statement in the drawScene() routine, each of which gives the value of one of the three primary components, *blue*, *green* and *red*.

Determine which of the three parameters of glColor3f() specifies the blue, green and red components by setting in turn each to 1.0 and the others to 0.0 (e.g., Figure 2.21 shows one case). In fact, further verify the following table for every possible combination of the values 0.0 and 1.0 for the primary components.

Call	Color
glColor3f(0.0, 0.0, 0.0)	Black
glColor3f(1.0, 0.0, 0.0)	Red
glColor3f(0.0, 1.0, 0.0)	Green
glColor3f(0.0, 0.0, 1.0)	Blue
glColor3f(1.0, 1.0, 0.0)	Yellow
glColor3f(1.0, 0.0, 1.0)	Magenta
glColor3f(0.0, 1.0, 1.0)	Cyan
glColor3f(1.0, 1.0, 1.0)	White

End

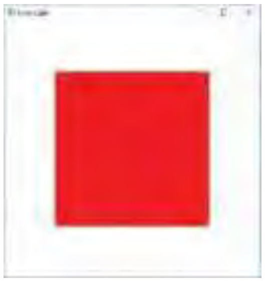

Figure 2.21: Screenshot of square.cpp with glColor3f(1.0, 0.0, 0.0).

Generally, the glColor3f(*red*, *green*, *blue*) call specifies the *foreground color*, or *drawing color* , which is the color applied to objects being drawn. The value of each color component, which ought to be a number between 0.0 and 1.0, determines its *intensity*. For example, glColor3f(1.0, 1.0, 0.0) is the brightest yellow while glColor3f(0.5, 0.5, 0.0) is a weaker yellow

Remark 2.9. The color values are each *clamped* to the range [0, 1]. This means that, if a value happens to be set greater than 1, then it's taken to be 1; if less than 0, it's taken to be 0.

Exercise 2.10. (Programming) Both glColor3f(0.2, 0.2, 0.2) and glColor3f(0.8, 0.8, 0.8) should be grays, having equal RGB intensities. Guess which is the darker of the two. Verify by changing the foreground color of square.cpp.

The call glClearColor(1.0, 1.0, 1.0, 0.0) in the setup() routine specifies the *background color* , or *clearing color* . Ignore for now the fourth parameter, which is the *alpha* value. The statement glClear(GL COLOR BUFFER BIT) in drawScene() actually clears the window to the specified background color, which means that every pixel in the color buffer is set to that color.

Experiment 2.8. Add the additional color declaration statement glColor3f(1.0, 0.0, 0.0) just after the existing one glColor3f(0.0, 0.0, 0.0) in the drawing routine of square.cpp so that the foreground color block becomes

```
glColor3f(0.0, 0.0, 0.0);
glColor3f(1.0, 0.0, 0.0);
```

The square is drawn red like the one in Figure 2.21 because the *current value* or *state* of the foreground color is red when each of its vertices is specified. End

Foreground color is one of a collection of variables, called *state variables*, which determine the state of OpenGL. Among other state variables are point size, line width, line stipple, material properties, etc. We'll meet several as we go along or you can refer to the *red book*[*] for a full list. OpenGL remains and functions in its current state until a declaration is made changing a state variable. For this reason, OpenGL is often called a *state machine*. The next couple of experiments illustrate important points about how state variables control rendering.

[*] The *OpenGL Programming Guide* [107] and its companion volume, the *OpenGL Reference Manual* [108], are the canonical references for the OpenGL API and affectionately referred to as the red book and blue book, respectively. Note that the on-line reference docs at www.opengl.org pretty much cover all that is in the blue book.

Experiment 2.9. Replace the polygon declaration part of square.cpp with the following to draw two squares:

```
glColor3f(1.0, 0.0, 0.0);
glBegin(GL_POLYGON);
   glVertex3f(20.0, 20.0, 0.0);
   glVertex3f(80.0, 20.0, 0.0);
   glVertex3f(80.0, 80.0, 0.0);
   glVertex3f(20.0, 80.0, 0.0);
glEnd();

glColor3f(0.0, 1.0, 0.0);
glBegin(GL_POLYGON);
   glVertex3f(40.0, 40.0, 0.0);
   glVertex3f(60.0, 40.0, 0.0);
   glVertex3f(60.0, 60.0, 0.0);
   glVertex3f(40.0, 60.0, 0.0);
glEnd();
```

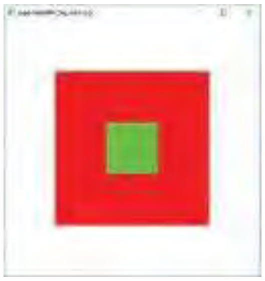

Figure 2.22: Screenshot of a green square drawn after (in the code) a red square.

A small green square appears inside a larger red one (Figure 2.22). Obviously, this is because the foreground color is red for the first square, but green for the second. One says that the color red *binds* to the first square – or, more precisely, to each of its four vertices – and green to the second square. These bound values specify the color *attribute* of either square. Generally, the values of those state variables which determine how it is rendered collectively form a primitive's attribute set.

Flip the order in which the two squares appear in the code by cutting the seven statements which specify the red square and pasting them after those to do with the green one. The green square is overwritten by the red one and no longer visible. This is because at the end of the day an OpenGL program is still a C++ program which processes code line by line, so objects are drawn in their *code order*.

End

Experiment 2.10. Replace the polygon declaration part of square.cpp with:

```
glBegin(GL_POLYGON);
   glColor3f(1.0, 0.0, 0.0);
   glVertex3f(20.0, 20.0, 0.0);
   glColor3f(0.0, 1.0, 0.0);
   glVertex3f(80.0, 20.0, 0.0);
   glColor3f(0.0, 0.0, 1.0);
   glVertex3f(80.0, 80.0, 0.0);
   glColor3f(1.0, 1.0, 0.0);
   glVertex3f(20.0, 80.0, 0.0);
glEnd();
```

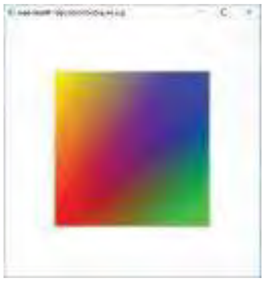

Figure 2.23: Screenshot of a square with differently colored vertices.

The different color values bound to the four vertices of the square are evidently *interpolated* over the rest of the square as you can see in Figure 2.23. In fact, this is most often the case with OpenGL: numerical attribute values specified at the vertices of a primitive are interpolated throughout its interior. In a later chapter we'll see exactly what it means to interpolate and how OpenGL goes about the task. End

Now that we have a square, as in Figure 2.23, which is not symmetric left to right or bottom to top, let's see what happens if we mess with what we were told in Remark 2.5, which was to set always the parameters of glOrtho(*left*, *right*, *bottom*, *top*, *near*, *far*) so that *left* < *right*, *bottom* < *top*, and *near* < *far*.

Exercise 2.11. (Programming) Return to the preceding experiment and flip the *near* and *far* values in the projection statement, precisely, change it to

```
glOrtho(0.0, 100.0, 0.0, 100.0, 1.0, -1.0)
```

Is there a change in what we see? Does it seem that we are viewing the square from the back so that the greenish corner is now at the lower left? *No* and *no*. The reason is that, in the shoot step, OpenGL always projects *up* the z-axis, i.e., in its positive direction. So, the viewing face is always the one with the higher z-value, which, given the glOrtho() statement above, effectively is now on the $z = -far = 1$ plane.

Restore the original *near* and *far* far values and flip *left* and *right*, and then *bottom* and *top*. Do you see differences? *Yes*. Can you explain them.

2.6 OpenGL Geometric Primitives

The geometric primitives – also called drawing primitives or, simply, primitives – of OpenGL are the parts that programmers use in Lego-like manner to create objects from the humblest to the incredibly complex. In fact, a thumbtack and a spacecraft would both be assembled from the same small family of OpenGL primitives. The only primitive we've seen so far though is the polygon. It's time to get acquainted with the whole family depicted in Figure 2.28.

Experiment 2.11. Replace glBegin(GL POLYGON) with glBegin(GL_POINTS) in square.cpp and make the point size bigger with a call to glPointSize(5.0) – the default size being 1.0 – so that the part drawing an object now is

```
glPointSize(5.0); // Set point size.
glBegin(GL POINTS);
    glVertex3f(20.0, 20.0, 0.0);
    glVertex3f(80.0, 20.0, 0.0);
    glVertex3f(80.0, 80.0, 0.0);
    glVertex3f(20.0, 80.0, 0.0);
glEnd();
```

See Figure 2.24. End

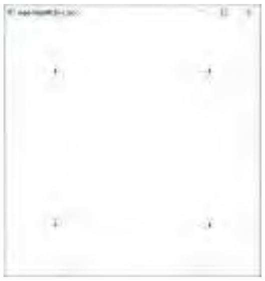

Figure 2.24: Screenshot of square.cpp using GL_POINTS instead of GL_POLYGON.

Experiment 2.12. Continue the previous experiment, replacing GL_POINTS with GL_LINES, GL_LINE_STRIP and, finally, GL_LINE_LOOP. See Figures 2.25-2.27. The thickness of lines is set by glLineWidth(*width*). Change the parameter value of this call in the program, currently the default 1.0, to see the difference. End

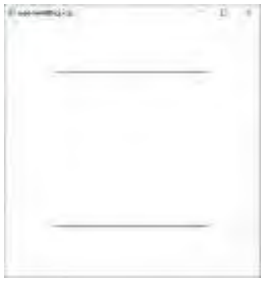

Figure 2.25: Screenshot of square.cpp using GL_LINES.

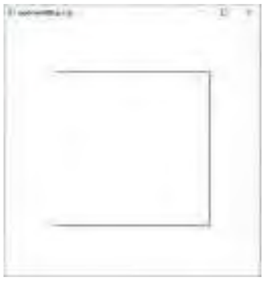

Figure 2.26: Screenshot of square.cpp using GL_LINE_STRIP.

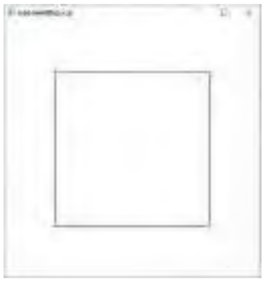

Figure 2.27: Screenshot of square.cpp using GL_LINE LOOP.

In the explanation that follows of how OpenGL draws each of the above primitives, assume that the n vertices declared in the code between glBegin(*primitive*) and glEnd() are $v_0, v_1, \dots, v_{n-1}$ in that order, i.e., the declaration of the primitive is of the form:

```
glBegin(primitive);
    glVertex3f(*, *, *); // v0
    glVertex3f(*, *, *); // v1
    ...
    glVertex3f(*, *, *); // vn−1
glEnd();
```

Refer to Figure 2.28 as you read.

GL_POINTS draws a point at each vertex

$$v_0, v_1, \dots, v_{n-1}$$

GL_LINES draws a *disconnected* sequence of straight line segments (henceforth, we'll simply use the term "segment") between the vertices, taken two at a time. In particular, it draws the segments

$$v_0v_1,\ v_2v_3,\ \dots,\ v_{n-2}v_{n-1}$$

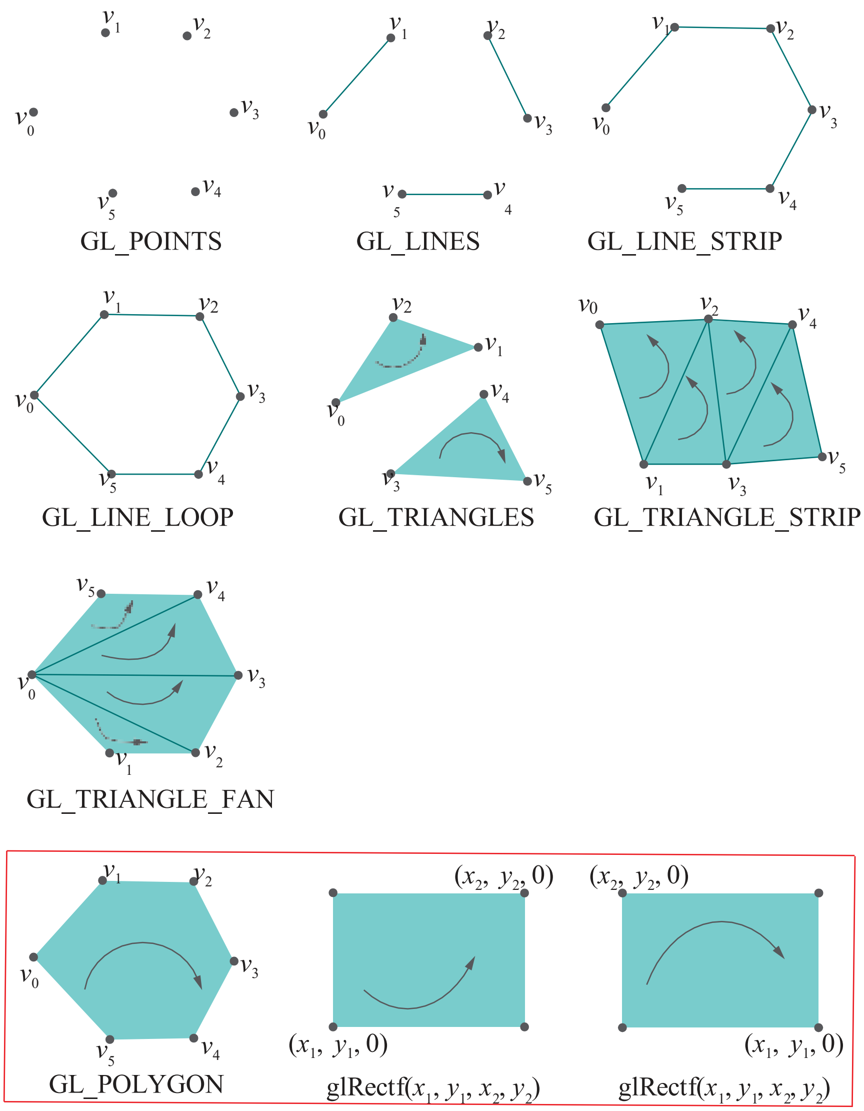

Figure 2.28: OpenGL's geometric primitives. Vertex order is indicated by a curved arrow. Primitives inside the red rectangle have been discarded from the core profile of later versions of OpenGL, e.g., 4.x; however, they are still accessible via the compatibility profile.

if n is even. If n is not even then the last vertex v_{n-1} is simply ignored.

GL_LINE STRIP draws the *connected* sequence of segments

$$v_0v_1,\ v_1v_2,\ \ldots,\ v_{n-2}v_{n-1}$$

Such a sequence is called a *polygonal line* or *polyline*.

GL_LINE_LOOP is the same as GL LINE STRIP, *except* that an additional segment $v_{n-1}v_0$ is drawn to complete a loop:

$$v_0v_1,\ v_1v_2,\ \ldots,\ v_{n-2}v_{n-1},\ v_{n-1}v_0$$

Such a segment sequence is called a *polygonal line loop*.

Remark 2.10. In world space points actually are 0-dimensional objects having zero size, while lines are 1-dimensional objects of zero width; in fact, values specified by glPointSize() and glLineWidth() are used only for rendering, the default for both being 1. Indeed, it would be rather hard to see a point rendered at zero size or a line at zero width!

Why does OpenGL provide separate primitives to draw polygonal lines and line loops when both can be viewed as a collection of segments and drawn using GL_LINES? For example,

```
glBegin(GL_LINE_STRIP);
    v0; v1; v2; v3;
glEnd();
```

is equivalent to

```
glBegin(GL_LINES);
    v0; v1; v1; v2; v2; v3;
glEnd();
```

The answer is first to avoid redundancy in vertex data. Secondly, possible rendering error is avoided as well because OpenGL does not know, for example, that the two v1s in the GL_LINES specification above are supposed to represent the same vertex, and may render them at slightly different locations because of differences in floating point round-off.

Exercise 2.12. (Programming) This relates to the brief discussion on interpolation at the end of Section 2.5. Replace the polygon declaration part of square.cpp with

```
glLineWidth(5.0);
glBegin(GL_LINES);
    glColor3f(1.0, 0.0, 0.0);
    glVertex3f(20.0, 20.0, 0.0);
    glColor3f(0.0, 1.0, 0.0);
    glVertex3f(80.0, 20.0, 0.0);
glEnd();
```

drawing a line segment between a red and a green vertex. Can you say what the color values should be at the midpoint (50.0, 20.0, 0.0) of the segment drawn? Check your answer by drawing a point with those color values just above the midpoint, say at (50.0, 21.0, 0.0), with the statements

```
glPointSize(5.0);
glBegin(GL_POINTS);
    glColor3f(*, *, *);
    glVertex3f(50.0, 21.0, 0.0);
glEnd();
```

and comparing.

On to triangles next.

Experiment 2.13. Replace the polygon declaration part of square.cpp with:

```
glBegin(GL_TRIANGLES);
    glVertex3f(10.0, 90.0, 0.0);
    glVertex3f(10.0, 10.0, 0.0);
    glVertex3f(35.0, 75.0, 0.0);
    glVertex3f(30.0, 20.0, 0.0);
    glVertex3f(90.0, 90.0, 0.0);
    glVertex3f(80.0, 40.0, 0.0);
glEnd();
```

See Figure 2.29. End

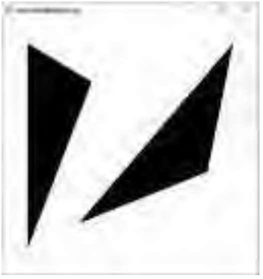

Figure 2.29: Screenshot of square.cpp using GL_TRIANGLES with new vertices.

GL_TRIANGLES draws a sequence of triangles using the vertices three at a time. In particular, the triangles are

$$v_0v_1v_2,\ v_3v_4v_5,\ \ldots,\ v_{n-3}v_{n-2}v_{n-1}$$

if n is a multiple of 3; if it isn't, the last one, or two, vertices are ignored.

The given order of the vertices for each triangle, in particular, v_0, v_1, v_2 for the first, v_3, v_4, v_5 for the second and so on, determines its *orientation* – whether clockwise (CW) or counter-clockwise (CCW) – as perceived by a viewer. Figure 2.28 indicates orientation with curved arrows (e.g., the top of the two triangles drawn for GL_TRIANGLES is CCW, while the bottom one CW, as perceived by a viewer at the reader's location).

The orientation of a 2D primitive, hence its vertex order, is important to specify because this enables OpenGL to decide which face, front or back, the viewer sees. We'll deal with this topic separately in Chapter 9. Till then disregard orientation when drawing.

GL_TRIANGLES is a *2-dimensional* primitive and, by default, triangles are drawn filled. However, one may choose a different drawing mode by applying the glPolygonMode(*face*, *mode*) command where *face* may be one of GL_FRONT, GL_BACK or GL_FRONT_AND_BACK, and *mode* one of GL_FILL, GL_LINE or GL_POINT. Whether a primitive is front-facing or back-facing depends, as said above, on its orientation. To keep matters simple for now, though, we'll use only GL_FRONT_AND_BACK in a glPolygonMode() call, which applies the given drawing mode to a primitive regardless of which face is visible. The GL_FILL option is, of course, the default for 2D primitives, while GL_LINE draws the primitive in *outline* (or *wireframe* as it's also called), and GL_POINT only the vertices.

In fact, it's often easier to decipher a 2D primitive by viewing it in outline, as we'll see in the following experiment introducing triangle strips.

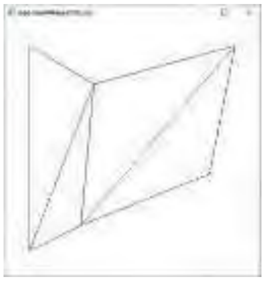

Figure 2.30: Screenshot of square.cpp using GL_TRIANGLE_STRIP with new vertices.

Experiment 2.14. Continue the preceding experiment by inserting the call glPolygonMode(GL_FRONT_AND_BACK, GL_LINE) in the drawing routine and, further, replacing GL_TRIANGLES with GL_TRIANGLE_STRIP. The relevant part of the display routine then is as below:

```
glPolygonMode(GL_FRONT_AND_BACK, GL_LINE);
glBegin(GL_TRIANGLE_STRIP);
   glVertex3f(10.0, 90.0, 0.0);
   glVertex3f(10.0, 10.0, 0.0);
   glVertex3f(35.0, 75.0, 0.0);
   glVertex3f(30.0, 20.0, 0.0);
   glVertex3f(90.0, 90.0, 0.0);
   glVertex3f(80.0, 40.0, 0.0);
glEnd();
```

See Figure 2.30. End

GL_TRIANGLE_STRIP draws a sequence of triangles – called a *triangle strip* – as follows: the first triangle is $v_0v_1v_2$, the second $v_1v_3v_2$ (v_0 is dropped and v_3 brought in), the third $v_2v_3v_4$ (v_1 dropped and v_4 brought in), and so on. Formally, the triangles in the strip are

$$v_0v_1v_2,\ v_1v_3v_2,\ v_2v_3v_4,\ \ldots,\ v_{n-3}v_{n-2}v_{n-1} \qquad \text{(if } n \text{ is odd)}$$

or

$$v_0v_1v_2,\ v_1v_3v_2,\ v_2v_3v_4,\ \ldots,\ v_{n-3}v_{n-1}v_{n-2} \qquad \text{(if } n \text{ is even)}$$

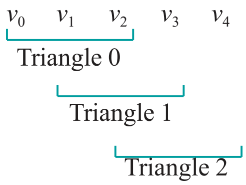

Figure 2.31: Sliding window picking the vertices of triangles in a strip.

As we know, the order of its vertices is important in determining a triangle's orientation, e.g., the second triangle $v_1v_3v_2$ in the strip is not the same as $v_1v_2v_3$. However, if we disregard order for a moment, the vertices of the strip's triangles are picked through a "sliding window" as in Figure 2.31.

Exercise 2.13. (Programming) Create a square annulus as in Figure 2.32(a) using a *single* triangle strip. You may first want to sketch the annulus on graph paper to determine the coordinates of its eight corners. The figure depicts one possible *triangulation* – division into triangles – of the annulus.
Hint: A solution is available in squareAnnulus1.cpp of Chapter 3.

Exercise 2.14. (Programming) Create the shape of Figure 2.32(b) using a single triangle strip. A partial triangulation is indicated.

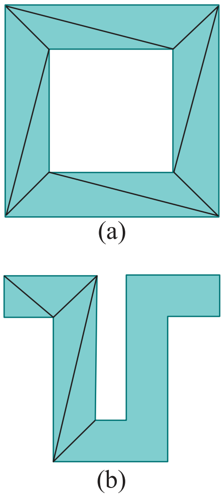

Figure 2.32: (a) Square annulus – the region between two bounding squares – and a possible triangulation (b) A partially triangulated shape.

We come to the third and final of the triangle-drawing primitives.

Experiment 2.15. Replace the polygon declaration part of square.cpp with:

```
glPolygonMode(GL FRONT_AND BACK, GL LINE);
glBegin(GL TRIANGLE_FAN);
   glVertex3f(10.0, 10.0, 0.0);
   glVertex3f(15.0, 90.0, 0.0);
   glVertex3f(55.0, 75.0, 0.0);
   glVertex3f(80.0, 30.0, 0.0);
   glVertex3f(90.0, 10.0, 0.0);
glEnd();
```

See Figure 2.33. **End**

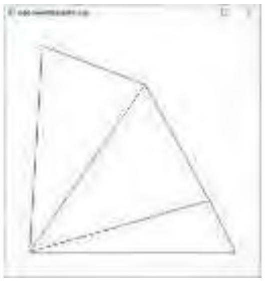

Figure 2.33: Screenshot of square.cpp using GL_TRIANGLE_FAN with new vertices.

GL_TRIANGLE FAN draws a sequence of triangles – called a *triangle fan* – around the first vertex as follows: the first triangle is $v_0v_1v_2$, the second $v_0v_2v_3$, and so on. The full sequence is

$$v_0v_1v_2,\ v_0v_2v_3,\ \ldots,\ v_0v_{n-2}v_{n-1}$$

Exercise 2.15. (Programming) Create a square annulus using *two* triangle fans. First sketch a triangulation different from that in Figure 2.32(a).

We've already met the polygon.

GL_POLYGON draws a polygon with the vertex sequence

$$v_0\ v_1 \ldots v_{n-1}$$

(n must be at least 3 for anything to be drawn).

Finally, more a macro than a true OpenGL primitive:

glRectf($x1$, $y1$, $x2$, $y2$) draws a rectangle lying on the $z = 0$ plane with sides parallel to the x- and y-axes. In particular, the rectangle has diagonally opposite corners at ($x1$, $y1$, 0) and ($x2$, $y2$, 0). The full list of four vertices is ($x1$, $y1$, 0), ($x2$, $y1$, 0), ($x2$, $y2$, 0) and ($x1$, $y2$, 0). The rectangle created is 2-dimensional and its vertex order depends on the situation of the two vertices ($x1$, $y1$, 0) and ($x2$, $y2$, 0) with respect to each other, as indicated by the two drawings at the lower right of Figure 2.28.

Note that glRectf() is a stand-alone call; it is not a parameter to glBegin() like the other primitives.

Figure 2.34: Screenshot of square.cpp using glRectf().

Experiment 2.16. Replace the polygon declaration part of square.cpp with

```
glRectf(20.0, 20.0, 80.0, 80.0);
```

to see the exact same square (Figure 2.34) of the original square.cpp. **End**

Important : The preceding two primitives, GL_POLYGON and glRectf(), have both been discarded from the core profile of later versions of OpenGL, e.g., 4.x, which we are going to study ourselves later in the book; however, they are accessible via the compatibility profile.

Why polygons and rectangles have been discarded is not hard to understand: both can be made from triangles, so are really redundant. The reason we do still use them in the early part of this book is because they afford an easily understood way to make objects – e.g., the square polygon of our very first program square.cpp is certainly more intuitive for a beginner than a triangle strip.

Exercise 2.16. (Programming) Replace the polygon of square.cpp first with a triangle strip and then with a triangle fan.

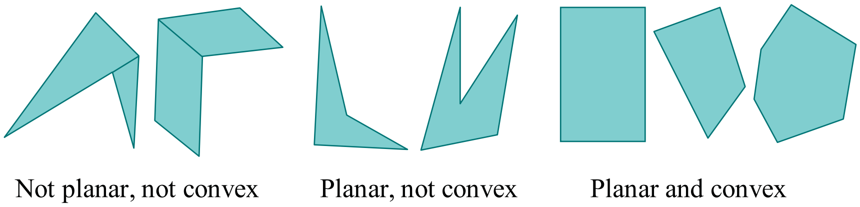
Not planar, not convex
Planar, not convex
Planar and convex

Figure 2.35: Polygons of various types.

It is important that if one does create a polygon, then one must be careful in ensuring that it is a *planar convex* figure, i.e., it lies on one plane and has no "bays" or "inlets" (see Figure 2.35); otherwise, rendering is unpredictable as we'll soon see. Therefore, even though we draw them occasionally for convenience, we recommend that the reader, in order to avoid rendering issues and to prepare for the fourth generation of OpenGL, altogether shun glRectfs and GL_POLYGONs in her own projects, and, instead, draw 2D objects using exclusively GL TRIANGLESs, GL TRIANGLE STRIPs and GL_TRIANGLE FANs.

In fact, following are a couple of experiments, the second one showing how polygon rendering can behave oddly indeed if one is not careful.

Experiment 2.17. Replace the polygon declaration of square.cpp with:

```
glBegin(GL_POLYGON);
   glVertex3f(20.0,  20.0,  0.0);
   glVertex3f(50.0, 20.0, 0.0);
   glVertex3f(80.0, 50.0, 0.0);
   glVertex3f(80.0, 80.0, 0.0);
   glVertex3f(20.0, 80.0, 0.0);
glEnd();
```

You see a convex 5-sided polygon (like the one in Figure 2.36(a)). End

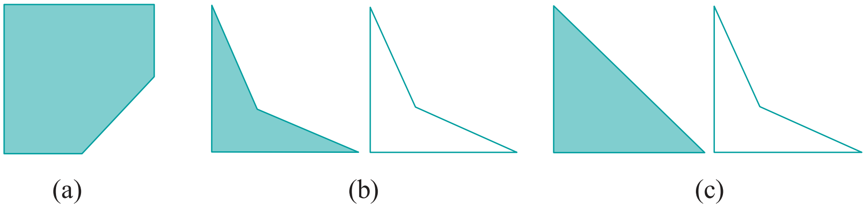
(a)
(b)
(c)

Figure 2.36: Outputs: (a) Experiment 2.17 (b) Experiment 2.18 (c) Experiment 2.18, vertices cycled.

Experiment 2.18. Replace the polygon declaration of square.cpp with:

```
glBegin(GL_POLYGON);
   glVertex3f(20.0,  20.0,  0.0);
   glVertex3f(80.0, 20.0, 0.0);
   glVertex3f(40.0, 40.0, 0.0);
   glVertex3f(20.0, 80.0, 0.0);
glEnd();
```

Display it *both* filled and outlined using appropriate glPolygonMode() calls. A non-convex quadrilateral is drawn in either case (Figure 2.36(b)). Next, keeping the same *cycle* of vertices as above, list them starting with glVertex3f(80.0, 20.0, 0.0) instead:

```
glBegin(GL_POLYGON);
   glVertex3f(80.0,  20.0,  0.0);
   glVertex3f(40.0, 40.0, 0.0);
   glVertex3f(20.0, 80.0, 0.0);
   glVertex3f(20.0, 20.0, 0.0);
glEnd();
```

Make sure to display it both filled and outlined. When filled it's a triangle, while outlined it's a non-convex quadrilateral (Figure 2.36(c)) identical to the one output earlier! Since the cycle of the vertices around the quad is unchanged, only starting at a different point, shouldn't the output still be as in Figure 2.36(b), both filled and outlined? End

We'll leave the apparent anomaly* of this experiment as a mystery to be resolved in Chapter 8 on triangulation. But, if you are impatient then refer to the hint provided with Exercise 2.9.

Exercise 2.17. (Programming) Verify, by cycling the vertices, that no such anomaly arises in the case of the convex polygon of Experiment 2.17.

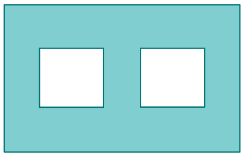

Figure 2.37: Double annulus.

Exercise 2.18. (Programming) Draw the double annulus (a figure '8') shown in Figure 2.37 using as few triangle strips as possible. Introduce extra vertices on the three boundary components, in addition to the original twelve, if you need to for a triangulation.

Note: Such additional vertices are called *Steiner vertices*. For example, Figure 2.38 shows six additional Steiner vertices allowing for a more even triangulation – desirable in certain applications – of a long thin rectangle, than just the original four.

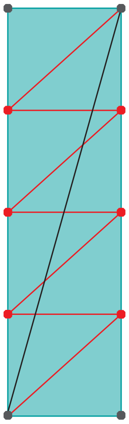

Figure 2.38: Black edge gives a triangulation, consisting of 2 long thin triangles, using only the rectangle's own 4 vertices; 6 red Steiner vertices and the red edges give a triangulation consisting of 8 nearly equal-sided triangles.

Remark 2.11. Here's an interesting semi-philosophical question. OpenGL claims to be a 3D drawing API. Yet, why does it not have a single 3D drawing primitive, e.g., cube, tetrahedron or such? All its primitives are 0-dimensional (GL POINTS), 1-dimensional (GL LINE*) or 2-dimensional (GL_TRIANGLE*).

The answer lies in how we humans (the regular ones that is and not supers with X-ray vision) perceive 3D objects such as cubes, tetrahedrons, chairs and spacecraft: *we see only the surface, which is two-dimensional* . It makes sense for a 3D API, therefore, to draw only as much as can be seen. Of course, OpenGL's "3Dness" lies in allowing us to make these drawings in 3D *xyz*-space.

2.7 Approximating Curved Objects

Looking back at Figure 2.28 we see that the OpenGL geometric primitives are composed of points, straight line segments and flat pieces, the latter being triangles, rectangles

*The rendering depends on the particular OpenGL implementation. However, all implementations that we are aware of show identical behavior.

and polygons. How, then, to draw curved objects such as discs, ellipses, spirals, beer cans and flying saucers? The answer is to *approximate* them with straight and flat OpenGL primitives well enough that the viewer cannot tell the difference. As a wag once put it, “Sincerity is a very important human quality. If you don’t have it, you *gotta* fake it!” In the next experiment we fake a circle.

Figure 2.39: Screenshot of circle.cpp.

Experiment 2.19. Run circle.cpp. Increase the number of vertices in the line loop

```
glBegin(GL LINE_LOOP);
   for(i = 0; i < numVertices; ++i)
   {
      glColor3f((float)rand()/(float)RAND_MAX,
                (float)rand()/(float)RAND_MAX,
                (float)rand()/(float)RAND MAX);
      glVertex3f(X + R * cos(t), Y + R * sin(t), 0.0);
      t += 2 * PI / numVertices;
   }
glEnd();
```

by pressing ‘+’ till it “becomes” a circle, as in the screenshot of Figure 2.39. Press ‘-’ to decrease the number of vertices. The randomized colors are a bit of eye candy. End

The vertices of the loop of circle.cpp, which lie evenly spaced on the circle, are collectively called a *sample of points* or, simply, *sample* from the circle. The loop itself evidently bounds a regular polygon. See Figure 2.40(a). Clearly, the denser the sample the better the loop approximates the circle.

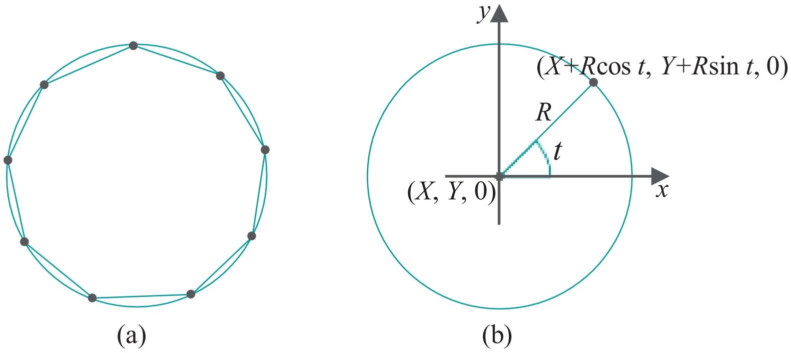

Figure 2.40: (a) A line loop joining a sample of points from a circle (b) Parametric equations for a circle.

The parametric equations of the circle implemented are

$$x = X + R\cos t,\ \ y = Y + R\sin t,\ \ z = 0,\quad 0 \le t \le 2\pi \qquad (2.1)$$

where $(X, Y, 0)$ is the center and R the radius. See Figure 2.40(b). A numVertices number of sample points, with coordinates $(X + R\cos t,\ Y + R\sin t,\ 0)$, equally spaced apart is generated by starting with the angle $t = 0$ and then incrementing it successively by $2\pi/$numVertices.

Observe that the vertex specifications occur within a loop construct, which is pretty much mandatory if there is a large number of vertices.

Incidentally, the program circle.cpp also demonstrates output to the command window, as well as non-trivial user interaction via the keyboard. The routine keyInput() is registered as the key handling routine in main() by the glutKeyboardFunc(keyInput) statement. Note the calls to glutPostRedisplay() in keyInput() asking the display to be redrawn after each update of numVertices.

Follow these conventions when writing OpenGL code:

1. Program the “Esc” key to exit the program.
2. Describe user interaction at two places:
   (a) The command window using cout().
   (b) Comments at the *top* of the source code.

Here’s a parabola.

Experiment 2.20. Run parabola.cpp. Press ‘+/-’ to increase/decrease the number of vertices of the approximating line strip. Figure 2.41 is a screenshot with enough vertices to make a smooth-looking parabola.

The vertices are equally spaced along the x-direction. The parametric equations implemented are

$$x = 50 + 50t,\ y = 100t^2,\ z = 0,\ -1 \le t \le 1$$

the constants being chosen so that the parabola is centered in the window. End

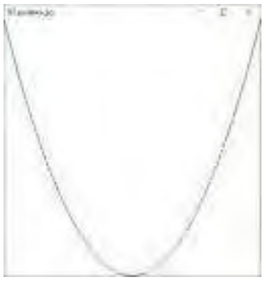

Figure 2.41: Screenshot of parabola.cpp.

Exercise 2.19. (Programming) Modify circle.cpp to draw a flat 3-turn spiral like the one in Figure 2.42.

Exercise 2.20. (Programming) Modify circle.cpp to draw a disc (i.e., a filled circle) by way of (a) a polygon and (b) a triangle fan.

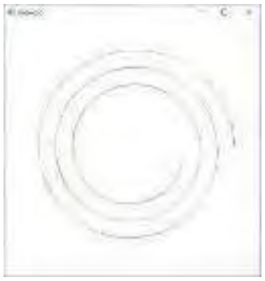

Figure 2.42: Flat spiral.

Exercise 2.21. (Programming) Draw a flat leaf like the one in Figure 2.43.

Exercise 2.22. (Programming) Modify circle.cpp to draw a circular annulus, like one of those shown in Figure 2.44, using a triangle strip. Don’t look at the program circularAnnuluses.cpp!

We’ll be returning shortly to the topic of approximating curved objects, but it’s on to 3D next.

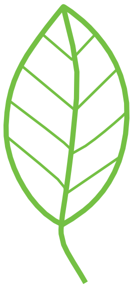

Figure 2.43: Flat leaf.

2.8 Three Dimensions, the Depth Buffer and Perspective Projection

The reader by now may be impatient to move on from the plane (pun intended) and simple to full 3D. Okay then, let’s get off to an easy start in 3-space by making use of the third dimension to fake a circular annulus. Don’t worry, we’ll be doing fancier stuff soon enough!

Experiment 2.21. Run circularAnnuluses.cpp. Three identical-looking red circular annuluses (Figure 2.44) are drawn in three *different* ways:

i) Upper-left: There is not a real hole. The white disc *overwrites* the red disc as it appears later in the code:

```
glColor3f(1.0, 0.0, 0.0);
drawDisc(20.0, 25.0, 75.0, 0.0);
glColor3f(1.0, 1.0, 1.0);
drawDisc(10.0, 25.0, 75.0, 0.0);
```

Note: The first parameter of the subroutine drawDisc() is the radius and the remaining three the coordinates of the center.

ii) Upper-right: There is not a real hole either. A white disc is drawn *closer* to the viewer than the red disc thus blocking it out:

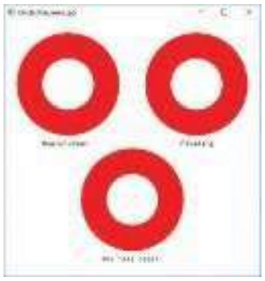

Figure 2.44: Screenshot of circularAnnuluses.cpp.

```
glEnable(GL_DEPTH_TEST);
glColor3f(1.0, 0.0, 0.0);
drawDisc(20.0, 75.0, 75.0, 0.0);
glColor3f(1.0, 1.0, 1.0);
drawDisc(10.0, 75.0, 75.0, 0.5);
glDisable(GL_DEPTH_TEST);
```

Observe that the z-value of the white disc's center is greater than the red disc's, bringing it closer to the viewing face. We'll discuss momentarily the mechanics of one primitive blocking out another.

iii) Lower: A true circular annulus with a real hole:

```
if (isWire) glPolygonMode(GL_FRONT, GL_LINE);
else glPolygonMode(GL_FRONT, GL_FILL);
glColor3f(1.0, 0.0, 0.0);
glBegin(GL_TRIANGLE_STRIP);
...
glEnd();
```

Press the space bar to see the wireframe of a triangle strip. End

Exercise 2.23. (Programming) Interchange in circularAnnuluses.cpp the drawing orders of the red and white discs – i.e., the order in which they appear in the code – in either of the top two annuluses. Which one is affected? (*Only the first!*) Why?

Remark 2.12. Note the use of a text-drawing routine in circularAnnuluses.cpp. OpenGL offers only rudimentary text-drawing capability but it often comes in handy, especially for annotation. We'll discuss text-drawing in fair detail in Chapter 3.

By far the most important aspect of circularAnnuluses.cpp is its use of the *depth buffer* , which allows objects nearer the eye to block out ones behind them, to draw the upper-right annulus. Following is an introduction to this critical 3D utility.

2.8.1 A Vital 3D Utility: The Depth Buffer

Enabling the depth buffer, also called the *z-buffer* , causes OpenGL to eliminate, prior to rendering, parts of objects that are *obscured* (or, *occluded*) by others.

Precisely, a point of an object is not drawn if its projection – think of a ray from that point – toward the viewing face is obstructed by another object. See Figure 2.45(a) for the making of the upper-right annulus of circularAnnuluses.cpp: the white disc obscures the part of the red disc behind it (because the projection is orthogonal, the obscured part is exactly the same shape and size as the white disc). This process is called *hidden surface removal* or *depth testing* or *visibility determination*.

Stated mathematically, the result of hidden surface removal in case of orthographic projection is as follows.

Fix an x-value X and a y-value Y value within the span of the viewing box. Consider the set S of points belonging to objects in the viewing box with their x-value equal to X and y-value equal to Y . Precisely, S is the set of points where the straight line L through $(X, Y, 0)$ parallel to the z-axis intersects objects in the viewing box. Clearly, S is of the form $S = \{(X, Y, z)\}$, where z varies depending on the intersected objects (it's empty if L intersects nothing in the viewing box). Let Z be the largest of these z-values, assuming S to be not empty. In other words, of points belonging to objects in the viewing box with x-value equal to X and y-value to Y , (X, Y, Z) has the largest z-value and lies closest to the viewing face.

Next, observe that all points in S project to the same point $P = (X, Y, -near)$, on the viewing face. Here, then, is the consequence of hidden surface removal: P is rendered with the color attributes of (X, Y, Z). The implication is that only (X, Y, Z),

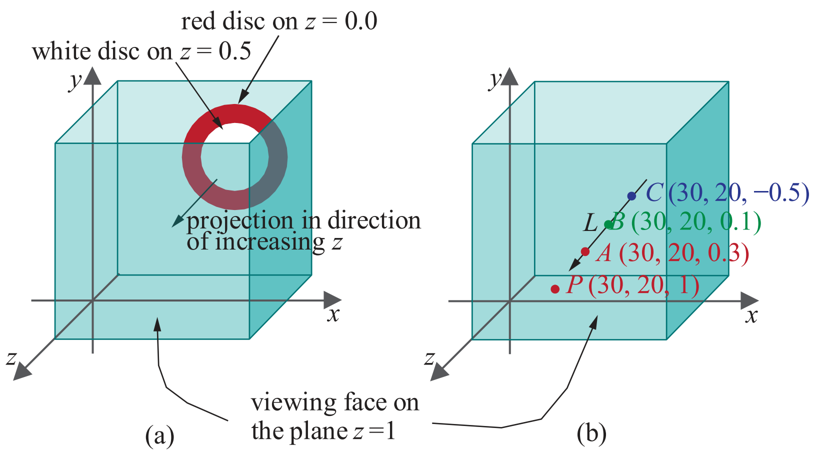

Figure 2.45: (a) The front white disc obscures part of the red one (b) The point A with largest z-value is projected onto the viewing plane so P is red.

closest to the viewing face, is drawn of the points in S, the rest, which are behind it, being obscured.

For example, in Figure 2.45(b), the three points A, B and C, colored red, green and blue, respectively, share the same first two coordinate values, namely, $X = 30$ and $Y = 20$. So, all three project along the line L to the same point P on the viewing face. As A has the largest z coordinate of the three, it obscures the other two and P, therefore, is drawn red.

The z-buffer itself is a block of memory in the GPU containing z-values, one per pixel. If depth testing is enabled, then, as a primitive is processed for rendering, the z-value of each of its points – or, more accurately, each of its pixels – is compared with that of the one with the same (x, y)-values currently resident in the z-buffer. If an incoming pixel's z-value is greater, then its RGB attributes and z-value replace those of the current one; if not, the incoming pixel's data is discarded.

For example, if the order in which the points of Figure 2.45(b) happen to appear in the code is C, A and B, here's how the color and z-buffer values at the pixel corresponding to P change:

```
draw C; // Pixel corresponding to P gets color blue
        // and z-value -0.5.
draw A; // Pixel corresponding to P gets color red
        // and z-value 0.3: A's values overwrite C's.
draw B; // Pixel corresponding to P retains color red
        // and z-value 0.3: B is discarded.
```

Remark 2.13. In actual implementation in the GPU, the value per pixel in the z-buffer is between 0 and 1, with 0 corresponding to the near face of the viewing box and 1 the far face. What happens is that, before recording them in the z-buffer, the system transforms (by a scaling, though not necessarily linear) world space z-values each to the range $[0, 1]$ with a flip in sign so that pixels farther from the viewing face have higher z-value. Consequently, following this transformation, lower values actually win the competition to be visible in the z-buffer. However, when writing OpenGL code we are operating in world space, where higher z-values in the viewing box are closer to the viewing face, and need not concern ourselves with this implementation particularity.

We ask you to note in circularAnnuluses.cpp the enabling syntax of hidden surface removal so that you can implement it in your own programs:

1. The GL_DEPTH_BUFFER_BIT parameter of glClear(GL_COLOR_BUFFER_BIT | GL_DEPTH_BUFFER_BIT) in the drawScene() routine causes the depth buffer to be cleared.

2. The command glEnable(GL_DEPTH_TEST) in the drawScene() routine turns hidden surface removal on. The complementary command is glDisable(GL_DEPTH_TEST).

3. The GLUT_DEPTH parameter of glutInitDisplayMode(GLUT_SINGLE | GLUT_RGB | GLUT_DEPTH) in main() causes the depth buffer to be initialized.

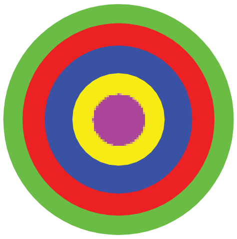

Figure 2.46: Bull's eye target.

Exercise 2.24. (Programming) Draw a bull's eye target as in Figure 2.46 by means of five discs of different colors, sizes and depths.

Exercise 2.25. (Programming) Here's a fun exercise related more to clipping than depth buffering though. The top two annuluses of circularAnnuluses.cpp are "fake" in that there is not a real hole in the disc. Can you make a fake annulus in yet another way by drawing first a filled disc as a triangle fan (e.g., as in Exercise 2.20(b)) and then repositioning only the center of the fan outside the viewing box?

Remark 2.14. The z-buffer, of course, is incredibly important in OpenGL's 3D scheme of things. However, it really will not be called upon to do much in the simple scenes with very few objects that we are going to be creating for a while. It's in busy scenes that the depth buffer comes into its own.

Remark 2.15. Before z-buffers started taking over the world with the advent of the first GPUs in the early 80s – by virtue of their simplicity and sheer speed derived from being implemented in GPU hardware – a more complex software technique based on so-called BSP trees was used extensively for hidden surface removal. We don't cover this technique ourselves in this book but an earlier edition had a detailed discussion which the interested reader will find extracted at the Downloads page of our website.

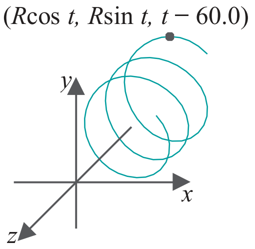

Figure 2.47: Parametric equations for a helix.

2.8.2 A Helix and Perspective Projection

We get more seriously 3D next by drawing a spiral or, more scientifically, a helix. A helix, though itself a 1-dimensional object – drawn as a line strip actually – can be made authentically only in 3-space.

Open helix.cpp but don't run it as yet! The parametric equations implemented are

$$x = R\cos t, \; y = R\sin t, \; z = t - 60.0, \quad -10\pi \le t \le 10\pi \tag{2.2}$$

See Figure 2.47. Compare these with Equation (2.1) for a circle centered at (0, 0, 0), putting $X = 0$ and $Y = 0$ in that earlier equation. The difference is that the helix climbs up the z-axis *simultaneously* as it rotates circularly with increasing t (so, effectively, it coils around the z-axis). Typically, one writes simply $z = t$ for the last coordinate; however, we tack on "−60.0" to push the helix far enough down the z-axis so that it's contained entirely in the viewing box.

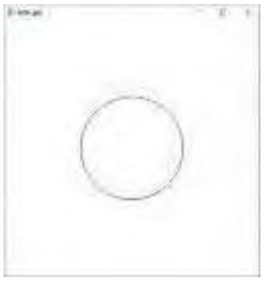

Figure 2.48: Screenshot of helix.cpp using orthographic projection with the helix coiling around the z-axis.

Exercise 2.26. Even before viewing the helix, can you say from Equation (2.2) how many times it is supposed to coil around the z-axis, i.e., how many full turns it is supposed to make?
Hint: One full turn corresponds to an interval of 2π along t.

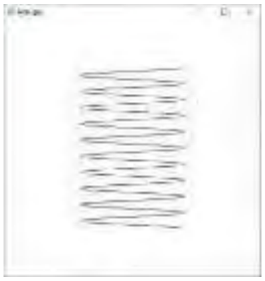

Figure 2.49: Screenshot of helix.cpp using orthographic projection with the helix coiling around the y-axis.

Experiment 2.22. Okay, run helix.cpp now. All we see is a circle as in Figure 2.48). There's no sign of any coiling up or down. The reason, of course, is that the orthographic projection onto the viewing face flattens the helix. Let's see if it makes a difference to turn the helix upright, in particular, so that it coils around the y-axis. Accordingly, replace the statement

```
glVertex3f(R * cos(t), R * sin(t), t - 60.0);
```

in the drawing routine with

```
glVertex3f(R * cos(t), t, R * sin(t) - 60.0);
```

Hmm, not a lot better (Figure 2.49). End

Because it squashes a dimension, typically, orthographic projection is not suitable for 3D scenes. OpenGL, in fact, provides another kind of projection, called *perspective projection*, more appropriate for most 3D applications.

Perspective projection is implemented with a glFrustum() call. Instead of a viewing box, a glFrustum(*left*, *right*, *bottom*, *top*, *near*, *far*) call sets up a *viewing frustum* – a frustum is a *truncated pyramid* whose top has been cut off by a plane parallel to its base – in the following manner (see Figure 2.50):

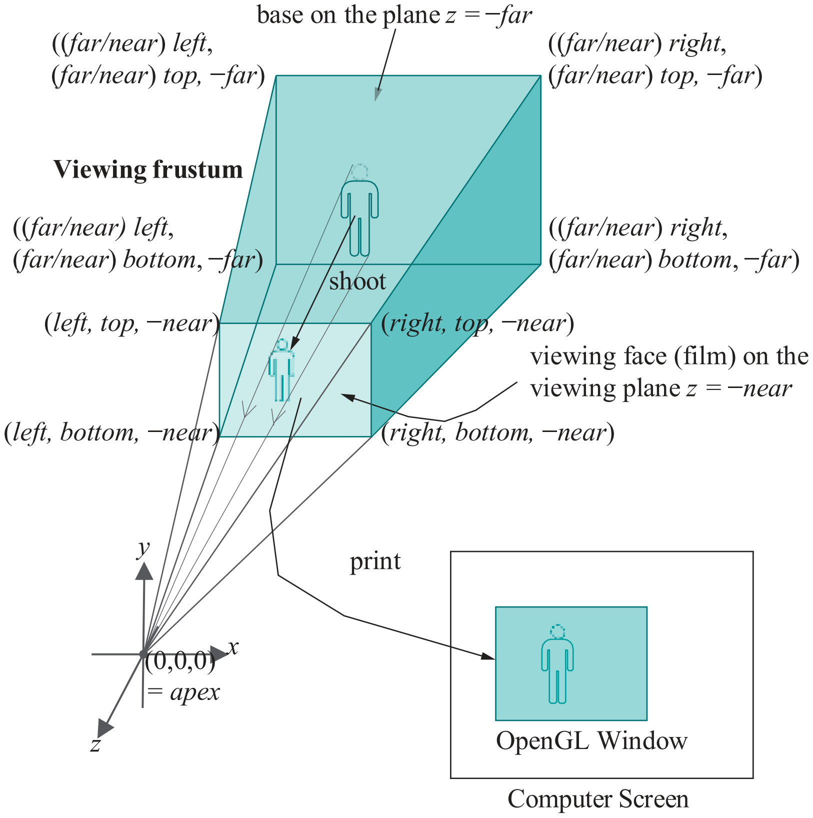

Figure 2.50: Rendering with glFrustum().

The apex of the pyramid is at the origin. The front face, or *viewing face*, of the frustum is the rectangle, lying on the plane $z = -near$, whose corners are (*left* , *bottom*, −*near*), (*right* , *bottom*, −*near*), (*left* , *top*, −*near*), and (*right* , *top*, −*near*). The plane $z = -near$ is the *viewing plane* – in fact, it's the plane which truncates the pyramid.

The four edges of the pyramid emanating from the apex pass through the four corners of the viewing face. The base or back face of the frustum is the rectangle whose vertices are precisely where the pyramid's four edges intersect the $z = -far$ plane. By proportionality with the front vertices, the coordinates of the base vertices are:

((*far*/*near*) *left*, (*far*/*near*) *bottom*, −*far*),
((*far*/*near*) *right*, (*far*/*near*) *bottom*, −*far*),
((*far*/*near*) *left*, (*far*/*near*) *top*, −*far*),
((*far*/*near*) *right*, (*far*/*near*) *top*, −*far*)

Values of the glFrustum() parameters are typically set so that the frustum lies symmetrically about the *z*-axis; in particular, *right* and *top* are chosen to be positive, and *left* and *bottom* their respective negatives. The parameters *near* and *far* should both be positive and *near* < *far* , which means the frustum lies entirely on the negative side of the z-axis with its base behind the viewing face.

Remark 2.16. An intuitive way to relate the box of glOrtho(*left*, *right*, *bottom*, *top*, *near*, *far*) with the frustum of glFrustum(*left*, *right*, *bottom*, *top*, *near*, *far*) is to note first that their front faces are identical and that the back face of the box is simply a copy of the front face shifted back, while the back face of the frustum is stretched as it's shifted back, the corners following rays from the origin.

Example 2.1. Determine the corners of the viewing frustum created by the call glFrustum(-15.0, 15.0, -10.0, 10.0, 5.0, 50.0).

Answer : By definition, the corners of the front face are $(-15.0, -10.0, -5.0)$, $(15.0, -10.0, -5.0)$, $(-15.0, 10.0, -5.0)$ and $(15.0, 10.0, -5.0)$. The x- and y-values of the vertices of the base (or back face) are scaled from those on the front by a factor of 10 (because *far*/*near* = 50/5 = 10). The base vertices are, therefore, $(-150.0, -100.0, -50.0)$, $(150.0, -100.0, -50.0)$, $(-150.0, 100.0, -50.0)$ and $(150.0, 100.0, -50.0)$.

Exercise 2.27. Determine the corners of the viewing frustum created by the call glFrustum(-5.0, 5.0, -5.0, 5.0, 5.0, 100.0).

The rendering sequence in the case of perspective projection is a two-step shoot-and-print, similar to orthographic projection. The shooting step again consists of projecting objects within the viewing frustum onto the viewing face, *except that the projection is no longer perpendicular* . Instead, each point is projected along the line joining it to the apex, as depicted by the light black rays from the bottom and top of the man in Figure 2.50.

Perspective projection causes *foreshortening* because objects farther away from the apex appear smaller (a phenomenon also called *perspective transformation*). For example, see Figure 2.51 where A and B are of the same height, but the projection pA is shorter than the projection pB.

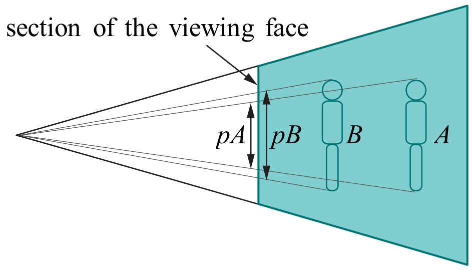

Figure 2.51: Section of the viewing frustum showing foreshortening.

The second rendering step of printing where the viewing face is proportionately scaled to fit onto the OpenGL window is exactly as for orthographic projection. Exactly as for orthographic projection as well, the scene is clipped to within the viewing frustum by the 6 planes that bound the latter.

Time now to see perspective projection work its magic!

Experiment 2.23. Fire up the original helix.cpp program. Replace orthographic projection with perspective projection; in particular, replace the projection statement

```
glOrtho(-50.0, 50.0, -50.0, 50.0, 0.0, 100.0);
```

with

```
glFrustum(-5.0, 5.0, -5.0, 5.0, 5.0, 100.0);
```

You can see a real spiral now (Figure 2.52). View the upright version as well (Figure 2.53), replacing

```
glVertex3f(R * cos(t), R * sin(t), t - 60.0);
```

with

```
glVertex3f(R * cos(t), t, R * sin(t) - 60.0);
```

A lot better than the orthographic version is it not?! End

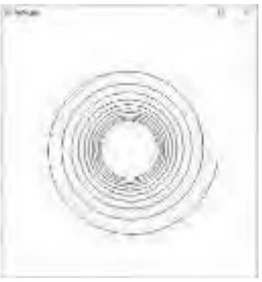

Figure 2.52: Screenshot of helix.cpp using perspective projection with the helix coiling up the z-axis.

Perspective projection is more realistic than orthographic projection as it mimics how images are formed on the retina of the eye by light rays traveling toward a point. And, in fact, it's precisely foreshortening which cues us humans to the distance of an object.

Remark 2.17. One can think of the apex of the frustum as the location of a *point camera* and the viewing face as its film.

Remark 2.18. One might think of orthographic and perspective projections *both* as being along lines of projection convergent to a single point, the *center of projection* (COP). In the case of perspective projection, this is a regular point with finite coordinates; however, for orthographic projection the COP is a "point at infinity" – i.e., infinitely far away – so that lines toward it are parallel.

Moreover, the sides of a viewing volume from back to front logically follow the lines of projection, so leading us from a box in the case of orthographic projection to a frustum in the case of perspective projection.

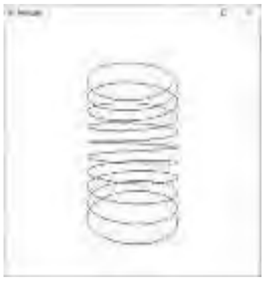

Figure 2.53: Screenshot of helix.cpp using perspective projection with the helix coiling up the y-axis.

Remark 2.19. There do exist 3D applications, e.g., in architectural design, where foreshortening amounts to distortion, so, in fact, orthographic projection is preferred.

Remark 2.20. It's because it captures the image of an object by intersecting rays projected from the object – either orthographically or perspectively – with a plane, which is similar to how a real camera works, that OpenGL is said to implement the *synthetic-camera* model.

Exercise 2.28. (Programming) Continuing from where we were at the end of the preceding experiment using helix.cpp, successively replace the glFrustum() call as follows, trying in each case to predict the change in the display caused by the change in the frustum before running the code:

(a) Move the back face back: glFrustum(-5.0, 5.0, -5.0, 5.0, 5.0, 120.0)

(b) Move the front face back: glFrustum(-5.0, 5.0, -5.0, 5.0, 10.0, 100.0)

(c) Move the front face forward: glFrustum(-5.0, 5.0, -5.0, 5.0, 2.5, 100.0)

(d) Make the front face bigger: glFrustum(-10.0, 10.0, -10.0, 10.0, 5.0, 100.0)

Parts (b) and (c) show, particularly, how moving the "film" causes the camera to zoom.

Exercise 2.29. Formulate mathematically how hidden surface removal should work in the case of perspective projection, as we did in Section 2.8.1 for orthographic projection.

Experiment 2.24. Run moveSphere.cpp, which simply draws a movable sphere in the OpenGL window. Press the left, right, up and down arrow keys to move the sphere, the space bar to rotate it and 'r' to reset.

The sphere appears distorted as it nears the boundary of the window, as you can see from the screenshot in Figure 2.54. Can you guess why? Ignore the code,

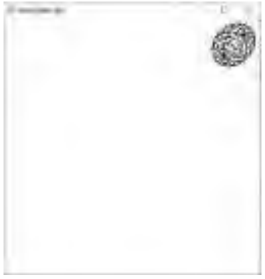

Figure 2.54: Screenshot of moveSphere.cpp.

especially unfamiliar commands such as glTranslatef() and glRotatef(), except for that projection is perspective.

This kind of *peripheral distortion* of a 3D object is unavoidable in any viewing system which applies perspective projection. It happens with a real camera as well, but we don't notice it as much because the field of view when snapping pictures is usually quite large with objects of interest tending to be centered, and the curved lens is designed to compensate as well. End

2.9 Drawing Projects

Here are a few exercises to stretch your drawing muscles. The objects may look rather different from what we have drawn so far, but as programming projects aren't really. In fact, you can probably cannibalize a fair amount of code from earlier programs.

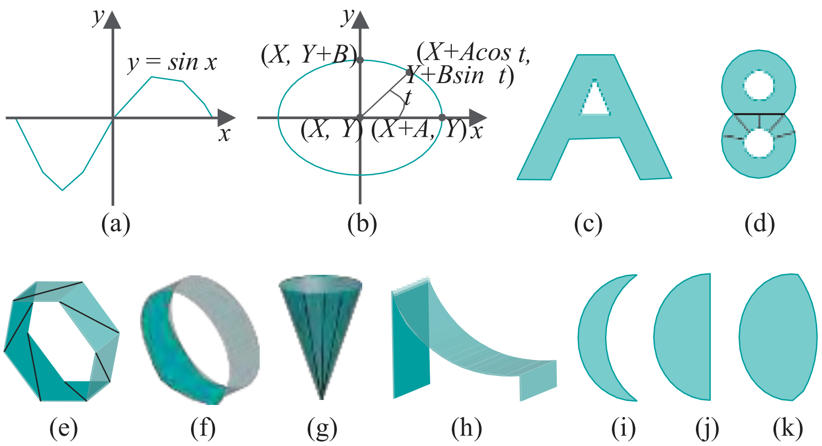

Figure 2.55: Draw these!

Exercise 2.30. (Programming) Draw a sine curve between $x = -\pi$ and $x = \pi$ (Figure 2.55(a)). Follow the strategy of circle.cpp to draw a polyline through a sample from the sine curve.

Exercise 2.31. (Programming) Draw an ellipse. Recall the parametric equations for an ellipse on the xy-plane, centered at (X, Y), with semi-major axis of length A and semi-minor axis of length B (Figure 2.55(b)):

$$x = X + A\cos t, \ \ y = Y + B\sin t, \ \ z = 0, \qquad 0 \le t \le 2\pi$$

Exercise 2.32. (Programming) Draw the letter 'A' as a *two-dimensional* figure like the shaded region in Figure 2.55(c). It might be helpful to triangulate it first on graph paper. Try to pack as many triangles into as few triangle strips as possible (because each drawing call costs in the GPU, but see the next experiment). Allow the user to toggle between filled and wireframe *a la* the bottom annulus of circularAnnuluses.cpp.

Note: Variations of this exercise may be made by asking different letters. Keep in mind that curvy letters like 'S' are harder than straight-sided ones.

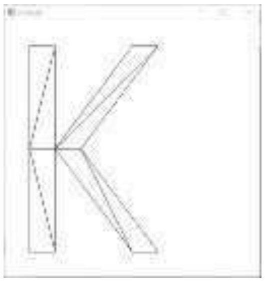

Figure 2.56: Screenshot of strangeK.cpp.

Experiment 2.25. Run strangeK.cpp, which shows how one might take the edict of minimizing the number of triangle strips a bit far. Press space to see the wireframe of a perfectly good 'K' (Figure 2.56).

Interestingly, though, the letter is drawn as a single triangle strip with 17 vertices within the one glBegin(GL_TRIANGLE_STRIP)-glEnd(). We ask the reader to parse this strip as follows: sketch the K on on a piece of paper, label the vertices $v_0, v_1, \ldots, v_{16}$ according to their code order (e.g., the lower left vertex of the straight side is v_0, to its right is v_1, and so on, and, yes, some vertices are labeled multiple times), and, finally, examine each one of the strip's 15 component triangles (best done by following the sliding window scheme as in Figure 2.31).

Did you spot a few so-called *degenerate* triangles, e.g., one with all its vertices along a straight line or with coincident vertices? Such triangles, which are not really 2D, are best avoided when drawing a 2D figure. End

Exercise 2.33. (Programming) Draw the number '8' as the 2D object in Figure 2.55(d). Do this in two different ways: (i) drawing 4 discs and using the z-buffer, and (ii) as a true triangulation, allowing the user to toggle between filled and wireframe. For (ii), a method of dividing the '8' into two triangle strips is suggested in Figure 2.55(d).

Note: Variations of part (ii) may be made by asking different numbers.

Exercise 2.34. (Programming) Draw a ring with cross-section a regular (equal-sided) polygon as in Figure 2.55(e), where a scheme to triangulate the ring in one triangle strip is indicated. Allow the user to change the number of sides of the cross-section. Increasing the number of sides sufficiently should make the ring appear cylindrical as in Figure 2.55(f). Use perspective projection and draw in wireframe.

Exercise 2.35. (Programming) Draw a cone as in Figure 2.55(g) where a possible triangulation is indicated. Draw in wireframe and use perspective projection.

Exercise 2.36. (Programming) Draw a children's slide as in Figure 2.55(h). Choose an appropriate equation for the cross-section of the curved surface – part of a parabola, maybe – and then "extrude" it sideways as a triangle strip. (If you did Exercise 2.34 then you've already extruded a polygon.) Draw in wireframe and use perspective projection.

Exercise 2.37. (Programming) Draw in a single scene a crescent moon, a half-moon and a three-quarter moon (Figures 2.55(i)-(k)). Each should be a true triangulation. Label each as well using text-drawing.

Remark 2.21. Your output from Exercises 2.34-2.36 may look a bit "funny", especially viewed from certain angles. For example, the ring viewed head-on down its axis may appear as two concentric circles on a single plane. This problem can be alleviated by drawing the object with a different alignment or, equivalently, changing the viewpoint. In Experiment 2.26, coming up shortly, we'll learn code for the user to change her viewpoint in real-time.

Remark 2.22. This thought may have occurred to the reader earlier, when we were discussing the viewing box or frustum: situating the front face of, say, the frustum very close to the eye (in other words, a *near* parameter value of glFrustum() of nearly zero) and the back face very far (in other words, a very large *far* parameter value) will create a large viewing space and less likelihood of inadvertent clipping.

However, beware! Increasing the distance between the near and far planes of the viewing space (box or frustum) causes loss in depth resolution because world space depths are transformed all to the range $[0, 1]$ in the z-buffer (see Remark 2.13). Moreover, in the case of the frustum there'll be loss of precision too if the front face is small – as it will be if close to the eye.

In fact, the user should try to push the front face as far back and bring the back face as close in as possible while keeping the scene within the viewing volume.

2.10 Approximating Curved Objects Once More

Our next 3-space drawing project is a bit more challenging: a hemisphere, which is a 2-dimensional object. We'll get in place, as well, certain design principles which will be expanded in Chapter 10 which is dedicated to drawing (no harm starting early).

Remark 2.23. A hemisphere is a 2-dimensional object because it is a surface. Recall that a helix is 1-dimensional because it's line-like. Now, both hemisphere and helix need 3-space to "sit in"; they cannot do with less. For example, you could sketch either on a piece of paper (2-space) but it would not be the real thing. On the other hand, a circle – another 1D object – does sit happily in 2-space.

Consider a hemisphere of radius R, centered at the origin O, with its circular base lying on the xz-plane. Suppose the spherical coordinates of a point P on this hemisphere are a longitude of θ (measured counter-clockwise from the x-axis when looking from the plus side of the y-axis) and a latitude of φ (measured from the xz-plane toward the plus side of the y-axis). See Figure 2.57(a). The Cartesian coordinates of P are by elementary trigonometry

$$(R\cos\varphi\cos\theta,\ \ R\sin\varphi,\ \ -R\cos\varphi\sin\theta) \tag{2.3}$$

The range of θ is $0 \leq \theta \leq 2\pi$ and of φ is $0 \leq \varphi \leq \pi/2$.

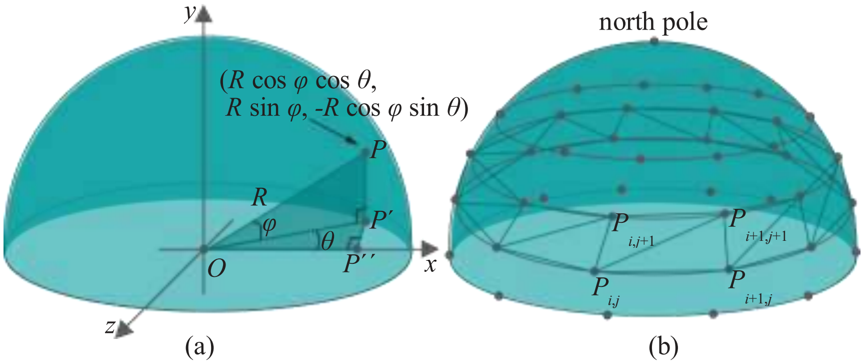

Figure 2.57: (a) Spherical and Cartesian coordinates on a hemisphere (b) Approximating a hemisphere with latitudinal triangle strips.

Exercise 2.38. Verify that the Cartesian coordinates of P are as claimed in (2.3).

Suggested approach: From the right-angled triangle OPP^{1} one has $|PP^{1}| = R\sin\varphi$ and $|OP^{1}| = R\cos\varphi$. $|PP^{1}|$ is the y-value of P. Next, from right-angled triangle $OP^{1}P^{11}$, find in terms of $|OP^{1}|$ and θ the values of $|OP^{11}|$ and $|P^{1}P^{11}|$. The first is the x-value of P, while the latter negated the z-value.

Sample the hemisphere at a mesh of $(p+1)(q+1)$ points P_{ij}, $0 \leq i \leq p$, $0 \leq j \leq q$, where the longitude of P_{ij} is $(i/p) * 2\pi$ and its latitude $(j/q) * \pi/2$. In other words, $p+1$ longitudinally equally-spaced points are chosen along each of $q+1$ equally-spaced latitudes. See Figure 2.57(b), where $p = 10$ and $q = 4$. The sample points P_{ij} are not all distinct. In fact, $P_{0j} = P_{pj}$, for all j, as the same point has longitude both 0 and 2π; and, the point P_{iq}, for all i, is identical to the north pole, which has latitude $\pi/2$ and arbitrary longitude.

The plan now is to approximate the circular band between each pair of adjacent latitudes with a triangle strip – such a strip will take its vertices alternately from either latitude. Precisely, we'll draw one triangle strip with vertices at

$$P_{0,j+1},\ \ P_{0j},\ \ P_{1,j+1},\ \ P_{1j},\ \ldots,\ \ P_{p,j+1},\ \ P_{pj}$$

for each j, $0 \leq j \leq q$ 1, for a total of q triangle strips. These q triangle strips together will approximate the hemisphere itself.

Experiment 2.26. Run hemisphere.cpp, which implements exactly the strategy just described. You can verify this from the snippet that draws the hemisphere:

```
for(j = 0; j < q; j++)
{
   // One latitudinal triangle strip.
   glBegin(GL_TRIANGLE STRIP);
      for(i = 0; i <= p; i++)
      {
         glVertex3f(R * cos((float)(j+1)/q * PI/2.0) *
                         cos(2.0 * (float)i/p * PI),
                    R * sin((float)(j+1)/q * PI/2.0),
                    -R * cos((float)(j+1)/q * PI/2.0) *
                         sin(2.0 * (float)i/p * PI));
         glVertex3f(R * cos((float)j/q * PI/2.0) *
                         cos(2.0 * (float)i/p * PI),
                    R * sin((float)j/q * PI/2.0),
                    -R * cos((float)j/q * PI/2.0) *
                         sin(2.0 *(float)i/p * PI));
      }
   glEnd();
}
```

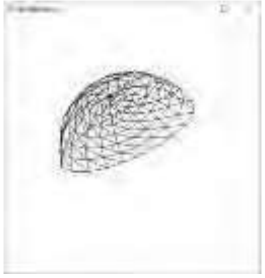

Figure 2.58: Screenshot of hemisphere.cpp.

Increase/decrease the number of longitudinal slices by pressing ‘P/p’. Increase/decrease the number of latitudinal slices by pressing ‘Q/q’. Turn the hemisphere about the axes by pressing ‘x’, ‘X’, ‘y’, ‘Y’, ‘z’ and ‘Z’. See Figure 2.58 for a screenshot. End

Experiment 2.27. Playing around a bit with the code will help clarify the construction of the hemisphere:

(a) Change the range of the hemisphere’s outer loop from

```
for(j = 0; j < q; j++)
```

to

```
for(j = 0; j < 1; j++)
```

Only the bottom strip is drawn. The keys ‘P/p’ and ‘Q/q’ still work.

(b) Change it again to

```
for(j = 0; j < 2; j++)
```

Now, the bottom two strips are drawn.

(c) Reduce the range of both loops:

```
for(j = 0; j < 1; j++)
...
      for(i = 0; i <= 1; i++)
      ...
```

The first two triangles of the bottom strip are drawn.

(d) Then, increase the range of the inner loop by 1:

```
for(j = 0; j < 1; j++)
...
      for(i = 0; i <= 2; i++)
      ...
```

The first four triangles of the bottom strip are drawn. End

There's syntax in hemisphere.cpp – none to do with the actual making of the hemisphere – which you may be seeing for the first time. The command glTranslatef(0.0, 0.0, -10.0) is used to move the hemisphere, drawn initially centered at the origin, into the viewing frustum, while the glRotatef() commands turn it. We'll be studying these so-called *modeling transformations* in Chapter 4 but you are encouraged to experiment with them even now as the syntax is fairly intuitive. The set of three glRotatef()s, particularly, comes in handy to re-align a scene.

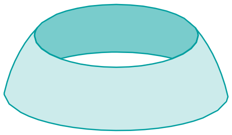
(a)

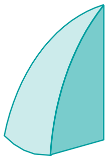
(b)

Figure 2.59: (a) Half a hemisphere (b) Slice of a hemisphere.

Exercise 2.39. (Programming) Modify hemisphere.cpp to draw:

(a) the bottom half of a hemisphere (Figure 2.59(a)).

(b) a 30° slice of a hemispherical cake (Figure 2.59(b)). Note that simply reducing the range of the inner loop of hemisphere.cpp produces a slice of cake without two sides and bottom, so these have to be added in separately to close up the slice.

Make sure the 'P/p/Q/q' keys still work.

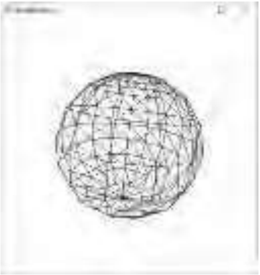

Figure 2.60: A wireframe sphere.

Exercise 2.40. A sphere, of course, can be made of two separate back-to-back hemispheres. However, try to manufacture it as one object with a simple modification of hemisphere.cpp so that the latitude spans a range of π instead of $\pi/2$. Your output might be something like Figure 2.60.

Exercise 2.41. (Programming) Just to get you thinking about animation, which we'll be studying in depth soon enough, guess the effect of replacing glTranslatef(0.0, 0.0, -10.0) with glTranslatef(0.0, 0.0, -20.0) in hemisphere.cpp. Verify.

And, here are some more things to draw.

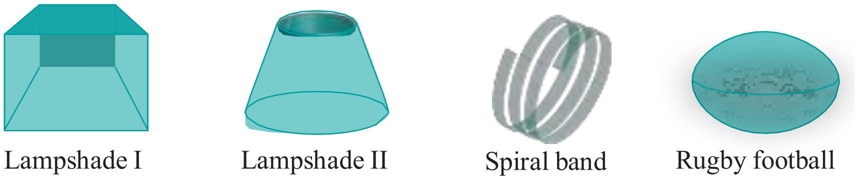

Figure 2.61: More things to draw.

Exercise 2.42. (Programming) Draw the objects shown in Figure 2.61. Give the user an option to toggle between filled and wireframe renderings. Borrow the glRotatef()s from hemisphere.cpp to allow an object to be turned.
Hint : A way to make the football, or ellipsoid, is to modify hemisphere.cpp to first make half an ellipsoid (a hemi-ellipsoid?). In fact, similarly to (2.3), a generic point on a hemi-ellipsoid is

$$(R_x \cos\varphi \cos\theta,\ R_y \sin\varphi,\ -R_z \cos\varphi \sin\theta)$$

where the constants R_x, R_y and R_z are the lengths of the semi-principal axes. Two hemi-ellipsoids back to back would then give a whole ellipsoid. Or, you could follow the idea of Exercise 2.40 to make it as one object.

Remark 2.24. Filled renderings of 3D scenes, even with color, rarely look pleasant in the absence of lighting. See for yourself by applying color to 3D objects you have drawn so far (remember to invoke a glPolygonMode(*, GL_FILL) call). For this reason, we'll draw mostly wireframe till Chapter 11, which is all about lighting. You'll have to bear with this. Wireframe, however, fully exposes the geometry of an object, which is not a bad thing when one is learning object design.

2.11 An OpenGL Program End to End

We have already touched on almost every command of square.cpp which is functional from a graphics points of view. However, let's run over the whole program to see all that goes into making OpenGL code tick.

We start with main():

1. glutInit(&argc, argv) initializes the FreeGLUT library. FreeGLUT [49], successor to GLUT (OpenGL Utility Toolkit), is a library of calls to manage a window and monitor mouse and keyboard input (the reason such a separate library is needed is that OpenGL itself is only a library of graphics calls).

2. glutInitContextVersion(4, 3);
   glutInitContextProfile(GLUT_COMPATIBILITY_PROFILE);

   tells FreeGLUT that the program will be wanting an OpenGL 4.3 *context* – this context being the interface between an instance of OpenGL and the rest of the system – which is backward-compatible in that legacy commands are implemented. This, for example, allows us to draw with the glBegin()-glEnd() operations from OpenGL 2.1, which do not belong in the core profile of OpenGL 4.3.

   Remark 2.25. If your graphics card doesn't support OpenGL 4.3 then the program may compile but not run as the system is unable to provide the context asked. What you might do in this case is thin the context by replacing the first line above with glutInitContextVersion(3, 3), or even glutInitContextVersion(2, 1), instead. Of course, then, programs using later-generation calls will not run, but you should be fine early on in the book.

3. glutInitDisplayMode(GLUT SINGLE | GLUT _RGBA) says that we'll be wanting an OpenGL context to support a single-buffered frame, each pixel having red, green, blue and alpha values.

4. glutInitWindowSize(500, 500);
   glutInitWindowPosition(100, 100);

   as we have already seen, set the size of the OpenGL window and the location of its top left corner on the computer screen.

5. glutCreateWindow("square.cpp") actually creates the OpenGL context and its associated window with the specified string parameter as title.

6. glutDisplayFunc(drawScene);
   glutReshapeFunc(resize);
   glutKeyboardFunc(keyInput);

   register the routines to call – so-called *callback routines* – when the OpenGL window is to be drawn, when it is resized, and when keyboard input is received, respectively.

7. glewExperimental = GL_TRUE;
   glewInit();

   initializes GLEW (the OpenGL Extension Wrangler Library) which handles the loading of OpenGL extensions, with the switch set so that extensions implemented even in pre-release drivers are exposed.

8. setup() invokes the initialization routine.

9. glutMainLoop begins the event-processing loop, calling registered callback routines as needed.

We have already seen that the only command in the initialization routine setup(), namely, glClearColor(1.0, 1.0, 1.0, 0.0), specifies the clearing color of the OpenGL window.

The callback routine to draw the OpenGL window is:

```
void drawScene(void)
{
    glClear(GL_COLOR_BUFFER_BIT);
    glColor3f(0.0, 0.0, 0.0);
    // Draw a polygon with specified vertices.
    glBegin(GL_POLYGON);
    ...
    glEnd();
    glFlush();
}
```

The first command clears the OpenGL window to the specified clearing color, in other words, paints in the background color. The next command glColor3f() sets the foreground, or drawing, color, which is used to draw the polygon specified within the glBegin()-glEnd() pair (we have already examined this polygon carefully). Finally, glFlush() forces all the commands in queue to actually execute – emptying or flushing the commands buffer as it were – which, in this case, means the polygon is drawn.

The callback routine when the OpenGL window is resized, and first created, is void resize(int w, int h). The window manager supplies the width w and height h of the resized OpenGL window (or, initial window, when it is first created) as parameters to the resize routine.

The first command

```
glViewport(0, 0, w, h);
```

of square.cpp's resize routine specifies the rectangular part of the OpenGL window in which actual drawing is to take place; with the given parameters it is the entire window. We'll be looking more carefully into glViewPort() and its applications in the next chapter.

The next three commands

```
glMatrixMode(GL PROJECTION);
glLoadIdentity();
glOrtho(0.0, 100.0, 0.0, 100.0, -1.0, 1.0);
```

activate the projection matrix stack, place the identity matrix at the top of this stack, and then multiply the identity matrix by the matrix corresponding to the final glOrtho() command. Don't worry if all this about matrices doesn't make much sense now – the takeway that the third statement above sets up the viewing box of square.cpp (as described in Section 2.2) is enough at this time. We'll be learning about OpenGL's matrix stacks in Chapters 4 and 5.

The final two commands

```
glMatrixMode(GL_MODELVIEW);
glLoadIdentity();
```

of the resize routine activate the modelview matrix stack and place the identity matrix at the top in readiness for modelview transformation commands in the drawing routine – commands which move objects, of which there happen to be none in square.cpp.

The callback routine to handle ASCII keys is keyInput(unsigned char key, int x, int y). When an ASCII key is pressed it is passed in the parameter char to this callback routine, as is the location of the mouse in the parameters x and y. All that keyInput of square.cpp does is terminate the program when the escape key is pressed. In the next chapter we'll see callback routines to handle non-ASCII keys, as well as interaction via the mouse.

As the reader might well guess, the guts of an OpenGL program are in its drawing routine. Interestingly, the initialization routine often pulls a fair load, too, because one would want to locate there tasks that need to be done once at start-up, e.g., setting up data structures. In fact, it's a common beginner's mistake to place initialization chores in the drawing routine, as the latter is invoked repeatedly if there is animation, leading to inefficiency.

The other routines, such as main() and the interactivity and reshape callbacks, are simple to code and, in fact, can often be copied from one program to the next.

Remark 2.26. Another popular library for use with OpenGL in order to manage a window and handle input events is GLFW [57], the name derived from "Graphics Library Framework", which can serve as an alternate to FreeGLUT. All our programs use FreeGLUT. However, for those who have prior experience with GLFW, or might be curious, we include below a GLFW version of square.cpp.

Experiment 2.28. You will need to configure your environment to include GLFW before running squareGLFW.cpp. How to do this is described in the comments at the top of the program file. This program has the exact same functionality as square.cpp, only with GLFW replacing FreeGLUT. Figure 2.62 is a screenshot. End

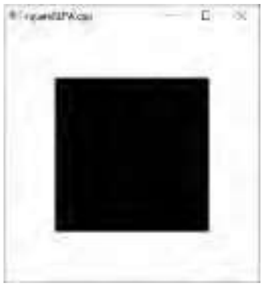

Figure 2.62: Screenshot of squareGLFW.cpp.

2.12 Summary, Notes and More Reading

In this chapter we began the study of 3D CG, looking at it through the "eyes" of OpenGL. OpenGL itself was presented to the extent that the reader acquires functional literacy in this particular API. The drawing primitives were probably the most important part of the API's vernacular.

We discovered as well how OpenGL functions as a state machine, attributes such as color defining the current state. Moreover, we learned that quantifiable attribute values, e.g., RGB color, are typically interpolated from the vertices of a primitive throughout its interior. We saw that OpenGL clips whatever the programmer draws to within a viewing volume, either a box or frustum.

Beyond acquaintance with the language, we were introduced as well to the synthetic-camera model of 3D graphics, which OpenGL implements via two kinds of projection: orthographic and perspective. This included insights into the world coordinate system, the viewing volume – box or frustum – which is the stage in which all drawings are made, the shoot-and-print rendering process to map a 3D scene to a 2D window, as well as hidden surface removal. We made a first acquaintance as well with another cornerstone of 3D graphics: the technique of simulating curved objects using straight and flat primitives like line segments and triangles.

Historically, OpenGL evolved from SGI's IRIS GL API, which popularized the approach to creating 3D scenes by drawing objects in actual 3-space and then rendering them to a 2D window by means of a synthetic camera. IRIS GL's efficiently pipelined architecture enabled high-speed rendering of animated 3D graphics and, consequently, made possible as well real-time interactive 3D. The ensuing demand from application developers for an open and portable (therefore, platform-independent) version of their API spurred SGI to create the first OpenGL specification in 1992, as well as a sample implementation. Soon after, the OpenGL ARB (Architecture Review Board), a consortium composed of a few leading companies in the graphics industry, was established to oversee the development of the API. Stewardship of the OpenGL specification passed in 2006 to the Khronos Group, a member-funded industry consortium dedicated to the creation of open-standard royalty-free API's. (That no *one* owns OpenGL is a good thing.) The canonical, and very useful, source for information about OpenGL is its own home page [106].

Microsoft has a non-open Windows-specific 3D API – Direct3D [92, 144] – which is popular among game programmers as it allows optimization for the pervasive Windows platform. However, outside of the games industry, where it nonetheless competes with

Direct3D, and leaving aside particular application domains with such high-quality rendering requirements that ray tracers are preferred, by far the dominant graphics API is OpenGL. The beginning graphics programmer should keep in mind though that recent versions of OpenGL and Direct3D are fairly alike in functionality – read an interesting comparison in Wikipedia [26]) – so migrating from one to the other is not hard.

It's safe to say that OpenGL is the de facto standard 3D graphics API. A primary reason for this, other than the extremely well-thought-out design, is OpenGL's portability. It's worth knowing as well that, despite its intended portability, OpenGL can take advantage of platform-specific and card-specific capabilities via so-called extensions, at the cost of clumsier code.

But wait, there's more! A lighter version of OpenGL, namely, OpenGL ES (for Embedded Systems), is to be found supporting mobile 3D apps on almost every Android smartphone. And, WebGL, a derivation again of OpenGL, is an emerging standard for 3D graphics on the web which runs on almost all browsers.

Perhaps the best reason for OpenGL to be *the* API of choice for students of 3D computer graphics is – and this is a consequence of its almost universal adoption by the academic, engineering and scientific communities – the sheer volume of learning resources available. Not least among these is the number of textbooks that teach computer graphics with the help of OpenGL. Search amazon.com with the keywords "computer graphics opengl" and you'll see what we mean. Angel [2], Buss [21], Govil-Pai [62], Hearn & Baker [71], Hill & Kelley [74] and McReynolds & Blythe [95] are some introductions to computer graphics via OpenGL that the author has learned much from.

Interestingly, nn unofficial clone of OpenGL, Mesa 3D [96], which uses the same syntax, was originally developed by Brian Paul for the Unix/X11 platform, but there are ports now to other platforms as well.

In case the reader prefers not to be distracted by code, here are a few API-independent introductions: Akenine-Möller, Haines & Hoffman [1], Foley et al. [47, 48], Marschner & Shirley [94], Watt [150], Xiang [157] and Xiang & Plastock [158]. Keeping different books handy in the beginning is a good idea as, often, when you are having trouble grasping one author's exposition of a topic, turning to another for help with that matter may clear the way.

With regard to the code which comes with this book, we don't make much use of OpenGL-defined data types, which are prefixed with GL, e.g., GLsizei, GLint, etc., though the red book advocates doing so in order to avoid type mismatch issues when porting. Fortunately, we have not yet encountered a problem in any implementation of OpenGL that we've tried.

In addition to the code which comes with this book, the reader should try to acquire OpenGL programs from as many other sources as possible, as an efficient way to learn the language – any language as a matter of fact – is by modifying live code. There are numerous resources on the web for code, as well as tutorials, 3D models and texture images. The OpenGL site [106] has pointers to several coding tutorials. The book by Wright, Lipchak & Haemel [132] is specifically about programming OpenGL and has numerous example programs. The red book comes with example code as well.

Hard-earned wisdom: Write experiments of your own to clarify ideas. Even if you are sure in your mind that you understand something, do write a few lines of code in verification. As the author has repeatedly been, you too might be surprised.

Part II

Tricks of the Trade

Chapter 3

An OpenGL Toolbox

Before getting to animation and other fun stuff in the next chapter, here are a few practical skills worth acquiring first. Our goal this chapter is to learn the following frequently-used OpenGL programming devices:

1. Vertex arrays and their drawing commands: storing geometric data in a single location for efficient access.
2. Vertex buffer objects: storage for vertex-related data on the graphics server to save client-to-server transfer time.
3. Vertex array objects: encapsulating the set of calls defining an object's vertex arrays.
4. Display lists: "macros" to store frequently-invoked pieces of code.
5. Drawing of text.
6. Programming the mouse – for button clicks, turning the wheel and mouse motion.
7. Programming non-ASCII keys.
8. Programming pop-up menus.
9. Line stipples: applying patterns to lines.
10. FreeGLUT objects: ready-made library objects.
11. Clipping planes: planes to clip a scene in addition to the automatic six that bound the viewing box or frustum.
12. Frustum, differently: gluPerspective() specifies a viewing frustum more intuitively than glFrustum() and with fewer parameters.
13. Viewports: specifiable parts of the OpenGL window to which a drawing is rendered.
14. Multiple windows: multiple top-level OpenGL windows.

None is particularly challenging or deep and the reader may choose to flip quickly through the pages to just see what each is about in order to be able to return later for how to implement when the need arises.

However, the exceptions we would make to this approach are the first three sections. The reader should master vertex arrays in Section 3.1 and begin using them right away. As for vertex buffer objects and vertex array objects in Sections 3.2-3.3, though we don't expect the user to code much of them at first, they are indispensable in the newer versions of OpenGL, e.g., 4.x, which we shall cover down the road, so the reader should at least make their acquaintance at this time.

The next fourteen sections follow the order of the list above.

3.1 Vertex Arrays and Their Drawing Commands

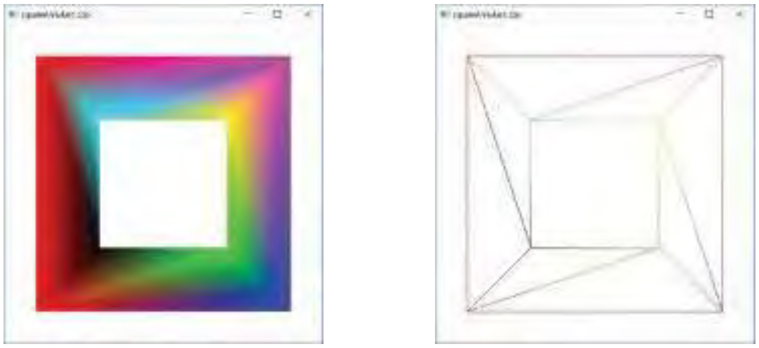

(a)

(b)

Figure 3.1: Screenshots of squareAnnulus1.cpp.

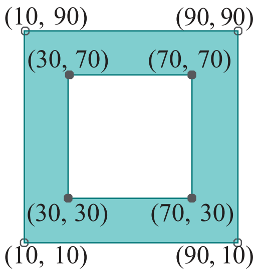

Figure 3.2: Square annulus (z coordinates all 0).

Experiment 3.1. Run squareAnnulus1.cpp. A screenshot is seen in Figure 3.1(a). Press the space bar to see the wireframe in Figure 3.1(b).

It is a plain-vanilla program which draws the square annulus diagrammed in Figure 3.2 with a single giant triangle strip containing 10 vertices and their color attributes (the last two vertices being identical to the first two in order to close the strip):

```
glBegin(GL_TRIANGLE_STRIP);
   glColor3f(0.0, 0.0, 0.0);
   glVertex3f(30.0, 30.0, 0.0); // Vertex 0
   glColor3f(1.0, 0.0, 0.0);
   glVertex3f(10.0, 10.0, 0.0); // Vertex 1
   glColor3f(0.0, 1.0, 0.0);
   glVertex3f(70.0, 30.0, 0.0); // Vertex 2
   ...
   glColor3f(0.0, 0.0, 0.0);
   glVertex3f(30.0, 30.0, 0.0); // Vertex 8 = Vertex 0
   glColor3f(1.0, 0.0, 0.0);
   glVertex3f(10.0, 10.0, 0.0); // Vertex 9 = Vertex 1
glEnd();
```

End

Experiment 3.2. Run squareAnnulus2.cpp.

It draws the same annulus as squareAnnulus1.cpp, except that the vertex coordinates and color data are now separately stored in two-dimensional global arrays, vertices and colors, respectively. Moreover, in each iteration, the loop

```
glBegin(GL_TRIANGLE_STRIP);
   for(int i = 0; i < 10; ++i)
   {
      glColor3fv(colors[i%8]);
      glVertex3fv(vertices[i%8]);
   }
glEnd();
```

retrieves a vector of coordinate values by the *pointer form* (also called *vector* form) of vertex declaration, namely, glVertex3fv(**pointer*), and as well a vector of color values with the pointer form glColor3fv(**pointer*). End

Compared with squareAnnulus1.cpp, an obvious efficiency gained in squareAnnulus2.cpp is in placing vertex and color data at one place in the code to be able simply to point to them from elsewhere. This allows the triangle strip block, though still containing 10 vertices and their colors, to be coded as a short loop.

It's always good practice to collect and place data for a program at a single location separate from the procedures which actually access the data. Redundancy and consequent errors tend to be eliminated, memory usage is more efficient, and it's easier to modularize and debug the procedures accessing data.

Helpfully, OpenGL offers specific devices – the *vertex array* data structures – which make it easy and efficient for the user to centralize and share data. Let's learn them from live code.

Experiment 3.3. Run squareAnnulus3.cpp.

It again draws the same colorful annulus as before. The coordinates and color data of the vertices are stored in global vertex arrays, vertices and colors, respectively, as in squareAnnulus2.cpp, except, now, the arrays are flat and not 2D (OpenGL assumes 1D arrays but, because of the way C++ stores arrays, we could, in fact, have specified vertices and colors as 2D arrays exactly as in squareAnnulus2.cpp if we had so chosen). End

Now, to the magic: within the triangle strip loop

```
glBegin(GL_TRIANGLE_STRIP);
   for(int i = 0; i < 10; ++i) glArrayElement(i%8);
glEnd();
```

the *i*th vector of values from both coordinates *and* color arrays are retrieved *simultaneously* with a single glArrayElement(*i*) call.

Note the steps in setting up the vertex arrays in the initialization routine:

1. Two vertex arrays are enabled by calling glEnableClientState(*array*), where *array* is, successively, GL_VERTEX_ARRAY and GL_COLOR_ARRAY, for vertex coordinate and color values, respectively. There are other possible values for the parameter *array* to store additional kinds of vertex data, e.g., normal values and texture coordinates.

2. The data for the two vertex arrays is specified with a call to glVertexPointer(*size*, *type*, *stride*, **pointer*) and to glColorPointer(*size*, *type*, *stride*, **pointer*). The parameter *pointer* is the address of the start of the data array, *type* declares the data type, *size* is the number of values per vertex (e.g., both our coordinate and color arrays store 3 values for each vertex) and *stride* is the byte offset between the start of the values for successive vertices (0 indicates specially that values for successive vertices are not separated, as is our case).

Experiment 3.4. Run squareAnnulus4.cpp.

The code is even more concise with the single draw call

```
glDrawElements(GL_TRIANGLE_STRIP, 10, GL_UNSIGNED_INT, stripIndices)
```

replacing the entire glBegin(GL_TRIANGLE_STRIP)-glEnd() block. End

The general form of this call is

glDrawElements(*primitive*, *countIndices*, *type*, **indices*) where parameter *primitive* is a geometric primitive, *indices* is the address of the start of an array of indices, *type* is the data type of the *indices* array and *countIndices* is the number of indices to use. What this call does is pick *countIndices* number of vertices for *primitive* from the enabled vertex arrays in the sequence specified by *indices*, equivalent, therefore, to the loop

```
glBegin(primitive);
   for(i = 0; i < countIndices; i++) glArrayElement(indices[i]);
glEnd();
```

Exercise 3.1. (Programming) Rewrite hemisphere.cpp of the last chapter to use a single vertex array and a loop of glDrawElements(GL_TRIANGLE_STRIP, . . .) commands.

When there are multiple objects in a scene it's convenient to keep their data separately in different vertex arrays, as in the following program.

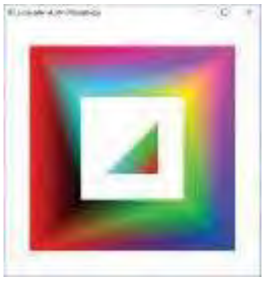

Figure 3.3: Screenshot of squareAnnulusAndTriangle.cpp.

Experiment 3.5. Run squareAnnulusAndTriangle.cpp, which adds a triangle inside the annulus of the squareAnnulus*.cpp programs. See Figure 3.3 for a screenshot. End

This program demonstrates the use of multiple vertex arrays. The vertex arrays vertices1 and colors1 contain the coordinate and color data, respectively, for the annulus, exactly as in squareAnnulus4.cpp.

The single vertex array vertices2AndColors2Interleaved for the triangle, on the other hand, is *interleaved* in that it contains both coordinate and color data together. When pointing to data for the triangle, the *stride* parameter of both the glVertexPointer() and glColorPointer() calls is set to 6 times the number of bytes in a float data item, as there are 6 floats (in particular, 3 coordinate values and 3 color values) between the start of successive coordinate or color vectors in the interleaved array.

The statement

```
glDrawArrays(GL_TRIANGLES, 0, 3)
```

drawing the triangle introduces a new drawing command as well to use with vertex arrays. Generally,

```
glDrawArrays(primitive, first, countVertices)
```

draws the geometric primitive *primitive*, using *countVertices* elements from the vertex array, starting with the element at position *first* . This is the command of choice when the drawing needs simply to process elements in a vertex array linearly, i.e., in code order, without needing to bounce around with something like an *indices* array supplying an intermediate level of indirection. Figure 3.4 diagrams the difference between ordered and indexed drawing.

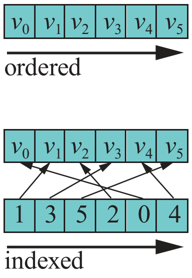
v_0 v_1 v_2 v_3 v_4 v_5
ordered
v_0 v_1 v_2 v_3 v_4 v_5
1 3 5 2 0 4
indexed

Figure 3.4: Example of ordered vs. indexed draw: ordered draw processes the vertices in the sequence $v_0v_1v_2v_3v_4v_5$, while indexed draw in the sequence $v_1v_3v_5v_2v_0v_4$.

Exercise 3.2. (Programming) Rewrite circle.cpp of the last chapter to use vertex arrays and a single glDrawArrays() command.

Exercise 3.3. (Programming) Here's a challenge: rewrite hemisphere.cpp to use a *single* glDrawArrays() command. Obviously, the trick is to set up one (long) vertex array "covering" the whole hemisphere (*hint*: think spiral).

Vertex arrays make for efficient, logical and conceptually clean OpenGL code. Figure 3.5 illustrates this (it shows additional vertex attributes also stored in vertex arrays – we'll be discussing these later). Moreover, they are *mandatory* in the latest versions of OpenGL, e.g., 4.x, which we'll be covering later on. *Make a habit of using vertex arrays starting now*!

Caveat : Henceforth, we'll be implementing vertex arrays consistently ourselves except, possibly, for programs where the overhead might detract from the main point of the program.

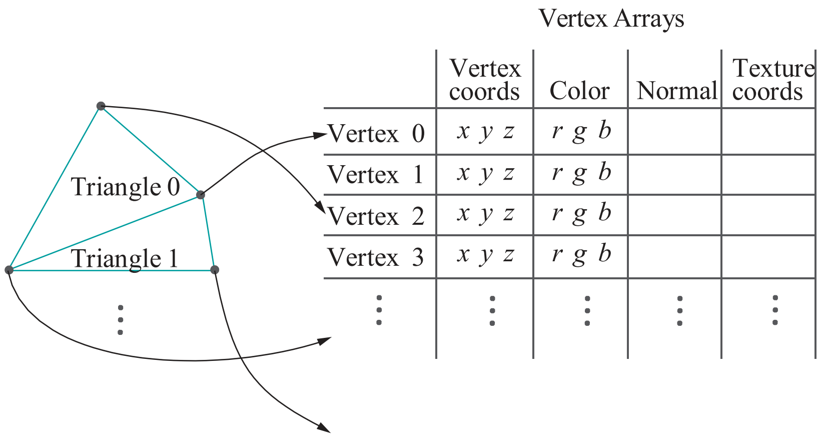

	Vertex coords	Color	Normal	Texture coords
Vertex 0	$x\ y\ z$	$r\ g\ b$		
Vertex 1	$x\ y\ z$	$r\ g\ b$		
Vertex 2	$x\ y\ z$	$r\ g\ b$		
Vertex 3	$x\ y\ z$	$r\ g\ b$		
⋮	⋮	⋮	⋮	⋮

Figure 3.5: Logical representation of data using vertex arrays: vertex data is in one area with primitives each defined as a list of pointers to vertices. In a glDrawElements() call, for example, the pointer values are in an indices array.

Remark 3.1. Keep in mind that the display routine is called repeatedly if there is animation. It's particularly inefficient, therefore, and, unfortunately, a common beginner's mistake to store static data in this routine, or perform computations there which actually can be done once initially and the results saved. The rule is to store vertex attributes in vertex arrays, while the initialization routine is the place for one-time computation.

Before closing this section we'll introduce a couple more drawing commands to use with vertex arrays. The first,

```
glMultiDrawElements(primitive, *countIndices, type, **indices,
                    countPrimitives)
```

is a powerlifter with the capacity of multiple glDrawElements(). In fact, the parameters of glMultiDrawElements() are much as you would expect in order to combine many

```
glDrawElements(primitive, countIndices, type, *indices)
```

calls, each drawing the same geometric primitive *primitive*: instead of one *countIndices* value, now there is an array **countIndices* of values; instead of an array **indices* of indexes, now there is an array of arrays ***indices*; finally, *countPrimitives*, of course, is the number of *primitive* s being drawn, i.e., the number of glDrawElements() being combined. The glMultiDrawElements() call so is equivalent to

```
for (int i = 0; i < countPrimitives; i++)
   glDrawElements(primitive, countIndices[i], type, indices[i]);
```

It's more efficient to draw an object composed of multiple instances of the same geometric primitive using one (or few) glMultiDrawElements() calls versus several glDrawElements(). Let's redo hemisphere.cpp from the last chapter using a single glMultiDrawElements() command.

Experiment 3.6. Run hemisphereMultidraw.cpp, whose sole purpose is to draw the loop

```
for(j = 0; j < q; j++)
{
   // One latitudinal triangle strip.
   glBegin(GL_TRIANGLE_STRIP);
   ...
}
```

of triangle strips of hemisphere.cpp using instead the single

```
glMultiDrawElements(GL_TRIANGLE_STRIP,   countIndices,
                     GL_UNSIGNED_BYTE, (const void **)indices, q)
```

command. Figure 3.6 is a screenshot. End

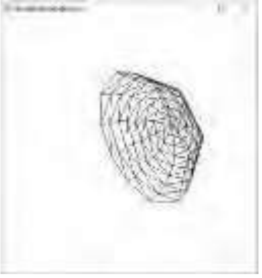

Figure 3.6: Screenshot of hemisphereMultidraw.cpp.

We'll leave the reader to plow through the rest of the code of hemisphereMultidraw.cpp, which is almost all dedicated to setting up the arrays for the glMultiDrawElements() call. Particularly, the reader should convince herself that fillIndices() does its job of filling the 2D array *indices* correctly (this is the part where one usually needs to be most careful in transitioning from glDrawElements() to glMultiDrawElements()).

Exercise 3.4. (Programming) If you drew any of the objects from Exercise 2.42 of the last chapter, redo the code to use glDrawElements(), or, if possible, glMultiDrawElements().

Finally,

glMultiDrawArrays(*primitive*, **first*, **countVertices*, *countPrimitives*)

is related to glDrawArrays() exactly as glMultiDrawElements() is related to glDrawElements(): a single glMultiDrawArrays() command encapsulating multiple glDrawArrays().

Exercise 3.5. (Programming) Draw the bull's eye of Exercise 2.24 of the last chapter using a single glMultiDrawArrays() call.

Remark 3.2. *Important* ! glBegin()-glEnd()-type drawing commands are for so-called *immediate mode* rendering, while glDrawElements(), glDrawArrays(), glMultiDrawElements(), glMultiDrawArrays() and a few more of their relatives (see the red book for a list) are for *retained mode* rendering. In immediate mode, the client (the machine running the program) forces rendering by the server (the GPU), while, in retained mode, the client provides the server only with instructions to perform and the data to use, allowing the latter to optimize prior to rendering.

Immediate mode drawing has been removed from OpenGL from version 3.1 on (though it's still accessible via the compatibility profile); only retained mode calls are available in the higher versions. *Therefore, we urge the reader to use retained mode commands as far as possible from now on. Stop using* glBegin()-glEnd()! However, we'll occasionally transgress this recommendation ourselves for the sake of simple code because setting up the array of indices, or the array of arrays of indices in the case of glMultiDraw* commands, can be a bit tricky and distracting.

Remark 3.3. Continuing on the theme of the preceding remark, the name of the game when issuing retained mode drawing calls to the GPU, is the fewer the better because of per-call initialization cost. So, try to pack us much geometry as possible into each draw call, preferring triangle strips to individual triangles – which means "stripifying" triangle meshes as much as possible – and preferring multidraw calls to single ones.

3.2 Vertex Buffer Objects

OpenGL's client-server model means that each time the server requires vertex data – e.g., coordinates, color or such to execute, say, a glDrawElements() call – it must be fetched from the client. On a PC, for example, this translates to a transfer across the bus connecting the CPU (the client holding the application and data) to the GPU (graphics processing unit, being the server which does the drawing). Now, accessing data across a bus is, typically, many times slower than accessing it locally. Moreover, the access might even be redundant if the same data had been retrieved for an earlier command and, subsequently, not changed. To save such inefficiency, *buffer objects* allow the programmer to explicitly ask that some particular set of data, typically, vertex-related, such as a vertex array, be shipped from the client to the server and stored there for future use. Figure 3.7 is a conceptualization.

We will focus now on buffer objects which store vertex data, such being called *vertex buffer objects* , or *VBOs*. Let's get straight to code showing how to create, initialize and update a VBO.

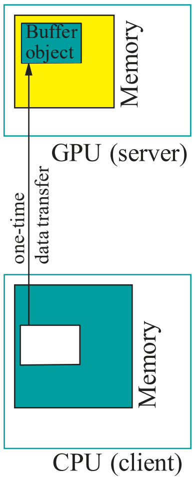

Figure 3.7: Buffer object logic.

Experiment 3.7. Fire up squareAnnulusVBO.cpp, which modifies squareAnnulus4.cpp to store vertex-related data in VBOs. There is a simple animation, too, through periodically changing color values in a VBO. Figure 3.8 is a screenshot, colors having already changed. End

Figure 3.8: Screenshot of squareAnnulusVBO.cpp.

Let's understand how squareAnnulusVBO.cpp works. The setup() routine is the one to look at first. The call

```
glGenBuffers(2, buffer)
```

returns two available buffer ids which we'll use to identify two VBOs in the array buffer. Generally, a call of the form glGenBuffers(*n*, *buffer*) returns *n* such ids. The binding command

```
glBindBuffer(GL_ARRAY_BUFFER, buffer[VERTICES])
```

activates the first VBO, buffer[VERTICES], the parameter GL ARRAY BUFFER declaring it to be for vertex data. Next,

```
glBufferData(GL_ARRAY_BUFFER, sizeof(vertices) + sizeof(colors),
             NULL, GL_STATIC_DRAW)
```

reserves sizeof(vertices) + sizeof(colors) bytes of space for the VBO currently bound to GL_ARRAY BUFFER, that being buffer[VERTICES], of course. The parameter NULL indicates that the buffer is not at this time initialized with data. The last parameter GL_STATIC_DRAW is a usage hint to the OpenGL system that the data will be specified once and used multiple times as a source for drawing commands.

The general form of the command glBufferData(*target*, *size*, **data*, *usage*) allocates *size* bytes of storage to the buffer object currently bound to *target* , filling it with application memory data pointed to by **data*, provided this pointer is not NULL, supplying, as well, the usage hint *usage*. The usage hint allows the system to optimize data storage for performance.

The next two commands

```
glBufferSubData(GL_ARRAY_BUFFER, 0, sizeof(vertices), vertices);
glBufferSubData(GL_ARRAY_BUFFER, sizeof(vertices), sizeof(colors),
                colors);
```

are update commands. In particular, we use them to update the VBO buffer[VERTICES] with coordinate and color values. What the command glBufferSubData(*target*, *offset*, *size*, **data*) does is copy *size* bytes of application data pointed to by **data* into the buffer object currently bound to *target*, starting at an offset of *offset* bytes from the start of the buffer. So, the two commands above evidently fill the first half of buffer[VERTICES] with vertex coordinate values and the latter half with color values.

Next,

```
glBindBuffer(GL_ELEMENT_ARRAY_BUFFER, buffer[INDICES]);
glBufferData(GL_ELEMENT_ARRAY_BUFFER, sizeof(stripIndices),
             stripIndices, GL_STATIC_DRAW);
```

activate the second VBO buffer[INDICES], the parameter GL ELEMENT ARRAY BUFFER declaring it to be for index data, and initialize it with data from the stripIndices array.

Vertex arrays are enabled next by

```
glEnableClientState(GL_VERTEX_ARRAY);
glEnableClientState(GL_COLOR_ARRAY);
```

Finally,

```
glVertexPointer(3, GL_FLOAT, 0, 0);
glColorPointer(3, GL_FLOAT, 0, (void *)(sizeof(vertices)));
```

specify vertex pointers as in the discussion following Experiment 3.3; *however* , the final parameter in both, instead of being a pointer to application memory as in earlier programs, e.g., squareAnnulus4.cpp, now is an offset relative to the start of the currently-bound VBO.

To the much simpler drawing routine next. The interesting thing to notice here is another buffer update method, different from glBufferSubData(). Firstly,

```
float* bufferData = (float*)glMapBuffer(GL_ARRAY_BUFFER,
                                        GL_WRITE_ONLY);
```

retrieves into the variable bufferData a pointer to the data store for the VBO currently bound to GL_ARRAY BUFFER, that being buffer[VERTICES]. The second parameter GL_WRITE ONLY says access will only be to write into the VBO. The general form of this command is glMapBuffer(*target*, *access*), where *target* is the target buffer object and *access* is one of GL_READ ONLY, GL WRITE ONLY and GL READ WRITE.

The loop

```
for (int i = 0; i < sizeof(colors)/sizeof(float); i++)
   bufferData[sizeof(vertices)/sizeof(float) + i]
   = (float)rand()/(float)RAND_MAX;
```

randomly updates color values in buffer[VERTICES], keeping in mind that the type of bufferData means that we'll be offsetting into the buffer storage in units of float size (not byte as earlier). Once updating is done,

```
glUnmapBuffer(GL_ARRAY_BUFFER)
```

releases the VBO, following which

```
glDrawElements(GL_TRIANGLE_STRIP, 10, GL_UNSIGNED_INT, 0);
```

draws the square annulus. Note, again, that the final parameter, instead of being a pointer to the start of the index array in application memory, is now an offset relative to the start of the (index data) VBO.

Comment out the for loop above for the buffer to be updated only in setup() with data from the vertices and colors arrays – of course, you'll see then the same square annulus as in squareAnnulus?.cpp.

The reader can at this time safely ignore the functioning of the little gadget animate(), which we include to periodically update color values and actually display the changed annulus.

Our next project is to buffer the vertex and index data of hemisphereMultidraw.cpp.

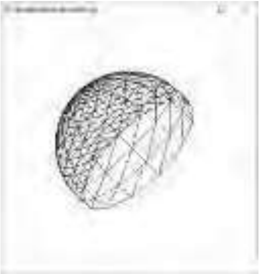

Figure 3.9: Screenshot of hemisphereMultidraw-VBO.cpp.

Experiment 3.8. Run hemisphereMultidrawVBO.cpp. A screenshot is in Figure 3.9. End

The code of hemisphereMultidrawVBO.cpp, which buffers the vertex and index data of hemisphereMultidraw.cpp along the lines of squareAnnulusVBO.cpp, should be intelligible to a reader who followed our analysis of the latter program. The one command, though, we would like to draw particular attention to is the program's only drawing command:

```
glMultiDrawElements(GL_TRIANGLE_STRIP, countIndices, GL_UNSIGNED_INT,
                    (const void **)offsets, LAT_SLICES);
```

In particular, note that the fourth parameter is now a pointer to the array *offsets* of offsets in the index VBO to the start of 1D index subarrays, one subarray per triangle strip.

Observe, as well, that the current program lacks the interactivity of hemisphereMultidraw.cpp, which allowed the user to alter the number of latitudinal and longitudinal slices. The reason is that different numbers of slices would require vertex and index arrays of different sizes and contents so, therefore, corresponding new VBOs which would have to be filled at run-time with data from the application, going against the "ship data once and use many times" precept underlying the utility of VBOs.

The problem of multiple data shipments might be circumvented by reserving space for one giant VBO, but this solution seems not particularly elegant. We shall, in fact, learn an efficient way to interactively refine the triangulation of an object when we come to the tessellation shaders of fourth generation OpenGL.

Exercise 3.6. Continue with Exercise 3.2 to redo the circle.cpp yet again, this time using VBOs to hold vertex data – a line loop of fixed size for the circle will do.

Exercise 3.7. (Programming) Continue with Exercise 3.5 to redo the bull's eye yet again, this time using VBOs to hold vertex data.

3.3 Vertex Array Objects

A busy scene with many objects, each coded up with its own vertex arrays, possibly buffered in VBOs as well, will likely require switching multiple times between these sets of arrays and buffers, leading to a proliferation of calls such as glBindBuffer() and glVertexPointer().

Since version 3.0, OpenGL provides a neat mechanism to deal with this problem: a *vertex array object* , or *VAO* , is a container to hold all the calls specifying one or more vertex arrays. So, once all these calls specifying a particular object's vertex arrays have been associated with a VAO, one need only activate that VAO prior to drawing the object; in other words, the VAO can be thought of as encapsulating the storage states associated with the object. Figure 3.10 indicates the scheme, though not all attributes may be present in every object. Let's get to code.

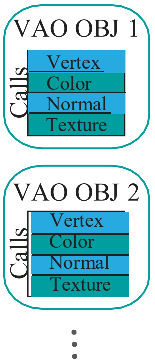

Figure 3.10: VAO logic.

Experiment 3.9. Run squareAnnulusAndTriangleVAO.cpp. This program builds on squareAnnulusVBO.cpp. We add to it the triangle from squareAnnulusAndTriangle.cpp in order to have two VAOs. Note, however, that we separate out the vertex coordinates and color arrays of the triangle, because interleaved, as in squareAnnulusAndTriangle.cpp, they are a bit trick to manage in a VBO. Otherwise, the outputs of the current program and squareAnnulusAndTriangle.cpp are identical – see Figure 3.11. End

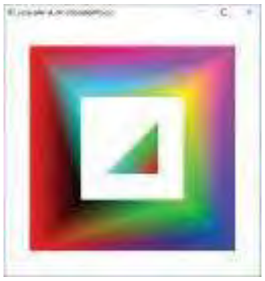

Figure 3.11: Screenshot of squareAnnulusAndTriangleVAO.cpp.

VAOs are simple to code. The call

```
glGenVertexArrays(2, vao)
```

in the initialization routine of squareAnnulusAndTriangleVAO.cpp returns two available ids for VAOs in the array vao. Generally, a call of the form glGenVertexArrays(n, vao) returns n such ids.

Next, the first block of statements bracketed by a // BEGIN...-// END... comment pair, namely,

```
// BEGIN bind VAO id vao[ANNULUS] ...
glBindVertexArray(vao[ANNULUS]);
glGenBuffers(2, buffer);
---
glVertexPointer(3, GL_FLOAT, 0, 0);
glColorPointer(3, GL_FLOAT, 0, (void *)(sizeof(vertices1)));
// END bind VAO id vao[ANNULUS].
```

begins with the binding command glBindVertexArray(vao[ANNULUS]), which activates the first VAO vao[ANNULUS]. Then, associated to this VAO are the rest of the calls in the above block, which are copied line for line from squareAnnulusVBO.cpp, in particular, from the block dedicated to setting up the VBOs and vertex arrays for the square annulus in the latter program.

The next block of statements bracketed by a comment pair, in particular,

```
// BEGIN bind VAO id vao[TRIANGLE] ...
glBindVertexArray(vao[TRIANGLE]);
glGenBuffers(1, buffer);
...
glVertexPointer(3, GL_FLOAT, 0, 0);
glColorPointer(3, GL_FLOAT, 0, (void *)(sizeof(vertices2)));
// END bind VAO id vao[TRIANGLE].
```

likewise associates to the VAO vao[TRIANGLE] all the calls after the initial binding, defining vertex arrays for the triangle.

Let's see now the drawing routine, much simplified courtesy the VAOs. The two blocks of statement pairs in

```
glBindVertexArray(vao[ANNULUS]);
glDrawElements(GL_TRIANGLE_STRIP, 10, GL_UNSIGNED_INT, 0);

glBindVertexArray(vao[TRIANGLE]);
glDrawArrays(GL_TRIANGLES, 0, 3);
```

successively activate the VAOs corresponding to the annulus and triangle, and draws them. Clearly, prepacking the definition of their respective storage states into VAOs in setup() has saved us a lot of calls in drawing the annulus and triangle in drawScene() (a saving which would have been even greater had there been multiple occurrences of either object).

Note that glBindVertexArray(*vaoID)* creates a new VAO if *vaoID* has been freshly returned by a glGenVertexArrays() call (as in our setup()) and associates with it subsequent vertex array specifications. On the other hand, if *vaoID* is the id of an already-created VAO (as in drawScene()), then glBindVertexArray(*vaoID)* activates that VAO.

Exercise 3.8. (Programming) The VAOs of both annulus and triangle in squareAnnulusAndTriangleVAO.cpp share the same buffer array. Why is this not a problem?
Hint: buffer is just a location for the system to return available buffer ids.

Exercise 3.9. (Programming) Put the VBOs and related data of the hemisphere of Experiment 3.8 into a VAO and draw a sphere as one hemisphere on top of another.

Exercise 3.10. (Programming) Continue with Exercise 3.6 putting all the data for the circle into a VAO.

Remark 3.4. *Important* ! Having thus introduced VBOs and VAOs we are, oddly enough, going to counsel the reader against using them. *For now* ! The reason is that the simple (low poly count) programs she, presumably, is going to be writing for a while will hardly benefit from their usage, not really justifying, therefore, the added layer of complexity. It's best to focus on the fundamentals at this stage. Just keep the resource in mind for when your data sets get big.

So that you know, though, VBOs and VAOs will truly come into their own when we study shader-based OpenGL, where using them is *mandatory*! Not to worry though as they are nothing conceptually difficult as we have seen and a bit of review is all we'll need at that time to get back up to speed.

3.4 Display Lists

A set of commands, e.g., to define an object such as a wheel or robot arm, which is invoked repeatedly, can be cached in a so-called *display list* . The display list is stored on the machine which runs the display unit and, often, pre-compiled and optimized. When the particular set of commands needs to be invoked, the program simply calls the display list rather than reissue them.

Display lists are particularly efficient in a client-server environment where the two communicate over a bus or network and a goal is to minimize traffic. Once a display list has been saved by the server (the machine running the display unit), it can be invoked on a single command from the client (the machine running the program). Another advantage of display lists is that they provide a logical way to encapsulate objects (think classes of objects in C++).

Experiment 3.10. Run helixList.cpp, which shows six copies of the same helix, variously transformed and colored. Figure 3.12 is a screenshot. End

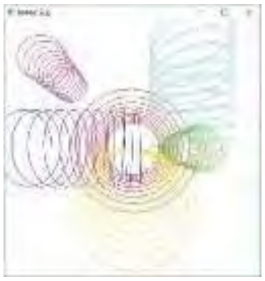

Figure 3.12: Screenshot of helixList.cpp.

Here's the snippet from the initialization routine of helixList.cpp which creates the display list to draw the helix:

```
aHelix = glGenLists(1);
glNewList(aHelix, GL COMPILE);
glBegin(GL LINE STRIP);
for(t = -10 * PI; t <= 10 * PI; t += PI/20.0)
   glVertex3f(20 * cos(t), 20 * sin(t), t);
glEnd();
glEndList();
```

The call glGenLists(*range*) returns the base (start) value of a block of size *range* of available display list indices. If a block of size *range* is not available, 0 is returned. The set of commands to be cached in a display list – a helix-drawing routine in the case of helixList.cpp – is grouped between a glNewList(*listName*, *mode*) and a glEndList() statement. The parameter *listName* – aHelix in helixList.cpp – is the index which identifies the list. The parameter *mode* may be GL_COMPILE (only store, as in the program) or GL COMPILE AND_EXECUTE (store and execute immediately).

Finally, the drawing routine of helixList.cpp invokes glCallList(aHelix) six times to execute the display list. The glPushMatrix()-glPopMatrix() statement pairs, as also the modeling transformations (viz., glTranslatef(), glRotatef(), glScalef()) within these pairs, are used to position and scale copies of the helix – you can ignore them for now as they are not relevant to display lists as such.

Exercise 3.11. (Programming) Put the hemisphere-drawing routine of hemisphere.cpp into a display list and call the list twice to make a sphere (apply the scaling transform glScalef(1.0, -1.0, 1.0) to flip the second hemisphere).

Exercise 3.12. (Programming) Make a ring of concentric circles of multiple colors on the *xy*-plane by repeatedly calling a display list containing a circle-drawing routine based on circle.cpp. Scale each invocation of the circle by a factor of *u* with a call to glScalef(*u*, *u*, 1.0).

There is a special mechanism in OpenGL to execute several display lists together.

Experiment 3.11. Run multipleLists.cpp. See Figure 3.13 for a screenshot. Three display lists are defined in the program: to draw a red triangle, a green rectangle and a blue pentagon, respectively. End

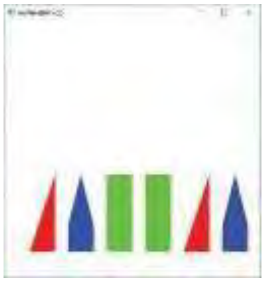

Figure 3.13: Screenshot of multipleLists.cpp.

The call glCallLists(*n*, *type*, **offsets*) causes *n* display list executions (*n* is 6 in the program). The indices of the lists to be executed are obtained by adding the current display list base – this base is specified by glListBase(*base*) – to the successive offset values of type *type* in the array pointed by *offsets*.

Remark 3.5. Each of the three display lists in multipleLists.cpp ends with a command of the form glTranslatef() in order to push the next drawing to the right. This is a strength of display lists that they can encapsulate transformation in addition to geometry.

Exercise 3.13. (Programming) Modify multipleLists.cpp to additionally draw a vertical black line separating each object and the next. The line itself should be in a display list.

3.5 Drawing Text

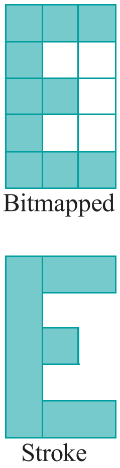

Figure 3.14: Bitmapped versus stroke text.

Graphical text can be of two types: *bitmapped* (also called *raster*) and *stroke* (also called *vector*). Characters of bitmapped text are defined as a pattern of on and off bits in a rectangular block, while characters of stroke text are created using line primitives. For example, in Figure 3.14, the letter 'E' is represented as a bitmap consisting of 10 on bits and 5 off in a 3×5 raster, as well as in stroke form as a union of four (rather thick) straight segments.

The FreeGLUT library offers both bitmapped and stroke characters. The calls glutBitmapCharacter(**font*, *character*) and glutStrokeCharacter(**font*, *character*) render *character* in the specified *font*.

Fonts available for bitmapped characters include:

GLUT_BITMAP_8_BY_13
GLUT_BITMAP_9_BY_15
GLUT_BITMAP_TIMES_ROMAN_10
GLUT_BITMAP_TIMES_ROMAN_24
GLUT_BITMAP_HELVETICA_10
GLUT_BITMAP_HELVETICA_12
GLUT_BITMAP_HELVETICA_18

Fonts available for stroke characters include:

GLUT_STROKE_ROMAN
GLUT_STROKE_MONO_ROMAN

Stroke characters offer an advantage over bitmapped ones in that they can be scaled in size and rotated, because line segments can be so transformed, whereas bitmapped characters, being fixed patterns on rectangular blocks of pixels, are always aligned with the axes and cannot be changed in size.

Figure 3.15: Screenshot of fonts.cpp.

Experiment 3.12. Run fonts.cpp. Displayed are the various fonts available through the FreeGLUT library. See Figure 3.15. End

The canonical routine we use to draw bitmapped text is the following:

```
void writeBitmapString(void *font, char *string)
{
   char *c;
   for (c = string; *c != '\0'; c++) glutBitmapCharacter(font, *c);
}
```

Accordingly, a subsequent call block

```
glRasterPos3f(p, q, r);
writeBitmapString(font, string);
```

renders *string* in bitmapped *font* starting from position (p, q, r) in world coordinates. Keep in mind that these coordinates are changed by prior modelview transformations, e.g., glTranslatef(), glRotatef() and such, though, as we said earlier, the bitmapped text itself is always drawn axis-aligned.

Our canonical routine to draw stroke text is

```
void writeStrokeString(void *font, char *string)
{
   char *c;
   for (c = string; *c != '\0'; c++) glutStrokeCharacter(font, *c);
}
```

which renders the text starting from (0, 0, 0) in world coordinates. Note that, in addition to modelview transformations, one can apply a glLineWidth() call to alter the thickness of stroke characters as well, as FreeGLUT uses GL_LINE* primitives to draw them.

Exercise 3.14. (Programming) Locate the labels of circularAnnuluses.cpp in the white center of each annulus (you may have to split the labels into more than one line to fit them).

3.6 Programming the Mouse

The mouse can be programmed to respond to button clicks, motion and the wheel turning.

Clicks

Experiment 3.13. Run mouse.cpp. Click the left mouse button to draw points on the canvas and the right one to exit. Figure 3.16 is a screenshot of "OpenGL" scrawled in points. End

Figure 3.16: Screenshot of mouse.cpp.

A mouse callback routine *mouse_callback_func*() is registered to handle mouse events by the FreeGLUT statement glutMouseFunc(*mouse callback_func*) in the main routine. In the case of mouse.cpp, the callback is mouseControl():

```
void mouseControl(int button, int state, int x, int y)
{
   if (button == GLUT LEFT BUTTON && state == GLUT DOWN)
      points.push_back( Point(x, height - y, pointSize) );
   if (button == GLUT RIGHT BUTTON && state == GLUT_DOWN) exit(0);
   glutPostRedisplay();
}
```

The callback routine, as ours above, has the form generally *mouse callback_func*(*button*, *state*, *x*, *y*), where *button* is one of:

GLUT_LEFT_BUTTON, GLUT RIGHT BUTTON, GLUT MIDDLE BUTTON

and *state* is one of:

GLUT_UP, GLUT DOWN

Moreover, the coordinates (x, y) return the location in the OpenGL window at which the mouse event occurs. They are measured similarly as for screen coordinates – recall from Section 2.3 that screen coordinates are measured in pixels starting from the origin at the upper-left corner of the screen with the x-axis heading right and the y-axis down – except that in the case of a mouse click the origin is at the upper-left corner of the OpenGL window, rather than screen. Units are still pixels and the x-axis still heads right and the y-axis down. See Figure 3.17. This necessitates care when using the coordinates of a mouse event in the OpenGL program itself, because there is no *a priori* connection between the former and the world coordinates used by the latter.

In particular, note the following two steps in mouse.cpp:

1. The call

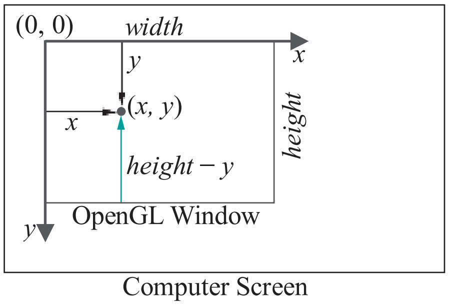

Figure 3.17: Mouse OpenGL window axes and event coordinates (black), y-correction for OpenGL (green).

```
glOrtho(0.0, w, 0.0, h, -1.0, 1.0);
```

in the reshape routine resize(w, h) ties screen coordinates to world coordinates by making the dimensions of the viewing face *equal* the actual physical dimensions of the OpenGL window, the latter being passed to the reshape routine via the parameters w and h. Because viewing face and OpenGL window are now the same size in their respective coordinate systems (world and screen), effectively, one unit along the viewing face along either the x- or y-axis is a pixel.

The only correction remaining to be made is owing to the y-axis being "upside down" going from one coordinate system to the other. This is done next.

2. The statement

```
points.push back( Point(x, height - y) );
```

in the mouse callback routine to store points in the points vector when the mouse is clicked makes the final correction from the event's screen coordinates to world coordinates, as (x, y) on the screen corresponds to $(x, height - y, 0)$ in the world.

Remark 3.6. A point of note in mouse.cpp is the use of an STL vector to store Point objects. STL stands for the *Standard Template Library*, a C++ library of container classes, e.g., vector, list, set, and so forth, together with routines to manipulate container objects. It is a part of the current ANSI C++ standard. The STL is extremely useful and saves a lot of repetitive programming. Readers not already familiar with the STL are well-advised to pick it up. There's no need to devote time separately for this purpose. Keeping a book like Schildt [126] handy while you code should be enough.

Exercise 3.15. (Programming) Write a program to draw a circle on a canvas after two left clicks of the mouse. The first click picks the center and the second a point on the circle.

Motion

Experiment 3.14. Run mouseMotion.cpp, which enhances mouse.cpp by allowing the user to drag the newly created point using the mouse with the left button still pressed. End

The additional capability of mouseMotion.cpp is obtained as follows. First, when the left mouse button is clicked, the mouse callback routine mouseControl() stores a point at the clicked position in the variable currentPoint of type Point. Only when the button is released is the new point added to the points vector by the same routine.

In the interim, between the press and release of the left mouse button, if the mouse moves, then its motion is tracked by the mouse motion callback routine mouseMotion():

```
void mouseMotion(int x, int y)
{
    currentPoint.setCoords(x, height - y);
    glutPostRedisplay();
}
```

This routine simply keeps updating the coordinates of currentPoint with the current location of the mouse as the latter moves with the button pressed. The result is that this point, which is drawn separately in the drawScene() routine, travels with the mouse. Note that, just as the mouse callback is registered in main(), so is the motion callback, the latter by glutMotionFunc(mouseMotion).

One can also track so-called *passive* motion of the mouse – when it moves with no button pressed – via a passive motion callback function, which is registered in main with a glutPassiveMotionFunc() call.

Exercise 3.16. (Programming) Enhance the previous circle-drawing exercise by allowing the user to view the changing circle as the mouse is dragged with the second click.

Exercise 3.17. (Programming) Modify mouseMotion.cpp to make a program which allows the user to sketch on a canvas.

Turning the Wheel

Experiment 3.15. Run mouseWheel.cpp, which further enhances mouseMotion.cpp with the capability to change the size of the last point drawn by turning the mouse wheel. End

The wheel callback routine

```
void mouseWheel(int wheel, int direction, int x, int y)
{
    (direction > 0) ? tempSize++ : tempSize--;
    points.back().setSize(tempSize);
    glutPostRedisplay();
}
```

reads the *wheel* number, which is 0 if there is a single wheel, the *direction* of rotation, which is either +1 or −1, and the location (x, y) of the mouse in screen coordinates. The callback routine then sets to tempSize the size of the current point, which is the last element of the vector points; moreover, tempSize increases or decreases by one for every step the wheel rotates, depending on the rotation direction. And, of course, the wheel callback routine is registered in main() by glutMouseWheelFunc(mouseWheel).

Exercise 3.18. (Programming) Further enhance the circle-drawing program by allowing the user to change the circle's size by scrolling the mouse wheel.

3.7 Programming Non-ASCII Keys

In various programs to date, we've already interacted with the OpenGL window through keyboard entry by registering a handling function *keyboard handling_func*() in the main routine via a call to glutKeyboardFunc(*keyboard_handling func*). To interact with non-ASCII keys such as the arrow, F, and page up and down keys, one needs likewise to register a handling function *special key_handling_func*() with a call to glutSpecialFunc(*special key handling_func*).

Experiment 3.16. Run moveSphere.cpp, a program we saw earlier in Experiment 2.24. Figure 3.18 is a screenshot. Press the left, right, up and down arrow keys to move the sphere, the space bar to rotate it and 'r' to reset.

Note how the specialKeyInput() routine is written to enable the arrow keys to change the location of the sphere. Subsequently, this routine is registered in main() as the handling routine for non-ASCII entry. End

Figure 3.18: Screenshot of moveSphere.cpp.

Exercise 3.19. (Programming) Write a program to cycle through the FreeGLUT fonts applied to the string "I am having so much fun with OpenGL it can't be legal!" by pressing the left and right arrow keys.

3.8 Menus

The FreeGLUT library provides pop-up menus.

Experiment 3.17. Run menus.cpp. Press the right mouse button for menu options which allow you to change the color of the initially red square or exit. Figure 3.19 is a screenshot. End

Figure 3.19: Screenshot of menus.cpp.

We'll define the menu-related calls generally first before explaining their role in menus.cpp.

glutCreateMenu(*menu function*) creates a menu, registers *menu_function*() as its callback function, and returns a unique integer identifying the menu – to be used by any higher-level menu which may call the current one.

glutAddMenuEntry(*tag*, *returned value*) creates a menu item labeled *tag* which, when clicked, returns *returned_value* to the callback function *menu_function*() of the menu itself. This callback, therefore, must be of the form *menu function*(*type of returned value*).

glutAddSubMenu(*tag*, *sub menu*) is similar to glutAddMenuEntry(), except that when *tag* is clicked a sub-menu pops up whose id is *sub menu*. Evidently, the statement creating a sub-menu must precede that for a higher-level menu which calls it, as the former's id must be known in order to create the latter. Consequently, menus must be created "bottom-up".

glutAttachMenu(*button*) attaches the menu to a mouse button.

To our program menus.cpp now. The routine makeMenu() is the one to look at. The first block of statements

```
int sub_menu;
sub_menu = glutCreateMenu(color_menu);
glutAddMenuEntry("Red", 2);
glutAddMenuEntry("Blue",3);
```

creates a menu with id sub_menu, callback color_menu(), and two items labeled "Red" and "Blue" which return 2 and 3, respectively, to color menu() in order to change the color of the square to red or green.

The next block

```
glutCreateMenu(top_menu);
glutAddSubMenu("Color", sub_menu);
glutAddMenuEntry("Quit",1);
```

creates a menu (whose id is not of interest as it's not going to become a sub of another menu) with callback top_menu() and two items labeled "Color" and "Quit", the first being the menu with id sub menu created above, which thus becomes a sub-menu, and the second returning 1 to top_menu() which causes the program to exit.

Finally

```
glutAttachMenu(GLUT_RIGHT_BUTTON);
```

causes the menu to pop up on clicking the right mouse button.

Exercise 3.20. (Programming) Enhance menus.cpp to add two more items to the top-level pop-up menu:

(a) A "Mode" option allowing the rectangle to be shown either "Outlined" or "Filled".

(b) A "Size" option which leads to two sub-menu options "Width" and "Height", either of which has options "Small", "Medium" and "Large".

3.9 Line Stipples

One can create *stippled* , i.e., broken, lines in OpenGL by specifying and applying a stipple pattern.

Experiment 3.18. Run lineStipple.cpp. Press the space bar to cycle through five different stipples. A screenshot is shown in Figure 3.20. End

Figure 3.20: Screenshot of lineStipple.cpp.

Stippling is enabled with a call to glEnable(GL_LINE_STIPPLE) and disabled by calling glDisable(GL_LINE_STIPPLE). The stipple pattern itself is specified by glLineStipple(*factor*, *pattern*).

Parameter *pattern* is a hex string of the form 0x$X_3X_2X_1X_0$ where each X_i is a hexadecimal symbol, equivalent, therefore, to 4 bits. Thus $X_3X_2X_1X_0$ represents a 16-bit string, say, $a_{15}a_{14} \dots a_0$. Parameter *factor* is a positive integer.

The stipple pattern is applied as follows: if a_0 is 1, then the first *factor* pixels starting from the first vertex of the line primitive are set on; if a_0 is 0, the first *factor* pixels are off. If a_1 is 1, the next *factor* pixels of the line are on; if a_1 is 0, they are off. And so on Note that the lower bits of the stipple pattern come first and that the effect of *factor* is simply to scale the pattern.

For example, suppose the stipple is specified by glLineStipple(1, 0x5555), as is the second stipple of lineStipple.cpp. Since 0x5555 = 0101010101010101, alternate pixels of the line are on and off with the first one being on. See Figure 3.21(a).

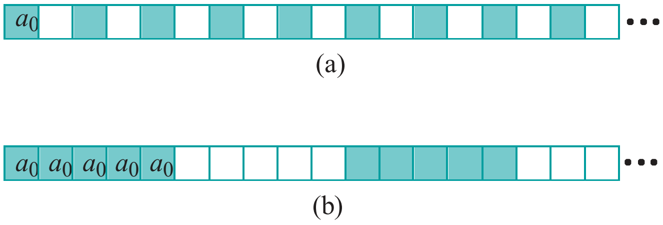

(a)

(b)

Figure 3.21: Line stipple specified by (a) glLineStipple(1, 0x5555) (b) glLineStipple(5, 0x5555).

If the stipple is specified by glLineStipple(5, 0x5555), as the fifth stipple of lineStipple.cpp, then alternate groups of five pixels on the line are on and off. See Figure 3.21(b).

Exercise 3.21. (Programming) Apply the different line stipples of lineStipple.cpp to the circle of circle.cpp.

FreeGLUT stroke characters can be stippled to interesting effect as well, as GL_LINE* primitives are used to draw them.

Exercise 3.22. (Programming) Display the text "I am having so much fun with OpenGL it can't be legal!" using variously stippled stroke fonts.

A 2D Drawing Program

Experiment 3.19. Run canvas.cpp, a simple program to draw on a flat canvas with menu and mouse functionality.

Left click on an icon to select it. Then left click on the drawing area to draw – click once to draw a point, twice to draw a line or rectangle. Right click for a pop-up menu. Figure 3.22 is a screenshot. End

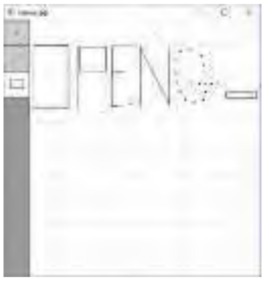

Figure 3.22: Screenshot of canvas.cpp.

Exercise 3.23. (Programming) Enhance canvas.cpp:

(a) Add a polyline (multi-segment line) drawing capability. Create a suitable icon. Left clicking this icon picks the polyline option. Subsequent left clicks pick successive segment endpoints until a middle click completes the polyline.

(b) Add a circle drawing capability. After left clicking the circle icon, the next two left clicks pick the center and a point on the circle, respectively, following which the circle is drawn.

(c) Add a regular (equal-sided) hexagon drawing capability. After left clicking the hexagon icon, the next two left clicks pick the center and a vertex, respectively, following which the hexagon is drawn.

(d) For the existing line segment and rectangle options, as well as for the new polyline, circle and hexagon options, use mouse motion tracking to allow the user to see the newly-created primitive change in real-time as the mouse moves, before it is saved with a final click.

(e) Add functionality to input text from the keyboard.

(f) Give options for the grid size in the pop-up menu.

(g) Add color options through the pop-up menu.

(h) Add an outlined/filled option through the pop-up menu.

(i) For the preceding three parts, make the pop-up menu depend on where the mouse is right-clicked. In particular, the color option should be available when any of the primitive icons on the left is clicked; the filled option, on the other hand, should appear only upon clicking icons of the 2D primitives, namely, the rectangle, circle and hexagon; finally, if the click is on the drawing area, then the options are, simply, grid-clear-quit (grid having a size sub-menu as well). For the color and filled options, the icon should change as well to represent the choice made.

A way to make the pop-up menu location-sensitive is by having the mouse callback routine, rather than the main routine, call the menu-making routine, so that the latter can access mouse event coordinates.

(j) Nothing to do with drawing as such but to get you to revisit vertex arrays in the first section, note that the drawGrid() routine draws lines over a for loop of vertices. Use vertex array commands instead.

3.10 FreeGLUT Objects

The FreeGLUT library offers a collection of standard objects for the programmer to use. Each is available in two flavors: solid and wireframe. The respective calls are shown in the table below. The objects are all drawn centered at the origin. The parameters, as present, determine the object's size and the fineness of its mesh. All the FreeGLUT objects are depicted in wireframe in Figure 3.23.

Solid	Wireframe
glutSolidSphere(*radius*, *slices*, *stacks*)	glutWireSphere(*radius*, *slices*, *stacks*)
glutSolidCube(*size*)	glutWireCube(*size*)
glutSolidCone(*base*, *height*, *slices*, *stacks*)	glutWireCone(*base*, *height*, *slices*, *stacks*)
glutSolidTorus(*inRadius*, *outRadius*, *sides*, *rings*)	glutWireTorus(*inRadius*, *outRadius*, *sides*, *rings*)
glutSolidDodecahedron(*void*)	glutWireDodecahedron(*void*)
glutSolidOctahedron(*void*)	glutWireOctahedron(*void*)
glutSolidTetrahedron(*void*)	glutWireTetrahedron(*void*)
glutSolidIcosahedron(*void*)	glutWireIcosahedron(*void*)
glutSolidTeapot(*size*)	glutWireTeapot(*size*)

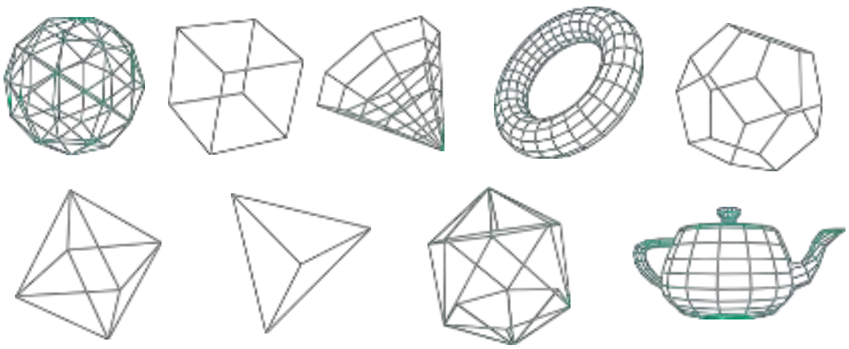

Figure 3.23: Wireframe FreeGLUT objects.

Experiment 3.20. Run glutObjects.cpp. Press the arrow keys to cycle through the various FreeGLUT objects and ‘x/X’, ‘y/Y’ and ‘z/Z’ to turn them. Figure 3.24 shows the teapot. End

Figure 3.24: Screenshot of glutObjects.cpp.

3.11 Clipping Planes

We saw in Section 2.4 that OpenGL clips a scene to within a viewing volume (box or frustum), a process which can be thought of as clipping the scene off on one side of each of the six planes which bound that volume. These six planes, called *clipping planes*, are automatically implied by the projection statement, such as glOrtho() or glFrustum(), which defines the box or frustum. However, the programmer can specify additional clipping planes.

The call

glClipPlane(GL_CLIP_PLANE*i*, **equation*);

specifies an *i*th additional clipping plane, where *equation* points to an array $\{A, B, C, D\}$ specifying the coefficients of the equation

$$Ax + By + Cz + D = 0$$

of the new clipping plane. If this plane is enabled with the call glEnable(GL_CLIP_PLANE*i*), then the points (x, y, z) of objects which lie in the open *half-space*

$$Ax + By + Cz + D < 0$$

are clipped off; equivalently, only those points (x, y, z) of objects lying in the closed half-space

$$Ax + By + Cz + D \geq 0$$

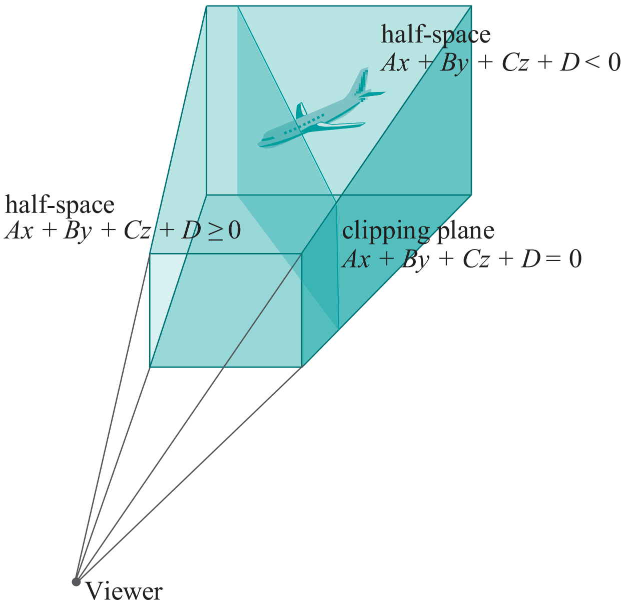

Figure 3.25: A clipping plane (not actually drawn by OpenGL) clipping a plane in half.

are rendered. The ith additional clipping plane is disabled with a call to glDisable(GL_CLIP_PLANEi). The clipping plane itself, of course, is never drawn. In Figure 3.25, for example, only the front part of the aircraft will be visible.

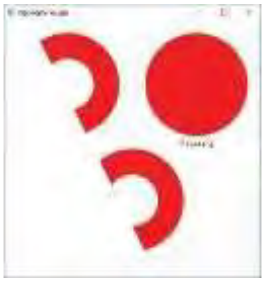

Figure 3.26: Screenshot of clippingPlanes.cpp.

Experiment 3.21. Run clippingPlanes.cpp, which augments circularAnnuluses.cpp with two additional clipping planes which can be toggled on and off by pressing ‘0’ and ‘1’, respectively.

The first plane (GL_CLIP_PLANE0) clips off the half-space $-z + 0.25 < 0$, i.e., $z > 0.25$, removing the floating white disc of the annulus on the upper-right. The second one (GL_CLIP_PLANE1) clips off the half-space $x + 0.5y < 60.0$, which is the space below an angled plane parallel to the z-axis. Figure 3.26 is a screenshot of both clipping planes activated. End

Exercise 3.24. (Programming) Change the equation of GL_CLIP_PLANE1 of clippingPlanes.cpp so that enabling both clipping planes leaves only the red disc of the upper-right annulus visible.

Example 3.1. Replace the data

```
double eqn0[4] = {0.0, 0.0, -1.0, 0.25};
```

for GL_CLIP_PLANE0 of clippingPlanes.cpp with

```
double eqn0[4] = {0.0, 0.0, 1.0, -0.25};
```

Apparently, we are replacing $-z + 0.25 = 0$ with $z - 0.25 = 0$, which are both equations of the same plane. Why, then, is the result of clipping different for the two?

Answer : The half-space clipped, given the equation $-z + 0.25 = 0$, is $-z + 0.25 < 0$, i.e., $z > 0.25$. On the other hand, the half-space clipped, given the equation $z - 0.25 = 0$, is $z - 0.25 < 0$, i.e., $z < 0.25$.

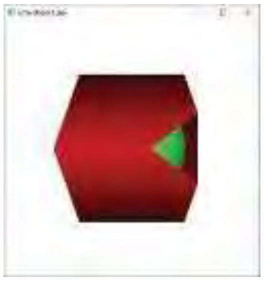

Figure 3.27: Screenshot of sphereInBox1.cpp with a corner clipped off.

Exercise 3.25. (Programming) Add a clipping plane to sphereInBox1.cpp of Chapter 11 to clip off a corner of the box, revealing the sphere inside. Ignore lighting and other calls that may not make sense now. All you need really are the coordinates of the corners of the box in the array vertices. Place the statements defining the clipping plane just after the gluLookAt() statement.

Your output should look like Figure 3.27.

Exercise 3.26. (Programming) Add a clipping plane to moveSphere.cpp to turn the movable sphere into a movable hemisphere.

Keep in mind that a clipping plane isn't object-specific but acts across the whole scene, so one must be careful to disable it after its target object is drawn.

Clipping planes cause OpenGL not to display parts of an object which are otherwise computed. For example, if one draws a hemisphere by clipping off half a FreeGLUT sphere, then OpenGL first computes geometric data (vertices, etc.) for the entire sphere and then suppresses the part on one side of the clipping plane before rendering. See Figure 3.28. Clearly, this is doubly inefficient for the suppressed part, as OpenGL computes the location of each of that part's vertices, *and then* computes again to decide that they are actually invisible! Clipping planes though are ideal for the purpose of displaying a *cut-away view* of an object, as in Figure 3.27.

Bottom line: Use clipping planes as a viewing and not a drawing device.

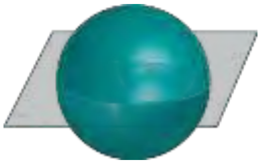

Figure 3.28: Clipping a sphere to make a hemisphere: the clipped half is computed *and* suppressed.

3.12 Frustum, Differently

The statement

gluPerspective(*fovy*, *aspect*, *near*, *far*);

calls a utility library (GLU) routine built on top of glFrustum(), the perspective projection command introduced in Section 2.8. It creates a viewing frustum as does glFrustum(). However, the frustum is specified differently:

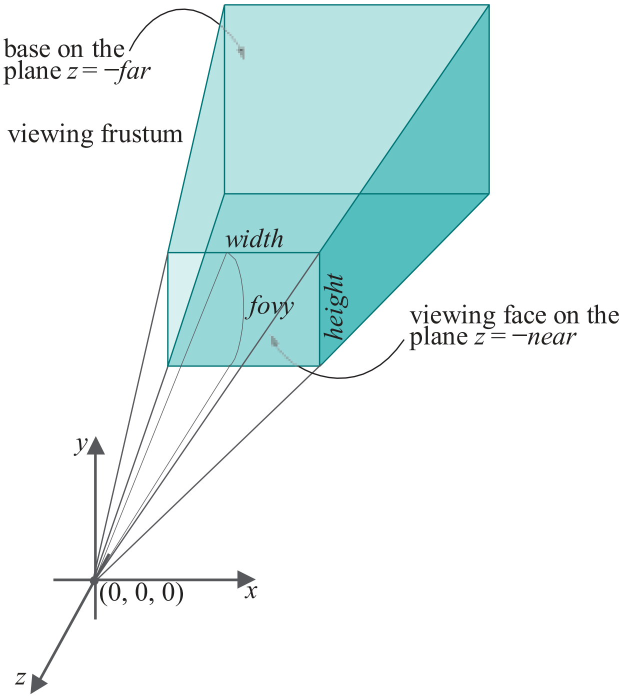

Figure 3.29: Viewing frustum created by gluPerspective(*fovy*, *aspect*, *near*, *far*).

The parameter *fovy* , called the *field of view angle*, is the angle subtended along the *yz*-plane at the apex of the pyramid (of which the frustum is a truncation); *aspect* is the *aspect ratio* = *width*/ *height* of the front face of the frustum; and *near* and *far* remain as for glFrustum(). See Figure 3.29. These four parameters it turns out are, in fact, enough for OpenGL to determine the eight vertices of a frustum which is *symmetric* about the *z*-axis, in other words, a frustum corresponding to a

```
glFrustum(left, right, bottom, top, near, far);
```

call where *left* = −*right* and *bottom* = −*top*. Such frustums are, in fact, most typical in applications and rarely does one have occasion to create one not symmetric about the *z*-axis.

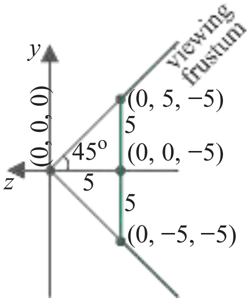

Figure 3.30: Section by the *yz*-plane (i.e., *x* = 0 plane) of the viewing frustum (bold) created by glFrustum(-5.0, 5.0, -5.0, 5.0, 5.0, 100.0).

Example 3.2. The projection statement of hemisphere.cpp from Chapter 2 is the symmetric

```
glFrustum(-5.0, 5.0, -5.0, 5.0, 5.0, 100.0);
```

Determine the equivalent gluPerspective() call.

Answer : The aspect ratio of the front face of the frustum created by glFrustum(-5.0, 5.0, -5.0, 5.0, 5.0, 100.0) is 1 as both its width (= *right* − *left*) and height (= *top* − *bottom*) are 10.0. To determine *fovy*, see Figure 3.30, which shows the section of the viewing frustum by the *yz*-plane. By elementary trigonometry the half-angle at the apex is 45° , so that *fovy* = 90.0. Therefore, the equivalent call is

```
gluPerspective(90.0, 1.0, 5.0, 100.0);
```

Let's check this out.

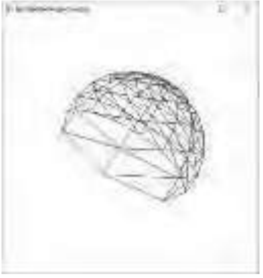

Figure 3.31: Screenshot of hemispherePerspective.cpp.

Experiment 3.22. Run hemispherePerspective.cpp, which replaces the original glFrustum() statement (still there in comments) of hemisphere.cpp with the gluPerspective() statement just computed. Figure 3.31 is a screenshot. The output of the program with either the original glFrustum() call or the equivalent gluPerspective() is same, as it should be. End

Exercise 3.27. Change the *near* value of the projection statement of hemispherePerspective.cpp as follows:

```
glFrustum(-5.0, 5.0, -5.0, 5.0, 10.0, 100.0);
```

Determine the equivalent gluPerspective() call.

Exercise 3.28. Determine the equivalent glFrustum() call of the following projection statement:

```
gluPerspective(60.0, 2.0, 10.0, 100.0);
```

Hint: Use trigonometry in the *yz*-section to determine first the *top* and *bottom* values and then the aspect ratio to determine *left* and *right*.

Whether to define a perspective projection with glFrustum() or gluPerspective() is a matter of personal taste. As we've seen, they are equivalent provided one is interested only in frustums symmetric about the *z*-axis.

However, a convenience of gluPerspective() in certain applications arises from the fact that the aspect ratio of the viewing face is an explicit parameter, making it easy to bind to the aspect ratio of the OpenGL window itself. This comes in handy if you recall the final step of the rendering process when the viewing face is scaled to fit onto the OpenGL window – resulting in distortion if the aspect ratios of the two differ. Let's see this in code.

Experiment 3.23. Run again hemispherePerspective.cpp.

The initial OpenGL window is a square 500×500 pixels. Drag a corner to change its shape, making it tall and thin. The hemisphere is distorted to become ellipsoidal (Figure 3.32(a)). Distortion is identical with either

```
glFrustum(-5.0, 5.0, -5.0, 5.0, 5.0, 100.0);
```

or

```
gluPerspective(90.0, 1.0, 5.0, 100.0);
```

as the two statements are equivalent. Next, replace the projection statement with

```
gluPerspective(90.0, (float)w/(float)h, 5.0, 100.0);
```

which sets the aspect ratio of the viewing frustum equal to that of the OpenGL window. Resize the window – the hemisphere is no longer distorted (Figure 3.32(b))! End

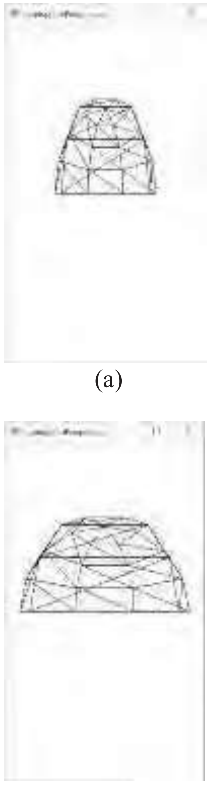

(a)

(b)

Figure 3.32: Screenshots of hemispherePerspective.cpp, window squished, with projection statement (a) glFrustum(-5.0, 5.0, -5.0, 5.0, 5.0, 100.0) or gluPerspective(90.0, 1.0, 5.0, 100.0) and (b) gluPerspective(90.0, (float)w/(float)h, 5.0, 100.0).

3.13 Viewports

The *viewport* of a scene is that region of the OpenGL window in which it is drawn. By default, it is the entire window. However, a glViewPort() call may be used to draw to a smaller rectangular subregion.

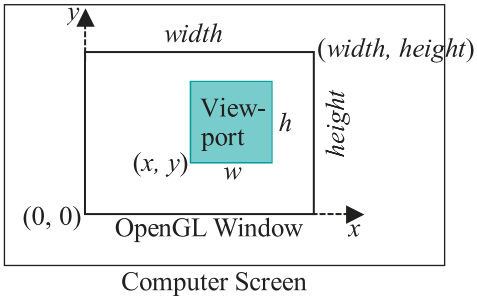

Figure 3.33: Viewport specified by glViewport(x, y, w, h).

The call glViewport(x, y, w, h) specifies the viewport as the rectangular subregion of the OpenGL window which has its lower-left corner at the point (x, y), and is of width w and height h. Units are pixels and the coordinates in the OpenGL window are such that the origin is located at the lower-left corner, the increasing direction of the x-axis is rightwards, and that of the y-axis upwards. See Figure 3.33.

Multiple viewports can be created in a single OpenGL window by invoking more than one glViewport() call in the drawing routine. The contents of a particular viewport are defined by the statements following its defining glViewport() call and before the next one (if any).

Experiment 3.24. Run viewports.cpp where the screen is split into two viewports, one defined by glViewport(0, 0, width/2.0, height) and the other by glViewport(width/2.0, 0, width/2.0, height), with contents a square and a circle, respectively. Figure 3.34 is a screenshot, where it should be clear from the parameters of the two glViewport() calls why the viewports are as seen.

A vertical black line is drawn by the program at the left end of the second viewport to separate the two. As the aspect ratio of both viewports differs from that of the viewing face, the square and circle are squashed laterally. End

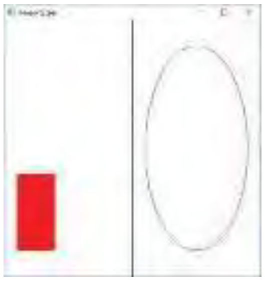

Figure 3.34: Screenshot of viewports.cpp.

Viewports are particularly useful in games to show split-screen views of different scenes, or perhaps the same scene from different cameras. We'll see a nice application of this in the program spaceTravel.cpp coming up in the next chapter, where the user maneuvers a spacecraft through an asteroid field with a split-screen view in the OpenGL window – one from a global fixed camera and the other from the craft itself.

Exercise 3.29. (Programming) Change the orthographic projection statement of viewports.cpp so that the square and circle are no longer distorted.

Exercise 3.30. (Programming) Create a 2×2 grid of four equally-sized viewports with one of the words "This", "is", "so" and "easy" in each. Add lines to separate the viewports.

3.14 Multiple Windows

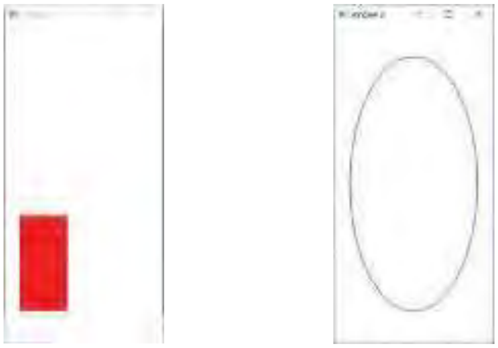

Figure 3.35: Screenshot of multipleWindows.cpp.

The glutCreateWindow() call of the FreeGLUT library may be invoked more than once in the main routine to create multiple top-level OpenGL windows. Properties such as the display routine, resize routine, etc., of each top-level window may be specified independently. On to code.

Experiment 3.25. Run multipleWindows.cpp, which creates two top-level windows (Figure 3.35). As you see in main(), after the size and position of the first window is specified, it is created with the call glutCreateWindow("window 1"), following which a block of four statements specify its initialization, display, resize and keyboard routines, respectively. The first three of these routines are unique to the first window while the second is shared by both.

The second window is then likewise created after its size and position are specified.
End

Exercise 3.31. (Programming) Create three top-level windows with red, green and blue backgrounds, and containing the words "Red", "Green" and "Blue", respectively.

3.15 Summary, Notes and More Reading

In this chapter we learned a number of different coding utilities, none difficult, but all useful. Vertex arrays and their access commands are particularly important for efficient OpenGL code and the reader should make a practice of using them. The coverage of syntax was by no means complete, nor was it meant to be.

For OpenGL utilities the reader should refer to the red and blue books for a full description. FreeGLUT's home page [49] doesn't seem to have much by way of documentation but Lighthouse 3D [89] has a tutorial on FreeGLUT's predecessor GLUT which applies to FreeGLUT.

Keep in mind that the purpose of GLUT originally, as of FreeGLUT now, is to provide a few easy-to-use platform-independent utilities to build a simple GUI, not a full-featured suite. Programmers who do require sophisticated interfaces should employ platform-specific utilities, e.g., the MFC Library for Windows. Readers may also find helpful Paul Rademacher's GLUI User Interface Library [59], which provides a collection of GLUT-based utilities such as buttons and checkboxes. Trolltech's Qt [145] may be of interest to those planning commercial-grade GUIs.

Part III

Movers and Shapers

Taylor & Francis

Taylor & Francis Group

http://taylorandfrancis.com

CHAPTER 4

Transformation, Animation and Viewing

The goal for this chapter is to understand how to move and manipulate objects, and maneuver the camera, skills essential to making movies and games. The modeling transformations of OpenGL – including translation, scaling and rotation – control object motion, while the viewing transformation manages the camera. We'll examine the syntax of the transformation commands and how they are composed and applied to achieve animation. To efficiently and creatively animate it's essential to have some grasp of its implementation, so we'll examine parts of OpenGL's animation engine as well. An experiment-discuss-repeat approach is used throughout, each new idea introduced and illustrated with the help of live code.

When objects move, especially in an interactive and unscripted environment like that of a game, they can collide. We'll discuss collision detection, therefore, in the context of animation. Related to animation as well is the notion of the orientation of an object, which we'll see how to quantify.

Section 4.1 introduces the three modeling transformations – translation, rotation and scaling. Sections 4.2 and 4.3 discuss composing transformations and how such composition places multiple objects relative to one another. The modelview matrix stack facilitates the application of transformations to multiple objects, as we see in Section 4.4. Section 4.5 analyzes a few instructional animation programs and concludes with a bunch of exercises.

The viewing transformation is introduced in Section 4.6. After grasping its functioning we find that a viewing transformation is actually a bit of a "fake", being simulated by OpenGL with the help of modeling transformations. An understanding of the viewing transformation leads to a preliminary discussion in Section 4.6, as well, of orientation and how it is specified by Euler angles. We present as well an application of the viewing transformation to animate a camera, together with rudimentary collision detection, in a space-travel program.

More animation code, including programs to develop key-frame animation sequences for a man-like articulated figure, as well as simple shadow animation, is presented in Section 4.7.

Section 4.8 describes methods to enable a user to choose an object on the screen with a mouse-like device, a facility critical in interactive programs like games. Section 4.9 concludes the chapter with a summary, notes and suggestions for more reading.

This chapter is a longish slog but it gets you well on the way to designing realistic 3D applications.

4.1 Modeling Transformations

Translation, scaling and rotation, the so-called *modeling transformations* of OpenGL, are applied to objects to change their location and shape.

4.1.1 Translation

Experiment 4.1. Run box.cpp, which shows an axis-aligned – i.e., with sides parallel to the coordinate axes – FreeGLUT wireframe box of dimensions 5 × 5 × 5. Figure 4.1 is a screenshot. Note the foreshortening – the back of the box appears smaller than the front – because of perspective projection in the viewing frustum specified by the glFrustum() statement.

Comment out the statement

```
glTranslatef(0.0, 0.0, -15.0);
```

What do you see now? *Nothing*! We'll explain why momentarily. End

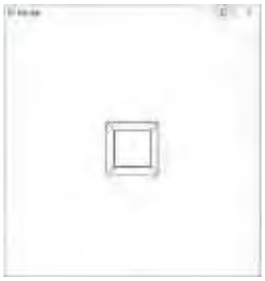

Figure 4.1: Screenshot of box.cpp.

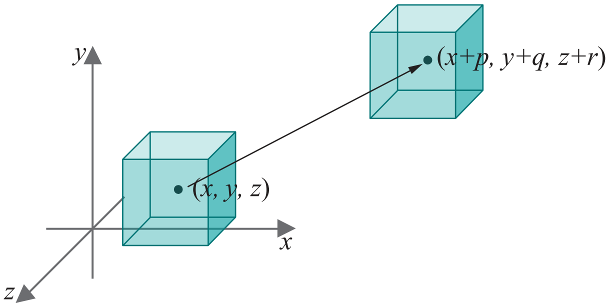

Figure 4.2: Translation: glTranslatef(p, q, r).

The *translation* command glTranslatef(p, q, r) translates an object *p* units in the *x*-direction, *q* units in the *y*-direction and *r* units in the *z*-direction. Precisely, each point (*x, y, z*) of the object is mapped to the point (*x* + *p, y* + *q, z* + *r*), which, of course, is the result of the vector addition (*x, y, z*) + (*p, q, r*). This all happens in world space so coordinates are in the world system (flip back to Section 2.2 if you need to jog your memory about world space). See Figure 4.2, which also shows a whole box translated by glTranslatef(p, q, r).

Returning to box.cpp, the command glutWireCube(5.0) itself creates a box of side length 5 centered at the origin, with vertices, therefore, at (±2.5, ±2.5, ±2.5), each vertex corresponding to one of the eight possible combinations of signs. The box clearly lies entirely outside the viewing frustum specified by glFrustum(-5.0, 5.0, -5.0, 5.0, 5.0, 100.0) – in fact, entirely on the clipped side of the viewing plane *z* = −5. However, glTranslatef(0.0, 0.0, -15.0) pushes the box 15 units in the −*z* direction, to place it inside the viewing frustum and make it visible (see Figure 4.3). That is why commenting out this statement results in a blank window.

Experiment 4.2. Successively replace the translation command of box.cpp with the following, making sure that what you see matches your understanding of where the command places the box. Keep in mind foreshortening, as well as clipping to within the viewing frustum.

1. glTranslatef(0.0, 0.0, -10.0) (see Figure 4.4)
2. glTranslatef(0.0, 0.0, -5.0)
3. glTranslatef(0.0, 0.0, -25.0)
4. glTranslatef(10.0, 10.0, -15.0)

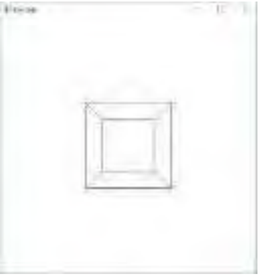

Figure 4.4: Screenshot of box.cpp with glTranslatef(0.0, 0.0, -10.0) instead (compare Figure 4.1).

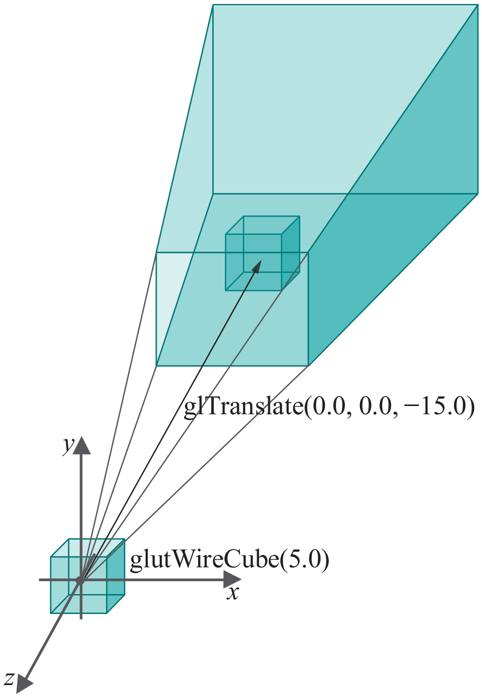

Figure 4.3: Translating into the viewing frustum.

End

Exercise 4.1. To what point is (−2.0, 3.0, 9.0) transformed by glTranslatef(3.0, 1.0, -8.0)?

Exercise 4.2. What is the OpenGL translation that takes (3.0, −1.0, 2.0) to (3.0, 5.0, 9.0)?

4.1.2 Scaling

Experiment 4.3. Add a scaling command, in particular, replace the modeling transformation block of box.cpp with:

```
// Modeling transformations.
glTranslatef(0.0, 0.0, -15.0);
glScalef(2.0, 3.0, 1.0);
```

Figure 4.5 is a screenshot – compare with the unscaled box of Figure 4.1.

End

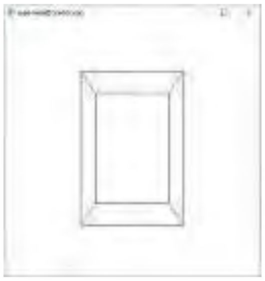

Figure 4.5: Screenshot of Experiment 4.3.

Remark 4.1. The glTranslatef(0.0, 0.0, -15.0) call is retained to "kick" the scaled box into the viewing frustum.

Precisely, the *scaling* command glScalef(u, v, w) maps each point (x, y, z) of an object to the point (ux, vy, wz). This has the effect of *stretching* objects by a factor of u in the x-direction, v in the y-direction, and w in the z-direction. See Figure 4.6.

Let's see how the box is transformed by scaling in the preceding experiment. The vertices of the scaled box are obtained from the original ones by the transformation $(x, y, z) \mapsto (2x, 3y, 1z)$. For example, $(2.5, 2.5, 2.5) \mapsto (5.0, 7.5, 2.5)$, $(-2.5, 2.5, 2.5) \mapsto (-5.0, 7.5, 2.5)$, and so on. So, the new vertices are $(\pm 5.0, \pm 7.5, \pm 2.5)$, which gives a $10 \times 15 \times 5$ box as one would expect from applying glScalef(2.0, 3.0, 1.0) to a $5 \times 5 \times 5$ box.

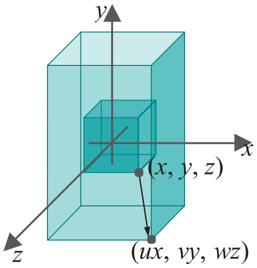

Figure 4.6: Scaling: glScalef(u, v, w).

Experiment 4.4. An object less symmetric than a box is more interesting to work with. Care for some teapot? Accordingly, change the modeling transformation and object definition part of box.cpp to:

```
// Modeling transformations.
glTranslatef(0.0, 0.0, -15.0);
glScalef(1.0, 1.0, 1.0);

glutWireTeapot(5.0); // Teapot.
```

Of course, glScalef(1.0, 1.0, 1.0) does nothing and we see the original unscaled teapot (Figure 4.7).

Next, successively change the scaling parameters by replacing the scaling command with the ones below. In each case, make sure your understanding of the command matches the change that you see in the shape of the teapot.

1. glScalef(2.0, 1.0, 1.0)
2. glScalef(1.0, 2.0, 1.0)
3. glScalef(1.0, 1.0, 2.0)

End

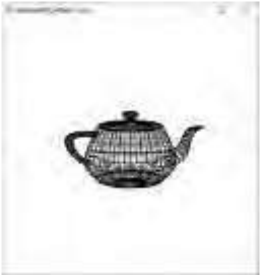

Figure 4.7: Screenshot of initial configuration of Experiment 4.4.

Exercise 4.3. (Programming) Continuing with the preceding experiment, try to guess first, for the scalings below, each of which has at least one negative parameter, the difference you will see from the initial configuration shown in Figure 4.7.

4. glScalef(-1.0, 1.0, 1.0)

   Hint: The transformation $(x, y, z) \mapsto (-x, y, z)$ is a mirror-like reflection about the yz-plane. See Figures 4.8 and 4.9.

5. glScalef(1.0, -1.0, 1.0)
6. glScalef(1.0, 1.0, -1.0)
7. glScalef(-1.0, -1.0, 1.0)

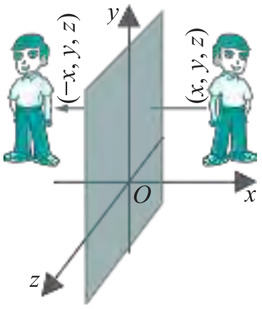

Figure 4.8: Reflection in the yz-plane.

Exercise 4.4. (Programming) Continue with the preceding exercise and replace the scaling command with the following, each of which has a zero parameter:

8. glScalef(1.0, 1.0, 0.0)

Hint: The transformation

$$(x, y, z) \mapsto (1x, 1y, 0z) = (x, y, 0)$$

"collapses" all z-values to 0.0, flattening the teapot on to the xy-plane.

9. glScalef(1.0, 0.0, 1.0)
10. glScalef(0.0, 1.0, 1.0)

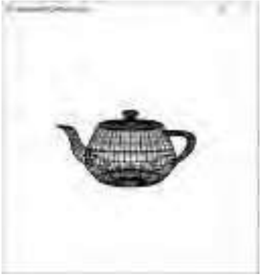

Figure 4.9: Screenshot of Experiment 4.4 with glScalef(-1.0, 1.0, 1.0) instead (compare Figure 4.7).

The last two make a flattened teapot too, but we see only a line because we are viewing it edgewise.

A scaling transformation where one or more of the scaling factors is zero is said to be *degenerate*. Although not common, there is the occasional application where a degenerate scaling transformation comes in handy. We'll see one such in drawing a shadow later this chapter in Experiment 4.37, the idea simply being for the flattened version of an object to simulate its shadow.

Exercise 4.5. To what point is $(-2.0, 3.0, 9.0)$ transformed by glScalef(3.0, 1.0, -8.0)?

Exercise 4.6. What is the OpenGL scaling that transforms $(3.0, -1.0, 2.0)$ to $(3.0, 5.0, 9.0)$?

We have so far scaled only FreeGLUT wire cubes and teapots, whose own axes are aligned with the coordinate axes, so that, effectively, they are only stretched and not skewed. Let's try one that's not so aligned.

Experiment 4.5. Replace the cube of box.cpp with a square whose sides are not parallel to the coordinate axes. In particular, replace the modeling transformation and object definition part of that program with:

```
// Modeling transformations.
glTranslatef(0.0, 0.0, -15.0);
// glScalef(1.0, 3.0, 1.0);

glBegin(GL LINE LOOP);
   glVertex3f(4.0, 0.0, 0.0);
   glVertex3f(0.0, 4.0, 0.0);
   glVertex3f(-4.0, 0.0, 0.0);
   glVertex3f(0.0, -4.0, 0.0);
glEnd();
```

See Figure 4.10(a). Uncomment the scaling. Now, see Figure 4.10(b). The square seems skewed to a parallelogram. End

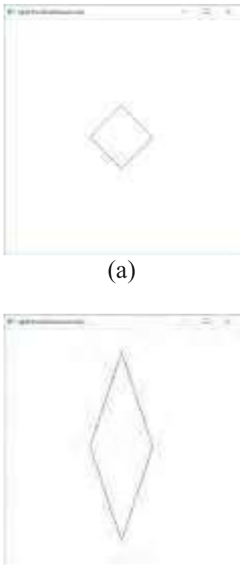
(a)

(b)

Figure 4.10: Screenshots of Experiment 4.5: (a) before scaling (b) after.

Exercise 4.7. Verify by elementary geometry that the unscaled line loop of the preceding experiment forms a square with sides of length $4\sqrt{2}$ angled at 45° to the axes. Next, verify that the scaling skews the square to a non-rectangular parallelogram.

4.1.3 Rotation

Experiment 4.6. Add a rotation command by replacing the modeling transformation and object definition part – we prefer a teapot – of box.cpp with:

```
// Modeling transformations.
glTranslatef(0.0, 0.0, -15.0);
glRotatef(60.0, 0.0, 0.0, 1.0);

glutWireTeapot(5.0);
```

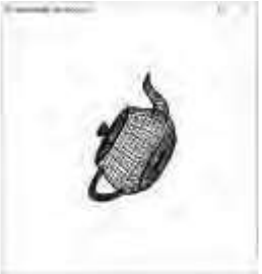
Figure 4.11: Screenshot for Experiment 4.6.

Figure 4.11 is a screenshot.

The *rotation* command glRotatef(A, p, q, r) rotates an object about an axis from the origin $O = (0, 0, 0)$ to the point (p, q, r). The amount of rotation is A°, measured CCW (counter-clockwise) looking *from* (p, q, r) to the origin. In this experiment, then, the rotation is 60° CCW looking down the z-axis. End

If the intuitive idea you have of rotating a point P about an axis is of the point turning along an imaginary cylinder on that axis as in Figure 4.12, then, well, you are perfectly correct. What we'll do next, though, is describe the rotation glRotatef(A, p, q, r) of P as a physical process for which we, hopefully, can find a formula.

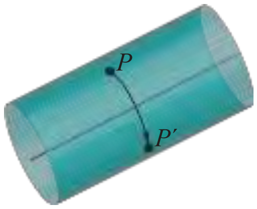

Figure 4.12: Turning along a cylinder.

Refer to Figure 4.13 as you read on. Assume $(p, q, r) = O$ so that the axis l through (p, q, r) and the origin O can indeed be drawn; in fact, if $(p, q, r) = O$ then glRotatef(A, p, q, r) is not a valid operation. Now, first, if the given point P lies on l itself then the situation is simple – the rotation does not move it. Suppose, then, that P does not lie on l. Here's how it's mapped by the rotation:

1. Drop the perpendicular from P to the point Q on l. Denote as L the segment PQ. L lies on a plane h perpendicular to l through Q.

2. Locate a viewer at V far enough along l, on the side of (p, q, r), as to be able to see h when looking toward the origin.

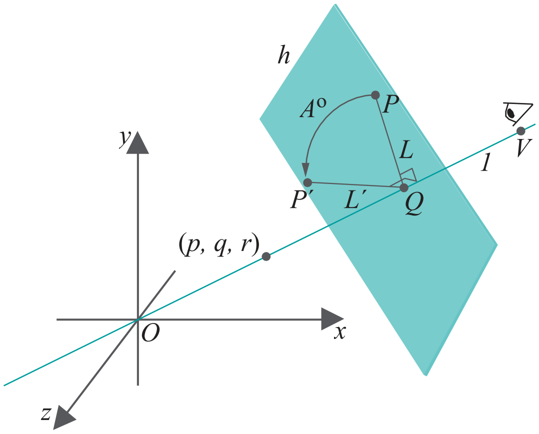

Figure 4.13: Rotation: glRotatef(A, p, q, r). The point P is rotated according to the 4-step process in the text.

3. Rotate the segment L about Q, on the plane h, an angle A° counter-clockwise as measured by the viewer.

4. If L^1 is the new position of L after rotation, then P is mapped to the corresponding endpoint P^1 of L^1.

Note: In Experiment 4.6, the axis of rotation, the z-axis, happens to intersect the object rotated, which is the teapot.

Experiment 4.7. Continuing with Experiment 4.6, successively replace the rotation command with the ones below, in each case trying to match what you see with your understanding of how the command should turn the teapot. (It can occasionally be a bit confusing because of the perspective projection.)

1. glRotatef(60.0, 0.0, 0.0, -1.0)

2. glRotatef(-60.0, 0.0, 0.0, 1.0)

3. glRotatef(60.0, 1.0, 0.0, 0.0)

4. glRotatef(60.0, 0.0, 1.0, 0.0)

5. glRotatef(60.0, 1.0, 0.0, 1.0)

End

The alert reader probably noticed in the 4-step definition of rotation earlier, that the purpose of the point (p, q, r), apart from specifying the axis l joining it to the origin, is to specify the *side* of the origin on l that the viewer is located. If (p, q, r) were replaced by another point (p^1, q^1, r^1) on l on the same side of O as (p, q, r), then the rotation would be *exactly same*. This is illustrated in the next experiment.

Experiment 4.8. Appropriately modify the code of Experiment 4.6 to compare the effects of each of the following pairs of rotation commands:

1. glRotatef(60.0, 0.0, 0.0, 1.0) and glRotatef(60.0, 0.0, 0.0, 5.0)

2. glRotatef(60.0, 0.0, 2.0, 2.0) and glRotatef(60.0, 0.0, 3.5, 3.5)

3. glRotatef(60.0, 0.0, 0.0, -1.0) and glRotatef(60.0, 0.0, 0.0, -7.5)

There is no difference in each case. One concludes that the rotation command glRotatef(A, p, q, r) is equivalent to glRotatef(A, ap, aq, ar), where a is any *positive* scalar. End

Exercise 4.8. Relate the three commands glRotatef(A, p, q, r), glRotatef($-A, p, q, r$) and glRotatef($A, \beta p, \beta q, \beta r$), where β is a *negative* scalar.

Unfortunately, even though the physical process of rotation is simple, the mathematical formula for how a point $P = (x, y, z)$ is mapped by an arbitrary rotation glRotatef(A, p, q, r) is complicated – in fact, significantly more so than the corresponding formulae in case of translation and scaling. Nevertheless, we'll ask the reader to derive it in the three simple cases where the rotation is about a coordinate axis. We'll defer the general case to the next chapter.

Exercise 4.9. Deduce the formula for how $P = (x, y, z)$ is mapped by each of the rotations:

(a) glRotatef(A, 1.0, 0.0, 0.0)

(b) glRotatef(A, 0.0, 1.0, 0.0)

(c) glRotatef(A, 0.0, 0.0, 1.0)

Part answer : See Figure 4.14 for (c). The axis of rotation is the z-axis. The point $P = (x, y, z)$ is mapped to $P^1 = (x^1, y^1, z^1)$. We'll find expressions for x^1, y^1 and z^1 in terms x, y, z and the angle parameter A.

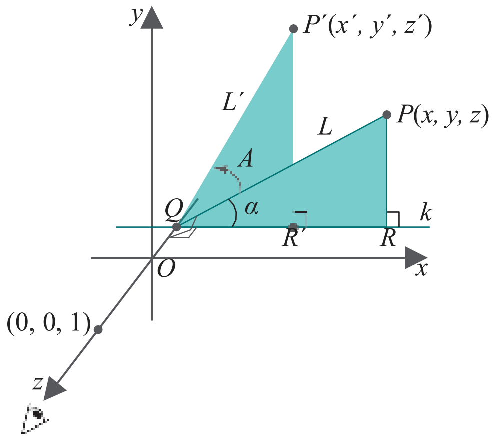

Figure 4.14: glRotatef(A, 0.0, 0.0, 1.0).

Draw $L = PQ$, the perpendicular from P to the z-axis. Further, draw the line k through Q parallel to the x-axis and the perpendicular PR from P to k. Say, $\angle PQR = \alpha$. Considering the sides QR and RP, respectively, of the triangle PQR, we have

$$\begin{aligned} x &= |L| \cos \alpha \\ y &= |L| \sin \alpha \end{aligned}$$

Now, the rotated segment $L^1 = P^1Q$ makes an angle of $\alpha + A$ with k, so that $\angle P^1QR^1 = \alpha + A$, where R^1 is the foot of the perpendicular from P^1 to k. Therefore,

$$\begin{aligned} x^1 &= |L^1| \cos(\alpha + A) = |L| \cos(\alpha + A) \\ y^1 &= |L^1| \sin(\alpha + A) = |L| \sin(\alpha + A) \end{aligned}$$

as $|L^1| = |L|$ because rotation does not change length. Apply trigonometric formulae to expand the rightmost sides of the two equations above:

$$\begin{aligned} x^1 &= |L| \cos \alpha \cos A - |L| \sin \alpha \sin A = x \cos A - y \sin A \\ y^1 &= |L| \cos \alpha \sin A + |L| \sin \alpha \cos A = x \sin A + y \cos A \end{aligned}$$

using the expressions for x and y derived earlier. And, of course,

$$z^1 = z$$

because rotation about the z-axis does not change the z-value.

Exercise 4.10. To what point is (2.0, 3.0, 9.0) transformed by

(a) glRotatef(90.0, 0.0, 0.0, 1.0)?

(b) glRotatef(90.0, 0.0, 0.0, 5.0)?

(c) glRotatef(90.0, 0.0, 0.0, -5.0)?

(d) glRotatef(60.0, 0.0, 0.0, 1.0)?

(e) glRotatef(180.0, 0.0, 1.0, 0.0)?

(f) glRotatef(45.0, 1.0, 0.0, 0.0)?

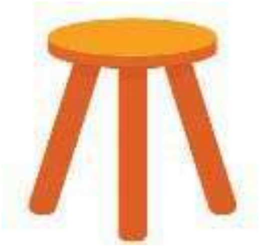

Figure 4.15: 3-legged stool.

Exercise 4.11. (Programming) Draw the three-legged stool of Figure 4.15. For the legs, first create one in a display list and then draw it three times rotated appropriately.

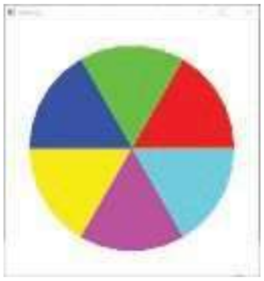

Figure 4.16: Disc with 6 colored sectors.

Exercise 4.12. (Programming) Draw the colorful disc of Figure 4.16 in a method similar to the previous exercise.

4.2 Composing Modeling Transformations

In most of the previous experiments we applied successively more than one modeling transformation to an object – a translation plus one other – but never explained exactly how it is that OpenGL goes about *composing* multiple transformations. There is magic to this as we'll see, but first a motivating experiment and an exercise.

Experiment 4.9. Apply three modeling transformations by replacing the modeling transformations block of box.cpp with:

```
// Modeling transformations.
glTranslatef(0.0, 0.0, -15.0);

glTranslatef(10.0, 0.0, 0.0);
glRotatef(45.0, 0.0, 0.0, 1.0);
```

It seems the box is *first* rotated 45° about the z-axis and *then* translated right 10 units. See Figure 4.17(a). The first translation glTranslatef(0.0, 0.0, -15.0), of course, serves to "kick" the box down the z-axis into the viewing frustum.

Next, interchange the last two transformations, namely, the rightward translation and the rotation, by replacing the modeling transformations block with:

```
// Modeling transformations.
glTranslatef(0.0, 0.0, -15.0);

glRotatef(45.0, 0.0, 0.0, 1.0);
glTranslatef(10.0, 0.0, 0.0);
```

It seems that the box is now *first* translated right and *then* rotated about the z-axis causing it to rise. See Figure 4.17(b). End

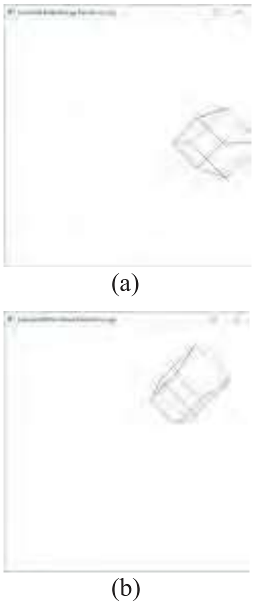

(a)

(b)

Figure 4.17: Screenshots from Experiment 4.9.

Exercise 4.13. (Programming) Again, apply three modeling transformations, this time by replacing the modeling transformations block of box.cpp with:

```
// Modeling transformations.
glTranslatef(0.0, 0.0, -15.0);
glRotatef(45.0, 0.0, 0.0, 1.0);
glScalef(1.0, 3.0, 1.0);
```

Next, interchange the rotation and scaling by replacing the modeling transformation block with:

```
// Modeling transformations.
glTranslatef(0.0, 0.0, -15.0);
glScalef(1.0, 3.0, 1.0);
glRotatef(45.0, 0.0, 0.0, 1.0);
```

Keeping the conclusions of the preceding experiment in mind can you explain what you see?

Apparently transformations are applied to an object in *backward* order through the code from where the object is created! This is correct and, hopefully, once it's explained how the OpenGL engine composes transformations, will not seem as idiosyncratic as it might at first.

We need, though, a quick acquaintance first with a concept which will be discussed in depth in the next chapter – that transformations correspond to matrices. We'll present here just enough that the reader can follow along as our goal is simply a conceptual understanding of how transformations are composed.

A vertex $V = (x, y, z)$ is represented in OpenGL as a 4 × 1 column matrix

$$\begin{bmatrix} x \\ y \\ z \\ 1 \end{bmatrix}$$

Take that extra 1 in the 4th row for granted for now – it comes from V's so-called homogeneous coordinates being $(x, y, z, 1)$. We'll use V to denote the column matrix above as well.

Moreover, every modeling transformation t – be it a translation, scaling or rotation – is represented by a 4 × 4 matrix of the form

$$M = \begin{bmatrix} a_{11} & a_{12} & a_{13} & a_{14} \\ a_{21} & a_{22} & a_{23} & a_{24} \\ a_{31} & a_{32} & a_{33} & a_{24} \\ a_{41} & a_{42} & a_{43} & a_{44} \end{bmatrix}$$

Applying this transformation to the vertex V consists of multiplying V from the left by the transformation matrix. In particular, V is transformed by t to the vertex $t(V)$ where

$$\begin{aligned} t(V) = MV &= \begin{bmatrix} a_{11} & a_{12} & a_{13} & a_{14} \\ a_{21} & a_{22} & a_{23} & a_{24} \\ a_{31} & a_{32} & a_{33} & a_{24} \\ a_{41} & a_{42} & a_{43} & a_{44} \end{bmatrix} \begin{bmatrix} x \\ y \\ z \\ 1 \end{bmatrix} \\ &= \begin{bmatrix} a_{11}x + a_{12}y + a_{13}z + a_{14} \\ a_{21}x + a_{22}y + a_{23}z + a_{24} \\ a_{31}x + a_{32}y + a_{33}z + a_{24} \\ a_{41}x + a_{42}y + a_{43}z + a_{44} \end{bmatrix} \end{aligned}$$

Here's an example.

Example 4.1. The transformation t_1 given by the translation command glTranslatef(5.0, 0.0, 0.0) corresponds to the matrix

$$M_1 = \begin{bmatrix} 1.0 & 0.0 & 0.0 & 5.0 \\ 0.0 & 1.0 & 0.0 & 0.0 \\ 0.0 & 0.0 & 1.0 & 0.0 \\ 0.0 & 0.0 & 0.0 & 1.0 \end{bmatrix}$$

This is verified by the multiplication

$$\begin{bmatrix} 1.0 & 0.0 & 0.0 & 5.0 \\ 0.0 & 1.0 & 0.0 & 0.0 \\ 0.0 & 0.0 & 1.0 & 0.0 \\ 0.0 & 0.0 & 0.0 & 1.0 \end{bmatrix} \begin{bmatrix} x \\ y \\ z \\ 1 \end{bmatrix} = \begin{bmatrix} x+5.0 \\ y \\ z \\ 1 \end{bmatrix}$$

Similarly, verify that the transformation t_2 given by the translation command glTranslatef(0.0, 10.0, 0.0) corresponds to the matrix

$$M_2 = \begin{bmatrix} 1.0 & 0.0 & 0.0 & 0.0 \\ 0.0 & 1.0 & 0.0 & 10.0 \\ 0.0 & 0.0 & 1.0 & 0.0 \\ 0.0 & 0.0 & 0.0 & 1.0 \end{bmatrix}$$

Now, if one applies t_2 followed by t_1 to a vertex V, then V is mapped as follows:

$$V \mapsto t_1(t_2(V)) = M_1(M_2V) = (M_1M_2)V$$

(associativity of matrix multiplication was applied in the second equality). The skeptical reader may multiply matrices as below to verify that

$$\begin{aligned} (M_1M_2)V &= \begin{bmatrix} 1.0 & 0.0 & 0.0 & 5.0 \\ 0.0 & 1.0 & 0.0 & 0.0 \\ 0.0 & 0.0 & 1.0 & 0.0 \\ 0.0 & 0.0 & 0.0 & 1.0 \end{bmatrix} \begin{bmatrix} 1.0 & 0.0 & 0.0 & 0.0 \\ 0.0 & 1.0 & 0.0 & 10.0 \\ 0.0 & 0.0 & 1.0 & 0.0 \\ 0.0 & 0.0 & 0.0 & 1.0 \end{bmatrix} \begin{bmatrix} x \\ y \\ z \\ 1 \end{bmatrix} \\ &= \begin{bmatrix} 1.0 & 0.0 & 0.0 & 5.0 \\ 0.0 & 1.0 & 0.0 & 10.0 \\ 0.0 & 0.0 & 1.0 & 0.0 \\ 0.0 & 0.0 & 0.0 & 1.0 \end{bmatrix} \begin{bmatrix} x \\ y \\ z \\ 1 \end{bmatrix} \\ &= \begin{bmatrix} x+5.0 \\ y+10.0 \\ z \\ 1 \end{bmatrix} \end{aligned}$$

which indeed corresponds to how (x, y, z) is transformed by the code sequence

```
glTranslatef(5.0, 0.0, 0.0);
glTranslatef(0.0, 10.0, 0.0);
```

Put simply, the matrix of the composition of two transformations is the product of their matrices. This generalizes. If one applies successively the transformations $t_n, t_{n-1}, \dots, t_1$ (in that order, t_n being first) to a vertex V, then it is mapped to

$$t_1(t_2(\dots t_n(V)\dots)) = M_1(M_2(\dots(M_nV)\dots)) = (M_1M_2\dots M_n)V \qquad (4.1)$$

where matrix M_i corresponds to transformation t_i, $1 \leq i \leq n$, and, again, the second equality uses associativity of matrix multiplication. *One sees that the matrix of the composition of transformations is precisely the product of the matrices corresponding to the individual transformations.*

We now have enough to explain exactly how OpenGL itself goes about composing transformations. Consider the code sequence:

```
modelingTransformation 1; // t1
modelingTransformation 2; // t2
modelingTransformation 3; // t3
...
modelingTransformation n-1; // tn-1
modelingTransformation n; // tn
object;
```

where the transformation t_i corresponds to the command modelingTransformation i.

Now, OpenGL maintains a 4 × 4 *modelview matrix*, call it M, which initially is the identity

$$I = \begin{bmatrix} 1.0 & 0.0 & 0.0 & 0.0 \\ 0.0 & 1.0 & 0.0 & 0.0 \\ 0.0 & 0.0 & 1.0 & 0.0 \\ 0.0 & 0.0 & 0.0 & 1.0 \end{bmatrix}$$

As the drawing routine is processed during run-time, the matrix of each successive modeling transformation encountered is multiplied from the *left* by the current modelview matrix, the product becoming the new modelview matrix. For example, assuming the matrix of t_i is M_i and that there were no earlier transformations, the successive values of the modelview matrix M for the code sequence above are indicated in the comments below:

```
                                 // $M = I$, initially
modelingTransformation 1;        // $M = IM_1 = M_1$
modelingTransformation 2;        // $M = M_1M_2$
modelingTransformation 3;        // $M = M_1M_2M_3$
...
modelingTransformation n-1; // $M = M_1M_2 \dots M_{n-1}$
modelingTransformation n;        // $M = M_1M_2 \dots M_{n-1}M_n$
object;
```

Keep in mind that it is *just the one* modelview matrix M above whose value is changing. Moreover, an object drawing statement is processed by multiplying the object's vertices from the left by the current modelview matrix, e.g., for the code sequence above, each vertex V of object is transformed as follows:

$$V \mapsto MV = (M_1 M_2 \dots M_{n-1} M_n)V$$

However, by associativity

$$\begin{aligned} (M_1 M_2 \dots M_{n-1} M_n)V &= M_1(M_2(\dots M_{n-1}(M_nV)\dots)) \\ &= t_1(t_2(\dots t_{n-1}(t_n(V)\dots)) \end{aligned}$$

We see, from the last line of the preceding equation, that transformation t_n is applied to V, then t_{n-1} and so on, until, finally, t_1, *indeed backward in code order*!

The conclusion, then, is that the backward order in which OpenGL applies transformations is simply a consequence of the particular, and perfectly logical, way it processes their matrices. It may take a little getting used to, but (trust us) by the end of this chapter you will be quite comfortable applying multiple transformations.

Example 4.2. Let's build on the earlier Example 4.1. We saw there that the matrix corresponding to glTranslatef(5.0, 0.0, 0.0) is

$$M_1 = \begin{bmatrix} 1.0 & 0.0 & 0.0 & 5.0 \\ 0.0 & 1.0 & 0.0 & 0.0 \\ 0.0 & 0.0 & 1.0 & 0.0 \\ 0.0 & 0.0 & 0.0 & 1.0 \end{bmatrix}$$

and that corresponding to glTranslatef(0.0, 10.0, 0.0) is

$$M_2 = \begin{bmatrix} 1.0 & 0.0 & 0.0 & 0.0 \\ 0.0 & 1.0 & 0.0 & 10.0 \\ 0.0 & 0.0 & 1.0 & 0.0 \\ 0.0 & 0.0 & 0.0 & 1.0 \end{bmatrix}$$

Moreover, the matrix corresponding to glScalef(2.0, 1.0, 3.0) is easily verified to be

$$M_3 = \begin{bmatrix} 2.0 & 0.0 & 0.0 & 0.0 \\ 0.0 & 1.0 & 0.0 & 0.0 \\ 0.0 & 0.0 & 3.0 & 0.0 \\ 0.0 & 0.0 & 0.0 & 1.0 \end{bmatrix}$$

And, the matrix corresponding to glRotatef(90.0, 0.0, 1.0, 0.0) – easy to see if the reader did Exercise 4.9(b) – is

$$M_4 = \begin{bmatrix} 0.0 & 0.0 & 1.0 & 0.0 \\ 0.0 & 1.0 & 0.0 & 0.0 \\ -1.0 & 0.0 & 0.0 & 0.0 \\ 0.0 & 0.0 & 0.0 & 1.0 \end{bmatrix}$$

Therefore, assuming no earlier transformations, following the first four statements in the code sequence

```
glTranslatef(5.0, 0.0, 0.0);
glTranslatef(0.0, 10.0, 0.0);
glScalef(2.0, 1.0, 3.0);
glRotatef(90.0, 0.0, 1.0, 0.0)
glBegin(GL POINTS);
   glVertex3f(4.0, 0.0, 0.0);
glEnd();
```

the current modelview matrix is

$$M_1 M_2 M_3 M_4 = \begin{bmatrix} 0.0 & 0.0 & 2.0 & 5.0 \\ 0.0 & 1.0 & 0.0 & 10.0 \\ -3.0 & 0.0 & 0.0 & 0.0 \\ 0.0 & 0.0 & 0.0 & 1.0 \end{bmatrix}$$

which the reader can verify by multiplying the four matrices herself. The four transformations in the preceding code sequence, accordingly, map the vertex $(4.0, 0.0, 0.0)$ to the point given by

$$\begin{bmatrix} 0.0 & 0.0 & 2.0 & 5.0 \\ 0.0 & 1.0 & 0.0 & 10.0 \\ -3.0 & 0.0 & 0.0 & 0.0 \\ 0.0 & 0.0 & 0.0 & 1.0 \end{bmatrix} \begin{bmatrix} 4.0 \\ 0.0 \\ 0.0 \\ 1.0 \end{bmatrix} = \begin{bmatrix} 5.0 \\ 10.0 \\ 12.0 \\ 1.0 \end{bmatrix}$$

which, in fact, is $(5.0, 10.0, -12.0)$. Let's now "unpack" the 4 × 4 matrix to the left above and write

$$\begin{aligned} \begin{bmatrix} 5.0 \\ 10.0 \\ 12.0 \\ 1.0 \end{bmatrix} &= \begin{bmatrix} 0.0 & 0.0 & 2.0 & 5.0 \\ 0.0 & 1.0 & 0.0 & 10.0 \\ -3.0 & 0.0 & 0.0 & 0.0 \\ 0.0 & 0.0 & 0.0 & 1.0 \end{bmatrix} \begin{bmatrix} 4.0 \\ 0.0 \\ 0.0 \\ 1.0 \end{bmatrix} \\ &= (M_1 M_2 M_3 M_4) \begin{bmatrix} 4.0 \\ 0.0 \\ 0.0 \\ 1.0 \end{bmatrix} \\ &= M_1 \left(M_2 \left(M_3 \left(M_4 \begin{bmatrix} 4.0 \\ 0.0 \\ 0.0 \\ 1.0 \end{bmatrix} \right) \right) \right) \end{aligned}$$

So, the point $(5.0, 10.0, -12.0)$ is obtained from $(4.0, 0.0, 0.0)$ by first applying glRotatef(90.0, 0.0, 1.0, 0.0), then glScalef(2.0, 1.0, 3.0), then .... In fact, we ask the reader next to verify the algebraic deduction above geometrically.

Exercise 4.14. Check, first, that glRotatef(90.0, 0.0, 1.0, 0.0) takes (4.0, 0.0, 0.0) to (0.0, 0.0, 4.0): do this *visually* , not by matrix multiplication, e.g., sketch the *xyz*-axes on a pieces of paper, draw a point a little to the right on the *x*-axis, then see how it rotates 90° CCW about the *y*-axis. Applying glScalef(2.0, 1.0, 3.0) next is easy: scale the coordinate values of (0.0, 0.0, 4.0) by 2, 1 and 3, respectively, to get to (0.0, 0.0, 12.0). See Figure 4.18. Complete this process for a geometric verification that the block of four transforms of the preceding example indeed take the vertex (4.0, 0.0, 0.0) to (5.0, 10.0, −12.0).

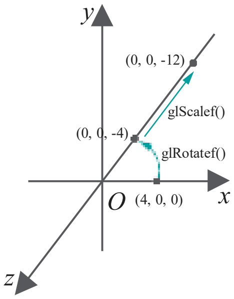

Figure 4.18: Sketching transformations.

At the risk of belaboring the point, the reason beginners often have trouble with a transformation sequence like

```
glTranslatef(...);
glTranslatef(...);
glScalef(...);
glRotatef(...);
```

is in thinking that the code being processed one line after another – which it is – means that a translation is applied (to something), then another translation (to that same thing), then a scaling, and so on. *It does not* . Rather, each line, one after another, simply updates the modelview matrix by a multiplication. Finally, when an object is encountered, it – or, more accurately, all its vertices – are multiplied by the current modelview matrix, which results in all the transformations which have been multiplied thus far into that matrix applying successively (backward) to the object.

Another particularly important point to note is that matrices corresponding to successive modeling transformations being multiplied into one matrix, the current modelview matrix, means that OpenGL is effectively *composing multiple modeling transformations into one transformation*. In other words, whether one transformation is applied to an object, or ten, or a hundred, the object's vertices are multiplied each by *one* matrix. This is key to OpenGL's run-time efficiency.

In the discussion above of how modeling transformations change objects, we had implicitly been treating the latter as unitary, with transformations coming either before or after an object. In fact, though, objects are multiple lines of code each in a program. So, what happens when a transformation statement ends up *inside* an object? We find out in the following experiment.

Experiment 4.10. Modify the code of Experiment 4.5 to draw a square with a short line segment above it, both translated to the right; precisely, replace the modeling transformation and object definition part of box.cpp with:

```
// Modeling transformations.
glTranslatef(0.0, 0.0, -15.0);
glTranslatef(10.0, 0.0, 0.0);

glBegin(GL_LINE LOOP);
glVertex3f(4.0,   0.0,   0.0);
glVertex3f(0.0, 4.0, 0.0);
glVertex3f(-4.0, 0.0, 0.0);
glVertex3f(0.0, -4.0, 0.0);
glEnd();

glBegin(GL LINES);
glVertex3f(0.0, 8.0, 0.0);
glVertex3f(0.0, 10.0, 0.0);
glEnd();
```

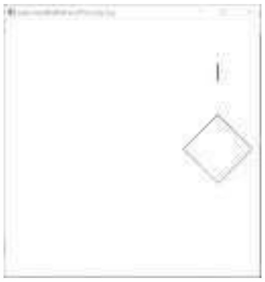

Figure 4.19: A square and a segment.

See Figure 4.19. Now, move the second translation statement glTranslatef(10.0, 0.0, 0.0) to just after the glBegin(GL LINE LOOP) statement. Are the square and segment still translated rightward? *No*! Experiment with a few more placements of glTranslatef(10.0, 0.0, 0.0).

The conclusion is that OpenGL indeed treats objects as unitary: rogue transformation statements within a glBegin(GL_*primitive*)-glEnd() pair are ignored.

End

Remark 4.2. There is one other kind of transformation, in addition to the three modeling transformations, which can modify the modelview matrix – the *viewing transformation* gluLookAt(). We'll discuss viewing transformations in Section 4.6. Modelview matrices, in fact, get their name from these two kinds of transformations.

Exercise 4.15. For each of the following, give the (x, y, z) coordinates of the point to which the center (0.0, 0.0, 0.0) of the sphere is transformed by the given piece of code in the display routine (note that the parameters of the sphere are irrelevant). Do *not* apply matrix multiplication at all. Use paper and pencil instead *a la* Exercise 4.14.

(a)
```
glTranslatef(0.0, 2.0, 2.0);
glTranslatef(4.0, 0.0, 2.0);
glutWireSphere(2.0, 10, 8);
```

(b)
```
glRotatef(90.0, 0.0, 0.0, 1.0);
glTranslatef(4.0, 0.0, 0.0);
glutWireSphere(2.0, 10, 8);
```

(c)
```
glRotatef(90.0, 1.0, 0.0, 0.0);
glTranslatef(4.0, 0.0, 0.0);
glRotatef(90.0, 0.0, 0.0, 1.0);
glutWireSphere(2.0, 10, 8);
```

(d)
```
glRotatef(90.0, 1.0, 0.0, 0.0);
glRotatef(90.0, 0.0, 1.0, 0.0);
glTranslatef(4.0, 0.0, 0.0);
glutWireSphere(2.0, 10, 8);
```

(e)
```
glScalef(1.0, 2.0, 3.0);
glRotatef(45.0, 1.0, 0.0, 0.0);
glRotatef(90.0, 0.0, 0.0, 1.0);
glTranslatef(4.0, 0.0, 0.0);
glutWireSphere(2.0, 10, 8);
```

(f)
```
glRotatef(90.0, 0.0, 0.0, 1.0);
glRotatef(45.0, 1.0, 0.0, 0.0);
glRotatef(90.0, 0.0, 1.0, 0.0);
glTranslatef(4.0, 0.0, 0.0);
glutWireSphere(2.0, 10, 8);
```

(g)
```
glRotatef(-90.0, 1.0, 1.0, 0.0);
glTranslatef(4.0, 0.0, 0.0);
glutWireSphere(2.0, 10, 8);
```

(h)
```
glRotatef(180.0, 2.0, 1.0, 0.0);
glTranslatef(4.0, 0.0, 0.0);
glutWireSphere(2.0, 10, 8);
```

Part answer: (a) $(4.0, 2.0, 4.0)$ (b) $(0.0, 4.0, 0.0)$.

Example 4.3. Replace the object definition statement

```
glutWireCube(5.0); // Box.
```

of box.cpp with

```
glRectf(5.0, 5.0, 10.0, 10.0); // Square
```

to draw, instead of a box centered at the origin, an axis-aligned square some ways north-east of it, centered at $(7.5, 7.5, 0.0)$.

Now, add transformation(s) to rotate the square 45° counter-clockwise about its *own center*, as indicated in Figure 4.20(a).

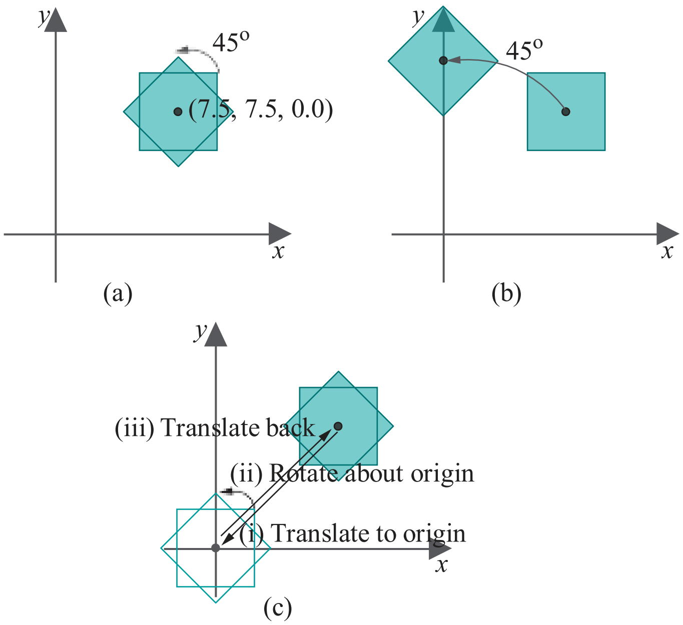

Figure 4.20: Rotating a square about its own center.

Answer : Inserting the command glRotatef(45.0, 0.0, 0.0, 1.0) just before glRectf() will not do as it rotates the square about the origin, and not its own center, as shown in Figure 4.20(b). What one must do instead (see Figure 4.20(c)) is first (i) translate the square so that its center is at the origin, then (ii) rotate it about the origin and, finally, (iii) translate it back. This is equivalent to the following modeling transformation block:

```
// Modeling transformations.
glTranslatef(0.0, 0.0, -15.0);

glTranslatef(7.5, 7.5, 0.0); // Translate back.
glRotatef(45.0, 0.0, 0.0, 1.0); // Rotate about origin.
glTranslatef(-7.5, -7.5, 0.0); // Translate to origin.
```

Such a maneuver is unavoidable as OpenGL's own rotations, as we know from Section 4.1.3, are always about an axis through the origin, such being called a *radial* axis. Therefore, a non-radial axis needs to be translated to the origin and back again in order to be rotated about. This "tricky" maneuver and its variants come up so often that we'll give them a collective name: the Trick.

Exercise 4.16. (Programming) As in the preceding example, replace the object definition statement

```
glutWireCube(5.0); // Box.
```

of box.cpp with

```
glRectf(5.0, 5.0, 10.0, 10.0); // Square
```

Now, scale the square so that its center is unchanged, but its shape changes to a rectangle of aspect ratio 2. Use the Trick.

Exercise 4.17. Prove that a composition of multiple translations is a single translation and that a composition of multiple scalings is a single scaling.

Remark 4.3. A composition of multiple rotations is a single rotation as well, but this is much harder to prove generally and we'll leave it to Chapter 5.

Exercise 4.18. What is the *inverse* of a translation? Specifically, what modeling transformation composed with a translation glTranslatef(*p*, *q*, *r*) "undoes" its effect, so that all points remain stationary? How about scalings and rotations? What are their inverses?

4.3 Placing Multiple Objects

We next consider the vital problem of applying modeling transformations to place multiple objects in a desired manner *relative* to one another.

Experiment 4.11. Replace the entire display routine of the original box.cpp with:

```
void drawScene(void)
{
    glClear(GL COLOR_BUFFER BIT);
    glColor3f(0.0, 0.0, 0.0);
    glLoadIdentity();

    // Modeling transformations.
    glTranslatef(0.0, 0.0, -15.0);
    // glRotatef(45.0, 0.0, 0.0, 1.0);
    glTranslatef(5.0, 0.0, 0.0);

    glutWireCube(5.0); // Box.

    //More modeling transformations.
    glTranslatef(0.0, 10.0, 0.0);

    glutWireSphere(2.0, 10, 8); // Sphere.

    glFlush();
}
```

See Figure 4.21(a) for a screenshot. The objects are a box and a sphere.

End

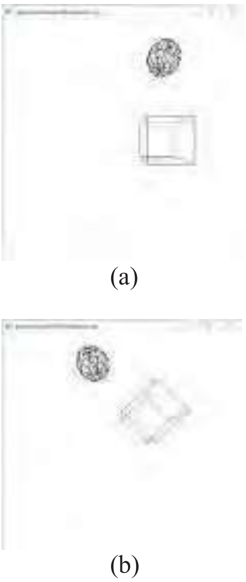
(a)

(b)

Figure 4.21: Screenshots: (a) Experiments 4.11 and (b) 4.12.

Let's understand the placement of the box and sphere in the preceding experiment individually first and then with respect to each other.

It's actually fairly straightforward to understand the placements individually. For example, to place the sphere, work backwards from where it's created in the code, applying to it the successive modeling transformations (all being translations in this case) encountered, and ignoring the one non-transformation statement glutWireCube() on the way. The result is that the sphere is centered at (5.0, 10.0, −15.0). Likewise, the box is seen to be centered at (5.0, 0.0, −15.0).

The relative placement in this case is not difficult either. Clearly, the sphere is transformed by glTranslatef(0.0, 10.0, 0.0) – which is the transformation "between them" – with respect to the box. The result is that the sphere's center is 10 units vertically above the box's.

Experiment 4.12. Continuing with the previous experiment, uncomment the glRotatef() statement. Figure 4.21(b) is a screenshot. End

Again, the individual placements are fairly straightforward. Working backwards from where it is created we see that, after being translated to (5.0, 10.0, 0.0), the sphere is rotated 45° counter-clockwise about the *z*-axis and, of course, finally pushed 15 units in the −*z* direction. We'll not compute the exact final coordinates of its center. The individual placement of the box is simple to parse as well and left to the reader.

It's the relative placement which is particularly interesting in this case. The sphere is no longer vertically above the box, though the transformation between them is still glTranslatef(0.0, 10.0, 0.0). Before trying to explain what's going on, let's return to the basics for a moment.

Consider the code sequence below which draws two objects:

```
modelingTransformation 1;     // $t_1$
modelingTransformation 2;     // $t_2$
...
modelingTransformation n-1; // $t_{n-1}$
modelingTransformation n;     // $t_n$
object1;
modelingTransformation n+1; // $t_{n+1}$
...
modelingTransformation m;     // $t_m$
object2;
```

Assuming that the transformation t_i specified by modelingTransformation i corresponds to the matrix M_i, for $1 \leq i \leq m$, the successive values of the modelview matrix M are indicated below:

```
                              // $M = I$, initially
modelingTransformation 1;     // $M = IM_1 = M_1$
modelingTransformation 2;     // $M = M_1M_2$
...
modelingTransformation n-1; // $M = M_1M_2 \dots M_{n-1}$
modelingTransformation n;     // $M = M_1M_2 \dots M_{n-1}M_n$
object1;                     // $M$ does not change
modelingTransformation n+1; // $M = M_1M_2 \dots M_{n-1}M_nM_{n+1}$
...
modelingTransformation m;     // $M = M_1M_2 \dots M_{n-1}M_nM_{n+1} \dots M_m$
object2;
```

Accordingly, each vertex V of the final object2 call is transformed according to:

$$V \mapsto (M_1 \dots M_{m-1}M_m)V = t_1(\dots t_{m-1}(t_m(V))\dots) \quad (4.2)$$

exactly as we would expect by working backwards in the code from object2. Now, how about the placement of object2 *with respect to* object1?

Let's repeat the transformation for a vertex V of object2 by stepping backward through the right side of Equation (4.2): first transform V by t_m to $t_m(V)$, then by t_{m-1} to $t_{m-1}(t_m(V))$, ..., then by t_{n+1} to $t_{n+1}(\dots t_{m-1}(t_m(V))\dots)$. *Stop*!

At this time object1 is drawn. Imagine that a part of object1 is a set of three directed line segments (drawn, say, using GL_LINES), aligned with the three world coordinate axes and calibrated identically. These lines are said to represent the *local coordinate system* of object1. See Figure 4.22 (depicting the box and sphere of the preceding experiment). So, at the time of its creation the local coordinate system of object1 coincides with the world coordinate system.

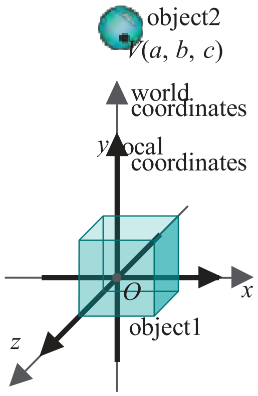

Figure 4.22: Local system (bold) coincides with the global (thin) initially. The global system is fixed.

Further, suppose at the time of object1's creation that the so-far transformed V, i.e., $t_{n+1}(\dots t_{m-1}(t_m(V))\dots)$, is located at (a, b, c) in the local coordinates of object1 (same as world coordinates, of course, at that moment).

Let's get back now to applying transformations backwards from where we had stopped. Next was t_n. Now, t_n applies to *both* V and object1. Three cases arise according to the type of t_n.

1. t_n is a translation specified by glTranslatef(p, q, r):

   This translation applies to V and object1 and, so, to the local coordinate system of the latter as well. That is, they all "move together". Therefore, the location (a, b, c) of V with respect to the local coordinate system of object1 does not change. The location of V in world coordinates, of course, changes to $(a+p, b+q, c+r)$.

2. t_n is a rotation specified by glRotatef(A, p, q, r):

   Same argument as for translation. Again, the location (a, b, c) of V with respect to the local coordinate system of object1 does not change.

3. t_n is a scaling specified by glScalef(u, v, w):

   The location of V in world coordinates is changed by the scaling to (ua, vb, wc). However, as the same scaling applies to the axes of the local coordinate system of object1 – particularly the units calibrating them – the location (a, b, c) of V with respect to this system again does not change.

   Sci-fi analogy : Prior to an experiment in a lab you measure yourself with a tape to be 6 feet tall. The experiment goes horribly wrong and radiation causes you to shrink by a factor of 12, leaving you at a Lilliputian 6 inches. However, if everything around you including the tape shrank by exactly the same factor, you would still believe yourself to be 6 feet.

Continue, applying transformations $t_{n-1}, t_{n-2}, \dots t_1$, successively, and reason as above for each. The conclusion is that the location of V at the point (a, b, c) of the local coordinate system of object1 at the time of the latter's creation is not altered by any subsequent transformation, i.e., those in the code prior to object1. Neither, obviously, is it changed by transformations in the code after object2, because their corresponding matrices multiply into the modelview matrix only after both object 1 and object 2 have already been drawn. We have, therefore, the following:

Proposition 4.1. *If* object1 *precedes* object2 *in code, then the location of* object2 *in the local coordinate system of* object1 *is determined by the transformation statements between the two and nothing else.*

What the proposition says is that, if object1 precedes object2 in code, then the latter is *frozen* in the former's coordinate system at a position determined solely by the transformation statements between the two. Accordingly, moving object2 *with respect to* object1 requires changing transformations between them. The practical importance of this, as we'll see, cannot be over-emphasized.

Let's try and understand now the relative position of the sphere with respect to the box in Experiment 4.12 in light of the preceding proposition. We'll do this by the oft-useful technique of deconstructing code by incrementally adding back transformations after stripping them first all away.

Experiment 4.13. Repeat Experiment 4.12. The modeling transformation and object definition part are as below:

```
// Modeling transformations.
glTranslatef(0.0, 0.0, -15.0);
glRotatef(45.0, 0.0, 0.0, 1.0);
glTranslatef(5.0, 0.0, 0.0);

glutWireCube(5.0); // Box.

//More modeling transformations.
glTranslatef (0.0, 10.0, 0.0);

glutWireSphere (2.0, 10, 8); // Sphere.
```

First, comment out the last two statements of the first modeling transformations block as below (the first translation is always needed to place the entire scene in the viewing frustum):

```
// Modeling transformations.
glTranslatef(0.0, 0.0, -15.0);
// glRotatef(45.0, 0.0, 0.0, 1.0);
```

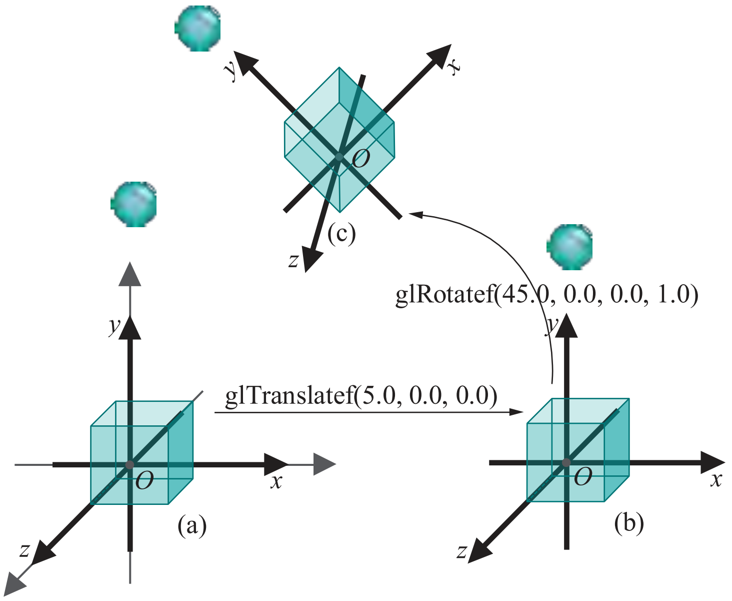

Figure 4.23: Transitions of the box, the box's local coordinates system (bold) and the sphere. The (thin) world coordinate system, which never changes, coincides with the box's initial local.

```
// glTranslatef(5.0, 0.0, 0.0);

glutWireCube(5.0); // Box.

//More modeling transformations.
glTranslatef (0.0, 10.0, 0.0);

glutWireSphere (2.0, 10, 8); // Sphere.
```

The output is as depicted in Figure 4.23(a).

Next, uncomment glTranslatef(5.0, 0.0, 0.0) as below:

```
// Modeling transformations.
glTranslatef(0.0, 0.0, -15.0);
// glRotatef(45.0, 0.0, 0.0, 1.0);
glTranslatef(5.0, 0.0, 0.0);

glutWireCube(5.0); // Box.

//More modeling transformations.
glTranslatef (0.0, 10.0, 0.0);

glutWireSphere (2.0, 10, 8); // Sphere.
```

The output is as in Figure 4.23(b). Finally, uncomment glRotatef(45.0, 0.0, 0.0, 1.0) as follows:

```
// Modeling transformations.
glTranslatef(0.0, 0.0, -15.0);
glRotatef(45.0, 0.0, 0.0, 1.0);
glTranslatef(5.0, 0.0, 0.0);

glutWireCube(5.0); // Box.

//More modeling transformations.
glTranslatef (0.0, 10.0, 0.0);

glutWireSphere (2.0, 10, 8); // Sphere.
```

```
glFlush();
```

The result is seen in Figure 4.23(c). Figure 4.23 shows the box's local coordinate system as well after each transition. Observe that the sphere is *always* 10 units vertically above the box in the latter's coordinate system, as one would expect from the glTranslatef (0.0, 10.0, 0.0) call between the two. End

The following program should solidify the reader's understanding of how Proposition 4.1 governs relative placement.

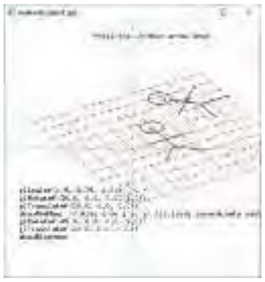

Figure 4.24: Screenshot of relativePlacement.cpp after all transformations from the scaling down have been executed.

Experiment 4.14. Run relativePlacement.cpp. Pressing the up arrow key once causes the last statement, viz., drawBlueMan, of the following piece of code to be executed:

```
glScalef(1.5, 0.75, 1.0);
glRotatef(30.0, 0.0, 0.0, 1.0);
glTranslatef(10.0, 0.0, 0.0);
drawRedMan; // Also draw grid in his local coordinate system.
glRotatef(45.0, 0.0, 0.0, 1.0);
glTranslatef(20.0, 0.0, 0.0);
drawBlueMan;
```

With each press of the up arrow we go back a statement and successively execute that statement *and* the ones that follow it. The statements executed are in black text, the rest gray. Pressing the down arrow key goes forward a statement. Figure 4.24 is a screenshot after all transformations from the scaling on have been executed. End

The torso and arms of both men are aligned along their respective local coordinate axes (only the x and y we care about, z being 0 always). The world coordinate axes which never change are drawn in cyan. At the time of the red man's creation also drawn is a 10 × 10 red grid of boxes in his local coordinate system, the sides of each box being 5 units.

With each transformation going back from the red man's creation, observe – focus on a point like the blue man's origin and trust your eyes – how the blue man stays static in the red man's local coordinate system. A simple calculation shows that the blue man's origin is actually at $(20/\sqrt{2}, 20/\sqrt{2}) \approx (14.14, 14.14)$ in the red man's system. Even when scaling skews the red man's system so that it's not rectangular any more, the blue man skews the same way as well, staying put in the red system. Proposition 4.1 is not to be denied!

Exercise 4.19. For the following two pieces of code in the drawing routine give (x, y, z) coordinates of the point to which the center of the sphere is transformed. Explain as well the relative positions of the sphere and box.

(a)
```
glRotatef(90.0, 1.0, 0.0, 0.0);
glutWireCube(1.0);
glRotatef(90.0, 0.0, 0.0, 1.0);
glTranslatef(4.0, 0.0, 0.0);
glutWireSphere(2.0, 10, 8);
```

(b)
```
glTranslatef(2.0, 0.0, 0.0);
glScalef(2.0, 2.0, 2.0);
glutWireCube(1.0);
glRotatef(90.0, 0.0, 1.0, 0.0);
glTranslatef(0.0, 0.0, 4.0);
glutWireSphere(2.0, 10, 8);
```

If you're impatient to get to animation hang on – there's one final piece to get in place!

4.4 Modelview Matrix Stack and Isolating Transformations

The modelview matrix, which we have described as being modified by modeling transformations by multiplication on the right, is actually the topmost one of a *modelview matrix stack* . This particular matrix is called the *current modelview matrix* . In fact, OpenGL maintains three different matrix stacks: modelview, projection and texture. A glMatrixMode(*mode*) command, where *mode* is GL MODELVIEW, GL_PROJECTION or GL TEXTURE, determines which stack is currently active.

Here's an experiment to motivate use of the modelview matrix stack:

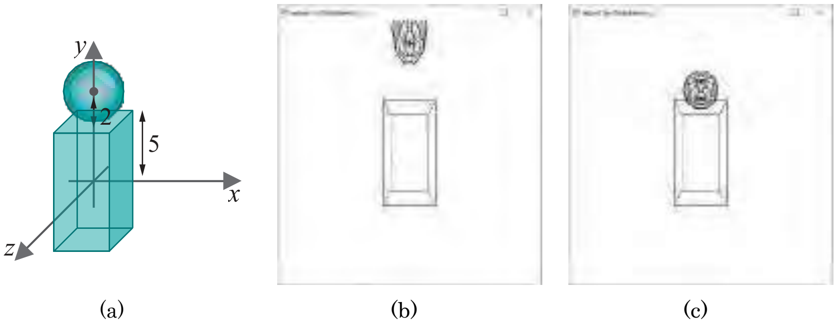

(a) (b) (c)

Figure 4.25: Planning a head on a torso: (a) The plan (b) Drawn without isolating the scaling (c) After isolating the scaling.

Experiment 4.15. We want to create a human-like character. Our plan is to start by drawing the torso as an elongated cube and placing a round sphere as its head directly on top of the cube (no neck for now). To this end replace the drawing routine of box.cpp with:

```
void drawScene(void)
{
    glClear(GL_COLOR_BUFFER_BIT);
    glColor3f(0.0, 0.0, 0.0);
    glLoadIdentity();

    glTranslatef(0.0, 0.0, -15.0);

    glScalef(1.0, 2.0, 1.0);
    glutWireCube(5.0); // Box torso.

    glTranslatef(0.0, 7.0, 0.0);
    glutWireSphere(2.0, 10, 8); // Spherical head.

    glFlush();
}
```

Our calculations are as follows: (a) the scaled box is 5× 10× 5 and, being centered at the origin, is 5 units long in the $+y$ direction; (b) the sphere is of radius 2; (c) therefore, if the sphere is translated 5 + 2 = 7 in the $+y$ direction, then it should sit exactly on top of the box (see Figure 4.25(a)).

It doesn't work: the sphere is no longer round and is, moreover, some ways above the box (Figure 4.25(b)). Of course, because the sphere is transformed by glScalef(1.0, 2.0, 1.0) as well! So, what to do? A solution is to *isolate* the scaling by placing it within a *push-pop pair* as below:

```
    ---
    glTranslatef(0.0, 0.0, -15.0);
```

```
glPushMatrix();
glScalef(1.0, 2.0, 1.0);
glutWireCube(5.0); // Box torso.
glPopMatrix();

glTranslatef(0.0, 7.0, 0.0);
glutWireSphere(2.0, 10, 8); // Spherical head.
---
```

The resulting screenshot is Figure 4.25(c), which shows a round head on a neckless torso as desired. End

What the glPushMatrix() command does is make a *copy* of the current (i.e., current topmost) matrix in the modelview matrix stack and place it on top of the stack; consequently, immediately upon execution of a glPushMatrix(), the two top matrices of the stack are identical. The glPopMatrix() statement, on the other hand, deletes the topmost matrix of the modelview matrix stack so the one underneath becomes the current one.

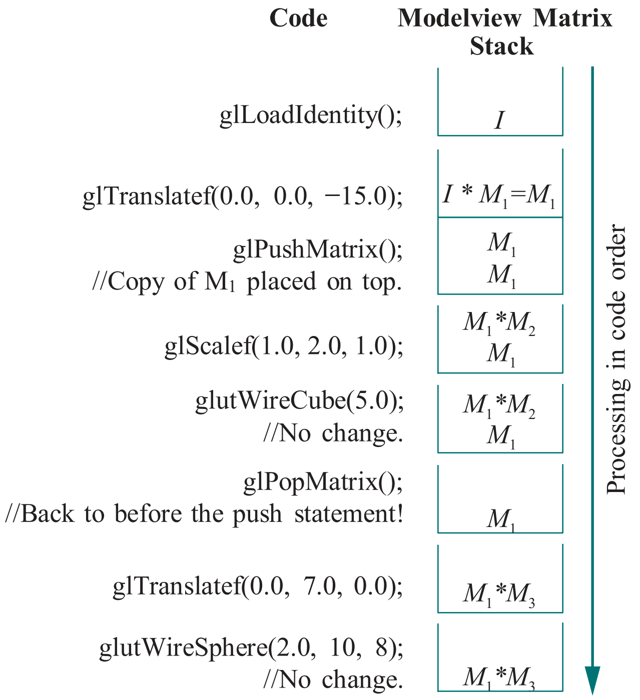

```
glLoadIdentity();
glTranslatef(0.0, 0.0, −15.0);
glPushMatrix();
//Copy of M1 placed on top.
glScalef(1.0, 2.0, 1.0);
glutWireCube(5.0);
//No change.
glPopMatrix();
//Back to before the push statement!
glTranslatef(0.0, 7.0, 0.0);
glutWireSphere(2.0, 10, 8);
//No change.
```

Figure 4.26: Transitions of the modelview matrix stack.

Let's follow the modelview matrix stack through the code above. Assume that the matrix corresponding to the translation glTranslatef(0.0, 0.0, -15.0) is M_1, to glScalef(1.0, 2.0, 1.0) is M_2, and to glTranslatef(0.0, 7.0, 0.0) is M_3. The transitions of the stack are shown in Figure 4.26, starting from the top.

As you see, the push-pop pair *stores* the current modelview matrix *prior* to the scaling transformation and then *restores* it once the cube has been drawn, effectively localizing the effect of the scaling to only the cube.

Exercise 4.20. Give (x, y, z) coordinates of the points to which the centers of the four spheres are located by the drawing routine below, assuming no prior transformations.

```
glPushMatrix();
```

```
glTranslatef(2.0, 0.0, 0.0);
glutWireSphere(2.0, 10, 8); // Sphere A

glPushMatrix();
glScalef(2.0, 2.0, 2.0);
glutWireSphere(2.0, 10, 8); // Sphere B
glPopMatrix();

glPushMatrix();
glRotatef(90.0, 1.0, 0.0, 0.0);
glTranslatef(0.0, 0.0, 4.0);
glutWireSphere(2.0, 10, 8); // Sphere C
glPopMatrix();

glTranslatef(0.0, 4.0, 0.0);
glutWireSphere(2.0, 10, 8); // Sphere D

glPopMatrix();
```

Remark 4.4. It's recommended programming practice to enclose all the transformations in the drawing routine in one giant push-pop pair, as in the preceding exercise, so that at the end of the routine the modelview matrix stack is guaranteed to revert to its initial state of containing a single identity matrix (though, admittedly, we don't follow this ourselves).

4.5 Animation

We're there! Animation in computer graphics is really a sequence of still frames, just like in a movie reel, smoothness being achieved by rendering frames rapidly one after another, each a little different from its predecessor. Successive frames are created by a "transform-and-draw" loop: the scene is redrawn after transformations in the drawing routine change the location or shape, or both, of objects in the scene.

4.5.1 Animation Technicals

Before analyzing animated programs we need first to explain a couple of animation-related technicalities.

Controlling Animation

There are three simple methods to control animation in OpenGL:

1. Interactively, via keyboard or mouse input, with the help of their callback routines to invoke transformations.

   Experiment 4.16. Run rotatingHelix1.cpp where each press of space calls the increaseAngle() routine to turn the helix. Note the glutPostRedisplay() command in increaseAngle() which asks the screen to be redrawn. Keeping the space bar pressed turns the helix continuously. Figure 4.27 is a screenshot.
   End

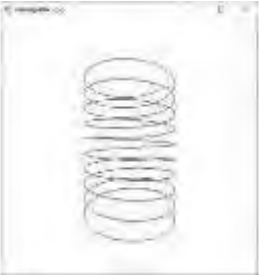

Figure 4.27: Screenshot of rotatingHelix1.cpp.

2. Automatically, by specifying a function idle_function, called the *idle function*, with the statement glutIdleFunc(idle function). The idle function is called whenever no OpenGL event is otherwise pending.

   Experiment 4.17. Run rotatingHelix2.cpp, a slight modification of rotatingHelix1.cpp, where pressing space causes the routines increaseAngle() and NULL (do nothing) to be alternately specified as idle functions.

   The speed of animation is determined by the processor's speed and availability to execute the idle function – the user cannot influence it. End

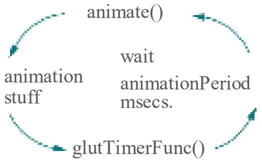

Figure 4.28: Animation control in rotatingHelix3.cpp.

3. Semi-automatically, by specifying a routine *timer_function*, called the *timer function*, with a call to glutTimerFunc(*period*, *timer_function*, *value*). The timer function is called *period* milliseconds after the glutTimerFunc() statement is executed and with the parameter *value* being passed to it.

Experiment 4.18. Run rotatingHelix3.cpp, another modification of rotatingHelix1.cpp, where the particular timer function animate() calls itself recursively after animationPeriod number of msecs., by means of its own glutTimerFunc(animationPeriod, animate, 1) statement.

The parameter value 1 passed to animate() is not used in this program. The routine increaseAngle() called by animate() turns the helix as before. Figure 4.28 shows the animation scheme.

The user can vary the speed of animation by changing the value of animationPeriod by pressing the up and down arrow keys. End

The speed of animation or, equivalently, *frame rate*, which is the rate at which the screen is redrawn with new frames, cannot be increased arbitrarily, e.g., by lowering the value of animationPeriod in rotatingHelix3.cpp, because redrawing the scene takes some minimum amount of time, depending on its complexity and the speed of the GPU.

Moreover, the frame rate can never exceed the monitor's installed refresh rate, which is the rate at which it can refresh all the pixels of its screen, i.e., change their color values to those corresponding to the next frame. Particularly, if the monitor's refresh rate is nHz, i.e., n refreshes a second, then the maximum achievable fps (frames per second) is n as well. The next program shows how to count the fps with help of OpenGL.

Experiment 4.19. Run rotatingHelixFPS.cpp, which enhances rotatingHelix3.cpp adding the routine frameCounter() to count the number of times the drawScene() routine is called, equivalently, the number of frames drawn, per second. The "fps" is output every second to the debug window.

Caveat: The number of frames drawn per second by the GPU to the color buffer, i.e., the number of completions of drawScene() per second, may not equal exactly the number of frames drawn to the screen per second, the true fps. See Remark 4.8 a little further on, for example, for what may happen if a fast GPU is up against a slower monitor.

The way the fps is output is with drawScene() incrementing the global frameCount every time it is called, and frameCounter() outputting the value of frameCount each second – note that frameCounter() calls itself every second because of its glutTimerFunc(1000, frameCounter, 1) statement – while simultaneously resetting the value of frameCount to 0. The if conditional in frameCounter() is so that no fps is output when it is first called from setup() with value passed being 0. End

Remark 4.5. We'll be using exclusively the third method above, with a call to glutTimerFunc(), in our animated programs. Finer control over the speed of animation, however, might be obtained by actually measuring the time elapsed since the last frame and then drawing the current frame with animation variables incremented depending upon this value.

The user can calculate the time difference between frames by accessing the system clock each frame or calling glutGet(GLUT ELAPSED_TIME) which returns the number of milliseconds elapsed since glutInit() was called.

Double Buffering

The second technicality critical to smooth animation is *double buffering*.

A color buffer is a space, almost always in GPU memory, which stores the RGBA values for raster pixels, typically, 8 bits for each of R, G, B and A for a total of 32 bits per pixel. So, it is a color buffer which holds the data for a single frame and is read when that frame is drawn to the monitor.

Space for two color buffers is provided in a double-buffered system in such a manner that one buffer, the *viewable buffer*, holds the frame currently displayed on the monitor while the next frame is being drawn in the second buffer, the *drawable buffer*. When the drawing of the frame in the drawable buffer is complete, the buffers are swapped, so that the next frame now becomes viewable and, at the same time, the one following it begins to be drawn. This *draw-and-swap* loop repeats through the animation. Figure 4.29 illustrates the process.

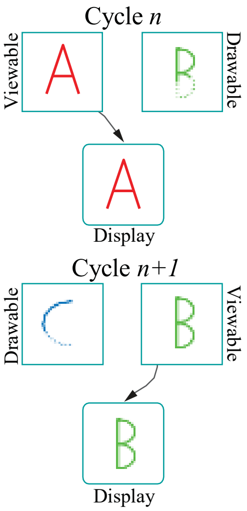

Figure 4.29: Successive cycles in double buffering.

Terminology: The viewable buffer is often called the *front buffer* or *main buffer*, while the drawable buffer is called the *back buffer* or *swap buffer*. Either buffer is also called a *refresh buffer*.

Double buffering greatly improves the quality of animation by hiding transition between successive frames from the viewer. With single buffering, on the other hand, the viewer "sees" the next frame being drawn in the same buffer that contains the current one. The result can be unpleasant *ghosting*, so called because a prior image persists while the next is being created.

The double buffering display mode is enabled by calling glutInitDisplayMode() in main with GLUT_DOUBLE as one of the arguments (instead of GLUT_SINGLE *and* inserting a call to glutSwapBuffers() at the end of the drawing routine (*instead of* glFlush()). The rotatingHelix*.cpp programs are all double buffered.

Experiment 4.20. Disable double buffering in rotatingHelix2.cpp by replacing GLUT_DOUBLE with GLUT_SINGLE in the glutInitDisplayMode() call in main, and replacing glutSwapBuffers() in the drawing routine with glFlush(). Ghostly is it not?! End

Remark 4.6. Double buffering, typically, is implemented in the GPU, both buffers being located in VRAM, the swap being effected by simply changing the value of the pointer to the start of displayable data in the VRAM. This method of going back and forth between the location of the two buffers is called *ping-pong buffering*.

Remark 4.7. There is a difference between the "draw" in the transform-and-draw animation loop described at the start of this section as how animation is implemented, and the "draw" in the draw-and-swap loop described above as how double buffering operates. The first is a programmer-instigated operation – typically, with a glutPostRedisplay() call – in which the world space is projected and scaled (recall shoot-and-print from Chapter 2) *and* rasterized into the color buffer. On the other hand, the "draw" in draw-and-swap actually draws the screen, in particular, the OpenGL window, with the contents of the color buffer – a more appropriate term for this then might be "render". We alluded, in fact, to this difference in Experiment 4.19.

Remark 4.8. The draw-and-swap loop to render frames may result in visual artifacts if the loop's rate is not in sync with the monitor's installed refresh rate.

For example, if the rate at which the GPU is drawing frames is 80 per second while the monitor's refresh rate is 60Hz, i.e., 60 per second, then the GPU takes only 0.0125 secs. to create a frame, while the slower monitor takes 0.0167 secs. to display one. So, if the back buffer is swapped with the front buffer as soon as the drawing of the former is complete, then the monitor starts to show a new frame when only 75% (= 0.0125/0.0167) of the previous one has been rendered, resulting, possibly, in distracting *screen tearing*.

Screen tearing can be avoided by imposing so-called *vertical synchronization*, or *v-sync*, which allows the back buffer to be swapped with the front buffer only after the latter has been entirely rendered, in other words, after the monitor has refreshed.

V-sync has issues of its own, though, the most glaring one in a double buffered system being that the GPU has to be locked out of writing to a back buffer which is waiting for a *vertical blank interrupt* , or *VBI* , which is the signal that monitor refresh has completed. Not only then is the GPU forcibly under-utilized, there is lag too between the time of a frame's drawing and when it is displayed. This problem can be alleviated somewhat by implementing *triple buffering* , where there are two back buffers instead of one and the GPU proceeds immediately to drawing the next frame in the other back buffer after completing the current frame in one. The GPU continues going back and forth between the two back buffers till a VBI occurs, when the most recently completed back buffer is swapped to the front.

Keep in mind that enabling v-sync, as also triple buffering, *cannot* be done from within OpenGL. One must access the window management system for this purpose.

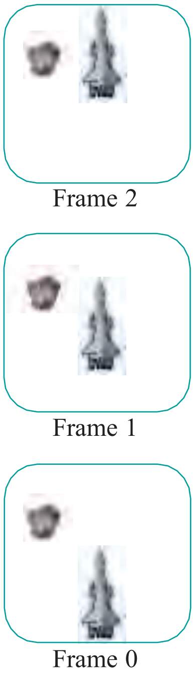
Frame 2

Frame 1

Frame 0

Figure 4.30: Animation in CG is frame by (static) frame, each created anew by the user.

Before proceeding to code, the difference between animation in CG and the real world bears belaboring, as it can appear unintuitive at first. Animation in CG does *not* consist of issuing a command like move the spacecraft image up at a speed of 100 pixels/sec; rather, it consists of issuing a command to create and render a (static) frame with the spacecraft in its current position, then to create a new (static) frame with the spacecraft drawn at a position an amount X (to be determined by the programmer) ahead of its old one and render this frame, then to create yet another frame with the craft moved forward another X and render, and so on (see Figure 4.30). In other words, animation is *frame by frame*. Depending on X and the frame rate is the speed at which the craft appears to progress up the monitor.

Moreover, each frame is drawn from scratch, pixel by pixel, with nothing taken from the previous frame. So, for example, we can't ask that pixels corresponding to the stationary asteroid in Figure 4.30 be "kept as they are" from Frame 0 on, while we redraw only the spacecraft; rather, each successive frame is entirely new. An interesting consequence of this is that we could render the (rather odd) sequence Frame 0, Frame 2, Frame 1 from Figure 4.30 with exactly the same computational effort as the (more authentic) Frame 0, Frame 1, Frame 2. In the real world, of course, the spacecraft moves from Frame 0 to Frame 1 and then to Frame 2, each frame being an *actual* temporal precursor of the next; not so in CG, where each frame is drawn independently, the rendering sequence being as the programmer cares to choose.

4.5.2 Animation Code

Ball Flying About a Torus

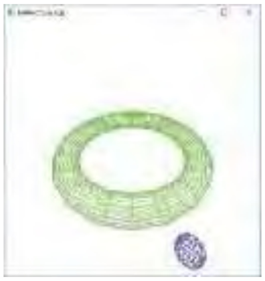
Figure 4.31: Screenshot of ballAndTorus.cpp.

Experiment 4.21. Run ballAndTorus.cpp. Press space to start the ball both flying around (longitudinal rotation) and in and out (latitudinal rotation) of the torus. Press the up and down arrow keys to change the speed of the animation. Press 'x/X', 'y/Y' and 'z/Z' to change the viewpoint. Figure 4.31 is a screenshot.

The animation of the ball is interesting and we'll deconstruct it. Comment out all the modeling transformations in the ball's block, except the last translation, as follows:

```
// Begin revolving ball.
// glRotatef(longAngle, 0.0, 0.0, 1.0);

// glTranslatef(12.0, 0.0, 0.0);
// glRotatef(latAngle, 0.0, 1.0, 0.0);
// glTranslatef(-12.0, 0.0, 0.0);

glTranslatef(20.0, 0.0, 0.0);

glColor3f(0.0, 0.0, 1.0);
glutWireSphere(2.0, 10, 10);
// End revolving ball.
```

The ball is centered at (20, 0, 0), its start position, by glTranslatef(20.0, 0.0, 0.0). See Figure 4.32. There is no animation even if you press space.

The ball's intended latitudinal rotation is in and out of the circle C_1 through the middle of the torus. C_1's radius, called the *outer radius* of the torus, is 12.0, as specified by the second parameter of glutWireTorus(2.0, 12.0, 20, 20). Moreover, C_1 is centered at the origin and lies on the xy-plane. Therefore, ignoring longitudinal motion for now, the latitudinal rotation of the ball *from its start position* is about the line L through (12, 0, 0) parallel to the y-axis (L being tangent to C_1). This rotation will cause the ball's center to travel along the circle C_2 centered at (12, 0, 0), lying on the xz-plane, of radius 8.

As glRotatef() always rotates about a radial axis, how does one obtain the desired rotation about L, a non-radial line? Employ the Trick (see Example 4.3 if you don't remember). First, translate left so that L is aligned along the y-axis, then rotate about the y-axis and, finally, reverse the first translation to bring L back to where it was. This means uncommenting the corresponding three modeling transformations as below:

```
// Begin revolving ball.
// glRotatef(longAngle, 0.0, 0.0, 1.0);

glTranslatef(12.0, 0.0, 0.0);
glRotatef(latAngle, 0.0, 1.0, 0.0);
glTranslatef(-12.0, 0.0, 0.0);

glTranslatef(20.0, 0.0, 0.0);

glColor3f(0.0, 0.0, 1.0);
glutWireSphere(2.0, 10, 10);
// End revolving ball.
```

Press space to view only latitudinal rotation.

Note: The two consecutive translation statements could be combined into one, but then the code would be less easy to parse.

Finally, uncomment glRotatef(longAngle, 0.0, 0.0, 1.0) to implement longitudinal rotation about the z-axis. The angular speed of longitudinal rotation is set to be five times slower than that of latitudinal rotation – the increments to longAngle and latAngle in the animate() routine being 1° and 5° , respectively. This means the ball winds in and out of the torus five times before it completes one trip around. End

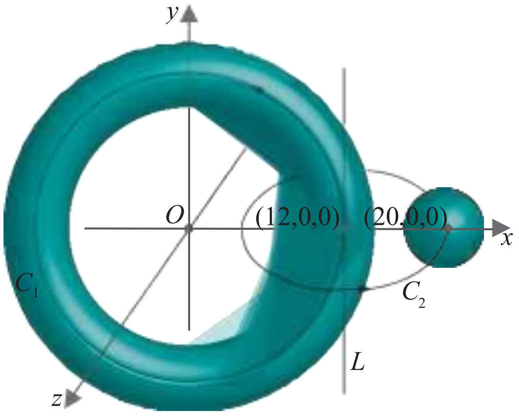

Figure 4.32: The ball's axis of latitudinal rotation from its start position is L.

Exercise 4.21. (Programming) It's instructive as well to uncomment one by one the three modeling transformations used to apply the Trick in the preceding experiment, rather than all together. So uncomment glTranslatef(-12.0, 0.0, 0.0) first, then glRotatef(latAngle, 0.0, 1.0, 0.0) and, last, glTranslatef(12.0, 0.0, 0.0). Check if animation can be activated and explain the output at each step.

Exercise 4.22. (Programming) Now here's something rather funny. Actually, what we'll show is not an uncommon accidental error. Cut the glLoadIdentity() call from the drawing routine of ballAndTorus.cpp and paste it as the last line of the window reshape routine (as, say, in square.cpp).

Oops! The ball and torus speed away together and are out of sight pretty quickly. Explain.
Hint : The current modelview matrix is not automatically cleared to identity between successive calls to the drawing routine.

Exercise 4.23. (Programming) Add a red and a yellow ball to the existing blue ball so that the three are always 120° from each other longitudinally and follow a similar rotate-revolve path one after the other.
Hint : Copy and paste the revolving ball code a couple of times, making sure to isolate each instance with a glPushMatrix()-glPopMatrix() pair, and add in appropriate glRotatef(*, 0.0, 0.0, 1.0) calls.

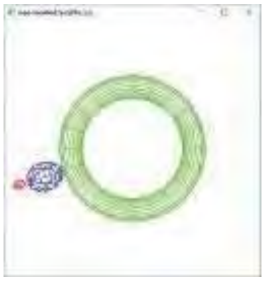

Figure 4.33: Screenshot from Experiment 4.22.

Experiment 4.22. We want to add a satellite which tags along with the ball of ballAndTorus.cpp. The following piece of code added to the end of the drawing routine – just after // End revolving ball. – does the job:

```
glTranslatef(4.0, 0.0, 0.0);

// Satellite
glColor3f(1.0, 0.0, 0.0);
glutWireSphere(0.5, 5, 5);
```

See Figure 4.33 for a screenshot. For a revolving satellite add the following instead:

```
glRotatef(10*latAngle, 0.0, 1.0, 0.0);
glTranslatef(4.0, 0.0, 0.0);

// Satellite
glColor3f(1.0, 0.0, 0.0);
glutWireSphere(0.5, 5, 5);
```

Observe how Proposition 4.1 is being applied in both cases to determine the motion of the satellite *relative to the* ball by means of transformation statements between the two.
End

Exercise 4.24. (Programming) Thinking that the Trick should be invoked to revolve the satellite about the ball in the preceding experiment, exactly as was done to obtain the latitudinal rotation of the ball itself, suppose we code the satellite as below instead:

```
// Trick code block.
glTranslatef(4.0, 0.0, 0.0);
glRotatef(10*latAngle, 0.0, 1.0, 0.0);
glTranslatef(-4.0, 0.0, 0.0);

glTranslatef(4.0, 0.0, 0.0);

// Satellite.
glColor3f(1.0, 0.0, 0.0);
glutWireSphere(0.5, 5, 5);
```

The satellite still follows the ball, but does *not* revolve about it. Why?
Hint : A good way to verify your answer is to stop the ball from moving by commenting out both glRotatef()s in its definition block and observing only the satellite.

Exercise 4.25. (Programming) Continuing with Experiment 4.22, add a second satellite. Both should revolve around the ball, but in different orbits.

Throwing a Ball

Experiment 4.23. Run throwBall.cpp, which simulates the motion of a ball thrown with a specified initial velocity subject to the force of gravity. Figure 4.34 is a screenshot partway through the ball's flight.

Press space to toggle between animation on and off. Press the right/left arrow keys to increase/decrease the horizontal component of the initial velocity, up/down arrow keys to likewise change the vertical component of the initial velocity and the page up/down keys to change the gravitational acceleration. Press 'r' to reset. The values of the initial velocity components and of gravitational acceleration are displayed on the screen.

End

Figure 4.34: Screenshot of throwBall.cpp.

The equation determining the horizontal distance traveled by the ball in throwBall.cpp, in terms of time t, is

$$x(t) = ht$$

where h is the horizontal component of the initial velocity (by integrating $\frac{dx}{dt} = h$, taking initial $x = 0$); that determining vertical distance traveled is

$$y(t) = vt - \frac{g}{2}t^2$$

where v is the vertical component of the initial velocity and g is gravitational acceleration (by integrating $\frac{dv}{dt} = -g$, and then again $\frac{dy}{dt} = v$, taking initial $y = 0$).

Motion is simulated by repeatedly redrawing the ball at the new location it's mapped to by glTranslatef($x(t)$, $y(t)$, 0), incrementing t by 1 each time step.

Remark 4.9. The techniques to animate the spheres in ballAndTorus.cpp and throwBall.cpp are interesting to compare. One could say that the former is "physical" while the latter "equational". It would certainly be possible though a bit hard to make the former equational as well.

Exercise 4.26. (Programming) Animate a ball thrown toward and bouncing off a wall. See Figure 4.35. The initial force on the ball is horizontal – allow the user to change the amount of this force. Also allow the user to adjust gravitational acceleration and the "springiness" of the ball. Animation can end when the ball hits the floor (if you are brave you could continue with it bouncing on some more).

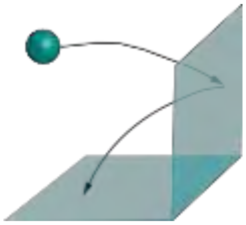

Figure 4.35: Ball bouncing off wall.

Ball Facing Friction

Experiment 4.24. Run ballAndTorusWithFriction.cpp, which modifies ballAndTorus.cpp to simulate an invisible viscous medium through which the ball travels. Press space to apply force to the ball. It has to be kept pressed in order to continue applying force. The ball comes to a gradual halt after the space bar is released. Increase or decrease the level of applied force by using the up and down arrow keys. Increase or decrease the viscosity of the medium using the page up and down keys. Press 'x/X', 'y/Y' and 'z/Z' to rotate the scene. Figure 4.36 is a screenshot. The values of the applied force and viscous drag are shown at the top. End

Figure 4.36: Screenshot of ballAndTorusWithFriction.cpp.

All the work of applying viscous friction to the ball is in animate(). In particular, the equation of motion implemented takes the frictional drag (or, equivalently, deceleration) on the ball of ballAndTorusWithFriction.cpp to be proportional to its velocity, a valid assumption from physics [52]. So, the equation is

$$\textit{drag-deceleration} = \textit{drag} * \textit{velocity}$$

where the *drag* (in real life) is a constant depending on the medium through which the object moves, as well as its shape. When space is pressed, the external acceleration applied is applied_acceleration, resulting in the net acceleration calculated in the line of code

```
acceleration = applied_acceleration - drag*velocity;
```

When space is not pressed, there is no applied acceleration but only frictional drag, so the equation is instead

```
acceleration = -drag*velocity;
```

At every time step we find the change in velocity from the equation

$$\frac{\Delta(velocity)}{\Delta(time)} = acceleration$$

which is certainly true in the limit as $\Delta(time) \to 0$. However, we approximate change through a unit time step by setting $\Delta(time) = 1$ to get

$$\Delta(velocity) = acceleration$$

which is implemented by the program statement

```
velocity += acceleration;
```

Finally, change per time step in the latAngle and longAngle variables is proportional to the current velocity via

```
latAngle += 5.0 * velocity;
...
longAngle += 1.0 * velocity;
```

Exercise 4.27. (Programming) Simulate a ball falling through air, landing upon and continuing on through a viscous medium such as water.

You need not simulate splashing. To differentiate air and water simply use color, e.g., the upper half of your window may be white, and the lower blue.

Remark 4.10. The last two programs, throwBall.cpp and ballAndTorusWithFriction.cpp, demonstrate simple applications of the fascinating field of *physics in graphics*, popularly called *game physics*, which is critical to realistic animation. Plausible simulation of such phenomena as a wall of bricks crashing down, clothes and hair blowing in the wind, a drop of water rolling off a leaf, and smoke, fire and explosions, to mention a few, all require the programmer to take into account the real-world physics of the setting. Accordingly, nowadays a so-called *physics engine*, to handle real-world simulations, is invariably part of a computer game of any complexity. Special effects in a Hollywood production, too, are almost always physics in graphics in action. Evidently, in real-time applications there are two overarching and competing considerations in this discipline – realism versus computational efficiency.

Popular books for the interested reader include Bourg & Bywalec [19], Eberly [39] and Szauer [143].

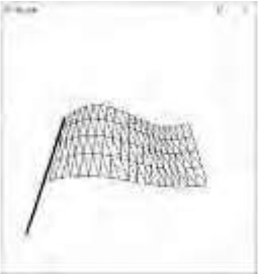

Figure 4.37: Screenshot of flag.cpp.

Fluttering Flag

Experiment 4.25. Run flag.cpp, which simulates a flag fluttering in the wind. Press space to start the animation, the up and down arrow keys to change its speed, and 'x/X', 'y/Y' and 'z/Z' to rotate the viewpoint. Figure 4.37 is a screenshot.

End

Observe first a fundamental difference between this animation and the previous ones this section. The flag *changes shape* through the animation, while the animated object in each of the earlier experiments, a ball, never changed shape but moved always as a rigid object.

So, how is the flag created and its shape changed? Geometrically, as can be seen from the glBegin(GL TRIANGLE_STRIP). . . glEnd() block in the drawing routine, the flag is a rectangular sheet comprising four triangle strips each with 40 triangles. The vertices of the flag are taken from a vertex array which is populated by a fillVertexArray() routine with the following statements:

```
int k = 0;
for (int j = 0; j <= q; j++)
   for (int i = 0; i <= p; i++)
   {
      vertices[k++] = -20.0 + 40.0 * (float)i/p;
      vertices[k++] = 5.0 * sin(s + (float)i/p * 1.8 * PI) -
                           5.0 * sin(s);
      vertices[k++] = -10.0 + 20.0 * (float)j/q;
   }
```

The first statement in the inner for loop scales the flag to occupy the range from −20 to 20 along the x-axis – in fact, denoting (float)i/p by t, we see that t varies from 0 to 1 as **i** varies from 0 to p, so that x varies from −20 to 20. The third statement likewise scales the flag to occupy −10 to 10 in the z-direction.

It is the second statement which makes the waviness of the flag by writing the y-values of its vertices as a sine function of t, in particular,

$$y = 5\sin(s + 1.8\pi t) - 5\sin s \tag{4.3}$$

where s is a shift variable. Let's ignore the last “ −5 sin s” for now, so that the equation becomes simply

$$y = 5\sin(s + 1.8\pi t)$$

Because t varies from 0 to 1 as **i** varies from 0 to p, the equation above draws the piece of a sine curve from $x = s$ to $x = s + 1.8\pi$ (the scaling factor of 5 in front is just to size the flag suitably). As the animate() routine increments s, this drawn arc, always ranging 1.8π along the x-direction, moves right along the sine curve. See Figure 4.38. Or, equivalently, one could think of the sine curve itself traveling leftward as an arc of it from a fixed window is drawn. This movement is exactly what creates the waves in the profile of the flag.

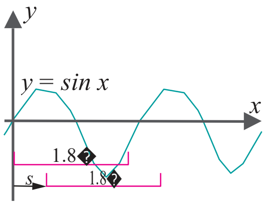

Figure 4.38: Window shifting right across a sine curve.

Now, let's return to the original equation (4.3): the “ −5 sin s” is tacked on so that the value at the $t = 0$ end of the flag is fixed, in particular, the value is always 0, for we want the edge attached to the pole to be motionless.

Why did we choose the x-range of the drawn arc of the sine curve to be of size 1.8π, instead of a full 2π-period? We'll leave the reader to look into this in the following exercise.

Exercise 4.28. (Programming) Change the x-range of the drawn arc of the sine curve to be of length 2π instead 1.8π by changing the second statement of the inner for loop in fillVertexArray() to

```
vertices[k++] = 5.0 * sin(s + (float)i/p * 2.0 * PI) - 5.0 * sin(s);
```

You might want to change the statement of the if (isAnimate) block in the animate() routine to s += 2.0*PI/p as well, so that the s-increment matches a segment of the curve, but this is not critical. What do you see? Both short sides of the flag are now motionless, which obviously is not authentic.

Exercise 4.29. (Programming) Return to the original flag.cpp and delete the adjusting factor “$-$ 5 sin s” of (4.3) by changing the second statement of the inner for loop in fillVertexArray() to

```
    vertices[k++] = 5.0 * sin(s + (float)i/p * 1.8 * PI);
```

It's clear now why the adjusting factor is needed is it not?

Exercise 4.30. (Programming) The program flag.cpp simulates fluttering certainly but isn't particularly authentic. A real flag in the wind would not wave perfectly uniformly; there would be the occasional randomness. Moreover, it would unlikely to be smooth throughout, rather developing a crinkle now and then.

Can you hack a little more authenticity into flag.cpp, particularly focusing on fillVertexArray()? See though the next remark.

Remark 4.11. Modeling a flag is an example of cloth physics, a subdiscipline of physics in graphics whose most important application evidently is in dressing characters in interactive games. Achieving authentic results can get pretty hairy too, with a piece of cloth typically modeled as a fine mesh of discrete mass-carrying particles, each connected to adjacent ones with springs.

Clown Head

Our next project is a program, which we'll develop incrementally, to draw a clown's head.

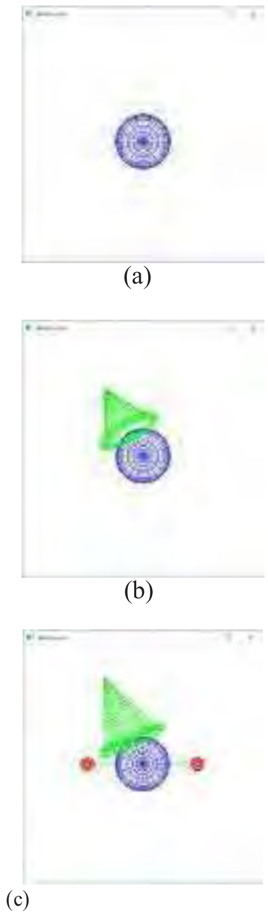

Figure 4.39: Screenshot of (a) clown1.cpp (b) clown2.cpp (c) clown3.cpp.

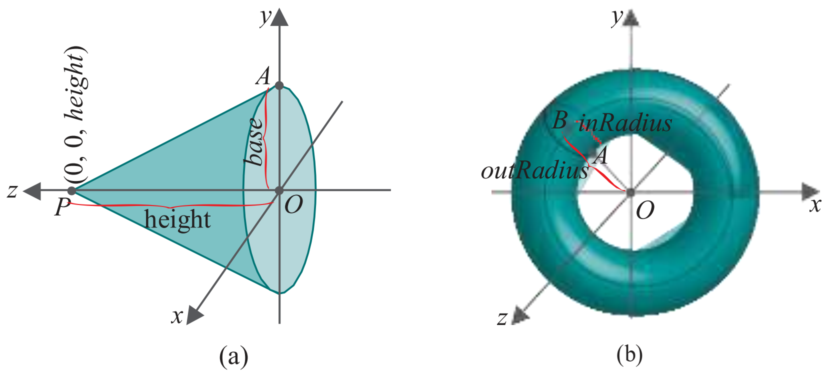

Figure 4.40: (a) Cone drawn by glutWireCone(*base*, *height*, *slices*, *stacks*) (b) Torus drawn by glutWireTorus(*inRadius*, *outRadius*, *sides*, *rings*). Note that the axes are depicted differently in either diagram.

Experiment 4.26. We start with only a blue sphere for the head by running clown1.cpp (see note next) which has the drawing routine below:

Note: clown1.cpp and clown2.cpp are not separate programs but incremental stages of clown3.cpp which is in ExperimenterSource/Chapter4. Currently, clown3.cpp is functionally actually clown1.cpp, drawing just a blue sphere because additions corresponding to clown2.cpp and clown3.cpp are commented out. The program indicates clearly the parts added by clown2.cpp and clown3.cpp, so uncomment them to get those programs.

```
void drawScene(void)
{
   glClear(GL COLOR_BUFFER BIT);
   glLoadIdentity();

  // Place scene in frustum.
   glTranslatef(0.0, 0.0, -9.0);

   // Head.
   glColor3f(0.0, 0.0, 1.0);
```

```
    glutWireSphere(2.0, 20, 20);

    glutSwapBuffers();
}
```

Figure 4.39(a) is a screenshot.

Next, we want a green conical hat. The command glutWireCone(*base*, *height*, *slices*, *stacks*) draws a wireframe cone of base radius *base* and height *height*. The base of the cone lies on the xy-plane with its axis along the z-axis and its apex pointing in the positive direction of the z-axis. See Figure 4.40(a). The parameters *slices* and *stacks* determine the fineness of the mesh (not shown in the figure).

Accordingly, insert the lines (as entire clown2.cpp is already in clown3.cpp, you might want to simply uncomment the selected lines):

```
    // Hat.
    glColor3f(0.0, 1.0, 0.0);
    glutWireCone(2.0, 4.0, 20, 20);
```

in clown1.cpp after the call that draws the sphere, so that the drawing routine becomes:

```
void drawScene(void)
{
    glClear(GL COLOR_BUFFER BIT);
    glLoadIdentity();

    // Place scene in frustum.
    glTranslatef(0.0, 0.0, -9.0);

    // Head.
    glColor3f(0.0, 0.0, 1.0);
    glutWireSphere(2.0, 20, 20);

    // Hat.
    glColor3f(0.0, 1.0, 0.0);
    glutWireCone(2.0, 5.0, 20, 20);

    glutSwapBuffers();
}
```

Not good! Because of the way glutWireCone() aligns, the hat covers the clown's face. This is easily fixed. Translate the hat 2 units up the z-axis and rotate it −90° about the x-axis to arrange it on top of the head. Finally, rotate it a rakish 30° about the z-axis! Here's the modified drawing routine of clown1.cpp at this point:

```
void drawScene(void)
{
    glClear(GL COLOR_BUFFER BIT);
    glLoadIdentity();

    // Place scene in frustum.
    glTranslatef(0.0, 0.0, -9.0);

    // Head.
    glColor3f(0.0, 0.0, 1.0);
    glutWireSphere(2.0, 20, 20);

    // Transformations of the hat.
    glRotatef(30.0, 0.0, 0.0, 1.0);
    glRotatef(-90.0, 1.0, 0.0, 0.0);
    glTranslatef(0.0, 0.0, 2.0);
    // Hat.
    glColor3f(0.0, 1.0, 0.0);
    glutWireCone(2.0, 5.0, 20, 20);

    glutSwapBuffers();
}
```

Let's add a brim to the hat by attaching a torus to its base. The command glutWireTorus(*inRadius*, *outRadius*, *sides*, *rings*) draws a wireframe torus of inner radius *inRadius* (the radius of a circular section of the torus), and outer radius *outRadius* (the radius of the circle through the middle of the torus). The axis of the torus is along the z-axis and centered at the origin. See Figure 4.40(b). Insert the call glutWireTorus(0.2, 2.2, 10, 25) right after the call that draws the cone, so the drawing routine becomes:

```
void drawScene(void)
{
    glClear(GL COLOR_BUFFER BIT);
    glLoadIdentity();

    // Place scene in frustum.
    glTranslatef(0.0, 0.0, -9.0);

    // Head.
    glColor3f(0.0, 0.0, 1.0);
    glutWireSphere(2.0, 20, 20);

    // Transformations of the hat and brim.
    glRotatef(30.0, 0.0, 0.0, 1.0);
    glRotatef(-90.0, 1.0, 0.0, 0.0);
    glTranslatef(0.0, 0.0, 2.0);

    // Hat.
    glColor3f(0.0, 1.0, 0.0);
    glutWireCone(2.0, 5.0, 20, 20);

    // Brim.
    glutWireTorus(0.2, 2.2, 10, 25);

    glutSwapBuffers();
}
```

Observe that the brim is drawn suitably at the bottom of the hat and stays there despite modeling transformations between head and hat – a consequence of Proposition 4.1.

To animate, let's spin the hat about the clown's head by rotating it around the y-axis. We rig the space bar to toggle between animation on and off and the up/down arrow keys to change speed. All updates so far are included in clown2.cpp. Figure 4.39(b) is a screenshot.

What's a clown without little red ears that pop in and out?! Spheres will do for ears. An easy way to bring about oscillatory motion is to make use of the function sin(*angle*) which varies between -1 and 1. Begin by translating either ear a unit distance from the head, and then repeatedly translate each a distance of sin(*angle*), incrementing *angle* each time.

Note: A technicality one needs to be aware of in such applications is that angle is measured in *degrees* in OpenGL syntax, e.g., in glRotatef(*angle*, *p*, *q*, *r*), while the C++ math library assumes angles to be given in *radians*. Multiplying by $\pi/180$ converts degrees to radians.

The ears and head are physically separate, though. Let's connect them with springs! Helixes are springs. We borrow code from helix.cpp, but modify it to make the length of the helix 1, its axis along the x-axis and its radius 0.25. As the ears move, either helix is scaled along the x-axis so that it spans the gap between the head and an ear. The completed program is clown3.cpp, of which a screenshot is seen in Figure 4.39(c).
End

Exercise 4.31. (Programming) Comment out the push-pop pair isolating the hat and brim in clown3.cpp. Explain the new situation of the ears.

Exercise 4.32. Proposition 4.1 came before our discussion of push-pop pairs, so the assumption there is that there are none. Must we revise the proposition to take into account possible push-pop pairs? If so how?

Blooming Flower

Experiment 4.27. Run floweringPlant.cpp, an animation of a flower blooming. Press space to start and stop animation, delete to reset, and 'x/X', 'y/Y' and 'z/Z' to change the viewpoint. Figure 4.41 is a screenshot.
End

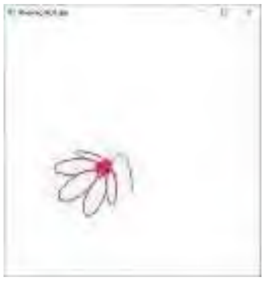

Figure 4.41: Screenshot of floweringPlant.cpp in mid-bloom.

The stem of the plant consists of four straight segments, the sepal (base of the flower) is modeled as a hemisphere, while the six petals are copies of the same circle. Both hemisphere and circle are reshaped by scaling during animation. The routines drawHemisphere() and drawCircle to draw the two are adapted from hemisphere.cpp and circle.cpp, respectively.

As calls to display lists cannot be parametrized at run-time, the two defining a sepal and a petal have to be placed, unfortunately, in the drawing routine to allow them access to the changing global animation parameter t – in fact, indirectly through the variables hemisphereScaleFactor, petalAspectRatio and petalOpenAngle at the top of drawScene(), which change with t.

The parameters involved in configuring the stem, sepal and petal all change from a start value to an end one via linear interpolation using the animation parameter t. For example,

```
hemisphereScaleFactor = (1 - t) * 0.1 + t * 0.75
```

linearly changes hemisphereScaleFactor from 0.1 to 0.75 as t goes from 0 to 1.

Exercise 4.33. (Programming) Defining a display list in the drawing routine, as in floweringPlant.cpp, in order to parametrize it at run-time is unpleasant. A way around in floweringPlant.cpp, for example, would be to define sepal and petal classes (in the manner of the Point class in mouse.cpp) with member variables whose values can be specified at run-time. Try this.

4.5.3 Animation Projects

Exercise 4.34. (Programming) Starting from clown3.cpp, add to the clown's head a comical conical nose which changes in length and color, as well as eyes that rotate and change in size and color.

Exercise 4.35. (Programming) Animate a ball *rolling* down a fixed flat inclined plane. See Figure 4.42(a). The ball should not slip or slide. Make the plane a wireframe mesh of triangles and the ball a wireframe sphere, as well, so that relative motion is apparent.

Exercise 4.36. (Programming) Add physics to the preceding exercise by allowing the incline of the plane to be changed even as the ball rolls down, the latter's speed depending obviously on the angle of inclination.

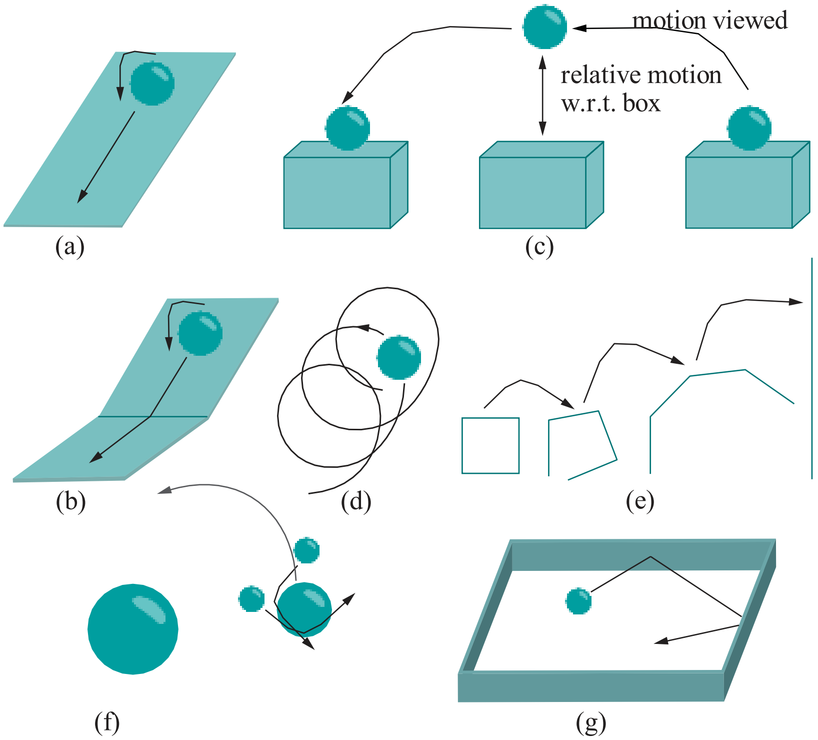

Figure 4.42: (a) Ball rolling down one plane (b) Ball rolling down two planes (c) Ball bouncing on a box (d) Ball traveling along a helix (e) Four segments opening from a square into a straight line (f) Solar system with a sun, one planet and two moons (g) Pool table with one ball.

Exercise 4.37. (Programming) Yet another extension of Exercise 4.35: add another plane at the bottom so that the ball rolls from the first onto the second. See Figure 4.42(b).

Exercise 4.38. (Programming) Roll a ball down the curved children's slide of Exercise 2.36 of Chapter 2, if you did that particular exercise.

Exercise 4.39. (Programming) Animate a ball bouncing up and down a box which itself moves in a straight line. See Figure 4.42(c).
Hint : First, code the straight-line motion of the box and, then, that of the ball *relative* to the box, being straight, too. The resultant motion of the ball as viewed in the OpenGL window, which is, of course, same as that seen by a stationary external observer, is parabolic. Incidentally, Remark 4.9 earlier about physical vs. equational animation is relevant here.

Exercise 4.40. (Programming) Make a ball travel a helical path. See Figure 4.42(d). Do this physically, *a la* ballAndTorus.cpp, and not equationally.

Exercise 4.41. (Programming) Animate four straight segments, which initially bound a square, smoothly opening into a straight line. See Figure 4.42(e), where the initial, final and two intermediate positions are depicted.
Hint: See the stem of floweringPlant.cpp.

Exercise 4.42. (Programming) Creating a solar system is a canonical exercise for beginning 3D programmers. First, animate a solitary planet, with two moons, in elliptic orbit around a stationary sun. See Figure 4.42(f). The planet rotates about its own axis as well, while its moons revolve about it at different speeds and on different orbital planes. Then, add more planets.

Exercise 4.43. (Programming) A spinning cube is another popular animation project which the reader likely has already encountered on-line (if not, a web search is in order). Make a spinning cube. Define the cube with glutWireCube() and control its rotation with mouse clicks (so that the cube wants to rotate "toward" the click).

Exercise 4.44. (Programming) Add a leaf to floweringPlant.cpp and make the whole blow in the wind.

Exercise 4.45. (Programming) Create an animated garden with the help of floweringPlant.cpp.

Exercise 4.46. (Programming) Make a lone cue ball travel on a pool table. The table should simply be a rectangle enclosed by four low walls – no need to make pockets. See Figure 4.42(g).

The ball should initially be stationary at a fixed position on the table. Then allow the user, with the help of a simple visual interface, to choose a direction and speed to get the ball moving – you don't need to draw a cue stick.

Animate the subsequent motion of the ball as it *rolls* along the surface of the table and *bounces* off its sides. You can either choose not to program in any deceleration, so that the ball keeps moving at uniform speed, or to incorporate frictional resistance to ultimately bring it to rest. Making the both the ball and table surface wireframe mesh will make the movement clear.

4.6 Viewing Transformation

We begin our discussion of the viewing transformation gluLookAt(), whose function is to arrange OpenGL's (imaginary) camera, by systematically deciphering its somewhat non-trivial syntax.

4.6.1 Understanding the Viewing Transformation

Think of the OpenGL camera as located at the origin with its lens pointing down the $-z$ direction (the *line of sight*) and with its top aligned along the $+y$ direction (the *up direction*). This, in fact, is the *default pose* of the OpenGL camera. See Figure 4.44(a).

Keep in mind, though, that the OpenGL camera is merely a *conceptual* device! The rendering we see of drawn objects is determined solely, as described in Chapter 2, by the shape of the viewing box or frustum, which in turn is decided by the programmer-specified projection statement (e.g., glOrtho() and glFrustum()). Figure 4.44(b) reminds us of the process. There is *no* camera as such!

Nevertheless, it appeals to the intuition to imagine that what we're viewing is through a camera. In the case of a viewing frustum, particularly, one can imagine a point camera at the origin with the film lying in front of it on the viewing face, as indicated in Figure 4.44(b). It's intuitive as well to think of changing the view by moving and turning the camera. This is exactly where the viewing transformation gluLookAt() comes in.

Now, the command gluLookAt(*eyex*, *eyey*, *eyez*, *centerx*, *centery*, *centerz*, *upx*, *upy*, *upz*) *simulates* – mark the word *simulates* – OpenGL's camera first being moved to the location *eye* = (*eyex* , *eyey* , *eyez*), then pointed at *center* = (*centerx* , *centery* , *centerz*), and, finally, rotated about its line of sight (*los*) – the line joining *eye* to *center* – so that its up direction is one determined from *up* = (*upx* , *upy* , *upz*). See Figure 4.43. We'll see shortly how the up direction is, in fact, determined by *up*.

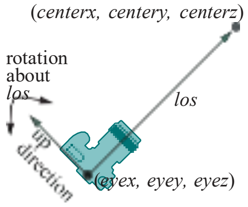

Figure 4.43: Camera pose determined by gluLookAt(*eyex*, *eyey*, *eyez*, *centerx*, *centery*, *centerz*, *upx*, *upy*, *upz*).

Remark 4.12. The viewing transformation gluLookAt() logically then is a function of *three* parameters, each a 3D point or vector.

Remark 4.13. For now, we ask the reader to assume that we have a viewing frustum defined by a glFrustum() statement, rather than a viewing box by glOrtho(), as the point camera is logically placed at the origin in the case of the former, but it's not evident where to place it for the latter. However, this apparent problem will be sorted out as soon as the working of gluLookAt() becomes clear.

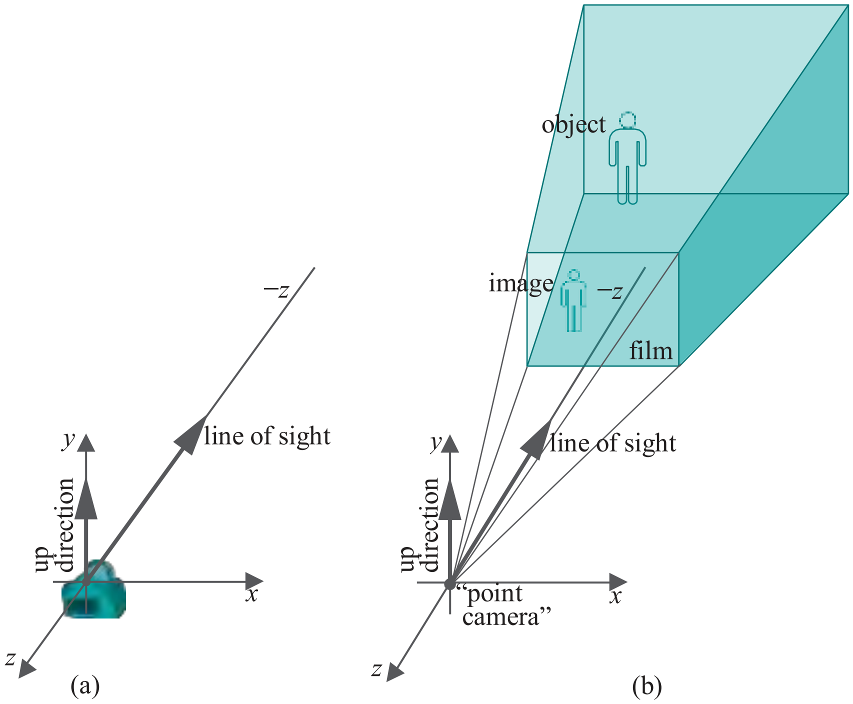

Figure 4.44: (a) The (conceptual) OpenGL camera's default pose (b) A (conceptual) point camera at the origin with film on the viewing plane of the frustum.

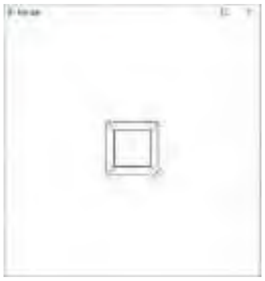

Figure 4.45: Screenshot of box.cpp with gluLookAt() instead of glTranslatef().

Experiment 4.28. Replace the translation command

```
glTranslatef(0.0, 0.0, -15.0)
```

of box.cpp with the viewing command

```
gluLookAt(0.0, 0.0, 15.0, 0.0, 0.0, 0.0, 0.0, 1.0, 0.0)
```

There is no change in what is viewed (Figure 4.45). In fact, the commands glTranslatef(0.0, 0.0, -15.0) and gluLookAt(0.0, 0.0, 15.0, 0.0, 0.0, 0.0, 0.0, 1.0, 0.0) are *exactly equivalent*. End

To understand why the two statements are equivalent, note that gluLookAt(0.0, 0.0, 15.0, 0.0, 0.0, 0.0, 0.0, 1.0, 0.0) takes the *eye* to (0, 0, 15), looking down the *z*-axis toward the *center* at (0, 0, 0), the frustum (whose apex is the eye) traveling with it. Assume the camera's up direction remains unchanged. Now, compare Figures 4.46(a) and (b): should the box appear different in the first (the frustum translated back) than the second (the box translated forward)? *No*, because its position relative to the frustum is the same in both.

The convenience of the command gluLookAt() over glTranslatef() in this program is that we have been able to arrange the camera according to how we want to shoot the box, rather than moving the box itself.

As box.cpp with gluLookAt() instead of glTranslatef(), as in the preceding experiment, is used often, the modified program is stored as boxWithLookAt.cpp.

Experiment 4.29. Continue the previous experiment, or run boxWithLookAt.cpp, successively changing only the parameters *centerx*, *centery*, *centerz* – the middle three – of the gluLookAt() call to the following:

1. 0.0, 0.0, 10.0

2. 0.0, 0.0, −10.0

3. 0.0, 0.0, 20.0

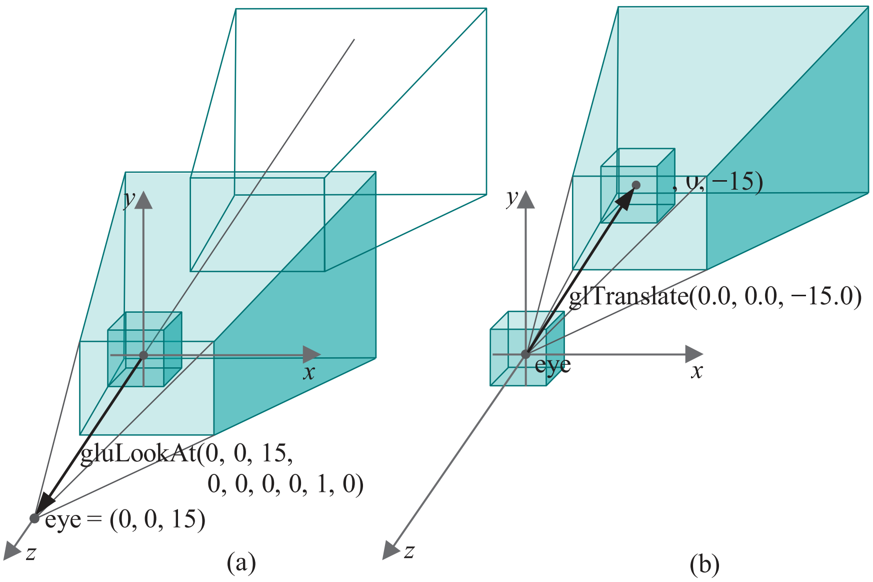

Figure 4.46: (a) gluLookAt(): the outlined frustum is the original viewing frustum, the solid one is where it's translated by the gluLookAt() call, the box doesn't move. (b) glTranslatef(): the viewing frustum doesn't move, rather the box is translated by the glTranslatef() call.

4. 0.0, 0.0, 15.0

End

The view does not change with the two parameter sets 1 and 2 of the experiment as the viewer's line of sight from eye to center does not change. Figures 4.47(a) and (b) show the respective configurations. Set 3 (Figure 4.47(c)) produces a blank screen because the eye is looking the "wrong way". The last set (Figure 4.47(d)) confuses OpenGL because eye and center coincide, making it impossible to decide a line of sight. Again a blank screen appears. Note in all cases that the shape of the frustum is not changed by gluLookAt(), only its placement and alignment.

Here are a few more *center* sets for you to try.

Exercise 4.47. (Programming) Restore the original boxWithLookAt.cpp program with its gluLookAt(0.0, 0.0, 15.0, 0.0, 0.0, 0.0, 0.0, 1.0, 0.0). Next, successively change only the parameters *centerx*, *centery*, *centerz* – the middle three of gluLookAt() – to the following, drawing diagrams as in Figure 4.47 to explain what is seen in each case:

1. 5.0, 0.0, 0.0 (*Answer*: See Figure 4.47(e))
2. −5.0, 0.0, 0.0
3. 0.0, 5.0, 0.0
4. 0.0, −5.0, 0.0
5. 5.0, 5.0, 0.0

Let's change the *eye* next, which still is pretty much the same game as changing *center*.

Exercise 4.48. (Programming) Restore the original boxWithLookAt.cpp program with its gluLookAt(0.0, 0.0, 15.0, 0.0, 0.0, 0.0, 0.0, 1.0, 0.0) call. Then replace the box with a glutWireTeapot(5.0), a non-symmetric object. Next, successively change only the parameters *eyex*, *eyey*, *eyez* – the first three of gluLookAt() – to the following, drawing diagrams as in Figure 4.47 to explain what is seen in each case:

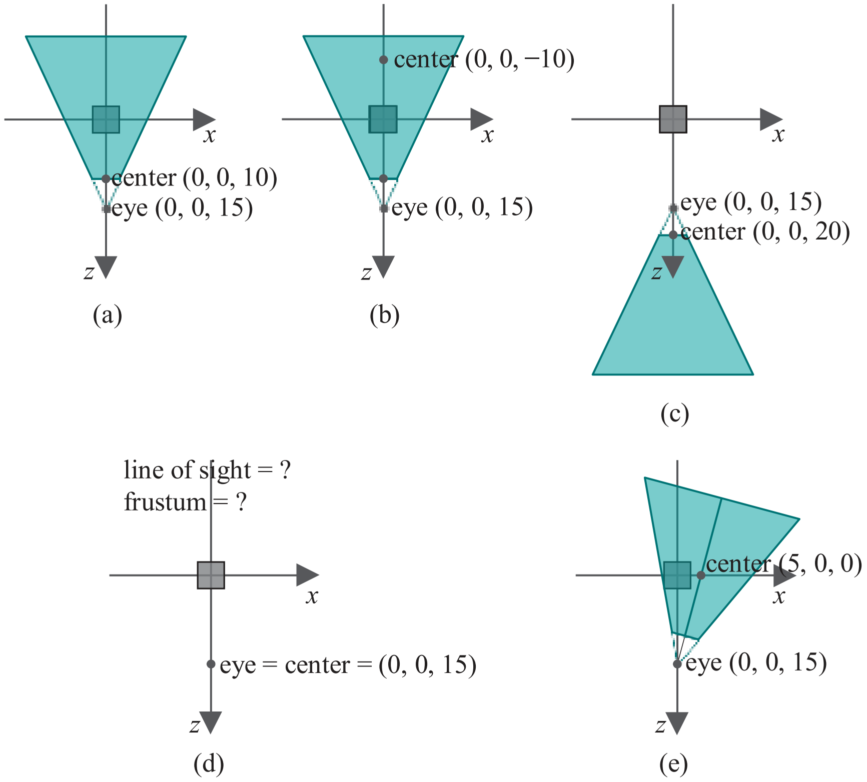

Figure 4.47: Sectional diagrams of the (simulated) configuration of the eye and frustum for various gluLookAt() calls in boxWithLookAt.cpp.

1. 0.0, 0.0, 10.0

2. 0.0, 0.0, 25.0

3. 0.0, 0.0, −15.0

4. 15.0, 0.0, 15.0

5. 15.0, 0.0, 0.0

6. 15.0, 15.0, 15.0

Let's get a feel now for how the up vector $up = (upx, upy, upz)$ works.

Experiment 4.30. Restore the original boxWithLookAt.cpp program with its gluLookAt(0.0, 0.0, 15.0, 0.0, 0.0, 0.0, 0.0, 1.0, 0.0) call and, again, first replace the box with a glutWireTeapot(5.0). Run: a screenshot is shown in Figure 4.48(a). Next, successively change the parameters upx , upy , upz – the last three parameters of gluLookAt() – to the following:

1. 1.0, 0.0, 0.0 (Figure 4.48(b))

2. 0.0, −1.0, 0.0 (Figure 4.48(c))

3. 1.0, 1.0, 0.0 (Figure 4.48(d))

Screenshots of the successive cases are shown in Figures 4.48(b)-(d). The camera appears to *rotate* about its line of sight, the z-axis, so that its up direction points along the up vector (upx, upy, upz) each time. End

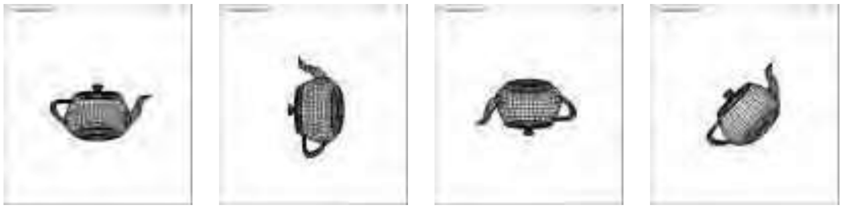
(a) (b) (c) (d)

Figure 4.48: Screenshots from Experiment 4.30.

Before we can state the rule for how the *up* vector determines the camera's up direction generally, here are some facts about the dot product of vectors which we'll need. Skip this part if you already have dot product basics.

Sidebar on Dot Products

The *dot product* (also called *scalar product*) of two vectors u and v in $\mathbb{R}^3$ is a scalar, denoted $u \cdot v$, defined as follows:

(a) if either of u or v is zero, then $u \cdot v$ is zero;

(b) if not, then the value of $u \cdot v$ is $|u||v| \cos\theta$, where θ is the angle between u and v.

See Figure 4.49.

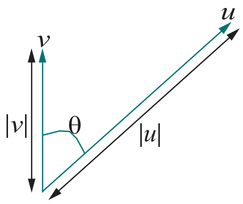

Figure 4.49: Taking the dot product: $u \cdot v = |u||v| \cos\theta$.

It turns out that $u \cdot v$ is given by the following simple formula, where $u = (u_x, u_y, u_z)$ and $v = (v_x, v_y, v_z)$:

$$u \cdot v = u_x v_x + u_y v_y + u_z v_z \tag{4.4}$$

This makes the dot product useful in calculating angles between pairs of vectors.

Example 4.4. Determine the angle θ between the two vectors $u = (1, 0, 2)$ and $v = (-2, 3, 4)$.

Answer:

$$|u||v| \cos\theta = u \cdot v = u_x v_x + u_y v_y + u_z v_z = 1 * -2 + 0 * 3 + 2 * 4 = 6$$

Therefore,

$$\cos\theta = \frac{6}{|u||v|} = \frac{6}{\sqrt{1^2 + 0^2 + 2^2}\ \sqrt{(-2)^2 + 3^2 + 4^2}} = \frac{6}{\sqrt{5}\sqrt{29}} \approx 0.49827$$

which gives $\theta \approx 60.11439^\circ$.

Exercise 4.49. Determine the angle between each pair from the three vectors $(1, 0, 0)$, $(\frac{1}{\sqrt{2}}, \frac{1}{\sqrt{2}}, 0)$ and $(\frac{1}{\sqrt{3}}, \frac{1}{\sqrt{3}}, \frac{1}{\sqrt{3}})$.

Exercise 4.50. Prove the following about dot products where u, v and w are any three vectors and c any scalar:

(a) Assuming that they are both non-zero, u and v are perpendicular if and only if $u \cdot v = 0$ (*perpendicularity test*)

(b) $u \cdot u = |u|^2$

(c) $u \cdot v = v \cdot u$ (*dot product is commutative*)

(d) $(cu) \cdot v = u \cdot (cv) = c(u \cdot v)$

(e) $u \cdot (v + w) = u \cdot v + u \cdot w$ (*dot product distributes over a sum*)

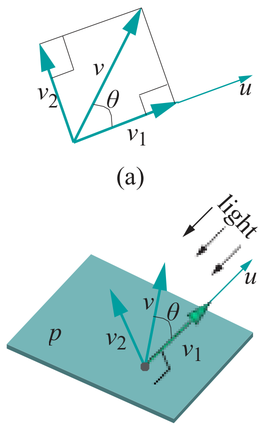

(a)

(b)

Figure 4.50: (a) Splitting v into components v_1 and v_2, parallel and perpendicular to u, respectively (b) v_2 as the "shadow" of v on a plane p perpendicular to u.

(f) $|u \cdot v| \leq |u||v|$

A particularly useful application of the dot product is when one wants to split a given vector v as $v = v_1 + v_2$, where the components v_1 and v_2 are, respectively, parallel and perpendicular to another given non-zero vector u. See Figure 4.50(a). An intuitive way to think of v_2 is as the shadow of v cast on a plane p perpendicular to u by a light shining from the direction of u, as depicted in Figure 4.50(b); $v_1 = v - v_2$, on the other hand, can be thought of as the part of v "following" u.

The component v_1 is the orthogonal projection of v onto the line of u, so its *signed length* is (see the triangle with sides v and v_1 in Figure 4.50(a))

$$|v| \cos\theta = \frac{|u||v| \cos\theta}{|u|} = \frac{u \cdot v}{|u|}$$

where θ is the angle between u and v. Multiplying the value of the signed length by the unit vector in the direction of u, which is $u/|u|$, one obtains the formula for v_1:

$$v_1 = \frac{u \cdot v}{|u|^2} u \tag{4.5}$$

The formula for the component v_2 of v that is perpendicular to u follows, as the sum of v_1 and v_2 is v:

$$v_2 = v - v_1 = v - \frac{u \cdot v}{|u|^2} u \tag{4.6}$$

The preceding formulae have particularly simple forms if u is a unit vector as we spell out in the trivial exercise following.

Exercise 4.51. If u is a unit vector and v arbitrary, prove the following:

(a) The component of v parallel to u is $v_1 = (u \cdot v)\, u$.

(b) The component of v perpendicular to u is $v_2 = v - (u \cdot v)\, u$.

Example 4.5. Split $v = (-2, 3, 4)$ into components parallel and perpendicular to $u = (1, 0, 2)$.

Answer: The component parallel to u is

$$v_1 = \frac{u \cdot v}{|u|^2} u = \frac{6}{5}(1, 0, 2) = (1.2, 0, 2.4)$$

and that perpendicular to u is

$$v_2 = v - v_1 = (-2, 3, 4) - (1.2, 0, 2.4) = (-3.2, 3, 1.6)$$

The following worked example shows a neat matrix expression for the component of one vector parallel to another.

Example 4.6. Show that if $u = [u_x\ u_y\ u_z]^T$ and $v = [v_x\ v_y\ v_z]^T$ are two vectors in $\mathbb{R}^3$, such that u is not zero, then the component v_1 of v parallel to u is given by

$$v_1 = \frac{1}{|u|^2} \begin{bmatrix} u_x^2 & u_x u_y & u_x u_z \\ u_x u_y & u_y^2 & u_y u_z \\ u_x u_z & u_y u_z & u_z^2 \end{bmatrix} v$$

(T standing for transpose, $[\ldots]^T$ is a vector written as a column matrix).

Answer: We have that the component of v parallel to u is

$$\begin{aligned}
v_1 &= \frac{u \cdot v}{|u|^2}\, u && \text{(shown earlier in (4.5))} \\
&= \frac{1}{|u|^2}(u^T v)u && (u^T v \text{ is a scalar equal to } u \cdot v\text{, the lone entry in} \\
& && \text{the } 1 \times 1 \text{ product matrix } u^T v) \\
&= \frac{1}{|u|^2}\, u(u^T v) && (\text{as } (u^T v)u = u(u^T v)\text{, where } u^T v \text{ denotes a scalar} \\
& && \text{on the LHS here and a } 1 \times 1 \text{ matrix on the RHS)} \\
&= \frac{1}{|u|^2}(uu^T)v && \text{(by associativity)} \\
&= \frac{1}{|u|^2}\begin{bmatrix} u_x^2 & u_xu_y & u_xu_z \\ u_xu_y & u_y^2 & u_yu_z \\ u_xu_z & u_yu_z & u_z^2 \end{bmatrix} v && (\text{multiplying } u \text{ and } u^T \text{ as matrices})
\end{aligned}$$

For a more thorough discussion of dot products refer to any book on linear algebra, e.g., Banchoff and Wermer [7].

Back to OpenGL

It's simple now to explain how OpenGL uses the *up* = (*upx, upy, upz*) vector to align the top of its camera – in other words, determine its up direction – upon the call gluLookAt(*eyex*, *eyey*, *eyez*, *centerx*, *centery*, *centerz*, *upx*, *upy*, *upz*).

Denote the camera's line of sight vector (*centerx, centery, centerz*) − (*eyex, eyey, eyez*) by *los*. Now, evidently the camera's true up direction has to be perpendicular to the *los*: just think of a real camera which can spin about its *los*, with its lens always pointing down the *los* and its top perpendicular to the *los*.

Accordingly, what OpenGL does is split *up* into components up_1 and up_2 parallel and perpendicular, respectively, to *los*. The up direction is then taken to be up_2. In particular, think of the camera, which is located at *eye* = (*eyex, eyey, eyez*) and pointing down *los*, as being rotated about *los* till its top points in the direction parallel to up_2.

For an example, see Figure 4.51. Imagine the camera lying with its back on this page (call it the plane *p*) facing up, so that the line of sight *los* emerges perpendicularly from *p* (toward the reader). The specified *up* vector is drawn in the figure starting from the camera, as also its components up_1 and up_2, the latter lying on the page. The camera, then, is rotated about *los* with its back always on the page till its top points along up_2.

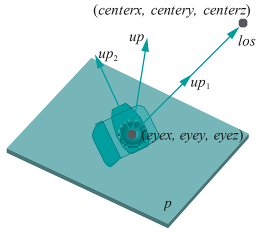

Figure 4.51: The camera is seen face-forward so that its back-plane *p* lies on the page. The line of sight *los* comes perpendicularly up from the page toward the reader. The components of the vector *up*, parallel and perpendicular to *los*, respectively, are up_1 and up_2 (the latter lying on the page).

Remark 4.14. A common mistake is to think of the up direction as the one from *eye* to *up*, in other words, equal to (*upx, upy, upz*) − (*eyex, eyey, eyez*), in analogy to how *los* is determined. *It is not*! In fact, *up* = (*upx, upy, upz*) is *itself* the up direction. So, when finding its components parallel and perpendicular to *los*, imagine both starting at the same point. If you prefer to think of this start point as the point camera, simply imagine the vector *up* = (*upx, upy, upz*) to be parallely transported from the origin to start there; of course, then the component up_2, perpendicular to *los*, starts at the point camera too and it's convenient to imagine the camera rotating about its line of sight to align its top with up_2.

The magnitude of *up* or of up_2 is of no consequence as long as it's not zero, because it's only the direction that matters in aligning the top; if either is zero, then OpenGL is unable to determine the alignment and renders a blank screen.

Exercise 4.52. Of course, if *up* is zero then its component up_2 is zero. Can it happen that *up* is non-zero and yet up_2 is zero?

Experiment 4.31. Replace the wire cube of boxWithLookAt.cpp with a glutWireTeapot(5.0) and replace its gluLookAt() call instead with:

```
gluLookAt(0.0, 0.0, 15.0, 0.0, 0.0, 0.0, 1.0, 1.0, 1.0)
```

The vector *los* = (0.0, 0.0, 0.0) − (0.0, 0.0, 15.0) = (0.0, 0.0, −15.0), which is down the z-axis. The component of *up* = (1.0, 1.0, 1.0), perpendicular to the z-axis, is (1.0, 1.0, 0.0), which, therefore, is the up direction. Is what you see the same as Figure 4.48(d), which, in fact, is a screenshot for gluLookAt(0.0, 0.0, 15.0, 0.0, 0.0, 0.0, 1.0, 1.0, 0.0)? End

Exercise 4.53. (Programming) Change (*upx*, *upy*, *upz*) of gluLookAt() in boxWithLookAt.cpp to (0.0, 0.0, 1.0). What do you see? *Nothing*! Why?

Exercise 4.54. Compute the direction of the top of the camera for each of the following viewing transformations:

(a) gluLookAt(0.0, 0.0, 5.0, 5.0, 0.0, 0.0, 0.0, 1.0, 1.0)

(b) gluLookAt(0.0, 5.0, 5.0, 0.0, 0.0, 0.0, 1.0, 1.0, 1.0)

(c) gluLookAt(10.0, 5.0, 5.0, 0.0, 5.0, 0.0, 5.0, 1.0, 1.0)

(d) gluLookAt(10.0, 10.0, 5.0, 0.0, 5.0, 0.0, 1.0, 2.0, 3.0)

Part answer:

(a) The line of sight vector

$$\begin{aligned} los &= (centerx, centery, centerz) - (eyex, eyey, eyez) \\ &= (5, 0, 0) - (0, 0, 5) = (5, 0, -5) \end{aligned}$$

The component of $up = (0, 1, 1)$ perpendicular to los is

$$\begin{aligned} up_2 &= up - \frac{los \cdot up}{|los|^2} los \\ &= (0, 1, 1) - \frac{(5, 0, -5) \cdot (0, 1, 1)}{50} (5, 0, -5) \\ &= (0, 1, 1) + \frac{1}{10} (5, 0, -5) \\ &= (0.5, 1, 0.5) \end{aligned}$$

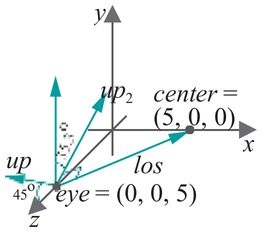

Figure 4.52: Solution to Exercise 4.54(a).

which, therefore, is the direction of the top of the camera. It is perpendicular, of course, to the line of sight and, as easily verified, rotated about 35.3° from the direction of the y-axis, the default top direction. See Figure 4.52.

The answer can be verified by alternately plugging

```
gluLookAt(0.0, 0.0, 5.0, 5.0, 0.0, 0.0, 0.0, 1.0, 1.0)
```

and

```
gluLookAt(0.0, 0.0, 5.0, 5.0, 0.0, 0.0, 0.5, 1.0, 0.5)
```

into boxWithLookAt.cpp to see the same (partly clipped) box shown in Figure 4.53. Incidentally, make sure you understand why the *up* vector is drawn as it is in Figure 4.52 – refer to Remark 4.14 if you need to.

Figure 4.53: Checking the solution to Exercise 4.54(a).

Remark 4.15. Collectively, the modeling transformations glTranslatef(), glRotatef() and glScalef() and the viewing transformation gluLookAt() are called *modelview transformations*.

Exercise 4.55. (Programming) Program a camera flying at a height over a sequence of balls arranged along the x-axis, looking ahead and down at them. See Figure 4.54, where coordinates for the eye and center are suggested.

Exercise 4.56. (Programming) Place a wire teapot centered at the origin. Program a camera which can be moved by the user anywhere on an imaginary sphere enclosing the teapot, the direction of the camera being always toward the origin. Appropriately program keys to move the camera. See Figure 4.55, where a couple of positions of the camera are indicated.

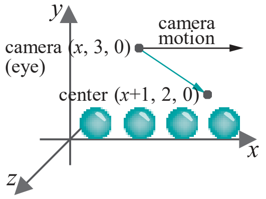

Figure 4.54: Camera flying over balls.

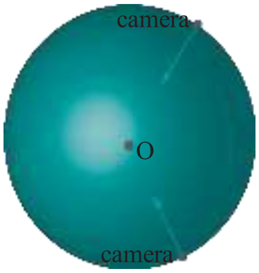

Figure 4.55: Camera rotated on an imaginary sphere enclosing a teapot.

4.6.2 Simulating a Viewing Transformation with Modeling Transformations

You can skip this section on a first reading.

When we introduced gluLookAt() we said that it *simulates* OpenGL camera movement. This is exactly right. The OpenGL camera *never* leaves its default pose at the origin with its lens pointing down the $-z$ direction and with its top aligned along the $+y$ direction. In other word, the viewing frustum (or box) stays put at where it was first created with glFrustum() (or glOrtho()).

In fact, the viewing transformation is simulated by replacing it with an equivalent sequence of modeling transformations. We actually saw a simple example of this earlier in Section 4.6.1 where the commands gluLookAt(0.0, 0.0, 15.0, 0.0, 0.0, 0.0, 0.0, 1.0, 0.0) and glTranslatef(0.0, 0.0, -15.0) were found to be equivalent.

Here's a motivating thought experiment for the general case:

You are out on an open field with a friend and a camera. She stands 10 meters in front of you, but looking through the viewfinder you think she should be, say, 3 meters closer. There are two options: (1) you, i.e., the camera, translate (walk) 3 meters toward her, or (2) she, i.e., the scene, translates 3 meters toward you. See the top left of Figure 4.56. The picture is same in either case. Ignore the backdrop, as it's a homogeneous open field!

Here's another way to arrive at the equivalence of the two options. Say you had already applied (1) when the guy you had borrowed the camera from starts yelling that it's really expensive and would you mind not moving it around but just keep it where it was first set up. In other words, you have to manage by rearranging the scene instead. So, to undo the effect of (1) and bring the camera back to its original position, you apply the reverse of (1) to *both* camera and scene (so as not to alter the picture). The result, of course, is the same as applying just (2) in the first place. See the two diagrams in the big box on the lower left of Figure 4.56.

Looking through the viewfinder again, you feel it'll be a nicer composition if your friend stands not at the center of the frame but to a side. Again, (1) you can rotate the camera, say, 45° *clockwise*, or (2) your friend can sidle 45° *counter-clockwise* along a circle centered where you are, as in the top right of Figure 4.56. The picture is exactly the same in either case. And, again, one can imagine arriving at (2) by first applying (1), and then undoing it by applying the reverse of (1) to both camera and scene, as the two diagrams in the big box on the lower right of Figure 4.56 indicate.

It should now be fairly straightforward understanding the equivalence of a viewing transformation to a sequence of modeling transformations. The transformation

gluLookAt(*eyex, eyey, eyez, centerx, centery, centerz, upx, upy, upz*)

asks that the camera be (i) first translated to the position (*eyex*, *eyey*, *eyez*), then, (ii) rotated at that position till it's pointing at (*centerx*, *centery*, *centerz*) and, finally, (iii) rotated about its line of sight till its up direction is parallel to the vector up_2, the component of (*upx*, *upy*, *upz*) perpendicular to the line of sight.

Let's move the camera as asked. Figure 4.57(a) shows the resulting configuration. Next – it's the owner yelling again – we'll restore the camera to its default pose by

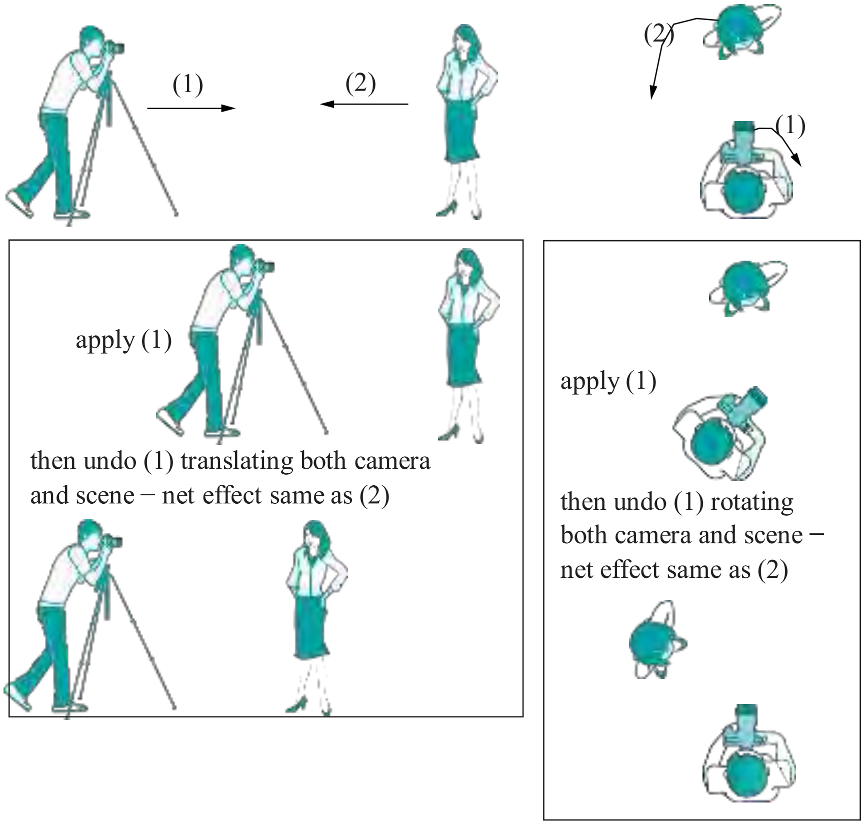

Figure 4.56: Relative movement of the camera and scene.

incrementally undoing its movements, moving instead the scene as in the preceding thought experiment. The sum total, then, of these reverse movements to bring the camera back to default will be equivalent to the viewing transform.

The first translation is undone by applying glTranslatef($-eyex$, $-eyey$, $-eyez$). The camera is then at the origin, but still pointing parallel to the line of sight vector

$$los = (centerx, centery, centerz) - (eyex, eyey, eyez)$$

and with its top still parallel to up_2. See Figure 4.57(b).

Suppose that p is a plane that contains both los and the z-axis – shaded in the figure. If los does not lie along the z-axis, then p is unique; if it does, then p can be any plane that contains the common line. Choose a non-zero vector $w = (wx, wy, wz)$ perpendicular to p, i.e., w is perpendicular to both los and the z-axis. Let A be the angle from los to $-z$ on the plane p measured counter-clockwise when looking down from w.

Note: Of course, if los lies along the z-axis then we need to do a 180° rotation only if it is pointing in the $+z$ direction; otherwise, if it is pointing already in the $-z$ direction there is nothing to do.

Applying glRotatef(A, wx, wy, wz) then rotates the camera till its line of sight matches the $-z$ direction. Moreover, its top then is parallel to the vector, call it up^1_2, which is the result of glRotatef(A, wx, wy, wz) applied to up_2.

Now, up^1_2, the new top direction, is perpendicular to the z-axis because the same rotation glRotatef(A, wx, wy, wz) was applied in the previous step to los and up_2, which were perpendicular, to obtain the vector toward $-z$ and up^1_2, respectively. Therefore, up^1_2 lies on the xy-plane. See Figure 4.57(c) where the camera is seen from the negative side of the z-axis.

Finally, all that remains to restore the camera to its default position is a rotation

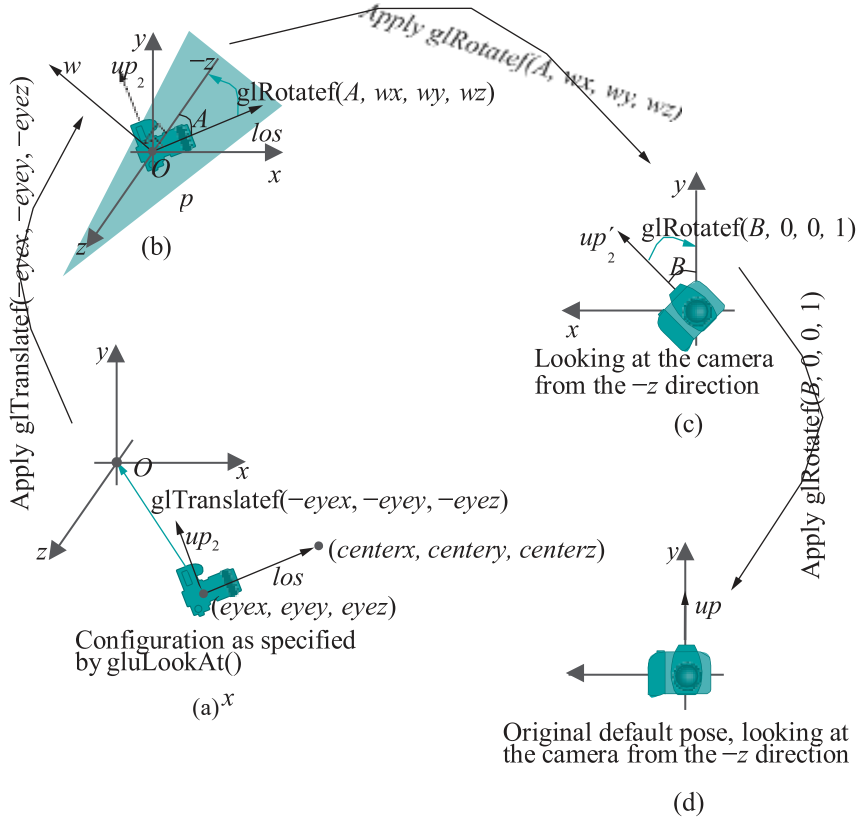
Apply glRotatef(A, wx, wy, wz)
y
w
up
2
−z
glRotatef(A, wx, wy, wz)
A
los
O
x
p
z
(b)
Apply glTranslatef(−eyex, −eyey, −eyez)
y
up′
2
glRotatef(B, 0, 0, 1)
B
x
Looking at the camera
from the −z direction
(c)
Apply glRotatef(B, 0, 0, 1)
y
O
x
glTranslatef(−eyex, −eyey, −eyez)
z
up2
(centerx, centery, centerz)
los
(eyex, eyey, eyez)
Configuration as specified
by gluLookAt()
(a)
x
y
up
Original default pose, looking at
the camera from the −z direction
(d)

Figure 4.57: Restoring the camera from gluLookAt(*eyex*, *eyey*, *eyez*, *centerx*, *centery*, *centerz*, *upx*, *upy*, *upz*) to its default pose: green arrows indicate intended movements, which actually applied take the camera to the next configuration in the sequence (a)-(d).

glRotatef(B, 0.0, 0.0, 1.0), of angle B about the z-axis, to align its top along $+y$. See Figure 4.57(d).

We conclude that the viewing transformation

gluLookAt(*eyex*, *eyey*, *eyez*, *centerx*, *centery*, *centerz*, *upx*, *upy*, *upz*)

is, indeed, equivalent to a sequence of modeling transformations, in particular, a translation followed by two rotations:

```
glRotatef(B, 0.0, 0.0, 1.0);
glRotatef(A, wx, wy, wz);
glTranslatef(−eyex, −eyey, −eyez);
```

We do not attempt to express the parameters A, B, wx, wy and wz in terms of the parameters $eyex$, $eyey$, . . ., upz of the gluLookAt() command. Generally, this would be a tedious computation, but for simple settings of the camera it is not as the experiment next shows.

Experiment 4.32. Replace the one modeling transformation statement of box.cpp with the block:

```
gluLookAt(0.0, 0.0, 15.0, 15.0, 0.0, 0.0, 0.0, 1.0, 0.0);

// glRotatef(45.0, 0.0, 1.0, 0.0);
// glTranslatef(0.0, 0.0, -15.0);
```

Run. Next, both comment out the viewing transformation and uncomment the two modeling transformations following it. Run again. The displayed output, shown in Figure 4.58, is the same in both cases. The reason, as Figures 4.59(a)-(c) explain, is that the viewing transformation is equivalent to the modeling transformation block. In particular, the former is undone by the latter. End

Figure 4.58: Screenshot from Experiment 4.32.

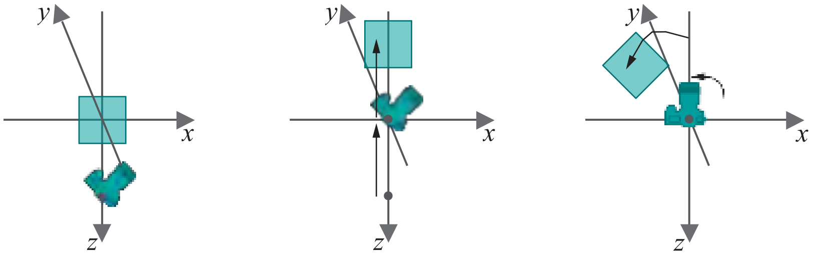

gluLookAt(0.0, 0.0, 15.0,
15.0, 0.0, 0.0, 0.0, 1.0, 0.0);
(a)

glTranslatef(0.0, 0.0, −15.0);
(b)

glRotatef(45.0, 0.0, 1.0, 0.0);
glTranslatef(0.0, 0.0, −15.0);
(c)

Figure 4.59: Viewing transformation equivalent to a sequence of modeling transformations.

Exercise 4.57. **(Programming)** Replace the modeling transformation statement of box.cpp with:

```
gluLookAt(-30.0, 0.0, 30.0, 0.0, 0.0, 0.0, 0.0, 1.0, 0.0);

// glRotatef(45.0, 0.0, 1.0, 0.0);
// glTranslatef(30.0, 0.0, -30.0);
```

Draw diagrams as in Figure 4.59 to show the equivalence of the viewing transformation and the modeling transformation block following it.

Exercise 4.58. Show that the viewing transformation

```
gluLookAt(30.0, 0.0, 30.0, 0.0, 0.0, 0.0, 1.0, 0.0, -1.0);
```

is equivalent to the sequence

```
glRotatef(90, 0.0, 0.0, 1.0);
glRotatef(45, 0.0, -1.0, 0.0);
glTranslatef(-30.0, 0.0, -30.0);
```

of modeling transformations. Pay particular attention to the alignment of the top of the camera.

Exercise 4.59. The sequence of modeling transformations equivalent to a given viewing transformation is not unique. In fact, for the preceding exercise find a sequence of modeling transformations, different from the one given, yet equivalent to the viewing transformation there.

Exercise 4.60. What sequence of modeling transformations is equivalent to each of the following viewing transformations:

(a) gluLookAt(0.0, 0.0, 0.0, -15.0, 0.0, 15.0, 0.0, 1.0, 0.0)

(b) gluLookAt(0.0, 0.0, 15.0, 0.0, 0.0, 0.0, 1.0, 0.0, 0.0)

(c) gluLookAt(0.0, 0.0, 15.0, -15.0, 0.0, 0.0, 1.0, 0.0, -1.0)

(d) gluLookAt(0.0, 0.0, 15.0, 0.0, 1.0, 14.0, 0.0, 1.0, 0.0)

(e) gluLookAt(0.0, 0.0, 15.0, 0.0, 1.0, 14.0, 1.0, 0.0, 0.0)

Part answer:

(c) One solution:

```
glRotatef(90, 0.0, 0.0, 1.0);
glRotatef(-45, 0.0, 1.0, 0.0);
glTranslatef(0.0, 0.0, -15.0);
```

Exercise 4.61. What is the viewing transformation equivalent to the following sequence of modeling transformations:

```
glRotatef(45.0, 0.0, 1.0, 0.0);
glTranslatef(0.0, 0.0, -5.0);
```

Remark 4.16. It's invariably good programming practice for there to be at most a single viewing transformation in a program, which comes in the code before all modeling transformations; in other words, the viewing transformation is applied last. Logically, this means that objects are drawn first and placed as desired with respect to each other using modeling transformations and, then, a gluLookAt() is applied *finally* to transport the *entire* scene together.

Exercise 4.62. A programmer writes the following at the top of his drawing routine:

```
gluLookAt(0.0, 10.0, 10.0, 0.0, 0.0, 0.0, 0.0, 1.0, 0.0);
gluLookAt(0.0, 0.0, 15.0, 0.0, 0.0, 0.0, 0.0, 1.0, 0.0);
```

As it is bad practice to have two gluLookAt() statements like this, replace them with one gluLookAt() having the same effect.

Exercise 4.63. A programmer writes the following at the top of his drawing routine:

```
glRotatef(45.0, 0.0, 1.0, 0.0);
gluLookAt(10.0, 0.0, 10.0, 0.0, 0.0, 0.0, 0.0, 1.0, 0.0);
```

However, a transformation preceding the gluLookAt() statement in the drawing routine is bad practice – gluLookAt() should be the first transformation. So, combine the above two statements into one gluLookAt() having the same effect.

Exercise 4.64. A program A.cpp places a sphere with

```
gluLookAt(0.0, 0.0, 10.0, 0.0, 0.0, 0.0, 0.0, 1.0, 0.0);
glutWireSphere(2.0, 10, 8);
```

with the viewing frustum defined by

```
glFrustum(-5.0, 5.0, -5.0, 5.0, 5.0, 100.0);
```

while program B.cpp places a sphere with

```
gluLookAt(0.0, 0.0, 55.0, 0.0, 0.0, 0.0, 0.0, 1.0, 0.0);
glutWireSphere(2.0, 10, 8);
```

with the viewing frustum defined by

```
glFrustum(-5.0, 5.0, -5.0, 5.0, 50.0, 100.0);
```

Assume no other modelview transformation applies to the sphere in either program and that the OpenGL windows are declared to be of the same square size in both. Does the sphere appear to be of the same size in both programs or bigger in one?

Remark 4.17. Earlier this section, in Remark 4.13 we asked the reader to assume that we had a viewing frustum defined by a glFrustum() statement, rather than a glOrtho()-defined viewing box, because a point camera is logically placed at the origin in case of the former, but it's not clear where to place it for the latter.

So what happens when one applies gluLookAt() in the drawing routine when the projection statement, in fact, is a glOrtho()? The answer, as the reader has probably already guessed, is that OpenGL simply replaces the viewing transformation with its corresponding sequence of modeling transformations *whatever* may be the projection statement.

Remark 4.18. We have been insistent that the viewing transformation gluLookAt()'s purported manipulation of the camera is simulated entirely by modeling transformations. Indeed, we showed in this section how this can be done. But, is this *really* what OpenGL does? For, it's plausible that OpenGL actually does move the viewing frustum, with the camera at its apex, as directed by a gluLookAt() call, rather than apply any modeling transformations. For example, is Figure 4.46(a) or (b) in Section 4.6.1 the "truth"? How to decide?

Here's how. Modeling transformations change the current modelview matrix at the top of the modelview matrix stack. The viewing frustum, on the other hand, is determined by the current projection matrix at the top of the projection matrix stack, which is altered, among others, by projection statements such as glFrustum(). A way to find out then what really happens inside the OpenGL engine is to read both the current modelview and projection matrices, both before and after issuing a gluLookAt(), and see which changes.

So what does happen? Only the current modelview matrix changes! The current projection matrix remains at the value it had prior to the gluLookAt() call. Take this in good faith now – you'll be able to verify the claim when we learn to access the modelview and projection matrix stacks in Chapter 5. In fact, we'll see then that the modelview matrix changes exactly as if multiplied on the right by the matrices corresponding to a sequence of modeling transformations equivalent to the given viewing transformation.

Remark 4.19. An interesting upshot of all this is that viewing transformations are not really needed, as any such transformation can always be manufactured from modeling transformations. Later versions of OpenGL, as we shall see, take this thought to heart, discarding gluLookAt() altogether.

4.6.3 Orientation and Euler Angles

This section may be skipped on a first reading. You will need it, though, before Section 6.4 about animating orientation with the help of Euler angles.

The viewing transformation leads nicely to a method of specifying the orientation of a camera. Recall the conclusion in Section 4.6.2 that the viewing transformation

gluLookAt($eyex$, $eyey$, $eyez$, $centerx$, $centery$, $centerz$, upx, upy, upz)

is equivalent to a translation followed by two rotations:

glRotatef(B, 0.0, 0.0, 1.0);
glRotatef(A, wx, wy, wz);
glTranslatef($-eyex$, $-eyey$, $-eyez$);

The axis of the particular rotation glRotatef(A, wx, wy, wz) is variable and depends on the line of sight. It was chosen, in fact, perpendicular to both line of sight and the z-axis. It's possible, however, to find a translation followed by a sequence of rotations, each about a *fixed* axis, equivalent to the given viewing transformation. In particular, one can show that

gluLookAt($eyex$, $eyey$, $eyez$, $centerx$, $centery$, $centerz$, upx, upy, upz)

is equivalent to:

```
glRotatef(−γ, 0.0, 0.0, 1.0);
glRotatef(−β, 0.0, 1.0, 0.0);
glRotatef(−α, 1.0, 0.0, 0.0);
glTranslatef(−eyex, −eyey, −eyez);
```

where rotations are each about a coordinate axis, for suitable angles α, β and γ (the minus signs are for simpler notation later on). Here's how.

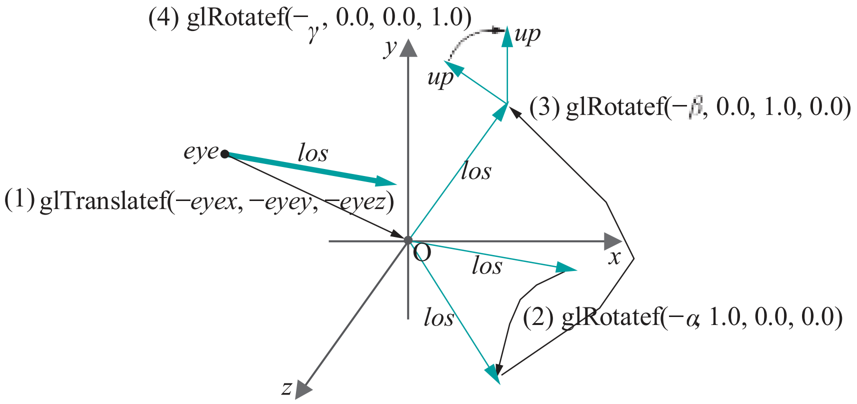
(4) glRotatef(−γ, 0.0, 0.0, 1.0)
y
up
up
(3) glRotatef(−β, 0.0, 1.0, 0.0)
eye
los
los
(1) glTranslatef(−eyex, −eyey, −eyez)
O
los
x
los
(2) glRotatef(−α, 1.0, 0.0, 0.0)
z

Figure 4.60: Applying a translation (1) and rotations (2)-(4) about the three coordinate axes, indicated by thin black arrows, to bring the camera back from gluLookAt(*eyex*, *eyey*, *eyez*, *centerx*, *centery*, *centerz*, *upx*, *upy*, *upz*) to its default pose. The original line of sight is bold. The up direction is shown only at the end.

Figure 4.60 – an all-in-one version of Figure 4.57 – shows, as we explain below, that the sequence of four transformations below restores the camera to its default pose from the one specified by

gluLookAt(*eyex*, *eyey*, *eyez*, *centerx*, *centery*, *centerz*, *upx*, *upy*, *upz*)

so, indeed, they are equivalent. Figure 4.60 looks busy but it's not hard to read. The best way is to start with the bold vector indicating the camera's initial configuration and follow the sequence (1)-(4) of transformations one by one:

(1) glTranslatef(−*eyex*, −*eyey*, −*eyez*) to bring the eye to the origin.

(2) glRotatef(α,1.0, 0.0, 0.0) to rotate the *los* about the x-axis till it lies on the xz-plane.

(3) glRotatef(−β, 0.0, 1.0, 0.0) to rotate the *los* about the y-axis till it points down the $-z$ direction.

(4) glRotatef(γ, 0.0, 0.0, 1.0) to rotate the camera about its *los* (now pointing down the z-axis) till its top is aligned in the $+y$ direction.

Remark 4.20. Evidently, from the above, we can reduce the number of parameters required to specify camera movement from the nine of gluLookAt() to only six: α, β, γ, *eyex* , *eyey* and *eyez*. This indicates redundancy in the construction of gluLookAt(), but it has the virtue of being intuitive to use.

Example 4.7. Express the viewing transformation

```
gluLookAt(0.0, 0.0, 0.0, 1.0, 1.0, 0.0, -1.0, 1.0, 0.0);
```

as a sequence of rotations about the coordinate axes (no translation is needed as the eye is already at the origin).

Answer:

```
glRotatef(90.0, 0.0, 0.0, 1.0);
glRotatef(135.0, 0.0, 1.0, 0.0);
glRotatef(90.0, 1.0, 0.0, 0.0);
```

See Figure 4.61 for how the camera is restored to its default pose by these three rotations.

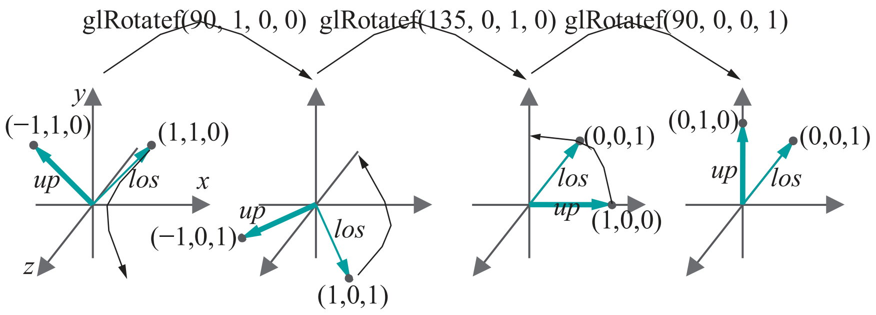

Figure 4.61: Solution to Example 4.7: the configuration of the camera given by gluLookAt(0.0, 0.0, 0.0, 1.0, 1.0, 0.0, -1.0, 1.0, 0.0) is at left; lines of sight are indicated by thin green arrows while up vectors by thick green ones; rotations are both annotated at the top and indicated in the figures themselves by thin black arrows, the result of each rotation being the *next* configuration.

Exercise 4.65. What sequence of rotations would have been found by the method of Section 4.6.2 as equivalent to the viewing transformation of the preceding example? Would they all have been about the coordinate axes?

If its first three parameters (*eyex*, *eyey*, *eyez*) = (0, 0, 0), then a gluLookAt()'s translational component is zero, so that it alters only a camera's orientation, or pose. From the preceding discussion, such a gluLookAt() call is equivalent to a sequence

glRotatef($-\gamma$, 0.0, 0.0, 1.0);
glRotatef($-\beta$, 0.0, 1.0, 0.0);
glRotatef($-\alpha$, 1.0, 0.0, 0.0);

for some angles α, β and γ. In the opposite direction, therefore, the orientation of the camera resulting from this particular gluLookAt() call can be obtained *from* its default pose by applying the inverse of the above sequence, viz.,

glRotatef(α, 1.0, 0.0, 0.0);
glRotatef(β, 0.0, 1.0, 0.0);
glRotatef(γ, 0.0, 0.0, 1.0);

The angles α, β and γ are called the camera's *Euler angles*. Euler angles, therefore, determine the camera's orientation: specifically, if they are α, β and γ, then the camera's orientation is obtained by applying first glRotatef(γ, 0.0, 0.0, 1.0), then glRotatef(β, 0.0, 1.0, 0.0) and, finally, glRotatef(α, 1.0, 0.0, 0.0) to its default pose.

Euler angles are not unique. For example, it's clear in Figure 4.60 that glRotatef($-\alpha\pm 180^\circ$, 1.0, 0.0, 0.0) could have been applied in Step (2), instead of glRotatef($-\alpha$, 1.0, 0.0, 0.0), to still place the camera's *los* on the *xz*-plane. So the orientation given by Euler angles α, β and γ is the same as the ones given by $\alpha\pm 180^\circ$, β^1 and γ^1, for some, possibly, new β^1 and γ^1.

Exercise 4.66. What are the Euler angles of a camera

(a) at the origin pointing at (1, 0, 0)?

(b) at the origin pointing at (1, 1, 1)?

(c) at (1, 0, 0) pointing at (1, 1, 1)?

In each case assume the up vector to be $(0, 1, 0)$. To determine the Euler angles of a camera not at the origin simply translate it first to the origin, moving the vector up parallely.

Part answer:

(a) 0°, −90°, 0° (one possible answer).

We'll see more of Euler angles when we discuss animating the orientation of rigid objects in Chapter 6.

4.6.4 Viewing Transformation and Collision Detection in Animation

Our next program makes use of viewing transformations to simulate a moving camera in an animated environment. It also has another aspect of interest, particularly to those programming interactive applications such as games, namely, collision detection.

Experiment 4.33. Run spaceTravel.cpp. The left viewport shows a global view from a fixed camera of a conical spacecraft and 48 stationary spherical asteroids arranged in a 6×8 grid. The right viewport shows the view from a front-facing camera attached to the tip of the craft.

Press the up and down arrow keys to move the craft forward and backward and the left and right arrow keys to turn it. Approximate collision detection is implemented to prevent the craft from crashing into an asteroid. See Figure 4.62 for a screenshot after the spacecraft has traveled and turned a bit. The frame rate of the program is shown in the debug window.

The asteroid grid can be changed in size by redefining ROWS and COLUMNS. The probability that a particular row-column slot is filled is specified as a percentage by FILL_PROBABILITY – a value less than 100 leads to a non-uniform distribution of asteroids. End

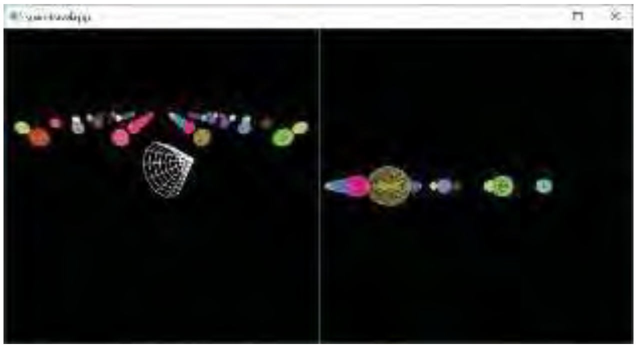

Figure 4.62: Screenshot of spaceTravel.cpp.

We'll discuss next the two most interesting aspects of spaceTravel.cpp: (a) the viewing transformation which defines the scene, viewed through a camera carried by the craft, in the right viewport, and (b) collision detection.

Viewing Transformation

The shape of the craft is defined by the glutWireCone(5.0, 10.0, 10, 10) statement; precisely, it is a cone of base radius 5 and height 10. The configuration of the spacecraft is specified by the values of $xVal$, $zVal$ and $angle$, all three global variables of spaceTravel.cpp. Figure 4.63(a) is a generic configuration in section along the xz-plane. The coordinates of the center of the craft's base are $(xVal, 0, zVal)$, while

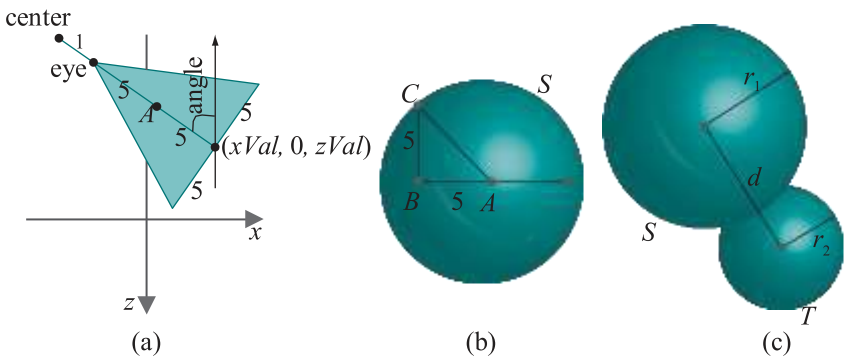

Figure 4.63: Spacecraft diagrams.

the angle its axis makes with the negative z-direction is *angle*. The middle A of the craft's axis will be of use in collision detection.

The camera for the right viewport is situated at the tip of the craft pointing straight ahead. It's straightforward trigonometry, now, to calculate the coordinates of *eye*, i.e., the tip of the craft, and of an imaginary point *center* to which it points, located 1 unit ahead along the craft's axis:

$$\begin{aligned} eye &= (\, xVal - 10\sin(angle),\ 0,\ zVal - 10\cos(angle)\,) \\ center &= (\, xVal - 11\sin(angle),\ 0,\ zVal - 11\cos(angle)\,) \end{aligned}$$

These equations for *eye* and *center* explain the parameters of the gluLookAt() command for the right viewport in the drawScene() routine.

Collision Detection

Collision detection as implemented in spaceTravel.cpp is simple though approximate. The spacecraft is enclosed in an imaginary bounding sphere S centered at the middle A of the cone's axis, with radius equal to the distance $|AC|$ from A to a point C on the boundary of its base. See Figure 4.63(b).

If B is the center of the base, then it follows from the dimensions of the cone that $|AB| = |BC| = 5$; therefore,

$$|AC| = \sqrt{|AB|^2 + |BC|^2} = \sqrt{50} = 7.071\ldots$$

Accordingly, we specify the radius of S to be 7.072 (slightly larger, in fact, than $|AC|$). The coordinates of the center A of S are obtained by trigonometry from Figure 4.63(a):

$$A = (\, xVal - 5\sin(angle),\ 0,\ zVal - 5\cos(angle)\,)$$

To detect collision between the spacecraft and an asteroid T, we detect instead collision between the craft's bounding sphere S and T. It's easy to determine if there is a collision between the two spheres S and T: compare the distance d between their centers with the sum $r_1 + r_2$ of their radii; there is collision if $d \leq r_1 + r_2$ (e.g., as in Figure 4.63(c)), and not otherwise. The corresponding check is implemented in the routine checkSpheresIntersection(). This collision-detection test is approximate, in fact, conservative, as the craft's bounding sphere may intersect an asteroid even if the craft itself doesn't (as, in fact, in Figure 4.63(c)). The reason, of course, for implementing such approximate collision detection is that exactly determining if the craft collides with an asteroid requires much more computation which would slow matters down at run-time (mathematically inclined readers may want to ponder an exact calculation).

The up and down arrow keys are programmed to move the craft a distance of 1 in either direction along its axis, and the left and right arrows to turn the craft an angle of 5°, *only if* there'll not be a collision with an asteroid in the new position.

Remark 4.21. Collision detection in real-time is requisite in many game-like applications and the trade-off between accuracy and computational efficiency is always an issue.

Exercise 4.67. (Programming) Modify spaceTravel.cpp as follows:

(a) Make the left viewport the view from the front of the spacecraft (currently, it's the right one).

(b) Make one of the asteroids the "big golden asteroid" by drawing it larger than the others and painting it suitably. Make it glow as well by oscillating the intensity of its color.

(c) Place a camera whose location is fixed a distance above the golden asteroid and which turns to track the spacecraft, i.e., it's aimed always toward the craft. Show the view from the golden asteroid's camera in the right viewport.

(d) When the spacecraft reaches the big golden asteroid, flash the text "You have found gold!".

Exercise 4.68. (Programming) Modify spaceTravel.cpp as follows:

(a) All asteroids currently are colored spheres. Make them more interesting by using FreeGLUT objects, e.g., tetrahedron, octahedron, etc., or design your own.

(b) Currently, the spacecraft moves interactively. Change this to program an automated tour which takes a fixed but zig-zag path through the asteroids and returns to the start position. Plan a path so that the craft comes close to a few interesting asteroids, visible in the right viewport. Pressing space should start/stop the journey.

(c) Currently, the camera on the craft always points straight ahead. Program occasional rotation of the camera, e.g., when the craft passes a strange asteroid, pan the camera to keep it in view.

Exercise 4.69. (Programming) Place a camera on top of the rolling ball of Exercise 4.35, pointing always down the plane. This camera does *not* rotate with the ball, but stays always at the top, so its motion is entirely linear. (How would you even install such a camera in real life? CG though is delightfully free of mundane constraints!)

Place a box just beyond the bottom of the plane so that the ball's camera sees an approaching object. Place an additional fixed camera on the box pointing at the planeto observe the ball. See Figure 4.64. Give a split-screen view as in spaceTravel.cpp. Apply a patchwork of colors to both ball and box to liven up the camera views.

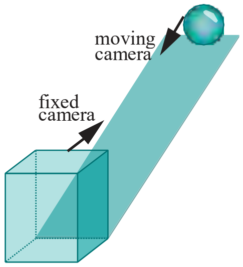

Figure 4.64: Ball rolling toward a box.

The following experiment is to whet your appetite for the topic of *frustum culling* , critical to the efficient rendering of complex scenes with large numbers of objects.

Experiment 4.34. Run spaceTravel.cpp after increasing both ROWS and COLUMNS to 100. The spacecraft now begins to respond so slowly to key input that its movement seems clunky, unless, of course, you have a very powerful machine (in which case, increase the values of ROWS and COLUMNS even more).

In fact, on our fairly fast desktop, there was almost no lag in response to key presses with the original 6×8 grid of asteroids – for example, we got a steady frame rate of 25 fps by keeping the up arrow key pressed, sending the craft straight ahead. However, we could never exceed 3 fps through the 100 × 100 grid. End

The reason for the degradation in the 100 × 100 grid is that, every time an arrow key is pressed, OpenGL processes 10,000 asteroids, which is an enormous amount of computing. However, of these 10,000 only a few (about 100, or 1%) are ultimately rendered, as you can roughly count on the screen. The rest, of course, are outside the viewing frustum and clipped.

Unfortunately, by the time the decision to clip is made in the graphics pipeline, a large amount of computation time has already been invested. Frustum culling is a technique to reduce this burden on OpenGL, whereby the programmer leverages her knowledge of the scene to efficiently pre-filter objects lying beyond the frustum, not letting them into the pipeline in the first place.

We'll discuss frustum culling in detail in Section 6.1. However, there's really not much more by way of prerequisites needed to read that particular section, so if you're anxious to learn this technique, which is so important in coding games, feel free to jump right there.

We are not done yet with animation, though, and have a bunch more fun code for you.

4.7 More Animation Code

4.7.1 Animating an Articulated Figure

Our next project is a "studio" to develop animation sequences for an articulated figure.

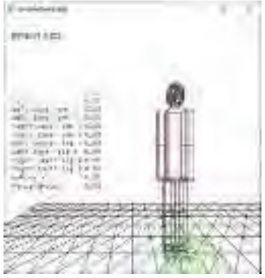

Figure 4.65: Screenshot of animateMan1.cpp.

Experiment 4.35. Run animateMan1.cpp. This is a fairly complex program to develop a sequence of key frames for a man-like figure, which can subsequently be animated. In addition to its spherical head, the figure consists of nine box-like body parts which can rotate about their joints. Figure 4.65 shows the opening screen. All parts are wireframe. End

Let's learn how the program works first before studying the code itself. There are two modes, develop and animate, and the program starts in the develop mode with the man facing you with his currently highlighted part, the torso, colored red. The rest of the body is black. Press the space bar to cycle through the man's movable parts, successively highlighting each. There are nine such, all OpenGL wire cubes: the torso, the upper and lower arms on either side, and the upper and lower legs on either side.

Rotate the currently highlighted part by pressing the page-up and page-down keys. To move the man as a whole press the left/right and up/down arrow keys. The angles at which the 9 movable parts are currently rotated, as well as the vertical and horizontal translational components of the man as a whole, are shown as text data in the window in develop mode.

While arranging the man into a desired configuration, you can rotate your own viewpoint by pressing 'r/R', or zoom in and out pressing 'z/Z'.

Once the first configuration is completed to your satisfaction, press 'n'. This creates a new configuration which cannot be seen immediately as it's a copy of the previous one. Press, say, the right arrow key to move the new configuration and separate it from the previous one. The (current) new configuration is bright, while the other(s) are ghosted. Again, use the space key to select a part, the page-up and page-down keys to rotate that part, and the arrow keys to move the entire configuration until it is arranged suitably.

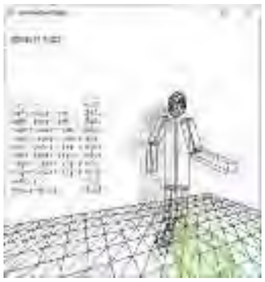

Figure 4.66: Screenshot of animateMan1.cpp in develop mode.

Press 'n' creating new configurations until the key frames sequence is complete. Figure 4.66 shows a screenshot part way through the develop mode. You can edit the sequence at any time as follows.

Press the tab key to cycle through the sequence of configurations – the currently selected configuration is bright, while the rest ghosted. Press backspace to reset the currently selected configuration, delete to remove it altogether, or you can rearrange it using keys as already described.

When the key frames sequence is complete, pressing 'a' begins an animation which cycles through the configurations. Pressing the up or down arrow keys speeds up or slows down the animation. Pressing 'a' again returns the program to develop mode.

Switching to animation mode also causes the program to write out to the file animateManDataOut.txt successive configurations of the animation sequence, stored currently in the vector manVector, for future use. Configuration are stored in successive lines of animateManDataOut.txt, each consisting of 11 floating point values – partAngles[0]-[8], upMove and forwardMove – the same as are displayed on the screen in develop mode.

Experiment 4.36. Run animateMan2.cpp. This is simply a pared-down version of animateMan1.cpp, whose purpose is to animate the sequence of configurations listed in the file animateManDataIn.txt, likely generated from the develop mode of animateMan1.cpp. Press 'a' to toggle between animation on/off. As in animateMan1.cpp, pressing the up or down arrow key speeds up or slows down the animation. The camera functionalities via the keys 'r/R' and 'z/Z' remain as well. Think of animateMan1.cpp as the studio and animateMan2.cpp as a movie theater.

The current contents of animateManDataIn.txt cause the man to do a handspring over the ball. Figure 4.67 is a screenshot. End

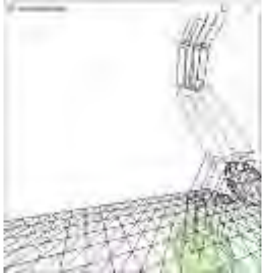

Figure 4.67: Screenshot of animateMan2.cpp.

Now let's look at the code of animateMan1.cpp. From an OpenGL point of view, most interesting possibly is the drawing of a configuration by the function Man::draw(). The best way to understand it is to analyze the successive placement of parts. We'll do this our usual way of deconstructing a program by first commenting out most of it and then restoring code piece by piece.

Accordingly, first comment out all parts except the torso as below:

```
// Function to draw man.
void Man::draw()
{
   if (highlight||animateMode) glColor3fv(highlightColor);
   else glColor3fv(lowlightColor);

   glPushMatrix();

   // Up and forward translations.
   glTranslatef(0.0, upMove, forwardMove);

   // Torso begin.
   if (highlight && !animateMode) if (selectedPart == 0)
      glColor3fv(partSelectColor);

   glRotatef(partAngles[0], 1.0, 0.0, 0.0);

   glPushMatrix();
   glScalef(4.0, 16.0, 4.0);
   glutWireCube(1.0);
   glPopMatrix();
   if (highlight && !animateMode) glColor3fv(highlightColor);
   // Torso end.

   /*
   // Head begin.
   -
   -
   -
   // Right upper and lower leg with foot end.
   */

   glPopMatrix();
}
```

Next, uncomment the head and successive body parts – with each it will be clear how it's being placed with respect to existing ones.

The creation of the camera as an object of the Camera class may be of interest as well and we'll leave the reader to relate the parameter values of the gluLookAt() command to the member variables viewDirection and zoomDistance of the Camera class.

Much of the rest of the code consists simply of managing and using manVector, which stores the sequence of configurations.

Remark 4.22. Even though he himself is 3D, the man moves and rotates his parts always parallel to the yz-plane, so he's not really capable of 3D motion!

Exercise 4.70. (Programming) Use animateMan*.cpp to animate a character kicking a football.

Exercise 4.71. (Programming) Enhance animateMan*.cpp:

(a) The character's body parts, except for the head, are currently all cubes. Make them more realistically rounded using cylinders.

(b) Add movement to the character's feet, which are currently fixed with respect to his lower legs. Give him movable hands as well.

(c) As remarked earlier, all the character's movements are currently parallel to a single plane. Enhance to true 3D.

Exercise 4.72. (Programming) Stick a (POV) camera to the front of the man's head and give a split-screen view of what he sees as he advances through an animation sequence and what is seen from a separate fixed camera focused on him.

Exercise 4.73. (Programming) By scaling individual body parts, create a second character who looks different from the first, though with identical functionality. Make a simple movie with the two, switching occasionally to the POV camera of either.

Exercise 4.74. (Programming) Smoothly animating even a short movie requires several key frames (approximately 24 per second). However, the "important" ones are likely far fewer in number. For example, if a man kicks a ball, these are probably his wound-up pose ready to kick, the pose when his foot makes contact with the ball, a follow-through pose having kicked and, possibly, a few more in between to guide the sequence; certainly, far fewer than the 72 or so key frames needed for even a 3-second kicking sequence.

A movie-maker, therefore, saves a lot of tedious labor by simply drawing the important key frames, leaving an interpolating routine to fill in enough frames to make the animation smooth, a process called *tweening*.

Write a simple tweening routine based on animateMan*.cpp. In particular, use linear interpolation to fill configurations – each being an 11-vector of floats – in between successive programmer-created ones.

4.7.2 Simple Orthographic Shadows

When the scaling transformation was introduced at the beginning of this chapter we said that degenerate scalings have the occasional application. Here's one to create and animate simple shadows.

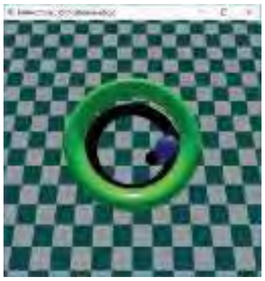

Figure 4.68: Screenshot of ballAndTorusLitOrthoShadowed.cpp.

Experiment 4.37. Run ballAndTorusLitOrthoShadowed.cpp of Chapter 11. This program, obviously based on ballAndTorus.cpp, has lighting, as well as shadows drawn on a checkered floor. Press space to start the ball traveling around the torus and the up and down arrow keys to change its speed. Figure 4.68 is a screenshot. End

Ignore the calls to do with lighting which may not make sense at this time. They are (oddly enough) not at all relevant to how the shadows are drawn, which is what we'll understand next.

Note, first, that the routine drawFlyingBallAndTorus() repositions the ball and torus from ballAndTorus.cpp horizontally so that their shadow, thrown supposedly by a distant overhead light source, falls on the floor which lies on the xz-plane. Assuming the light source vertically far above is important, as it justifies drawing the shadows as if cast by rays parallel to the y-axis, in other words, as parallel, or, orthographic, projections onto the floor – called *orthographic shadows*. The actual shadow drawing itself is quite simple – the following few lines in the drawing routine do the trick:

```
glPushMatrix();
glScalef(1.0, 0.0, 1.0);
drawFlyingBallAndTorus(1);
glPopMatrix();
```

The argument value 1 to drawFlyingBallAndTorus() causes both ball and torus to be drawn black, while the degenerate scaling command glScalef(1.0, 0.0, 1.0) collapses the y-values of all their vertices to 0, creating a flat black object which is precisely their projection on the xz-plane (the floor's plane) from light rays parallel to the y-axis.

Remark 4.23. Since ballAndTorusLitOrthoShadowed.cpp evidently contains code to light the scene, one might think that OpenGL would have calls to compute shadows. This is not the case: *OpenGL does not automatically compute secondary consequences of lighting such as shadows and reflection*. These have to be implemented separately by the programmer. The reason for this will be apparent when we study OpenGL's lighting model in Chapter 11.

Remark 4.24. Note that the ball's shadow on the torus is missing, even when it flies directly above. Our simple-minded projective flatten-and-blacken method doesn't run to drawing shadows on curved surfaces. We'll learn a way to do this, however, later on in Section 13.10 on shadow mapping.

4.8 Selection and Picking

Strictly speaking, this section does not fit in a chapter about animation and viewing. However, countless animated applications ask the user to pick and move an object on the screen with a mouse or mouse-like device (shoot-em-up games come to mind). We thought it important, therefore, to explain how to implement such interactivity.

Unfortunately, picking an object on the screen – which, effectively, means deciding to which object a picked pixel belongs – is not a simple operation given how the synthetic-camera pipeline functions. Particularly, objects enter the pipeline, are processed and emerge each as a set of fragments (fragment = pixel + color values), which are then rendered to the screen. Figure 4.69 is a conceptual diagram.

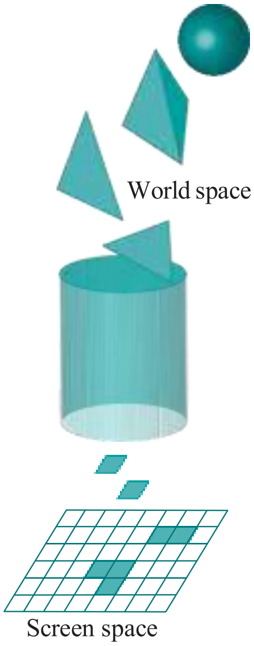

Figure 4.69: OpenGL's synthetic-camera pipeline (highly simplified!).

The pipeline is not designed to be reversible, so there's no easy way to "climb back up" from screen space to world space and say to which object a given pixel belongs. How then does one go about picking? Fortunately, OpenGL provides support for picking as well as a process it calls selection, which, in fact, enables picking. Let's begin with selection.

4.8.1 Selection

The idea underlying selection is simple. In a nutshell, it is to allow the user to specify a viewing volume and to then select the objects that intersect, or *hit* , this volume. To this end the user must first enter a rendering mode, called *selection mode*, by invoking glRenderMode(GL_SELECT). In selection mode nothing is drawn to the frame buffer; rather, primitives are processed simply to determine their intersections with the specified viewing volume and generate so-called *hit records*.

To help determine from a hit record the primitive, or primitives, which produced it, OpenGL provides a so-called *name stack* which the user manipulates. The user can load names on to the name stack in a manner that establishes correspondence between primitives and names.

A hit record contains the contents of the name stack at the time of its creation so, based upon the correspondence between primitives and names, one can determine those involved in the hit. Let's get to specifics with the help of live code.

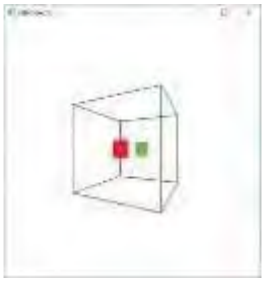

Figure 4.70: Screenshot of selection.cpp.

Experiment 4.38. Run selection.cpp, which is inspired by a similar program in the red book. It uses selection mode to determine the identity of rectangles, drawn with calls to drawRectangle(), which intersect the viewing volume created by the projection statement glOrtho (-5.0, 5.0, -5.0, 5.0, -5.0, 5.0), this being a 10 ×10 10×axis-aligned box centered at the origin. Figure 4.70 is a screenshot. Hit records are output to the command window. In the discussion following, we parse the program carefully. End

We'll call the viewing volume glOrtho(-5.0, 5.0, -5.0, 5.0, -5.0, 5.0), used to "select" the rectangles intersecting it, the *selection volume*. Note that it is different from the program's own viewing volume defined by the glFrustum(-5.0, 5.0, -5.0, 5.0, 5.0, 100.0) call in the resize() routine.

Displayed by the drawConfiguration routine is the outline of the selection volume and two rectangles, one red and one green, both inside it. If you don't trust the perspective view of the scene in Figure 4.70, as probably you shouldn't, verify from the parameters of the drawRectangle() call that the two rectangles indeed lie inside the selection volume.

The selectHits() routine, which comes next in the code, is where all the action is. Let's step through it carefully. The first statement

```
glSelectBuffer(1024, buffer);
```

specifies the array, called the *hit buffer*, to store hit records, as well as its size in bytes. The next statement

```
glRenderMode(GL_SELECT);
```

makes OpenGL enter selection mode. The next block of statements

```
glMatrixMode(GL PROJECTION);
glPushMatrix();
glLoadIdentity();
glOrtho(-5.0, 5.0, -5.0, 5.0, -5.0, 5.0);
glMatrixMode(GL MODELVIEW);
glLoadIdentity();
```

causes the matrix mode to change to projection, the current projection matrix (i.e., the one defined in the resize() routine) to be saved, that corresponding to the selection volume for hit testing to be placed on top of the projection matrix stack and, finally, modelview matrix mode to be re-entered and the current modelview matrix set to identity.

The statement pair next, viz.,

```
glInitNames();
glPushName(0);
```

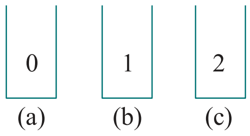

Figure 4.71: Name stack configurations: (a) Initial (b) When the red rectangle is drawn (c) When the green rectangle is drawn.

initializes an empty name stack and pushes the name 0 on it (names are always non-negative integers). We'll not be using 0 to name any primitive, but push it on so that we have something to replace with "real" names when using glLoadName(). The initial configuration is depicted in Figure 4.71(a).

The following set of commands both manipulates the name stack and correspondingly "draws" primitives. Keep in mind that in selection mode nothing is *actually* drawn to the frame buffer, in other words, nothing is seen to happen.

```
glLoadName(1);
drawRectangle(0.0, 0.0, 3.0, 1.0, 0.0, 0.0); // Rectangle 1 (red).

glLoadName(2);
drawRectangle(0.0, 0.0, -3.0, 0.0, 1.0, 0.0); // Rectangle 2 (green).
```

Figures 4.71(b) and (c) depict the name stack as it is at the time of drawing of the red and green rectangles, respectively. The next statement

```
hits = glRenderMode(GL_RENDER);
```

returns OpenGL to the default rendering mode where objects are indeed drawn to the frame buffer, at the same time returning the number of hit records currently in the hit buffer. Note that the return value of glRenderMode() has meaning only when transiting out of selection mode or another mode called feedback, which we'll not use, and not when leaving rendering mode. Finally,

```
glMatrixMode(GL_PROJECTION);
glPopMatrix();
glMatrixMode(GL_MODELVIEW);
```

restore the projection matrix from the resize() routine and return OpenGL to modelview matrix mode.

As selectHits() was being executed, hit records were written into the hit buffer following rules we'll describe next. A hit record is written into the hit buffer when *both* of the following conditions hold:

(a) A name stack manipulation or glRenderMode() command is encountered, *and*

(b) a hit has occurred (i.e., a primitive drawn that intersects the selection volume) since the previous instance of such a command.

Note: The hit record is written just *before* the command of item (a) is executed.

Each hit record contains four fields in the following order:

1. The number of names in the name stack at the time of writing the record.

2. The minimum z-value of vertices belonging to primitives which have hit the selection volume since the last hit record was written. This value is normalized by dividing by the depth of the selection volume to a number in the range [0, 1], which is then multiplied by $2^{32}-1$, rounded, and stored in the hit record as a 32-bit unsigned integer.

3. The maximum z-value of vertices belonging to primitives which have hit the selection volume since the last hit record was written, stored likewise.

4. The sequence of the names in the name stack at the time of writing the record with the bottom one first. (This sequence may be empty.)

It is the processHitBuffer() routine, called by drawScene(), which steps through the hit buffer, outputting its contents to the command window. Items 2 and 3 above, the minimum and maximum z-values of vertices, are normalized back to between 0 and 1 by dividing by $2^{32}-1$.

There are two hit records, as you can see in the command window. The first one (1, 0.2, 0.2{, }1) was generated just before executing the glLoadName(2) call because the latter is a name stack manipulation command itself and because a hit (the red rectangle) occurred after the previous name stack manipulation command (glLoadName(1)).

The contents of this record are easy to understand if one observes first that the configuration of the name stack at the time of the record's creation was as in

Figure 4.71(b). Accordingly, the one name '1' on this stack explains the first and last entries of the record (1, 0.2, 0.2{, 1}). Moreover, the depth of *all* vertices of the red rectangle from the front face of the viewing box is 2, which becomes 2/10 = 0.2 when normalized by division by the box's depth, explaining the second and third entries.

The second hit record $(1, 0.8, 0.8, \{2\})$ is generated just before processing the

```
hits = glRenderMode(GL RENDER);
```

statement, and we leave the reader to parse its contents.

Keep in mind that the rectangles of selection.cpp are actually drawn on screen because the drawConfiguration() routine called by drawScene() has copies of them.

The following exercises should, hopefully, fully clarify how hit records are generated.

Exercise 4.75. (Programming) Add one more rectangle, but in two different ways. First, insert the statement

```
drawRectangle(0.0, 0.0, 0.0, 0.0, 0.0, 1.0);
```

in the selectHits() routine (a) *just before* the glPushName(0) call (and after glInitNames()), and (b) *just after* glPushName(0). What are the hit records generated in each case? When is each of these hit records generated?

Part answer : In either case a new hit record comes before the two from the original program. When the statement is before glPushName(0), the new record is $(0, 0.5, 0.5, \{\})$ with an empty name list.

Exercise 4.76. (Programming) Continuing the preceding exercise, now move the rectangle-drawing statement

```
drawRectangle(0.0, 0.0, 0.0, 0.0, 0.0, 1.0);
```

to just after the statement that draws the first (red) rectangle. Explain the hit records, particularly, the z-values of the first one.

Exercise 4.77. (Programming) Restore the original selection.cpp program, but then change the command to draw the red rectangle to

```
drawRectangle(5.5, 0.0, 3.0, 1.0, 0.0, 0.0);
```

(mind that the change should be in both drawConfiguration() and selectHits()). Should the hit records stay the same? Verify.

Exercise 4.78. (Programming) Continuing the preceding exercise, next change the command to draw the red rectangle to

```
drawRectangle(7.5, 0.0, 3.0, 1.0, 0.0, 0.0);
```

Now, explain the hit records. This exercise, in fact, illustrates the idea we suggested at the start of the section, namely, that the name stack can be used to determine which objects hit the selection volume. In particular, here we "named" the red rectangle 1 and the green one 2 and the one hit record tells us it is the green one that intersects the selection box.

Exercise 4.79. (Programming) Restore the original selection.cpp program and insert the pair of name stack manipulation commands

```
glPushName(3);
glPushName(4);
```

right after the statement that draws the second (green) rectangle. Say now what's wrong with the following statement: "The glRenderMode(GL RENDER) call will cause the hit record $(1, 0.8, 0.8, \{2, 3, 4\})$ to be output." Check by running.

Exercise 4.80. (Programming) Restore the original selection.cpp program and add the name stack manipulation command

```
glPushName(3);
```

between the glLoadName(2) call and the statement that draws the green rectangle. Predict the output before running.

We see then a way of tagging an object with multiple names (in this case the green rectangle with 2 and 3) which is particularly useful in a scene where there is a hierarchy of objects. For example, we may want to tag the tail fin of the fourth aircraft with the names 4 and 7, if 7 is the part number of a tail fin.

Exercise 4.81. (Programming) The one remaining name stack manipulation command, which we have not used yet, is glPopName(), whose action the user can easily guess.

Insert a glPopName() statement in the selectHits() routine of selection.cpp in such a manner that the second hit record generated is $(0, 0.8, 0.8, \{\})$.

4.8.2 Picking

Now that we have an understanding of the selection process, let's move on to picking, which is really selection plus a little help from OpenGL in setting up a selection volume to track a user-specified point on the screen.

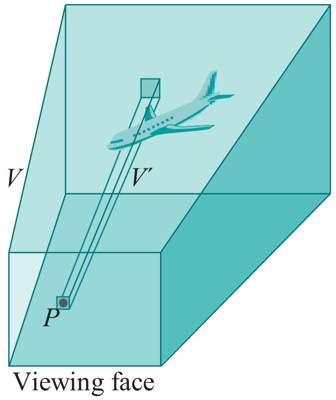

Figure 4.72: Clicking P "hits" the aircraft because the latter intersects $V^!$.

Figure 4.72 illustrates the idea. V is the viewing frustum defined by the projection statement of a program. Objects are, therefore, drawn to the OpenGL window following perspective projection to the viewing face of V (we'll identify V's viewing face with the OpenGL window without harm, because going from one to the other is a simple scaling).

Accordingly, one can find objects picked from choosing a point P in the OpenGL window by determining those that intersect a long thin frustum like V^1 whose base is centered at P, because it's precisely these objects whose projections intersect P. Of course, there's some error depending on the size of V^1, the thinner being V^1 the more accurate the picking. And, obviously, it's in detecting intersection with V^1 that selection comes in.

Fortunately, in addition to the selection mechanism discussed last section, there's even more help to be had from OpenGL in creating a suitable selection volume for use in picking: the GLU routine gluPickMatrix() defines a selection volume that is a frustum of user-specified size centered at a user-specified point. Here's how it works. The sequence of commands

```
glLoadIdentity();
```

```
gluPickMatrix(pickX, pickY, width, height, viewport);
glFrustum(); or gluPerspective(); or glOrtho();
```

where the last statement is copied from the program's resize routine, causes the top matrix of the projection matrix stack to be replaced by one corresponding to a selection volume whose front face is a *width* × *height* rectangle centered at the point of the OpenGL window with (window) coordinates equal to *pickX* and *pickY* , respectively. Moreover, the last parameter points to an integer array *viewport[4]* which contains the x and y coordinates of the viewport and its width and height, in that order; it is set by calling glGetIntegerv(GL_VIEWPORT, *viewport*). Functionally, the gluPickMatrix() command actually generates a matrix, called the *pick matrix*.

Let's get to work using the pick mechanism in a simple game-like application.

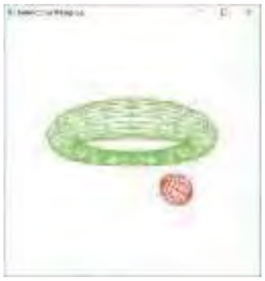

Figure 4.73: Screenshot of ballAndTorusPicking.cpp moments after the ball has been clicked.

Experiment 4.39. Run ballAndTorusPicking.cpp, which preserves all the functionality of ballAndTorus.cpp upon which it is based and adds the capability of picking the ball or torus with a left click of the mouse. The picked object blushes. See Figure 4.73 for a screenshot. End

The drawBallAndTorus() routine of ballAndTorusPicking.cpp is pretty much the whole drawScene() routine of ballAndTorus.cpp, except with two main differences:

(a) In selection mode, glLoadName() is invoked to tag the torus with the name 1 and the ball with name 2.

(b) If one of the torus or ball is picked – the name being contained in the global closestName – it is painted red for as long as the global highlightFrames is greater than 0.

The mouse callback pickFunction() is written along the lines of selectHits() of selection.cpp. The important difference is that the selection volume for hits is specified with help of a gluPickMatrix() call. And, of course, instead of drawing rectangles as in selection.cpp, it's drawBallAndTorus() which is executed in selection mode.

The routine findClosestHit() called by pickFunction() is an interesting modification of the processHitBuffer() routine of selection.cpp. In case there is more than one hit record, implying that both ball and torus fell under the mouse click, findClosestHit() compares their min-z fields to determine the one closer to the viewer.

Note: Sometimes the ball or torus doesn't light up on what seems like a definite click or the farther one lights up when both fall under the same mouse click. That's because the click, or, rather, its selection volume, slipped between mesh wires! Possible solutions include making the meshes finer or the picking less sensitive by increasing the *width* and *height* parameters of gluPickMatrix() from the current values of 3 for both.

Picking plus dragging with mouse motion (see Section 3.6 for the latter) make a potent duo. Give it a go in the next exercise.

Exercise 4.82. (Programming) Enhance canvas.cpp, from the previous chapter, so that figures in the drawing area can be picked and moved.

Exercise 4.83. (Programming) Referring again to Exercise 4.23, where you added two more balls to ballAndTorus.cpp, now add the functionality of being able to pick any of the four objects *a la* ballAndTorusPicking.cpp.

Exercise 4.84. (Programming) Create a game, be it a shoot-em-up or drag-em-down or Use your imagination.

4.9 Summary, Notes and More Reading

If animation is like a car, then we've just got our driver's license. In this chapter we learned the basics of the modeling and viewing transformations and how to use them to move objects and change their shape, as well as to manipulate the camera. We also peeked under the hood at OpenGL's engine, particularly in order to understand how transformations are composed and how they are used to place objects relative to one another. Collision detection, which is often crucial in interactive game programming, was discussed in the context of animation. We also began a discussion of orientation and Euler angles which will be continued in a more advanced chapter on animation. We learned as well the techniques of selection and picking, essential in interactive environments. And we saw plenty of live code along the way.

The topics covered in this chapter are at the very heart of computer graphics. Every introduction to the subject will have some coverage – see, for example, any of the introductory references, both OpenGL-based and API-independent, listed in Section 2.12 – differing perhaps in style and extent. So the reader has several options for an alternative point of view. She may also find useful the on-line tutorials listed at the OpenGL site [106].

Collision detection is also to a greater or lesser extent covered in most introductory CG books, often in the context of ray tracing, which is a technique of rendering where light rays are followed from source to collision with an object (and possibly reflection again). For further reading about collision detection, however, the reader is well-advised to consult books on game programming, where it is especially important. See, e.g., Lengyel [87] and van Verth & Bishop [148]. Specialized books on collision detection include Ericson [43] and van den Bergen [147]. An extensive repository of resources on collision detection, including research papers and code, is at the UNC Gamma Research Group website [146].

This chapter is also a lead-in to the extremely important discipline of physics in graphics (popularly called game physics), which includes the study of multi-body kinematics and dynamics of rigid and deformable bodies, among other topics from real-world physics. Real-time game physics is particularly important in the creation of realistic interactive games. Introductory books for the interested reader include Bourg & Bywalec [19] and Eberly [39].

Undoubtedly, the best way for the reader to build on this chapter is to write lots and lots of animation code. In fact, this is a good time for her to begin, if she hasn't already done so, a significant project, e.g., a game or movie. She can get the essentials in place now and then embellish her project as we go along – with more complex objects, color, light and texture. Aspiring game programmers, too, should be pleasantly surprised to find their understanding of animation carrying over to engines such as Unity – they will be racing through concepts like transforms (yes, translations, rotations and scalings), coordinate systems (world and local) and so forth with déjà vu. Impromptu exercise: explain the relationship between Unity child and parent object in OpenGL terms. In fact, developing a game using an engine would make for a terrific practical project in parallel with learning OpenGL.

Taylor & Francis

Taylor & Francis Group

http://taylorandfrancis.com

CHAPTER 5

Inside Animation: The Theory of Transformations

We studied transformations and their application to animation in Chapter 4. The goal for this chapter is to understand the underlying theory. We want to check under the hood of the graphics engine and learn exactly how transformations are implemented. What we'll encounter is the mathematics of geometric transformations.

We begin our discussion of geometric transformations in Section 5.1 in the simple surroundings of Flatland (2-dimensional space), the objective being to get concepts in place and prove results that will extend fairly easily later on to the real 3D world. This program starts in Sections 5.1.1-5.1.4 with the expression of familiar geometric transformations, in particular, translations, scalings, rotations and reflections, by means of matrices.

Next, we briefly interrupt our pursuit of 2D geometric transforms to digress in Section 5.2 into linear algebra, particularly for an understanding of affine transformations. Affine transformations will provide a unifying perspective of all the geometric transformations that we encounter. In Sections 5.2.1-5.2.3 we define affine transformations as a generalization of linear transformations, prove that they are particularly pleasant in their geometric behavior, understand the central role they play in the design of a graphics API such as OpenGL and, finally, learn the use of homogeneous coordinates to facilitate the application of affine transformations.

We resume our study of 2D geometric transforms in Section 5.3 with our newfound knowledge of affine transformations. We begin in 5.3.1 by placing the transformations of Section 5.1 in context as affine geometric transformations. In 5.3.2 comes the notion of Euclidean transformations, and their subclass of rigid transformations, neither of which distorts the shape of an object. Consequently, these are the transformations to use to animate rigid objects.

Geometric transformations of the real world or 3-space – transformations that OpenGL actually implements – is the topic of Section 5.4. The development parallels that of the previous section on 2D transformations. Matrix expressions for translations, scalings and reflections generalize easily from their 2D counterparts in Sections 5.4.1-5.4.2 and 5.4.4. 3D rotations, however, require considerably more work in the longish 5.4.3.

Observing in 5.4.5 that translations, scalings and rotations about radial axes are fundamental affine transformations, in the sense that they can be used to generate all other affine transformations, lends insight into the design of a CG animation engine. We realize that, however exciting the game or movie is that we happen to be enjoying, most of what is going on inside the GPU is the distinctly unglamorous activity of multiplying matrices by matrices and vectors by matrices – many many times and very very fast! We learn to access and manipulate the OpenGL modelview matrix stack in 5.4.6. Euclidean and rigid 3D transformations are discussed next in Section 5.4.7.

We conclude in Section 5.5 with a summary, notes and suggestions for further reading.

Prerequisite: We assume for this chapter familiarity with basic linear algebra as, say, would be found in a first college course or in a multitude of introductory texts, e.g., [7, 50, 75, 82, 86, 140] and others. Section 5.2 asks familiarity as well with the basics of convex sets, again from an introductory geometry text or our own Chapter 7, particularly Sections 7.1-7.2, which the reader can flip through even now.

Note to the reader about projection transformations : This chapter is devoted to the theory of modelview transformations. You will find a thorough coverage of projection transformations and their matrices in Chapter 20.

You can safely defer this somewhat theoretical chapter to a second pass through the book.

5.1 Geometric Transformations in 2-Space

We begin discussion of geometric transformations in 2D space, rather than real-life 3D, in order to develop our intuition in a simpler setting. Much of what we say and prove, though, will generalize fairly easily to 3D.

5.1.1 Translation

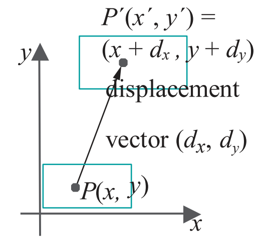

Figure 5.1: Translation.

A translation is specified by a *displacement vector* $D = [d_x\, d_y]^T$, which is added to the location vector of a point. Precisely, the image of the point $P = [x\ y]^T$ by this translation is $P' = [x'\ y']^T$, where

$$\begin{bmatrix} x' \\ y' \end{bmatrix} = \begin{bmatrix} x \\ y \end{bmatrix} + \begin{bmatrix} d_x \\ d_y \end{bmatrix} = \begin{bmatrix} x + d_x \\ y + d_y \end{bmatrix} = \begin{bmatrix} 1 & 0 \\ 0 & 1 \end{bmatrix} \begin{bmatrix} x \\ y \end{bmatrix} + \begin{bmatrix} d_x \\ d_y \end{bmatrix}$$

(T standing for transpose, $[\ldots]^T$ is a vector written as a column matrix). See Figure 5.1. Concisely:

$$P' = \begin{bmatrix} 1 & 0 \\ 0 & 1 \end{bmatrix} P + D \qquad (5.1)$$

The matrix multiplication may seem redundant, but it serves to put the RHS in a general form which will soon prove useful.

Terminology : We'll use the coordinate notation (x, y) and the matrix notation $[x\ y]^T$ for a point interchangeably, particularly preferring the latter when we want to treat the point's location as a vector.

Exercise 5.1. Prove that the composition of translations is a translation and that the inverse of a translation is another translation.

Part answer : We'll prove that the composition of translations is again a translation the long way, using the matrix form of the translation equation, but it's good practice. So suppose the translations t_1 and t_2 are specified by the displacement vectors D_1 and D_2, respectively. Then

$$\begin{aligned} (t_1 \circ t_2)(P) &= t_1(t_2(P)) = t_1\left(\begin{bmatrix} 1 & 0 \\ 0 & 1 \end{bmatrix} P + D_2 \right) \\ &= \begin{bmatrix} 1 & 0 \\ 0 & 1 \end{bmatrix} \left(\begin{bmatrix} 1 & 0 \\ 0 & 1 \end{bmatrix} P + D_2 \right) + D_1 \\ &= \begin{bmatrix} 1 & 0 \\ 0 & 1 \end{bmatrix} P + D_2 + D_1 = \begin{bmatrix} 1 & 0 \\ 0 & 1 \end{bmatrix} P + (D_2 + D_1) \end{aligned}$$

proving that $t_1 \circ t_2$ is indeed a translation, specified by the displacement vector $D_2 + D_1$.

5.1.2 Scaling

A scaling is specified by a scaling factor s_x along the x-axis and a scaling factor s_y along the y-axis. The image of a point P by this scaling is the one whose x coordinate value is s_x times that of P and y coordinate value s_y times that of P (see Figure 5.2). Precisely, the image of $P = [x\ y]^T$ is $P' = [x'\ y']^T$, where

$$\begin{bmatrix} x' \\ y' \end{bmatrix} = \begin{bmatrix} s_x x \\ s_y y \end{bmatrix} = \begin{bmatrix} s_x & 0 \\ 0 & s_y \end{bmatrix} \begin{bmatrix} x \\ y \end{bmatrix}$$

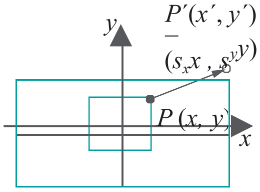

Figure 5.2: Scaling.

Concisely:

$$P' = \begin{bmatrix} s_x & 0 \\ 0 & s_y \end{bmatrix} P \qquad (5.2)$$

If either, or both, of the scaling factors s_x and s_y is zero, then the scaling is said to be *degenerate*; if neither is zero, it is *non-degenerate*. By a scaling we shall always mean a non-degenerate one, unless specifically stated otherwise.

Exercise 5.2. Show that the scaling given by Equation (5.2) is non-degenerate if and only if its matrix is non-singular (i.e., has non-zero determinant).

Exercise 5.3. Use Equation (5.2) to prove that the composition of scalings is a scaling and that the inverse of a non-degenerate scaling is another non-degenerate scaling. Are degenerate scalings invertible?

5.1.3 Rotation

A rotation about the origin is specified by an angle θ measured counter-clockwise as seen by a viewer V located on the positive side of the z-axis (in a hypothetical right-handed 3D coordinate system made by adding a z-axis to the x- and y-axes of the given 2D plane). See Figure 5.3(a).

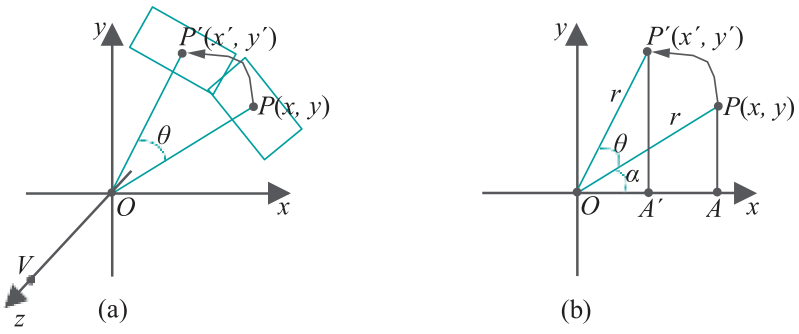

Figure 5.3: Rotation.

Remark 5.1. We had to add the z-axis, as well as a viewer on a particular side of it, because it's not enough to simply say that a rotation on the xy-plane is counter-clockwise: the same rotation appears counter-clockwise from one side and clockwise from the other. In the future, to avoid tedious language, we'll always assume that a viewer is located at a point such as V, on the positive side of the z-axis.

We want to calculate the image $P' = [x'\ y']^T$ of the point $P = [x\ y]^T$ by this rotation. The method is exactly the same as the solution given for Exercise 4.9(c), in the case of a 3D rotation about the z-axis. The reader can refer again to that exercise or deduce herself the following equations from Figure 5.3(b):

$$\begin{aligned} x &= OA = r\cos a \\ y &= PA = r\sin a \end{aligned}$$

which are used in

$$\begin{aligned} x^1 &= OA^1 = r\cos(a+\theta) = r\cos a\cos\theta - r\sin a\sin\theta \\ &= x\cos\theta - y\sin\theta \\ y^1 &= P^1A^1 = r\sin(a+\theta) = r\cos a\sin\theta + r\sin a\cos\theta \\ &= x\sin\theta + y\cos\theta \end{aligned}$$

Therefore, the image of $P = [x\ y]^T$ by a rotation of angle θ counter-clockwise about the origin is $P^1 = [x^1\ y^1]^T$, where

$$\begin{bmatrix} x^1 \\ y^1 \end{bmatrix} = \begin{bmatrix} x\cos\theta - y\sin\theta \\ x\sin\theta + y\cos\theta \end{bmatrix} = \begin{bmatrix} \cos\theta & -\sin\theta \\ \sin\theta & \cos\theta \end{bmatrix} \begin{bmatrix} x \\ y \end{bmatrix} \tag{5.3}$$

or, concisely,

$$P^1 = \begin{bmatrix} \cos\theta & -\sin\theta \\ \sin\theta & \cos\theta \end{bmatrix} P \tag{5.4}$$

The matrix in the preceding equation is often called a *rotation matrix*.

Example 5.1. Write the matrix form as in (5.4) of a counter-clockwise rotation by an angle of 60° about the origin. To which point is $[1\ {-2}]^T$ transformed by this particular rotation?

Answer: The given rotation will take $P = [x\ y]^T$ to $P^1 = [x^1\ y^1]^T$, where

$$P^1 = \begin{bmatrix} \cos 60^\circ & -\sin 60^\circ \\ \sin 60^\circ & \cos 60^\circ \end{bmatrix} P = \begin{bmatrix} 1/2 & -\sqrt{3}/2 \\ \sqrt{3}/2 & 1/2 \end{bmatrix} P$$

Therefore, $[1\ -2]^T$ is transformed to

$$\begin{bmatrix} 1/2 & -\sqrt{3}/2 \\ \sqrt{3}/2 & 1/2 \end{bmatrix} \begin{bmatrix} 1 \\ -2 \end{bmatrix} = \begin{bmatrix} 1/2+\sqrt{3} \\ -1+\sqrt{3}/2 \end{bmatrix} \approx \begin{bmatrix} 2.23 \\ -0.13 \end{bmatrix}$$

Exercise 5.4. Is the matrix of a rotation about the origin always non-singular?

Exercise 5.5. Determine the matrix expression for a counter-clockwise rotation by an angle θ about an arbitrary point $O^1 = [a\ b]^T$, not necessarily the origin.

Suggested approach: Use the Trick of Example 4.3 to express this rotation as a composition of three successive transformations:

1. A translation by the displacement vector $[-a\ -b]^T$ taking O^1 to the origin.
2. A counter-clockwise rotation by θ about the origin.
3. A translation by the displacement vector $[a\ b]^T$ restoring O^1 to its original position.

Next, compose the expressions corresponding to these three transformations (make sure to do this in the right order). The result will be a transformation of the form $P\ 1\!\to MP + D$.

Exercise 5.6. Determine the matrix expression for a rotation of 45° counter-clockwise about the point $[2\ 3]^T$.

Exercise 5.7. Use Equation (5.4) to prove that the composition of rotations about the origin is another such and that so is the inverse of a rotation about the origin.

Exercise 5.8. How about the composition of rotations about some fixed point other than the origin? Is this again a rotation about that point?

Example 5.2. Is the composition of rotations about *different* points necessarily equivalent to a *single* rotation about some one point?

Answer: Consider rotations r_1 and r_2, both of 180°, about the two points $O_1 = [0\ 0]^T$ and $O_2 = [1\ 0]^T$, respectively. We'll show that $r_2 \circ r_1$ is not a rotation about any point, answering the question asked in the negative.

It's easy to check (see Figure 5.4(a)) that $(r_2 \circ r_1)(O_1) = r_2(r_1(O_1)) = r_2(O_1) = [2\ 0]^T$, while $(r_2 \circ r_1)(O_2) = r_2(r_1(O_2)) = r_2([-1\ 0]^T) = [3\ 0]^T$.

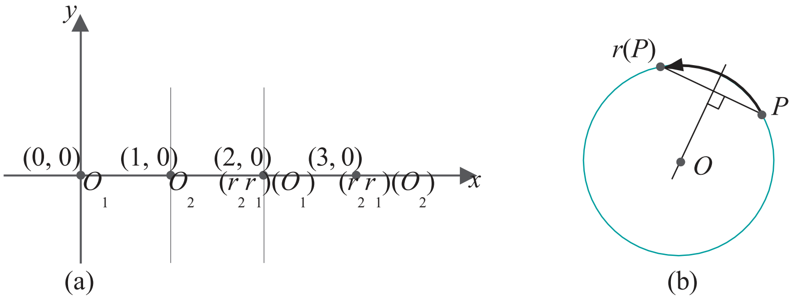

Figure 5.4: Illustrations for Example 5.2.

Next, observe that for any (non-identity) rotation r, and any point P which is not itself the center O of the rotation, O lies on the perpendicular bisector of the segment joining P and $r(P)$. Figure 5.4(b) indicates why.

Now, *if* $r_2 \circ r_1$ were indeed a rotation, its center, first, is not either O_1 or O_2, as both points are moved by $r_2 \circ r_1$. Therefore, its center must lie on the perpendicular bisector of the segment joining O_1 and $(r_2 \circ r_1)(O_1)$, as also on the perpendicular bisector of the segment joining O_2 and $(r_2 \circ r_1)(O_2)$. But this is not possible as the two bisectors are straight lines through $[1\ 0]^T$ and $[2\ 0]^T$, respectively, both parallel to the y-axis and, therefore, non-intersecting. One concludes that $r_2 \circ r_1$ is not a rotation about any point.

Exercise 5.9. The composition $r_2 \circ r_1$ of the preceding example, though not a rotation, is, nevertheless, a familiar kind of transformation. Can you identify it? *Hint*: It's a translation!

Exercise 5.10. Can you give an example where the composition of two (non-trivial) rotations about different points *is* equivalent to a single rotation about some point? *Hint*: Consider rotating 90° counter-clockwise around $[\ 1 -1]^T$ and then around $[1\ 1]^T$ the same amount. Show that this composition is equivalent to a rotation of 180° around the origin.

Remark 5.2. From the preceding two exercises we see one case where the composition of two rotations is a translation and one where it is again a rotation. It turns out that these are the only two possibilities in general. We'll prove this fact in Section 5.3.2, in particular, when we classify rigid transformations, and see an easy rule as well to decide the nature of a composition of rotations.

5.1.4 Reflection

The image of the point $P = [x\ y]^T$ by a reflection about a straight line l, called the *mirror*, is $P' = [x'\ y']^T$ such that:

(a) if P lies on l, then $P' = P$;

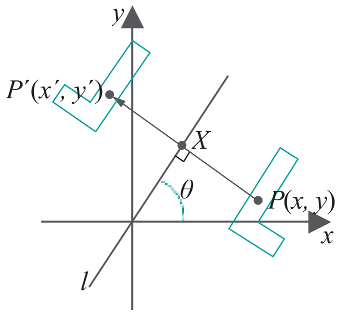

Figure 5.5: Reflection ($|XP| = |XP^!|$).

(b) if P does not lie on l, then P^1 is the point on the other side of l such that PP^1 is perpendicular to l, and P^1 is the same distance from l as P. See Figure 5.5.

A reflection is, therefore, specified by the mirror about which it occurs. Let's analyze first the reflection about a *radial* mirror l at an angle θ counter-clockwise from the positive direction of the x-axis (as depicted in Figure 5.5). We claim that reflection about l maps the point P to P^1 where

$$P^1 = \begin{matrix} \cos 2\theta & \sin 2\theta \\ \sin 2\theta & -\cos 2\theta \end{matrix} \ P \tag{5.5}$$

and leave the proof to the reader in the next exercise.

Note: A *radial* line or plane is one which passes through the origin.

Exercise 5.11. Verify Equation (5.5).

Suggested approach: Use the Trick to express this reflection as the composition of three successive transformations:

1. A rotation of $-\theta$ about the origin to align l along the x-axis.
2. A reflection about the x-axis. This is given by $[x\ y]^T$ 1→ $[x\ -\ y]^T$, which is simply scaling by a factor of 1 along the x-axis and -1 along the y-axis.
3. A rotation of θ about the origin to restore l to its original alignment.

Exercise 5.12. Write the matrix form, as in (5.5), of a reflection about the radial mirror at an angle of 30° to the positive x-axis. To which point is $[1\ 1]^T$ transformed by this reflection?

Exercise 5.13. What is the determinant of the matrix of a reflection about a radial mirror? Is the matrix always non-singular?

Exercise 5.14. Use the Trick to prove that a reflection about an arbitrary mirror, not necessarily radial, is a composition of two translations, two rotations about the origin and one scaling.

A consequence of the preceding exercise is that one of those highly-paid Flatland programmers developing a graphics API has only to implement translations, rotations about the origin, and scalings to get reflections for free.

Exercise 5.15. What is the inverse of a reflection?

Exercise 5.16. Show that any non-identity translation can be obtained by composing reflections about two parallel mirrors. Show that any non-identity rotation can be obtained by composing reflections about two intersecting mirrors. (The identity transformation itself can be obtained obviously by composing reflections about the same mirror twice.)

Shear

Shears, though not as important in the scheme of geometric transformations as the ones we have so far studied, nevertheless are worthy of discussion as they arise naturally from a distinctive physical process. Roughly, a shear is the distortion caused by placing a lump of putty between your palms, keeping the lower palm stationary and moving the upper palm parallel to the lower.

A 2D shear s is uniquely determined by two parameters: a directed line l called the *line of shear* and an angle a called the *angle of shear*.

Here's how a point $P \in \mathbb{R}^2$ is mapped to the point P^1 by s (see Figure 5.6(a)):

(a) If P lies on l, then it is unchanged.

(b) If P lies a distance of h left of l, then it moves parallel to l in the positive direction of l a distance of $h \tan a$.

(c) If P lies a distance of h right of l, then it moves parallel to l in the negative direction of l a distance of $h \tan a$.

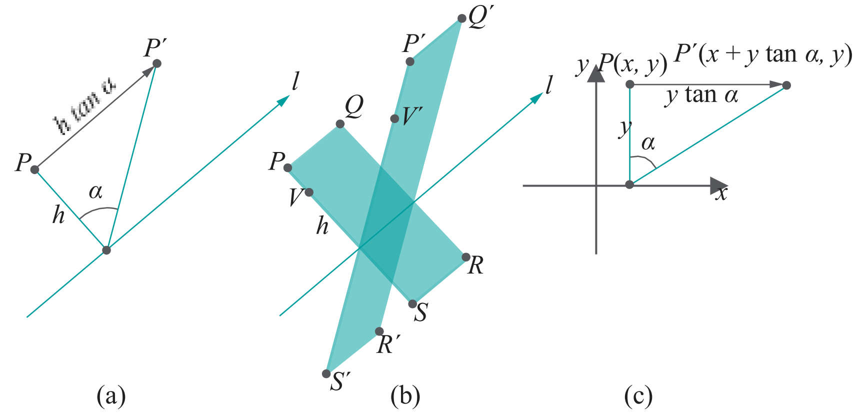

(a) (b) (c)

Figure 5.6: 2D shears: l is a directed line, a the angle of shear.

Note: Left or right is according to a viewer standing upright on the plane at a point of l, head pointing toward the positive z-axis (of a hypothetical right-handed coordinate system) and facing toward the direction of l.

Another way to think of the shear is as a force parallel to l which "bends" each perpendicular to it a fixed angle a. For example, the rectangle $PQRS$ in Figure 5.6(b) is sheared into the parallelogram $P^1Q^1R^1S^1$. The farther points are from l, the proportionately more they travel under the shear; e.g., compare $V \mapsto V^1$ and $P \mapsto P^1$ in Figure 5.6(b). Figure 5.7 shows a sheep.

Figure 5.7: Sheared sheep.

If the directed line l of the shear is the x-axis, then it is particularly simple to determine its transformation equation. Figure 5.6(c) shows this to be $[x\ y]^T \mapsto [x + y \tan a\ \ y]^T$.

Exercise 5.17. Write the 2×2 transformation matrix corresponding to a shear along the x-axis. Write the 2×2 transformation matrix corresponding to a shear along a radial line making an angle θ counter-clockwise from the x-axis.

Exercise 5.18. (Commutativity) Two transformations f_1 and f_2 are said to *commute* (or be *commutative*) if $f_1 \circ f_2 = f_2 \circ f_1$, in other words, if applying f_1 followed by f_2 is the same as applying f_2 followed by f_1.

(a) Do translations commute with each other?

(b) Do scalings commute with each other?

(c) Do rotations about the same point commute with each other?

(d) Does a rotation about one point commute with another about a different point?

(e) Do translations and rotations commute?

(f) Do reflections about two different mirrors *ever* commute? (*Hint*:Keep in mind the special case of perpendicular mirrors.)

(g) Does a shear along a radial axis commute with a rotation about the origin?

(h) What kind of translations does a shear along the directed line l commute with?

5.2 Affine Transformations

Before resuming our pursuit of geometric transformations in 2-space, we change pace a bit to learn about affine transformations because they will provide a unifying framework in which to locate the seemingly disparate geometric transformations that we have encountered (and will encounter).

5.2.1 Affine Transformations Defined

Affine transformations are a natural generalization of linear transformations, obtained by tacking on an additional translation to a non-singular linear transformation. We'll give the next couple of definitions in arbitrary dimensions – this generality costing nothing in difficulty. Down the road, of course, we can specialize to R^2 or R^3 depending on the setting.

For the record, here's the definition of a linear transformation, which is our starting point.

Definition 5.1. The *linear transformation* f^M of R^m, with the $m \times m$ *defining matrix*

$$M = \begin{bmatrix} a_{11} & a_{12} & \dots & a_{1m} \\ a_{21} & a_{22} & \dots & a_{2m} \\ & \dots & \dots & \\ a_{m1} & a_{m2} & \dots & a_{mm} \end{bmatrix}$$

is the transformation f^M : R$^m \to$ R^m specified by the equation

$$f^M(P) = MP, \qquad P \in \mathrm{R}^m \tag{5.6}$$

In other words, f^M maps $P = [x_1\ x_2 \dots\ x_m]^T$ to $f^M(P) = [x^1{}_1\ x^1{}_2\ \dots\ x^1{}_m]^T$, where

$$\begin{aligned} x^1{}_1 &= a_{11}x_1 + a_{12}x_2 + \dots + a_{1m}x_m \\ x^1{}_2 &= a_{21}x_1 + a_{22}x_2 + \dots + a_{2m}x_m \\ &\dots\ \dots \\ x^1{}_m &= a_{m1}x_1 + a_{m2}x_2 + \dots + a_{mm}x_m \end{aligned} \tag{5.7}$$

Note: It's called a linear transformation because the power on each x_i on the right of (5.7) is 1, i.e., each x^1_i is a linear combination of the x_is.

A linear transformation is said to be non-singular according as it's defining matrix is so.

Definition 5.2. An *affine transformation* of R^m is a transformation g : R$^m \to$ R^m specified by an equation of the form

$$g(P) = f^M(P) + D = MP + D \tag{5.8}$$

for $P \in$ R^m, where f^M is a non-singular linear transformation of R^m and D is an m-vector. The matrix M, which is non-singular, is called the *defining matrix* of g. The vector D is called the *translational component* of g.

Accordingly, if

$$M = \begin{bmatrix} a_{11} & a_{12} & \dots & a_{1m} \\ a_{21} & a_{22} & \dots & a_{2m} \\ & \dots & \dots & \\ a_{m1} & a_{m2} & \dots & a_{mm} \end{bmatrix} \text{ is non-singular and } D = \begin{bmatrix} d_1 \\ d_2 \\ \dots \\ d_m \end{bmatrix} \text{ arbitrary,}$$

then the affine transformation g defined by $g(P) = MP + D$ maps $P = [x_1\ x_2\ \dots\ x_m]^T$ to $g(P) = [x^1{}_1\ x^1{}_2\ \dots\ x^1{}_m]^T$, where

$$\begin{aligned} x^1{}_1 &= a_{11}x_1 + a_{12}x_2 + \dots + a_{1m}x_m + d_1 \\ x^1{}_2 &= a_{21}x_1 + a_{22}x_2 + \dots + a_{2m}x_m + d_2 \\ &\dots\ \dots \\ x^1{}_m &= a_{m1}x_1 + a_{m2}x_2 + \dots + a_{mm}x_m + d_m \end{aligned} \tag{5.9}$$

If its translational component is zero, then an affine transformation evidently reduces to a non-singular linear transformation. Conversely, a non-singular linear transformation is an affine transformation with zero translational component.

Example 5.3. $g : \mathbb{R}^2 \to \mathbb{R}^2$ given by

$$g([x\ y]^T) = \begin{bmatrix} 2 & 1 \\ 0 & 4 \end{bmatrix} [x\ y]^T + [4\ 6]^T$$

is affine. Writing out the formula for g we have

$$g([x\ y]^T) = \begin{bmatrix} 2x + y + 4 \\ 4y + 6 \end{bmatrix}$$

So, e.g.,

$$g([-1\ 2]^T = [4\ 14]^T \quad \text{and} \quad g([0\ 3]^T = [7\ 18]^T$$

Exercise 5.19. What are the images of the points $[0\ 0\ 0]^T$ and $[1\ -1\ 1]^T$ by the affine transformation $g : \mathbb{R}^3 \to \mathbb{R}^3$ given by

$$g([x\ y\ z]^T) = \begin{bmatrix} -1 & -2 & 3 \\ 4 & 0 & 2 \\ 0 & -3 & 1 \end{bmatrix} [x\ y\ z]^T + [-1\ 6\ 3]^T\ ?$$

The next example says that an affine transformation is respectful of convex combinations.

Example 5.4. Show that an affine transformation g of $\mathbb{R}^m$ preserves convex combinations and barycentric coordinates in that

$$g(c_1P_1 + c_2P_2 + \dots + c_kP_k) = c_1g(P_1) + c_2g(P_2) + \dots + c_kg(P_k)$$

for any m-vectors P_i and scalars c_i, $1 \le i \le k$, such that $0 \le c_i \le 1$ and $c_1 + c_2 + \dots + c_k = 1$.

Answer: Suppose that $g(P) = MP + D$, where M is the defining matrix and D the translational component of g. Then

$$\begin{aligned} g(c_1P_1 + c_2P_2 + \dots + c_kP_k) &= M(c_1P_1 + c_2P_2 + \dots + c_kP_k) + D \\ &= M(c_1P_1 + c_2P_2 + \dots + c_kP_k) + \\ &\quad (c_1 + c_2 + \dots + c_k)D \\ &\quad (\text{because } c_1 + c_2 + \dots + c_k = 1) \\ &= c_1MP_1 + c_2MP_2 + \dots + c_kMP_k + \\ &\quad c_1D + c_2D + \dots + c_kD \\ &= c_1(MP_1 + D) + c_2(MP_2 + D) + \dots + \\ &\quad c_k(MP_k + D) \\ &= c_1g(P_1) + c_2g(P_2) + \dots + c_kg(P_k) \end{aligned}$$

Exercise 5.20. Prove that an affine transformation which fixes the origin (i.e., maps the origin to itself) is a non-singular linear transformation.

Exercise 5.21. Prove that the composition of affine transformations is again an affine transformation.

Exercise 5.22. Determine the affine transformation $g_1 \circ g_2$, where

$$g_1(P) = \begin{bmatrix} 2 & 1 \\ 0 & 4 \end{bmatrix} P + [4\ 6]^T \quad \text{and} \quad g_2(P) = \begin{bmatrix} -1 & 3 \\ 1 & -2 \end{bmatrix} P + [-1\ 0]^T$$

Example 5.5. An affine transformation g is always invertible. In fact, if g is defined by $g(P) = MP + D$, then show that its inverse, also affine, is given by

$$g^{-1}(Q) = M^{-1}Q - M^{-1}D$$

Answer: For any $P \in \mathbb{R}^m$, we have

$$(g^{-1} \circ g)(P) = g^{-1}(g(P)) = M^{-1}g(P) - M^{-1}D = M^{-1}(MP + D) - M^{-1}D = P$$

proving that $g^{-1} \circ g$ is the identity on $\mathbb{R}^m$. Likewise, it can be seen that $g \circ g^{-1}$ is the identity, proving that g^{-1} as defined above indeed is the inverse of g.

Exercise 5.23. Determine the inverse of the affine transformation g of $\mathbb{R}^2$ given by

$$g([x\ y]^T) = \begin{bmatrix} 2 & 1 \\ 0 & 4 \end{bmatrix} [x\ y]^T + [4\ 6]^T$$

The following important proposition says that affine transformations are particularly well-behaved from a geometric point of view, in particular, that they preserve straightness, planarity, parallelism and convexity.

Proposition 5.1.

(a) *An affine transformation g of $\mathbb{R}^2$ maps straight lines to straight lines. Moreover, it maps parallel straight lines to parallel straight lines and intersecting straight lines to intersecting straight lines.*

(b) *An affine transformation g of $\mathbb{R}^2$ maps convex sets to convex sets. Moreover, it maps the convex hull of $\{P_1, P_2, \ldots, P_k\}$ to the convex hull of $\{f^M(P_1), f^M(P_2), \ldots, f^M(P_k)\}$.*

(c) *An affine transformation g of $\mathbb{R}^3$ maps straight lines to straight lines and planes to planes. Moreover, it maps parallel straight lines to parallel straight lines, intersecting straight lines to intersecting straight lines, parallel planes to parallel planes and intersecting planes to intersecting planes.*

(d) *An affine transformation g of $\mathbb{R}^3$ maps a convex set lying on one plane of $\mathbb{R}^3$ to a convex set on another plane. Moreover, it transforms the convex hull of a set of points $\{P_1, P_2, \ldots, P_k\}$ on one plane to the convex hull of $\{g(P_1), g(P_2), \ldots, g(P_k)\}$ lying on another plane.*

Figure 5.8 illustrates the actions of an affine transformation in $\mathbb{R}^3$.

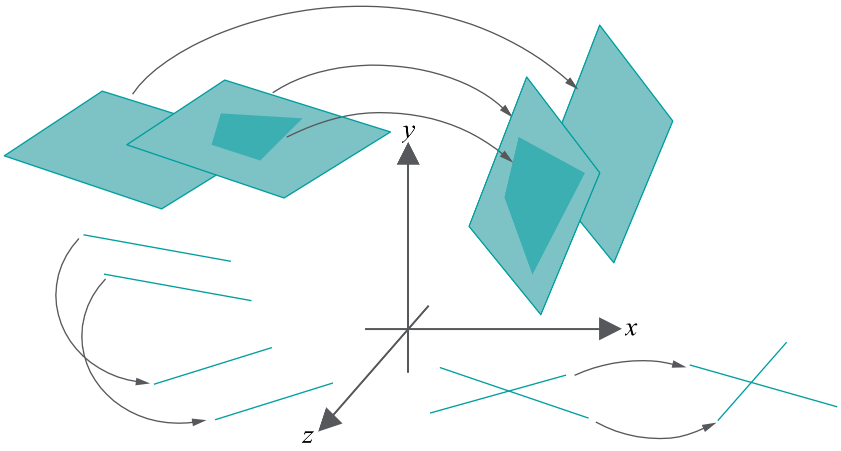

Figure 5.8: Affine transformation in R³.

Proof. (a) Say $g(P) = MP + D$, for $P \in \mathrm{R}^2$, where M is a non-singular 2×2 matrix and D a column 2-vector.

Suppose, first, that the equation of a given straight line l in R^2 is $ax + by = c$, which can be written as $[a\ b][x\ y]^T = c$. If the point $[x\ y]^T$ is on l, let's see where its image $g([x\ y]^T) = M[x\ y]^T + D$ lies. Now

$$([a\ b]\,M^{-1})\,(M\,[x\ y]^T + D) = [a\ b][x\ y]^T + [a\ b]M^{-1}D = c + [a\ b]M^{-1}D$$

Writing $[a^1\ b^1] = [a\ b]M^{-1}$ and writing $c^1 = c + [a\ b]M^{-1}D$, using $[a\ b][x\ y]^T = c$, the preceding equation gives

$$[a^1\ b^1]\,(M\,[x\ y]^T + D) = c^1$$

which shows that if $[x\ y]^T$ lies on l, then $g([x\ y]^T)$ lies on the straight line $[a^1\ b^1][x\ y]^T = c^1$, proving that the image $g(l)$ of l is indeed a straight line.

Say next that l and l^1 are two parallel straight lines in R^2, whose equations can then be written as $[a\ b][x\ y]^T = c$ and $[a\ b][x\ y]^T = d$, respectively, where $c /= d$.

From the first part of the proof it's seen that $g(l)$ is the straight line whose equation is

$$[a^1\ b^1][x\ y]^T = c^1, \quad \text{where} \quad [a^1\ b^1] = [a\ b]M^{-1} \quad \text{and} \quad c^1 = c + [a\ b]M^{-1}D$$

Likewise, $g(l^1)$ is the straight line whose equation is

$$[a^1\ b^1][x\ y]^T = d^1, \quad \text{where} \quad [a^1\ b^1] \quad \text{is as above and} \quad d^1 = d + [a\ b]M^{-1}D$$

Moreover, it follows from $c /= d$, that $c^1 = d^1$. We conclude that $g(l)$ and $g(l^1)$ are indeed parallel straight lines.

Finally, it's easy to see that two straight lines l and l^1 which intersect at P are mapped by g to straight lines which intersect at $g(P)$.

(b) Again, say, $g(P) = MP + D$, for $P \in \mathrm{R}^2$, where M is a non-singular 2×2 matrix and D a column 2-vector.

Suppose, first, that S is a convex subset of R^2. To prove that $g(S)$ is convex as well, it is sufficient to show that $cP + (1 - c)Q \in g(S)$, given two points P and Q in $g(S)$ and c in $0 \leq c \leq 1$.

Since $P, Q \in g(S)$, there exist $P^1, Q^1 \in S$ such that $g(P^1) = P$ and $g(Q^1) = Q$. As S is convex $cP^1 + (1 - c)Q^1 \in S$. Applying g to both sides of the preceding inclusion we have that $g(cP^1 + (1-c)Q^1) \in g(S)$, but

$$\begin{aligned}
g(cP^1 + (1-c)Q^1) &= M(cP^1 + (1-c)Q^1) + D \\
&= M(cP^1 + (1-c)Q^1) + cD + (1-c)D \\
&= cMP^1 + cD + (1-c)MQ^1 + (1-c)D \\
&= c(MP^1 + D) + (1-c)(MQ^1 + D) \\
&= cg(P^1) + (1-c)g(Q^1) \\
&= cP + (1-c)Q
\end{aligned}$$

proving that indeed $cP + (1-c)Q \in g(S)$, so that the latter is a convex set.

We leave the proof of the second part of (b) as well as those of (c) and (d) to the reader.

Exercise 5.24. Does an affine transformation of R^2 or R^3 necessarily map radial lines to radial lines or radial planes to radial planes? How about a linear transformation?

5.2.2 Affine Transformations and OpenGL

Proposition 5.1 says that affine transformations preserve straightness, flatness and convexity, among other properties, because they keep straight lines straight, planes plane and convex sets convex. It's not hard to see, if one works through the proof, that this is a consequence of the fact that their defining Equations (5.9) (shown again below)

$$\begin{aligned}
x^1{}_1 &= a_{11}x_1 + a_{12}x_2 + \ldots + a_{1m}x_m + d_1 \\
x^1{}_2 &= a_{21}x_1 + a_{22}x_2 + \ldots + a_{2m}x_m + d_2 \\
&\ldots \ldots \\
x^1{}_m &= a_{m1}x_1 + a_{m2}x_2 + \ldots + a_{mm}x_m + d_m
\end{aligned}$$

are of degree one, in particular, that the maximum degree of a variable x_i on the right side of each of these equations is one.

Here's an example of what happens if this were not the case, and if even we go to degree two.

Example 5.6. The quadratic transformation h of R^2 defined by $h([x\ y]^T) = [x\ y^2]^T$ doesn't necessarily keep straight lines straight. In fact, we'll show that it maps at least one straight segment into an arc of a parabola.

Write the transformation as

$$\begin{aligned}
x^1 &= x \\
y^1 &= y^2
\end{aligned}$$

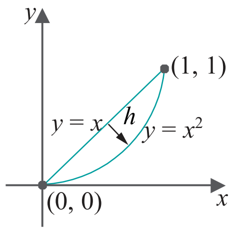

Figure 5.9: Quadratic transform h of R^2 takes a straight segment to a parabolic arc.

Now consider how the straight line

$$y = x$$

is mapped. We have, using the preceding 3 equations

$$y^1 = y^2 \Longrightarrow y^1 = x^2 \Longrightarrow y^1 = x^{12}$$

which is the equation of a parabola. It follows that h maps the straight segment between $(0, 0)$ and $(1, 1)$ to the arc of the parabola $y = x^2$ joining the same two points, as shown in Figure 5.9.

One notices, further, that affine transformations are the *most general* class of transformations of degree one, because the right side of each one of the Equations (5.9) has its full complement of terms possible up to degree one – specifically, *every* x_i is present with degree one and there is, as well, the constant term d_i of degree zero.

One concludes that not only do affine transformations of R^2 or R^3 (or, in fact, R^m in general) preserve straightness, flatness and convexity, they are the most general class of transformations to do so. Put another way, one cannot hope to go beyond affine transformations if these properties are not to be broken.

What has all this to do with OpenGL? Because they preserve straightness, flatness and convexity, affine transformations preserve as well the primitives of OpenGL, in particular, they map primitives of one type to another of the same type. The following exercise asks the reader to prove the specifics of this claim.

Exercise 5.25. Given an affine transformation g of R^2 or R^3, prove that

(a) g maps the straight segment joining two points P and Q to the straight segment joining $g(P)$ and $g(Q)$.

(b) g maps the triangle with vertices at P, Q and R to the triangle with vertices at $g(P)$, $g(Q)$ and $g(R)$.

(c) g maps the n-sided polygon with vertices at $P_1, P_2, \ldots, P_n$ to the n-sided polygon with vertices at $g(P_1), g(P_2), \ldots, g(P_n)$. If the original polygon is planar, then so is the transformed one. If the original polygon is convex, then so is the transformed one.

Hint: Use Proposition 5.1.

Non-affine transformations may not treat OpenGL primitives with quite as much respect, as the following exercise shows.

Exercise 5.26. We already saw in Example 5.6 the non-affine quadratic transformation h of R^2, given by $h([x\ y]^T) = [x\ y^2]^T$, take a straight segment to a parabolic arc. How does h transform the triangle with corners at (0, 0), (1, 0) and (1, 1)? Figure 5.10 is a gentle hint.

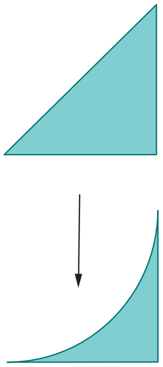

Figure 5.10: Non-affine transformation of a triangle.

Now, it's desirable for a graphics API such as OpenGL to implement only modeling transformations which preserve its drawing primitives – specifically, mapping each one to another of the same type. Why? Consider OpenGL in particular. At the rendering end of its pipeline are evidently modules to render points, segments and triangles (mind that even a general polygon is triangulated prior to rendering). Suppose, then, that a particular scene is specified by the programmer as a list of n primitives:

$$primitive1,\ primitive2,\ \ldots,\ primitiveN$$

where each $primitiveI$, $1 \leq I \leq N$, is a point, segment or triangle. The scene is rendered essentially in a simple loop:

```
for ($I$ = 1;  $I$ ≤ $N$;  $I$++) render $primitiveI$
```

where each iteration invokes the appropriate primitive rendering module.

Suppose, next, that a modeling transformation g is applied to the scene. The transformed scene is given by the list:

$$g(primitive1),\ g(primitive2),\ \ldots,\ g(primitiveN)$$

If g preserves primitives, then $g(primitiveI)$ is of the same class as $primitiveI$, for $1 \leq I \leq N$, and the transformed scene is rendered in the loop

```
for ($I$ = 1;  $I$ ≤ $N$;  $I$++) render $g(primitiveI)$
```

invoking the same modules as before.

On the other hand, if g doesn't map primitives of one class to another of the same, e.g., if a triangle can change to something that is no longer one, as in Figure 5.10, then the situation becomes significantly more complicated. In this case, either there have to be modules to render all possible target objects of all drawing primitives, or modules to approximate them using existing primitives, or, maybe, a combination of both. See Figure 5.11 for the good and bad.

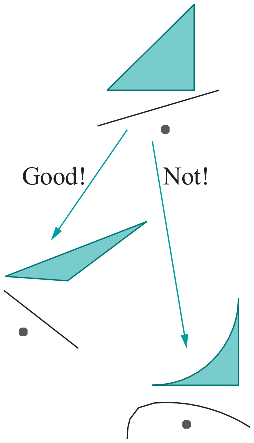

Figure 5.11: Good and bad transformations from an API programmer's point of view.

If the API designer is understandably reluctant to open this particular can of worms, then she should restrict herself to modeling transformations which do keep primitives within their class. In case of OpenGL, this calls for transformations taking points to points, straight segments to straight segments, triangles to triangles and, preferably, convex polygons to convex polygons (the latter so that a straightforward fan triangulation maps to a corresponding one). However, even given these constraints, the designer would reasonably want the widest collection of transformations as possible at her disposal. From Exercise 5.25 and the discussion preceding it we see that what she's asking for, in fact, is the class of transformations of degree one, in other words, *affine transformations*.

And, indeed, we shall see in this chapter that the designers of OpenGL have implemented, barring a few degenerate calls, exactly the class of affine transformations as their modeling transformations.

5.2.3 Affine Transformations and Homogeneous Coordinates

Despite their virtues listed in the previous two sections, there is potentially a serious computational problem with applying affine transformations rather than linear ones. The source lies in the difference in how the two are defined. A linear transformation is given by an equation of the form

$$f^M(P) = MP$$

while an affine transformation by one of the form

$$g(P) = MP + D$$

The former is expressed as a single matrix-vector multiplication, while the latter by a matrix-vector multiplication *followed* by a vector-vector sum. It is the additional sum step which cascades when composing affine transformations.

For example, if $f^{M_1}, f^{M_2}, f^{M_3}, \ldots$ are linear transformations of $\mathbb{R}^m$, then for an m-vector P,

$$\begin{aligned} f^{M_1}(P) &= M_1 P \\ (f^{M_2} \circ f^{M_1})(P) &= (M_2 M_1) P \\ (f^{M_3} \circ f^{M_2} \circ f^{M_1})(P) &= (M_3 M_2 M_1) P \qquad (5.10) \end{aligned}$$

and so on. On the other hand, if $g_1, g_2, g_3, \ldots$ are affine transformations of $\mathbb{R}^m$ given by $g_1(P) = M_1 P + D_1$, $g_2(P) = M_2 P + D_2$, $g_3(P) = M_3 P + D_3, \ldots$, respectively, then for an m-vector P,

$$\begin{aligned} g_1(P) &= M_1 P + D_1 \\ (g_2 \circ g_1)(P) &= (M_2 M_1) P + M_2 D_1 + D_2 \\ (g_3 \circ g_2 \circ g_1)(P) &= (M_3 M_2 M_1) P + M_3 M_2 D_1 + M_3 D_2 + D_3 \qquad (5.11) \end{aligned}$$

It's not hard to see that the number of matrix operations grows quadratically with the number n of affine transformations $g_n \circ \ldots \circ g_2 \circ g_1$ being composed, versus linearly in the case $f^{M_n} \circ \ldots \circ f^{M_2} \circ f^{M_1}$ of linear transformations. Composing affine transformations, at least by means of equations as above, therefore, is highly inefficient. There is an elegant way, however, to rectify the problem. It is with the help of so-called homogeneous coordinates.

Definition 5.3. A point

$$P = [x_1 \; x_2 \; \ldots \; x_m]^T$$

belonging to $\mathbb{R}^m$ is represented in *homogeneous coordinates* by *any* $m+1$-tuple of the form

$$[cx_1 \; cx_2 \ldots \; cx_m \; c]^T$$

where c is a *non-zero* scalar. Homogeneous coordinates, therefore, are not unique. And, note they live one dimension higher.

Example 5.7. Possible homogeneous coordinates of the point $P = [3\ 7]^T \in \mathbb{R}^2$ include $[3\ 7\ 1]^T$, $[16.5\ 38.5\ 5.5]^T$, $[-6\ -14\ -2]^T$, etc.

For our current purposes, though, it's good enough to fix the scalar c in Definition 5.3 to be 1. We'll have use for the general c later when studying projective spaces. So, for the present, assume that the point

$$P = [x_1 \; x_2 \; \ldots \; x_m]^T$$

is represented in homogeneous coordinates by

$$[x_1 \; x_2 \; \ldots \; x_m \; 1]^T$$

For example, $[3\ 7]^T$ would be homogenized to $[3\ 7\ 1]^T$. To save space we'll often write $[x_1 \; x_2 \ldots \; x_m \; 1]^T$ as $[P\ 1]^T$.

Observe now that Equations (5.9)

$$\begin{aligned}
x'_1 &= a_{11}x_1 + a_{12}x_2 + \ldots + a_{1m}x_m + d_1\\
x'_2 &= a_{21}x_1 + a_{22}x_2 + \ldots + a_{2m}x_m + d_2\\
&\ldots\ldots\\
x'_m &= a_{m1}x_1 + a_{m2}x_2 + \ldots + a_{mm}x_m + d_m
\end{aligned}$$

defining an affine transformation g are equivalent to the *single* matrix equation

$$\begin{bmatrix} x'_1\\ x'_2\\ \ldots\\ x'_m\\ 1 \end{bmatrix} = \begin{bmatrix} a_{11} & a_{12} & \ldots & a_{1m} & d_1\\ a_{21} & a_{22} & \ldots & a_{2m} & d_2\\ & \ldots & \ldots & & \\ a_{m1} & a_{m2} & \ldots & a_{mm} & d_m\\ 0 & 0 & 0 & 0 & 1 \end{bmatrix} \begin{bmatrix} x_1\\ x_2\\ \ldots\\ x_m\\ 1 \end{bmatrix}$$

(as is easily verified by multiplying the two matrices on the right). Concisely:

$$\begin{bmatrix} g(P)\\ 1 \end{bmatrix} = \begin{bmatrix} P'\\ 1 \end{bmatrix} = \begin{bmatrix} M & D\\ 0 & 1 \end{bmatrix} \begin{bmatrix} P\\ 1 \end{bmatrix} \qquad (5.12)$$

Presto! Computation of the affine transformation g, which earlier required a matrix-vector multiplication followed by a vector-vector addition, has now become a *single* matrix-vector multiplication with the use of homogeneous coordinates and, albeit, a bigger matrix. The translational component has, evidently, been subsumed into the one extra dimension of the larger matrix.

Example 5.8. The affine transformation $g : \mathbb{R}^2 \to \mathbb{R}^2$ given by

$$g\left(\begin{bmatrix} x\\ y \end{bmatrix}\right) = \begin{bmatrix} x'\\ y' \end{bmatrix} = \begin{bmatrix} 2 & 1\\ 0 & 4 \end{bmatrix} \begin{bmatrix} x\\ y \end{bmatrix} + \begin{bmatrix} 4\\ 6 \end{bmatrix}$$

can be written using homogeneous coordinates as

$$\begin{bmatrix} x'\\ y'\\ 1 \end{bmatrix} = \begin{bmatrix} 2 & 1 & 4\\ 0 & 4 & 6\\ 0 & 0 & 1 \end{bmatrix} \begin{bmatrix} x\\ y\\ 1 \end{bmatrix}$$

Let's give it a check for, say, the point $[1\ 1]^T$. Now,

$$g\left(\begin{bmatrix}1\\1\end{bmatrix}\right) = \begin{bmatrix}2 & 1\\0 & 4\end{bmatrix}\begin{bmatrix}1\\1\end{bmatrix} + \begin{bmatrix}4\\6\end{bmatrix} = \begin{bmatrix}7\\10\end{bmatrix}$$

and with homogeneous coordinates

$$\begin{bmatrix}2 & 1 & 4\\0 & 4 & 6\\0 & 0 & 1\end{bmatrix}\begin{bmatrix}1\\1\\1\end{bmatrix} = \begin{bmatrix}7\\10\\1\end{bmatrix}$$

the RHS of the preceding equation indeed being the homogenization of the RHS of the one before it.

Exercise 5.27. Express the affine transformation g of $\mathbb{R}^2$ given by

$$g\left(\begin{bmatrix}x\\y\end{bmatrix}\right) = \begin{bmatrix}-1 & 2\\-3 & 0\end{bmatrix}\begin{bmatrix}x\\y\end{bmatrix} + \begin{bmatrix}2\\1\end{bmatrix}$$

as a single matrix vector multiplication using homogeneous coordinates.

The composition of affine transformations is drastically simplified with use of homogeneous coordinates. For example, the third equation of (5.11), which had a cascading RHS, now becomes

$$\begin{bmatrix}(g_3 \circ g_2 \circ g_1)(P)\\1\end{bmatrix} = \left(\begin{bmatrix}M_3 & D_3\\0 & 1\end{bmatrix}\begin{bmatrix}M_2 & D_2\\0 & 1\end{bmatrix}\begin{bmatrix}M_1 & D_1\\0 & 1\end{bmatrix}\right)\begin{bmatrix}P\\1\end{bmatrix}$$

the number of matrix operations growing linearly with the number of affine transformations being composed, instead of quadratically.

Exercise 5.28. If you did Exercise 5.22, then you have determined the affine transformation $f \circ g$, where

$$f(P) = \begin{bmatrix}2 & 1\\0 & 4\end{bmatrix}P + [4\ 6]^T \quad \text{and} \quad g(P) = \begin{bmatrix}-1 & 3\\1 & -2\end{bmatrix}P + [-1\ 0]^T$$

Now, verify your answer by multiplying the 3×3 matrices corresponding to f and g.

5.3 Geometric Transformations in 2-Space Continued

We resume our study of 2D geometric transformations, equipped now with a newfound grasp of affine transformations.

5.3.1 Affine Geometric Transformations

Are translations, scalings, rotations about the origin and reflections about radial mirrors, which we studied in the opening section, affine transformations? Of course, they all are! This follows easily from the non-singularity of the matrix on the RHS of each of the Equations (5.1), (5.2), (5.4) and (5.5).

Exercise 5.29. Prove that rotations about arbitrary points (not necessarily the origin) and reflections about arbitrary mirrors (not necessarily radial) are affine as well.

That translations, scalings, rotations and reflections are affine means they are geometrically well-behaved, preserving straightness, parallelism and convexity, as well. We record this fact as a proposition.

Proposition 5.2. *Let g be either a translation, a scaling, a rotation (about an arbitrary point) or a reflection (about an arbitrary mirror). Then:*

(a) g maps straight lines to straight lines. Moreover, it maps parallel straight lines to parallel straight lines and intersecting straight lines to intersecting straight lines.

(b) g maps convex sets to convex sets. Moreover, it maps the convex hull of $\{P_1, P_2, \ldots, P_k\}$ *to the convex hull of* $\{f^M(P_1), f^M(P_2), \ldots, f^M(P_k)\}$.

Proof. Follows from Proposition 5.1 for 2D affine transformations in general.

Geometric Transformation Equations Using Homogeneous Coordinates

In Section 5.2.3 we learned how to express an affine transformation as a single matrix-vector multiplication, after writing points in homogeneous coordinates. In the case of R^2 this means writing $P = [x\ y]^T$ as $[x\ y\ 1]^T$ or $[P\ 1]^T$ for short. Let's now rewrite Equations (5.1), (5.2), (5.4) and (5.5) of the basic 2D transformations using homogeneous coordinates:

Translation by displacement vector $[d_x\ d_y]^T$:

$$\begin{bmatrix} P' \\ 1 \end{bmatrix} = \begin{bmatrix} 1 & 0 & d_x \\ 0 & 1 & d_y \\ 0 & 0 & 1 \end{bmatrix} \begin{bmatrix} P \\ 1 \end{bmatrix} \tag{5.13}$$

Scaling by a factor of s_x along the x-axis and s_y along the y-axis:

$$\begin{bmatrix} P' \\ 1 \end{bmatrix} = \begin{bmatrix} s_x & 0 & 0 \\ 0 & s_y & 0 \\ 0 & 0 & 1 \end{bmatrix} \begin{bmatrix} P \\ 1 \end{bmatrix} \tag{5.14}$$

Rotation by an angle θ counter-clockwise about the origin:

$$\begin{bmatrix} P' \\ 1 \end{bmatrix} = \begin{bmatrix} \cos\theta & -\sin\theta & 0 \\ \sin\theta & \cos\theta & 0 \\ 0 & 0 & 1 \end{bmatrix} \begin{bmatrix} P \\ 1 \end{bmatrix} \tag{5.15}$$

Reflection about a radial mirror l at an angle of θ counter-clockwise from the positive x-axis:

$$\begin{bmatrix} P' \\ 1 \end{bmatrix} = \begin{bmatrix} \cos 2\theta & \sin 2\theta & 0 \\ \sin 2\theta & -\cos 2\theta & 0 \\ 0 & 0 & 1 \end{bmatrix} \begin{bmatrix} P \\ 1 \end{bmatrix} \tag{5.16}$$

Exercise 5.30. Write the 3× 3 matrix corresponding to each of the following affine transformations:

(a) Translation by the displacement vector $[-2\ 3]^T$.

(b) Scaling by a factor of 2 in the x-direction and 4 in the y.

(c) Counter-clockwise rotation by an angle of -45° about the origin.

(d) Reflection about the radial mirror making an angle of 30° measured counter-clockwise from the positive direction of the x-axis.

Factoring Affine Transformations

We know then that affine transformations include translations, scalings and rotations. But are they more than just these three special kinds of transformations? It's extremely important that the answer is *no* in the following sense: *any* affine transformation can be "made from" translations, scalings and rotations; precisely, any affine transformation can be expressed as a composition of transformations of just these three kinds. Here is the formal statement:

Proposition 5.3. *Any affine transformation of* $\mathbb{R}^2$ *is the composition in some order of translations, scalings and rotations about the origin.*

In particular, any affine transformation $g : \mathbb{R}^2 \to \mathbb{R}^2$ *can be factored into a composition* $g = g_4 \circ g_3 \circ g_2 \circ g_1$*, where* g_1 *is a rotation about the origin,* g_2 *a scaling,* g_3 *another rotation about the origin and* g_4 *a translation.*

Proof. Let

$$g(P) = MP + D$$

where $M = \begin{bmatrix} a_{11} & a_{12} \\ a_{21} & a_{22} \end{bmatrix}$ is g's non-singular 2×2 defining matrix and the 2-vector $D = \begin{bmatrix} d_x \\ d_y \end{bmatrix}$ is its translational component.

We claim first that it is possible to find 2×2 matrices M_1, M_2 and M_3, corresponding, respectively, to a rotation about the origin, a scaling and another rotation about the origin, such that

$$M = M_3 M_2 M_1$$

Say M_1 corresponds to a rotation by angle θ, M_2 to scaling by a factor of s_x along the x-axis and s_y along the y-axis, and M_3 to a rotation by angle φ. The preceding equation gives, therefore, that

$$\begin{bmatrix} a_{11} & a_{12} \\ a_{21} & a_{22} \end{bmatrix} = \begin{bmatrix} \cos\varphi & -\sin\varphi \\ \sin\varphi & \cos\varphi \end{bmatrix} \begin{bmatrix} s_x & 0 \\ 0 & s_y \end{bmatrix} \begin{bmatrix} \cos\theta & -\sin\theta \\ \sin\theta & \cos\theta \end{bmatrix} \qquad (5.17)$$

which we'll show next can be solved to find φ, θ, s_x and s_y.

Multiply the three matrices on the RHS of the preceding equation and then equate terms of the resulting matrix with the corresponding ones on the LHS to see that:

$$\begin{aligned} a_{11} &= s_x \cos\varphi \cos\theta - s_y \sin\varphi \sin\theta \\ a_{12} &= -s_x \cos\varphi \sin\theta - s_y \sin\varphi \cos\theta \\ a_{21} &= s_x \sin\varphi \cos\theta + s_y \cos\varphi \sin\theta \\ a_{22} &= -s_x \sin\varphi \sin\theta + s_y \cos\varphi \cos\theta \end{aligned} \qquad (5.18)$$

Four equations in four unknowns seems right. Check that:

$$\begin{aligned} a_{21} - a_{12} &= (s_x + s_y)\sin(\varphi + \theta) \\ a_{11} + a_{22} &= (s_x + s_y)\cos(\varphi + \theta) \\ a_{21} + a_{12} &= (s_x - s_y)\sin(\varphi - \theta) \\ a_{11} - a_{22} &= (s_x - s_y)\cos(\varphi - \theta) \end{aligned} \qquad (5.19)$$

Assuming for the moment that neither $a_{11} + a_{22}$ nor $a_{11} - a_{22}$ is zero, divide the first equation above by the second and the third by the fourth to get:

$$\begin{aligned} \tan(\varphi + \theta) &= \frac{a_{21} - a_{12}}{a_{11} + a_{22}} \\ \tan(\varphi \_ \theta) &= \frac{a_{21} + a_{12}}{a_{11} - a_{22}} \end{aligned} \qquad (5.20)$$

which implies:

$$\begin{aligned} \varphi + \theta &= \tan^{-1}\left(\frac{a_{21} - a_{12}}{a_{11} + a_{22}}\right) \\ \varphi - \theta &= \tan^{-1}\left(\frac{a_{21} + a_{12}}{a_{11} - a_{22}}\right) \end{aligned} \qquad (5.21)$$

These two equations can be solved to determine φ and θ. Furthermore, the values of $\varphi + \theta$ and $\varphi - \theta$ can then be substituted back into equation set (5.19) to determine equations for $s_x + s_y$ and $s_x - s_y$, which can then be solved to find s_x and s_y.

The earlier claim that (5.17) can be solved to find φ, θ, s_x and s_y is proved and, therefore, $M = M_3M_2M_1$, in the manner claimed at the start of the proof as well – *except* when either or both of $a_{11} + a_{22}$ and $a_{11} - a_{22}$ is 0, in which case Exercise 5.34 below helps verify the claim.

As $g(P) = MP + D = (M_3M_2M_1)P + D$ one concludes, finally, that indeed $g = g_4 \circ g_3 \circ g_2 \circ g_1$, where g_1 is the counter-clockwise rotation about the origin by an angle of θ, g_2 the scaling by a factor of s_x along the x-axis and s_y along the y-axis, g_3 the counter-clockwise rotation about the origin by an angle of φ and g_4 translation by the displacement vector D.

Since a non-singular linear transformation of $\mathbb{R}^2$ is simply an affine transformation with null translational component, we have also proved the following on the way to proving Proposition 5.3:

Proposition 5.4. *Any non-singular linear transformation of* $\mathbb{R}^2$ *is the composition successively of a rotation about the origin, a scaling and another rotation about the origin.*

Example 5.9. Factor the affine transformation

$$g(P) = \begin{bmatrix} 1 & \frac{\sqrt{3}}{2} \\ \frac{\sqrt{3}}{2} & 0 \end{bmatrix} P + \begin{bmatrix} 2 \\ 1 \end{bmatrix}$$

according to Proposition 5.3.

Answer: From Equations (5.21) we have

$$\varphi + \theta = \tan^{-1} 0 = 0^\circ \quad \text{and} \quad \varphi - \theta = \tan^{-1}\sqrt{3} = 60^\circ$$

which solve to

$$\varphi = 30^\circ \quad \text{and} \quad \theta = -30^\circ$$

Plugging the values of $\varphi + \theta$ and $\varphi - \theta$ into the second and fourth equations of (5.19) we have

$$1 = (s_x + s_y)\cos 0^\circ = s_x + s_y \quad \text{and} \quad 1 = (s_x - s_y)\cos 60^\circ = \frac{1}{2}(s_x - s_y)$$

which solve to

$$s_x = \frac{3}{2} \quad \text{and} \quad s_y = -\frac{1}{2}$$

(If the reader is wondering about the other two equations in (5.19) – the first and third – she may check that these are satisfied as well by the values found above for φ, θ, s_x and s_y.)

Therefore, $g = g_4 \circ g_3 \circ g_2 \circ g_1$, where g_1 is the clockwise rotation about the origin by an angle of 30°, g_2 the scaling by a factor of $\frac{3}{2}$ along the x-axis and $-\frac{1}{2}$ along the y-axis, g_3 the counter-clockwise rotation about the origin by an angle of 30°, and g_4 translation by the displacement vector $[2\ 1]^T$.

Exercise 5.31. Factor the affine transformation

$$g(P) = \begin{bmatrix} 1 & \frac{1}{2} \\ \frac{1}{2} & 0 \end{bmatrix} P + \begin{bmatrix} -1 \\ 1 \end{bmatrix}$$

according to Proposition 5.3.

Exercise 5.32. Is factorization according to Proposition 5.3 unique, or might there be affine transformations which can be so factored in more than one way?

Exercise 5.33. Give an example of an affine transformation g which itself is not a translation nor a scaling nor a rotation about the origin. Of course, g can be made by composing such transformations by the proposition.

Exercise 5.34. Fill in the gap in the proof of Proposition 5.3, where it was assumed (just after Equations (5.19)) that neither $a_{11} + a_{22}$ nor $a_{11} - a_{22}$ is zero. In particular, even if one or both of these quantities is zero, show how to proceed again from (5.19) to solve for φ, θ, s_x and s_y.

Hint : Suppose $a_{11} - a_{22} = 0$. The fourth equation of set 5.19 then says either $s_x = s_y$ or $\varphi = \theta \pm \pi/2$, or both. Suppose, firstly, $s_x = s_y$. Then the first and third equations of set 5.18 give

$$\begin{aligned} a_{11} &= s_x \cos(\varphi + \theta) \\ a_{21} &= s_x \sin(\varphi + \theta) \end{aligned}$$

which means $s_x = \sqrt{a_{11}^2 + a_{21}^2}$. And so on . . ..

Exercise 5.35. Following up on the previous exercise, factor the affine transformation

$$g(P) = \begin{bmatrix} \frac{1}{2} & \sqrt{3} \\ 0 & \frac{1}{2} \end{bmatrix} P$$

according to Proposition 5.3.

Exercise 5.36. Show that a shear along a radial line is a non-singular linear transformation of $\mathbb{R}^2$. Accordingly, factor the shear of angle 30° along the y-axis according to Proposition 5.4.

Remark 5.3. The reader may have noticed that we never used the non-singularity of M in the proof of Proposition 5.3. As a matter of fact, even if M is singular, it can be still written as $M = M_3 M_2 M_1$ as in the proposition, *except* that the scaling M_2 turns out to be degenerate.

Proposition 5.3 suggests that translations, scalings and rotations about the origin are fundamental in the sense that they can be used to generate *all* affine transformations, a particularly useful insight for anyone in Flatland trying to implement a graphics API. For, all such a programmer has to code is an implementation of each of those three special kinds of affine transformations, to get the rest automatically. (OpenGL's modeling transformations are beginning to look good aren't they?)

5.3.2 Euclidean and Rigid Transformations

Proposition 5.2 tells us that transformations such as translations, scalings, rotations and reflections are respectful of a bunch of geometric attributes, from straightness to convexity. How about that most important geometric attribute of all, though, namely, distance? We would say a transformation g *preserves distance* if it were true that, for any pair of points P and Q, the distance between $f(P)$ and $f(Q)$ is the same as that between P and Q.

One has only to consider scalings to see that distance is not preserved by transformations in general. However, there certainly are transformations that seem to preserve distance. Translations come to mind, as points are "carried together" by a translation, so neither pulled apart nor drawn closer together. Similar thoughts apply to rotations.

Distance-preserving transformations are important in animation because they preserve *shape* as well. In fact, an object's shape is not changed precisely when the distance between *every* pair of points belonging to it is not changed. See Figure 5.12. Comparing the pre-hit and post-hit heads, one observes that the distance between at least two pairs of points is different from those between the transformed pairs: the eyeballs, and P and Q. On the other hand, the distance between any pair of points of the book remains unchanged.

Transformations preserving distances are the ones, therefore, to use when animating *rigid* objects such as balls, bats (not the flying kind) and houses. They are important enough, in fact, to have been honored with the name of the great ancient geometer Euclid. Here's a formal definition.

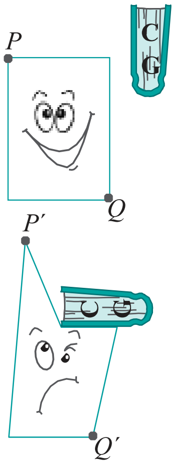

Figure 5.12: Square-headed student struck by a CG book: the shape of the head is distorted, but not that of the book.

Definition 5.4. A *Euclidean transformation* (also called *isometry*) of R^2 is one that preserves distance. Precisely, $f : R^2 \to R^2$ is Euclidean if $|f(P)f(Q)| = |PQ|$ for any two points $P, Q \in R^2$.

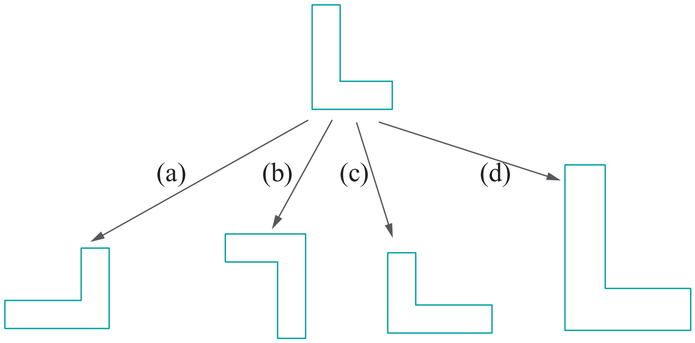

Figure 5.13: Transformations (a)-(c) are Euclidean, (d) is not.

See Figure 5.13 for three simple examples of Euclidean and one of non-Euclidean transformation. It may seem, as it cannot alter shape, that all a Euclidean transformation can do is "slide" an object around the plane, which, if true, would imply that it is merely a composition of translations and rotations. However, compare the Euclidean transformations in cases (a), (b) and (c) of Figure 5.13. The first two can certainly be obtained by sliding the top L around the page. However, it's not hard to convince oneself that (c) cannot and, therefore, is not a combination of translations and rotations.

Let's examine (c). As indicated in Figure 5.14, it can, in fact, be obtained by applying a reflection about a vertical mirror l, followed by translation and rotation. A reflection is required because (c) is a so-called orientation-reversing transformation. Here's the relevant definition:

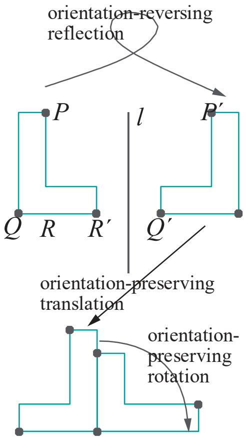
orientation-reversing reflection
P
l
P′
Q
R
R′
Q′
orientation-preserving translation
orientation-preserving rotation

Figure 5.14: Executing (c) of Figure 5.13 by a reflection about the mirror l followed by translation and rotation.

Definition 5.5. A Euclidean transformation f of R^2 is said to be *orientation-reversing* if there exist three non-collinear points P , Q and R in R^2 such that, looking at R^2 from a fixed side, one of the two sequences PQR and $f(P)f(Q)f(R)$ appears clockwise (CW) and the other counter-clockwise (CCW).

A Euclidean transformation that is not orientation-reversing is said to be *orientation-preserving*.

Orientation-preserving Euclidean transformations are also called *rigid transformations*.

Remark 5.4. The property of the transformation f described in the first paragraph of the preceding definition does not depend on the choice of the non-collinear points

P, Q and R. In fact, as we'll see, if for *some* three non-collinear points P, Q and R it is true that PQR and $f(P)f(Q)f(R)$ appear oriented differently, then this is true for *any* three non-collinear points.

Rigid transformations are so called because they model the physical motion of a rigid object restricted always to a plane – such motion can never reverse orientation. Conceptually, reversing orientation requires the object to be "lifted off the plane, flipped and placed back."

The sequence PQR in Figure 5.14 appears CCW to the reader, while that of their images $P^1Q^1R^1$ by reflection about l appears CW, proving that the reflection is indeed orientation-reversing and, therefore, not rigid.

Exercise 5.37. Show that a Euclidean transformation f preserves angles, i.e., $\angle ABC = \angle f(A)f(B)f(C)$, where A, B, C are any three points on the plane.

We'll see next how to determine algorithmically if PQR appears CW or CCW to a given viewer, which will in turn help decide if a transformation is orientation-preserving or not.

Lemma 5.1. *Let $P = [x_1\ y_1]^T$, $Q = [x_2\ y_2]^T$ and $R = [x_3\ y_3]^T$ be three points on the plane. Define the scalar D by*

$$D = x_1y_2 - x_2y_1 + x_2y_3 - x_3y_2 + x_3y_1 - x_1y_3 = \begin{matrix} x_1 & x_2 & x_3 \\ y_1 & y_2 & y_3 \\ 1 & 1 & 1 \end{matrix}$$

the rightmost term being called the discriminant determinant.

Let V be a viewer on the positive side of the z-axis of a hypothetical right-handed system. We have then the following:

1. *If $D = 0$, then P, Q and R are collinear.*
2. *If $D < 0$, then V perceives the order PQR as CW.*
3. *If $D > 0$, then V perceives the order PQR as CCW.*

Note: The column vectors of the discriminant determinant are the coordinates of P, Q and R, respectively, homogenized; so, it can be written

$$D = \begin{matrix} P & Q & R \\ 1 & 1 & 1 \end{matrix}$$

Proof. We'll first prove the lemma assuming that $R = O$, the origin, in which case

$$D = \begin{matrix} x_1 & x_2 & 0 \\ y_1 & y_2 & 0 \\ 1 & 1 & 1 \end{matrix} = x_1y_2 - x_2y_1$$

If $P = O$ as well, then P, Q and R are trivially collinear, and it's easily seen that the determinant $D = 0$, too, which falls into case 1 of the lemma. Accordingly, suppose that $P /= O$ as in Figure 5.15. Now, the straight line l through P and R has the equation $x_1y - y_1x = 0$.

If Q does not lie on l, then whether PQR appears CW or CCW to V depends on which half-plane of l contains Q. In particular, if Q lies in the half-plane $x_1y - y_1x > 0$ – the case depicted in the figure – then PQR appears CCW to V; if in the half-plane $x_1y - y_1x < 0$, then CW. Plugging in Q's coordinates means that PQR appears CCW to V if $x_1y_2 - y_1x_2 > 0$ and CW if $x_1y_2 - y_1x_2 < 0$. Of course, $x_1y_2 - y_1x_2 = 0$ if Q lies on l, in which case P, Q and R are collinear. As $D = x_1y_2 - y_1x_2$, we've proved the lemma assuming $R = O$.

The case of arbitrary R can be reduced to that of $R = O$ by applying the translation $-R$ to all three points, because the relative dispositions of P, Q and R

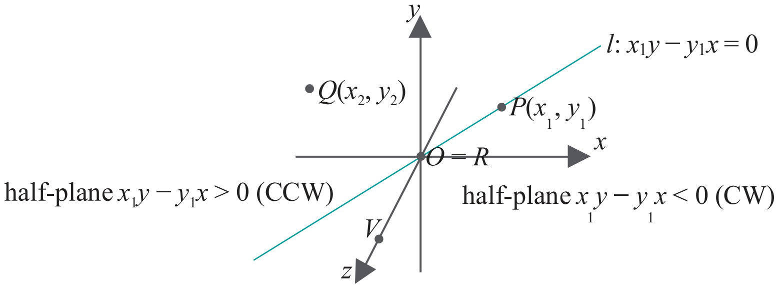
y
l: $x_1y - y_1x = 0$
$Q(x_2, y_2)$
$P(x_1, y_1)$
x
$O = R$
half-plane $x_1y - y_1x > 0$ (CCW)
half-plane $x_1y - y_1x < 0$ (CW)
V
z

Figure 5.15: The orientation of PQR perceived by V depends on the half-plane of l containing Q (Q is depicted here in the half-plane $x_1y - y_1x > 0$).

as they appear to V are the same as those of $P- R$, $Q- R$ and $R- R$ (= O). Now, $P -R = [x_1 -x_3 \; y_1 -y_3]^T$ and $Q -R = [x_2 -x_3 \; y_2 -y_3]^T$, and we leave it to the reader to use the case $R = O$ to finish up the proof.

Exercise 5.38. Verify the lemma for the following triples by plotting the points on paper:

(a) $P = [1\ 0]^T$, $Q = [0\ 1]^T$, $R = [0\ 0]^T$

(b) $P = [-1 - 1]^T$, $Q = [-2\ 1]^T$, $R = [3\ 4]^T$

The following proposition is intuitively clear but, nevertheless, has to be proved formally.

Proposition 5.5. *A translation or a rotation about an arbitrary point is a rigid transformation of 2-space. A reflection about an arbitrary mirror is an orientation-reversing Euclidean transformation of 2-space.*

Proof. We'll prove first that a translation t by the displacement vector $D = [d_x\ d_y]^T$ preserves both distance and orientation.

Let $P = [x_1\ y_1]^T$ and $Q = [x_2\ y_2]^T$ be two points in R^2. The images of P and Q by t are, respectively, $P^1 = P + D = [x_1 + d_x\ y_1 + d_y]^T$ and $Q^1 = Q + D = [x_2 + d_x\ y_2 + d_y]^T$. Now,

$$|PQ| = \overline{(x_1 - x_2)^2 + (y_1 - y_2)^2}$$

and

$$\begin{aligned} |P^1Q^1| &= \overline{\underline{((x_1 + d_x) - (x_2 + d_x))}^2 + ((y_1 + d_y) - (y_2 + d_y))^2} \\ &= (x_1 - x_2)^2 + (y_1 - y_2)^2 \end{aligned}$$

proving t indeed preserves distance.

Let $P = [x_1\ y_1]^T$, $Q = [x_2\ y_2]^T$ and $R = [x_3\ y_3]^T$ be three points in R^2, and V a viewer on the positive side of the z-axis. Lemma 5.1 says that PQR are collinear, appear CW to V, or CCW to V, according as the determinant

$$D = \begin{matrix} x_1 & x_2 & x_3 \\ y_1 & y_2 & y_3 \\ 1 & 1 & 1 \end{matrix}$$

is equal to, less than, or greater than 0.

The images of P, Q and R by t are $P^1 = P + D = [x_1 + d_x\ \ y_1 + d_y]^T$, $Q^1 = Q + D = [x_2 + d_x\ y_2 + d_y]^T$ and $R^1 = R + D = [x_3 + d_x\ y_3 + d_y]^T$, respectively. By another application of Lemma 5.1, $P^1Q^1R^1$ are collinear, appear CW to V, or CCW to V, according as the determinant

$$D^1 = \begin{matrix} x_1 + d_x & x_2 + d_x & x_3 + d_x \\ y_1 + d_y & y_2 + d_y & y_3 + d_y \\ 1 & 1 & 1 \end{matrix}$$

is equal to, less than, or greater than 0.

However, subtracting d_x times the third row of D^1 from its first and d_y times the third row from the second, we see that, in fact, $D = D^1$. It follows that the relative dispositions of PQR and of $P^1Q^1R^1$ (either CCW or CW) with respect to V are identical, giving the conclusion that t indeed preserves orientation.

The proofs for rotations and reflections are left to the reader.

Exercise 5.39. Scalings in general are not Euclidean transformations, but for certain choices of scaling factors they are. List these choices and for each say if it preserves or reverses orientation.

Exercise 5.40. Show that the composition of two Euclidean transformations is Euclidean and that of two rigid transformations is rigid.

Exercise 5.41. Show that the composition of two orientation-reversing Euclidean transformations is an orientation-preserving Euclidean transformation (in other words, rigid). Show that the composition of an orientation-preserving and an orientation-reversing Euclidean transformation is orientation-reversing.

We saw in Proposition 5.3 that an affine transformation can be factored as a composition of translations, scalings and rotations about the origin. The following proposition shows how Euclidean and rigid transformations can be factored. The first part verifies our intuition that a rigid transformation slides an object around the plane by translation and rotation, while the second says that a Euclidean transformation is at most one reflection away from being rigid.

Proposition 5.6. *A rigid transformation of* R^2 *keeping the origin fixed is a rotation about the origin, while an arbitrary rigid transformation is a composition of a rotation about the origin followed by a translation.*

A Euclidean transformation of R^2 *is a composition of a rotation about the origin, followed by a translation, possibly followed again by a reflection.*

Proof. Consider, first, a rigid transformation $f : R^2 \rightarrow R^2$ keeping the origin fixed, i.e., $f(O) = O$. Let $P \in R^2$ be different from the origin. By the distance-preserving property

$$|OP| = |f(O)f(P)| = |Of(P)|$$

so both P and $f(P)$ lie on a circle c centered at O. See Figure 5.16(a) or (b). Say the angle from OP to $Of(P)$ is θ measured counter-clockwise. We'll show for any point $Q \in R^2$ that its image $f(Q)$ is obtained by rotating Q counter-clockwise by an angle of θ about the origin as well, proving the claim that f is a rotation about the origin.

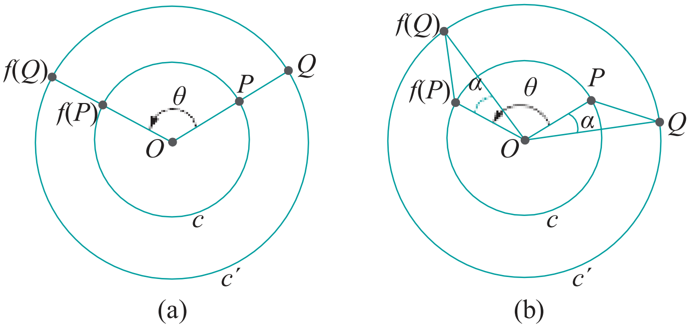

Figure 5.16: Illustrations for the proof of Proposition 5.6.

Let Q be an arbitrary point on the plane. Without loss of generality assume $Q = O$. Reasoning as before, then, both Q and $f(Q)$ lie on some circle c^1 centered at O. By the distance-preserving property

$$|PQ| = |f(P)f(Q)|$$

Consider first the case that Q lies on the straight line through O and P (Figure 5.16(a)). Because $P|Q = |f(|P)f(Q)$,| it's seen that $f(Q)$ lies at the intersection with c^1 of the straight line through O and $f(P)$, as all other points on c^1 are at a distance more than $|PQ|$ from $f(P)$. In this case, $f(Q)$ is indeed obtained by rotating Q counter-clockwise by an angle of θ about the origin.

Next, consider the case that Q does not lie on the straight line through O and P. First, suppose that the vertex order POQ appears CCW to the viewer (Figure 5.16(b)). Let the angle POQ be a. The congruence of the triangles POQ and $f(P)Of(Q)$, a consequence of the distance-preserving property, implies that angle $f(P)Of(Q)$ is a as well. Furthermore, f being rigid preserves orientation, so $f(P)Of(Q)$ appears CCW to the viewer as well. It follows from simple angular arithmetic that $f(Q)$ is θ counter-clockwise about the origin from Q.

If the vertex order POQ appears CW instead, a similar conclusion can still be reached. This completes the proof that a rigid transformation keeping the origin fixed is a rotation about the origin.

Suppose, next, that f is an arbitrary rigid transformation, not necessarily fixing the origin. Let $f(O) = O^1$ and t be translation by the displacement vector O^1O. Then the transformation $f^1 = t\circ f$ is a rigid transformation such that $f^1(O) = O$, i.e., fixing the origin. Therefore, as proved earlier, f^1 is a rotation about the origin. Consequently, $f = t^{-1} f\circ^1$ is a rotation about the origin followed by a translation, proving the statement of the proposition about arbitrary rigid transformations and completing the proof of the first paragraph.

Note: If f is itself a translation then, of course, the rotation f^1 about the origin is the identity, i.e., zero rotation.

For the second paragraph of the proposition, suppose that f is an orientation-reversing Euclidean transformation, because if f is orientation-preserving, then it is rigid, and there is nothing to prove after the first paragraph.

Let w be a reflection about any mirror, an orientation-reversing Euclidean transformation by Proposition 5.5. Then $f^1 = w\circ f$, being a composition of two orientation-reversing Euclidean transformations, is rigid by Exercise 5.41. By the first part of the proposition, f^1 is a rotation about the origin followed by a translation, implying that $f = w^{-1}\circ f^1$ is the composition of a rotation about the origin, followed by a translation and, then, a reflection. This completes the proof of the second paragraph.

Exercise 5.42. Apply the proposition to show that a rigid transformation which keeps

(a) no point fixed is a translation.

(b) exactly one point fixed is a rotation (about the fixed point as center).

(c) more than one point fixed is the identity (which, therefore, keeps every point fixed, so also is a zero translation and a zero rotation).

Exercise 5.43. Use Exercises 5.16 and 5.42 to prove that any Euclidean transformation can be obtained by composing reflections about at most three mirrors.

Exercise 5.44. At the end of Section 5.1.3 we saw one case that the composition of two rotations (about arbitrary centers) is a translation and one where it is again a rotation. Use Exercise 5.42 to prove now that these are the only two possibilities in general for the composition of two rotations.

Moreover, show how to decide which case arises by proving:

1. The composition of two rotations, either both counter-clockwise or both clockwise, one of angle θ_1 and one of angle θ_2, about arbitrary centers, is a translation if either $\theta_1 = \theta_2 = 0$ or $\theta_1 + \theta_2 = 2\pi$ (assume $0 \leq \theta_1, \theta_2 < 2\pi$); otherwise, it is a rotation.

2. The composition of two rotations, one counter-clockwise of angle θ_1 and the other clockwise of angle θ_2, about arbitrary centers, is a translation if $\theta_1 = \theta_2$ (assume $0 \leq \theta_1, \theta_2 < 2\pi$); otherwise, it is a rotation.

Proposition 5.7. *Affine, Euclidean and rigid transformations of 2-space are related by the following inclusions, which are each proper:*

$$\textit{rigid transforms} \subset \textit{Euclidean transforms} \subset \textit{affine transforms}$$

Proof. The first inclusion follows from the definitions. It is proper because a reflection about any mirror is Euclidean but not rigid.

From Proposition 5.6 it follows that a Euclidean transformation is a composition of affine transformations (because translations, rotations and reflections are all affine) and, therefore, itself affine, proving the second inclusion. The inclusion is proper because a scaling by factors not all of unit magnitude is affine but not Euclidean.

Remark 5.5. An interesting perspective on the proposition is to think of affine transformations as being made from translations, rotations, reflections and scalings; Euclidean transformations from translations, rotations and reflections; and rigid transformations from translations and rotations.

The worked example next implies that Definition 5.5 about whether a Euclidean transformation reverses or preserves orientation is, in fact, independent of the choice of the three non-collinear points P, Q and R.

Example 5.10. Suppose that an affine transformation g of R^2 maps *some* three non-collinear points P , Q and R in a manner that, looking at R^2 from a fixed side, one of the sequences PQR and $g(P)g(Q)g(R)$ appears CW and the other CCW.

Show, then, that for *any* three non-collinear points X, Y and Z, one of the sequences XYZ and $g(X)g(Y)g(Z)$ appears CW and the other CCW, looking at R^2 from the same side.

Answer: Use homogeneous coordinates to write $[g(W)\ 1]^T = M[W\ 1]^T$, where M is a fixed non-singular 3× 3 matrix, and $W = [x\ y]^T$ is an arbitrary point of the plane. Suppose that $P = [x_1\ y_1]^T$, $Q = [x_2\ y_2]^T$ and $R = [x_3\ y_3]^T$. Consider the equation

$$M \begin{bmatrix} x_1 & x_2 & x_3 \\ y_1 & y_2 & y_3 \\ 1 & 1 & 1 \end{bmatrix} = \begin{bmatrix} x'_1 & x'_2 & x'_3 \\ y'_1 & y'_2 & y'_3 \\ 1 & 1 & 1 \end{bmatrix}$$

in matrices, which gives the following

$$det(M) * \begin{matrix} x_1 & x_2 & x_3 \\ y_1 & y_2 & y_3 \\ 1 & 1 & 1 \end{matrix} = \begin{matrix} x'_1 & x'_2 & x'_3 \\ y'_1 & y'_2 & y'_3 \\ 1 & 1 & 1 \end{matrix}$$

relating determinants. Now, $[x'_1\ y'_1\ 1]^T = M[x_1\ y_1\ 1]^T = M[P\ 1]^T = [g(P)\ 1]^T$. Likewise, $[x'_2\ y'_2\ 1]^T = [g(Q)\ 1]^T$ and $[x'_2\ y'_2\ 1]^T = [g(R)\ 1]^T$. Therefore, the preceding equation can be written

$$det(M) * \begin{matrix} P & Q & R \\ 1 & 1 & 1 \end{matrix} = \begin{matrix} g(P) & g(Q) & g(R) \\ 1 & 1 & 1 \end{matrix}$$

Considering the signs of the three determinants above, and applying Lemma 5.1, one sees that PQR and $g(P)g(Q)g(R)$ appear differently oriented, from a fixed side of the plane, if and only if $det(M)$ is negative. But, then, by similar calculations, exactly the same would be true of XYZ and $g(X)g(Y)g(Z)$, for any points X, Y and Z.

Exercise 5.45. Does the affine transformation of Example 5.8 preserve or reverse orientation?

5.4 Geometric Transformations in 3-Space

Finally, the real world. Our discussions will mirror those of the previous section. In fact, extending translations, scalings and reflections from 2D to 3D is almost automatic. We'll pay our dues, though, for entering 3-space with a fair bit of work on rotations.

5.4.1 Translation

A translation is specified by a displacement vector $D = [d_x\, d_y\, d_z]^T$. The image of the point $P = [x\ y\ z]^T$ by this translation is $P^1 = [x + d_x\ y + d_y\ z + d_z]^T$ (see Figure 5.17).

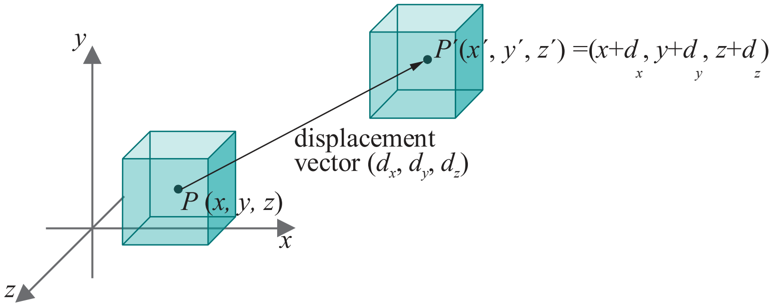
y
x
z
P′(x′, y′, z′) =(x+d_x, y+d_y, z+d_z)
displacement vector (d_x, d_y, d_z)
P (x, y, z)

Figure 5.17: Translation.

Equivalently,

$$P^1 = P + D = \begin{bmatrix} 1 & 0 & 0 \\ 0 & 1 & 0 \\ 0 & 0 & 1 \end{bmatrix} P + D$$

which in homogeneous form, analogous to the 2D version (5.13), is

$$\begin{bmatrix} P^1 \\ 1 \end{bmatrix} = \begin{bmatrix} 1 & 0 & 0 & d_x \\ 0 & 1 & 0 & d_y \\ 0 & 0 & 1 & d_z \\ 0 & 0 & 0 & 1 \end{bmatrix} \begin{bmatrix} P \\ 1 \end{bmatrix} \tag{5.22}$$

For the record, the 4 × 4 matrix corresponding to translation by the displacement vector $[d_x\ d_y\ d_z]^T$ is denoted $T(d_x, d_y, d_z)$ and given by

$$T(d_x, d_y, d_z) = \begin{bmatrix} 1 & 0 & 0 & d_x \\ 0 & 1 & 0 & d_y \\ 0 & 0 & 1 & d_z \\ 0 & 0 & 0 & 1 \end{bmatrix} \tag{5.23}$$

Exercise 5.46. Write the 4 × 4 matrix corresponding to translation by the displacement vector $[3\ 0\ -1]^T$.

Exercise 5.47. Use Equation (5.22) to prove that the composition of translations is a translation and that the inverse of a translation is a translation as well.

Note: By default we're in 3-space from now on and all exercises and examples are in 3D.

5.4.2 Scaling

A scaling is specified by scaling factors s_x, s_y and s_z along the x-, y- and z-axis, respectively. The image of the point $P = [x\ y\ z]^T$ by this scaling is $P^1 = [s_x x\ s_y y\ s_z z]^T$ (see Figure 5.18).

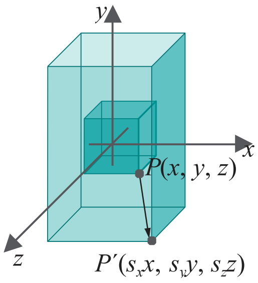

Figure 5.18: Scaling.

Without further ado we write the 4 × 4 matrix corresponding to this scaling as (compare the 2D Equation (5.14))

$$S(s_x, s_y, s_z) = \begin{bmatrix} s_x & 0 & 0 & 0 \\ 0 & s_y & 0 & 0 \\ 0 & 0 & s_z & 0 \\ 0 & 0 & 0 & 1 \end{bmatrix} \qquad (5.24)$$

If any one or more of the scaling factors s_x, s_y and s_z is zero, the scaling is said to be *degenerate*; otherwise, it is *non-degenerate*. Clearly, a scaling is non-degenerate if and only if its matrix is non-singular. By a scaling we shall always mean a non-degenerate one, unless stated otherwise.

Exercise 5.48. Write the 4× 4 matrix corresponding to scaling by the factors −1, 3 and 4 along the x-, y- and z-axis, respectively.

Exercise 5.49. Use (5.24) to prove that the composition of scalings is a scaling and that the inverse of a non-degenerate scaling is a non-degenerate scaling.

5.4.3 Rotation

Warning upfront : This section is much longer than the corresponding Section 5.1.3 on 2D rotations as there's much more to going around in 3D!

A rotation about a radial axis is specified by (a) a directed line l through the origin, which is the axis of rotation, and (b) the angle θ of the rotation.

We'll describe as a physical process how such a rotation maps a point P. First, if P lies on the axis l itself, then it does not move. Suppose, then, that P does not lie on l. Here's how it's mapped by the rotation (see Figure 5.19):

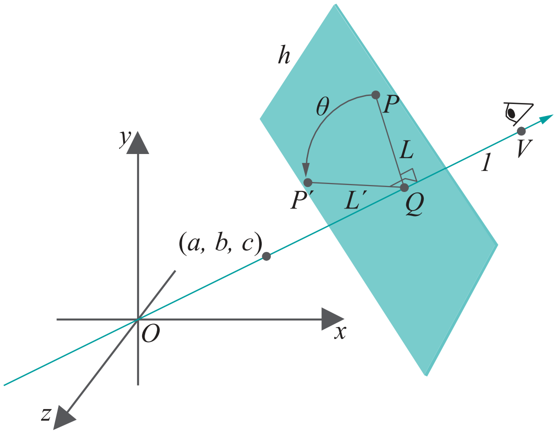

Figure 5.19: Rotation.

1. Drop the perpendicular from P to the point Q on l. Denote as L the segment PQ. L lies on the plane h perpendicular to l through Q.

   Note that Figure 5.19 has Q and h on the positive side of l, but they could very well be on the other side, or even touching the origin, depending on where P is.

2. Locate a viewer at V far enough in the positive direction of l as to be able to see h when looking toward the origin.

3. Rotate the segment L about Q, on the plane h, an angle θ counter-clockwise, as measured by the viewer.

4. If L^1 is the new position of L after rotation, then P is mapped to the corresponding endpoint P^1 of L^1.

Remark 5.6. Giving a single point (a, b, c), not equal to the origin, is enough to specify the directed radial line l through it, as indicated in Figure 5.19. Therefore, all that remains to specify a rotation about l is the angle θ. This, of course, is exactly how the OpenGL command glRotatef(θ, a, b, c) works, as described earlier in Section 4.1.3.

Rotation about the Coordinate Axes

The matrices corresponding to rotations in 3D *about the coordinate axes* are straightforwardly deduced from the 2D equation (5.3), reproduced below

$$\begin{bmatrix} x^1 \\ y^1 \end{bmatrix} = \begin{bmatrix} \cos\theta & -\sin\theta \\ \sin\theta & \cos\theta \end{bmatrix} \begin{bmatrix} x \\ y \end{bmatrix} \tag{5.25}$$

where $[x^1\ y^1]^T$ is the image of $[x\ y]^T$ by a rotation on the xy-plane by an angle of θ about the origin, measured counter-clockwise by a viewer V on the positive side of the z-axis (Figure 5.20(a)).

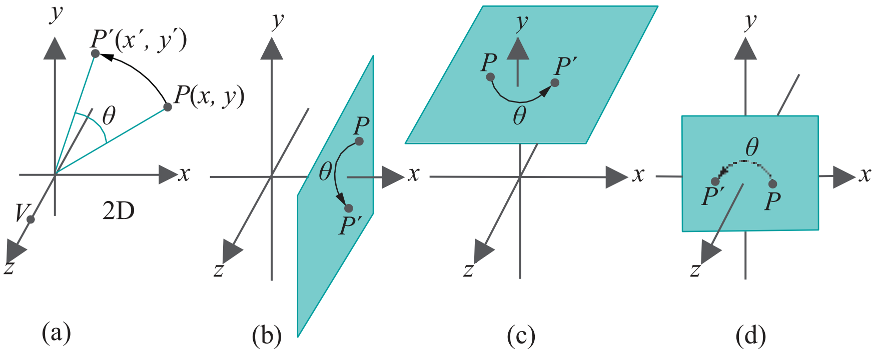

Figure 5.20: (a) 2D rotation on the xy-plane (b)-(d) 3D rotations about the coordinate axes.

Next, in 3D, rotation about the x-axis by an angle θ (Figure 5.20(b)) maps a point $P = [x\ y\ z]^T$ to the point $P^1 = [x^1\ y^1\ z^1]^T$, where

(a) $x^1 = x$, because P travels parallel to the yz-plane, so its x value never changes.

(b) $[y\ z]^T \mapsto [y^1\ z^1]^T$ is precisely as for a *2D rotation* by an angle θ CCW about the origin on the yz-plane, looking from the positive side of the x-axis.

To apply (b), replace x with y and y with z in (5.25), to get

$$\begin{bmatrix} y^1 \\ z^1 \end{bmatrix} = \begin{bmatrix} \cos\theta & -\sin\theta \\ \sin\theta & \cos\theta \end{bmatrix} \begin{bmatrix} y \\ z \end{bmatrix}$$

Therefore, the 4×4 matrix of 3D rotation about the x-axis is

$$R_x(\theta) = \begin{bmatrix} 1 & 0 & 0 & 0 \\ 0 & \cos\theta & -\sin\theta & 0 \\ 0 & \sin\theta & \cos\theta & 0 \\ 0 & 0 & 0 & 1 \end{bmatrix} \tag{5.26}$$

Rotation about the y-axis by an angle θ (Figure 5.20(c)) maps a point $P = [x\ y\ z]^T$ to the point $P^1 = [x^1\ y^1\ z^1]^T$, where:

(a) $y^1 = y$

(b) $[x\ z]^T \mapsto [x^1\ z^1]^T$ is as for a 2D rotation by an angle θ CCW about the origin on the xz-plane, looking from the positive side of the y-axis.

We have to be careful, though, in applying (5.25). In fact, compare Figure 5.20(a) with Figure 5.20(c) to observe that the role of x in the 2D figure is played by z in the 3D one, that of the 2D y by the 3D x, and, of course, that of the 2D z (the viewer's axis) by the 3D y. (You can verify this by scratching out the current labels on the axes in Figure 5.20(a), relabeling them as just suggested, and then "mentally" turning the system to match Figure 5.20(c).) So, (5.25) gives

$$\begin{bmatrix} z^1 \\ x^1 \end{bmatrix} = \begin{bmatrix} \cos\theta & -\sin\theta \\ \sin\theta & \cos\theta \end{bmatrix} \begin{bmatrix} z \\ x \end{bmatrix}$$

or, equivalently,

$$\begin{bmatrix} x^1 \\ z^1 \end{bmatrix} = \begin{bmatrix} \cos\theta & \sin\theta \\ -\sin\theta & \cos\theta \end{bmatrix} \begin{bmatrix} x \\ z \end{bmatrix}$$

Finally, since y is fixed, we have

$$R_y(\theta) = \begin{bmatrix} \cos\theta & 0 & \sin\theta & 0 \\ 0 & 1 & 0 & 0 \\ -\sin\theta & 0 & \cos\theta & 0 \\ 0 & 0 & 0 & 1 \end{bmatrix} \qquad (5.27)$$

We ask the reader to verify that the matrix of rotation about the z-axis by an angle θ (Figure 5.20(d)) is

$$R_z(\theta) = \begin{bmatrix} \cos\theta & -\sin\theta & 0 & 0 \\ \sin\theta & \cos\theta & 0 & 0 \\ 0 & 0 & 1 & 0 \\ 0 & 0 & 0 & 1 \end{bmatrix} \qquad (5.28)$$

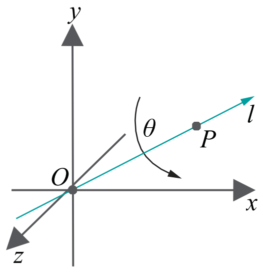

Figure 5.21: Rotating about an arbitrary radial axis.

Exercise 5.50. Write the 4×4 matrix corresponding to rotation by an angle of 30° about the y-axis.

Rotation about an Arbitrary Radial Axis

It is a bit of work to find the matrix corresponding to rotation about an arbitrary axis through the origin. But it's important enough that we'll do it in two different ways. The first is mainly geometric and fairly intuitive. The second involves a bit of algebraic legerdemain, so it is a little less intuitive, but the final form it yields is more compact than that of the first.

Let the axis of rotation be specified as the directed line l through the origin O toward a point $P = (a, b, c)$ (/= O), and the angle of rotation as θ. See Figure 5.21. To simplify computation we'll assume that P is a unit vector, i.e., $|P| = a^2 + b^2 + c^2 = 1$. There is no loss in generality because, if P is not of unit length, we can always divide it by $|P|$ to obtain a unit vector specifying the same rotation. Our goal is to compute the matrix, denote it $R_P(\theta)$ or, simply, $R_{a,b,c}(\theta)$, corresponding to this rotation.

Remark 5.7. To be honest, at this point we don't even know if a rotation about an arbitrary radial axis has a matrix representation at all, in other words, if it is a linear transformation!

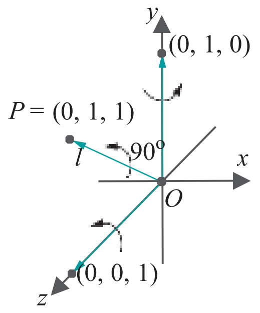

Figure 5.22: Adding rotational axes?

Before we proceed, here's a possible temptation and, then, an exercise to squelch it. Can't we simply "add rotational axes" like vectors? For example, isn't it true, say, that glRotatef(90.0, 0.0, 1.0, 1.0) is the same as glRotatef(90.0, 0.0, 1.0, 0.0) followed by glRotatef(90.0, 0.0, 0.0, 1.0) or, maybe, the other way around? See Figure 5.22. Certainly, translations do work this way. E.g., glTranslatef(0.0, 1.0, 1.0) is, indeed, glTranslatef(0.0, 1.0, 0.0) followed by glTranslatef(0.0, 0.0, 1.0), or vice versa, which means the matrix of the first translation is the product of the those of the second two.

If rotational axes could be so added, then writing the matrix corresponding to glRotatef(90.0, 0.0, 1.0, 1.0) would be equally simple: it would be the product of the matrices corresponding to glRotatef(90.0, 0.0, 1.0, 0.0) and glRotatef(90.0, 0.0, 0.0, 1.0) in some order, both matrices easily written from what we know already about rotating about the coordinate axes. The following exercise shows that this approach is not valid.

Exercise 5.51. Prove that we *cannot* , in general, add rotational axes. In fact, show that glRotatef(90.0, 0.0, 1.0, 1.0) is neither glRotatef(90.0, 0.0, 1.0, 0.0) followed by glRotatef(90.0, 0.0, 0.0, 1.0), nor the other way around.
Hint : If, say, glRotatef(90.0, 0.0, 1.0, 1.0) were equal to the transformation glRotatef(90.0, 0.0, 1.0, 0.0) followed by glRotatef(90.0, 0.0, 0.0, 1.0), then the two would move all points identically. Consider the point (0, 1, 1). How is it moved by glRotatef(90.0, 0.0, 1.0, 1.0)? By glRotatef(90.0, 0.0, 1.0, 0.0) followed by glRotatef(90.0, 0.0, 0.0, 1.0)? And then reversing the order?

A Method to Compute the Rotation Matrix Which Is Mainly Geometric

Even though we can't quite add axes, the plan is still to express the rotation of θ about the radial axis l as a composition of rotations about the coordinate axes. We'll use the Trick. First we'll apply rotations to align l along one of the coordinate axes, then rotate by θ about that coordinate axis and, last, undo the initial rotations to bring l back where it was. For our plan to work, of course, the rotations to align l along a coordinate axis must themselves be about coordinate axes!

Here's a simple motivating experiment.

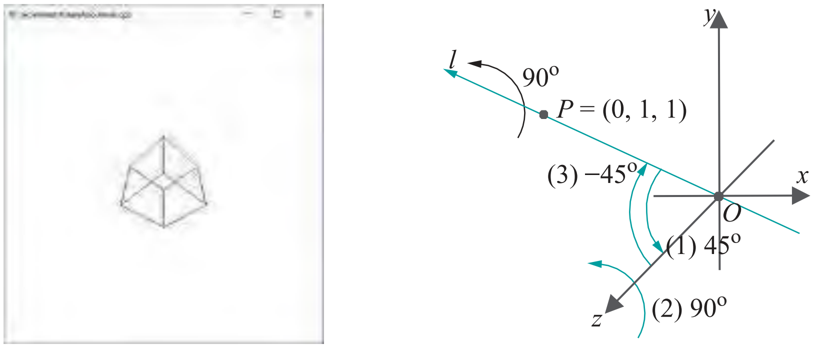

(a) (b)

Figure 5.23: Experiment 5.1: (a) Screenshot of output (b) Trick-based rotation scheme: the green-arrow transforms combine to give the black-arrow one.

Experiment 5.1. Fire up box.cpp and insert a rotation command – in fact, the same one as in the previous exercise – just before the box definition so that the transformation and object definition part of the drawing routine becomes:

```
// Modeling transformations.
glTranslatef(0.0, 0.0, -15.0);

glRotatef(90.0, 0.0, 1.0, 1.0);
glutWireCube(5.0); // Box.
```

The rotation command asks to rotate 90° about the line l from the origin through $(0, 1, 1)$. See Figure 5.23(a) for the displayed output.

Let's try now, instead, to use the strategy suggested above to express the given rotation in terms of rotations about the coordinate axes. Figure 5.23(b) illustrates the following simple scheme. One can align l along the z-axis by rotating it 45° about the x-axis. Therefore, the given rotation should be equivalent to (1) a rotation of 45° about the x-axis, followed by (2) a rotation of 90° about the z-axis followed, finally, by a (3) rotation of -45° about the x-axis.

Give it a whirl. Replace the single rotation command glRotatef(90.0, 0.0, 1.0, 1.0) with a block of three as follows:

```
glRotatef(-45.0, 1.0, 0.0, 0.0);
glRotatef(90.0, 0.0, 0.0, 1.0);
glRotatef(45.0, 1.0, 0.0, 0.0);
```

Seeing is believing, is it not?! End

Returning to the general problem, let's plan to align l along the z-axis in a manner that $P = (a, b, c)$ maps to the point $P^{11} = (0, 0, 1)$ on the positive side of the z-axis. We accomplish this by applying two successive rotations (see Figure 5.24):

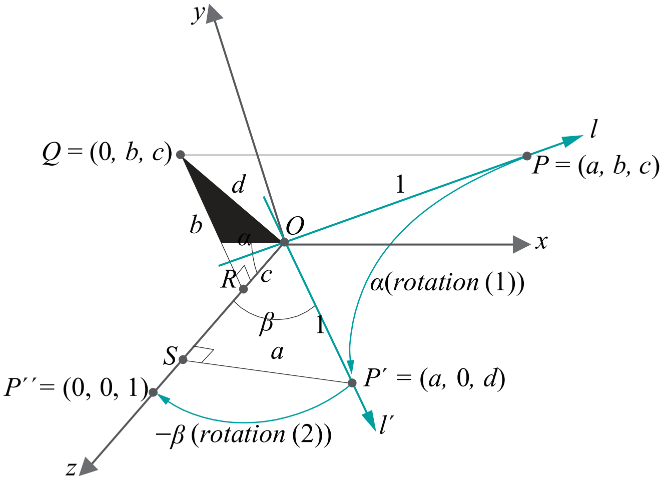

Figure 5.24: Aligning l along the z-axis.

(1) Rotate l an angle a about the x-axis onto a line l^1 on the xz-plane, taking P to P^1.

(2) Rotate l^1 an angle $-\beta$ about the y-axis till it's aligned along the z-axis, taking P^1 to P^{11} (the minus sign in front of β is because the rotation is CW).

Note: The choice of the z-axis as l's final alignment was arbitrary – it could have been any of the three coordinate axes.

We must determine a and β. In fact, we'll simply determine the sine and cosine of both, which is sufficient to write the matrices $R_x(a)$ and $R_y(-\beta)$ corresponding to the rotations (1) and (2), respectively.

Observe that the angle a that OP turns by rotation (1) about the x-axis is the same as the angle between its projection OQ on the yz-plane and the positive direction of the z-axis. In fact, imagine OQ as the "shadow" of OP cast on the yz-plane by a light shining down the x-axis – as OP turns so does its shadow, and by the same amount.

The coordinates of Q are $[0\ b\ c]^T$ as Q is the projection of $[a\ b\ c]^T$ on the yz-plane. Drop the perpendicular from Q to the point R on the z-axis. The angle QOR then is equal to a. We see from the coordinates of Q that $|OR| = c$ and $|RQ| = b$. Denoting

$|OQ|$ by d, it follows from the right-angled triangle ORQ that $d = \sqrt{b^2 + c^2}$. Therefore, *assuming that* $d \neq 0$, we have $\sin\alpha = \frac{b}{d}$ and $\cos\alpha = \frac{c}{d}$.

Note: We don't lose any generality in assuming $d \neq 0$, because $d = 0$ means $Q = O$, which in turn means P is on the x-axis, implying that l lies along the x-axis as well, in which case we already know the matrix for rotation about l.

We can now use Equation (5.26) to write the matrix of rotation (1) as

$$R_x(\alpha) = \begin{bmatrix} 1 & 0 & 0 & 0 \\ 0 & \cos\alpha & -\sin\alpha & 0 \\ 0 & \sin\alpha & \cos\alpha & 0 \\ 0 & 0 & 0 & 1 \end{bmatrix} = \begin{bmatrix} 1 & 0 & 0 & 0 \\ 0 & c/d & -b/d & 0 \\ 0 & b/d & c/d & 0 \\ 0 & 0 & 0 & 1 \end{bmatrix}$$

After rotation (1), l coincides with l' on the xz-plane, and P with P'. The x coordinate of P' is a, the same as that of P, because rotation about the x-axis leaves this value unchanged; the z coordinate is d because rotation by α about the x-axis causes OQ, the shadow of OP whose length is d, to coincide with OS, the projection of OP' on the z-axis; the y coordinate, of course, is 0 as P' lies on the xz-plane.

Therefore, $P' = [a\ 0\ d]^T$, which means that in the right-angled triangle OSP', $|OS| = d$, $|SP'| = a$, and, therefore, $|OP'| = \sqrt{a^2 + d^2} = \sqrt{a^2 + b^2 + c^2} = 1$ (the latter evident as well from the fact that OP' is the unit vector OP rotated). Moreover, angle $P'OS = \beta$, where β is the angle turned by l' to align along the z-axis in rotation (2) above. From the triangle OSP' we have, then, $\sin\beta = a$ and $\cos\beta = d$.

We can now use Equation (5.27) to write the matrix of rotation (2) as

$$R_y(-\beta) = \begin{bmatrix} \cos(-\beta) & 0 & \sin(-\beta) & 0 \\ 0 & 1 & 0 & 0 \\ -\sin(-\beta) & 0 & \cos(-\beta) & 0 \\ 0 & 0 & 0 & 1 \end{bmatrix} = \begin{bmatrix} d & 0 & -a & 0 \\ 0 & 1 & 0 & 0 \\ a & 0 & d & 0 \\ 0 & 0 & 0 & 1 \end{bmatrix}$$

Returning to our original Trick-based plan, the first step of aligning l along the z-axis is accomplished, then, by the composition $R_y(-\beta)\, R_x(\alpha)$. The next, of rotating by θ about the z-axis, is simply a matter of applying $R_z(\theta)$. Finally, the initial rotations aligning l along the z-axis are undone by the inverse transformation $(R_y(-\beta)\, R_x(\alpha))^{-1} = R_x(\alpha)^{-1}\, R_y(-\beta)^{-1} = R_x(-\alpha)\, R_y(\beta)$.

Putting everything together we have, finally,

$$\begin{aligned} R_{a,b,c}(\theta) &= R_x(-\alpha)\, R_y(\beta)\, R_z(\theta)\, R_y(-\beta)\, R_x(\alpha) \\ &= \begin{bmatrix} 1 & 0 & 0 & 0 \\ 0 & c/d & b/d & 0 \\ 0 & -b/d & c/d & 0 \\ 0 & 0 & 0 & 1 \end{bmatrix} \begin{bmatrix} d & 0 & a & 0 \\ 0 & 1 & 0 & 0 \\ -a & 0 & d & 0 \\ 0 & 0 & 0 & 1 \end{bmatrix} \\ &\quad \begin{bmatrix} \cos\theta & -\sin\theta & 0 & 0 \\ \sin\theta & \cos\theta & 0 & 0 \\ 0 & 0 & 1 & 0 \\ 0 & 0 & 0 & 1 \end{bmatrix} \begin{bmatrix} d & 0 & -a & 0 \\ 0 & 1 & 0 & 0 \\ a & 0 & d & 0 \\ 0 & 0 & 0 & 1 \end{bmatrix} \\ &\quad \begin{bmatrix} 1 & 0 & 0 & 0 \\ 0 & c/d & -b/d & 0 \\ 0 & b/d & c/d & 0 \\ 0 & 0 & 0 & 1 \end{bmatrix} \end{aligned} \tag{5.29}$$

The five matrices on the RHS above can be multiplied to give a single matrix, which would then be the value of $R_{a,b,c}(\theta)$ in terms of a, b, c and θ (mind, $d = \sqrt{b^2 + c^2}$, assumed non-zero). However, we'll not do so as the next method to calculate $R_{a,b,c}(\theta)$ gives a more concise form directly.

Exercise 5.52. Is rotation about an arbitrary radial axis a linear transformation? If so, is it always non-singular, or can it be singular?

Exercise 5.53. Use the Trick to write a rotation about an arbitrary axis l, not necessarily radial, as a seven-matrix product.

Example 5.11. (a) Determine the 4 × 4 matrix corresponding to a 90° rotation about the radial axis l directed toward the point $P = [1\ 1\ 1]^T$, which corresponds to the OpenGL command glRotatef(90.0, 1.0, 1.0, 1.0).

(b) Express glRotatef(90.0, 1.0, 1.0, 1.0) as a composition of five successive rotations about the coordinate axes and experimentally verify.

Answer:

(a) The unit vector along l in the direction of P is $\overline{P} = [\frac{1}{\sqrt{3}}\ \frac{1}{\sqrt{3}}\ \frac{1}{\sqrt{3}}]^T$. Accordingly, keeping the notation used above,

$$a = b = c = \frac{1}{\sqrt{3}}, \quad d = \sqrt{b^2 + c^2} = \frac{\sqrt{2}}{\sqrt{3}} \text{ and, of course, } \theta = \pi/2.$$

Plugging these values into (5.29) we get the required matrix as

$$R_{\overline{P}}(\theta) = \begin{bmatrix} 1 & 0 & 0 & 0 \\ 0 & \frac{1}{\sqrt{2}} & \frac{1}{\sqrt{2}} & 0 \\ 0 & -\frac{1}{\sqrt{2}} & \frac{1}{\sqrt{2}} & 0 \\ 0 & 0 & 0 & 1 \end{bmatrix} \begin{bmatrix} \frac{\sqrt{2}}{\sqrt{3}} & 0 & \frac{1}{\sqrt{3}} & 0 \\ 0 & 1 & 0 & 0 \\ -\frac{1}{\sqrt{3}} & 0 & \frac{\sqrt{2}}{\sqrt{3}} & 0 \\ 0 & 0 & 0 & 1 \end{bmatrix} \begin{bmatrix} 0 & -1 & 0 & 0 \\ 1 & 0 & 0 & 0 \\ 0 & 0 & 1 & 0 \\ 0 & 0 & 0 & 1 \end{bmatrix}$$

$$\begin{bmatrix} \frac{\sqrt{2}}{\sqrt{3}} & 0 & -\frac{1}{\sqrt{3}} & 0 \\ 0 & 1 & 0 & 0 \\ \frac{1}{\sqrt{3}} & 0 & \frac{\sqrt{2}}{\sqrt{3}} & 0 \\ 0 & 0 & 0 & 1 \end{bmatrix} \begin{bmatrix} 1 & 0 & 0 & 0 \\ 0 & \frac{1}{\sqrt{2}} & -\frac{1}{\sqrt{2}} & 0 \\ 0 & \frac{1}{\sqrt{2}} & \frac{1}{\sqrt{2}} & 0 \\ 0 & 0 & 0 & 1 \end{bmatrix}$$

$$= \begin{bmatrix} \frac{1}{3} & \frac{1}{3} - \frac{1}{\sqrt{3}} & \frac{1}{3} + \frac{1}{\sqrt{3}} & 0 \\ \frac{1}{3} + \frac{1}{\sqrt{3}} & \frac{1}{3} & \frac{1}{3} - \frac{1}{\sqrt{3}} & 0 \\ \frac{1}{3} - \frac{1}{\sqrt{3}} & \frac{1}{3} + \frac{1}{\sqrt{3}} & \frac{1}{3} & 0 \\ 0 & 0 & 0 & 1 \end{bmatrix}$$

after some tedious computation.

(b) Now, (5.29) says that

$$R_{\overline{P}}(\theta) = R_x(-\alpha)\ R_y(\beta)\ R_z(\theta)\ R_y(-\beta)\ R_x(\alpha)$$

where $\alpha = \sin^{-1} \frac{b}{d} = \sin^{-1} \frac{1}{\sqrt{2}} = 45°$ and $\beta = \sin^{-1} a = \sin^{-1} \frac{1}{\sqrt{3}} = 35.26°$. So,

$$R_{\overline{P}}(\theta) = R_x(-45°)\ R_y(35.26°)\ R_z(90°)\ R_y(-35.26°)\ R_x(45°)$$

which means glRotatef(90.0, 1.0, 1.0, 1.0) is equivalent to the sequence

```
glRotatef(-45.0, 1.0, 0.0, 0.0);
glRotatef(35.26, 0.0, 1.0, 0.0);
glRotatef(90.0, 0.0, 0.0, 1.0);
glRotatef(-35.26, 0.0, 1.0, 0.0);
glRotatef(45.0, 1.0, 0.0, 0.0);
```

We'll leave verification along the lines of Experiment 5.1 to the reader.

Exercise 5.54. Determine the 4×4 matrix corresponding to a 90° rotation about the radial axis l directed toward the point $[0\ 1\ 1]^T$, which corresponds to the OpenGL command glRotatef(90.0, 0.0, 1.0, 1.0). (Recall that in Experiment 5.1 we had already written glRotatef(90.0, 0.0, 1.0, 1.0) as a composition of rotations about the coordinate axes.)

Exercise 5.55. (a) Determine the 4×4 matrix corresponding to a 45° rotation about the radial axis l directed toward the point $[1\ {-1}\ 1]^T$, which corresponds to the OpenGL command glRotatef(45.0, 1.0, -1.0, 1.0).

(b) Express glRotatef(45.0, 1.0, -1.0, 1.0) as a composition of five successive rotations about the coordinate axes and experimentally verify.

Before discussing the second method to compute the matrix corresponding to rotation about an arbitrary axis, here are some facts about cross-products that we'll need. Skip this part if you are already familiar with cross-products of vectors.

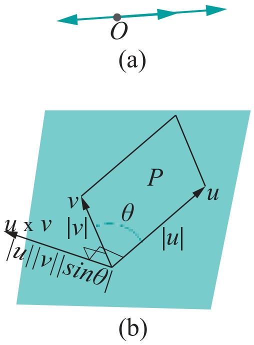

Figure 5.25: (a) Three non-zero collinear vectors drawn from the origin (b) Taking the cross-product.

Sidebar on Cross-Products

The *cross-product* (also called *vector product*) of two vectors u and v in $\mathbb{R}^3$ is another vector, denoted $u \times v$, defined as follows:

(a) If u and v are collinear, then $u \times v$ is the zero vector.

Note: Two vectors are collinear if and only if any one is a scalar (positive, zero or negative) multiple of the other. Therefore, if at least one of the vectors is zero, the two are trivially collinear. (Figure 5.25(a) shows an example of three non-zero vectors, each pair being collinear.)

(b) If u and v are not collinear, then $u \times v$ is the vector whose (a) magnitude is $|u||v||\sin\theta|$, where θ is the angle between u and v, and (b) direction is perpendicular to the plane spanned by u and v, such that u, v and $u \times v$ form a right-handed system. See Figure 5.25(b).

Here's another way to think of the cross-product. The magnitude $|u||v||\sin\theta|$ of the cross-product is nothing but the area of the parallelogram P with u and v as adjacent sides. The area of this parallelogram is, in fact, zero if and only if u and v are collinear. Consequently, the following is an alternate definition: $u \times v$ is the vector whose magnitude is the area of the parallelogram P with u and v as adjacent sides; if the magnitude is non-zero, then the direction of $u \times v$ is perpendicular to P, such that u, v and $u \times v$ form a right-handed system.

If $u = [u_x\ u_y\ u_z]^T$ and $v = [v_x\ v_y\ v_z]^T$, a formula for the cross-product is the following:

$$u \times v = [u_y v_z - v_y u_z \quad v_x u_z - u_x v_z \quad u_x v_y - v_x u_y]^T \tag{5.30}$$

A convenient way to remember this formula is with the help of a determinant, as you are asked to show in the following exercise.

Exercise 5.56. If

$$u = u_x\mathrm{i} + u_y\mathrm{j} + u_z\mathrm{k} \text{ and } v = v_x\mathrm{i} + v_y\mathrm{j} + v_z\mathrm{k}$$

where i, j and k are the unit vectors in the directions of the positive x-, y- and z-axes, show that

$$u \times v = \begin{vmatrix} \mathrm{i} & u_x & v_x \\ \mathrm{j} & u_y & v_y \\ \mathrm{k} & u_z & v_z \end{vmatrix} \tag{5.31}$$

Example 5.12. Determine the cross-product $[2\ 1\ 0]^T \times [1\ {-2}\ 4]^T$.

Answer:

$$[2\ 1\ 0]^T \times [1\ \ -2\ 4]^T = \begin{vmatrix} i & 2 & 1 \\ j & 1 & 2 \\ k & 0 & 4 \end{vmatrix} = 4i - 8j - 5k = [4\ -8\ -5]^T$$

Exercise 5.57. Determine the cross-product $[3\ -1\ 2]^T \times [-1\ 0\ 3]^T$.

Exercise 5.58. Write the result of the cross-product of every ordered pair from the three vectors i, j and k (there are 9 such products if you include products of vectors with themselves).

Remark 5.8. An easy way to remember the answer to the preceding exercise is the following:

The cross-product of any of i, j and k with itself is the zero vector. For the product of two different ones from i, j and k, keep in mind the cyclic order i → j → k → i. Then, if two successive elements in this order are multiplied, the result is the next; if two successive elements are multiplied in reverse order, then the result is the negative of the next element. For example, $j \times k = i$ and $k \times j = -i$.

Exercise 5.59. Prove the following about cross-products, where u, v and w are any three vectors, and c an arbitrary scalar:

(a) u and v are collinear if and only if $u \times v = 0$ (*collinearity test*)

Note: The "only if" direction follows from the definition of cross-product; "if" needs to be proved.

(b) $u \times u = 0$

(c) $u \times v = -(v \times u)$ (*cross-product is anti-commutative*)

(d) It may not be true that $(u \times v) \times w = u \times (v \times w)$ (*cross-product is not associative*). Give an example of u, v and w where it isn't true.

(e) $(cu) \times v = u \times (cv) = c(u \times v)$

(f) $u \times (v + w) = u \times v + u \times w$ and $(v + w) \times u = v \times u + w \times u$ (*cross-product distributes over a sum*)

Exercise 5.60. Prove that if u is a unit vector and v arbitrary, then the vector $(u \times v) \times u$ is the component of v perpendicular to u.

Interestingly, it turns out, as the next example shows, that a cross-product with one fixed vector is a linear transformation.

Example 5.13. Show for a fixed vector $u = u_x i + u_y j + u_z k$ that the transformation of $\mathbb{R}^3$ defined by $v \mapsto u \times v$ is linear.

Answer: Check from the formula (5.30) for $u \times v$ that

$$u \times v = Mv$$

where

$$M = \begin{bmatrix} 0 & -u_z & u_y \\ u_z & 0 & -u_x \\ -u_y & u_x & 0 \end{bmatrix}$$

which proves that $v \mapsto u \times v$ is indeed linear, with defining matrix M.

A Method to Compute the Rotation Matrix Which Is Part Geometry and Part Algebra

The problem statement again:

The axis of rotation is the directed line l through the origin toward another point $P = [a\ b\ c]^T$ and the angle of rotation is θ. The goal is to compute the matrix $R_{a,\,b,\,c}(\theta)$ corresponding to this rotation. As before, we assume without loss that $|P| = 1$.

Obviously, we're interested in how the rotation transforms a point, but this is equivalent to asking how it transforms the position vector of the point, i.e., the vector with its start at the origin and end at the point. Accordingly, let the image of a vector X by the given rotation be $f(X)$. See Figure 5.26, all vectors starting at the origin. First, split X as

$$X = X_1 + X_2$$

into components X_1 and X_2 parallel and perpendicular, respectively, to l. See Figure 5.27.

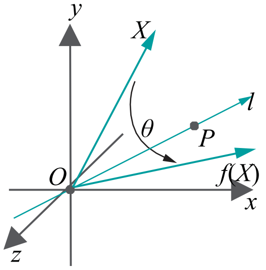

Figure 5.26: The vector $f(X)$ is obtained by rotating X an angle of θ about the radial line l.

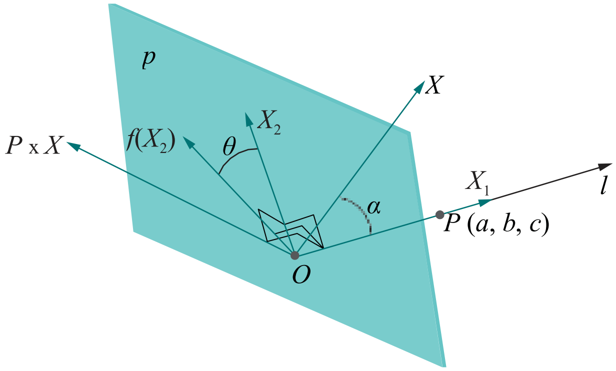

Figure 5.27: X_1 and X_2 are components of X parallel and perpendicular, respectively, to l; X_2, $f(X_2)$ and $P \times X$ all lie on the plane p through O perpendicular to l. X_2 and $P \times X$ are mutually perpendicular as well.

Since a rotation is a linear transformation, we have

$$f(X) = f(X_1) + f(X_2) \tag{5.32}$$

As X_1 lies on l, rotation about l leaves it unchanged. So

$$f(X_1) = X_1 \tag{5.33}$$

Now, X_2 lies on the plane p through O perpendicular to l and rotates by an angle θ about l, to $f(X_2)$. Therefore, $f(X_2)$ lies on p as well. We'll assume for now that X_2 is non-zero, meaning that X is not parallel to l, for, otherwise, $f(X) = f(X_1) = X_1$ and there's nothing more to do.

Observe that the vector $P \times X$, being perpendicular to l, lies on p too; moreover, $P \times X$ is perpendicular to X_2 as it is perpendicular to the plane containing P and X, which contains X_2 as well. It follows, then, that the plane p is spanned by the two perpendicular vectors X_2 and $P \times X$. Consequently, these two specify coordinate axes on p. Let's determine the coordinates of $f(X_2)$ with respect to these axes, equivalently, the components of $f(X_2)$ parallel to X_2 and to $P \times X$.

The component of $f(X_2)$ parallel to X_2 has signed length $|f(X_2)| \cos\theta$. Moreover, the unit vector in the direction of X_2 is $X_2/|X_2|$. Therefore, the component of $f(X_2)$ parallel to X_2 is

$$|f(X_2)| \cos\theta * X_2/|X_2| = X_2 \cos\theta \tag{5.34}$$

using the fact that $|f(X_2)| = |X_2|$, because $f(X_2)$ is X_2 rotated.

Let a be the angle between P and X. Then, the component of $f(X_2)$ parallel to $P \times X$ has signed length

$$\begin{aligned} |f(X_2)| \sin\theta &= |X_2| \sin\theta \quad \text{(using again } |f(X_2)| = |X_2|) \\ &= |X \sin a| \sin\theta \\ &= |P||X|| \sin a| \sin\theta \quad (\text{as } |P| = 1) \\ &= |P \times X| \sin\theta \quad \text{(by definition of the cross-product)} \end{aligned}$$

The unit vector in the direction of $P \times X$ is $(P \times X)/|P \times X|$. It follows that the component of $f(X_2)$ parallel to $P \times X$ is

$$|P \times X| \sin\theta \ * (P \times X)/|P \times X| = (P \times X) \sin\theta \tag{5.35}$$

Adding its components parallel to X_2 and $P \times X$ with help of (5.34) and (5.35), we conclude that

$$f(X_2) = X_2 \cos\theta + (P \times X) \sin\theta \tag{5.36}$$

Plugging the values from (5.33) and (5.36) into (5.32) we see that

$$\begin{aligned} f(X) &= X_1 + X_2 \cos\theta + (P \times X) \sin\theta \\ &= X_1 + (X - X_1) \cos\theta + (P \times X) \sin\theta \\ &= X \cos\theta + X_1(1 - \cos\theta) + (P \times X) \sin\theta \end{aligned} \tag{5.37}$$

Note: The preceding equation is valid even if X_2 is the zero vector, for, then, $X = X_1$ and $P \times X = 0$, so that the equation says $f(X) = X$, which is correct. So we're completely general from here on.

Use the results of Example 4.6 and Example 5.13 to replace X_1 and $P \times X$, respectively, with their equivalent matrix products:

$$\begin{aligned} f(X) &= \cos\theta \begin{bmatrix} 1 & 0 & 0 \\ 0 & 1 & 0 \\ 0 & 0 & 1 \end{bmatrix} X + (1 - \cos\theta) \begin{bmatrix} a^2 & ab & ac \\ ab & b^2 & bc \\ ac & bc & c^2 \end{bmatrix} X + \\ &\quad \sin\theta \begin{bmatrix} 0 & -c & b \\ c & 0 & -a \\ -b & a & 0 \end{bmatrix} X \\ &= \left(\begin{bmatrix} a^2 & ab & ac \\ ab & b^2 & bc \\ ac & bc & c^2 \end{bmatrix} + \cos\theta \begin{bmatrix} 1-a^2 & -ab & -ac \\ -ab & 1-b^2 & -bc \\ -ac & -bc & 1-c^2 \end{bmatrix} + \right. \\ &\quad \left. \sin\theta \begin{bmatrix} 0 & -c & b \\ c & 0 & -a \\ -b & a & 0 \end{bmatrix} \right) X \end{aligned} \tag{5.38}$$

Finally, adding the matrices in the parentheses and writing the result in homogeneous coordinates, we get another form for the rotation matrix, different from the earlier geometrically-derived (5.29), as a single matrix rather than a 5-matrix product, though their values must obviously be equal:

$$R_{a,b,c}(\theta) = \begin{bmatrix} a^2(1-\cos\theta)+\cos\theta & ab(1-\cos\theta)-c\sin\theta & ac(1-\cos\theta)+b\sin\theta & 0 \\ ab(1-\cos\theta)+c\sin\theta & b^2(1-\cos\theta)+\cos\theta & bc(1-\cos\theta)-a\sin\theta & 0 \\ ac(1-\cos\theta)-b\sin\theta & bc(1-\cos\theta)+a\sin\theta & c^2(1-\cos\theta)+\cos\theta & 0 \\ 0 & 0 & 0 & 1 \end{bmatrix} \tag{5.39}$$

Remark 5.9. One can replace X_1 in (5.37) by $(X \cdot P)P$, as X_1 is the component of X parallel to the vector P of unit length (see Exercise 4.51(a)). The resulting equation

$$f(X) = X\cos\theta + (X \cdot P)P(1 - \cos\theta) + (P \times X)\sin\theta \qquad (5.40)$$

is called *Rodrigues' rotation formula*.

Exercise 5.61. Verify the result of Example 5.11 by computing the rotation matrix using Equation (5.39) instead of (5.29).

Exercise 5.62. Verify your answer to Exercise 5.54 by computing the rotation matrix using Equation (5.39) instead of (5.29).

Remark 5.10. An exercise which may have been conspicuous by its absence so far is to show that the composition of two rotations about radial axes is also a rotation about a radial axis. Unfortunately, though true, this is not easy to prove.

In fact, unlike its 2D counterpart, it's not even intuitive that it is true. For example, is it evident that, say, a rotation of 45° about the x-axis followed by another, say, of 30° about the y-axis is a rotation about some axis in the first place? We'll prove that rotations do, in fact, compose to rotations using properties of rigid transformations in Section 5.4.5.

Whew, we told you this section was going to be long! It turned out to be fairly technical, too. We'll be coasting downhill the rest of the way and, believe it or not, get to see some code before long.

5.4.4 Reflection

The image of the point $P = [x\ y\ z]^T$ by reflection about a plane p, called the *mirror*, is $P^1 = [x^1\ y^1\ z^1]^T$ such that:

(a) if P lies on p, then $P^1 = P$;

(b) if P does not lie on p, then P^1 is the point on the other side of p such that PP^1 is perpendicular to p, and P^1 is the same distance from p as P. See Figure 5.28.

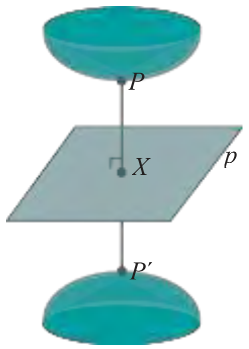

Figure 5.28: Reflection about plane p $(|XP| = |XP^!|)$.

Reflection about the xy-plane is simply scaling by the factors $s_x = 1$, $s_y = 1$ and $s_z = -1$. Its matrix, therefore, is

$$M = S(1, 1, -1) = \begin{bmatrix} 1 & 0 & 0 & 0 \\ 0 & 1 & 0 & 0 \\ 0 & 0 & -1 & 0 \\ 0 & 0 & 0 & 1 \end{bmatrix} \qquad (5.41)$$

Exercise 5.63. Let p be an arbitrary plane mirror. Use the Trick to show that the matrix corresponding to reflection about p is of the form

$$M_1^{-1} M_2^{-1} S(1, 1, -1) M_2 M_1$$

where M_1 corresponds to a translation and M_2 to a rotation about a radial axis. You don't need to find exact values for M_1 and M_2.

Exercise 5.64. Write the 4 × 4 matrix corresponding to reflection about the plane $x - z = 0$.

Exercise 5.65. What is the result of composing reflections about the same mirror? What transformation is the result of composing reflections about two parallel mirrors? About two perpendicular mirrors? What is the inverse of a reflection?

Shear

Thinking back to the analogy made in our discussion of 2D shears at the end of Section 5.1, imagine again placing a lump of putty between your palms and then moving one palm parallel to the other. In proper 3D there are three choices to make: (1) how to initially align your palms in space with putty between them, (2) which direction to move, say, the upper palm, but keeping it parallel to the fixed lower one and, finally, (3) how far to move the upper palm. Accordingly, a 3D shear s is uniquely determined by three parameters: a plane p called the *plane of shear* , a directed line l called the *line of shear* , which is parallel to p, and an angle a called the *angle of shear*.

The action of s is equivalent to that of "infinitely many" 2D shears applied to parallel planes. Here's how (see Figure 5.29)(a)):

Given a point $P \in R^3$, let q be the unique plane containing P which is both perpendicular to the plane p of shear s *and* parallel to the line l of shear s. Therefore, q intersects p in a directed line, denote it l^1, parallel to l. P , then, is transformed by s to the point P^1 *exactly* as it would by the particular 2D shear s^1, on the plane q, specified by the directed line l^1 and the angle a.

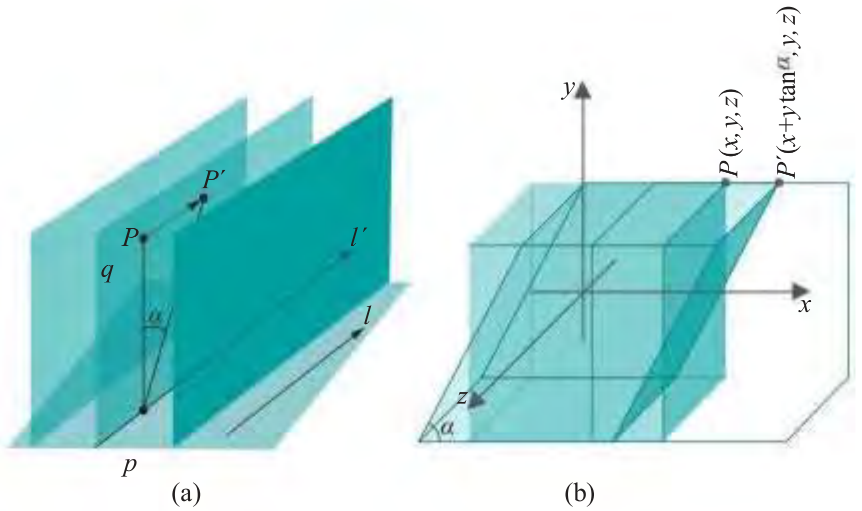

Figure 5.29: (a) A 2D slice of a 3D shear on the plane q and two more "copies" of q (b) A shear along the xz-plane whose line is the x-axis.

In other words, imagine 3D space "sliced" into infinitely many parallel planes, each perpendicular to p and parallel to l, and s as the "union of identical 2D shears" on each of these slices (Figure 5.29)(a) depicts two more slices parallel to q).

Example 5.14. Figure 5.29(b) depicts a 3D shear along the xz-plane whose line is the x-axis and angle a, shearing a cube into a parallelepiped. It's not hard to see that the equation of this shear is as follows:

$$P^1 = \begin{bmatrix} 1 & \tan a & 0 & 0 \\ 0 & 1 & 0 & 0 \\ 0 & 0 & 1 & 0 \\ 0 & 0 & 0 & 1 \end{bmatrix} P$$

Exercise 5.66. What is the 4 × 4 transformation matrix of a 3D shear along the xy-plane, whose line is the x-axis and angle a?

Exercise 5.67. What is the 4 × 4 transformation matrix of a 3D shear along the xz-plane, whose line is the z-axis and angle a?

Exercise 5.68. (Commutativity)

(a) Do translations commute with each other?

(b) Do scalings commute with each other?

(c) Do rotations about the same radial axis commute with each other?

(d) Does a rotation about one radial axis commute with another about a different radial axis?

(e) Do translations and rotations commute?

(f) Do reflections about two different mirrors ever commute?

(g) Do shears and translations ever commute?

(h) Do shears and rotations ever commute?

5.4.5 Affine Geometric Transformations

From Equations (5.23), (5.24), (5.39) and (5.41) and judicious applications of the Trick one sees that translations, rotations about arbitrary axes, scalings and reflections about arbitrary mirrors are all affine transformations of 3-space. Consequently, one has the following 3D analogue of Proposition 5.2 about their geometric niceness.

Proposition 5.8. *Let g be either a translation, a scaling, a rotation (about an arbitrary radial axis) or a reflection (about an arbitrary mirror). Then:*

(a) g maps straight lines to straight lines and planes to planes. Moreover, it maps parallel straight lines to parallel straight lines, intersecting straight lines to intersecting straight lines, parallel planes to parallel planes and intersecting planes to intersecting planes.

(b) g maps a convex set on one plane to a convex set on another plane. Moreover, it transforms the convex hull of a set of points $\{P_1, P_2, \ldots, P_k\}$ on one plane to the convex hull of $\{g(P_1), g(P_2), \ldots,$ $g(P_k)\}$ lying on another plane.

Proof. Follows from Proposition 5.1(c)-(d) about affine transformations in $\mathbb{R}^3$.

Translations, rotations, scalings and reflections are all affine. In the opposite direction, the following analogues of the 2D Propositions 5.3 and 5.4 are true as well, though there seem to be no “low-level” proofs similar to the 2D ones. Fairly sophisticated linear algebra appears unavoidable. So at this time we’ll only state Propositions 5.9 and 5.10, deferring the proof of the latter to later in this chapter as optional reading for the mathematically inclined. Mind that Proposition 5.9 follows straightforwardly from Proposition 5.10.

Proposition 5.9. *Any affine transformation of $\mathbb{R}^3$ is the composition in some order of translations, scalings and rotations about radial axes.*

In particular, an affine transformation $g : \mathbb{R}^3 \to \mathbb{R}^3$ can be factored into a composition $g = g_4 \circ g_3 \circ g_2 \circ g_1$, where g_1 is a rotation about a radial axis, g_2 a scaling, g_3 another rotation about a radial axis and g_4 a translation.

Proposition 5.10. *Any non-singular linear transformation of $\mathbb{R}^3$ is the composition successively of a rotation about a radial axis, a scaling and another rotation about a radial axis.*

Exercise 5.69. Prove that a shear along a radial plane is a non-singular linear transformation of 3-space, while an arbitrary 3D shear is an affine transformation. Conclude that any 3D shear is a composition of translations, scalings and rotations about radial axes.

OpenGL and Affine Transformations

The importance of Proposition 5.9, particularly to the design of an API like OpenGL, cannot be overstated. The modeling transformations one creates using OpenGL are compositions of translations (glTranslatef()), scalings (glScalef(), excluding for the moment degenerate calls) and rotations about a radial axis (glRotatef()). The whole collection, therefore, is affine as a composition of affine transformations is affine. Proposition 5.9 tells us that, conversely, any affine transformation of 3-space is a composition of translations, scalings and rotations about a radial axis and, so, may be implemented in OpenGL.

Conclusion: barring degenerate scalings, *the modeling transformations one can create in OpenGL are precisely the affine transformations of 3-space and nothing else*. And, as we argued in Section 5.2.2, this is a welcome situation both from the API designer's point of view of being able to implement a simple rendering engine, and the application programmer's point of view of having a comprehensive set of transformations at her disposal.

Example 5.15. Express the affine transformation

$$f([x\, y\;\; z]^T) = [-y\;\; x\;\; z+2]^T$$

as a composition of OpenGL transformations.

Answer: The mapping by f is the composition

$$[x\, y\; z]^T \mapsto [-y\;\; x\;\; z]^T \mapsto [-y\;\; x\;\; z+2]^T$$

Now, the first map is easily seen to be a rotation of $\pi/2$ about the z-axis, while the second is a translation of 2 in the z-direction. We have, therefore, the required block of OpenGL transformations:

```
glTranslatef(0.0, 0.0, 2.0);
glRotatef(90.0, 0.0, 0.0, 1.0);
```

Exercise 5.70. Express each of the following affine transformations as a composition of OpenGL transformations:

(a) $f([x\; y\; z]^T) = [y\;\; x\;\; z]^T$

(b) $f([x\; y\; z]^T) = [y\;\; z\;\; x]^T$

(c) $f([x\; y\; z]^T) = [x-y\;\;\; x+y\;\;\; -z]^T$

Verifying the Matrices Generated by OpenGL

Appendix E of the red book lists the matrices which OpenGL generates for the modeling transformations.

The translation and scaling matrices are simple and seen to agree with Equations (5.23) and (5.24), respectively. We leave it to the reader to verify that the rotation matrix R which OpenGL generates for the rotation transformation glRotate{fd}($a,\; x,\; y,\; z$) is equivalent to that of Equation (5.39); in fact, the red book expresses it in the form of the prior more expansive Equation (5.38).

Incidentally, it's clear now and worth emphasizing that the composition of modelview transformations is implemented in the OpenGL engine as 4 × 4 matrix multiplication, and the actual transformation of a vertex, of course, is a matrix-vector multiplication. In fact, it's not an oversimplification to say that a graphics card animates as fast as it multiplies matrices.

Projection Transformations

There is another set of transformations which OpenGL implements as 4 × 4 matrix multiplication as well: these are the projection transformations used to transform the viewing box (respectively, frustum) created by a glOrtho() (respectively, glFrustum()) call into a cubical so-called canonical viewing box.

However, we defer consideration of projection transformations to Chapter 20 because transformation at least of a frustum into a box cannot be done affinely, but requires an understanding of projective spaces (if the transformation matrix is not to be pulled out of a hat). Nevertheless, a reader with some math preparation who is eager to see all of OpenGL's matrices can proceed to Chapter 20 right away as it may be read independently. Moreover, it is written in a manner to be at least accessible to the reader even without much projective math under her belt.

5.4.6 Accessing and Manipulating the Current Modelview Matrix

Finally, we surface from deep theory to see – *code*!

There are four commonly-used methods to access the current modelview matrix, i.e., the matrix at the top of the OpenGL modelview matrix stack, three to change its value and one to read it. After setting the matrix mode to GL MODELVIEW with the command glMatrixMode(GL_MODELVIEW) if need be, the call

1. glLoadIdentity() sets the current modelview matrix to the identity matrix I_4.

2. glLoadMatrix(**matrixData*) sets the current modelview matrix to the 4 × 4 matrix whose elements are listed in the one-dimensional array pointed by **matrixData* in column-major order (which means elements of the first column are listed first in order of increasing row, then those of the second column and so on).

3. glMultMatrix(**matrixData*) multiplies the current modelview matrix on the right by the 4 × 4 matrix whose elements are listed in column-major order in the one-dimensional array pointed by **matrixData*.

4. glGetFloatv(GL MODELVIEW_MATRIX, **modelviewMatrixData*) stores the 16 elements of the current modelview matrix in column-major order in the one-dimensional array pointed by **modelviewMatrixData*.

Experiment 5.2. Run manipulateModelviewMatrix.cpp. Figure 5.30 is a screenshot, although we are now really more interested in the transformations in the program rather than its visual output.

The displayModelviewMatrix() routine outputs the current modelview matrix to the C++ window in conventional rectangular form. It is invoked four times in drawScene(), first right after the glLoadIdentity() command, and then successively after the gluLookAt(), glMultMatrixf() and glScalef() calls. We'll see next if the four output values match our understanding of theory. End

Figure 5.30: Screenshot from Experiment 5.2.

As expected, the first matrix output by the program, after the glLoadIdentity() command, is the identity

$$I_4 = \begin{bmatrix} 1 & 0 & 0 & 0 \\ 0 & 1 & 0 & 0 \\ 0 & 0 & 1 & 0 \\ 0 & 0 & 0 & 1 \end{bmatrix}$$

The gluLookAt(0.0, 0.0, 10.0, 0.0, 0.0, 0.0, 0.0, 1.0, 0.0) command next is equivalent to glTranslatef(0.0, 0.0, -10.0), whose matrix, from Equation (5.23), is

$$T(0, 0, -10) = \begin{bmatrix} 1 & 0 & 0 & 0 \\ 0 & 1 & 0 & 0 \\ 0 & 0 & 1 & -1 \\ 0 & 0 & 0 & 1 \end{bmatrix}$$

Therefore, after the gluLookAt() call the current modelview matrix should equal

$$\begin{bmatrix} 1 & 0 & 0 & 0 \\ 0 & 1 & 0 & 0 \\ 0 & 0 & 1 & 0 \\ 0 & 0 & 0 & 1 \end{bmatrix} \begin{bmatrix} 1 & 0 & 0 & 0 \\ 0 & 1 & 0 & 0 \\ 0 & 0 & 1 & -10 \\ 0 & 0 & 0 & 1 \end{bmatrix} = \begin{bmatrix} 1 & 0 & 0 & 0 \\ 0 & 1 & 0 & 0 \\ 0 & 0 & 1 & -10 \\ 0 & 0 & 0 & 1 \end{bmatrix}$$

which indeed is the second matrix output.

Next, glMultMatrixf(matrixData) multiplies the current modelview matrix on the right by the matrix

$$M = \begin{bmatrix} 0.707107 & -0.707107 & 0 & 0 \\ 0.707107 & 0.707107 & 0 & 0 \\ 0 & 0 & 1 & 0 \\ 0 & 0 & 0 & 1 \end{bmatrix}$$

where $0.707107 \approx 1/\sqrt{2}$, so M corresponds to a rotation of 45° about the z-axis. The third matrix output then is, as expected,

$$\begin{bmatrix} 1 & 0 & 0 & 0 \\ 0 & 1 & 0 & 0 \\ 0 & 0 & 1 & -10 \\ 0 & 0 & 0 & 1 \end{bmatrix} \begin{bmatrix} 0.707107 & -0.707107 & 0 & 0 \\ 0.707107 & 0.707107 & 0 & 0 \\ 0 & 0 & 1 & 0 \\ 0 & 0 & 0 & 1 \end{bmatrix} =$$

$$\begin{bmatrix} 0.707107 & -0.707107 & 0 & 0 \\ 0.707107 & 0.707107 & 0 & 0 \\ 0 & 0 & 1 & -10 \\ 0 & 0 & 0 & 1 \end{bmatrix}$$

The final matrix output is after the call glScalef(1.0, 2.0, 1.0), a scaling by a factor of 2 along the y-axis. From Equation (5.24)

$$S(1, 2, 1) = \begin{bmatrix} 1 & 0 & 0 & 0 \\ 0 & 2 & 0 & 0 \\ 0 & 0 & 1 & 0 \\ 0 & 0 & 0 & 1 \end{bmatrix}$$

which multiplies the third matrix output on the right to indeed give the final output matrix as

$$\begin{bmatrix} 0.707107 & -0.707107 & 0 & 0 \\ 0.707107 & 0.707107 & 0 & 0 \\ 0 & 0 & 1 & -10 \\ 0 & 0 & 0 & 1 \end{bmatrix} \begin{bmatrix} 1 & 0 & 0 & 0 \\ 0 & 2 & 0 & 0 \\ 0 & 0 & 1 & 0 \\ 0 & 0 & 0 & 1 \end{bmatrix} =$$

$$\begin{bmatrix} 0.707107 & -1.414214 & 0 & 0 \\ 0.707107 & 1.414214 & 0 & 0 \\ 0 & 0 & 1 & -10 \\ 0 & 0 & 0 & 1 \end{bmatrix}$$

Exercise 5.71. (Programming) Replace the gluLookAt() statement in manipulateModelviewMatrix.cpp with the following

```
gluLookAt(0.0, 10.0, 10.0, 0.0, 0.0, 0.0, 0.0, 1.0, 0.0);
```

Theoretically verify the correctness of the modelview matrix output by the program after the new gluLookAt() statement.
Hint : The new gluLookAt() statement is simulated as a translation by displacement vector $[0\ -10\ -10]^T$, followed by a rotation of 45° about the x-axis.

Exercise 5.72. (Programming) Verify your answer to Exercise 5.54 by comparing it with the output from an appropriately modified manipulateModelviewMatrix.cpp.

Exercise 5.73. (Programming) What is the current modelview matrix after the following piece of code in the drawing routine:

```
glMatrixMode(GL_MODELVIEW);
glLoadIdentity();
glScalef(1.0, 2.0, 2.0);
glTranslatef(2.0, 1.0, 0.0);
glRotatef(90.0, 1.0, 0.0, 0.0);
```

Find the answer theoretically by multiplying appropriate 4×4 matrices and then verify with the help of manipulateModelviewMatrix.cpp.

Exercise 5.74. (Programming) Verify your answers to Exercise 4.60(a)-(e) by using manipulateModelviewMatrix.cpp to find the matrix corresponding to the given gluLookAt() call, as well as that corresponding to the composed sequence of modeling transformations which you gave as being equivalent.

Exercise 5.75. (Programming) In Remark 4.18 we claimed that, following a gluLookAt() call, the current modelview matrix changes by multiplication by the simulating modeling transformations, but that the current projection matrix does not change at all.

The part about the current modelview matrix seems true from what we have just seen in Experiment 5.2.

We ask the reader to verify the claim about the current projection matrix, particularly for the program manipulateModelviewMatrix.cpp, by reading the current projection matrix, both before and after the gluLookAt() statement with the help of glGetFloatv(GL_PROJECTION_MATRIX, **projectionMatrixData*) calls.

5.4.7 Euclidean and Rigid Transformations

We have definitions analogous to the 2D case for Euclidean and rigid transformations of 3-space. Euclidean transformations are important because they preserve distance and, therefore, shape as well.

Definition 5.6. A *Euclidean transformation* (also called *isometry*) f of $\mathbb{R}^3$ is such that $|f(P)f(Q)| = |PQ|$ for any two points $P, Q \in \mathbb{R}^3$.

For the discussion of orientation coming up next, we need first to know when triples of vectors in 3-space are right-handed or left-handed.

Definition 5.7. An ordered triple of non-coplanar vectors $\{u, v, w\}$, each assumed originating from the same point O, is said to form a *right-handed system* (or, simply, be *right-handed*) if the rotation of u about O toward v, along the plane containing u and v, and along the smaller of the angles between the two, appears counter-clockwise to a viewer watching from the endpoint of w; otherwise, it is said to be *left-handed* . See Figures 5.31(a) and (b) for examples.

Remark 5.11. We actually first discussed handedness in the context of coordinate systems way back in Section 2.2.

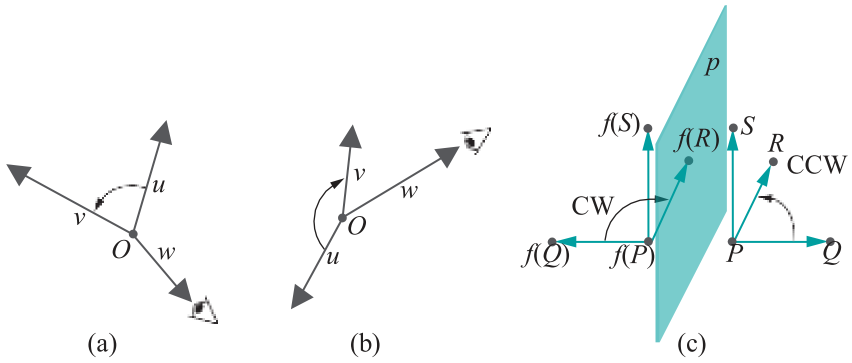

Figure 5.31: (a) $\{u, v, w\}$ is right-handed (b) $\{u, v, w\}$ is left-handed (c) The reflection f about the plane p is orientation-reversing, because the triple $\{PQ, PR, PS\}$ is right-handed, while the triple of images $\{f(P)f(Q), f(P)f(R), f(P)f(S)\}$ is left-handed.

Remark 5.12. Another term for handedness – more scientific-sounding, but less used – is *chirality*.

Definition 5.8. A Euclidean transformation f of $\mathbb{R}^3$ is said to be *orientation-reversing* if there exist four non-coplanar points P, Q, R and S in $\mathbb{R}^3$ such that one of the two ordered triples of vectors $\{PQ, PR, PS\}$ and $\{f(P)f(Q), f(P)f(R), f(P)f(S)\}$ is right-handed, while the other is left-handed.

A Euclidean transformation that is not orientation-reversing is said to be *orientation-preserving*.

Orientation-preserving Euclidean transformations are called *rigid transformations*.

Remark 5.13. The property of the transformation f described in the first paragraph of the definition above does not depend on the choice of the non-coplanar points: we'll see that if it is true for *some* four non-coplanar points P, Q, R and S in $\mathbb{R}^3$ that one of $\{PQ, PR, PS\}$ and $\{f(P)f(Q), f(P)f(R), f(P)f(S)\}$ is right-handed, while the other left-handed, then it is true for *any* four non-coplanar points.

Example 5.16. The reflection f of Figure 5.31(c) about the plane p is an orientation-reversing Euclidean transformation.

Exercise 5.76. Scalings in general are not Euclidean transformations, but with certain choices of scaling factors they are. List these choices and for each say if the scaling preserves or reverses orientation.

Exercise 5.77. Show that the composition of two Euclidean transformations is Euclidean and that of two rigid transformations is rigid.

Exercise 5.78. Show that the composition of two orientation-reversing Euclidean transformations is an orientation-preserving Euclidean transformation (in other words, rigid). Show that the composition of an orientation-preserving and an orientation-reversing Euclidean transformation is orientation-reversing.

The following result gives a way to decide if an ordered triple of vectors is right-handed or left-handed.

Lemma 5.2. *Assuming that the coordinate axes themselves form a right-handed system, then an ordered triple $\{u, v, w\}$ of non-coplanar vectors, where $u = [u_x\ u_y\ u_z]^T$, $v = [v_x\ v_y\ v_z]^T$ and $w = [w_x\ w_y\ w_z]^T$, is right-handed or left-handed according as the determinant*

$$\begin{matrix} u_x & v_x & w_x \\ u_y & v_y & w_y \\ u_z & v_z & w_z \end{matrix}$$

is greater or less than zero (it cannot be zero as $\{u, v, w\}$ is non-coplanar).

Proof. The proof is not difficult, but uses more linear algebra than we would like to assume at this time, so we ask the reader to refer to a text such as [7].

The next exercise, analogue of the 2D Example 5.10, implies that Definition 5.8 about a Euclidean transformation reversing or preserving orientation is independent of the choice of the four non-coplanar points P, Q, R and S.

Exercise 5.79. Suppose that an affine transformation f of $\mathbb{R}^3$ maps some four non-coplanar points P , Q, R and S in $\mathbb{R}^3$ such that one of the two ordered triples of vectors $\{PQ, PR, PS\}$ and $\{f(P)f(Q), f(P)f(R), f(P)f(S)\}$ is right-handed, while the other is left-handed.

Show, then, that for any four non-coplanar points, P^1, Q^1, R^1 and S^1, one of the two ordered triples of vectors $\{P^1Q^1, P^1R^1, P^1S^1\}$ and $\{f(P^1)f(Q^1), f(P^1)f(R^1), f(P^1)f(S^1)\}$ is right-handed, while the other is left-handed.
Hint : Use the same approach as for Example 5.10. You will need as well to apply the preceding lemma.

Next is the 3D analogue of the 2D Proposition 5.5.

Proposition 5.11. *A translation or a rotation about an arbitrary axis is a rigid transformation of 3-space. A reflection about an arbitrary mirror is an orientation-reversing Euclidean transformation of 3-space.*

Proof. The proof that a 3D translation t is distance-preserving is exactly similar to the 2D version in the proof of Proposition 5.5. That t is orientation-preserving is even simpler, because the two ordered triples of vectors $\{PQ, PR, PS\}$ and $\{t(P)t(Q), t(P)t(R), t(P)t(S)\}$ are identical for any four points P, Q, R and S in $\mathbb{R}^3$.
We'll leave the reader to prove the claims for rotations and reflections.

The following is the 3D version of the 2D Proposition 5.6.

Proposition 5.12. *A rigid transformation of* $\mathbb{R}^3$ *keeping the origin fixed is a rotation about a radial axis, while an arbitrary rigid transformation of* $\mathbb{R}^3$ *is a composition of a rotation about a radial axis followed by a translation.*

A Euclidean transformation of $\mathbb{R}^3$ *is a composition of a rotation about a radial axis followed by a translation, possibly followed again by a reflection.*

Proof. The first statement of the proposition can be proved using linear algebra, but more interesting is to apply elementary arguments along the lines of Proposition 5.6. In fact, we ask the reader who doesn't mind wallowing in a bit of geometry to follow the approach suggested below to make a proof herself. If you are not so inclined it won't hurt to skip the proof altogether.

Suggested approach: Show first that a rigid transformation f of 3-space fixing the origin O is a rotation about a radial axis as follows:

If f is the identity, then it is trivially a rotation.

If f is not the identity, then suppose that P is a point such that $f(P) = P$. There are three possibilities:

(a) $f(f(P))$ /= P.
Argue that the three points P, $f(P)$ and $f(f(P))$ cannot be collinear. Therefore, they belong to a unique plane p. Show that the line l through O perpendicular to p is the axis of f; further, the angle of rotation θ is the angle between the perpendiculars from P and $f(P)$ to l. See Figure 5.32(a).

(b) $f(f(P)) = P$ and the line l^1 joining P and $f(P)$ does not contain O.
Show in this case that the line l through O perpendicular to l^1 is the axis of f; furthermore, the angle of rotation is π. See Figure 5.32(b).

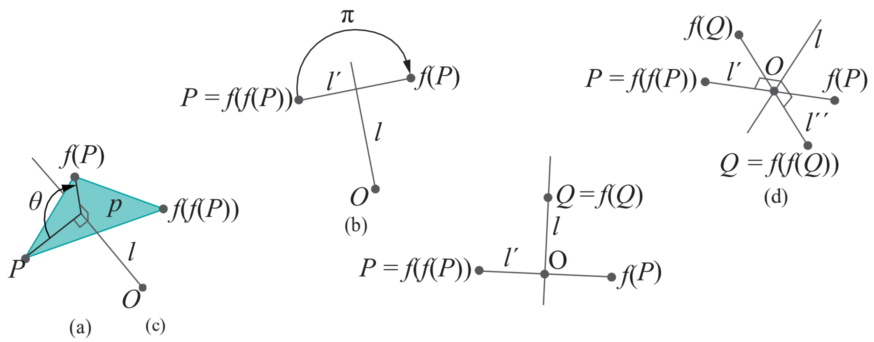

Figure 5.32: Finding the axis of a rigid transformation that fixes the origin.

(c) $f(f(P)) = P$ and the line l^1 joining P and $f(P)$ does contain O.

In this case, let Q be a point not lying on l^1.

If $f(Q) = Q$, then show that the line l through O and Q is the axis of f and the angle of rotation is π. See Figure 5.32(c).

If $f(Q) = Q$, then assume that $f(f(Q)) = Q$ and that the line l^{11} joining Q and $f(Q)$ contains O, for, if not, this case is equivalent to one of (a) or (b). Then show that the line l through O perpendicular to both l and l^1 is the axis and the angle of rotation is π. See Figure 5.32(d).

The rest of the proposition follows easily from the first part.

Remark 5.14. The first part of Proposition 5.12, that a rigid transformation of R^3 which keeps the origin fixed is a rotation about a radial axis, is often called Euler's Rotation Theorem. It is actually one of several theorems, proved by the great eighteenth century Swiss mathematician Leonhard Euler, bearing his name.

Finally, here's the 3D analogue of the 2D Proposition 5.7.

Proposition 5.13. *Affine, Euclidean and rigid transformations of 3-space are related by the following inclusions, which are each proper:*

$$\textit{rigid transforms} \subset \textit{Euclidean transforms} \subset \textit{affine transforms}$$

Proof. We leave this to the reader.

A proposition whose proof we kept putting off, because of its apparent difficulty, is now all of a sudden simple to prove:

Proposition 5.14. *The composition of two rotations about radial axes in 3-space is another such.*

Proof. Let f_1 and f_2 be rotations about radial axes in 3-space. By Proposition 5.11 they are rigid transformations and, moreover, both fix the origin. By Exercise 5.77 the composition $f_1 \circ f_2$ is rigid, and it obviously fixes the origin because both f_1 and f_2 do so. Proposition 5.12 then completes the proof.

Exercise 5.80. Consider reflections through *points*. For example, the reflection through the origin corresponds to the transformation $[x\ \ y\ ]\,z]^T \!-\![\ \cancel{x}\ \ y\ {-z}]^T$. This transformation is clearly affine, in fact, linear. Is it Euclidean? Rigid? How about reflections through arbitrary points?

Sketch how the boy of Figure 4.8 of the last chapter would be transformed by reflection through the origin.

Proof of Proposition 5.10

This section is only for those with a good knowledge of linear algebra and may be safely skipped by others with no consequences to their learning of CG.

Lemma 5.3. *A special orthogonal transformation of* R^3*, i.e., one whose matrix is orthogonal with determinant 1, is a rotation about a radial axis.*

Proof. It's easy to verify that a linear transformation f of R^3 defined by an orthogonal matrix of determinant 1 preserves both distance and orientation. Therefore, it is rigid and the lemma follows from Proposition 5.12.

The author learned the proof of the following lemma from T. K. Mukherjee [100].

Lemma 5.4. *For any non-singular real $n \times n$ matrix M, there exist special orthogonal matrices P and Q and a real diagonal matrix D with all non-zero entries such that*

$$M = PDQ$$

Proof. Consider the product MM^T . As it is symmetric, by a standard result of linear algebra there exists a real orthogonal matrix P such that

$$P^{-1}(MM^T)P = D^1$$

where D^1 is a diagonal matrix.

Moreover, MM^T is positive definite, which implies that D^1 is as well. Therefore, each element of the diagonal of D^1 is positive. Let $D = \sqrt{D^1}$. In particular, if $D^1 = [d^1_i]$, then $D = [d_i]$, where d_i is the positive square root of $d^1{}_i$

Accordingly,

$$P^{-1} MM^T P = D^2$$

It follows that

$$\begin{aligned} I &= D^{-1} (P^{-1} MM^T P) D^{-1} = (D^{-1}P^{-1}M) (M^T PD^{-1}) \\ &= (D^{-1}P^{-1}M) (D^{-1}P^{-1}M)^T \end{aligned}$$

as $(D^{-1})^T = D^{-1}$ and $(P^{-1})^T = P$.

Writing

$$Q = D^{-1}P^{-1}M$$

we have from the above that $QQ^T = I$, so Q is orthogonal

Now

$$M = PDQ$$

and we can assume that both P and Q are, in fact, special orthogonal, for, if either is not, then it can be multiplied by a diagonal matrix with determinant -1, viz.,

$$R = \begin{pmatrix} -1 & 0 & 0 & \dots & 0 \\ 0 & 1 & 0 & \dots & 0 \\ 0 & 0 & 1 & \dots & 0 \\ & & & \ddots & \\ 0 & 0 & 0 & \dots & 1 \end{pmatrix}$$

and, correspondingly, D multiplied by R^{-1} (=R).

The two lemmas combine to establish Proposition 5.10.

Remark 5.15. Proposition 5.10 and its 2D sibling Proposition 5.4 are both deducible as cases of the Singular Value Decomposition Theorem. For an account of this fundamental theorem of linear algebra see, for example, Roman [121].

5.5 Summary, Notes and More Reading

In this chapter we opened up the graphics animation engine to find out what makes it tick. The short answer is 4×4 matrix multiplication and we learned why.

Each modeling transformation corresponds to an affine transformation of 3-space, which is represented using homogeneous coordinates by a 4× 4 matrix. The composition of modeling transformations corresponds to multiplication of their matrices. Viewing transformations, being compositions of modeling transformations as well, each corresponds to a 4 ×4 matrix too. We learned the particular matrix representations of basic geometric transformations such as translation, scaling, rotation and reflection.

We learned as well that the modeling transformations of OpenGL – translation, scaling and rotation – were chosen for good reasons by the designers of the API. Not only are these transformations affine, but they combine to generate all affine transformations.

We studied certain particularly useful subclasses of affine transformations. One was that of shape-preserving transformations, the Euclidean transformations, which in turn include rigid transformations that model the motion of rigid objects in space. Another special class of affine transformations which we studied was that of the shears.

We learned to access and manipulate OpenGL's modelview matrix stack as well, allowing us to program transformations directly into the stack if need be, rather than through calls to OpenGL's own modeling transformations.

Till Chapter 4 we were primarily interested in *using* OpenGL. Now we have an understanding of the *working* of this API as well. True, familiarity, say, with the functioning of an internal combustion engine does not necessarily make one a superior driver; however, it certainly does help one better understand technical issues, which has its value.

One topic the knowledgeable reader might think missing from this chapter on transformations is discussion of the so-called projection transformation in the graphics pipeline – which is critical to the shoot part of the shoot-and-print rendering paradigm from Chapter 2 – and how it is implemented by means of mathematical projective transformations. However, we thought it best to introduce the projection transformation as an application of projective spaces later in the book in Chapter 20. The reason is that the choice of the particular transformations applied in the graphics pipeline is hard to motivate without an understanding of projective spaces.

For further reading about geometric transformations the reader is recommended to Mortenson [98] and Yaglom's series [159, 160, 161]. Articles about transformations and their role in computer graphics, written in recreational style and yet very informative, can be found in the books by Blinn [16, 17] and Glassner [54, 55].

CHAPTER 6

Advanced Animation Techniques

The goal for this chapter is to learn techniques to cope with two major issues that arise often in animation projects. The first is managing large worlds where the polygon count may painfully slow down the rendering pipeline. The programmer can help ease the logjam by pre-filtering objects lying outside the camera's field of view. This process is called frustum culling and we describe how to do it by means of space partitioning in Section 6.1. The related process of occlusion culling, where objects blocked from the camera's view by other objects are filtered, is the topic of Section 6.2. This section discusses, in particular, occlusion queries for the purpose of occlusion culling, as well as so-called conditional rendering based on the outcome of occlusion queries.

Before proceeding to the next issue we interject the short Section 6.3, which presents timer queries, syntactically related to occlusion queries, which help the programmer profile the performance of particular sections of code.

The second major issue is that of animating the orientation of an object. In Chapter 4 we learned all about animating motion, coding balls and boxes that flew, fell, spun and revolved around one another. But how about animating orientation or pose? For example, an aircraft maneuvering in a dogfight or a camera tracking a scene. Changing orientation involves modeling transformations as well, particularly rotation, but first one must develop a method to *quantify* orientation, just as (x, y, z) quantify position. Only then can come the question of moving between two orientations.

In Section 6.4 we learn how to use Euler angles – which we first encountered in Section 4.6.3 – to quantify orientation in 3D. Animating between a pair of orientations given by their Euler angle tuples is possible but, as we shall see, potentially problematic. A more sophisticated approach is with the use of quaternions. This is the topic of Section 6.5, which begins with an introduction to the mathematics of quaternions, and then goes on to describe their application to representing and animating orientation.

There is a fair amount of theory in this chapter but it is tremendously important practically and we back it all the way with code.

6.1 Frustum Culling by Space Partitioning

Frustum culling is *de rigueur* for game programmers or, for that matter, anyone creating scenes with large polygon counts. We'll motivate the proceedings by rerunning Experiment 4.34.

Experiment 6.1. First, run the program spaceTravel.cpp of Chapter 4 with its current values of ROWS and COLUMNS, determining the size of the asteroid grid, as 8 and 6, respectively. Move the spacecraft with the arrow keys.

Next, increase both ROWS and COLUMNS to 100. Figure 6.1 is a screenshot. The spacecraft now begins to respond sluggishly to the arrow keys, at least on a typical desktop. You may have to pump up even more the values of ROWS and COLUMNS if yours is exceptionally fast. End

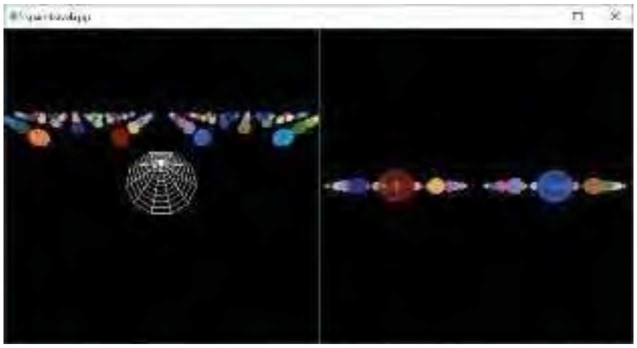

Figure 6.1: Screenshot of spaceTravel.cpp with a 100 × 100 array of asteroids.

Let's first do a back-of-the-envelope calculation to understand what's happening. Assuming the viewable space of spaceTravel.cpp to be a box of sides 250 units, significantly larger, in fact, than the actual viewing frustum defined by the glFrustum(-5.0, 5.0, -5.0, 5.0, 5.0, 250.0) statement of the program, and noting that asteroids are 30 units apart in both the x and z directions, one deduces that at most 9*9=81 asteroids are viewable in either viewport at any given time. That's not a lot for OpenGL to draw. In fact, set ROWS to 9 and COLUMNS to 9 to find no perceptible slowdown. So what's going on? Why the slowdown in simply *creating* a larger asteroid field?

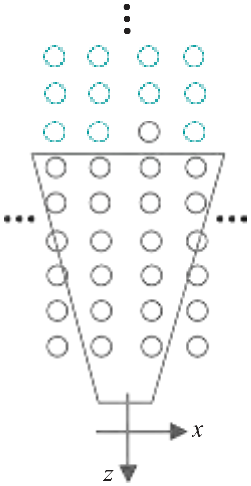

Figure 6.2: Tiny part of an asteroid field inside the viewing frustum.

A moment's consideration of the rendering pipeline reveals the answer. At every redisplay, in other words, every arrow press, the ROWS × COLUMNS number of asteroids in arrayAsteroids[ROWS][COLUMNS] are *all* – in fact, their *collective polygons* are *all* – zapped first with the modelview matrix, then with the projection matrix, and *then* those which fall outside the viewing volume are clipped, and the rest projected to the viewing face and rendered. Specifically, if ROWS and COLUMNS are both 100, then the polygons of all 10,000 asteroids, several hundred thousand in total, enter the rendering pipeline before only those belonging to approximately 80 are drawn. That's more than 99% of the polygons, each incurring computational cost in the pipeline, ultimately not making it to the screen. Figure 6.2, where the triple black dots represent dozens of columns or rows of asteroids, pictures the situation. Talk about waste!

It's not OpenGL's fault though. OpenGL finds out which polygons belong on-screen and which off only *after* transforming and clipping, operations well into the pipeline. However, the programmer can help by pre-identifying as many objects as possible which do not intersect the viewing frustum, which means that they will end up being clipped, and not letting them into the pipeline in the first place. This is a process called *frustum culling*, which consists, then, of adding to the program routines to check if an object intersects the frustum and filtering through to be drawn only those which do or, equivalently, culling those which do not. So, from a programming point of view the drawing routine has a part that looks like

```
for (each object Obj in the scene)
    if (Obj passes the test to check if it intersects the frustum)
        draw Obj;
```

Keep in mind that the test must be fast or the objective of speeding up the rendering process is defeated. However, here's a critical observation which can help devise a fast test. It does *not* have to be 100% accurate: false positives (objects passing the test which actually don't intersect the frustum) will not compromise the program's integrity, but false negatives will.

6.1.1 Space Partitioning

The most straightforward way to frustum cull is to test each object individually if it intersects the frustum. This may, in fact, give decent speed-up if the objects are simple enough that the combined cost of testing them all is still cheap.

However, frustum culling is typically more efficient if space is first partitioned in a hierarchical manner into cells which each contain only a few objects. Cost-effective partitioning must be driven by the distribution of the objects – subdividing into smaller ones only cells containing many objects. Once space is partitioned, frustum culling can be accomplished by hierarchically checking cells to determine if they intersect the frustum and passing to the drawing routine objects belonging only to those which do. This approach is based on a few premises:

(a) That partitioning space and determining the distribution of the objects in individual cells is primarily a one-time pre-processing cost, which is true if most objects in the scene are static. The few moving objects, in this case, can be passed mandatorily to the drawing routine.

(b) That the cells are of a shape easy to check for intersection with the frustum.

(c) That the hierarchical nature of the partition leads to efficiency because, if a cell is found not to intersect the frustum, then its sub-cells and the objects which they contain can all be eliminated from further consideration, a process called *pruning*.

(d) That the partitioning process is efficient in that, if a cell contains only a few objects, then it is not subdivided, so that the final partition reflects the distribution of the objects in space.

There's more than one way to hierarchically partition space, but intuitively simplest is the *octree* for 3-space and its analogue, the *quadtree*, for 2-space. We'll explain quadtree-based space partitioning using the scenario of spaceTravel.cpp as a running example because we have, in fact, an implementation in the program spaceTravelFrustumCulled.cpp.

6.1.2 Quadtrees

Note, first, that spaceTravel.cpp is essentially a 2D problem as the spacecraft, asteroids and frustum can all be projected onto the xz-plane and intersection testing done on that plane – observe that the spacecraft has no motion in the y-direction. Therefore, a quadtree is appropriate for spaceTravel.cpp even though, nominally, the scene is 3D.

A quadtree partitions 2-space into axis-aligned squares, the collection having the hierarchy of a tree. In frustum culling applications the root node corresponds to a square large enough to contain all objects that might potentially be culled.

Terminology: We'll use the terms "node" and "square" interchangeably in the context of quadtrees.

Figure 6.3(a) illustrates a hypothetical projected scenario of spaceTravel.cpp (an irregular distribution of asteroids is obtained by setting FILL_PROBABILITY, the percentage probability that a particular row-column slot is filled, to a value less than 100). The craft itself is ignored because it moves; therefore, it's always passed into the pipeline.

To begin with, the root square of the quadtree is chosen big enough to bound the entire asteroid field. Subsequently, at each level, each square *may* be subdivided – if so, into four equal sub-squares (quadrants). The criterion to subdivide is determined by the programmer. What we'll do in the spaceTravel.cpp scenario is subdivide a square if it intersects more than one asteroid.

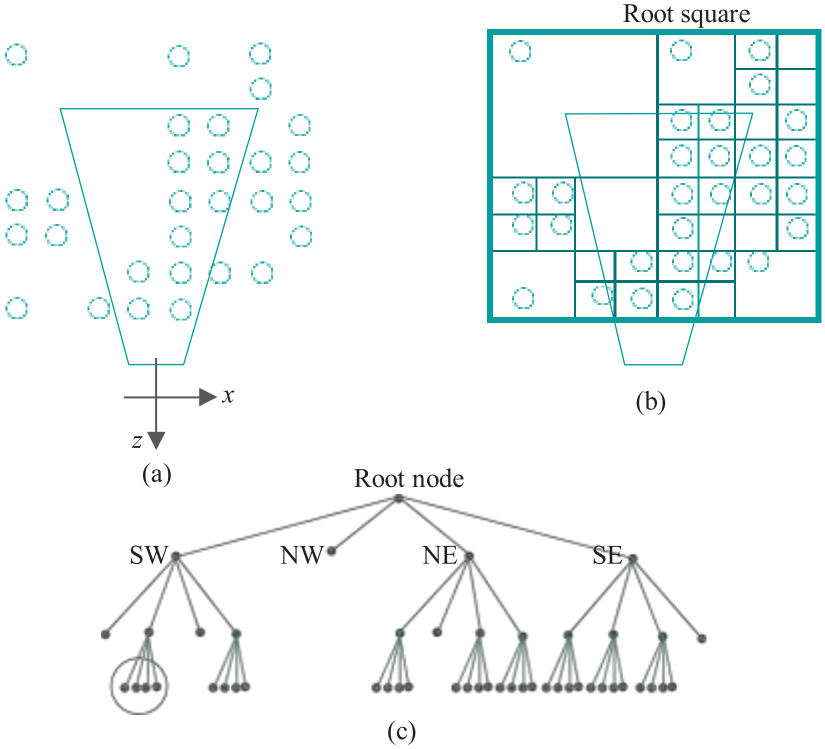

Figure 6.3: (a) Projection of the asteroids and the frustum of spaceTravel.cpp onto the *xz*-plane. (b) Corresponding quadtree squares (the root square is bold) (c) The tree structure with children at each node drawn SW, NW, NE, SE from left to right; the nodes in the red circle are *some* of those pruned when checking intersection with the frustum.

If a square is subdivided, then its four quadrants become its children in the tree hierarchy and are denoted SW, NW, NE and SE according to their location in the parent square. Given our condition for when to subdivide, leaf squares – those which are not further subdivided – evidently intersect either one asteroid or none.

The squares of the quadtree corresponding to the arrangement of asteroids in Figure 6.3(a) are shown in Figure 6.3(b) and the underlying tree structure in Figure 6.3(c).

Once the quadtree is built, culling is straightforward: check, starting at the root, for squares that intersect the frustum; if a non-leaf square intersects the frustum, then recursively process its children; if a leaf square intersects the frustum, then pass its asteroid (if any) to the drawing routine. (Readers familiar with computational geometry – e.g., see [10] – will find this process reminiscent of querying a kd-tree.)

Let's verify how the premises (a)-(d) for space partitioning, mentioned earlier, are fulfilled by a quadtree for spaceTravel.cpp:

(a) The asteroids are all static while the spacecraft is the only object which is not, so we'll build a one-time quadtree for the asteroids, while the craft itself will always be passed to the drawing routine.

In the second viewport the camera moves, which, as we know, is implemented by actually transforming the scene. However, in order not to have to update the quadtree structure, we'll treat the viewing frustum itself as moving, attached to the front of the spacecraft, as in Figure 6.4.

(b) The cells are each a square, a shape easy to test for intersection with the trapezoidal projection of a frustum.

(c) Several of the nodes, even in the simple example of Figure 6.3 are pruned. E.g., the ones inside the red circle are pruned because their parent does not intersect the frustum.

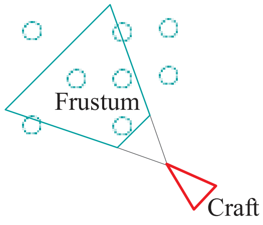

Figure 6.4: Spacecraft carrying a viewing frustum "attached" to its front.

(d) It can be seen from Figure 6.3 that the spatial distribution of the quadtree squares indeed tracks that of the asteroids.

Exercise 6.1. Indicate all the nodes of the tree of Figure 6.3 which are pruned when checking intersection with the frustum.

6.1.3 Implementation

Experiment 6.2. Run spaceTravelFrustumCulled.cpp, which enhances spaceTravel.cpp with optional quadtree-based frustum culling. Pressing space toggles between frustum culling enabled and disabled. As before, the arrow keys maneuver the craft.

The current size of the asteroid field is 100×100. Move the craft around toggling between frustum culling off and on. Dramatic isn't it, the speed-up from frustum culling?!

Note: When the number of asteroids is large, the display may take a while to come up because of pre-processing to build the quadtree structure.

End

We have already described in the previous section the plan to enhance spaceTravel.cpp with quadtree-based frustum culling. Here are specifics in spaceTravelFrustumCulled.cpp.

The quadtree asteroidsQuadtree is an object of the Quadtree class containing nodes belonging to the QuadtreeNode class. The member function numberAsteroidsIntersected() of the class QuadtreeNode helps decide for each quadtree square if it is to be subdivided, while the member list asteroidList stores for each leaf square the asteroid (if any) intersecting it. Observe that the root square of the quadtree is initially chosen big enough to bound the entire asteroid field – see the setting of the initialSize variable of the setup() routine

In addition to checkSpheresIntersection() from the original spaceTravel.cpp, used in asteroidCraftCollisiond() to detect (approximately) intersection between the spacecraft and an asteroid, routines from the program intersectionDetectionRoutines.cpp are invoked for other intersection tests. In particular, checkQuadrilateralsIntersection() determines if the frustum in either viewport intersects a quadtree square, while checkDiscRectangleIntersection() if an asteroid intersects a quadtree square.

In Figure 6.3, asteroids lie either entirely inside or outside a square. This need not be the case in general, of course, and in our code an asteroid straddling the boundary of a quadtree square is associated with it.

With large numbers of asteroids, the speed-up through frustum-culling is clearly enormous. Even so, our implementation spaceTravelFrustumCulled.cpp is minimal and there are further optimizations to be made. We ask the reader to explore a couple in the next exercise.

Exercise 6.2. (Programming) A large quadtree costs both in RAM space and pre-processing time. Try the following two options in spaceTravelFrustumCulled.cpp to control its size:

(a) The size of the quadtree tends to grow exponentially with its height. Accordingly, set a *cut-off depth* beyond which nodes cannot be partitioned.

(b) The criterion for subdividing a square, currently if it intersects more than one asteroid, can be made stricter by setting a larger threshold for the number to be intersected, again reducing the size of the quadtree.

Exercise 6.3. (Programming) Currently, spaceTravelFrustumCulled.cpp checks for intersection between the spacecraft and *every* asteroid. Use the quadtree to improve on this. In particular, check only for collision between the craft and each asteroid associated with a leaf square that the craft intersects.

Exercise 6.4. (Programming) Design a busy scene, maybe part of a game, and draw it using frustum culling.

6.1.4 More about Space Partitioning

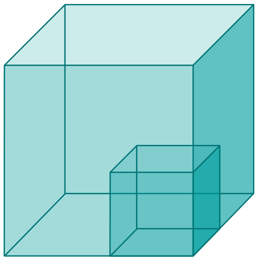

Figure 6.5: An octree cube and one of its 8 octants.

Octrees are a straightforward generalization of quadtrees to 3-space – space is partitioned into a tree-like hierarchy of axis-aligned cubes. Each cube in an octree can be partitioned into 8 child octants (see Figure 6.5).

Quadtrees and octrees are not the only ways to partition space. There are more sophisticated data structures such as kd-trees, range trees and BSP (Binary Space Partitioning) trees, which can be applied in two and higher dimensions.

Moreover, applications of space partitioning are not limited to frustum culling either. Another important one is collision detection. The principle is that two objects can intersect only if they belong to the same or adjacent cells; accordingly, one can pre-process and pass only "nearby" pairs to the, typically, costly intersection-checking routines.

Dynamic scenes with multiple mobile objects are a challenge for any space partitioning application. Options include predictively locating moving objects in cells if there is prior knowledge of their trajectories, followed, possibly, by a repartitioning of space or a redistribution of objects to cells.

Bottom line: There is overhead both in code and pre-processing in setting up a space-partitioning structure, but if the application is appropriate, e.g., frustum culling a busy but mostly static scene, the bang for the buck is enormous.

6.2 Occlusion

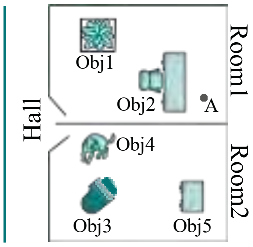

Figure 6.6: Two rooms off a hall. A black bounding box is shown containing the first object.

Often, a programmer's global view of a scene allows her to conclude for a given position of the camera that certain objects are *occluded* , i.e., blocked from view, and, therefore, need not be sent into the rendering pipeline. For example, in the scene of Figure 6.6 of two rooms opening to a hall, if the camera is inside one room, then objects in the other are always occluded by the wall in between.

6.2.1 Querying and Culling

Given the setting of Figure 6.6, part of the drawing routine could then be as the pseudo-code below:

```
if (camera is in Room1)
{
    draw Obj1;
    draw Obj2;
}
if (camera is in Room2)
{
    draw Obj3;
    draw Obj4;
    draw Obj5;
}
```

This technique of *occlusion culling* can improve immensely efficiency of rendering, as can be imagined if, say, the objects in Figure 6.6 are many and complex. In the code above, occlusion culling is implemented by the programmer herself from a fairly coarse global understanding of the scene. Evidently, she could dig even deeper and implement more refined tests, e.g., one which determines that a camera at location A will find Obj1 occluded by Obj2, applying, possibly, geometric intersection tests of the kind used in spaceTravelFrustumCulled.cpp.

OpenGL itself provides a powerful device to help with occlusion culling: one can set up a so-called *occlusion query* to determine if an object is visible after depth testing. Before we get to an actual example, here's the general idea.

In a situation as depicted in Figure 6.6, the camera being at A, before attempting to render (the complex) Obj1, query if its bounding box, the (much simpler) black rectangle, is visible. If the bounding box is visible, then render Obj1; if not, don't. The expectation is that in more configurations than not, the added investment in querying occlusion for a simple object is more than offset by being able, subsequently, to toss a complex one from the pipeline. Let's get to code.

Experiment 6.3. Run occlusion.cpp, which initially shows only a green rectangle. Use the arrow keys to move a solid red cube into view from behind the rectangle. Press the space bar, which is a toggle, to reveal a blue wire sphere contained in the box. See Figure 6.7. The sphere plays the role of a complex "occludee", while the cube is its simple bounding box, and the rectangle is the "occluder".

We'll analyze this program next. End

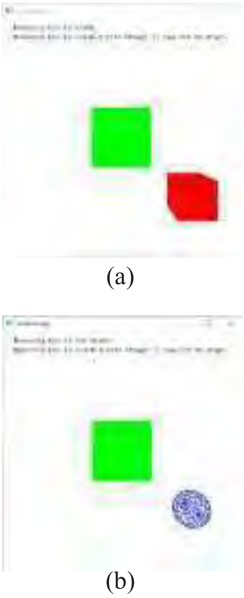

(a)

(b)

Figure 6.7: Screenshots of occlusion.cpp with the (a) box drawn (b) not drawn.

The call glGenQueries(1, &query) in the setup routine generates a query object, storing its id in the global query.

The drawing routine begins with a piece of code to draw the obscuring green rectangle. Next comes the block to draw the bounding box enclosed in a query:

```
glBeginQuery(GL_SAMPLES_PASSED, query);
if (!boxDrawn)
{
    glColorMask(GL_FALSE, GL_FALSE, GL_FALSE, GL_FALSE);
    glDepthMask(GL_FALSE);
}
glColor3f(1.0, 0.0, 0.0);
glutSolidCube(1.0);
if (!boxDrawn)
{
    glDepthMask(GL_TRUE);
    glColorMask(GL_TRUE, GL_TRUE, GL_TRUE, GL_TRUE);
}
glEndQuery(GL_SAMPLES_PASSED);
```

Ignore the four masking statements for now; we'll explain these later. So, what the block above does is simple: the command glBeginQuery(GL SAMPLES-PASSED, query) starts the counting of samples – as we're not multisampling, a sample is simply a fragment – which pass the depth test, then the box is drawn, and, finally, the complementary call glEndQuery(GL SAMPLES-PASSED) stops the counting. Evidently, then, the query counts fragments of the box passing the depth test.

Next comes

```
while (!resultAvailable) glGetQueryObjectuiv(query,
                                 GL_QUERY_RESULT_AVAILABLE, &resultAvailable);
```

Now, the glGetQueryObjectuiv(..., GL QUERY RESULT-AVAILABLE, ...) above places a Boolean in resultAvailable saying if the query has, in fact, completed counting. For, observe that, especially if multiple queries are being run, it is quite possible that all the drawing commands before a glEndQuery() did not complete before the fragment total was retrieved, in which case the latter value may not be accurate. So, the while loop in the statement above spins until the query has indeed completed.

The next statement in the drawing routine

```
glGetQueryObjectuiv(query, GL_QUERY_RESULT, &result);
```

retrieves the total number of fragments counted by the query, now guaranteed to be correct, and places it in result. Obviously, if this number is more than zero, then the box, the only object for which depth-test passed fragments were counted, is visible. The following

```
if (result)
{
   glColor3f(0.0, 0.0, 1.0);
   glutWireSphere(0.5, 16, 10);
}
```

then draws the sphere only if the box is visible.

Messages at the top left of the display indicate if the bounding box is being drawn and if it is visible, even though it may not actually be drawn.

Now, in practical applications we would not want an object's bounding box to be drawn – once queried for visible fragments it has served its purpose and should be ejected from the pipeline. However, in order to run tests we keep the option of drawing the box in occlusion.cpp by toggling the space bar. This is where the four masking statements, conditional on the box not being drawn, in the glBeginQuery()-glEndQuery() block above, come into play.

In particular, if boxDrawn is false, we first disable writes to the color buffer prior to rendering the box so that indeed it cannot display. Moreover, we obviously want the box to compete in depth tests with the green rectangle in order to resolve our query; however, we do *not* want it to update the depth buffer (when it wins) because, at time of drawing the actual scene, the sphere should compete only with the green rectangle, certainly not its own bounding box. For this reason, we further emasculate the box by setting the depth mask so that it cannot write the depth buffer. The masks are reset once the box is drawn.

Is the program really doing what it's supposed to when the box is behind the green rectangle, which is suppress rendering of the sphere? A neat way to check this is to make the box smaller by replacing glutSolidCube(1.0) with glutSolidCube(0.25). Of course, the box no longer bounds the sphere, but moving it toward the back of the rectangle we that the sphere indeed disappears the instant the box does.

Next is an interesting exercise showing a limitation of the query-based rendering process.

Exercise 6.5. (Programming) Move the block

```
glPushMatrix();
...
glRectf(-0.5, -0.5, 0.5, 0.5);
glPopMatrix();
```

drawing the green rectangle from the top of the drawScene() routine to just after where the sphere is drawn, i.e., just before the message-writing block. Next, as suggested just before this exercise, replace glutSolidCube(1.0) with glutSolidCube(0.25) to make a smaller box in order to check if the sphere disappears with the box. *No*, it no longer does. Why?

The moral to be drawn from the preceding exercise is that at the end of the day OpenGL code runs linearly always, so no point in the code can see what's ahead. Of course, the output will never be invalidated no matter where the query is placed to test visibility. However, an occlusion test might be useless if potential occluders haven't been drawn yet. The programmer should keep this in mind as queries carry significant overhead themselves.

Exercise 6.6. (Programming) If you move the box in occlusion.cpp out of the display, i.e., out of the viewing frustum, then the occlusion query indicates it to be invisible – of course, because no fragment even made it to the depth test, let alone past.

So, it seems such queries might be applied to frustum culling as well. Do you think this would be as efficient as what we do, for example, in spaceTravelFrustumCulled.cpp, which is use a quadtree to filter out asteroids outside the frustum?
Hint : Consider where clipping and depth-testing occur in the rendering pipeline (you might want to peek ahead to Chapter 21, especially the diagram of the fixed-function pipeline in Figure 21.10, where depth-testing is one of the per-fragment operations).

6.2.2 Conditional Rendering

OpenGL versions 3.0 and on support *conditional rendering* which makes for even more efficient handling of the query outcome. Conditional rendering allows the programmer to specify that a particular block of drawing statements is to be executed only if a particular query result comes back positive. This obviates the need for explicit glGetQueryObject* calls on the programmer's part to fetch the result or determine if a query had completed. Code then is simpler, and, more importantly, the query and its outcome can be handled *entirely within* the GPU – e.g., without having to ship values of variables like result or resultAvailable in occlusion.cpp back to the application for further instruction.

The following reworking of occlusion.cpp invokes conditional rendering, but, otherwise, is functionally equivalent to the original.

Experiment 6.4. Run occlusionConditionalRendering.cpp. The major change from occlusion.cpp is in the following code block in the drawing routine, where the rendering of the sphere is made conditional upon the outcome of the query with id query. The parameter GL_QUERY_WAIT says to wait for the query to complete.

```
glBeginConditionalRender(query, GL_QUERY_WAIT);
glColor3f(0.0, 0.0, 1.0);
glutWireSphere(0.5, 16, 10);
glEndConditionalRender();
```

Programmed into the block above is what to render depending on the query outcome. There is no need, therefore, for user-instigated determination of results, so the variables result and resultAvailable are now gone. End

6.3 Timer Queries and Performance Measurememt

Now that we have learned all these cool gadgets, and will be learning many more, it would be nice to be able to evaluate their performance. Counting the frame rate, which we learned how to do in Chapter 4 and, in fact, applied to spaceTravel.cpp to quantify the slowdown in going from a small asteroid field to a large one, is one way. However, the frame rate simply tells the speed at which the whole program runs, but doesn't allow the developer to zoom in to profile parts of the code to see which are guzzling the most cycles and might, therefore, bear optimization. This is where timer queries, related syntactically to the occlusion queries of the preceding section come in, and this short section shows how to set them up. Let's get straight to code.

Experiment 6.5. Run spaceTravelFrustumCulledTimerQuery.cpp. The program is simply spaceTravelFrustumCulled.cpp enhanced with timer queries to count the total time per frame spent in drawing the asteroids in both left and right viewports. This is output in milliseconds to the debug window. Figure 6.8 is a screengrab of the latter where, despite the small size, the reader might still be able to make out the transition from three-digit values to single digits and back to three, as we switch from frustum culling off to on and then off again. Read on to see how timer queries have, in fact, been incorporated into this program. End

Figure 6.8: Screenshot of the debug window of spaceTravelFrustumCulledTimerQuery.cpp.

The generation of query ids – two in the case of spaceTravelFrustumCulledTimerQuery.cpp – in the initialization routine is same as for occlusion.cpp. Next, observe that code drawing asteroids in the left viewport is bracketed within a timer query:

```
glBeginQuery(GL_TIME_ELAPSED, query[0]);

... // Asteroid drawing code.

glEndQuery(GL_TIME_ELAPSED);
while (!resultAvailable[0]) glGetQueryObjectuiv(query[0],
                              GL_QUERY_RESULT_AVAILABLE,
                              &resultAvailable[0]);
glGetQueryObjectui64v(query[0], GL_QUERY_RESULT, &timeLeftViewport);
```

The querying statements above should, in fact, be familiar from occlusion.cpp. The difference, of course, is that glBeginQuery(GL_TIME_ELAPSED, ...) activates a query starting the counting of system time, rather than fragments as would glBeginQuery(GL_SAMPLES_PASSED, ...). The result of this query evidently is the time spent in drawing the asteroids in the left viewport.

Code drawing asteroids in the right viewport is similarly bracketed within another timer query. The sum of the times from the two viewports is written to the debug window each frame. Note that the elapsed system time is counted by OpenGL in nanoseconds, so we divide by 10^6 to convert to milliseconds.

6.4 Animating Orientation Using Euler Angles

The lead-in to this section is the discussion of viewing transformations in Section 4.6, particularly orientation and Euler angles in 4.6.3, so you might want to review this earlier material.

6.4.1 Euler Angles and the Orientation of a Rigid Body

Consider this for a second: it's no different to locate and orient a camera in 3-space than it is to locate and orient an aircraft, spacecraft or any other freely-movable rigid object. The gluLookAt() command simply happens to provide intuitive syntax to use, in particular, with a camera, namely, translate to ($eyex$, $eyey$, $eyez$), point at ($centerx$, $centery$, $centerz$) and turn about the line of sight according to the (upx, upy, upz) value. As you can see from Figure 6.9, the captain of a spacecraft could use similar syntax to steer her ship.

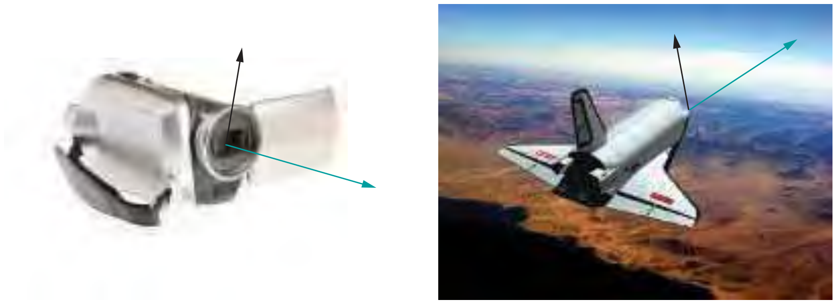

Figure 6.9: Video camera and spacecraft: line of sight is green, up is black.

Accordingly, replace the camera with an arbitrary rigid object B. Assume that the location of B is fixed or, more precisely, that the location of a point P belonging to B is fixed, say, at the origin – see Figure 6.10(a), where the point P at the corner of an L-shaped B is fixed at the origin. One might think of the long leg of the L as the line of sight and the short one as the up direction of a camera.

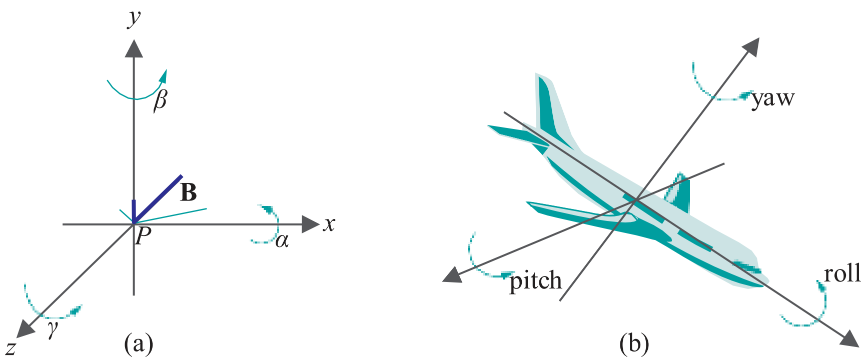

Figure 6.10: (a) Orienting an object in space with respect to fixed axes – the fixed reference orientation of the L is bold blue, another orientation is green (b) Orienting an aircraft with respect to local axes "carried" by it.

Now we are exactly at the point in Section 4.6.3 that we considered a gluLookAt() command with zero translational component, i.e., (*eyex* , *eyey* , *eyez*) = (0, 0, 0). From discussions in that section, the orientation of B is specified by *Euler angles* α, β and γ such that it can be obtained from a fixed reference orientation – in the case of the OpenGL camera this is its default pose – by applying the following rotation sequence:

```
glRotatef(α, 1.0, 0.0, 0.0);
glRotatef(β, 0.0, 1.0, 0.0);
glRotatef(γ, 0.0, 0.0, 1.0);
```

Remark 6.1. The yaw, pitch and roll of an aircraft to which pilots refer are nothing but Euler angles, the difference being that the axis system is carried by the aircraft itself (e.g., the roll axis is the line through the middle of the craft from tail to nose). See Figure 6.10(b).

6.4.2 Animating Orientation

It seems, then, that animating orientation is a matter simply of changing Euler angles. This is true.

Experiment 6.6. Run eulerAngles.cpp, which shows an L, similar to the one in Figure 6.10(a), whose orientation can be interactively changed.

The initial orientation (Figure 6.11) of the L is analogous to the default pose of the OpenGL camera. Pressing 'x/X', 'y/Y' and 'z/Z' changes the L's Euler angles and delete resets. The Euler angle values are displayed on-screen. End

Figure 6.11: Screenshot of eulerAngles.cpp initially.

Remark 6.2. If the commands

```
glRotatef(Xangle, 1.0, 0.0, 0.0);
glRotatef(Yangle, 0.0, 1.0, 0.0);
glRotatef(Zangle, 0.0, 0.0, 1.0);
```

in eulerAngles.cpp to change the Euler angles look familiar, well, we've been using similar ones since the second chapter to rotate scenes.

It all seems easy enough so far. However, things can get rather strange with Euler angles. Run eulerAngles.cpp, or use paper and pencil, to determine the two orientations of the L specified by the following distinct tuples of Euler angles (all angles are in degrees in this section):

(a) $\alpha = 0$, $\beta = 90$, $\gamma = 0$

(b) $\alpha = -90$, $\beta = 90$, $\gamma = 90$

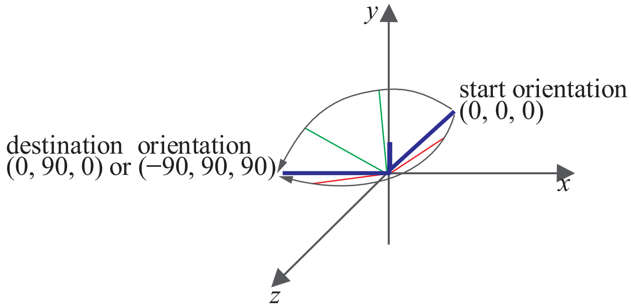

Figure 6.12: The bold blue start orientation is given by the Euler angle tuple (0, 0, 0) and the bold blue destination one by either (0, 90, 0) or (−90, 90, 90). Intermediate orientations (green) in the linear interpolation between (0, 0, 0) and (0, 90, 0) all lie on the *xz*-plane, while those (red) between (0, 0, 0) and (−90, 90, 90) arc below it.

The two orientations are identical, both equal to the destination orientation of Figure 6.12, with the L's long leg along the −*x* direction and short leg along +*y*. Imagine now that the L is a spacecraft we want to take from its start orientation specified by the Euler angle tuple (0, 0, 0) to the destination one specified by either of the tuples (a) or (b).

What comes to mind naturally is a linear interpolation between the start and destination orientations, exactly as if one had to translate the spacecraft from a start to a destination *location*, except that, instead of intermediate positions, one has now intermediate orientations. However, the ambiguity in representing the destination leads to a surprise we see next.

6.4.3 Problems with Euler Angles: Gimbal Lock and Ambiguity

Figure 6.13: Screenshot of interpolateEulerAngles.cpp.

Experiment 6.7. Run interpolateEulerAngles.cpp, which is based on eulerAngles.cpp. It simultaneously interpolates between the tuples (0, 0, 0) and (0, 90, 0) and between (0, 0, 0) and (−90, 90, 90). Press the left and right arrow keys to step through the interpolations (delete resets). For the first interpolation (green L) the successive tuples are (0, *angle*, 0) and for the second (red L) they are (−*angle*, *angle*, *angle*), *angle* changing by 5 at each step in both, between 0 and 90.

The paths are different! The green L seems to follow the intuitively straighter path by keeping its long leg always on the *xz*-plane as it rotates about the *y*-axis, while the red L arcs below the *xz*-plane, as diagrammed in Figure 6.12. Figure 6.13 is a screenshot of interpolateEulerAngles.cpp part way through the interpolation.
End

Two different paths arise in the program, of course, because of the non-unique representation of the destination orientation by Euler angles. Are (0, 90, 0) and (−90, 90, 90) the only tuples of Euler angles that represent this particular destination? Emphatically not, as we see next!

Use eulerAngles.cpp to see that any tuple of the form (−*A*, 90, *A*) represents the same configuration as (0, 90, 0) and (−90, 90, 90): the *A* rotation about the *x*-axis seems always to cancel the *A* rotation about the *z*-axis to make an equivalence to (0, 90, 0). It's not hard to understand why. The first rotation that is applied, viz., glRotatef(*A*, 0.0, 0.0, 1.0), twists the L about its long leg lying along the *z*-axis, the second glRotatef(90, 0.0, 1.0, 0.0) rotates the long leg to line it up with *x*-axis, so that the final glRotatef(−*A*, 1.0, 0.0, 0.0) again twists the L about its long leg, but equally and oppositely to the first rotation.

We've run into the problem of *gimbal lock* which afflicts the Euler angle representation of orientation. Let's get a better understanding of this phenomenon.

Experiment 6.8. Run eulerAngles.cpp again.

Press ‘x’ and ‘X’ a few times each – the L turns longitudinally. Reset by pressing delete. Press ‘y’ and ‘Y’ a few times each – the L turns latitudinally. Reset. Press ‘z’ and ‘Z’ a few times each – the L twists. There appear to be three physical *degrees of freedom* of the L derived from rotation about the three coordinate axes which we might descriptively term, respectively, longitudinal, latitudinal and twisting.

Now, from the initial configuration of eulerAngles.cpp press ‘y’ till $\beta = 90$. Next, press ‘z’ or ‘Z’ – the L twists. Then press ‘x’ or ‘X’ – the L still twists! **End**

Even with β fixed in eulerAngles.cpp one would expect two degrees of freedom to remain, viz., twisting *and* longitudinal. However, because of the particular value of β, namely, 90, which takes the L from the z-axis to the x-axis, we seem to have lost the longitudinal one.

Well, physical space hasn’t changed and all three degrees of freedom are obviously still there for the taking. It’s simply because of the particular value of β that the other two Euler angles α and γ both “act on the same degree of freedom”, causing loss of access to the remaining one.

This *apparent* loss of a degree of freedom is precisely gimbal lock, and it’s the reason as well for the multiple representations of the destination orientation of the L in interpolateEulerAngles.cpp – rotations about the x- and z-axes, both acting on the same degree of freedom when $\beta = 90$, can cancel one another.

Exercise 6.7. Show that gimbal lock also arises when $\beta = -90$.

Even though infinitely many different representations of an orientation occur only at the two gimbal lock values of $\beta = \pm 90$, there’s actually instability near these values as well. In fact, two paths beginning and ending at nearby orientations which happen to be close to gimbal lock values can differ widely.

Exercise 6.8. **(Programming)** Verify the preceding remark by modifying interpolateEulerAngles.cpp to simultaneously interpolate between the Euler angle tuples $(0, 0, 0)$ and $(5, 95, 0)$ and the tuples $(0, 0, 0)$ and $(-95, 85, 95)$.

Moreover, there’s another pesky problem with Euler angles: that of *non-unique*, in fact, *dual* representation of *every* orientation. To begin with, mentally visualize, or run eulerAngles.cpp, to see that the Euler angle tuple $(180, 180, 180)$ is equivalent to the Euler angle tuple $(0, 0, 0)$, both representing the initial orientation of the L.

This generalizes:

Proposition 6.1. *Given any particular values of α, β and γ, the Euler angle tuples (α, β, γ) and $(\alpha + 180, -\beta + 180, \gamma + 180)$ are equivalent in that they both represent the same orientation.*

(Note the minus sign in front of the β in the second tuple.)

Proof. We’ll not prove this formally but leave the reader to “visually verify” it by comparing the orientation of the L of eulerAngles.cpp, as specified by the Euler angle tuples (α, β, γ) and $(\alpha + 180, -\beta + 180, \gamma + 180)$, for a few different values of α, β and γ.

Of course, an Euler angle tuple (α, β, γ) is always equivalent to the Euler angle tuple $(\alpha \pm 360, \beta \pm 360, \gamma \pm 360)$ for any choice of the pluses and minuses, simply because angular degree arithmetic is modulo 360. However, the equivalence of the Euler angle tuples (α, β, γ) and $(\alpha + 180, -\beta + 180, \gamma + 180)$ is *not* a consequence of angular arithmetic, but a true *geometric duality* intrinsic to Euler angles.

Exercise 6.9. **(Programming)** Modify interpolateEulerAngles.cpp to simultaneously interpolate between the initial orientation $(0, 90, 0)$ and the destination orientation represented dually by the distinct Euler angle tuples $(0, 0, 0)$ and $(180, 180, 180)$.

Again, the two paths are different.

All this is not the best news if one is in the business of animating the orientation of a camera or rigid body, as one then wants to be able to *uniquely* choose representations of the start and destination orientations in order to interpolate between the two, just as one has unique (x, y, z)-coordinates of any position in world space. It turns out that there, in fact, is a more efficient representation of orientation by means of mathematical thingies called quaternions, in which case there's never gimbal lock and, though there's still an issue with ambiguous representation, it's one that can be elegantly resolved prior to interpolation. Quaternions and their application to orientation are the topic of the next section.

6.5 Quaternions

We are going now to get past the problems arising in animating orientation with Euler angles, which we saw in the last section, with the use of quaternions instead. The misapprehension of quaternions as forbidding math, fairly common amongst game programmers, is unfortunate, not only because it is interactive applications like games which stand to benefit most from their use, but because quaternions are not hard to learn and actually easy to use once you do.

6.5.1 Quaternion Math 101

Quaternions were invented by the Irish mathematician William Hamilton in the mid-1900s as part of his investigation into 3D mechanics. Think of them as complex numbers on steroids. Whereas complex numbers extend the reals with one imaginary i, a square root of -1, quaternions add three such numbers i, j and k, all square roots of -1. Formally:

Definition 6.1. A *quaternion* q is a number of the form

$$q = w + xi + yj + zk$$

where w, x, y and z are real numbers

It's often written as $q = w + \mathrm{v}$, where w is the *real* or *scalar* part, while $\mathrm{v} = xi + yj + zk$ is the *vector* or *pure quaternion* part. A quaternion of the form $q = xi+yj+zk$, with a zero scalar part, is also called a pure quaternion.

Terminology : In this section vector parts will be denoted in bold to distinguish them from the scalar (except for i, j and k themselves, as there's little risk of ambiguity with the three).

The set of quaternions is commonly denoted H in honor of its inventor.

The real numbers are a subset of the quaternions, the real w being identified with the quaternion w $(= w + 0i + 0j + 0k)$ with a zero vector part.

Example 6.1. Some quaternions:

$$2 - 3.4i + 4.8j + 2k, \quad -i + \sqrt{2}k, \quad 10.9, \quad -6.3j, \; 0$$

Quaternions are added component-wise, just as complex numbers:

Definition 6.2. The *sum* of two quaternions $q_1 = w_1 + x_1i + y_1j + z_1k$ and $q_2 = w_2 + x_2i + y_2j + z_2k$ is the quaternion

$$q_1 + q_2 = (w_1 + w_2) + (x_1 + x_2)i + (y_1 + y_2)j + (z_1 + z_2)k$$

Exercise 6.10. Add the quaternions

(a) $2 - 3.4i + 4.8j + 2k$ and $-6.3j$

(b) $-i + \frac{1}{\sqrt{2}}k$ and $\frac{1}{\sqrt{2}}k$

The "square root of -1" property kicks in when multiplying quaternions. Here are the rules to keep in mind:

$$i^2 = j^2 = k^2 = -1$$

$$\begin{array}{ll} ij = k & ji = -k \\ jk = i & kj = -i \\ ki = j & ik = -j \end{array}$$

They're not hard to remember. The square of i, j and k each is -1. For the rest, simply keep in mind the cyclic order $i \to j \to k \to i$. If two successive elements in this order are multiplied, the result is the next element; if two successive elements are multiplied in reverse order, the result is the negative of the next element. This second rule is a replica of that of taking the cross-product of two different ones from the three unit vectors i, j and k (see Remark 5.8).

When multiplying two quaternions, it's a matter of "presuming" distributivity of multiplication over addition and using the preceding rules. Here's an example:

Example 6.2.

$$\begin{aligned} (2 - 3i + 2j)(3 + i - k) &= 2(3 + i - k) - 3i(3 + i - k) + 2j(3 + i - k) \\ &= 2 * 3 + 2 * i + 2 * -k - 3i * 3 - 3i * i \\ &\quad -3i * -k + 2j * 3 + 2j * i + 2j * -k \\ &= 6 + 2i - 2k - 9i + 3 - 3j + 6j - 2k - 2i \\ &= 9 - 9i + 3j - 4k \end{aligned}$$

We have "presuming" in quotes above because distributivity really has to be proved given a *definition* of multiplication. Here's that definition which, of course, is based on looking ahead to distributivity: the product of two quaternions $q_1 = w_1 + x_1 i + y_1 j + z_1 k$ and $q_2 = w_2 + x_2 i + y_2 j + z_2 k$ is

$$\begin{aligned} q_1 q_2 = {} & (w_1 w_2 - x_1 x_2 - y_1 y_2 - z_1 z_2) + (w_1 x_2 + x_1 w_2 + y_1 z_2 - z_1 y_2)\, i \\ & (w_1 y_2 + y_1 w_2 - x_1 z_2 + z_1 x_2) j + (w_1 z_2 + z_1 w_2 + x_1 y_2 - y_1 x_2) k \end{aligned} \tag{6.1}$$

Exercise 6.11. Multiply

$$(4 + 2i + 2j - k)(1 - k)$$

Exercise 6.12. Prove the following:

(a) The addition of quaternions is commutative and associative. In particular,

$$q_1 + q_2 = q_2 + q_1 \quad \text{and } (q_1 + q_2) + q_3 = q_1 + (q_2 + q_3)$$

for any three quaternions q_1, q_2 and q_3.

(b) The multiplication of quaternions is associative and, moreover, distributes both ways over addition. In particular,

$$(q_1 q_2) q_3 = q_1 (q_2 q_3), \; q_1 (q_2 + q_3) = q_1 q_2 + q_1 q_3, \; (q_2 + q_3) q_1 = q_2 q_1 + q_3 q_1$$

for any three quaternions q_1, q_2 and q_3.

(c) The multiplication of quaternions is *not* commutative. In particular, it need not be true that $q_1 q_2 = q_2 q_1$ for two quaternions q_1 and q_2. Give an example.

(d) The additive identity is 0 and the multiplicative identity 1. In particular,

$$q + 0 = 0 + q = q = q1 = 1q$$

for any quaternion q.

There is a useful shorter expression for the product of two quaternions in terms of vector operations:

Exercise 6.13. Prove that if $q_1 = w_1 + \mathrm{v}_1$ and $q_2 = w_2 + \mathrm{v}_2$, then

$$q_1q_2 = w_1w_2 - \mathrm{v}_1 \cdot \mathrm{v}_2 + w_1\mathrm{v}_2 + w_2\mathrm{v}_1 + \mathrm{v}_1 \times \mathrm{v}_2 \qquad (6.2)$$

where and $\times$ represent the vector dot and cross-product, respectively, and we treat the pure quaternion part $\mathrm{v} = xi + yj + zk$ of a quaternion $q + \mathrm{v}$ as the geometric vector $x\mathrm{i} + y\mathrm{j} + z\mathrm{k}$ when applying these products.

Similar to complex numbers, quaternions each have a magnitude and a conjugate.

Definition 6.3. The *magnitude* of the quaternion $q = w + xi + yj + zk$, denoted $|q|$, is the non-negative value of the square root

$$\sqrt{w^2 + x^2 + y^2 + z^2}$$

Therefore, if we write $q = w + \mathrm{v}$, then its magnitude $|q| = \sqrt{w^2 + |\mathrm{v}|^2}$, where $|\mathrm{v}|$ denotes as usual the magnitude of the vector v. A *unit quaternion* is one with magnitude 1.

Definition 6.4. The *conjugate* of the quaternion $q = w+xi+yj+zk$ is the quaternion

$$\bar{q} = w - xi - yj - zk$$

In other words, if $q = w + \mathrm{v}$ then its conjugate $\bar{q} = w - \mathrm{v}$.

And, as with complex numbers, a quaternion and its conjugate and magnitude are related:

Exercise 6.14. Prove that $q\bar{q} = \bar{q}q = |q|^2$.

Definition 6.5. The *inverse* of a quaternion q, if it exists, is the quaternion q^{-1} such that

$$qq^{-1} = q^{-1}q = 1$$

Exercise 6.15. Use Exercise 6.14 to prove that a quaternion q has an inverse if and only if it is non-zero, in which case

$$q^{-1} = \frac{\bar{q}}{|q|^2}$$

Therefore, $q^{-1} = \bar{q}$ for a unit quaternion q.

Example 6.3. Determine the inverse of the quaternion $q = 1 + i + j + k$.

Answer:

$$q^{-1} = \frac{\bar{q}}{|q|^2} = \frac{1 - i - j - k}{1^2 + 1^2 + 1^2 + 1^2} = \frac{1}{4}(1 - i - j - k)$$

Exercise 6.16. Determine the inverses of the quaternions

(a) j

(b) $\sqrt{3}i + \sqrt{2}k$

(c) $-1 + i + 2j - k$

Exercise 6.17. Prove the following if q_1 and q_2 are quaternions and c a scalar:

(a) $\overline{(q_1q_2)} = \overline{q_2}\,\overline{q_1}$

(b) $(cq_1)^{-1} = c^{-1}q_1^{-1}$, provided both c and q_1 are non-zero.

(c) $(q_1q_2)^{-1} = q_2^{-1}q_1^{-1}$, provided both q_1 and q_2 are non-zero.

(d) $|q_1q_2| = |q_1||q_2|$

6.5.2 Quaternions and Orientation

So what do quaternions have to do with orienting a rigid body? The answer comes by way of the rotation transformation. Recall from the last section that the orientation of a rigid object B is specified by Euler angles α, β and γ such that the specified orientation can be obtained from a fixed reference orientation by applying the following sequence of rotations:

```
glRotatef(α, 1.0, 0.0, 0.0);
glRotatef(β, 0.0, 1.0, 0.0);
glRotatef(γ, 0.0, 0.0, 1.0);
```

Now, we know from Proposition 5.14 that the composition of rotations about radial axes is another such. Therefore, the three above can be combined into a *single* rotation

```
glRotatef(θ, x, y, z)
```

for some angle θ and some values of x, y and z.

It follows that, instead of Euler angles, one can represent an orientation in 3D by means of a single 3D rotation about some radial axis. Moreover, it turns out that each quaternion, as we shall see, represents a 3D rotation about some radial axis as well. The conclusion, then, is that each quaternion represents a 3D orientation. The next proposition says how a quaternion determines a 3D rotation.

Note: In what follows we'll often identify the quaternions i, j and k with their vector counterparts i, j and k, respectively. It should be clear from the context whether we mean a quaternion or vector.

Proposition 6.2. *Suppose the axis of a 3D rotation is specified by the directed line l through the origin O toward a point $P = [a\ b\ c]^T$ and the angle of rotation is θ. Assume that $|P| = 1$. Denote the unit vector OP = ai + bj + ck by* u. (See Figure 6.14.)

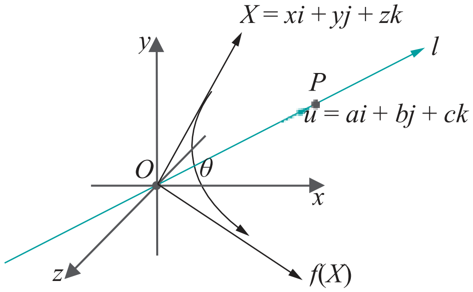

Figure 6.14: The vector f(X) is obtained by rotating X about the line l.

If X $= xi + yj + zk$ *is an arbitrary vector in* $\mathbb{R}^3$ *then the image of* X, *call it* f(X), *by the given rotation is*

$$f(\mathrm{X}) = q\,\mathrm{X}\,q^{-1} \tag{6.3}$$

where q is the unit quaternion

$$q = \cos\frac{\theta}{2} + \mathrm{u}\sin\frac{\theta}{2} \tag{6.4}$$

Note: We're treating the vector $X = xi + yj + zk$ as a pure quaternion in the product on the RHS of (6.3).

Let's put the proposition into context first. It gives yet another way to determine the image $f(X)$ of a vector X by rotation of an angle θ about a radial axis l. The first, which we derived in Section 5.4.3, expressed $f(X)$ as the matrix product $R_{a,\,b,\,c}(\theta)\,X$, where $R_{a,\,b,\,c}(\theta)$ was, in fact, given in a couple of different ways by the equations (5.29) and (5.39). Now, instead of a matrix, we manufacture a unit quaternion q such that the rotated vector $f(X)$ is $q\,X\,q^{-1}$ (this operation of pre-multiplying by an element and then post-multiplying by its inverse is called an *inner automorphism* by that element). The proof itself is a straight slog.

Proof. As q is a unit quaternion, its inverse is

$$q^{-1} = \bar{q} = \cos\frac{\theta}{2} - u\sin\frac{\theta}{2}$$

Repeatedly applying the multiplication formula (6.2) we get the following equations:

$$\begin{aligned}
&q\,X\,q^{-1}\\
&= \left(\cos\frac{\theta}{2} + u\sin\frac{\theta}{2}\right) X \left(\cos\frac{\theta}{2} - u\sin\frac{\theta}{2}\right)\\
&= \left(-(u\cdot X)\sin\frac{\theta}{2} + X\cos\frac{\theta}{2} + (u\times X)\sin\frac{\theta}{2}\right)\left(\cos\frac{\theta}{2} - u\sin\frac{\theta}{2}\right)\\
&= \ -(u\cdot X)\sin\frac{\theta}{2}\cos\frac{\theta}{2} + (u\cdot X)\sin\frac{\theta}{2}\cos\frac{\theta}{2} + (u\times X)\cdot u\sin^2\frac{\theta}{2}\\
&\quad + (u\cdot X)\,u\sin^2\frac{\theta}{2} + X\cos^2\frac{\theta}{2} + (u\times X)\sin\frac{\theta}{2}\cos\frac{\theta}{2}\\
&\quad + (u\times X)\sin\frac{\theta}{2}\cos\frac{\theta}{2} - ((u\times X)\times u)\sin^2\frac{\theta}{2}
\end{aligned}$$

Of the eight terms summed in the final expression, the first two cancel, while the third is 0 because $u\times X$ is perpendicular to u. Let $X = X_1 + X_2$, where X_1 and X_2 are the components of X parallel and perpendicular, respectively, to u. Use the facts that $X_1 = (u\cdot X)\,u$ and $X_2 = X - X_1 = (u\times X)\times u$, which we know from Exercises 4.51 and 5.60, respectively, to further simplify the final expression:

$$\begin{aligned}
q\,X\,q^{-1} &= X_1\sin^2\frac{\theta}{2} + X\cos^2\frac{\theta}{2} + (u\times X)\sin\frac{\theta}{2}\cos\frac{\theta}{2}\\
&\quad + (u\times X)\sin\frac{\theta}{2}\cos\frac{\theta}{2} - (X - X_1)\sin^2\frac{\theta}{2}\\
&= X\left(\cos^2\frac{\theta}{2} - \sin^2\frac{\theta}{2}\right) + 2X_1\sin^2\frac{\theta}{2} + 2(u\times X)\sin\frac{\theta}{2}\cos\frac{\theta}{2}\\
&= X\cos\theta + X_1(1-\cos\theta) + (u\times X)\sin\theta \qquad (6.5)
\end{aligned}$$

Comparing (6.5) with the formula (5.37) derived for $f(X)$ in Section 5.4.3 completes the proof.

So, indeed, we have the correspondence:

orientation → radial rotation → quaternion

Example 6.4. Let's verify the preceding proposition in the case of rotating the vector i by an angle of $\pi/2$ about the axis k.

It's easily checked by hand that this particular rotation takes i to j.

Next, to use the proposition, write first $u = k$, $X = i$ and $\theta = \pi/2$. This gives the quaternion

$$q = \cos\frac{\theta}{2} + u\sin\frac{\theta}{2} = \frac{1}{\sqrt{2}} + \frac{1}{\sqrt{2}}k$$

Therefore, by the proposition the image of i by the rotation of $\pi/2$ about axis k is

$$\begin{aligned} qXq^{-1} &= \left(\frac{1}{\sqrt{2}} + \frac{1}{\sqrt{2}}k\right) i \left(\frac{1}{\sqrt{2}} - \frac{1}{\sqrt{2}}k\right) \\ &= \left(\frac{1}{\sqrt{2}}i + \frac{1}{\sqrt{2}}j\right)\left(\frac{1}{\sqrt{2}} - \frac{1}{\sqrt{2}}k\right) \\ &= \frac{1}{2}i + \frac{1}{2}j + \frac{1}{2}j - \frac{1}{2}i \\ &= j \end{aligned}$$

which, indeed, matches what we checked.

Exercise 6.18. Verify the proposition in the case of rotating the vector $i + k$ by an angle of π about j.

Proposition 6.2 says that every radial rotation corresponds to a unit quaternion. How about the other way around: does every unit quaternion correspond to a radial rotation in the sense that it gives that rotation by an inner automorphism? The answer is yes:

Proposition 6.3. *Let $q = w + xi + yj + zk$ be a unit quaternion. If $q = \pm 1$, then $X \mapsto qXq^{-1}$ is the identity transformation, i.e., a zero rotation about an arbitrary axis. If $q \neq \pm 1$, then there exists a unique pair (u, θ), such that u is a unit vector and $\theta \in (0, 2\pi)$, and such that*

$$q = \cos\frac{\theta}{2} + u \sin\frac{\theta}{2},$$

which implies that $X \mapsto qXq^{-1}$ is a rotation by angle θ about the radial axis directed along u.

Proof. If $q = 1$ or $q = -1$ then it's obvious that $X \mapsto qXq^{-1}$ is the identity transformation.

Suppose, then, that $q \neq \pm 1$. As $w^2 + x^2 + y^2 + z^2 = |q|^2 = 1$, we must have $-1 \leq w \leq 1$. However, if $w = \pm 1$, then we would have $x = y = z = 0$, giving $q = \pm 1$, contradicting our assumption. One deduces, therefore, that $-1 < w < 1$, implying that there is a unique $\theta/2 \in (0, \pi)$ – equivalently, a unique $\theta \in (0, 2\pi)$ – such that $\cos\frac{\theta}{2} = w$. Accordingly, we have $\sin\frac{\theta}{2} = \sqrt{1 - w^2}$, where the RHS is the positive square root. It follows that

$$\begin{aligned} q &= w + xi + yj + zk \\ &= w + \left(\frac{x}{\sqrt{1-w^2}}i + \frac{y}{\sqrt{1-w^2}}j + \frac{z}{\sqrt{1-w^2}}k\right)\sqrt{1-w^2} \\ &= \cos\frac{\theta}{2} + u\sin\frac{\theta}{2} \end{aligned}$$

where

$$u = \frac{x}{\sqrt{1-w^2}}i + \frac{y}{\sqrt{1-w^2}}j + \frac{z}{\sqrt{1-w^2}}k$$

is a unit vector because $x^2 + y^2 + z^2 = 1 - w^2$. The conclusion in the last line of the proposition now follows from an application of Proposition 6.2.

Example 6.5. Determine the rotation corresponding to the unit quaternion

$$\frac{1}{\sqrt{3}}i + \frac{1}{\sqrt{3}}j + \frac{1}{\sqrt{3}}k$$

and write it in OpenGL form.

Answer: We want to express

$$q = \frac{1}{\sqrt{3}}i + \frac{1}{\sqrt{3}}j + \frac{1}{\sqrt{3}}k$$

in the form

$$\cos\frac{\theta}{2} + \mathrm{u}\sin\frac{\theta}{2}$$

Following the preceding proposition, write

$$q = w + xi + yj + zk \quad \text{where} \quad w = 0 \quad \text{and} \quad x = y = z = \frac{1}{\sqrt{3}}$$

Now,

$$\cos\theta/2 = w = 0 \implies \theta/2 = \frac{\pi}{2} \implies \theta = \pi$$

and

$$\mathrm{u} = \frac{x}{\sqrt{1-w^2}}i + \frac{y}{\sqrt{1-w^2}}j + \frac{z}{\sqrt{1-w^2}}k = \frac{1}{\sqrt{3}}i + \frac{1}{\sqrt{3}}j + \frac{1}{\sqrt{3}}k$$

It follows that the given quaternion corresponds to the OpenGL rotation (up to round-off error)

```
glRotatef(180.0, 0.58, 0.58, 0.58)
```

Exercise 6.19. Determine the rotation corresponding to the unit quaternion

$$\frac{1}{\sqrt{2}} + \frac{1}{2}i + \frac{1}{2}k$$

and write it in OpenGL form.

We prove next a couple of useful facts related to Proposition 6.2:

Proposition 6.4. *(a) If the rotation f_1 corresponds to the quaternion q_1 and the rotation f_2 to q_2, then the composed rotation $f_1 \circ f_2$ corresponds to the product q_1q_2.*

In other words, rotations can be composed by multiplying their corresponding quaternions.

(b) If q is a unit quaternion and c an arbitrary non-zero scalar, then the transformation

$$X \mapsto (cq)\,X\,(cq)^{-1}$$

is equivalent to the rotation

$$X \mapsto q\,X\,q^{-1}$$

In other words, q and any non-zero scalar multiple cq give the same rotation by inner automorphism.

Proof. (a) For a vector X,

$$\begin{aligned}(f_1 \circ f_2)(X) &= f_1(f_2(X)) = q_1(q_2\,X\,q_2^{-1})q_1^{-1} \\ &= (q_1q_2)\,X\,(q_2^{-1}q_1^{-1}) = (q_1q_2)\,X\,(q_1q_2)^{-1}\end{aligned}$$

completing the proof.

(b) Since $(cq)^{-1} = c^{-1}q^{-1}$, the equalities

$$(cq)\,X\,(cq)^{-1} = (cq)\,X\,(c^{-1}q^{-1}) = (cc^{-1})q\,X\,q^{-1} = q\,X\,q^{-1}$$

complete the proof (note, for the second equality, that a scalar can be moved in and out of a product with impunity).

Exercise 6.20. Let f_1 be a rotation of 60° about the x-axis and f_2 a rotation of 90° about the y-axis. Determine the composed rotations $f_1 \circ f_2$ and $f_2 \circ f_1$ (by giving their respective axis and amount of rotation).

Part answer : The plan is to go from rotation space to quaternion space, multiply and return to rotation space.

Proposition 6.2 tells us that rotation f_1 corresponds to the quaternion

$$q = \cos\frac{\theta}{2} + u \sin\frac{\theta}{2}$$

where $u = i$ and $\theta = \pi/3$. In other words, f_1 corresponds to

$$\frac{\sqrt{3}}{2} + \frac{1}{2}i$$

Likewise, f_2 corresponds to

$$\frac{1}{\sqrt{2}} + \frac{1}{\sqrt{2}}j$$

By Proposition 6.4(a), $f_1 \circ f_2$ corresponds to

$$\left(\frac{\sqrt{3}}{2} + \frac{1}{2}i\right)\left(\frac{1}{\sqrt{2}} + \frac{1}{\sqrt{2}}j\right) = \frac{\sqrt{3}}{2\sqrt{2}} + \frac{1}{2\sqrt{2}}i + \frac{\sqrt{3}}{2\sqrt{2}}j + \frac{1}{2\sqrt{2}}k$$

Applying Proposition 6.3 to determine the rotation corresponding to the above quaternion, one finds after some calculation $f_1 \circ f_2$ to be glRotatef(104.48, 0.45, 0.77, 0.45) written as an OpenGL rotation up to round-off error.

We leave the reader to apply the same method to $f_2 \circ f_1$.

Proposition 6.4 has a couple of interesting consequences.

Firstly, part (a) has an implication for computational efficiency. If a rotation is represented by a matrix, as in Equation (5.39), then the complexity of composing two rotations, equivalent to multiplying the corresponding matrices, is dominated by 27 scalar multiplications – treating the matrix of (5.39) as 3 × 3 because the fourth row and column don't add complexity and observing that each of the 9 entries of the product involves 3 multiplications.

On the other hand, if a rotation is represented by a quaternion, then composing two rotations, equivalent to multiplying the corresponding quaternions by Proposition 6.4(a), requires 16 scalar multiplications. The conclusion is that an efficient way, in fact, to compose multiple rotations is via quaternion representation.

Secondly, a consequence of part (b) of the proposition is a mathematically useful, though somewhat abstract, representation of 3D rotations. Note, first, that the set H of quaternions is in one-to-one correspondence with 4D space R^4 via the association $w + xi + yj + zk \leftrightarrow [w\ x\ y\ z]^T$. We can, therefore, identify H with R^4 and refer to points of the latter as quaternions.

Now, Proposition 6.4(b) says that all non-zero quaternions on a given radial line in R^4 correspond to the same rotation, as they differ one from another by a scalar multiple. It can also be verified that non-zero quaternions on distinct radial lines correspond to different rotations.

So here's a summary of the situation. Quaternions are in one-to-one correspondence with points of R^4. Each non-zero quaternion also corresponds *uniquely* to a rotation of 3-space, which it gives by inner automorphism. Rotations, on the other hand, are not as "faithful" because each corresponds to infinitely many quaternions, in fact, a whole radial line's worth (except that the origin O does not correspond to a rotation). See Figure 6.15. Rotations of 3-space, therefore, are in one-to-one correspondence with the set of radial lines in R^4.

If one is uncomfortable with identifying rotations of R^3 with lines in R^4, then here's a way to identify them with points instead: since a radial line of R^4 intersects

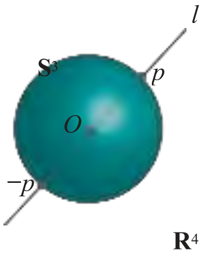

Figure 6.15: The unit sphere S^3 in R^4 with a radial line l, representing a rotation of R^3, passing through a pair of antipodal points.

S^3, the unit sphere of R^4, in a pair of *antipodal* , or, diametrically opposite, points, rotations are in 1-1 correspondence with the points of S^3, *provided* one is willing to undertake the mental trick of identifying each antipodal pair as a single point. S^3 with its antipodal points identified is actually the so-called projective 3-space P^3, so, finally, one identifies the space of 3D rotations with P^3.

Incidentally, note that since the space H of all quaternions is identified with R^4, the space of unit quaternions identifies with the unit sphere S^3 of R^4.

Quaternion to Rotation Matrix

Proposition 6.3 enables us to find the unique rotation corresponding to a unit quaternion in terms of its axis and rotation angle. However, in various applications, e.g., when using OpenGL, the rotation matrix itself is more useful. We ask the reader to find the 4 × 4 rotation matrix corresponding to a given quaternion by completing the solution to the following exercise.

Exercise 6.21. Show that the 4 × 4 matrix representing the rotation corresponding to the unit quaternion

$$q = w + xi + yj + zk$$

is

$$\begin{bmatrix} w^2 + x^2 - y^2 - z^2 & 2xy - 2wz & 2xz + 2wy & 0 \\ 2xy + 2wz & w^2 - x^2 + y^2 - z^2 & 2yz - 2wx & 0 \\ 2xz - 2wy & 2yz + 2wx & w^2 - x^2 - y^2 + z^2 & 0 \\ 0 & 0 & 0 & 1 \end{bmatrix} \qquad (6.6)$$

Part answer : Verify first the case when $q = \pm 1$ (keep in mind that this implies that $w = \pm 1$ and that $x = y = z = 0$). Suppose, next, that $q \neq \pm 1$. Proposition 6.3 says, then, that q gives, by inner automorphism, the rotation of angle θ about the unit vector u where

$$\cos\frac{\theta}{2} = w \quad \text{and} \quad \mathrm{u} = (x/\sqrt{1 - w^2})\, i + (y/\sqrt{1 - w^2})\, j + (y/\sqrt{1 - w^2})\, k$$

In Section 5.4.3 – see Equation (5.39) – we derived the following matrix corresponding to a rotation of angle θ about the radial axis l toward the point $P = [a\ b\ c]^T$, where $|P| = 1$.

$$R_{a,b,c}(\theta) = \begin{bmatrix} a^2(1-\cos\theta)+\cos\theta & ab(1-\cos\theta)-c\sin\theta & ac(1-\cos\theta)+b\sin\theta & 0 \\ ab(1-\cos\theta)+c\sin\theta & b^2(1-\cos\theta)+\cos\theta & bc(1-\cos\theta)-a\sin\theta & 0 \\ ac(1-\cos\theta)-b\sin\theta & bc(1-\cos\theta)+a\sin\theta & c^2(1-\cos\theta)+\cos\theta & 0 \\ 0 & 0 & 0 & 1 \end{bmatrix}$$

We ask the reader to finish the exercise by deriving the matrix (6.6) after plugging the following into the matrix expression above for $R_{a,b,c}(\theta)$:

$$\begin{aligned} a &= x/\sqrt{1 - w^2} \\ b &= y/\sqrt{1 - w^2} \\ c &= z/\sqrt{1 - w^2} \\ 1 - & \qquad {}^2\frac{\theta}{2} \\ \cos\theta &= 2\cos^2\frac{\theta}{2} - 1 = 2w^2 - 1 \\ \sin\theta &= 2\sin\frac{\theta}{2}\cos\frac{\theta}{2} = 2w\sqrt{1 - w^2} \end{aligned}$$

Spherical Linear Interpolation

Let's return to our original objective of applying quaternions to the animation of orientation. We have a 3-step strategy: (1) represent the start and end orientations corresponding, say, to the rotations f_1 and f_2 by unit quaternions, q_1 and q_2, respectively; (2) interpolate between the two in quaternion space, traveling from q_1 to q_2 along a path of unit quaternions as well; (3) finally, map this path back to a path in the space of rotations from f_1 to f_2, which, of course, is equivalent to a path in the space of orientations between the original start and end ones. Figure 6.16(a) is a conceptual diagram (numbers in parentheses indicate steps).

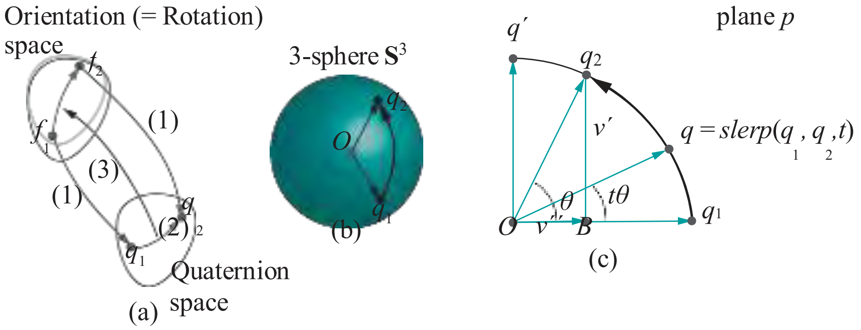

Figure 6.16: (a) Conceptual plan to use quaternion space to interpolate in orientation space (numbers in parentheses indicate steps) (b) The geodesic path from q_1 to q_2 on S^3 (c) Slerping from q_1 to q_2.

Figure 6.16(b) shows the representing unit quaternions q_1 and q_2 as points on the unit sphere S^3 of R^4, the latter being identified with the set H of all quaternions. A shortest path on S^3 between q_1 and q_2 is along a great circle – a *great circle* is the intersection of a radial plane with S^3. A shortest path itself is called a *geodesic* path. If q_1 and q_2 are not antipodal, then there is a unique geodesic path joining them; if they are antipodal, then there are infinitely many (each half a great circle).

Remark 6.3. It helps the intuition to think of shortest paths on the surface of the Earth, where the situation is exactly the same, only one dimension lower.

Suppose, first, that q_1 and q_2 are not antipodal. We want to interpolate at a constant angular rate from q_1 to q_2 along the unique geodesic joining them. This is called *spherical linear interpolation*, or *slerp* for short. Even though q_1 and q_2 are points of R^4, the slerp between them takes place entirely on the unique 2D plane p containing the two and the origin. See Figure 6.16(c).

Suppose that θ is the smaller of the angles between q_1 and q_2 on the great circle containing them. The point q, an angle of $t\theta$ from q_1 toward q_2 on that same circle, is denoted $slerp(q_1, q_2, t)$. As t varies from 0 to 1, $slerp(q_1, q_2, t)$ travels from q_1 to q_2. We seek, therefore, a formula for $slerp(q_1, q_2, t)$.

Let q^1 be the unit quaternion on the plane p on the same side of q_1 as q_2 and such that Oq^1 is perpendicular to Oq_1 (this assumes, additionally, that q_2 /= q_1, for slerping between them is trivial otherwise). Drop the perpendicular from q_2 to the point B on Oq_1 and denote the 4-vector Bq_2 by v^1 and OB by v^{11}.

Observe, first, that

$$|v^1| = |q_2| \sin\theta = \sin\theta \quad \text{and} \quad |v^{11}| = |q_2| \cos\theta = \cos\theta$$

because $|q_2| = 1$. Moreover, $v^{11} = |v^{11}| q_1$, because q_1 is the unit vector parallel to v^{11}, which means $v^{11} = q_1 \cos\theta$. Therefore, we have

$$v^1 = q_2 - v^{11} = q_2 - q_1 \cos\theta$$

Since q^1 is of unit length and parallel to v^1, we have as well

$$q^1 = \frac{v^1}{|v^1|} = \frac{v^1}{\sin\theta} = \frac{q_2 - q_1 \cos\theta}{\sin\theta}$$

(that q_1 and q_2 are neither equal nor antipodal ensures that θ and $\sin\theta$ are bothnon-zero). Therefore,

$$\begin{aligned} q = slerp(q_1, q_2, t) &= q_1 \cos(t\theta) + q^1 \sin(t\theta) \\ &\qquad \text{(adding the components of } q \text{ along } q_1 \text{ and } q^1\text{)} \\ &= q_1 \cos(t\theta) + \frac{q_2 - q_1 \cos\theta}{\sin\theta} \sin(t\theta) \\ &= q_1 \left(\cos(t\theta) - \frac{\cos\theta}{\sin\theta} \sin(t\theta)\right) + q_2 \frac{\sin(t\theta)}{\sin\theta} \\ &= q_1 \frac{\sin((1-t)\theta)}{\sin\theta} + q_2 \frac{\sin(t\theta)}{\sin\theta} \qquad (6.7) \end{aligned}$$

which gives the formula sought for $slerp(q_1, q_2, t)$ (note that θ, the angle between them, is easily determined from q_1 and q_2).

Remark 6.4. Expectedly, linear interpolation has not been able to escape the ugly diminutive *lerp* in the CG literature, with the obvious formula

$$lerp\,(q_1, q_2, t) = (1 - t)q_1 + tq_2$$

Interpolating Orientations via Quaternions

We now have all the pieces in place to implement the following scheme to interpolate between two orientations corresponding to the rotations f_1 and f_2:

1. Go from rotation space to quaternion space by finding unit quaternions q_1 and q_2 corresponding to f_1 and f_2, respectively.

2. Observe that both q_2 and $-q_2$ represent the same rotation but one of the two makes an angle of at most $\pi/2$ with q_1 and the other an angle at least $\pi/2$. We want to interpolate to the one closer to q_1, in case the two are at different angular distances.

   Accordingly, determine $q_1 \cdot q_2$. If its value is negative, then the angle between q_1 and q_2 is greater than $\pi/2$, in which case set $q_2 = -q_2$; otherwise, leave it as it is.

   Note: It's in this last step that we resolve the problem from potentially ambiguous representation of a rotation. In fact, it is only when q_1 and q_2 are orthogonal that both q_2 and $-q_2$ are at the same angle of $\pi/2$ from q_1, and we *could* choose either. The last step above finesses this choice by leaving q_2 unchanged in this case. However, see Exercise 6.22 below.

   Recall in this connection how much more troublesome were ambiguous Euler angle representations in the last section.

3. Compute $slerp(q_1, q_2, t)$, t varying from 0 to 1.

4. Return to rotation space by computing the rotation $f(t)$ corresponding to $slerp(q_1, q_2, t)$. Then $f(t)$ interpolates between the rotations f_1 and f_2 (equivalently, the corresponding orientations).

Exercise 6.22. Show that if q_1 and q_2 are orthogonal then ambiguity is *inherent*, in that the orientation corresponding to one is a rotation of 180° about some axis of the orientation corresponding to the other. In this case, rotating one way about that axis, to change one orientation to the other, is exactly symmetric to going the other way, and there is no procedure to prefer one over the other. For example, consider the two ways of going from the orientation AB to AB^1 of the solid straight arrow in Figure 6.17.

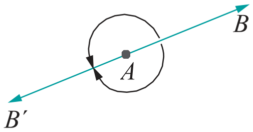

Figure 6.17: Changing the orientation from AB to AB^1 is inherently ambiguous.

Time for code.

Experiment 6.9. Run quaternionAnimation.cpp, which applies the preceding ideas to animate the orientation of our favorite rigid body, an L, with the help of quaternions. Press 'x/X', 'y/Y' and 'z/Z' to change the orientation of the blue L, whose current Euler angles are shown on the display. Its start orientation is the initially stationary red L. See Figure 6.18 for a screenshot.

Pressing enter at any time begins an animation of the red L from its initial disposition to the blue's current orientation. Press the up and down arrow keys to change the speed and delete to reset. End

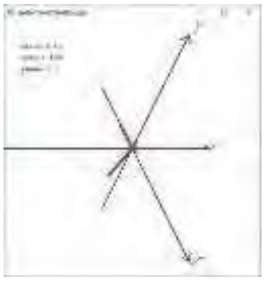

Figure 6.18: Screenshot of quaternionAnimation.cpp.

The routine eulerAnglesToQuaternion() of the program determines the unit quaternion corresponding to an orientation specified by three Euler angles, by computing first the unit quaternion corresponding to the rotation about the coordinate axis connoted by each Euler angle, and then multiplying the three.

The routine slerp() implements formula (6.7), except for the following "hack" to avoid problems with division by zero, or near-zero numbers, when θ is small. Applying the approximation $\sin a$ '::: a for small a, formula (6.7) is modified as follows if $\theta \leq 0.000001$:

$$\begin{aligned} slerp(q_1, q_2, t) &= q_1 \frac{\sin((1-t)\theta)}{\sin\theta} + q_2 \frac{\sin(t\theta)}{\sin\theta} \\ &= q_2 \frac{(1-t)\theta}{\theta} + q_2 \frac{t\theta}{\theta} = (1-t)q_1 + tq_2 \end{aligned}$$

(the value 0.000001 having been chosen arbitrarily).

The routine quaternionToRotationMatrix() gets us back to rotation space with help of (6.6) to find the 4 × 4 rotation matrix corresponding to a given quaternion.

Exercise 6.23. (Programming) Extend quaternionAnimation.cpp to animate the motion of a rigid body, say a spacecraft, from a start disposition to a user-specified target disposition which can differ *both* in location and orientation from the start. Transformation should be simultaneous in both position and orientation.

The utility of quaternions in interactive animation cannot be over-emphasized and they should be in every game programmer's tool kit. For instance, try to do what quaternionAnimation.cpp does *without* using quaternions (good luck!).

6.6 Summary, Notes and More Reading

In this chapter we learned a few CG techniques which are especially important from a practical point of view. Particularly indispensable to programmers of heavily-populated environments are the methods of frustum culling and occlusion culling. For further reading, books on game programming, e.g., Lengyel [87] and Eberly [38], will, typically, contain descriptions of structures such as quadtrees, octrees, kd-trees and BSP trees in the context of frustum culling, occlusion culling and collision detection. An excellent computational geometry reference for space partitioning data structures, including range trees and kd-trees, is the one by de Berg et al. [10]. Samet [123] is a must for anyone seeking to learn about spatial data structures in depth. See Slater et al. [137] and the paper by Kumar et al. [85] for literature on the important problem of partitioning a space encompassing a dynamic scene.

We learned how to animate orientation with the use of both Euler angles and quaternions. This will come in handy in camera control and rigid body animation. The Euler angle representation, as we saw, suffers from certain problems, surmounted subsequently by the slick mathematics of quaternions. The books by Buss [21], Lengyel [87] and Watt [150], among others, contain discussions of Euler angles and quaternions and their relation to rigid-body kinematics. The ones by Hanson [65] and Kuipers [84] are all about quaternions and their applications.

Part IV

Geometry for the Home Office

CHAPTER 7

Convexity and Interpolation

It's time now to get some of the geometric concepts underlying 3D modeling and lighting in place before we reach those particular chapters. We've seen programs where colors, defined at the vertices of a primitive, are mixed and spread throughout the primitive's interior. This is done by means of interpolation. In this chapter we'll study the exact mechanics of the interpolation process.

Section 7.1 motivates the process of interpolation with simple examples. Section 7.2 gets to the heart of the matter by showing first that line segment and triangle primitives are particularly suited for interpolation because of the property they share that any point of such a primitive can be uniquely represented as a so-called convex combination of its vertices. Section 7.3 shows precisely how this property is used by OpenGL to interpolate values such as color.

The geometric property which some objects have of being convex is closely related to interpolation. Section 7.4 defines convexity and the convex hull of a set of points and applies them to understanding if objects more complicated than line segments and triangles, e.g., polygons in general, can be equally easily interpolated. We see that the answer is no and that line segments and triangles are indeed special. We conclude with Section 7.5.

This chapter and the next two on triangulation and orientation, respectively, are closely related and should be read one after another. The material is somewhat mathematical. However, the math involved is geometric, which means that it can be "seen to work", and not particularly abstract. The importance of these three chapters at the conceptual foundation of 3D computer graphics cannot be overemphasized.

Having said this, though, it's true that this particular chapter will be fairly light reading for someone already familiar with linear interpolation and convexity, possibly from an earlier math class. If this is the case, then flip quickly through the pages – make sure the parts to do with OpenGL make sense – and move on. Conversely, if you find the math in the proof of some proposition bogging you down, feel free to skip the proof just making sure you understand what the proposition is trying to say.

7.1 Motivation

OpenGL has three favorites among its several drawing primitives: points, segments (by segment we'll always mean a straight line segment) and triangles. This is not owing to some idiosyncrasy of its specification as an API, but for a deeper reason.

We've already seen that material values such as color, specified at a primitive's vertices, are apparently interpolated throughout its interior. So here, briefly, is why points, segments and triangles are favored: they have the property that every point inside each can be *unambiguously* (or, *uniquely*, same thing) represented in terms of its vertices. This makes it possible for values like color defined at the vertices to be *unambiguously* – therefore, *automatically* , by means of a program – interpolated throughout the primitive. We'll clarify all this soon, but we begin with a simple example.

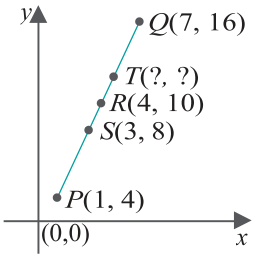

Figure 7.1: Points that split segment PQ.

Example 7.1. Using graph paper if you like, draw the segment PQ joining the point P , with coordinates (1, 4), to the point Q, with coordinates (7, 16). See Figure 7.1. Measure off the midpoint R of the segment. Verify that its coordinates are as indicated in the figure. Since the midpoint is halfway from either endpoint it does make sense that the coordinates of R are an exact average of those of P and Q, viz.,

$$\frac{1}{2} * (1,4) + \frac{1}{2} * (7,16) = \left(\frac{1}{2} * 1 + \frac{1}{2} * 7, \frac{1}{2} * 4 + \frac{1}{2} * 16\right) = (4,10)$$

How about the point S a third of the way from P to Q? Again, measure it off and see if the coordinates shown in the figure are correct. S splits PQ in the ratio $\frac{2}{3} : \frac{1}{3}$, where it's $\frac{2}{3}$ toward P from Q and $\frac{1}{3}$ toward Q from P. Ergo, S's coordinates are

$$\frac{2}{3} * (1,4) + \frac{1}{3} * (7,16) = \left(\frac{2}{3} * 1 + \frac{1}{3} * 7, \frac{2}{3} * 4 + \frac{1}{3} * 16\right) = (3,8)$$

Exercise 7.1. We ask you to calculate the coordinates of T , which is two-thirds of the way from P to Q, and verify by actual measurement.

Interestingly, P itself, which splits PQ in the ratio 1 : 0, has coordinates

$$1 * (1,4) + 0 * (7,16) = (1,4)$$

while Q, which splits PQ in the ratio 0 : 1, has coordinates

$$0 * (1,4) + 1 * (7,16) = (7,16)$$

It seems then that in the expression

$$X = c * (1,4) + (1 - c) * (7,16)$$

the variable c acts as a "dial" which can be turned from 1 to 0 to move the point X from P to Q.

Here's an exercise to get you thinking about using an expression like the last one to interpolate material properties.

Exercise 7.2. If the end vertex P of the segment in the preceding example is specified red (RGB = (1, 0, 0)) and Q green (RGB = (0, 1, 0)), then what should the colors be at the midpoint R? At the point S?

7.2 Convex Combinations

We said at the beginning of the last section that points, segments and triangles are favored by OpenGL. In fact, they are *the* building blocks of OpenGL. Even quadrilaterals and polygons in general, as we'll see, are first sub-divided into triangles before being processed. We informally described a property shared by these three primitives – that each point belonging to one has a unique expression in terms of its vertices – which makes unambiguous interpolation possible. We'll formalize this next for segments and then triangles (points as we shall see are trivial to deal with).

Segments

Proposition 7.1. *If P and Q are two points in* $\mathbb{R}^3$, *then a point V lies on the segment PQ if and only if it can be expressed as*

$$V = c_1P + c_2Q$$

where $0 \leq c_i \leq 1$, *for both* $i = 1$ *and* $i = 2$, *and where* $c_1 + c_2 = 1$.

Further, if P and Q are distinct – so that PQ does not degenerate to a point – then this expression for V is unique.

Before the proof, take a second to match the proposition with the example of the previous section: the points P, Q, R, S and T on the segment PQ could each indeed be expressed in the form $c_1P + c_2Q$, where c_1 and c_2 lie between 0 and 1, and add up to 1.

Proof. For the first part of the proposition, suppose initially that $P \quad Q$ so that PQ is a non-degenerate segment. Consider a point V on this segment. The vector $V - P$ clearly is parallel to the vector $Q - P$ (see Figure 7.2). Therefore, one is obtained from the other by multiplying by the ratio of their lengths:

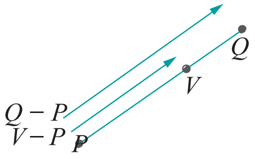

Figure 7.2: Illustration for the proof of Proposition 7.1.

$$V - P = \frac{|V - P|}{|Q - P|}(Q - P) \implies V - P = c(Q - P)$$
$$\implies V = (1 - c)P + cQ$$

where c denotes $\frac{|V-P|}{|Q-P|}$ Note then that $0 \leq c \leq 1$, as $|V - P| \leq |Q - P|$. Writing $c_1 = 1 - c$ and $c_2 = c$ we have, indeed, that

$$V = c_1P + c_2Q$$

where $0 \leq c_i \leq 1$, for both $i = 1$ and $i = 2$, and, moreover, $c_1 + c_2 = 1$. This proves the "only if" direction of the first part, provided $P /= Q$.

Conversely, for the "if" direction, assuming again $P \quad Q$, suppose that

$$V = c_1P + c_2Q$$

where $0 \leq c_i \leq 1$, for both $i = 1$ and $i = 2$, and $c_1 + c_2 = 1$. Then writing $c = c_2$ we have

$$V = (1 - c)P + cQ = P + c(Q - P) \tag{7.1}$$

V is seen to be the point at a distance of $c|Q - P|$ from P in the direction of Q. As $0 \leq c \leq 1$, V indeed lies on the segment joining P and Q. This completes the proof of the first part of the proposition when $P \quad Q$. If $P = Q$, the first part is actually trivial to prove because the segment PQ degenerates to a point (so any point on it is P itself – we leave the rest to the reader).

For the second part regarding uniqueness, suppose that the point V on PQ can be expressed as both $V = c_1P + c_2Q$ and $V = d_1P + d_2Q$, where $c_1 + d_1 = d_1 + d_2 = 1$. Then

$$V = c_1P + c_2Q = d_1P + d_2Q \implies (c_1 - d_1)P = (d_2 - c_2)Q \tag{7.2}$$

From $c_1 + c_2 = d_1 + d_2 = 1$ we have that $c_1 - d_1 = d_2 - c_2$. Therefore, if these two equal quantities are not 0 we could multiply Equation (7.2) by $\frac{1}{c_1 - d_1}$ $(= \frac{1}{d_2 - c_2})$ to deduce that $P = Q$, contradicting the hypothesis of the second part. We are led to conclude that $c_1 - d_1 = d_2 - c_2 = 0$, so that $c_1 = d_1$ and $c_2 = d_2$, proving that the expression for V in the proposition is indeed unique.

Remark 7.1. To minimize notation we wrote the endpoints of the segment in the proposition as single variables P and Q. Of course, one could write out their coordinates as, say, $P = (p_x, p_y, p_z)$ and $Q = (q_x, q_y, q_z)$ and, correspondingly, the equation for V in the statement of the proposition as

$$(v_x, v_y, v_z) = c_1(p_x, p_y, p_z) + c_2(q_x, q_y, q_z) = (c_1 p_x + c_2 q_x,\ c_1 p_y + c_2 q_y,\ c_1 p_z + c_2 q_z)$$

For example, if $P = (1, 4, 3)$ and $Q = (2, 5, 2)$, then the proposition says that points on the segment PQ are of the form

$$(c_1 + 2c_2, 4c_1 + 5c_2, 3c_1 + 2c_2), \quad \text{where } 0 \leq c_1, c_2 \leq 1 \text{ and } c_1 + c_2 = 1.$$

Remark 7.2. We assumed for the proposition that points lie in the "real world" $\mathbb{R}^3$, but the proposition holds in arbitrary dimensional space $\mathbb{R}^n$ as well, because nothing in its proof requires $n = 3$. A point $P = (p_x, p_y, p_z, \ldots)$ in $\mathbb{R}^n$ simply has n coordinates.

Remark 7.3. We could have saved ourselves a variable and written $V = cP + (1 - c)Q$, instead of $V = c_1P + c_2Q$, because $c_1 + c_2 = 1$, but chose not to in order to have separate variables for the coefficients of P and Q. This keeps our notation consistent with the proposition for triangles coming up soon.

Definition 7.1. A point V of the form

$$V = c_1P + c_2Q$$

where $0 \leq c_i \leq 1$, for both $i = 1$ and $i = 2$, and where $c_1 + c_2 = 1$, is said to be a *convex combination* – or *barycentric combination* – of P and Q. The scalars c_1 and c_2 are called the *barycentric coordinates* of V.

The following corollary then is just a rewrite of the first part of Proposition 7.1.

Corollary 7.1. *The segment joining two points P and Q in* $\mathbb{R}^3$ *consists of all their convex combinations.*

A point $V = c_1P + c_2Q$ on the segment PQ can be usefully thought of as a *weighted sum* of P and Q, where the barycentric coordinates c_1 and c_2 are the weights – or influence, or ownership, if you will – of P and Q, respectively, on the location of V. The next exercise follows up on this idea.

Exercise 7.3. Suppose that $V = c_1P + c_2Q$ lies on the segment PQ in $\mathbb{R}^3$.

(a) If $c_1 = c_2 = \frac{1}{2}$, *prove* that V is the midpoint of PQ; in other words, if the weights of P and Q on V are equal, then it's in the middle of the two. (We saw an illustration, though not proof, of this in Example 7.1.)

Suggested approach:

Without using vectors: Say $P = (p_x, p_y, p_z)$ and $Q = (q_x, q_y, q_z)$. Then

$$V = \frac{1}{2}(p_x, p_y, p_z) + \frac{1}{2}(q_x, q_y, q_z) = \left(\frac{p_x + q_x}{2}, \frac{p_x + q_x}{2}, \frac{p_x + q_x}{2}\right)$$

Determine the distance between P and V and between Q and V using the formula for distance between a pair of points, and find that the two are equal.

Note: The distance between the points (x, y, z) and (x^1, y^1, z^1) is

$(x - x^1)^2 + (y - y^1)^2 + (z - z^1)^2$.

Using vectors: $V - P = (\frac{1}{2}P + \frac{1}{2}Q) - P = \frac{1}{2}Q - \frac{1}{2}P$. Similarly, determine $Q - V$ and find that it equals $V - P$.

(b) Prove generally that $|PV| : |VQ|$ equals $c_2 : c_1$.

(c) If $c_1 > c_2$, prove that V is closer to P than Q, and vice versa.

Exercise 7.4. Say P /= Q and that $V = c_1P + c_2Q$, where c_1 and c_2 are *any* real numbers such that $c_1 + c_2 = 1$ (the condition that the c_i's must lie between 0 and 1 being dropped). Show then that V may be any point on the (infinite) straight line through P and Q.

Hint: $V = (1 - c_2)P + c_2Q = P + c_2(Q - P)$. How does this point change as c_2 varies?

Exercise 7.5. The previous exercise says that points on the whole infinite straight line through P and Q (given P Q) are of the form $c_1P + c_2Q$, where $c_1 + c_2 = 1$. We already know that points on this line *between* P and Q additionally satisfy $0 \leq c_1, c_2 \leq 1$. How about those on either side of PQ – what are the conditions on c_i? See Figure 7.3.

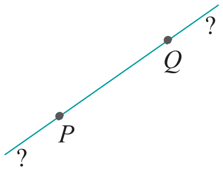

Figure 7.3: What are the conditions on c_1 and c_2 for $V = c_1P + c_2Q$ to lie on either side of PQ?

Triangles

Statements analogous to Proposition 7.1 can be proved for triangles as well:

Proposition 7.2. *If P, Q and R are three points in* $\mathbb{R}^3$, *then a point V lies on the triangle PQR if and only if it can be expressed as*

$$V = c_1P + c_2Q + c_3R$$

where $0 \leq c_i \leq 1$, *for* $1 \leq i \leq 3$, *and where* $c_1 + c_2 + c_3 = 1$.

Further, if P, Q and R are not collinear – so that PQR does not degenerate to a segment or a point – then this expression for V is unique.

Proof. For the first part of the proposition, suppose initially that the triangle PQR is non-degenerate, in other words, that P, Q and R are not collinear. Consider a point V on this triangle.

If $V = P$, then, of course, $V = 1P + 0Q + 0R$, which is an expression of the form required.

If $V = P$, suppose that the straight line from P through V intersects the edge QR at V^1 (see Figure 7.4). As V lies on the segment joining P and V^1 the previous proposition gives an expression

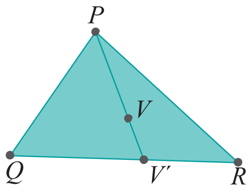

Figure 7.4: Illustration for the proof of Proposition 7.2.

$$V = c^1_1 P + c^1_2 V^1 \tag{7.3}$$

where $0 \leq c^1_i \leq 1$, for $i = 1$ and $i = 2$, and $c^1_1 + c^1_2 = 1$.

Again, by the previous proposition, since V^1 lies on the segment joining Q and R,

$$V^1 = c^{1\,1}_1 Q + c^{1\,1}_2 R \tag{7.4}$$

where $0 \leq c^{11}_i \leq 1$, for $i = 1$ and $i = 2$, and $c^{11}_1 + c^{11}_2 = 1$.

We have using both (7.3) and (7.4) that

$$\begin{aligned} V &= c^1_1 P + c^1_2(c^{1\,1}_1 Q + c^{1\,1}_2 R) \\ &= c^1_1 P + c^1_2 c^{1\,1}_1 Q + c^1_2 c^{1\,1}_2 R \end{aligned}$$

Writing $c_1 = c^1_1$, $c_2 = c^1_2 c^{1\,1}_1$ and $c_3 = c^1_2 c^{1\,1}_2$, we see that

$$V = c_1P + c_2Q + c_3R \tag{7.5}$$

where it may be checked easily that $0 \leq c_i \leq 1$, for $1 \leq i \leq 3$, and, moreover, that $c_1 + c_2 + c_3 = c^1_1 + c^1_2 c^{1\,1}_1 + c^1_2 c^{1\,1}_2 = c^1_1 + c^1_2(c^{1\,1}_1 + c^{1\,1}_2) = c^1_1 + c^1_2\ 1 = 1$. This proves the "only if" direction of the first part, provided PQR is not degenerate; we leave the proof in case PQR is degenerate (so, either it is a point or a segment) to the reader.

We leave the proof of the "if" direction and of the uniqueness of the expression in the case that PQR is non-degenerate to the reader as well.

Definition 7.2. A point V of the form

$$V = c_1P + c_2Q + c_3R$$

where $0 \le c_i \le 1$, for $1 \le i \le 3$, and where $c_1 + c_2 + c_3 = 1$, is said to be a *convex combination* – or *barycentric combination* – of P, Q and R. The scalars c_1, c_2 and c_3 are called the *barycentric coordinates* of V.

The following corollary is a rewrite of the first part of Proposition 7.2.

Corollary 7.2. *The triangle with vertices at P, Q and R in* $\mathbb{R}^3$ *consists of all their convex combinations.*

Similarly as for a segment, a point $V = c_1P + c_2Q + c_3R$ on the triangle PQR can be thought of as a weighted sum of P, Q and R, where the barycentric coordinates c_1, c_2 and c_3 are the respective weights.

Exercise 7.6. Suppose that $V = c_1P + c_2Q + c_3R$ lies on the triangle PQR. Where is V when

(a) one of the c_i's is 1 and the other two are 0?

(b) one of the c_i's is 0 and the other two equal to $\frac{1}{2}$?

(c) all the c_i's are equal to $\frac{1}{3}$?

Example 7.2. If $P = (0, 0, 0)$, $Q = (20, 0, 0)$ and $R = (20, 30, 0)$, does the point $V = (10, 20, 0)$ lie on the triangle PQR? If so, express V as a convex combination of the three vertices.

Answer: Let's try to solve the equations

$$\begin{aligned} V &= c_1P + c_2Q + c_3R \\ c_1 + c_2 + c_3 &= 1 \end{aligned}$$

The first gives

$$(10, 20, 0) = c_1(0, 0, 0) + c_2(20, 0, 0) + c_3(20, 30, 0)$$

Equating the values in each coordinate on either side of the above equation we get the following (the equation in the z coordinate contributes nothing and is not written):

$$\begin{aligned} 20c_2 + 20c_3 &= 10 \\ 30c_3 &= 20 \end{aligned}$$

With the additional

$$c_1 + c_2 + c_3 = 1$$

one solves the three equations simultaneously to find that

$$c_1 = \frac{1}{2}, \quad c_2 = -\frac{1}{6}, \quad c_3 = \frac{2}{3}$$

As the c_i's do not all lie between 0 and 1 we conclude that V is not a convex combination of P, Q and R and, therefore, does not lie on the triangle PQR.

Exercise 7.7. If $P = (0, 0, 0)$, $Q = (20, 0, 0)$ and $R = (20, 30, 0)$, does the point $V = (15, 15, 0)$ lie on the triangle PQR? If so, express V as a convex combination of the three vertices.

Exercise 7.8. What if $V = c_1P + c_2Q + c_3R$, where c_i, $1 \le i \le 3$, are *any* real numbers such that $c_1 + c_2 + c_3 = 1$ (the condition that the c_i's must lie between 0 and 1 being dropped)? Where does V lie?

Exercise 7.9. If $P = (30, 50, 45)$, $Q = (40, 20, 5)$ and $R = (30, 20, 0)$, which of the points $V = (35, 25, 20)$, $V^{1} = (35, 25, 15)$ and $V^{11} = (28, 80, 89)$ lie on the triangle PQR? Which of them lie on the plane containing P, Q and R, but not on the triangle PQR?

Exercise 7.10. In Figure 7.5, points D, E and F are midpoints of the edges PQ, QR and RP, respectively. Are points in the triangle DEF a special kind of convex combination of P, Q and R? Precisely, if $V \in DEF$ is expressed as $V = c_1P + c_2Q + c_3R$, what restrictions, if any, are there on the values that the c_i can have?

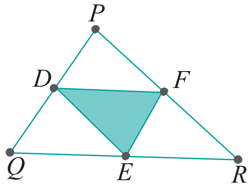

Figure 7.5: A triangle DEF with vertices at the midpoints of the edges of a larger triangle.

Exercise 7.11. So, what about points? Do we really have to find an analogue to Propositions 7.1 and 7.2 for points in R^3 or is this a non-issue?

7.3 Interpolation

It is straightforward now to explain how OpenGL interpolates property values, specified at the vertices, through the interiors its favorite primitives. Let's begin with a non-degenerate triangle $P_1P_2P_3$.

Suppose that the RGB color tuples at the vertices P_1, P_2 and P_3 are specified by the programmer to be (R_1, G_1, B_1), (R_2, G_2, B_2) and (R_3, G_3, B_3), respectively. Let V be any point of $P_1P_2P_3$. See Figure 7.6.

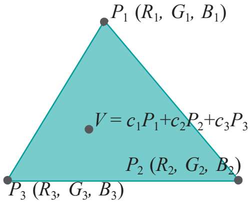

Figure 7.6: Color values specified at the vertices P_1, P_2 and P_3 of a triangle are interpolated at V.

By Proposition 7.2, there is a unique expression

$$V = c_1P_1 + c_2P_2 + c_3P_3 \qquad (7.6)$$

of V as a convex combination of the vertices P_1, P_2 and P_3. OpenGL, in fact, computes this expression, particularly, the values of c_1, c_2 and c_3. The color at V is then set to

$$\begin{aligned} & c_1(R_1, G_1, B_1) + c_2(R_2, G_2, B_2) + c_3(R_3, G_3, B_3) \qquad (7.7)\\ = \ & (c_1R_1 + c_2R_2 + c_3R_3,\ c_1G_1 + c_2G_2 + c_3G_3,\ c_1B_1 + c_2B_2 + c_3B_3) \end{aligned}$$

Simply put, OpenGL uses the weight of each vertex on the location of V as its weight on the color of V as well. As the weights c_1, c_2 and c_3 are unique, the interpolation process is *unambiguous* (and, therefore, *programmable*).

OpenGL performs an exactly similar computation to interpolate color values specified at the end vertices of a non-degenerate line segment to its interior. In the case of the third of OpenGL's favorite primitives, the point, there is obviously nothing to interpolate.

This method of interpolating color values in a CG context is called *smooth shading*, or *Gouraud shading* for its inventor Henri Gouraud – "shading" because it pertains to coloring the inside of a triangle.

Remark 7.4. From a math point of view, what we call interpolation is often (more accurately) referred to as *linear interpolation* because the interpolation parameters enter as linear variables – i.e., with power one – in the expression for the interpolated value; e.g., the c_i's in the expression for V in Equation (7.6), viz., $V = c_1P_1 + c_2P_2 + c_3P_3$.

Remark 7.5. Color values aren't the only ones to be interpolated. In fact, any attribute specified *numerically* at a triangle's vertices can be interpolated through its interior. For example, in Phong's shading model, normal vector values defined at a triangle's vertices are interpolated.

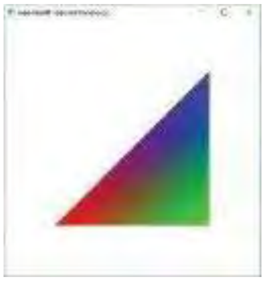

Figure 7.7: Screenshot of Experiment 7.1.

Experiment 7.1. Replace the polygon declaration part of our old favorite square.cpp with the following:

```
glBegin(GL TRIANGLES);
   glColor3f(1.0, 0.0, 0.0);
   glVertex3f(20.0, 20.0, 0.0);
   glColor3f(0.0, 1.0, 0.0);
   glVertex3f(80.0, 20.0, 0.0);
   glColor3f(0.0, 0.0, 1.0);
   glVertex3f(80.0, 80.0, 0.0);
glEnd();
```

Observe how OpenGL interpolates vertex color values throughout the triangle. Figure 7.7 is a screenshot. We'll check next if it's doing this the way described above. End

Exercise 7.12. For the triangle of Experiment 7.1 calculate the RGB colors at the point (70.0, 50.0, 0.0) inside it according to the interpolation process. Verify your answer by drawing a point with those colors at (70.0, 50.0, 0.0), the point being that you should not be able to see this point!

Exercise 7.13. Show by computation that the interpolated color value at the *centroid* (whose barycentric coordinates are all equal) of the triangle of Experiment 7.1 is a darkish gray. Again, verify your answer by drawing a point of that color at the centroid.

Exercise 7.14. If the vertices of a triangle at $P = (0, 0, 0)$, $Q = (20, 0, 0)$ and $R = (20, 30, 0)$ are colored red, cyan and magenta, respectively, what is the color at the point $(15, 15, 0)$?

Exercise 7.15. A polygon is created with the following piece of code:

```
glBegin(GL_POLYGON);
   glColor3f(1.0, 0.0, 0.0);
   glVertex3f(20.0, 20.0, 0.0); // P
   glColor3f(0.0, 1.0, 0.0);
   glVertex3f(80.0, 20.0, 0.0); // Q
   glColor3f(0.0, 0.0, 1.0);
   glVertex3f(80.0, 80.0, 0.0); // R
   glColor3f(1.0, 1.0, 0.0);
   glVertex3f(50.0, 100.0, 0.0); // S
   glColor3f(0.0, 1.0, 1.0);
   glVertex3f(20.0, 80.0, 0.0); // T
glEnd();
```

What are the RGB colors at the point (50.0, 90.0, 0.0)?
Hint : Recall that OpenGL draws a polygon after triangulating it as a triangle fan with the first vertex of the polygon, in code order, the center of the fan. And check that $(50.0, 90.0, 0.0)$ lies in the triangle *PRS*.

Remark 7.6. It's clear from the per-triangle color interpolation process that the computation involved in rendering a scene is at the least proportional to its triangle count. In animated applications, in particular, where the scene is repeatedly re-rendered, an important objective then is to minimize this count without compromising visual quality – hence, the "cost" of a model said to be its triangle count (often, somewhat inaccurately called polygon count or polycount).

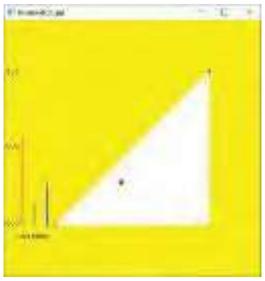

Figure 7.8: Screenshot of interpolation.cpp.

Experiment 7.2. Run interpolation.cpp, which shows the interpolated colors of a movable point inside a triangle with red, green and blue vertices. The triangle itself is drawn white. See Figure 7.8 for a screenshot.

As the arrow keys are used to move the large point, the height of each of the three vertical bars on the left indicates the weight of the respective triangle vertex on the point's location. The color of the large point itself is interpolated (by the program) from those of the vertices. End

Exercise 7.16. (**Programming**) Replace the triangle declaration of interpolation.cpp with:

```
glBegin(GL_TRIANGLES);
    glColor3f(1.0, 0.0, 0.0);
    glVertex3f(20.0, 20.0, 0.0);
    glColor3f(0.0, 1.0, 0.0);
    glVertex3f(80.0, 20.0, 0.0);
    glColor3f(0.0, 0.0, 1.0);
    glVertex3f(80.0, 80.0, 0.0);
glEnd();
```

The movable large point is no longer visible except when it pokes out of the triangle. Why?

Exercise 7.17. (**Programming**) The interpolation procedure described above requires the triangle or segment to be non-degenerate. Find out by writing code how OpenGL draws a degenerate segment or triangle.
Hint: It doesn't!

Exercise 7.18. It is easy to test a segment with vertices at $P = (x_1, y_1, z_1)$ and $Q = (x_2, y_2, z_2)$ for degeneracy: simply check if the end vertices are identical, i.e., if $x_1 = x_2$ and $y_1 = y_2$ and $z_1 = z_2$.

How about a triangle? How does one test if the triangle with vertices at $P = (x_1, y_1, z_1)$, $Q = (x_2, y_2, z_2)$ and $R = (x_3, y_3, z_3)$ is degenerate?

Hint: PQR is degenerate if and only if at least one of the two vectors $Q - P$ and $R - P$ is zero, *or*, if they are parallel. It's easy to test if one of them is zero; if not, their being parallel implies that each is a multiple of the other.

Exercise 7.19. If you know about determinants, then write a succinct condition for the degeneracy of a triangle lying on the xy-plane with vertices at $P = (x_1, y_1)$, $Q = (x_2, y_2)$ and $R = (x_3, y_3)$, using a single determinant.

Remark 7.7. A practical application of interpolation to rendering must take into account the fact that screen space is not actually a 2D continuum but, in practice, a rectangular array, called a *raster*, of finitely many pixels. Each pixel is not a point either but a square of non-zero size.

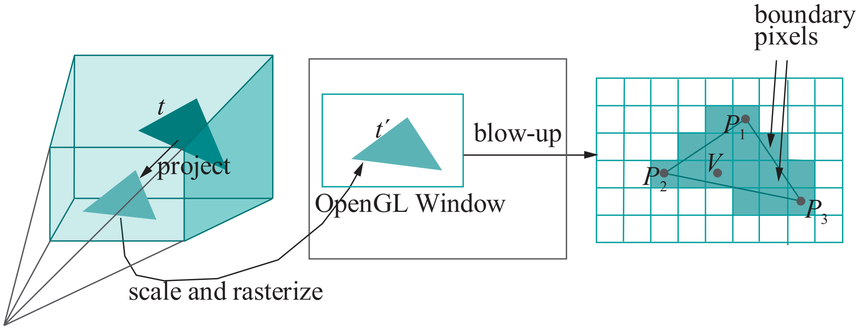

Figure 7.9: Project, scale and rasterize.

We know – see the discussion of shoot-and-print in Section 2.2 – that a primitive object, such as a triangle t, drawn in the viewing volume is projected to the volume's front and, then, scaled to its image t^1 on the OpenGL window. See the left and middle diagrams of Figure 7.9. The image t^1 is what we see and is actually *rendered* as a set of pixels – the shaded ones in the raster on the right of Figure 7.9, admittedly at a rather lousy resolution. A part of the print process, called *rasterization* or *scan conversion*, in fact, consists of choosing and coloring the pixels to render t^1.

We'll be studying rasterization algorithms in depth later on, but it's worth noting a couple of issues at this time in relation to interpolation. Since a pixel is a square that contains not one point, but infinitely many, OpenGL must pick a representative one at which to interpolate the color values from the vertices and then set the entire pixel RGB to those particular values.

For a pixel in the interior of the primitive, a valid choice is its center point, e.g., V on the right of Figure 7.9 for the pixel to which it belongs. The color of that pixel is then determined by formula (7.7), viz.,

$$c_1(R_1, G_1, B_1) + c_2(R_2, G_2, B_2) + c_3(R_3, G_3, B_3)$$

where $V = c_1P_1 + c_2P_2 + c_3P_3$, and the programmer-specified color at P_i is (R_i, G_i, B_i), for $1 \leq i \leq 3$.

Coloring boundary pixels is more complicated, as both foreground and background colors need to be taken into account. In practice, depending on if effects such as antialiasing are in force, weights may be decided by the area of the pixel occupied by the primitive and the background, respectively. For example, compare the two boundary pixels pointed at by arrows in the right of Figure 7.9: the lower one should give greater weight to the foreground color (that of the triangle) than the background, while the opposite is the case for the upper pixel.

The reader may have been wondering the following for a while now. It seems points, segments and triangles can be programmably interpolated, but how about quadrilaterals and, in general, polygons with more than three vertices? Isn't it true that points belonging to such figures have unique expressions in terms of their vertices as well, in which case they can be programmably interpolated too? In other word, can't we formulate an analogue to Proposition 7.2 for polygons with more than just the three vertices of a triangle? The answer is no, as we'll see. First, though, let's learn about convexity and the convex hull, which will lead to the answer and more.

7.4 Convexity and the Convex Hull

There's nothing about convex combinations in Definitions 7.1 and 7.2 that's specific to two or three points. They can be defined for arbitrary numbers of points:

Definition 7.3. If $F = \{P_1, P_2, \dots, P_k\}$ is a set of k points, then a point V of the form

$$V = c_1P_1 + c_2P_2 + \dots + c_kP_k$$

where $0 \leq c_i \leq 1$, for $1 \leq i \leq k$, and where $c_1 + c_2 + \dots + c_k = 1$, is said to be a *convex combination* – or *barycentric combination* – of F. The scalars c_i, $1 \leq i \leq k$, are the *barycentric coordinates* of V.

From now on, though, we'll work mostly on the plane $\mathbb{R}^2$ to keep our discussion (and figures) simple and, more importantly, because there's little need to do anything with convexity in higher dimensions in OpenGL. However, most everything we say and prove will hold in $\mathbb{R}^3$ and higher too.

Corollaries 7.1 and 7.2 tell us that the convex combinations of two points in $\mathbb{R}^2$ (actually $\mathbb{R}^3$ in the statements of the propositions but they are true on the plane $\mathbb{R}^2$ too) form the segment joining them and those of three points the triangle with corners at these points. How about an arbitrary set $F = \{P_1, P_2, \dots, P_k\}$ of points on the plane? What object is formed by its convex combinations? To answer the question we need first to define convexity.

Definition 7.4. A set S of points is said to be *convex* if, for any two points $P, Q \in S$, it is true that the segment $PQ \subset S$; in other words, if it is true that, if the endpoints of a segment are in S, then the segment itself is contained in S.

See Figure 7.10 for examples of both convex and non-convex sets on the plane. Intuitively, convexity ensures that the object has neither holes nor depressions.

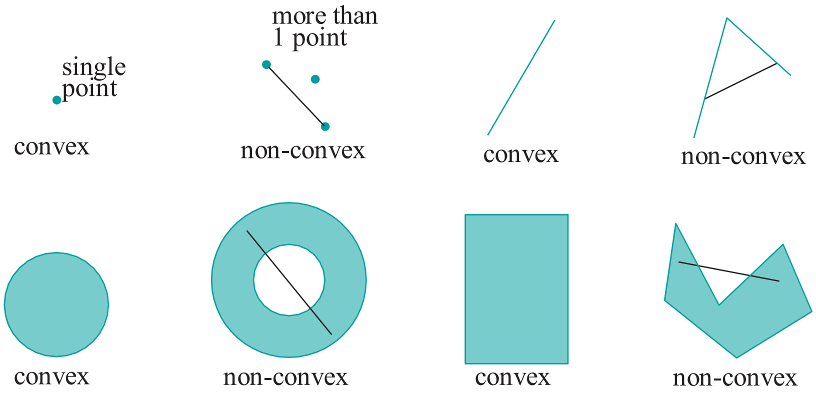

Figure 7.10: Convex and non-convex subsets of R^2 – non-convexity is indicated by an example of a black line with endpoints in the object but that itself is not contained in it.

Exercise 7.20. Prove that points, segments and triangles are always convex.

Exercise 7.21. Prove that the entire plane R^2 is itself convex. What about a *half-plane*, i.e., the part of the plane to only one side of a straight line? Assume it is a *closed* half-plane (i.e., one which includes its border straight line).

Exercise 7.22. Prove that the intersection of (any number of) convex sets is again convex. Is the union of two convex sets necessarily convex?

A polygon which happens to be a convex set is, of course, a *convex polygon*. Convex polygons are particularly important in OpenGL. As we noted even in the second chapter, a programmer should ensure that polygons he draws with GL POLYGON calls are convex; otherwise, rendering is unpredictable (we'll see why in the next chapter).

Exercise 7.23. Show that it's possible to tell if a (plane) polygon is convex by measuring the internal angle at each vertex.
Hint : Compare the two polygons at the lower right of Figure 7.10, one of which is convex and the other not.

Exercise 7.24. For the four non-convex figures shown in Figure 7.10, fill them out *minimally* to make them convex; in particular, for each, shade in on the page itself an additional area as small as possible which, together with the original, forms a convex figure.

Part answer: See Figure 7.11.

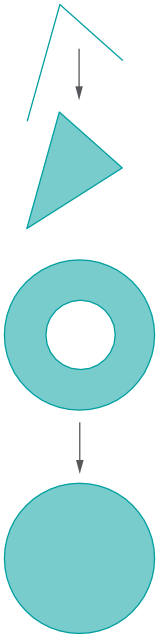

Figure 7.11: Part answer to Exercise 7.24.

The previous exercise leads to the consideration of the *smallest* possible convex set which contains a given planar set F – obtained by "filling out the holes and depressions" of F. If F is convex already then there's nothing to do as, obviously, F is the smallest convex set containing itself. But does there always exist a smallest convex set containing an arbitrary F?

Consider the collection of *all* convex sets containing a given set F. This collection includes certainly the whole plane itself and, possibly, many other sets. Now, the intersection, call it X, of this collection surely contains F as each member does. And Exercise 7.22 tells us that X is convex as well. Moreover, X is no bigger than any convex set C containing F, because C was one of the collection that was intersected to derive X in the first place. So the answer is yes, there always exists a smallest convex set containing a given planar set F: it is simply the intersection of all convex sets containing F. This leads to the definition next.

Definition 7.5. The smallest convex set containing a given set F on the plane is called its *convex hull*, denoted $ch(F)$.

Remark 7.8. Obviously, a set F is convex if and only if it is its own convex hull, i.e., if and only if $F = ch(F)$.

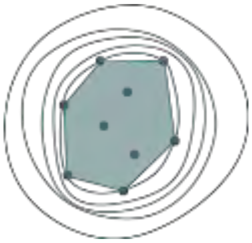

Figure 7.12: A rubber band snapping to bound the convex hull of the nails.

The intersection of infinitely many convex sets is a rather abstract notion. It's more intuitive to think of $ch(F)$ as the "limit" of a shrinking sequence of convex sets containing F. Imagine sticking a nail at each point of F (assuming for the moment that F is finite set of points). Then, stretch a rubber band around all the nails and release it. See Figure 7.12. When the rubber band becomes taut it bounds the convex hull of F. Figure 7.13 shows the convex hulls of a few small sets of points and (the rightmost) that of a segment and a point.

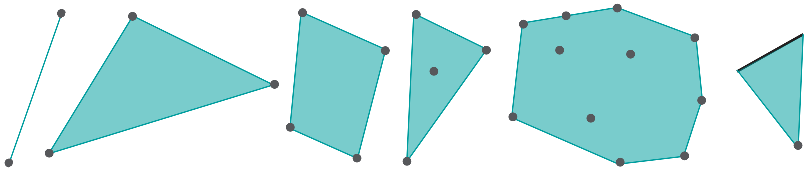

Figure 7.13: Convex hulls.

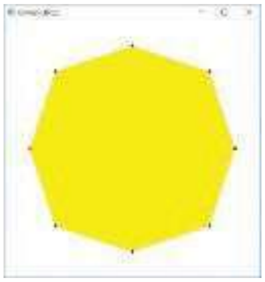

Figure 7.14: Screenshot of convexHull.cpp.

Experiment 7.3. Run convexHull.cpp, which shows the convex hull of 8 points on a plane. Use the space bar to select a point and the arrow keys to move it. Figure 7.14 is a screenshot.

Note: The program implements a very inefficient (but easily coded) algorithm to compute the convex hull of a set F as the union of all triangles with vertices in F.
End

Example 7.3. What is the convex hull of the set consisting of two opposite edges of a parallelogram? How about that consisting of two adjacent edges?

Answer: The whole (filled) parallelogram. The triangle on the two edges.

Exercise 7.25. What are the convex hulls of the figures +, × and ÷?

Exercise 7.26. Earlier, in Exercise 7.21, you showed that a closed half-plane H is convex. Can you find two straight lines S and T, not necessarily finite, such that $H = ch(S \cup T)$?

We relate next convex hulls to convex combinations.

Proposition 7.3. *Given a set $F = \{P_1, P_2, \dots, P_k\}$ of k points in* $\mathbb{R}^2$, *$ch(F)$ is exactly the set of convex combinations of F.*

Proof. We'll prove first that the set X of convex combinations of F is a convex set. As X obviously contains F, a consequence will be that $ch(F) \subseteq X$, because $ch(F)$ is the smallest convex set containing F.

Accordingly, given $V, V^1 \in X$, we have to show that the segment VV^1 lies in X. As V and V^1 are convex combinations of F, they can be written as

$$V = \sum_{i=1}^{k} c_i P_i \quad \text{and} \quad V^1 = \sum_{i=1}^{k} c_i^1 P_i$$

where $0 \le c_i, c_i^1 \le 1$, for each i, and $\sum_{i=1}^{k} c_i = \sum_{i=1}^{k} c_i^1 = 1$. A point W on the segment VV^1 is of the form

$$W = dV + d^1V^1$$

where $0 \le d, d^1 \le 1$ and $d + d^1 = 1$. Therefore,

$$W = d\sum_{i=1}^{k} c_iP_i + d^1\sum_{i=1}^{k} c_i^1P_i = \sum_{i=1}^{k}(dc_i + d^1c_i^1)P_i$$

It's easily verified that $0 \le dc_i + d^1c_i^1 \le 1$, for each i. Moreover, $\sum_{i=1}^{k}(dc_i + d^1c_i^1) = d\sum_{i=1}^{k} c_i + d^1\sum_{i=1}^{k} c_i^1 = d.1 + d^1.1 = 1$. One concludes that W is a convex combination of F as well and, therefore, belongs to X. As W was an arbitrary point of VV^1, we have proved that VV^1 indeed lies in X and, therefore, X is convex.

Next, we'll prove that any convex set Y containing F contains X as well. This will imply that $ch(F) \supset X$, which, together with the proof above that $ch(F) \subset X$, will complete the proof of the proposition.

In fact, we'll prove by induction that Y contains all convex combinations of the sets $\{P_1, P_2, \ldots, P_r\}$, for $r = 1, 2, \ldots, k$ (the case $r = k$ will, of course, prove that Y contains X). Starting the induction at $r = 1$ is trivial as the only convex combination of $\{P_1\}$ is P_1, which belongs to F and, therefore, to Y.

Suppose, inductively, that Y contains all convex combinations of the set $\{P_1, P_2, \ldots, P_r\}$, for some r, $1 \le r \le k - 1$. Let $V = \sum_{i=1}^{r+1} c_iP_i$ be a convex combination of $\{P_1, P_2, \ldots, P_r, P_{r+1}\}$. We'll prove that $V \in Y$, completing the induction. We can assume that $c_{r+1} < 1$, because, if $c_{r+1} = 1$, then $V = P_{r+1}$ which trivially belongs to Y. Now,

$$\begin{aligned} V &= \sum_{i=1}^{r} c_iP_i + c_{r+1}P_{r+1} \\ &= c(\sum_{i=1}^{r} \frac{c_i}{c}P_i) + c_{r+1}P_{r+1} \end{aligned}$$

writing $c = \sum_{i=1}^{r} c_i$, which is not 0 as $c_{r+1} < 1$.

Since $\sum_{i=1}^{r} \frac{c_i}{c} = \frac{\sum_{i=1}^{r} c_i}{c} = 1$, apply the inductive hypothesis to conclude that the point

$$V^1 = \sum_{i=1}^{r} \frac{c_i}{c}P_i$$

is in Y. Next, use the preceding expression for V^1 to rewrite the earlier equation for V as

$$V = cV^1 + c_{r+1}P_{r+1}$$

which is a convex combination of V^1 and P_{r+1}, because $c + c_{r+1} = 1$, and so lies on the segment V^1P_{r+1}. Since Y is a convex set containing both V^1 and P_{r+1}, it contains the segment V^1P_{r+1} and, therefore, V as well.

The proof of the proposition is complete.

Extreme Points

The reader, contemplating again Figure 7.13, will note that some of the points of the fourth and fifth point sets lie at the corners of their respective hulls, while others are inside or elsewhere on the boundary. Here's a definition that classifies points accordingly.

Definition 7.6. If a point P of a set F of points on the plane is such that the convex hulls of F and $F - \{P\}$(i.e., F with P deleted) are the same, then P is said to be a *non-extreme* point of F; otherwise, it is an *extreme point* of F.

Remark 7.9. Colloquially, non-extreme points are “expendable” in that the elimination of any one doesn’t affect the convex hull. However, removing an extreme point will change the hull; it will, in fact, become smaller.

So, only the three corner points of the triangle of the fourth figure and the seven of the polygon of the fifth figure of Figure 7.13 are extreme.

Exercise 7.27. What are the extreme points of a set of, say, 10 points chosen arbitrarily from a circle (i.e., from the boundary of a disc)?

Exercise 7.28. A set of, say, 10 points is chosen from the boundary of a rectangle. At most how many of these can be extreme?

Interpolation and Convexity

We’ve covered a fair amount of the theory of convexity so far. Let’s pause to take stock of how it impacts our understanding of the interpolation process. In particular, let’s return to the question posed at the end of Section 7.3 if there’s an analogue of Proposition 7.2 for polygons with more than three vertices. Let’s start at just one over with four vertices. So, we are looking for a proposition along the lines:

If P, Q, R and S are four points in $\mathbb{R}^3$, then a point V lies on the quadrilateral $PQRS$ if and only if it can be expressed as

$$V = c_1P + c_2Q + c_3R + c_4S$$

where $0 \leq c_i \leq 1$, for $1 \leq i \leq 4$, and where $c_1 + c_2 + c_3 + c_4 = 1$.

Further, if P, Q, R and S satisfy “some” conditions, then this expression for V is unique.

We run into trouble right off the bat: even the reference to “*the* quadrilateral $PQRS$” may not be legitimate! At issue is planarity as the following example illustrates.

Example 7.4. Say, a quadrilateral $q = PQRS$ is made starting from a square of side 1 unit on the xy-plane and then lifting one vertex a unit in the z-direction. Specifically, say, the vertices of q are $P = (1, 1, 0)$, $Q = (2, 1, 0)$, $R = (2, 2, 1)$ and $S = (1, 2, 0)$. So, P, Q and S lie on the xy-plane, while R is one unit above.

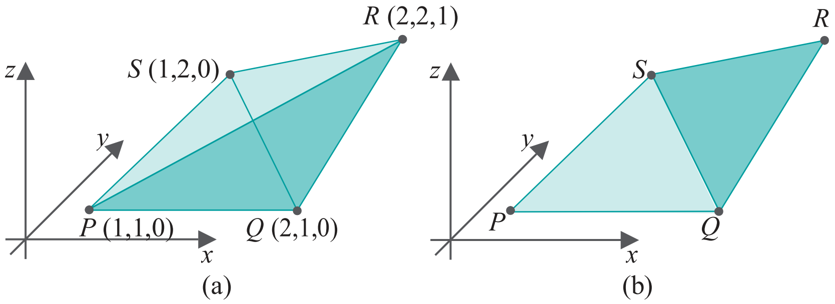

Figure 7.15: A non-planar quad q drawn in two different ways.

Now, which is q: is it the union of the two triangles PQR and PSR (Figure 7.15(a)) or is it the union of the two triangles QPS and QRS (Figure 7.15(b))? These two shapes are completely disjoint except for the shared boundary (appropriately bending a sheet of paper will convince you of this).

There is nothing special of the points chosen in the example above; in fact, they are perfectly representative of four non-coplanar points, because any three such points are always on a plane, while the fourth off it. We conclude that four points not all one plane cannot even uniquely specify a quadrilateral.

Well, if non-planarity is the enemy then let’s restrict to points all on a plane, in particular, to planar quads (after all, we did say even back in Chapter 2 that OpenGL polygons should be planar and convex). In which case, the following example is indeed to do with a quad which is both planar and convex.

Example 7.5. Consider the square $PQRS$ in Figure 7.16, obtained from the previous example by keeping R on the xy-plane. $PQRS$ is evidently planar, lying on the xy-plane, and convex. Observe now that the point V has at least two distinct expressions as a convex combination of P, Q, R and S:

(i) $V = 0.25P + 0.5Q + 0.0R + 0.25S$, obtained by computing for V as belonging to the triangle PQS (so the coefficient of R is 0).

(ii) $V = 0.5P + 0.25Q + 0.25R + 0.0S$, obtained by computing for V as belonging to the triangle PQR (so the coefficient of S is 0).

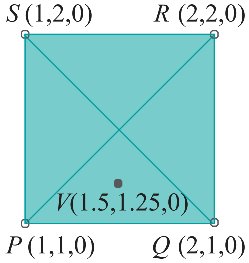

Figure 7.16: V has at least two expressions as a convex combination of P, Q, R and S.

We see, therefore, that the second part of the proposed proposition, where we seek a unique expression for V as a convex combination of P, Q, R and S, fails.

Again, the reader should easily convince herself with a few sketches that there's nothing especially devious about the square. She will see that *all* quadrilaterals on the plane – both convex *and* non-convex – contain points with non-unique expression as a convex combination of its vertices. This is very bad news from the point of view of rendering because it means that there is no unambiguous (in other word, programmable) way in which to interpolate values, such as color, which are defined at the vertices of a quad, into its interior. E.g., which set of weights would one use to interpolate at V in the preceding example: (0.25, 0.5, 0.0, 0.25) or (0.5, 0.25, 0.25, 0.0)?

And, of course, the situation doesn't improve with more than four points. We conclude that no analogue of Proposition 7.2 can be proved for polygons with more than three vertices.

So, to recount, we have the very nice Propositions 7.1 and 7.2 for segments and triangles, respectively, allowing for programmable interpolation. For points, of course, interpolation is a non-issue. Moreover, points, segments and triangles are always planar and convex. Polygons with more than three vertices might, however, be non-planar and non-convex, and, further, they never allow programmable interpolation.

It's clear then why OpenGL favors points, segments and triangles, and why, in fact, these three kinds of primitives are the building blocks for all drawing. Indeed, as we observed even in Chapter 2, OpenGL first triangulates an arbitrary polygon as a triangle fan before drawing. Moreover, polygons made using GL POLYGON have been discarded altogether from newer versions of OpenGL. We urge even readers using versions of OpenGL which allow drawing polygons to instead apply various triangle calls, including strips and fans, in order to avoid problems in case a polygon is not planar or convex.

7.5 Summary, Notes and More Reading

In this chapter we learned that points, segments and triangles are preferred by a drawing API such as OpenGL for the reason that their interiors can be unambiguously interpolated from their vertices. This led to exploring the definition of a convex combination and the notions of convexity and a convex hull.

To learn more about convexity and related algorithms the place to look is the computational geometry literature. The introductory computational geometry texts by de Berg et al. [10] and O'Rourke [110] are good starting points. The mathematical introduction to computer graphics by Buss [21] has a chapter on averaging and interpolation and an interesting discussion of convexity as well.

Taylor & Francis
Taylor & Francis Group
http://taylorandfrancis.com

Chapter 8

Triangulation

To create a 3D object in CG one assembles its surface, or a good likeness, with help of 2D primitives. For example, the seemingly 3D solid ball and torus in the screenshot Figure 8.1, seen originally in Chapter 4, are actually depicted by their respective *2D surfaces*. Note that the calls glut*Solid*Sphere() and glut*Solid*Torus() in ballAndTorusLitOrthoShadowed.cpp to draw these surfaces refer to *filled* triangles, not solid 3D objects. Boris's head in Figure 8.2 is a mesh of quads.

Figure 8.1: Screenshot of ballAndTorusLitOrthoShadowed.cpp.

Figure 8.2: Mesh of Boris's head (courtesy of Sateesh Malla at www.sateeshmalla.com).

The triangle, as we learned in the previous chapter, is the preferred of OpenGL's 2D primitives. It turns out, though, that simply cobbling together a collection of triangles which resembles the desired object may not be good enough. In order to avoid problems at the time of rendering the collection must follow certain rules. The goal of this chapter is to formulate these rules and understand their importance.

Section 8.1 begins by listing the rules that make a collection of triangles a so-called triangulation. After several examples of triangulations and non-triangulations it then explains the logic behind these rules, in particular, why they make a collection behave predictably at the time of rendering. The next section is a brief discussion of so-called Steiner vertices and how they are included to improve the quality of a triangulation. Section 8.3 explains OpenGL's own somewhat simple-minded triangulation mechanism and the consequent importance of making sure that all polygons specified in a program are convex – or, better yet, doing away with polygon calls altogether and using only triangles. Section 8.4 concludes.

This short chapter, together with its sisters Chapter 7 on convexity and interpolation and Chapter 9 on orientation, goes to the geometric core of CG.

8.1 Definition and Justification

Definition 8.1. Suppose T is a collection of triangles whose union is an object X. Then T is said to be a *triangulation* of X if, given any two different triangles t_1 and t_2 from T, exactly one of the following three is true:

1. t_1 and t_2 are disjoint, i.e., do not intersect at all.

2. t_1 and t_2 intersect in a vertex of both.

3. t_1 and t_2 intersect in an edge of both.

Informally, triangles in a triangulation are asked to intersect "nicely" or not at all. If T is a triangulation of X then X is said to be *triangulated* by T.

A collection of triangles may be such that its union is X, but without being a triangulation of X according to the preceding rules – such a collection is called an *invalid triangulation* of X.

Remark 8.1. We should probably call triangulations "valid triangulations" to make the contrast with invalid ones clear, but that would be cumbersome.

Figure 8.3(a) shows the triangulation of a non-convex polygon. In Figure 8.3(b), $\{ABC, ADC\}$ is a triangulation of the rectangle $ABCD$.

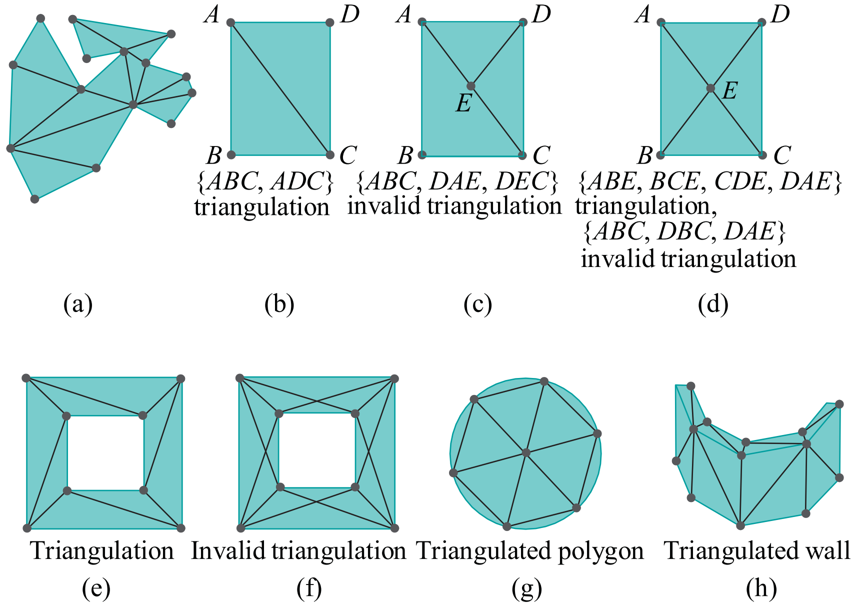

{ABC, ADC} triangulation

{ABC, DAE, DEC} invalid triangulation

{ABE, BCE, CDE, DAE} triangulation,
{ABC, DBC, DAE} invalid triangulation

(a) (b) (c) (d)

Triangulation (e)

Invalid triangulation (f)

Triangulated polygon (g)

Triangulated wall (h)

Figure 8.3: Triangulations.

In Figure 8.3(c), $\{ABC, DAE, DEC\}$ is an invalid triangulation of $ABCD$ as ABC intersects DAE in AE, which is an edge of DAE, but *not* of ABC (it is only *part* of the edge AC). Generally, if the vertex of one triangle lies on another, then it should be a vertex of the second triangle as well, or there is a violation of the triangulation rules.

In Figure 8.3(d), $\{ABE, BCE, CDE, DAE\}$ is a triangulation of $ABCD$, while $\{ABC, DBC, DAE\}$ is an invalid triangulation because ABC and DBC intersect in a triangle EBC, which, of course, is neither an edge nor vertex of either.

Figure 8.3(e) is a familiar triangulation of a square annulus, while Figure 8.3(f) is an often drawn invalid triangulation. Figure 8.3(g) is a triangulated polygon approximating a disc. The approximation may be made closer by increasing the number and decreasing the size of the sides of the boundary polygon. Likewise, the wall of Figure 8.3(h) may be made to appear smoothly curved by increasing the number of flat panels and making them narrower.

Triangulation is not a unique process and the same object may have multiple triangulations.

Exercise 8.1. Draw a different triangulation of the polygon of Figure 8.3(a). Does the number of triangles change?

Exercise 8.2. Can you give a formula for the number of triangles that any triangulation of a simple polygon with n vertices must have? Assume that there is no triangle vertex other than those from the original polygon (e.g., like Figure 8.3(a), but unlike Figure 8.3(d) where vertex E doesn't belong to the input rectangle).

Why the rules for triangulation? As long as a collection of triangles looks like the desired object why should one care if it happens to be a triangulation according to Definition 8.1 or not?

To answer this question consider the invalid triangulation $\{ABC, DBC, DAE\}$ of the rectangle in Figure 8.3(d). Say the programmer has specified color values at the vertices A-E. These are interpolated separately through the three triangles ABC, DBC and DAE. What happens though in the region EBC of overlap of the two triangles ABC and DBC? The color of EBC is determined by the one of triangles ABC and DBC which appears *later* in the code, as its color values overwrite those of the earlier one. This exact situation is implemented in the following experiment.

Experiment 8.1. Run invalidTriangulation.cpp, which implements exactly the invalid triangulation $\{ABC, DBC, DAE\}$of the rectangle in Figure 8.3(d). Colors have been arbitrarily fixed for the five vertices A-E. Press space to interchange the order that ABC and DBC appear in the code. Figure 8.4 shows the difference. End

Exercise 8.3. (Programming) Theoretically, in Figure 8.3(c) a similar ambiguity arises in the coloring of the segment AC, depending on the order of the triangles ABC, DAE and DEC in the code. Try to write code like invalidTriangulation.cpp to demonstrate this.

Interestingly, you will most likely find that the expected ambiguity does not arise in practice. The reason is that, at the time of rasterization, pixels on the edge shared between two abutting polygons are assigned uniquely to one or the other, independent of code order, by the polygon rasterizing algorithm (we'll see how in Section 14.4). Accordingly, color values of these border pixels are obtained each from its "owning" polygon and there is no ambiguity.

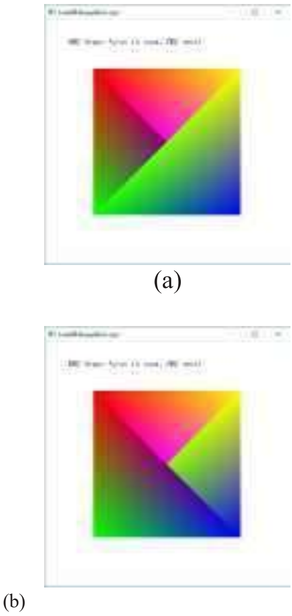

Figure 8.4: Screenshots of invalidTriangulation.cpp with two different drawing orders: (a) ABC drawn first in code, DBC next (b) DBC drawn first, ABC next.

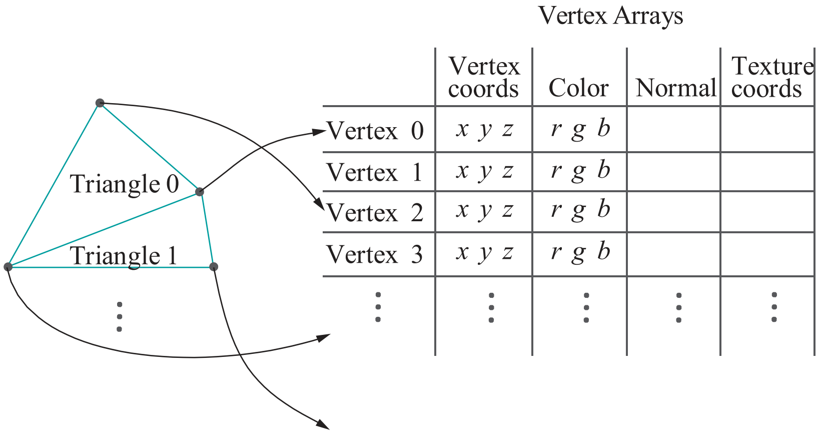

Vertex Arrays

	Vertex coords	Color	Normal	Texture coords
Vertex 0	x y z	r g b		
Vertex 1	x y z	r g b		
Vertex 2	x y z	r g b		
Vertex 3	x y z	r g b		
⋮	⋮	⋮	⋮	⋮

Figure 8.5: Logical representation of data using vertex arrays: vertex data is in one area with primitives each defined as a list of pointer to vertices (copy of Figure 3.5).

Generally, though, it is not desirable that the rendering of an object might be sensitive to the order in which the collection of triangles composing it *happens* to appear in the code. From a designer's perspective it should be enough to simply specify (a) a set of vertices with color and other data at each, and (b) a collection of triangles with corners pointing at these vertices, in other words, vertex adjacency data. Figure 3.5, copied above in Figure 8.5, depicts this ideal conceptually.

It should *not* be necessary to additionally specify a particular order on the collection of triangles. For example, in Figure 8.5, the order of the array of triangles (or, for that matter, vertices) should not matter – the relationships between the two is all the designer should need to care about. We have now the following proposition which the reader is asked next to prove.

Proposition 8.1. *If the collection of triangles composing an object satisfies the properties of a triangulation, then its image is independent of the order in which the triangles are rendered, i.e., independent of their code order.*

Exercise 8.4. Prove the proposition just stated.

Suggested approach: Let t_1 and t_2 be two triangles of a triangulation. If they don't intersect then, of course, they cannot conflict in coloring a region and code order between them does not matter at all. If they intersect in a vertex v of both, then there cannot be a conflict to be resolved by code order either, because colors are specified per-vertex so that both t_1 and t_2 want to color v identically. If they intersect in an edge, ...

8.2 Steiner Vertices and the Quality of a Triangulation

A vertex used in the triangulation of an input object which is not a vertex of the object itself is called a *Steiner vertex* . For example, E is a Steiner vertex of the triangulation $\{ABE, BCE, CDE, DAE\}$ of the rectangle $ABCD$ of Figure 8.3(d). Even though they may not be necessary per se in order to triangulate, Steiner vertices are often inserted to improve the "quality" of a triangulation.

Roughly, a good triangulation is one where there are few long and thin triangles, called *slivers*, and where most triangles are of nearly equal size and relatively small with respect to the entire object. We'll not try to formalize any further the notion of the quality of a triangulation, but here's a hypothetical situation to explain how it can impact rendering.

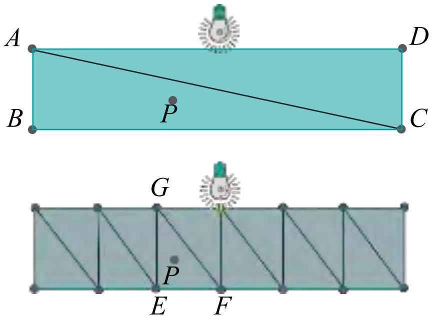

Figure 8.6: Triangulations of different quality.

Consider the long rectangular floor $ABCD$, triangulated as in the top of Figure 8.6. Located just above the middle is a lamp emitting white light – one can indeed create light sources in OpenGL, as we'll see. The vertices A, B, C and D are not particularly well-lit being distant from the lamp; say the color tuple computed at each is (0.5, 0.5, 0.5). Recalling that OpenGL interpolates the values evaluated at its vertices over the interior of a triangle, the color at *every* point of $ABCD$ turns out then to be (0.5, 0.5, 0.5), even though, realistically, a point in its interior near the middle, such as P, should appear brighter.

Unfortunately, the sliver ABC causes what should be a local brightness (or lack thereof) to propagate globally. Such a problem can often be alleviated by improving the triangulation – e.g., the lower one of Figure 8.6 which uses Steiner vertices. There, the color intensities computed at E, F and G will be greater owing to proximity to the light source, so the interpolated values at P greater too.

Exercise 8.5. Typical triangulations of a disc that come to mind are shown in Figures 8.7(a) and (b), but in either the problem with slivers becomes severe with an increasing number of edges. Can you suggest a better quality of triangulation? Maybe so that most of the disc is covered with "good" triangles and only a small area with slivers.

Exercise 8.6. Triangulate the double annulus depicted in Figure 8.7(c) using exactly one triangle strip, with the help of Steiner vertices.

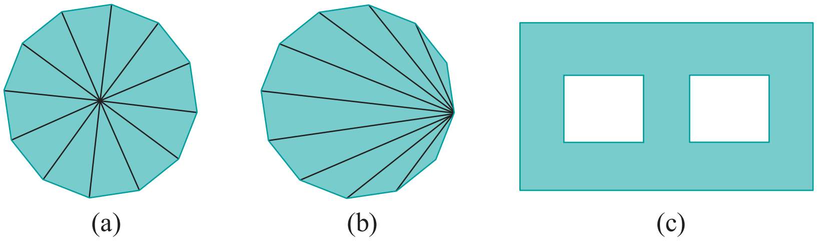

Figure 8.7: (a) and (b) Triangulations of a disc (c) Double annulus.

Exercise 8.7. Can the invalid triangulation of Figure 8.3(f) be made valid with use of Steiner vertices?

8.3 Triangulation in OpenGL and the Trouble with Non-Convexity

We'll now resolve the mystery which arose in Experiment 2.18 of Chapter 2. Here's the experiment again.

Experiment 8.2. Replace the polygon declaration of square.cpp with:

```
glBegin(GL_POLYGON);
   glVertex3f(20.0, 20.0, 0.0);
   glVertex3f(80.0, 20.0, 0.0);
   glVertex3f(40.0, 40.0, 0.0);
   glVertex3f(20.0, 80.0, 0.0);
glEnd();
```

Display it *both* filled and outlined using appropriate glPolygonMode calls. A non-convex quadrilateral is drawn in either case (Figure 8.8(a)).

Next, keeping the *same* cycle of vertices as above, list them starting with glVertex3f(80.0, 20.0, 0.0) instead:

```
glBegin(GL_POLYGON);
   glVertex3f(80.0, 20.0, 0.0);
   glVertex3f(40.0, 40.0, 0.0);
   glVertex3f(20.0, 80.0, 0.0);
   glVertex3f(20.0, 20.0, 0.0);
glEnd();
```

Make sure to display it both filled and outlined. When filled it's a triangle, while outlined it's a non-convex quadrilateral identical to the one output earlier (see Figure 8.8(b))! Because the cyclic order of the vertices is unchanged, shouldn't it be as in Figure 8.8(a) both filled and outlined? End

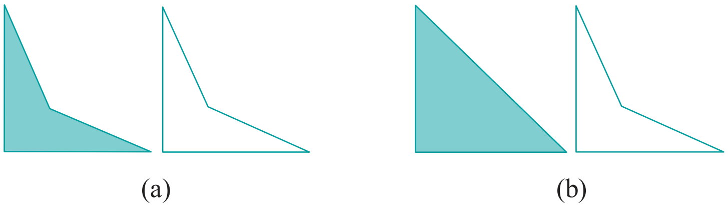

Figure 8.8: Outputs: (a) Experiment 8.2 (b) Experiment 8.2, vertices cycled.

Here is what's happening. When OpenGL is asked to draw a *filled* polygon P with n vertices $v_0, v_1, \ldots, v_{n-1}$, it renders a fan of $n-2$ triangles around the first vertex v_0, exactly as though the call was made using the primitive GL_TRIANGLE_FAN instead of GL_POLYGON; in particular, the triangles of the fan are $v_0v_1v_2$, $v_0v_2v_3$, . . ., $v_0v_{n-2}v_{n-1}$.

Now, if the polygon $P = v_0v_1 \ldots v_{n-1}$ is convex then the fan around v_0 is a triangulation of P. In fact, if P is convex then it does not matter how the cycle of vertices is listed, i.e., at which vertex it starts: the fan around the first vertex, or any vertex for that matter, is *always* a triangulation of P. For example, Figures 8.9(a) and (b) show the triangulation fans corresponding to cyclically rotated listings of the vertices of a convex pentagon.

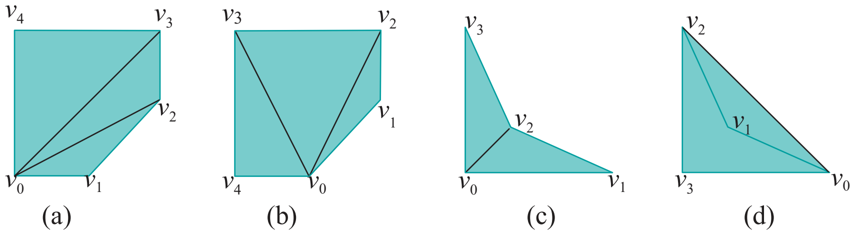

(a) (b) (c) (d)

Figure 8.9: Triangle fans.

Remark 8.2. That OpenGL seeks to triangulate the polygon before rendering is understandable given, from what we learned in Chapter 7, that it can then unambiguously interpolate property values from the vertices through the interior of individual triangles.

However, if the polygon $P = v_0v_1 \ldots v_{n-1}$ is not convex then there is no guarantee that the fan $v_0v_1v_2$, $v_0v_2v_3$, . . ., $v_0v_{n-2}v_{n-1}$ is a triangulation of P. For example, the listing $v_0v_1v_2v_3$ in Figure 8.9(c) of the vertices of the non-convex quadrilateral as in the preceding experiment does, in fact, give the fan triangulation $\{v_0v_1v_2,\ v_0v_2v_3\}$. However, the fan from the cyclically rotated listing in Figure 8.9(d) not only does not give a triangulation, it does not even give an invalid triangulation, as the union of the triangles $v_0v_1v_2$ and $v_0v_2v_3$ is $v_0v_2v_3$ itself, which is larger than the input quadrilateral $v_0v_1v_2v_3$! This explains the differing filled outputs of Experiment 8.2.

It's accordingly vital to ensure that a filled polygon specified using GL_POLYGON is convex; otherwise, rendering is unpredictable and may even be incorrect depending on the vertex listing. In fact, as we have said before: avoid polygons, using triangles instead; indeed, newer versions of OpenGL (like 4.x, which we'll be studying soon) have discarded polygons altogether.

When asked to draw a polygon in outline, OpenGL draws a line loop using the given vertex sequence, which is always valid however the vertices are listed. This explains the correctness of the outlined outputs in both cases in Experiment 8.2.

Important : As the reader may easily verify, a triangle strip specified with GL_TRIANGLE_STRIP and a triangle fan with GL_TRIANGLE_FAN are automatically valid triangulations provided they don't self-intersect, so use these constructs as much as possible.

Remark 8.3. Why doesn't OpenGL do something more than a simple-minded fan triangulation? For example, it could implement an algorithm which outputs something like the triangulation in Figure 8.3(a) of a non-convex polygon. The answer is that OpenGL's mandate is to be an efficient and portable 3D rendering API, for which reason it specifies only low-level operations and simple drawing primitives. Complex algorithms like triangulation are left to the programmer. Moreover, triangulations *should be* the programmer's call because she is the one to choose their quality.

Exercise 8.8. If v_0, v_1, v_2 and v_3 are at the corners of a rectangle on the plane, is any *triangle strip* drawn on these vertices a valid triangulation or does the order in which they are specified matter? How about if v_3 is lifted slightly above the plane?

Exercise 8.9. (Programming) Replace the polygon declaration of square.cpp with:

```
glBegin(GL_POLYGON);
   glColor3f(0.0, 0.0, 0.0);
   glVertex3f(80.0, 20.0, 0.0);
   glColor3f(1.0, 0.0, 0.0);
   glVertex3f(40.0, 40.0, 0.0);
   glColor3f(0.0, 0.0, 0.0);
   glVertex3f(20.0, 80.0, 0.0);
   glVertex3f(20.0, 20.0, 0.0);
glEnd();
```

It's actually the second listing of the polygon of Experiment 8.2 with all vertices, except the second, colored black, while the second vertex itself is colored red. The rendered figure is all black with no sign of red at all. Why?

Exercise 8.10. **(Programming)** Replace the polygon declaration of square.cpp with the following piece of code specifying a non-convex pentagon:

```
glBegin(GL_POLYGON);
   glVertex3f(50, 10, 0);
   glVertex3f(40, 50, 0);
   glVertex3f(10, 60, 0);
   glVertex3f(90, 60, 0);
   glVertex3f(60, 50, 0);
glEnd();
```

Sketch the pentagon on graph paper first and then predict the filled output each time as you rotate the vertices cyclically.

Even in the case of a convex polygon, different triangulations may lead to different renderings as the following exercise illustrates.

Exercise 8.11. **(Programming)** Replace the polygon declaration of square.cpp with the following to make a colored pentagon:

```
glBegin(GL_POLYGON);
   glColor3f(0.0, 0.0, 0.0);
   glVertex3f(20.0, 20.0, 0.0);
   glVertex3f(50.0, 20.0, 0.0);
   glVertex3f(80.0, 50.0, 0.0);
   glVertex3f(80.0, 80.0, 0.0);
   glColor3f(1.0, 0.0, 0.0);
   glVertex3f(20.0, 80.0, 0.0);
glEnd();
```

All the vertices are black except the last one listed, which is red. Next, cyclically rotate the vertices, *preserving* their colors:

```
glBegin(GL_POLYGON);
   glColor3f(0.0, 0.0, 0.0);
   glVertex3f(50.0, 20.0, 0.0);
   glVertex3f(80.0, 50.0, 0.0);
   glVertex3f(80.0, 80.0, 0.0);
   glColor3f(1.0, 0.0, 0.0);
   glVertex3f(20.0, 80.0, 0.0);
   glColor3f(0.0, 0.0, 0.0);
   glVertex3f(20.0, 20.0, 0.0);
glEnd();
```

Explain the difference in rendering. Verify your understanding by calculating the color of the point (50.0, 70.0, 0.0) in either pentagon and actually drawing a point of that color at (50.0, 70.0, 0.0) (which should then be invisible).
Hint: See Figures 8.9(a) and (b).

Exercise 8.12. A polygon with more than three vertices might be worse than non-convex – it might even be non-planar. Explain what might happen with different fan triangulations of such a "polygon", particularly using Example 7.4 of the last chapter.

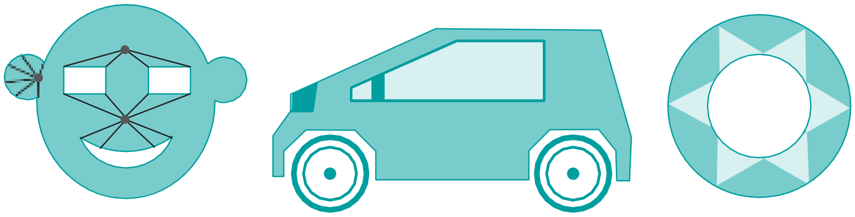

Figure 8.10: Objects to draw: the mask and annulus are flat, while the car is 3D showing only a side view.

Exercise 8.13. (Programming) Draw the objects in Figure 8.10 after first triangulating them. Allow rendering both filled and wireframe.

Make true holes for the eyes and mouth of the mask, which is a flat object. In addition to the vertices you'll need on the circular arcs in order to approximate the rounded regions, it may be useful to situate Steiner vertices in the interior of the mask as well (possible strategic locations are indicated in the figure).

Make the car simple and boxy. Keep in mind that it is 3D and depicted in Figure 8.10 is just a side view. In fact, copy code from hemisphere.cpp to rotate an object so that the car may be viewed from all angles.

For the flat decorated annulus, make sure that the triangles comprising the darkly shaded part are separate from those the lightly shaded part.

8.4 Summary, Notes and More Reading

In this chapter we learned the importance of triangulation and the potential problems arising from an invalid one. We learned as well of OpenGL's somewhat cavalier default attitude toward triangulation and the actually good reasons for it.

For more on the topic, computational geometry literature, in particular, deals extensively with theory of triangulation – and tetrahedralization, its 3D equivalent – as well as practical algorithms for both. There are practical algorithms to triangulate a simple plane polygon with n vertices in $O(n \log n)$ time. You will find them described in de Berg et al. [10] and O'Rourke [110], both good introductions to computational geometry in general. The CGAL [27] library is a marvelous source of ready-to-use algorithms for various geometric applications, including triangulation.

Mesh generation, as triangulation is often called, is obviously key to object creation in computer graphics. We'll be seeing much more of this process as we go along and Chapter 10 on design is mostly devoted to the topic.

An advanced text on mesh generation is by Edelsbrunner [41]. The proceedings of the annual Meshing Roundtable Conference organized by Sandia National Laboratories [76] is a source for the latest developments in the field.

CHAPTER 9

Orientation

The notion of orientation is vitally important in CG when drawing 3D scenes but, unfortunately, often confusing for the beginner. OpenGL itself makes critical use of orientation to determine the visible side of a surface. Note that the word "orientation" in the current context relates to handedness, e.g., clockwise or counter-clockwise, as we shall see, and has nothing to do with the orientation of a camera as discussed in Section 4.6.3, where the word meant pose or arrangement. The goal for this chapter is an understanding of orientation and its utility in CG.

The first section motivates the concept of orientation with a benign thought experiment. Section 9.2 describes how OpenGL applies orientation to determine the particular side of a 2D primitive which the viewer sees and then renders it with that side's specified material properties. If an object is specified as a collection of triangles, as in a triangulation, the question then arises of consistently orienting the collection. This is the topic of Section 9.3. Section 9.4 describes how OpenGL can make use of orientation to improve the efficiency of its rendering pipeline by culling certain triangles belonging to a closed surface, a procedure called back-face culling. In Section 9.5 we see how geometric transformations affect the perceived orientation of a primitive. We conclude in Section 9.6.

Although the three are conceptual in nature without a lot of excitement by way of programming, this chapter and the two preceding ones form a good part of the geometric core of CG.

9.1 Motivation

A thought experiment:

You and your friend, environmentally-conscious types both, are headed separately toward a meeting of the Tree Huggers' Union. The meeting is out in the open in a field with, well, lots of trees and no other landmarks. There is, though, a triangle of long helium-filled balloons with the letters T, H and U at the corners floating high above the meeting site. See Figure 9.1 (ignore superman with a spray can and the sheet in the middle for now).

Now, you want to meet up with your friend before running into the crowd. So while walking you call him on his cell phone to try to figure out how he is currently situated with respect to you. How do you do this?

As both can see the balloons, a start is to determine if you are on the same side or not. Unfortunately, the letters at the corners (carefully chosen, of course) are of no help as they each look the same from either side.

What you can do, though, is ask your friend, "Does the vertex sequence THU – that's T→H→U – appear CW (clockwise) or CCW (counter-clockwise) from where

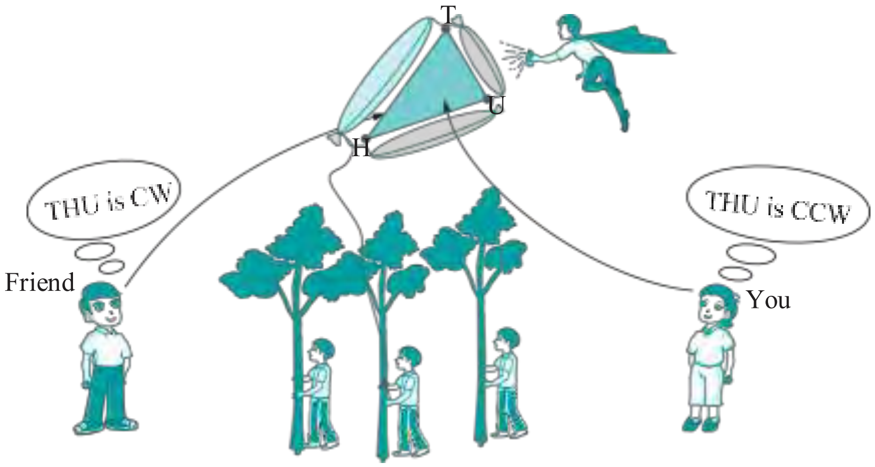

Figure 9.1: Meeting of the Tree Huggers' Union.

you are?" If the orientation appears the same for both, then you are on the same side of the balloons; if not, you are on opposite sides.

OpenGL, as well, must determine for each triangle if the viewer currently sees one side or the other. And, as we'll see, it does so in an exactly similar manner. We'll understand as well the reason for this (seemingly) roundabout method.

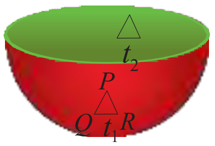

Figure 9.2: A bowl of two colors.

Why does OpenGL need to distinguish sides in the first place? Because they may have properties (e.g., outlined/filled, color, etc.) specified differently by the programmer and OpenGL is obliged to display accordingly. For example, if the inside of a triangulated bowl is green and the outside red, then the two sides of every triangle composing it are colored differently as well. Given a viewpoint, OpenGL must determine the visible side of each triangle and render it with the appropriate color. See Figure 9.2. From the current (reader's) viewpoint the red side of triangle t_1 and the green side of triangle t_2 are visible. If the viewpoint travels 180° around the bowl, then the visible side is reversed for both.

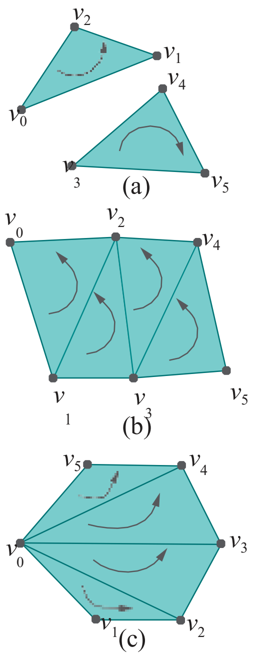

Figure 9.3: Ordered triangles and triangle strip.

9.2 OpenGL Procedure to Determine Front and Back Faces

Here then is the procedure that OpenGL follows.

(1) First, it obtains the vertex orders of each 2D primitive *from the code*. For example, the declaration

```
glBegin(GL TRIANGLES);
   v0; v1; v2; v3; v4; v5;
glEnd();
```

specifies the order of the vertices of the first triangle as v0, v1, v2 and that of the second as v3, v4, v5 (these orders, in fact, are part of the GL TRIANGLES definition; see Section 2.6). See Figure 9.3(a). For other examples, the declaration

```
glBegin(GL TRIANGLE STRIP);
   v0; v1; v2; v3; v4; v5;
glEnd();
```

specifies the vertex orders of the four successive triangles in the strip as v0, v1, v2 and v1, v3, v2 and v2, v3, v4 and v3, v5, v4 (Figure 9.3(b)) and

```
glBegin(GL_POLYGON);
   v0; v1; v2; v3; v4; v5;
glEnd();
```

specifies v0, v1, v2 and v0, v2, v3 and v0, v3, v4 and v0, v4, v5 (Figure 9.3(c)). And, similarly, each 2D primitive imposes an order on the vertices of its component triangles.

(2) Second, OpenGL determines for each component triangle if the order of its vertices as determined in Step (1) is *perceived* as CW or CCW by the viewer. This is said to be the *orientation* of the triangle with respect to the viewer.

OpenGL can make this determination because it knows both the location of the viewer – at the origin in case of perspective projection and at some point on the viewing face (it doesn't matter which) in case of orthographic projection – and those of the triangle's vertices. For example, in Figure 9.4, if the vertex order of the triangle is P, Q, R, then it is perceived as CCW by the viewer. We'll see later in this section an algorithm to output its orientation given an ordered input triangle.

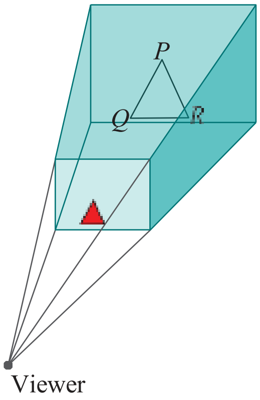

Figure 9.4: PQR is oriented CCW to the viewer, so it's rendered (as the red triangle on the viewing face) according to properties for its front face.

(3) Finally, those triangles whose orientation the viewer perceives as CCW are presumed to be *front-facing* , i.e., the viewer is presumed by OpenGL to see their front faces, while those whose orientation is perceived as CW are *back-facing* . This is actually the default, which can be flipped with a glFrontFace(GL_CW) call. Front-facing triangles then are rendered with properties specified for their front faces, and back-facing ones with those for their back faces.

For example, if the vertex order of triangle t_1 in Figure 9.2 happens to be P, Q, R and the viewer is the reader, then OpenGL determines that this triangle is oriented CCW with respect to the viewer, who sees, therefore, the front face. Accordingly, t_1 is rendered red, assuming that the code indeed specifies that front-facing triangles are red. In Figure 9.4 we show the red rendering on the viewing face itself, pretending that it is the OpenGL window.

The reader may wonder at this point why one needs to invoke a *particular* viewpoint to distinguish sides. In real life the inside of the bowl (which is *absolute* and does not depend on the location of any viewer) is painted green and the outside (absolute as well) red. Subsequently, what a viewer sees is determined simply by the laws of nature, in particular, how light from the bowl travels to her eyes.

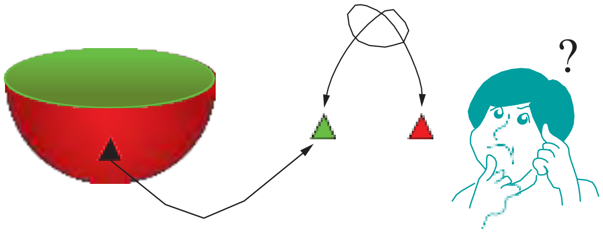

Figure 9.5: Was the inside of the bowl red or green?

Why doesn't OpenGL try and simulate this phenomenon? The answer is that, yes, it is true that the inside and outside of the bowl are absolute irrespective of the viewer, but *only after the entire bowl has been created* ! If one breaks off a tiny piece of the bowl – a tiny nearly flat triangle, if you will – and shows it to someone who has never seen the whole, then it is not possible for that person to decide which side of the piece originally lay on the bowl's inside and which the outside (Figure 9.5). OpenGL has no global notion of objects either as it simply draws them triangle by triangle, and, therefore, requires direction from the programmer as to which side of each triangle is which.

The three-step procedure described above provides exactly a mechanism for such direction to OpenGL. Let's return to the thought experiment at the start of the section and assume that there is a giant triangular sheet of paper attached to the balloons (as in Figure 9.1) which you know is colored differently on either side. Then, of course, you could ask your friend, "What color do you see up there?" instead of "Does the vertex sequence THU appear CW or CCW from where you are?" The point is that the two questions are exactly equivalent in that those who perceive a particular orientation see a particular side and vice versa.

Continuing with this line of thought, suppose as you are walking that you notice a man high up about to spray-paint the sides of the triangular paper and he has a cell phone which you can call. You could then either ask him to arbitrarily paint one side green and the other red, which would at least serve the purpose of locating your friend, or you could ask him to paint *your* side red and the *other* side green, which is equivalent to you (the programmer) dictating that "CCW-seers" see red and "CW-seers" green.

There are three points worth emphasizing:

(a) A real-life 2D object (like a piece of paper) actually has two physical sides regardless of which an observer sees. This is not true of OpenGL, whose objects are all, of course, virtual. An OpenGL 2D primitive such as a triangle consists simply of data, e.g., vertex coordinates, color values, etc., residing inside the computer.

When asked to draw, OpenGL determines *if* the viewer is *supposed* to see the front or the back face according to the procedure described earlier and then *renders* the primitive with properties specified for that face.

(b) The terms "front-facing" and "back-facing" are simply used to indicate one side and the other. There is no *intrinsic* front or back of an OpenGL triangle or other virtual 2D primitive. If we didn't use these terms, we would have to say things like "the side which the viewer sees when the order v0v1v2 appears clockwise from the origin".

(c) OpenGL draws primitives *individually*. It has no global understanding of objects formed by these primitives *together*.

Exercise 9.1. If a triangle t is specified by

glBegin(GL_TRIANGLES); v_0; v_1; v_2; glEnd();

where the vertices are as below, in each case determine which side of t, front or back, a viewer at the origin sees, assuming the default of glFrontFace(GL_CCW):

(a) $v_0 = (1, 0, 0)$, $v_1 = (0, 1, 0)$, $v_2 = (0, 0, 1)$

Answer:

The back face because $v_0v_1v_2$ appears CW from O. See Figure 9.6.

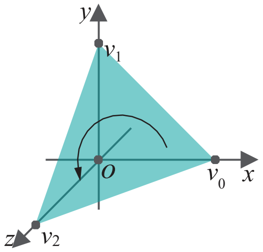

Figure 9.6: $v_0v_1v_2$ appears CW from O.

(b) $v_0 = (0, 1, 0)$, $v_1 = (1, 0, 0)$, $v_2 = (0, 0, 1)$

(c) $v_0 = (-1, 0, 0)$, $v_1 = (0, -1, 0)$, $v_2 = (0, 0, -1)$

(d) $v_0 = (1, 1, 1)$, $v_1 = (1, 1, -2)$, $v_2 = (-1, 1, -2)$

Exercise 9.2. A tacit assumption in all of the preceding discussion is that a viewer at a particular location sees, in fact, *only one* side – front or back – of a 2D primitive. For example, if a viewer could see both sides of a triangle, then is it front or back facing (or both)? So, is the assumption that only one side is visible a valid one? *Hint*: A triangle is always *flat* (planar), while a polygon should be specified to be so.

Definition 9.1. Two orders of the vertices of a polygon are said to be *equivalent* if one can be *cyclically rotated* into the other.

It follows that the sequence of vertices around any given polygon can be written in exactly *two* inequivalent orders. For example, the sequence of vertices around the quadrilateral q of Figure 9.7 can be written in eight different ways:

$$\begin{array}{cccc} v_0v_1v_2v_3 & v_1v_2v_3v_0 & v_2v_3v_0v_1 & v_3v_0v_1v_2 \\ v_0v_3v_2v_1 & v_3v_2v_1v_0 & v_2v_1v_0v_3 & v_1v_0v_3v_2 \end{array}$$

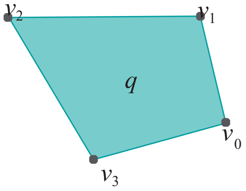

Figure 9.7: A quadrilateral.

The orders on the top line are all equivalent to each other, while those on the second all to each other as well, and none on the first equivalent to any on the second. The notion of equivalence is important precisely because of the fact that a viewer on one side of a polygon perceives equivalent orders of vertices as either all CW or all CCW.

Experiment 9.1. Replace the polygon declaration part of square.cpp of Chapter 2 with:

```
glPolygonMode(GL_FRONT, GL_LINE);
glPolygonMode(GL_BACK, GL_FILL);
glBegin(GL_POLYGON);
   glVertex3f(20.0, 20.0, 0.0);
   glVertex3f(80.0, 20.0, 0.0);
   glVertex3f(80.0, 80.0, 0.0);
   glVertex3f(20.0, 80.0, 0.0);
glEnd();
```

This simply adds the two glPolygonMode() statements to the original square.cpp. In particular, they specify that front-facing polygons are to be drawn in outline and back-facing ones filled. Now, the order of the vertices is (20.0, 20.0, 0.0), (80.0, 20.0, 0.0), (80.0, 80.0, 0.0), (20.0, 80.0, 0.0), which appears CCW from the viewing face. Therefore, the square is drawn in outline (Figure 9.8).

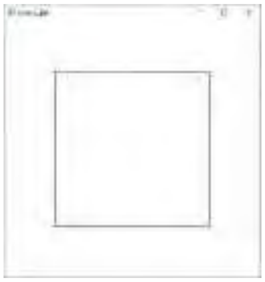

Figure 9.8: Screenshot of first part of Experiment 9.1.

Next, rotate the vertices cyclically so that the declaration becomes:

```
glPolygonMode(GL_FRONT, GL_LINE);
glPolygonMode(GL_BACK, GL_FILL);
glBegin(GL_POLYGON);
   glVertex3f(20.0, 80.0, 0.0);
   glVertex3f(20.0, 20.0, 0.0);
   glVertex3f(80.0, 20.0, 0.0);
   glVertex3f(80.0, 80.0, 0.0);
glEnd();
```

As the vertex order remains equivalent to the previous one, the square is still outlined.

Reverse the vertex listing next:

```
glPolygonMode(GL_FRONT, GL_LINE);
glPolygonMode(GL_BACK, GL_FILL);
glBegin(GL_POLYGON);
   glVertex3f(80.0, 80.0, 0.0);
   glVertex3f(80.0, 20.0, 0.0);
   glVertex3f(20.0, 20.0, 0.0);
   glVertex3f(20.0, 80.0, 0.0);
glEnd();
```

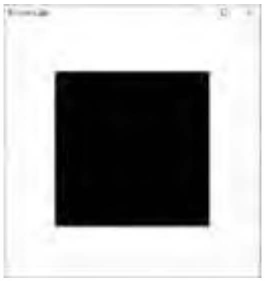

Figure 9.9: Screenshot of third part of Experiment 9.1.

The square is drawn filled as the vertex order now appears CW from the front of the viewing box (Figure 9.9). End

Exercise 9.3. (Programming) Continuing with the preceding experiment (after the last part) add the following statements just before the polygon declaration.

```
glTranslatef(50.0, 0.0, 0.0);
glRotatef(180.0, 0.0, 1.0, 0.0);
glTranslatef(-50.0, 0.0, 0.0);
```

Explain what you observe (Figure 9.8).

Exercise 9.4. (Programming) If the polygon declaration part of square.cpp is replaced with the following piece of code, then is an outlined or filled triangle seen? Try to answer first without running the program.

```
glFrontFace(GL_CW);
glPolygonMode(GL_FRONT, GL_LINE);
glPolygonMode(GL_BACK, GL_FILL);
glBegin(GL_TRIANGLES);
   glVertex3f(80.0, 10.0, -1.0);
   glVertex3f(90.0, 75.0, 1.0);
   glVertex3f(15.0, 10.0, 0.5);
glEnd();
```

Remark 9.1. Before we get to Chapter 11 and learn about material properties and how to color the sides of an object differently, we'll have to do with distinguishing them by the distinctly unglamorous means of drawing one in outline and the other filled.

Algorithm to Decide the Orientation Perceived by a Viewer

An algorithmic question, that we did not address then, arose earlier in this section in Step (2) of OpenGL's procedure to determine the side of a primitive a viewer sees: given a viewpoint and a primitive with its vertices ordered, how to decide if the given order appears CW or CCW? We invite the reader to answer this for herself in the following exercise, with a fair amount of input from our end.

Exercise 9.5. Assume that the viewpoint is at the origin O and that the vertices of a triangle are $P = (x_1, y_1, z_1)$, $Q = (x_2, y_2 z_2)$ and $R = (x_3, y_3, z_3)$. See Figure 9.10. Determine if the viewer at O perceives the order PQR as CCW or CW.

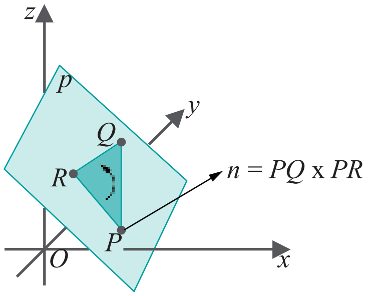

Figure 9.10: The plane p contains the triangle PQR: the orientation of PQR depends on which side of p the viewer is located.

If you don't do the exercise do at least read the conclusion below in terms of the determinant D.

Suggested approach: Supposing, first, that P, Q and R are not collinear, i.e., PQR is a non-degenerate triangle, determine the equation $ax + by + cz + d = 0$ of the unique plane p containing P, Q and R.

A point (x, y, z) lies on p if $ax+by+cz+d = 0$. A point lies in one (open) half-space of p, i.e., on one side of p, or the other, depending on whether $ax + by + cz + d < 0$ or $ax + by + cz + d > 0$.

Observe, next, that a viewer located *on* p sees triangle PQR "edge-on", in other words, as a line and not a triangle, so the question of orientation does not arise. A viewer not on p, on the other hand, perceives the orientation of PQR depending on the half-space she is in: particularly, all viewers inside one half-space perceive CCW, while those in the other CW.

Therefore, the perception at viewpoint O, in particular, depends on whether O lies on p or, if not, on which side.

Finally, conclude the following:
Let D be the determinant

$$\begin{matrix} x_1 & x_2 & x_3 \\ y_1 & y_2 & y_3 \\ z_1 & z_2 & z_3 \end{matrix}$$

1. If $D = 0$, then either (a) P , Q and R are collinear, in which case PQR is a degenerate triangle and the question of an orientation of PQR does not arise, or (b) O lies on the plane p containing P , Q and R, so that the viewer at O sees triangle PQR edge-on and, again, the question of orientation does not arise.

2. If $D > 0$, then the viewer at O perceives the order PQR as CW.

3. If $D < 0$, then the viewer at O perceives the order PQR as CCW.

Another approach is with the use of cross-products, by observing that $n = PQ \times PR$ is normal to the plane p and, in fact, points to the half-space where observers perceive PQR as CCW. Therefore, if the eye direction vector PO makes an angle of less than 90° with n – placing it in the same half-space as n – then the viewer at O perceives the order PQR as CCW as well; if greater, then as CW (in the configuration depicted in the figure the angle is, in fact, greater than 90°). Whether the angle between the two vectors n and PO is greater or less than 90° can be decided from the sign of the dot product $n \cdot PO$.

Exercise 9.6. Does a viewer at the origin perceive the order PQR of the points $P = (-1, 2, 0)$, $Q = (3, 2, 2)$ and $R = (-3, -8, 6)$ as CW or CCW?

Exercise 9.7. Does a viewer at the point $O^1 = (1, 3, 2)$ perceive the order PQR of the points $P = (3, 7, 5)$, $Q = (4, 1, 2)$ and $R = (0, 1, 2)$ as CW or CCW?

Exercise 9.8. Relate Lemma 5.1 to the answer to Exercise 9.5.

9.3 Consistently Oriented Triangulation

The notion of orientation gets even more interesting when one considers a collection of triangles, as in a triangulation. The issue arises then of *consistency* . We have the following definition:

Definition 9.2. Suppose an order is given of the vertices of each triangle belonging to some triangulation T of an object X. iTs said to be *consistently oriented* if any two triangles ofTwhich share an edge order that edge oppositely; otherwiseT, is *inconsistently oriented*.

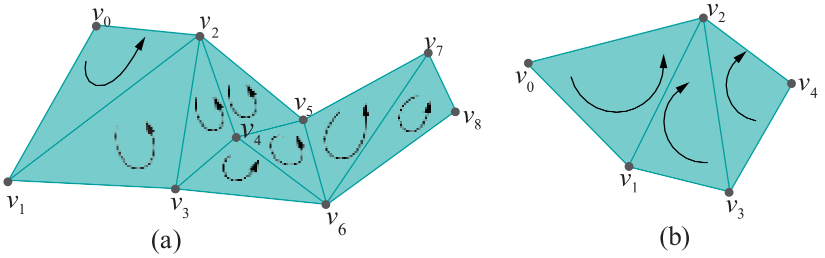

Figure 9.11: (a) Consistently oriented triangulation (b) Inconsistently oriented triangulation.

Figure 9.11(a) shows a consistently oriented triangulation. For example, the edge shared by the two triangles $v_0v_1v_2$ and $v_1v_3v_2$ is ordered v_1v_2 by the first and v_2v_1

by the second. The triangulation of Figure 9.11(b) is not consistently oriented as the edge shared by the two leftmost triangles is ordered v_1v_2 by both.

Intuitively, triangles in a consistently oriented triangulation of X appear oriented either all CW or all CCW "looking at one side of X". What exactly does this mean?

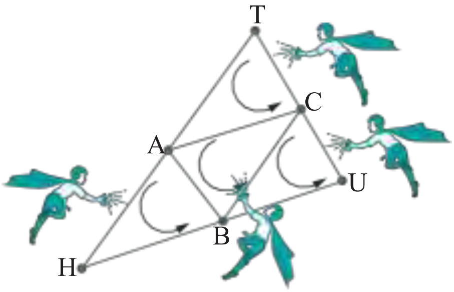

Figure 9.12: OpenGL spray-painting bots.

Let's return again to the earlier thought experiment at the point when you were about to call the painter. Looking up again you make out that the large triangular sheet is actually composed of four smaller ones and that there's a painter for each, so you'll have to call them separately (Figure 9.12). Moreover, all that you are allowed to specify to each is the order of his triangle's vertices – e.g., you can specify to the painter at the top his vertex order as either C → A → T or T → A → C – for these painters are nothing but OpenGL bots that have been programmed to do the following:

Determine if you perceive the order that you just called in as CCW or CW; if CCW then paint your side red, if not green.

Clearly, the onus then is on you to call in the four orders so that the small triangles are consistently oriented or else your side of the large triangle will be colored disparately.

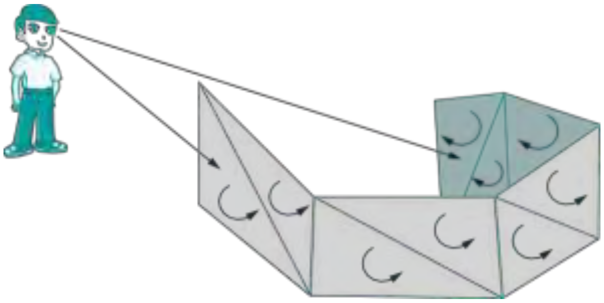

Figure 9.13: Man looking at both sides of a consistently oriented wall.

Are we saying that an observer at a given position can see only one side of a consistently oriented surface? Not at all. For example, the man in Figure 9.13 can see parts of both sides of the consistently oriented triangulated wall. However, he sees a change in side, according to the CW/CCW rule, only across boundary edges, never across an internal edge – which is physically authentic. If the wall were not consistently oriented, though, then this would not be the case. For example, the reader using the CW/CCW rule would believe herself to be seeing two different sides of the polygon of Figure 9.11(b) along the edge v_1v_2.

Recall again the bowl of Figure 9.2 with its inside green and outside red. If it's created in OpenGL as a triangulation, the programmer should then (a) specify that all front faces are of one color and back faces of the other, *and* (b) ensure consistent orientation of the triangulation so that the entire inside and entire outside appear of the desired colors, respectively.

In fact, the preceding rule should apply to all surfaces that we create. Here's what can happen if it doesn't.

Experiment 9.2. Replace the polygon declaration part of square.cpp with:

```
glPolygonMode(GL_FRONT, GL_LINE);
glPolygonMode(GL_BACK, GL_FILL);
glBegin(GL_TRIANGLES);
    // CCW
    glVertex3f(20.0,  80.0,  0.0);
    glVertex3f(20.0,  20.0,  0.0);
    glVertex3f(50.0,  80.0,  0.0);

    //CCW
    glVertex3f(50.0,   80.0,  0.0);
    glVertex3f(20.0,  20.0,  0.0);
    glVertex3f(50.0,  20.0,  0.0);

    // CW
    glVertex3f(50.0,   20.0,  0.0);
    glVertex3f(50.0,  80.0,  0.0);
    glVertex3f(80.0,  80.0,  0.0);

    // CCW
    glVertex3f(80.0,   80.0,  0.0);
    glVertex3f(50.0,  20.0,  0.0);
    glVertex3f(80.0,  20.0,  0.0);
glEnd();
```

The specification is for front faces to be outlined and back faces filled, but, as the four triangles are not consistently oriented, we see both outlined and filled triangles (Figure 9.14(a)). End

Experiment 9.3. Continuing the previous experiment, next replace the polygon declaration part of square.cpp with:

```
glPolygonMode(GL_FRONT, GL_LINE);
glPolygonMode(GL_BACK, GL_FILL);
glBegin(GL_TRIANGLE_STRIP);
    glVertex3f(20.0, 80.0, 0.0);
    glVertex3f(20.0, 20.0, 0.0);
    glVertex3f(50.0, 80.0, 0.0);
    glVertex3f(50.0, 20.0, 0.0);
    glVertex3f(80.0, 80.0, 0.0);
    glVertex3f(80.0, 20.0, 0.0);
glEnd();
```

The resulting triangulation is the same as before, but, as it's consistently oriented, we see only outlined front faces (Figure 9.14(b)). End

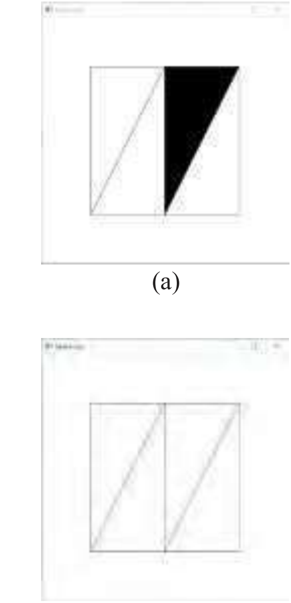
(a)

(b)

Figure 9.14: Screenshots for (a) Experiment 9.2 and (b) Experiment 9.3.

In the next experiment we see an example of a consistently oriented object, both sides of which are visible.

Experiment 9.4. Run squareOfWalls.cpp, which shows four rectangular walls enclosing a square space. The front faces (the outside of the walls) are filled, while the back faces (the inside) are outlined. Figure 9.15(a) is a screenshot.

The triangle strip of squareOfWalls.cpp consists of eight triangles which are consistently oriented, because triangles in a strip are *always* consistently oriented. End

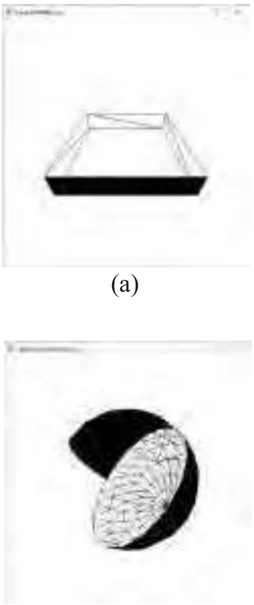

(a)

(b)

Figure 9.15: Screenshots of (a) squareOfWalls.cpp (b) threeQuarterSphere.cpp.

Experiment 9.5. Run threeQuarterSphere.cpp, which adds one half of a hemisphere to the bottom of the hemisphere of hemisphere.cpp. The two polygon mode calls ask the front faces to be drawn filled and back ones outlined. Turn the object about the axes by pressing 'x', 'X', 'y', 'Y', 'z' and 'Z'.

Unfortunately, the ordering of the vertices is such that the outside of the hemisphere appears filled, while that of the half-hemisphere outlined. Figure 9.15(b) is a screenshot. Likely, this would not be intended in a real design application where one would, typically, expect a consistent look throughout one side.

Such mixing up of orientation is not an uncommon error when assembling an object out of multiple pieces. Fix the problem in the case of threeQuarterSphere.cpp in four different ways:

(a) Replace the loop statement

```
for(i = 0; i <= p/2; i++)
```

of the half-hemisphere with

```
for(i = p/2; i >= 0; i--)
```

to reverse its orientation.

(b) Interchange the two glVertex3f() statements of the half-hemisphere, again reversing its orientation.

(c) Place the additional polygon mode calls

```
glPolygonMode(GL_FRONT, GL_LINE);
glPolygonMode(GL_BACK, GL_FILL);
```

before the half-hemisphere so that its back faces are drawn filled.

(d) Call

```
glFrontFace(GL_CCW)
```

before the hemisphere definition and

```
glFrontFace(GL_CW)
```

before the half-hemisphere to change the front-face default to be CW-facing for the latter.

Of the four, either (a) or (b) is to be preferred because they go to the source of the problem and repair the object, rather than hide it with the help of state variables, as do (c) and (d). End

It is not hard to orient consistently when creating objects in OpenGL because the primitives themselves tend to help. Verify from the definition of the drawing primitives in Section 2.6 that the set of triangles created by a call to GL_TRIANGLE_STRIP or GL_TRIANGLE_FAN is, in fact, consistently oriented. Therefore, a GL_TRIANGLE_STRIP or a GL_TRIANGLE_FAN call guarantees consistent orientation, at least for that particular set of triangles, so it's a good idea to use as many such as possible.

Non-Orientable Surfaces

Before concluding this section, mention must be made of non-orientability. There do exist surfaces which can be triangulated but *never* consistently oriented. The most famous two, the Möbius band and Klein bottle, are depicted in Figure 9.16. Such surfaces are said to be *non-orientable*. Surfaces for which consistently oriented triangulations do exist are *orientable*.

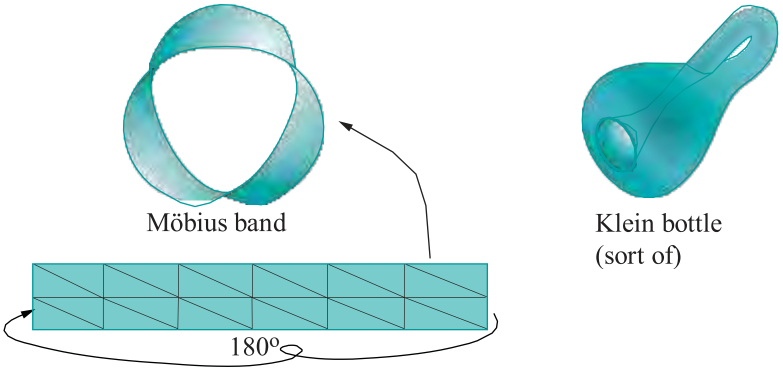

Figure 9.16: Non-orientable surfaces.

Experiment 9.6. Make a Möbius band as follows.

Take a long and thin strip of paper and draw two equal rows of triangles on one side to make a triangulation of the strip as in the bottom of Figure 9.16. Turn the strip into a Möbius band by pasting the two end edges together after twisting one 180°. The triangles you drew on the strip now make a triangulation of the Möbius band.

Try next to orient the triangles by simply drawing a curved arrow in each, in a manner such that the entire triangulation is consistently oriented. Were you able to?!

End

We have less to worry about with the Klein bottle, at least as far as real-world applications are concerned, because it cannot be created in 3-space. It needs at least 4D space to hold it properly. In fact, if you see Figure 9.16, the long neck of the bottle slips into the fourth dimension as it turns back to enter inside the bottle without, therefore, self-intersecting (a feat impossible in 3D space).

Further formalization of the notion of orientability requires knowledge of topology, but what we have discussed so far is ample from the point of view of first-level computer graphics. By the way, in case non-orientability looks like a potential can of worms, rest assured you will almost never encounter a non-orientable surface in the wild.

9.4 Culling Obscured Faces

Consider a *closed* surface such as a sphere, cube or torus, i.e., a surface that bounds a solid. See the first three surfaces Figure 9.17. For example, the sphere bounds a ball, the torus bounds a solid torus and the box bounds a cube. If a closed surface is opaque, then a viewer outside of it sees only one side, no matter where she is located, while a viewer inside sees the other. Closedness is essential here, otherwise, a viewer may be able to see both sides, e.g., as the reader can see for the hemisphere or cylinder in Figure 9.17.

Such a situation where closedness blocks off a side of a surface is replicated in OpenGL by ensuring a consistently oriented triangulation of the given surface. For example, suppose the outside of the sphere of Figure 9.17 is painted red, and the inside green. Suppose, too, it's consistently oriented so that the orientation of the

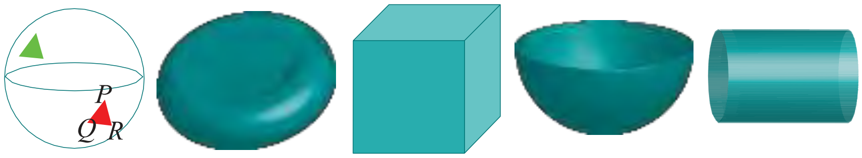

Figure 9.17: First three closed surfaces, next two non-closed. The closed sphere is not shaded in order to reveal the inside; the green back face of a triangle is not visible from outside the sphere.

triangle PQR appears CCW, as shown in the figure, to a viewer outside the sphere (e.g., the reader). Then *any* viewer outside the sphere sees only front-facing (assuming the default of CCW = front-facing) triangles and never any back-facing ones (e.g., the green back face of the other triangle in the figure) because, for such a viewer, all back faces are on the inside and hidden behind front-facing triangles. The precise opposite is true for viewers inside the sphere who see only back-facing triangles.

Now, OpenGL cannot know if a surface is closed or not because this is a global decision to be made *after* the *entire* surface has been drawn (e.g., if even one triangle were missing from the sphere then it would no longer be closed). Closedness cannot, therefore, be determined by an API which simply draws one triangle after another. As a result, what happens, for example, in the case of the sphere above with the viewer outside, is that OpenGL processes *every* triangle, oblivious of the global picture, only to subsequently discard back-facing ones at the time of hidden surface removal because it's only then that OpenGL discovers back-facing triangles to be obscured by front-facing ones.

In such as situation then, knowing a viewer is outside the closed sphere, the programmer can help OpenGL be more efficient by directing it to not process any further a triangle as soon as it's been determined to be back-facing. This is called *back-face culling* or *polygon culling*.

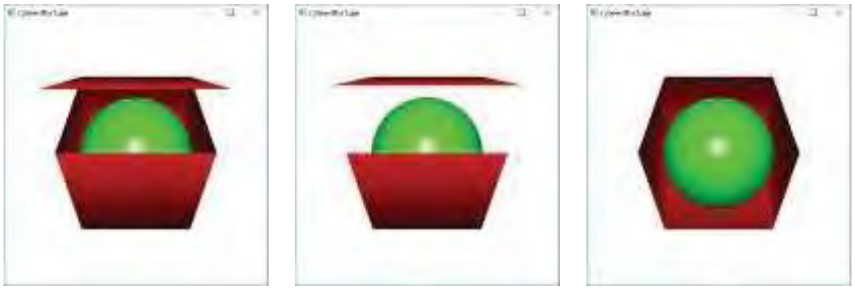

(a) (b) (c)

Figure 9.18: Screenshots for (a) Experiment 9.7 (b) Experiment 9.7 (disable culling commented out) (c) Experiment 9.8.

Experiment 9.7. Run sphereInBox1.cpp of Chapter11, which draws a green ball inside a red box. Press up or down arrow keys to open or close the box. Figure 9.18(a) is a screenshot of the box partly open.

Ignore the statements to do with lighting and material properties for now. See the statements before and following where the sphere is drawn with a glutSolidSphere(). Culling is enabled with a call to glEnable(GL CULL _FACE) and disabled with glDisable(GL CULL _FACE). The command glCullFace(*face*) where *face* can be GL_FRONT, GL BACK or GL FRONT AND BACK – it is, in fact, GL_BACK in the program – is used to specify if front-facing or back-facing or all triangles are to be culled. Therefore, back-facing triangles of the sphere, which evidently are all hidden behind front-facing ones, are indeed culled.

Comment out the glDisable(GL CULL FACE) call and open the box. Oops! Some sides of the box have disappeared as you can see in Figure 9.18(b). The reason, of course, is that the state variable GL_CULL_FACE is set when the drawing routine is called the first time so that all back-facing triangles, including those belonging to the box, are eliminated on subsequent calls.

End

Exercise 9.9. We know that back-facing triangles of a closed surface are obscured from a viewer outside. Is the converse true, in particular, are all obscured triangles necessarily back-facing?

Experiment 9.8. Here's a trick often used in 3D design environments like Maya and Studio Max to open up a closed space. Suppose you've finished designing the exterior of a house and now want to work inside it, e.g., to make interior walls and fittings. A good way to do this is to remove only those exterior walls which obscure your view of the interior and leave the rest; that the obscuring walls are either *all* front-facing or *all* back-facing means a cull will do the trick. Let's see this in action.

Insert the pair of statements

```
glEnable(GL_CULL_FACE);
glCullFace(GL_FRONT);
```

in the drawing routine of sphereInBox1.cpp just before the first glDrawElements() call. The top and front sides of the box are not drawn, leaving its interior visible. Figure 9.18(c) is a screenshot.

End

9.5 Transformations and the Orientation of Geometric Primitives

We know now how OpenGL uses the vertex order to determine the orientation of a primitive perceived by a viewer and, accordingly, the face seen, front or back. A reader, recollecting the theory of transformations, particularly Section 5.4.7 about orientation-preserving Euclidean transformations (i.e., rigid transformations) and orientation-reversing ones, may have already thought about and guessed the answer to the following question: how do these transformations affect the perceived orientation of a geometric primitive?

Answer : An orientation-preserving Euclidean transformation preserves the viewer's perceived orientation of the primitive, while an orientation-reversing one reverses it. An experiment will help make this clear.

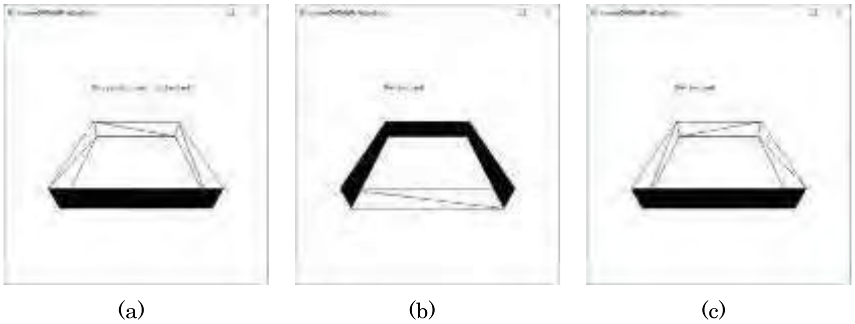

Figure 9.19: Screenshots from Experiment 9.9: (a) Original (b) Wrongly reflected (c) Correctly reflected.

Experiment 9.9. Run squareOfWallsReflected.cpp, which is squareOfWalls.cpp with an additional block of code before the drawing of the wall, including a glScalef(-1.0, 1.0, 1.0) call, to reflect the scene about the yz-plane:

```
if (isReflected)
{
   ...
   glScalef(-1.0, 1.0, 1.0);
   // glFrontFace(GL_CW);
}
else
{
   ...
   // glFrontFace(GL_CCW);
}

// Draw walls as a single triangle strip.
glBegin(GL_TRIANGLE_STRIP);
...
```

The original walls are as in Figure 9.19(a). Press space to reflect. Keeping in mind that front faces are filled and back faces outlined, it seems that glScalef(-1.0, 1.0, 1.0) not only reflects, but turns the square of walls inside out as well, as you can see in Figure 9.19(b). End

Well, of course! The viewer's (default) agreement with OpenGL is that if she perceives a primitive's vertex order as CCW, then she is shown the front, if not the back. Reflection about the yz-plane, an orientation-reversing Euclidean transformation, flips all perceived orientations, so those primitives whose front the viewer used to see now have their back to her, and vice versa.

We likely want the reflection to transform the primitives but not simultaneously change their orientation. This is easily done by revising the viewer's agreement with OpenGL with a call to glFrontFace(GL CW). Accordingly, uncomment the two glFrontFace() statements in the reflection block. Now the reflection looks right, as shown in Figure 9.19(c). The primitives are clearly still being reflected about the yz-plane, but front and back stay the same.

9.6 Summary, Notes and More Reading

In this chapter we learned how OpenGL applies orientation to determine that side of a 2D primitive which is visible. We saw as well the importance of consistently orienting a triangulation. The technique of back-face culling to improve efficiency in rendering a closed surface was a useful addition to our repertoire. We learned as well how orientation-preserving and orientation-reversing transformations impact the orientation of a primitive.

Although our discussion of orientation at the elementary level is ample for the practical programmer, a fairly sophisticated mathematical setting is required to formalize the concept of the orientability of a surface. The interested reader is urged to look up an introductory topology text. The two by Munkres [101, 102], as well as the one by Singer & Thorpe [136], are classics. Incidentally, the mathematically-inclined student of CG will find many things of use in topology. One has only to scan the latest ACM SIGGRAPH papers [133] to see the heavy application of topological ideas in cutting-edge CG. Two introductory texts on the emerging area of computational topology are by Edelsbrunner [40] and Edelsbrunner and Harer [42].

Part V

Making Things Up

Taylor & Francis
Taylor & Francis Group
http://taylorandfrancis.com

CHAPTER 10

Modeling in 3D Space

The goal for this chapter is to systematically study the modeling of objects in 3D space in order to be able to populate the movies, games and other scenes that we create.

As OpenGL has only straight and flat drawing primitives, curved objects must necessarily be approximated. We'll develop general strategies to manufacture approximations of both curves and surfaces. We'll examine in depth certain special classes of curves and surfaces especially important in applications. Particular attention will be paid to Bézier primitives because of their utility, as well as the easy-to-use OpenGL syntax available to code them. Another popular class we'll study is that of fractals. Although we'll delve into some of the mathematics underlying curves and surfaces, we'll never be far from practical code: throughout this chapter are numerous illustrative programming examples and exercises.

We begin in Section 10.1 with the modeling of curves. The first two subsections, 10.1.1 and 10.1.2, describe how a curve is specified by equations, either implicitly or parametrically. A strategy to draw a curve as a polyline approximation is the topic of 10.1.3. We discuss polynomial and rational parametrizations of curves in 10.1.4, as they are computationally more efficient than other kinds. The conic sections, including parabolas, ellipses and hyperbolas, comprise a very important and commonly-occurring class of curves that we investigate briefly in 10.1.5. Section 10.1.6 is a short introduction to the mathematics of curves, particularly giving a rigorous definition of what it means to be a curve, and discussing continuity and regularity. This section can and probably should be skipped on a first reading.

We move on to surfaces in Section 10.2. We present the following 2D primitives in an informal order of increasing drawing complexity: polygons, meshes, planar surfaces and general surfaces. Subsections 10.2.1-10.2.3 describe the first three, which are straightforward to draw. The next two subsections, 10.2.4 and 10.2.5, discuss the specification of a general surface and how to model one as a mesh approximation.

The powerful technique of making a surface by sweeping a curve is the topic of 10.2.6. In 10.2.7 we pause to apply our newly-acquired skills in a bunch of modeling projects. We continue our study of surfaces in 10.2.8, discussing a special class of swept surfaces, called ruled surfaces. This class includes bilinear patches and generalized cones and cylinders. The generalization of conic sections to 3D, the quadric surfaces, is described in 10.2.9. Objects of the GLU library which are somewhat inappropriately called the GLU quadrics are introduced in 10.2.10. The beautifully symmetric regular polyhedra, or Platonic solids as they are often called, are presented in 10.2.11. Section 10.2.12 parallels 10.1.6 in a formal discussion of surfaces and the properties of continuity and regularity – and the same recommendation applies that it be skipped on a first reading.

Although we'll be discussing Bézier theory in depth in a later chapter, it turns out that a fair amount of design with Bézier curves and surfaces can be accomplished even with limited theoretical understanding. Therefore, in keeping with our aim in this chapter of equipping the reader with as many practical modeling techniques as possible, Section 10.3 introduces Bézier design – curves in 10.3.1 and surfaces in 10.3.2.

Yet another very practical technique, that of importing into a program models created externally, typically with 3D modeling software like Maya, Studio Max or Blender, is the topic of Section 10.4. In particular, we show how to import models defined in the OBJ file format.

Fractal curves, ubiquitous in nature, and so often used to create surreal shapes by designers, are discussed in Section 10.5.

This is a long chapter because we tried to make it as complete as possible, but parts may certainly be skipped on a first reading. In fact, we provide the occasional suggestion ourselves as to what to skip. However, the reader should really obey her taste: if it's fun reading, keep reading; if not, move on.

10.1 Curves

One-dimensional objects are unions of straight and curved segments. See Figure 10.1. Parts composed of straight segments can be drawn exactly in an OpenGL environment – one would invoke the GL LINES, GL LINE STRIP and GL LINE LOOP primitives. Curved segments, on the other hand, have to be approximated.

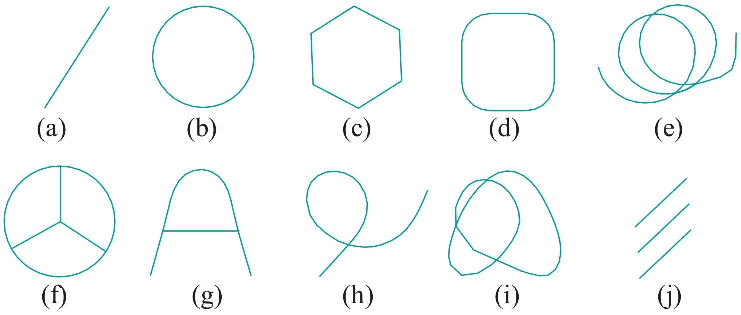

Figure 10.1: One-dimensional objects.

We'll formalize the process of approximating a curve with a polygonal line. However, let's first see how to mathematically specify a curve.

Terminology: The term "curve" itself can mean any segment, curved or straight.

10.1.1 Specifying Plane Curves

We begin with *plane curves*, which are those that lie on a plane (mathematically, 2-dimensional space, denoted R^2). There are two ways to specify such a curve, implicit and parametric.

Implicit

A plane curve c is specified *implicitly* by the equation

$$F(x, y) = 0 \qquad (10.1)$$

if the points of c are those whose coordinates (x, y) satisfy this equation. $F(x, y) = 0$ is said to be the *implicit equation* of c, and the curve c the *graph* of this equation. An implicit equation, therefore, gives a *Boolean condition* for points on the curve to satisfy: a point (a, b) lies on the curve $F(x, y) = 0$ if $F(a, b) = 0$; it doesn't if $F(a, b)$ /= 0.

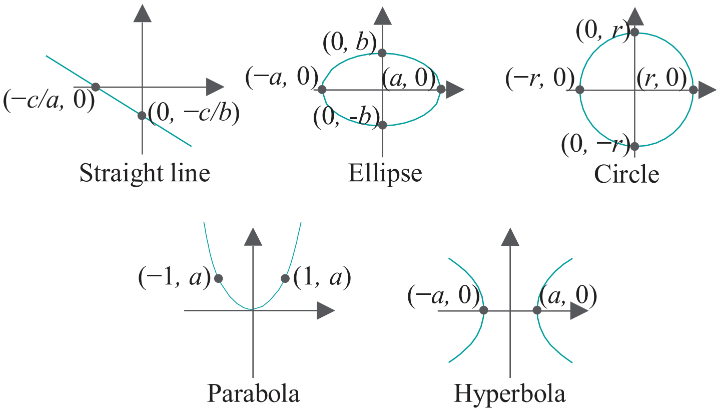

Figure 10.2: Graphs of familiar plane curves (curves are fairly accurate sketches but not exact plots).

Example 10.1. Here are examples of implicit equations of curves. Five familiar ones first (see Figure 10.2, which shows a few points on the graph of each as well):

(a) Straight line: $ax + by + c = 0$

(b) Ellipse: $\frac{x^2}{a^2} + \frac{y^2}{b^2} = 1$

(c) Circle (special case of ellipse): $x^2 + y^2 = r^2$

(d) Parabola: $y = ax^2$

(e) Hyperbola: $\frac{x^2}{a^2} - \frac{y^2}{b^2} = 1$

Remark 10.1. An implicit equation is often written in the form $F(x, y) = G(x, y)$ with the RHS not necessarily equal to 0, but, of course, it can be rearranged as $F(x, y) - G(x, y) = 0$.

The following two exotic curves (Figure 10.3) may not be as familiar:

(f) Witch of Agnesi: $y(x^2 + 4) = 8$

(g) Lemniscate of Bernoulli: $(x^2 + y^2)^2 = x^2 - y^2$

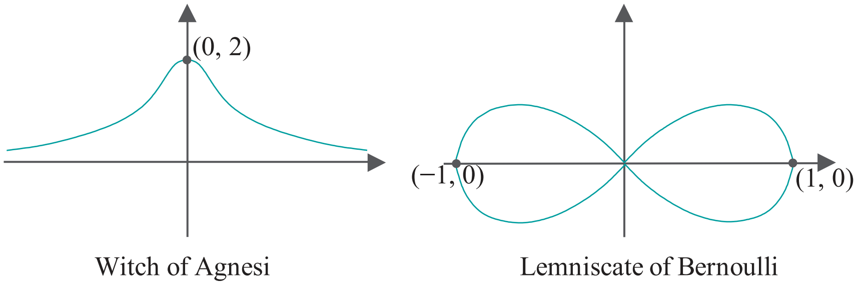

Figure 10.3: A couple of exotic curves.

Parametric

A plane curve c is specified *parametrically*, or *explicitly*, by the two equations

$$x = f(t), \quad y = g(t), \quad \text{where } t \in T \tag{10.2}$$

if the points of c are those whose coordinates (x, y) satisfy $x = f(t)$ and $y = g(t)$, for some value of $t \in T$, where T is a given set called the *parameter space*, or *parameter* *domain*. Typically, T is an interval of the real line R, bounded or unbounded, e.g., $[-\pi, \pi]$, $[0, \infty]$ and $(-\infty, \infty)$.

The functions f and g are called *parameter functions* and t the *parameter variable*. Mathematically, as as a set on the plane, the curve $c = \{(f(t), g(t)) : t \in T\}$.

Remark 10.2. Sometimes, a curve c is thought of as a function from T to the plane R^2 defined by $c(t) = (f(t), g(t))$, for $t \in T$, rather than as the set of points $c = \{f(t), g(t)) : t \in T\}$ lying on the plane, which, of course, is simply the image of the function. The context should make it clear if the curve is being treated as a set or function.

Example 10.2. Here are parametrizations of the curves earlier given implicitly in Example 10.1:

(a) Straight line: $x = t$, $y = -\frac{a}{b}t - \frac{c}{b}$ $t \in (-\infty, \infty)$, assuming $b \neq 0$.

(b) Ellipse: $x = a\cos t$, $y = b\sin t$, $t \in [-\pi, \pi]$.

Observe that the two different parameter values $t = -\pi$ and $t = \pi$ map to the same point $(-a, 0)$ on the ellipse, which is by no means illegal. A larger parameter space, e.g., $(-\infty, \infty)$ would cause even more overlap of parameter images. The half-open parameter interval $[-\pi, \pi)$ causes no overlap, but is a bit ungainly.

There's nothing special about $[-\pi, \pi]$ other than that it's symmetric about the origin. Any other closed interval of size 2π would do as well, e.g., $[0, 2\pi]$.

(c) Circle: $x = r\cos t$, $y = r\sin t$, $t \in [-\pi, \pi]$.

(d) Parabola: $x = t$, $y = at^2$, $t \in (-\infty, \infty)$.

(e) Hyperbola: $x = a\sec t$, $y = b\tan t$, $t \in [-\pi, -\pi/2) \cup (-\pi/2, \pi/2) \cup (\pi/2, \pi]$.

As you may check, the parameter space is simply $[-\pi, \pi]$ *minus* the two values $\pm\pi/2$, where sec and tan become "infinite".

(f) Witch of Agnesi: $x = 2t$, $y = \frac{2}{1+t^2}$, $t \in (-\infty, \infty)$. Alternately, $x = 2\tan t$, $y = 2\cos^2 t$, $t \in (-\frac{\pi}{2}, \frac{\pi}{2})$.

(g) Lemniscate of Bernoulli: $x = \frac{\cos t}{1+\sin^2 t}$, $y = \frac{\cos t \sin t}{1+\sin^2 t}$, $t \in [-\pi, \pi]$.

Exercise 10.1. Prove that parametrizations of Example 10.2 are indeed those of the curves given implicitly in Example 10.1.

Hint : Plug the parametric forms for x and y into the implicit equation and verify the equality, e.g., for the circle

$$x^2 + y^2 = (r\cos t)^2 + (r\sin t)^2 = r^2(\cos^2 t + \sin^2 t) = r^2$$

Whereas an implicit equation $F(x, y) = 0$ for a curve gives a Boolean check for points "claiming" to be on the curve, a parametric representation is more functional. If a curve c is given parametrically by the equations $x = f(t)$ and $y = g(t)$, where $t \in T$, one can think of the image $(f(t), g(t))$ of the parameter value t as traveling along c, as t travels along the parameter domain. For example, as t goes from $-\pi$ to π, the point $(a\cos t, b\sin t)$ sweeps around the ellipse $\frac{x^2}{a^2} + \frac{y^2}{b^2} = 1$ from $(-a, 0)$ and back again.

In summary, while an implicit specification $F(x, y) = 0$ is ideal for *verifying* if a given point lies on a curve c, it's not as useful for the purpose of *generating* points on c; it is exactly the opposite in the case of a parametric specification such as $x = f(t)$, $y = g(t)$, $t \in T$.

Example 10.3. (a) Verify if the points $(1, 0)$ and $(1, -1)$ lie on the Lemniscate of Bernoulli.

(b) Generate three distinct points on the Lemniscate of Bernoulli.

Answer: (a) Plugging $(1, 0)$ and $(1, -1)$ successively into the implicit equation $(x^2 + y^2)^2 = x^2 - y^2$, one sees that the first point lies on the curve, while the second doesn't.

(b) Plugging $t = 0$, $\pi/4$ and $\pi/2$ successively into the parametric equations

$$x = \frac{\cos t}{1 + \sin^2 t} \quad y = \frac{\cos t \sin t}{1 + \sin^2 t}$$

one gets the points $(1, 0)$, $(\frac{\sqrt{2}}{3}, \frac{1}{3})$ and $(0, 0)$ on the curve.

A parametric representation is to be preferred to an implicit for drawing as it enables the programmer to efficiently generate sample points on the curve. Going from one kind of representation to another often requires a bit of mathematical dexterity. The following two exercises are not particularly difficult though.

Exercise 10.2. An astroid, a curve traced by a fixed point on a circle rolling inside another circle of four times the diameter (see Figure 10.4), is given by the implicit equation

$$x^{\frac{2}{3}} + y^{\frac{2}{3}} - 1 = 0$$

Find parametric equations.

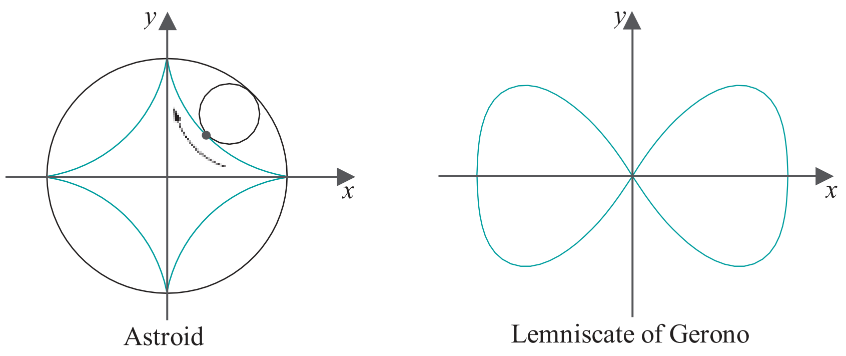

Astroid

Lemniscate of Gerono

Figure 10.4: More exotic curves.

Exercise 10.3. Parametric equations for another exotic curve, the Lemniscate of Gerono (see Figure 10.4), are

$$x = \cos t, \; y = \cos t \sin t, \; t \in [-\pi, \pi]$$

Find an implicit equation.

Remark 10.3. Neither the implicit nor parametric specification of a curve is ever unique. For example, the unit circle can be written implicitly as both $x^2 + y^2 = 1$ and $2x^2 + 2y^2 = 2$, or parametrically as $x = \cos t$, $y = \sin t$, $t \in [-\pi, \pi]$ and $x = \cos(t/2)$, $y = \sin(t/2)$, $t \in [-2\pi, 2\pi]$.

10.1.2 Specifying Space Curves

The extra dimension they have in which to move makes curves in 3-space $\mathbb{R}^3$ – the real world – more interesting than their plane counterparts. Such curves are called *space curves*.

Implicit

The implicit specification of a space curve requires two equations:

$$\begin{aligned} F(x, y, z) &= 0\,, \\ G(x, y, z) &= 0 \end{aligned} \qquad (10.3)$$

The reason for two equations rather than the one as in the case of a plane curve is as follows. $\mathbb{R}^3$ itself – unconstrained by any equations – is of dimension 3. However, each additional equation imposed reduces the resulting object's dimension by one. For example, points of $\mathbb{R}^3$ satisfying the one equation

$$x^2 + y^2 + z^2 - 1 = 0$$

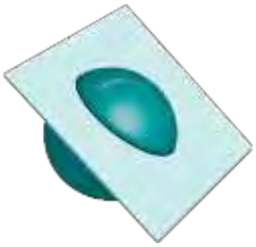

Figure 10.5: A sphere and a plane intersect in a circle.

make a sphere, a surface of dimension 2. Adding the equation of, say, the plane $x + y + z - 1 = 0$, one obtains the circle

$$\begin{aligned} x^2 + y^2 + z^2 - 1 &= 0, \\ x + y + z - 1 &= 0 \end{aligned}$$

which is a curve of dimension 1 at the intersection of the two (Figure 10.5). Generally, two equations imposed on $\mathbb{R}^3$ give an object of dimension $3 - 2 = 1$, a curve.

Plane curves, of course, are space curves too, and if the implicit equation of a plane curve is already known to be $F(x, y) = 0$, then it can be written as a space curve by means of the two equations

$$\begin{aligned} F(x, y) &= 0, \\ z &= 0 \end{aligned}$$

Remark 10.4. We have used the term "dimension" without defining it formally. We'll not do so at this time as it would take us too far afield, but think intuitively of an object's dimension as the number of "independent directions of movement" – "degrees of freedom" would be apt as well – on it.

For example, there is only one independent direction of movement on a curve (mind that forward and backward are not independent, but merely the negative of one another). A surface allows two independent directions of movement. True, there are infinitely many directions of movement from any given point on a surface, but at most any two are independent. For example, take a point on a sphere – using only latitude and longitude one can represent any direction starting from it.

Remark 10.5. Of course, Equation (10.1), $F(x, y) = 0$, for the implicit equation of a plane curve follows the principle of using equational constraints to reduce dimension, as well. Particularly, one equation reduces the dimension two of a plane to that of one of a curve.

Exercise 10.4. What space curve is

$$\begin{aligned} x^2 + y^2 &= 1, \\ x + z &= 1 \end{aligned}$$

Describe or sketch the curve.

Exercise 10.5. What space curve is

$$\begin{aligned} x^2 + y^2 + z^2 &= 1, \\ x^2 + y^2 + z^2 - 2x &= 0 \end{aligned}$$

Describe or sketch the curve.

Parametric

The parametric, or explicit, specification of a space curve is similar to that of a plane one except, as one would expect, another parameter function is required to determine the z coordinate value:

$$x = f(t), \; y = g(t), \; z = h(t), \; t \in T \qquad (10.4)$$

Given a plane curve, its parametric equations in 2-space are extended to 3-space, to make it a space curve, simply by adding $z = 0$.

Similarly as for a plane curve, a space curve can be thought of as the function from the parameter domain T to $\mathbb{R}^3$ defined by $c(t) = (f(t), g(t), h(t))$, rather than the set of points $\{(f(t), g(t), h(t)) : t \in T\}$ lying in $\mathbb{R}^3$.

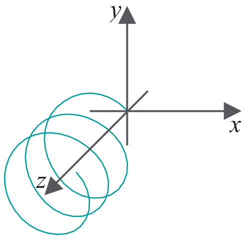

Figure 10.6: Helix.

Example 10.4. Parametric equations for a helix whose axis is along the z-axis (Figure 10.6) are

$$x = r\cos t, \; y = r\sin t, \; z = t, \; t \in \mathbb{R}$$

which, in fact, we used (slightly modified) to draw one in Section 2.8.2.

Example 10.5. Parametric equations for a general straight line in space are

$$x = a_1 t + b_1, \; y = a_2 t + b_2, \; z = a_3 t + b_3, \; t \in \mathbb{R}$$

where the $a_i, b_i, 1 \le i \le 3$, are constants.

Example 10.6. Give implicit equations for the helix of Example 10.4.

Answer:

$$\begin{aligned} x - r\cos z &= 0 \\ y - r\sin z &= 0 \end{aligned}$$

Exercise 10.6. Give parametric equations for the infinite straight line through (p_x, p_y, p_z) and (q_x, q_y, q_z). How is the parameter space restricted if we are interested only in the finite segment *between* the two points?

Exercise 10.7. Sketch using pencil and paper the curve, called a *conical helix* , specified parametrically by

$$x = t\cos t, \; y = t\sin t, \; z = t, \; t \in (-\infty, \infty)$$

10.1.3 Drawing Curves

Drawing a curve from its parametric equations is straightforward. We did this in Chapter 2 for a few particular curves, in particular, the circle, parabola and helix. We'll describe next the procedure for a general space curve c given parametrically by

$$x = f(t), \; y = g(t), \; z = h(t), \quad t \in T \qquad (10.5)$$

Assume that the parameter domain T is $[a, b]$, a closed interval. The point $(f(t), g(t), h(t))$ on c is denoted $c(t)$.

It's useful to imagine T as being part of the real line and to imagine c as lying in a "separate" 3-space. The parameter equations together $c(t) = (f(t), g(t), h(t))$ can then be thought of as a map from the former to the latter or, more vividly, to lift and shape T into c. See Figure 10.7.

A sample

$$a = t_0 < t_1 < \ldots < t_n = b$$

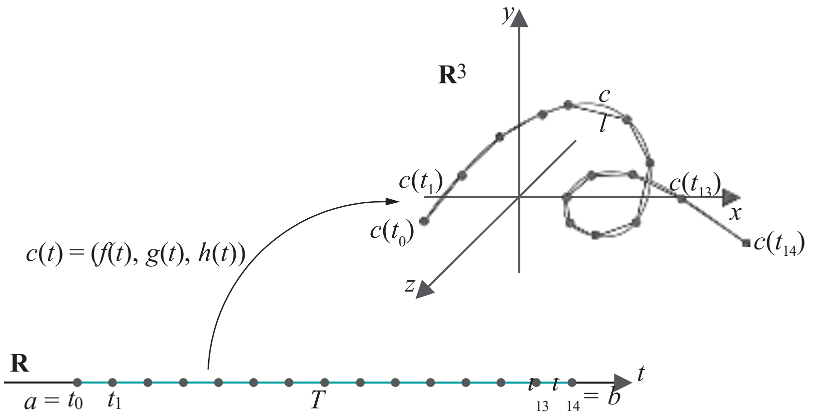

Figure 10.7: Parameter space $T = [a, b]$ mapped to a curve c. The sample grid on T, as well as its corresponding mapped sample on c, has 15 points (not all labeled). The polyline l connecting the mapped sample approximates c.

of $n+1$ points from $[a, b]$ is called a *sample grid* on $[a, b]$ (note that the end points a and b are always included in the sample). It maps to a sample

$$c(t_0), c(t_1), \dots, c(t_n)$$

of $n+1$ points of c, called the *mapped sample*.

The polyline l joining, successively, $c(t_0), c(t_1), \dots, c(t_n)$ is an approximation of c. Each individual segment $c(t_{i-1})c(t_i)$, $1 \le i \le n$, of l approximates the arc of c between $c(t_{i-1})$ and $c(t_i)$. The sample grid and its corresponding mapped sample in Figure 10.7 contain 15 points each.

Keep in mind that a sample which is uniformly spaced along $[a, b]$ may *not* map to one which is uniformly spaced along c. For, the length of the arc of c between $c(t_{i-1})$ and $c(t_i)$ depends not only on the length of the interval $[t_{i-1}, t_i]$, but also on the "speed" of $c(t)$ with respect to t. We see next an example of this.

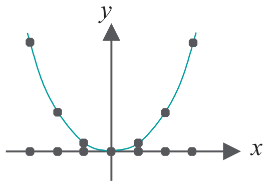

Figure 10.8: A uniformly sampled parabola $y = x^2$.

Example 10.7. Figure 10.8 shows the parabola $y = x^2$. The seven sample points on the real line are uniformly spaced, but their images on the curve are not because the rate of change of y with respect to x – equaling $\frac{dy}{dx} = 2x$ for the parabola – increases away from the origin.

Exercise 10.8. (Programming) Compare the outputs of circle.cpp, helix.cpp and parabola.cpp, all in Chapter 2.

The sample is chosen uniformly from the parameter space in all three programs. The output quality is good for both the circle – after pressing '+' a sufficient number of times for a dense enough sample – and the helix. The parabola, however, shows a difference in quality between its curved bottom and straighter sides, the sides becoming smoother more quickly than the bottom. In curves such as this one may want to sample non-uniformly, in particular, more densely from parts of greater curvature in order to keep the polyline approximation close always to the curve.

Can you do this for the parabola? *Harder* : think of an automatic way to sample the parameter space of a curve for a good approximation, e.g., possibly by progressively refining a starting sample in order to reduce the "error" between curve and polyline.

Here's another simple curve-drawing program.

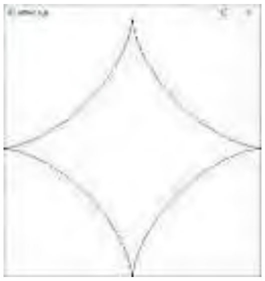

Figure 10.9: Screenshot of astroid.cpp.

Experiment 10.1. Run astroid.cpp which modifies circle.cpp to implement instead the parametric equations

$$x = \cos^3 t, \; y = \sin^3 t, \; z = 0, \; 0 \le t \le 2\pi$$

for the astroid of Exercise 10.2. Figure 10.9 is a screenshot. End

Exercise 10.9. (Programming) Draw the Lemniscate of Bernoulli with the help of the parametric equations given in Example 10.2(g).

Exercise 10.10. (Programming) Draw the conical helix of Exercise 10.7.

Exercise 10.11. (Programming) Draw a curve with a repeating pattern like that of Figure 10.10(a). The two arcs of the "shark's fin" could be parts of circles. Your program should allow the user to specify the number of repetitions.

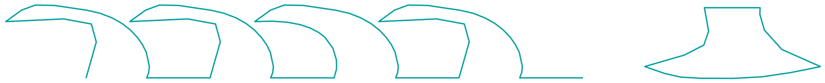

(a) (b)

Figure 10.10: (a) Curve with a repeating pattern (b) Ax head.

Exercise 10.12. (Programming) Draw an ax head as in Figure 10.10(b).

Exercise 10.13. (Programming) The *twisted cubic* is a space curve given parametrically by the equations

$$x = t, \ y = t^2, \ z = t^3$$

Draw a part of it near the origin.

Exercise 10.14. (Programming) Animate the drawing of an astroid, as described in Exercise 10.2, as the curve traced by a point of a circle rolling inside another four times as large. The popular children's drawing toy called Spirograph can draw an astroid, among other curves.

Superellipses

A class of plane curves which generalizes both the ellipse and the astroid is that of the *superellipses*, invented by Lamé in 1818, given by the implicit equation:

$$\frac{x}{a}^{n} + \frac{y}{b}^{n} = 1$$

where a, b and n each is a positive constant.

Note: Because the exponent n can be fractional, the modulus signs are to avoid imaginaries if x or y is negative.

Figure 10.11 shows a few superellipses for $a = b = 1$ – when their equation is $|x|^n + |y|^n = 1$ – and different values of n. Generally, if $a = b$, the superellipse is called a *supercircle*. When $n = 1$ the supercircle is a square, when $n > 1$ it's convex outwards, and when $n < 1$ concave outwards.

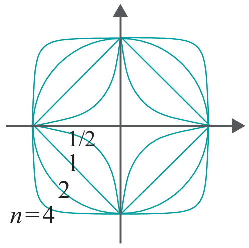

Figure 10.11: Supercircles $|x|^n + |y|^n = 1$, for $n = 1/2, 1, 2, 4$.

Exercise 10.15. Justify the claim that superellipses generalize both ellipses and astroids.

Exercise 10.16. Deduce the parametric equations of a superellipse.

Exercise 10.17. (Programming) Write a program to draw a supercircle $|x|^n + |y|^n = 1$, allowing the user to choose n.

10.1.4 Polynomial and Rational Parametrizations

This section may be skipped on a first reading.

A *rational function* is the ratio of two polynomials. For example,

$$\frac{1+2t}{1-t+t^2-t^3} \quad \text{and} \quad \frac{x}{1+x} \tag{10.6}$$

are rational functions of t and x, respectively. A *polynomial function* is, of course, simply a special case of a rational function where the denominator is 1, e.g.,

$$1+2t-3t^2+4t^3 \quad \text{and} \quad x^3 \tag{10.7}$$

Unlike polynomial functions, rational functions may become undefined, which happens when their denominator vanishes. The first rational function of (10.6) is undefined at $t = 1$ and the second at $x = 1$.

If the parameter functions of a curve c are all rational, then it is said to be a *rational curve* and to have a *rational parametrization*; if they are, in fact, all polynomial, then c is a *polynomial curve* with a *polynomial parametrization*. E.g., Examples 10.2 (a) and (d) give polynomial parametrizations, while the first part of (f) a rational one.

The parametrization

$$x = r\cos t, \quad y = r\sin t, \quad t \in [-\pi, \pi]$$

of Example 10.2(c) of the circle $x^2 + y^2 = r^2$ uses trigonometric functions and is called, of course, a *trigonometric parametrization*. It turns out that there's an alternate rational parametrization of the circle, with one so-called singularity, as the reader is asked to show in the following exercise.

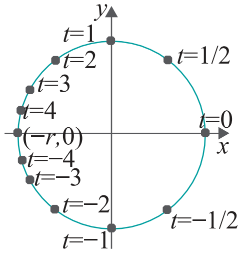

Figure 10.12: Points on a circle from a rational parametrization.

Exercise 10.18. Show, first, that

$$x = r\frac{1-t^2}{1+t^2} \quad \text{and} \quad y = r\frac{2t}{1+t^2}$$

satisfy $x^2 + y^2 = r^2$ for all values of t.

By plotting a few values of (x, y) for values of $t = 0, \pm 1, \pm 2, \ldots$ (see Figure 10.12) convince yourself that

$$x = r\frac{1-t^2}{1+t^2}, \quad y = r\frac{2t}{1+t^2}, \quad t \in (-\infty, \infty)$$

is a parametrization of the entire circle of radius r centered at the origin *minus* the point $(-r, 0)$. The one point $(-r, 0)$, which the parametrization "cannot reach," is called a *singularity* of the curve (with respect to this particular parametrization).

Polynomial and rational parametrizations are often preferred to trigonometric ones in applications because the former can be computed exactly (up to round-off error) while a trigonometric function can at best be approximated by a series. For example, the *infinite* power series $1 - x^2/2! + x^4/4! - x^6/6! + \ldots$ must be summed to some finite number of terms to determine $\cos x$ to desired accuracy. Moreover, the number of arithmetic operations in computing even the finite part of the power series, typically, is significantly larger than in computing the corresponding rational parametric expression.

Exercise 10.19. (Programming) Draw a unit circle centered at the origin with the help of a rational parametrization. Avoid the problem of the singularity at $(-r, 0)$ in the previous exercise, as well as the infinite parameter domain there, by using the equations

$$x = \frac{1-t^2}{1+t^2}, \quad y = \frac{2t}{1+t^2}, \quad t \in [-1, 1]$$

to draw the right half semi-circle and

$$x = -\frac{1-t^2}{1+t^2}, \quad y = \frac{2t}{1+t^2}, \quad t \in [-1, 1]$$

to draw the left half.

Exercise 10.18 gave a rational parametrization of a circle. Is there a polynomial parametrization which might, in fact, be computationally better because it does not require the expensive division operation? The answer is no, as is shown in the following.

Example 10.8. Prove that no non-trivial arc of the circle $x^2 + y^2 = r^2$ has a polynomial parametrization.

Answer : Suppose, if possible, that $x = f(t)$ and $y = g(t)$ is a polynomial parametrization of a non-trivial arc of a circle. Then $f(t)$ and $g(t)$ are polynomial functions such that

$$f(t)^2 + g(t)^2 = r^2 \tag{10.8}$$

If $f(t)$ and $g(t)$ are both constants, i.e., neither contains a power of t, then $(f(t), g(t))$ is just one point and certainly cannot represent a non-trivial arc. Therefore, either one or both of the two functions must contain a power of t. Let t^m be the highest power of t in $f(t)$ or $g(t)$. Write

$$f(t) = a_m t^m + a_{m-1} t^{m-1} + \ldots a_0 \quad \text{and} \quad g(t) = b_m t^m + b_{m-1} t^{m-1} + \ldots b_0$$

where at least one of a_m and b_m is non-zero. Then

$$f(t)^2 + g(t)^2 = (a_m^2 + b_m^2) t^{2m} + \text{ lower powers of } t$$

where the coefficient of t^{2m} is non-zero, in fact, positive, because at least one of a_m and b_m is non-zero.

We see, then, that the LHS of (10.8) contains a non-zero power of t, but, in this case, it cannot equal the RHS which is only scalar, proving that a non-trival arc of the circle $x^2 + y^2 = r^2$ indeed has no polynomial parametrization.

10.1.5 Conic Sections

This section may be skipped on a first reading.

The ellipse, parabola and hyperbola are well-known members of a special class of plane curves called *conic sections* or, simply, *conics*. A conic is nothing but the graph on the plane of a quadratic equation in two variables, typically written:

$$Ax^2 + Bxy + Cy^2 + Dx + Ey + F = 0 \tag{10.9}$$

(At least one of A, B and C should not be zero, or the equation is no longer that of a quadratic.)

Conditions on the coefficients determine the type of conic. If the quantity $B^2\ 4AC$, called the *discriminant* of the conic, is less than zero, then the conic is an ellipse, if it is zero then a parabola, and if it is greater than zero then a hyperbola. If $A = C$ are non-zero and $B = 0$ we get a circle, which is a special case of the ellipse. However, in all cases, there are *degenerate* instances when the equation is that of a point, straight line(s), or nothing at all, as the reader is asked to find for herself next.

Exercise 10.20. Show that the following are equations of degenerate conics by determining their graphs:

$$x^2 + 2y^2 + 1 = 0, \qquad x^2 + y^2 = 0, \qquad x^2 + 2xy + y^2 = 0, \qquad x^2 - y^2 = 0$$

In each case say as well if it is a degenerate ellipse, circle, parabola or hyperbola.

Conics arise frequently in design applications. Consequently, it's useful that they all have polynomial or rational parametrizations. In fact, any non-degenerate conic can be transformed by translation and rotation to one of the four normalized forms in the table below (pictured in Figure 10.13):

Conic	Implicit	Polynomial or Rational Parametrization	Singu-larity
Ellipse	$\frac{x}{a^2} + \frac{y}{b^2} = 1$	$x = a\frac{1-t}{1+t^2}, y = b\frac{2t}{1+t^2}, t \in (-\infty, \infty)$	$(-a, 0)$
Circle	$x^2 + y^2 = r^2$	$x = r\frac{1-t}{1+t^2}, y = r\frac{2t}{1+t^2}, t \in (-\infty, \infty)$	$(-r, 0)$
Parabola	$y = ax^2$	$x = t, y = at^2, t \in (-\infty, \infty)$	None
Hyperbola	$\frac{x^2}{a^2} - \frac{y^2}{b^2} = 1$	$x = a\frac{1+t}{1-t^2}, y = b\frac{2t}{1-t^2}, t \in (-\infty, \infty) - \{-1, 1\}$	$(-a, 0)$

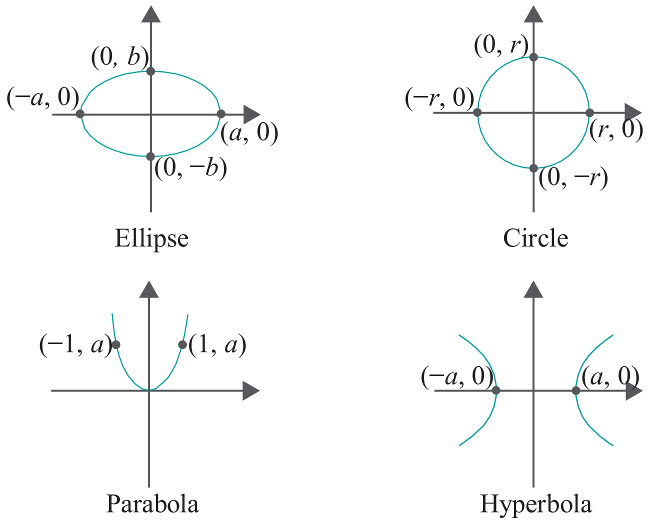

Figure 10.13: Conic sections.

Geometric Construction

There is a rather neat geometric construction of the conics which, in fact, explains why they are called conic sections. Consider the double cone C formed from all the lines through the origin intersecting a circle c centered some distance vertically above the origin. See Figure 10.14(a).

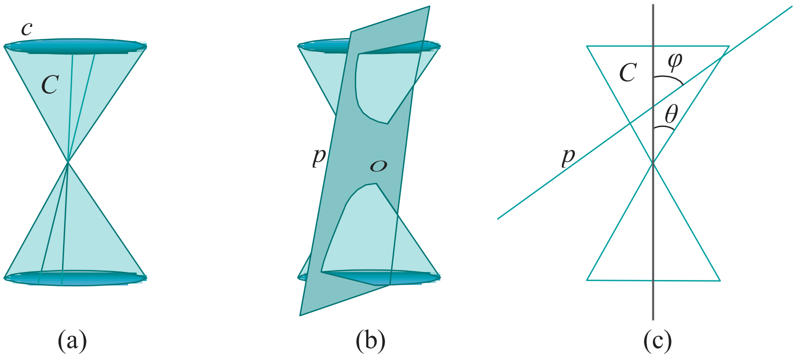

Figure 10.14: (a) A double cone C showing two lines on it passing through the origin (b) A hyperbolic section of C by a non-radial plane p (c) Cross-sectional view of a non-radial plane p intersecting C.

Now, the section of C by a non-radial plane p aligned as in Figure 10.14(b) is a hyperbola (a *non-radial* line or plane is one that does not pass through the origin). A hyperbola is not the only curve that can be sectioned off a double cone, as the reader is asked to show next.

Exercise 10.21. Using paper and pencil draw three non-radial planes so that their intersections with a double cone, whose vertex is the origin, are a circle, ellipse and parabola, respectively.

Let's try to determine precisely the section of the double cone C by some given plane p. Assume that the half-angle at the vertex of C is θ and that the angle between p and the axis of C is φ. A typical cross-sectional view is drawn in Figure 10.14(c).

First, suppose that p is non-radial, as in Figure 10.14(c). We have then the following: *the section of C by p is an ellipse, parabola or hyperbola according as $\theta < \varphi$, $\theta = \varphi$ or $\theta > \varphi$*. We'll leave the reader to convince herself of this fact by mentally rotating the plane p of Figure 10.14(c), where, in fact, currently $\theta < \varphi$.

Exercise 10.22. Suppose now that p is *radial*. Determine the three different *degenerate* conic sections that arise, again according as θ <=> φ.

10.1.6 Curves More Formally

This section may be skipped on a first reading.

As we make our living in computer graphics drawing curves and surfaces, it's reasonable to try and understand some of their underlying mathematical formalism. We'll make a start with curves in this section. The theory of curves is a vast area within mathematics. Our objective in contrast is modest: to bring across a few definitions and results we believe most relevant to graphics applications, and in as intuitive a manner as possible.

We assume that you have some basic calculus. In other words, statements such as the function $f(x) = x^2$ is continuous and derivable (derivable, differentiable, same thing), that its derivative is the function $f^{1}(x) = 2x$, and that its tangent at the point $(1, 1)$ has gradient 2 all make sense to you. Good!

Moving on, we'll first examine some "holes" in the rules given earlier to specify a curve. We'll then try to fix these and motivate in the process a more rigorous definition.

An implicit equation of the form $F(x, y) = 0$ on the plane may well specify an object that does not agree with our notion of what a curve should be. For example, $x^2 - y^2 = 0$ specifies two intersecting straight lines. See Figure 10.15(a). Writing $x^2 - y^2 = 0$ as $(x - y)(x + y) = 0$ explains the graph. And $x^2 + y^2 = 0$ defines just the single point $(0, 0)$, as in Figure 10.15(b)!

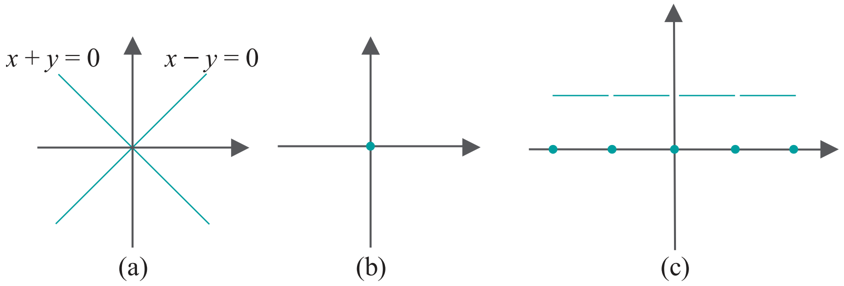

Figure 10.15: Non-curves: (a) $x^2 - y^2 = 0$ (b) $x^2 + y^2 = 0$ (c) $y = 0$, if x is an integer, 1 otherwise (gaps in the blue line indicate missing points).

Parametric equations may not fare better. The following is contrived certainly but makes the point:

$$x = t, \quad y = \begin{array}{l} 0, \ t \text{ is an integer} \\ 1, \ t \text{ is not an integer} \end{array}, \quad t \in \mathrm{R}$$

define a disconnected union of points and straight segments (Figure 10.15(c)).

It seems, therefore, that the definition earlier of implicit and parametric curves simply by sets of equations might not be enough to comply always with our intuition at least of what a curve should be. To motivate a better definition, contemplate again the one-dimensional objects in Figure 10.1. All, except (f), (g) and (j), seem to match the notion of a curve as being the *trajectory of a continuously-moving point*. We'll build on this simple observation.

In fact, we begin with the following definition of so-called C^0-continuity:

Definition 10.1. A real-valued function f defined on a closed interval T is said to be C^0-*continuous* or, simply, C^0, if it is continuous on T.

Remark 10.6. Yes, the definition simply re-christens what we know already as continuous. The reason to do this is that we'll soon be encountering so-called higher orders of continuity, to be called C^1, C^2, etc.

Remark 10.7. As the only functions that we consider are real-valued we won't explicitly say this any more.

Remark 10.8. A closed interval (like T in the preceding definition) is either bounded of the form $[a, b]$ or unbounded in one direction of the form $(-\infty, b]$ or $[a, \infty)$ or unbounded in both when it can only be $(-\infty, \infty)$ (i.e., R).

The C^0-continuity of functions leads to the definition of C^0 curves:

Definition 10.2. Three C^0 functions f, g and h defined on a closed interval T give the following C^0-*parametrization* of a space curve c:

$$x = f(t), \;\; y = g(t), \;\; z = h(t), \;\; t \in T$$

The curve c itself is the set of all image points $\{ (f(t), g(t), h(t)) : t \in T \}$ If a curve c has a C^0-parametrization, then it is said to be C^0-*continuous* or, simply, C^0.

Remark 10.9. An equivalent definition of a C^0 plane curve is obtained by dropping the "$z = h(t)$" term. Henceforth, we'll stick to 3D and give definitions only for space curves.

Example 10.9. The parametrization

$$x = t, \qquad y = \begin{cases} 0, & t \text{ is an integer} \\ 1, & t \text{ is not an integer} \end{cases}, \qquad t \in \mathrm{R}$$

given earlier is not C^0 as y is not a continuous function of t.

Example 10.10. The single point $(0, 0)$ defined implicitly by $x^2 + y^2 = 0$ is, strangely enough, a C^0 curve. For, it has the C^0-parametrization

$$x = 0, \; y = 0, \;\; t \in (-\infty, \infty)$$

on the plane, the constant functions $x = 0$ and $y = 0$ being continuous.

Example 10.11. All the parametrizations given in Example 10.2, except for the hyperbola, are C^0. The problem with the hyperbola is that its parameter space is not a (single) closed interval as we require. See the next exercise.

Exercise 10.23. Parametrize either of the two wings of the hyperbola of Example 10.2(e) so that each is a C^0 curve defined on a closed interval.

Example 10.12. Even though there are no actual parametrizations given there to go by, it's believable that, except for (f), (g) and (j), the one-dimensional objects of Figure 10.1 are each a C^0 curve. The problem with those three seems to be that each is composed of more than one trajectory.

Exercise 10.24. How about the astroid of Exercise 10.2 and the Lemniscate of Gerono of Exercise 10.3? Are they C^0?

Exercise 10.25. Is the graph of the following function C^0?

$$y = \begin{matrix} 0, & x \leq 0 \\ 1, & x > 0 \end{matrix}$$

Exercise 10.26. Is the graph of the function $y = |x|$ C^0?

Because of the continuity conditions, a C^0 curve is at least minimally well-behaved. However, it may still not fit our intuition of how a "nice" curve should be. For example, it's hard to think of the one-point $x^2 + y^2 = 0$ of Example 10.10 as a curve; the hexagon of Figure 10.1(c), though better, has six hard corners where it's not curvy or smooth.

To capture the notion of smoothness we ask that a curve not only possess a tangent at every point, but that the tangent turn continuously along the curve as well. This leads to the following two definitions:

Definition 10.3. A function f defined on a closed interval T is said to be C^1-*continuous* or, simply, C^1 if its derivative f^1 exists and is continuous on T; equivalently, if f^1 exists and is C^0 on T.

Definition 10.4. Three C^1 functions f, g and h defined on a closed interval T give the following C^1-*parametrization* of a curve c:

$$x = f(t), \;\; y = g(t), \;\; z = h(t), \;\; t \in T$$

The curve c itself is the set of all image points $\{ (f(t), g(t), h(t)) : t \in T \}$. If a curve c has a C^1-parametrization, then it is said to be C^1-*continuous* or, simply, C^1.

If, additionally, the three derivatives f^1, g^1 and h^1 never vanish together at any point of $[a, b]$, then the parametrization is said to be *regular*, and c is said to be a *regular curve.*

Because derivability implies continuity, C^1 curves and regular curves are C^0 as well. Regularity is nice enough for most CG applications. Why? Because regularity assures the smoothness of a curve c in the following sense:

(a) The tangent line to c at any point $c(t) = (f(t), g(t), h(t))$ exists. In fact, it is parallel to the vector $c^1(t) = (f^1(t), g^1(t), h^1(t))$, which is non-zero because we know that the derivatives of the parameter functions do not vanish simultaneously (see Figure 10.16(a)). The existence of a tangent line everywhere on c means that it has a well-defined *direction* at every point.

(b) Since f^1, g^1 and h^1 are continuous, $c^1(t) = (f^1(t), g^1(t), h^1(t))$ is continuous along c, which means that, not only does the tangent line exist at all points of c, it turns continuously along c as well. In other words, c cannot have a corner where its direction changes abruptly as in Figure 10.16(b) or the hexagon.

The upshot is that a regular curve appears smooth when drawn.

Note: We have used the term "smooth" as an informal descriptor. There are technical definitions of a "smooth function" and a "smooth curve" which will come up shortly.

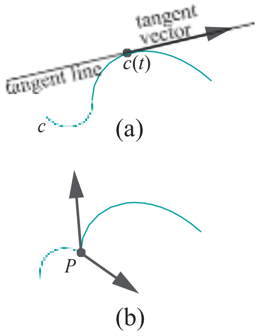

Figure 10.16: (a) A smooth curve (b) A non-smooth curve with a corner at P where the tangent changes direction abruptly.

It's precisely the non-vanishing property of $c^1(t)$ which is not guaranteed by mere C^1-continuity, as opposed to regularity, as we see in the following example.

Example 10.13. The astroid of Exercise 10.2 has parametric equations

$$x = \cos^3 t, \;\; y = \sin^3 t, \;\; t \in [0, 2\pi]$$

As $x = \cos^3 t$ and $y = \sin^3 t$ are continuous functions of t, the astroid is C^0. Now

$$\frac{dx}{dt} = -3\cos^2 t \sin t, \quad \frac{dy}{dt} = 3\sin^2 t \cos t$$

which are continuous functions of t as well, proving that the astroid is C^1 too. However, as both $\frac{dx}{dt}$ and $\frac{dy}{dt}$ vanish at $t = 0, \frac{\pi}{2}, \pi$ and $\frac{3\pi}{2}$, the astroid is not regular. In fact, it has cusps at precisely these four parameter values. Intuitively, as well, one sees that a point traveling along the astroid has to abruptly reverse direction on reaching a cusp.

Exercise 10.27. How about the Lemniscate of Gerono of Exercise 10.3? Is it C^0, C^1, regular?

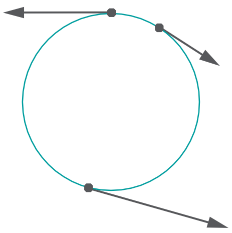

Figure 10.17: Tangent vectors to a circle.

The (non-zero) vector $c^1(t) = (f^1(t), g^1(t), h^1(t))$ is called a *tangent vector* to a regular curve $c(t) = (f(t), g(t), h(t))$. We say *a* tangent vector because any non-zero multiple of $c^1(t)$, i.e., a vector collinear with it, is tangent at $c(t)$ as well. For example, Figure 10.17 shows tangent vectors, intentionally drawn of varying lengths and inconsistently oriented, at three points of a circle.

Example 10.14. Consider the helix given by the parametrization

$$x = \cos t, \ y = \sin t, \ z = t, t \in \mathrm{R}$$

A tangent vector at the point $(\cos t, \sin t, t)$ of the helix is by differentiation $(-\sin t, \cos t, 1)$, which never vanishes, so the helix is regular.

Exercise 10.28. The stationary curve $x^2 + y^2 = 0$, $t \in (-\infty, \infty)$, which is just the point $(0, 0)$, we saw earlier to be C^0. Is it C^1? Regular?

Exercise 10.29. What about the hexagon of Figure 10.1(c)? Is it C^0? C^1? Imagine a parametrization for it by "stringing" together parametric equations for its straight sides.

Exercise 10.30. What is a tangent vector to the graph of the function $y = f(x)$ on the xy-plane at the point $(x, f(x))$? Assume f to be differentiable.

Exercise 10.31. Is the graph of the function

$$y = \begin{cases} x^3, & x < 0 \\ x^2, & x \geq 0 \end{cases}$$

C^0? C^1? Regular? The point of interest obviously is the origin.

Exercise 10.32. (Programming) Animate the non-regularity of the astroid. In particular, draw the asteroid and animate its tangent vector, moving along the curve with changing t, as an arrow from $(\cos^3 t, \sin^3 t)$ to $(\cos^3 t - 3\cos^2 t \sin t, \ \sin^3 t + 3\sin^2 t \cos t)$.

The tangent vector shrinks to zero at each cusp and grows again as it leaves the cusp.

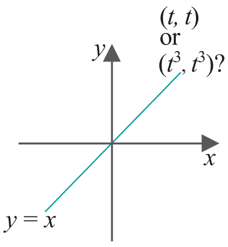

Figure 10.18: Good and bad parametrizations.

It is important to keep in mind that a curve is regular (or C^0, or C^1) *if* there is *some* parametrization according to the respective definition. For example, the curve c on the plane given by the parametric equations

$$x = y = t, \quad t \in (-\infty, \infty) \tag{10.10}$$

is regular as $c^1(t) = (1, 1)$ for all t. (Yes, it's the straight line $y = x$ drawn in Figure 10.18.)

However, the same straight line is defined by the cubic equations

$$x = y = t^3, \quad t \in (-\infty, \infty) \tag{10.11}$$

but now regularity is lost at the origin (verify)!

In fact, to finesse the issue of finding the "best" parametrization, mathematical texts often define a curve to be the set of parameter functions itself, rather than the image, so, e.g., (10.10) and (10.11) would actually represent different curves, thus avoiding ambiguity over continuity.

If the reader is now wondering, no, there is no parametrization which will make either the hexagon or the astroid regular, though we'll not try to prove these facts.

The following intuitive proposition suggests how two regular curves can join end to end so that their union is regular.

Proposition 10.1. *If two regular curves c_1 and c_2 meet at the point P, which is an endpoint of both, and if their tangent vectors at P are collinear, then the curve $c_1 \cup c_2$ is regular as well (Figure 10.19).*

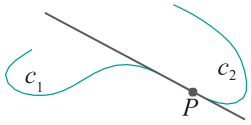

Figure 10.19: Two regular curves which share a tangent line at a common endpoint join to make one regular curve.

Proof. We leave it to the reader.

Hint : One must find a regular parametrization for the union $c_1 \cup c_2$. Change the parametrization of one of the curves, say c_1, from $t \mapsto c_1(t)$ to $t \mapsto at \mapsto c_1(at)$, choosing the constant a so that c_1's tangent vector at P becomes identical to that of c_2 (such rescaling of the parameter necessitates that the parameter interval be resized as well). Finally, "move" one parameter interval to abut the other.

Exercise 10.33. Prove that the two helixes

$$x = \cos t, \ \ y = \sin t, \ \ z = t, \ \ t \in [0, 10\pi]$$

and

$$x = 2 + \cos t, \ \ y = -\sin t, \ \ z = t - \pi, \ \ t \in [\pi, 10\pi]$$

meet at their common endpoint $(1, 0, 0)$, corresponding to $t = 0$ of the first curve and $t = \pi$ of the second, and share there a tangent vector. Can you come up with a single parametrization for the union of the two?

We can loosen up the definition of regularity to be a bit more inclusive.

Definition 10.5. A curve c is said to be *piecewise regular* if it can be made by sequentially joining a finite number of regular curves *end to end*.

In other words, a piecewise regular curve is regular except, possibly, for a finite number of corners inside it.

Example 10.15. Of those 1D objects depicted in Figures 10.1, the hexagon (c) is piecewise regular but not regular, while (f), (g) and (j) are not even piecewise regular. The others are all regular curves.

Exercise 10.34. What about the curves of Figures 10.3 and 10.4? Identify those that are piecewise regular but not regular.

We define next a regular one-dimensional object as composed of pieces that are each a regular curve, except that they are not required to be joined end to end as for a piecewise regular curve.

Definition 10.6. A *regular one-dimensional object* is a finite union of regular curves.

In other words, even though composed of pieces that are regular, a regular one-dimensional object may not have the property of a curve that it can be continuously traversed end to end.

Example 10.16. Figures 10.1(f), (g) and (j) are regular one-dimensional objects, but not piecewise regular curves. So are the letters 'K', 'Q' and 'X'. Of these six, note that all are *connected* except for Figure 10.1(j), which consists of three distinct components.

We have the obvious proper inclusions

$$\text{regular curves} \subset \text{piecewise regular curves} \subset \text{regular 1D objects}$$

Remark 10.10. Curves arising in real life – strings, wires, rubber bands, edges of a car or aircraft – are almost invariably piecewise regular, if not regular. Likewise, one-dimensional objects we see around us are almost all regular one-dimensional.

As expected, there are higher orders of continuity (C^0 is said to be zero-order, C^1 first-order) one can define as well, pretty much in the obvious manner:

Definition 10.7. A function f defined on a closed interval T is said to be C^m-*continuous* or, simply, C^m, where $m \geq 1$, if all of its derivatives of order m and less exist and are continuous on T.

A function f that is C^m-continuous for all m, no matter how large, is said to be C^∞-*continuous* or, simply, C^∞. C^∞ functions are also called *smooth*.

Definition 10.8. Three C^m functions (m can be ∞ as well) f, g and h defined on a closed interval T give the following C^m-*parametrization* of a curve c:

$$x = f(t),\ \ y = g(t),\ \ z = h(t),\ \ t \in T$$

The curve c itself is the set of all image points $\{ (f(t), g(t), h(t)) : t \in T \}$. If a curve c has a C^m-parametrization, then c is said to be C^m-*continuous* or, simply, C^m. If it has a C^∞-parametrization, then c is said to be *smooth*.

Remark 10.11. C^m-continuity implies C^n continuity for any $n < m$.

Remark 10.12. It is usual to assume regularity in addition to C^m-continuity, if $m \geq 1$.

Exercise 10.35. How continuous is a polynomial curve, in other words, what is the maximum order of continuity it possesses?

C^2 is about the highest order of continuity which can be distinguished visually. Even so, the lack of C^2-continuity is not as easy for the eye to catch as the lack of C^0 or C^1-continuity, which is, typically, obvious. The labeled continuity of all the curves of Figure 10.20, except the third, is probably easy to understand.

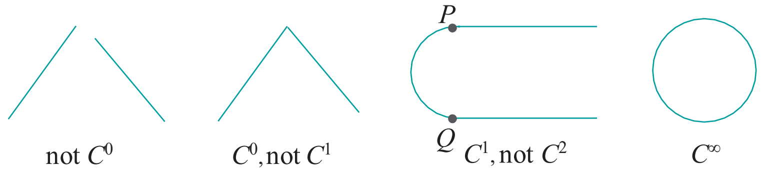

Figure 10.20: Various orders of continuity.

The third one is C^1-continuous but loses C^2-continuity at the two points P and Q where the half-circle meets straight segments, because the tangent stops turning abruptly at these two points, its rate of change dropping from uniform to zero.

An interesting application of C^2-continuity arises in planning the motion of a camera. We ask the reader to see this for herself in the following two exercises.

Exercise 10.36. Verify that the graph of the function (encountered earlier in Exercise 10.31)

$$y = \begin{array}{ll} x^3, & x < 0 \\ x^2, & x \geq 0 \end{array}$$

is not C^2 because of a second-order discontinuity at the origin.

Exercise 10.37. (Programming) Use gluLookAt() to simulate the view of a simple scene (populated, say, by spheres) from a camera moving along the graph of the preceding exercise and pointing always along its tangent. See Figure 10.21. Move the camera by uniformly incrementing its x-value at each time step.

The viewer perceives a jolt as the camera passes the origin. The reason is as follows. Even though the *path* of the camera is smooth, in that it is C^1, the *direction* of the camera, which is along the *tangent* to this path, does not turn smoothly past the origin because of the C^2-discontinuity there. Moreover, the location of the camera and its direction together determine the scene, so a discontinuity in either is echoed in the animation.

Bottom line: (Regular) C^1 is good enough for a curve to appear smooth, while smooth camera movement should be (regular) C^2.

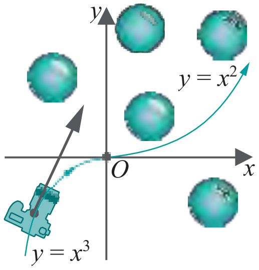

Figure 10.21: Camera moving along a path with a C^2-discontinuity at the origin O.

10.2 Surfaces

Two-dimensional objects are composed of surfaces. Analogously to the situation for one-dimensional objects, parts of a two-dimensional object which cannot be drawn exactly using triangles – OpenGL's fundamental 2D primitives as we know – must be approximated.

We'll discuss two-dimensional objects in an informal taxonomy ordered by increasing complexity from the point of view of drawing.

10.2.1 Polygons

The simplest two-dimensional object is the familiar polygon. By a polygon we shall always mean, unless stated otherwise, a *simple planar polygon*, i.e., one which lies on a plane and whose boundary consists of a single component which is a non-self-intersecting loop of straight line segments. All the polygons in Figure 10.22 are planar. However, (a) and (b) are non-simple polygons, while (c) and (d) are simple.

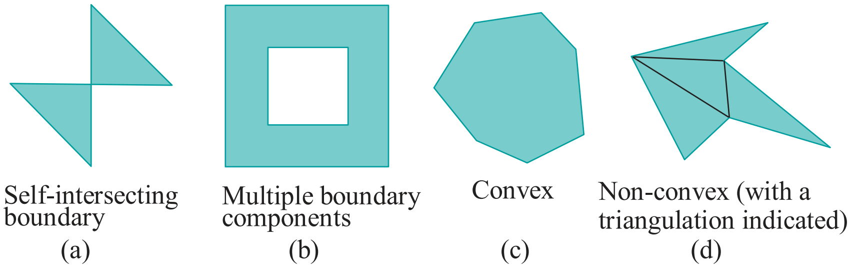
Self-intersecting boundary
(a)
Multiple boundary components
(b)
Convex
(c)
Non-convex (with a triangulation indicated)
(d)

Figure 10.22: (a) and (b) Non-simple planar polygons (c) and (d) Simple planar polygons (what we call polygons).

A convex polygon, e.g., Figure 10.22(c), can be drawn as a single GL POLYGON primitive. A non-convex polygon should be drawn after decomposing it into convex pieces, otherwise (recall from Section 8.3) it may not render correctly. Figure 10.22(d) is an example of a non-convex polygon decomposed into triangles, in other words, *triangulated* . It's recommended, in fact, that *all* polygons, convex or otherwise, be first triangulated and then drawn using GL_TRIANGLE* primitives (this being mandatory, in fact, in higher versions of OpenGL where the only 2D primitives are triangles or collections thereof).

10.2.2 Meshes

The next simplest kind of two-dimensional object is a *polygonal mesh* or, simply, *mesh*, also called a *polyhedral surface*. A mesh is a union of convex polygons satisfying the following two conditions:

1. Any two polygons in the union are either disjoint or intersect in a vertex of both or intersect in an edge of both.

   Note: This is a repetition of the condition for a collection of triangles to be a triangulation (see Definition 8.1) and motivated likewise to ensure deterministic rendering.

2. The neighborhood around each vertex is "sheet-like".

   We said the taxonomy would be informal. We'll not try to define what it means exactly for a neighborhood around a vertex to be sheet-like, leaving it instead to the reader's intuition with a few suggestive examples coming next.

Figure 10.23(a) is part of a hexagonal tiling of the plane with the shaded piece in the middle missing. Figure 10.23(b) is the surface of a glass with a hexagonal base and six rectangular walls. Figure 10.23(c) is the surface of an octahedron. Evident from the drawings themselves, all three objects are unions of convex polygons satisfying the first condition above. Moreover, for any vertex V belonging to any one of them, one can imagine fitting a small rubber sheet exactly onto the surface in an area around V, for an informal verification of the second condition above. Therefore, Figures 10.23(a)-(c) are meshes.

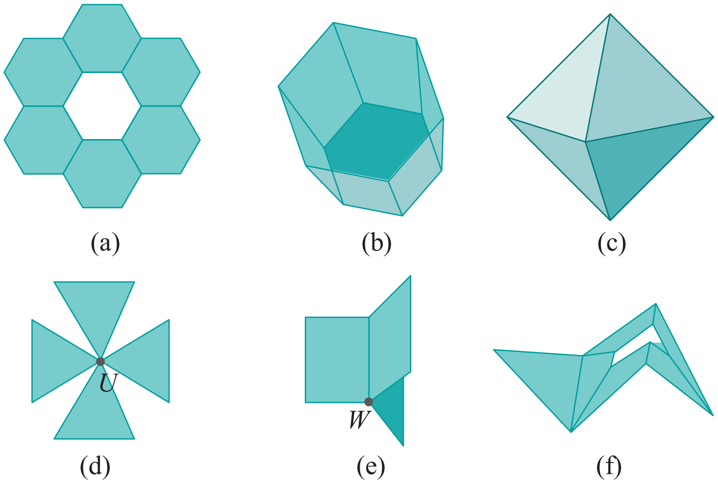

Figure 10.23: (a), (b) and (c) Meshes (d) and (e) Not meshes: parts around vertices U and W are not sheet-like (f) Your call.

Both Figures 10.23(d) and (e) clearly satisfy the first condition to be a mesh as well. However, Figure 10.23(d) fails the second condition because it's crimped at U– no rubber sheet, no matter how pliable, can be squeezed to a point. Figure 10.23(e), which consists of three rectangles sharing an edge, is not a mesh either because it has multiple panels around W. One would have to tear a sheet into pieces to cover a neighborhood of W.

Exercise 10.38. Is Figure 10.23(f) a mesh?

Remark 10.13. In mathematical terms condition 2 above is for a mesh to be a so-called topological manifold, which guarantees a certain respectability to shapes that a mesh can take. However, more math along these lines, though fascinating, is something a CG practitioner can comfortably live without.

The convex polygons comprising a mesh are its *faces*. The *boundary* of a mesh consists of those edges with a polygon on only one side. The mesh of Figure 10.23(a) has two boundary components (one inside bordering the missing hexagon and the other on the outside with three edges from each hexagon); that of Figure 10.23(b) has one boundary component (the rim of the glass); and that of Figure 10.23(c) has no boundary. A mesh with no boundary, a *closed* mesh as such is called, bounds a solid figure. For example, the closed mesh of Figure 10.23(c) bounds an octahedron.

From an OpenGL point of view, in fact, it's best the faces of a mesh be all triangles. Such a mesh is called a *triangular mesh*. Of course, any mesh can be made triangular by triangulating each face.

Drawing a mesh is, of course, simply a matter of drawing each of its polygonal faces. Again, the recommendation is that each face be triangulated first, if it's not already a triangle, and then drawn using GL_TRIANGLE* primitives. Because of the first condition for a mesh, the rendering is consistent whatever order the faces be drawn (for why, see the discussion in Section 8.1 of the reasons for the rules for a triangulation).

In fact, a moment's consideration of its primitives indicates that the *only* 2D objects OpenGL can draw *exactly* are meshes and unions of meshes. Others have to be approximated. So for the remaining two classes of 2D objects we will be trying to find good mesh approximations.

Example 10.17. Figures 10.23(d) and (e) are not meshes as we have seen. But are they a union of meshes?

Answer : Easily yes. For example, Figure 10.23(d) is the union of four meshes, each consisting of a single triangle.

10.2.3 Planar Surfaces

A planar surface is a generalization the first object in our 2D taxonomy, that being the polygon which lies on a plane and whose boundary consists of a single component which is a non-self-intersecting loop of straight line segments. A planar surface is simply a surface which lies on a plane and with no further restrictions. It may have multiple components as, too, may its boundary and the latter may be composed of both straight and curved parts. See Figure 10.24.

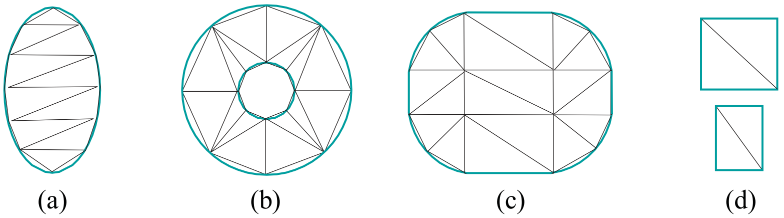

Figure 10.24: Planar surfaces with green boundary; the second one has one component but two boundary components; the last one has two components and two boundary components. The black edges belong to approximating meshes.

The drawing of a general planar surface can be reduced to that of drawing an approximating mesh by the following approach:

1. Apply the technique of Section 10.1.3 to make polyline approximations of the curved edges on the surface's boundary. Together with the boundary's existing straight edges, these polylines then bound a (possibly, non-simple) planar polygon, or a union of such if there are multiple components, approximating the surface.

2. Triangulate the approximating polygon(s). The result is a triangular mesh approximation of the surface.

The black edges in Figures 10.24(a)-(d) clarify the approach.

Exercise 10.39. (Programming) Draw a rounded rectangle as in Figure 10.24(c).

Exercise 10.40. (Programming) Draw a likeness in wireframe of the chair in Figure 10.25.

First of all, assume the panels to be all of zero thickness. So, for example, the seat is a flat rounded quad, while all four legs are bow-shaped planar surfaces. The only part that's evidently not planar, even at zero thickness, is the back rest, but it's not hard to approximate if one doesn't mind stealing a part slice from the hemisphere of Chapter 2. Be sure to use the symmetries: the two front legs are identical, as are the two (longer) back legs, so make only one of each.

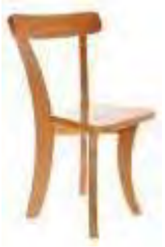

Figure 10.25: Wooden chair.

10.2.4 General Surfaces

More general surfaces, which may be neither planar nor a union of polygons, are drawn by approximation by triangular meshes as well. But, let's see first how a general surface s is specified, harking back to the specification of curves in Sections 10.1.1 and 10.1.2. An *implicit specification* consists of an equation

$$F(x, y, z) = 0 \tag{10.12}$$

such that points of the surface s are those whose coordinates (x, y, z) satisfy this equation.

Note: The logic here is the same as in Section 10.1.2, the one equation $F(x, y, z) = 0$ reducing the dimension of 3-space to the two of a surface.

A *parametric*, or *explicit*, *specification* consists of three equations

$$x = f(u, v), \ \ y = g(u, v), \ \ z = h(u, v), \ \text{where} \ (u, v) \in W \tag{10.13}$$

the parameter space W being a subset of the plane R^2. In this case, the points of s are those whose coordinates (x, y, z) satisfy $x = f(u, v)$, $y = g(u, v)$ and $z = h(u, v)$, for some value of $(u, v) \in W$. There are two parameter variables for a surface, versus one for a curve, because it is of dimension two.

The point $(f(u, v), g(u, v), h(u, v))$ on the surface s is often denoted $s(u, v)$.

Example 10.18. The (infinitely long circular) cylinder with its axis along the z-axis, and a circular cross-section of radius 1, is given by the implicit equation

$$x^2 + y^2 - 1 = 0$$

It's also given by the parametric equations

$$x = \cos u, \ y = \sin u, \ \ z = v, \ \ (u, v) \in [-\pi, \pi] \times (-\infty, \infty)$$

where the parameter space is an infinitely long rectangular subset of the plane.

Figure 10.26 shows a finite part of the parameter space, namely, the rectangle bounded by the lines $u = \pm\pi$ and $v = \pm 1$, as well as the corresponding part of the cylinder.

Again, as we did for a curve, one can imagine $s(u, v) = (f(u, v), g(u, v), h(u, v))$ as lifting and shaping the plane rectangle on the left of Figure 10.26 into the cylinder.

If the parameter variables are u and v, then the image on the surface s, of a straight line $v = \beta$ in the parameter space, is a curve, denoted $s(v = \beta)$, called a *u-parameter curve* of s; in other words, a u-parameter curve is traced on s by fixing the parameter v and varying u. Similarly, the image $s(u = a)$ on s, of the line $u = a$, is called a *v-parameter curve*.

The u-parameter curves of the cylinder of the preceding example are circles, while the v-parameter curves are vertical straight lines. One curve of either class is shown on the right of Figure 10.26.

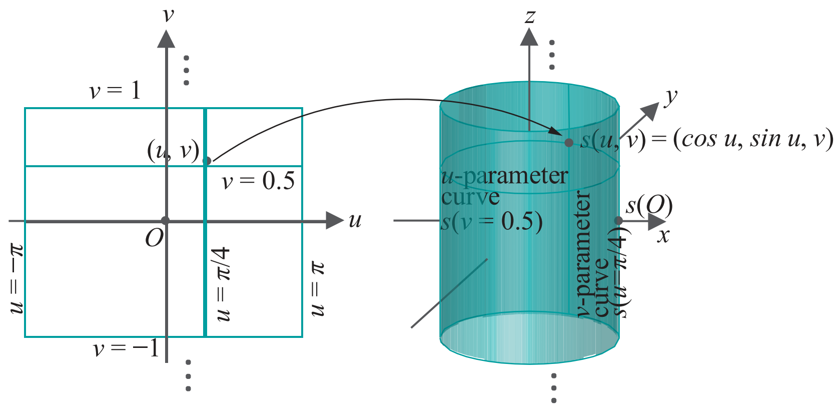
v
v = 1
(u, v)
v = 0.5
u
O
u = −π
u = π/4
u = π
v = −1
z
y
s(u, v) = (cos u, sin u, v)
u-parameter curve s(v = 0.5)
s(Q)
x
v-parameter curve s(u=π/4)

Figure 10.26: Parametric mapping of a circular cylinder s.

One can imagine a surface s either as the union of its u-parameter curves $s(v=\beta)$ as β varies, or the union of its v-parameter curves $s(u=a)$ as a varies, each over its respective range. For example, the infinite cylinder of the preceding example is the union of its u-parameter circles as the corresponding parameter β varies in $-\infty(\infty)$, while the finite part depicted in Figure 10.26 is the union as β varies in $[-1, 1]$. Saying it more graphically, the infinite cylinder is *swept* by its u-parameter circle as β changes from $-\infty$ to ∞. Complementarily, it's swept by its v-parameter straight lines as a varies from $-\pi$ and π.

Exercise 10.41. The implicit equation $x^2 + y^2 = 1$ of the cylinder of the preceding example did not involve z at all. In fact, it's the equation of a circle on the xy-plane applied to 3-space. Generally, if the implicit equation of a plane curve is $F(x, y) = 0$, then what surface is represented by the same equation in 3-space?

10.2.5 Drawing General Surfaces

The strategy to approximate a surface is similar to that for a curve. However, instead of straight line segments approximating sub-arcs of a curve, triangles are used to approximate small patches of the surface and a triangular mesh the entire surface. We make the assumption that the parametric specification of a surface s is given as

$$x = f(u, v), \quad y = g(u, v), \quad z = h(u, v), \quad (u, v) \in W \tag{10.14}$$

where the parameter space W is the plane rectangle $[a, b] \times [c, d]$. Think then of the parametric equations as shaping the rectangle W from uv-space into s in xyz-space (Figure 10.26 shows a rectangle being morphed into a cylinder).

Sample W at the $(p+1)(q+1)$ points

$$(u_i, v_j), \quad 0 \le i \le p, \quad 0 \le j \le q$$

of a *rectangular sample grid* where

$$a = u_0 < u_1 < \ldots < u_p = b$$
$$c = v_0 < v_1 < \ldots < v_q = d$$

The *mapped sample*

$$s(u_i, v_j), \quad 0 \le i \le p, \quad 0 \le j \le q$$

of $(p+1)(q+1)$ points of s are used as vertices of a triangular mesh approximation of s. This mesh consists of the following $2pq$ triangular faces:

$$s(u_i, v_{j+1})\, s(u_i, v_j)\, s(u_{i+1}, v_{j+1}) \text{ and } \quad s(u_{i+1}, v_{j+1})\, s(u_i, v_j)\, s(u_{i+1}, v_j),$$

for $0 \leq i \leq p-1$, $0 \leq j \leq q-1$. (Note that ABC denotes the triangle with vertices at A, B and C.)

Each mesh face approximates a patch of the surface. In particular, the face with corners at the images of the vertices of a grid triangle approximates the image of that triangle on the surface. Spelling this out for the two triangles listed above: the face $s(u_i, v_{j+1})\ s(u_i, v_j)\ s(u_{i+1}, v_{j+1})$ approximates the patch $s(\ (u_i, v_{j+1})\ (u_i, v_j)\ (u_{i+1}, v_{j+1}))$ which is the image on s of the grid triangle $(u_i, v_{j+1})\ (u_i, v_j)\ (u_{i+1}, v_{j+1})$; likewise, the face $s(u_{i+1}, v_{j+1})\ s(u_i, v_j)\ s(u_{i+1}, v_j)$ approximates the patch $s(\ (u_{i+1}, v_{j+1})\ (u_i, v_j)\ (u_{i+1}, v_j))$.

It's easiest to understand this visually. Let's use again the circular cylinder

$$x = \cos u,\ \ y = \sin u,\ \ z = v,\ \ (u, v) \in [-\pi, \pi] \times [-1, 1]$$

from the previous example. Refer to Figure 10.27. Sample points in the parameter space are seen at the upper left and the corresponding mapped sample points on the cylinder at the upper right (here, $p = 6$ and $q = 4$). The triangles of the mesh along a band of the cylinder are shown at the upper right as well (for clarity, upright edges of the triangles are green, the others black).

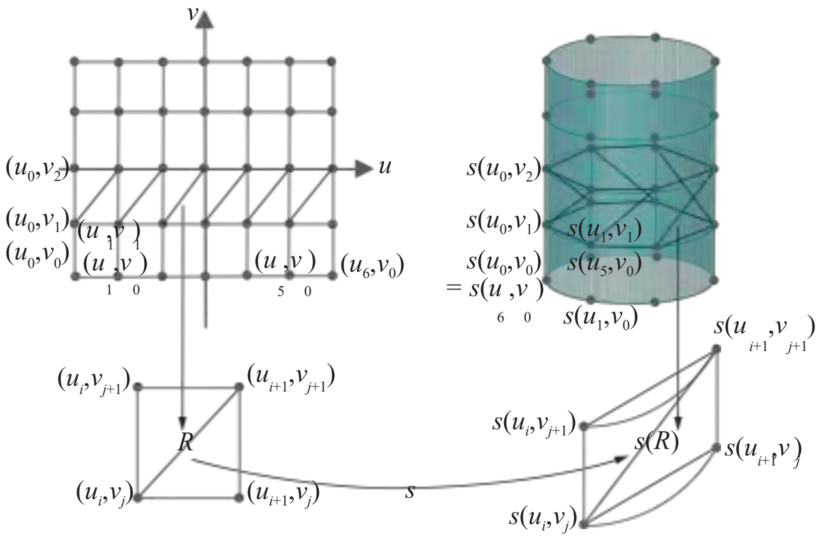

Figure 10.27: Triangular mesh approximation of a circular cylinder. *Upper*: A uniform sample grid on the parameter rectangle and its corresponding mapped sample on the cylinder. Only a few points are labeled. Vertices of a triangle strip on the rectangle maps to those of a strip approximating a band of the cylinder. *Lower*: A map from a grid rectangle to a patch of the cylinder.

The lower left and right diagrams are blow-ups, respectively, of a grid rectangle R, with corners at (u_i, v_{j+1}), (u_i, v_j), (u_{i+1}, v_j), (u_{i+1}, v_{j+1}), and the patch $s(R)$ of the cylinder which is its image. The two triangles $s(u_i, v_{j+1})\ s(u_i, v_j)\ s(u_{i+1}, v_{j+1})$ and $s(u_{i+1}, v_{j+1})\ s(u_i, v_j)\ s(u_{i+1}, v_j)$ of the mesh together approximate $s(R)$.

Cylinder

Figure 10.28: Screenshot of cylinder.cpp.

Experiment 10.2. Run cylinder.cpp, which shows a triangular mesh approximation of a circular cylinder, given by the parametric equations

$$x = f(u, v) = \cos u, \qquad y = g(u, v) = \sin u, \qquad z = h(u, v) = v,$$

for $(u, v) \in [-\pi, \pi] \times [-1, 1]$. Pressing arrow keys changes the fineness of the mesh. Press 'x/X', 'y/Y' or 'z/Z' to turn the cylinder itself. Figure 10.28 is a screenshot.
End

The approximating mesh of cylinder.cpp is constructed according to the method above. However, a minor technicality is that the parameter space of the program is taken to be the square $[0, 1] \times [0, 1]$, rather than the parameter rectangle $[-\pi, \pi] \times [-1, 1]$ of the definition, so the former has first to be scaled to the latter. In fact, see the definitions of the functions f, g and h in the program:

```
float f(int i, int j)
{
   return ( cos( (-1 + 2*(float)i/p) * PI ) );
}

float g(int i, int j)
{
   return ( sin( (-1 + 2*(float)i/p) * PI ) );
}

float h(int i, int j)
{
   return ( -1 + 2*(float)j/q );
}
```

The expression returned by f first applies the mapping $u \mapsto (-1+2u)\pi$ to scale $[0, 1]$ to $[-\pi, \pi]$, then applies cos; likewise, the expression returned by g applies $u \mapsto (-1+2u)\pi$, then sin; the expression returned by h applies $v \mapsto -1 + 2v$ to scale $[0, 1]$ to $[-1, 1]$. Figure 10.29 diagrams the scheme.

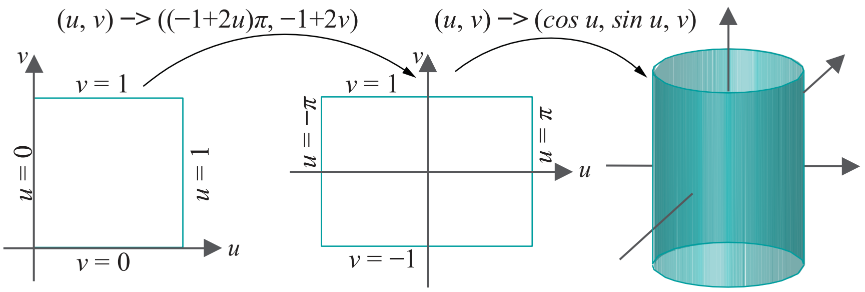

Figure 10.29: The composed mapping implemented in cylinder.cpp: first the parameter space is scaled, then mapped to the cylinder.

The most important part of cylinder.cpp's implementation of the drawing strategy of Section 10.2.5 is that the coordinate values $(i/p, j/q)$ run over a uniformly-spaced $(p + 1) \times (q + 1)$ grid of sample points in $[0, 1] \times [0, 1]$, as the integer argument i runs from 0 to p, and j from 0 to q. Correspondingly, $(f(i, j), g(i, j), h(i, j))$ run over the mapped sample points on the cylinder itself. These mapped sample coordinate values are written into a vertex array by the fillVertexArray() routine. Triangles corresponding to each row of the grid in parameter space are drawn as a single triangle strip in the drawing routine, so that there are q triangle strips consisting of $2p$ triangles each.

Let's revisit next a surface we had first drawn in Experiment 2.26 of Chapter 2 to put it into the perspective of our general drawing strategy.

Exercise 10.42. (Programming) Run hemisphere.cpp from Chapter 2, which draws a triangulated hemisphere. Figure 10.30 is a screenshot. Press 'p/P' and 'q/Q' to coarsen or refine the triangulation. The parametric equations of the hemisphere implemented in the program are

$$x = R\cos\varphi\cos\theta, \qquad y = R\sin\varphi, \qquad z = -R\cos\varphi\sin\theta,$$

for $0 \le \theta \le 2\pi$ and $0 \le \varphi \le \pi/2$.

Figure 10.30: Screenshot of hemisphere.cpp.

Does the program use the drawing strategy of cylinder.cpp above? *Yes, it does.* Accordingly, alter only the f, g and h function definitions of cylinder.cpp to obtain a program equivalent to hemisphere.cpp.

This is really useful: you can write down *any* set of parametric equations you like and implement the corresponding surface with the help of the template of cylinder.cpp. *All that changes in the program are the function definitions* f, g *and* h. If you have a shape in mind then, of course, first deduce appropriate functions.

Helical Pipe

Experiment 10.3. Without really knowing what to expect (honestly!) we tweaked the parametric equations of the cylinder to the following:

$$x = \cos u + \sin v,\ \ y = \sin u + \cos v,\ \ z = u, \qquad (u, v) \in [-\pi, \pi] \times [-\pi, \pi]$$

It turns out the resulting shape looks like a helical pipe – run helicalPipe.cpp. Figure 10.31 is a screenshot.

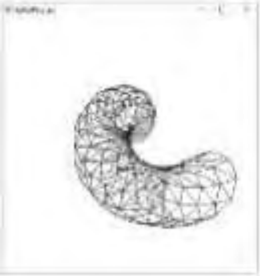

Figure 10.31: Screenshot of helicalPipe.cpp.

Functionality is the same as for cylinder.cpp: press the arrow keys to coarsen or refine the triangulation and 'x/X', 'y/Y' or 'z/Z' to turn the pipe.

Looking at the equations again, it wasn't too hard to figure out how this particular surface came into being. See the next exercise. End

Exercise 10.43. Why do the parametric equations of the preceding experiment create a helical pipe?
Hint: The equation of the surface is

$$s(u, v) = (\cos u + \sin v, \sin u + \cos v, u) = (\cos u, \sin u, u) + (\sin v,\ \cos v,\ 0)$$

Note now that $u \mapsto (\cos u, \sin u, u)$ gives a helix, while $v \mapsto (\sin v, \cos v, 0)$ a circle.

Exercise 10.44. (Programming) Changing only the functions f, g and h of cylinder.cpp, draw wireframe surfaces resembling those in Figure 10.32.

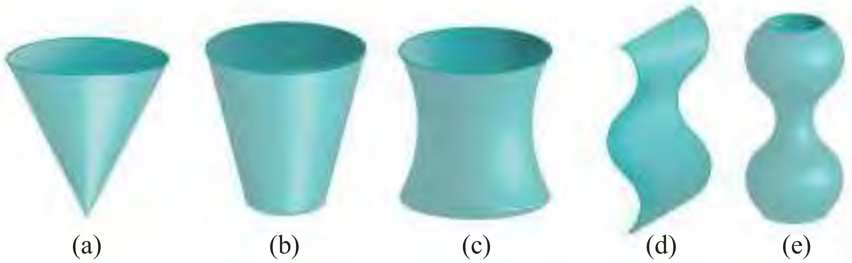

Figure 10.32: Draw these by modifying cylinder.cpp.

Exercise 10.45. (Programming) Nothing to do with drawing as such but practice in preparation for the newest OpenGL we'll be covering from Chapter 15, which no more has glBegin()-glEnd() type commands: replace the glBegin(GL_TRIANGLE_STRIP)-glEnd() loop in cylinder.cpp with *one* glMultiDrawElements(GL_TRIANGLE_STRIP, ...) call as in hemisphereMultidraw.cpp of Chapter 3. In fact, you might be able to use a good part of the code from the latter program.

10.2.6 Swept Surfaces

A powerful design method to create surfaces is by *sweeping* a curve. For example, consider the circular cylinder of Figure 10.33(a). One can think of it as the surface

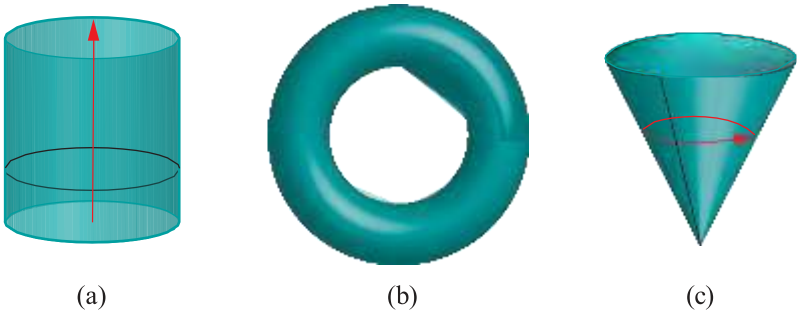

Figure 10.33: Swept surfaces: trajectories red, profiles black.

swept by a circle traveling upward, its center moving along a vertical line; precisely, the cylinder is the union of all copies of the circle as it travels.

The curve that sweeps the surface is called its *profile curve* or, simply, *profile*. The path followed by the profile is the *trajectory* . The trajectory is actually the path of a point on the profile, or some point fixed with respect to it, such as the center of the circle sweeping the cylinder. The surface itself is the *swept surface*.

A torus (Figure 10.33(b)) is swept by a circular profile itself traveling along a circular trajectory. When the trajectory is a circle, the swept surface is called a *surface of revolution*. A cone (Figure 10.33(c)) is a surface of revolution swept by a straight segment profile in a circular trajectory about the cone's axis.

When the trajectory is a straight segment, as in the case of the cylinder swept by a circle, the resulting surface is said to be an *extrusion*, or *extruded surface*, obtained by *extruding* the profile curve. In this case the profile is often called the *base curve*.

Exercise 10.46. Our description of a cylinder was as an extrusion of a circle. Can it be conceived of as a surface of revolution as well? If so, what are the profile and trajectory curves?

Exercise 10.47. How about a sphere, a hemisphere, an ellipsoid (egg shape) and (the surface of) a cube? Are they surfaces of revolution, extrusions, . . .?

The advantage of being able to describe a surface as a swept surface – and many familiar surfaces, in fact, are swept – is that its parametric equations are often, then, easy to deduce from those of its profile and trajectory curves. We see a few examples of this next.

Torus

Example 10.19. Let's compute the parametric equations of a torus described as follows. The profile is a circle c of radius r, whose center revolves along a circular trajectory C. C itself is of radius R, centered at the origin O and lying on the xy-plane. Each configuration of c, as it revolves, lies on a plane containing the z-axis and a radius of C. See Figure 10.34, where both the torus and a section through it are drawn.

A point P on the torus is specified by two angles θ and φ as follows:

(a) θ is the angle made with the x-axis by the radius OO' of C from its center (the origin) to the center of the configuration of c containing P.

(b) φ is the angle made by $O'P$, the radius of the configuration of c containing P , with the extension of OO'.

Let P' be the projection of P on the xy-plane and P'' be the projection of P' on the x-axis. Now, the x coordinate of P is

$$\begin{aligned} OP'' &= OP' \cos\theta = (OO' + O'P')\cos\theta = (OO' + O'P\cos\varphi)\cos\theta \\ &= (R + r\cos\varphi)\cos\theta \end{aligned}$$

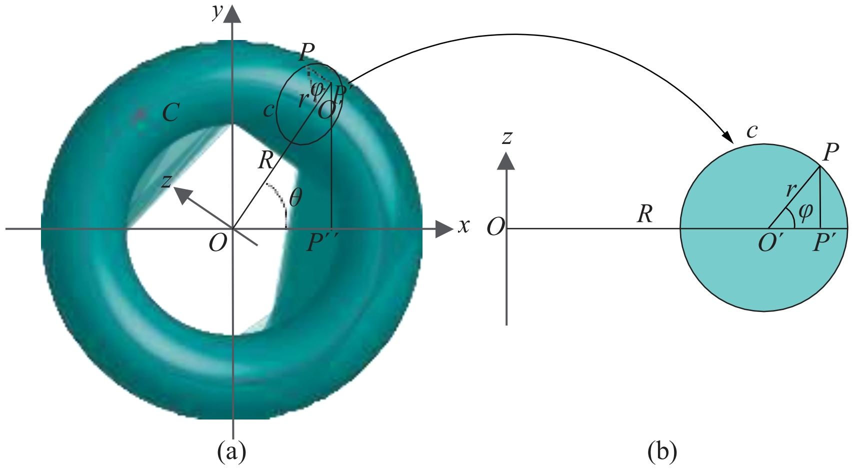

Figure 10.34: Computing parametric equations of a torus: (a) Profile circle c revolves along trajectory circle C (b) Sectional view of the left diagram along the plane containing the z-axis and OO^1.

and its y coordinate is

$$\begin{aligned} P^1P^{11} &= OP^1 \sin\theta = (OO^1 + O^1P^1)\sin\theta = (OO^1 + O^1P\cos\varphi)\sin\theta \\ &= (R + r\cos\varphi)\sin\theta \end{aligned}$$

and its z coordinate is

$$P^1P = O^1P\sin\varphi = r\sin\varphi$$

These give the parametric equations of the torus as

$$x = (R+r\cos\varphi)\cos\theta, \quad y = (R+r\cos\varphi)\sin\theta, \quad z = r\sin\varphi, \quad -\pi \le \theta, \varphi \le \pi \quad (10.15)$$

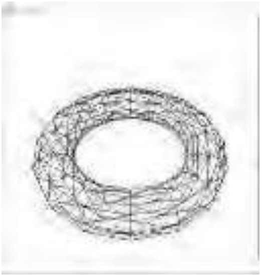

Figure 10.35: Screenshot of torus.cpp.

Experiment 10.4. Run torus.cpp, which applies the parametric equations deduced above within the template of cylinder.cpp (simply swapping the new f, g and h function definitions into the latter program). The radii of the circular trajectory and the profile circle are set to 2.0 and 0.5, respectively. Figure 10.35 is a screenshot.

Functionality is the same as for cylinder.cpp: press the arrow keys to coarsen or refine the triangulation and 'x/X', 'y/Y' or 'z/Z' to turn the torus. End

Experiment 10.5. Run torusSweep.cpp, modified from torus.cpp to show the animation of a circle sweeping out a torus. Press space to toggle between animation and on and off. Figure 10.36 is a screenshot part way through the animation. End

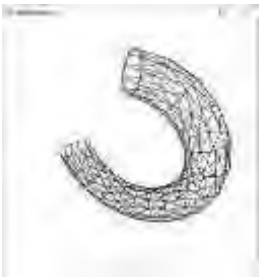

Figure 10.36: Screenshot of torusSweep.cpp.

Exercise 10.48. (Programming) Plump a *toroidal helix* – which is a helix coiling around a torus (Figure 10.37(a)) – into a pipe (Figure 10.37(b)). Allow the user to choose the number of times the pipe coils before closing. No need to draw the torus itself.

Suggested approach: Begin by using the parametric equations of the torus itself as determined in Example 10.19, namely,

$$x = (R + r\cos\varphi)\cos\theta, \quad y = (R + r\cos\varphi)\sin\theta, \quad z = r\sin\varphi, \quad -\pi \le \theta, \varphi \le \pi$$

to find those for the toroidal helix.

The torus, being a surface, has the two degrees of freedom represented by θ and φ. For a curve lying on it, φ should depend on θ, leaving only a single degree of freedom. The function $\varphi = n\theta$ yields a helix coiling n times around the torus before closing.

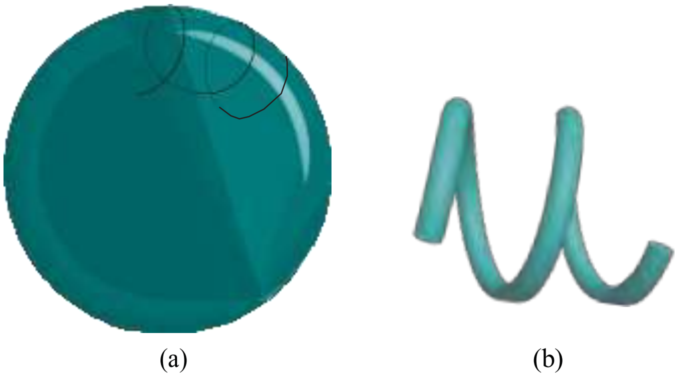

Figure 10.37: (a) Part of a toroidal helix (b) Part of a toroidal helix pipe.

Substituting, then, for φ in the equation above, one gets the parametric equations of a toroidal helix:

$$x = (R + r\cos(n\theta))\cos\theta,\ \ y = (R + r\cos(n\theta))\sin\theta,\ \ z = r\sin(n\theta),\ -\pi \leq \theta \leq \pi$$

To plump the toroidal helix into a pipe, observe that the pipe is swept by a circle c traveling along the toroidal helix; Experiment 10.3 might help here too.

Exercise 10.49. (Programming) For the mathematically inclined, a fun programming exercise is to draw a (p, q)-*torus knot*, where the user specifies p and q. You may have to look up torus knots – they are not hard at all though. The output of this program can be beautiful, especially for large p and q.

Table

We'll draw next a table as the surface of revolution swept by revolving a profile curve c about the y-axis. The profile c is a polygonal line composed of seven segments starting at the point A and ending at B, as shown in Figure 10.38(a), where it currently lies on the xy- plane. The trajectory of any point of c is a circle centered on the y-axis.

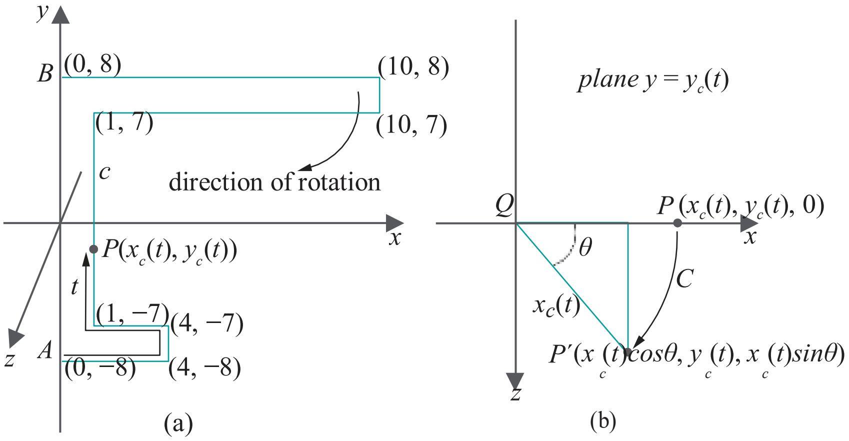

Figure 10.38: (a) Table's profile curve lying on the xy-plane with the z-coordinates, all 0, not written (b) A point on the profile curve after a rotation θ CW about the y-axis.

We'll parametrize c first by using the length t along c measured from A to P as the parameter value for a point P on c. Accordingly, the x coordinate $x_c(t)$ of a point with parameter value t is given below, as can be verified from a straightforward reading of Figure 10.38(a).

$$x_c(t) = \begin{cases} t, & 0 \le t \le 4 \\ 4, & 4 \le t \le 5 \\ 9 - t, & 5 \le t \le 8 \\ 1, & 8 \le t \le 22 \\ t - 21, & 22 \le t \le 31 \\ 10, & 31 \le t \le 32 \\ 42 - t, & 32 \le t \le 42 \end{cases}$$

Likewise, the y coordinate $y_c(t)$ is given by:

$$y_c(t) = \begin{cases} -8, & 0 \le t \le 4 \\ t - 12, & 4 \le t \le 5 \\ -7, & 5 \le t \le 8 \\ t - 15, & 8 \le t \le 22 \\ 7, & 22 \le t \le 31 \\ t - 24, & 31 \le t \le 32 \\ 8, & 32 \le t \le 42 \end{cases}$$

When c revolves an angle of θ clockwise about the y-axis from its start configuration on the xy-plane, then a point P on c with coordinates $(x_c(t), y_c(t), 0)$ rotates an angle of θ on a circle on the plane $y = y_c(t)$, centered at $Q = (0, y_c(t), 0)$ to a new point P^1. See Figure 10.38(b) where C is part of the circular trajectory of P. Since $|QP^1| = |QP| = |x_c(t)|$, the coordinates of P^1 are $(x_c(t) \cos \theta, y_c(t), x_c(t) \sin \theta)$.

Therefore, parametric equations for the table are

$$x = x_c(t) \cos \theta, \quad y = y_c(t), \quad z = x_c(t) \sin \theta, \quad 0 \le t \le 42 \text{ and } -\pi \le \theta \le \pi \quad (10.16)$$

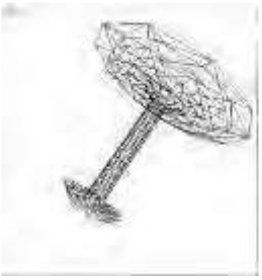

Figure 10.39: Screenshot of table.cpp.

Experiment 10.6. The preceding equations are implemented in table.cpp, again using the template of cylinder.cpp. Press the arrow keys to coarsen or refine the triangulation and 'x/X', 'y/Y' or 'z/Z' to turn the table. See Figure 10.39 for a screenshot of the table.

Note that the artifacts at the edges of the table arise because sample points may not map exactly to corners $(0, -8), (4, -8), \dots, (0, 8)$ of the profile drawn in Figure 10.38(a) – which can be avoided by including always t values 0, 4, 5, 8, 22, 31, 32 and 42 in the sample grid. End

Exercise 10.50. (Programming) Modify table.cpp to eliminate the artifacts at the edges in the manner suggested above.

Doubly-Curled Cone

Next is an experiment where the alignment of the profile curve varies as it travels along its trajectory. We want to make a "doubly-curled" cone, much like a cone made by curling a sheet of paper so that the edges don't meet, but that one wraps inside the other.

Let's write first the parametric equations for a plain-vanilla cone obtained by revolving a straight segment profile c of length 1 about the z-axis, with one end of c fixed at the origin, and with c making an angle of A with the xy-plane. We'll leave the reader to verify, using Figure 10.40(a), that the coordinates of the point P at a distance t from the origin along c, after the latter has revolved an angle of θ CCW from an original configuration on the xz-plane, are given by:

$$x = t \cos A \cos \theta, \quad y = t \cos A \sin \theta, \quad z = t \sin A, \qquad 0 \le t \le 1 \text{ and } 0 \le \theta \le 2\pi$$

To make the cone doubly-curled we'll bring the profile c in toward the z-axis as it rotates, by increasing its angle with the xy-plane. Moreover, we'll rotate c twice about the z-axis to make a double curl.

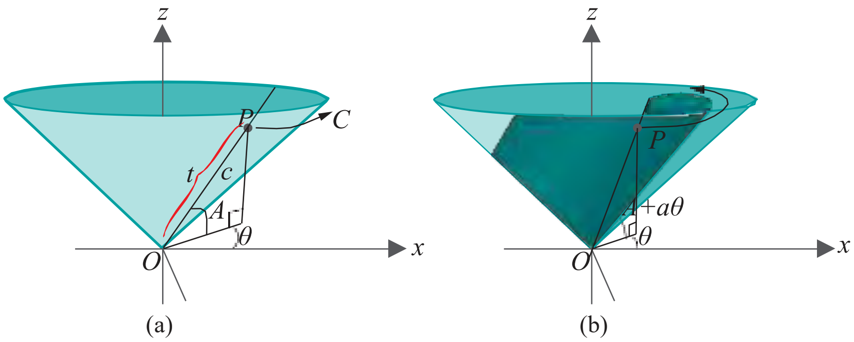

Figure 10.40: (a) A cone and (b) a doubly-curled cone as swept surfaces. The direction of the y-axis is into the page. $|OP| = t$.

A simple way to bring c in uniformly is to increment A, the angle that it makes with the xy-plane, by a multiple $a\theta$ of the amount of c's rotation. Figure 10.40(b) indicates the plan and it's straightforward to modify the parametric equations of the plain cone to write those of the doubly-curled:

$$x = t\cos(A + a\theta)\cos\theta,\ \ y = t\cos(A + a\theta)\sin\theta,\ \ z = t\sin(A + a\theta),$$

for $0 \le t \le 1$ and $0 \le \theta \le 4\pi$.

Experiment 10.7. The plan above is implemented in doublyCurledCone.cpp, again using the template of cylinder.cpp, with the value of A set to $\pi/4$ and a to 0.05. Press the arrow keys to coarsen or refine the triangulation and 'x/X', 'y/Y' or 'z/Z' to turn the cone. Figure 10.41 is a screenshot. End

Figure 10.41: Screenshot of doublyCurledCone.cpp.

Exercise 10.51. (Programming) Modify doublyCurledCone.cpp to change as well the length of the revolving segment c as it sweeps the cone.

Exercise 10.52. A *superellipsoid* is given generally by the implicit equation

$$\frac{x}{a}^{n} + \frac{\ }{b}^{n} + \frac{y}{c} = 1 \qquad (10.17)$$

where a, b, c and n are each a positive constant. It's an extension to 3D of the superellipse of Section 10.1.3.

In fact, a special type of superellipsoid is obtained as a surface of revolution by simply revolving a superellipse about either the x- or y-axis. Accordingly, deduce the parametric equations of the superellipsoid obtained by revolving the superellipse

$$\frac{x}{a}^{n} + \frac{\ }{b}^{y} = 1$$

about the y-axis.

Exercise 10.53. (Programming) Draw a superellipsoid obtained by revolving a superellipse, allowing the user to choose parameters.

Extruded Helix

For the record, here's a simple example of extrusion.

Experiment 10.8. Run extrudedHelix.cpp, which extrudes a helix, using yet again the template of cylinder.cpp. The parametric equations of the extrusion are

$$x = 4cos(10\pi u),\ \ y = 4sin(10\pi u),\ \ z = 10\pi u + 4v,\ 0 \le u, v \le 1$$

the constants being chosen to size the object suitably. As the equation for z indicates, the base helix is extruded parallel to the z-axis. Figure 10.42 is a screenshot. End

Figure 10.42: Screenshot of extrudedHelix.cpp.

Exercise 10.54. (Programming) Can you extrude the panels of the chair of Exercise 10.40, all of which you were then asked to draw flat, to make them now truly solid?

Drawing Projects

Here are real-life 3D projects for your drawing pleasure.

Exercise 10.55. (Programming) Draw the objects depicted in Figure 10.43: wine glass, vase, helmet with visor, extruded 'A', arch. Draw in wireframe.

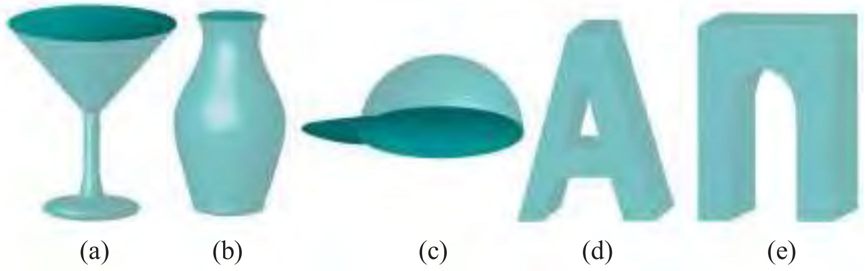

Figure 10.43: Stuff to draw.

Exercise 10.56. (Programming) Draw your name in 3D text.

Exercise 10.57. (Programming) Draw the six different chess pieces.

Exercise 10.58. (Programming) You have a chair from Exercise 10.40 (or Exercise 10.54) and a table from Experiment 10.6. Can you place these into animateMan1.cpp of Experiment 4.35, and get the man to walk up to the chair, sit and lean forward with his elbows on the table?

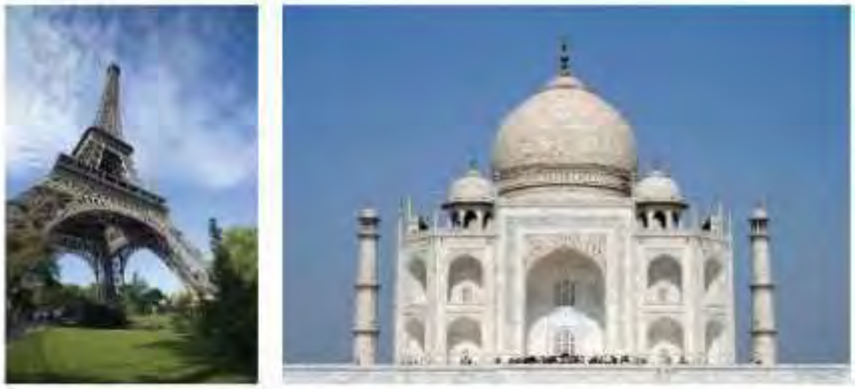

Figure 10.44: Model these?

Exercise 10.59. (Programming) Make a likeness of an interesting structure at the place where you live, e.g., building, bridge, multi-level highway crossing, train station, or some famous one, e.g., the Eiffel Tower or Taj Mahal shown in Figure 10.44. Ignore architectural details but try to be as faithful as possible to the large-scale geometry.
Hint: The Eiffel Tower and Taj Mahal may seem daunting at first, but there are multiple symmetries in each which can be exploited to simplify the design process.

Consider the Eiffel Tower. The base has four identical panels reminiscent of the arch of Exercise 10.55 a little earlier. As for the tower above the base, it has fourfold symmetry. Once a suitable profile curve has been chosen for one of the four identical edges of the tower – its designer Gustave Eiffel used an exponential equation in order for the structure to be able to withstand severe wind forces – it's a matter of placing this curve four times, rotated 90° each time, and filling identical wireframes between successive pairs. Don't forget display lists from Section 3.4 in your design process.

The Taj Mahal has arches as well and multiple symmetries and surfaces of revolution.

You can skip the rest of Section 10.2 on a first reading and go directly to Section 10.3 on Bézier curves and surfaces. The reason is that Sections 10.2.8-10.2.11 deal with special classes of surfaces which can be left to explore later at leisure, while 10.2.12 is about the theory of surfaces which can be deferred as well.

10.2.8 Ruled Surfaces

A *ruled surface* is a swept surface whose profile curve is a straight line. In other words, a ruled surface is traced by a straight line traveling through space. Each instance of the profile line is called a *ruling* . See Figure 10.45, which is an intuitively simple example; generally, the rulings need not be parallel as we'll soon see.

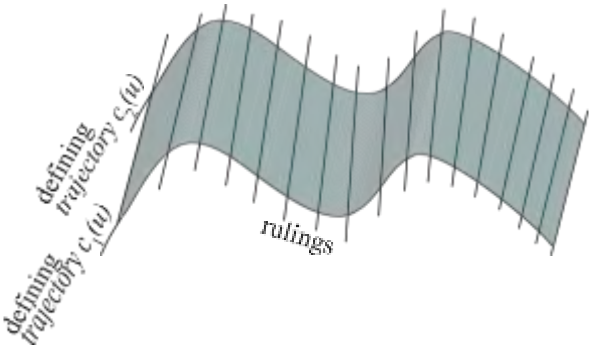

Figure 10.45: A ruled surface showing several rulings and two defining trajectories.

The parametrization of a ruled surface is particularly simple. Say that the paths of two distinct points on the profile line are $c_1(u)$ and $c_2(u)$, $u \in [a, b]$, respectively, each called a *defining trajectory* of the surface. A parametrization then is

$$s(u, v) = (1 - v)c_1(u) + vc_2(u), \qquad u \in [a, b], \; v \in (-\infty, \infty) \tag{10.18}$$

where u varies over the defining trajectories, and v over the (infinite) straight line through a pair of corresponding points on the two. If we want only the part of the surface *between* the defining trajectories, then we have to restrict the parameter space as follows:

$$s(u, v) = (1 - v)c_1(u) + vc_2(u), \qquad u \in [a, b], \; v \in [0, 1] \tag{10.19}$$

Various kinds of surfaces arise as ruled surfaces. Here are three interesting ones.

Bilinear Patches

A *bilinear patch* is a ruled surface whose defining trajectories c_1 and c_2 are straight line segments both. The bilinear patch itself lies between the two trajectories. See Figure 10.46. Suppose the endpoints of c_1 are p_1 and q_1, so that it can be parametrized $c_1(u) = (1 - u)p_1 + uq_1$, $0 \leq u \leq 1$, while the endpoints of c_2 are p_2 and q_2, and it is parametrized $c_2(u) = (1 - u)p_2 + uq_2$, $0 \leq u \leq 1$. Plugging these equations into (10.19) we get the equations of a bilinear patch:

$$s(u, v) = (1 - u)(1 - v)\, p_1 + u(1 - v)\, q_1 + (1 - u)v\, p_2 + uv\, q_2, \qquad u, v \in [0, 1] \tag{10.20}$$

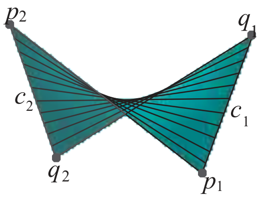

Figure 10.46: Bilinear patch.

Counter-intuitively, even though a bilinear patch is made of a family of straight rulings joining points again on two straight segments c_1 and c_2, it need not be flat, as the next experiment shows. In fact, it's flat only when c_1 and c_2 are coplanar; otherwise, it is a curved surface.

Experiment 10.9. Run bilinearPatch.cpp, which implements precisely Equation (10.20). Press the arrow keys to refine or coarsen the wireframe and ‘x/X’, ‘y/Y’ or ‘z/Z’ to turn the patch. Figure 10.47 is a screenshot. End

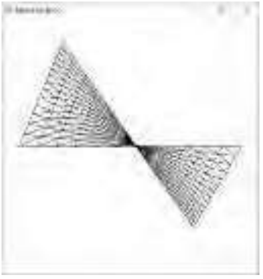

Figure 10.47: Screenshot of bilinearPatch.cpp.

Generalized Cones

A *generalized cone* is a ruled surface, one of whose defining trajectories is an arbitrary curve c, while the other is stationary, in other words, a single point p, which should not belong to c. The cone is said to be *over* c with *apex* at p. See Figure 10.48 for three examples. Unless the qualifier “generalized” is used, the curve c is typically presumed closed. Often, informally meant by the term cone is the familiar *right circular cone*, which is a cone over a circle c whose apex is located on the line which is through the center of c and perpendicular to its plane.

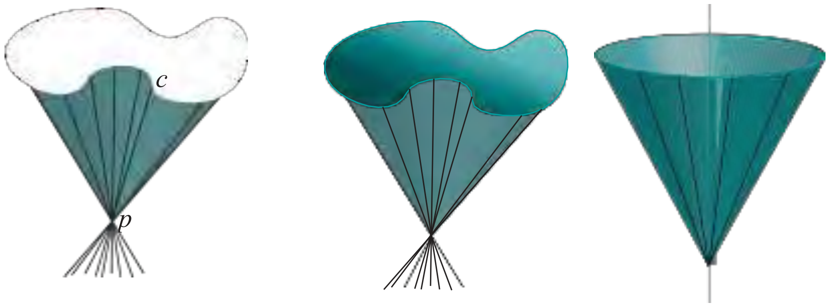

Generalized cone Cone (on a closed curve) Right circular cone

Figure 10.48: Generalized cones: (a) over a non-closed curve (b) over a closed curve (c) right circular cone.

The equation of the part of the generalized cone between its trajectories – a part like those depicted in Figure 10.48 – is obtained by plugging $c_1(u) = p$ for the trajectory stationary at the apex p, and $c_2(u) = c(u)$ for the other, into (10.19):

$$s(u, v) = (1 - v)p + vc(u), \qquad u \in [a, b], \;\; v \in [0, 1] \tag{10.21}$$

Evidently, all rulings pass through the apex p, at $v = 0$.

Exercise 10.60. (Programming) Draw a cone over the astroid of astroid.cpp.

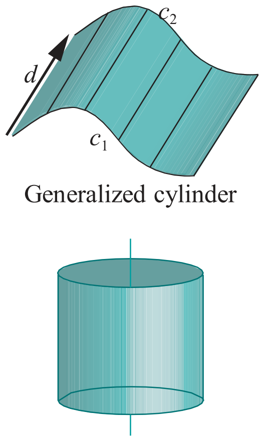

Generalized cylinder

Right circular cylinder

Figure 10.49: A generalized cylinder and a special case.

Generalized Cylinders

A *generalized cylinder* is a ruled surface whose defining trajectories c_1 and c_2 are translates of one another. See Figure 10.49. Most often, by a cylinder one means the familiar *right circular cylinder* , where c_1 and c_2 are circles whose centers are joined by a line perpendicular to the plane of both.

The equation for the generalized cylinder is obtained by writing the equation of one trajectory as $c(u)$ and the other as $c(u) + d$, where $u \in [a, b]$, and d is the vector translating the first trajectory to the second. Plugging these equations into (10.19) we get the generalized cylinder as

$$s(u, v) = (1 - v)c(u) + v(c(u) + d) = c(u) + vd, \qquad u \in [a, b], \;\; v \in [0, 1] \tag{10.22}$$

The rulings are evidently all parallel to the vector d.

Exercise 10.61. Are generalized cylinders the same as extrusions?

Exercise 10.62. (Programming) Draw a generalized cylinder using an astroid as a trajectory.

10.2.9 Quadric Surfaces

As we saw in 10.1.5, conics are curves on a plane given by a quadratic equation in two variables. *Quadric surfaces* or, simply, *quadrics*, are their generalization to one dimension higher. They are surfaces in 3D space given by a quadratic equation in *three* variables:

$$Ax^2 + By^2 + Cz^2 + Dyz + Ezx + Fxy + Px + Qy + Rz + H = 0$$

Excluding degenerate instances (e.g., $x^2 + y^2 + z^2 = 0$, which gives a single point) a quadric is of one of the nine kinds shown in Figure 10.50. In fact, any non-degenerate quadric can be transformed by translation and rotation to one of the normalized forms in the following table, corresponding each to one of those pictured in Figure 10.50.

Quadric	Implicit Equation
Ellipsoid	$\frac{x^2}{a^2} + \frac{y^2}{b^2} + \frac{z^2}{c^2} = 1$
Elliptic Paraboloid	$\frac{x^2}{a^2} + \frac{y^2}{b^2} - z = 0$
Hyperbolic Paraboloid	$\frac{x^2}{a^2} - \frac{y^2}{b^2} - z = 0$
Hyperboloid (1 sheet)	$\frac{x^2}{a^2} + \frac{y^2}{b^2} - \frac{z^2}{c^2} = 1$
Hyperboloid (2 sheets)	$\frac{x^2}{a^2} - \frac{y^2}{b^2} - \frac{z^2}{c^2} = 1$
Elliptic Cone	$\frac{x^2}{a^2} + \frac{y^2}{b^2} - \frac{z^2}{c^2} = 0$
Elliptic Cylinder	$\frac{x^2}{a^2} + \frac{y^2}{b^2} = 1$
Parabolic Cylinder	$y = ax^2$
Hyperbolic Cylinder	$\frac{x^2}{a^2} - \frac{y^2}{b^2} = 1$

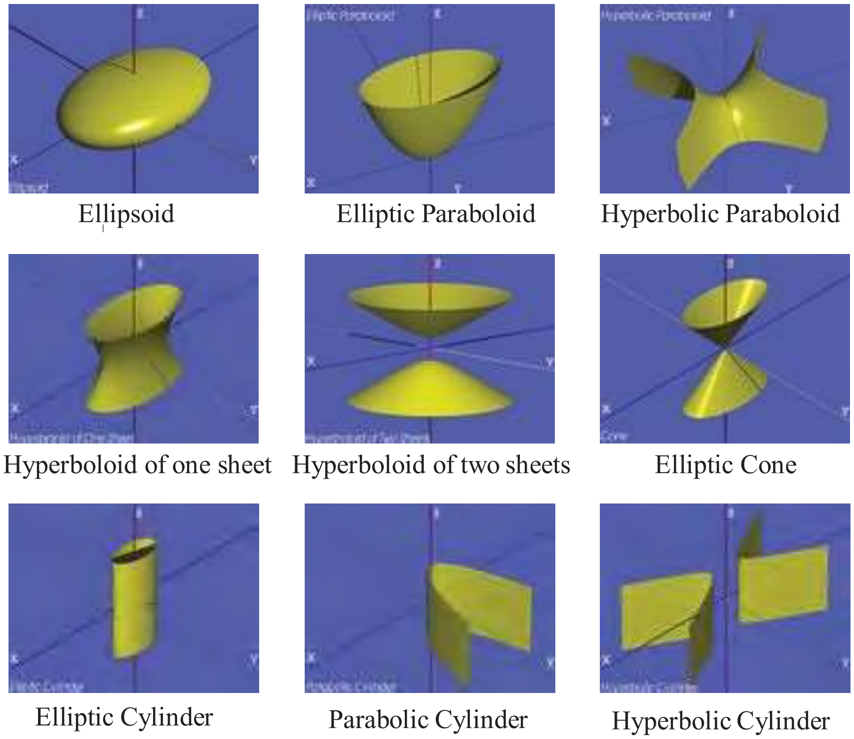
Ellipsoid
Elliptic Paraboloid
Hyperbolic Paraboloid
Hyperboloid of one sheet
Hyperboloid of two sheets
Elliptic Cone
Elliptic Cylinder
Parabolic Cylinder
Hyperbolic Cylinder

Figure 10.50: The nine non-degenerate quadric surfaces (from Wikimedia).

A sphere is, of course, a special case of an ellipsoid. The hyperbolic paraboloid, for an obvious reason, is often called a *saddle surface*. The three cylindrical quadrics along the bottom row are probably the least interesting, as they are merely extrusions of plane conics. Parametrization, both trigonometric and rational, of the quadrics are not hard to derive.

Example 10.20. Find both trigonometric and rational parametrizations of the ellipsoid.

Answer: We begin with the ellipsoid's implicit equation

$$\frac{x^2}{a^2} + \frac{y^2}{b^2} + \frac{z^2}{c^2} = 1$$

A trigonometric parametrization is

$$x = a\cos\theta\cos\varphi,\ y = b\sin\theta\cos\varphi,\ z = c\sin\varphi,\ \theta \in [-\pi, \pi],\ \varphi \in [-\pi/2, \pi/2]$$

while a rational one is

$$x = a\frac{1 - u^2 + v^2}{1 + u^2 + v^2},\ y = b\frac{2uv}{1 + u^2 + v^2},\ z = c\frac{2u}{1 + u^2 + v^2},\ u, v \in (-\infty, \infty)$$

with a singularity at $(-a, 0, 0)$.

Exercise 10.63. Find trigonometric and rational parametrizations of the elliptic paraboloid.

Remark 10.14. If $a = b$ in the equation of the elliptic paraboloid – the equation becomes $\frac{x^2}{a^2} + \frac{y^2}{a^2} - z = 0$ in this case – then it's actually a surface of revolution obtained from revolving a parabola around its axis. This special case of an elliptic paraboloid is called a *circular paraboloid*. It is the shape used in mirrors behind headlamps because light from a bulb placed at its focal point reflects in a parallel beam.

Drawing the quadrics is simple. We'll use a trigonometric parametrization to draw next the hyperboloid of one sheet.

Experiment 10.10. Run hyperboloid1sheet.cpp, which draws a triangular mesh approximation of a single-sheeted hyperboloid with the help of the parametrization

$$x = \cos u \sec v,\quad y = \sin u \sec v,\quad z = \tan v,\quad u \in [-\pi, \pi],\quad v \in (-\pi/2, \pi/2)$$

Figure 10.51(a) is a screenshot. In the implementation we restrict v to $[-0.4\pi, 0.4\pi]$ to avoid $\pm\pi/2$ where sec is undefined. End

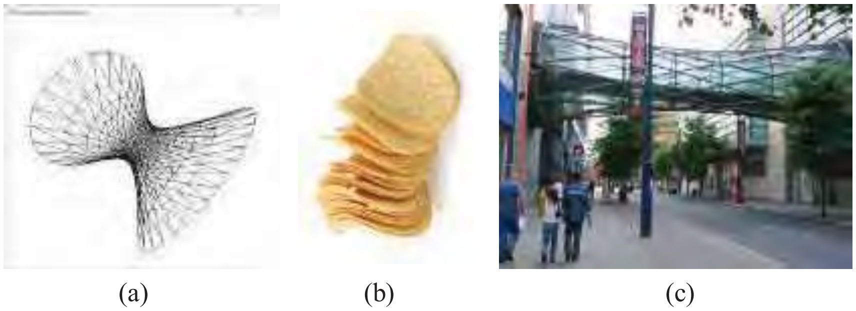
(a) (b) (c)

Figure 10.51: (a) Screenshot of hyperboloid1sheet.cpp (b) Edible hyperbolic paraboloids (c) Hyperboloid footbridge over Corporation Street in Manchester in England supported by its rulings (courtesy of Patrick Litherland).

It's interesting that a few of the non-degenerate quadrics are ruled surfaces as well and, therefore, traced by a straight line traveling through space. The ones on the bottom row of Figure 10.50 are evidently so. We'll prove a less obvious case.

Example 10.21. Show that the hyperbolic paraboloid is a ruled surface.

Answer: We'll work with the instance s given by the implicit equation

$$x^2 - y^2 = z$$

as setting the coefficients all equal to 1 simplifies calculations (without costing in generality). Write the equation as

$$(x+y)(x-y) = z$$

Setting $u = x+y$ and $v = x-y$ then leads to the following parametrization of s:

$$x = \frac{u+v}{2}, \quad y = \frac{u-v}{2}, \quad z = uv, \quad u, v \in (-\infty, \infty) \tag{10.23}$$

Now, a u-parameter curve of s is obtained by fixing $v = \beta$:

$$x = \frac{u+\beta}{2}, \quad y = \frac{u-\beta}{2}, \quad z = \beta u, \quad u \in (-\infty, \infty)$$

which is a straight line as x, y and z are all three linear in u. Therefore, s is swept by a straight line profile, particularly the u-parameter curve for $v = \beta$, as β varies, proving it is indeed ruled. Evidently, it's *doubly-ruled* , the u-parameter curves and v-parameter curves defining distinct symmetric families of rulings.

In fact, it gets even more interesting! Two defining trajectories for s can be obtained as the v-parameter curves corresponding to a couple of distinct values of u, because they intersect each u-parameter curve in a distinct pair of points. Accordingly, set u equal to 0 and 1 in Equation (10.23) to get, respectively, the equations

$$x = \frac{v}{2}, \quad y = -\frac{v}{2}, \quad z = 0, \quad v \in (-\infty, \infty)$$

and

$$x = \frac{1+v}{2}, \quad y = \frac{1-v}{2}, \quad z = v, \quad v \in (-\infty, \infty)$$

which are both straight lines. So a hyperbolic paraboloid is a ruled surface with straight-line defining trajectories, which means it's a bilinear patch as in Section 10.2.8.

Exercise 10.64. Prove that the single-sheeted hyperboloid is doubly-ruled. Figure 10.51(c) illustrates how this fact is applied to build a bridge – note the two sets of steel rulings and how they intersect in a grid. You likely have seen baskets woven in the shape of single-sheeted hyperboloids as well.

Exercise 10.65. (Programming) Animate a straight line segment sweeping out a single-sheeted hyperboloid.

10.2.10 GLU Quadric Objects

We are already familiar with several FreeGLUT library objects such as spheres, cubes and cones which are ready-to-use for 3D drawing. The OpenGL Utility Library GLU provides additional routines to create four kinds of so-called quadric objects: sphere, tapered cylinder, annular disc and partial annular disc. See Figure 10.52.

Experiment 10.11. Run gluQuadrics.cpp to see all four GLU quadrics. Press the left and right arrow keys to cycle through the quadrics and 'x/X', 'y,Y' and 'z/Z' to turn them. The images in Figure 10.52 were, in fact, generated by this program. End

Remark 10.15. It's a bit unfortunate that OpenGL chooses to render the quadrics quadrilateralized, rather than triangulated.

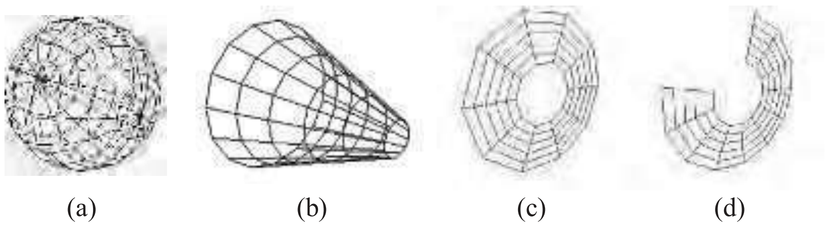

Figure 10.52: GLU quadrics: (a) Sphere (b) Tapered cylinder (c) Annular disc (d) Partial annular disc.

Here's how the syntax works (refer to Figure 10.53):

1. gluSphere(**qobj*, *radius*, *slices*, *stacks*)

   Draws a *sphere* of radius *radius* centered at the origin. The parameters *slices* and *stacks* determine the fineness of the quadrilateralization.

   Note: The parameter *qobj* in this case, and in the following, points to a quadric object.

2. gluCylinder(**qobj*, *baseRadius*, *topRadius*, *height*, *slices*, *stacks*)

   Draws a *tapered cylinder* with its axis along the z-axis, whose base is a circle of radius *baseRadius* lying on the $z = 0$ plane and whose top a circle of radius *topRadius* lying on the $z =$ *height* plane. If either *baseRadius* or *topRadius* is zero then the object is a cone; if these two parameters are equal it is a plain-vanilla (right circular) cylinder. The parameters *slices* and *stacks* determine the fineness of the quadrilateralization.

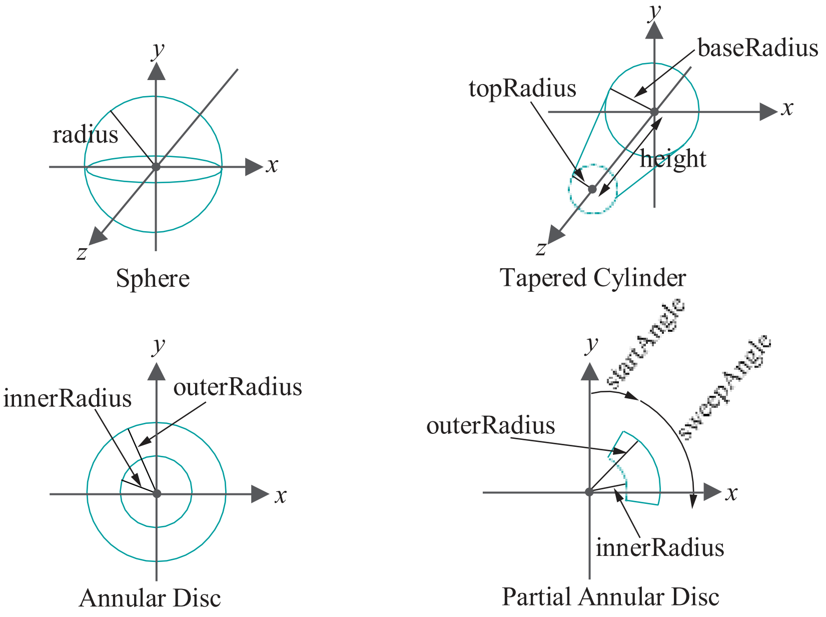

Figure 10.53: Defining the GLU quadrics.

3. gluDisk(**qobj*, *innerRadius*, *outerRadius*, *slices*, *rings*)

   Draws an *annular disc* centered at the origin and lying on the $z = 0$ plane, whose inner boundary is of radius *innerRadius* and outer boundary of radius *outerRadius*. The parameters *slices* and *rings* determine the fineness of the quadrilateralization.

4. gluPartialDisk(**qobj*, *innerRadius*, *outerRadius*, *slices*, *rings*, *startAngle*, *sweepAngle*)

   Draws a *partial annular disc*: precisely, the sector of the annular disc defined by gluDisk(**qobj*, *innerRadius*, *outerRadius*, *slices*, *rings*), starting from angle *startAngle* and ending at *startAngle* + *sweepAngle*, where either angle is measured clockwise (looking from the $+z$-direction) along the xy-plane starting from the y-axis.

GLU calls of the form gluQuadric*(**qobj*, *) determine various properties of the quadric. For example, the call gluQuadricDrawStyle(qobj, GLU LINE) causes the quadric to be rendered in wireframe.

Remark 10.16. The GLU quadrics are somewhat ambitiously named. Although they are each a part of one of the mathematical quadric surfaces described in the preceding section, they will hardly help in drawing the more complex ones.

10.2.11 Regular Polyhedra

To begin with here's a definition of a particular kind of polygon which should be familiar:

Definition 10.9. A *regular polygon* is a simple planar polygon whose sides are of equal length and which has equal interior angles at its vertices.

A regular polygon with n sides is convex and its vertices are spaced equally along a circle, called its *circumscribed circle*, at an angle of $2\pi/n$ apart (Figure 10.54). The larger the n, the more closely the polygon approximates its circumscribed circle (as we saw in circle.cpp in Chapter 2).

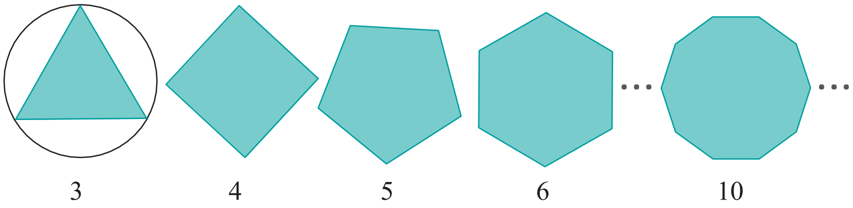

Figure 10.54: Regular polygons with number of sides indicated. The triangle shows its circumscribed circle.

Exercise 10.66. What is the interior angle at a vertex of an n-sided regular polygon?

Exercise 10.67. Show that if the condition "and which has equal interior angles at its vertices" is dropped from the definition of a regular polygon, then we could make one not belonging to the family of Figure 10.54.

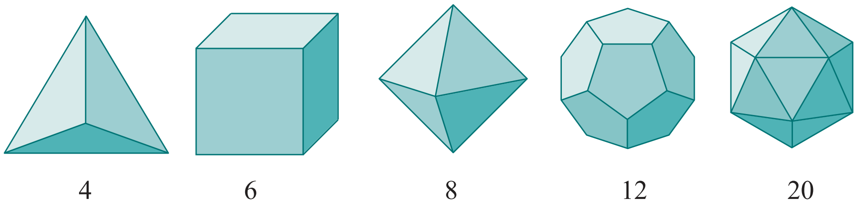

Figure 10.55: The five regular polyhedra with the number of faces indicated.

Regular polyhedra are a generalization of regular polygons to three dimensions. Here first is the definition of a polyhedron based on that of a polygonal mesh (see Section 10.2.2).

Definition 10.10. A *polyhedron* is a solid object whose boundary is a polygonal mesh (in other words, a solid whose faces are all convex polygons).

Definition 10.11. A *regular polyhedron* is a polyhedron all of whose faces are identical regular polygons.

Because of the symmetry constraints on their faces, there exist only five different regular polyhedra, ignoring difference in size. They are the *tetrahedron*, *hexahedron* (familiarly, *cube*), *octahedron*, *dodecahedron* and *icosahedron* in order of increasing number of faces. See Figure 10.55.

Geometric data for the five in numerical form is collected in the following table.

	Faces	Edges	Vertices	Edges of a face	Faces at a vertex
Tetrahedron	4	6	4	3	3
Hexahedron (cube)	6	12	8	4	3
Octahedron	8	12	6	3	4
Dodecahedron	12	30	20	5	3
Icosahedron	20	30	12	3	5

The hexahedron is bounded by squares, the dodecahedron by regular pentagons and the remaining three by equilateral triangles. The value (m, n) for a regular polyhedron, where m is the number of edges of a face and n the number of faces meeting at a vertex – the items in the last two columns of the table – is called its *Schläfli symbol*. The five different Schläfli symbols are (3, 3), (4, 3), (3, 4), (5, 3) and (3, 5), and each uniquely identifies a regular polyhedron. It's not an accident, as we'll see, that the reverse of each Schläfli symbol is another.

Remark 10.17. Regular polyhedra are also called *Platonic solids* because they were known to Plato, as recorded in his Timaeus dialogues. In fact, archeological finds suggest that these beautiful shapes were familiar to even earlier people.

Modeling Regular Polyhedra

There's an easy way to draw regular polyhedra using OpenGL: call them from the FreeGLUT library! All five are available as FreeGLUT objects.

Experiment 10.12. Run glutObjects.cpp, a program we originally saw in Chapter 3. Press the left and right arrow keys to cycle through the various FreeGLUT objects and 'x/X', 'y/Y' and 'z/Z' to turn them. Among other objects you see all five regular polyhedra, both in solid and wireframe. End

However, in case you are the hardy do-it-yourself type, what you need to know is in the following few pages.

Experiment 10.13. Run tetrahedron.cpp. The program draws a wireframe tetrahedron of edge length 2 2 which can be turned using the 'x/X', 'y/Y' and 'z/Z' keys. Figure 10.56 is a screenshot. End

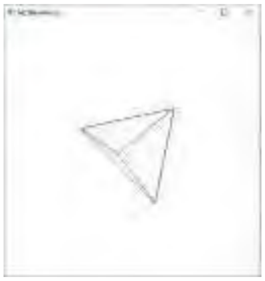

Figure 10.56: Screenshot of tetrahedron.cpp.

The coordinates of the vertices of the tetrahedron of tetrahedron.cpp, as well as the indices of the vertices comprising each of its triangular faces, are listed in the following two global arrays:

```
// Vertex coordinate vectors for the tetrahedron.
   static float vertices[] =
   {
        1.0,   1.0,   1.0, // V0
       -1.0,   1.0,  -1.0, // V1
        1.0,  -1.0,  -1.0, // V2
       -1.0,  -1.0,   1.0  // V3
   };
```

```
// Vertex indices for the four triangular faces.
static int triangleIndices[4][3] =
{
    {1, 2, 3}, // F0
    {0, 3, 2}, // F1
    {0, 1, 3}, // F2
    {0, 2, 1}  // F3
};
```

For example, the face $F0$ is a triangle with corners at the vertices $V1$, $V2$ and $V3$.

Here's similar data for a cube of edge length 2:

Cube

Vertex	Coordinates
$V0$	$(1, 1, 1)$
$V1$	$(1, 1, -1)$
$V2$	$(1, -1, -1)$
$V3$	$(1, -1, 1)$
$V4$	$(-1, 1, 1)$
$V5$	$(-1, 1, -1)$
$V6$	$(-1, -1, -1)$
$V7$	$(-1, -1, 1)$

Face	Vertices
$F0$	$(V3,\ V0,\ V1,\ V2)$
$F1$	$(V2,\ V1,\ V5,\ V6)$
$F2$	$(V6,\ V5,\ V4,\ V7)$
$F3$	$(V7,\ V4,\ V0,\ V3)$
$F4$	$(V1,\ V0,\ V5,\ V4)$
$F5$	$(V3,\ V2,\ V6,\ V7)$

You may be wondering why we bothered at all with the totally trivial cube. The reason is that a cube sets up modeling an octahedron by way of the beautiful relationship of *duality* between regular polyhedra.

Duality

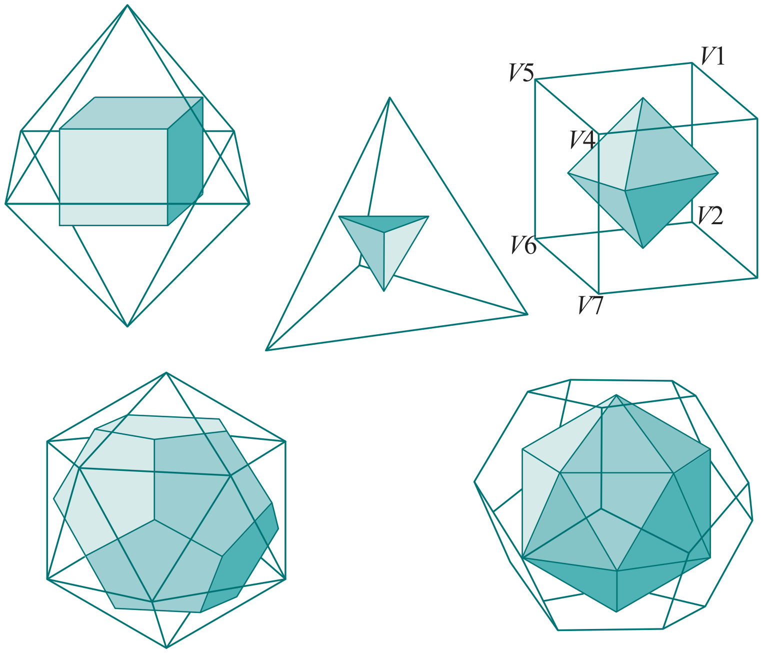

Figure 10.57: The five regular polyhedra each containing its inscribed dual (the cube is labeled to help with Exercise 10.68).

The *dual* of a regular polyhedron P is the polyhedron P^1 *inscribed* in P as follows:

(a) For each face f of P there is a vertex of P^1, called f's dual, located at the center of f.

(b) For each edge e of P there is an edge of P^1, called e's dual, joining the dual of the two faces of P adjacent to e.

(c) For each vertex v of P there is a face of P^1, called v's dual, with vertices at the duals of the faces of P that meet at v.

See Figure 10.57. Fascinatingly enough, it turns out that the dual of a regular polyhedron is another regular polyhedron. Cubes and octahedrons are duals of one another, as are dodecahedrons and icosahedrons, while tetrahedrons are self-dual.

It's clear from the construction that a regular polyhedron and its dual have the same number of edges, while the number of vertices of one equals the number of faces of the other. Moreover, their Schläfli symbols are flips one of the other.

Returning to the drawing of regular polyhedra, it's easy now to compute the data for the octahedron dual to the cube whose data we listed earlier. In fact, we leave the reader to verify data for the dual octahedron in the next exercise.

Exercise 10.68. Verify the data for the octahedron, dual to the cube whose data was listed earlier, as given in the two tables just below. Note that the vertex V^1i of the octahedron is the dual of the face Fi of the cube, while the face F^1j of the octahedron dual of the face Vj of the cube. Moreover, the edge length of this particular octahedron is 2.

Octahedron

Vertex	Coordinates
V^10	$(1, 0, 0)$
V^11	$(0, 0, -1)$
V^12	$(-1, 0, 0)$
V^13	$(0, 0, 1)$
V^14	$(0, 1, 0)$
V^15	$(0, -1, 0)$

Face	Vertices
F^10	(V^10, V^14, V^13)
F^11	(V^14, V^10, V^11)
F^12	(V^15, V^11, V^10)
F^13	(V^15, V^10, V^13)
F^14	(V^12, V^13, V^14)
F^15	(V^11, V^12, V^14)
F^16	(V^12, V^11, V^15)
F^17	(V^15, V^13, V^12)

Part answer: In addition to the data for the cube, refer as well to the diagram of the octahedron inscribed in the labeled cube in Figure 10.57.

V^10, dual of the face $F0$, is located at the center of $F0$. Its coordinates, therefore, are

$$\begin{aligned}\frac{1}{4}(V3 + V0 + V1 + V2) &= \frac{1}{4}\big((1, -1, 1) + (1, 1, 1) + (1, 1, -1) + (1, -1, -1) \big)\\ &= (1, 0, 0)\end{aligned}$$

F^10, dual of the vertex V^10, has vertices that are the duals of the faces of the cube that contain $V0$. From the cube's table the faces containing $V0$ are $F0$, $F3$ and $F4$. Therefore, F^10 has vertices V^10, V^13 and V^14.

Solve the following two problems using the data for an icosahedron in the two tables the next page.

Exercise 10.69. (Programming) Draw an icosahedron.

Exercise 10.70. (Programming) Use duality to compute the data for a dodecahedron from that of an icosahedron. In fact, write a short program for this purpose which takes as input the icosahedron data.

Icosahedron

Vertex	Coordinates
$V0$	$(0,1,X)$
$V1$	$(0,1,-X)$
$V2$	$(1,X,0)$
$V3$	$(1,-X,0)$
$V4$	$(0,-1,-X)$
$V5$	$(0,-1,X)$
$V6$	$(X,0,1)$
$V7$	$(-X,0,1)$
$V8$	$(X,0,-1)$
$V9$	$(-X,0,-1)$
$V10$	$(-1,X,0)$
$V11$	$(-1,-X,0)$

Note: The constant $X = (\sqrt{5}-1)/2$ is the reciprocal of the golden ratio. Its value is approximately 0.618.

Face	Vertices
$F0$	$(V6, V2, V0)$
$F1$	$(V2, V6, V3)$
$F2$	$(V3, V6, V5)$
$F3$	$(V6, V7, V5)$
$F4$	$(V0, V7, V6)$
$F5$	$(V8, V2, V3)$
$F6$	$(V1, V2, V8)$
$F7$	$(V2, V1, V0)$
$F8$	$(V10, V0, V1)$
$F9$	$(V9, V10, V1)$
$F10$	$(V8, V9, V1)$
$F11$	$(V4, V8, V3)$
$F12$	$(V3, V5, V4)$
$F13$	$(V11, V4, V5)$
$F14$	$(V10, V11, V7)$
$F15$	$(V0, V10, V7)$
$F16$	$(V4, V11, V9)$
$F17$	$(V8, V4, V9)$
$F18$	$(V11, V5, V7)$
$F19$	$(V10, V9, V11)$

10.2.12 Surfaces More Formally

The material in this section is fairly theoretical though we do our best to motivate it practically. We suggest skipping it on a first reading of the book and returning later.

In addition to calculus 101, a basic understanding of partial derivatives is required in order to formalize the notion of surfaces, particularly that of the regular surfaces. If you're not familiar with partial derivatives then a math class or calculus book, e.g., Stewart [139] or Schaum's Outlines [4, 155], is the place to pick the stuff up. We have a handy primer ourselves in Section 11.10 (independent of the rest of that chapter).

Recall that a C^0 curve was defined as the continuous image of a closed interval. Defining a surface as the continuous image of, say, a rectangle seems then a reasonable thing to do.

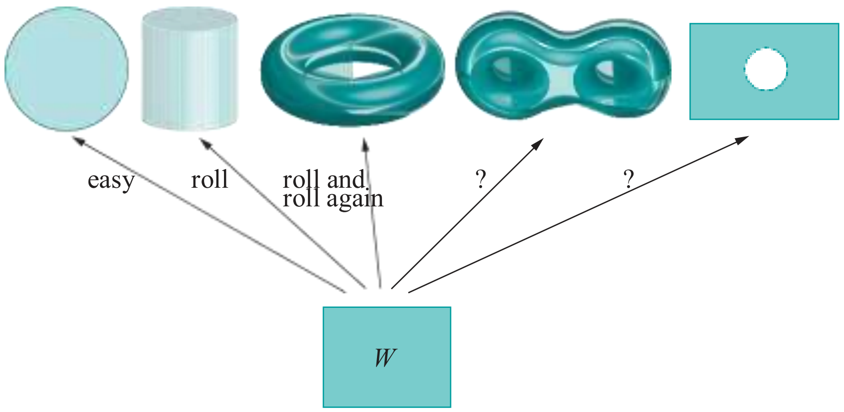

Figure 10.58: Mapping a rectangle onto surfaces.

This does indeed pass muster for simple surfaces. See Figure 10.58. It's straightforward to map the rectangle W continuously onto the disc. The cylinder is not much harder, requiring the parametric functions to roll up W – mapping an edge onto the opposite one. The torus can be made in an additional step from the cylinder, by mapping the cylinder's opposite ends onto each other. How about the double torus though, which is certainly a surface? Is it apparent how to map W onto a double torus? Or, consider something as simple as the punctured rectangle, also a surface. How can one map the (unpunctured) rectangle W onto a punctured one in a continuous manner?

It's not quite clear, then, if the view of a surface as simply the image of a rectangle can be successful. Well, even if it might not succeed *globally*, it does *locally*. Huh?

Figure 10.59: Patting gray a double torus.

Here's a thought experiment to explain what we mean. Straighten and bring the fingers of your right hand together so that it looks like an ellipse. Actually, let's pretend that it's the rectangle W of Figure 10.58. A question now: if you coated your palm and fingers with gray ink could you color each of the surfaces of Figure 10.58 all gray by patting repeatedly? Pats are allowed to overlap. Ignore size constraints as well – think of your palm or any of the surfaces to be as small or large as you like. After a couple of minutes, then, the double torus may look like Figure 10.59.

Well, . . .? We're hoping your answer is yes, that you could pat each of the surfaces fully gray. What would that mean then? Exactly that the surfaces can each be covered by patches, each of which is a continuous image of a rectangle – continuous in the sense that you'll probably have to bend and squeeze your palm a lot, but not do anything drastic like poke a hole through it or squeeze part of it to a point! In other words, per patch (locally!) the surface is indeed the continuous image of a rectangle.

We're close to a definition of a surface. First, though, we have to formalize the notion of a so-called C^0 coordinate patch.

Definition 10.12. A C^0 *coordinate patch* in $\mathbb{R}^3$ is specified by three real-valued C^0 functions f, g and h, all defined on a closed rectangle $W = [a, b]\times[c, d]$ on the plane, such that the function

$$(u, v) \mapsto (f(u, v), g(u, v), h(u, v))$$

from W to its image B is one-to-one. The image set

$$B = \{(f(u, v), g(u, v), h(u, v)) : (u, v) \in W\}$$

itself is called a C^0 coordinate patch in $\mathbb{R}^3$.

Remark 10.18. The one-to-one condition ensures that B is topologically equivalent to W, which is stronger than if B were merely a continuous image of W. The examples next clarify this.

Example 10.22. Assume W to be the rectangle $[-1, 1]\times[-1, 1]$ on the plane. Refer to Figure 10.60 for diagrams of the following functions from W.

(a)

$$(u, v) \mapsto (u, v, u^2 + v^2)$$

specifies a coordinate patch that covers the bottom part of a paraboloid.

(b)

$$(u, v) \mapsto (\cos u, \sin u, v)$$

specifies a coordinate patch that covers part of a cylinder.

(c)

$$(u, v) \mapsto (u, 0, |u|v)$$

continuously maps the rectangle onto the union of two triangles on the xy-plane *but* is not one-to-one – the entire segment $\{0\}\times[-1, 1]$ of W is mapped to the single point $(0, 0, 0)$ – so does not specify a coordinate patch.

The union cannot be patted gray either, as you can squeeze your palm as thin as you like, but never to a point.

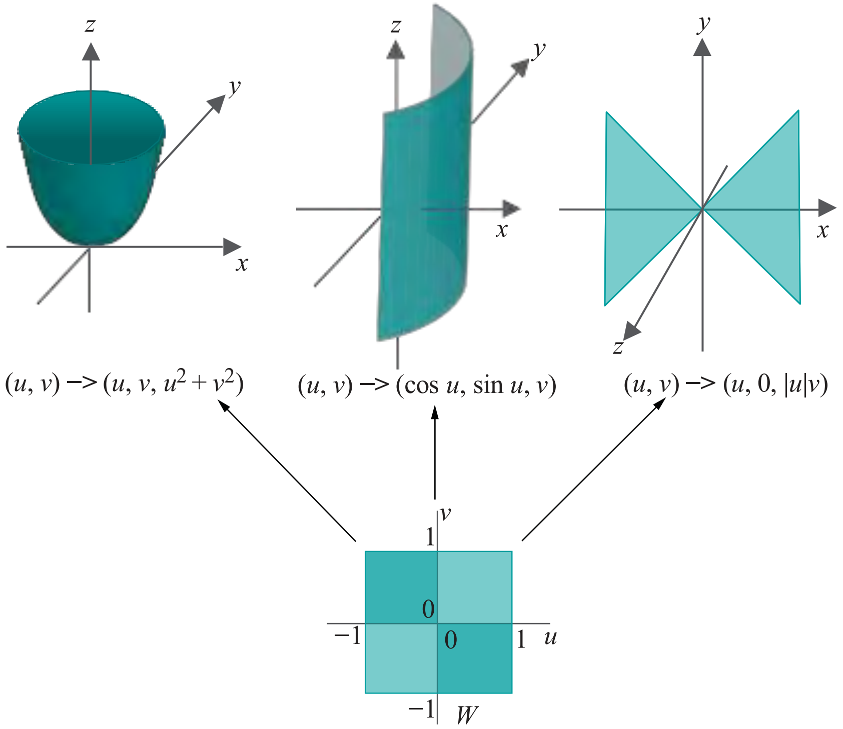

Figure 10.60: Functions $(u, v) \mapsto (f(u, v),\ g(u, v),\ h(u, v))$ and their images.

We employ coordinate patches next to define surfaces.

Definition 10.13. A subset s of $\mathbb{R}^3$ is a C^0 *surface* if there is a collection B of C^0 coordinate patches in $\mathbb{R}^3$ such that

(a) the union of the coordinates patches in B equals s, and

(b) for each point $P \in s$, a sufficiently small neighborhood of P – i.e., consisting of points within a distance δ of P for some small positive δ – lies inside a single coordinate patch belonging to B.

Remark 10.19. Patches in B can overlap. B can be an infinite collection.

Remark 10.20. A C^0 surface is said to be a *two-dimensional topological manifold* or *topological surface.*

The first condition of the definition formalizes the intuition of a surface being covered by "rectangle-like" patches. The second one is to eliminate the sort of pathology shown in Figure 10.61. The object s consisting of two intersecting planes should not qualify as a surface – even though it can evidently be covered by patches – as it's not of a single "sheet". In fact, a neighborhood of P , no matter how small, consists of two intersecting fragments, which can never lie in a single coordinate patch, violating condition (b) above.

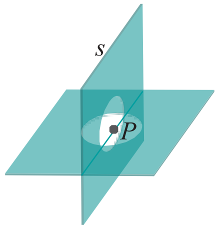

Figure 10.61: Any neighborhood of P will consist of two intersecting fragments, which cannot lie in one coordinate patch.

Exercise 10.71. Is the union of two triangles touching at a vertex, as in the top right of Figure 10.60, a topological surface?

Example 10.23. What is the minimum number of coordinate patches required to cover the cylinder

$$x = \cos u,\ \ y = \sin u,\ \ z = v,\ \ (u, v) \in [-\pi, \pi] \times [-1, 1]$$

to prove that it's a C^0 surface according to Definition 10.13? You don't have to write equations for the coordinate patches. Just sketch them on the cylinder.

Answer : Two coordinate patches are sufficient. Figure 10.62(a) indicates one patch covering a sector of more than 180°. Another patch that's a mirror image of this one would cover the rest of the cylinder. The two would overlap, of course.

One coordinate patch by itself will never do. Although this is fairly evident given the shape of the cylinder, a proof requires topology (in particular, the fact that the cylinder is not "homeomorphic" to a rectangle). Thus, two patches is the minimum.

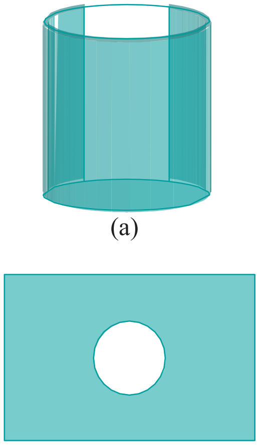
(a)

(b)

Figure 10.62: (a) One coordinate patch wrapping almost all the way around a cylinder (b) A punctured square.

Exercise 10.72. The two coordinate patches of the preceding example overlapped significantly. To avoid "waste" suppose we had two patches that each spanned 180°, covering exactly one half of the cylinder, one a mirror image of the other. Their intersection would then consist of two line segments.

Would these two patches do to prove a cylinder to be a C^0 surface?

Exercise 10.73. How about the following punctured square lying on the xy-plane?

$$[-1, 1] \times [-1, 1] \times \{0\} - \{(x, y, 0) : x^2 + y^2 < 0.5\}$$

See Figure 10.62(b). Note that it's closed with two boundary components – an outside one bounding the square and an inside one bounding the missing disc. How many coordinate patches does one need to prove that it's a C^0 surface? Answer with a sketch.

Exercise 10.74. Consider the following *open* disc (i.e., missing its boundary) lying on the xy-plane:

$$\{(x, y, 0) : x^2 + y^2 < 1\}$$

How does one cover it with coordinate patches to prove that it's a C^0 surface?

Suggested approach: A finite number of coordinate patches will not do. Find, first, a continuous mapping of a closed rectangle W to the closed disc

$$D_r = \{(x, y, 0) : x^2 + y^2 \leq 1 - 1/r\}$$

for any $r \geq 2$, to make D_r a coordinate patch. Consider, then, the union $\cup_{r=2}^{\infty} D_r$.

Exercise 10.75. Revisit the definition of a mesh at the start of Section 10.2.2 and make the second condition precise so that a mesh is always a topological surface.

Defining C^m surfaces for values of m greater than zero is the next natural step and not hard. One must first define the C^m continuity of a function of more than one variable. Not surprisingly, this involves partial derivatives. Compare the following with Definition 10.7 of the C^m-continuity of a function of a single variable.

Definition 10.14. A function f defined on a closed rectangle $W = [a, b] \times [c, d]$ on the plane is said to be C^m-*continuous* or, simply, C^m, where $m \geq 1$, if all of its partial derivatives of order m and less exist and are continuous on W.

Next, C^m coordinate patches will obviously invoke C^m functions of two variables, while imposing an additional condition of so-called regularity will help when it comes to defining tangent planes:

Definition 10.15. A C^m *coordinate patch* in $\mathbb{R}^3$, where $m \geq 1$, is specified by three real-valued C^m functions f, g and h, all defined on a closed rectangle $W = [a, b] \times [c, d]$ on the plane, such that the function

$$(u, v) \mapsto (f(u, v), g(u, v), h(u, v))$$

from W to its image B is one-to-one. The image set

$$B = \{(f(u, v), g(u, v), h(u, v)) : (u, v) \in W\}$$

itself is called a C^m coordinate patch.

If, additionally, the two vectors

$$\left[\frac{\partial f}{\partial u}\ \ \frac{\partial g}{\partial u}\ \ \frac{\partial h}{\partial u}\right]^T \quad \text{and} \quad \left[\frac{\partial f}{\partial v}\ \ \frac{\partial g}{\partial v}\ \ \frac{\partial h}{\partial v}\right]^T \tag{10.24}$$

are linearly independent – i.e., if they are both non-zero and are not collinear – for every $(u, v) \in W$, then the coordinate patch is said to be *regular*.

It's usual to consider regular C^m coordinate patches, when $m \geq 1$, rather than just C^m. Accordingly, here's the definition of a surface covered by such patches:

Definition 10.16. A subset s of $\mathbb{R}^3$ is a *regular C^m surface*, where $m \geq 1$, if there is a collection $\mathcal{B}$ of regular C^m coordinate patches in $\mathbb{R}^3$ such that

(a) the union of the coordinate patches in $\mathcal{B}$ equals s, and

(b) for each point $P \in s$, all points of s sufficiently close to P lie in a single coordinate patch belonging to $\mathcal{B}$.

A regular C^m surface, $m \geq 1$, is often simply called a *regular surface*. A regular surface that is C^m for any m, no matter how large, is regular C^∞, also called *smooth*.

Recall that the regularity condition in the case of a curve – that the tangent vector never vanishes – ensures a meaningful tangent direction at each of its points. The regularity condition for a surface ensures likewise that a meaningful *tangent plane* exists at each point P, this being the plane p spanned by the two vectors of (10.24) (computed at that point of the coordinate patch whose image is P). See Figure 10.63. Moreover, any non-zero vector t on p is a *tangent vector* to the surface s at P.

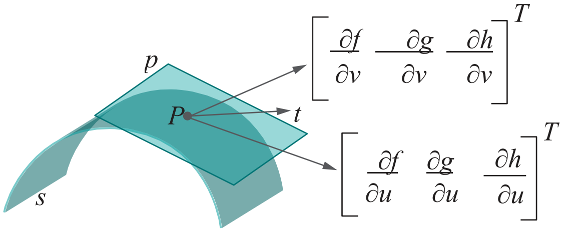
p
P
t
s
$\left[\frac{\partial f}{\partial v}\ \ \frac{\partial g}{\partial v}\ \ \frac{\partial h}{\partial v}\right]^T$
$\left[\frac{\partial f}{\partial u}\ \ \frac{\partial g}{\partial u}\ \ \frac{\partial h}{\partial u}\right]^T$

Figure 10.63: The non-zero linearly independent vectors $\left[\frac{\partial f}{\partial u}\ \frac{\partial g}{\partial u}\ \frac{\partial h}{\partial u}\right]^T$ and $\left[\frac{\partial f}{\partial v}\ \frac{\partial g}{\partial v}\ \frac{\partial h}{\partial v}\right]^T$ span the tangent plane p at P. Any non-zero vector t lying on p is a tangent vector.

Figure 10.64 shows four surfaces of various orders of continuity. All labels should be clear except maybe for the second one, which is a cylinder capped by a hemisphere. This surface is regular C^1 but not regular C^2, for precisely the same reason that the third curve of Figure 10.20 is C^1 and not C^2 (we'll leave the reader to revisit the explanation there if need be).

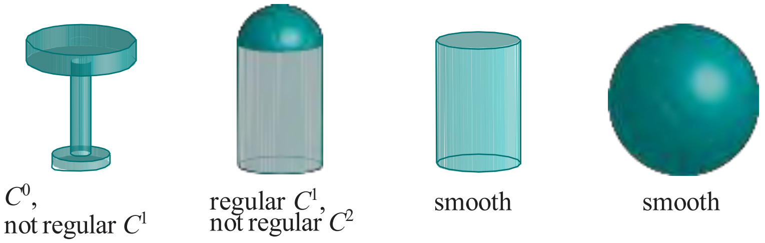

Figure 10.64: Various orders of surface continuity.

The table in Figure 10.64 is not regular, though it is composed of regular pieces. It would be nice to have a definition of piecewise regularity to apply to such surfaces. However, formulating an analogue of Definition 10.5 of piecewise regular curves is not straightforward, as it isn't clear what it means to join a number of surfaces end to end. The following definition finesses the problem.

Definition 10.17. A *piecewise regular surface* in $\mathbb{R}^3$ is a C^0 surface that is the union of finitely many regular surfaces.

The requirement of C^0-continuity in the definition assures the sheet-like nature of the union. The table is then piecewise regular, but the intersecting planes of Figure 10.61 are not as they don't form a C^0 surface.

Exercise 10.76. Is the surface of a regular polyhedron C^0, C^1, piecewise regular, . . .?

We finish up with a definition of regular two-dimensional objects analogous to Definition 10.6 of regular one-dimensional objects, which does apply to the intersecting planes of Figure 10.61, and pretty much everything else one is likely to run into in 3D graphics.

Definition 10.18. A *regular two-dimensional object* is a finite union of regular surfaces.

And, for the record we have the proper inclusions

$$\text{regular surfaces} \subset \text{piecewise regular surfaces} \subset \text{regular 2D objects}$$

10.3 Bézier Phrase Book

Bézier and NURBS (Non-Uniform Rational B-Spline) curves and surfaces are two special classes of curves and surfaces widely used in 3D design. Their utility to the applications programmer lies in the ability to sculpt a primitive in an intuitive manner by manipulating so-called control points, rather than by devising equations (the equations do exist but are created and managed transparently by the API). Several 3D modeling systems, in fact, allow the user to *interactively* design Bézier and NURBS primitives in a WYSIWYG environment. OpenGL, however, offers both in a sparser code-it-yourself manner.

There is a fair amount of theory underlying the two, which is the reason for their effectiveness in the first place, and it's important that designers have a reasonable understanding in order to use them effectively. We'll study polynomial Bézier and NURBS theory in depth in Chapters 17-18. The rational version of both classes of primitives is developed in Chapter 20.

Although it is most convenient to design Bézier and NURBS primitives in a WYSIWYG environment, nevertheless, with a little effort fairly complex designs can be coded in raw OpenGL. In fact, it is good practice for the beginner to do so in order to get a hands-on feel for the design process.

Polynomial Bézier curves and surfaces, in particular, are quite intuitive and it's perfectly possible to learn their OpenGL syntax and begin design even before fully grasping the theory. Unfortunately, such is not the case with NURBS primitives in general, or even rational Bézier primitives, as it's difficult to make sense of their OpenGL syntax without some theoretical understanding.

In keeping, therefore, with the goal of this chapter to acquaint the reader with as many 3D design techniques as possible, we'll discuss polynomial OpenGL Bézier primitives – both curves and surfaces – without, for now, much of the theory.

10.3.1 Curves

A *Bézier curve* c is specified by a sequence $P_0, P_1, \dots, P_n$ of *control points* in 3-space, whose number $n+1$ is called the *order* of c. The curve starts at the first control point P_0, ends at the last P_n and approaches, but does not necessarily pass through, the intermediate ones. Think of the intermediate control points as "attractors" which the designer pushes around molding the shape of c. See Figure 10.65, a screenshot of the program bezierCurves.cpp, which we'll be discussing momentarily, showing six control points and their Bézier curve (the curvy line).

Specifying its control points defines a Bézier curve c in a particular parametric form

$$x = f(t), \;\; y = g(t), \;\; z = h(t), \text{ where } t \in [t_1, t_2]$$

though we'll leave discussing what exactly are the Bézier parameter functions f, g and h to Chapter 17.

Experiment 10.14. Run bezierCurves.cpp. Press the up and down arrow keys to select an order between 2 and 6 on the first screen. Press enter to proceed to the next screen where the control points initially lie on a straight line. Press space to select a control point and then the arrow keys to move it. Press delete to start over. Figure 10.65 is a screenshot for order 6. Obviously, the control points always lie on a plane, keeping matters simple for now.

In addition to the black Bézier curve, drawn in light gray is its *control polygon*, the polyline through successive control points. Note how the Bézier curve tries gently, without hard corners, to track its control polygon's shape. End

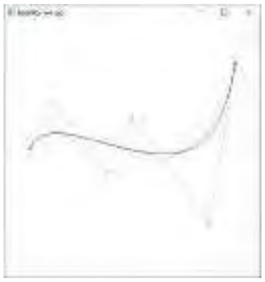

Figure 10.65: Screenshot of bezierCurves.cpp with six control points, showing both the Bézier curve and its control polygon.

We'll let OpenGL maintain the parameter equations of a Bézier curve, as it's evidently doing in the program above, and focus ourselves on learning the syntax involved in drawing such a curve. In fact, we'll do this with the help of the following two simpler programs.

Experiment 10.15. Run bezierCurveWithEvalCoord.cpp, which draws a fixed Bézier curve of order 6. See Figure 10.66 for a screenshot. There is no interaction. End

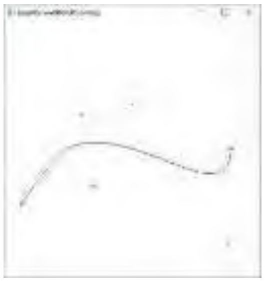

Figure 10.66: Screenshot of bezierCurveWithEvalCoord.cpp.

The pair of statements

```
glMap1f(GL MAP1 VERTEX 3, 0.0, 1.0, 3, 6, controlPoints[0]);
glEnable(GL_MAP1 VERTEX_3);
```

in the initialization routine of bezierCurveWithEvalCoord.cpp specify and enable the Bézier curve. The command

glMap1f(*target*, *t1*, *t2*, *stride*, *order*, **controlPoints*)

defines what OpenGL calls a *one-dimensional Bézier evaluator*, the dimension being that of a curve. Depending on how the parameter *target* is specified, the evaluator can be used to generate data for position, color, texture or normal direction. For now, we'll use it only to generate positional data and, accordingly, set *target* to GL_MAP1 VERTEX 3: the '1' is the dimension of the evaluator, while '3' calls for x, y and z coordinate values.

The parameters *t1* and *t2* specify the endpoints of the parameter interval of the curve, so for the program above this interval is $[0, 1]$. Parameter *order* specifies the number of control points, this being 6 above. The coordinate values of the control points are to be found in the array pointed by *controlPoints*, while *stride* is the number of floating point values between the start of the data set for one control point and that of the next in the array, this being 3 above to account for x, y and z values.

An evaluator of the form glMap1f(*target*, ...) must be enabled with a corresponding glEnable(*target*) command.

The Bézier curve itself of bezierCurveWithEvalCoord.cpp is drawn – or, more precisely, approximated – as a line strip joining vertices returned by calls to glEvalCoord1f((GLfloat)i/50.0). Generally, glEvalCoord1f(t) evaluates the coordinates of the point on the Bézier curve corresponding to the value t in the parameter interval.

Exercise 10.77. (Programming) Guess what will be displayed if the line strip definition in the drawing routine of bezierCurveWithEvalCoord.cpp is changed to either of the two below:

(a)
```
glBegin(GL_LINE_STRIP);
   for (i = 0; i <= 25; i++) glEvalCoord1f( (float)i/50.0 );
glEnd();
```

(b)
```
glBegin(GL_LINE_STRIP);
   for (i = 0; i <= 4; i++) glEvalCoord1f( (float)i/4.0 );
glEnd();
```

As Bézier curves are most often sampled evenly through the parameter interval, OpenGL provides a convenient way to do so, as we see in the next experiment.

Experiment 10.16. Run bezierCurveWithEvalMesh.cpp. This program is similar to bezierCurveWithEvalCoord.cpp except that, instead of calls to glEvalCoord1f(), the pair of statements

```
glMapGrid1f(50, 0.0, 1.0);
glEvalMesh1(GL_LINE, 0, 50);
```

are used to draw exactly the same approximating polyline.

The call glMapGrid1f(n, $t1$, $t2$) specifies an *evenly-spaced* grid of $n+1$ sample points in the parameter interval, starting at $t1$ and ending at $t2$. So, the sample points returned by glMapGrid1f(50, 0.0, 1.0) are 0.0, 0.02, 0.04, . . . , 1.0. The call glEvalMesh1($mode$, $p1$, $p2$) works in tandem with the glMapGrid1f(n, $t1$, $t2$) call. For example, if $mode$ is GL_LINE, then it draws a line strip through the mapped sample points, starting with the image of the $p1$th sample point and ending at the image of the $p2$th one. End

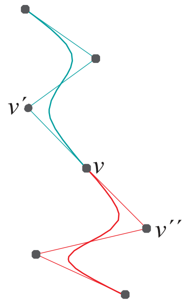

Figure 10.67: Two Bézier curves meet smoothly (actually, C^1-continuously) at a common endpoint.

End Tangents

Not only does a Bézier curve contain its first and last control points, the tangent at the first control point is along the straight line joining the first two control points. In other words, it lies along the first segment of the control polygon. Likewise, the tangent at the other end lies along the last control polygon segment. This makes it possible to join two Bézier curves which meet at a common end control point v in a C^1-continuous manner, by arranging v and its adjacent control points in either curve so that all three are on a straight line, which, of course, means that their control polygons meet smoothly at the common endpoint. See Figure 10.67.

Figure 10.68: Screenshot of bezierCurveTangent.cpp.

Experiment 10.17. Run bezierCurveTangent.cpp. The blue curve may be shaped by selecting a control point with the space key and moving it with the arrow keys. Check that the two curves meet in a visually smooth way when their control polygons meet smoothly. Figure 10.68 is a screenshot of such a configuration. End

10.3.2 Surfaces

From Bézier curves to Bézier surfaces is straightforward. A *Bézier surface* (also called *Bézier patch*) s is specified by an $(n+1) \times (m+1)$ array of control points P_{ij}, $0 \leq i \leq n$, $0 \leq j \leq m$. The surface passes through the four "corner" control points $P_{00}, P_{n0}, P_{0m}, P_{nm}$, but not necessarily the others which, nevertheless, act as attractors. Let's continue the discussion with live code in front.

Experiment 10.18. Run bezierSurface.cpp, which allows the user herself to shape a Bézier surface by selecting and moving control points originally in a 6 × 4 grid. Drawn in black actually is a 20 × 20 quad mesh approximation of the Bézier surface. Also drawn in light gray is the *control polyhedron*, which is the polyhedral surface with vertices at control points.

Press the space and tab keys to select a control point. Use the left/right arrow keys to move the selected control point parallel to the x-axis, the up/down arrow keys to move it parallel to the y-axis, and the page up/down keys to move it parallel to the z-axis. Press 'x/X', 'y/Y' and 'z/Z' to turn the surface. Figure 10.69 is a screenshot. End

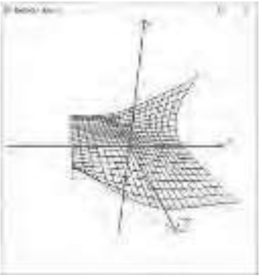

Figure 10.69: Screenshot of bezierSurface.cpp, showing both the surface mesh and its control polyhedron.

Specifying the control points array causes the Bézier surface s to be defined in a parametric form

$$x = f(u, v),\ \ y = g(u, v),\ \ z = h(u, v),\ \text{ where } (u, v) \in [u_1, u_2] \times [v_1, v_2]$$

We'll see in Chapter 17 how the functions f, g and h are obtained. The statement

```
glMap2f(GL MAP2 VERTEX 3, 0, 1, 3, 4, 0, 1, 12, 6,
        controlPoints[0][0]);
```

in the drawing routine of bezierSurface.cpp specifies the Bézier surface, while

```
glEnable(GL MAP2_VERTEX 3);
```

enables it.

The syntax of the command

```
glMap2f(target, u1, u2, ustride, uorder, v1, v2, vstride,
        vorder, *controlPoints)
```

defining a *two-dimensional Bézier evaluator*, or Bézier surface, is a logical extension of that for a one-dimensional evaluator, taking into account the extra dimension. Like its one-dimensional counterpart, a two-dimensional evaluator can be used to generate data for position, color, texture or normal direction. We'll restrict ourselves to positional data for the present, setting *target* to GL MAP2_VERTEX 3 (indicating a 2D surface in 3D space).

The values $u1$ and $u2$ specify the endpoints of the u-parameter interval and $v1$ and $v2$ those of the v-parameter interval. The parameter *uorder* is $m + 1$, the number of columns of the control points array P_{ij}; *vorder* is $n + 1$, the number of rows.

The coordinate values of the control points are located in the array pointed by *controlPoints*. The parameter *ustride* is the number of floating point values between the starts of the data sets for control points P_{ij} and $P_{i,j+1}$; *vstride* is the number of floating point values between the starts of the data sets for control points P_{ij} and $P_{i+1,j}$.

The parameter values of the glMap2f() statement of bezierSurface.cpp should now be clear, except, possibly for *vstride* – it is 12 because between the starts of the data sets for successive control points on one column are those for four control points, traveling row-wise, each having x, y and z values.

The pair of statements

```
glMapGrid2f(20, 0.0, 1.0, 20, 0.0, 1.0);
glEvalMesh2(GL LINE, 0, 20, 0, 20);
```

are analogous in functionality to glMapGrid1f() and glEvalMesh1() discussed in the context of drawing Bézier curves. In particular,

```
glMapGrid2f(numberU, u1, u2, numberV, v1, v2)
```

specifies a $(numberU + 1) \times (numberV + 1)$ grid of sample points in the parameter rectangle, evenly spaced along both rows and columns, each row starting with u-value $u1$ and ending with u-value $u2$, and each column starting with v-value $v1$ and ending with v-value $v2$. The call glEvalMesh2(*mode*, *p1*, *p2*, *q1*, *q2*)

works in tandem with the glMapGrid2f(*numberU*, *u1*, *u2*, *numberV*, *v1*, *v2*) call in a manner which we'll leave the reader to decipher from a comparison with the working of glEvalMesh1() in the case of a Bézier curve.

Remark 10.21. It's a minor design flaw of OpenGL that a Bézier surface is approximated with a stack of quad strips, rather than triangle strips.

Remark 10.22. The u-parameter curves and v-parameter curves of a Bézier surface are (no surprise) Bézier curves. Think of the parameter u as being associated with (i.e., varying along) the rows of the control points array, and v with the columns. Accordingly, for a fixed i, the points $P_{i0}, P_{i1}, \ldots, P_{im}$ on the ith row are the control points of a u-parameter curve. The order of a u-parameter curve, therefore, is $m+1$, which is the parameter *uorder* of glMap2f(). Likewise, for a fixed j, $P_{0j}, P_{1j}, \ldots, P_{nj}$ are the control points of a v-parameter curve, whose order is $n+1$, the parameter *vorder* of glMap2f().

Remark 10.23. There is a glEvalCoord2f() call available as well, analogous to glEvalCoord1f(), to evaluate the coordinates of a point on the surface corresponding to parameter point (u, v).

Next is an example of how to make a target shape by manipulating the control points of a Bézier surface.

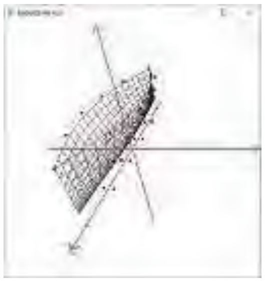

Figure 10.70: Screenshot of bezierCanoe.cpp.

Experiment 10.19. Run bezierCanoe.cpp. Repeatedly press the right arrow key for a design process that starts with a rectangular Bézier patch, and then edits the control points in each of three successive steps until a canoe is formed. The left arrow reverses the process. Press 'x/X', 'y/Y' and 'z/Z' to turn the surface.

The initial configuration is a 6×4 array of control points placed in a rectangular grid on the xz-plane, making a rectangular Bézier patch.

The successive steps are:

(1) Lift the two end columns of control points up in the y-direction and bring them in along the x-direction to fold the rectangle into a pocket.

(2) Push the middle control points of the end columns outwards along the x-direction to plump the pocket into a "canoe" with front and back still open.

(3) Bring together the two halves of each of the two end rows of control points to stitch closed the erstwhile open front and back. Figure 10.70 is a screenshot after this step.

End

Bicubic Bézier Patches and How to Join Them

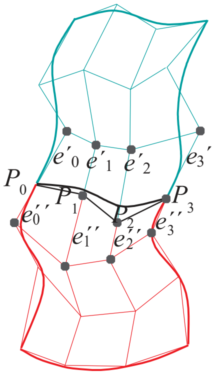

Figure 10.71: Two bicubic Bézier patches meet smoothly (actually, C^1-continuously) along the shared black boundary curve; their control polyhedrons meet along the shared black polyline.

Most often invoked in design are Bézier surfaces specified by a 4 × 4 array of control points, called *bicubic Bézier patches*. Complex shapes can be made by connecting multiple such patches. A similar principle applies to joining two bicubic patches – in fact, arbitrary Bézier patches – C^1-continuously, which often is acceptably "smooth", as applies to joining two Bézier curves C^1-continuously. First, two patches are contiguous if they share a common end row or end column of control points, in which case their control polyhedrons abut along that row or column. For the two patches to join C^1-continuously, one further requires every pair of edges, one from either control polyhedron, meeting at a vertex of the shared border but not lying on the border itself, to be collinear.

For example, in Figure 10.71 two bicubic patches meet along a common boundary (Bézier) curve specified by their shared control points P_0, P_1, P_2 and P_3, which also specify the shared 3-edge border of their control polyhedrons. In fact, $P_0P_1P_2P_3$ is the control polygon of the shared boundary curve. The edges of the control polyhedrons on either side which meet at the border, viz., the pairs e^1_i and e^{11}_i, for $0 \le i \le 3$, are collinear, so the patches join C^1-continuously.

Utah Teapot

Probably the most famous object ever made from bicubic Bézier patches is the *Utah Teapot* , created originally by Martin Newell, then a computer graphics Ph.D. student at the University of Utah, in 1975. As the story goes, Newell was casting about for a fairly complex object to use as a testbed for the various rendering algorithms which were being developed at that time of the dawn of the modern CG era, when he sat down one evening to tea with his wife Sandra. The rest as they say is history.

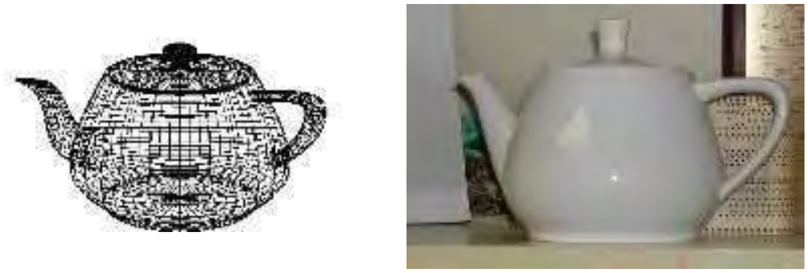

Figure 10.72: FreeGLUT library's version of the Utah teapot and Martin Newell's original porcelain Melitta model (from Wikimedia).

Run glutObjects.cpp, a program we originally saw in Chapter 3.

Though no longer considered particularly challenging an object to render, the teapot nevertheless has become a CG icon (often snuck into CGI scenes in commercial movies as an in-joke of the programmers). Newell's original design consisted of 28 patches and had neither a bottom nor a rim for the lid to rest on. The current incarnation, available from the FreeGLUT library and one of the objects drawn by our program glutObjects.cpp of Chapter 3, as seen in wireframe on the left of Figure 10.72, has both. It consists of 32 patches and a total of 306 different control points – 12 patches specify the body of the teapot, 4 the handle, 4 the spout, 8 the lid and 4 the bottom. Patches which meet obviously share control points, those composing the same part of the teapot joining smoothly based on the principle described earlier.

The original porcelain teapot which inspired Martin Newell, part of the Melitta tea set at the Newells' home in Utah in the 70s, is now on exhibit at the Computer History Museum in California. A picture is on the right of Figure 10.72. The current Bézier impression, in fact, is squatter than the original. To know why and for an entertaining account of the teapot's evolution read Crow's article [31], which gives control points data as well.

Torpedo

Experiment 10.20. Run torpedo.cpp, which shows a torpedo composed of a few different pieces, including bicubic Bézier patch propeller blades:

(i) Body: GLU cylinder.

(ii) Nose: hemisphere.

(iii) Three fins: identical GLU partial discs.

(iv) Backside: GLU disc.

(v) Propeller stem: GLU cylinder.

(vi) Three propeller blades: identical bicubic Bézier patches (control points arranged by trial-and-error).

Press space to start the propellers turning. Press 'x/X', 'y/Y' and 'z/Z' to turn the torpedo. Figure 10.73 is a screenshot. End

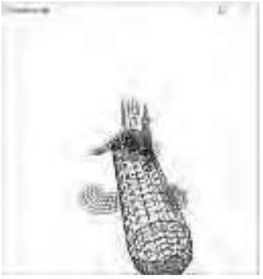

Figure 10.73: Screenshot of torpedo.cpp.

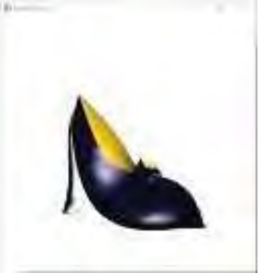

Figure 10.74: Bézier lady's shoe (courtesy of Pongpon Nilaphruek).

Exercise 10.78. (Programming) Model a fairly complex everyday object using using at least one Bézier patch in your design; of course, parts of your object can be non-Bézier. For example, a shoe is about as everyday as it gets. Figure 10.74 is a screenshot of a shoe designed using three different Bézier patches by a student in the author's class at AIT in Thailand. Amongst other objects which come to mind are cups, lamps, faucets and clothes irons.

Try to emulate Newell by using only bicubic patches, making your object a "quilt" of such.

Exercise 10.79. (Programming) Animate a river scene with several boats. Modify the canoe from bezierCanoe.cpp for a couple of different kinds of boats and put them in display lists and place (scaled and colored) copies on the river. Give a split screen view, one global from the bank and one from a particular boat.

Exercise 10.80. (Programming) Animate a roller coaster scene with one simple empty car (or a train of cars), populating the space around the coaster with flying spheres, teapots and such, and give a split screen view, one global and one from a car.

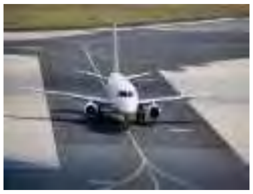

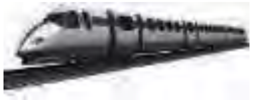

Figure 10.75: Aircraft and express train.

Exercise 10.81. (Programming) Model the aircraft (Figure 10.75) and make it fly. Parts like the wings, tail and fins can be panels of zero thickness, as can be the jet engine cases. Ignore logos and details. These can be textured in later. Focus on large-scale geometry.

Exercise 10.82. (Programming) Model a running version of the express train (Figure 10.75).

Exercise 10.83. (Programming) Make a recognizable replica of some familiar automobile.

Remark 10.24. Rational Bézier curves and surfaces, which we shall study in Chapter 20, are a superclass of their polynomial versions that we studied this section. As design primitives they are more powerful too because each control point has not only a location but a scalar *weight* as well, which influences its "pull" on the curve or surface, the greater the weight the more the pull. For instance, to draw a polynomial Bézier primitive's shape toward a control point we need to move the latter away from the primitive, while, in the case of a rational primitive, we can simply raise the control point's weight, leaving it stationary, leading to a more elegant design process.

10.4 Importing Objects

Though, as we said at the start of the last section on Bézier modeling, that it's our opinion a new programmer profits from creating objects "by hand" in the minimalist OpenGL environment, it is true too that designing complicated objects and busy scenes in this manner can be inefficient. So, once the programmer "knows what she is doing" we do recommend that she learn a WYSIWYG 3D modeling software package like Maya, Studio Max or Blender (the latter being freeware) in order to take on larger projects.

To this end, in this section we are going to show how to import into an OpenGL program 3D models written in the OBJ file format. This format was developed by Wavefront Technologies for use in its Advanced Visualizer animation package. Our reason for preferring OBJ – there are several alternate formats defining 3D objects – is its simplicity and that almost all modeling packages, including the three mentioned above, can export in the OBJ format. The ability to import objects from a specialized design environment, of course, will enhance dramatically the OpenGL programmer's capabilities. Let's get a sense of this right away.

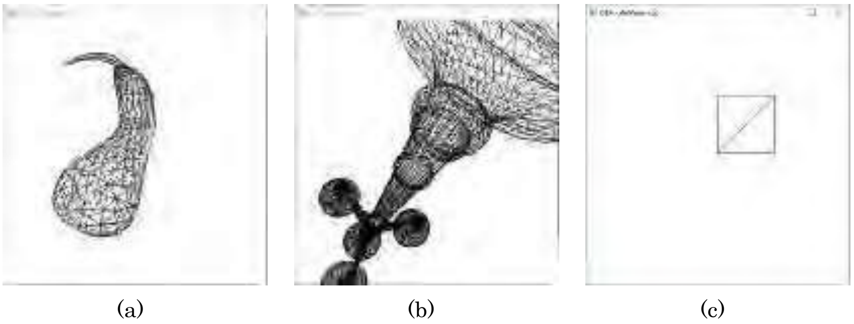

(a) (b) (c)

Figure 10.76: Screenshot of OBJmodelViewer.cpp displaying a (a) gourd (b) lamp (c) rectangle.

Experiment 10.21. Run OBJmodelViewer.cpp. Press 'x'-'Z' to turn the object, currently a gourd. See Figure 10.76. Replace gourd.obj with lamp.obj as parameter to loadOBJ() in setup() to see a lamp, or with rectangle.obj to see a simple test object.

You can load the other OBJ model files from the site where we obtained the gourd and lamp (see README.txt in the program's directory), as well as those you might find in the numerous OBJ model galleries on the web, or make yourself using a 3D design package.

Note, however, that our object-loading routine loadOBJ() is barebones, reading, as we'll soon see, only the physical coordinates of an object's vertices, as well as its mesh structure, the latter being displayed by the program. It *ignores* additional vertex attributes such as texture coordinates and normal values so the program as now can neither display texture nor handle lighting. Nevertheless, the program is fairly robust and should draw at least the wireframe for any OBJ model. End

Before delving into OBJmodelViewer.cpp let's understand first the OBJ file format, or at least as much of it as will serve our purpose in this book (the reader is referred to on-line resources for a full specification).

OBJ File Format

The OBJ file format is a way to specify polygonal meshes in 3-space together, possibly, with attributes, such as texture coordinates and normal values amongst others, which determine how each face is rendered. Each OBJ file is a sequence of lines, the starting characters of each line determining what that line specifies. Keeping in view the simple OBJ file rectangle.obj, located in the directory OBJModelViewer and shown below, which draws the triangulated rectangle in Figure 10.76(c), let's see the kinds of lines there may be.

```
# rectangle.obj
# specified intentionally in an odd way;
# ...
v 0.0 0.0 0.0
v 1.0 0.0 0.0
f 1/1/2 2/2/1 3/2/1 4/3/2
v 1.0 1.0 0.0
vt 0.4 0.5
v 0.0 1.0 0.0
vt 0.2 0.9
vn 0.1 0.2 0.1
vn 0.4 0.1 0.3
vt 0.3 0.3
```

A line beginning with a

- # is a comment line, e.g., the first line of rectangle.obj.

- v specifies the x, y and z coordinates of a vertex, e.g., the fourth line of rectangle.obj specifies a vertex at $(0.0, 0.0, 0.0)$. A fourth w-coordinate in a v-line is optional.

- vt specifies the s and t texture coordinates of a vertex, e.g, the eighth line of rectangle.obj specifies $s = 0.4$ and $t = 0.5$. A third texture coordinate in a vt-line is optional (note that OBJmodelViewer.cpp doesn't process such lines).

- vn specifies the x, y and z values of a vertex normal, e.g., the eleventh line of rectangle.obj specifies the normal vector $(0.1, 0.2, 0.1)$ (OBJmodelViewer.cpp doesn't process such lines either).

- f specifies a polygonal face as a sequence of three or more vertices, each vertex itself specified by a sequence of numbers separated by slashes, successive vertex sequences separated by space.

  Most generally, a vertex sequence is of the form $v/vt/vn$, where v is the vertex index, vt the texture coordinates index and vn the normal values index (OBJmodelViewer.cpp doesn't process vt and vn values). E.g., the sixth line of rectangle.obj specifies a quad whose first vertex is given by the sequence 1/1/2, the second by 2/2/1, the third by 3/2/1, and the fourth by 4/3/2.

  The first vertex 1/1/2 of the face has (x, y, z)-coordinates $(0.0, 0.0, 0.0)$ corresponding to the first of the v-lines, texture coordinates $(0.4, 0.5)$ corresponding to the first of the vt-lines, and normal values $(0.4, 0.1, 0.3)$ corresponding to the second of the vn-lines; the second vertex 2/2/1 has (x, y, z)-coordinates $(1.0, 0.0, 0.0)$ corresponding to the second of the v-lines, texture coordinates $(0.2, 0.9)$ corresponding to the second of the vt-lines, and normal values $(0.1, 0.2, 0.1)$ corresponding to the first of the vn-lines; and, similarly, for the last two vertices.

  Observe that the vertex index v in the sequence $v/vt/vn$ corresponds to the vth in the list of v-lines in the OBJ file, starting with index 1 for the first v-line; these v-lines are not necessarily consecutive in the file though, typically, they are grouped together as in gourd.obj and lamp.obj. Similar rules hold for the texture coordinates index vt and normal values index vn.

  Only the vertex index is mandatory for each vertex of a face; the texture coordinates and normal values indices are not. A face with only vertex indices is of the form $f\ v1\ v2\ v3\ \ldots$ (no slashes); one with only vertex and texture coordinates indices is of the form $f\ v1/vt1\ v2/vt2\ v3/vt3\ \ldots$; while, one with only vertex and normal values indices is of the form $f\ v1//vn1\ v2//vn2\ v3//vn3$ E.g, the one face of rectangle.obj could be specified with the line f 1 2 3 4 if we choose to drop texture and normal data.

There is more to a full definition of the OBJ file format but above is the crux of it and all that we'll need.

Let's examine OBJmodelViewer.cpp next. All the heavy lifting of importing an OBJ file is done by the routine loadOBJ(), which, as one might expect, essentially is a long exercise in string processing.

After the OBJ file is opened at the start of loadOBJ() as an ifstream object, it is processed line by line in the giant loop

```
while ( getline(inFile, line) ) {.......}
```

The block

```
if (line.substr(0, 2) == "v ") {......}
```

at the top of the while loop reads the x, y and z values from a v-line into the vector of floats verticesVector. A fourth w-value is ignored even if present in a v-line.

The next block

```
else if (line.substr(0, 2) == "f ") { ... }
```

which processes f-lines is more complex because it doesn't simply read the sequence of vertices per face, but, additionally, determines the vertices of successive triangles in a fan triangulation of the face, pushing them into facesVector.

The vertices of the first triangle of the fan are the first three vertices of the face; the vertices of the second triangle are the first, third and fourth vertices of the face; the vertices of the third triangle are the first, fourth and fifth vertices of the face; and, so on. The vertex indices of the current triangle of the fan are always in the variables vertexIndex1, vertexIndex2 and vertexIndex3. See Figure 10.77, where the current triangle evidently is the third of the fan. Note that a vertex index is detected as a character following a white space in an f-line and, moreover, always decremented by one so that the range of indices in facesVector starts from 0. Further, observe that lines other than v- and f-lines are *not* processed and, within an f-line, texture coordinates indices and normal values indices are *not* read even if there, though the program can obviously be enhanced to do so.

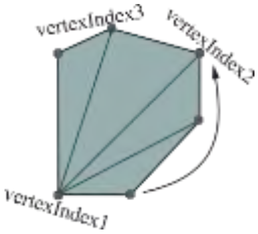

Figure 10.77: Fan triangulation of a face by loadOBJ() (the third triangle of the fan is currently being processed).

The setup routine copies values from the vectors verticesVector and facesVector to the arrays vertices and faces, respectively, and initializes a vertex array. Finally, the drawing routine has now only to invoke a single glDrawElements() command to draw the object whose polygonal faces are each drawn as a fan of triangles.

We invite the reader next to exercise her new-found capability.

Exercise 10.84. (Programming) Create an animated scene with multiple objects obtained from OBJ galleries across the web. In this connection, we recommend the *Open 3D Model Viewer* [104], a freely-downloadable OBJ model previewer with an easy-to-use interface, for the reader to inspect models before loading them into her own program.

Now, one can easily imagine an OBJ file with vertex values such that the object is awkwardly placed inside OBJmodelViewer.cpp's viewing frustum (lamp.obj, in fact) or, possibly, even entirely outside it and, therefore, invisible. We ask the reader next to address this problem with the help of so-called bounding boxes.

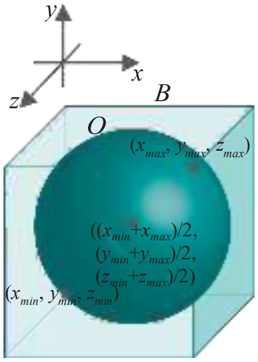

Figure 10.78: Bounding box B of a sphere O.

Suppose the smallest of the x-values of the points comprising an object O is x_{min}, the largest of the x-values is x_{max}, and that y_{min}, y_{max}, z_{min} and z_{max} are similarly defined. Then, the *bounding box* of O is the axis-aligned box B with diagonally opposite corners at $(x_{min}, y_{min}, z_{min})$ and $(x_{max}, y_{max}, z_{max})$. Of course, B is nothing but the smallest axis-aligned box containing O, its left face lying on the plane $x = x_{min}$, right face on the plane $x = x_{max}$, and so on. See Figure 10.78 which shows the bounding box of a sphere.

Now, the x-span of O clearly is $[x_{min}, x_{max}]$, the y-span is $[y_{min}, y_{max}]$ and the z-span is $[z_{min}, z_{max}]$, while a proxy for the center of O may very well be taken to be the center of B, this being $((x_{min} + x_{max})/2, (y_{min} + y_{max})/2, (z_{min} + z_{max})/2)$ (in the case of a sphere, its bounding box's center is its own center).

Note: Sometimes, loosely, any axis-aligned box containing O, not just the smallest, is called *a* bounding box of O.

Exercise 10.85. (Programming) Enhance OBJmodelViewer.cpp with translation and scaling commands whose parameters, determined from the bounding box of the object specified by the OBJ file, cause that object to be centralized in the viewing frustum.

Remark 10.25. Another weakness of OBJmodelViewer.cpp, as can be seen from the glDrawElements() command in the drawing routine, is that it draws individual triangles. More efficient, requiring fewer draw calls, would be to draw triangle strips. However, this requires first "stripifying" the OBJ mesh triangles, i.e., assembling triangle strips from them, a highly non-trivial process itself. We'll leave the interested reader to look up the literature on triangle stripification.

Remark 10.26. To the student who is planning to do some amount of designing for an OpenGL environment we recommend the *Open Asset Import Library* (Assimp) [105], an open source library to import various 3D model formats (including, of course, OBJ). Assimp links particularly well with OpenGL running in a Visual C++ setting.

10.5 Fractals

Fractals are fun, but not essential to design. You can safely skip this section if you are in a hurry to progress through the book.

A *fractal* shape, or just fractal for short, is one that possesses the characteristic of *self-similarity*. A canonical example of a fractal in nature is a coastline. The sketch on the left of Figure 10.79 is that of a hypothetical stretch of a hundred miles of coastline, as it may appear from an aircraft. To its right is a view zoomed in on a part of maybe about ten miles, seen from a low-flying aircraft, showing bays and inlets. Rightmost is an even closer zoom-in on a stretch of one mile of beach showing its own features. One notices the similarity across different levels of resolution – fractal self-similarity – in the undulations of the coastline. Clouds, trees and neural systems of animals are among a multitude of other naturally occurring fractals.

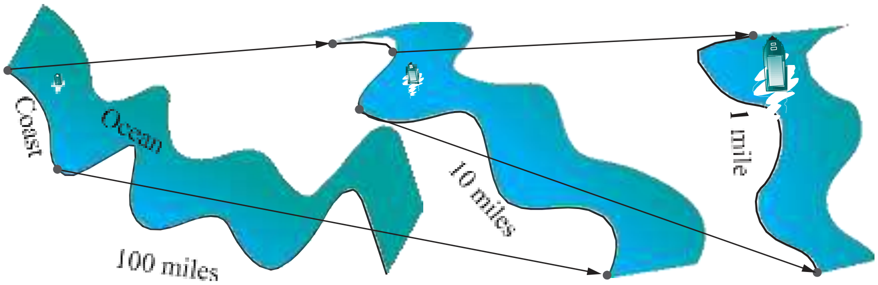

Figure 10.79: A coastline at increasing degrees of resolution: pairs of arrows indicate a blow-up.

Self-similarity lends itself immediately to programming by recursion. We'll give a semi-formal definition of fractal curves which makes self-similarity explicit. Our goal is not mathematical rigor, but a reasonable framework within which to write recursive code. The running example we'll use is a classic fractal curve – the *Koch curve* – invented by the Swedish mathematician Helge von Koch.

The first step in defining a fractal curve is to specify a *source* curve s. The location and orientation of s are not fixed: it can be placed freely anywhere on the plane if we are drawing in 2D or space if in 3D. In the case of the Koch curve, s is a straight line segment on a fixed plane. See the top diagram in Figure 10.80.

The next step is to specify a rule to generate a *sequel* curve s^1 from the source curve. The sequel is rigidly associated with the source in that, if the location and orientation of s are fixed, then so are those of s^1. The sequel for a Koch curve, in particular, is obtained by deleting the middle one-third segment of the source s and replacing it with two edges of an equilateral triangle such that the third edge would occupy the position of the now-deleted middle third. See the second diagram from the top in Figure 10.80. This particular 4-segment polyline sequel is called the *Koch polyline*.

The third and final step is to specify a rule to allow iterative reproduction of the sequel curves. In particular, for a sequel s^1 this rule specifies a finite set $\{s_1, s_2, \ldots, s_n\}$ of curves that are each a "transformed" copy of the source s. We'll not try to be precise as to how exactly they are transformed. It's best to imagine them being such that the s_i each are similar in shape to the source s, differing only in scale and location, which is the most common situation. Moreover, each s_i, $0 \leq i \leq n$, is rigidly associated with s^1 in that, if the location and orientation of s^1 are fixed, then so are those of s_i. The s_i, $0 \leq i \leq n$, are said to be the source curves *associated* with the

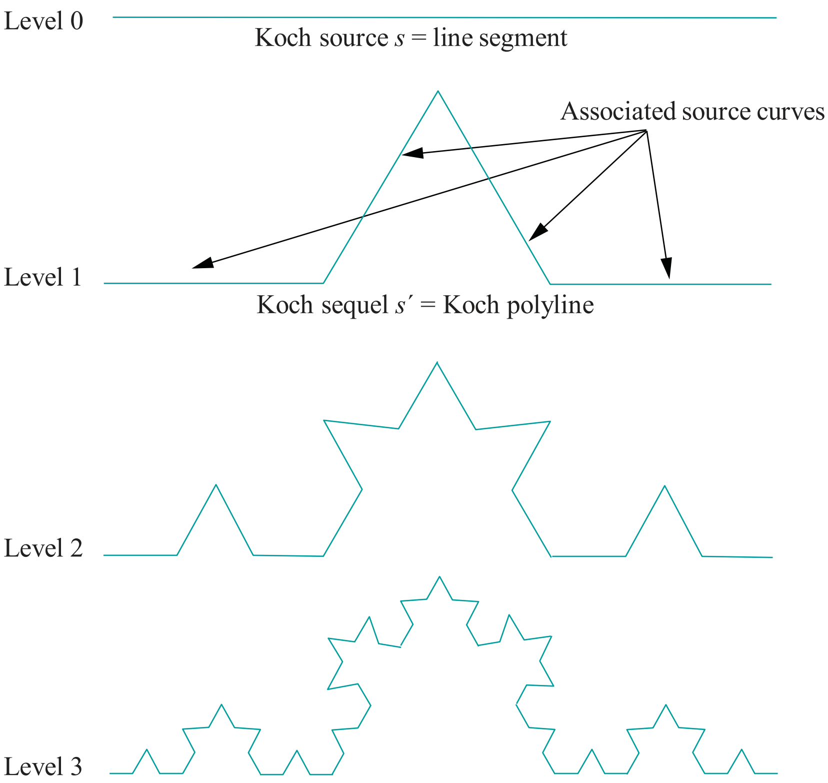
Level 0
Koch source s = line segment
Associated source curves
Level 1
Koch sequel s' = Koch polyline
Level 2
Level 3

Figure 10.80: Koch curves.

sequel. In the case of the Koch curve, the associated source curves are simply the four segments of the Koch polyline, as indicated in Figure 10.80, each obviously a scaled version of the Koch source.

We are now ready to recursively produce the fractal curve to any desired level. Level 0 is a fixed copy s of the source. Level 1 is s replaced with its sequel s^1. Level 2 is s^1 replaced with the union of the sequels of its associated sources $s_1, s_2, \ldots, s_n$, with the proviso that transformed copies of the source each generate equally transformed copies of the sequel. Level 3 and higher are obtained by repeating the procedure. Figure 10.80 shows the Koch curves till level 3.

The following program demonstrates the flexibility afforded by the framework just described.

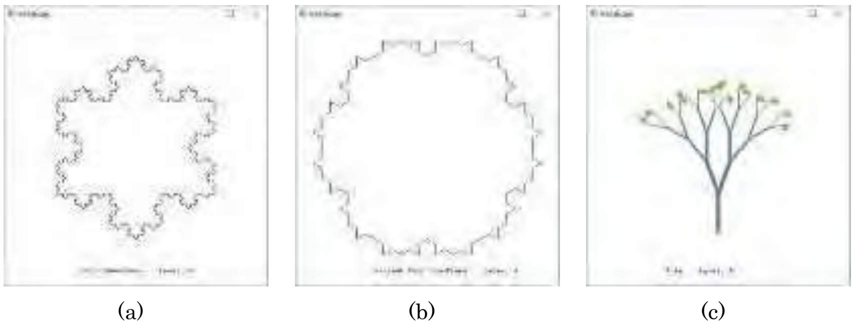

(a) (b) (c)

Figure 10.81: Screenshots from fractals.cpp: (a) Koch snowflake (b) Variant Koch snowflake (c) Tree.

Experiment 10.22. Run fractals.cpp, which draws three different fractal curves – a Koch snowflake, a variant of the Koch snowflake and a tree – all within the framework above, by simply switching source-sequel specs. Press the left/right arrow keys to cycle through the fractals and the up/down arrow keys to change the level of recursion. Figure 10.81 shows all three at level 4. End

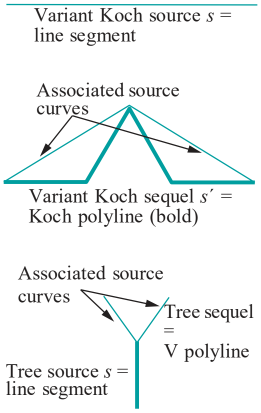
Variant Koch source s = line segment
Associated source curves
Variant Koch sequel s' = Koch polyline (bold)
Associated source curves
Tree sequel = V polyline
Tree source s = line segment

Figure 10.82: The variant Koch curve and fractal tree.

The first curve of fractals.cpp drawn is the so-called *Koch snowflake* which consists of three Koch curves, each starting with one edge of an equilateral triangle as its level 0 source.

The *variant Koch snowflake* is produced as the Koch snowflake, except that it uses a variant Koch curve whose definition differs in just one place from a Koch curve: the source and sequel of a variant Koch curve are the same as for a Koch curve; however, the associated sources of the sequel are the two segments joining the end vertices of the polyline to its middle. See the upper two diagrams in Figure 10.82. Observe that it's not necessary that the associated sources be parts of the sequel.

The source for the fractal tree is a straight line segment as well, the initial copy being vertical. The sequel is a V-shaped two-segment polyline located atop the source, the length of each segment being a specified fraction (the constant RATIO in the program) of the length of the corresponding source, with a specified angle (the constant ANGLE) between them. The sources associated with the sequel are its two segments. See the bottom diagram of Figure 10.82.

The tree is produced by drawing the original vertical source line segment, as also the succeeding sequels at *all* levels, till the highest level of recursion. Note the difference here with the Koch curve and its variant, *only* the highest-level sequels being drawn in the case of the latter two. Moreover, sequels at successive levels of the fractal tree are drawn thinner – not part of the fractal definition. The final drawing is also adorned with leaves – not part of the fractal structure either – which are quadrilaterals at random angles at the ends of the top-level V's.

The program combines all three fractals by providing different member functions for each in the classes Source and Sequel.

Exercise 10.86. (Programming) Create a non-uniform tree by adding randomization so that not all sequels are drawn.

Exercise 10.87. (Programming) The variant Koch snowflake drawn in fractals.cpp self-intersects at high enough levels. Draw an "interesting" variation of the snowflake which doesn't self-intersect.

Exercise 10.88. (Programming) Draw a fractal cloud.

Exercise 10.89. (Programming) Draw a fractal flower.

Exercise 10.90. We formalized and drew fractal curves. How about fractal *surfaces*?

10.6 Summary, Notes and More Reading

In this chapter we learned how to create a range of objects in 3D space. Of course, we had been creating objects earlier, but in this chapter we studied 3D drawing techniques systematically. These included polygonal line approximation of curves and mesh approximation of surfaces. Special classes of curves and surfaces particularly useful in drawing, including conics and quadrics, swept and ruled surfaces, regular polyhedra, Bézier curves and surfaces, and fractals were discussed. We were, as well, introduced at an elementary level to the mathematical theory underlying curves and surfaces. In addition to manufacturing objects inside an OpenGL program, we learned a way to import into it external objects, created, possibly, in specialized design environments.

The dictum that practice makes perfect applies particularly to drawing. The more drawing projects one completes the better one will know how to proceed on the next one, not to mention the reusable object parts and code one will begin to accumulate.

Now is also the time for a student with CG ambitions to explore professional modeling packages like Maya and Studio Max. Mastery of at least one such package is essential to an aspiring CG programmer. This chapter together with the material on animation from Chapter 4 should also get intending game programmers off to a flying start in using engines such as Unity and Unreal, because they will begin with a thorough grasp of the fundamentals.

A great thing about drawing scenes for movies and games is that if it walks like a duck and talks like a duck, then it *is* a duck. We have already taken advantage of this notion in faking curved objects with the help of straight and flat primitives. There's more to it though as the following example shows.

On the top of Figure 10.83 is what seems a perfectly respectable T-pipe of a sort one might find at a plumbing goods store. The picture at the bottom though reveals how it's drawn – by pushing one GLU cylinder into another so that an end of it protrudes inside (run fakeT.cpp). This is unlikely to be an acceptable industrial design of a T-pipe, but for the purposes of 3D graphics it is. Consider the saving in complexity. Authentic industrial design would require a hole whose boundary is a non-planar loop to be excised in one cylinder and an end of the other pared to match – neither trivial operations at all!

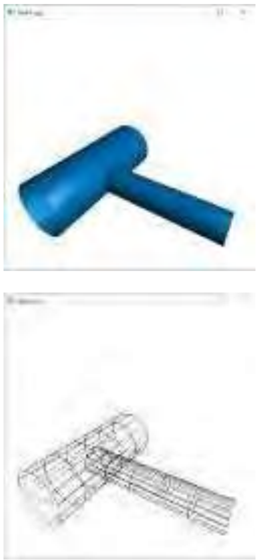

Figure 10.83: A T-pipe simulated by sticking one GLU cylinder into another.

One is reminded of the amusing story of a farmer and a mathematics professor traveling together on a train through the countryside. The farmer looking out of the window remarks to the professor, "The sheep look like they've just been sheared." The ever-precise professor replies, "Well, we can say only that the sides that we see have been sheared. We cannot make claims about what is invisible." In CG one can indeed get away with shearing only the sides that the viewer sees. This liberation from real-world rectitude (or even rationality!) throws the doors wide open to creativity. If you are working on a game or a movie, now is the time to enhance it with various objects. And, if you are getting a bit tired now of wireframe, it won't be long – a bit more than a page as a matter of fact – before we begin to color and illuminate!

Figure 10.84: Sheared? But, what about the other side?

All introductory texts on 3D graphics have parts devoted to drawing curves and surfaces in 3-space. Books containing a more specialized treatment of modeling include Farin [45], the two by Mortenson [97, 99] and Rogers & Adams [120]. They all include discussions of the Bézier primitives as well. In Simmons [135]) the reader will find more about conics and quadrics. The author's own paper [64] is a mathematical investigation of a rather curious irregularity of regular polyhedra.

Keep in mind that we are not at all done with modeling ourselves. This chapter laid the groundwork. More of the theory of Bézier curves and surfaces comes in Chapter 17. Chapter 18 is about B-spline curves and surfaces, which are staples in modern design. That chapter discusses the polynomial version of B-splines, while NURBS – non-uniform rational B-splines, the most general version – are a topic of the later Chapter 20. Chapter 19 is about Hermite curves and patches, which interpolate – i.e., actually pass through – their control points, rather than merely approximate.

The reader interested in the mathematical theory of curves and surfaces, especially those wishing at some point to get into the research end of 3D graphics, should refer to math books such as Lipschutz [90] and Pressley [117] for a fairly soft introduction to differential geometry, while the books by Do Carmo [36], Kreyszig [83], O'Neill [109] and Singer & Thorpe [136] are written at a higher level.

Our account of fractals, though basic, has probably enough for the person who primarily wants to draw them. There are several excellent books to learn more about this popular topic. In addition to Mandelbrot's classic [93], which had seminal influence in formalizing fractals and attracting popular interest, a couple of more recent ones are by Barnsley [8] and Falconer [44].

Part VI

Lights, Camera, Equation

Taylor & Francis
Taylor & Francis Group
http://taylorandfrancis.com

CHAPTER 11

Color and Light

Our objects so far have mostly looked as if they plan to stay home and watch the game. It's time now to dress up and go party. The goal for this chapter is to learn how to use light sources to illuminate a scene and complementarily define material properties of objects to determine how they appear when lit.

We begin with a brief discussion of the theory of vision and color models in Section 11.1, learning particularly about the RGB color model so important in CG, as well as a few other models which pop up occasionally, such as CMY, CMYK and HSV. In Section 11.2 we study Phong's lighting model and how it conceives of light coming off an object as comprised of three components – ambient, diffuse and specular – based on the nature of their reflectance. This section concludes with a formula to derive the RGB intensities of the light reflected at a vertex based on Phong's model.

We move on to OpenGL in Section 11.3 and see how faithfully it implements Phong's model. And, we begin extensively to experiment and code. Section 11.4 describes OpenGL's so-called lighting model – not to be confused with Phong's lighting model – which sets certain environmental parameters. Directional light sources, located far from the scene, and positional lights, located in or near it, are discussed in Section 11.5, as is the related notion of attenuation of light over distance. Spotlights are the topic of Section 11.6. At this point we have all the parts needed to formulate in Section 11.7 the famous lighting equation which OpenGL actually implements to calculate color intensities at a lit vertex.

We discuss the two so-called shading models OpenGL offers, smooth and flat, in Section 11.8. The former familiarly interpolates the vertex colors through a primitive, while the latter is a somewhat idiosyncratic discrete coloring scheme. Animation of light sources is the topic of Section 11.9.

Specifying appropriate surface normals is critical to good lighting. OpenGL can sometimes help with automatic normals, but often the user is on her own and the task can require a fair amount of calculation. Before we begin with normal computation proper, we have an introduction in Section 11.10 to the calculus of partial derivatives, to the extent required to calculate tangent planes and normals to the kinds of surfaces typical in CG.

The long Section 11.11 is devoted to computing and applying surface normals to lighting. It begins by following the informal taxonomy of 2D objects introduced in Section 10.2, and moves on to Bézier and quadric surfaces for which automatic normals are available.

Section 11.12 contains a discussion of an alternate shading model proposed by Phong, which is more sophisticated (and more computation-intensive) than OpenGL's smooth shading.

Section 11.13 is a whole bunch of exercises. In fact, the reader will find few programming exercises before that section as we decided to collect them in one place after getting most of the theory and experiments out of the way. However, this does not mean that the interested reader should not attempt them earlier. She should keep an eye on Section 11.13 as she reads to see what comes within reach. We conclude with Section 11.14.

11.1 Vision and Color Models

We begin with a bit of the physics and biology underlying color and its perception.

Electromagnetic (EM) radiation consists of oscillating electric and magnetic fields moving through space. It is produced by the motion of electrically charged particles. From a physics point of view, EM radiation can be treated dually as waves or a stream of massless particles called photons traveling through a vacuum at the speed of light. EM radiation is characterized by its frequency or, equivalently, wavelength, the inverse of frequency. The EM *spectrum* consists of EM radiation of all possible frequencies. Visible light is a (very small) part of this spectrum. See Figure 11.1.

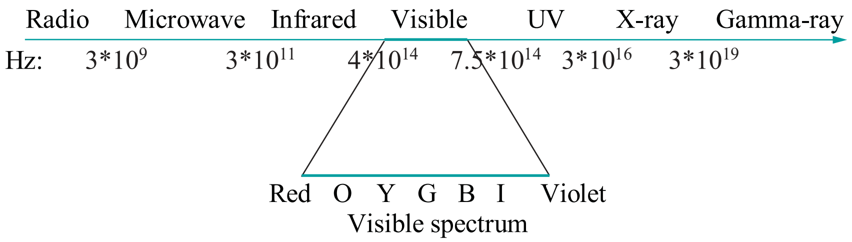

Figure 11.1: EM spectrum indicating approximate frequency ranges in Hz.

Visible light emitted from a source is rarely pure, i.e., of one particular frequency. Rather, there is an intensity distribution across the entire visible spectrum, and the perceived color depends on the particular distribution. Light from a source with an intensity distribution, for example, as in Figure 11.2(a), would be perceived as blue, as this color's intensity dominates, while one with the distribution of Figure 11.2(b) would appear white, because white is a mix of all colors in the visible spectrum.

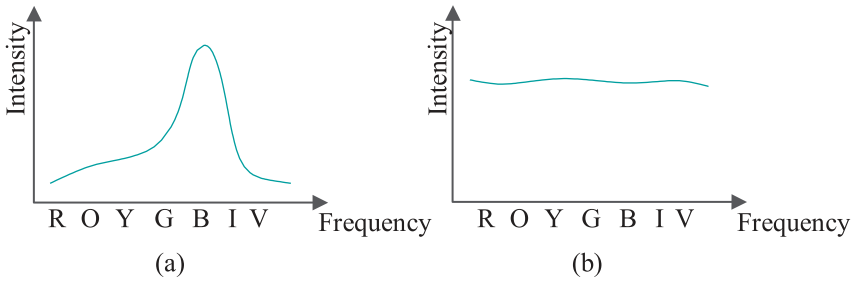

Figure 11.2: Intensity distributions across the visible spectrum: (a) appears blue (b) appears white.

We humans can see because of millions of light-sensitive cells embedded in the retina of our eyes (see Figure 11.3 for a simplified anatomy). These cells are of two kinds, rod and cone. Rod cells are sensitive to low-intensity light, but not its frequency, which accounts for our night vision, as well as the fact that we have particular difficulty distinguishing colors in the dark.

Cone cells, on the other hand, are stimulated only by fairly bright light, but can efficiently distinguish frequencies in the visible light spectrum, enabling us to perceive color. In fact, there are three kinds of cones – red, green and blue – according to the color of the light that most stimulates them. This is the basis of the *tristimulus* theory

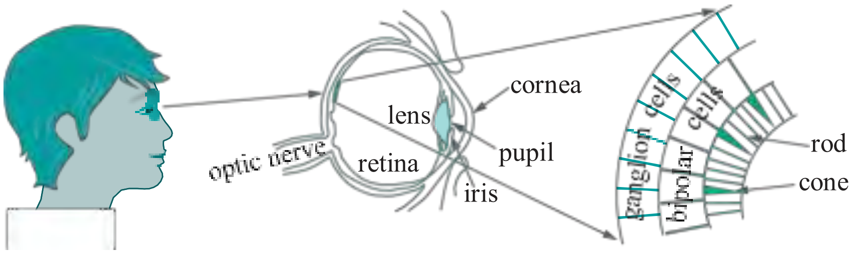

Figure 11.3: The human eye.

of human vision that perceived color is the net effect of the stimulation of these three kinds of cells.

11.1.1 RGB Color Model

A consequence of the tristimulus theory is the ubiquitous *RGB color model* : each color is represented as a sum of the three *primary colors* , red, green and blue, and each with a certain intensity, typically a value between 0 and 1 (for this reason RGB is called an *additive color model*). Typically, a color is denoted by a *color tuple* (r, g, b), where each component is the respective primary color's intensity.

Note: An intensity distribution curve, as those in Figure 11.2, one corresponding to each primary color, has been standardized by the International Commission on Illumination (CIE, from its French name Commission Internationale de L'Éclairage), as also a standard to convert intensity distributions across the visible spectrum to RGB triplets.

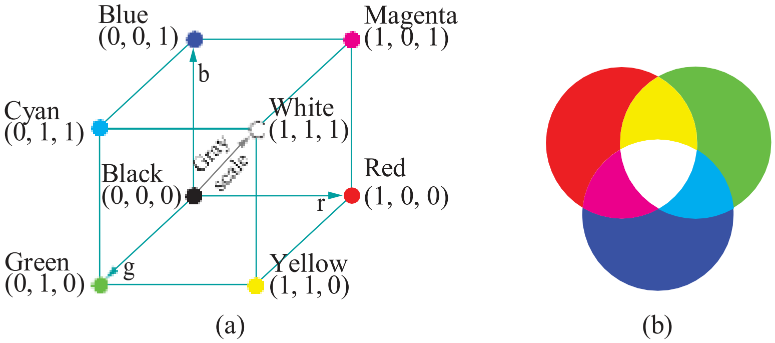

Figure 11.4: (a) The RGB color cube (b) Venn diagram combining colors.

The RGB color space can be depicted as a cube, called a *color cube*, as in Figure 11.4(a), with axes corresponding to R, G and B values. The origin $(0, 0, 0)$ of the cube corresponds to black, while its diagonally opposite vertex $(1, 1, 1)$ to white, which, of course, is the maximal equal mix of red, green and blue. The other three diagonally opposite pairs each corresponds to a primary color and its complement (the complement of a color being that which with it combines to produce white). The straight line segment from black to white, each point (x, x, x) of which has equal parts of the primary colors, represents the gray scale. Figure 11.4(b) is a popularly drawn Venn diagram, where discs correspond to primary colors and their intersections are colored according to the mixing of the primaries.

The mechanics of the "addition" of colors in the RGB model is interesting. The color cube, for instance, indicates that an equal mix of red (which is $(1, 0, 0)$) and green ($(0, 1, 0)$) produces yellow ($(1, 1, 0)$). The reason for this is that the sensation produced in the human eye by a mix of two lights, one whose red frequency dominates and another whose green dominates, is similar to that produced by a single light dominant in the yellow frequency. This is a consequence of how our optic nerves react to the stimulation of particular combinations of cone cells, *not* because the frequencies of red and green combine according to some law of physics to produce that of yellow! The RGB model, therefore, rests more on the biology of human vision than the physics of light.

RGB Color Model and Computer Graphics

The RGB model is implemented in the millions of color display units around us, including computer monitors, which are almost all LCD nowadays with a few CRT still in use. From a CG programmer's point of view though, as we shall see, the exact display technology is of little importance.

A CRT (cathode-ray tube) monitor has phosphors of the three primary colors located at each one of a rectangular array of pixels, and three electron guns that each fires a beam at phosphors of one color. A mechanism to aim and control their intensities causes the beams to travel together row by row, striking successive pixels in order to excite the RGB phosphors at each to values specified for it in the color buffer. See Figure 11.5(a).

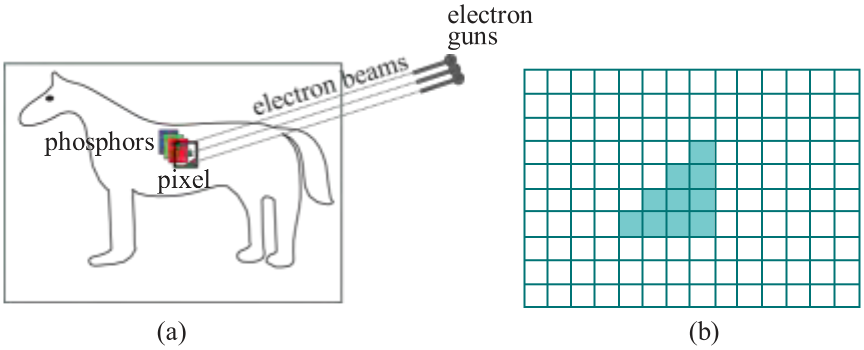

Figure 11.5: (a) Color CRT monitor with electron beams aimed at a pixel with phosphors of the 3 primaries (b) A raster of pixels showing a (very low-res) rasterized triangle.

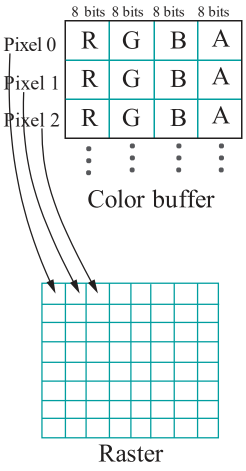

Figure 11.6: Pixel color intensities read from color buffer.

Pixels in an LCD (liquid crystal display) monitor, on the other hand, each consist of three subpixels made of liquid crystal molecules, which separately filter through light of only one primary color. The amount of primary color emerging through each subpixel is controlled by an electric charge, whose intensity in turn is determined by the corresponding value in the color buffer.

From the standpoint of OpenGL and, indeed, most CG applications, what is most important is that the pixels in a monitor are, in fact, arranged in a rectangular array, called a *raster* , as depicted in Figure 11.5(b), each pixel's color determined by three values, each between 0 and 1, determining red, green and blue intensities, respectively.

The number of rows and columns in the raster determines the monitor's resolution. This rectangular layout is the basis of the lowest-level CG algorithms, the so-called raster algorithms, which actually select and color the pixels to represent user-specified shapes such as lines and triangles on the monitor. Figure 11.5(b), for example, shows the rasterization of a right-angled triangle (with terrible jaggies because of the low resolution). We'll be studying raster algorithms in fair depth ourselves in Chapter 14.

Further relevant to CG programming is that a memory location called the *color buffer*, either in the computer's CPU or graphics card, contains, typically, 32 bits of data per raster pixel – 8 bits for each of RGB and 8 for the alpha value (used for blending). It is the RGB values in the color buffer which determine the corresponding raster pixel's color intensities – 0-255 (for 8 bits) mapping linearly to the intensity range 0-1. Figure 11.6 is a logical depiction. The values in the color buffer are read by the raster – at which time the raster is said to be refreshed – at a rate called the monitor's refresh rate. Beyond this, the technology underlying a particular display, be it CRT, LCD or something else, matters little to the graphics programmer.

11.1.2 CMY and CMYK Color Models

The *CMY color model* , whose augmentation CMYK is typically used in color printing, is a *subtractive color model* . CMY stands for cyan, magenta and yellow, and they are, respectively, the complements of red, green and blue. For example, cyan reflects blue and green but absorbs (or subtracts) red. Likewise, magenta and yellow subtract green and blue, respectively. Accordingly, cyan, magenta and yellow are referred to as the *subtractive primaries*. The color cube and Venn diagram for the CMY color model are depicted in Figure 11.7.

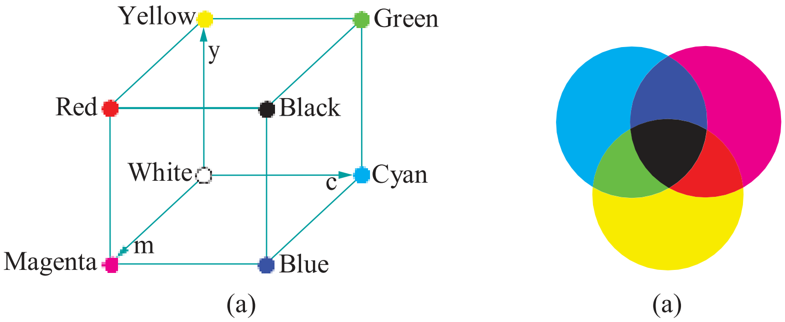

(a)

(a)

Figure 11.7: (a) The CMY color cube (b) Venn diagram of the CMY model.

Going between the RGB and CMY color spaces is simple:

$$\begin{bmatrix} c \\ m \\ y \end{bmatrix} = \begin{bmatrix} 1 \\ 1 \\ 1 \end{bmatrix} - \begin{bmatrix} r \\ g \\ b \end{bmatrix} \quad \text{and} \quad \begin{bmatrix} r \\ g \\ b \end{bmatrix} = \begin{bmatrix} 1 \\ 1 \\ 1 \end{bmatrix} - \begin{bmatrix} c \\ m \\ y \end{bmatrix} \qquad (11.1)$$

Ink of the color of each of the three subtractive primaries is coated as a grid of dots (called a *screen*) on a sheet of paper during printing. The relative proportions of CMY ink at each dot determine the amounts of light of various frequencies subtracted there; the remaining light emerges through the ink layers and imparts to the dot its perceived color.

However, in practice, the combination of CMY ink to produce RGB color does not work as well as Equations (11.1) might suggest. The CMY pigments in printer toner cartridges are never pure enough that an equal mix produces 100% black or even proper shades of gray. In addition to this technical problem there is an economic one too: making blacks and grays, by far the most common colors in printing, by mixing colored inks is expensive. Modern color printers, accordingly, supplement their CMY inks with a black ink so that blacks and the gray scale may be produced directly without mixing, the resulting process being called *four-color printing*.

The CMY model augmented with black is called the *CMYK color model* (for reasons to do with printing terminology black is denoted by K rather than B). Conversion formulae between the CMYK color space and the RGB and CMY color spaces are more complicated than those between the latter two and we'll not discuss them here. However, drawing and image editing programs, such as GNU's GIMP (freeware [53]), which offer both RGB and CMYK models will automatically convert between them.

A practical point to note is that mapping from RGB to CMYK is often device-dependent and rarely 100% accurate, which is why CMYK print-outs are frequently significantly different from the original RGB display. Keep this in mind if you are preparing a color document on your computer to print out on paper. Moreover, the space of colors representable in the RGB and CMYK color models – their *gamuts*

– are not identical either, so some colors simply cannot be transferred exactly from monitor to paper (or vice versa).

11.1.3 HSV (or HSB) Color Model

The RGB color model, though pretty much ingrained into applications around us, is not particularly intuitive for the mixing of colors. For example, what RGB values should an artist combine for a jungle green, sunset orange, ocean blue, . . .? The *HSV color model* was created by Alvy Ray Smith, one of the co-founders of Pixar Corporation, in 1978 as a more user-friendly alternative for designers. HSV is the abbreviation for hue, saturation and value. The model is also called *HSB*, where B stands for brightness.

The HSV model gets past the problem of having to numerically mix primaries by allowing the designer to choose a color's "coloredness" (that which we perceive as jungle green, sunset orange, ocean blue, etc.) directly with a *single* parameter, the *hue*. The hue parameter space is circular and often called the *color wheel*.

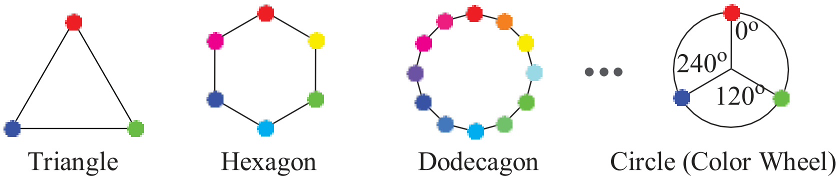

Figure 11.8: Hues on a triangle, hexagon, dodecagon and circle (color wheel).

Here's how the color wheel is derived. See Figure 11.8. Begin with a triangle with corners representing the red, green and blue hues. Double the number of vertices to make a hexagon and fill in the middle hues, yellow, cyan and magenta (e.g., yellow is an equal mix of red and green, so midway between them). Again, double to a dodecagon, adding new hues by interpolating between successive hues of the hexagon. Continuing the process leads to a continuum of hues in a circle. A position on this circle – or, the color wheel as it's called – thus represents a particular hue. Typically, red, green and blue are located at 0° , 120° and 240° , respectively.

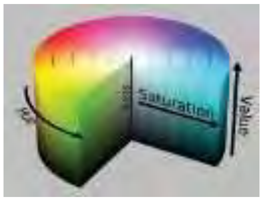

Figure 11.9: HSV coordinates cylinder (thanks SharkD for a Creative Commons license; we modified).

The hue parameter, though, by itself is insufficient to specify a color. Two other parameters are required as well. The *saturation* of a color, typically given as a percentage, represents its purity. The higher the saturation the richer and more vibrant the color appears; conversely, less saturated colors (called *desaturated*) appear faded and grayish. The final parameter is *value*, given as a percentage as well, representing a color's intensity or brightness. All three parameters are often represented in cylindrical coordinates (see Figure 11.9) where hue is measured along the circular boundary of the cylinder, saturation is the distance from cylinder's axis, while value is the distance along the axis.

11.1.4 Summary of the Models

In drawing applications the predominant model is RGB and we'll not have use for any other through the rest of this book. It's useful, though, to have a nodding acquaintance with models which may occasionally pop up elsewhere. With CMY, CMYK and HSV we have covered the ones the user is most likely to encounter. CMYK, in fact, becomes particularly important when one goes from drawing to printing. There are other color models not used as much, such as Lab (an option in Adobe's Photoshop) and HLS (for hue, lightness, saturation).

The gold standard among color models was established by the CIE (International Commission on Illumination) in 1931. It's the *CIE XYZ model* , also called the *CIE 1931 model* , where the X, Y and Z parameters represent, respectively, three theoretical primaries, each corresponding to a particular intensity distribution standardized by the CIE. Although not seen in practical interfaces, the CIE XYZ color model is used to calibrate implementations of the other ones.

11.2 Phong's Lighting Model

A model of interaction between light sources and objects is called a *lighting model* (or *reflection model*, or *illumination model*). In 1975 Vietnamese computer scientist Phong Bui Tuong [112] invented a particular lighting model, now known by his name, which is currently the one most widely used in practice. Despite the subsequent development of more authentic lighting models, e.g., Cook-Torrance [28], ray tracing, etc., Phong's has endured in popularity, especially because it delivers realistic lighting at moderate computational cost. OpenGL implements Phong's model. But, before we start coding up light let's first get an understanding of the model.

11.2.1 Phong Basics

In Phong's model the light reflected off an object O is the sum of three components – *ambient* , *diffuse* and *specular* – based on the *reflectance* properties of its surface. We'll describe each component next before explaining how to specify and calculate them.

Ambient: Ambient reflectance models O's reflection of background light striking it from multiple directions. For this reason ambient light is scattered equally in all directions from the surface of O as well. See Figure 11.10(a).

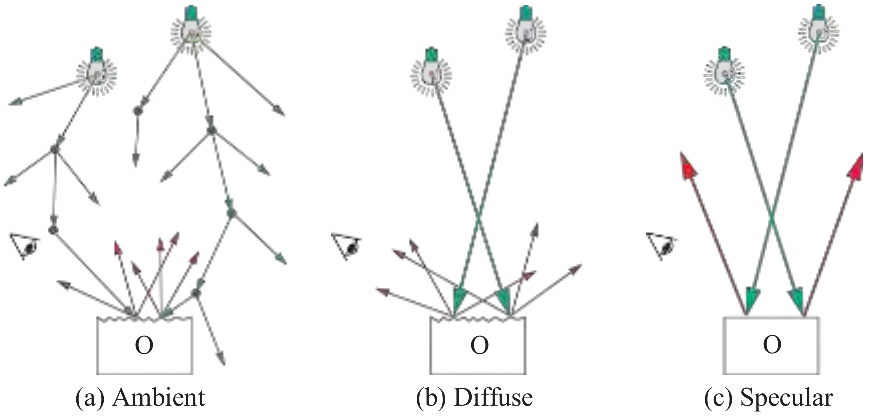

(a) Ambient
(b) Diffuse
(c) Specular

Figure 11.10: Ambient, diffuse and specular reflectance: incident light drawn green, reflected red.

Of the light sources in the environment – e.g., lamps and the sun – a part of the light from each is presumed ambient in that it's scattered in the environment, e.g., by minute particles such as dust, effectively becoming part of background light before striking O. The direction of the light's source, therefore, is lost in that part of it which is ambient. Neither does it matter where the viewer is located because of the scattered reflection from the surface of O, presumed equal in all directions. In practical terms, the ambient component models that part of light which supplies constant illumination throughout a scene. An example of a familiar light source which is mostly ambient is a tube lamp recessed behind a frosted panel (the material of the panel serving to scatter light rather than let through a focused beam).

In addition to the ambient parts of each light source, there is presumed to be a *global ambient light* as well, from no particular identifiable source, i.e., "true" background light. For example, when modeling a scene inside a building, we can adjust the global ambient to account for light from outside through doors and windows, without trying to model every possible light source such as the sun and street lights, which would be very complex indeed.

The total ambient component of the light reflected from an object O is the sum of what it reflects of the ambient parts from each source, plus what it reflects of the global ambient. Informally (we'll be getting to more precise equations soon):

ambient reflectance from O = (reflectance of ambient part from each light source) + reflectance of global ambient

Diffuse: Diffuse reflectance specifically models the fine-scale graininess of the surface: the diffuse part of light from a particular source is presumed to travel in a coherent beam toward O and then be scattered equally in all directions by diffuse reflectance from the surface of O. See Figure 11.10(b). Therefore, the direction of the light source does matter in the case of diffuse reflectance, but not that of the viewer. Practically, the diffuse component models the "soft" part of the light with little focus as it comes off an object, e.g., that reflected off polished wood or silky fabric.

The total diffuse component of light reflected from O is the sum of the reflectances of the diffuse parts from each source:

diffuse reflectance from O = (reflectance of diffuse part from each light source)

Specular: Specular reflectance models the shininess of the surface: the specular part of light from a particular source is presumed to travel in a coherent beam toward O and then be reflected in mirror-like manner, again in a coherent beam, by specular reflectance from the surface of O. See Figure 11.10(c). Both the direction of the light source and the viewer matter in the case of specular reflectance. Specular light is "hard" light with a focus, e.g., that from a beam bouncing off a polished metal surface.

The total specular component of the light reflected from O is the sum of the reflectances of the specular parts from each source:

specular reflectance from O = (reflectance of specular part from each light source)

Remark 11.1. Because specular reflection is mirror-like, while the ambient and diffuse reflections are due to scattering from the surface of the object, the color of specularly reflected light depends primarily on that of the source itself, while those of the ambient and diffusely reflected on the native color of the object, as well as the light source.

Remark 11.2. The split of light into the three components of ambient, diffuse and specular according to reflectance is *independent* of the split into the primary color components of red, green and blue, in that each of the ambient, diffuse and specular components has RGB subcomponents and all nine subcomponents can be independently set. Or, one can equivalently say that each of RGB has ambient, diffuse and specular subcomponents which can all be independently set. In other words, you can think of light as being split as in Figure 11.11(a) or Figure 11.11(b) – it does not matter. Yet another way this is often phrased is by saying that color and reflectance splits are *orthogonal*.

A final component of light emerging from O is not reflected.

Emissive: The emissive component of light from an object O is that which is "manufactured" at O and unrelated to external light sources or the global ambient light. An example of an emissive object would be a lamp or the headlight of an automobile.

Extremely important : In OpenGL implementations emissive light is perceived *only* by the viewer and does *not* illuminate other objects, in other words, it does *not* make O a light source for the rest of the environment.

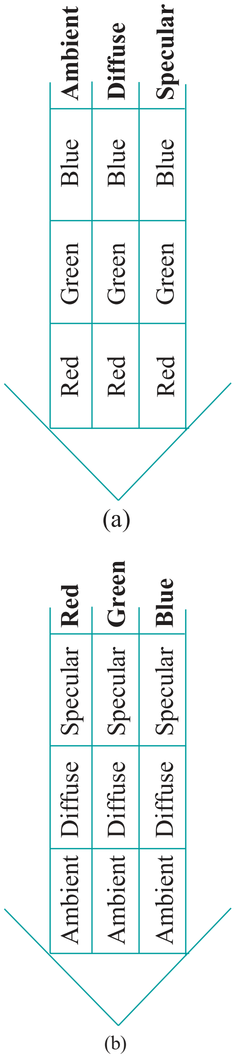

Figure 11.11: Orthogonal splitting of light: (a) Reflectance followed by color (b) Color followed by reflectance.

11.2.2 Specifying Light and Material Values

OpenGL allows several light sources to be specified – the exact number depending on the implementation. For each of the, say, N specified light sources L^i, $0 \le i \le N-1$, the RGB intensities of each of its ambient, diffuse and specular components can be set to between 0 and 1, for nine values altogether per light source. These are written, typically, in a 3 × 3 *light properties matrix*:

$$\begin{bmatrix} L^i_{amb,\,R} & L^i_{amb,\,G} & L^i_{amb,\,B} \\ L^i_{diff,\,R} & L^i_{diff,\,G} & L^i_{diff,\,B} \\ L^i_{spec,\,R} & L^i_{spec,\,G} & L^i_{spec,\,B} \end{bmatrix} \qquad (11.2)$$

Similarly, for each object O or, more precisely, each vertex V of O, one can set *scaling factors*, or, *reflectance values* as they are also called, between 0 and 1 to determine how much of each component of the incident light is reflected, for again nine values, contained in a 3 × 3 *material properties matrix*:

$$\begin{bmatrix} V_{amb,\,R} & V_{amb,\,G} & V_{amb,\,B} \\ V_{diff,\,R} & V_{diff,\,G} & V_{diff,\,B} \\ V_{spec,\,R} & V_{spec,\,G} & V_{spec,\,B} \end{bmatrix} \qquad (11.3)$$

Setting nine color values for every vertex in a scene may seem daunting at first but, in fact, will turn out not that hard because of OpenGL's behavior as a state machine, whereby property values remain same until they are explicitly altered. These nine reflectance values represent the object's color: the higher one is, the more of the corresponding incoming light is reflected, so the more of that color the object appears to be.

The RGB values of the global ambient light are contained in a 3-vector called the *global ambient light vector*:

$$[globAmb_R \quad globAmb_G \quad globAmb_B] \qquad (11.4)$$

The RGB values of the emissive light from a vertex V is a 3-vector called the *emissive light vector*:

$$[V_{emit,\,R} \quad V_{emit,\,G} \quad V_{emit,\,B}] \qquad (11.5)$$

11.2.3 Calculating the Reflected Light

We come now to calculating each component of the reflected light.

Ambient

Calculating the ambient component emerging from a vertex V owing to a particular light source consists simply of scaling the light's ambient intensity by V's ambient reflectance. So, if the original intensity of the ambient light of some primary color from a source L (or the global ambient) is I, then that of its reflection from the surface at V is

$$I * material\ ambient\ scaling\ factor \qquad (11.6)$$

The *material ambient scaling factor* is the fraction of the incident ambient light that the material reflects. It is nothing but the ambient reflectance value $V_{amb,\,X}$, where X may be R, G or B, in the first row of the material properties matrix. An example will clarify use of the equation.

Example 11.1. Say the intensities of the ambient light from source L are given by

$$L_{amb,\,R} = 0.4, \quad L_{amb,\,G} = 0.9, \quad L_{amb,\,B} = 0.2$$

and the ambient reflectances of V by

$$V_{amb,\,R} = 0.9, \quad V_{amb,\,G} = 0.9, \quad V_{amb,\,B} = 0.1$$

Then the intensity of red light emanating from V owing to the L ambient is

$$L_{amb,\ R} * V_{amb,\ R} = 0.36$$

and the intensity of green light emanating from V owing to the L ambient is

$$L_{amb,\ G} * V_{amb,\ G} = 0.81$$

and the intensity of blue light emanating from V owing to the L ambient is

$$L_{amb,\ B} * V_{amb,\ B} = 0.02$$

Exercise 11.1. Continuing the preceding if, in addition to the source L, the global ambient light vector is

$$[0.2\ 0.2\ 0.2]$$

calculate the RGB light emanating from V owing to the L ambient *and* the global ambient.

Diffuse

Calculation of the diffuse component of the light reflected from V is more complex than that of the ambient as, not only must the incident light be scaled by the reflectance at V, but its direction taken into account as well. The latter is done by measuring the angle between the direction of the light source and the normal to the surface at V.

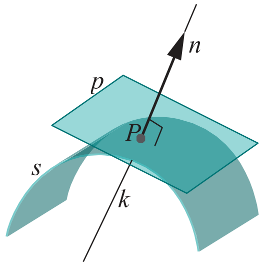

Figure 11.12: A normal vector n to a surface s at P lies along the normal line k there and is perpendicular to the tangent plane p at P.

Remark 11.3. A line k is *normal* to a surface s at the point P if it is perpendicular to the tangent plane p of s at P. Any non-zero vector n parallel to k is a *normal vector* to s at P. See Figure 11.12. (Think intuitively of the tangent plane as a hard board pressed to touch s at P.)

The light source L is modeled as a point. Further, the surface of the object O around the illuminated vertex V is assumed flat; in fact, it's taken to coincide with its own tangent plane at V. See Figure 11.13(a). Diffuse light is reflected in all directions from V.

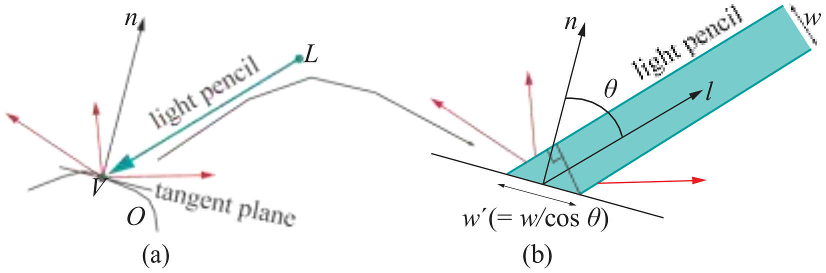

Figure 11.13: Calculating the diffuse component: (a) A light pencil from a point source L hits the surface, represented by its tangent plane at V (b) A blow-up of the pencil.

One observes from the blow-up in Figure 11.13(b) that a pencil of light of cross-sectional width w from L illuminates an area of width w^1, which is, typically, greater than w. In this figure, θ is the angle between a direction vector l from V toward the light source L, called the *light direction vector*, and an outward normal vector n at V. The angle θ is called the *angle of incidence* of the light. We ask the reader to show next, by elementary trigonometry in Figure 11.13(b), that the width $w^1 = w/\cos\theta$.

Exercise 11.2. Verify the claim just made about the width of the area illuminated by a light of width w being $w^1 = w/\cos\theta$.
Hint : Consider the right-angled triangle at the bottom of the pencil in Figure 11.13(b) with the right angle marked. The length of one side next to the right angle is w and that of the hypotenuse w^1.

Since the area illuminated is greater by a factor of $1/\cos\theta$ than the cross-sectional area of the light pencil, the intensity of the light is diminished by a factor of $1/\cos\theta$, i.e., from I to $I/(1/\cos\theta) = \cos\theta * I$. Accordingly, if the original intensity of the diffuse light of some primary color emanating from the light source L is I, then that of its reflection from the surface of O at V is

$$\cos\theta * I * \textit{material diffuse scaling factor} \tag{11.7}$$

The *material diffuse scaling factor*, given by the values $V_{diff,\,X}$, where X is R, G or B, in the second row of material properties matrix, determines the fraction of the incident diffuse light the material reflects.

Example 11.2. Say the intensities of the diffuse light from source L are given by

$$L_{diff,\,R} = 0.3,\ L_{diff,\,G} = 1.0,\ L_{diff,\,B} = 1.0$$

and the diffuse reflectances of a vertex V by

$$V_{diff,\,R} = 0.8,\ V_{diff,\,G} = 1.0,\ V_{diff,\,B} = 0.8$$

and that the angle θ of incidence at V is 60° .

Then the intensity of red light emanating from V owing to the L diffuse is

$$\cos\theta * L_{diff,\,R} * V_{diff,\,R} = 0.5 * 0.3 * 0.8 = 0.12$$

Likewise, the intensity of the green light emanating from V owing to the L diffuse is

$$\cos\theta * L_{diff,\,G} * V_{diff,\,G} = 0.5$$

and the intensity of the blue light emanating from V owing to the L diffuse is

$$\cos\theta * L_{diff,\,B} * V_{diff,\,B} = 0.4$$

Remark 11.4. The relationship that the intensity of the reflected light varies as the cosine of the angle of incidence is known as *Lambert's law* . It is Lambert's law which explains why early mornings and late evenings, when the sun is lower in the sky, are cooler and darker than mid-day.

Specular

For specular light, as in the case of diffuse light, the light source L is modeled as a point and the surface of O identified with its tangent plane at the illuminated vertex V . An outward normal vector to the surface of O at V is n. In case of specular light, though, unlike for diffuse light, the eye comes into the equation. It is modeled as the point E.

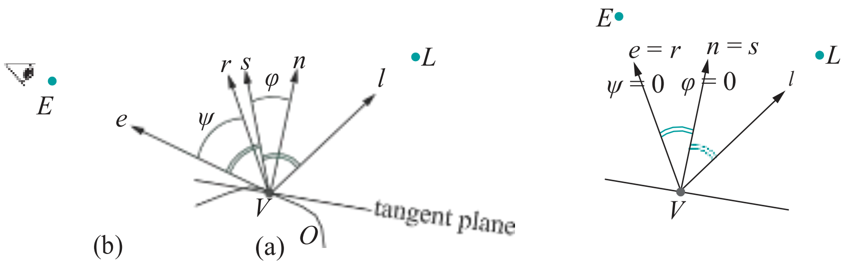

Figure 11.14: Calculating the specular component: (a) The light direction vector l, eye direction vector e, halfway vector s, normal vector n and reflection vector r (b) The special case when reflection is in the direction of the eye. (Double arcs indicate equal angles.)

The direction vector from V toward the light source L is l and the direction vector from V toward the eye E is e. Further, let s be a vector, called a *halfway vector* , which bisects the angle between l and e. The angle between s and the outward normal vector n is φ. See Figure 11.14(a) (ignore r and ψ for the moment).

We'll next state a relationship between the intensity of the reflected specular light and that of the incident which may seem unintuitive at first, but motivation will soon be apparent:

If the intensity of the specular light of some primary color emanating from the light source L is I, then that of its reflection from the surface of O at V is

$$\cos^f \varphi * I * \mathit{material\ specular\ scaling\ factor} \qquad (11.8)$$

where f $0 \geq$ is a scalar, called the *shininess exponent* ; φ is the angle between the halfway vector and the outward normal vector; the *material specular scaling factor* is a value $V_{spec,\,X}$ read from the material properties matrix, determining the fraction of the incident specular light the material reflects.

Here's what's happening. If the surface of O is *perfectly* mirror-like, then a ray of light from L to V reflects according to the laws of reflection, which say that the normal to O at V , the incident ray and the reflected ray all lie on the same plane and, moreover, that the incident and reflected rays make the same angle with the normal. So, in the case of a perfect mirror, if the eye E is located in the direction of reflection, given by the *reflection vector* r, then it perceives all of the incident light from L, if not no light at all. Now, see again Figure 11.14(a) for r. The figure should really have double arcs between the pair r and n and the pair l and n, as well, to indicate equal angles, but that would have made it too cluttered.

Say, ψ is the angle the reflection vector makes with the eye direction vector e, as depicted in Figure 11.14(a). Now, Figure 11.14(b) shows the particular case of the general Figure 11.14(a) when O is a perfect mirror and the eye is actually situated in the direction of reflection, so that $\psi = 0$. Observe, in this case, that the halfway vector is aligned with the normal, in other words, $\varphi = 0$ as well.

Most real surfaces, however, are not perfectly mirror-like and do not reflect light only along the direction of reflection, but, rather, spread it *about* that direction with an intensity which diminishes with increasing angle. In other words, maximum intensity is perceived by the viewer in a configuration as in Figure 11.14(b); nevertheless, even in a general configuration as in Figure 11.14(a), the eye receives light, though, with intensity inversely related to ψ.

This suggests that the intensity of specular reflection be modeled by the formula

$$\mathit{angular\ attenuation\ factor} * I * \mathit{material\ specular\ scaling\ factor} \qquad (11.9)$$

where the *angular attenuation factor*, in fact, is in inverse relationship with ψ.

Phong suggested the angular attenuation factor $\cos^f \psi$, where the exponent f is larger the more mirror-like (i.e., shiny) the surface is. His considerations were empirical rather than based on actual physics. In particular, $\cos \psi$ is a function of ψ which is at its maximum of 1 when $\psi = 0$ and drops off as ψ increases, behavior expected of the angular attenuation factor. The function $\cos^f \psi$ shows also the same behavior, but more markedly, as f increases. In particular, the larger the value of f the more rapid the drop from the value of 1 as ψ increases from 0. See Figure 11.15. Practically, the shinier the surface the more rapidly the light diminishes away from the direction of reflection.

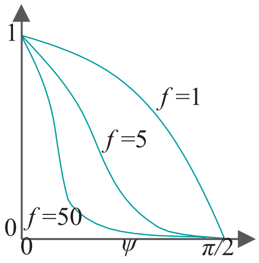

Figure 11.15: Graphs of $\cos^f \psi$ for different values of f (not exact plots).

The angle ψ is often replaced by φ, the angle between the halfway vector s and the normal vector n, because φ is easier to compute and because it is legitimate to do so given the following linear relation between the two.

Example 11.3. Show that $\psi = 2\varphi$.

Answer : Label the angles from the tangent plane to the light direction, the reflection and eye direction vectors θ_1, θ_2 and θ_3, respectively, as in Figure 11.16.

The angle to the halfway vector, then, is $(\theta_1 + \theta_3)/2$, implying that the angle between the halfway vector and the normal is $\varphi = (\theta_1 + \theta_3)/2 - \pi/2$.

By laws of reflection, the angle between the light vector and the normal, which is $\pi/2 - \theta_1$, is the same as the angle between the normal and the reflection vector, which is $\theta_2 - \pi/2$. Now, $\pi/2 - \theta_1 = \theta_2 - \pi/2$ gives $\theta_2 = \pi - \theta_1$, which, in turn, implies that the angle between the eye direction vector and the reflection vector is $\psi = \theta_3 - \theta_2 = \theta_3 - (\pi - \theta_1) = \theta_1 + \theta_3 - \pi$. That $\psi = 2\varphi$ now follows.

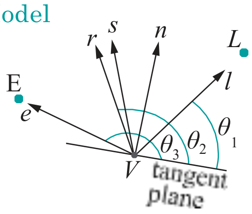

Figure 11.16: Proving $\psi = 2\varphi$.

Given the relationship between φ and ψ contained in the preceding example, substituting $\cos^f \varphi$ for $\cos^f \psi$ as the angular attenuation factor in Equation (11.9) makes no qualitative difference. The result of the substitution, in fact, is Equation (11.8), which is now fully justified.

Remark 11.5. The alert reader may have spotted the tacit assumption in the above, particularly, Figures 11.14(a) and 11.16, that the eye, and so the eye direction vector as well, lies on the same plane as the normal and the light; obviously, in general it does not have to.

However, we'll leave the mathematically-inclined to ponder if Equation (11.8) is still an acceptable approximation in all cases. Keep in mind that this equation is meant to capture *plausibly* the effect of specular lighting, not necessarily exactly. The still skeptical reader might want to defer judgement until Section 11.3 when we run experiments actually implementing OpenGL's lighting model.

Example 11.4. Give a formula for the halfway vector s in terms of the light direction vector l and the eye direction vector e from V, which are, of course, the two vectors that s bisects. Assume that both l and e are of unit length. Give s as a unit vector as well.

Answer: See Figure 11.17, where $l = \overrightarrow{OA}$, $e = \overrightarrow{OB}$, and where $l + e$ is drawn with the help of the parallelogram law of addition of vectors. Since| $|l = |e| = 1$, all four sides of the parallelogram $OACB$ are of unit length as well. A consequence is that corresponding sides of the triangles OAC and OBC are of equal lengths. The two triangles are, therefore, congruent, so $\angle AOC = \angle BOC$. One concludes that the vector $l + e$ bisects l and e.

Accordingly, the unit halfway vector

$$s = \frac{l + e}{|l + e|} \quad \text{(provided that } l + e \text{ is not the zero vector)}$$

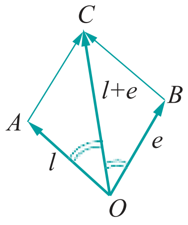

Figure 11.17: The vector $l + e$ bisects l and e.

Remark 11.6. When a vector u is used to represent a direction, so that its magnitude is not of importance, it is often convenient to scale it to unit length, a step called *normalizing* u. Normalization of a non-zero vector u (note that a vector representing a direction cannot be zero) consists simply of dividing it by its length, in other words, replacing u by $u/|u|$.

Exercise 11.3. Give a simple formula, in an OpenGL setting, for the eye direction vector e from a vertex V, denoting V's position vector by V too. Accordingly, rewrite the formula for the halfway vector of the preceding example in terms of l and v.

Hint : The OpenGL eye is always at the origin, so e is the vector from V to the origin, which is just the opposite of the vector from the origin to V.

It's interesting that calculation of the reflected light never actually required determination of the reflection vector r itself. It's not hard though to find r as we see next.

Exercise 11.4. Suppose that n is the unit (outward) normal vector and l the unit light direction vector at a vertex V. Prove that the unit vector r in the direction of reflection is given by the equation

$$r = 2(n \cdot l)n - l \qquad (11.10)$$

Part answer : According to the laws of reflection we have to verify that r lies on the plane of l and n and makes the same angle with n as l. We must also prove that r is of unit length.

That r lies on the plane of l and n follows from its formula above, because of the linear dependence of r on l and n. Now

$$|r|^2 = r \cdot r = (2(n \cdot l)n - l) \cdot (2(n \cdot l)n - l) = 4(n \cdot l)^2 - 4(n \cdot l)^2 + l \cdot l = |l|^2 = 1$$

proving that r indeed is a unit vector.

We'll leave the reader to prove that r makes the same angle with n as l makes by computing its dot product with n.

Example 11.5. Say the intensities of the specular light from source L are given by

$$L_{spec,\ R} = 1.0,\ L_{spec,\ G} = 1.0,\ L_{spec,\ B} = 1.0$$

and the specular reflectances of a vertex V by

$$V_{spec,\ R} = 0.0,\ V_{spec,\ G} = 1.0,\ \ V_{spec,\ B} = 0.6$$

and that the angle φ between the halfway vector and the outward normal vector at V is 60° and that the shininess exponent is 2.0.

Then the intensity of the red light emanating from V owing to the L specular is

$$\cos^f \varphi * L_{spec,\ R} * V_{spec,\ R} = 0.5^2 * 1.0 * 0.0 = 0.0$$

Likewise, the intensity of the green light emanating from V owing to the L specular is

$$\cos^f \varphi * L_{spec,\ G} * V_{spec,\ G} = 0.25$$

and the intensity of the blue light emanating from V owing to the L specular is

$$\cos^f \varphi * L_{spec,\ B} * V_{spec,\ B} = 0.15$$

To summarize, then, for each vertex V and each light source L:

(a) Reflected ambient light from V is the ambient component of light from L scaled by the ambient reflectance at V (Equation (11.6)).

(b) Reflected diffuse light from V is the diffuse component of light from L scaled by both the diffuse reflectance at V and the cosine of the angle of incidence at V (Equation (11.7)).

(c) Reflected specular light from V is the specular component of light from L scaled both by the specular reflectance at V and the cosine of the angle between the halfway vector and the normal at V raised to a power equal to the shininess exponent at V (Equation (11.8)).

11.2.4 First Lighting Equation

At the end of the day we need, of course, a color vector for each vertex V in the scene, in other words, values for R, G and B at V, so that OpenGL can color triangles in the scenes by interpolating their vertex color values into their interior, as we learned how to do in Chapter 7. The color vector at vertex V is obtained by adding – for each of R, G and B – contributions of the ambient, diffuse and specular reflected light at V due to *all* light sources *plus* the emitted light at V. The corresponding equation, the so-called *lighting equation*, is straightforwardly written from the formulae of the last section.

Assume that we are given the values of the lighting properties matrix (11.2) for each of the N light source L^i, $0 \leq i \leq N - 1$, the material properties matrix (11.3) for the vertex V, the global ambient light vector (11.4), as well as the emissive light vector (11.5) at V. Further, denote the normalized light direction and halfway vectors corresponding to light source L^i at vertex V by l^i and s^i, respectively. Denote the normalized outward surface normal vector at V by n and its shininess exponent by f.

Here, then, is the lighting equation giving the color intensity V_X at V, where X may be any of RGB:

$$\begin{aligned} V_X \ = \ & V_{emit,\,X} \ + \\ & globAmb_X * V_{amb,\,X} \ + \\ & \sum_{i=0}^{N-1} \Big(L^i_{amb,\,X} * V_{amb,\,X} \ + \\ & \quad \max\{l^i \cdot n,\ 0\} * L^i_{diff,\,X} * V_{diff,\,X} \ + \\ & \quad (\max\{s^i \cdot n,\ 0\})^f * L^i_{spec,\,X} * V_{spec,\,X} \Big) \end{aligned} \qquad (11.11)$$

Notes:

1. The dot product of two unit vectors gives the cosine of the angle between them.

2. The reason for the max$\{*\ 0\}$ terms is not to allow a negative multiplier, which would imply the physically impossible phenomenon of light being subtracted. For example, $l^i \cdot n$ is negative when the angle between l^i and n is greater than 90°, which means that the light source L^i is behind the surface on which V is located, contributing zero light, rather than negative light.

3. If the RHS sums to more than 1, for any of X equal to R, G or B, then it is clamped to 1.

The lighting equation simply collects the components that we have already discussed separately. The first summand on the RHS is the emissive component; the second the global ambient scaled by the ambient reflectance; the third is a summation over the N light sources of the values of the reflected ambient, diffuse and specular components. Observe, as well, that all the variables on the RHS are explicitly programmer-specified, except l^i and s^i, which are computed by OpenGL from the positions of the light sources (which, of course, the programmer specifies).

Equation (11.11) is actually a first draft. The final lighting equation of OpenGL, which we'll see soon, enhances it by taking into account the attenuation of light over distance, as well as the spotlight effect, where light from a source emerges as a cone, rather than in all directions.

Exercise 11.5. There are two light sources, L^0 and L^1, the respective values of whose lighting properties matrices are

$$\begin{bmatrix} 0.0 & 0.0 & 0.0 \\ 0.7 & 0.1 & 0.1 \\ 0.7 & 0.1 & 0.1 \end{bmatrix} \quad \text{and} \quad \begin{bmatrix} 0.0 & 0.0 & 0.0 \\ 0.1 & 0.7 & 0.1 \\ 0.1 & 0.7 & 0.1 \end{bmatrix}$$

The material properties matrix at a vertex V is

$$\begin{bmatrix} 0.1 & 0.8 & 0.9 \\ 0.1 & 0.8 & 0.9 \\ 1.0 & 1.0 & 1.0 \end{bmatrix}$$

Furthermore, the shininess exponent of the surface at V is 2.0, the unit outward normal vector at V is

$$[0.0\ 1.0\ 0.0]^T$$

and the emissive light vector at V is

$$[0.01\ 0.0\ 0.0]^T$$

The position vectors of L^0, L^1, V and the eye are, respectively,

$$[0.0\ 5.0\ 5.0]^T,\ [5.0\ 5.0\ 5.0]^T,\ [0.0\ 0.0\ 5.0]^T \text{ and } [0.0\ 0.0\ 0.0]^T$$

The global ambient light vector is

$$[0.1\,0.1\,0.1]^T$$

Fill out color values at V in the table below.

	R	G	B
Emission			
Global Ambient			
Ambient			
Diffuse			
Specular			
Total (color vector at V)			

Remark 11.7. *Important* ! Phong's lighting model is *local* . As you can see from Equation 11.11, the color at a vertex V depends only on the external light source values, as well as values, particularly, material properties and the normal vector, at V *itself* . Other vertices in the scene do *not* enter into the equation at all. So, for example, no account is taken of whether V is obscured from a light source by another object (shadows), or of light that strikes V not directly from a light source but having bounced off other objects (reflection and secondary lighting).

Consider Figure 11.18: the color at vertex V is determined by plugging in the values of the variables on the right of Equation 11.11. In particular, the light direction vector l, i.e., the unit vector in the direction from V to the light source L, is calculated by OpenGL simply from the coordinates of V and L *without* checking that an actual ray from V along l, in fact, is blocked by the surface s_2, meaning that V is in s_2's shadow. One sees then that this kind of "oblivious" use of Equation 11.11, effectively, lights s_1 as if s_2 did not exist!

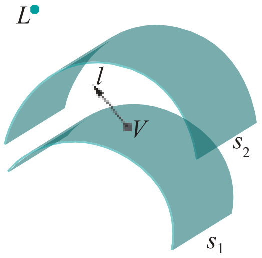

Figure 11.18: Light ray from V toward L, along l, is blocked by s_2.

Colloquially, local models like OpenGL do not consider object-object light interaction, only light-object. If the programmer wants shadows, reflections and such, then she'll have to code them in herself, e.g., as in ballAndTorusLitOrthoShadowed.cpp, which we first ran way back in Section 4.7.2, where simple-minded shadowing is seen with the use of degenerate scaling. We'll have more to say about applying secondary effects ourselves as we go along.

Additionally, we will discuss two global lighting models, different from Phong's, viz., ray tracing and radiosity, where shadows, reflections and other secondary effects are automatically captured, in Chapter 21.

11.3 OpenGL Light and Material Properties

Time for code!

The mapping from Phong's lighting model to OpenGL syntax is pretty much one-to-one. For each light source the user defines the values in the lighting properties matrix (11.2), as also the values in the material properties matrix (11.3) for each vertex. The global ambient vector (11.4) is user-defined as well. The user, too, defines the shininess exponent f, the emission color vector (11.5) and, very importantly, the normal vector at each vertex. If you are worrying that that's a lot of values to specify to light a scene, don't! Remember that OpenGL is a state machine, so material properties – which are state variables – persist in their current setting until explicitly changed, making it convenient for the programmer to apply the same properties to all vertices of a single object. Moreover, OpenGL has sensible defaults for values the programmer doesn't care to define.

Exercise 11.6. Show that the light and material properties noted above are sufficient, in fact, for OpenGL to compute the color vector at every vertex using lighting equation (11.11).
Hint : OpenGL can compute the direction vector at a vertex V toward light source L from the coordinates of V and L; it can compute the eye direction vector from the coordinates of V and the eye E (the latter, typically, being $(0, 0, 0)$); the halfway vector, of course, can be derived from the light and eye direction vectors.

Experiment 11.1. Run sphereInBox1.cpp. Press the up-down arrow keys to open or close the box. Figure 11.19 is a screenshot of the box partly open. We'll use this program as a running example to explain much of the OpenGL lighting and material color syntax.
End

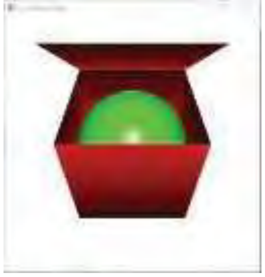

Figure 11.19: Screenshot of sphereInBox1.cpp.

11.3.1 Light Properties

Properties of light sources are set by statements of the form:

glLight*(*light*, *parameter*, *value*)

where *light* is the label of the light source (viz., GL LIGHT0, GL LIGHT1, . . .) and its particular *parameter* set to *value*.

The properties of the single light source of sphereInBox1.cpp are specified by the following statements in the setup() routine:

```
glLightfv(GL LIGHT0, GL AMBIENT, lightAmb);
glLightfv(GL LIGHT0, GL DIFFUSE, lightDifAndSpec);
glLightfv(GL LIGHT0, GL SPECULAR, lightDifAndSpec);
glLightfv(GL LIGHT0, GL POSITION, lightPos);
```

The values of GL AMBIENT, GL DIFFUSE and GL SPECULAR – lightAmb, lightDifAndSpec and (repeat) lightDifAndSpec, respectively, above – are 4-vectors representing RGBA components. The fourth component, the alpha value, should always be 1.0 for a light source.

Typically, the diffuse and specular color vectors, i.e., the values of the GL DIFFUSE and GL SPECULAR parameters, respectively, are set identically to values perceived as the actual color of the light source. So, these values, particularly{ 1.0, 1.0, 1.0, 1.0 }of lightDifAndSpec for the light source of sphereInBox1.cpp make it a bright white.

It's simplifying, as well, to consolidate all light source ambients – their GL AMBIENT values – into the global ambient; in other words, set light source ambient colors all to 0.0 and adjust the one global ambient light vector. We follow this approach in all our lit programs, explaining the value s{et 0.0, 0.0, 0.0, 1.0}of lightAmb in sphereInBox1.cpp.

The value x{, y, z, w}of GL POSITION specifies the location $[x\ y\ z\ w]^T$ of the light source in homogeneous coordinates. If $w = 0$ then the light source is said to be positional and is located at world coordinates

$$[x/w\ y/w\ z/w]^T$$

The value of lightPos being {0.0, 1.5, 3.0, 1.0 }, the single positional light source of sphereInBox1.cpp is at $[0.0\ 1.5\ 3.0]^T$, which is just above and some ways in front of the box. We'll see what happens if $w = 0$ in Section 11.5 when we discuss directional light sources.

Note that *no visible object* is ever created by OpenGL at the location of a light source! This location is simply a point used for the purpose of lighting calculation. If you want the light to appear to be from a lamp or car headlight or some such source you'll have to model that object and position it yourself.

Global ambient light in sphereInBox1.cpp is set with the statement

```
glLightModelfv(GL LIGHT MODEL AMBIENT, globAmb);
```

in the setup() routine, where the second parameter globAmb points to the global ambient vector, whose value is the mild white {0.2, 0.2, 0.2, 1.0}.

Finally, mind that lighting calculation is enabled with the call glEnable-(GL_LIGHTING) and individual lights with calls to glEnable(GL_LIGHT*i*).

Exercise 11.7. Show that nothing, in fact, is lost according to the first lighting equation (11.11) by setting all light source ambient colors to 0.0. In particular, prove that, however the light source ambients are initially set, they can all be reset to 0.0 and the global ambient adjusted accordingly so that the color computed at each vertex by (11.11) remains unchanged.

11.3.2 Material Properties

Material properties at a vertex are set by statements of the form:

glMaterial*(*face*, *parameter*, *value*)

where the *parameter* of *face* is set to *value*. The value of face can be GL ERONT, GL BACK or GL FRONT_AND BACK for both faces.

Material properties of the box of sphereInBox1.cpp are specified by the following statements in the drawScene() routine:

```
glMaterialfv(GL FRONT AND BACK, GL AMBIENT AND DIFFUSE, matAmbAndDif1);
glMaterialfv(GL_FRONT AND BACK, GL SPECULAR, matSpec);
glMaterialfv(GL FRONT AND_BACK, GL SHININESS, matShine);
```

In fact, these properties apply to *all* eight vertices of the box because no property is changed until after the drawing of the box is complete.

As for a light source, the values of GL AMBIENT, GL_DIFFUSE and GL_SPECULAR for a material are 4-vectors representing RGBA components. The A, or alpha, components are currently all set to the default value of 1.0 – they pertain to blending which is not done in this chapter.

Typically, the ambient and diffuse color vectors are set identically to values to be perceived as an object's native color. OpenGL makes it convenient to do so via the GL AMBIENT AND DIFFUSE parameter, which, in fact, is how the ambient and diffuse values of the box are both set to the red {0.9, 0.0, 0.0, 1.}0 contained in matAmbAndDif1. However, the ambient and diffuse values may be set separately as well using GL AMBIENT and GL DIFFUSE.

As specular light is obtained from reflection from the light source, it's reasonable to set an object's GL SPECULAR value either to a white {1.0, 1.0, 1.0, 1.0} fully reflecting the incident specular light, as for the box, the value being in matSpec, or a shade of gray {γ, γ, γ, 1.0}, *equally* diminishing each color component.

The value of GL_SHININESS – 50.0 for the box, contained in matShine – is, of course, the shininess exponent *f* of the first lighting equation (11.11). Its value must be in the range [0.0, 128.0]. The default is 0.0, which causes no angular attenuation of specular reflectance.

The emissive color at a vertex can be set using the GL EMISSION parameter, but we choose to leave it at the default of 0{.0, 0.0, 0.0, 1.0}, in other words, there is no emission at any vertex in sphereInBox1.cpp.

Finally, remaining is to define the normals at the eight vertices of the box. In fact, these are contained in the global normals[] array and pointed to by a normals vertex array as is seen from the two statements

```
glEnableClientState(GL_NORMAL_ARRAY);
...
glNormalPointer(GL_FLOAT, 0, normals);
```

in the drawing routine. We'll be discussing our choice of the particular normal values for the box's vertices as part of a systematic discussion of normals in Section 11.11.

Exercise 11.8. (Programming) What are the material ambient, diffuse, specular and emissive values and the shininess exponent of the sphere of sphereInBox1.cpp? Note that OpenGL automatically supplies normals for FreeGLUT objects.

Remark 11.8. Our conventions essentially reduce the specification of the nine components each of the light properties and material properties matrices to that of just three, in particular, *one* RGB triple for either. Particularly, for each light source, we set the diffuse and specular values to one identical RGB triple, leaving the ambient black (only the global ambient being adjusted). For each vertex, the ambient and diffuse values are set to the same RGB triple, while the specular is made white, reflecting all specular light (though this might be adjusted to a shade $\{\gamma, \gamma, \gamma, 1.0\}$ of gray, equally scaling each specular component).

Remark 11.9. As stated at the start of the chapter, programming exercises are mostly collected in Section 11.13. However, this should not deter the reader from visiting that section as she reads and attempting those which seem within reach.

11.3.3 Experimenting with Properties

The two programs lightAndMaterial1.cpp and lightAndMaterial2.cpp allow the user to experiment with various material and light properties. Both show a blue ball lit by two lights, one white and one green, whose positions are indicated by small wire spheres. Figure 11.20 shows screenshots of both the programs.

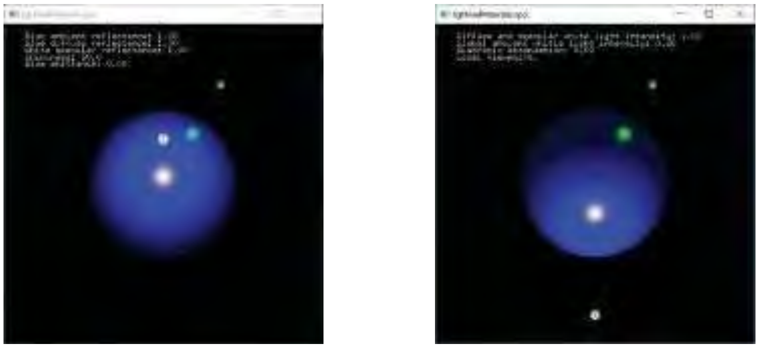

(a) (b)

Figure 11.20: Screenshots of (a) lightAndMaterial1.cpp (b) lightAndMaterial2.cpp.

Using the first program one can change material properties of the blue ball, as well as move it. The second program, on the other hand, allows properties of the white light to be controlled, as also those of the global ambient, and enables the user to rotate the white light in addition to moving the blue ball. Text messages show property values. Let's take a quick tour of the two before experimenting with properties.

Experiment 11.2. Run lightAndMaterial1.cpp.

The ball's current ambient and diffuse reflectances are identically set to a maximum blue o{f 0.0, 0.0, 1.0, 1.}0 , its specular reflectance to the highest gray level { 1.0, 1.0, 1.0, 1}.0 (i.e., white), shininess to 50.0 and emission to zero{0.0, 0.0, 0.0, 1.0}.

Press 'a/A' to decrease/increase the ball's blue Ambient reflectance and 'd/D' to change likewise its Diffuse reflectance. Pressing 's/S' decreases/increases the gray level of its Specular reflectance. Pressing 'h/H' decreases/increases its sHininess, while pressing 'e/E' decreases/increases the blue component of the ball's Emission. The page up and down keys move the ball while 'r' returns it to its original position. End

Experiment 11.3. Run lightAndMaterial2.cpp.

The white light's current diffuse and specular are identically set to a maximum of {1.0, 1.0, 1.0, 1.0} and it gives off zero ambient light. The green light's attributes are fixed at a maximum diffuse and specular of {0.0, 1.0, 0.0, 1.0}, again with zero ambient. The global ambient currently is a low intensity gray at {0.2, 0.2, 0.2, 1.0}.

Press 'w' to toggle the White light off and on and 'g' to toggle likewise the Green light. Press 'd/D' to decrease/increase the gray level of the white light's Diffuse and specular intensity (the ambient intensity never changes from zero). Pressing 'm/M' decreases/increases the gray intensity of the global aMbient. Move the ball with the page up and down keys. Rotate the white light about the ball's *original* position by pressing the arrow keys (it does not follow the ball if the latter is moved).

The program has added functionality which we'll need later. End

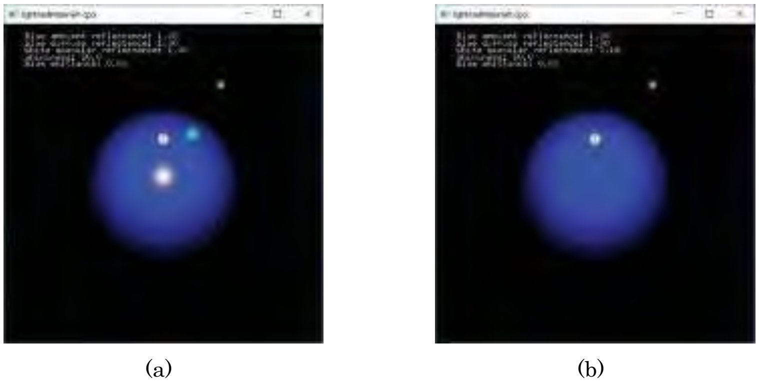
(a) (b)

Figure 11.21: Screenshots of lightAndMaterial1.cpp with specular reflectance value (a) 1.00 (b) 0.15.

Experiment 11.4. Run lightAndMaterial1.cpp.

Reduce the specular reflectance of the ball. Both the white and green highlights begin to disappear, as it's the specular components of the reflected lights which appear as specular *highlights* (or, *glint*). See Figure 11.21. End

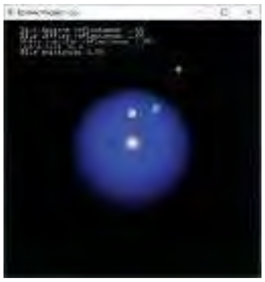

Figure 11.22: Screenshot of lightAndMaterial1.cpp with shininess exponent 80.0.

Exercise 11.9. (Programming) The specular highlight is sharpened or blunted, respectively, by increasing or decreasing the shininess exponent (see Figures 11.22 and 11.23). Why?

Hint: The higher the shininess exponent the more rapidly the specular light diminishes as the reflection vector rotates away from the eye direction (recall the definition of the angular attenuation factor $\cos^f \psi$ in Section 11.2.3).

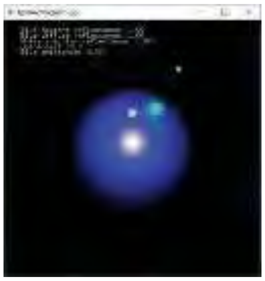

Figure 11.23: Screenshot of lightAndMaterial1.cpp with shininess exponent 20.0.

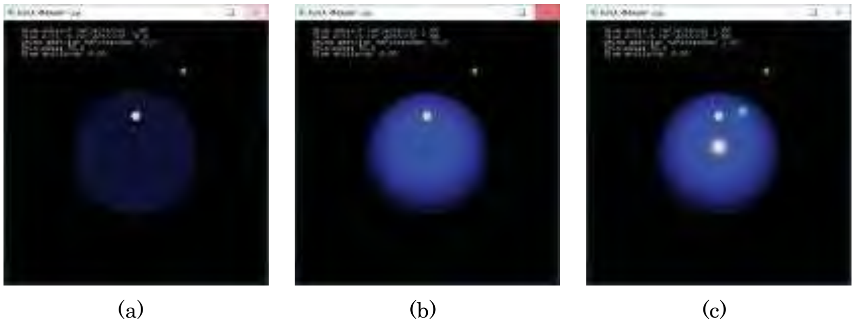
(a) (b) (c)

Figure 11.24: Screenshots of lightAndMaterial1.cpp: (a) Only ambient reflectance (b) Ambient and diffuse (c) Ambient, diffuse and specular.

Experiment 11.5. Restore the original values of lightAndMaterial1.cpp.

Reduce the diffuse reflectance gradually to zero. The ball starts to lose its roundness and brightness until it looks like a flat glassy disc. The reason for this is that ambient intensity, which does not depend on eye or light direction, is uniform across vertices of the ball and cannot, therefore, provide the perception of depth that obtains from a contrast in color values across the surface. Diffuse light, on the other hand, which varies in intensity across the surface depending on how the normal turns, cues the viewer to depth or "3Dness".

Even though there is a specular highlight, sensitive to both eye and light direction, it's too localized to provide much depth contrast. Reducing the shininess does spread the highlight but the effect is not a realistic perception of depth.

Figure 11.24 shows the ball starting with only ambient reflectance, then successively adding in diffuse and specular. End

Remark 11.10. Watch an artist sketch a portrait and you'll see how carefully she shades the base of the nose where it meets the face. This is precisely to apply diffuse light to make the nose appear to rise from the face.

Moral: Diffusive light lends three-dimensionality.

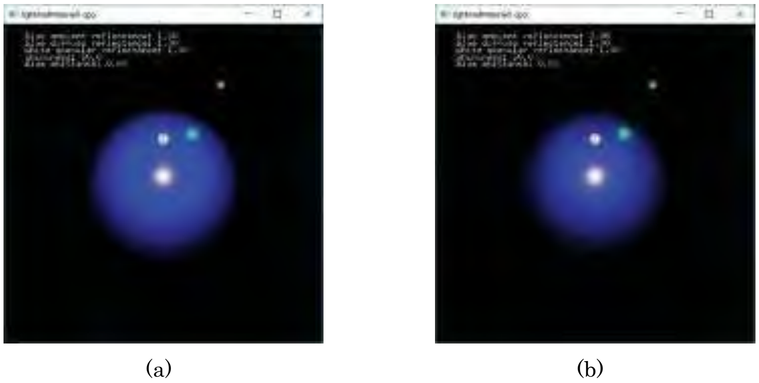

Figure 11.25: Screenshots of lightAndMaterial1.cpp with ambient reflectance value (a) 1.00 (b) 0.05.

Experiment 11.6. Restore the original values of lightAndMaterial1.cpp.

Now reduce the ambient reflectance gradually to zero. The ball seems to shrink! See Figure 11.25. This is because the vertex normals rotate away from the light direction (and viewer) near the visible edges of the ball, scaling down the diffuse reflectance there (recall the cos θ term in the diffusive reflectance equation (11.7)). The result, with no ambient light to offset the reduction in diffuse, is that the ends of the ball are dark. End

Moral: Ambient light provides a level of uniform lighting over a surface.

Experiment 11.7. Restore the original values of lightAndMaterial1.cpp.

Reduce both the ambient and diffuse reflectances to nearly zero. See Figure 11.26. It's like the cat disappearing, leaving only its grin! End

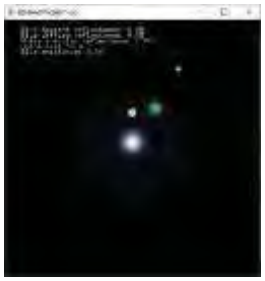

Figure 11.26: Screenshot of lightAndMaterial1.cpp with ambient and diffuse reflectances both 0.05.

Moral: Specular light is for highlights and not much else.

Exercise 11.10. (Programming) Restore the original values of lightAndMaterial1.cpp.

Reduce all three of the ball's diffuse, ambient and specular reflectances to nearly zero and raise its emissive light intensity. It does appear to glow but also appears flat. See Figure 11.27. Why?

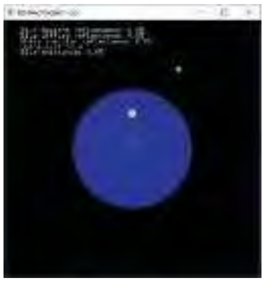

Figure 11.27: Screenshot for Exercise 11.10.

Experiment 11.8. Run lightAndMaterial1.cpp with its original values.

With its current high ambient, diffuse and specular reflectances the ball looks a shiny plastic (Figure 11.28(a)). Reducing the ambient, diffuse and specular reflectances somewhat makes for a heavier and less plastic appearance (Figure 11.28(b)). Restoring the ambient and diffuse to higher values, but reducing the specular reflectance makes it a less shiny plastic (Figure 11.28(c)). Low values for all three of ambient, diffuse and specular reflectances give the ball a somewhat wooden appearance (Figure 11.28(d)).

But, of course, the eyes of the beholder have final say, which means that color and light are art as much as science. End

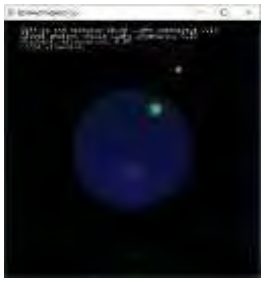

Figure 11.29: Screenshot of lightAndMaterial2.cpp with the white light's diffuse and specular values both 0.1.

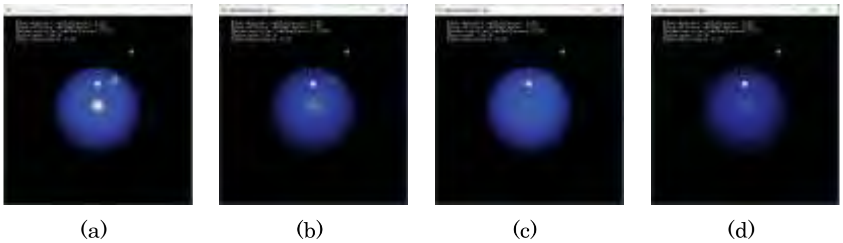

Figure 11.28: Screenshots of lightAndMaterial1.cpp with ambient, diffuse and specular reflectance values: (a) 1.00, 1.00, 1.00 (b) 0.75, 0.75, 0.5 (c) 1.0, 1.0, 0.25 (d) 0.6, 0.6, 0.1.

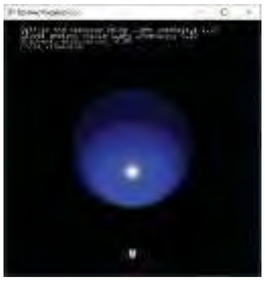

Figure 11.30: Screenshot of lightAndMaterial2.cpp: white light on, green off.

Experiment 11.9. Run lightAndMaterial2.cpp.

Reduce the white light's diffuse and specular intensity to nearly 0. The ball becomes a flat dull blue disc with only the green highlight prominent (Figure 11.29). This is because the ball's diffuse (and ambient) is blue and cannot reflect the green light's diffuse component, causing the ball thereby to lose almost all diffuse light and, consequently, three-dimensionality.

Raising the white global ambient brightens the ball, but it still looks flat in the absence of diffusive light. End

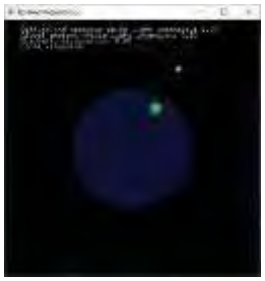

Figure 11.31: Screenshot of lightAndMaterial2.cpp: white light off, green on.

Exercise 11.11. (Programming) Explain the significant difference in what is seen when the white light is on and the green off (Figure 11.30) in lightAndMaterial2.cpp versus oppositely when the white light is off and the green on (Figure 11.31).

11.3.4 Color Material Mode

Remember glColor*() which we used to set vertex color in the dark days before there were light sources? Now that glMaterial*() allows us to set all sorts of material properties, including color, per vertex, it seems there's no use any more for glColor*(). Well, it turns out that the good folk at OpenGL Inc. found a way to keep it on the payroll.

Here's how. Suppose you're in the not uncommon situation coloring a scene where only a particular color attribute, say the ambient and diffuse reflectances of the front faces, changes from one object to the next, other attributes remaining constant. What you can do in this case, instead of repeatedly calling glMaterialfv(GL_FRONT, GL_AMBIENT AND DIFFUSE, *value*), is to:

1. Enable the so-called *color material mode* with a call to glEnable(GL_COLOR_MATERIAL).

2. Call glColorMaterial(GL FRONT, GL AMBIENT AND DIFFUSE), which tells OpenGL to use the current color, set by glColor*(), to determine the front-face ambient and diffuse color values.

Generally, the glColorMaterial() call can be of the form glColorMaterial(*face*, *parameter*) where *face* can be GL_ FRONT, GL_ BACK or GL_ FRONT _AND _-BACK, and *parameter* one of GL_AMBIENT, GL_DIFFUSE, GL AMBIENT _AND_ DIFFUSE, GL_SPECULAR or GL EMISSION.

3. Make a call to glColor*() to set the front-face ambient and diffuse color from one object to the next.

Experiment 11.10. Run spotlight.cpp. The program is primarily to demonstrate spotlighting, the topic of a forthcoming section. Nevertheless, press the page-up key to see a multi-colored array of spheres. Figure 11.32 is a screenshot.

Currently, the point of interest in the program is the invocation of the color material mode for the front-face ambient and diffuse reflectances by means of the last two statements in the initialization routine, viz.,

```
glEnable(GL COLOR_MATERIAL);
glColorMaterial(GL FRONT, GL AMBIENT AND_DIFFUSE);
```

and subsequent coloring of the spheres in the drawing routine by glColor4f() statements. End

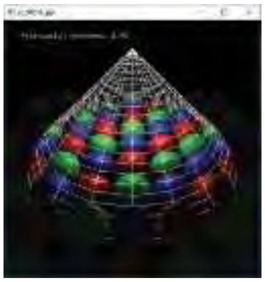

Figure 11.32: Screenshot of spotLight.cpp.

11.4 OpenGL Lighting Model

The so-called OpenGL *lighting model* sets certain environmental parameters. This terminology, even though used in the red book, is somewhat unfortunate as it may suggest laws of interaction between light and objects, or a relation with Phong's model – neither of which is true. The four parameters the OpenGL lighting model sets are the following:

1. The global ambient light with the statement

   glLightModel*(GL LIGHT MODEL AMBIENT, *globAmb*)

   where *globAmb* is the global ambient light vector. This we've seen already.

2. Whether to use a local or infinite viewpoint for lighting calculation.

   See again the lighting equation (11.11). The halfway vector s^i at a vertex, one for each light source, is the unit vector bisecting the angle between the direction vector l^i to the light source L^i and the direction vector e to the eye.

   The OpenGL eye being fixed at the origin $[0\ 0\ 0]^T$, we can take (the unnormalized) $e = -V$, denoting a vertex V 's position vector by V as well. Clearly, then, e changes from one vertex to another. However, it simplifies lighting computation to keep e constant, particularly $e = [0\ 0\ 1]^T$, equivalent to *assuming* an eye which is infinitely far up the z-axis and so, effectively, in the same direction from every vertex. See Figure 11.33. This simplification, often, still gives adequately authentic lighting.

   The OpenGL default viewpoint, in fact, is infinite. For lighting calculation to be done using a local viewpoint instead – i.e., with the eye at the origin – call

   glLightModel*(GL LIGHT MODEL LOCAL_VIEWER, GL_TRUE)

   which is what we do in the setup() routines of both sphereInBox1.cpp and lightAndMaterial1.cpp, while lightAndMaterial2.cpp provides an option. The local viewpoint is more realistic at the expense of greater computation.

   Remark 11.11. The chosen light model viewpoint is used *only for lighting calculations*. The viewing frustum or box stays unchanged. Therefore, in the case of a frustum, for instance, we still *see the scene* from the eye at the origin.

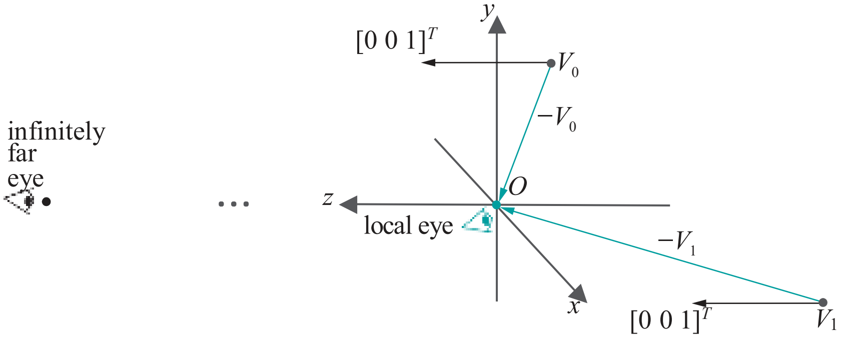

Figure 11.33: Local versus infinite viewpoint: the eye direction vector from each vertex toward the infinite viewpoint is black, while that toward the local viewpoint is green. V_i denotes both a vertex and its position vector.

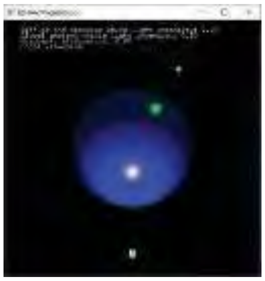

Figure 11.34: Screenshot of lightAndMaterial2.cpp: local viewpoint.

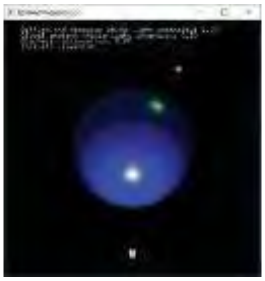

Figure 11.35: Screenshot of lightAndMaterial2.cpp: infinite viewpoint.

Remark 11.12. The direction vector l to the light source, too, changes from vertex to vertex if the source is positional, i.e., if w 0 in the value $[x\ y\ z\ w]^T$ of the source's GL_POSITION. However, a simplification exactly similar to that of assuming an infinite viewpoint can be achieved, not by tweaking the OpenGL lighting model, but by making the light directional by setting $w = 0$. We'll discuss this next section.

Experiment 11.11. Run lightAndMaterial2.cpp. Press 'l' or 'L' to toggle between the Local and the infinite viewpoint in lightAndMaterial2.cpp. See Figures 11.34 and 11.34 for screenshots. End

Exercise 11.12. (Programming) The change between local and infinite viewpoints in the preceding experiment seems to be only in the highlights, in other words, only the specular reflection. Why?

3. Whether to enable two-sided lighting.

The OpenGL default is to perform lighting calculations for each polygon based on its specified GL_FRONT face parameter values and its specified vertex normals, *regardless* if it is front or back facing. As the user likely sets material properties and normal values with the front faces of polygons in mind, results tend to be unrealistic for those whose back faces happen to be visible. So, when back faces might be visible, the command to use is

```
glLightModel*(GL_LIGHT_MODEL_TWO_SIDE, GL_TRUE)
```

which causes OpenGL to

(a) use the GL_BACK (or GL_FRONT_AND_BACK) parameter values to color back-facing polygons, *and*

(b) *reverse* the specified vertex normal for back-facing polygons.

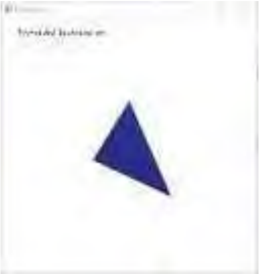

Figure 11.36: Screenshot of litTriangle.cpp showing the back face with two-side lighting on.

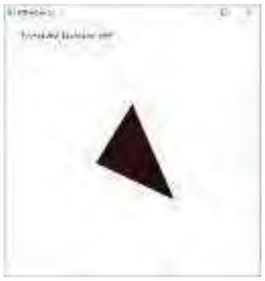

Figure 11.37: Screenshot of litTriangle.cpp showing the back face with two-side lighting off.

Experiment 11.12. Run litTriangle.cpp, which draws a single triangle, whose front face is coded to be red and back blue, initially front-facing and lit two-sided. Press the left and right arrow keys to turn the triangle and space to toggle two-sided lighting on and off. See Figures 11.36 and 11.37 for screenshots.

Notice how the back face is dark when two-sided lighting is disabled – this is because the normals are pointing oppositely of the way they should be. End

Exercise 11.13. (Programming) Comment out the statement enabling two-sided lighting in sphereInBox1.cpp, predicting what will be different before running.

4. Whether to apply specular light before or after texturing.

   The following remarks will be more meaningful after the discussion of textures in the next chapter.

   The OpenGL default is to apply textures *following* lighting calculations, which can cause specular highlights to be smothered. However, the command

```
glLightModel*(GL LIGHT MODEL COLOR CONTROL,
                GL SEPARATE SPECULAR COLOR)
```

   makes OpenGL

   (a) separately produce two colors at each vertex: a primary color calculated from all incoming non-specular components and a secondary color from all incoming specular components,

   (b) combine only the primary color with texture color at the time of texture mapping and, finally,

   (c) add in the secondary color to the result of the previous step, which assures the specular highlights.

11.5 Directional Lights, Positional Lights and Attenuation of Intensity

Directional and Positional Light Sources

We know that the value of the GL POSITION parameter of a light source L specifies its location $[x\ y\ z\ w]^T$ in homogeneous coordinates.

If $w = 0$, then the light source is called *positional*, or *local*, or *point*, and located at world coordinates $[x/w\ y/w\ z/w]^T$. This is the kind of source we have used so far. And, in this case, the (unnormalized) light direction vector at a vertex V is

$$l = [x/w \quad y/w \quad z/w]^T - V \qquad \text{(denoting } V\text{'s position vector by } V \text{ as well)}$$

which, of course, varies with V. See Figure 11.38.

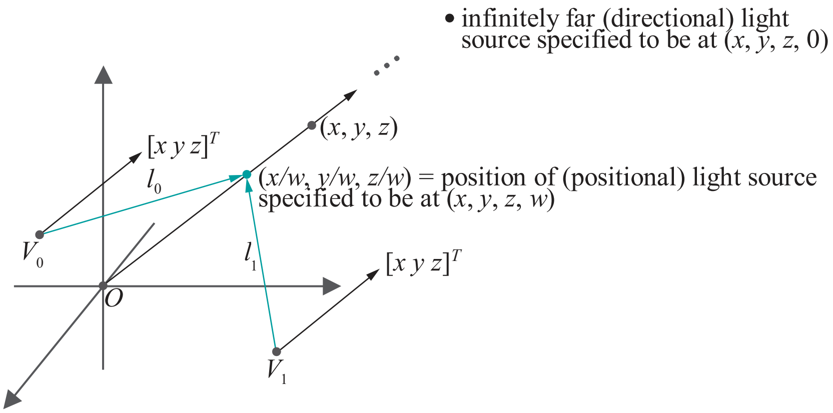
• infinitely far (directional) light
source specified to be at (x, y, z, 0)
(x, y, z)
[x y z]^T
l_0
(x/w, y/w, z/w) = position of (positional) light source
specified to be at (x, y, z, w)
V_0
l_1
[x y z]^T
O
V_1

Figure 11.38: Directional versus positional light: the direction vector from each vertex toward the directional light is black and parallel to the direction of the directional light, while that toward the positional light is green.

However, if $w = 0$, then the light source is *directional* and assumed located at an infinite distance in the direction of $[x\ y\ z]^T$ from the origin, in which case the light direction vector at *every* vertex is the same $[x\ y\ z]^T$.

When modeling a scene, a positional light is one which is located within it or nearby, e.g., a street light or car headlight, while a directional light is far removed, e.g., the sun. Evidently, lighting calculation is cheaper for directional sources. The default value for GL_POSITION is $[0\ 0\ 1\ 0]^T$, which defines a directional light shining down from high up the z-axis.

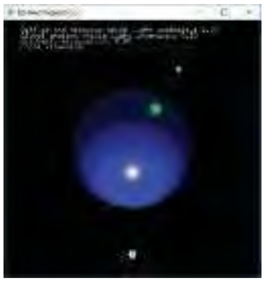

Figure 11.39: Screenshot of lightAndMaterial2.cpp: positional light source at white ball.

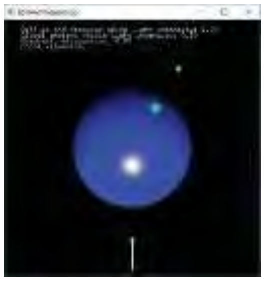

Figure 11.40: Screenshot of lightAndMaterial2.cpp: directional light source along white arrow.

Experiment 11.13. Press 'p' or 'P' to toggle between Positional and directional white light in lightAndMaterial2.cpp. The white wire sphere indicates the positional light, while the white arrow the incoming directional light. See Figures 11.39 and 11.40. Keep in mind that you can both move the ball and rotate the light position. End

Exercise 11.14. Explain the difference in how the ball looks in Figures 11.39 and 11.40.

Attenuation of Light

In the real world, the intensity of light from a source diminishes with distance from the source following an inverse square law. This phenomenon, called *distance attenuation*, can be modeled in OpenGL as well by a multiplicative *distance attenuation factor*

$$\frac{1}{k_c + k_l d + k_q d^2}$$

where d is the distance from the light source and k_c, k_l and k_d are the values of the light parameters GL CONSTANT ATTENUATION, GL LINEAR ATTENUATION and GL QUADRATIC ATTENUATION, respectively. These values are set by statements of the form

glLightf(GL LIGHTi, GL CONSTANT ATTENUATION, k_c);
glLightf(GL LIGHTi, GL LINEAR ATTENUATION, k_l);
glLightf(GL LIGHTi, GL QUADRATIC ATTENUATION, k_q);

The default values are $k_c = 1$ and $k_l = k_q = 0$, which imply no attenuation over distance at all.

Attenuating the intensity of a directional light over distance is not meaningful as it's already infinitely far from every vertex; therefore, changing attenuation parameters from the default has no effect for such a source.

Experiment 11.14. Run lightAndMaterial2.cpp. The current values of the constant, linear and quadratic attenuation parameters are 1, 0 and 0, respectively, so there's no attenuation. Press 't/T' to decrease/increase the quadratic aTtenuation parameter. Linear attenuation is always zero.

Move the ball by pressing the page up/down keys to observe the effect of attenuation. Figure 11.41 shows the ball some ways off with no attenuation and then with some amount of attenuation in the case of both a positional and a directional light. End

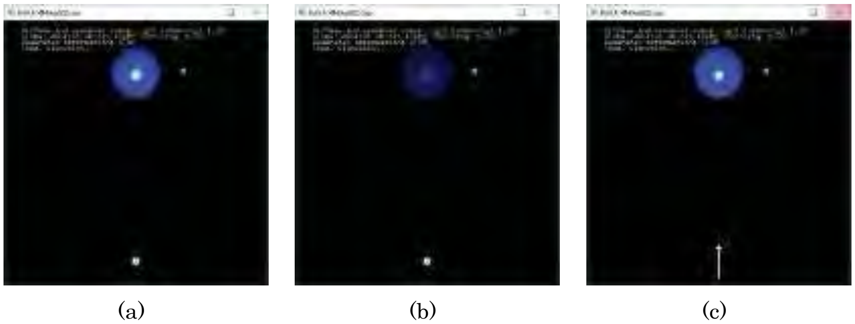

(a) (b) (c)

Figure 11.41: Screenshots of lightAndMaterial2.cpp: (a) No attenuation (b) Quadratic attenuation 0.05 (c) Quadratic attenuation 0.05 but light changed to directional.

11.6 Spotlights

The default for a light source is that it's *regular* , emitting in all directions (a fancy descriptor would be *omnidirectional*). This can be altered by turning it into a *spotlight* , in which case the emitted light is in the shape of a cone, the purpose being, of course, to simulate a real-life spotlight illuminating a limited area.

Figures 11.42(a) and (b) show, respectively, plane sections of the light from a regular source and a spotlight.

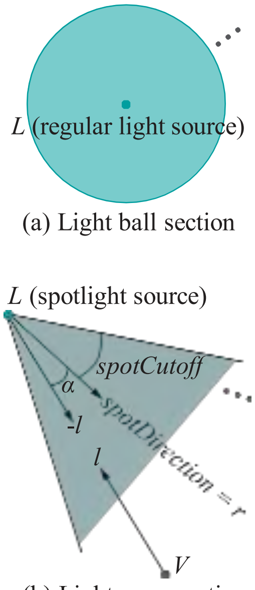

(a) Light ball section

(b) Light cone section

Figure 11.42: Partial plane sections of (a) regular light (b) spotlight.

Experiment 11.15. Run spotlight.cpp, which shows a bright white spotlight illuminating a multi-colored array of spheres. Figure 11.43 is a screenshot.

Press the page up/down arrows to increase/decrease the angle of the light cone. Press the arrow keys to move the spotlight. Press 't/T' to change the spotlight attenuation exponent (to be explained soon). A white wire mesh is drawn separately along the light cone boundary. End

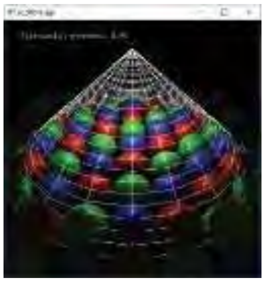

Figure 11.43: Screenshot of spotLight.cpp (with attenuation exponent 2.0).

The first step to turning a light source L into a spotlight is to specify the *half-angle* at the apex of the light cone, called the *spotlight cutoff angle*, with a command

glLightf(GL LIGHT0, GL SPOT CUTOFF, *spotCutoff*)

which, in fact, sets the spotlight cutoff angle to the value *spotCutoff* . The whole light cone angle then is 2*spotCutoff* . The spotlight cutoff angle should be between 0.0 and 90.0. The default is the special value of 180.0, meaning that L is not a spotlight, but a regular source emitting in all directions ($2 * 180^\circ$ being 360°). The initial value of the spotlight cutoff angle in spotlight.cpp, in fact, is 10° , as the reader may check from the glLightf(..., GL SPOT CUTOFF, ...) statement in the drawScene() routine.

The next step is to specify the *spotlight direction* or, more specifically, that of the axis of its cone with a command

glLightfv(GL LIGHT0, GL SPOT DIRECTION, *spotDirection*)

which sets the axis in a direction parallel to the vector $[x\ y\ z]^T$, if *spotDirection* is set to $\{x, y, z\}$. The default value of *spotDirection* is $\{0.0, 0.0, -1.0\}$, aiming the spotlight down the negative z-axis. It is set to $\{0.0, -1.0, 0.0\}$ in spotlight.cpp, pointing the spotlight in the negative y-direction.

The final step is to set the *spotlight attenuation exponent*, which controls the distribution of intensity through the light cone, with a command

glLightfv(GL LIGHT0, GL SPOT EXPONENT, *spotExponent*)

If the spotlight attenuation exponent is h and the angle between the axis of the light cone and the direction from the light source L toward vertex V is α, as in Figure 11.42(b), then the intensity of light at V is attenuated by the multiplicative factor $\cos^h \alpha$. This, of course, presumes that V lies within the light cone in the first place; if not, of course, no light reaches V from L at all. Note that a vector from L toward V is, simply, $-l$, the negative of the light direction vector at V . The spotlight attenuation exponent is set to 2.0, initially, in spotlight.cpp.

The logic behind the spotlight attenuation exponent is exactly same as that for the shininess exponent in the calculation of specular reflection in Equation (11.8) – so that the greater the value h of the attenuation exponent, the more rapidly the intensity of the spotlight diminishes away from the cone's axis. Equivalently, the greater h the more concentrated or focused the spotlight. OpenGL's default value for the spotlight attenuation exponent is 0, implying no attenuation at all.

Experiment 11.16. Run again spotlight.cpp. Observe the darkening of the balls near the cone boundary as the attenuation exponent is increased by pressing 'T'. Figure 11.44 is a screenshot with the attenuation exponent equal to 10.0. Compare this with the Figure 11.43 where the exponent was 2.0. End

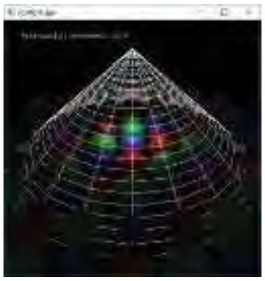

Figure 11.44: Screenshot of spotLight.cpp (with attenuation exponent 10.0).

Exercise 11.15. A spotlight should always be positional. Why?

For use in the upcoming final OpenGL light equation, let's write a single complete formula for a *spotlight attenuation factor* or, briefly, *saf*, at a vertex V, for a given light source L. Denote the unit vector along the spotlight axis, i.e., the normalized value of the spotlight direction, by r. Assume that l, the light direction vector at V, is normalized as well. Denote the spotlight cutoff angle by *spotCutoff* and the spotlight attenuation exponent by h. Then we have:

$$saf = \begin{cases} 1 \;, & \text{if } spotCutoff = 180.0 \\ 0 \;, & \text{if } -l \cdot r < \cos(spotCutoff) \\ (-l \cdot r)^h \;, & \text{otherwise} \end{cases} \tag{11.12}$$

Here's how to parse the formula.

The first line is the case when L, in fact, is not a spotlight, so there's no angular attenuation.

For the second line, refer to Figure 11.42(b) as you read on. Note that $-l$ is the unit vector from L toward V. Therefore, $-l \cdot r = \cos a$, where a is the angle between the axis of the light cone and the direction of V from L. Now, if $\cos a < \cos(spotCutoff)$, then $a > spotCutoff$, which means that V lies outside the light cone and gets no light. This explains the second line.

The third line, of course, gives the multiplicative angular attenuation factor $\cos^h a$.

Note: A spotlight could be distance attenuated, as well as angle attenuated.

Exercise 11.16. Why isn't it necessary to write $(\max\{-l \cdot d, 0\})^h$, instead of just $(-l \cdot d)^h$, in Equation (11.12) in a manner similar to the first lighting equation (11.11)?

11.7 OpenGL Lighting Equation

We now have the two additional pieces needed to enhance the first lighting equation (11.11) to the form which is, in fact, used by OpenGL to calculate RGB color intensities at a vertex V, namely, distance attenuation and spotlight attenuation. The enhancement is straightforward.

All symbols from the first lighting equation retain the same meaning. Additionally, d^i denotes the distance of V from the ith light source; k_c^i, k_l^i and k_q^i denote, respectively, the constant, linear and quadratic attenuation parameters for the ith light source; and saf^i is the spotlight attenuation factor for the ith light source at the vertex V, as given by Equation (11.12).

So, finally, here it is, the grand ole lighting equation of OpenGL:

$$\begin{aligned} V_X \;=\;& V_{emit,\,X} \;+ \\ & globAmb_X * V_{amb,\,X} \;+ \\ & \sum_{i=0}^{N-1} \frac{1}{k_c^i + k_l^i d^i + k_q^i (d^i)^2} * saf^i * \\ & \qquad L^i_{amb,\,X} * V_{amb,\,X} \;+ \\ & \qquad \max\{l^i \cdot n,\, 0\} * L^i_{diff,\,X} * V_{diff,\,X} \;+ \\ & \qquad (\max\{s^i \cdot n,\, 0\})^f * L^i_{spec,\,X} * V_{spec,\,X} \end{aligned} \tag{11.13}$$

where V_X is the color intensity at V, X being any of RGB.

The additions to the first lighting equation (11.11) are exactly the two multiplicative terms on the third line of the current equation, representing distance attenuation and spotlight attenuation, respectively.

Remark 11.13. We must revisit Exercise 11.7 at this time. Its implication that all individual light source ambients can be consolidated into the global ambient is not true any more if one uses Equation (11.13) instead of Equation (11.11), because the same light source can contribute different amounts of ambient light to different vertices owing to distance and spotlight attenuation.

Nevertheless, the simplification of setting all individual light source ambients to zero, and adjusting only the global, is almost always worth the mild damage to authenticity.

Exercise 11.17. If there is a single directional light source in an OpenGL program, which is not distance attenuated, which of the three – ambient, diffuse and specular – reflectance components at its vertices is changed by *translating* an object?

Exercise 11.18. If there is a single positional light source in an OpenGL program, which is not a spotlight and not distance attenuated, which of the three – ambient, diffuse and specular – reflectance components at an object's vertex can change by moving the light source? By translating the object?

Exercise 11.19. Which of the three components – ambient, diffuse and specular – of light reflected from a vertex V are affected if the normal at V is altered?

11.8 OpenGL Shading Models

A *shading model* is a method to shade, or color, the interiors of primitives. Keep in mind that Phong's lighting model, as implemented through the OpenGL lighting equation, determines colors *only* at the vertices of primitives, but says nothing about how to spread them inside. OpenGL's default shading model, called *smooth shading* or *Gouraud shading*, is to linearly interpolate color values computed at its vertices through a primitive's interior. In fact, we discussed at length in Section 7.2 the mechanics of linear interpolation.

An alternate simplistic shading model, called *flat shading*, is available, as well, in OpenGL. It is specified by a call to

```
glShadeModel(GL FLAT)
```

The default of smooth shading is restored by calling

```
glShadeModel(GL SMOOTH)
```

When flat shading, even if the color values differ across the vertices of a primitive, OpenGL chooses *one* of them, called the *provoking vertex* , and applies its color to the entire primitive. For example, the provoking vertex of a triangle is its first (according to the order of the vertices in the code). In a triangle strip, the provoking vertex of the i th triangle is the $i + 2$ th vertex. The reader is referred to the red book for a full description of provoking vertices for each primitive type.

Flat shading sometimes can be a reasonable alternative, particularly in the absence of lighting. Computationally it's, of course, far less expensive than smooth shading as there's no interpolation to do. An interesting application of flat shading is in applying "discrete" color schemes which, often, is difficult with smooth shading. The following experiment is an illustration.

Experiment 11.17. Run checkeredFloor.cpp, which creates a checkered floor drawn as an array of flat shaded triangle strips. See Figure 11.45. Flat shading causes each triangle in a strip to be painted with the color of the last of its three vertices, according to the order of the strip's vertex list.

End

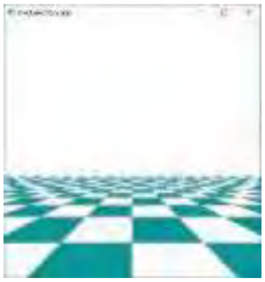

Figure 11.45: Screenshot of checkeredFloor.cpp.

Exercise 11.20. (Programming) Try and replicate the checkered floor of the preceding experiment using smooth shading instead of flat.

11.9 Animating Light

There are three ways that the spatial properties of a light source can be animated:

1. By moving its position.
2. By changing its direction if it's a spotlight.
3. By changing the light cone angle if it's a spotlight.

We've already seen light motion in two programs in this chapter – lightAndMaterial2.cpp and spotlight.cpp – the light source being moved by the arrow keys in both programs, while the cone angle is altered in spotlight.cpp with the page up/down keys.

Things to keep in mind are:

(a) A light source's position vector, specified by a **glLightfv(***light*, GL_ POSITION, *lightPos*) statement, is transformed by the value of the current modelview matrix by multiplication from the left. (See Section 4.2 if you need to review modelview matrices.)

Effectively, then, modelview transformations in the code prior to the glLightfv(*light*, GL POSITION, *lightPos*) statement apply to a light's position, exactly as if it were a vertex position specified by a glVertex3f() statement.

(b) Likewise, a spotlight source's direction vector, specified by the **glLightfv(***light*, GL_SPOT_ DIRECTION, *spotDirection*) statement, is transformed by the value of the current modelview matrix by multiplication from the left.

For example, as the light source of sphereInBox1.cpp is positioned by the glLightfv(GL LIGHT0, GL POSITION, lightPos) statement in the initialization routine setup(), it is unaffected by any modelview transformations in drawScene(). However, both lights of lightAndMaterial1.cpp are positioned in the display routine following the viewing command gluLookAt(), so their positions are, in fact, transformed by gluLookAt(), which means that the lights stay static relative to the scene, no matter if the viewpoint is changed by altering parameters in gluLookAt(). The light positions of lightAndMaterial2.cpp are similarly transformed by its own gluLookAt().

Prior to the positioning of the white light of lightAndMaterial2.cpp are a couple of rotation commands as well, which, therefore, turn it; likewise, the spotlight of spotlight.cpp is positioned in the display routine after the viewing transformation and a user-specified translation.

Remark 11.14. We've discussed animating only spatial attributes of a light source. Obviously, color values can be animated as well.

11.10 Partial Derivatives, Tangent Planes and Normal Vectors 101

This section is an introduction to the calculus sometimes required to calculate normals to surfaces. It is not mandatory reading. We suggest you skip this section initially and consult it later if need be.

Actually, if you know how to compute derivatives of a function of a single variable, e.g., $f(x) = x^2$ or $f(x) = \sin x$, as we'll assume you do, you already know how to compute partial derivatives. Because . . .

Definition 11.1. Suppose that f is a function of more than one variable $x, y,$ The *partial derivative* of f with respect to one of these variables, say x, is the derivative of f as a function *only* of x, assuming the other variables all fixed. The partial derivative of f with respect to x is denoted $\frac{\partial f}{\partial x}$.

Example 11.6. Evaluate the partial derivatives of

$$f(x, y) = x^2 + y^2$$

at the point (1, 2).

Answer: We have

$$\frac{\partial f}{\partial x}(x, y) = 2x, \qquad \frac{\partial f}{\partial y}(x, y) = 2y$$

Therefore,

$$\frac{\partial f}{\partial x}(1, 2) = 2, \qquad \frac{\partial f}{\partial y}(1, 2) = 4$$

Remark 11.15. Often $\frac{\partial f}{\partial x}(x, y)$ is simply written $\frac{\partial f}{\partial x}$, e.g., the first two equations of the preceding answer could be written

$$\frac{\partial f}{\partial x} = 2x, \qquad \frac{\partial f}{\partial y} = 2y$$

Example 11.7. Evaluate the partial derivatives of

$$f(x, y) = x^2 \sin y$$

at the point $(1, \pi/2)$.

Answer: We have

$$\frac{\partial f}{\partial x} = 2x \sin y, \qquad \frac{\partial f}{\partial y} = x^2 \cos y$$

Therefore,

$$\frac{\partial f}{\partial x}(1, \pi/2) = 2, \qquad \frac{\partial f}{\partial y}(1, \pi/2) = 0$$

Exercise 11.21. Evaluate the partial derivatives of

$$f(x, y, z) = xz + \sin x \cos y \cos z + y$$

at the point $(\pi/2, \pi, 0)$.

Exercise 11.22. Evaluate the partial derivatives of

$$f(x, y) = xy$$

at the point (2, 3).

Exercise 11.23. Evaluate the partial derivatives of

$$f(x, y, z) = x \cos y + y \cos z + z \cos x$$

at the point $(\pi/2, 0, \pi/2)$.

The reader may wonder that if the partial derivative $\frac{\partial f}{\partial x}$, for example, is obtained by differentiating f with respect to the single variable x, assuming the others fixed, then why do those other variables pop up again in the expression for $\frac{\partial f}{\partial x}$? Here's the reason.

Consider the function $f(x, y) = x^2 \sin y$ of Example 11.7 above. Fixing y at, say, the value $\pi/6$ gives the function $f(x, \pi/6) = x^2/2$, while fixing y at $\pi/2$ gives the function $f(x, \pi/2) = x^2$. Both $f(x, \pi/6)$ and $f(x, \pi/2)$ are functions of the one variable x, but they are *different* functions because y's been fixed at two *different* values.

Moreover,

$$\frac{\partial f}{\partial x}(x, \pi/6) = \frac{\mathrm{d}}{\mathrm{d}x}(x^2/2) = x \quad \text{and} \quad \frac{\partial f}{\partial x}(x, \pi/2) = \frac{\mathrm{d}}{\mathrm{d}x}(x^2) = 2x$$

are different as well, as they are derivatives of different functions. This is why $\frac{\partial f}{\partial x}$ depends on y, as well as on x.

So far so good. At least calculating partial derivatives is no different from calculating ordinary derivatives. But what do partial derivatives mean geometrically (in “real life”, that is)?

To answer this, let’s see first how ordinary derivatives specify the tangent to a curve in the case of both implicit and parametric declarations.

(a) *Implicit*: Suppose a plane curve is given by the equation

$$y = f(x)$$

Then the value of

$$\frac{\mathrm{d}f}{\mathrm{d}x}$$

at $x = a$ is the gradient of the tangent line to the curve at the point $(a, f(a))$.

For example, the gradient of the tangent line l at the point $(1, 1)$ of the parabola

$$y = x^2$$

is 2 as

$$\frac{\mathrm{d}}{\mathrm{d}x}(x^2) = 2x$$

which equals 2 when x is 1. See Figure 11.46(a). Moreover, any non-zero vector along l, e.g., $v = [1\ 2]^T$, is a tangent vector to the parabola at $(1, 1)$.

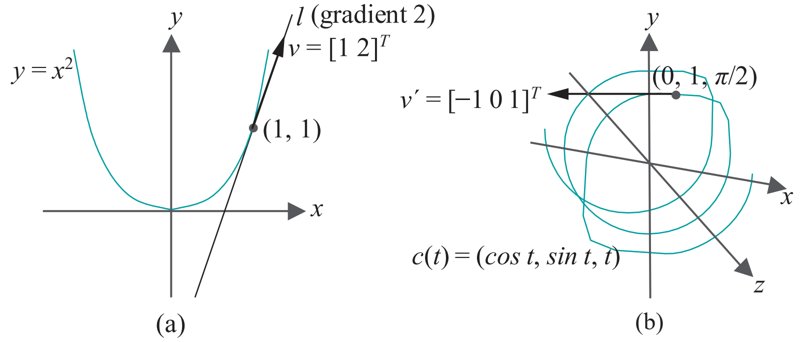

Figure 11.46: Tangents: (a) Tangent line l and tangent vector v to the parabola $y = x^2$ at $(1, 1)$ (b) Tangent vector v^1 to the helix $c(t) = (\cos t,\ \sin t,\ t)$ at $(0,\ 1,\ \pi/2)$.

(b) *Parametric*: Suppose a curve in 3-space is given by

$$c(t) = (f(t), g(t), h(t))$$

Then the value of the vector

$$c^1(t) = \left[\frac{\mathrm{d}f}{\mathrm{d}t}\ \frac{\mathrm{d}g}{\mathrm{d}t}\ \frac{\mathrm{d}h}{\mathrm{d}t}\right]^T$$

at $t = a$ is a tangent vector to the curve at the point $(f(a), g(a), h(a))$.

For example, a tangent vector v^1 to the helix

$$c(t) = (\cos t,\ \sin t,\ t)$$

at the point $(0, 1, \pi/2)$, corresponding to $t = \pi/2$, is $[-1\ 0\ 1]^T$, as

$$\left[\frac{d}{dt}(\cos t) \quad \frac{d}{dt}(\sin t) \quad \frac{d}{dt}(t)\right]^T = [-\sin t \quad \cos t \quad 1]^T$$

which equals $[-1\ 0\ 1]^T$ when $t = \pi/2$. See Figure 11.46(b).

Remark 11.16. In the above and in what follows we ignore the possibility of singularities where the tangent does not even exist, e.g., if the tangent vector $c^1(t) = 0$.

It turns out that, just as the computation of partial derivatives is based on computing ordinary derivatives, their geometric significance obtains from that of ordinary derivatives too. Here's how:

(a) *Implicit* : Consider $z = f(x, y)$, a function of two variables. It defines a surface s in 3-space, called the graph of f. (*Note*: This form is more easily visualized than the most general $F(x, y, z) = 0$ for a surface in 3-space.)

Now, if we fix y at, say, the value b, then $z = f(x, b)$ gives a curve c on s; in fact, c is the section of s by the plane $y = b$. See Figure 11.47(a). (In terms of the discussion in Section 10.1.2, c's implicit specification consists of the two equations $z = f(x, y)$ and $y = b$.)

Now, $z = f(x, b)$ is the equation of the *plane* curve c, which can be thought of as lying on the xz-plane, for $y = b$ is a copy of the xz-plane. Moreover, by definition, the value of $\frac{\partial f}{\partial x}$ at (a, b) is the value at a of the ordinary derivative $\frac{d}{dx}f(x, b)$. Therefore, applying now the geometric interpretation earlier of the derivative of a plane curve given implicitly, we see that the value of $\frac{\partial f}{\partial x}$ at (a, b) is the gradient of the tangent line l_1, at the point $P = (a, b, f(a, b))$, to the sectional curve $z = f(x, b)$ of s.

In fact, l_1 is tangent to the surface s at P, as well, and any non-zero vector t_1 along l_1 is a tangent vector to s at P.

Likewise, the value of $\frac{\partial f}{\partial y}$ at (a, b) is the gradient of the tangent line l_2, at the point $P = (a, b, f(a, b))$, to the curve $z = f(a, y)$, which is the section of s by the plane $x = a$ (Figure 11.47(b)); moreover, l_2 is tangent to the surface s at P and any non-zero vector t_2 along l_2 is a tangent vector to s at P.

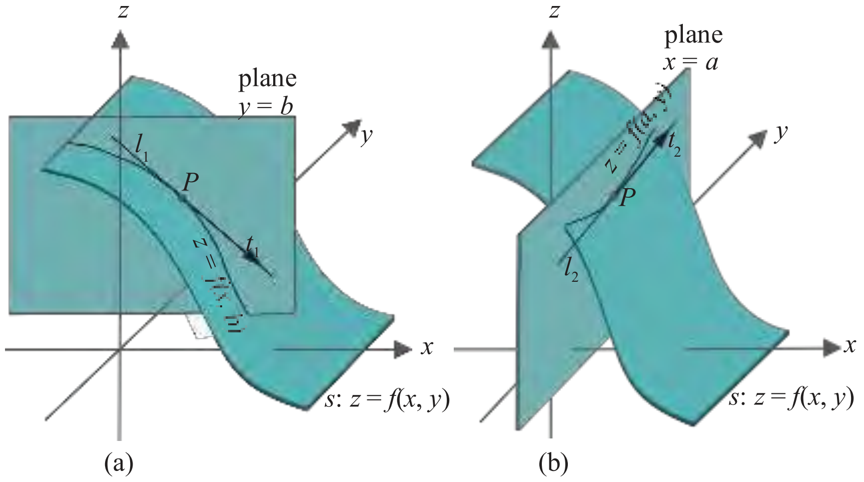

Figure 11.47: Section of the graph s of $z = f(x, y)$ by the (a) plane $y = b$, giving the tangent line l_1 and the tangent vector t_1 at $P = (a, b, f(a, b))$, (b) plane $x = a$, giving the tangent line l_2 and tangent vector t_2 at P.

(b) *Parametric*:

Consider next the surface s specified by the parametric equations

$$x = f(u, v), \;\; y = g(u, v), \;\; z = h(u, v), \;\; (u, v) \in W$$

where $W = [u_1, u_2] \times [v_1, v_2]$ is a rectangle in uv parameter space. The function $(u, v) \mapsto s(u, v) = (f(u, v), g(u, v), h(u, v))$ maps W to the surface s in 3-space. See Figure 11.48.

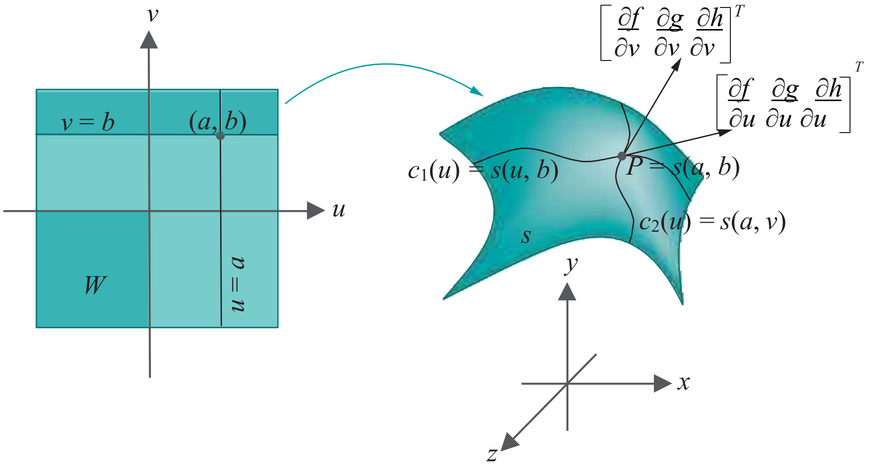
$\left[\frac{\partial f}{\partial v} \; \frac{\partial g}{\partial v} \; \frac{\partial h}{\partial v}\right]^T$
$\left[\frac{\partial f}{\partial u} \; \frac{\partial g}{\partial u} \; \frac{\partial h}{\partial u}\right]^T$
v
$v = b$
(a, b)
u
W
$u = a$
$c_1(u) = s(u, b)$
$P = s(a, b)$
$c_2(u) = s(a, v)$
s
y
x
z

Figure 11.48: The surface s is the image of a parameter rectangle W by the map $(u, v) \mapsto s(u, v) = (f(u, v), g(u, v), h(u, v))$ with tangents to the parameter curves on s at the point $P = s(a, b)$.

Fix a point $(a, b) \in W$. The image of the line $v = b$ by s is the u-parameter curve c_1 in 3-space with equation

$$c_1(u) = (f(u, b), \;\; g(u, b), \;\; h(u, b)), \;\; u \in [u_1, u_2]$$

From the geometric interpretation earlier of the ordinary derivative in the case of a space curve given parametrically, the tangent vector to this curve is

$$c'_1(u) = \left[\frac{d}{du} f(u, b) \quad \frac{d}{du} g(u, b) \quad \frac{d}{du} h(u, b)\right]^T$$

at $u \in [u_1, u_2]$. However, the RHS just above is by definition equal to

$$\left[\frac{\partial f}{\partial u}(u, b) \quad \frac{\partial g}{\partial u}(u, b) \quad \frac{\partial h}{\partial u}(u, b)\right]^T$$

We conclude that the value of the vector $\left[\frac{\partial f}{\partial u} \; \frac{\partial g}{\partial u} \; \frac{\partial h}{\partial u}\right]^T$ at the point (a, b) is a tangent vector to the u-parameter curve $c_1(u) = s(u, b)$ at the point $P = s(a, b)$ on s; in fact, it is, as well, a tangent vector to the surface s at P. Likewise, the value of the vector $\left[\frac{\partial f}{\partial v} \; \frac{\partial g}{\partial v} \; \frac{\partial h}{\partial v}\right]^T$ at the point (a, b) is a tangent vector to the v-parameter curve $c_2(v) = s(a, v)$ at the point P and a tangent vector to s at P.

So, we see that, just as an ordinary derivative on a curve specifies its tangent, partial derivatives can be used to specify tangents to a surface. In fact, they can give even more geometric information about the surface, in particular, by determining the tangent plane, as well as normals, as we see next.

Definition 11.2. If two tangent vectors, say t_1 and t_2, at a point P on a surface s are linearly independent – in other words, they are not collinear – then they span a plane p, called the *tangent plane* to the surface at P. The line l perpendicular to p through P is said to be the *normal line* to s at P and any non-zero vector lying on this line a *normal vector* to s at P. See Figure 11.49.

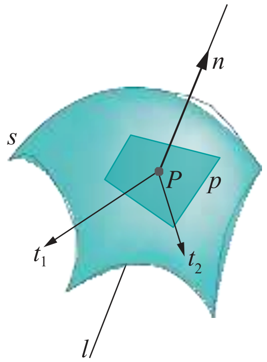

Figure 11.49: Tangent vectors t_1 and t_2 span the tangent plane p at point P on the surface s; l is the normal line and n a normal vector.

A tangent plane to a surface is precisely the analogue of a tangent line to a curve. A thin straight stick pressed to a plane wire curve aligns itself along the tangent line at the point of contact; likewise, a thin flat board pressed to a surface in 3-space aligns itself along the tangent plane at the point of contact.

Example 11.8. Determine the tangent plane and a normal vector at the point $P = (1, 2, 5)$ to the paraboloid s given by

$$z = x^2 + y^2$$

Answer : We can do this in two different ways depending on if we use the given implicit form or write a parametric one. Let's do both. See Figure 11.50 as we proceed.

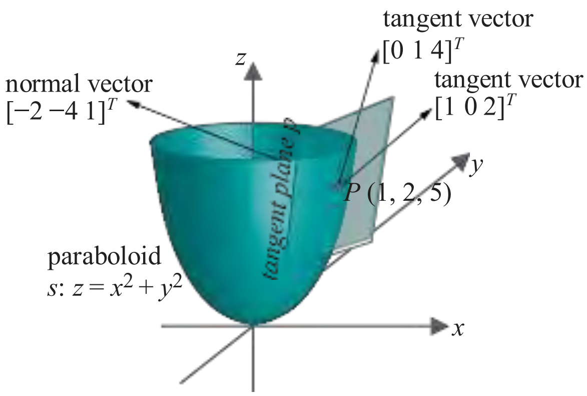

Figure 11.50: Tangent vectors, tangent plane and normal vector at the point $(1, 2, 5)$ to the paraboloid $z = x^2 + y^2$.

The implicit form of s is $z = f(x, y) = x^2 + y^2$. So, from earlier discussion, a tangent line to s at P, which is also a tangent line to the sectional curve $z = f(x, 2)$ at P, has gradient $\frac{\partial f}{\partial x}(1, 2) = 2$, as $\frac{\partial f}{\partial x} = 2x$. Therefore, a tangent vector to s at P on this tangent line is $[1\ 0\ 2]^T$, noting that that tangent line has gradient 2 lying on (a copy of) the xz-plane, which implies that any vector on it has z-component twice its x-component and y-component zero.

Likewise, a vector at P tangent to s, as well as to its sectional curve $z = f(1, y)$, is $[0\ 1\ 4]^T$. So, we have found two tangent vectors to s at P. Before proceeding further, let's see what we can do with a parametric form next.

It's easy first to write s in the parametric form

$$x = f(u, v) = u, \quad y = g(u, v) = v, \quad z = h(u, v) = u^2 + v^2 \tag{11.14}$$

the point P corresponding to the parameter values $u = 1$ and $v = 2$. From discussion earlier, we have that a tangent vector to s at P, which, in fact, is a tangent vector to the u-parameter curve on s at P, is the value of $\frac{\partial f}{\partial u}\ \frac{\partial g}{\partial u}\ \frac{\partial h}{\partial u}^{T} = [1\ 0\ 2u]^T$ at $(1, 2)$. This gives the tangent vector $[1\ 0\ 2]^T$. Likewise, one finds the vector $[0\ 1\ 4]^T$ tangent to the v-parameter curve on s at P, as well as to s itself at P.

So, we get the same two vectors $[1\ 0\ 2]^T$ and $[0\ 1\ 4]^T$ tangent to s at P using either the implicit or parametric form for s. Continuing, then, the tangent plane p to s at P is spanned by these two vectors. Precisely, p consists of all vectors of the form $a[1\ 0\ 2]^T + \beta[0\ 1\ 4]^T$, where a and β are any two reals.

A normal vector to s at P is perpendicular to its tangent plane there and, therefore, to both spanning vectors $[1\ 0\ 2]^T$ and $[0\ 1\ 4]^T$. It is obtained, then, as the cross-product of the latter two (cross-products of vectors were reviewed in Section 5.4.3), viz.,

$$[1\ 0\ 2]^T \times [0\ 1\ 4]^T = [-2\ -4\ 1]^T$$

Remark 11.17. Computing the tangent plane at a point of a surface and computing a normal vector there are evidently equivalent.

Exercise 11.24. Determine the tangent plane and a normal vector to the circular cylinder

$$x = \cos u, \;\; y = \sin u, \;\; z = v$$

at the point corresponding to the parameter values $(u, v) = (\pi/4, 3)$.

Exercise 11.25. Determine the tangent plane and a normal vector to the saddle-shaped surface (hyperbolic paraboloid is the mathematical name)

$$z = xy$$

at the point $(2, 3, 6)$.

Exercise 11.26. (Programming) Draw the paraboloid of Example 11.8 and its tangent plane at some point. The paraboloid should be wireframe and the tangent plane a finely meshed rectangle. Allow the user to press the arrow keys to slide the tangent plane over the paraboloid.

Normals from Function Gradients

There's a neat way to compute directly a normal vector at a point of a surface s given by an implicit equation of the most general form

$$F(x, y, z) = 0$$

without determining the tangent plane first: a normal vector to s at the point P is given by the value at P of the so-called *gradient* of F, denoted $grad(F)$ and defined by

$$grad(F) = \left[\frac{\partial F}{\partial x} \;\; \frac{\partial F}{\partial y} \;\; \frac{\partial F}{\partial z}\right]^T$$

We'll not prove that $grad(F)$ is indeed normal to the surface $F(x, y, z) = 0$, referring the reader instead to books on vector calculus, e.g., Schey [125] and Spiegel [138], for, not only the proof, but more about the gradient, as well as its related functions *divergence* and *curl*.

Example 11.9. Determine a normal vector to the paraboloid

$$z = x^2 + y^2$$

at the point $(1, 2, 5)$.

Answer: Write the implicit equation in the form

$$F(x, y, z) = z - x^2 - y^2 = 0$$

Then

$$grad(F) = \left[\frac{\partial F}{\partial x} \;\; \frac{\partial F}{\partial y} \;\; \frac{\partial F}{\partial z}\right]^T = [-2x\ -2y\ \ 1]^T$$

Therefore, a normal vector at the point $(1, 2, 5)$ is $[-2\ -4\ 1]^T$, which is obtained from putting $x = 1$ and $y = 2$ in the preceding equation. This result checks with Example 11.8.

Exercise 11.27. Verify your answer to Exercise 11.24 by finding a normal vector to the cylinder using the *grad* function. You must write an implicit equation for the cylinder first.

11.11 Computing Normals and Lighting Surfaces

Look carefully at the OpenGL lighting equation (11.13) once more. Outside of a bunch of user-specified color properties, the only data needed to compute the color intensities at a vertex V of an object O consists of the location of V, the locations of the light sources *and* the normal vector n at V.

The location of V, of course, is part of the user's design of O itself. As for the light sources, typically, they are few and can be located with a fair amount of flexibility for the desired level of illumination. Remaining is the normal vector n, which the user is free to set as well to whatever value she chooses. However, for authentic lighting it should actually be perpendicular to the surface of O at V or at least nearly so. For example, the choice of the normal vector n at the vertex V (outward along a radius) of the sphere in Figure 11.51 seems good, though either of the other two vectors drawn could conceivably have been picked as well without OpenGL complaining.

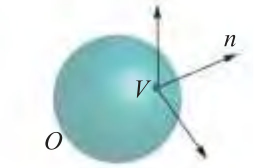

Figure 11.51: Three vectors at a vertex on a sphere, one of which has been chosen as the normal.

We'll discuss computing surface normals following the informal taxonomy of 2D objects in Section 10.2 before moving on to Bézier and quadric surfaces for which OpenGL provides automatic normals.

11.11.1 Polygons and Planar Surfaces

Polygons in particular, and planar surfaces in general, are the simplest. The normal at each vertex is simply normal to the plane itself containing the surface. In particular, unit vertex normals are all identical across a given side of the surface.

So how does one determine the normal direction to a plane p? If two non-collinear vectors u and v are known to lie on p, then the cross-product $u \times v$ is normal to p (cross-products were reviewed in Section 5.4.3). For example, two adjacent edges of a simple plane polygon, assuming they do not happen to lie on one line, determine non-collinear vectors u and v spanning the plane p containing the polygon. In Figure 11.52, $u = P_1 - P_0$ and $v = P_4 - P_0$ span p and $n = u \times v$ is normal to p.

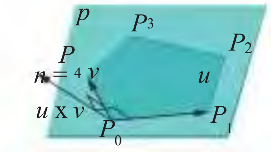

Figure 11.52: Vector n is normal to the plane p.

Exercise 11.28. Determine a normal to the plane p of the triangle with vertices at

$$P_0 = [0\ 3\ 5]^T, \quad P_1 = [1\ -2\ 0]^T, \quad P_2 = [3\ 3\ 3]^T$$

11.11.2 Meshes

Polygonal meshes are of interest next. Let's work with real examples.

Experiment 11.18. Run again sphereInBox1.cpp. The normal vector values at the eight box vertices of sphereInBox1.cpp, placed in the array normals[], are

$$[\pm 1/\sqrt{3}\ \ \pm 1/\sqrt{3}\ \ \pm 1/\sqrt{3}]^T$$

each corresponding to one of the eight possible combinations of signs. End

The choice of the normals in sphereInBox1.cpp is easily motivated. The box being situated symmetrically about the origin, the normal values are chosen as unit vectors along the lines from the origin to each of the eight vertices, which indeed give the values above. The box is depicted in Figure 11.53(a), where only the normal vector at the lower-right vertex V of the front face is shown: it is the green arrow n drawn by extending OV a unit distance from V.

In fact, probably a better rationale for this particular choice of normals, not depending on symmetry, is that the one at each vertex is the normalized *average* of the unit outward normals to the three faces meeting at that vertex. For example, in Figure 11.53(a) the unit outward normals to f_1, f_2 and f_3, the three faces which meet at V, are $[1\ 0\ 0]^T$, $[0\ 0\ 1]^T$ and $[0\ -1\ 0]^T$, respectively, whose average is $[1/3\ \ -1/3\ \ 1/3]^T$, which normalizes to $[1/\sqrt{3}\ \ -1/\sqrt{3}\ \ 1/\sqrt{3}]^T$, which one can verify from the code is indeed the value of the normal at V in sphereInBox1.cpp.

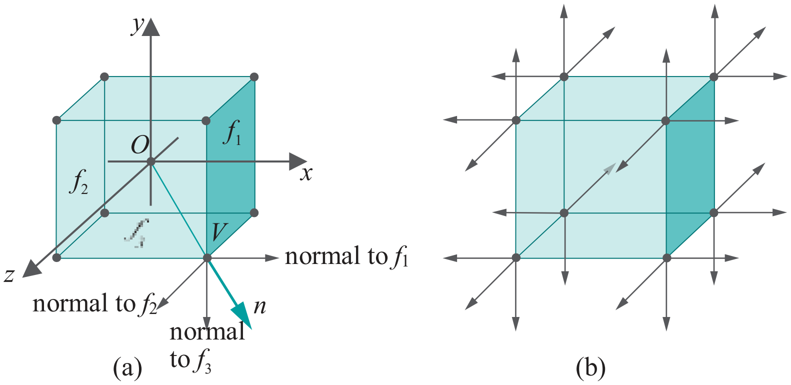

Figure 11.53: (a) The box of sphereInBox1.cpp with the averaged normal vector n at vertex V, together with the normals to the three faces that meet at V (f_1 right face, f_2 front face, f_3 bottom face) (b) The unaveraged normals of sphereInBox2.cpp.

Although they possess the virtue of symmetry and being averages, none of the box normals of sphereInBox1.cpp is even close to perpendicular to a face of the box. This consideration leads to another approach – to set the normal at each vertex of a face as a normal to that face itself. This is implemented as an option in sphereInBox2.cpp.

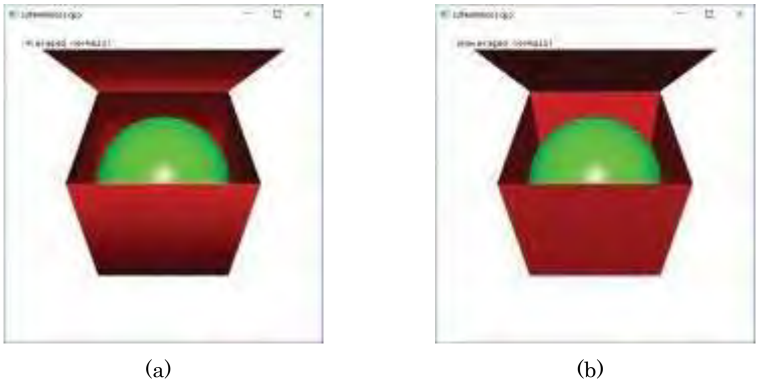

Figure 11.54: Screenshot of sphereInBox2.cpp: (a) Averaged box normals (b) Unaveraged box normals.

Experiment 11.19. Run sphereInBox2.cpp, which modifies sphereInBox1.cpp. Press the arrow keys to open or close the box and space to toggle between two methods of drawing normals.

The first method is the same as that of sphereInBox1.cpp, specifying the normal at each vertex as an average of incident face normals. The second creates the box by first drawing one side as a square with the normal at each of its four vertices identically specified to be the unit vector perpendicular to that square, then placing that square in a display list and, finally, drawing it six times appropriately rotated. Figure 11.53(b) shows the vertex normals to the three incident faces at each vertex. Figure 11.54 shows screenshots of the box created with and without averaged normals.

End

The contrast in output between the two ways of defining box normals in sphereInBox2.cpp is clear and the reason not hard to understand. The first method softens the edges because the averaged normal at each vertex is shared by all its three adjacent faces. Consequently, the interpolation of color values in each face's interior continues smoothly across its boundary.

The second method is significantly different. As each face is drawn separately with the normals at all its four vertices equal and perpendicular to the face itself, interpolation in the interior results in the entire face being colorized as if with that one normal value throughout. Moreover, this normal value turns abruptly 90° from one face to the next. The upshot is that there is a marked difference in color intensities, as well, from one face to the next, throwing the edges between them into sharp relief. Which approach to choose depends on the effect desired.

Remark 11.18. Using the second method, colors at pixels along an edge are defined differently by its two adjacent faces, while pixel colors at a vertex are defined differently, in fact, by its three adjacent faces. At these pixels, therefore, code order determines which color prevails. This is not desirable, but it is not a serious issue because such "ambiguous" pixels lie only on edges and vertices, but not in the interior of faces, the latter constituting by far the bulk of the figure.

Versions of the averaging approach implemented sometimes to achieve greater realism use a *weighted* average rather than a straight one. Two possibilities are:

(a) Weight the normal to each face incident at a vertex with the angle that face subtends at the vertex. In Figure 11.55, five faces meet at the vertex V subtending angles θ_1, θ_2, . . . , θ_5, respectively. Therefore, the angle-weighted average value of the normal at V is:

$$n = \frac{\theta_1 n_1 + \theta_2 n_2 + \theta_3 n_3 + \theta_4 n_4 + \theta_5 n_5}{\theta_1 + \theta_2 + \theta_3 + \theta_4 + \theta_5}$$

(b) Weight the normal to each face incident at a vertex with the area of that face. The areas of the five faces in Figure 11.55 meeting at V are A_1, A_2, . . . , A_5, respectively. The area-weighted average value of the normal at V is then:

$$n = \frac{A_1 n_1 + A_2 n_2 + A_3 n_3 + A_4 n_4 + A_5 n_5}{A_1 + A_2 + A_3 + A_4 + A_5}$$

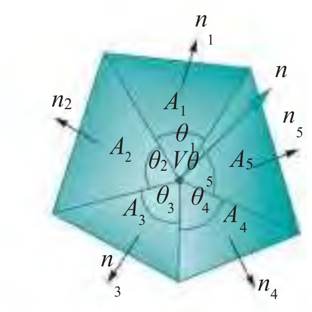

Figure 11.55: Weighted average of normals: θ_i are angles, A_i area, n_i face normals and n a weighted average normal at V.

Important : Whatever approach you adopt to compute normals, make sure, as a last step, to normalize each to unit length (easy enough – just divide each by its length). The reason is that OpenGL uses the dot product to compute the cosine of the angle between two vectors (see Equation (11.13)), which is correct *if* both are of unit length.

Example 11.10. For the trash can mesh whose vertices are given in Figure 11.56, compute the unit normals to the three faces adjacent to the vertex V. Then compute the (unweighted) average of these three normals and normalize to unit length.

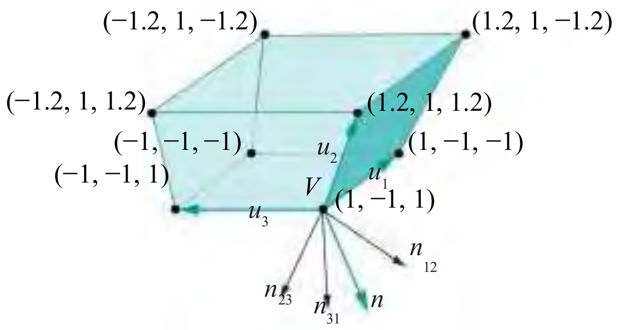

Figure 11.56: Trash can of five quadrilateral sides. The vectors n_{12}, n_{23} and n_{31} from V are normals to V's adjacent faces, while n is the averaged normal.

Answer: The three edge vectors emanating from V are:

$$\begin{aligned} u_1 &= [1\ \ -1\ \ -1]^T - [1\ \ -1\ \ 1]^T = -2k \\ u_2 &= [1.2\ \ 1\ \ 1.2]^T - [1\ \ -1\ \ 1]^T = 0.2i + 2j + 0.2k \\ u_3 &= [-1\ \ -1\ \ 1]^T - [1\ \ -1\ \ 1]^T = -2i \end{aligned}$$

Therefore, the outward unit normal to the face with edges u_1 and u_2 is

$$n_{12} = (u_1 \times u_2) \,/\, |u_1 \times u_2| = (4\mathrm{i} - 0.4\mathrm{j}) \,/\, \sqrt{4^2 + 0.4^2} \approx 0.995\mathrm{i} - 0.0995\mathrm{j}$$

and that to the face with edges u_2 and u_3 is

$$n_{23} = (u_2 \times u_3) \,/\, |u_2 \times u_2| = (-0.4\mathrm{j} + 4\mathrm{k}) \,/\, \sqrt{4^2 + 0.4^2} \approx -0.0995\mathrm{j} + 0.995\mathrm{k}$$

while the outward unit normal to the face with edges u_3 and u_1, the bottom face, is easily seen to be

$$n_{31} = -\mathrm{j}$$

The normalized average of these normals is

$$\begin{aligned} n &= (n_{12} + n_{23} + n_{31}) \,/\, |n_{12} + n_{23} + n_{31}| \\ &\approx (0.995\mathrm{i} - 1.199\mathrm{j} + 0.995\mathrm{k}) \,/\, \sqrt{0.995^2 + 1.199^2 + 0.995^2} \\ &\approx 0.538\mathrm{i} - 0.649\mathrm{j} + 0.538\mathrm{k} \end{aligned}$$

Exercise 11.29. (Programming) Use data from the preceding example to replace the box of sphereInBox2.cpp with a trash can. Omit the sphere. Let the user choose between averaged and unaveraged normals. Allow the can to be rotated keeping the light source fixed.

11.11.3 General Surfaces

As a general surface is drawn by approximating it with a polygonal mesh, the thought comes to mind to simply use the methods of the preceding section to find normals. Precisely, (a) formulate a mesh approximation of the surface and (b) specify the normal at each vertex as an average of those of its incident faces (we really want to use an average here, especially if the original surface is smooth, to avoid lighting discontinuities between adjacent faces).

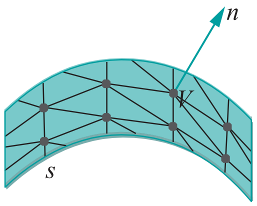

Figure 11.57: Normal vector n to the surface s at a vertex V of its mesh approximation.

This approach is perfectly reasonable if the surface is known to the user only by its mesh approximation. However, if one knows, say, a parametric representation of the original surface, why not get the normals from the "horse's mouth" – that being the parametrization itself? In other words, use the parametrization to *analytically* compute the normals at the mesh vertices. This makes for stable normals independent of the vagaries of the particular mesh approximation, not to mention those of the averaging process. For example, working from the mesh approximation of the surface s in Figure 11.57, the normals to the six faces incident at vertex V must be averaged to determine the normal n at V. However, knowledge of s itself could enable a direct computation without reference to any particular triangulation.

So let's see how to compute normals analytically. We're going to assume in the following that you know that the tangent plane at the point $s(u, v)$ to a surface s given parametrically by the equations

$$x = f(u, v),\ y = g(u, v),\ z = h(u, v)$$

is spanned by the two vectors

$$\begin{bmatrix} \frac{\partial f}{\partial u} & \frac{\partial g}{\partial u} & \frac{\partial h}{\partial u} \end{bmatrix}^T \quad \text{and} \quad \begin{bmatrix} \frac{\partial f}{\partial v} & \frac{\partial g}{\partial v} & \frac{\partial h}{\partial v} \end{bmatrix}^T$$

evaluated at (u, v) (provided they are not collinear). Moreover, a normal vector to s at $s(u, v)$ is the cross-product

$$\begin{bmatrix} \frac{\partial f}{\partial u} & \frac{\partial g}{\partial u} & \frac{\partial h}{\partial u} \end{bmatrix}^T \times \begin{bmatrix} \frac{\partial f}{\partial v} & \frac{\partial g}{\partial v} & \frac{\partial h}{\partial v} \end{bmatrix}^T \qquad (11.15)$$

evaluated at (u, v). If you need to brush up, Section 11.10 was a review of the needed calculus.

Denote the normalized value of the vector (11.15) – obtained by dividing it by its magnitude – by

$$[f_n(u, v) \quad g_n(u, v) \quad h_n(u, v)]^T \tag{11.16}$$

which, therefore, is a unit normal to s at $s(u, v)$.

Finally, we'll specify either $[f_n(u, v)\ g_n(u, v)\ \ h_n(u, v)]^T$ or its reverse, $[-f_n(u, v) \quad -g_n(u, v) \quad -h_n(u, v)]^T$, as the unit normal at $s(u, v)$ depending on which direction is appropriate for front-facing triangles. There's not much to worry about making a wrong choice in this last step, as it'll be plenty clear from the viewable output! Let's get to work on a benign surface first.

Cylinder

Example 11.11. Consider the circular cylinder $s(u, v)$ with parametric equations

$$x = \cos u, \;\; y = \sin u, \;\; z = v, \;\; \text{where } (u, v) \in [-\pi, \pi] \times [-1, 1]$$

We drew it using these equations in cylinder.cpp of Experiment 10.2. To color and light now, let's do normal calculations. The vectors spanning the tangent plane at $s(u, v)$ are

$$\left[\frac{\partial x}{\partial u} \;\; \frac{\partial y}{\partial u} \;\; \frac{\partial z}{\partial u}\right]^T = \left[\frac{\partial(\cos u)}{\partial u} \;\; \frac{\partial(\sin u)}{\partial u} \;\; \frac{\partial v}{\partial u}\right]^T = [-\sin u \quad \cos u \quad 0]^T$$

and

$$\left[\frac{\partial x}{\partial v} \;\; \frac{\partial y}{\partial v} \;\; \frac{\partial z}{\partial v}\right]^T = \left[\frac{\partial(\cos u)}{\partial v} \;\; \frac{\partial(\sin u)}{\partial v} \;\; \frac{\partial v}{\partial v}\right]^T = [0 \; 0 \; 1]^T$$

so a normal vector is

$$[-\sin u \quad \cos u \quad 0\,]^T \times [\;0 \;\; 0 \;\; 1\;]^T = [\;\cos u \quad \sin u \quad 0]^T$$

which happens to be normalized already. So, in the terminology of (11.16), for the cylinder,

$$f_n(u, v) = \cos u, \; g_n(u, v) = \sin u, \; h_n(u, v) = 0$$

We'll add this normal data to cylinder.cpp next.

Experiment 11.20. Run litCylinder.cpp, which builds upon cylinder.cpp using the normal data calculated above, together with color and a single directional light source. Press 'x/X', 'y/Y' and 'z/Z' to turn the cylinder. The functionality of being able to change the fineness of the mesh approximation has been dropped. Figure 11.58 is a screenshot. End

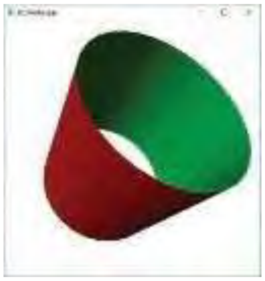

Figure 11.58: Screenshot of litCylinder.cpp.

Compare the two programs cylinder.cpp and litCylinder.cpp – it's not really a lot of code from the first to the second. Essentially, the additions are (a) the fn(), gn() and hn() normal component functions as calculated above, (b) the fillNormalArray() function to fill the array normals[], and (c) a bunch of routine code specifying light and material properties, which can be kept similar across most programs with lighting. So the extra code arising from analytic normal computation is really in (a) and (b), about 20 lines all told. Not too bad, huh? And it gets better. As we used the template of cylinder.cpp to draw various surfaces, simply swapping in new f(), g() and h() functions according to the given parametrization, so we can use litCylinder.cpp as a template for lit applications, additionally swapping in new fn(), gn() and hn() functions for new surfaces.

Exercise 11.30. (Programming) Reverse the normals of litCylinder.cpp by changing their specification in the fillNormalArray() routine as follows:

```
   normals[k++] = -fn(i,j);
   normals[k++] = -gn(i,j);
   normals[k++] = -hn(i,j);
```

Not good! As we remarked earlier, wrongly-directed normals are easy to spot. Can you fix the problem caused by the normal values above by a minimal amount of code change *only* in the drawing routine?
Hint: Think orientation, in particular, reversing the orientation of the strip triangles.

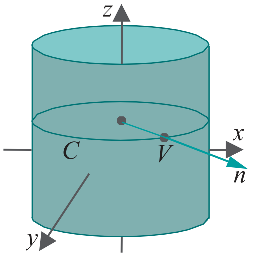

Figure 11.59: Normal n to a cylinder.

Exercise 11.31. It's a bit late now, but do we really need partial derivatives, as in Example 11.11, to determine the normal to the cylinder at the point $V = (\cos u, \sin u, v)$?

The outward normal to the cylinder at V evidently lies along a radius of the circle C which is the section of the cylinder through V by a plane perpendicular to its axis. See Figure 11.59. Use this to compute the parametric equation for a unit normal vector to the cylinder without any calculus.

Often, as in the preceding exercise, normals to a surface can be determined by elementary geometric considerations. Unfortunately, this does not seem to be the case with the doubly-curled cone of Experiment 10.7.

Doubly-curled Cone

Let's light the doubly-curled cone of doublyCurledCone.cpp. Its parametric equations are

$$x = t\cos(A + a\theta)\cos\theta, \;\; y = t\cos(A + a\theta)\sin\theta, \;\; z = t\sin(A + a\theta),$$

where $0 \leq t \leq 1$ and $0 \leq \theta \leq 4\pi$. A somewhat tedious calculation gives a normal to the cone as

$$\begin{aligned}\left[\frac{\partial x}{\partial\theta}\;\frac{\partial y}{\partial\theta}\;\frac{\partial z}{\partial\theta}\right]^T \times \left[\frac{\partial x}{\partial t}\;\frac{\partial y}{\partial t}\;\frac{\partial z}{\partial t}\right]^T \\ = [-at\sin\theta + t\sin(A + a\theta)\cos(A + a\theta)\cos\theta, \\ at\cos\theta + t\sin(A + a\theta)\cos(A + a\theta)\sin\theta, \\ -\,t\cos^2(A + a\theta)]^T\end{aligned} \tag{11.17}$$

Moreover, the length of this normal is

$$t\sqrt{a^2 + \cos^2(A + a\theta)} \tag{11.18}$$

Dividing the normal (11.17) by its length (11.18) gives a unit normal to the cone.

Figure 11.60: Screenshot of litDoublyCurledCone.cpp.

Experiment 11.21. The program litDoublyCurledCone.cpp, in fact, applies the preceding equations for the normal and its length. Press 'x/X', 'y/Y', 'z/Z' to turn the cone. See Figure 11.60 for a screenshot.

As promised, litDoublyCurledCone.cpp is pretty much a copy of litCylinder.cpp, except for the new f(), g(), h(), fn(), gn() and hn() functions, as also the new normn() to compute the normal's length.

End

Exercise 11.32. Verify Equations (11.17) and (11.18) for the normal and its magnitude of the doubly-curled cone.

Programmed Normal Calculation

Exact normals deduced from the equation of a surface – as in the preceding examples of the cylinder and doubly-curled cone – are the most honest as we have observed. Nevertheless, if one wishes to avoid admittedly often tedious calculations, then the next program, a reworking of litCylinder.cpp, shows a simple *programmable* way to find *approximate* normals to a surface mesh.

Experiment 11.22. Run litCylinderProgrammedNormals.cpp. Press 'x/X', 'y/Y', 'z/Z' to turn the cylinder. Figure 11.61 is a screenshot. End

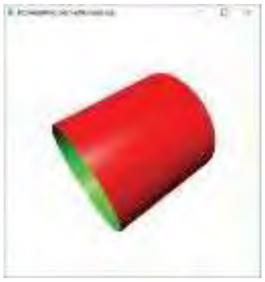

Figure 11.61: Screenshot of litCylinderProgrammedNormals.cpp.

Let's understand now the normal calculations in litCylinderProgrammedNormals.cpp. Refer to Figure 11.62 as you read.

The chord vector, call it $t1(i,j)$, from the vertex with parameters $(i-1,j)$ to that with parameters $(i+1,j)$, is taken as the approximation to the tangent $\frac{\partial x}{\partial u}\ \frac{\partial y}{\partial u}\ \frac{\partial z}{\partial u}^{T}$ at the vertex V with parameters (i,j); likewise, the chord vector $t2(i,j)$ from the vertex with parameters $(i,j-1)$ to the one with parameters $(i,j+1)$ is taken as an approximation to the tangent $\frac{\partial x}{\partial v}\ \frac{\partial y}{\partial v}\ \frac{\partial z}{\partial v}^{T}$ at V. Care, of course, must be taken at the boundaries of the parameter domain as $\pm i$ 1 or $j\pm 1$ may got out of bounds. For example, what we do if V has maximum j-parameter value, so that $j+1$ is out of bounds, is take the chord vector from the vertex with parameters $(i,j-1)$ to V itself (the green arrow in Figure 11.62) as the approximation to the tangent $\frac{\partial x}{\partial v}\ \frac{\partial y}{\partial v}\ \frac{\partial z}{\partial v}^{T}$ at V.

Next, the approximate normal $un(i,j)$ at V is taken to be the cross-product $t1(i,j)\times t2(i,j)$. Dividing $un(i,j)$ by its length $nl(i,j)$ gives a normalized approximate normal at V. Evidently, the closer the mesh vertices, i.e., the finer the mesh, the better the tangent and normal approximations.

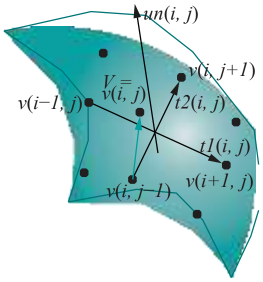

Figure 11.62: Approximate tangents and normal.

The neat thing about litCylinderProgrammedNormals.cpp, of course, is that the approximate normals are calculated automatically from the base functions $f()$, $g()$ and $h()$ defining the surface. Therefore, one can cut and paste in any set of $f(u,v)$, $g(u,v)$ and $h(u,v)$ into the litCylinderProgrammedNormals.cpp template to instantly illuminate the corresponding surface, normals done and dusted transparently!

It is important to note that the method of litCylinderProgrammedNormals.cpp is applicable only if the surface is defined parametrically by

$$x = f(u,v),\ \ y = g(u,v),\ \ z = h(u,v)$$

over a (triangulated) rectangular grid mesh as in Figure 11.63(a). It is *not* valid for an arbitrary triangular mesh, e.g., an irregular one as in Figure 11.63(b).

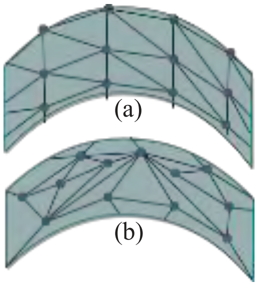

Figure 11.63: A (triangulated) rectangular grid mesh and an irregular triangular mesh.

However, we can still take recourse to the suggestion at the start of the section of approximating the normal to a vertex V as an average of the normals of faces incident at V – a process which may be automated for *all* meshes, with no restriction, given only a description of the mesh. We ask the reader to prove this for the particular triangulation of litCylinderProgrammedNormals.cpp.

Remark 11.19. An irregular mesh may arise, for example, from triangulating the point cloud acquired from a laser scan of some real 3D object, such as a statue.

Exercise 11.33. (Programming) Write a new version of litCylinderProgrammedNormals.cpp where vertex normals are automatically approximated as the averages of normals of incident faces. Observe that, given a surface approximated as a stack of triangle strips, as in this program, each vertex, typically, will have six incident faces (Figure 11.63(a)). However, this may not be the case for an arbitrary triangular mesh (Figure 11.63(b)).

11.11.4 FreeGLUT, Bézier and Quadric Surfaces

Life is about to get considerably easier! Normals come for free with FreeGLUT surfaces – OpenGL computes them automatically without being asked. Here's our workhorse ball and torus from Chapter 4 now lit (and orthographically shadowed).

Figure 11.64: Screenshot of ballAndTorusLitOrthoShadowed.cpp.

Experiment 11.23. Run ballAndTorusLitOrthoShadowed.cpp. Press space to start the ball traveling around the torus and the up and down arrow keys to change its speed. Figure 11.64 is a screenshot.

The only user-provided normal in the program is the unit vector in the $+y$-direction for the checkered floor; normals are automatic for the ball and torus, FreeGLUT objects both. The shadows are the result of simple degenerate scaling calls, as discussed in Section 4.7.2. End

Bézier surfaces are not much harder. All one has to do is type in the command glEnable(GL_AUTO_NORMAL) for OpenGL to automatically calculate unit normals at the vertices of a Bézier surface which has been created using glMap2f(GL_MAP2_VERTEX_3, . . .) and glEnable(GL_MAP2_VERTEX_3). Let's see this in action.

Canoe

Experiment 11.24. Run litBezierCanoe.cpp. Press 'x/X', 'y/Y', 'z/Z' to turn the canoe. You can see a screenshot in Figure 11.65.

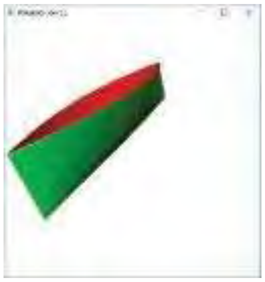

Figure 11.65: Screenshot of litBezierCanoe.cpp.

This program illuminates the final shape of bezierCanoe.cpp of Experiment 10.19 with a single directional light source. Other than the expected command glEnable(GL_AUTO_NORMAL) in the initialization routine, an important point to notice about litBezierCanoe.cpp is the reversal of the sample grid along the u-direction. In particular, compare the statement

```
glMapGrid2f(20, 1.0, 0.0, 20, 0.0, 1.0)
```

of litBezierCanoe.cpp with

```
glMapGrid2f(20, 0.0, 1.0, 20, 0.0, 1.0)
```

of bezierCanoe.cpp. This change reverses the directions of one of the tangent vectors evaluated at each vertex by OpenGL and, consequently, that of the normal (which is the cross-product of the two tangent vectors).

Modify litBezierCanoe.cpp by changing

```
glMapGrid2f(20, 1.0, 0.0, 20, 0.0, 1.0);
```

back to bezierCanoe.cpp's

```
glMapGrid2f(20, 0.0, 1.0, 20, 0.0, 1.0);
```

Wrong normal directions! The change from bezierCanoe.cpp is necessary. Another solution would be to leave glMapGrid2f() as it is in bezierCanoe.cpp, instead making a call to glFrontFace(GL_CW). End

The lesson to take from this is that if you obtain normals automatically from OpenGL, then you might have to subsequently alter their orientation for authenticity, which is not unreasonable because OpenGL cannot know which side was intended to be the front.

Remark 11.20. If the user wishes to define her own normals for a Bézier surface, she can do so with a glMap2f(GL_MAP2_NORMAL, . . .) call. We'll not have occasion to do this ourselves.

Quadrics are simple too. The call

```
gluQuadricNormals(qobj, GLU_SMOOTH)
```

automatically generates a normal at each vertex of the quadric pointed by qobj.

The next program we'll look at is a fairly substantial animation which invokes both glEnable(GL_AUTO_NORMAL) for Bézier surface normals and gluQuadricNormals(qobj, GLU_SMOOTH) for quadric surfaces. It also has a FreeGLUT solid cube for which OpenGL sets up normals automatically.

Movie with a Ship and a Torpedo

Experiment 11.25. Run shipMovie.cpp. Pressing space starts an animation sequence which begins with a torpedo traveling toward a moving ship and ends on its own after a few seconds. Press space again at any time to stop the animation. Figure 11.66 is a screenshot as the torpedo nears the ship. End

Figure 11.66: Screenshot of shipMovie.cpp.

There are a few different objects in shipMovie.cpp. The hull of the ship is obviously inspired by the Bézier canoe of the previous experiment. The deck is a flat Bézier surface lying parallel to the xz-plane – all its control points' y-values, in fact, being identical – designed to fit the hull. Each of the ship's three storeys is a cylindrical quadric, as is its chimney.

The torpedo should be familiar from the program torpedo.cpp of Experiment 10.20. Each of the four grayish boats in the background is a couple of quads, while the sea itself is a solid green cube.

The smoke from the chimney is a simple-minded so-called *particle system*; in particular, we render a sequence of quadric discs in point mode and hack in a coloring and animation scheme.

Remark 11.21. The reason OpenGL can help with the normals of FreeGLUT objects, Bézier surfaces and quadrics is that it knows the equation of the whole surface – in fact, it's drawing the surface based on this internally-generated equation – making it possible, therefore, for OpenGL to calculate normals. For an arbitrary mesh, however, OpenGL has no notion of the global surface the programmer is trying to approximate and, moreover, it's certainly not going to attempt an ad hoc method *a la* litCylinderProgrammedNormals.cpp.

11.11.5 Transforming Normals

When a surface is transformed by modelview transformations, so are its normals, but not as straightforwardly as its vertices (which we know are simply multiplied from the left by the transformation matrix). Let's see how normals are transformed by each of the fundamental transformations – translation, rotation and scaling.

1. Translation:

   A translation leaves a normal vector at a vertex unchanged because the normal simply translates parallely (see Figure 11.67(a)).

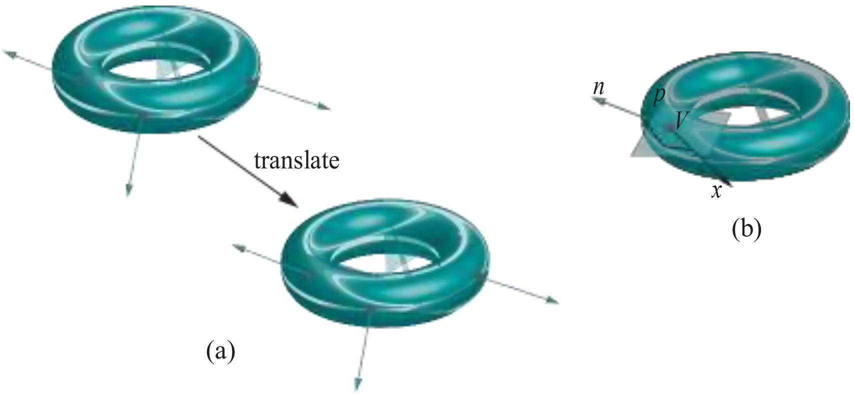

Figure 11.67: (a) Vertex normals translate parallely as the torus is translated (b) The normal n at V is perpendicular to any vector x which lies on the tangent plane p at V.

2. Rotation and Scaling:

   These cases are not as simple and require a bit of calculation.

A rotation or non-degenerate scaling, say t, corresponds to a non-singular 3 × 3 defining matrix in $\mathbb{R}^3$, say N. Suppose that n is a normal vector at a vertex V of an object O. Therefore, n is perpendicular to any arbitrary vector, say x, tangent to the surface of O at V (see Figure 11.67(b)).

Now, if we apply t, it will transform all the vertices of O, *as well as* vectors tangent to O's surface, by multiplication on the left by N.

Note: To convince yourself that tangent vectors are transformed identically with vertices, think of a tangent vector as connecting two vertices infinitesimally close together on the surface of O. Therefore, these two vertices "carry" the tangent vector with them.

So, x is transformed to Nx. We would, therefore, like to transform n to a vector perpendicular to Nx. Since n is perpendicular to x, we already have $n\ x = 0$, which is equivalent to $n^T x = 0$, the latter being a matrix equation (note that 3-vectors are represented as 3 × 1 columns matrices). It follows that

$$n^T (N^{-1}N)x = n^T x = 0$$

Therefore,

$$0 = n^T (N^{-1}N)x = (n^T N^{-1})(Nx) = ((N^{-1})^T n)^T (Nx)$$

invoking rules of matrix algebra. One sees that $((N^{-1})^T n) \cdot Nx = 0$, so $(N^{-1})^T n$ is indeed perpendicular to Nx.

The conclusion, then, is that the appropriate transformation to apply to the normal vector n, under a rotation or non-degenerate scaling corresponding to the matrix N, is left multiplication by $(N^{-1})^T$, i.e., $n \mapsto (N^{-1})^T n$.

OpenGL actually transforms normals as just described. If the current modelview matrix is

$$M = \begin{bmatrix} a_{11} & a_{12} & a_{13} & a_{14} \\ a_{21} & a_{22} & a_{23} & a_{24} \\ a_{31} & a_{32} & a_{33} & a_{24} \\ a_{41} & a_{42} & a_{43} & a_{44} \end{bmatrix}$$

then "erasing" the translational part, which, as we know, has no impact on the normal, leaves its upper-left 3 × 3 submatrix

$$N = \begin{bmatrix} a_{11} & a_{12} & a_{13} \\ a_{21} & a_{22} & a_{23} \\ a_{31} & a_{32} & a_{33} \end{bmatrix}$$

and, in fact, the matrix $(N^{-1})^T$, called the *normal matrix*, is used to transform normals by multiplication from the left. Mind that an OpenGL normal is always a 3D vector, never homogenized to 4D, so that left-multiplication by the 3 × 3 matrix N is a valid operation.

Note: It's valid to go from the 4 × 4 modelview matrix M to the 3 × 3 normal matrix N by erasing a row and a column as above provided that the last row of M is [0 0 0 1], which indeed would be the case unless the programmer herself has been loading strange matrices into the modelview matrix stack.

Remark 11.22. By elementary matrix algebra we have always $(N^{-1})^T = (N^T)^{-1}$, so in OpenGL context the normal matrix is often called the *inverse transpose*, or *transpose inverse*, matrix, being one and the same.

Exercise 11.34. Given a unit normal vector n to start with, can the transformation $n \mapsto (N^{-1})^T n$ change its length in case the normal matrix $(N^{-1})^T$ was derived from the transformation matrix M of a rotation? Of a scaling?

Hint: No. Yes.

Exercise 11.35. We gave above a general formula for how a normal vector is transformed. Ignoring the formula for a moment, can you deduce from elementary considerations what should happen in the particular case of a rotation? Then relate your answer to the formula.

11.11.6 Normalizing Normals

Normalizing a (non-zero) vector means dividing it by its magnitude to obtain a vector with the same direction, but of unit length. We've already seen that it's important to specify normalized normals because OpenGL uses the dot product to compute the cosine of the angle between two vectors, which is correct if they are both of unit length.

Here's a simple modification of litTriangle.cpp to show what can happen if one is careless.

Experiment 11.26. Run sizeNormal.cpp based on litTriangle.cpp.

The ambient and diffuse colors of the three triangle vertices are set to red, green and blue, respectively. The normals are specified separately as well, initially each of unit length perpendicular to the plane of the triangle.

However, pressing the up/down arrow keys changes (as you can see) the size, but not the direction, of the normal at the red vertex. Observe the corresponding change in color of the triangle. Figure 11.68 is a screenshot.

End

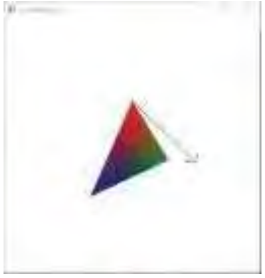

Figure 11.68: Screenshot of sizeNormal.cpp.

There are, typically, two reasons why normals turn out not normalized:

(a) The user does not specify them of unit length in the first place.

(b) Even if they are specified of unit length, a subsequent application of a scaling transformation changes the length (see Exercise 11.34).

If the user is not inclined to write code to ensure normals of unit length, there's a way to ask OpenGL's help. Calling glEnable(GL NORMALIZE) causes OpenGL to normalize all normal vectors before lighting calculation. Beware, though, it's not a particularly efficient call and should be avoided if possible.

Experiment 11.27. Run sizeNormal.cpp after placing the statement glEnable(GL NORMALIZE) at the end of the initialization routine. Press the up/down arrow keys. The triangle no longer changes color (though the white arrow still changes in length, of course, because its size is that of the program-specified normal). End

There's a cheaper renormalization call, glEnable(GL RESCALE NORMAL), which we'll leave the reader to look up, which can be used if originally unit normals were provided, that were subsequently all changed by the *same* scaling transformation.

11.12 Phong's Shading Model

Recall from Section 11.8 that a shading model is a method to color the interior of a primitive. A shading model, first proposed by Phong, different from the two which OpenGL offers – these being smooth (or, Gouraud) and flat shading – though computationally more intensive, significantly improves the realism of a rendered image.

Note: Phong's shading model should not be confused with his lighting model, which we know already that OpenGL implements.

Instead of computing light values only at a primitive's vertices and then interpolating through its interior as in Gouraud shading, Phong suggested (a) interpolate the vertex normal values through the primitive, and then (b) compute light values at each pixel using the interpolated normals.

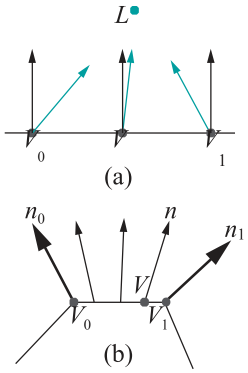

Figure 11.69: (a) Light direction vectors are green, normals black (b) User-specified normals are bold, interpolated normals thin.

Let's understand first where Phong was coming from with an example. See Figure 11.69(a), where V_0 and V_1 are the vertices of a primitive of which V is a point in the interior, the normals at both V_0 and V_1 are perpendicular to V_0V_1 and L is a light source (the light direction vectors are green, normals black). Gouraud shading, OpenGL's default, would compute the light intensities at V_0 and V_1 and interpolate them at V. Now, the location of L causes the angle of incidence at V_0 and V_1 to be large, lowering, therefore, the diffuse intensities (the "3D-making" part of light) at both as well. Consequently, the interpolated diffuse intensity at V is low too; however, this is physically inaccurate because the true angle of incidence at V is small. Therefore, the problem is of a local intensity propagating globally, one which we actually encountered earlier in the context of the quality of a triangulation in Section 8.2, where the cause was a sliver.

Now, Phong shading solves the problem of the example above because it computes the light intensity at V *itself* after interopolating there the normal values from V_0 and V_1, which works out correctly as the interpolated normal at V (perpendicular to the segment V_0V_1 as well and, in this case, the true normal) gives a small angle of incidence.

A more typical picture of interpolated normals is as in Figure 11.69(b), where the bold arrows are user-specified unit normals and the thin ones interpolated. If the unit normals specified at V_0 and V_1 are, in fact, n_0 and n_1, respectively, and if barycentric coordinates of the point V are given by

$$V = c_0V_0 + c_1V_1$$

then the (normalized) normal value n at V is computed to be

$$n = (c_0n_0 + c_1n_1) / |c_0n_0 + c_1n_1|$$

(provided the denominator is not zero). Of course, we draw line primitives in Figure 11.69 for convenience; practically, a lit primitive will be a triangle, the barycentric expression $V = c_0V_0 + c_1V_1 + c_2V_2$ and the equation for the interpolated normal $n = (c_0n_0 + c_1n_1 + c_2n_2) / |c_0n_0 + c_1n_1 + c_2n_2|$.

The color values of a pixel which happens to be centered at V are then computed in Phong's model using the lighting equation (11.13), where, now, the normal value n is interpolated as above and the color values $V_{*,X}$ are interpolated from the vertices as well, as, too, are the light direction and halfway vectors l^i and s^i.

Remark 11.23. OpenGL's default process of computing lit values at vertices followed by a Gouraud shading of the interior is often called *per-vertex* lighting to contrast it with the *per-pixel* (also called, *per-fragment*) lighting of Phong shading.

OpenGL itself, as we know, offers only flat and Gouraud shading as automatic shading options. However, the OpenGL Shading Language, or GLSL, allows individual pixels to be programmed, which means the programmer herself can code in Phong shading. We'll be doing precisely this as an application when we get to fourth generation OpenGL in Chapter 15 and see for ourselves the enhanced realism.

Exercise 11.36. Even before we get to coding Phong, here's a question to think of. The problem of the example earlier motivating Phong shading could conceivably be solved, as well, along the lines of Section 8.2 with a finer triangulation. So which do you like: a high poly triangulation with Gouraud or low poly with Phong? Think of both space and computation time.

Exercise 11.37. So, here's a point of view: "Phong shading simply passes the buck from the light intensities to the normals – instead of interpolating the former, it interpolates the latter. Therefore, Phong commits the sin of local-to-global propagation just as much Gouraud and there's no reason to believe it will do better." What do you say to this?

11.13 Lighting Exercises

Here's a bunch of exercises to light up your life. Feel free to pick and choose.

Exercise 11.38. (Programming) As Figure 11.61 shows, there is a distinct seam on the cylinder drawn by litCylinderProgrammedNormals.cpp of Experiment 11.22, not present in litCylinder.cpp. Why is this so? Can you fix the problem?

Exercise 11.39. (Programming) The doubly-curled cone of Experiment 11.21 would probably benefit from at least one more light source, particularly to brighten the inside. Code this in.

Exercise 11.40. (Programming) Program distance attenuation into spotlight.cpp. Add vertical motion capability to the light source to bring out the effect of distance attenuation.

And while you're at it, why not make the light emerge from a well at the bottom of a flying saucer?!

Exercise 11.41. (Programming) Extending the previous exercise: add capability to aim the spotlight of spotlight.cpp.

Exercise 11.42. (Programming) Our first experiment in this chapter ran sphereInBox1.cpp, which, though a useful workhorse, was rather bland. Jazz it up by replacing the single large ball with a small ball (or balls) bouncing around inside the box.

Exercise 11.43. (Programming) Add a satellite, shadowed too, to ballAndTorusLitOrthoShadowed.cpp, revolving around the ball *a la* Experiment 4.22.

Exercise 11.44. (Programming) If you made the spinning cube of Exercise 4.43 in Chapter 4, color and light it now. Make its shadow on the floor too. (You should not use a GLUT cube, but draw squares for each face.)

Exercise 11.45. (Programming) It's alway fun merging projects! So, merge ballAndTorusLitOrthoShadowed.cpp and sphereInBox1.cpp by "placing" the former in the box of the latter; in other words, opening the box reveals a torus with a ball flying around it.

Exercise 11.46. (Programming) Color and light the helical pipe of Experiment 10.3 in two different ways:

(a) Using exact normals found with calculus.

(b) Using approximate normals with help of the template of litCylinderApproximateNormals.cpp.

Exercise 11.47. (Programming) Color and light the table of Experiment 10.6. You don't really need any calculus in order to compute the normals to the various component surfaces – which happen each to be either cylindrical or flat. Make sure to choose normals so that edges appear sharp.

Exercise 11.48. (Programming) Color and light the single-sheeted hyperboloid of Experiment 10.10.

Exercise 11.49. (Programming) Revisit your drawing projects from Chapter 10 and color and light the objects.

Exercise 11.50. (Programming) In Exercise 10.79 you animated a river scene using the canoe of bezierCanoe.cpp to make boats. Illuminate the scene now.

Exercise 11.51. (Programming) Animate a night street scene. Buildings and cars can be boxy. Make sure to use emission to create authentic street lights.

Exercise 11.52. (**Programming**) The program shipMovie.cpp of Experiment 11.25 bears improvement. Try at least the following:

(a) Add detail to the ship.

(b) Make the water more realistic, possibly by adding movement, variation in color, etc.

(c) Put stars and a moon in the sky.

(d) Improve the smoke particle system.

(e) Make a particle system to simulate water spray from the torpedo's propeller.

Exercise 11.53. (**Programming**) Paint and light the character of animateMan*.cpp of Section 4.7.1 in surroundings less bland than a plane with a ball.

11.14 Summary, Notes and More Reading

In Chapters 4, 5 and 6 we learned to animate objects, in Chapter 10 to draw them (systematically), and now we have begun to "dress them up" with color and light. In this chapter we learned the underlying color and lighting models which OpenGL implements, the related syntax, and how to use them to specify light sources and material properties, as well as related environmental parameters. The technical issue of normal computation was an important part of our program too. We'll continue this theme in the next chapter when we learn of yet another technique to decorate an object, texturing.

For a further reference on coloring models, the somewhat encyclopedic Wyszecki and Stiles [156] is frequently cited as the bible of color science. The books by Berns [11] and Jackson et al. [77] are probably easier to read though.

Since the publication of Phong's model in 1975 [112] several other lighting models, both local and global, have been proposed. Local models like Phong's do not consider object-object light interaction, while global ones do, thereby displaying secondary effects such as shadows and reflections. Lighting models are often deployed in an application-specific manner, certain models being more realistic in rendering particular material properties and finishes.

A few of the local models which appeared after Phong's are Blinn [14], Cook-Torrance [28], He et al. [69, 70], Nayar-Oren [103], Poulin-Fournier [114] and Schlick [127]. However, the only local model which we discuss or use in this book is Phong's.

The two most commonly implemented global models are ray tracing [3, 151] and radiosity [60], which as a matter of fact complement each other. Global models, though much more realistic than local ones, are notoriously computation-intensive, so rarely apt for interactive applications. However, they are almost always used when frames can be created off-line, as in movies. We discuss both ray tracing and radiosity in Chapter 21.

It's sobering, though, to realize that the only reason OpenGL's local lighting model is used in interactive applications is that its demand on the GPU is low enough that frames can be generated in real-time, something which as yet the more authentic but labor-intensive global models cannot manage. However, with GPU capabilities advancing by leaps and bounds each generation one wonders if the days of local lighting models (and, heaven forbid, OpenGL!) are numbered.

The theory of lighting models necessarily involves a fair amount of physics and mathematics. The reader interested in learning more is best advised to start with advanced books such as those by Akenine-Möller, Haines & Hoffman [1], Buss [21] and Watt [150] and then proceed to original research papers, as the area is particularly active. The canonical source for the latest in CG research in general is the annual ACM SIGGRAPH conference [133].

CHAPTER 12

Texture

We continue to explore methods to attire objects, which we began in the last chapter with color and light. The topic of this chapter is texturing. Textures are a vital part of the wardrobe available to designers. Texturing makes it possible to create lifelike scenes at acceptable costs. It's an enormously important technique in modern-day CG. We'll examine how texturing is implemented in OpenGL and various aspects of texturing in practice. Textures can be combined, as well, with color and light to good effect, as we'll see.

We cover the basics of loading and applying textures in Section 12.1. The so-called texture map, determined by texture coordinates in a texture space, which in turn specifies how a texture is painted onto an object is introduced in Section 12.2. Sections 12.3 and 12.4 discuss setting various texturing parameters, including the very important ones to control filtering. Specifying the texture map for various surfaces is the topic of Section 12.5. We discuss the texture matrix and its application to animating textures in Section 12.6. Section 12.7 explains how to combine texture with light and color. We learn to mix more than one texture in Section 12.8 and the rather striking technique of rendering to a texture in Section 12.9 before, finally, concluding in Section 12.10.

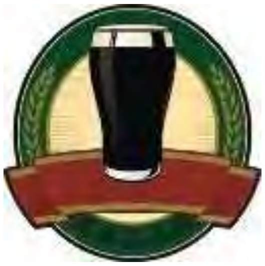

Figure 12.1: Beer can label.

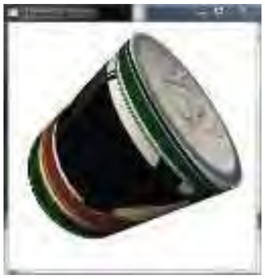

Figure 12.2: Screenshot of can with textured label and top.

12.1 Basics

Texturing a surface consists essentially of painting a picture onto it, a process which can be used to two advantages when programming graphics:

(a) *Authenticity* : Realistically depicting an object which happens to be painted in real life, requires painting the surface that models the object as well.

For example, the beer label of Figure 12.1 has been textured onto the surface of a cylinder to make a realistic-looking beer can in Figure 12.2.

(b) *Illusion of geometric detail* : Instead of trying to faithfully recreate an object with geometric primitives, painting a picture of it in a scene might very well achieve a realistic result at a fraction of the cost in the number of triangles.

For example, instead of modeling the individual blades of a grass in a field, which would require a massive number of triangles, paint one picture of a field (Figure 12.3) onto a single rectangle; instead of modeling individual trees in the backdrop of a scene, paint pictures of trees (Figure 12.4) onto appropriately located polygons. The top of the can of Figure 12.2, including the fairly complex pop tab, is a texture too (an image of a can top, in fact).

Figure 12.3: Grassy field.

Figure 12.4: Trees on white background.

Typically, a texture is an image, which is applied to a polygon or a mesh. The pixels in the texture are called *texels*, each texel storing color values, such as 24-bit

RGB or 32-bit RGBA, just as their counterpart pixels in the frame buffer. The texture itself can be an external image which is imported into an OpenGL program or one generated internally by the program itself. The former often is called an *external* texture while the latter a *procedural* , or *synthetic*, texture. Once loaded though there is no difference between the two. Let's run a program using both kinds.

Experiment 12.1. Run texturedSquare.cpp, which loads an external image of a shuttle launch as one texture and generates internally a chessboard image as another.

The program paints both the external and the procedural texture onto a square polygon. Figure 12.5 shows the two. Press space to toggle between them, the left and right arrow keys to turn the square and delete to reset.

As one rotates the square one sees the texture image front-facing on the front of the square, while the image is seen from behind on its backside. End

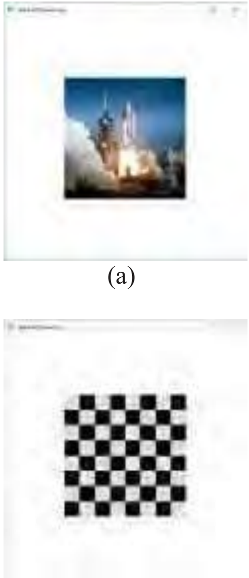
(a)

(b)

Figure 12.5: The two textures of texturedSquare.cpp: shuttle launch (external, from NASA) and chessboard (procedural).

Note: *Important* ! Our texture programs are written to input, as textures images, files in the *Windows BMP* format, in particular, uncompressed 24-bit unindexed color RGB BMP files. Image files in other formats must, therefore, first be converted, which can be done using image-editing software such as Windows Paint, GIMP and Adobe Photoshop. The input file, though, is stored *internally* in the program in a 32-bit RGBA format, the A (alpha) field allowing for possible use in blending applications. Note that so-called NPOT (non-power-of-two) textures, whose width or height are not powers of two, can be read by our programs as well – earlier versions of OpenGL did not allow NPOT textures.

Note: Our own texture images are all in the folder ExperimenterSource/Textures.

Let's start to understand the texture-related OpenGL commands in texturedSquare.cpp. First, the call

```
glGenTextures(2, texture);
```

in the setup() routine returns two texture ids in the array texture. Generally, a call of the form glGenTextures(*n*, *texture*) returns *n* such ids. Next, setup() calls

```
loadTextures();
```

which will be our template routine for importing external textures for all future programs. This routine first creates storage and loads the texture image launch.bmp with the statements

```
imageFile *image[1];
image[0] = getBMP("../../Textures/launch.bmp");
```

In particular, the imageFile structure, defined in getBMP.h, stores the width and height of an image file, as well as a sequence of bytes comprising the pixel RGB and, possibly, A values. The getBMP() routine, which is in a separate source, reads an external BMP image file and stores it in an object of type imageFile. We'll briefly describe the logic of getBMP() at the end of this section. Next, loadTextures() creates a new 2D *texture object* with id texture[0] with the statement

```
glBindTexture(GL_TEXTURE_2D, texture[0]);
```

Then

```
glTexImage2D(GL_TEXTURE_2D, 0, GL_RGBA, image[0]->width,
   image[0]->height, 0, GL_RGBA, GL_UNSIGNED_BYTE, image[0]->data);
```

specifies the texture image for the currently bound texture object, this being, of course, texture[0]. Generally,

```
glTexImage2D(target, level, internalFormat, width, height, border,
                externalFormat, type, *pointer);
```

specifies the texture image pointed to by *pointer* , which is of format *externalFormat* and data type *type*; the kind of texture is *target* , the mipmap level (to be discussed later) is *level*, the size of the texture image is *width*×*height*, while *internalFormat* tells OpenGL how to store the image data; *border* is a legacy parameter which must be 0.

Ignore, for now, the final four parameter-setting commands of the form glTexParameteri() in the loadTextures() routine – they are, in fact, the topics of Sections 12.3 and 12.4.

Returning to setup(), the call next is

```
loadChessboardTexture();
```

this routine first calling createChessboard() to create as procedural texture a chessboard image in the 64×64×4 array chessboard of RGBA values (each square of the board is represented by an 8×8×4 subarray of chessboard, consisting either of all black or all white color values) and then binding the chessboard image to texture[1] exactly similarly to how loadTextures() bound the launch image to texture[0]. Finally, setup() concludes with

```
glTexEnvf(GL_TEXTURE_ENV, GL_TEXTURE_ENV_MODE, GL_REPLACE);
glEnable(GL_TEXTURE_2D);
```

specifying the texture environment parameters – in this case, asking that the texture replace the surface's current color values – and activating texturing.

On to the drawScene() next. The call

```
glBindTexture(GL_TEXTURE_2D, texture[id]);
```

activates texture object texture[id] (in fact, binding a previously created texture object makes it active). The polygon drawing command of drawScene() which specifies the so-called texture coordinates of each vertex, in fact, is what we'll discuss in detail the next section, but first a couple of light exercises.

Exercise 12.1. (Programming) Replace the image of the launch with others downloaded from the web.

Exercise 12.2. (Programming) Write a routine createStripedBoard() that generates the image of a striped board, depicted in Figure 12.6, in a 64×64×4 RGBA array.

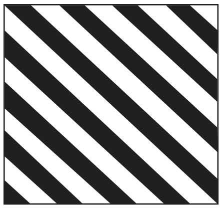

Figure 12.6: A striped board.

Remark 12.1. Much more can be done in generating textures internally than creating just a static image such as a chessboard or a striped board. In fact, as we'll see later this chapter, OpenGL can actually render to a texture, in other words, a texture can act as a "paper-thin screen" on which to show an OpenGL movie!

How getBMP() Works

The reader is referred to on-line sources for a full specification of the BMP file format. What is relevant for our purposes in the specfication of an uncompressed 24-bit unindexed color RGB BMP file (the most commonly occurring) is shown in Figure 12.7: after 10 bytes from the start is a 4-byte field containing the byte offset to the start of the image data; after 18 bytes from the start are the image's width and height in successive 4-byte fields; the image data is stored in the order BGR, one byte per color, so three bytes per pixel; moreover, the image data is stored one pixel row after another, each row being *4-byte aligned* , meaning that if the number of bytes in a row is not a multiple of four, then it is padded with zero-bytes till it is so.

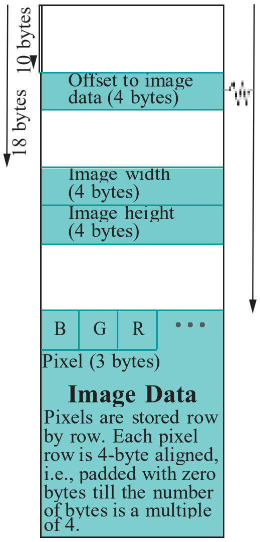
10 bytes
18 bytes
Offset to image data (4 bytes)
Image width (4 bytes)
Image height (4 bytes)
B
G
R
• • •
Pixel (3 bytes)
Image Data
Pixels are stored row by row. Each pixel row is 4-byte aligned, i.e., padded with zero bytes till the number of bytes is a multiple of 4.

Figure 12.7: BMP file format.

The logic of getBMP() should be fairly easy to follow now. The offset to the image data and its width and height are read into the variables offset, w and h, respectively. Next, the number of zero-bytes of padding at the end of each pixel row is computed and stored in padding. Then, the image data is actually read into tempStore, an object of type imageFile.

Two imageFile objects are readied for possible output. The first outRGB is filled from tempStore after stripping the zero-byte padding off each row and reversing the bytes from BGR to RGB in each pixel. The second output file outRGBA is simply made from outRGB by copying the RGB data *and* adding an extra A byte per pixel which is set to all 1s. It is outRGBA which getBMP() finally returns.

12.2 Texture Space, Coordinates and Map

A texture, once loaded, occupies the unit square with corners at (0,0), (1,0), (1,1) and (0,1) of an imaginary (virtual) plane called *texture space*. This is regardless of whether the original texture image is equal-sided or not. If it is not, then it is scaled (virtually, of course) to fit the square, as illustrated in Figure 12.8. The axes of texture space are usually denoted *s* and *t*. As one would expect, the left-to-right direction of the image is aligned in the positive direction of the *s*-axis, while its bottom-to-top direction is aligned along the positive direction of the *t*-axis.

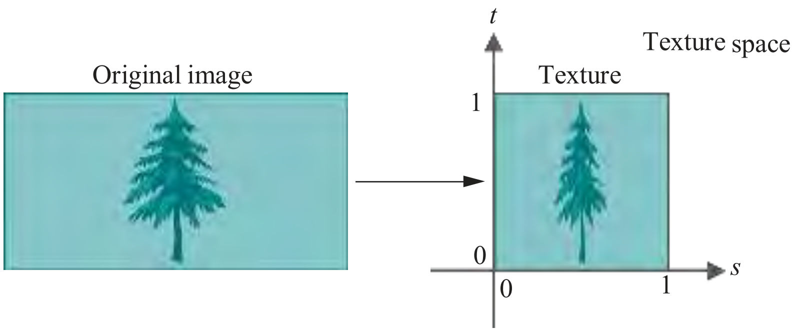

Figure 12.8: An image stored as a texture in a unit square of texture space.

Each of the four statements within the glBegin(GL POLYGON)–glEnd() pair of the following piece of code, from the drawing routine of texturedSquare.cpp, maps the vertex of a polygon to a point in texture space.

```
glBegin(GL POLYGON);
   glTexCoord2f(0.0, 0.0); glVertex3f(-10.0, -10.0, 0.0);
   glTexCoord2f(1.0, 0.0); glVertex3f(10.0, -10.0, 0.0);
   glTexCoord2f(1.0, 1.0); glVertex3f(10.0, 10.0, 0.0);
   glTexCoord2f(0.0, 1.0); glVertex3f(-10.0, 10.0, 0.0);
glEnd();
```

The first statement, for example, maps the vertex at (−10.0, −10.0, 0.0) of world space to the point (0.0, 0.0) of texture space. The coordinates of the mapped point in texture space are called the *texture coordinates* of the vertex. The mapping of the polygon vertices to texture space is interpolated throughout the polygon to obtain the so-called *texture map*, which, therefore, is a map from a part of world space (that occupied by the polygon) to texture space. The texture, finally, is painted onto the polygon by applying to each point of the polygon the RGB color values of its image by the texture map.

Exercise 12.3. In texturedSquare.cpp, what are the texture coordinates of the following points of the world-space square?

(a) (0.0, 0.0, 0.0)

(b) (5.0, 5.0, 0.0)

(c) (10.0, 0.0, 0.0)

Part answer : (a) (0.5, 0.5), as the midpoint (0.0, 0.0, 0.0) of the world-space square maps to the midpoint of the texture square by the linearity of interpolation.

Experiment 12.2. Replace every 1.0 in each glTexCoord2f() command of texturedSquare.cpp with 0.5 so that the polygon specification is:

```
glBegin(GL POLYGON);
   glTexCoord2f(0.0, 0.0); glVertex3f(-10.0, -10.0, 0.0);
   glTexCoord2f(0.5, 0.0); glVertex3f(10.0, -10.0, 0.0);
   glTexCoord2f(0.5, 0.5); glVertex3f(10.0, 10.0, 0.0);
   glTexCoord2f(0.0, 0.5); glVertex3f(-10.0, 10.0, 0.0);
glEnd();
```

The lower left quarter of the texture is interpolated over the square (Figure 12.9 for a screenshot and Figure 12.13(a) for the texture map). Make sure to see both the launch and chessboard textures! End

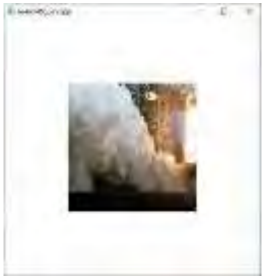

Figure 12.9: Screenshot of Experiment 12.2.

Experiment 12.3. Restore the original texturedSquare.cpp and delete the last vertex from the polygon so that the specification is that of a triangle:

```
glBegin(GL POLYGON);
   glTexCoord2f(0.0, 0.0); glVertex3f(-10.0, -10.0, 0.0);
   glTexCoord2f(1.0, 0.0); glVertex3f(10.0, -10.0, 0.0);
   glTexCoord2f(1.0, 1.0); glVertex3f(10.0, 10.0, 0.0);
glEnd();
```

Exactly as expected, the lower-right triangular half of the texture is interpolated over the world-space triangle (Figure 12.10 and Figure 12.13(b)).

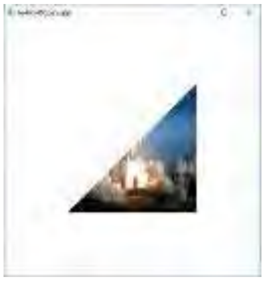

Figure 12.10: Screenshot of Experiment 12.3: lower-right triangular half of texture not skewed.

Change the coordinates of the last vertex of the world-space triangle to (0.0, 10.0, 0.0):

```
glBegin(GL POLYGON);
   glTexCoord2f(0.0, 0.0); glVertex3f(-10.0, -10.0, 0.0);
   glTexCoord2f(1.0, 0.0); glVertex3f(10.0, -10.0, 0.0);
   glTexCoord2f(1.0, 1.0); glVertex3f(0.0, 10.0, 0.0);
glEnd();
```

Interpolation is clearly evident now. Parts of both launch and chessboard are skewed by texturing, as the triangle specified by texture coordinates (still the lower-right half) is not similar to its world-space counterpart (Figure 12.11 and Figure 12.13(c)).

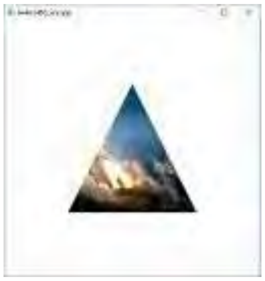

Figure 12.11: Screenshot of Experiment 12.3: lower-right triangular half of texture skewed.

Continuing, change the texture coordinates of the last vertex of the triangle to (0.5, 1.0):

```
glBegin(GL POLYGON);
   glTexCoord2f(0.0, 0.0); glVertex3f(-10.0, -10.0, 0.0);
   glTexCoord2f(1.0, 0.0); glVertex3f(10.0, -10.0, 0.0);
   glTexCoord2f(0.5, 1.0); glVertex3f(0.0, 10.0, 0.0);
glEnd();
```

The textures are no longer skewed as the triangle in texture space is similar to the one being textured (Figure 12.12 and Figure 12.13(d)). End

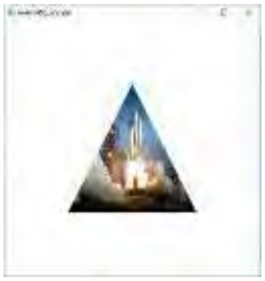

Figure 12.12: Screenshot of Experiment 12.3: middle triangle of texture not skewed.

Experiment 12.4. Restore the original texturedSquare.cpp and replace launch.bmp with cray2.bmp, an image of a Cray 2 supercomputer.

View the texture images in the Textures folder and note their sizes: the launch is 512 × 512 pixels while the Cray 2 is 512 × 256. As you can see, the Cray 2 (original texture is Figure 12.14) is now scaled by half width-wise to fit the square polygon (screenshot is Figure 12.15). End

Exercise 12.4. (Programming) Change the polygon specs of texturedSquare.cpp so that the Cray 2 is no longer distorted.

Figure 12.14: Original Cray texture image.

Figure 12.15: Screenshot of Experiment 12.4.

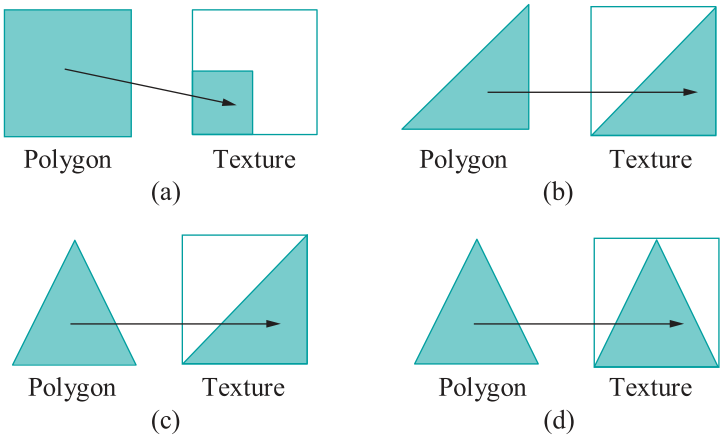

Figure 12.13: Texture maps.

Experiment 12.5. Restore the original texturedSquare.cpp and then change the coordinates of only the third world-space vertex of the textured polygon to $(20.0, 0.0, 0.0)$:

```
glBegin(GL POLYGON);
   glTexCoord2f(0.0, 0.0); glVertex3f(-10.0, -10.0, 0.0);
   glTexCoord2f(1.0, 0.0); glVertex3f(10.0, -10.0, 0.0);
   glTexCoord2f(1.0, 1.0); glVertex3f(20.0, 0.0, 0.0);
   glTexCoord2f(0.0, 1.0); glVertex3f(-10.0, 10.0, 0.0);
glEnd();
```

The launch looks odd. The rocket rises vertically, but the flames underneath are shooting sideways! Toggle to the chessboard and it's instantly clear what's happening Figure 12.16 shows both textures. End

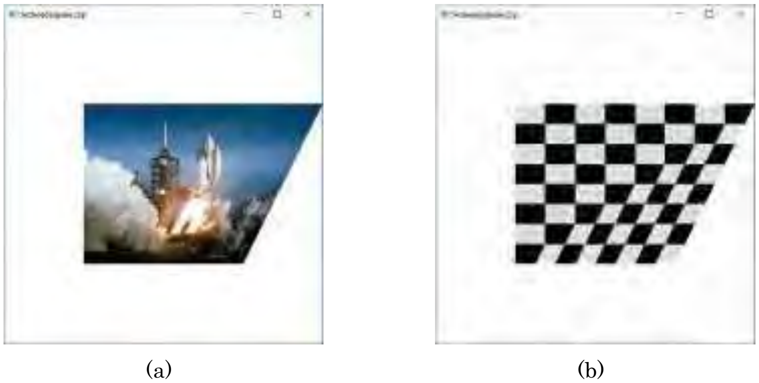

Figure 12.16: Screenshots from Experiment 12.5.

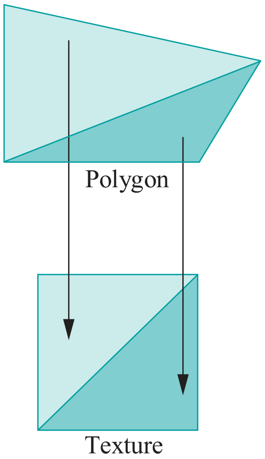

Figure 12.17: Each of the two texture triangles is interpolated over the corresponding polygon triangle.

The polygon and the texture have evidently been triangulated *equivalently* – in particular, triangles in a fan-triangulation around the first vertex of one correspond to those in a fan-triangulation around the first vertex of the other via the texture map – each triangle of the texture subsequently being *separately* interpolated over the corresponding triangle of the polygon (see Figure 12.17). Corresponding triangles in this case, though, are not similar in shape causing the perceived distortion.

When we had said a little earlier that the texture map is obtained by interpolating over the polygon the mapping from its vertices to points in texture space, we had not taken into account the fact that there is no unambiguous way to do such an interpolation over the entire polygon if it has more than three sides (recall discussions to this effect in Section 7.4). We see now that OpenGL gets past this problem by interpolating the vertex texture coordinates over each triangle separately of a fan-triangulation of the polygon, which comes as no surprise as we've seen before OpenGL draw and color polygons in a similar manner. Of course, the issue does not arise at all if, as always recommended, one avoids polygons and draws only triangular primitives.

Exercise 12.5. (Programming) Change the polygon specs in texturedSquare.cpp to map a 5-sided polygon in world space to a 5-sided polygon in texture space:

```
glBegin(GL_POLYGON);
    glTexCoord2f(0.0, 0.0); glVertex3f(-10.0, -10.0, 0.0);
    glTexCoord2f(1.0, 0.0); glVertex3f(10.0, -10.0, 0.0);
    glTexCoord2f(1.0, 0.5); glVertex3f(20.0, 0.0, 0.0);
    glTexCoord2f(0.5, 1.0); glVertex3f(0.0, 10.0, 0.0);
    glTexCoord2f(0.0, 1.0); glVertex3f(-10.0, 0.0, 0.0);
glEnd();
```

Can you make out the triangulations in world and texture space, as well as the correspondence between triangles?

12.3 Repeating and Clamping

So far we've been careful to keep texture coordinates in the range [0, 1], along both the *s*- and *t*-axes. What happens if they slip outside? Let's find out.

Experiment 12.6. Restore the original texturedSquare.cpp and change the texture coordinates of the polygon as follows:

```
glBegin(GL POLYGON);
    glTexCoord2f(-1.0, 0.0); glVertex3f(-10.0, -10.0, 0.0);
    glTexCoord2f(2.0, 0.0); glVertex3f(10.0, -10.0, 0.0);
    glTexCoord2f(2.0, 2.0); glVertex3f(10.0, 10.0, 0.0);
    glTexCoord2f(-1.0, 2.0); glVertex3f(-10.0, 10.0, 0.0);
glEnd();
```

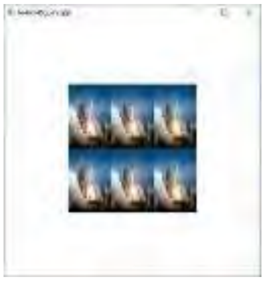

Figure 12.18: Screenshot of Experiment 12.6.

It seems that the texture space is *tiled* with the texture. See Figure 12.18.

In particular, the texture seems repeated in every unit square of texture space with integer vertex coordinates. As the world-space polygon is mapped to a 3 × 2 rectangle in texture space, it is painted with six copies of the texture, each scaled to an aspect ratio of 2:3. The scheme itself is indicated Figure 12.19. End

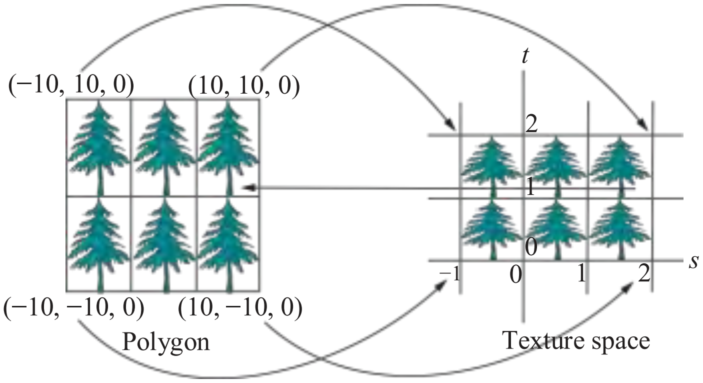

Figure 12.19: Tiling of texture space. The curved arrows indicate the texture map. The straight arrow indicates the painting of one tile onto a sub-rectangle of the polygon; other tiles similarly paint corresponding sub-rectangles.

Experiment 12.7. Change again the texture coordinates of texturedSquare.cpp by replacing each −1.0 with −0.5:

```
glBegin(GL _POLYGON);
   glTexCoord2f(-0.5, 0.0); glVertex3f(-10.0, -10.0, 0.0);
   glTexCoord2f(2.0, 0.0); glVertex3f(10.0, -10.0, 0.0);
   glTexCoord2f(2.0, 2.0); glVertex3f(10.0, 10.0, 0.0);
   glTexCoord2f(-0.5, 2.0); glVertex3f(-10.0, 10.0, 0.0);
glEnd();
```

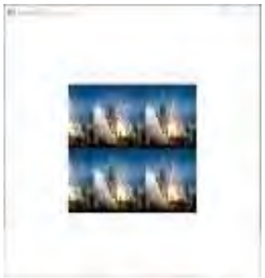

Figure 12.20: Screenshot of Experiment 12.7.

Again it's apparent that the texture space is tiled with the specified texture and that the world-space polygon is painted over with its rectangular image in texture space. See Figure 12.20. End

That the texture space is tiled with the texture is because of the following two statements in both the loadTextures() and loadChessboardTexture() routines of texturedSquare.cpp, specifying the *wrapping mode* to be *repeated* in both *s*- and *t*-directions:

```
glTexParameteri(GL TEXTURE 2D, GL TEXTURE WRAP S, GL REPEAT);
glTexParameteri(GL TEXTURE 2D, GL TEXTURE WRAP T, GL REPEAT);
```

Another wrapping mode, instead of repeated, is *clamped to the edge*.

Experiment 12.8. Restore the original texturedSquare.cpp and then change the texture coordinates as below, which is the same as in Experiment 12.6:

```
glBegin(GL POLYGON);
   glTexCoord2f(-1.0, 0.0); glVertex3f(-10.0, -10.0, 0.0);
   glTexCoord2f(2.0, 0.0); glVertex3f(10.0, -10.0, 0.0);
   glTexCoord2f(2.0, 2.0); glVertex3f(10.0, 10.0, 0.0);
   glTexCoord2f(-1.0, 2.0); glVertex3f(-10.0, 10.0, 0.0);
glEnd();
```

Next, replace the GL REPEAT parameter in the

```
glTexParameteri(GL TEXTURE 2D, GL TEXTURE WRAP S, GL REPEAT);
```

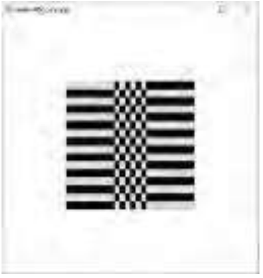

Figure 12.21: Screenshot from Experiment 12.8.

statement of both the loadlTextures() and loadChessboardTexture() routines with GL CLAMP TO EDGE so that the statement becomes

```
glTexParameteri(GL TEXTURE 2D, GL TEXTURE WRAP S, GL CLAMP TO EDGE);
```

This causes the wrapping mode to be clamped to the edge in the *s*-direction. It's probably easiest to understand what happens in this mode by observing, in particular, the chessboard texture. See Figure 12.21: points of the square with texture coordinate *s*-value is greater than 1 (i.e., points in the right one-third of the square) each get their color values from the point on the right edge of the texture with the same *t*-value. In other words, the right edge of the texture, where $s = 1$, is repeated along every column of the square whose texture s is greater than 1. Likewise, the left edge of the texture, where $s = 0$, is repeated along every column of the square whose texture s is less than 1. End

Experiment 12.9. Continue the previous experiment by clamping to the edge the texture along the *t*-direction as well. In particular, replace the GL REPEAT parameter in the

```
glTexParameteri(GL TEXTURE 2D, GL TEXTURE WRAP T, GL REPEAT);
```

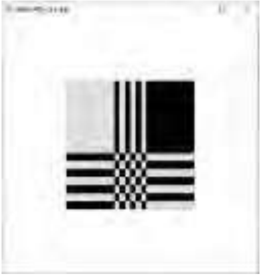

Figure 12.22: Screenshot from Experiment 12.9.

statements with GL CLAMP TO EDGE. We leave the reader to parse the output (Figure 12.22). End

The repeating option is appropriate to tile the surface of an object with a particular pattern, e.g., a wall with a brick pattern, a table with a wood grain pattern, the ground with a grass pattern and so on, while clamping is appropriate for painting a single copy of the texture, e.g., the facade of a building onto a rectangle, with the texture boundary, typically, aligned with the rectangle boundary.

There exist wrapping modes other than repeated and clamped to the edge, but we'll not have occasion to use them and refer the interested reader to the OpenGL specs.

12.4 Filtering

Experiment 12.10. Run fieldAndSky.cpp, where a grass texture is tiled over a horizontal rectangle and a sky texture clamped to a vertical rectangle. There is the added functionality of being able to transport the camera over the field by pressing the up and down arrow keys. Figure 12.23 shows a screenshot.

As the camera travels, the grass seems to *shimmer* – *flash* and *scintillate* are terms also used to describe this phenomenon. This is our first encounter with the *aliasing* problem in texturing. Any visual artifact which arises owing to the finite resolution of the display device, or, equivalently, the "large" size of individual pixels – at least to the extent that they are discernible to the human eye – is said to be caused by aliasing. End

Figure 12.23: Screenshot of fieldAndSky.cpp.

Let's try and understand why shimmer is caused by aliasing. Recall that the texture map is obtained by interpolating through each world triangle the texture coordinates specified at its vertices. Subsequently, each point of the triangle is colored with the values of its mapped texture point. However, a technicality arises at this stage we did not consider earlier. Color values in the computer are *not* associated per *point* , either in the screen polygon or the texture image. In reality, they are associated one set (RGB or RGBA) per per *pixel* in the display, as also one ser per *texel* in the texture, pixels and texels being finite-sized squares, rather than points.

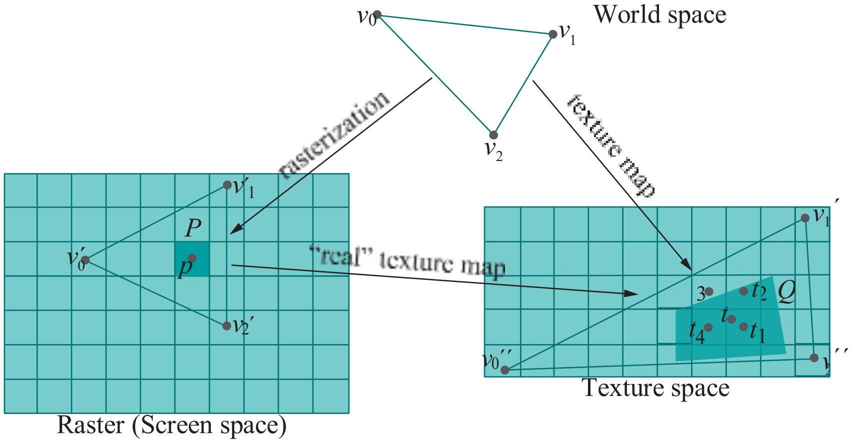

Figure 12.24: The aliasing problem in texture mapping. A single pixel P is mapped to a quadrilateral Q covering many texels (minification).

Now, once the polygon has been rasterized – i.e., its set of corresponding pixels determined – the texture map is unlikely to map pixels to texels in a one-to-one manner. The situation, more typically, is as depicted in Figure 12.24, where the triangle $v_1v_2v_3$ in world space is mapped to the raster (i.e., screen space) triangle $v'_1v'_2v'_3$ via the rasterization process and to the texture space triangle $v''_1v''_2v''_3$ via the texture map. These two maps (downwards in the figure) induce the "real" texture map from raster to texture space (left to right) which takes pixels to texels (precisely, this map is rasterization reversed followed by the texture map).

Now, in Figure 12.24, the dark pixel P in the raster happens to map to the dark quadrilateral Q in texture space (note that the composed map from raster to texture space is not necessarily affine and may distort shape). As Q intersects multiple texels, how should OpenGL choose color values for P ? Particularly, which texel should OpenGL sample to apply its particular color values to P?

Here's a reasonable solution: if the texture map takes the center p of P to the point t in texture space, then sample the texel whose center is nearest to t. In Figure 12.24, then, the sampled texel would be the one centered at t_1, so this texel's colors would be applied to P. In fact, this is precisely the so-called *filtering* option specified by the GL_NEAREST value in the following two parameter-setting commands in both the statement blocks that bind the grass and sky textures of the loadTextures() routine of fieldAndSky.cpp:

```
glTexParameteri(GL_TEXTURE_2D, GL_TEXTURE_MIN_FILTER, GL_NEAREST);
glTexParameteri(GL_TEXTURE_2D, GL_TEXTURE_MAG_FILTER, GL_NEAREST);
```

(We'll discuss the difference between MIN and MAG filters momentarily.)

The reason for the shimmer observed in fieldAndSky.cpp is now not hard to grasp. See again Figure 12.24. Suppose that the object in world space moves a small distance so that its rasterization changes a small amount as well, causing the map from raster to texture space to map p to, say, a new point just to the left of t, closer to the pixel center t_4 than t_1. Accordingly, by the GL_NEAREST filtering principle, there is a switch in the color values at pixel P, sampled now from the texel centered at t_4, rather than the one at t_1. It's exactly these relatively large discrete changes in pixel colors arising from minute movements of the world object which cause shimmer.

Figure 12.24 itself suggests a way to ameliorate the problem: instead of sampling color values from just the one texel centered at t_1, sample all the four texels whose centers (particularly, t_1, t_2, t_3 and t_4) surround t and average. This smooths the color transitions and, in fact, is offered by OpenGL as the GL_LINEAR filtering option.

Remark 12.2. The basis for linear filtering is exactly the same as for moving averages in statistics. For example, as part of analyzing the stock market, one may chart average values over a sliding window of size one week or month, instead of daily values, in order to smooth out near-term fluctuations.

Experiment 12.11. Change to linear filtering in fieldAndSky.cpp by replacing every GL_NEAREST with GL_LINEAR. The grass still shimmers though less severely. The sky seems okay with either GL_NEAREST or GL_LINEAR. End

The process of sampling color values for pixels based on the texture map is called filtering. OpenGL offers a few different filtering options, in addition to GL_NEAREST and GL_LINEAR, allowing the user to trade between speed and output quality. OpenGL makes a distinction, as well, between *minification* and *magnification* when filtering.

Minification occurs when a pixel is mapped onto multiple texels as in Figure 12.24 as a consequence, typically, of a textured surface moving into the distance to occupy a smaller part of the screen or, equivalently, the viewer zooming out. For example, as an aircraft flies away from the camera, the texels comprising its logo occupy an increasingly smaller region of the screen, until, when the craft is far enough, multiple texels begin to occupy single pixels (which is equivalent to the texture map taking a single pixel to multiple texels).

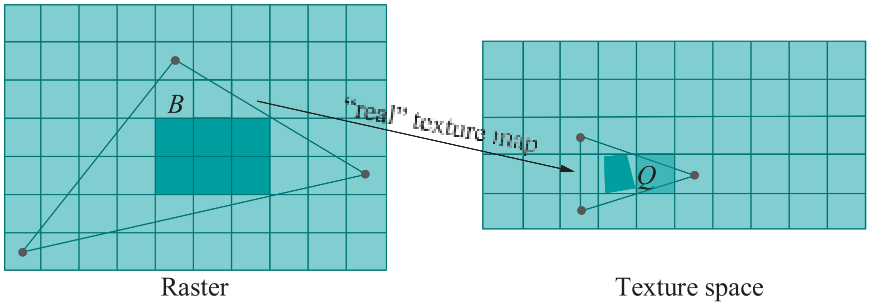

Figure 12.25: A block B of many pixels is mapped to a quadrilateral Q inside a single texel (magnification).

Magnification, related to zooming in, of course, is the inverse phenomenon where the pixel-to-texel mapping is many-to-one as in Figure 12.25.

The statement

```
glTexParameteri(GL_TEXTURE_2D, case, filter)
```

causes the filtering option *filter* to be applied in the case of minification or magnification, according as the value of *case* is GL_TEXTURE_MIN_FILTER or GL_TEXTURE_MAG_FILTER. For example, with the commands

```
glTexParameteri(GL_TEXTURE_2D, GL_TEXTURE_MIN_FILTER, GL_NEAREST);
glTexParameteri(GL_TEXTURE_2D, GL_TEXTURE_MAG_FILTER, GL_NEAREST);
```

fieldAndSky.cpp asks for the nearest filter in the case of either minification or magnification.

In the case of minification, particularly, OpenGL offers an array of filtering options, in addition to nearest and linear, based on *pre-assigning* a set of textures to be used at different levels of minification. The idea, conceived by Lance Williams [153], is clever yet simple. Starting with the original texture, the *base texture*, a set of textures of progressively lower resolution, called *mipmaps*, is prepared. These mipmaps are either computed by OpenGL by an averaging process – we'll see momentarily how – or supplied by the programmer.

Subsequently, during run-time, OpenGL maps a geometric primitive, based upon the size it occupies in the raster, to that particular mipmap which affords a nearly one-to-one correspondence between pixels and texels, rather than the one-to-many which would occur if the base texture were used. This (a) saves on run-time filtering computation, and (b) assures quality (provided mipmaps are initially well-chosen).

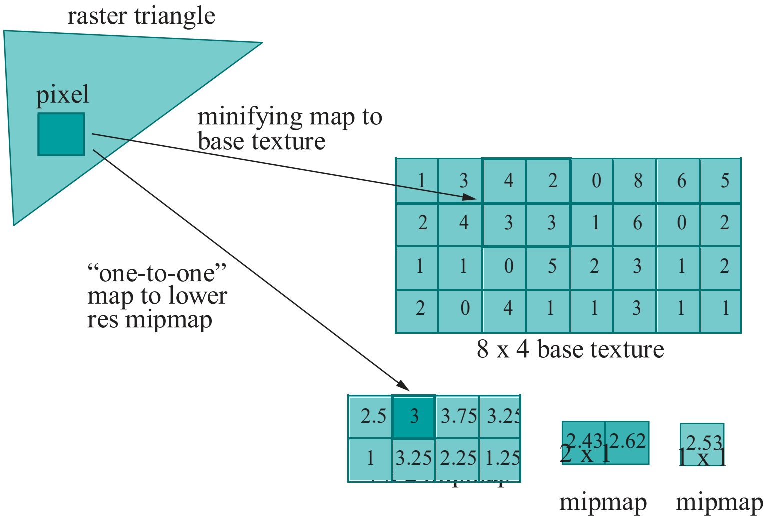

Figure 12.26: Mipmapping.

Figure 12.26 illustrates the idea with an idealized example. The base texture is of resolution 8×4 with a single scalar color value at each texel. Mipmaps of successively lower resolution till 2×1 are computed by averaging the color values in 2×2 squares of texels, until, finally, the 1×1 mipmap is computed by averaging the two color values in the 2×1 mipmap. For example, the value 3 in the dark texel in the 4×2 mipmap is the average of the four values in the dark square of texels in the 8×4 mipmap. A set of mipmaps is often called a *pyramid* of mipmaps – think of them stacked one on top of the other, highest resolution at the bottom to the lowest at the top.

Now, when the raster triangle of Figure 12.26 is mapped to the base texture, minification apparently causes the dark pixel to map to the dark square of texels, which requires run-time linear filtering to return the color value 3. On the other hand, if it is mapped to the 4×2 mipmap, then there is no minification and the color value of 3 is returned *without* run-time filtering. For this reason mipmaps are often called *pre-filtered* textures.

Generally, if a base texture of resolution $2^m \times 2^n$ is to be mipmapped, then OpenGL requires mipmaps of resolution $2^{m-1} \times 2^{n-1}$, $2^{m-2} \times 2^{n-2}$, . . ., obtained by halving both width and height, until one of the dimensions becomes 1; subsequently, if the other dimension is still greater than 1, then it must be repeatedly halved and mipmaps provided for each resolution down to 1 × 1.

Exercise 12.6. If the base texture is 4 × 8 with color values at the texels as follows

1	0	4	2
3	2	1	5
0	1	2	6
8	2	7	7
2	3	1	2
6	4	3	8
7	3	6	1
3	5	0	2

then find all the mipmaps down to the one of lowest resolution.

Example 12.1. What is the total space required to store all the mipmaps for a base texture of resolution $2^m \times 2^n$? What is the ratio of this space to that required for only the base texture?

Answer: Suppose without loss of generality that $m \geq n$. The total number of texels in all the mipmaps is

$$2^m \times 2^n + 2^{m-1} \times 2^{n-1} + \ldots + 2^{m-n+1} \times 2 + 2^{m-n} \times 1$$
$$+ 2^{m-n-1} + 2^{m-n-2} + \ldots + 1$$

(the first line above bringing one dimension down to 1, the second the next)

$$= 2^{m-n}(1 + 2^2 + \ldots + 2^{2n}) + (1 + 2 + \ldots + 2^{m-n-1})$$
$$= 2^{m-n}(2^{2n+2} - 1)/3 + 2^{m-n} - 1$$
$$= \frac{4}{3} 2^{m+n} + \frac{2}{3} 2^{m-n} - 1$$

The space required is, therefore, the above quantity multiplied by the number of bits per texel.

Now, the number of texels in the base texture is $2^m \times 2^n = 2^{m+n}$ and

$$\frac{4}{3} 2^{m+n} + \frac{2}{3} 2^{m-n} - 1 < \frac{4}{3} 2^{m+n} + \frac{2}{3} 2^{m+n} = 2 \times 2^{m+n}$$

so the ratio of the space required for all the mipmaps to that only for the base texture is less than 2.

Example 12.1 implies that mipmapping offers efficiency and quality at a cost of at most twice the amount of space. Once mipmaps have been set, OpenGL has four filtering options, in addition to GL_NEAREST and GL_LINEAR, available for use in case of minification. In order of increasing quality *and* computational cost they are:

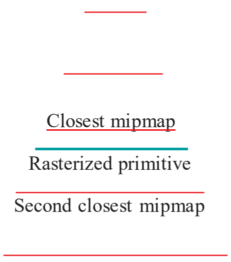

Figure 12.27: Red segments represent mipmaps decreasing in resolution upward, the green one the rasterized primitive.

(1) GL_NEAREST_MIPMAP_NEAREST: Applies the mipmap that's a closest fit resolution-wise to the rasterized primitive and then uses the GL_NEAREST filtering option within that mipmap.

Figure 12.27 is a conceptual representation of a rasterized primitive relative to a pyramid of mipmaps.

(2) GL_LINEAR_MIPMAP_NEAREST: Applies the mipmap that's a closest fit resolution-wise to the rasterized primitive and then the GL_LINEAR filtering option within that mipmap.

(3) GL_NEAREST_MIPMAP_LINEAR: Finds the two mipmaps that are closest resolution-wise to the rasterized primitive, then uses the GL_NEAREST filtering option within either mipmap to produce two sets of color values and, finally, takes a weighted average of the two sets.

(4) GL_LINEAR_MIPMAP_LINEAR: Finds the two mipmaps that are closest resolution-wise to the rasterized primitive, then uses the GL_LINEAR filtering option within either mipmap to produce two sets of color values and, finally, takes a weighted average of the two sets.

Mipmaps are *not* used in the case of magnification because, with the viewer zooming in, one wants only the highest resolution, namely, the base texture. Accordingly, the only two filters available in the case of magnification are GL_NEAREST and GL_LINEAR applied, of course, to the base texture.

Terminology : In OpenGL speak a *texture object* comprises a texture together with its associated parameters, specified by glTexParameter[i/f]() commands, such as the filter and wrapping options.

It's time to see mipmapping in action. Generating mipmaps automatically is simple. The command glGenerateMipmap(*target*) – implemented in OpenGL 3.0 and on – generates a full set of mipmaps for the texture associated with *target* as in the following program.

Experiment 12.12. Run fieldAndSkyFiltered.cpp, identical to fieldAndSky.cpp except for additional filtering options. Press the up/down arrow keys to move the camera and the left/right ones to cycle through filters for the grass texture. Messages at the top identify the current filters. Screenshots of the weakest and strongest filters applied are in Figure 12.28. End

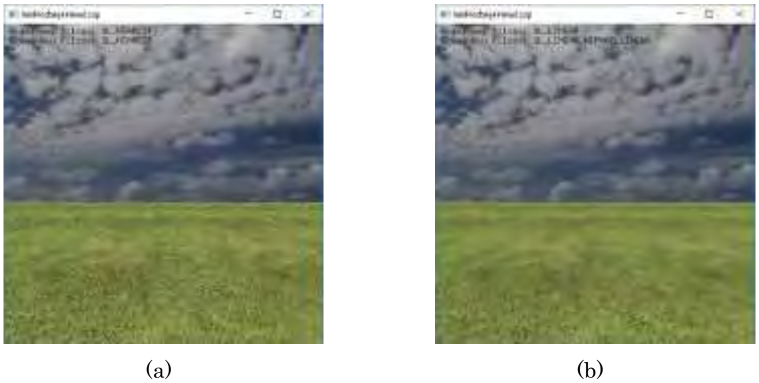
(a)

(b)

Figure 12.28: Screenshots of fieldAndSkyFiltered.cpp: (a) Weakest filter (b) Strongest filter.

The loadTextures() routine of fieldAndSkyFiltered.cpp loads the same grass image as six different textures with the min filter ranging from GL_NEAREST to GL_LINEAR_MIPMAP_LINEAR. The mag filter used is GL_NEAREST when the min filter is GL_NEAREST as well; otherwise, it's GL_LINEAR. The sky texture is not mipmapped.

The call

```
glGenerateMipmap(GL_TEXTURE_2D);
```

in loadTextures(), occurring just after glTexImage2D(), when binding the grass texture with each of the four min filters GL_NEAREST_MIPMAP_NEAREST and higher, generates mipmaps.

As one sees, the more expensive filters do nearly eliminate shimmering, but at the same time tamp down possibly desirable sharpness. For example, blades of grass can be distinguished easily in Figure 12.28(a), where the weakest filter is applied, but this is not so in Figure 12.28(b), which applies the strongest.

We have a couple more programs for you to experiment with mipmaps and filters.

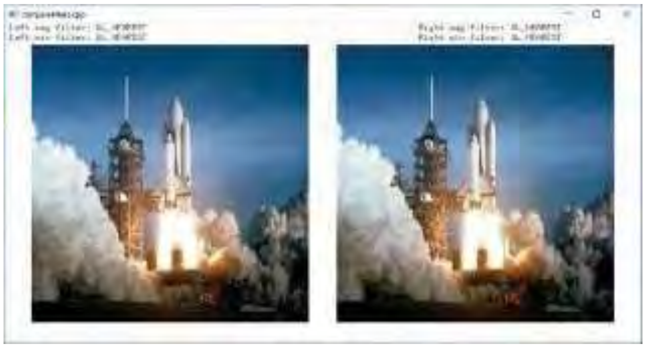

Left mag filter: GL_NEAREST
Left min filter: GL_NEAREST

Right mag filter: GL_NEAREST
Right min filter: GL_NEAREST

Figure 12.29: Screenshot of compareFilters.cpp initially.

Experiment 12.13. Run compareFilters.cpp, where one sees side-by-side identical images of a shuttle launch bound to a square. Press the up and down arrow keys to move the squares. Press the left arrow key to cycle through filters for the image on the left and the right arrow key to do likewise for the one on the right. Messages at the top say which filters are currently applied. Of course, if one of the four mipmap-based min filters – GL_NEAREST_MIPMAP_NEAREST through GL_LINEAR_MIPMAP_LINEAR – is applied, then the particular mipmap actually chosen by OpenGL depends on the screen space currently occupied by the square. Figure 12.29 is a screenshot of the initial configuration.

Compare, as the squares move, the quality of the textures delivered by the various min filters. For example, apply the GL_NEAREST min filter to the image on the left and GL_LINEAR_MIPMAP_LINEAR to that on the right and press the up key to move both away – the contrast between the shimmer on the left and its absence on the right is dramatic. End

An unavoidable artifact of filtering using mipmaps is that of *popping* when one mipmap is replaced with another. The next program illustrates this in a purposely dramatic manner.

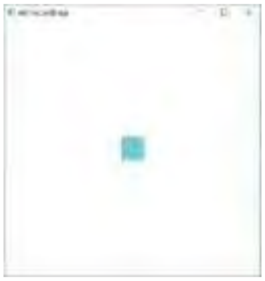

Figure 12.30: Screenshot of mipmapLevels.cpp after the first pop.

Experiment 12.14. Run mipmapLevels.cpp, where the mipmaps are supplied by the program, rather than generated automatically with glGenerateMipmap(). The mipmaps are very simple: just seven differently colored square images, created by the routine createMipmaps(), starting with the blue 64 × 64 mipmapRes64 down to the black 1 × 1 mipmapRes1. Subsequently, commands of the form

```
glTexImage2D(GL_TEXTURE_2D, level, GL_RGBA, width, height,
                        0, GL_RGBA, GL_UNSIGNED_BYTE, image);
```

in the routine loadMipmaps() each binds a $width \times height$ mipmap *image* to the current texture object, starting with the highest resolution image (which, of course, would be the original texture image in the case of an imported texture) at *level* 0, and with each successive image of lower resolution having one higher *level* all the way up to 6.

Move the square using the up and down arrow keys. As it grows smaller a change in color indicates a change in the currently applied mipmap. Figure 12.30 is screenshot after the first change. As the min filter setting is GL_NEAREST_MIPMAP_NEAREST, a unique color, that of the closest mipmap, is applied to the square at any given time. End

Remark 12.3. OpenGL offers options in addition to those that we have discussed to fine-tune mipmapping. The interested reader is referred to the chapter on textures in the red book.

Remark 12.4. Mipmapping is one of a class of LOD (*level-of-detail*) methods, or *multiresolution* methods as they are also called, which are important in graphics from the point of view of run-time efficiency.

Representing objects by polygonal meshes of varying levels of refinement is another practically important LOD application and one related to the drawing methods that we studied in Chapter 10. For example, if the camera is close to a spacecraft, then one may want a "base mesh" of thousands, or even millions, of triangles to be rendered. However, after the ship has flown some distance off to occupy a smaller portion of the screen, a mesh with fewer triangles may not only be visually adequate, but, in fact, desirable both for quicker rendering and to avoid aliasing artifacts. Accordingly, it's often advantageous to pre-compute a set of meshes for a moving object, exactly as mipmaps for a texture, with varying numbers of triangles.

Instead of a spacecraft, we have a cow at three different levels of resolution in Figure 12.31, starting from the highest at left, and then simplified twice with the help of mesh simplification software [23] co-developed by the author.

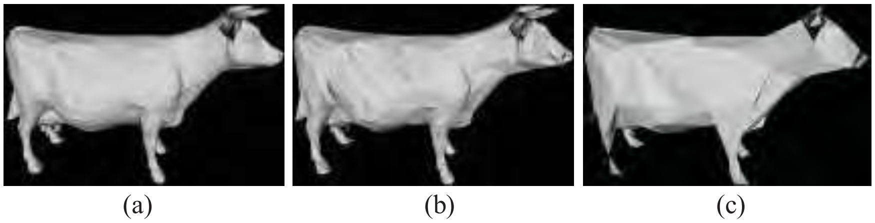

Figure 12.31: Cow at 3 different resolutions: (a) 5804 (b) 1772 (c) 328 triangles.

There's an extensive literature on LOD methods, of which a good starting point would be the book by Luebke et al. [91].

Figure 12.32: Screenshot of texturedTorus.cpp.

12.5 Specifying the Texture Map

Our programs so far have been simple from the point of view of specifying the texture map. The surfaces textured were all polygons, so that all we had to was specify texture coordinates at the corners. How about more complicated surfaces? It's actually surprisingly straightforward if the surface is parametrized – we can leverage the parametrization to derive texture coordinates.

12.5.1 Parametrized Surfaces

Experiment 12.15. Run texturedTorus.cpp, which shows a high-calorie donut made from mapping a sugary texture onto a torus. Figure 12.32 is a screenshot. Press 'x'-'Z' to turn the torus. End

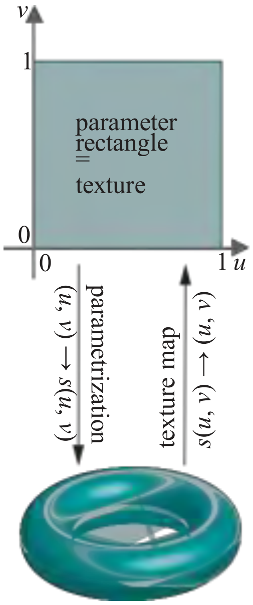

Figure 12.33: Texturing a torus by identifying the parameter rectangle with the texture.

The program texturedTorus.cpp is based on torus.cpp of Experiment 10.4. As i runs from 0 to p and j from 0 to q, $(i/p, j/q)$ runs over sample points in $[0, 1]\times[0, 1]$, and $(f(i, j), g(i, j), h(i, j))$ – see the corresponding function definitions f(), g() and h() in the program – runs over mapped sample points on the torus, which are stored in a vertex array. Since the (i, j)th entry in the vertex array is the image of the point $(i/p, j/q)$ of the parameter rectangle $[0, 1]\times[0, 1]$ by the parameter map, an obvious texture map is to associate this very same image with the point $(i/p, j/q)$ of texture space, effectively identifying the parameter rectangle with the texture! See Figure 12.33. This is exactly what's done in texturedTorus.cpp by the routine fillTextureCoordArray(), which fills values into a *texture coordinates array* holding texture coordinates per vertex (just like vertex coordinates arrays hold (x, y, z) coordinates per vertex and color arrays hold RGB colors per vertex).

Exercise 12.7. (Programming) If you did Exercise 12.2 to create the synthetic striped board texture of Figure 12.6, apply it now to the torus of texturedTorus.cpp.

Exercise 12.8. (Programming) Texture the helical pipe of Experiment 10.3 to give it an appearance of rusted metal.

Exercise 12.9. (Programming) Texture the table of Experiment 10.6 with a wood grain texture.

12.5.2 Bézier and Quadric Surfaces

OpenGL can automatically generate texture coordinates for Bézier and quadric surfaces, as is demonstrated in the next experiment.

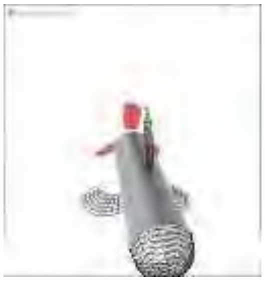

Figure 12.34: Screenshot of texturedTorpedo.cpp: propeller blades textured with checkered pattern, body with metal finish.

Experiment 12.16. Run texturedTorpedo.cpp, which textures parts of the torpedo of torpedo.cpp – from Experiment 10.20 – as you can see in the screenshot in Figure 12.34. Press space to start the propeller turning. End

Let's see first how propeller blade Bézier surface of texturedTorpedo.cpp is textured. In fact, we plan to do this exactly as we did the torus of Experiment 12.15 – by identifying parameter rectangle and texture. However, because of the way OpenGL is set up for Bézier texture coordinates generation, we are forced to this end in the slightly roundabout way discussed next.

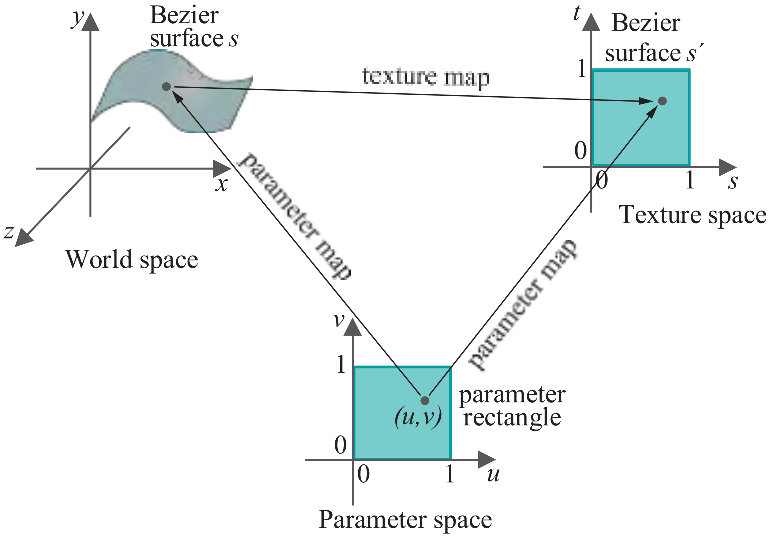

Figure 12.35: Texture mapping a Bézier surface via a Bézier surface in texture space. The parameter map on the right from parameter to texture space is the identity in the case of texturedTorpedo.cpp.

First, we have to create a Bézier surface s^1 in *texture space*. The statement

```
glMap2f(GL MAP2 TEXTURE COORD 2, 0, 1, 2, 2, 0, 1, 4, 2,
           texturePoints[0][0])
```

in the display list for the propeller blade in setup() does just this. The syntax of this statement is similar to that of the glMap2f(GL MAP2_VERTEX 3, . . .) we are already familiar with to create a world-space Bezier´ surface. Control points of s^1 stored in the texturePoints global array are (0, 0), (0, 1), (1, 0) and (1, 1), making s^1 nothing but the rectangle [0, 1]× [0, 1] in texture space. See Figure 12.35. Moreover, the bilinearity of the parametric mapping of s^1 (it's of order 2, or degree 1, along both u and v) implies that it is simply the identity map from the rectangle [0, 1] ×[0, 1] in parameter space to s^1 in texture space.

Observe, next, that the statement

```
glMap2f(GL_MAP2_VERTEX_3, 0, 1, 3, 3, 0, 1, 9, 4,
        controlPointsPropellerBlade[0][0])
```

in its display list defines the parameter space for the propeller blade Bézier surface to be [0, 1]×[0, 1], as well. Given, then, that the parameter spaces for the blade Bézier surface s in world space and the Bézier surface s^1 in texture space are identical, OpenGL defines the texture map between the two in the following simple manner: for each parameter point (u, v), the image of (u, v) on the blade surface s is mapped to the image of (u, v) on s^1 (see Figure 12.35). Given how s^1 itself is defined, evidently texture coordinates (u, v) are assigned to the image of the parameter point (u, v) on the blade Bézier surface, effectively identifying the texture with the parameter rectangle as we set out to do.

The two statements

```
glEnable(GL_MAP2 TEXTURE COORD 2);
glMapGrid2f(5, 0.0, 1.0, 5, 0.0, 1.0);
```

in the propeller blade's display list actually instigate texture coordinate generation at the image points on the world-space Bézier surface – the propeller blade in this case – of an evenly-spaced 5×5 grid in the parameter domain.

Getting OpenGL to generate texture coordinates for a quadric is even simpler. The statement

```
gluQuadricTexture(qobj, GL TRUE)
```

in the drawScene() routine of texturedTorpedo.cpp is all that it takes to automatically generate texture coordinates for the quadric torpedo body.

OpenGL's particular mechanism to generate texture coordinates for a Bézier surface affords flexibility. For example, by changing the control points of the texture-space surface and so its extent, one can paint the real-world surface with a different region of texture space. The next exercise asks you to try this.

Exercise 12.10. (Programming) Make the squares of the checkered pattern on the propeller blades of texturedTorpedo.cpp twice as big as they are currently by changing the program and not the texture.

Exercise 12.11. (Programming) Texture the parts of the torpedo of texturedTorpedo.cpp which are still wire mesh.

12.5.3 Spheres and Mercator Projection

Textured spheres are fairly common everyday objects, e.g., think of globes. So how are spheres textured? For this we need first to understand the *Mercator projection*, the most common way flat maps of the Earth are drawn.

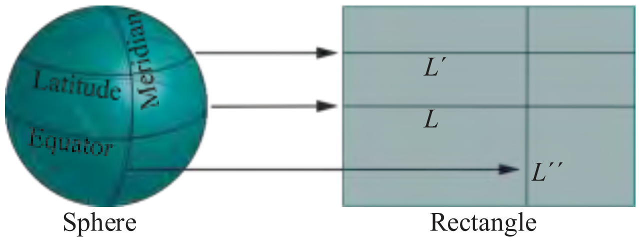

Figure 12.36: Mercator projection.

Imagine a sphere and a rectangular sheet of paper, the latter's height equaling the diameter of the sphere, held upright next to each other. See Figure 12.36. Then the Mercator projection from the sphere to the rectangle maps each latitude (circle) of the sphere to the horizontal segment across the rectangle at the same altitude, scaling each latitude to fit its segment in a such a manner that the image of each meridian (a longitudinal half-circle joining the poles) is a vertical segment through the rectangle. For example, in Figure 12.36, the equator maps to the segment L, while the other latitude drawn maps to the segment L^1, and the meridian drawn to the segment L^{11}. If the height of the rectangle is different from the diameter of the sphere then the Mercator projection evidently must incorporate a scaling in the vertical direction as well.

The Mercator projection obviously causes distortion which worsens as one moves away from the equator because increasingly smaller latitudes are mapped to equal-sized line segments (which is why world maps show Greenland, which is near the north pole, apparently larger than Australia when, in reality, it is a fraction of the size). There are issues, too, with singularities of the Mercator projection with which we won't concern ourselves – particularly that latitudinal circles can never map in a continuous one-to-one manner onto a line segment and, moreover, at the north and south poles the latitudes are no longer even circles, but points.

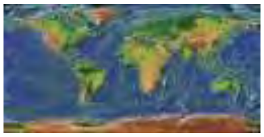

Figure 12.37: World map texture.

Textures which are meant to be applied to a sphere are usually obtained from a Mercator projection of the intended coloring of the sphere. We have, in fact, in earth.bmp a map of the Earth (see Figure 12.37) indeed made from a Mercator projection. The next program applies earth.bmp to a sphere, using the Mercator projection as a texture map.

Experiment 12.17. Run texturedSphere.cpp, which applies earth.bmp as texture to a sphere, the texture map being Mercator projection. Press 'x'-'Z' to turn the sphere. Figure 12.38 is a screenshot. **End**

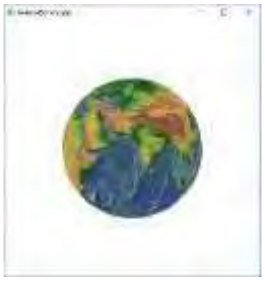

Figure 12.38: Screenshot of texturedSphere.cpp.

The programs is fairly straightforward. Firstly, we leave the reader to check that the parametrization of the sphere is an extension, as it were, of the parametrization of hemisphere.cpp of Chapter 2, making a surface from south pole to north pole, rather than just from equator to north pole.

Observe from the function definitions f, g and h that a generic point on the sphere's mesh is

$$R\cos\left(\frac{-\pi}{2}+\frac{j\pi}{q}\right)\cos\left(\frac{2i\pi}{p}\right),\ R\sin\left(\frac{-\pi}{2}+\frac{j\pi}{q}\right),$$
$$R\cos\left(\frac{-\pi}{2}+\frac{j\pi}{q}\right)\cos\left(\frac{2i\pi}{p}\right)$$

One sees, then, that fixing a y-value on the sphere, equivalent to staying on a given latitude, implies fixing a j-value on the rectangular sample grid, which is equivalent to staying on a horizontal line of grid points. Likewise, traversing a given meridian implies fixing an i-value on the sample grid, which is equivalent to staying on a vertical line of grid points.

Clearly, then, if we map the generic point above to the point (i, j) on the rectangular grid of size $p \times q$, we'll have a Mercator projection; moreover, mapping it to $(i/p, j/q)$ would give a Mercator projection to a unit square, which can very well be taken to be a texture. In fact, it is the latter projection which is implemented as the texture map in texturedSphere.cpp by the routine fillTextureCoordArray().

Remark 12.5. As the reader may have already noted, our texture map would have been no different if we had simply taken the sphere as a parametrized surface and proceeded following the earlier subsection on texture maps for such surfaces in general. However, knowing that our texture map, in fact, is a Mercator projection puts us on solid ground and allows us to apply spherical textures made from such projections (the most common kind available in texture libraries).

Exercise 12.12. (Programming) Look for a map of the moon on the web and use it to texture a sphere.

12.6 Texture Matrix and Animating Textures

Recall from Section 4.4 that the current modelview matrix, say M, the topmost one in the modelview matrix stack, transforms a vertex V by multiplication from the left, in particular, V $-MV$. Likewise, the *texture matrix stack* contains 4×4 *texture matrices*, the topmost one of which is the *current texture matrix* ; likewise, too, texture coordinates are transformed by multiplication from the left by the current texture matrix.

When being multiplied by the current texture matrix, texture coordinates are written as column vectors with four components, typically denoted $[s\ t\ r\ q]^T$. For example, texture coordinates represent points (s, t) in plane texture space for the 2D textures we have been using; however, extended to 4D, (s, t) would be written $[s\ t\ 0\ 1]^T$. As expected, by default, the current texture matrix is the 4 × 4 identity.

Texture mode is entered with a call to glMatrixMode(GL TEXTURE); subsequently, the texture matrix stack and current texture matrix can be manipulated with exactly the same commands, e.g., glPushMatrix(), glLoadIdentity(), glTranslatef(), etc., as their modelview counterparts. Indeed, by transforming texture coordinates one can animate a texture in various ways. Let's see a simple example.

Experiment 12.18. Run fieldAndSkyTextureAnimated.cpp, which animates the sky texture of fieldAndSky.cpp by applying translations to the current texture matrix. Press space to toggle between animation on and off. Figure 12.39 is a screenshot.
End

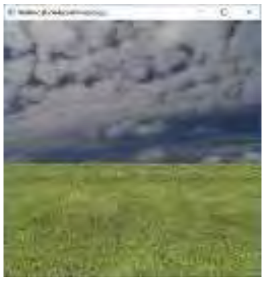

Figure 12.39: Screenshot of fieldAndSkyTextureAnimated.cpp.

The modification of fieldAndSky.cpp to make fieldAndSkyTextureAnimated.cpp is straightforward. In particular, the following block of code in the drawing routine of the latter does the trick by entering texture matrix mode and applying translations around a circle to rotate the sky texture:

```
// Enter texture mode and load identity.
glMatrixMode(GL_TEXTURE);
glLoadIdentity();
---

glTranslatef(0.1 * cos(angle), 0.1 * sin(angle), 0.0);

// Map the sky texture onto a rectangle parallel to the xy-plane.
glBindTexture(GL_TEXTURE_2D, texture[1]);
---

// Reenter modelview mode.
glMatrixMode(GL_MODELVIEW);
```

The rest of the modification of fieldAndSky.cpp is in managing the animation.

Exercise 12.13. (Programming) Continuing with Exercise 12.7 rotate the stripes in a screw-like manner around the torus which should look as if the torus itself is rotating oppositely.

12.7 Lighting Textures

By now the reader may be wondering if color and light can coexist with texture or if the two are mutually exclusive ways of adorning an object. The answer is indeed they can play well together and OpenGL, in fact, offers more than one way to make this happen. An option is selected using the following texture function call, typically located in the initialization routine:

```
glTexEnvf(GL TEXTURE_ENV, GL_TEXTURE ENV MODE, parameter)
```

If *parameter* is GL_REPLACE, as it has been in our programs thus far, then the texture colors *overwrite* the current primitive pixel colors (i.e, the primitive's own material colors as well as light sources in the environment are ignored).

The most common way, though, to combine color and light with texture is by setting *parameter* to GL_MODULATE, in which case OpenGL does the following:

(a) Computes RGB values at a primitive's vertices using OpenGL's lighting equation (11.13) and interpolates these through its interior – assuming that smooth shading is on – to determine the RGB values at each of its pixels.

(b) Uses the texture map to obtain RGB values from the texture at each of the primitive's pixels.

(c) Determines the final RGB values at each pixel as the *product* of the corresponding values from the preceding two steps.

In short, OpenGL *separately* computes RGB values for color and light as if there were no texture, and RGB values for texture as if there were no color and light and, finally, scales one with the other.

Example 12.2. If the RGB tuple at a pixel P is (0.5, 0.75, 0.1) as obtained by interpolation from vertex RGB values computed after lighting, while that determined at P from the texture via the texture map is (0.4, 0.5, 1.0), then the final color applied to P using the GL_MODULATE option is $(0.5 \times 0.4,\ 0.75 \times 0.5,\ 0.1 \times 1.0) = (0.2, 0.375, 0.1)$.

Experiment 12.19. Run fieldAndSkyLit.cpp, which lights the scene of fieldAndSky.cpp with help of the GL_MODULATE option. The light source is directional – imagine the sun – its direction being controlled with the left and right arrow keys, while its brightness can be changed using the up and down arrow keys. A white line indicates the direction and brightness of the sun. Figure 12.40(a) is an early morning screenshot.

The material colors are all white and the light is a uniform gray, which means essentially that the texture is modulated by the intensity of the light source, which can be controlled by changing its diffuse and specular $(d, d, d, 1)$ value or its direction at angle of θ to the ground. The normal to the horizontal grassy plane is vertically upwards. Strangely, we use the same normal for the sky's vertical plane, because using its "true" value toward the positive z-direction has the unpleasant, but not unexpected, consequence of a sky that doesn't darken together with land. End

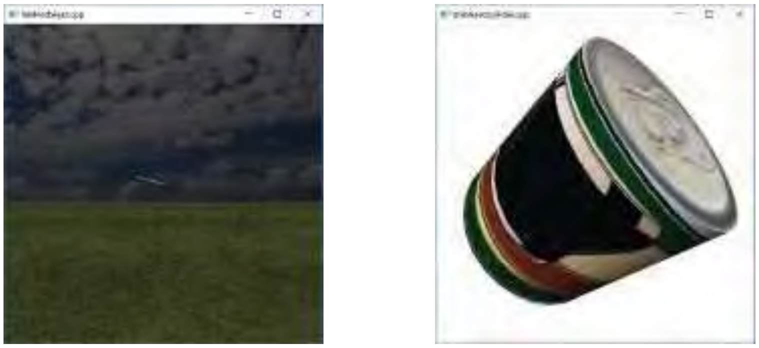

(a)

(b)

Figure 12.40: Screenshots of (a) fieldAndSkyLit.cpp and (b) litTexturedCylinder.cpp.

Experiment 12.20. Run litTexturedCylinder.cpp, which adds a label texture and a can top texture to litCylinder.cpp from the previous chapter. Press 'x'-'Z' to turn the can. Figure 12.40(b) is a screenshot.

Most of the program is routine – the texture coordinate generation is, in fact, a near copy of that in texturedTorus.cpp – except for the following lighting model command in setup() which we're invoking in a program for the first time:

```
glLightModeli(GL LIGHT MODEL COLOR CONTROL, GL SEPARATE SPECULAR COLOR)
```

We had briefly encountered this statement as an OpenGL lighting model option in Section 11.4. It causes a modification of OpenGL's GL MODULATE procedure: the specular color components are separated and not multiplied with the corresponding texture color components, as are the ambient and diffuse, but added in after. The result is that specular highlights are preserved rather than blended with the texture. Turning the can you do see the specular highlights, but if you care to comment out the statement above then they disappear. End

Exercise 12.14. (Programming) Close off the bottom of the cylinder of litTexturedCylinder.cpp with a metal-textured disc.

Exercise 12.15. (Programming) Light and texture the fluttering flag of flag.cpp (see Experiment 4.25 of Chapter 4).

Exercise 12.16. (Programming) Make the spinning cube of Exercise 11.44 into a spinning wooden crate by applying a texture like Figure 12.41 to each face. Keep the lighting and the shadow.

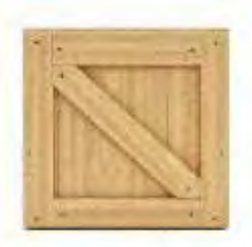

Figure 12.41: Wooden crate side.

Exercise 12.17. (Programming) Continue improvement of shipMovie.cpp, which you began in Exercise 11.52, now with the help of textures. There are numerous possibilities of which a few are:

(a) Texture the black back plane with the image of a night-time city skyline.

(b) Paint the surface of the sea with a water texture, possibly animated.

(c) Add detail to the ship by texturing it with images of parts of real ships.

(d) Texture the background boats. You may want to strategically place additional light sources.

Exercise 12.18. (Programming) Continue with Exercise 11.53 where you enhanced animateMan*.cpp with color and light, now using texture.

12.8 Multitexturing

OpenGL allows more than one texture to be applied to a polygon in a pipelined process, each texture being combined with its predecessor in programmer-specified manner. This so-called multitexturing makes possible myriad visual effects depending upon the textures and how they are combined. Let's get to work on a particular one – transforming a night sky into day – by interpolating between night and day sky textures, illustrating in the process the key steps in multitexturing.

Experiment 12.21. Run multitexture.cpp, which interpolates between night and day sky texture. Press the left/right arrow keys to transition between night and day. Figure 12.42 shows stages in the transition. End

Multitexturing requires more than one *texture unit* – a binding point for a texture to the OpenGL context – each with id of the form GL_TEXTUREi. Here's the block in the initialization routine of multitexture.cpp which initializes GL TEXTURE0:

```
glActiveTexture(GL TEXTURE0);
glEnable(GL TEXTURE 2D);
glBindTexture(GL_TEXTURE 2D, texture[0]);
glTexEnvi(GL TEXTURE_ENV, GL_TEXTURE ENV MODE, GL REPLACE);
```

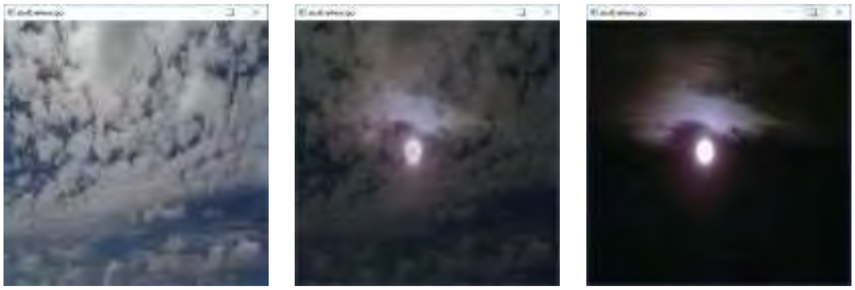

(a) (b) (c)

Figure 12.42: Screenshots of multitexture.cpp: (a) Mid-day (b) Late evening (c) Night.

The first statement selects GL_TEXTURE0 as the currently active texture unit, the second enables 2D texturing, the third binds texture object texture[0], containing the day sky image, to the active texture unit, while the last specifies that surface colors come from the active texture unit.

The block initializing GL_TEXTURE1, binding it to texture[1], containing the night sky image, is similar except for the last statement

```
glTexEnvi(GL_TEXTURE_ENV, GL_TEXTURE_ENV_MODE, GL_COMBINE);
```

where the third parameter GL_COMBINE, instead of GL_REPLACE as in the earlier GL_TEXTURE0 block, indicates that the texture unit GL_TEXTURE1 combines with GL_TEXTURE0 by the application of a *texture combiner function*. The second parameter of the next statement in the initialization routine

```
glTexEnvi(GL_TEXTURE_ENV, GL_COMBINE_RGB, GL_INTERPOLATE);
```

indicates that it defines the combiner function, while the third parameter means that this function, in fact, is interpolation. In particular, this interpolation is given by

$$Arg0 * Arg2 + Arg1 * (1 - Arg2)$$

which evidently interpolates between $Arg0$ and $Arg1$, the interpolation parameter being $Arg2$. The following final block of statements in the initialization routine specify the combiner's three arguments.

```
glTexEnvi(GL_TEXTURE_ENV, GL_SRC0_RGB, GL_TEXTURE0);
glTexEnvi(GL_TEXTURE_ENV, GL_OPERAND0_RGB, GL_SRC_COLOR);

glTexEnvi(GL_TEXTURE_ENV, GL_SRC1_RGB, GL_TEXTURE1);
glTexEnvi(GL_TEXTURE_ENV, GL_OPERAND1_RGB, GL_SRC_COLOR);

glTexEnvi(GL_TEXTURE_ENV, GL_SRC2_ALPHA, GL_CONSTANT);
glTexEnvi(GL_TEXTURE_ENV, GL_OPERAND2_ALPHA, GL_SRC_ALPHA);
```

The first statement says that the combiner's zeroth source has RGB values from the zeroth texture unit, while the second says that the zeroth operand, i.e., $Arg0$, reads its RGB values from the zeroth source. So, the two statements together imply that the $Arg0$ values are, in fact, GL_TEXTURE0's RGB.

The next two statements similarly set $Arg1$ values to GL_TEXTURE1's RGB, while the last two say that $Arg2$ is the alpha value of the texture environment variable GL_TEXTURE_ENV_COLOR, which is connoted by GL_CONSTANT.

Note: One sees that the setting of all three combiner arguments $Arg0$, $Arg1$ and $Arg2$ are through an intermediate combiner source, rather than directly from a texture unit or environment variable.

Next, observe that the two statements

```
glTexEnvfv(GL_TEXTURE_ENV, GL_TEXTURE_ENV_COLOR, constColor);
constColor[3] = alpha;
```

in the display routine specify that GL_TEXTURE_ENV_COLOR values are to be read from the global array constColor, and set its alpha value which, as we know from statements above, is equal to the interpolation parameter *Arg*2; note that GL_TEXTURE_ENV_COLOR RGB values are not set because they are never used.

The final piece is to specify independently the texture coordinates for the two texture units, which is done within the polygon definition in the display routine via statements of the form glMultiTexCoord2f(GL_TEXTUREi, *, *), e.g., the block

```
glMultiTexCoord2f(GL_TEXTURE0, 0.0, 0.0);
glMultiTexCoord2f(GL_TEXTURE1, 0.0, 0.0);
glVertex3f(-20.0, -20.0, 0.0);
```

says that the polygon vertex $(-20.0, -20.0, 0.0)$ has texture coordinates $(0.0, 0.0)$ for both texture units.

Whew, if you are thinking that multitexturing is convoluted then you will be glad to know that a program like multitexture.cpp will become almost embarrassingly simple with the use of shaders, as we'll see in Chapter 16, because we'll then be able to read texel values and do as we please with them in the fragment shader. In fact, for this reason glTexEnvf() is gone from OpenGL 3.3 and higher.

Figure 12.43: Mountain.

Figure 12.44: Fog.

Exercise 12.19. (Programming) In addition to interpolation, other texture combiners, e.g., modulation, addition and subtraction, can be used to create various effects. Apply modulation, which has the combiner function $Arg0 * Arg1$, with a call to glTexEnvi(GL_TEXTURE_ENV, GL_COMBINE_RGB, GL_MODULATE), to combine a mountain texture, such as Figure 12.43, with a fog texture, such as Figure 12.44. Animate the latter as well, to make the fog blow around the mountain.

12.9 Rendering to Texture with Framebuffer Objects

We are now going to see a rather spectacular capability of modern OpenGL, namely, that of rendering a scene at run-time to a texture. So, an application can conceivably apply a texture to a TV screen, a billboard, or, even, the side of a can, and run a movie on it. Rendering to a texture requires the use of so-called *framebuffer objects*, or FBOs, which have been part of the OpenGL core since version 3.0. Let's learn a bit about FBOs first.

Framebuffer Objects

The final destination of the OpenGL rendering pipeline is the framebuffer provided by the windowing system of the computer, the *default* framebuffer as it's called. This framebuffer actually consists of multiple separate buffers (Figure 12.45): color buffers with RGBA values, a depth buffer with z-values and a stencil buffer, which we'll be examining carefully the next chapter, which one can think of as having a counter per pixel. The default framebuffer is read by the screen, so determines what is displayed.

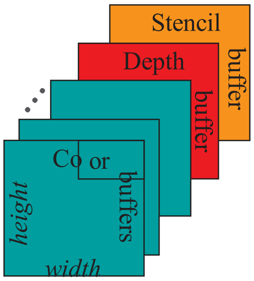

Figure 12.45: Framebuffer.

A framebuffer object or FBO, on the other hand, is a "pretend" framebuffer created by an application. An FBO lives in GPU memory, accessible to the OpenGL pipeline, as long as the application doesn't delete it. It has no connection with the windowing system and doesn't display; it's simply an application-created artifact.

In fact, an FBO is somewhat less than even a pretend framebuffer at the time of its creation: it comes with not a single color, depth or stencil buffer, but, rather, slots to attach these. So, it is the application's responsibility to attach buffers to an FBO as required. The utility of an FBO with appropriate buffers attached, of course, lies in that it can serve as an intermediate off-screen rendering station where the application can perform all kinds of processing without interfering with what's actually being displayed.

The slots to attach color buffers to an FBO are denoted GL_COLOR_ATTACHMENT*i*, where *i* runs from 0 to some system-determined maximum, the slot to attach a depth buffer is denoted GL_DEPTH_ATTACHMENT, while the slot to attach a stencil buffer is denoted GL_STENCIL_ATTACHMENT. See Figure 12.46 for an example of storage scheme for an FBO with four attachments – two color, one depth and one stencil. The buffers themselves may be either of two base forms, a texture or a so-called *renderbuffer*.

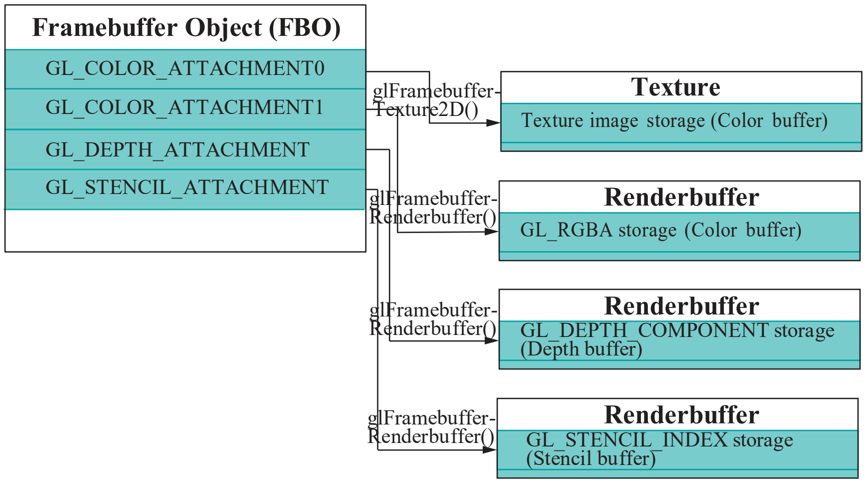
Framebuffer Object (FBO)
GL_COLOR_ATTACHMENT0
GL_COLOR_ATTACHMENT1
GL_DEPTH_ATTACHMENT
GL_STENCIL_ATTACHMENT
glFramebuffer-Texture2D()
Texture
Texture image storage (Color buffer)
glFramebuffer-Renderbuffer()
Renderbuffer
GL_RGBA storage (Color buffer)
glFramebuffer-Renderbuffer()
Renderbuffer
GL_DEPTH_COMPONENT storage (Depth buffer)
glFramebuffer-Renderbuffer()
Renderbuffer
GL_STENCIL_INDEX storage (Stencil buffer)

Figure 12.46: Scheme for an FBO with 4 attachments: the zeroth color attachment has texture storage; the first color attachment, depth attachment and stencil attachment each have renderbuffer storage.

A texture comes with its own storage, typically, for an image, which, nevertheless, can serve as a color, depth or stencil buffer. The command to attach a 2D texture as a color buffer, for example, to an FBO is of the form

```
glFramebufferTexture2D(GL_FRAMEBUFFER, GL_COLOR_ATTACHMENTi,
                       GL_TEXTURE_2D, textureID, mipmapLevel);
```

where the last two parameters, obviously, identify the texture and mipmap level.

A renderbuffer, on the other hand, is an object that has to be created and bound first and then its storage assigned with a command of the form

```
glRenderbufferStorage(GL_RENDERBUFFER, storageFormat, width, height);
```

where the second parameter *storageFormat* can be, for example, GL_RGBA for the object to function as a color buffer, or GL_DEPTH_COMPONENT for it to function as a depth buffer, or GL_STENCIL_INDEX for it to function as a stencil buffer. The last two parameters specify the renderbuffer's size. Finally, the renderbuffer is attached to an FBO with a command of the form

```
glFramebufferRenderbuffer(GL_FRAMEBUFFER, attachSlot,
                          GL_RENDERBUFFER, renderbufferID);
```

where *attachSlot* may be GL_COLOR_ATTACHMENT*i*, GL_DEPTH_ATTACHMENT or GL_STENCIL_ATTACHMENT, specifying the kind of buffer it will act as, and *renderbufferID* identifies the renderbuffer. The FBO of Figure 12.46 evidently has texture storage for its zeroth color attachment and renderbuffer storage for the next color attachment, as well as the depth and stencil attachments.

Note that FBOs and renderbuffers are themselves created and bound in usual OpenGL fashion with glGen...() and glBind...() commands.

The preceding overview of FBOs was not a complete specification – for this the reader ought to pick up the red book – but should be enough to get us going with most practical applications. Here, then, is one.

Our next program takes litTexturedCylinder.cpp from earlier this chapter, strips away lighting to keep it simple *and* replaces the beer label with a texture to which is rendered an animated scene like that of ballAndTorus.cpp from Chapter 4, the difference with the latter program essentially being that, instead of a torus we now have a long cylinder spanning the OpenGL window, so this cylinder, in fact, turns into a torus when the texture is wrapped around the can.

Experiment 12.22. Run renderedTexture.cpp. Press space to toggle the can label animation on and off and 'x'-'Z' to turn the can. Figure 12.47 is a screenshot.
End

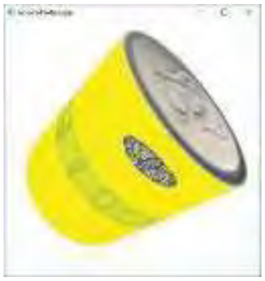

Figure 12.47: Screenshot of renderedTexture.cpp.

We'll narrate renderedTexture.cpp top down. The globals are from both litTexturedCylinder.cpp and ballAndTorus.cpp, taking into account the elimination of lighting from the former, which means no normals, and, moreover, that a GLU quadric cylinder replaces the torus in the latter, the ball rotating around this cylinder as it simultaneously translates parallely. A few obvious additional globals hold an FBO's id and size, a renderbuffer's id, as well as the size of the OpenGL window.

The routine loadTextures() next should be familiar, binding the can top image to texture[1]. Familiar, too, should be f(), g(), h(), fillVertexArray() and fillTextureCoordArray(), which are all copied from litTexturedCylinder.cpp. The setup() routine next is where it starts to get interesting. In fact, if the reader compares the two, then she will see that the top part between the two statements

```
glEnable(GL_DEPTH_TEST);
---
glEnable(GL_TEXTURE_2D);
```

is copied over from litTexturedCylinder.cpp's setup *minus* all calls to do with light, material properties and normal values; moreover, renderedTexture.cpp's setup is missing a glClearColor(), which we'll momentarily see why, and glTexEnvf()'s last parameter is GL REPLACE instead of GL_MODULATE because textures will not be mixed with material colors.

The next two calls

```
qobj = gluNewQuadric();
gluQuadricDrawStyle(qobj, GLU_LINE);
```

evidently define a wireframe quadric object, which in turn will be the cylinder and ball of the animation.

The next block of statements

```
glBindTexture(GL_TEXTURE_2D, texture[0]);
glTexImage2D(GL_TEXTURE_2D, ..., NULL);
---
glTexParameteri(GL_TEXTURE_2D, GL_TEXTURE_MIN_FILTER, GL_LINEAR);
```

standardly bind texture[0], setting its parameters, but leaving its image data uninitialized as can be seen from the NULL last parameter of the second command glTexImage2D() – this, of course, is because we'll be rendering to this texture ourselves.

The final seven statements initialize the FBO:

```
glGenRenderbuffers(1, &renderbuffer);
glBindRenderbuffer(GL_RENDERBUFFER, renderbuffer);
glRenderbufferStorage(GL_RENDERBUFFER, GL_DEPTH_COMPONENT,
                      framebufferWidth, framebufferHeight);
```

```
glGenFramebuffers(1, &framebuffer);
glBindFramebuffer(GL_FRAMEBUFFER, framebuffer);
glFramebufferTexture2D(GL_FRAMEBUFFER,   GL_COLOR_ATTACHMENT0,
                       GL_TEXTURE_2D, texture[0], 0);
glFramebufferRenderbuffer(GL_FRAMEBUFFER, GL_DEPTH_ATTACHMENT,
                          GL_RENDERBUFFER, renderbuffer);
```

The first two statements above create and bind a renderbuffer with eponymous id, while the third one declares it to be a depth buffer of the (fixed) size of the FBO. The fourth and fifth statements create and bind an FBO, while the sixth and seventh statements, respectively, attach to it texture[0] as color buffer and renderbuffer as depth buffer. So, we have now a 512×512-sized FBO with a color and a depth buffer ready to be drawn to.

The drawTextureScene() routine next, in fact, is the one which will draw to the FBO. Its top part bears attention first. There are three things to notice:

(a) Texturing is disabled through the routine because colors are applied with glColor3f(), not textures.

(b) The routine defines its own clearing color (yellow) to be used as background for the animation, different from the OpenGL window's clearing color (white).

(c) ballAndTorus.cpp's resize() routine is copied to the top because its viewing frustum is different from that of litTexturedCylinder.cpp, the "containing" program inside which this drawing routine lives.

The rest of the routine is adapted from ballAndTorus.cpp's drawing routine – we'll leave the reader to parse how the modeling transformations carry the ball around as well as parallel to the cylinder.

Next comes renderedTexture.cpp's own drawing routine drawScene(). The first three statements

```
glBindFramebuffer(GL_FRAMEBUFFER, framebuffer);
drawTextureScene();
glBindFramebuffer(GL_FRAMEBUFFER, NULL);
```

successively activate the FBO framebuffer, draw to it, and then restore the default (windowing system's) framebuffer, as the parameter NULL in the third statement indicates. Drawing to framebuffer, of course, means rendering to texture[0], its color buffer.

Next, the drawing routine sets its own clearing color (white) to be applied to the OpenGL window and also copies in litTexturedCylinder.cpp's resize() routine in order to invoke the latter's viewing frustum.

Finally, in the next two blocks of statements, exactly identical to the corresponding blocks in litTexturedCylinder.cpp's drawing routine, texture[0] is applied to the can cylinder and texture[1] to the can top, the former, of course, being the render target of drawTextureScene().

A final point of note is that, since its drawScene() has its own copy of frustum-defining commands, renderedTexture.cpp's resize() is reduced to a rump whose only function is to ship the OpenGL window dimensions to globals.

We'll be seeing another application of FBOs – to image manipulation – in the next chapter.

Exercise 12.20. (Programming) Model a TV set and show a movie.

Remark 12.6. *A texture may not always be an image*. What an odd thing to say at the end of a chapter of applying exclusively images as textures! But it may not appear so strange upon noting that texels are nothing but arrays of bits which, thus far, have been *interpreted* as RGBA values.

They don't have to be, e.g., we could very well interpret a 32-bit texel as a 32-bit floating point number representing, say, depth. Moreover, the hardware accelerated access to textures in the GPU – designed, particularly, for the texture map to be calculated rapidly – may be put to good use accessing other kinds of data, as well, effectively exploiting the texture as a rapid-access *look-up table*.

In fact, there are various applications of such non-image data textures. We'll soon be seeing one ourselves in the next chapter, where a so-called depth texture is used to store z-buffer values for the purpose of shadow mapping.

12.10 Summary, Notes and More Reading

Texturing, the process of painting an image onto the surface of an object, is of great practical importance in computer graphics. In this chapter we learned the basics of how to apply a texture, underlying principles of the texturing process and a fair number of techniques to effectively manage textures, amongst them being combining textures with lighting, multitexturing to combine multiple textures, as well as rendering to textures.

The seminal reference for textures in CG is Heckbert [72]. The article by Haeberli and Segal [67] is easily-readable and informative as well. More advanced CG books, e.g., the ones by Akenine-Möller, Haines & Hoffman [1] and Watt [150], all have sections on texturing that will take the reader beyond what she has learned in this chapter. The book by Reynolds and Blythe [95] is a good reference for texturing in OpenGL in particular. Texturing techniques are a field of active research and, as for CG research in general, the place to visit for the latest developments is the annual ACM SIGGRAPH conference [133].

Taylor & Francis
Taylor & Francis Group
http://taylorandfrancis.com

Chapter 13

Special Visual Techniques

And now for special effects! Special visual techniques are the topic of the next ten sections of this chapter. These include blending, fog, billboards, antialiasing and multisampling, point sprites, environment mapping, stencil buffer techniques, image manipulation, bump mapping and shadow mapping.

The goal of blending objects by combining their color values, the topic of Section 13.1, is primarily to engender translucency; however, blending can also be used in effects such as reflection and morphing. Section 13.2 shows how to use fog to cue the viewer to the distance of an object. This imparts realism to a scene, as does the technique of billboarding introduced in Section 13.3, a cost-effective way to create the illusion of a 3D object by means of its 2D image.

We'll learn in Section 13.4 how to antialias points and straight lines, as well as how to multisample polygons, in order to remove jaggedness in their rendering. Section 13.5 shows how to turn plain points into spectacular point sprites, multitudes of which can then combine to form particle systems. Environment mapping, the topic of Section 13.6, consists of texturing objects with images of their surroundings. We'll discuss two particular environment mapping techniques, namely, sphere mapping and cube mapping. The former is used make objects reflect their surroundings, while the latter to manufacture skyboxes so commonly used to backdrop games scenes.

The stencil buffer, described in Section 13.7, essentially, has a counter per pixel, which can be set and read to interesting effect. Section 13.8 discusses image manipulation, particularly with the help of an FBO. Bump mapping, which we'll study in Section 13.9, is a technique to add the illusion of detail to an object by altering its normals, but without changing its geometry. In Section 13.10 we learn the method of shadow mapping to create authentic shadows – a technique far more sophisticated than the simple flatten-and-blacken of Section 4.7.2. Section 13.11 concludes the chapter.

13.1 Blending

We'll spend a little time first assimilating the theory of blending before putting it into practice.

13.1.1 Theory

Our plan is to understand first how OpenGL operates without blending, and then with.

No Blending

Consider the following piece of pseudo-code and how OpenGL would process it without blending:

```
glClear(GL COLOR BUFFER_BIT | GL DEPTH BUFFER_BIT);
draw triangle $T$;
draw quad $Q$;
```

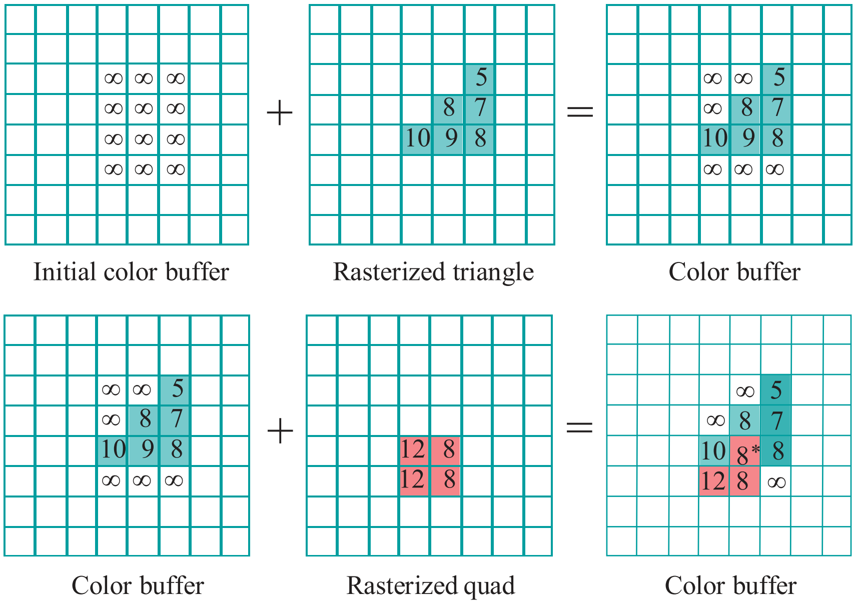

Initial color buffer | Rasterized triangle | Color buffer

Color buffer | Rasterized quad | Color buffer

Figure 13.1: Assuming depth testing on: T rasterized and rendered (upper row), followed by Q rasterized and rendered (lower row). The starred pixel is considered in an example below.

See Figure 13.1. The z-values in the depth buffer (aka z-buffer) are each initialized to a very large value by the glClear() command, as are values in the color buffer all to the clearing color, say, white. This initial configuration is depicted in the upper left grid, where pixels only in a region of interest are labeled with their z-values, unlabeled pixels all having ∞ z-value as well.

The triangle T is then *rasterized*, i.e., the set of pixels corresponding to T determined, and color and z-values computed for each – the upper middle grid showing hypothetical z-values. A raster pixel, together with its color values and z-value, is called a *fragment*.

OpenGL next *renders* T to the color buffer, which will be viewed when flushed to the screen, according to sets of rules depending on whether depth testing is on or not.

If *depth testing is enabled*, then the process is two-step:

1. The z-value of each of T's fragments, called a *source fragment*, is compared with that of the corresponding pixel, called the *destination pixel*, in the color buffer.

2. If the source fragment's z-value is less than that of the destination pixel, so that it's closer to the eye, then it passes the depth test and its color values *overwrite* the current color values of the destination pixel and its z-value overwrites the current z-value, as well; if the source fragment's z-value is not less than that of the destination pixel, then it fails the depth test and its color values and z-value are discarded, leaving all destination values unchanged.

   Note: That its z-value be less than that in the destination pixel is the default test that a source fragment has to pass in order to overwrite the destination. Other tests can be invoked with a call to glDepthFunc() (see the red book for a listing of possible tests).

If *depth testing is not enabled*, then the process is a simple single step:

1. Each one of T's fragments unconditionally overwrites the color values of its destination pixel. The z-values are not relevant and never change.

Given depth testing as enabled, the result of rendering T is depicted in the upper right grid in Figure 13.1, and also in the lower left. Following T, quad Q is rasterized (lower middle) and rendered (lower right) in an identical manner, Q replacing T in the two-step procedure above. One sees that three of Q's fragments pass the depth test and overwrite their destination pixels.

The Difference with Blending

Next, let's understand what happens *with* blending. The differences are precisely the following:

(a) In all the cases above – without blending, that is – where a source fragment's color values are supposed to overwrite those of its destination pixel, OpenGL instead *combines*, or *blends*, the two sets and applies the result to the destination pixel. We'll discuss momentarily how color values are, in fact, combined.

(b) In all the cases above, where the source fragment does not overwrite its destination pixel – e.g., if depth testing is on and its z-value is greater – then it's discarded as before.

(c) As for z-values, if depth testing is on, a source z-value lower than that of the destination replaces the latter, *regardless* if blending is in effect or not. If depth testing is not enabled, then, as before, z-values are irrelevant and never change, blending or not.

Here's how OpenGL combines color values in order to blend them in item (a) above. Say the source fragment's color values are (src_R, src_G, src_B), while those of the destination are (dst_R, dst_G, dst_B). Based upon the programmer's specifications, OpenGL assigns so-called *blending factors*, in particular, a scalar src_b to the source, and a scalar dst_b to the destination. It then determines the final color values of the destination pixel as a sum of the source and destination color vectors weighted by their respective blending factors, particularly, using the following *blending equation*:

$$\begin{aligned}(dst_R, dst_G, dst_B) &= src_b * (src_R, src_G, src_B) + \\ &\quad dst_b * (dst_R, dst_G, dst_B)\end{aligned} \tag{13.1}$$

We'll say soon how, in fact, the programmer specifies the blending factors, but first an example and an exercise.

Example 13.1. Consider the starred pixel in the lower right grid of Figure 13.1. Say its RGB color values prior to the rendering of Q, in particular, those of the corresponding pixel in the triangle T in the lower left grid, are $(0.6, 0.4, 0.2)$, while those of the corresponding pixel of the quad in the lower middle are $(0.5, 0.5, 0.5)$. Suppose as well that $src_b = 0.3$ and $dst_b = 0.7$ and that depth testing is on. What are the final color and depth values of the starred pixel if blending is not enabled? If it is?

Answer: Suppose, first, that blending is off. The source fragment's z of 8 being less than the destination's 9, it overwrites the destination's colors. Final color values of the starred pixel are, therefore, $(0.5, 0.5, 0.5)$.

Next, suppose blending is enabled. Since the source would overwrite the destination colors if blending were off, given that blending is, in fact, on, their color values are combined instead. The blending equation (13.1) gives the resulting values as

$$0.3 * (0.5, 0.5, 0.5) + 0.7 * (0.6, 0.4, 0.2) = (0.57, 0.43, 0.29) \tag{13.2}$$

The resulting z of 8 for the starred pixel is the same, though, both in blended and unblended applications, as it is determined only by competition in the depth buffer.

Exercise 13.1. How about the pixel just to the left of the starred one? What are its color and depth values with blending enabled, assuming that the color values in the corresponding pixels in the left and middle grids are the same as for the starred one in the preceding example and that blending factors are identical as well? Consider when depth testing is both on and off.

Specifying Blending Factors: Alpha

It's in assigning the blending factors that the programmer can make use of the *alpha* values, the A in RGBA. For example, the *blend function* command

```
glBlendFunc(GL SRC ALPHA, GL ONE MINUS SRC ALPHA)
```

causes OpenGL to set

$$src_b = src_A \quad \text{and} \quad dst_b = 1 - src_A$$

where src_A denotes the source fragment's alpha value. The consequence of this particular blend function, as one sees from plugging the blending factors into (13.1) to get

$$\begin{aligned}(dst_R, dst_G, dst_B) &= src_A * (src_R, src_G, src_B) + \\ &\quad (1 - src_A) * (dst_R, dst_G, dst_B)\end{aligned}$$

is that the greater the source's alpha the more its contribution to the final color or, equivalently, the more it retains of its own color, meaning, intuitively, the more *opaque* it is. E.g, in Example 13.1 above, if glBlendFunc(GL SRC ALPHA, GL ONE MINUS SRC ALPHA) had been called, then glColor4f(0.5, 0.5, 0.5, 0.3) for the quad Q would give blending parameters as in (13.2).

In general, blending factors are set by calling

```
glBlendFunc(srcFactor, dstFactor)
```

where the values of the parameters *srcFactor* and *dstFactor* tell OpenGL how to determine the source and destination blending factors, respectively. We've already seen that the value GL SRC ALPHA chooses the source alpha value src_A, while GL ONE MINUS SRC ALPHA chooses $1 - src_A$. Likewise, GL DST ALPHA and GL-ONE-MINUS-DST-ALPHA choose dst_A and $1 - dst_A$, respectively.

The reader is referred to the red book for a full list of possible values for *srcFactor* and *dstFactor* , though GL SRC ALPHA and GL ONE MINUS SRC ALPHA are, in fact, most commonly used. Moreover, any of these values may be used for either parameter, e.g., even GL SRC ALPHA for *dstFactor*, which would be an odd choice indeed.

Finally, the alpha value dst_A of the destination pixel changes, too, being combined from those of the source and destination by a blending equation exactly similar to (13.1), so we could rewrite the latter more comprehensively as

$$\begin{aligned}(dst_R, dst_G, dst_B, dst_A) &= src_b * (src_R, src_G, src_B, src_A) + \\ &\quad dst_b * (dst_R, dst_G, dst_B, dst_A) \qquad (13.3)\end{aligned}$$

Remark 13.1. The blending equation (13.3), though the default and most commonly used, isn't the only option in OpenGL to combine source and destination color values. Other formulae are available as well, which can be chosen by a call to the command glBlendEquation(). Moreover, certain parameter choices for glBlendFunc() allow (13.3) to be refined to apply different blending factors to each of R, G, B and A of the source, and to each of R, G, B and A of the destination. Refer to the red book for details.

13.1.2 Experiments

Experiment 13.1. Run blendRectangles1.cpp, which draws two translucent rectangles with their alpha values equal to 0.5 set by calls of the form glColor4f(*, *, *, 0.5), the red one being closer to the viewer than the blue one. The *code* order in which the rectangles are drawn can be toggled by pressing space. Figure 13.2 shows screenshots of either order. End

Blending is enabled in blendRectangles1.cpp with the call

```
glEnable(GL BLEND)
```

in the initialization routine and the blend function defined by

```
glBlendFunc(GL SRC ALPHA, GL ONE MINUS SRC ALPHA)
```

As depth testing is currently disabled by glDisable(GL DEPTH_TEST), if there were no blending, then the rectangle second in code would overwrite the one drawn first. Therefore, from our understanding of theory now, with blending on, their colors are combined instead.

As $src_A = 1 - src_A = 0.5$, no matter which rectangle is drawn first, the blending equation (13.3) gives simply

$$\begin{aligned}(dst_R, dst_G, dst_B, dst_A) &= 0.5 * (src_R, src_G, src_B, src_A) + \\ & \quad 0.5 * (dst_R, dst_G, dst_B, dst_A) \qquad (13.4)\end{aligned}$$

which is symmetric in source and destination. So, one may wonder why the one drawn second seems to dominate where the images intersect. The reason is that the rectangle drawn first is blended with the background white, diluting its color, while the second-drawn rectangle comes in at "full strength". Let's check that this is actually so in the next example.

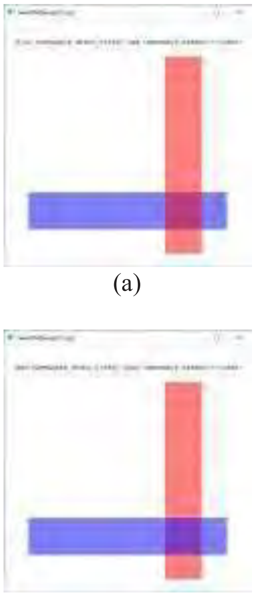
(a)

(b)

Figure 13.2: Screenshot of blendRectangles1.cpp with (a) the blue rectangle first in code (b) the red rectangle first in code.

Example 13.2. For blendRectangles1.cpp, in the case when the blue rectangle is drawn first, use the blending equations to compute the colors of each region of the composite output shape. Next, verify the color values experimentally.

Answer : For the two parts of the blue rectangle which are not intersected, (13.4) gives the RGBA vector as

$$0.5 * (0.0, 0.0, 1.0, 0.5) + 0.5 * (1.0, 1.0, 1.0, 0.0) = (0.5, 0.5, 1.0, 0.25)$$

because the source fragment vector is $(0.0, 0.0, 1.0, 0.5)$ and the destination (background) vector is $(1.0, 1.0, 1.0, 0.0)$.

Where the blue and red rectangles intersect, the RGBA vector is

$$0.5 * (1.0, 0.0, 0.0, 0.5) + 0.5 * (0.5, 0.5, 1.0, 0.25) = (0.75, 0.25, 0.5, 0.375)$$

because the source fragment vector is $(1.0, 0.0, 0.0, 0.5)$ and the destination vector is $(0.5, 0.5, 1.0, 0.25)$ as calculated above.

Note: Even though the destination alpha changes after the first blend, this does not matter subsequently as the program's particular blend function glBlendFunc(GL_SRC_-ALPHA, GL_ONE MINUS SRC ALPHA) means the source alpha is used always to define both source and destination blending factors.

We leave it to the reader to calculate the RGBA vector for the non-intersected parts of the red rectangle.

For experimental verification, draw a point inside each region with its calculated RGB values – the points should be invisible!

Exercise 13.2. (Programming) Change the alpha values of both rectangles in blendRectangles1.cpp successively to 0.0, 0.25, 0.75 and 1.0. Verify the color values in each region both theoretically and experimentally, as in the preceding example, for the case when alpha is 0.75.

Before proceeding to the next exercise, keep in mind that world space z-values are flipped in sign and scaled to the range 0 to 1 in OpenGL's depth buffer (we first saw this way back in Remark 2.13). Therefore, a larger z in world space – closer then to the front face of the viewing volume – transforms to a smaller z in the depth buffer, so winning the depth competition there.

Exercise 13.3. (Programming) Although there is a depth buffer in blendRectangles1.cpp, depth testing has been disabled. Enable it by replacing the call glDisable(GL_DEPTH_TEST) in setup() with glEnable(GL_DEPTH_TEST). Explain what you observe, first with blending disabled (replace glEnable(GL_BLEND) in setup() with glDisable(GL_BLEND)) and then enabled.
Hint : The world z of the red rectangle is 0.5, while that of the blue rectangle is 0.1, which means that the former wins the z-competition in their intersection. Therefore, here is the situation with *no* blending: if the blue rectangle is first in code, then the red rectangle values following will overwrite the blue's in their intersection; on the other hand, if the red rectangle is first in code, then the blue rectangle values are discarded. Now, refer to the theoretical discussion earlier to see what changes, given blending is *enabled*.

13.1.3 Opaque and Translucent Objects Together

Experiment 13.2. Run blendRectangles2.cpp, which draws three rectangles at different distances from the eye with depth testing enabled. The closest rectangle at $z = 0.5$ is vertical and a translucent red ($a = 0.5$), the next one at $z = 0.3$ is angled and opaque green ($a = 1$), while the farthest at $z = 0.1$ is horizontal and a translucent blue ($a = 0.5$). See Figure 13.3(a).

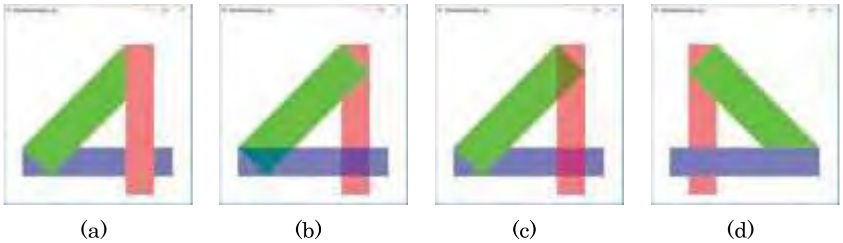

Figure 13.3: Screenshots of blendRectangles2.cpp: (a) Initial (b) With depth testing disabled (c) With depth testing re-enabled and rectangles re-ordered to blue, green, red in the code (d) New ordering seen from the $-z$-direction.

The scene is clearly not authentic as no translucency is evident in either of the two areas where the green and blue rectangles are behind the red. The fault is not OpenGL's as it is rendering as it's supposed to with depth testing, as we see next.
End

Example 13.3. Verify the claim just made that the program is doing as it's supposed to.

Answer: The program's drawing order is:

```
drawRedRectangle(); // Red rectangle closest to viewer, translucent.
drawGreenRectangle(); // Green rectangle second closest, opaque.
drawBlueRectangle(); // Blue rectangle farthest, translucent.
```

Once the red rectangle, the closest, is drawn, the green and blue both fail the depth test where they intersect the red, so there's no translucency apparent in those two regions (keep in mind that only if the source fragment passes the depth test does blending kick in).

Returning to the experiment, disabling depth testing doesn't help either, as the green blocks out the red (which it shouldn't as it's farther away), while it doesn't block out the blue (which it should as it's closer). See Figure 13.3(b).

Restoring depth testing and trying all 6 (=3!) possible orders to draw the rectangles, it's seen that the only one producing an authentic rendering is:

```
drawBlueRectangle(); // Blue rectangle farthest, translucent.
drawGreenRectangle(); // Green rectangle second closest, opaque.
drawRedRectangle(); // Red rectangle closest to viewer, translucent.
```

See Figure 13.3(c). As one would expect, both green and blue rectangles can be seen through the red, while the green blocks out the blue. The order that the primitives are drawn in code happens to be according to their distance from the viewer, starting with the farthest; moreover, with this order it doesn't matter if depth testing is on or off.

Exercise 13.4. Explain why the (farthest-to-nearest) blue-green-red drawing order is successful, regardless of whether depth testing is enabled or not.

Unfortunately, this method is not a particularly robust way to produce an authentic scene, as the farthest-to-nearest order depends on the viewpoint. For example, keeping the same blue-green-red drawing order, replace the viewing transformation

```
gluLookAt(0.0, 0.0, 0.0, 0.0, 0.0, -1.0, 0.0, 1.0, 0.0);
```

with

```
gluLookAt(0.0, 0.0, 0.0, 0.0, 0.0, 1.0, 0.0, 1.0, 0.0);
```

to view the rectangles from the $-z$-direction, which means now the blue is closest, the green next and the red farthest away. Oops! See Figure 13.3(d). The result is no longer authentic as the closest translucent blue rectangle blocks out both red and green, which, of course, it shouldn't. The reason for the breakdown is clearly that what used to be farthest-to-nearest rendering is now no longer.

Note: Interestingly, the original gluLookAt(. . . , -1.0, . . .) actually "does nothing" in that its simulating modeling transformation (recall Section 4.6.2) is just the identity, because the camera is in its default posture; however, gluLookAt(. . . , 1.0, . . .) causes the rectangles to be rotated 180° about the y-axis, so that subsequent projection to the viewing face effectively shows them from the back.

So, what is one to do to resolve the problem? Precisely, the following:

1. Enable depth testing.

2. Draw first the opaque objects. Because of depth testing they block one another out according to distance from viewpoint, as one would want.

3. Make the depth buffer read-only with a call to glDepthMask(GL_FALSE).

4. Draw next the translucent objects. As depth testing is still on, translucent objects farther than the nearest opaque one – which per-pixel has written the z-buffer – are discarded, again as one wants.

   However , as they can no longer update the z-buffer to their own z-values, closer translucent objects don't block out farther ones – which is what would happen if their z-values were recorded – but blend instead. In fact, all translucent objects, which are closer than the closest opaque one, blend successively into the latter. Exactly as the doctor ordered. See Figure 13.4 for what happens at a hypothetical pixel on the z-axis.

5. Restore the depth buffer's writability by calling glDepthMask(GL_TRUE).

   Note: The depth buffer is writable by default.

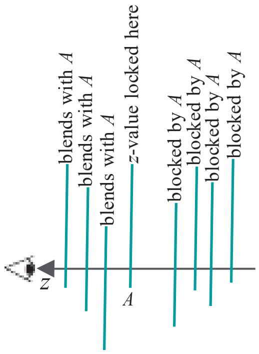

Figure 13.4: Opaque objects are hard lines, translucent objects are light ones. Consider the pixel on the z-axis: Closest opaque object is A. All objects behind A are blocked. Translucent objects in front of A blend into it.

Try it:

Experiment 13.3. Rearrange the rectangles and insert two glDepthMask() calls in the drawing routine of blendRectangles2.cpp as follows:

```
// Draw opaque objects, only one.
drawGreenRectangle();

glDepthMask(GL_FALSE); // Make depth buffer read-only.

// Draw translucent objects.
drawBlueRectangle();
drawRedRectangle();

glDepthMask(GL TRUE); // Make depth buffer writable.
```

Try both gluLookAt(. . ., 0.0, 0.0, -1.0, . . .) and gluLookAt(. . ., 0.0, 0.0, 1.0, . . .) to see the rectangles from the front and back. Interchange the drawing order of the two translucent rectangles as well. The scene is authentic in every instance.
End

Experiment 13.4. Run sphereInGlassBox.cpp, which makes the sides of the box of sphereInBox2.cpp glass-like by rendering them translucently. Only the unaveraged normals option of sphereInBox2.cpp is implemented. Press the up and down arrow keys to open or close the box and 'x/X', 'y/Y' and 'z/Z' to turn it.

The opaque sphere is drawn first and then the translucent box sides, after making the depth buffer read-only. A screenshot is Figure 13.5(a).
End

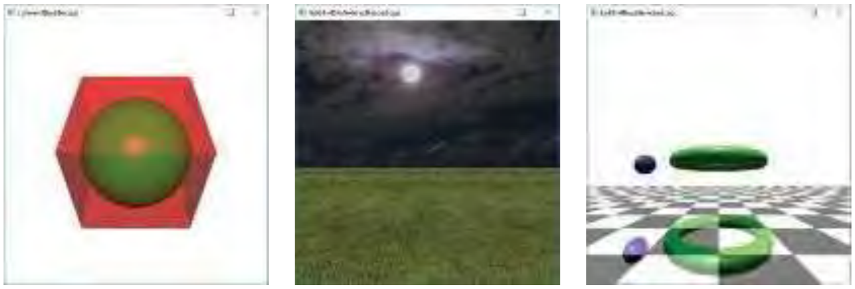

(a) (b) (c)

Figure 13.5: Screenshots of blended effects: (a) sphereInGlassBox.cpp (b) fieldAndSkyTexturesBlended.cpp (c) ballAndTorusReflected.cpp.

Exercise 13.5. (Programming) Inscribe a glass dodecahedron inside a glass icosahedron.

Exercise 13.6. (Programming) Make a solid ball travel through a glass helical pipe (see Experiment 10.3 for the helical pipe).

Exercise 13.7. (Programming) Make the ball of ballAndTorusLitOrthoShadowed.cpp of Chapter 11 to be of glass.

13.1.4 Blending Textures

There's no reason why textures cannot be blended – it's simply a matter of either one or both of the source fragment and destination pixels obtaining color values from a texture map. Here's a fun program doing just that.

Experiment 13.5. Run fieldAndSkyTexturesBlended.cpp, which is based on fieldAndSkyLit.cpp of the preceding chapter. Press the arrow keys to move the sun (actually, the direction of the light).

As the sun rises the night sky morphs into a day sky. Figure 13.5(b) shows late evening. Yes, we saw this very same morph in multitexture.cpp as an application of multitexturing, using the interpolation combiner, in Section 12.8. End

The program fieldAndSkyTexturesBlended.cpp is a straightforward application of alpha blending. We point out a few interesting features though:

(a) The sky rectangle is no longer lit as in fieldAndSkyLit.cpp because the night texture itself causes the sky to darken.

(b) Source blending factors all 1 (GL_ONE) and destination blending factors all 0 (GL_ZERO) enable the grass and night sky textures to initially paint their respective rectangles without dilution.

(c) The statements

```
if (theta <= 90.0) alpha = theta/90.0;
else alpha = (180.0 - theta)/90.0;
glColor4f(1.0, 1.0, 1.0, alpha);
```

in the drawing routine link alpha to the angle theta of the sun in the sky, so that the former increases from 0 to 1 as the sun rises from the horizon to vertically above.

(d) The day sky is blended into the night sky because both textures paint the same rectangle and because the prior disabling of depth testing allows an incoming fragment to write a destination pixel even if the former's z-value is equal the latter's (with depth testing on it has to be less in order to do so). The call glBlendFunc(GL SRC ALPHA, GL ONE MINUS SRC ALPHA) in the drawing routine sets the source (day sky) blending factor equal to alpha and the destination (night sky) blending factor to 1 - alpha.

Remark 13.2. The simple-minded alpha-morph just described should work fairly well if the transition required is mainly in the colors of a scene and not the geometry, because it is a straight linear interpolation between corresponding source and destination color values. For the same reason, one should not expect much from it by way of morphing *shapes*, as in the Terminator movies.

Exercise 13.8. (Programming) Morph a day image of a static scene (e.g., city skyline, mountainous landscape, etc.) to a night image. Intermediate images may help smooth the morph.

13.1.5 Creating Reflections

Another neat application of blending is to simulate reflection.

Experiment 13.6. Run ballAndTorusReflected.cpp, which builds on ballAndTorusLitOrthoShadowed.cpp. Press space to start the ball traveling around the torus and the up and down arrow keys to change its speed.

The reflected ball and torus are obtained by drawing them scaled by a factor of -1 in the y-direction, which creates their reflections in the xz-plane, and then blending the floor into the reflection. Figure 13.5(c) shows a screenshot. End

This method of manufacturing reflections with a scaling command is reminiscent of how shadows were drawn in ballAndTorusLitOrthoShadowed.cpp, and equally limited. E.g., it can never simulate the reflection of the ball in the torus. To exactly simulate such secondary lighting effects as reflections and shadows one must invoke a lighting model such as ray tracing, which is more sophisticated than OpenGL's and, currently, far too computation-intensive to run in real-time. The strength of OpenGL, of course, is that it offers interactive 3D graphics in real-time; moreover, despite a somewhat constrained lighting model, OpenGL often allows with a bit of effort for many effects, including reflection and shadows, to be fairly convincingly represented.

Exercise 13.9. (Programming) Draw the reflection of the ship of shipMovie.cpp in the sea.

Exercise 13.10. (Programming) Make the character of animateMan1.cpp walk along a shiny floor.

13.1.6 Motion Blur in World Space

The blurring of a moving object to give the impression of high speed can be simulated by blending in additional copies of the object just behind it.

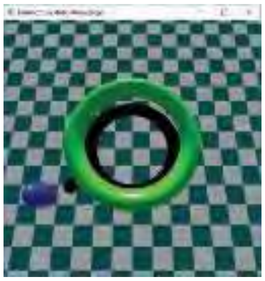

Figure 13.6: Screenshot of ballAndTorusMotionBlurred.cpp.cpp.

Experiment 13.7. Run ballAndTorusMotionBlurred.cpp, which enhances the ball of ballAndTorusLitOrthoShadowed.cpp with motion blur. Press space to start the ball traveling around the torus and the up and down arrow keys to change its speed. See Figure 13.6 for a screenshot.

Examine the drawing routine to see that the blur, in fact, is simulated by blending four additional copies of the ball behind it with alpha values decreasing with distance from the actual ball. End

Exercise 13.11. (Programming) Motion blur the plant of floweringPlant.cpp of Chapter 4 as it blooms – of course, you'll want to speed up the process!

Our method of motion blur by creating additional copies of the object in world space is not particularly efficient – each copy costs as it goes down the rendering pipeline. We'll see more efficient blurring, happening all in screen space, no redundant objects traveling down the pipeline, with the use of shaders in Chapter 16.

13.2 Fog

Fog is an *atmospheric effect* that OpenGL offers ready to use. What fog does is blend objects with a programmer-specified fog color so that the farther away an object is from the viewer the more the fog color dominates, the effect being of objects fading into the distance.

We'll explain how fog is implemented in OpenGL using yet another version of ballAndTorus.cpp as a running example.

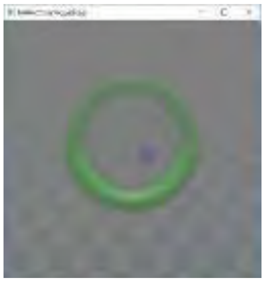

Figure 13.7: Screenshot of fieldAndSkyFogged.cpp with exponential fogging.

Experiment 13.8. Run ballAndTorusFogged.cpp, which enhances ballAndTorusLitOrthoShadowed.cpp from Chapter 11 with a gray fog. Figure 13.7 is a screenshot.

Press the delete key to toggle fog on and off, press space to toggle animation on and off, and the up/down arrows to change the ball's speed. End

The following block of fog-related calls are near the top of the initialization routine:

```
glFogfv(GL_FOG_COLOR, fogColor);
glFogi(GL_FOG_MODE, fogMode);
glFogf(GL_FOG_DENSITY, fogDensity);
glFogf(GL_FOG_START, fogStart);
glFogf(GL_FOG_END, fogEnd);
```

The *fog color* , the color blended with scene objects to create fog, is specified by the statement

glFogfv(GL FOG COLOR, *fogColor*)

where *fogColor* points to the fog color values (a medium gray in the program).

The user can set the *fog mode* to be one of three – GL LINEAR, GL EXP and GL EXP2 – by assigning that value to the parameter *fogMode* in

glFogi(GL FOG MODE, *fogMode*)

In the program the fog mode, in fact, is GL_EXP2. It is the fog mode which, together with a few associated parameters, determines the thickness of the fog. Here's how.

OpenGL invokes the fog mode and the z-distance of an incoming fragment from the eye to compute a number f, called the *fog factor*, which is used to blend the fragment with the fog color. The equation which determines the fog factor f depends on the fog mode as follows:

$$\begin{aligned} \text{GL\_LINEAR:} \quad f &= \frac{fogEnd - z}{fogEnd - fogStart} \\ \text{GL\_EXP:} \quad f &= e^{-(fogDensity * z)} \\ \text{GL\_EXP2:} \quad f &= e^{-(fogDensity * z)^2} \end{aligned} \tag{13.5}$$

The values of the parameters *fogDensity*, *fogStart* and *fogEnd* are user-specified as well by the statements:

glFogf(GL EOG DENSITY, *fogDensity*);
glFogf(GL EOG START, *fogStart*);
glFogf(GL FOG_END, *fogEnd*);

Their default values are 0.0, 1.0 and 1.0, respectively. In the program *fogDensity* is 0.05, while *fogStart* and *fogEnd* are, in fact, set to their defaults; note that because the fog mode is not GL LINEAR in the program currently, *fogStart* and *fogEnd* are not used.

One sees from Equations (13.5) that if fog mode is GL LINEAR, then *fogStart* and *fogEnd* give the two endpoints of a linear ramp along the z-axis along which the fog factor f decreases from 1 to 0; moreover, if fog mode is GL EXP or GL_EXP2 then *fogDensity* controls the (exponential or doubly exponential) rate of diminishment of f with increasing z – the greater *fogDensity* the more rapidly f diminishes. See Figure 13.8 for sketches of how f changes with z.

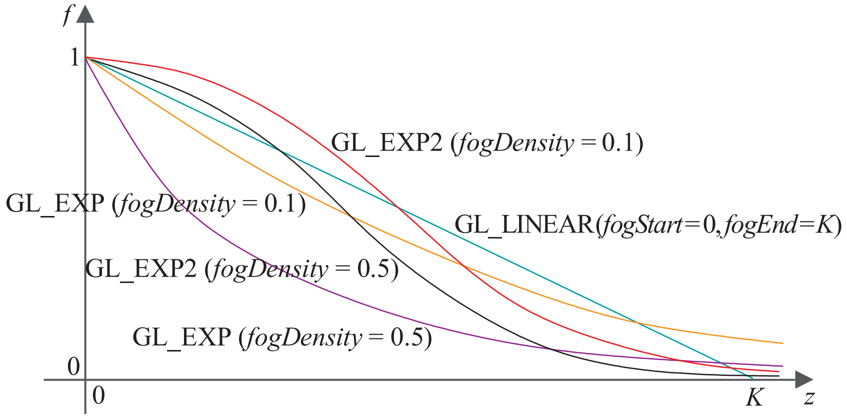

Figure 13.8: f versus z for various parameter values – the graphs are *not* mathematically exact. Values of *fogStart* and *fogEnd* are 0 and K, respectively.

After it's computed from (13.5), the incoming fragment's fog factor f is clamped in the range [0, 1]. OpenGL next blends the fog color tuple *fogColor* with the incoming fragment's color tuple C_{in}, using the equation

$$C_{dest} = (1 - f)\, fogColor + f\, C_{in}$$

to determine the color tuple C_{dest} of the destination pixel. The smaller the fog factor, therefore, the more the fog dominates and the fragment fades. One sees, as well, from the equations in (13.5) that fog modes GL LINEAR, GL_EXP and GL EXP2 in that order create increasingly thicker fog in general, though the constants in the equations have to be taken into account as well.

A final point of note is that fog is enabled or disabled with a call to glEnable(GL FOG) or glDisable(GL FOG), respectively, as can be seen in the drawing routine.

Exercise 13.12. (Programming) Experiment in ballAndTorusFogged.cpp with the other fog modes and their parameters by changing fogMode, fogDensity, fogStart and fogEnd.

Exercise 13.13. (Programming) Exercise 12.17 was about enhancing shipMovie.cpp. Fog can be used to good effect in the scene as well to depth cue the traveling torpedo and ship.

13.3 Billboarding

The technique of *billboarding* is to simulate a 3D object in a scene by placing an image of it as a texture on a rectangle, the *billboard* . The latter is then continuously rotated to keep it normal always to the direction of the viewer, giving the latter an illusion of the real object.

As long as the object is a peripheral one, e.g., trees, road sign or furniture in the background, the device of holding up an “impostor” 2D image is often authentic enough, thereby saving on the geometry required to make a real 3D version.

Experiment 13.9. Run billboard.cpp, where an image of two trees is textured onto an upright rectangle in a display list, and then the list called four times to arrange a staggered array of images from left to right. Press the space bar to turn billboarding on and off. See Figure 13.9 for screenshots.

As can be seen, billboarding causes a fairly convincing arc of trees to appear in the distance, while turning it off dispatches the illusion. End

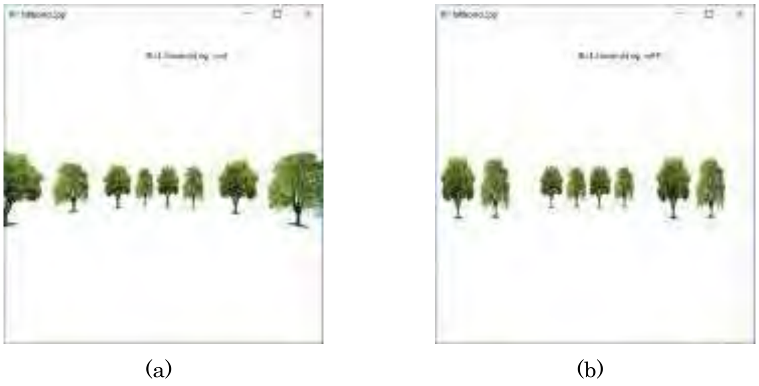
billboard.cpp
Billboarding on
billboard.cpp
Billboarding off

Figure 13.9: Screenshots of billboard.cpp: (a) Billboarding on (b) Billboarding off.

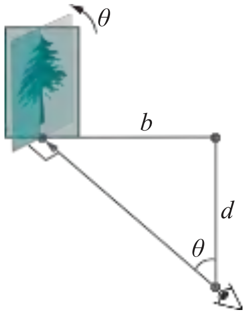

Figure 13.10: Billboarding: the original placement (bold border) of the billboard is rotated so its plane is normal to the direction of the viewer.

Each copy of the billboard rectangle of billboard.cpp is located in the scene by drawing it first on the xy-plane centered about the z-axis, and then translating it d units down the z-direction and b units left (Figure 13.10). Therefore, the angle θ that the billboard must be rotated about the vertical line through its center to keep it normal to the viewer's direction is given by

$$\theta = \tan^{-1}(b/d)$$

This particular rotation, in fact, is implemented if billboarding is on; otherwise, the billboard remains parallel to the xy-plane (the position indicated by the bordered rectangle in Figure 13.10).

Remark 13.3. One way to seamlessly fit a billboard into a scene is to paint its background texels a color matching the scene's backdrop (e.g., both are already white in the case of billboard.cpp). Another is to make the billboard's background texels transparent by setting their alpha values to 0 and then blend it onto the backdrop.

Exercise 13.14. (Programming) Hopefully, somewhere along the line you created a car. Make it now travel down a road against a billboarded backdrop of houses and trees.

13.4 Antialiasing Points and Lines, Multisampling Polygons

A straight line segment s specified, say, to be one pixel wide can be rasterized by selecting a set of fragments that best approximates it and setting each to the color specified for s, while unselected fragments remain of the background color. See Figure 13.11(a) for a particularly low-res example. Such discrete on/off rasterization protocols are computationally inexpensive, but tend to give poor visual quality at certain alignments of the segment owing to the jaggedness of the rasterization, the so-called *jaggies*.

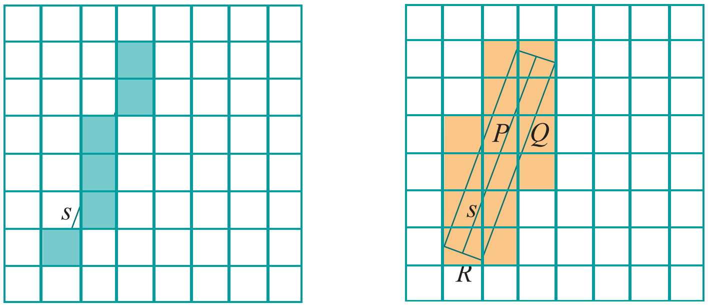

(a) (b)

Figure 13.11: (a) Dark fragments represent a rasterization of a line segment s, specified to be one pixel wide; jaggies are apparent (b) Shaded fragments are those intersected by the one-pixel wide rectangle R centered on s.

Jaggies are another example of *aliasing* , a visual artifact which arises because of the limited resolution of the display device (an earlier example of aliasing that we saw was that of texture shimmering in the previous chapter). Since a line segment not parallel to one of the axes can at best be approximated in a raster, one cannot hope to eliminate jaggies altogether. However, there are techniques to attenuate their visual impact, not surprisingly at the cost of extra computation.

13.4.1 Antialiasing

OpenGL, in particular, offers an *antialiasing* method for line segments based on blending with the help of so-called *coverage* values. Consider again the line segment s in Figure 13.11(a). A one-pixel wide rectangle R centered on s intersects the 14 fragments shaded in Figure 13.11(b). However, the area which R covers of each, called its *coverage* of that fragment, varies. For example, the coverage value of fragment P is more than twice that of Q.

When antialiasing is enabled, OpenGL draws the line by making an object consisting of the 14 intersected fragments, setting the color of all 14 to that of *s*, then multiplying the alpha value of each with its coverage and, finally, using the resulting weighted alpha to blend the fragment with the corresponding pixel already in the color buffer. The amount of the segment's color, therefore, blended into a destination pixel is proportional to the area of its source fragment covered by R. This has the effect of smoothing out the jaggies.

Points can be antialiased too. The mechanism is simpler – the point is rounded into a disc whose edge is smoothed by blending. The experiment next illustrates antialiasing of both a line and a point. In the process we'll learn an interesting fact about how points are rendered.

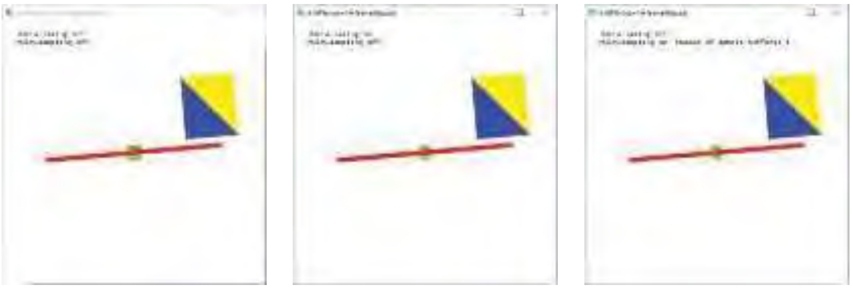

(a) (b) (c)

Figure 13.12: Screenshots of antiAliasing+Multisampling.cpp: (a) Antialiasing off, multisampling off (b) Antialiasing on, multisampling off (c) Antialiasing off, multisampling on.

Experiment 13.10. Run antiAliasing+Multisampling.cpp. Ignore the multisampling controls, as well as the blue-yellow rectangle, for now.

Focus on the red line segment and the green point, which are both either antialiased or not, 'a' or 'A' toggling between the two modes. The width of the line is changed by pressing 'l/L', while the size of the point with 'p/P'. The scene can be turned by the 'x'-'Z' keys and translated by pressing the arrow and page up/down keys.

Figures 13.12(a) and (b) show screenshots of antialiasing off and on, respectively. The effect of antialiasing is especially marked when the line is just shy of horizontal or vertical. End

Antialiasing is simple to implement in OpenGL. One has to enable blending, of course – done in drawScene() of antiAliasing+Multisampling.cpp when antialiasing is turned on. The blending factors GL SRC ALPHA and GL ONE MINUS SRC ALPHA defined in setup() are the usual choices. We apply the maximum alpha of 1.0 to both line and point. Line and point antialiasing are enabled, respectively, with glEnable(GL LINE SMOOTH) and glEnable(GL POINT SMOOTH); they are disabled, of course, by corresponding glDisable() calls.

Rendering points

Antialiasing rounds the green point, as we said earlier, but observe how its size and shape are never changed by translation or rotation. The reason is that a point is created zero-dimensional, so of zero size, in world space, then projected to the viewing face – equivalently, screen space – and *only there* given size as an $n \times n$ square of pixels (assuming the point is unaliased) centered at the projected point, where n, of course, may be specified by glPointSize(n).

Therefore, its position in world space, in particular, how near or far it is from the viewing face, has no bearing on a point's size or shape on the screen; and, of course, a point's "alignment" by rotation is a non-factor, too.

So, we see that, even though points are grouped with lines and triangles amongst OpenGL's fundamental drawing primitives, they are of a very different DNA, at least come the projection step of the rendering process.

Remark 13.4. There actually is a similar issue when rendering lines because a line in world space, being one-dimensional, has zero width. So, just like points, lines are imbued with a viewable size – width in the case of lines – only after arrival on screen by projection. This width, of course, can be set by the programmer with a call to glLineWidth().

So, one sees that, just as points "are made" on screen as squares of pixels, lines are made there, too, as (long thin) rectangles. This is the reason that rotating or translating a line never has visible effect on its width, which certainly would not be the case if the line were an actual rectangle in world space.

13.4.2 Multisampling

One can indeed call glEnable() with the parameter GL POLYGON SMOOTH to antialias polygons, particularly, their edges. However, the problem with this method is that, being based upon blending, polygons need to be properly sorted in the drawing routine as discussed in Section 13.1.3. OpenGL offers another antialiasing method, based on so-called *multisampling*, which not only avoids this constraint but is particularly effective at the border of a polygon or one between two.

In multisampling, color, depth and stencil values are computed at a sample of points in each fragment's area, stored in a dedicated sample buffer, to be subsequently *resolved* into one color to apply to that fragment. Figure 13.13 shows the idea using a simple 2 × 2 sampling scheme: the 12 shaded fragments generated by the triangle have their color, depth and stencil values sampled at four points each. So, one can think of multisampling as *virtually* increasing a screen's native resolution where an object is being drawn by, again, virtually splitting fragments into subfragments.

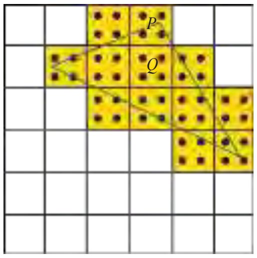

Figure 13.13: Multisampling using a 2×2 sampling scheme.

Though we'll not go into details of the process of resolving multiple sample values into one, it's seen even from Figure 13.13 how multisampling might be able to diminish jaggies. For example, fragment P would be a 50-50 mix of the triangle's color and the background color because two samples come from each, while Q would evidently be fully colored by the triangle. Let's observe multisampling in practice.

Experiment 13.11. Fire up again antiAliasing+Multisampling.cpp. Multisampling is toggled on/off, independently of antialiasing, by pressing 'm' or 'M'. Figures 13.12(c) is a screenshot with multisampling on.

Multisampling antialiases polygons particularly effectively and its effect in our program is best observed on the boundary of the blue-yellow rectangle, as well as the edge between its two colored triangular halves, particularly, when they are nearly horizontal or vertical. When multisampling is enabled, lines and points are antialiased regardless if GL POINT SMOOTH or GL LINE SMOOTH has been enabled, which you can see as well.

The number of sample buffers, shown at the top of program's window when multisampling is enabled, should be at least one, or there is effectively no multisampling and you may need to check the settings of your graphics card. End

Multisampling is simple to get going. First, one has to create an OpenGL window which supports multisampling: passing GLUT MULTISAMPLE as a parameter to glutInitDisplayMode() does the trick. Next, multisampling is enabled and disabled, respectively, with glEnable() and glDisable() given GL MULTISAMPLE as the parameter. That's it!

Keep in mind that multisampling comes at a high cost because of the additional processing per fragment. So, if you are particularly performance-conscious it might make sense to enable multisampling for polygons and disable it for lines and points, only antialiasing the latter two.

Exercise 13.15. The unaided human eye can resolve to a minimum size of approximately 0.1 mm. (about 0.004 inch). So, what resolution levels must a 24-inch desktop monitor reach in terms of number of pixels by number of pixels for aliasing problems and antialiasing algorithms to go the way of the VCR? What's your best guess as to how long it will take for technology to get there?

13.5 Point Sprites

From the last section we know that points are created dimensionless in world space, being given shape as a square of pixels only upon arrival by projection on screen space. Not particularly interesting is this? However, one can bring a point to life by turning it into a so-called *point sprite* (or, *sprite*, for short). A sprite is simply a point, usually of a relatively large size, with a texture mapped on to it.

Sprites are particularly useful in manufacturing *particle systems*, where a swarm of particles on the screen creates a certain visual effect, e.g., smoke, sparks, fireworks, and so on. Because they are always flat on the display, facing the viewer, sprites can be invoked as a sort of poor man's billboard as well. Sprites are easy to code. Let's have a look at the real thing.

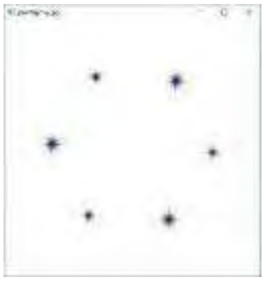

Figure 13.14: Screenshot of pointSprite.cpp.

Experiment 13.12. Fire up pointSprite.cpp. The space bar toggles animation on and off. The particle system of six sprites of fluctuating size, imprinted with the same star texture, spinning in a circle, is simple-minded, though, hopefully, suggestive of possibilities. Figure 13.14 is a screenshot. End

In addition to the usual commands to prepare a texturing environment, there are three new ones in the setup routine of pointSprite.cpp. The call

```
glTexEnvi(GL_POINT_SPRITE, GL_COORD_REPLACE, GL_TRUE)
```

enables texture interpolation across sprites, while the parameter GL_LOWER_LEFT in

```
glPointParameteri(GL_POINT_SPRITE_COORD_ORIGIN, GL_LOWER_LEFT)
```

causes the texture t-coordinate to increase from 0 to 1 from bottom to top of the sprite. The texture s-coordinate always increases 0 to 1 from left to right. Finally, as one would expect

```
glEnable(GL_POINT_SPRITE)
```

enables point sprites. With these three commands in place, all subsequent calls to glBegin(GL_POINTS)-glEnd() draw sprites painted with the currently bound texture.

If you were wondering how textures can be painted on round antialiased points, which happen to be sprites, the answer is that sprites *cannot* be antialiased.

Exercise 13.16. (Programming) The only other option for the second parameter of glPointParameteri(GL_POINT_SPRITE_COORD_ORIGIN, GL_LOWER_LEFT) is GL_UPPER_LEFT, causing the texture t-coordinate to increase from 0 to 1 from the top of the sprite to the bottom. The s-coordinate still increases from 0 to 1 from left to right.

Try GL_UPPER_LEFT instead of GL_LOWER_LEFT. It will be hard to spot the difference with the symmetric star texture, but using launch.bmp instead should make it clear.

Exercise 13.17. (Programming) Create the effect of sparks flying using a particle system of sprites.

13.6 Environment Mapping: Sphere Mapping and Cube Mapping

The purpose of *environment mapping* is to map the surroundings of a scene onto an object. For example, a shiny kettle with a painting of the kitchen mapped onto its surface would simulate reflection, as would a well-polished car painted over with a street scene. A somewhat different example would be trees painted onto strategically placed billboards to simulate the background of a playing field. Environment mapping is typically accomplished by capturing the environment in one or more texture images and then applying these suitably to scene objects.

In the next two sections we're going to study two popular environment mapping techniques, namely, *sphere mapping* and *cube mapping*, both of which OpenGL supports.

13.6.1 Sphere Mapping

The goal of sphere mapping is to simulate the reflection by an object of its environment, so it's a form of environment mapping often called *reflection mapping* . It's based on an approach invented by Blinn and Newell [18] which makes clever use of textures, but the basic idea is not hard. An image of the environment (presumed static) is captured in a texture or multiple textures, called the *environment map*. Subsequently, the particular texture and texture coordinates used to paint a vertex on the environment-mapped object are determined from the position of the viewer relative to the object.

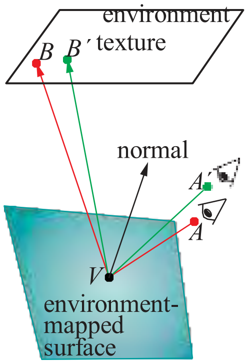

Figure 13.15: Blinn-Newell environment mapping principle: texture coordinates for a vertex V on an environment-mapped surface are obtained from the point on the texture image struck by the reflected ray originating from the eye.

Figure 13.15 illustrates the principle. The texture coordinates at the vertex V of an environment-mapped quad are determined by the point of the environment – more precisely, the corresponding point of the environment texture – seen by the viewer by reflection off the object. For example, when the viewer is at A, V is painted with the color values at B (red); when she moves to A^1, those of B^1 are used (green). The crux of the Blinn-Newell approach then is to *dynamically* compute texture coordinates, based on the laws of reflection, as the viewpoint changes.

Implementing sphere mapping using OpenGL is simple as the following program shows.

Experiment 13.13. Run sphereMapping.cpp, which shows the scene of a shuttle launch with a reflective rocket cone initially stationary in the sky above the rocket. Press the up and down arrow keys to move the cone. As the cone flies down, the reflection on its surface of the launch image changes. Figure 13.16 is a screenshot as it's about to crash to the ground. The environment texture applied obviously is launch.bmp. End

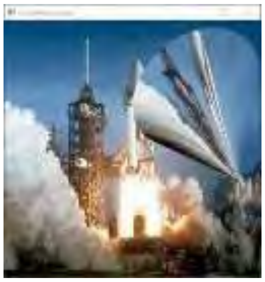

Figure 13.16: Screenshot of sphereMapping.cpp.

The two commands

```
glTexGeni(GL S, GL TEXTURE GEN MODE, GL SPHERE MAP);
glTexGeni(GL T, GL TEXTURE GEN MODE, GL SPHERE MAP);
```

in the initialization routine of sphereMapping.cpp ask OpenGL to use functions from its library to generate the s and t texture coordinates for sphere mapping.

The pair of commands

```
glEnable(GL TEXTURE_GEN S);
glEnable(GL TEXTURE_GEN T);
```

and its inverse

```
glDisable(GL TEXTURE_GEN S);
glDisable(GL TEXTURE_GEN T);
```

in the drawing routine, bracketing the drawing of the cone as a GLU quadric, enable and disable the use of these functions. That's pretty much all there is to implementing a sphere map. Note that at the time sphere mapping is activated the currently bound texture is the launch image, which, of course, is why it is the environment texture reflected in the cone.

Now, a reader watching the cone as it zooms down may ask how authentic actually is the reflection. Good question, and it leads us to how OpenGL computes sphere-mapped texture coordinates.

Imagine the environment around a vertex V of the reflective object arranged on a sphere S – from which concept the name sphere mapping is derived– centered at V; further, imagine a small mirror lying flat along the equatorial plane at V (Figure 13.17, where the reddish disc is the mirror). The eye looking at V, then, would see actually the point P where S is intersected by the reflection from V of the line of sight. However, OpenGL's only knowledge of the environment is from the user-provided environment texture occupying a unit square in texture space. So what it does is this: if the eye wants, by reflection, to see the point P in the spherical environment, OpenGL samples instead the point (s, t) in texture space which happens to be the image of P by OpenGL's sphere-mapping texture map.

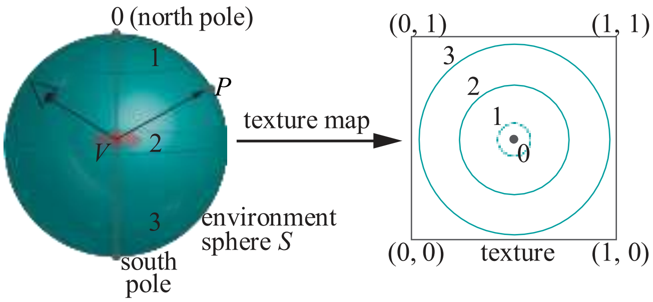

Figure 13.17: The sphere map texture map.

What, then, is this texture map? Well, first of all, it is very different from the Mercator projection of Section 12.5. In fact, see again Figure 13.17: the sphere-mapping texture map takes the north pole to the middle of the texture and latitudes south of it to increasingly larger circles centered at its middle, e.g., latitudes numbered 1, 2 and 3 map to the same-numbered circles in the texture (obviously, there is a singularity at the south pole). So, if the eye asks, by reflection, to see the north pole of the environment, then it's shown instead the middle of the texture. And, as the eye travels to see points farther and farther south, it's shown points farther and farther from the center of the texture. We do not go into futher detail here.*

Given this sphere-mapped scheme to present the environment to the viewer via a texture, what is the right way to prepare the texture? Practically speaking, how then should one photograph the environment in order to create the texture image? From the way the texture map is defined, a wide-angle snap taken from a camera situated near the object to be environment mapped and pointing up the z-axis of world space should be good.

To answer the question from a few paragraphs back, the reflection on the cone would have appeared more authentic if we had been able to use an image of the NASA site behind the photographer of the shuttle launch – now the cone somewhat implausibly reflects objects behind it off its front.

Exercise 13.18. (Programming) Sphere map the torpedo in shipMovie.cpp.

13.6.2 Cube Mapping

In cube mapping the environment is projected onto the faces of an equal-sided cube, or *skybox* as it's often called, the user having provided an image of each of the six faces – these six (necessarily square) images together form a *cube map*. Figure 13.18 shows cube map images captured at a location in the north of Sweden.

*Earlier editions of this book had a complete and rather mathematical account of sphere-mapped texture coordinates generation. However, we feel now that such a detailed exposition is not in keeping with the practical spirit of this chapter and, therefore, drop it. Nevertheless, we have put that matter at the Downloads page of the book's website for the interested reader.

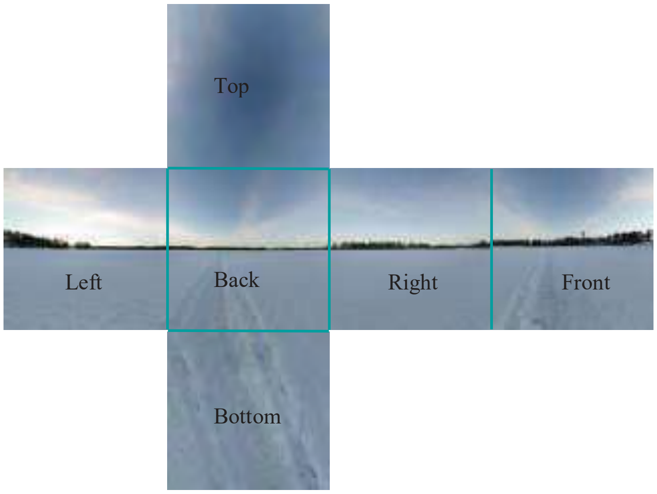

Figure 13.18: Cube map: images are rotated around the green edges to make a skybox. (Thanks Emil Persson, aka Humus, for a Creative Commons license.)

Imagine this page upright facing you; next, imagine rotating each of the top, left, bottom and right images of Figure 13.18 an angle of 90° toward you around the (green) edge between it and the back image, which stays fixed; finally, imagine the front image rotated about the edge between it and the right one to close off a skybox. If this box were big enough, then a viewer inside, near the middle, would think herself to be on a rather forbidding terrain. We see then that a skybox enclosing a scene can give it a backdrop in every direction. A reader at this time being reminded of billboards and thinking of a skybox as a family of billboards in space would not be far off.

Skyboxes are frequently implemented in games where a distant background stays static through the action occurring in the foreground. Let's see how to make a skybox from a cube map with a fair bit of help from OpenGL.

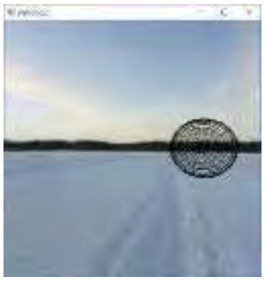

Figure 13.19: Screenshot of skybox.cpp.

Experiment 13.14. Run skybox.cpp, which creates a skybox using precisely the cube map of Figure 13.18. A wire ball, the only "real" object in the scene, has been placed inside the box.

The viewer is initially halfway between the middle of the box and the back, looking toward the latter. The up/down arrow keys translate the viewpoint, while the left/right and page up/down keys rotate it. Figure 13.19 is a screenshot.

Note that translations are constrained to keep the viewer far enough always from the background to preserve the illusion that it's real. End

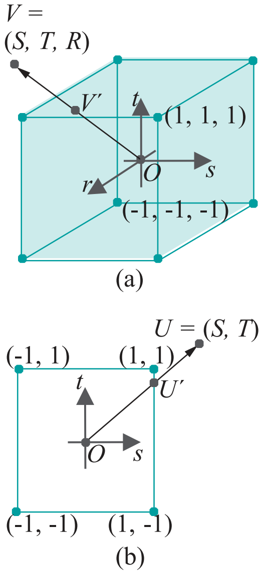

Figure 13.20: (a) A skybox intersected by a line toward V (only two corners of the skybox are labeled) (b) 2D "skysquare" intersected by a line toward U.

Before getting into the weeds of skybox.cpp, let's understand first the 3D texture coordinates the program uses to sample cube map textures with glTexCoord3f() calls. What we are familiar with to date are 2D texture coordinates specified with glTexCoord2f() calls at the vertices of, say, a triangle, which map the vertices to points in texture space. This map is then interpolated over the whole triangle to give the texture map, which in turn is used to sample the texture in order to color the triangle.

3D texture coordinates in the context of cube maps are very different. Think of a set of 3D texture coordinates, say (S, T, R), as defining a *direction* from the center O of a canonical skybox of side lengths 2 with vertex coordinates all ±1, made from the given cube map. In particular, it is the direction toward the point $V = (S, T, R)$, or, imagining V to be a vector, it is the direction along V. See Figure 13.20(a), where the axes of 3D texture space are s, t and r (only two diagonally opposite vertices are labeled to avoid clutter).

The line in the direction of V, assuming V is not null, intersects the skybox at a point V^{1}, lying obviously on one of the six faces, e.g., in Figure 13.20(a), V^{1} is at the top. So, by means of this point V^{1}, V determines a face of the box, *as well as* a point of it, in other words, a point on one of the six cube map textures. Effectively, then, we are back to the familiar situation of 2D texture coordinates specifying a point of a texture. (Of course, when V^1 is on an edge or at a corner of the skybox, there is ambiguity in the choice of the face to which it belongs, which one can resolve arbitrarily as this will affect only a relatively few pixels.)

Note: Observe a similarity with sphere mapping here in that we are using the Blinn-Newell idea to determine texture coordinates from the point where a particular ray intersects the texture.

So, given V how does one calculate V^1? It is easier to gain first an insight from the 2D version of the problem, a "skysquare" as drawn in Figure 13.20(b). For example, it's not hard to see that the line toward $U = (S, T)$ intersects the right side of the square if S is positive *and* the gradient T/S lies between -1 and 1, or, equivalently, if S is positive and $|T| \le |S|$; moreover, in this case the point of intersection $U^1 = (1, T/|S|)$. Similarly, the line toward (S, T) intersects the left side of the square if S is negative and $|T| \le |S|$, the point of intersection being $(-1, T/|S|)$. We'll leave the reader to fill in the rest in the following two exercises.

Exercise 13.19. In Figure 13.20(b), what are the respective conditions on (S, T) for the line toward it to intersect the top or bottom of the square. In either case, what are the coordinates of the point of intersection?

Exercise 13.20. Returning now to the original 3D box depicted in Figure 13.20(a), say how to determine the face intersected by the line toward (S, T, R), as well as the coordinates of the point of intersection.

Part answer : If the largest of $|S|$, $|T|$ and $|R|$ is $|S|$, and S is positive, then the line toward (S, T, R) intersects the right face at coordinates $(1, T/|S|, R/|S|)$.

Referring again to Figure 13.20(a), there's one easy last step from the coordinates of the point of intersection V^1 to texture coordinates on the face to which V^1 belongs, this being a transformation from the range $[-1, 1]$ of s, t and r along the surface of the canonical skybox to the range $[0, 1]$ of 2D texture coordinates. In fact, the affine transformation $x \mapsto (x + 1)/2$ does the trick. Let's give it all a whirl.

Example 13.4. Which texture of a cube map and what coordinates of that texture will be sampled at the centroid of the triangle in world space given the 3D texture coordinates $(-2, 2, -5)$, $(-1, 4, -3)$ and $(0, 0, -1)$, respectively, at its vertices?

Answer : By linear interpolation, the texture map has the value $((-2-1+0)/3, (2+4+0)/3, (-5-3-1)/3) = (-1, 2, -3)$ at the triangle's centroid. Now, the magnitude of the r-value of $(-1, 2, -3)$ is highest and it is negative. Therefore, the face $r = -1$, the back of the skybox, is sampled at coordinates $(-1/|-3|, 2/|-3|, -1) = (-1/3, 2/3, -1)$, meaning that the back face image is sampled at texture coordinates $((-1/3+1)/2, (2/3+1)/2) = (1/3, 5/6)$.

There's a quirk, though, to applying cube maps in OpenGL. Let's see this in the code of skybox itself. In particular, consider the block

```
glBegin(GL_POLYGON);
   glTexCoord3f(-1.0, 1.0, 1.0); glVertex3f(-50.0, -50.0, -25.0);
   glTexCoord3f(1.0, 1.0, 1.0); glVertex3f(50.0, -50.0, -25.0);
   glTexCoord3f(1.0, -1.0, 1.0); glVertex3f(50.0, 50.0, -25.0);
   glTexCoord3f(-1.0, -1.0, 1.0); glVertex3f(-50.0, 50.0, -25.0);
glEnd();
```

in the drawing routine specifying the one textured square of the code. Initially, as the reader can check from the zero values of the global transformation parameters, no modelview transformation is applied, so we should be looking (through the default OpenGL camera) down the frustum in the $-z$-direction at the *back face* of the skybox.

Noting that the square above lies on $z = -25$, it then is the back face. However, the $r = 1$ of the glTexCoord3f() coordinates indicates the square to be textured with the *front face* of the cube map.

Here is what's happening. Apparently, due to adaptation of certain specs from Pixar's RenderMan, the OpenGL skybox lives in a left-handed coordinate system. Ouch, but it's not too hard to reconcile with the right-handed OpenGL we know and love.

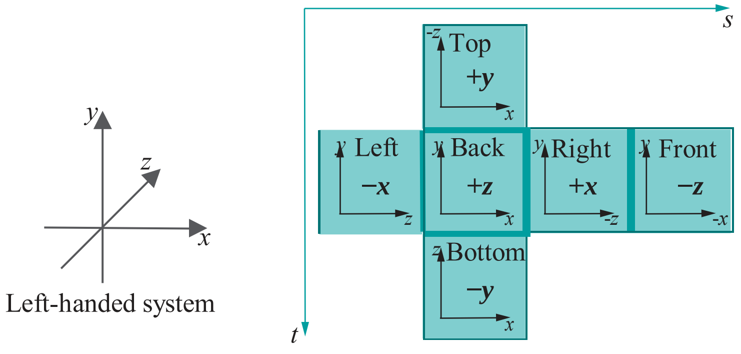

Figure 13.21: Texture coordinates on a cube map (modified from MSDN docs).

See Figure 13.21. It shows a generic skybox opened up – rotations are along the thick green edges – into a shape comprising six squares, just like the example we saw earlier in Figure 13.18. Let's understand the labeling of the six squares first.

E.g., consider the middle square with all thick green edges. It's the back face, so the $+z$-face if you reference the left-handed system drawn on the left, explaining the bold $+z$ label. Moreover, the left-to-right and bottom-to-top axes drawn on the square follow the x and y directions of the left-handed axes, explaining their x and y labels, respectively.

Next, consider the rightmost square and keep in mind again the left-handed system on the left. Being the front face, the rightmost square becomes the $-z$-face; moreover, after the square is rotated to take its position at the front of the box, the left-to-right axis on it reverses to point in the $-x$-direction of the left-handed system, while the bottom-to-top one stays pointing up the y-axis. This explains all the labels on this square. The reader can check that labels on the other four squares follow the same scheme.

Finally, texture s and t coordinates are oriented over the whole skybox by the two long green axes in Figure 13.21. Particularly, they define the way texture coordinates run in each of the six squares.

We are now in a position to understand the particular texture coordinates of skybox.cpp's square in the statement block above. We know this square should be imprinted with the back face of the skybox so imagine it, in fact, to be the back square in Figure 13.21: that this is the $+z$-face means r texture values all are 1; further, noting the orientation of the long green axes of Figure 13.21, one sees that s-values should increase with x, while t-values decrease with y. From the easy-to-read listing in Figure 13.22 of the vertex and texture coordinates of this square one finds that, indeed, s-values increase from -1 to 1 from left to right, while t-values decrease from 1 to -1 from bottom to top.

Run the program again: the opening view is indeed of posz.bmp, which, as we'll see momentarily, is stored as the $+z$ cube map texture in the program. Note that we don't see all of posz.bmp, as the reader will find if she opens posz.bmp in Textures/IceRiver. This is because the dimensions of the viewing frustum have been set so that it intersects the 100×100 textured square in a smaller 50×50 subsquare, as depicted in Figure 13.23, for the purpose of seamless viewing as the eye rotates.

Let's get to the rest of the code in skybox.cpp. In loadTextures()

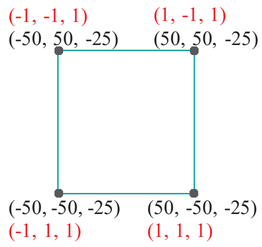

Figure 13.22: Initial textured square of skybox.cpp: vertex coordinates are black, texture coordinates red.

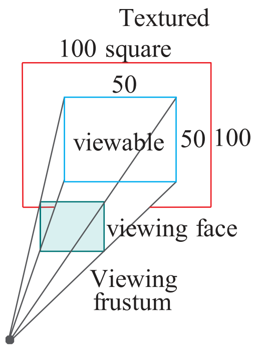

Figure 13.23: Viewing frustum sees only the blue-bordered part of the large red-bordered textured square.

```
glBindTexture(GL TEXTURE_CUBE MAP, textureCube);
for (int face = 0; face < 6; face++)
{
    int target = GL TEXTURE CUBE_MAP POSITIVE X + face;
    glTexImage2D(target, ...);
}
...
```

binds a cube map, the for-loop defining its components textures by taking advantage of the fact that GL TEXTURE CUBE_MAP POSITIVE X, GL... NEGATIVE_X, GL... POSITIVE Y, GL... NEGATIVE Y, GL... POSITIVE Z and GL... NEGATIVE Z are six successive system-defined integer values.

Moreover, we see here the final side effect of the texturing scheme of Figure 13.21: we had to switch the top and bottom textures, in particular, posy.bmp is the ground, while negy.bmp the sky. The reason for this reversal is that the texture *t*-value is 0 at the top of the skybox and 1 at the bottom.

Before moving on, let's recap the adjustments to be made setting up OpenGL cube maps:

1. Swap the top and bottom textures, in particular, glTexImage2D(GL TEXTURE_CUBE MAP POSITIVE Y, ...) and glTexImage2D(GL TEXTURE CUBE MAP_NEGATIVE_Y, ...) should specify the bottom and top images, respectively, of the skybox. This is the only physical change the programmer has to make.

2. Keep in mind when viewing the scene that the back of the skybox has the texture defined by glTexImage2D(GL_TEXTURE_ CUBE MAP POSITIVE Z, ...), while the front that defined by glTexImage2D(GL TEXTURE CUBE MAP NEGATIVE Z, ...).

That's it. Continuing with code, as expected, the setup routine enables cube mapping with glEnable(GL TEXTURE_CUBE MAP). On to the drawing routine next, where we see something interesting. Though the scene comprises images on all six sides of a sky box, as we can travel over rotating the viewpoint, there is no box drawn, but only one textured square.

To understand why, consider the skybox in Figure 13.24. When we look down the *z*-axis at the back of the box we see the textured square (a) with the sun. Rotating the camera left 90°, we see the textured square (b) with a tree, which we can imagine to be the same square as in (a), but differently textured. It seems, then, that we can always see correctly, even as the camera rotates, *provided* we pick up the texture coordinates specifying the region of the skybox we're *supposed* to see and apply them to a single stationary square. One can think of this square as a blank page on which is drawn whatever its texture coordinates, which keep changing, cause to be drawn. This is almost exactly the idea implemented in skybox.cpp's drawScene() as we see next.

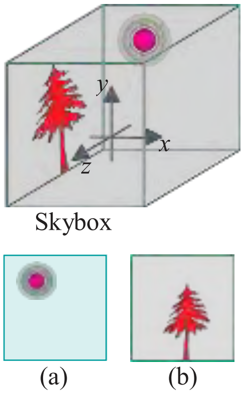

Skybox

(a) (b)

Figure 13.24: (a) Square textured with the back face of the skybox (b) Same square textured with the left face.

The viewing transfomation is defined as a composition

```
glRotatef(longAngle, 0.0, 1.0, 0.0);
glRotatef(latAngle, 1.0, 0.0, 0.0);
glTranslatef(0.0, 0.0, zVal);
```

at the top of drawScene(), which allows the eye to look in any direction and move forward and backward along that direction. Subsequently, with

```
glMatrixMode(GL_TEXTURE);
glLoadIdentity();
glRotatef(longAngle, 0.0, 1.0, 0.0);
glRotatef(latAngle, 1.0, 0.0, 0.0);
```

we enter texture matrix mode and apply the rotational component of the viewing transformation to the texture matrix, so that texture coordinates track that rotation. Next,

```
glMatrixMode(GL_MODELVIEW);
glPushMatrix();
glRotatef(-latAngle, 1.0, 0.0, 0.0);
glRotatef(-longAngle, 0.0, 1.0, 0.0);
glBindTexture(GL_TEXTURE_CUBE_MAP, textureCube);
glBegin(GL_POLYGON);
   glTexCoord3f(-1.0, 1.0, 1.0); glVertex3f(-50.0, -50.0, -25.0);
   ---
glEnd();
glPopMatrix();
```

re-enters modelview matrix mode, cancels out the rotational component of the earlier viewing transformation and draws the textured square. We keep the translational component as we do want foreshortening when moving the viewpoint away.

There are a couple more points of note. Firstly, we disable the depth buffer before drawing the textured square and enable it again after. The reason is that the square, supposedly in the background, should not z-compete with "real" foreground objects, so we don't allow it to update depth values, keeping these at $+\infty$. Secondly, the eye (this being world (0, 0, 0)) is not at the center of the skybox, which would have required it to be 50 units from the textured square, not the 25 it is now as can be seen from the z-coordinate values of -25 of the textured square; however, the current choice seems to give the better viewing experience.

Exercise 13.21. (Programming) The reader will find free-to-use cube map collections on the web (ours called IceRiver is from www.humus.name). Download a few and try them in skybox.cpp. Add animated activity in the foreground.

Exercise 13.22. (Programming) Environment map the hovering sphere of skybox.cpp using the very same cube map used to make the skybox, so that the sphere reflects its surroundings, via the following steps:

(1) Replace the GLUT sphere of skybox.cpp with the mesh sphere of texturedSphere.cpp of the previous chapter, so that we can access the vertices ourselves.

(2) Refer to Equation (11.10) of Chapter 11 for the formula for the direction of a reflected ray. Use this formula to calculate the direction that the eye of skybox.cpp will see by reflection off the sphere.

(3) Use the reflected direction calculated in the preceding step to apply 3D texture coordinates at vertices of the sphere.

13.7 Stencil Buffer Techniques

A space in memory reserved for pixel-related data is called a *buffer* . A computer system can have multiple buffers of different sizes for various purposes, though a given buffer will have an equal amount of space - in particular, the same number of bits - assigned to each pixel. We'll briefly introduce all the system buffers OpenGL supports and their uses before focusing in particular on the stencil buffer.

13.7.1 OpenGL Buffers

A modern OpenGL system supports three kinds of buffers: color, depth and stencil. Older systems had additionally accumulation buffers, but their purpose has been superseded by FBOs.

We already know well the *color buffer*, which stores primary RGB color values, as well as the alpha A value, typically to a precision of 8 bits each, for a total of 32 bits per pixel. Color buffers are the only ones of the buffers the user can directly draw into, and it is the final RGB values in some particular color buffer which are *flushed* to the screen for viewing.

In fact, there may be multiple color buffers. A double-buffered system has at least two – front (viewable) and back (drawable) – critical to smooth animation, as we learned in Section 4.5.1. If stereoscopic viewing is supported, there will be left and right color buffers, possibly even front-left, back-left, front-right and back-right, if combined with double buffering. The left buffers are shown to the left eye and the right ones to the right eye, typically with the user wearing special glasses. If the images in the left and right buffers are of the same scene captured by two cameras slightly offset one from the other, as are human eyes, a perception of 3D is created. Additionally, a system may have so-called auxiliary color buffers to store intermediate steps of a complicated rendering process.

Remark 13.5. Going, then, from monoscopic to stereoscopic viewing of an OpenGL scene, game or movie is a matter merely of plugging in a second camera, quite simple from a programming aspect.

We are also familiar with the *depth buffer* (or *z-buffer* as it's popularly called) which stores depth information, usually a 24-bit integer, per pixel. When depth testing is enabled, the depth buffer helps sort out objects according to their depth from the viewer along lines of sight, permitting nearer objects to obscure further ones in the rendering phase.

Less familiar to the reader might be the *stencil buffer* . This is a buffer used to tag pixels in the color buffer. The stencil buffer most often contains 8 bits, called tags, per pixel – effectively, then, a stencil buffer has a counter per pixel. The typical way to use the stencil buffer is to set the tags in a first phase when nothing is drawn to the screen and then employ these tags as controls in a second phase when actual drawing takes place. The tag values make possible various creative applications. We'll be studying the stencil buffer in fair detail shortly.

The collection of buffers in an OpenGL system, which is initialized simultaneously with the OpenGL context, is called its *default framebuffer* , or, simply, framebuffer. The reason for the default qualifier is that, as we saw in Section 12.9, the user can create so-called framebuffer objects (FBOs) in GPU memory, which act like framebuffers with color, depth and stencil components, but are not part of the windowing system and do not display.

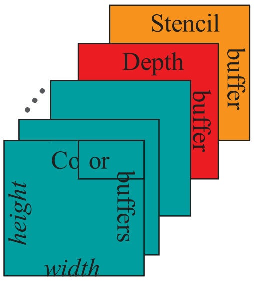

Figure 13.25:
Framebuffer.

Figure 13.25 shows a framebuffer containing the three kinds of buffers supported by OpenGL. The *width* ×*height* size, in terms of pixels, of all its constituent buffers must be equal and the same as that of the display device. This size is called the *resolution* of the frame buffer. The number of bits per pixel in a buffer determines the buffer's *precision*. E.g., a color buffer with 8 bits for each of RGB and A has a precision of 32 bits. Bits in the buffer in some particular bit position, between 0 to *precision*−1, form an array called a *bitplane*. So, of course, a buffer's precision is identical to its number of bitplanes.

Exercise 13.23. Suppose we want a graphics card which has four 32-bit precision color buffers for stereoscopic viewing with double-buffering, an auxiliary color buffer of similar precision, a 24-bit depth buffer and an 8-bit stencil buffer, all to support a 1024 × 768 resolution display. How much on-card memory are we asking for?

Remark 13.6. A given OpenGL implementation may not support all the possible buffers. One can determine which are supported, as well as the number of bitplanes in each, with the help of glGet*() calls, e.g., glGetIntegerv(GL_DEPTH_BITS, **pointer*) returns the number of bitplanes in the depth buffer. Check the blue book for the specs for such calls.

13.7.2 Using the Stencil Buffer

Applications using the stencil buffer usually set the *stencil bits*, or *tags* as they are called – typically there being 8 for each pixel – in a first phase, by means of a *stencil test* applied to each incoming fragment. Stencil testing is enabled by calling glEnable(GL_STENCIL_TEST). The particular test applied depends on a glStencilFunc() call. The stencil test is applied in the graphics pipeline just before the depth test and only if a fragment passes the stencil test does it proceed to the depth test. If a fragment fails either test then it is discarded from the drawing pipeline.

How the incoming fragments set tags depends on a glStencilOp() call which is typically paired with a glStencilFunc() call. Incoming fragments that fail the stencil test, those that pass the stencil test but fail the depth test and those that pass both tests can set tags differently. The color buffer, typically, is disabled during the tag-setting first phase so that nothing is actually rendered to the display.

Once the tags have been set, actual drawing to the display occurs in the second phase, when tags are read per incoming fragment and a stencil test applied to determine if it is to continue on down the pipeline. We'll describe next the mechanics of the twin commands glStencilFunc() and glStencilOp() before putting everything together in a program.

The **glStencilFunc(*func*, *ref*, *mask*)** command sets a comparison function *func* to use in the stencil test, as well as a reference value *ref* to compare the stencil tag with. For example, if *func* is GL_LESS, then the test passes if *ref* is less than the value of the stencil tag.

The reference value is clamped to the range $[0, 2^k-1]$ if the stencil buffer contains k bitplanes and the stencil tag, too, interpreted as an integer in the same range. However, prior to comparison, the *mask* is bitwise ANDed with both the reference value and the stencil tag. Effectively, therefore, comparison is between the two integers made from bits in the reference value and stencil tag, respectively, at positions corresponding to the on bits in the mask.

A couple of options for *func* make **glStencilFunc(*func*, ...)** essentially non-test; particularly, if *func* is GL_ALWAYS then the test always passes, while if it is GL_NEVER the test never passes.

Example 13.5. If the call is glStencilFunc(GL EQUAL, 0xFF, 0x3F) and the stencil tag corresponding to a fragment is 0xBF, then the fragment passes the stencil test because only the lower six bits of the mask are 1, and the reference value and the given stencil tag, in fact, agree in each of these positions.

Remark 13.7. The color and depth values of a fragment come from "outside" the pipeline, in that they are determined by where and how the object to which the fragment belongs is drawn by the programmer; not so the stencil tag value, which is whatever is contained in the corresponding position of the stencil buffer. In fact, values in the stencil buffer cannot be changed by drawing operations at all, only by glStencilOp() commands, as we shall see.

We shall henceforth use always a mask value of 1 (= 00000001, assuming an 8-bit stencil buffer), which means that the lowest bit of the reference value is compared with the lowest bit of the stencil tag, other bits of no matter.

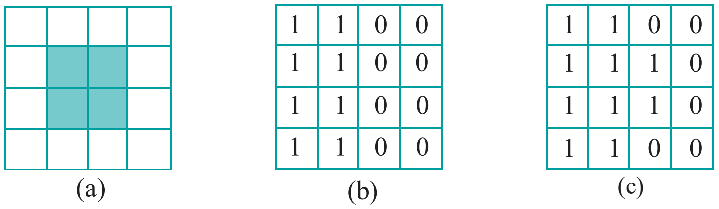

(a)

(b)

1	1	0	0
1	1	0	0
1	1	0	0
1	1	0	0

(c)

1	1	0	0
1	1	1	0
1	1	1	0
1	1	0	0

Figure 13.26: (a) Square R, which is drawn after calls to glStencilFunc(GL EQUAL, 1, 1) and glStencilOp(GL REPLACE, GL REPLACE, GL REPLACE) (b) Stencil buffer configuration before R is drawn (c) Stencil buffer configuration after R is drawn. Only each lowest bit in the stencil buffer is shown.

Example 13.6. The call glStencilFunc(GL EQUAL, 1, 1) allows a fragment to pass the stencil test only if the lowest bit in its corresponding stencil tag equals 1.

Suppose this, in fact, is the call prior to drawing the square R consisting of four fragments, as shown in Figure 13.26(a), and that the contents of the stencil buffer are as in Figure 13.26(b) (only the lowest bit of each tag is drawn). Then the left two fragments of R pass the stencil test and proceed on to the depth test, while the right two fail and are ejected from the pipeline. Ignore the right grid for now.

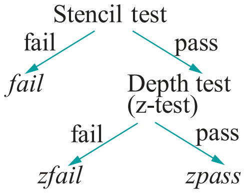

Figure 13.27: Potential outcomes for a fragment through the stencil and depth tests.

So, how is the result of a stencil test used? That’s where the glStencilOp() paired with a glStencilFunc() comes in. The values of the three parameters *fail*, *zfail* and *zpass* of a glStencilOp(*fail*, *zfail*, *zpass*) call‘ specify, respectively, how a stencil tag is updated in case the fragment fails the stencil test, passes the stencil test but fails the ensuing depth test, and passes both tests. Figure 13.27 indicates the testing scheme.

Values that we’ll use for a glStencilOp() parameter are GL KEEP, GL REPLACE and GL_INVERT which, respectively, keep the current stencil tag unchanged, replace it with the reference value, and invert it bitwise (for the full list of possible parameter values refer the red book). Note that *fail* ed and *zfail* ed fragments are ejected from the pipeline, even though they may update a tag.

Example 13.7. The call glStencilOp(GL REPLACE, GL REPLACE, GL_REPLACE) causes the stencil tag to be replaced with the reference value in all cases. If this call were indeed paired with glStencilFunc(GL EQUAL, 1, 1) prior to drawing the square R of Figure 13.26(a), then the stencil buffer would be updated as in Figure 13.26(c).

Exercise 13.24. Determine how the stencil buffer would be updated in the situation of Figure 13.26 if the call were glStencilOp(GL INVERT, GL REPLACE, GL_KEEP) instead of glStencilOp(GL REPLACE, GL REPLACE, GL REPLACE), and it was known that rectangle fragments all fail the depth test if they come to it. Assume that the call glStencilFunc(GL EQUAL, 1, 1) remains.

Drawing reflections in a constrained area is a canonical application of the stencil buffer which we illustrate next.

Experiment 13.15. Run ballAndTorusStenciled.cpp, based on ballAndTorusReflected.cpp. The difference is that in the earlier program the entire checkered floor was reflective, while in the current one the red floor is non-reflective except for a mirror-like disc lying on it. Pressing the arrow keys moves the disc and pressing the space key starts and stops the ball moving. As can be seen in the screenshot of Figure 13.28, the ball and torus are reflected only in the disc and nowhere else. End

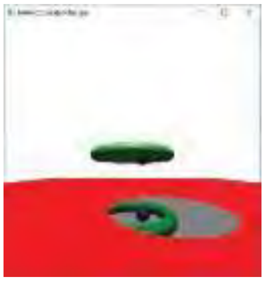

Figure 13.28: Screenshot of ballAndTorusStenciled.cpp.

The effect of restricted reflection in ballAndTorusStenciled.cpp is obtained using four successive pairs of glStencilFunc() and glStencilOp() calls in the drawing routine. The first pair

```
glStencilFunc(GL_ALWAYS, 1, 1);
glStencilOp(GL REPLACE, GL REPLACE, GL REPLACE);
```

causes the next drawing statement drawReflectiveDisc(xVal, zVal) to create a “mask” of the disc in the stencil buffer with 1’s at positions corresponding to a disc fragment and 0’s elsewhere. The reason for this is that the GL ALWAYS parameter value of glStencilFunc() ensures that every fragment of the disc passes the stencil test, while the second two GL REPLACE values of glStencilOp(), for *zfail* and *zpass*, respectively, ensure that the stencil tag corresponding to a disc fragment is always replaced with the reference value 1, regardless the result of the depth test. The remaining stencil tags remain at their clearing value 0 set by the call glClearStencil(0) in the initialization routine.

Note, as well, that both color and depth buffers are disabled prior to the drawReflectiveDisc(xVal, zVal) mask-creating call with appropriate glColorMask() and glDepthMask() commands, so that only the stencil buffer is updated and nothing is drawn to the screen by the first drawReflectiveDisc(xVal, zVal).

Once the mask of the disc in the stencil buffer has been created, actual drawing to the window commences. The color and depth buffers are accordingly enabled next. The second pair of stencil-buffer manipulating calls

```
glStencilFunc(GL EQUAL, 1, 1);
glStencilOp(GL KEEP, GL KEEP, GL KEEP);
```

causes the subsequent drawing statement drawFlyingBallAndTorus() to draw the reflected ball and torus in the mask area of the disc, because only fragments corresponding to this area pass the stencil test and proceed on down the pipeline. The contents of the stencil buffer are kept unchanged.

The next drawing statement, drawReflectiveDisc(xVal, zVal), actually draws (or, rather, blends) the disc onto the reflected ball and torus.

The third pair of stencil-buffer manipulating calls

```
glStencilFunc(GL NOTEQUAL, 1, 1);
glStencilOp(GL KEEP, GL KEEP, GL KEEP);
```

prevents the red quad drawn next from erasing the disc by allowing drawing only outside the area corresponding to the disc.

The final pair of stencil-buffer manipulating calls

```
glStencilFunc(GL ALWAYS, 1, 1);
glStencilOp(GL KEEP, GL KEEP, GL KEEP);
```

allows the real ball and torus to be drawn by a drawFlyingBallAndTorus() statement regardless of the stencil tags.

Exercise 13.25. (Programming) Reverse the roles of the floor and disc in ballAndTorusStenciled.cpp. In particular, make the floor reflective, while a movable red disc blocks reflection.

Exercise 13.26. (Programming) Draw the glass door of a roadside building reflecting a passing vehicle – all shapes in your scene being simple and boxy.

Exercise 13.27. (Programming) Create the effect of a user's view of some static scene blocked entirely by an opaque rectangle, except for a circular annulus cut out from the latter, so the user sees only through this annulus. The user can slide the rectangle about, or, equivalently, translate the annulus.

For more about drawing shadows and reflections with the help of the stencil buffer read Mark Kilgard's tutorial [80].

Scissor Test

The *scissor test* is simply a stencil test applied to a rectangular region of the display window. The command

glScissor(*x*, *y*, *width*, *height*)

specifies the lower left corner (*x*, *y*) of a *scissor rectangle* (also called *scissor box*), as well as its *width* and *height* , all in windows coordinates, such that only fragments inside the rectangle pass the scissor test. Scissoring is enabled and disabled, respectively, by glEnable(GL SCISSOR TEST) and glDisable(GL SCISSOR TEST). The reason for singling out this special case of stencilling as a separate test is that it can be highly optimized in the GPU.

Exercise 13.28. (Programming) Add in ballAndTorusStenciled.cpp a vertical rectangular mirror on the wall directly behind the torus with help of a scissor test.

Image Manipulation

OpenGL allows manipulation of images on the screen in various ways. Let's get right to a particularly powerful one using a framebuffer object (FBO) – review Section 12.9 for how to code up an FBO. Our object now is to move a texture image around the screen with help of the mouse. What we'll do is attach the texture as the color buffer of an FBO and then *blit* (i.e., bit copy) the color values from the FBO to the default, i.e., viewable, framebuffer.

Figure 13.29: Screenshot of imageManipulationFBO.cpp.

Experiment 13.16. Run imageManipulationFBO.cpp. An image of the numeral 1 appears at the bottom left of the OpenGL window. Clicking the mouse left button anywhere on the window will move the image to that location, while you can, as well, drag it with the left button pressed. Figure 13.29 is a screenshot of the initial configuration. End

In the setup routine of imageManipulationFBO.cpp, the block

```
imageFile *image[1];
image[0] = getBMP("../../Textures/number1.bmp");

glGenTextures(1, &texture);
glBindTexture(GL_TEXTURE_2D, texture);
glTexImage2D(GL_TEXTURE_2D, ...);
glTexParameteri(...);
...

glGenFramebuffers(1, &framebuffer);
glBindFramebuffer(GL_READ_FRAMEBUFFER, framebuffer);
glFramebufferTexture2D(GL_READ_FRAMEBUFFER, GL_COLOR_ATTACHMENT0,
                       GL_TEXTURE_2D, texture, 0);
```

binds the image of the number 1 to texture, which in turn is bound as the color buffer to the FBO frameBuffer. Next, in the drawing routine, the statements

```
glBindFramebuffer(GL_READ_FRAMEBUFFER, framebuffer);
glBindFramebuffer(GL_DRAW_FRAMEBUFFER, NULL);

glBlitFramebuffer(0, 0, textureWidth, textureHeight, rasterX,
                  rasterY, rasterX + textureWidth, rasterY +
                  textureHeight, GL_COLOR_BUFFER_BIT, GL_NEAREST);
```

define the blitting from the FBO to the default framebuffer. In particular, the first two statements specify the "from" and "to" buffers, these being the FBO frameBuffer and the default framebuffer, respectively. Lastly comes the glBlitFramebuffer() command, the first and second of whose 10 parameters are the xy-coordinates of the lower-left corner of the rectangular block of pixels to be copied, while the third and fourth are the xy-coordinates of the upper-right corner of this source rectangle; the next four parameters, likewise, specify the extent of the destination rectangle; the ninth parameter indicates the type of the buffers to be copied, while the last parameter is the filtering option to use if the image is scaled (in our case it is not, so we apply the simplest filter).

The reader can see from the parameter values of our call to glBlitFramebuffer() that we are blitting the entire texture image to a rectangle on the screen whose lower-left corner $(rasterX, rasterY)$ is determined by the user via the mouse.

Remark 13.8. Another command which the reader might find useful in connection with image manipulation, though we don't have occasion to use it, is glReadPixels(), which copies a rectangular array of pixel data from a frame buffer, the default or an FBO, to client memory. We'll leave the interested reader to refer to the red book for specs.

13.8

Exercise 13.29. (Programming) Blitting from one FBO to another is a powerful technique. However, it might be a bit of overkill in order only to drag a texture image around as in imageManipulationFBO.cpp. Do what this program does in a simpler way without invoking FBOs, particularly, by dragging a textured rectangle with the mouse.

When you do this it should be easy as well to fix the current "bug" that the mouse click always positions the lower-left of the image – allow it instead to pick the image at any point and drag.

Exercise 13.30. (Programming) Program a tile-moving game. See Figure 13.30. The object is to rearrange the four tiles from the configuration on the top to that on the bottom by *sliding* them around in the big rectangle – tiles may not be picked up – the white space at the bottom being available for intermediate moves. The user should be able to select and drag a tile with the mouse. Implement collision detection so that one tile cannot climb over another.

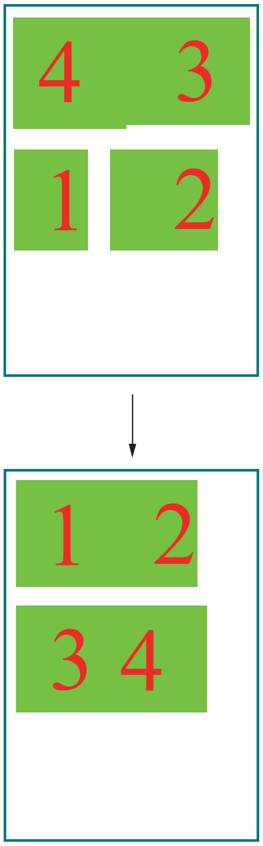

Figure 13.30: Rearrange the tiles from the order on the top to that on the bottom.

Exercise 13.31. (Programming) Code a simple image-editing program, where the user can load an image, tweak it and save (the command glReadPixels() might come in handy for the latter).

13.9 Bump Mapping

Blinn [15] developed an ingenious method, called *bump mapping* , to give the illusion of geometric detail on a surface, e.g., making it appear ridged or dimpled, by means of perturbing the surface normals, but *without* actually changing any geometry. The idea is to re-align the normals to the original surface so that light reflects from it *as if* it were detailed. A one-dimensional example will make matters clear.

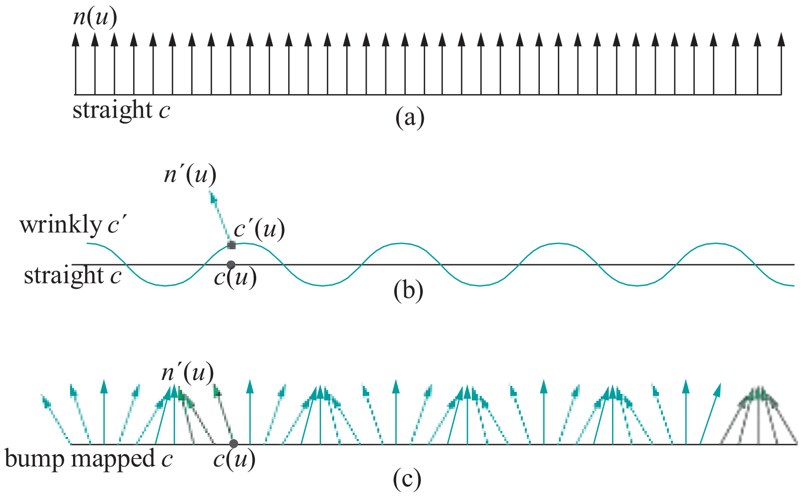

Figure 13.31: Bump mapping: (a) The original curve c and its true unit normals $n(u)$ (b) The wrinkled curve $c^{\prime}$ and its unit normal $n^{\prime}(u)$ at a single point $c^{\prime}(u)$ (c) Bump mapped c with redefined normals $n^{\prime}(u)$.

Consider the straight line c of Figure 13.31(a). The unit normals $n(u)$ at points $c(u)$ of c are identical vectors perpendicular to c (drawn in the figure at a discrete sequence of points).

Next, suppose that one wants to wrinkle c to make it look like the green curve c^1 of Figure 13.31(b). Actually wrinkling c entails replacing it with a multi-segment polyline approximation of c^1, an object substantially more complex than c. The bump mapping approach is to leave c as it is, but, instead, to redefine the normal at each point $c(u)$ so that it equals $n^1(u)$, the normal at the corresponding point $c^1(u)$ of c^1.

Figure 13.31(b) shows $n^1(u)$ at one point $c^1(u)$ of c^1, while Figure 13.31(c) shows the so-called *bump mapped* c with its perturbed normals.

The premise of bump mapping is that c with normals redefined to match those of c^1 will resemble c^1 when lit, because the reflection of light from a surface depends on the normals there. We describe next Blinn's method to compute the perturbed normals.

Suppose that s is a surface in 3-space defined parametrically on some domain W by

$$s(u, v) = (f(u, v), g(u, v), h(u, v))$$

so that the vector $n(u, v) = \frac{\partial s}{\partial u}(u, v) \times \frac{\partial s}{\partial v}(u, v)$ is normal to s at $s(u, v)$ (see Section 11.10 for a primer about partial derivatives and their application to finding tangents and normals to a surface).

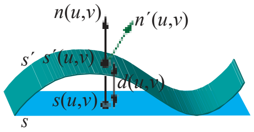

Figure 13.32: The bumped surface s^1 is obtained from s by displacing each point $s(u.v)$ a distance $d(u, v)$ along the normal $n(u, v)$ at $s(u, v)$.

Suppose, as well, that the desired (hypothetical) detailed surface s^1 is obtained from s by displacing each point $s(u, v)$ a distance $d(u, v)$ along $n(u, v)$. See Figure 13.32. The scalar-valued function $d(u, v)$ giving this displacement is called the *bump map*.

Accordingly,

$$s^1(u, v) = s(u, v) + d(u, v)n(u, v)$$

which we write more simply by dropping the arguments as

$$s^1 = s + dn \tag{13.6}$$

A normal n^1 to s^1 is given by

$$n^1 = \frac{\partial s^1}{\partial u} \times \frac{\partial s^1}{\partial v} \tag{13.7}$$

We evaluate n^1 next in terms of the original surface and the bump map. First, from (13.6),

$$\begin{aligned} \frac{\partial s^1}{\partial u} &= \frac{\partial s}{\partial u} + \frac{\partial d}{\partial u} n + d\frac{\partial n}{\partial u} \\ &'\!:: \frac{\partial s}{\partial u} + \frac{\partial d}{\partial u} n \end{aligned}$$

where the approximation in the second line is made by dropping the term $d\frac{\partial n}{\partial u}$, which is negligibly small on the assumptions that

(a) the displacement d is small, and

(b) $\frac{\partial n}{\partial u}$ is small as well, from the reasonable premise that the original surface s lacked detail and was fairly smooth, meaning that its normal value changed only slowly with u.

Likewise, one writes

$$\frac{\partial s^1}{\partial v} \ '\!:: \frac{\partial s}{\partial v} + \frac{\partial d}{\partial v} n$$

Plugging the preceding two approximations into (13.7) one gets

$$\begin{aligned} n^1 \ &'\!:: \left(\frac{\partial s}{\partial u} + \frac{\partial d}{\partial u} n\right) \times \left(\frac{\partial s}{\partial v} + \frac{\partial d}{\partial v} n\right) \\ &= \left(\frac{\partial s}{\partial u} \times \frac{\partial s}{\partial v}\right) + \frac{\partial d}{\partial u}\left(n \times \frac{\partial s}{\partial v}\right) - \frac{\partial d}{\partial v}\left(n \times \frac{\partial s}{\partial u}\right) \\ &= n + \frac{\partial d}{\partial u}\left(n \times \frac{\partial s}{\partial v}\right) - \frac{\partial d}{\partial v}\left(n \times \frac{\partial s}{\partial u}\right) \end{aligned} \tag{13.8}$$

which expresses the perturbed normal n^1 in terms of the original surface s, the original normal n and the bump map d. Finally, the new normal function for the bump mapped s^1 is obtained by normalizing n^1 to unit length.

Bump mapping comes into its own in the per-pixel lighting of Phong's shading model, which we discussed in Section 11.12, where normals defined at the vertices by Equation (13.8) vary linearly over the interior pixels, with lighting calculation done separately at each pixel. Unfortunately, Phong's shading model is not an option in pre-shader OpenGL, but can be implemented using the shaders of the newer generations. In fact, when we get to OpenGL 4.x later in the book, we shall implement the per-pixel lighting of Phong's model, and bump mapping itself will be a case study. Without per-pixel lighting bump mapping is at best awkward but, nevertheless, we do have a simple proof-of-concept program even now.

Experiment 13.17. Run bumpMapping.cpp, where a plane is bump mapped to make it appear corrugated. Press space to toggle between bump mapping turned on and off. Figure 13.33 shows screenshots. End

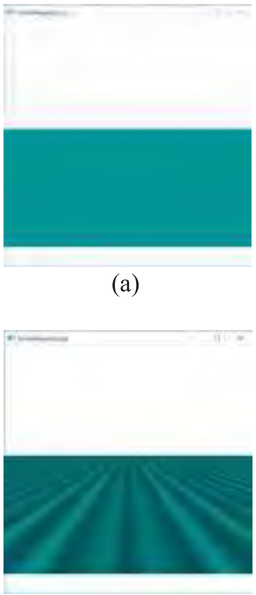
(a)

(b)

Figure 13.33: Screenshots of bumpMapping.cpp: bump mapping (a) off (b) on. The underlying geometry is a flat plane in both cases.

The equation of the plane in bumpMapping.cpp is

$$s(u, v) = (u, 0, -v)$$

the minus sign in front of v is so that the normal $n(u, v) = \frac{\partial s}{\partial u} \times \frac{\partial s}{\partial v} = (0, 1, 0)$ to the plane points in the upward y-direction. The bump map itself is taken to be the wave

$$d(u, v) = \sin(2u)$$

along the x-direction. We leave it to the reader to verify that with these equations for s and d, (13.8) gives

$$n^1(u, v) = (-2\cos(2u), 1, 0)$$

This formula for the perturbed normals to the plane is, in fact, implemented in bumpMapping.cpp when bump mapping is turned on, together with a call to glEnable(GL NORMALIZE) in initialization to normalize the normals.

13.10 Shadow Mapping

Recall Experiment 4.37 in Chapter 4, where we simulated a shadow by applying a degenerate scaling to flatten a ball and a torus. The method though simple was severely limited, the shadow of the ball not falling on the torus, for example. We'll now learn the far more sophisticated technique of *shadow mapping*, formulated by Lance Williams in his 1978 paper *Casting curved shadows on curved surfaces* [152], to authentically simulate shadows cast by a local light source.

Here's the idea. Consider a scene with a single point light source L. The lit region is the one to every point of which there is an unobstructed straight-line ray from L, in other words, it consists precisely of those points which would be visible from a camera located at L. Let's call such a camera L, too. See Figure 13.34.

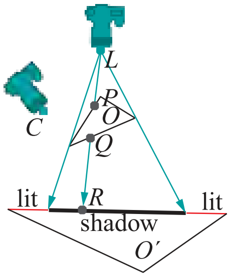

Figure 13.34: A camera and light source L at the same location; shadow cast by O on O' is thick dark; lit part of O' is red; C is the "real" program-defined camera.

Now, if we had access to the z-buffer for the scene as seen by L, then we could determine which fragments are shadowed by comparing their z-values to corresponding ones in the z-buffer: a fragment with z-value greater than the corresponding one in the z-buffer is hidden from L and, therefore, shadowed; otherwise, it is lit. E.g., if the scene in Figure 13.34 were drawn from the point of view of L, then the fragment corresponding to P would be the "winner" sitting in the z-buffer, while those corresponding to Q and R with higher z-values would be shadowed. Simple idea, no? But a major difficulty lurks.

Indeed, shadow mapping starts off in a first phase by drawing the scene as viewed by L and capturing the z-buffer values in a so-called *depth texture*. A depth texture storing z-values from a light source, in fact, is called a *shadow map*.

In the next phase, shadow mapping intends to draw the scene as viewed by the actual program-defined camera, call it C, comparing, as it does so, each incoming fragment's z-value, *w.r.t. the camera at* L, with the corresponding one saved in the shadow map to determine if it's shadowed or not.

But – here's the difficulty – when processing the scene for C, how does the pipeline on-the-fly determine the z-value of an incoming fragment w.r.t. L? In fact, as can be seen in Figure 13.34, z-values for C itself may have nothing to do with those for L, e.g., R is in P's shadow, the former having the larger z-value w.r.t. L, but they are not even on the same line of sight w.r.t. C.

How about modifying the first phase to store the z-values of *all* fragments w.r.t. L so that they can be read when processing w.r.t. C? Unfortunately, this is impossible given the working of the OpenGL pipeline – the depth competition in the z-buffer is *transparent* to the user, losing fragments being discarded silently, e.g., when Q and R lose to P from L's viewpoint in Figure 13.34, there is no way to retain their z-values. It is to solve this problem that the key insight of shadow mapping comes, as we see next.

Suppose, the program's camera C sees a vertex to be at $[x\ y\ z\ 1]^T$ in world space. Now, the vertex arrived at these coordinates after modeling transformations in the program followed by, say, a viewing transformation, namely, C's gluLookAt(). However, from L's viewpoint this last gluLookAt is "fake" – equivalent, as we know from Section 4.6, to a sequence of modeling transformations which are applied to the scene only to bring C to its default position at the origin, and which are *not* apparent to a second viewer, such as L.

For example, say the only modeling transformation applied to a scene is glTranslatef(10.0, 0.0, 0.0). Say, as well, the camera's viewing transformation is gluLookAt(0.0, 0.0, 10.0, 0.0, 0.0, 0.0, 0.0, 1.0, 0.0), which is equivalent to glTranslatef(0.0, 0.0, -10.0). Then, the combined transformation is glTranslatef(10.0, 0.0, -10.0). However, from the viewpoint of another viewer, who happens to watching, the scene is transformed by glTranslatef(10.0, 0.0, 0.0) *only*, and *not* glTranslatef(10.0, 0.0, -10.0). In other words, one needs to undo the program camera's viewing transformation in order to perceive the scene as by the second viewer.

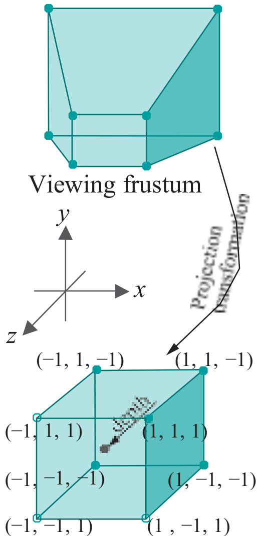

Figure 13.35: Viewing frustum transformed by the projection transformation into the canonical box.

Before proceeding further, we need a quick acquaintance with a concept which will be discussed in depth in Chapter 20. It is that the projection transformation (glOrtho(), glFrustum() or gluPerspective()), which is applied always after all modelview ones, transforms a viewing volume into the so-called canonical viewing box with corners at $(\pm 1, \pm 1, \pm 1)$, points in the viewing volume being transformed to points in the box (see Figure 13.35 for frustum-to-box). Moreover, the z-value of a (post-transform) fragment is its distance, or depth, from the canonical box's $z = -1$ face, this depth being scaled first from the range $[0, 2]$ to the range $[0, 1]$. Okay, backto shadow mapping.

Suppose, then, that C's viewing transformation, defined by its gluLookAt(), is V_C, while L's viewing transformation is V_L and L's projection transformation P_L (obviously L has no modeling transforms associated as it simply represents a camera). So, the point seen by C at world $[x\ y\ z\ 1]^T$ is "really" at $V_C^{-1}\ [x\ y\ z\ 1]^T$, after undoing C's gluLookAt(). To get to L's point of view, it is then transformed by L's gluLookAt() to $V_L\ V_C^{-1}[x\ y\ z\ 1]^T$, and, finally, by L's projection transformation to

$$P_L\ V_L\ V_C^{-1}\ [x\ y\ z\ 1]^T \qquad (13.9)$$

in the canonical box. Now, to scale the depth values from $[0, 2]$ to $[0, 1]$, in order to read z-values w.r.t. L, we simply scale the $2 \times 2 \times 2$ canonical box $[-1, 1] \times [-1, 1] \times [-1, 1]$ to the $1 \times 1 \times 1$ box $[0, 1] \times [0, 1] \times [0, 1]$ with the linear 2-transformation sequence

```
glTranslatef(0.5, 0.5, 0.5);
glScalef(0.5, 0.5, 0.5);
```

whose matrix, called the *bias matrix*, is

$$B = \begin{bmatrix} 0.5 & 0 & 0 & 0.5 \\ 0 & 0.5 & 0 & 0.5 \\ 0 & 0 & 0.5 & 0.5 \\ 0 & 0 & 0 & 1 \end{bmatrix}$$

Tacking B to the left of (13.9), we see finally how to determine the z-value, from L's perspective, of a point in world space which has been transformed to coordinates $[x\ y\ z\ 1]^T$ by a pipeline processing for camera C: it is the z-coordinate of the vector

$$B\ P_L\ V_L\ V_C^{-1}\ [x\ y\ z\ 1]^T \tag{13.10}$$

Time to turn theory into practice!

Experiment 13.18. Before running ballAndTorusShadowMapped.cpp you may want to run again ballAndTorusLitOrthoShadowed.cpp from Chapter 11, seen as well in Experiment 4.37 in Chapter 4, which implements a simple-minded blacken-and-flatten strategy to draw orthographic shadows on the floor cast by a distant overhead light source.

The scenes of the two shadowing programs are nearly identical, except that ballAndTorusShadowMapped.cpp shadow maps a local light source, whose position is indicated by a red sphere. Controls are identical too: press space to start the ball traveling around the torus and the up and down arrow keys to change its speed. As can even be seen in the screenshot of Figure 13.36, shadowing is far more authentic in ballAndTorusShadowMapped.cpp. End

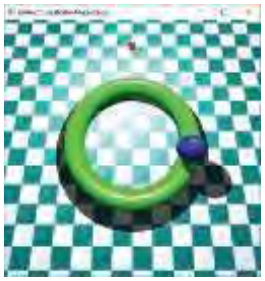

Figure 13.36: Screenshot of ballAndTorusShadowMapped.cpp.

We'll narrate ballAndTorusShadowMapped.cpp starting from the top. First come a bunch of globals whose purpose will be clear as we go along. The drawFlyingBallAndTorus(), drawCheckeredFloor() and animate() routines are copied from ballAndTorusLitOrthoShadowed.cpp, except now there is no option in the first one to blacken the ball and torus as this is not needed in the current program.

There are three points of note in the initialization routine next:

1. With glDepthFunc(GL_LEQUAL) the comparison in the z-buffer is set to "$\leq$", rather than the default "<", so that regions lit by the light source drawn in the third drawing pass can overwrite their ambiently-lit versions drawn earlier in the second pass.

2. The shadow map, i.e., depth texture, is created in a manner similar to image (RGB) textures, except now the two GL DEPTH COMPONENT format parameter values in the glTexImage2D() call indicate that it is a depth texture intended to store z-values.

3. The camera and the light's projection and viewing transformation matrices are computed and stored, respectively, in four globals, suggestively named cameraProjMat, . . ., lightViewMat. (By the light's transformations, of course, we mean those of a camera located there.) The matrix computations are done all in the modelview matrix stack, which doubles through the program as our personal matrix calculator! Indeed, it may seem odd to apply a gluPerspective() to the modelview stack, but it's not illegal and we care only about the value of the corresponding matrix.

   Moreover, parameters for the camera's and light's gluPerspective() and gluLookAt() commands, corresponding to their respective projection and viewing transformations, are user-set in the globals cameraFovy, . . ., cameraUp, lightFovy, . . ., lightUp.

   It's in setting the values of lightFovy, lightLookAt and lightUp that we settle a question which may have occurred earlier to the reader: if L is a regular light source, emitting in all directions, how do we determine a line of sight and up direction for a camera at L, in particular, parameters for its gluLookAt(), or viewing transformation? Well, we really can't. So, we imagine L as a spotlight (see Section 11.6) whose direction points down the y-axis, explaining the lightLookAt value of $(0.0, 0.0, 0.0)$, given its location lightPos of $(0.0, 30.0, 0.0)$; moreover, we choose L's cone angle to be 120°, explaining the lightFovy of 120.0; finally, L's up direction could be taken to be any vector perpendicular to its los – we choose lightUp to be (1.0, 0.0, 0.0).

Such approximation of a regular light source by a spotlight is valid in most scenes, where only a part of the light emitted, a cone if you will, is needed to illuminate the region of interest. Keep in mind that the treatment of L as a spotlight is only for the purpose of determining its parameters as a camera, e.g., as a light source GL_LIGHT0 in ballAndTorusShadowMapped.cpp is not a spotlight.

We'll leave the reader to convince herself that the remaining light* globals have been reasonably set, too.

The drawing routine next has four passes which we discuss one after another.

FIRST PASS: The shadow map's z-values are set in this pass. First, we load the light's projection and viewing transformation matrices to draw the scene from its viewpoint. Then, the viewport dimensions are set to match those of the shadow map so that there is one-to-one correspondence between pixels and texels. Rendering of the scene to the color buffer is disabled by passing GL FALSE parameters to glColorMask(), as we don't want to actually see the scene, but only fill the depth buffer.

Front faces are culled prior to drawing for efficiency because only back faces are enough from the light's viewpoint to determine shadows (e.g., in Figure 13.34 the shadow cast by O on O^1 is precisely that cast by its back face, the one containing Q). Finally, the scene is drawn and z-values captured in the shadow map using a glCopyTexImage2D() command.

SECOND PASS: This pass has actually nothing to do with shadow mapping, but is inserted for authenticity's sake: the whole scene is drawn with global ambient lighting, which illuminates all objects regardless of shadows.

First, the camera's projection and viewing transformation matrices are loaded. The viewport is set to the OpenGL window size and back face culling is enabled as usual for efficiency. Rendering to the color buffer is enabled as well because we want what we draw to contribute to what will be finally visible. Lighting is enabled prior to drawing the scene, but the local light source GL_LIGHT0 is *not* enabled, allowing only global ambient light into the pipeline.

THIRD PASS: Now, we'll draw with the local light source turned on, eliminating first, however, with help of the shadow map, fragments which are shadowed. Thus, the lit parts only, which were drawn with ambient lighting in the previous pass, are redrawn illuminated now by the light source.

First, the light source GL_LIGHT0 is enabled. Next, we want to calculate and apply the transformation matrix $B\,P_L\,V_L\,V_C^{-1}$ of (13.10). More than one step is needed. To begin with, the matrix product $B\,P_L\,V_L$, which we call the intermediate matrix, is calculated in the modelview matrix stack and saved in the global interMat by

```
glMatrixMode(GL_MODELVIEW);
glPushMatrix();
glLoadIdentity();
glTranslatef(0.5, 0.5, 0.5);
glScalef(0.5, 0.5, 0.5); // MV matrix value = B
glMultMatrixf(lightProjMat); // MV matrix value = B x P_L
glMultMatrixf(lightViewMat); // MV matrix value = B x P_L x V_L
glGetFloatv(GL_MODELVIEW_MATRIX, interMat);
```

Post-multiplying the intermediate matrix by V_C^{-1} and then using it to transform vertices is up next. Unfortunately, though, there is no inversion operation available in an OpenGL matrix stack. Still, there is another resource which solves our problem exactly. The automatic texture coordinate generation sequence

```
glEnable(GL_TEXTURE_GEN_X);
glTexGeni(GL_X, GL_TEXTURE_GEN_MODE, GL_EYE_LINEAR);
glTexGenfv(GL_X, GL_EYE_PLANE, eyePlaneParams);
```

X being any one of the four texture coordinates S, T, R and Q and *eyePlaneParams* pointing to a 4-vector $[p_x\ p_y\ p_z\ p_w]$, sets the value of X to

$$p^1_x x + p^1_y y + p^1_z z + p^1_w w$$

where $[x\ y\ z\ w]^T$ are the homogeneous coordinates of the current vertex, and where

$$[p^1_x\ p^1_y\ p^1_z\ p^1_w] = [p_x\ p_y\ p_z\ p_w]\, M^{-1}$$

M being the current modelview matrix. Now, consider the program. The current modelview matrix, in fact, is V_C. Moreover, the code sequence above is repeated once for X equal to each of the texture coordinates S, T, R and Q, with *eyePlaneParams* pointing to successive rows of the intermediate matrix $B\,P_L\,V_L$. It's not hard to check then that after this fourfold repetition

$$[S\ T\ R\ Q]^T = B\,P_L\,V_L\,V_C^{-1}\,[x\ y\ z\ w]^T \tag{13.11}$$

which is precisely the transformation the doctor ordered if you see again (13.10). So, the value of R on the left of (13.11) is the z-value from the light's viewpoint, which we must compare with the corresponding value in the shadow map. Happily, OpenGL has specialized support for such an operation as well. The three statements

```
glTexParameteri(GL_TEXTURE_2D,    GL_TEXTURE_COMPARE_MODE,
                         GL_COMPARE_R_TO_TEXTURE);
glTexParameteri(GL_TEXTURE_2D, GL_TEXTURE_COMPARE_FUNC, GL_LEQUAL);
glTexParameteri(GL_TEXTURE_2D, GL_DEPTH_TEXTURE_MODE, GL_ALPHA);
```

cause a fragment's R-value to be compared with the corresponding value – i.e., the one at location (S, T) – in the currently bound depth texture. The comparison passes if the former is less than or equal to the latter, failed comparisons generating an alpha value of 0, successful ones an alpha value of 1. At the end of these statements, then, shadowed fragments, which failed the comparison because of an R-value greater than their shadow map counterpart, will have an alpha value of 0, while lit fragments will have an alpha value of 1.

Finally, the two statements

```
glEnable(GL_ALPHA_TEST);
glAlphaFunc(GL_GREATER, 0.5);
```

prior to drawing the scene set up an alpha test which will be failed by fragments with an alpha value of 0, namely, shadowed ones. The net result is that the lit region is redrawn illuminated by the light source in this pass. Combined with the ambient lighting of the whole scene from the previous pass, shadow mapping is now complete.

FOURTH PASS: This is a trivial pass whose purpose is only to draw a red sphere at the light's position.

Finally, the reshape routine has a point of interest in that, instead of simply declaring a viewing frustum, it goes on to compute the frustum's projection matrix and accordingly update the cameraProjMat global, because it is this global from which the program obtains the camera's projection matrix. All the rest of the program is straightforward.

Note: Our implementation has a minor flaw from the point of view of Phong's lighting model of Chapter 11. For regions not shadowed we apply only the local light's diffuse and specular components because the result of applying the global ambient from the second pass is drawn over in the third. Phong's model, though, would have us keep and add to the global ambient.

Shadow mapping is a powerful and much-implemented real-time shadowing technique. However, a couple of its drawbacks are seen even in ballAndTorusShadowMapped.cpp. Firstly, aliasing is evidently an issue with the shadows – it is, in fact, inversely correlated to the resolution of the shadow map. Secondly, multiple drawing passes may become computationally taxing, especially with more than one light source.

Refinements of shadow mapping have been developed, though, in order to circumvent these issues. A popular alternative to shadow mapping, that of *shadow volumes*, was first developed by Crow [32] in 1977. The reader is referred to more advanced texts such as those by Akenine-Möller et al. [1] and McReynolds-Blythe [95], as well as the research literature, for more on shadow volumes and other techniques to create shadows.

Exercise 13.32. In the third pass of ballAndTorusShadowMapped.cpp we applied (13.10), which says that the transformation needed to determine its coordinates in the box [0, 1] × [0, 1] × [0, 1], from the light source's viewpoint, of a fragment which has been transformed by modeling transformations and the program camera's viewing transformation is $B\, P_L\, V_L\, V_C^{-1}\, [x\ y\ z\ 1]^T$.

Why did we ignore the program camera's projection transformation, in other words, why didn't we apply $B\, P_L\, V_L\, V_C^{-1}\, P_C^{-1}\, [x\ y\ z\ 1]^T$?

Exercise 13.33. (Programming) The third pass of ballAndTorusShadowMapped.cpp, as observed in the note above, kills the ambient reflectance of unshadowed objects. Fix this.

Exercise 13.34. (Programming) Shadow map sphereInBox1.cpp of Experiment 11.1.

The shadow mapping technique developed above was for a local light source. Shadows cast by such a source are called *perspective* or *projective*, as opposed to orthographic shadows cast by a distant light source. However, see the following exercise.

Exercise 13.35. (Programming) There is no reason the shadow mapping method can't be adapted to simulate orthographic shadows, in fact, more authentically than the flattening method of Section 4.7.2. Change ballAndTorusShadowMapped.cpp to draw orthographic shadows cast by a distant overhead light source.

13.11 Summary, Notes and More Reading

In this chapter we learned a few different visual techniques to help embellish our scenes, games and movies. It's worth emphasizing that visual techniques are as much an art as a science. Experience counts a lot in knowing how to get the "right effect", right being subjective in the first place. A lot of people out there are doing amazingly creative stuff. Although much of it is commercial, there's plenty of free stuff still to be found on the net, so collect code to save re-inventing the wheel and for inspiration. The OpenGL site [106] has numerous pointers.

It's worth noting that we've just crossed a milestone in the progression of this book. With only the significant exceptions of B-splines, NURBS and rational Bézier primitives, to come in later chapters, *we've mostly covered all in this book to do with coding pre-shader OpenGL*. Pre-shader OpenGL itself is a perfectly serviceable 3D API. Moreover, as we said at the start, a grasp of pre-shader OpenGL makes the modern shader-based versions much easier to learn. In particular, the reader is now well set to take on our own coverage of fourth generation OpenGL which begins in Chapter 15.

Of course, topics to come such as rasterization, Bézier, B-spline and NURBS theory, projective spaces, ray tracing and radiosity, among others, are extremely important for a solid understanding of CG. Nevertheless, it's heartening to realize how far we have come since the first chapter, particularly from the point of view of practical programming.

Part VII

Pixels, Pixels, Everywhere

CHAPTER 14

Raster Algorithms

In this chapter we are going to travel almost all the way to the other end of the graphics pipeline – from world space to just behind screen space – to understand some of the low-level processes which take place at the time primitives are transformed to pixels in the raster. In particular, the goal for this chapter is to learn algorithms to clip and rasterize lines and polygons. These are operations a user cannot herself call directly or interact with via a high-level API such as OpenGL, which is not a bad thing as she can devote herself then to modeling and animation. Nevertheless, it's useful to have a grasp overall of the functioning of the pipeline. We'll not attempt here a comprehensive coverage of raster algorithms, but focus instead on four which are commonly implemented and fairly representative.

First comes clipping, which is the process of determining the part of a primitive within some restricted area. We're already familiar with the functionality of OpenGL's clipping to a viewing volume and in this chapter we'll learn how the operation is implemented in two 2D cases, namely, those of a straight line segment and a convex polygon, both clipped to a rectangle. In particular, the Cohen-Sutherland line clipper is the topic of Section 14.1 and the Sutherland-Hodgman polygon clipper that of Section 14.2. Both clippers can be straightforwardly extended to 3D to clip a line segment or convex polygon against a box, the version actually implemented in the rendering pipeline.

Next, we'll investigate rasterization, the process of selecting and coloring pixels from the raster to represent a given primitive. We'll again limit ourselves to the two cases of straight segments and polygons. Moreover, we shall only be choosing pixels to comprise a primitive, leaving the problem of coloring them to a later chapter. Section 14.3 presents Bresenham's line rasterizer, actually as an improvement over the DDA (Digital Differential Analyzer) line rasterizing algorithm. Section 14.4 next discusses scan-based polygon rasterization. Section 14.5 concludes the chapter.

The reader impatient to keep up her momentum in coding OpenGL – the last chapter took us almost to the end of all there is in this book about classical OpenGL – and move onto OpenGL 4.x, the latest generation, which starts the next chapter, can indeed skip this one. What is covered here is not needed by a person who wants simply to write code. However, it is an important part of CG theory, which is why we placed the material here, just after reaching a milestone on the practical side.

14.1 Cohen-Sutherland Line Clipper

Straight line segments traveling down the OpenGL graphics pipeline are clipped to within an axis-aligned 3D viewing box prior to rasterization. Cohen-Sutherland is the classic algorithm for this purpose. Our exposition of Cohen-Sutherland, though, will be in 2D – clipping a segment to a rectangle – for the sake of simplicity. However, extension to a 3D version, where a segment is clipped to a box, is fairly straightforward.

Remark 14.1. How about clipping to a viewing volume which is not a box, but a frustum, as when the projection statement is glFrustum() or gluPerspective()? It turns out that in a stage in the pipeline, prior to clipping, the frustum is "straightened" into a box by a so-called projective transformation, so one need clip only to a box.

The inputs to (2D) Cohen-Sutherland are, then, the endpoints p_i and p_j of a straight line segment S on the xy-plane, and an axis-aligned rectangle R on the same plane bounded by the lines $x = a$, $x = b$, $y = c$ and $y = d$. R is called the *clipping rectangle*. The output consists of the endpoints $p^1{}_i$ and $p^1{}_j$ of the intersection $S \cap R$ of S with R if it is non-empty, and *empty* otherwise. The output is said to be the segment S clipped to R.

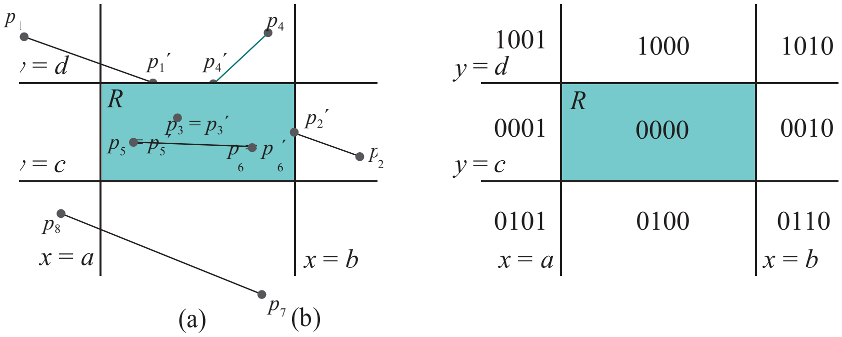

Figure 14.1: (a) A clipping rectangle R and four straight line segments with their parts clipped to R colored bold (b) Nine regions of the plane by outcode.

See Figure 14.1(a) for a diagram with four input segments with endpoints with labels of the form p_i, while their parts clipped to R are bold and have endpoint labels p_i^1; the output for $p_7 p_8$ is *empty*.

Outcodes and Trivial Termination

Critical to Cohen-Sutherland is a classification of points of the plane, according to their disposition with respect to the input rectangle R, by means of so-called outcodes. A point $p = (x, y)$ is said to have *outcode* the 4-bit string $k_3k_2k_1k_0$, whose value is determined by comparing the x- and y-values of p with those of the edges of R as follows:

- $k_0 = 0$, if $x \geq a$; $k_0 = 1$, if $x < a$
- $k_1 = 0$, if $x \leq b$; $k_1 = 1$, if $x > b$
- $k_2 = 0$, if $y \geq c$; $k_2 = 1$, if $y < c$
- $k_3 = 0$, if $y \leq d$; $k_3 = 1$, if $y > d$

It's easily seen that the four infinite straight lines, viz., $x = a$, $x = b$, $y = c$ and $y = d$, bounding R divide the plane into nine regions by outcode, as indicated in Figure 14.1(b): all points in each region have the outcode with which the region is labeled. For each of the lines $x = a$, $x = b$, $y = c$ and $y = d$, call the side of it containing R the *inside*, the other the *outside*. The line itself is included on its inside (so, e.g., the inside of $x = a$ is the closed half-plane $x \geq a$, while its outside is the open half-plane $x < a$). The rules above say, then, that each of the four lines determines one outcode bit of the four, which is 0 if the point is on its inside, 1 if it's outside.

Cohen-Sutherland begins with the first step of determining the outcodes o_i and o_j of the endpoints p_i and p_j, respectively, of the input segment S, using the rules above. The second step is to determine if one of the following two cases applies, when the algorithm can immediately return the answer and terminate:

(a) S lies entirely inside R. In this case, both outcodes o_i and o_j are 0000, which can be verified by performing the logical bitwise operation $o_i \vee o_j$ and checking that the result is false, i.e., 0000.

(b) S lies entirely outside one of the four straight lines bounding R. In this case, both outcodes must have a 1-bit in the same position, which can be verified by performing the operation $o_i \wedge o_j$ and checking that the result is true, i.e., *not* 0000.

If (a) holds, the algorithm *trivially accepts*, returning the endpoints of S itself; if (b) holds, it *trivially rejects*, returning *empty*.

Recursion

If the outcome of the second step is neither a trivial accept nor a trivial reject, then Cohen-Sutherland proceeds recursively as follows.

There exists a bit position where o_i and o_j differ for, otherwise, one of the cases (a) and (b) above would have occurred. Scan the bits of o_i and o_j from right to left to find the first (i.e., lowest) bit position, say the rth, where they differ. It follows that p_i and p_j lie on opposite sides of the infinite straight line bounding R, call it L, corresponding to the rth bit. Therefore, S intersects L and the algorithm calculates the point of intersection q. As they lie on opposite sides of L, exactly one of p_i and p_j lies inside L. The algorithm, then, calls itself recursively on the segment p_iq or p_jq, according as p_i or p_j is inside L. This is illustrated in the next example.

Example 14.1. Apply the Cohen-Sutherland algorithm to the segment p_1p_2 in Figure 14.1(a).

Answer : The rectangle R and segment p_1p_2 of Figure 14.1(a) are drawn separately in Figure 14.2. The outcodes of p_1 and p_2 are 1001 and 0010, respectively, and neither of the two conditions that terminate Cohen-Sutherland trivially holds.

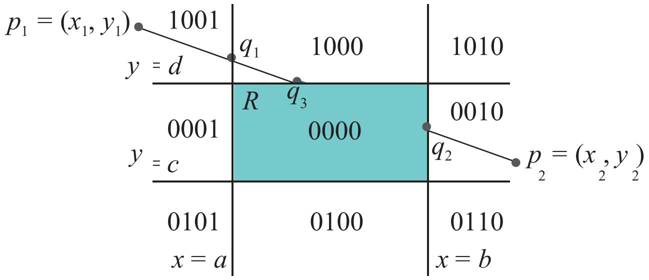

Figure 14.2: Cohen-Sutherland, called on segment p_1p_2, recursively calls itself on p_2q_1, q_1q_2 and q_2q_3, successively.

Scanning the bits of the two outcodes from right to left, they are seen to differ in the rightmost bit k_0, corresponding to the line $x = a$. Accordingly, the intersection q_1 of p_1p_2 with $x = a$ is determined. As p_2 lies inside $x = a$, a recursive call is made on the segment p_2q_1.

The outcodes of p_2 and q_1 are, respectively, 0010 and 1000. Again, there is no trivial termination. The rightmost bit at which the outcodes differ is k_1, so the intersection q_2 of p_2q_1 with $x = b$ is computed. As q_1 lies inside $x = b$, a recursive call is made next on the segment q_1q_2.

The outcodes of q_1 and q_2 are, respectively, 1000 and 0000. There is again no trivial termination. The rightmost bit the outcodes differ at is k_3, so the intersection q_3 of q_1q_2 with $y = d$ is computed. As q_2 lies inside $y = d$, a recursive call is made on the segment q_2q_3.

The outcodes of q_2 and q_3 are both 0000 and the call terminates trivially, returning q_2 and q_3.

Exercise 14.1. Apply Cohen-Sutherland to the other three segments in Figure 14.1(a).

Exercise 14.2. Show that the maximum number of times Cohen-Sutherland can recursively call itself on a single input segment is four. Give an example of a segment where, in fact, four calls are made.

Exercise 14.3. (**Programming**) Animate Cohen-Sutherland using OpenGL. Draw a fixed clipping rectangle R, but allow the user to specify the endpoints of an arbitrary segment. Subsequently, highlight its subsegments as they are recursively processed.

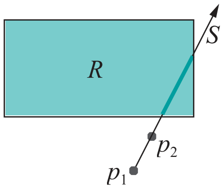

Figure 14.3: Clipping a semi-infinite segment to a rectangle.

The following two exercises extend Cohen-Sutherland.

Exercise 14.4. Extend Cohen-Sutherland to handle *semi-infinite* segments. A semi-infinite segment S is specified by one finite endpoint p_1 and another point p_2 in the *direction* of which it is infinite. See Figure 14.3.

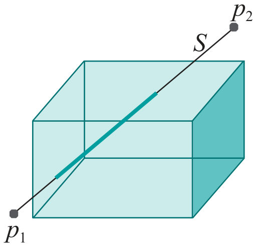

Figure 14.4: Clipping a line segment to an axis-aligned box.

Exercise 14.5. Extend Cohen-Sutherland to 3D: pseudo-code a 3D version to clip a straight-line segment S in 3-space against an axis-aligned box. See Figure 14.4. Obviously, 3D outcodes come into the picture. Extend your 3D clipper to handle semi-infinite segments as well.

3D Cohen-Sutherland (with refinements) is the clipper to be found in practical implementations of the OpenGL pipeline.

Complexity

The complexity of Cohen-Sutherland lies mainly in the intersection computation resulting if the logical operation on the outcodes in the second step fails to terminate the algorithm trivially. Suppose the endpoints of the input segment S are $p_1 = (x_1, y_1)$ and $p_2 = (x_2, y_2)$ as in Example 14.1 (see again Figure 14.2). The first intersection to be calculated is $q_1 = (a, y_3)$, where S and $x = a$ meet.

The slope-intercept form of the equation of the straight line on which S lies is

$$y = \frac{y_2 - y_1}{x_2 - x_1} x + x_1$$

assuming $x_1 \quad x_2$. Plugging $x = a$ into this equation we find

$$y = \frac{y_2 - y_1}{x_2 - x_1} a + x_1$$

Intersections of input segments with $x = b$, $y = c$ and $y = d$ can be found similarly as required.

If the input segments are pre-processed to determine their slope-intercept form, e.g., in the case above this entails pre-computing $\frac{y_2 - y_1}{x_2 - x_1}$, then, evidently, one floating point multiplication and one addition is performed per intersection finding.

Note: When pre-processing the slope-intercept form one has to be careful to check for vertical line segments, e.g., when $x_1 = x_2$ for the endpoints p_1 and p_2 above, for which this form is not defined. However, once detected, vertical segments are obviously easy to clip to any rectangle.

We know from Exercise 14.2 that a call to Cohen-Sutherland to clip an input segment spawns at most four more recursive calls. The conclusion then is that a call to Cohen-Sutherland may require four floating point multiplications and four additions for intersection computation per input segment in the worst case, which is fairly expensive. Refinements of Cohen-Sutherland, e.g., Liang-Barsky [88], invest in greater pre-processing in order to reduce subsequent intersection computation.

14.2 Sutherland-Hodgman Polygon Clipper

The Sutherland-Hodgman strategy for clipping a convex polygon P to a rectangle R is to successively clip off parts of P lying outside the four straight lines bounding R – the outside evidently being the side of the straight line not containing R. The process can be conceived of as a pipeline of four clippers, as in Figure 14.5.

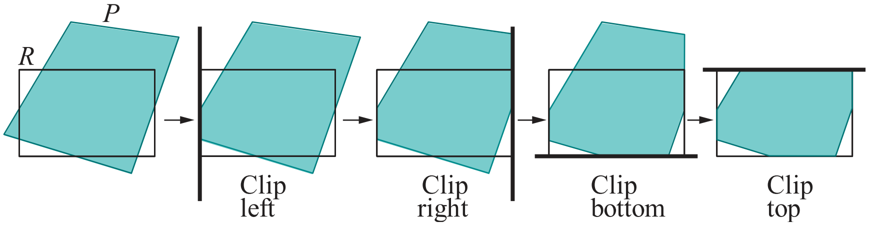

Figure 14.5: A pipeline of clippers.

Remark 14.2. There is no particular merit to the left-right-bottom-top ordering in Figure 14.5 – any other ordering could have been chosen.

The implementation of the four clippers is similar and we explain in detail only the leftmost one, which clips off outside the line bordering the left of R. In general, the input to this clipper is an ordered list $\{v_0, v_1, \ldots, v_n\}$ of the vertices of a convex polygon P and a vertical straight line L. See Figure 14.6. The output is an ordered list of vertices of the polygon P^1 resulting from clipping P off to the left of L.

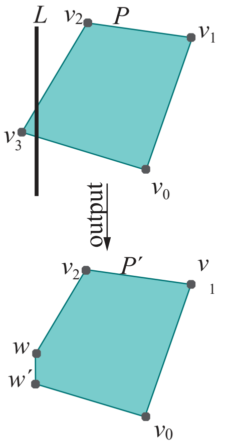

Figure 14.6: The left clipper in action: input = $\{v_0, v_1, v_2, v_3\}$, output = $\{v_0, v_1, v_2, w, w'\}$.

Output Rules for Left Clipper

The input list $\{v_0, v_1, \ldots, v_n\}$ of vertices is processed, in fact, in successive pairs, plus a final pair containing the first and last vertices, in particular, $v_0v_1, v_1v_2, \ldots, v_nv_0$. Equivalently, processing is edge by edge around the polygon P. Each edge outputs zero, one or two vertices to the output list. The output of an edge depends on the respective disposition of its end vertices with respect to L, in particular, if either is inside or outside L.

There is, therefore, a total of four possible dispositions. The four output rules, one corresponding to each disposition, are listed below. Refer to Figure 14.7 as you read (take v_{i+1} to be v_0, if v_i is v_n).

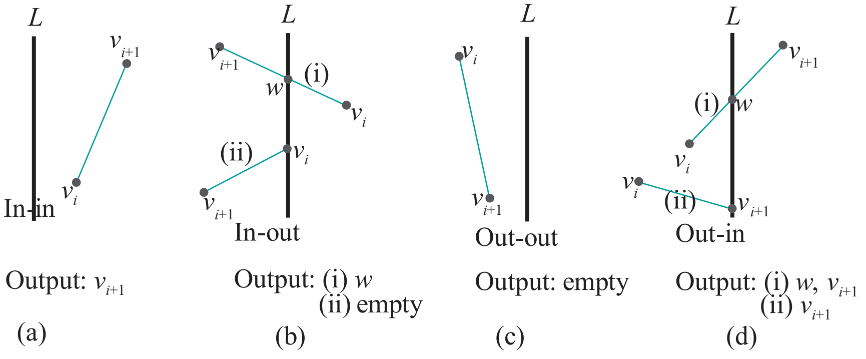

Figure 14.7: Output of an edge v_iv_{i+1} entering the left clipper. Note both in-out and out-in dispositions have two subcases: (i) where the vertex inside is properly on the inside of L, (ii) where the vertex inside lies *on* L.

(a) In-in: Both v_i and v_{i+1} are inside L. Output v_{i+1}.

(b) In-out: v_i is inside, while v_{i+1} outside L. There are two subcases, according as v_i lies right of L or on it:

(i) v_i is right of L: Output w, the point where the segment v_iv_{i+1} intersects L.

(ii) v_i lies on L: Output *empty*, i.e., zero vertices are output.

(c) Out-out: Both v_i and v_{i+1} are outside L. Output *empty*.

(d) Out-in: v_i is outside, while v_{i+1} inside L. There are two subcases, according as v_{i+1} lies right of L or on it:

(i) v_{i+1} is right of L: Output w, v_{i+1}, where w is the point where the segment v_iv_{i+1} intersects L (this is the only case when two vertices are output).

(ii) v_{i+1} lies on L: Output v_{i+1}.

Note: Rule (a) doesn't care if either v_i or v_{i+1} is on L or right of it.

Observe that, if L is $x = a$, it is easy to determine if a point is (strictly) inside, outside or on L by simply comparing its x-value with a. Therefore, it's easy as well to decide which of the four rules above to apply to each successive pair of vertices. We ask the reader next to determine the new vertex w, in case it arises, in the following exercise.

Exercise 14.6. Suppose $v_i = (x_i, y_i)$, $0 \leq i \leq n$, and L is the line $x = a$. Observe, from the rules above, that if a *new* vertex – one not belonging to the original input sequence – is at all output, then there is only one such. Give a formula to determine the new vertex.

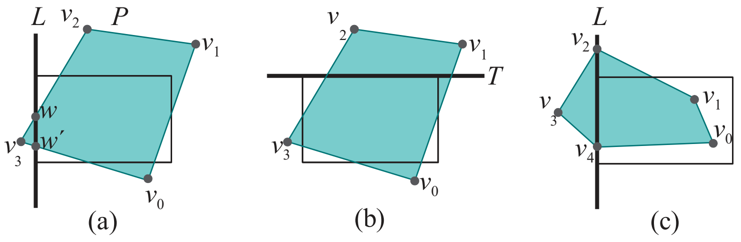

Figure 14.8: Applying the clipping rules.

Example 14.2. Let's apply the rules above to the initial polygon P, at the leftmost of Figure 14.5, and the vertical straight line L along the left edge of the rectangle R. See Figure 14.8(a). The output of successive vertex pairs is as follows:

$$\begin{array}{lcl}
v_0v_1 & \Rightarrow & v_1 \quad \text{(in-in)} \\
v_1v_2 & \Rightarrow & v_2 \quad \text{(in-in)} \\
v_2v_3 & \Rightarrow & w \ \text{(in-out (i))} \\
v_3v_0 & \Rightarrow & w^1, v_0 \quad \text{(out-in (i))}
\end{array}$$

Accordingly, the vertex list returned by the left clipper is $\{v_1, v_2, w, w^1, v_0\}$, which indeed is the sequence of vertices around the polygon resulting from clipping off the part of P outside L.

Exercise 14.7. Clip the initial polygon P of Figure 14.5 to the top, in other words, apply the top clipper to it first (see Figure 14.8(b)). Rules, similar exactly to those given already for the left clipper, apply to the top.

Exercise 14.8. Clip the polygon P of Figure 14.8(c) to the left.

Pipelining

Now that we understand the implementation of its individual clippers, we come to the beauty of the Sutherland-Hodgman algorithm: that it can be *pipelined* with all four clippers running in *parallel* , each one after the first using as input the output of its predecessor. This follows from observing that each clipper *incrementally* produces its output list as it *incrementally* consumes its input vertices. Therefore, the next clipper in the sequence does not have to wait till its predecessor completes processing – it can begin to operate *as soon* as it receives the first two vertices output by its predecessor.

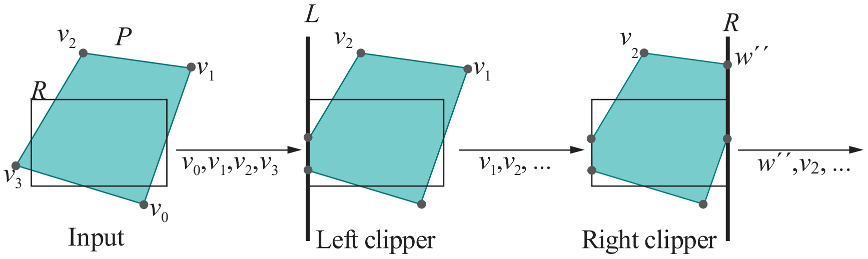

Figure 14.9: The right clipper consumes the first two vertices v_1 and v_2 entering into it from the left clipper to output $w^{!!}$ and v_2.

For example, we saw in Example 14.2 that the successive vertices output by the left clipper operating on P are $\{v_1, v_2, w, w^1, v_0\}$. Observe, now, that as soon as v_1 and v_2 enter the next clipper in the sequence – the right one according to the scheme in Figure 14.5 – the latter can process them to output w^{11}, v_2. See Figure 14.9, where the disposition of v_1 and v_2 with respect to L^1 is case (i) of out-in.

The Sutherland-Hodgman pipeline of four clippers is often implemented in hardware, the clippers being identical but separate modules.

Exercise 14.9. Assuming that each clipper takes unit time to perform the operation of applying one of the rules of Figure 14.7 to a pair of successive vertices and that vertices move from one clipper to the next in zero time, how long does it take for the clipping pipeline of Figure 14.5 to process the particular polygon P in that figure?

Exercise 14.10. (Programming) Code and creatively animate the Sutherland-Hodgman clipping pipeline.

Exercise 14.11. Extend Sutherland-Hodgman to 3D to clip a convex polygon against an axis-aligned box. This, in fact, is simpler than generalizing the Cohen-Sutherland line clipper to three dimensions, which we considered in Exercise 14.5, because the Sutherland-Hodgman output rules go through pretty much verbatim in one higher dimension, except that the part of the polygon to one side of a plane, rather than a line, is clipped off.

14.3 DDA and **Bresenham's** Line Rasterizers

Rasterization of a straight line segment consists of picking and coloring the pixels which will comprise it in the display window. However, both the DDA and Bresenham's line rasterizers we're going to study now only pick pixels. Coloring them, though, is a straightforward application of linear interpolation discussed in Chapter 7, except for the added twist of "perspective correction" needed in case of perspective projection, which we'll learn how to apply in Chapter 21. Selecting pixels then is the focus this chapter.

Let's take the raster to be a rectangular $m \times n$ grid of square pixels, each of side length one, located axis-aligned on a plane, so that the pixel centers have integer coordinates (i, j), $0 \leq i \leq m-1$ and $0 \leq j \leq n-1$. See Figure 14.10(a).

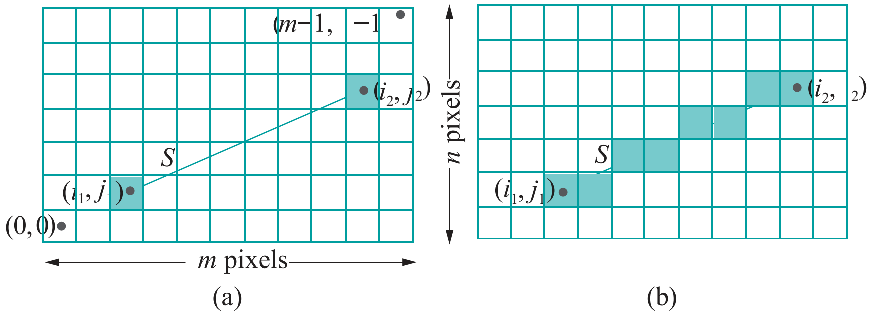

Figure 14.10: An $m \times n$ raster of pixels and a rasterized straight line segment.

We'll assume that both end vertices of an input segment S have already been projected and scaled onto the raster – shot on film and printed according to the analogy in the second chapter – so that they lie at the pixels centered at (i_1, j_1) and (i_2, j_2), respectively, as shown in Figure 14.10(a).

Note: Even though S is actually a segment in world space, we'll call its image on the raster as S as well – which of the two we mean should be clear from the context.

The rasterization task then is to choose the pixels between its two ends to represent S, as, say, in Figure 14.10(b). We can assume that one end of S lies strictly to the right of the other because, otherwise, either both ends are at the same pixel or one is vertically above the other, both cases being trivial to rasterize. Suppose, without loss of generality then, that (i_2, j_2) is to the right of (i_1, j_1), meaning $i_2 > i_1$. The line equation of S is:

$$\frac{y - j_1}{x - i_1} = \frac{j_2 - j_1}{i_2 - i_1} \quad \text{or} \quad y = m(x - i_1) + j_1 \tag{14.1}$$

where $m = \frac{j_2 - j_1}{i_2 - i_1}$ is the slope of S.

DDA Algorithm – Floating Point Heavy

We'll warm up with the very simple DDA (Digital Differential Analyzer) rasterization algorithm which Bresenham subsequently improves.

Remark 14.3. The rather fancy name Digital Differential Analyzer comes from Differential Analyzer, a class of mechanical machines invented in the 1800s to solve differential equations. A Digital Differential Analyzer, or DDA, is a digital version of the Differential Analyzer. The DDA line rasterizer implements an incrementing loop borrowed from the DDA, hence the name.

Suppose, first, that its slope m lies between -1 and 1, so that the input segment S makes an angle of at most 45° with the x-axis (as in Figure 14.10(a)). It's clear in this case that a rasterization of S should contain exactly one pixel per x-value within the x-span of S. Moreover, the equation on the right of (14.1) implies that the y-value along S increases by m as the x-value increases by 1. This motivates the following DDA algorithm:

```
// DDA Line  Rasterizer
// Assume i2 > i1 and -1 <= m <= 1
float y = j1;
float m = (j2 - j1)/(i2 - i1);
for (int x = i1; x <= i2; x++)
{
    pickPixel(x,  round(y));
    y += m;
}
```

Note: Due to obvious typesetting constraints we write variables such as i_1 and j_1 as i1 and j1 in the code snippet.

The algorithm starts with the pixel centered at (i_1, j_1), then increases the x-value by 1 and the y-value by m at each step, until x equals i_2. The function pickPixel(*, *) evidently chooses the pixel with its parameters as coordinates; in the routine above its y-value is rounded first to an integer so that a legitimate pixel center is picked.

Experiment 14.1. Run DDA.cpp, which is pretty much a word for word implementation of the DDA algorithm above. A point of note is the *simulation* of the raster by the OpenGL window: the statement gluOrtho2D(0.0, 500.0, 0.0, 500.0) identifies "pixel-to-pixel" the viewing face with the 500×500 OpenGL window (a "pixel" of the viewing face being a 1×1 square with corners at integer coordinates).

There's no interaction and the endpoints of the line are fixed in the code at (100, 100) and (300, 200). Figure 14.11 is a screenshot. End

Figure 14.11: Screenshot of DDA.cpp.

Exercise 14.12. (Programming) The restriction on the slope m in the DDA rasterizer can be removed by noting that a rasterization of S should contain exactly one pixel per y-value in its y-span, if it makes an angle of more than 45°, but at most 90°, with the x-axis.

Accordingly, rewrite DDA.cpp so that there are no restrictions at all and that it interactively accepts arbitrary input end vertices (i_1, j_1) and (i_2, j_2).

The problem with the DDA algorithm is that it invokes two floating point operations per loop iteration – an addition and a rounding – floating point operations being computationally expensive.

Bresenham's Algorithm – Eliminating Floating Points

Bresenham's algorithm avoids floating point operations altogether. Here's the idea in a nutshell. The algorithm incrementally picks one pixel after another starting with the left end vertex of S, the smarts being in using the location of the current pixel to cost-effectively deduce that of the next.

Assume first that the slope of S satisfies $0 < m < 1$; we'll handle other cases later. Given this constraint, there is exactly one pixel of S for each x-value within its x-span.

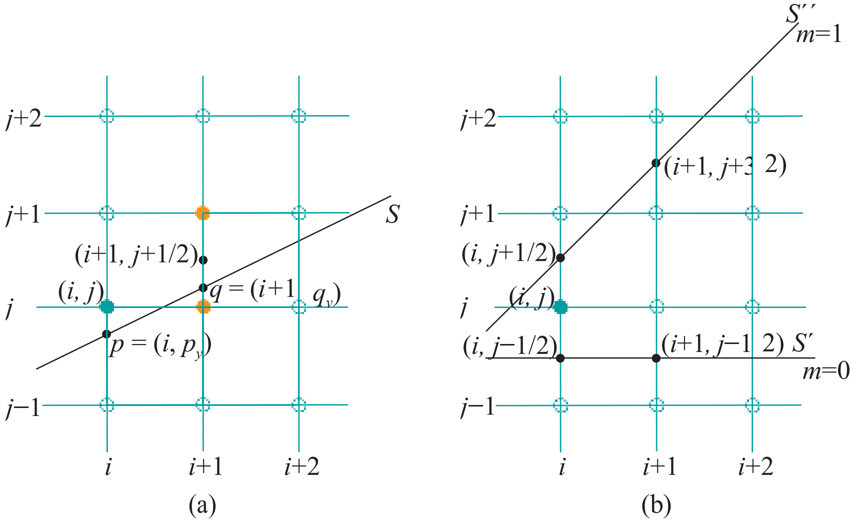

Figure 14.12: The larger circles are pixel centers. (a) Pixel (i, j) shown filled green has just been chosen, the two candidate pixels for the next step are filled orange (b) Diagram for Example 14.3.

Suppose that pixel (i, j) has just been picked – pixel (i, j) means, of course, the pixel centered at (i, j) – in the one-after-one selection process. See Figure 14.12(a), where only pixel centers are shown in a grid. One can assume that the point $p = (i, p_y)$ of the intersection of S with the line $x = i$ is at least as close to (i, j) as it is to the center of any other pixel on the line $x = i$, for, otherwise, pixel (i, j) would not have been chosen. In other words, $j - \frac{1}{2} \leq p_y \leq j + \frac{1}{2}$ (Figure 14.12(a) happens to $p_y < j$.) These inequalities, together with the condition $0 < m < 1$ on the gradient of S, imply that S intersects $x = i+1$ at the point $q = (i+1, q_y)$, where $j - \frac{1}{2} < q_y < j + \frac{3}{2}$, as we'll show next.

Example 14.3. Prove the inequalities claimed on q_y in the preceding statement.

Answer: Let the line S^1 go through $(i, j - \frac{1}{2})$ with gradient 0 and the line S^{11} go through $(i, j + \frac{1}{2})$ with gradient 1. See Figure 14.12(b), where S^1 and S^{11} are shown but not S. Since $j - \frac{1}{2} \leq p_y \leq j + \frac{1}{2}$ and $0 < m < 1$, S lies strictly between S^1 and S^{11} to the right of $x = i$, so intersecting $x = i+1$ at a point $q = (i+1, q_y)$ strictly between the points where S^1 and S^{11} intersect $x = i+1$. It's straightforward geometry to see that S^1 intersects $x = i+1$ at $(i+1, j - \frac{1}{2})$ and S^{11} intersects $x = i+1$ at $(i+1, j + \frac{3}{2})$. It follows that, indeed, $j - \frac{1}{2} < q_y < j + \frac{3}{2}$.

As $j - \frac{1}{2} < q_y < j + \frac{3}{2}$, the pixel to choose when x is incremented to $i+1$ is either $(i+1, j)$ or $(i+1, j+1)$, depending on which of the two is closer to q. Now, q is closer to $(i+1, j)$ if the midpoint $(i+1, j+\frac{1}{2})$ between the two candidate pixels is above S (the situation depicted in Figure 14.12(a)); on the other hand, it's closer to $(i+1, j+1)$ if the midpoint is below S.

Evidently, then, we need to determine the disposition of $(i+1, j+\frac{1}{2})$ with respect to S. So, how does one generally determine the disposition of some given point (x, y) with respect to S? Rewrite the equation of S, on the left of Equation (14.1), as

$$(i_2 - i_1)y - (j_2 - j_1)x + i_1 j_2 - i_2 j_1 = 0$$

Denote the LHS of the preceding equation by $D^1(x, y)$, i.e.,

$$D^1(x, y) = (i_2 - i_1)y - (j_2 - j_1)x + i_1 j_2 - i_2 j_1 \qquad (14.2)$$

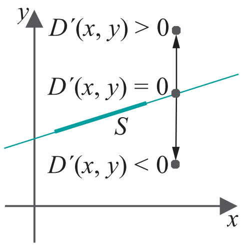

Figure 14.13: Discriminating the position of a point with respect to a segment: S is bold, while the straight line through it is thin.

Therefore, if (x, y) satisfies $D^1(x, y) = 0$, then the point (x, y) lies on the straight line containing S. In fact, it lies on S itself if, additionally, its x-value lies within the x-span of S. Furthermore, (x, y) lies above that straight line if $D^1(x, y) > 0$ and below if $D^1(x, y) < 0$ (see Figure 14.13).

Exercise 14.13. Verify the claim made in the last statement.

Hint: Consider a point (x, y) lying on the straight line containing S, so that $D^1(x, y) = 0$. If only its y-value is increased to raise it above the line, then the value of $D^1(x, y)$ increases because the coefficient of y in the formula (14.2) for $D^1(x, y)$ is positive.

For a reason which will soon be apparent, we'll use

$$D(x, y) = 2D^1(x, y) = 2(i_2 - i_1)y - 2(j_2 - j_1)x + 2(i_1 j_2 - i_2 j_1) \qquad (14.3)$$

whose sign is always the same as that of $D^1(x, y)$, as the *discriminant* to determine the disposition of (x, y) with respect to the straight line on S.

Returning to the question of which of the candidate pixels $(i+1, j)$ or $(i+1, j+1)$ to choose when $x = i+1$, we see the answer now as:

- Choose $(i+1, j)$ if $D(i+1, j+\frac{1}{2}) > 0$ (when the midpoint $(i+1, j+\frac{1}{2})$ between the candidate pixels lies above S, implying that S is closer to the center of the lower one).
- Choose $(i+1, j+1)$ if $D(i+1, j+\frac{1}{2}) < 0$ (complementary to the first case).
- Choose $(i+1, j+1)$ if $D(i+1, j+\frac{1}{2}) = 0$ (this choice being made arbitrarily as S is equidistant from the centers of both candidates).

We near the crux of Bresenham's algorithm, which is to use the old value of D to compute its new value after x is incremented once again to $i+2$. There are two cases:

(a) $D(i+1, j+\frac{1}{2}) > 0$, which implies, according to the pixel-choosing process just described, that $(i+1, j)$ was chosen when $x = i+1$.

Repeating the reasoning that took us from $x = i$ to $x = i+1$, we see that the two candidate pixels when $x = i+2$ are $(i+2, j)$ and $(i+2, j+1)$; moreover, $(i+2, j)$ is chosen if $D(i+2, j+\frac{1}{2}) > 0$ and $(i+2, j+1)$ if $D(i+2, j+\frac{1}{2}) \leq 0$. As for the new value of the discriminant, we ask the reader to verify from (14.3) that it can be calculated from its previous value by:

$$D(i+2, j+\frac{1}{2}) = D(i+1, j+\frac{1}{2}) - 2(j_2 - j_1) \qquad (14.4)$$

(b) $D(i+1, j+\frac{1}{2}) \leq 0$, which implies that $(i+1, j+1)$ was chosen when $x = i+1$. The two candidate pixels when $x = i+2$ are now $(i+2, j+1)$ and $(i+2, j+2)$; moreover, $(i+2, j+1)$ is chosen if $D(i+2, j+\frac{3}{2}) > 0$ and $(i+2, j+2)$ if $D(i+2, j+\frac{3}{2}) \leq 0$. Again, we ask the reader to verify that:

$$D(i+2, j+\frac{3}{2}) = D(i+1, j+\frac{1}{2}) + 2(i_2 - i_1 - j_2 + j_1) \qquad (14.5)$$

We are now at the crux of Bresenham's algorithm: Equations (14.4) and (14.5) together say how D changes as x is incremented by 1. It only remains to get the algorithm started by initializing D. The first pixel picked is at the left endpoint (i_1, j_1) of S. Accordingly, the candidate pixels for the next value of x, namely, $x = i_1 + 1$, are (i_1+1, j_1) and (i_1+1, j_1+1), whose midpoint is $(i_1, j_1+\frac{1}{2})$. Therefore, the first value of D is

$$D(i_1+1, j_1+\frac{1}{2}) = i_2 - i_1 - 2(j_2 - j_1) \qquad (14.6)$$

using (14.3). It's here that taking $D(x, y) = 2D^1(x, y)$, rather than $D^1(x, y)$ itself, pays off because $D^1(i_1+1, j_1+\frac{1}{2}) = \frac{1}{2}(i_2 - i_1) - (j_2 - j_1)$ may be fractional (remember, we want to stay away from floating points).

With (14.4)-(14.6) all pieces now are in place to implement Bresenham's strategy: initialize D using (14.6) and then successively increment it with the help of (14.4)-(14.5), picking at each step the next pixel based on the sign of D. Here's code:

```
// Bresenham's Line Rasterizer
// Assume i2 > i1 and 0 < m < 1
int y = j1;
int diff1 = -2*(j2 - j1);
int diff2 =  2*(i2 - i1 - j2 + j1);
int D = i2 - i1 - 2*(j2 - j1);
for (int x = i1; x <= i2; x++)
{
    pickPixel(x, y);
    if (D > 0) D += diff1;
    else {y++; D += diff2;}
}
```

Compare this with the DDA algorithm earlier which required floating point rounding and addition – there's nary a floating point value in sight in Bresenham's procedure! Bresenham is extremely efficient and, often, implemented in the graphics card itself for even higher rendering speeds.

Exercise 14.14. Use Bresenham's Line Rasterizer as coded above to pick the pixels on the straight line segment joining pixel centers (9, 17) and (25, 25).

Part answer : We'll get the reader started. Set $(i1, j1) = (9, 17)$ and $(i2, j2) = (25, 25)$ in the code above. Accordingly,

$$\begin{aligned} diff1 &= -2 * (j2 - j1) = -16 \\ diff2 &= 2 * (i2 - i1 - j2 + j1) = 16 \\ D &= i2 - i1 - 2 * (j2 - j1) = 0 \quad \text{(initially)} \end{aligned}$$

The first pixel picked is the left endpoint $(9, 17)$. As $D = 0$, the next pixel picked is $(10, 18)$ and D changes to $D + diff2 = 16 > 0$. Therefore, the next pixel picked is $(11, 18)$ and D changes to $D + diff1 = 0, \ldots$.

The reader should sketch the rasterization on graph paper and verify that it indeed starts and ends at the given endpoints.

Exercise 14.15. (Programming) We ask the reader now to implement Bresenham's algorithm, simulating the raster using the OpenGL window, as in DDA.cpp. Remove, as well, the assumptions in our formulation of Bresenham's algorithm. In particular, allow the two input end vertices (i_1, j_1) and (i_2, j_2) to be arbitrary.

Moreover, ensure that your program is not sensitive to the order that the end vertices are input. In other words, the rasterization should be identical if (i_1, j_1) and (i_2, j_2) are swapped in the routine. This is as a user would expect: it should not matter in what order the end vertices happen to appear in the segment definition in code.

14.4 Scan-Based Polygon Rasterizer

We'll describe a commonly-implemented scan-based rasterization algorithm to draw a polygon, or *fill* it, as is commonly said, because pixels comprising the interior of the polygon are selected (oddly enough, a selected pixel is often said to be filled too, as it is "filled" with the color values of the polygon).

The notion of scanning arises from CRT technology where an electron gun repeatedly scans the screen, pixel row by pixel row. One row of pixels is called a *scan line*. Although rasterization algorithms are implemented when filling pixels in the frame buffer and have nothing to do with the front-end display technology, this particular algorithm for polygon rasterization happens to mimic the scan process, hence the CRT reference.

A central part of the scan-based algorithm is to use the so-called *parity test*, also called the *inside-outside test* , to determine if a point lies inside or outside a polygon P.

Parity Test

Here's the idea behind the test. Suppose P is a simple planar polygon, i.e., one which lies on a plane and whose boundary is a single line loop which doesn't self-intersect. Let q be a point known to lie outside P (possibly, by choosing q's x- or y-value to be very large). Now, suppose we wish to determine if another given point p lies inside or outside P . Consider the ray R from q to p. The ray, obviously, starts from outside P . Upon its first intersection (if any) with the boundary of P , R enters P ; upon its second intersection with the boundary of P , it exits P ; upon its third intersection, it re-enters P; and so on. See Figure 14.14.

This leads to the following test to decide if p lies inside P or outside.

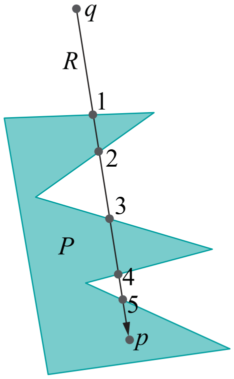

Figure 14.14: Intersections of R with the boundary of P are labeled with their respective ranks.

Parity Test : If the ray R from a point q, known to lie outside P , to some given point p, intersects the boundary of P an odd number of times, then p lies inside P , while if it intersects the boundary of P an even number of times, then P lies outside P . We assume, when applying the parity test, that p itself does not lie *on* the boundary of P , i.e., it is either inside or outside.

The parity of the number of intersections of R with the boundary of P, odd or even, is often called the *parity* of p. So the parity test may be rephrased to say that points of odd parity lie inside P, while those of even parity outside.

Note: If R does not intersect the boundary of P at all, then P's parity is that of zero, which is even, and, of course, p lies outside P.

Exercise 14.16. For the five points p_1, p_2, p_3, p_4, p_5 in Figure 14.15, use the parity test to verify where they lie with respect to P. The rays from an outside point q are already drawn.

Consider how you would reconcile the singularities seen in the case of p_3 and p_4 – note, in particular, how the rays from q to these two points intersect P – with the parity test as stated above. We'll be discussing this matter in some detail momentarily.

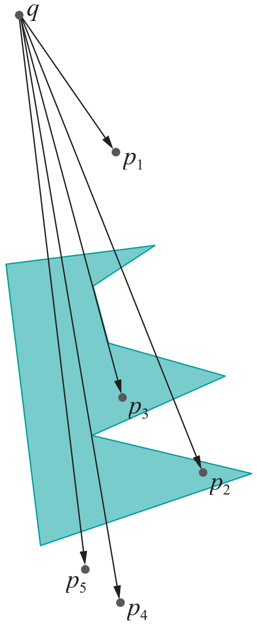

Figure 14.15: Testing parity: the points p_3 and p_4 require handling a singularity.

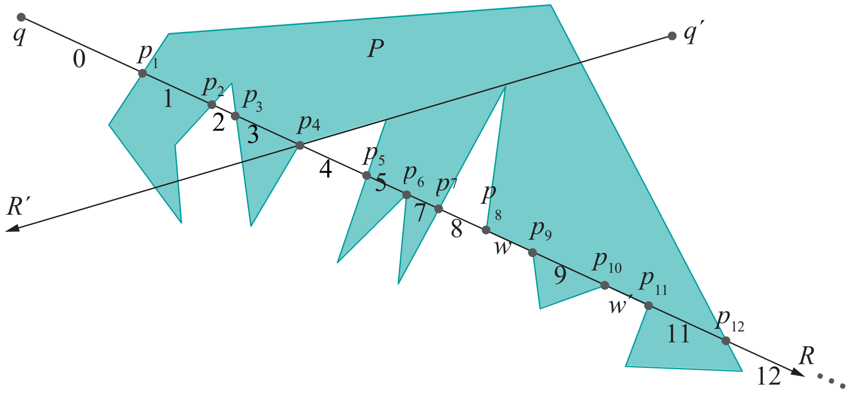

Figure 14.16: Applying the parity test: the integer label beneath a segment of R indicates the number of intersections of R with the boundary of P prior to reaching that segment.

See Figure 14.16. The integer label beneath each segment of the semi-infinite ray R from q indicates the number of intersections of R with the boundary of P before it reaches that segment – modulo a few conventions to be discussed. Therefore, all points in the *interior* of a segment share the same parity, that of its number (the restriction to the interior is to avoid endpoints lying on the boundary of P, whose parity is not defined). For example, points in the interior of qp_1 have even parity, those in the interior of p_1p_2 odd parity, and so on. The segments w and w^1 are not numbered because they each lie entirely on the boundary.

One has to be careful, evidently, when counting intersections, to take into account edges such as w and w^1 lying all on R, as well as points such as p_6 where the ray intersects a vertex of the polygon. Here are the conventions to follow, and which have been followed in Figure 14.16, to ensure that these singularities are handled correctly.

Conventions for Singularities:

(a) When the ray R passes through a vertex v, but neither of the edges adjacent to v lie along R, there are two cases:

(i) these two edges lie on opposite sides of R, when v is a proper intersection point and counted once (p_4 in Figure 14.16, explaining the difference of 1 in the edge numbers on either side of p_4);

(ii) these two edges lie on the same side of R, when R *touches* P at v, and v is counted as two intersections (p_6, explaining the difference of 2 in the edge numbers on either side of p_6).

(b) When the ray R passes through a vertex v and *one* of the edges, say e, adjacent to v lies along R (we'll assume that successive edges of P are never collinear, so that both edges adjacent to v cannot lie on R):

(i) the two edges adjacent to e lie on opposite sides of R, in which case count the entire edge e as one intersection (edge w in Figure 14.16, explaining the difference of 1 in the edge numbers before and after w);

(ii) the two edges adjacent to e lie on the same side of R, in which case count the entire edge e as two intersections (w^1, explaining the difference of 2 in the edge numbers before and after w^1).

In other words, case (b) is the same as (a) if one imagines e as one giant vertex.

The reader can now check in Figure 14.16 if indeed the parity of the segments of R identify correctly whether points in their interior lie inside or outside P.

Exercise 14.17. Label the segments of the ray R^1 emanating from the point q^1 in Figure 14.16 following the conventions for singularities, just like R, and verify the correctness of the parity test.

Exercise 14.18. (Programming) Implement the parity test. Allow the user to select a polygon P , as well as a test point p, by clicking on the OpenGL window. Automatically choose a point q outside P . Then display the working of the test with some creative animation.

It's easy now to explain the strategy of the scan-based polygon-filling algorithm. Each scan line in the context of the algorithm is imagined to be horizontal ray starting to the left of a row of pixels and heading right, pixels along it chosen to fill a given polygon P according to the parity test (Figure 14.17 shows one such scan line). In particular, each scan line is split into segments, each with endpoints at intersections with the boundary of P . Moreover, pixels in one segment all have the same parity. The result is alternate runs of pixels filling and not filling P.

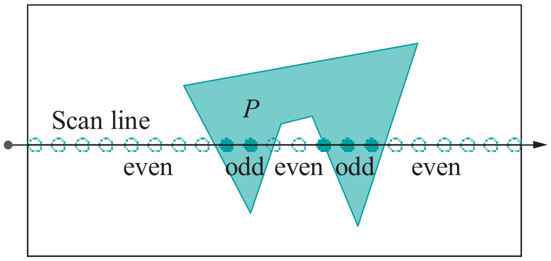

Figure 14.17: The scan line as a ray with parities along segments indicated, (solid) pixels filling the polygon according to the parity test. Two boundary pixels are filled according to the edge ownership rule discussed further in the text.

Before we proceed to specify exactly a scan-based polygon filling algorithm, we need first to resolve how to deal with pixels which happen to lie on the boundary of a polygon, whose parity, therefore, is indeterminate. We do this next.

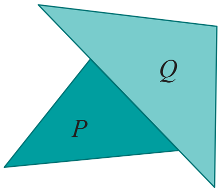

Figure 14.18: Abutting polygons.

Ownership of Boundary Pixels

One must be cautious in scan-based filling about pixels lying *on* the boundary of a polygon. For example, given a couple of *abutting* polygons – ones whose edges overlap, e.g., P and Q in Figure 14.18 – one has to decide ownership of the pixels along the overlapping part, which, in turn, decides the coloring of these pixels. Clearly, it is desirable to do this in a consistent manner, independent of the order in which the polygons happen to appear in the code.

For example, if each polygon coming down the OpenGL pipeline is awarded ownership of all its boundary pixels, then the color of shared boundary pixels depends, in fact, on the order in which the abutting polygons appear in the code, the color of the one coming last prevailing. At the other extreme, if boundary pixels are excluded altogether from a polygon, then gaps may arise in the rendering.

If one follows the rules of triangulation as described in Chapter 8, then there will be no anomalies, as we saw then, if every triangle simply owns its boundary. However, the intention here is to set up rules robust enough to hold in all situations, even in the case of an invalid triangulation as in Figure 14.18. A simple and oft-implemented rule to resolve the ownership of a polygon's boundary and, therefore, boundary pixels, is the following:

Edge Ownership Rule: Among its non-horizontal edges, a polygon owns only the *left* edges, while, among its horizontal edges, it owns only the *bottom* ones.

Note: A left edge of a polygon is one such that its interior lies to the right of the edge. Keep in mind that a left edge does not have to be physically located at a left extreme of the polygon. Similar remarks apply to right, bottom and top edges. Figure 14.19 labels the edges of the (lightly-colored) polygon P accordingly.

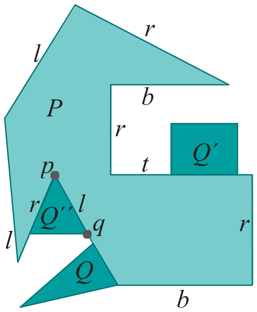

Figure 14.19: The non-horizontal edges of P are labeled left (l) or right (r), while the horizontal ones top (t) or bottom (b).

In Figure 14.19, by the edge ownership rule, P owns the pixels on the part of the edge it shares with Q, while those on the part of the edge it shares with Q^1 are owned by the latter. The two pixels in Figure 14.17 on the boundary of the polygon P have been processed according to this rule as well.

The rule above does not resolve the ownership question in every case. Ambiguities remain, e.g., the vertex p in Figure 14.19 is on a left (and a right) edge of both P and Q^{11}, which means both polygons have a claim to it; likewise, the reader may see that the ownership of q is in dispute, too.

Obviously, then, the edge ownership rule needs to be enhanced to handle such cases. This is left to the particular implementation of OpenGL as the API specs themselves do not lay down any laws. However, we'll leave the reader to convince herself with a few sketches that such singular points as p and q will likely be rare if the primitives are triangles or even convex polygons (as we recommend all drawn polygons to be; note that P isn't convex), and, of course, there'll be no such singularities at all if the entire drawing is a valid triangulation (as is our best recommendation). Therefore, the way an OpenGL implementation chooses to resolve the coloring of the few pixels corresponding to such singular points should not have much impact visually even, say, on a non-HD 1024 × 768 monitor.

Exercise 14.19. If the expected ambiguity in edge color did not arise in Exercise 8.3, then say how this may be explained by the edge ownership rule above.

14.4.1 Algorithms

Assume that P is a simple polygon input as the list of its edges, each edge specified by the coordinates of its end vertices. Here's a first cut at an algorithm to rasterize P:

Scan-based Polygon-filling Algorithm (Version 1)

```
for each scan line s
{
    1. for each non-horizontal edge e of P intersecting s
          determine and output the intersection between s and e;
    2. sort the intersection points output by the preceding step
       from left to right along s in a list $p_1, \dots, p_k$;
    3. fill, as belonging to P, pixels strictly between each of the pairs
       $p_1$ and $p_2$, $p_3$ and $p_4$, ...;
    4. if a pixel coincides with a $p_i$, which means it's a boundary pixel,
       fill it or not according as $i$ is odd or even;
    5. for each horizontal edge $e$ intersecting $s$
          include/exclude $e$ according as it is a bottom/top edge;
}
```

Note: Identical intersection points output by statement 1 can be arbitrarily sorted amongst themselves in statement 2.

The reader will agree that this algorithm is at least an honest attempt to implement the scan-based strategy: the first three statements inside the bracketed for loop apply the parity test to select alternate runs of pixels to fill, while the fourth statement applies the edge ownership rule to left and right edges, and the fifth applies it to bottom and top edges.

However, upon a more careful examination, Version 1 is seen to have three significant flaws:

(1) When a scan line passes through a vertex whose adjacent edges are non-horizontal and lie on either side of the scan line, that vertex is output twice as an intersection point by the for loop of statement 1, in violation of clause (i) of convention (a) for singularities listed earlier. (Outputting a vertex twice, though, if its adjacent non-horizontal edges are on the same side of the scan line is in accordance with the convention.)

For example, in Figure 14.20(a), the sorted list of intersection points for scan line s is $\{p_1, p_2, p_3, p_4, p_5\}$, where p_3 (= p_4) appears twice on the list, once as an intersection with the edge e and once as an intersection with edge e^1, leading to pixels between p_4 and p_5 being wrongfully left unfilled by statement 3.

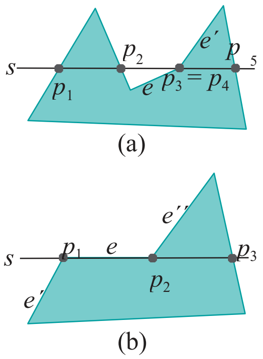

(a)

(b)

Figure 14.20: Problems with Version 1.

(2) If a pixel coincides with more than one p_i – in particular, if it's at a vertex adjacent to two non-horizontal edges – how do we decide to include/exclude it when executing statement 4?

For example, in Figure 14.20(a), do we treat the pixel at the vertex shared by e and e^1 as a p_i with an odd subscript (i.e., p_3), or even subscript (p_4), at the time of processing statement 4?

(3) There may be ambiguity in rendering pixels along a horizontal edge because its vertices are those as well of its non-horizontal neighbors and will be processed as such for the scan line upon which it lies.

For example, in Figure 14.20(b), pixels in the interior of the horizontal edge e (strictly between p_1 and p_2) are filled when processing scan line s at statement 3, because s's sorted list of intersections is $\{p_1, p_2, p_3\}$. However, when processing e itself at statement 5, we find that these pixels should be excluded, as e is a top edge.

It looks like rescuing Version 1 will be tricky, but it turns out, in fact, that a fix is not hard at all. Just add in the following two rules:

(i) For a non-horizontal edge, don't list the intersection of a scan line with the upper endpoint of that edge.

(ii) Don't process horizontal edges at all.

That's it! Here's the amended algorithm.

Scan-based Polygon-filling Algorithm (Version 2)

```
for each scan line $s$
{
    1. for each non-horizontal edge $e$ of $P$ intersecting $s$ determine
       the intersection point between $s$ and $e$ and output it if it is
       *not* the upper endpoint of $e$;
    2. sort the points from the preceding step from left to right along $s$
```

```
        in a list $p_1, \dots, p_k$;
3.      fill, as belonging to $P$, pixels *strictly* between each of the pairs
        $p_1$ and $p_2$, $p_3$ and $p_4$, ...;
4.      if a pixel coincides with a *single* $p_i$, which means it's a boundary
        pixel, fill it or not according as $i$ is odd or even;
5.      if a pixel coincides with *more than one* $p_i$, which also means it's
        a boundary pixel, fill it;
}
```

We'll soon see why this version is correct, but let's take it for a spin first. Figure 14.21 shows how many times each intersection point along the boundary of a polygon P is output by statement 1 of Version 2, which, of course, is the number of times it appears in the sorted list made by statement 2. Based on these labels is an exercise next to run the new version (with a part answer).

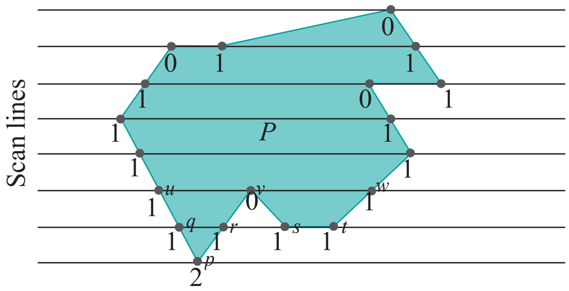

Figure 14.21: Eight scan lines showing their intersections with the polygon boundary and the number of times each intersection point is output by statement 1 of algorithm Version 2. Not all vertices and intersection points are not named to avoid clutter.

Exercise 14.20. Describe how pixels are filled along each of the eight scan lines drawn in Figure 14.21 by Version 2.

Part answer: We'll assume first that all the vertices of P are located exactly at pixels.

Bottom scan line: The sorted list on this scan line, after statements 1 and 2, is $\{p, p\}$. The pixel at p is filled by statement 5; all others on the scan line are not.

Second scan line: The sorted list (statements 1 and 2) is $\{q, r, s, t\}$. All pixels strictly between q and r and strictly between s and t are filled (statement 3). If there is a pixel at q, it is filled (statement 4). The pixel at s is filled (statement 4 again). All other pixels on the scan line are not filled.

Third scan line: The sorted list (statements 1 and 2) is $\{u, w\}$. All pixels strictly between u and w are filled (statement 3). (This means the pixel at v is filled.) If there is a pixel at u, it is filled (statement 4). All other pixels on the scan line are not filled.

As the reader may have surmised from completing the exercise, the new version gets past the three problems of the earlier one as follows:

(1) Ignoring upper endpoints eliminates the first flaw.

(2) If pixel coincides with more than one p_i then it must be included, removing the ambiguity underlying the second flaw.

(3) Noting that the pixels on a horizontal edge lie, as well, between the endpoints of the two non-horizontal edges adjacent to it suggests that we can leave off separately processing horizontal edges altogether. Version 2 does so, resolving the last flaw.

Exercise 14.21. How are the problems with Version 1, as indicated particularly in Figures 14.20(a) and (b), resolved in Version 2?

14.4.2 Optimizing Using Edge Coherence – Active Edge List

Version 2 is pretty much ready to go as long as a couple of statements requiring efficient implementation in code are kept in mind: in particular, statements 1 and 2 to determine and sort the intersection points of a scan line with polygon edges. Doing these two tasks from scratch per scan line – which wouldn't be efficient at all – can be avoided if one exploits so-called *edge coherence*.

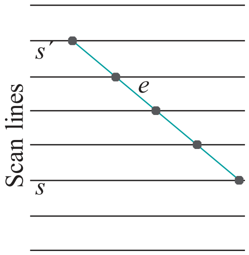

Figure 14.22: Edge coherence.

This simple but very useful concept is illustrated in Figure 14.22, which shows an edge e straddling a run of scan lines. Now, if scan lines are processed in order, say from bottom to top, then e first appears in the intersection list for scan line s, remains in the intersection list for each scan line until s^1 and then disappears forever. Moreover, the intersection of e with successive scan lines clearly travels uniformly along the x-direction.

Consideration of edge coherence leads to the creation and maintenance of a particular dynamic data structure, called the *active edge list* (AEL). The AEL is a linked list of records, one record for each non-horizontal edge e which intersects the *current* scan line s – hence the qualifier "active", the AEL changing from scan line to scan line – *below* e's upper endpoint. The record for an edge e contains three data items:

1. The y-value of the upper endpoint of e.

2. The reciprocal $1/m$ of e's gradient (as e can't be horizontal, m 0).

3. The x-value of the intersection of e with s.

The reason for choosing these particular items will become apparent as we learn to process the AEL. The AEL, additionally, is sorted according to the left to right order of the intersections of its member edges with s, a left edge (of the polygon) preceding a right one if their intersections with s coincide. Observe that the first two items of each record are static, depending only on the particular edge e, while the value of the third item varies as s sequences through successive scan lines.

See Figure 14.23, which shows a polygon P in a 19 × 11 raster, as well as the AEL values at scan lines 0, 4 and 5. For example, the data values in the first record of the bottom configuration arise because it corresponds to the edge joining vertices at (12, 7) and (13, 0), the reciprocal of whose gradient, therefore, is $1/7$ -0.143, and which intersects scan line 0 at x-value 13.

Exercise 14.22. Verify the data items in every record of each of the three AEL values shown in Figure 14.23.

Exercise 14.23. Calculate the AEL value at scan line 7 (mind upper endpoints).

What is important now is that given the value of the AEL for a scan line s, it's straightforward to apply Version 2 to compute the runs of filled pixels along s by traversing the AEL from left to right, reading off the third data value from successive records.

Initialization – Edge Table

All that's left to do, then, is initialize the AEL data structure and say how to update it from scan line to scan line. To this end, a bit of pre-processing first is needed to put the non-horizontal edges of the input polygon P into a data structure called the *edge table* (ET).

The ET is an array of linked lists, one for each scan line. The linked list for a scan line consists of one record for each non-horizontal edge which has a lower endpoint on that scan line. Each record is exactly similar in structure to an AEL record and, in fact, the first two data items are identical – the y-value of the upper endpoint of e and the reciprocal $1/m$ of e's gradient – while the third contains the x-value of the lower

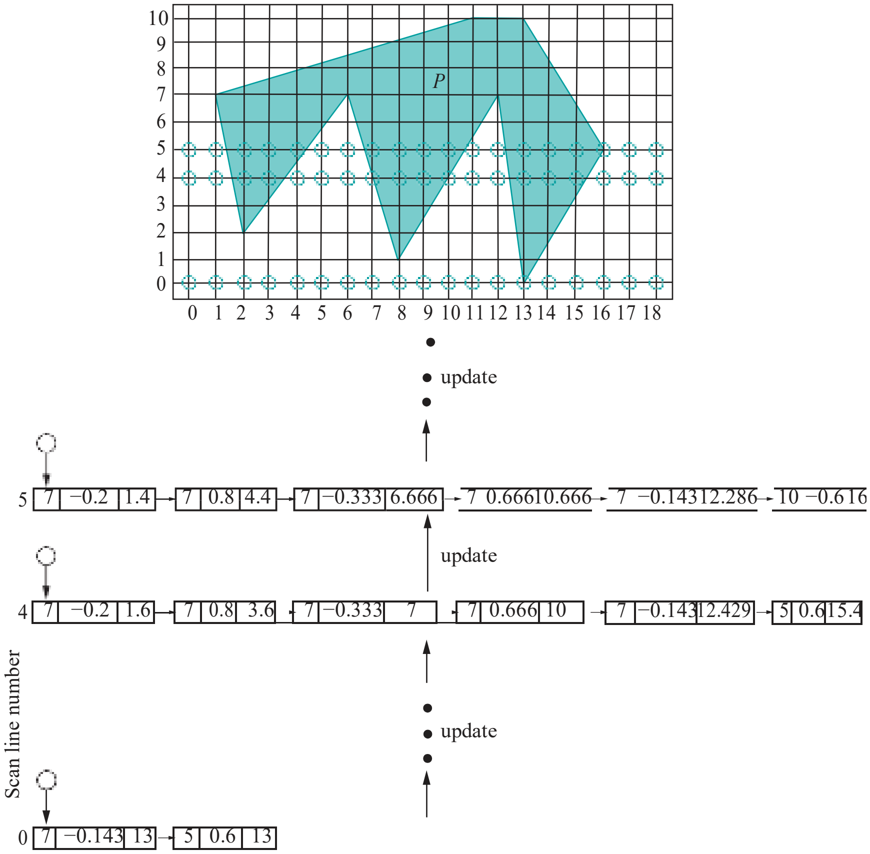

Figure 14.23: The AEL values at scan lines 0, 4 and 5 for a polygon P in a 19 × 11 raster (end null pointers not shown). Pixels are drawn as hollow circles only for these three scan lines.

endpoint of the edge. Moreover, records in each list are sorted in increasing order of their corresponding lower endpoints, with a left polygon edge again preceding a right one if their lower endpoints coincide. Of course, the list for a scan line on which no non-horizontal edge has a lower endpoint is empty.

Figure 14.24 shows the ET for the polygon P of Figure 14.23. The ET is evidently a static data structure created easily from a bucket sort of the non-horizontal edges keyed on their lower y-value.

Processing the AEL

With the ET in hand, processing the AEL is straightforward. Set $j = -1$, the number of an imaginary scan line just below the drawing area and initialize the AEL to empty. To update the AEL from scan line j to scan line $j + 1$, do the following:

```
Updating the AEL
for each record in the AEL successively from left to right
{
        1. if the first data value (i.e., the $y$-value of the upper endpoint of the
        corresponding edge) equals $j + 1$, delete the record;
        2. else, update the third data value (i.e., the $x$-value of the intersection
        of the edge with the scan line) by adding to it the second data value
        (i.e., the reciprocal of the edge's gradient);
}
if the ET list for scan line $j + 1$ is not empty, merge that list with the AEL using the
third data value as the key;
```

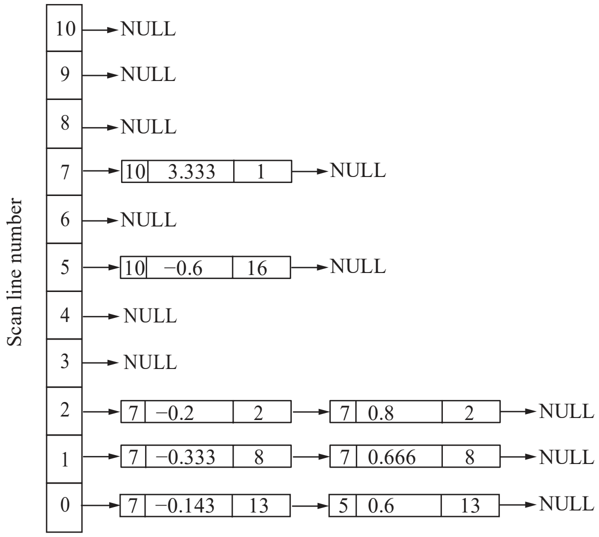
Scan line number
10 NULL
9 NULL
8 NULL
7 | 10 | 3.333 | 1 | NULL
6 NULL
5 | 10 | −0.6 | 16 | NULL
4 NULL
3 NULL
2 | 7 | −0.2 | 2 | 7 | 0.8 | 2 | NULL
1 | 7 | −0.333 | 8 | 7 | 0.666 | 8 | NULL
0 | 7 | −0.143 | 13 | 5 | 0.6 | 13 | NULL

Figure 14.24: Edge table for the polygon P of Figure 14.23.

The reader is asked next to prove the one fact required to assure the validity of the AEL update procedure.

Exercise 14.24. Show that the third data value is correctly computed for each record in the new AEL by the update procedure.

Exercise 14.25. Refer to Figure 14.23. Apply the update procedure to compute the AEL values for scan lines 0 through 7.

Exercise 14.26. Write pseudo-code to expand the Scan-based Polygon-filling Algorithm (Version 2) to include both initialization of the ET and subsequent AEL-driven processing. Apply this algorithm to fill the pixels in P on scan lines 0, 4 and 5 of Figure 14.23.

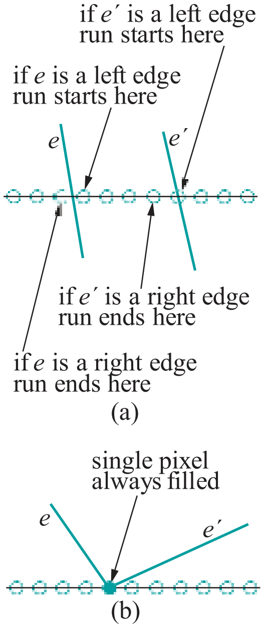
if e' is a left edge run starts here
if e is a left edge run starts here
e
e'
if e' is a right edge run ends here
if e is a right edge run ends here
(a)
single pixel always filled
e
e'
(b)

Figure 14.25: (a) Typical dispositions of a left and right edge with respect to a run of pixels (b) The one exceptional case where a left and a right edge meet at a common lower endpoint.

If you're coming to this polygon-filling algorithm fresh from Bresenham's line rasterizer, then alarm bells are probably going off in your head right now about floating point computation. And rightly so. The update procedure for the AEL as just described does require a floating point addition in its step 2 to update a record. This, in fact, can be avoided by optimizing the implementation. We'll let you figure out how in the next exercise.

Exercise 14.27. To cut floating points from Version 2, observe that, generally, a run of filled pixels along a given scan line s will (1) start at the intersection of a left edge e with s if there is a pixel at the intersection or, if not, at the pixel just after the intersection, *and* (2) end at the pixel before the intersection of a right edge e with s, even if there is a pixel at the intersection. See Figure 14.25(a). The one exceptional case – easily detected – is shown in Figure 14.25(b).

Therefore, instead of the floating point x-value, call it X, of the intersection of a segment e with a scan line s, one can store in AEL records the smallest integer greater than or equal to X if e is a left edge, or the largest integer strictly less than X if it is a right edge.

Accordingly, suggest a new form of the AEL with no floating point data items and a method to update it.

Remark 14.4. Primitive rasterization in OpenGL is particularly simple as it entails rasterizing only triangles and sets of contiguous triangles (particularly, strips and fans). Keep in mind that even OpenGL polygons are first automatically fan-triangulated.

Flood-fill

The scan-based polygon rasterization algorithm does not explicitly draw (i.e., fill) a polygon P's boundary given its vertices. Rather, its output is directly a set of pixels filling an area corresponding to P. Another approach to rasterizing P is, in fact, to fill first its boundary by, say, repeatedly applying Bresenham's line rasterizer to each edge, and then fill its interior.

Once the boundary of P has been fill, a particularly intuitive algorithm to fill its interior is the so-called *flood-fill* algorithm. Here's how flood-fill works:

Start with a pixel p known to be in P's interior, found, possibly, by following a ray through the raster and applying the parity test. Fill p. Then examine four of p's neighboring pixels, in particular, the ones to its north, south, east and west. Of these pixels, which are said to be *4-adjacent* to p, fill those that don't belong to the boundary and have not yet been filled. Next, examine the pixels 4-adjacent to the ones just filled and, again, fill those that don't belong to the boundary and have not yet been filled. Continue in this manner until no more pixels can be filled. See Figure 14.26 for the initial configuration and the next two steps of a flood-fill.

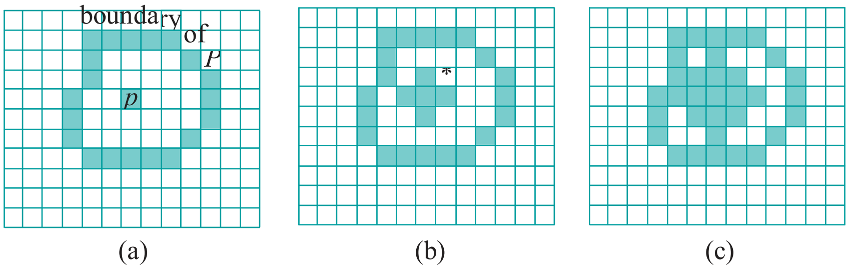

Figure 14.26: Flood-fill: (a) Initially (b) Fill pixels 4-adjacent to p (c) Fill pixels 4-adjacent to the ones filled in the previous step. The starred pixel of (b) is examined by both its south and west neighbors at this step.

Exercise 14.28. In how many more steps after Figure 14.26(c) does the flood-fill algorithm terminate?

Coding flood-fill is simple and we ask the reader to do this next.

Exercise 14.29. Assume that initially all pixels in the raster were of background_color, that a line rasterizer was subsequently invoked on the edges of an input polygon P to set its boundary pixels to foreground_color, and that the pixel at location (x, y) is known to be in the interior of P.

Pseudo-code a recursive flood-fill procedure to set pixels in the interior of P to foreground_color as well.

Now, the flood-fill algorithm will fill exactly the interior of a polygon P provided that

(a) it is *4-connected*, in that any pair of pixels in P's interior can be joined by a path of pixels, each consecutive pair of which is 4-adjacent, and

(b) no pixel in P's interior is 4-adjacent to a pixel outside P, i.e., one neither on P's boundary nor in its interior.

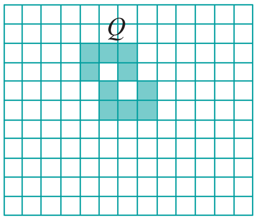

Figure 14.27: Flood-fill fails on the polygon Q whose boundary is drawn.

Polygon P of Figure 14.26 satisfies conditions (a) and (b) and flood-fill indeed terminates after filling its whole interior.

On the other hand, the boundary of a polygon Q where flood-fill will not succeed is shown in Figure 14.27. Evidently, Q's interior is not 4-connected and, whichever of its two pixels is chosen to start with, flood-fill will terminate after filling only that one. It might seem from this example, then, that one need only enhance flood-fill to examine all eight neighbors of the current pixel, which are said to be *8-adjacent* to it, instead of only the 4-adjacent ones. However, care is needed. For, consider the two interior pixels of Q. Both are 8-adjacent to pixels outside Q. Therefore, a simple-minded enhancement of flood-fill could “leak” and fill the whole raster.

Exercise 14.30. We’ve already seen conditions, namely, (a) and (b) above, for flood-fill through 4-adjacent neighbors to work correctly. However, conditions involving properties of the interior of a polygon P would, typically, be harder to check than ones related only to its boundary, the latter, in fact, being the input to flood-fill. So, come up with an easy-to-verify condition on the boundary of P and a possibly modified flood-fill algorithm guaranteed to fill exactly the interior of P.

Flood-fill is not efficient, particularly compared to scan-based filling. A reason is that flood-fill examines the same pixel repeatedly as a neighbor of different ones. For example, the starred pixel in Figure 14.26(b) is examined twice in the second step, once by its south neighbor and once by its west neighbor. Nevertheless, flood-fill is simple to implement and, moreover, can be applied even to curved non-polygonal shapes, once the shape’s boundary has been identified. For this reason many paint programs allow the user to flood-fill a “blob”.

14.5 Summary, Notes and More Reading

In this chapter we learned a few important algorithms from deep in the graphics pipeline. These included line and polygon clipping, as well as the raster-conversion of these primitives. This knowledge will hardly impact our programming of graphics, particularly because high-level API’s like OpenGL allow no access to these algorithms. Still, as students of CG, not just OpenGL, it’s good to have some understanding of what goes on at the far end of the pipeline. And, in Section 21.1, when we assemble the entire synthetic-camera rendering pipeline, clipping and rasterization algorithms will be incorporated into its final stage.

The algorithms in this chapter are all from the foundational period of modern CG, particularly the sixties and early seventies. The Cohen-Sutherland line clipper is from Sketchpad [141], the pioneering interactive CG system Sutherland developed in 1963. The Sutherland-Hodgman polygon clipper [142] is from that period as well, as is Bresenham’s line rasterizer [20], the latter originally being proposed as a method to plot lines on real paper using a computer-controlled pen. The scan-based filling techniques migrated from pen-plotters to raster displays as well.

The classic books by Foley et al. [47] and Rogers [119] contain extensive discussions of various raster algorithms, while the two by Akenine-Möller, Haines & Hoffman [1] and Watt [150] describe modern-day implementations.

Part VIII

Programming Pipe Dreams

CHAPTER 15

OpenGL 4.3, Shaders and the Programmable Pipeline: Liftoff

Programmers mutiny! We're going to throw off our shackles and take over the engine room!

The first radical advancement of OpenGL, since its creation in 1992, was the inclusion of shaders in OpenGL 2.0, released in 2004. Shaders are ancillary programs, attached to an OpenGL program, that run on the GPU and are written by the user to supplant parts of the graphics pipeline formerly of fixed-functionality. They are written in a C-like language called the OpenGL Shading Language (abbreviated GLSL).

Historically, shaders evolved as a response to the increasing capabilities of GPUs and the need to expose these to the application programmer. Before the standardization of the GLSL for shaders a programmer had to write code in vendor-specific language to access individual GPU features – a difficult and inefficient task at best. Just as high-level programming languages like C evolved from assembly in order to hide low-level calls from the developer and give her a structured environment, so did the GLSL.

As a language the GLSL is based on C, so coding will not be an issue for us. In addition to much of C's functionality, the GLSL necessarily has specialized ones for shaders to interact with each other, as well as with the application OpenGL program to which they are attached.

The first version of the GLSL, included in OpenGL 2.0 in 2004, was GLSL 1.1. Since then both OpenGL and the GLSL have progressed in tandem through several versions to, now, OpenGL and GLSL 4.x, where x will be at least 6 when this book is released (since OpenGL 3.3, released in 2010, OpenGL and GLSL version numbers have matched). In this chapter and the next we are, in fact, going to reference particularly OpenGL version 4.3 and its sister GLSL 4.3 because graphics cards with support for 4.3 seem the most common at the time of this writing; moreover, advances in the higher 4.x's are only going to be in specialized features.

With this chapter and the next, we intend to take the reader from the fixed-functionality pre-shader OpenGL thus far in this book to a comprehensive treatment of core 4.3. We are sure though that she will agree as she goes along that pre-shader OpenGL was well worth the effort, even if her goal all along was mastery of the latest version, because the shared fundamentals are best learned in fixed-functionality with generous support from the API itself.

Section 15.1 is an overview of the programmable pipeline with a brief discussion of its most significant consequences to the actual writing of OpenGL code. GLSL, particularly its data types, is introduced in Section 15.2. In Section 15.3 we take apart our first 4.3 program to see what makes it tick – this program, in fact, is a rewrite of our very first OpenGL program, square.cpp of Chapter 2, now using shaders. Animation, lighting and textures, as managed in the 4.3 pipeline, are the topics, respectively, of Sections 15.4, 15.5 and 15.6. We conclude with Section 15.7.

15.1 New Pipeline for OpenGL

We discuss the role of shaders in the programmable pipeline and changes in OpenGL as it has grown to accommodate shaders.

15.1.1 Shaders in the Rendering Pipeline

There are four possible *shader stages* in the programmable pipeline: vertex, tessellation, geometry and fragment. Each stage, except tessellation, corresponds to a single shader program written in the GLSL; the tessellation stage can consist of two shader programs, namely, tessellation control and tessellation evaluation.

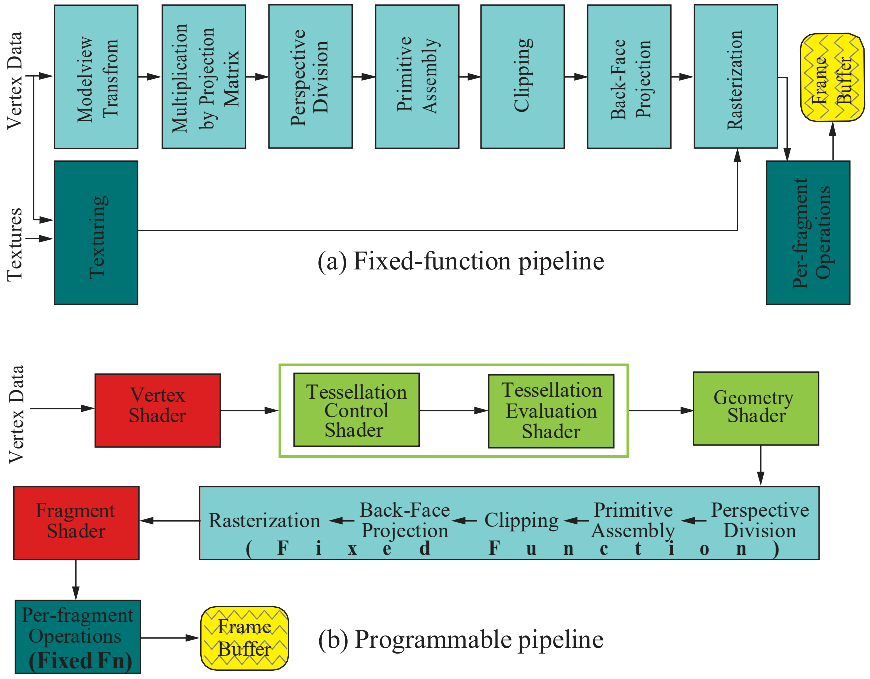

(a) Fixed-function pipeline

(b) Programmable pipeline

Figure 15.1: OpenGL pipelines.

Figure 15.1(a) shows the fixed-function OpenGL pipeline, which should be mostly intelligible to the reader even now – we'll be looking carefully at each of its stages and its implementation in Chapter 21. At the moment, though, our interest solely is in understanding the transition to the programmable pipeline, shown in Figure 15.1(b), from a coding perspective.

Observe, first, that the fixed-function sequence from perspective division to rasterization remains intact in the programmable pipeline, but now there are three shading stages before this sequence, namely, vertex, tessellation and geometry, in that order; moreover, the fragment shader comes just after this fixed-function sequence and before the per-fragment operations, the latter also remaining from fixed-function. Fixed-function's texturing path, as we'll find, has been subsumed into the fragment shader. Let's make a quick first acquaintance of the shaders.

Vertex shader: This is a mandatory shading stage which was part of the original programmable pipeline specification in OpenGL 2.0. The vertex shader runs once per input vertex, processing the data associated with the vertex, e.g., world coordinates, color values, normal values, texture coordinates. At minimum, this shader must output (homogeneous) (x, y, z, w)-coordinates for each vertex. How should it do this?

At this time, we'll need a brief acquaintance with a concept which will be dealt with in depth in Chapter 20. It is that the projection transformation (glOrtho(), glFrustum() or gluPerspective()), which is applied always after all modelview ones, transforms a viewing volume into the so-called canonical viewing box with corners at $(\pm 1, \pm 1, \pm 1)$, points in the volume being transformed to points in the box (see Figure 15.2 for frustum-to-box). Moreover, it accomplishes this by multiplying each (modelview-transformed) vertex's homogeneous $(x, y, z, 1)$-coordinates by a 4×4 matrix, the so-called *projection matrix* corresponding to the particular projection transformation.

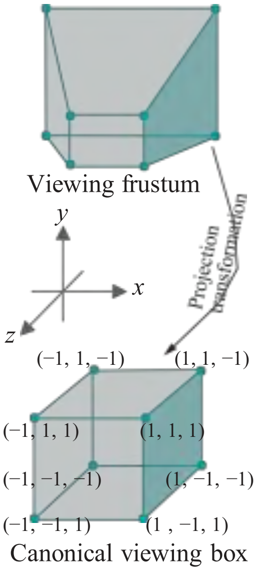

Figure 15.2: Viewing frustum transformed by the projection transformation into the canonical box.

So, typically, the vertex shader outputs (x, y, z, w)-coordinates for each vertex by multiplying its programmer-specified initial world $(x, y, z, 1)$-coordinates by the modelview and projection matrices, in that order. This makes perfect sense if you see the first two stages of the fixed-function pipeline in Figure 15.1, which, in fact, have been supplanted by the vertex shader. Mind that the vertex shader must have, i.e., the programmer must specify, the *actual* matrices corresponding to modelview and projection transformations, not just the transformations themselves as in fixed-function (e.g., instead of a glTranslatef(), its corresponding 4×4 matrix must be given).

Tessellation shader: This is an optional stage comprising two shaders, the tessellation control and evaluation shaders. In fact, even the tessellation control shader is optional and tessellation shading can be done with only the tessellation evaluation shader. Tessellation shading was introduced in OpenGL 4.0 for the purpose of LOD (level-of-detail) management. It can adaptively refine or coarsen an object's mesh – tessellation is the fancy word for mesh – e.g., adding more and smaller triangles as the object comes closer to the eye.

Geometry shader: This is yet another optional stage, following tessellation in the pipeline, but, actually, introduced earlier in OpenGL 3.2. The geometry shader allows the programmer to transform the original geometry, e.g., replacing triangles with lines, or new triangles of a different size, or replacing lines with points, and such. Such radical alteration of an object is done, typically, for specialized effects.

Fragment shader: This is a mandatory shading stage which, like the vertex shader, was part of the original programmable pipeline of OpenGL 2.0. The fragment shader runs once per output fragment, either setting its color or discarding it (which means the fragment is not drawn). The output fragment may, however, be further changed by per-fragment operations (the most important of which is depth testing) coming after the fragment shader, before finally being written to the frame buffer.

Typically, a fragment shader will compute at least the interpolated color values per fragment from color values received per vertex from the vertex shader. If there is texturing, though, then it is an additional responsibility of the fragment shader to calculate appropriate fragment colors based on the bound texture.

15.1.2 New OpenGL

As shaders have evolved so has OpenGL, the shared aim being to (a) leverage the computational power of the GPU to the maximum, and (b) minimize traffic, particularly, transfer of vertex data, along the relatively slow CPU-GPU bus. To this end, numerous new features have been added in the progression through versions from (pre-shader) OpenGL 1.0 to OpenGL version 4.3 as, at the same time, several old ones were deprecated or altogether discarded. We'll obviously be seeing these differences as we code 4.3. Nevertheless, it's worth noting even now a few with significantly large footprints on programming:

1. *Elimination of immediate mode (viz.,* glBegin()-glEnd()*) drawing*: 4.3 allows only retained-mode drawing calls of the glDraw*() and glMultiDraw*() type. The reason is not hard to understand from the following analogy.

Compare issuing a stream of instructions via cell phone to a friend in a supermarket along the lines of "Got the milk? Good! Now, pick up a loaf of whole wheat from across the aisle. Great! Frosted Flakes next in cereals on aisle 9 . . ." with, instead, setting her off once and for all with a shopping list which she can herself optimize together with other stuff she might have to buy.

The first option might make sense if your buddy happens to be a bit thick like the first GPUs from a few decades ago, but certainly not if she is as quick as even the low-end ones nowadays.

Fortunately, we switched (well, mostly) from immediate mode to retained way back in Section 3.1, though our motivation then was separating data out of drawing procedures more so than efficient GPU usage.

2. *Requirement that all data must be stored in buffer objects*: We met buffer objects a long time ago too, in Section 3.2, learning even then their utility in saving CPU-GPU traffic by providing GPU-side storage for vertex and pixel data. That section was about VBOs (vertex buffer objects), while the next, Section 3.3, was about VAOs (vertex array objects) which help encapsulate the buffer objects related to a given geometric object.

   At the end of Section 3.3 we, in fact, counseled the user against coding VBOs and VAOs then because the added complexity would detract from our focus on fundamentals at the time. Now, though, the situation is reversed: VBOs and VAOs are *compulsory* in 4.3 because the whole point is to get the GPU to save and work on all the data it can. We, therefore, pause for the following.

   Exercise 15.1. (Programming) Review Section 3.2 and Section 3.3 on VBOs and VAOs, respectively, and do the exercises therein.

   It's important to be comfortable with their usage before starting to code 4.3.

3. *Elimination of modelview and projection transformation commands* : glTranslatef(), glRotatef(), glScalef() and gluLookAt() are all gone from 4.3, the creation and management of the modelview matrix stack now the responsibility of the programmer who has to write, store and operate on the matrices herself (don't worry, we'll import a library to help with this!).

   The principle behind this change is that the vertex shader already allows the user access to vertex coordinates and the ability to change them, so why not give her full charge, instead of leaving some coordinate processing to fixed-function.

   No more too are glFrustum() and gluPerspective(), the creation and management of the projection matrix stack being the programmer's duty as well.

4. *Do-it-yourself lighting* : glLight*() and glMaterial*() commands? All gone from 4.3. You have to calculate the color values at lit vertices yourself and then if, say, you want to Gouraud (i.e., smooth) shade the interiors of triangle, you're going to have to do that yourself too (no, there is no glShadeModel() either).

   Again, this makes sense if one observes that lighting is all about coloring pixels, which is exactly what the fragment shader is for.

One might conclude that shaders tend to put the programmer in a master-slave relationship with herself.

Defining the OpenGL Context

With changing OpenGL versions, there is naturally demand often from consumers for usability of code written in an older version, as equally from developers to protect their products from rapid obsolescence. For this reason, since OpenGL 3.0, there is a fairly refined way that one can ask an *OpenGL context* from the operating system (think of an OpenGL context as the interface between an instance of OpenGL and the drivers and hardware which run it).

Firstly, the command

```
glutInitContextVersion(major, minor)
```

specifies the OpenGL version number *major.minor*. Next

```
glutInitContextProfile(profile)
```

where *profile* can be GLUT_CORE_PROFILE or GLUT_COMPATIBILITY_PROFILE, specifies the profile. The core profile excludes all features discarded from the specification of the current or earlier versions, while the compatibility profile includes them all (in other words, it allows backward-compatibility). This is why all our programs thus far, which declared a version 4.3 compatibility profile with the statements

```
glutInitContextVersion(4, 3);
glutInitContextProfile(GLUT_COMPATIBILITY_PROFILE);
```

in main() were able to use legacy pre-4.3 commands. From now on, at least in this chapter and the next, we'll be replacing the above block with

```
glutInitContextVersion(4, 3);
glutInitContextProfile(GLUT_CORE_PROFILE);
glutInitContextFlags(GLUT_FORWARD_COMPATIBLE);
```

which asks for a 4.3 core profile; further, the last statement asks for forward-compatibility, which means excluding features marked for deprecation in the current version, thus guaranteeing compatibility with future versions.

15.2 GLSL Basics

We'll come to grips in earnest with shaders in the next section but before that our goal in this one is to give an overview of their language, the GLSL.

To begin with, GLSL has the "Cish" (though, not exactly C) *basic data types*:

float	32-bit floating point number
double	64-bit floating point number
int	signed 32-bit integer
uint	unsigned 32-bit integer
bool	Boolean (true/false)

GLSL has, as well, the *aggregate data types* vectors and matrices to more accurately support OpenGL functionality. Particularly, 2-, 3- and 4-component vectors are available in each of the five basic types:

float:	vec2	vec3	vec4
double:	dvec2	dvec3	dvec4
int:	ivec2	ivec3	ivec4
uint:	uvec2	uvec3	uvec4
bool:	bvec2	bvec3	bvec4

Moreover, GLSL implements floating point and double matrices:

float:	mat2x2	mat2x3	mat2x4
	mat3x2	mat3x3	mat3x4
	mat4x2	mat4x3	mat4x4
	mat2	mat3	mat4
double:	dmat2x2	dmat2x3	dmat2x4
	dmat3x2	dmat3x3	dmat3x4
	dmat4x2	dmat4x3	dmat4x4
	dmat2	dmat3	dmat4

Note that mat*pxq* and dmat*pxq* have each *p* columns and *q* rows (*not p* rows and *q* columns per math convention); mat*p* and dmat*p* are square of size *p*.

Construction and initialization of both the basic and aggregate types are pretty much along the lines one would expect coming from C, e.g.,

```
vec4 color;
color = vec4(1.0, 0.0, 1.0, 1.0);
vec3 rgbColor = vec3(color); // rgbColor has the first
                             // three components of color
```

A matrix, e.g.,

$$M = \begin{bmatrix} 1.0 & 3.0 & 5.0 \\ 2.0 & 4.0 & 6.0 \end{bmatrix}$$

can be initialized in multiple ways including

```
mat3x2 M = mat3x2(1.0, 2.0, 3.0, 4.0, 5.0, 6.0); // Column major!
```

and

```
vec2 column0 = vec2(1.0, 2.0);
vec2 column1 = vec2(3.0, 4.0);
vec2 column2 = vec2(5.0, 6.0);
mat3x2 M = mat3x2(column0, column1, column2);
```

There's a simple way to initialize a scalar matrix, e.g.,

```
mat2 M = mat2(3.0);
```

sets

$$M = \begin{bmatrix} 3.0 & 0.0 \\ 0.0 & 3.0 \end{bmatrix}$$

Accessing the components of an aggregate type is Cish too (e.g., v[i] and M[i][j] retrieve elements of a vector and matrix, respectively). Additionally, one has the particularly OpenGL-friendly way of accessing the components of a vector via the corresponding member of any one of the following three sets of so-called *accessors*:

```
x, y, z, w          r, g, b, a          s, t, p, q
```

Particularly, if *v* is a vec4 variable then *v.x* (or *v.r* or *v.s*) is its first component, *v.y* (or *v.g* or *v.t*) its second component, and so on. The above sets of accessors, of course, are meant to be used in connection with position coordinates, color values and texture coordinates, respectively. The sets cannot be mixed, though, in the same statement. The "." in the middle is often called the *swizzle* operator. The following snippet illustrates both traditional access and *swizzling*, which is the use of the swizzle operator to access and, possibly, rearrange components.

```
vec4 pos1 = vec4(1.0, 2.0, 3.0, 4.0);
float xVal = pos1[0]; // xVal = 1.0
float xVal = pos1.x; // xVal = 1.0
float yVal = pos1.y; // yVal = 2.0
float yVal = pos1.g; // yVal = 2.0

vec4 pos2 = pos1.yxzw; // Swizzling: pos2 = (2.0, 1.0, 3.0, 4.0)
vec4 pos3 = pos1.rrba; // Swizzling: pos3 = (1.0, 1.0, 3.0, 4.0)
vec4 pos4 = vec4(pos1.xyz, 5.0); // pos4 = (1.0, 2.0, 3.0, 5.0).
vec2 pos5 = pos1.xy; // pos5 = (1.0, 2.0).
vec4 pos6 = pos1.xgga; // Illegal: mixing accessors from two sets.
```

One can swizzle on the left-hand side as well, but repeated components are disallowed, e.g.,

```
vec4 pos1 = vec4(1.0, 2.0, 3.0, 4.0);
pos1.xy = vec2(5.0, 6.0); // pos1 = (5.0, 6.0, 3.0, 4.0).
pos1.yx = vec2(5.0, 6.0); // pos1 = (6.0, 5.0, 3.0, 4.0).
pos1.xx = vec2(5.0, 6.0); // Illegal: x is repeated.
```

Here is a snippet illustrating access of elements of a matrix:

```
mat3x2 M = mat3x2(1.0, 2.0, 3.0, 4.0, 5.0, 6.0);
vec2 column2 = M[2]; // column2 = vec2(5.0, 6.0)
float xTan = M[2][1]; // xTan = 6.0
float xTan = M[2].y; // xTan = 6.0
```

Note: Keep in mind the column-major order for matrices! The usual convention in math is that $M[i][j]$ is the element in row i and column j; in GLSL it's the element in column i and row j.

The fun with GLSL vectors and matrices starts with applying the operators "$*$" and "+" between them, when they start behaving as in linear algebra, e.g.,

```
mat2 M = mat2(1.0, 2.0, 3.0, 4.0);
mat2 N = mat2(1.0, 0.0, 0.0, 2.0);
mat2 P = M + N; // P = mat2(2.0, 2.0, 3.0, 6.0)
P = M * N; // P = mat2(1.0, 2.0, 6.0, 8.0)

vec2 U = vec2(1.0, 2.0);
vec2 V = M * U; // V = vec2(7.0, 10.0)
vec2 W = U * M; // W = vec2(5.0, 11.0)
```

Note: A vector multiplied by a matrix from the left is treated as a one-column matrix; a vector multiplied by a matrix from the right is treated as a one-row matrix. See the next exercise.

Exercise 15.2. Show that multiplying a vector from the right by a matrix is equivalent to multiplying it from the left by the transposed matrix.

The *complex data types* structures (struct) and arrays ([ ]), functioning as in C, are implemented in GLSL as well. Additionally, and usefully, one can query the length of an array with help of the Java-like length method, e.g., if the array A contains 10 elements then A.length() returns 10.

Variable types discussed thus far are all *transparent* in that they can be read and written directly. GLSL has a class of *opaque* types, as well, which can be accessed only via built-in functions. Opaque variables are always handles to other objects. The only opaque type that we'll use is sampler2D, a handle to a 2D texture.

Variable declarations may be preceded by at most one of the *storage qualifiers* listed in Table 15.1 with their definitions. For example, the declaration

const	Read-only variable whose value is fixed after initialization.
in	Variable whose value is input from a previous shader stage or the application program.
out	Variable whose value is output to a subsequent shader stage.
uniform	Variable whose value is supplied to the shader by the application and is constant across a primitive.
buffer	Variable whose storage is shared across all shader invocations so can be read and written by them all.
shared	Variable shared within a local work group (only compute shaders).

Table 15.1: Storage Qualifiers.

```
in vec4 colors;
```

in the fragment shader would mean that the value of colors comes from the vertex shader, assuming that the tessellation and geometry shaders are absent. In this case, there would be the matching declaration

```
out vec4 colors;
```

in the vertex shader.

A *conceptual* classification of variables is as *attribute* or *uniform*: attribute variables (or, simply, attributes) are those that vary from vertex to vertex, while uniform variables (or, uniforms) vary from primitive to primitive (just like its namesake storage qualifier, of course). The coordinates of a vertex are classic examples of an attribute variable; the modelview matrix is an example of a uniform; color, e.g., could be attribute if we define a different color for each vertex, or uniform if we choose to keep colors constant across objects.

A typical example of the declaration of an attribute variable in the vertex shader is

```
layout(location=1) in vec4 coordinates;
```

which, in fact, introduces the *layout qualifier* which in/out variables, uniforms and buffers may have additionally. Generally, the syntax of a layout qualifier is of the form

layout(*param1* or *param1* = *value*, *param2*, ...) *variable definition*

where the parameter values specify properties of the variable. E.g., the value of location indicates the buffer which supplies the values of the variable.

An example of a uniform declaration which might be in the vertex shader, as well, is

```
uniform mat4 modelViewMatrix;
```

The fragment shader might declare

```
uniform sampler2D aTexture;
```

as a handle to a texture.

We'll leave it at this for now. Don't worry if the definitions don't all make sense at this time. It should all come together when we get to live GLSL code in a bit. However, if you are interested in a fuller specification of the language, then see the red book or, even better, refer to the horse's mouth, that being the GLSL spec sheet at opengl.org.

Remark 15.1. In early 2015, Khronos released an assembly-like *intermediate* language, acronymed SPIR-V for Standard Portable Intermediate Representation - V, to write shaders – intermediate because the goal is for various high-level languages to compile to SPIR-V. A main purpose for a unique low-level intermediary was standardization as different platforms may compile a high-level language like GLSL somewhat differently. Other advantages of SPIR-V include a potentially smaller distribution size for multi-shader projects and the ability to obfuscate the source shader in order to protect intellectual property.

Programmers intending to produce SPIR-V shader files typically code first in a high-level language like GLSL, subsequently compiling to SPIR-V with the help of third-party tools. We'll leave the interested reader to consult the red book for how to integrate SPIR-V shaders into an OpenGL program.

15.3 First Core GL 4.3 Program (Dissected)

For our first program we'll *shaderize* our trusty guinea pig from way back when, namely, square.cpp – we coin the rather ugly verb "shaderize" to indicate converting one of our existing pre-shader programs to compliance with forward-compatible core 4.3. Shaderizing the simple square.cpp, making sure we understand well each step, should set us on our 4G way.

Experiment 15.1. Fire up the application program squareShaderized.cpp, which comes with its two sidekick shaders, the imaginatively named vertexShader.glsl and fragmentShader.glsl, located in the subfolder Shaders. Not only is the functionality of squareShaderized.cpp – drawing a black square over white background, see Figure 15.3 – *exactly* that of square.cpp, but, as we'll see, so are its internals *modulo* shaders. End

Figure 15.3: Screenshot of squareSaderized.cpp.

We're going to step through the code of squareShaderized.cpp line by line from top to bottom, but first point out the three statements

```
glutInitContextVersion(4, 3);
glutInitContextProfile(GLUT_CORE_PROFILE);
glutInitContextFlags(GLUT_FORWARD_COMPATIBLE);
```

in main(), which assert that the program is compliant with the 4.3 *forward-compatible core* profile vs. the 4.3 *compatibility* (i.e., backward-compatibility) profile in all earlier programs. We're fully committed to 4th generation OpenGL then tossing all legacy commands.

Okay, so back to the top of squareShaderized.cpp. First, to better manage buffer data we set up the Vertex structure

```
struct Vertex
{
   float coords[4];
   float colors[4];
};
```

with one array field for (x, y, z, w) coordinates and another for RGBA colors. Next, to manage matrices – 4.3 asks us to do modelview and projection matrices ourselves – we define the Matrix4x4 structure

```
struct Matrix4x4
{
   float entries[16];
};
```

to hold the 16 entries of a 4×4 matrix. Keep in mind that GLSL is the language of shaders, not the application program, so data types such as mat4 are not available, though we'll find a way around this in our next program. We define next the 4× 4 identity matrix

```
static const Matrix4x4 IDENTITY_MATRIX4x4 =
{
   {
      1.0, 0.0, 0.0, 0.0,
      0.0, 1.0, 0.0, 0.0,
      0.0, 0.0, 1.0, 0.0,
      0.0, 0.0, 0.0, 1.0
   }
};
```

as a constant. Next, a couple of enums, namely,

```
static enum buffer {SQUARE VERTICES};
static enum object {SQUARE};
```

contain names for buffer and vertex array objects, respectively.

Then, we have a block of global variables:

```
static Vertex squareVertices[] =
   {
      { { 20.0, 20.0, 0.0, 1.0 }, { 0.0, 0.0, 0.0, 1.0 } },
      { { 80.0, 20.0, 0.0, 1.0 }, { 0.0, 0.0, 0.0, 1.0 } },
   { { 20.0, 80.0, 0.0, 1.0 }, { 0.0, 0.0, 0.0, 1.0 } },
   { { 80.0, 80.0, 0.0, 1.0 }, { 0.0, 0.0, 0.0, 1.0 } }
};

static   Matrix4x4
   modelViewMat,
   projMat;

static unsigned int
   programId,
   vertexShaderId,
   fragmentShaderId,
   modelViewMatLoc,
   projMatLoc,
   buffer[1],
   vao[1];
```

First, above, come the coordinates (same as in square.cpp) and color values (black) for the four vertices of the square to be drawn. Then, we declare our very own modelview and projection matrices. We'll explain the seven unsigned int variables declared next as they are initialized later on. After this, the function readShader() to read an external shader text file into a character string in the program is one whose innards are not of particular interest here.

On to the initialization routine setup() next where there's plenty going on, which we discuss carefully below.

Compiling and Linking Shaders

After the mandatory glClearColor(), the first part of setup() compiles and links the two shaders into a single shader program executable. Here's the first block of statements from this part:

```
char* vertexShader = readShader("Shaders/vertexShader.glsl");
vertexShaderId = glCreateShader(GL_VERTEX_SHADER);
glShaderSource(vertexShaderId, 1, (const char**) &vertexShader,
               NULL);
glCompileShader(vertexShaderId);
```

The first statement reads the text file vertexShader.glsl containing the vertex shader into the character string vertexShader, while the next creates an empty vertex shader object, returning a non-zero id in vertexShaderId. The third statement sets the source code of the shader object with id vertexShaderId to the value of the character string vertexShader, the second and fourth parameters of glShaderSource() indicating there is only one null-terminated string. The last statement compiles the source code for shader id vertexShaderId. So, on completion of this block we have a compiled vertex shader object.

The second block of statements processes likewise the fragment shader source file fragmentShader.glsl to produce a compiled fragment shader object with id fragmentShaderId.

The final block

```
programId = glCreateProgram();
glAttachShader(programId, vertexShaderId);
glAttachShader(programId, fragmentShaderId);
glLinkProgram(programId);
glUseProgram(programId);
```

of the first part of setup() is fairly self-explanatory. The first statement creates an empty shader program object, returning its non-zero id in programId, the next two statements attach the shader objects identified by vertexShaderId and fragmentShaderId to the program object identified by programId, while the final two statements, respectively, link the shader objects attached to the program object with id programId to create an executable shader program object and install it within the current rendering context. The entire process is diagrammed in Figure 15.4.

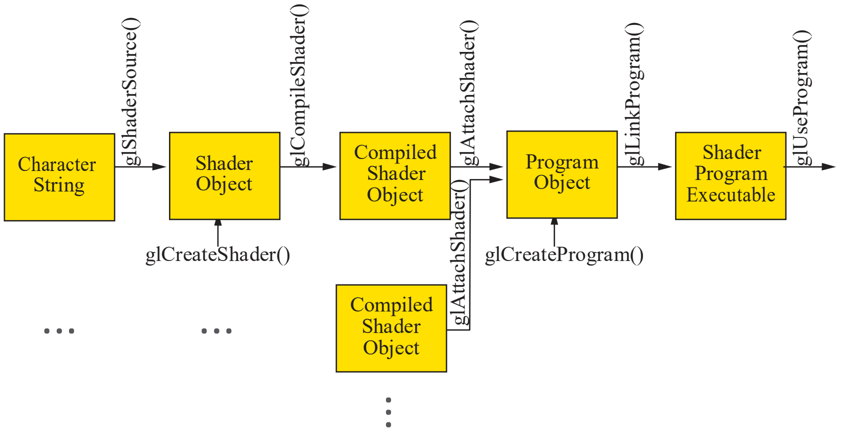

Figure 15.4: Process to create a shader program executable.

Initializing Data and Communicating with the Vertex Shader

The second part of the setup() routine sets up and initializes both a VAO (vertex array object) and VBO (vertex buffer object) and associates the data in the latter with variables in the vertex shader. Now, we are going to assume that, having reviewed Sections 3.2 and 3.3, the reader understands how, in fact, the first block of statements

```
glGenVertexArrays(1, vao);
glGenBuffers(1, buffer);
glBindVertexArray(vao[SQUARE]);
glBindBuffer(GL_ARRAY_BUFFER, buffer[SQUARE_VERTICES]);
glBufferData(GL_ARRAY_BUFFER, sizeof(squareVertices),
             squareVertices, GL_STATIC_DRAW);
```

creates the VAO with id vao[SQUARE] containing the buffer with id buffer[SQUARE_VERTICES], filling the latter with the square's vertex data.

Here, then, is the next block which, critically, is the first step connecting the application program to the vertex shader:

```
glVertexAttribPointer(0, 4, GL_FLOAT, GL_FALSE, sizeof(Vertex), 0);
glEnableVertexAttribArray(0);
glVertexAttribPointer(1, 4, GL_FLOAT, GL_FALSE, sizeof(Vertex),
                      (void*)offsetof(Vertex, colors));
glEnableVertexAttribArray(1);
```

Let's begin to understand it. Generally, the command

glVertexAttribPointer(*index*, *size*, *type*, *normalized*, *stride*, *pointer*)

specifies where and how data for the shader attribute at location *index* is to be accessed. The number of data components to be read per vertex attribute is in *size*, while *type* is the data type of a component. The Boolean *normalized* specifies if the component values are to be normalized prior to access. Finally, *stride* is the byte offset between the data sets for successive vertices, and *pointer* is the byte offset from the start of the currently-bound buffer object to the start of the data set for the first vertex.

Time now to quickly bring the vertex shader vertexShader.glsl, which executes once per input vertex, into the picture. The statements

```
layout(location=0) in vec4 squareCoords;
layout(location=1) in vec4 squareColors;
```

at the top of the vertex shader declare the vec4 attribute variables squareCoords and squareColors, respectively, the storage qualifier in indicating that both get data values from the application program (in this case, actually, a GPU-side buffer filled by the application program). The variable squareCoords is at location 0 and squareColors at location 1.

So, the glVertexAttribPointer(0, ...) statement above in the application program causes the vertex shader to read four floats (a vec4, in other words) for squareCoords per vertex from buffer[SQUARE_VERTICES], starting from the beginning of the buffer, with a stride of sizeof(Vertex) (i.e., the size of data for one vertex) between data sets.

Likewise, glVertexAttribPointer(1, ...) means the shader will read four floats per vertex for squareColors from buffer[SQUARE_VERTICES] starting from byte offset offsetof(Vertex, colors) (i.e., the offset of the colors field in the Vertex structure) with the same stride of sizeof(Vertex).

Think of it this way: the glBufferData() call earlier brought the squareVertices data over to the GPU simply as an array of floats with "no meaning" as such, while the two glVertexAttribPointer() calls tell the GPU how actually to read and use the data.

The statements glEnableVertexAttribArray(0) and glEnableVertexAttribArray(1) above, in the application program as well, activate the vertex attributes at locations 0 and 1, i.e., squareCoords and squareColors, respectively.

See Figure 15.5 for a diagram of how the application program and vertex shader link up. Continuing with setup(), the final two blocks set the modelview matrix and projection matrix, respectively, and connect them to the vertex shader. Let's look at the last block first:

```
Matrix4x4 projMat =
{
   {
      0.02, 0.0,  0.0, -1.0,
      0.0,  0.02, 0.0, -1.0,
      0.0,  0.0, -1.0,  0.0,
      0.0,  0.0,  0.0,  1.0
   }
};
projMatLoc = glGetUniformLocation(programId, "projMat");
glUniformMatrix4fv(projMatLoc, 1, GL_TRUE, projMat.entries);
```

The reader should take in good faith now that the matrix corresponding to the projection command of square.cpp, viz., glOrtho(0.0, 100.0, 0.0, 100.0, -1.0, 1.0), is, indeed, the value of projMat as defined in the first line above (the calculations are in Example 20.1 of Chapter 20). At this time we swing over once more to the vertex shader to note the two uniform declarations

```
uniform mat4 modelViewMat;
uniform mat4 projMat;
```

Returning to the application program snippet above, glGetUniformLocation() in the second statement returns the location of the shader uniform variable named projMat, within the (current) program object programId, into the variable projMatLoc.

The last command glUniformMatrix4fv() updates the uniform at the location given by its first parameter, namely, projMatLoc – this uniform, indeed, being projMat by the previous line – with the value pointed by its fourth parameter, namely, that of the application program (member) variable projMat.entries. Moreover, the second parameter of glUniformMatrix4fv() specifies that there is one matrix to update,

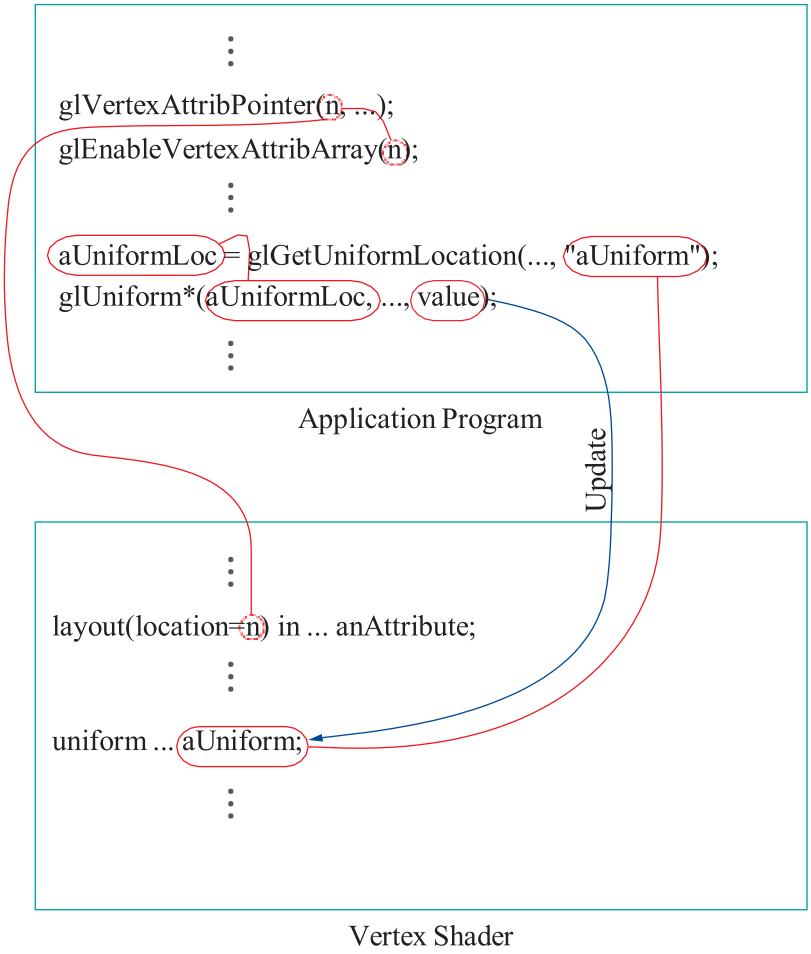
glVertexAttribPointer(n, ...);
glEnableVertexAttribArray(n);
aUniformLoc = glGetUniformLocation(..., "aUniform");
glUniform*(aUniformLoc, ..., value);
Application Program
Update
layout(location=n) in ... anAttribute;
uniform ... aUniform;
Vertex Shader

Figure 15.5: Linkages between the application program and vertex shader. During run-time, the source data for the attribute variables are read from GPU buffers, while uniform values are shipped from the CPU by the application program.

while the third specifies to use the transpose of projMat in updating (because GLSL matrices are stored in column-major order).

Note: As the application program and shaders have different name spaces, we can use identical names (e.g., projMat above) for application and shader variables, when this makes sense, without risk of ambiguity.

The next-to-last block of setup() sets the modelview matrix and links it to the vertex shader in a process exactly similar to that for the projection matrix.

Remaining Routines

The drawing routine drawScene() is extremely simple: the one non-trivial call glDrawArrays(GL_TRIANGLE STRIP, 0, 4) draws the square as a 4-vertex (2-triangle) triangle strip. Keep in mind that immediate mode drawing, precisely, glBegin()-glEnd() code, has been banished from 4.3 – instead, we must use retained mode calls of the glDraw*() and glMultiDraw*() variety – and the only 2D primitives are triangles and their strip and fan relatives, there being no polygons.

The window reshape routine resize() in squareShaderized.cpp is simpler, too, than in square.cpp as the vertex shader has now charge of the projection and modelview matrices: the one statement glViewport(0, 0, w, h) sets the viewport to the entire OpenGL window.

The keyInput() routine is unchanged from square.cpp, while the only change in main(), as we noted right at the start, is from (backward-) compatibility to forward-compatible core profile.

Finally, we examine the two shaders, both of which, fortunately, are fairly minimal.

Vertex Shader

The first line of the vertex shader is the preprocessor command

```
#version 430 core
```

which declares the shader's version of GLSL to be 4.3 core. We've already discussed the four vertex shader variables declared in

```
layout(location=0) in vec4 squareCoords;
layout(location=1) in vec4 squareColors;

uniform mat4 modelViewMat;
uniform mat4 projMat;
```

in connection with the application program – these four variables, in fact, form the communication interface between the application program and the vertex shader. The remaining vertex shader variable, declared

```
out vec4 colorsExport;
```

to match with the fragment shader declaration

```
in vec4 colorsExport;
```

is used evidently to communicate color values from the vertex to the fragment shader. Moreover, as can be seen from its main routine

```
void main(void)
{
    gl_Position = projMat * modelViewMat * squareCoords;
    colorsExport = squareColors;
}
```

our vertex shader really does little work. The first line applies modelview and then projection transformation on input vertex world coordinates, writing the result into the *built-in variable* gl_Position – built-in variables are system-defined variables which shaders use to communicate with fixed-function pipeline stages. In fact, it is gl_Position which continues into the fixed-function perspective division stage of the pipeline (see again Figure 15.1(b), noting there is neither a tessellation nor a geometry shader attached to squareShaderized.cpp). The second line of main() simply copies the input color values into the colorsExport variable for output to the fragment shader.

Fragment Shader

The first line

```
#version 430 core
```

of the fragment shader is the same preprocessor GLSL version declaration as in the vertex shader. Next,

```
in vec4 colorsExport;
```

expectedly matches the namesake colorsExport of type out in the vertex shader. Lastly,

```
out vec4 colorsOut;
```

is declared to output the color values of a fragment.

Remark 15.2. OpenGL automatically identifies the fragment shader's output variable – it must have exactly one such and of type vec4 – as supplying the fragment's final color values.

The one-line main routine

```
void main(void)
{
    colorsOut = colorsExport;
}
```

simply copies the color values input from the vertex shader into colorsExport over to colorsOut for output. Such a shader is often called a *pass-through* shader because its only purpose is to relay incoming values on to the next stage of the pipeline.

However, there is a bit more going on in that one line in main than meets the eye. The fragment shader receives color values from the vertex shader per *vertex*, while it outputs them per *fragment* (remember, a fragment shader runs once per fragment). So, how does it propagate values from vertices to fragments? Interpolation seems the answer, and indeed is the case with this fragment shader though, evidently, the process is being done with a bit of behind-the-scenes help from fixed-function because there is no pertinent code in the fragment shader.

smooth	Perspectively correct interpolation. This is the default. Works exactly the same as glShadeModel(GL_SMOOTH), the default shading model (see Section 11.8)) in pre-shader OpenGL.
noperspective	Linear interpolation without perspective correction (rarely used).
flat	No interpolation: all fragments given same color value, which is that of the *provoking vertex* (see discussion of flat shading in Section 11.8) of the triangle. Works like glShadeModel(GL_FLAT) in pre-shader OpenGL.

Table 15.2: Interpolation Qualifiers.

The GLSL actually offers options for coloring interior fragments of a triangle in the form of three *interpolation qualifiers* – namely, smooth, noperspective and flat – whose respective functions are described in Table 15.2. The default is smooth, as is the case currently, though it has no effect as such because all vertices of the square are colored identically. However, we ask the reader next to make modifications to compare the smooth and flat options.

Exercise 15.3. (Programming) Change the color values of the square's four vertices in squareShaderized.cpp to red, green, blue and yellow, respectively. Smooth interpolation should now be evident. Next, change the declaration of the colorsExport variable in the vertex shader to

```
flat out vec4 colorsExport;
```

and in the fragment shader to

```
flat in vec4 colorsExport;
```

Does what you see tally with the rule for provoking vertices of triangles in a strip described in Section 11.8?

Finally, we are done with our first forward-compatible GL 4.3 core program! A long slog it was but well worth the effort because subsequent programs are going to follow pretty much the same template. Before moving on though here are a couple for you to write.

Exercise 15.4. (Programming) Shaderize squareAnnulus4.cpp from Chapter 3.

Exercise 15.5. (Programming) Shaderize hemisphereMultidrawVBO.cpp from Chapter 3.

15.4 Animation

We move right on to animation. Now, as we have seen, 4.3 asks us to manage our own modelview and projection matrices; in fact, there is no gl*modelingTransform*() or gl*projectionTransform*() at our disposal. We are on our own. To save doing a bunch of 4 × 4 matrix computation in code, therefore, we first import the GLM library.

OpenGL Mathematics (GLM)

GLM, standing for OpenGL Mathematics, is a freely downloadable [58] header-only C++ library for graphics applications meant to replicate the math functionality of the GLSL. So, a programmer familiar with the GLSL will automatically be able to use GLM. However, not only does GLM simulate GLSL math, it (amongst other things) provides replacements for discarded OpenGL functions such as glTranslatef(), glRotatef(), and the like.

If you created your programming environment following the installation guide at the book's website http://www.sumantaguha.com, then you already have GLM ready to use. If you didn't, then refer to the guide and install GLM as we'll be using it in all our programs from now on. With GLM in place we are all set for our first 4.3 animation program, a shaderization, in fact, of Chapter 4's ballAndTorus.cpp.

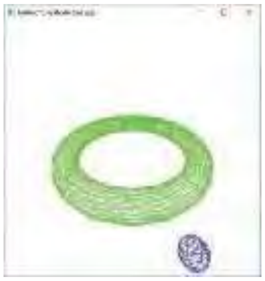

Figure 15.6: Screenshot of ballAndTorusShaderized.cpp.

Experiment 15.2. Run ballAndTorusShaderized.cpp. The program's two shaders are vertexShader.glsl and fragmentShader.glsl. If you care to run ballAndTorus.cpp again you see that the functionality of ballAndTorusShaderized.cpp is exactly same: space toggles animation on and off, the up and down arrow keys change its speed, and 'x'-'Z' turn the scene. Figure 15.6 is a screenshot. End

The code is not hard to understand – in fact, it's mostly made up of pieces from older programs. Firstly, though, note the GLM headers included near the top. Further, use of the glm namespace saves us, for example, from writing glm::vec4 instead of, simply, vec4. Included as well is the header file prepShader.h which lists function declarations from the separate source prepShader.cpp, the latter containing the routines to create the shader program executable, all of which we have already seen in squareShaderized.cpp.

Sadly, the GLUT objects we saw in Section 3.10 are no longer available in 4.3 so we'll have to make our own ball and torus. For the ball we pretty much copy in code from hemisphereMultidrawVBO.cpp of Chapter 3, which draws a hemisphere using VBOs to hold vertex and index arrays, modifying only the code to fill the vertex coordinates array so that mesh vertices run from latitude $-\pi/2$ to $\pi/2$, instead of just 0 to $\pi/2$ – see our separate source sphere.cpp included via the header sphere.h.

Similarly, we have a source torus.cpp and header torus.h to initialize the torus. In fact, for the torus we refer back to torus.cpp of Chapter 10 for the mesh vertex coordinates. Now, comparing sphere.cpp and torus.cpp, one sees that only their respective functions fill*Obj*VertexArray(), filling their vertex coordinates arrays, differ depending on the object's geometry, while the remaining functions are identical save for naming. Hopefully, then, drawing our own objects in future will not be hard if we follow this template. Observe, as well, that both sphere.cpp and torus.cpp use the Vertex structure defined in the header file vertex.h.

The first block of globals of ballAndTorusShaderized.cpp, from latAngle to animationPeriod, are animation-related parameters copied over from ballAndTorus.cpp. Following these are blocks of global storage for sphere and torus data, and, finally, a couple of blocks, familiar from squareShaderized.cpp, containing uniform values and locations, in addition to shader, buffer and VAO ids. And, there, in fact, the reader will spot our use of the GLSL types vec4 and mat4, courtesy the GLM.

The first few blocks of statements of the initialization routine, where we create the shader program executable, call functions to initialize data for a sphere and a torus, and create VAOs and VBOs to hold this data should also be clear from squareShaderized.cpp. Let's move on then to the block

```
projMatLoc = glGetUniformLocation(programId,"projMat");
projMat = frustum(-5.0, 5.0, -5.0, 5.0, 5.0, 100.0);
glUniformMatrix4fv(projMatLoc, 1, GL_FALSE, value_ptr(projMat));
```

where the projection matrix uniform is set. The first line retrieves the location of the uniform projMat in the vertex shader. The second line sees our first use of a GLM function. As the user might guess, frustum(*left*, *right*, *bottom*, *top*, *near*, *far*) returns the matrix corresponding to glFrustum(*left*, *right*, *bottom*, *top*, *near*, *far*). The third line updates that uniform's value with the value of projMat – note the GLM call value ptr(*variable*) which returns a pointer to *variable*'s storage.

The next block of setup() sets the sphere and torus color uniforms in the fragment shader, their values being obtained from sphere.h and torus.h, respectively. In the final block, we obtain the locations of the modelview matrix and object name uniforms for future reference.

On to the drawing routine next where the modelview transformations are, in fact, copied line for line from ballAndTorus.cpp, except, of course, that they now are implemented with the help of GLM, rather than pre-shader OpenGL calls. Here are the first couple:

```
modelViewMat = mat4(1.0);
modelViewMat = translate(modelViewMat, vec3(0.0, 0.0, -25.0));
```

The first statement, equivalent to glLoadIdentity(), sets the modelview matrix to the 4 × 4 identity. To understand the next, note that the GLM call translate(*matrix*, vec3(*p*, *q*, *r*)) returns the result of post-multiplying *matrix* by the matrix corresponding to glTranslatef(*p*, *q*, *r*). Effectively, then, the second statement post-multiplies the current value of the modelview matrix modelViewMat with the matrix corresponding to the translation glTranslatef(0.0, 0.0, -25.0).

Keeping in mind that the GLM calls rotate() and scale() are proxies for glRotatef() and glScalef(), respectively, exactly as how translate() is a proxy for glTranslatef(), the reader should have no difficulty following the rest of the modelview transformation sequence. Note, though, that GLM, unlike OpenGL, counts all angles in radians, entailing calls of the form radians(*angle*) to change *angle* from degrees to radians in our code.

Observe that, prior to drawing either the sphere or torus with the respective glMultiDrawElements(GL TRIANGLE_STRIP, ...) call, the modelViewMat uniform value is updated with a glUniformMatrix4fv(modelViewMatLoc, ...) statement so that the correct modelview transformation is applied. Updated, as well, with a glUniform1ui(objectLoc, ...) statement, is the object uniform value in both shaders with the name of the object to be drawn – the value of object determines in the vertex shader if the vec4 coordinates variable coords reads its values from the attribute variable sphCoords or torCoords, while in the fragment shader it determines if the vec4 output color values colorsOut are read from the uniform sphColor or torColor. However, see the insightful Exercise 15.6 below.

Except for resize() and main(), both of which are standard with nothing of interest, the remaining routines of ballAndTorusShaderized.cpp are copied over from ballAndTorus.cpp.

Note: Observe that the uniform object has been declared identically in both vertex and fragment shader. Their values will be updated simultaneously too.

Note: As enum isn't a part of GLSL 4.3, we are unable to replicate the enum object {SPHERE, TORUS}declaration of the application program, but define the values of SPHERE and TORUS in both shaders via preprocessor directives.

Exercise 15.6. (Programming) Observe that the vertex shader of ballAndTorusShaderized.cpp doesn't really need to "know" if a set of coords comes from the sphere or the torus because it does the same with coords in either case. Neither does it need for coordinate values coming from the sphere and torus to be associated to different in variables, because the vertex shader, which runs once per vertex, is in no danger of "mixing up" sphere and torus coordinates. Therefore, at the cost of a bit of clarity one could amend the program as follows:

Firstly, change the last two lines of the block associating torus data with the vertex shader in the setup() routine to

```
glVertexAttribPointer(0, 4, GL_FLOAT, GL_FALSE, sizeof(Vertex), 0);
glEnableVertexAttribArray(0);
```

associating torus coordinates to the same in variable at vertex shader location 0 as sphere coordinates. Secondly, shorten the vertex shader routine to

```
#version 430 core
layout(location=0) in vec4 coords;
uniform mat4 projMat;
uniform mat4 modelViewMat;
void main(void)
{
   gl_Position = projMat * modelViewMat * coords;
}
```

Execute now to see the program run as before.

So, we can dispense with the object-based if-clause in the vertex shader. If we could do the same in the fragment shader, then we could as well remove all statements to do with objectLoc in the application program. Could we?

Exercise 15.7. Why can't GLUT calls to draw objects from pre-shader OpenGL be included as such in 4.3?
Hint: Immediate mode . . ..

Exercise 15.8. Doesn't using GLM to recreate fixed-function commands defeat the whole purpose of programmable pipelines?!

Exercise 15.9. (Programming) Shaderize floweringPlant.cpp from Chapter 4.

Exercise 15 10. (Programming) If you did animation projects from Section 4.5.3 then shaderize at least a couple of them now.

15.5 Lighting

As noted in Section 15.1.2 on the major facets of the newer OpenGL, 4.3 asks us to do our own lighting – which is good and bad. The bad, or rather tedious, is that, even for classical lighting, we have to implement ourselves the OpenGL lighting equation, which used to be a free service of the fixed-function pipeline. To be fair though, this is just a one-time job writing the appropriate shader, which can then be reused. The good is that, now that we can write our own equations, we can actually go beyond classical lighting to fancier effects.

Our first case study will be bump mapping, first encountered as a special effect in Section 13.9. The idea of bump mapping is to give an illusion of detail to a surface by perturbing its normals so that light reflects off it as though it were actually detailed. We applied this idea in Experiment 13.17 of Section 13.9 to make a plane appear corrugated in the program bumpMapping.cpp. We remarked then that bump mapping is particularly effective with the per-pixel lighting of Phong's shading model, where normal values are interpolated across primitives, rather than being fixed at vertices as in classical lighting (aka per-vertex lighting). However, the fixed-function pipeline cannot do Phong shading; on the other hand, we can program the pipeline of 4.3 to do so.

So, here's the plan: first, we'll shaderize bumpMapping.cpp which'll mean essentially setting up per-vertex lighting ourselves; then, simply to reinforce our ideas, we'll shaderize litCylinder.cpp of Experiment 11.20 of Section 11.11; finally, we'll move definitively beyond fixed-function by applying per-pixel lighting to the setting of bumpMapping.cpp.

15.5.1 Per-Vertex Lighting

Per-vertex lighting comprises Phong lighting at each vertex, governed by the OpenGL lighting equation, followed by Gouraud (smooth) shading to interpolate colors through triangles. Per-vertex lighting is the default of the fixed-function pipeline and is what we have used in all our lit programs to date, including, of course, bumpMapping.cpp.

Let's see then how to write a shader to implement per-vertex lighting with no assistance from fixed-function.

Experiment 15.3. Run bumpMappingShaderized.cpp. Interaction is the same as bumpMapping.cpp: press space to toggle between bump mapping on and off. Figure 15.7(b) is a screenshot with bump mapping enabled, evidently identical to that of bumpMapping.cpp in Figure 15.7(a). End

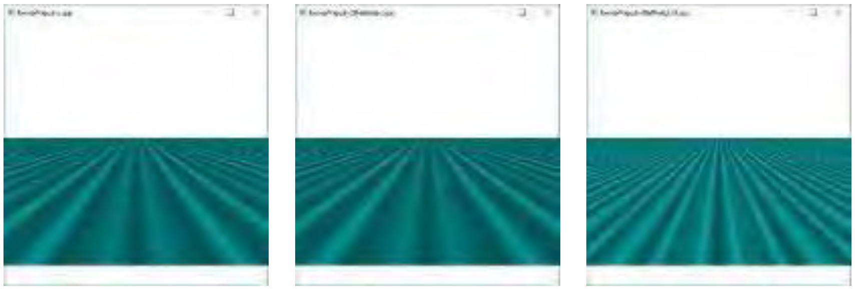

(a) (b) (c)

Figure 15.7: Screenshots of (a) bumpMapping.cpp (b) bumpMappingShaderized.cpp (c) bumpMappingPerPixelLight.cpp.

So, let's understand the code of bumpMappingShaderized.cpp. Note, first, that the structure Vertex defined in vertex.h now has fields for the normal and bump mapped normal, in addition to position. The two simple new header files light.h and material.h define the structures Light and Material to hold light and material properties, respectively. In bumpMappingShaderized.cpp, light0 of type Light holds light property values, planeFandB of type Material holds material property values (identical for the front and back of the plane), and globAmb holds the global ambient vector, all these being copied from bumpMapping.cpp.

The vertices of the program's plane mesh, formed from of a stack of triangle strips exactly as in bumpMapping.cpp, are filled in by the function fillPlaneVertexArray()

in plane.cpp. As promised, this is the only function which differs based on object geometry from the corresponding one in sphere.cpp or torus.cpp of the previous program. However, note that fillPlaneVertexArray() fills in, as well, the values of two kinds of normals, the“real” planeVertices[k].normal and the bump mapped planeVertices[k].bumpedNormal. The real normal is a unit vector in the y-direction at every vertex as in bumpMapping.cpp, while the bump mapped normal varies according to a formula copied again from bumpMapping.cpp.

Moving on to setup(), it does first the routine chores of creating the shader program executable, as well as the VAO and VBOs associated with the plane. Then, as expected, the plane coordinate, real normal and bump mapped normal values are input via glVertexAttribPointer()-glEnableVertexAttribArray() statement pairs to attribute variables in the vertex shader – namely, planeCoords, planeNormal and planeBumpedNormal at locations 0, 1 and 2, respectively. Next, setup() sets the projection matrix uniform, while the locations of the modelview matrix and normal matrix uniforms are retrieved for future reference. The toggle isBumpMapped uniform is set as well.

In the final few blocks of setup(), light property values, the global ambient and material property values are copied, respectively, from the variables light0, globAmb and planeFandB in the application program to corresponding fields in like-named structure uniforms in the vertex shader.

The drawing routine is mundane save, possibly, for the calculation of the normal matrix, following Section 11.11.5, as the transpose inverse of the upper-left 3 × 3 submatrix of the modelview matrix in the line

```
normalMat   =   transpose(inverse(mat3(modelViewMat)));
```

On to the vertex shader next where all of the action is. At this time the reader may want to review the short Section 11.7 on the OpenGL lighting equation as we’ll pretty much be implementing the latter line for line. Here’s the first part of the vertex shader’s main():

```
normal = (isBumpMapped == 1)? planeBumpedNormal : planeNormal;
normal = normalize(normalMat * normal);
lightDirection = normalize(vec3(light0.coords));
eyeDirection =  vec3(0.0, 0.0, 1.0);
halfway = (length(lightDirection + eyeDirection) == 0.0f) ?
                    vec3(0.0) : (lightDirection + eyeDirection)/
                    length(lightDirection + eyeDirection);
```

The first line reads into the variable normal the real or bumped normal values depending on the value of the toggle isBumpMapped, while the second line transforms the normal by the normal matrix and then (re-)normalizes it. The third line sets the light direction vector as the xyz-values of the light’s position, the w-value of 0 implying that the light is directional.

Since bumpMapping.cpp has an infinite viewpoint (the pre-shader default) for lighting calculation, we accordingly set the eye direction vector pointing up the z-axis in the fourth line. The last line sets the halfway vector as the unit vector in the direction of the sum of the light direction and eye vectors (using the formula from Example 11.4) with a zero-division check first.

Here’s the final part of the vertex shader’s main(), except for the routine setting of gl_Position:

```
fAndBEmit  =  planeFandB.emitCols;
fAndBGlobAmb = globAmb * planeFandB.ambRefl;
fAndBAmb = light0.ambCols * planeFandB.ambRefl;
fAndBDif = max(dot(normal, lightDirection), 0.0f) *
              light0.difCols * planeFandB.difRefl;
fAndBSpec = pow(max(dot(normal, halfway), 0.0f),
                    planeFandB.shininess)  *
                    light0.specCols * planeFandB.specRefl;
fAndBColsExport =   vec4(vec3(min(fAndBEmit + fAndBGlobAmb +
                    fAndBAmb + fAndBDif + fAndBSpec,
                    vec4(1.0))), 1.0);
```

We ask the reader to now refer to the OpenGL lighting equation (11.13) to see that the above implements that equation term for term, except there is no distance or spotlight attenuation as these are absent from bumpMapping.cpp too. The last statement which sums the color terms and writes them into fAndBColsExport for output to the fragment shader clamps, in a slightly screwy manner, the individual RGB values to a maximum of 1, and sets the A value to 1.

The fragment shader is pass-through, the default smooth interpolation qualifier of the input variable fAndBColsExport assuring Gouraud shading.

Not too hard was that?! Let's shaderize litCylinder.cpp from Chapter 11 next just for fun.

Experiment 15.4. Run litCylinderShaderized.cpp. Interaction is the same as litCylinder.cpp: press the 'x'-'Z' keys to turn the cylinder. Figure 15.8 is a screenshot. End

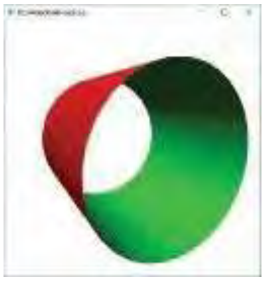

Figure 15.8: Screenshot of litCylinder-Shaderized.cpp.

If you followed bumpMappingShaderized.cpp there's not much really which needs to be explained in litCylinderShaderized.cpp.

Recalling that litCylinder.cpp activated two-sided lighting with the command

```
glLightModeli(GL_LIGHT_MODEL_TWO_SIDE, GL_TRUE)
```

as expected one finds two sets of Material values in litCylinderShaderized.cpp versus the one in bumpMappingShaderized.cpp; in particular, these are cylFront for the front (actually, outside) of the cylinder and cylBack for the back (inside), which are input, respectively, to like-named structure uniforms in the vertex shader.

Lighting calculations in the vertex shader of litCylinderShaderized.cpp are almost exactly as in that of bumpMappingShaderized.cpp, too, except now there are two sets of calculations, identical save for normal reversal, to determine, respectively, front and back colors, both of which are output to the fragment shader. The pass-through fragment shader outputs either the front or back color depending on the value of the Boolean built-in gl_FrontFacing which is true if the current fragment belongs to a front-facing triangle, false otherwise.

The one difference, though, in the lighting calculations themselves is because litCylinder.cpp, unlike bumpMapping.cpp, asks for a local viewpoint for lighting calculation with the command

```
glLightModeli(GL_LIGHT_MODEL_LOCAL_VIEWER, GL_TRUE);
```

To this end, litCylinderShaderized.cpp's vertex shader statement

```
eyeDirection = -1.0 * normalize(vec3(modelViewMat * cylCoords));
```

sets the eye direction vector as the unit vector in the direction from the vertex (in its current location in world space after transformation by the modelview matrix) to the origin.

Finally, returning once more to the application program litCylinderShaderized.cpp, we point out another minor change. In order to be faithful to the command

```
gluPerspective(60.0, (float)w/(float)h, 1.0, 50.0);
```

in litCylinder.cpp's resize() routine, litCylinderShaderized.cpp uses the OpenGL window's width and height, obtained from its own resize() routine via the globals width and height, respectively, to set the projection matrix in drawScene() with

```
projMat = perspective(60.0f, (float)width/(float)height, 1.0f,
                      50.0f);
```

Exercise 15.11. (Programming) Shaderize spotlight.cpp from Chapter 11.

15.5.2 Per-Pixel Lighting

Finally, we are going write a 4.3 program to do something that the fixed-function pipeline could never, namely, Phong shading, or, per-pixel lighting, as it's popularly called. You might want, though, to first review the discussion of Phong shading in Section 11.12.

In per-pixel lighting (a) vertex normal values are interpolated through each triangle, and then (b) light values are computed at each pixel using the interpolated normals. Let's bump map the exact same plane of bumpMappingShaderized.cpp, but now applying per-pixel lighting instead.

Experiment 15.5. Run bumpMappingPerPixelLight.cpp. Again, press space to toggle between bump mapping on and off. Figure 15.7(c) is a screenshot. The program, its associated C++ source and header files are all *exactly* same as for bumpMappingShaderized.cpp – the difference is only in the shaders! End

A comparison of the shaders of bumpMappingPerPixelLight.cpp with those of bumpMappingShaderized.cpp reveals quickly the former's modus operandi. The star turn is now the fragment shader's: the lighting equation statements are brought over from the vertex shader to the fragment shader, which, as well, gets light and material property values directly from the application program *and imports normal values from the vertex shader* . This last is crucial. The default smooth interpolation qualifier of the input variable normalExport causes normal values to be interpolated through each triangle, following which the lighting equation gives precisely Phong shading.

Compare the identical Figures 15.7(a) and (b) with Figure 15.7(c) to see the crisper waves on the plane of the latter, a consequence of its more sophisticated shading model.

Looking back over the last few programs, it seems coding shader-based lighting is mostly a matter of implementing by hand theory learned earlier in Chapter 11.

Exercise 15.12. (Programming) Apply per-pixel lighting to litCylinder.cpp. Compare the result with litCylinderShaderized.cpp which is per-vertex lit. Do you see a difference? How about the highlights?

Exercise 15.13. (Programming) Write a per-pixel lit version of lightAndMaterial1.cpp. Make sure to take into account distance attenuation and that both lights are positional.

15.6 Textures

Textures can not only be imported into the programmable pipeline with ease, but manipulated there by the programmer to great effect as well. Let's start simple, shaderizing fieldAndSkyFiltered.cpp from Chapter 12 on textures, which the reader might want to quickly review at this time.

Experiment 15.6. Run fieldAndSkyFilteredShaderized.cpp. As in fieldAndSkyFiltered.cpp press the up and down arrow keys to move the viewpoint. However, unlike the earlier program, fieldAndSkyFilteredShaderized.cpp implements (to keep it simple) only one fixed filter for the grass texture and no options. Figure 15.9 is a screenshot. End

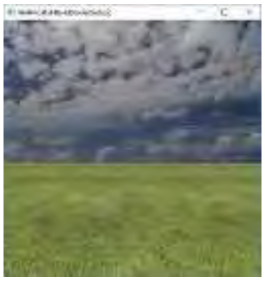

Figure 15.9: Screenshot of fieldAndSkyFilteredShaderized.cpp.

Let's see if texturing in 4.3 is indeed straightforward. First off note that, as expected, the structure Vertex defined in vertex.h now has a field for texture coordinates.

The initialization routine of fieldAndSkyFilteredShaderized.cpp loads the sky and grass images with

```
image[0] = getBMP("../../Textures/grass.bmp");
image[1] = getBMP("../../Textures/sky.bmp");
```

and then generates two texture ids with

```
glGenTextures(2, texture);
```

The next statement block, binding the grass texture to texture unit zero, is

```
glActiveTexture(GL_TEXTURE0);
glBindTexture(GL_TEXTURE_2D, texture[0]);
glTexImage2D(GL_TEXTURE_2D, 0, GL_RGBA, image[0]->width,
             image[0]->height,    0,    GL_RGBA,
             GL_UNSIGNED_BYTE, image[0]->data);
glTexParameteri(GL_TEXTURE_2D,  GL_TEXTURE_WRAP_S,  GL_REPEAT);
glTexParameteri(GL_TEXTURE_2D,  GL_TEXTURE_WRAP_T,  GL_REPEAT);
glTexParameteri(GL_TEXTURE_2D, GL_TEXTURE_MIN_FILTER,
                GL_LINEAR_MIPMAP_LINEAR);
glTexParameteri(GL_TEXTURE_2D, GL_TEXTURE_MAG_FILTER, GL_LINEAR);
glGenerateMipmap(GL_TEXTURE_2D);
grassTexLoc = glGetUniformLocation(programId, "grassTex");
glUniform1i(grassTexLoc, 0);
```

The first statement above selects GL_TEXTURE0 as the active texture unit, the second binds the 2D texture object texture[0] to this unit, the third sets the image data to that of grass, the next four set texture parameters, while the eighth statement generates the mipmaps required for the GL_LINEAR_MIPMAP_LINEAR min filter. All of these statements, thus far, should be familiar from Chapter 12.

It's the last two statements which connect the grass texture to the fragment shader. The second last statement reads the location of grassTex, a uniform of type sampler2D, in particular, a handle to a 2D texture, in the fragment shader; the last statement links grassTex to texture unit GL_TEXTURE0. At the end, it's fair simply to think of grass.bmp becoming the texture grassTex in the fragment shader.

A similar block of statements binds the sky texture to texture unit one, image sky.bmp becoming texture skyTex. And that's it for the application program as far as texture-related statements are concerned. The action moves to the fragment shader next, where the relevant statements are

```
---
in vec2 texCoordsExport;

uniform sampler2D grassTex;
uniform sampler2D skyTex;
uniform uint object;

---
void main(void)
{
   fieldTexColor = texture(grassTex, texCoordsExport);
   skyTexColor = texture(skyTex, texCoordsExport);

   if (object == FIELD) colorsOut = fieldTexColor;
   if (object == SKY) colorsOut = skyTexColor;
}
```

Firstly, the in variable texCoordsExport reads vertex texture coordinates from its namesake out variable in the vertex shader, which in turn obtains them from one of the two vertex attribute arrays fieldTexCoords and skyTexCoords, depending on if the current object is FIELD or SKY; moreover, these two attribute arrays are filled via glVertexAttribPointer() commands in the application program with texture values from the globals fieldVertices and skyVertices, respectively.

Let's examine the main routine next. Now, generally, texture(*sampler*, *texCoords*) is a built-in GLSL *texture lookup function* which samples the colors at the location *texCoords* of the texture space corresponding to the texture bound to *sampler*.

So, for example, the first statement in main() above returns in fieldTexColor the color values of the grass texture at location texCoordsExport, the latter being interpolated from the texture coordinates at the field's vertices; in other words, fieldTexColor are the color values at texCoordsExport, the latter being precisely the point in texture space corresponding to the current fragment by the texture map (which is exactly consistent with how we understood texture coordinates to work in Section 12.1). The rest of main() in the fragment shader should now be clear.

Note: The value of texCoordsExport is, in fact, interpolated from the vertex texture coordinates of the field by the (default) smooth interpolation qualifier of the input variable texCoordsExport.

Let's shaderize a couple more earlier texture programs: texturedTorus.cpp from Section 12.5 specified texture coordinates of a parametrized surface, a torus, using, in fact, the surface's own parametrization, while litTexturedCylinder.cpp from Section 12.7 combined texturing with light.

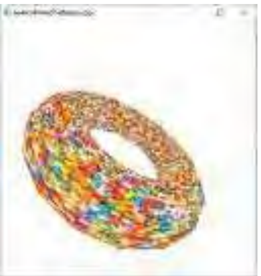

Figure 15.10: Screenshot of texturedTorusShaderized.cpp.

Experiment 15.7. Run texturedTorusShaderized.cpp. As in texturedTorus.cpp press 'x'-'Z' to turn the torus. See Figure 15.10 for a screenshot.

The point to note in textureTorusShaderized.cpp is how the associated source torus.cpp defines texture coordinates for the torus following exactly texturedTorus.cpp. Beyond that the application program and shaders should be easily understood. End

Experiment 15.8. Run litTexturedCylinderShaderized.cpp. The same beer can is drawn twice, per-vertex lit on the left and per-pixel lit on the right. Press 'x'-'Z' to turn the two cans simultaneously to able to compare per-vertex and per-vertex lighting on the same disposition of the can. Figure 15.11 is a screenshot. We discuss the program below. End

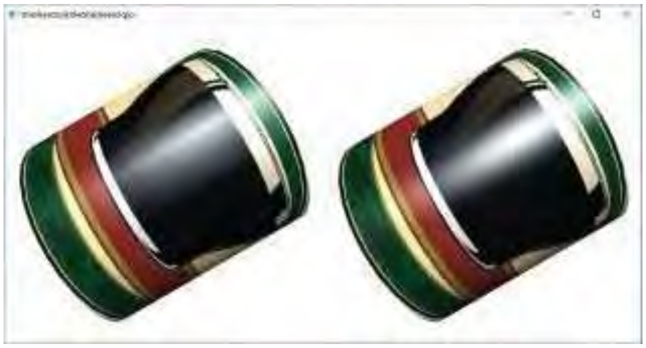

Figure 15.11: Screenshot of litTexturedCylinderShaderized.cpp: per-vertex lighting on the left, per-pixel lighting on the right.

Obviously, litTexturedCylinderShaderized.cpp and its shaders piggyback, respectively, on the earlier litCylinderShaderized.cpp and its shaders. So, let's see where the two differ owing to litTexturedCylinderShaderized.cpp's texturing.

Focus on per-vertex lighting first, which was the only kind applied in litCylinderShaderized.cpp. One notes that the front and back color values of litCylinderShaderized.cpp were both calculated in the vertex shader and exported to the fragment shader, which chose which of the two to apply based on if a triangle was front or back facing, as determined by the value of the built-in variable gl_FrontFacing.

Now, litTexturedCylinderShaderized.cpp's vertex shader does the same *except* that it additionally separates out the specular component of the computed light for front and back faces in frontSpecExport and backSpecExport, respectively, while the rest of the light for these two faces is in frontAmbDiffExport and backAmbDiffExport, again respectively. For the reason for this, refer back to the statement

```
glLightModeli(GL_LIGHT_MODEL_COLOR_CONTROL,
              GL_SEPARATE_SPECULAR_COLOR);
```

in litTexturedCylinder's initialization routine asking that specular colors be added in only after mixing the texture with the non-specular colors (in order not to dilute specular highlights as was discussed in Section 11.4 on the OpenGL lighting model).

Returning to litTexturedCylinderShaderized.cpp, all four color variables frontAmbDiffExport, frontSpecExport, backAmbDiffExport and backSpecExport are exported from its vertex shader to its fragment shader, the latter executing

```
colorsOut = gl_FrontFacing?
            (frontAmbDiffExport * texColor + frontSpecExport) :
            (backAmbDiffExport * texColor + backSpecExport);
```

in case of per-vertex lighting. One sees that the non-specular color component of both front and back is combined with the texture color by *multiplication*, as asked by glTexEnvf(..., GL MODULATE) in litTexturedCylinder's initialization routine, *after* which the specular component is added in, as commanded by glLightModeli(..., GL SEPARATE SPECULAR COLOR).

Per-pixel lighting in litTexturedCylinderShaderized.cpp, too, separates non-specular and specular color components, multiplying the former by texture color and then adding in the latter, calculations this time happening in the fragment shader.

Exercise 15.14. (Programming) Shaderize texturedTorpedo.cpp from Chapter 12. Texturing the Bézier propeller blades is the challenge.

Exercise 15.15. (Programming) Here's an issue that might have come to the reader's mind even when reading pre-shader texturing in Chapter 12, but which we never dealt with then. See for example Figure 15.12. The inside of the can doesn't look right. Modify litTexturedCylinderShaderized.cpp to apply a metal aluminum texture to the entire inside of the can, the need being obviously to texture back and front faces differently.

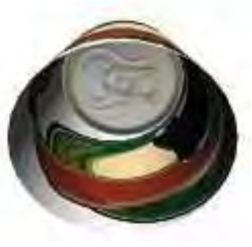

Figure 15.12: Part of screenshot of litTexturedCylinderShaderized.cpp showing inside of can.

FBOs and Rendering to Texture

FBOs (framebuffer objects), the virtual framebuffers we first discussed in Section 12.9, are fully supported in GL 4.3. We ask the reader to recreate the application of an FBO in rendering to a texture.

Exercise 15.16. (Programming) Shaderize renderedTexture.cpp.

15.6.1 Procedural Textures

A *procedural texture*, as we first saw in Section 12.1, is one which is created within the program, rather than imported. In that earlier pre-shader section we created a chessboard texture in the program texturedSquare.cpp by setting a 64×64 array of RGBA values. Now, with the power of the GLSL at our disposal, especially in the fragment shader where colors are finalized, we can do much more, as we see in a simple program.

Experiment 15.9. Run proceduralTexture.cpp. Press 'x'-'Z' to turn the beer can and space to toggle between a procedurally textured whole can and one with a grid of rectangular holes. Screenshots are in Figure 15.13. We'll discuss the program's working next. End

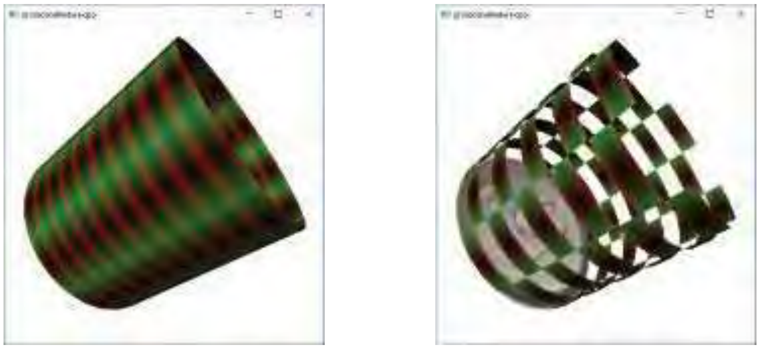
(a) (b)

Figure 15.13: Screenshots of proceduralTexture.cpp: (a) Whole can procedurally textured (b) With pieces missing.

Clearly, proceduralTexture.cpp is based on litTexturedCylinderShaderized.cpp, in particular, keeping only per-vertex lighting from the earlier program and dispensing with the can label texture as the cylinder is to be procedurally textured. The magic is all in proceduralTexture.cpp's fragment shader. Here's its main:

```
void main(void){
if (object == CYLINDER){
texColor = abs(fract(10.0 * texCoordsExport.s) - 0.5) * greenColor +
              abs(fract(10.0 * texCoordsExport.t) - 0.5) * redColor;
if (renderHoles == 1) if((int(floor(10.0 * texCoordsExport.s)) +
                          int(floor(10.0  *  texCoordsExport.t))) % 2
                      == 1) discard;}
if (object == DISC) ...
colorsOut = gl_FrontFacing? ... }
```

Of the two statements within the **if** (object == CYLINDER){... } block, the first specifies the procedural texture while the second conditionally makes the holes. Let's understand them.

Note, first, that the expressions 10.0*texCoordsExport.s and 10.0*texCoordsExport.t effectively scale the range of the texture coordinates s and t, respectively, from [0, 1] to [0, 10], giving us a bit more room for manipulation. Next, note that on any interval of the form $[N, N+1]$, where N is an integer, the value of the expression abs(fract(x) $-$0.5) decreases from 0.5 when $x = N$ at the left end to 0 when $x = N+0.5$ in the middle, and then increases again to 0 when $x = N+1$ at the right end.

The reader can see now how the statement texColor = ... actually makes the procedural texture: it splits the unit texture square into a 10× 10 grid of 100 equal subsquares in each of which the green channel decreases from 0.5 to 0 from the left end to the middle and then increases again to 0.5 at the right end; likewise, the red channel decreases from 0.5 at the bottom to 0 in the middle and then increases again to 0.5 at the top. The result is the banded green-red texture pattern on the cylinder.

The statement **if** (renderHoles == 1) ..., next, invokes the GLSL discard command – which causes the processing of the current fragment to stop with no buffers updated, effectively making it disappear from the pipeline – to erase half the squares from the 10× 10 grid based on the parity of the s and t values at a square's lower-left corner.

There is nothing of particular interest in the last two statements which, successively, apply the can top texture and output the final fragments colors.

Exercise 15.17. (Programming) Apply a procedural texture to the can top as well.

15.6.2 Specular Maps

The do-it-yourself lighting of 4.3 offers limitless possibilities. Here's an effect pretty much impossible in fixed-function. See again the per-pixel lit beer can of litTexturedCylinderShaderized.cpp on the right of Figure 15.11: the specular highlight stretches all the way from the bottom to the top. Say, though, we want only the black-painted part of the label – the glass filled with beer – to be glossy and specularly reflective, while the rest of the label to be matte finished.

So, we did the following. We used an image editing software (GIMP) to select the black region of the can label and color it actually white, while the rest we colored black. The resulting texture is what we'll use as a so-called *specular map*. Figure 15.14 shows the original can label and Figure 15.15 the specular map made from it. This map will allow us to control the specular component of the reflected light as in the following program.

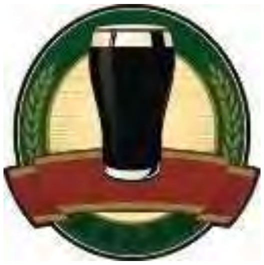

Figure 15.14: Can label.

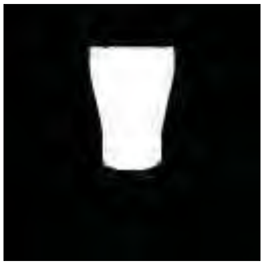

Figure 15.15: Specular map (from editing the can label).

Experiment 15.10. Run specularMapping.cpp. Press 'x'-'Z' to turn the beer can and space to toggle between specular mapping off and on. The program is obviously based on litTexturedCylinderShaderized.cpp, in particular, keeping only per-pixel lighting from the earlier program.

Screenshots are in Figure 15.16, specular mapping being off on the left and on to the right. Evidently, specular mapping indeed restricts the highlight to the black part of the label. We see how next. End

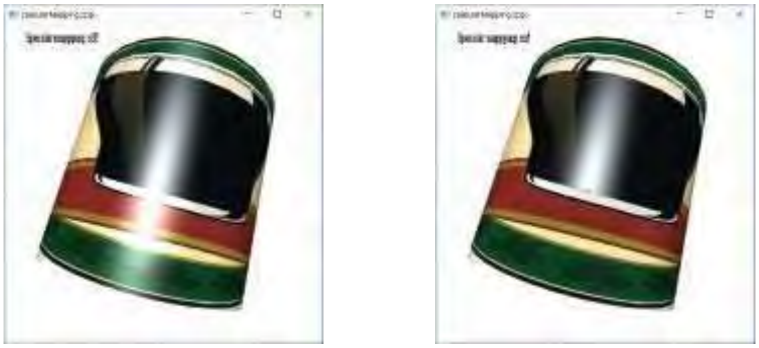

specularMapping.cpp

Specular mapping: off

specularMapping.cpp

Specular mapping: on

(a)

(b)

Figure 15.16: Screenshots of specularMapping.cpp: (a) Specular mapping off (b) Specular mapping on.

The working of specularMapping.cpp is simple to understand if you see the part

```
if (isSpecularMapped == 1 && object == CYLINDER &&
    texture(canLabelSpecularMapTex, texCoordsExport).r < 1.0)
    colorsOut = gl_FrontFacing? (frontAmbDiff*texColor) :
                                  (backAmbDiff*texColor);
else if (object != RECTANGLE)
    colorsOut = gl_FrontFacing?(frontAmbDiff*texColor + frontSpec):
                                 (backAmbDiff*texColor + backSpec);
else
    colorsOut = texColor;
```

which determines the fragment color at the bottom of the fragment shader's main(). The first clause of the if-else ladder says that, if specular mapping is on, then the specular component is not to be mixed into the regions of the cylinder where the specular map is black (for which it's enough to check if the red channel is less than 1, as the code does). Otherwise, specular highlight is mixed in provided the object is not the rectangle at the top left of the image on to which text is textured.

The program specularMapping.cpp shows a simple instance of a specular map – essentially using it to store a Boolean determining if to apply specular reflection or not. Obviously, one can do more. A popular application of a specular map, in fact, is to store a shininess exponent which varies over the scene.

15.6.3 Normal Maps

We shall now see yet another application of a texture map to store non-image data, in particular, normal vectors. A texture containing normal data is called a *normal map*.

What we're going to do is revisit bumpMappingPerPixelLight.cpp to store its bump mapped normals – which were calculated from a sine-wavy bump map of a plane in Section 13.9 – in a normal map and then read them from that normal map within the fragment shader. Let's get to the program first and we'll explain afterward a potential virtue of this apparently needless detour through a texture.

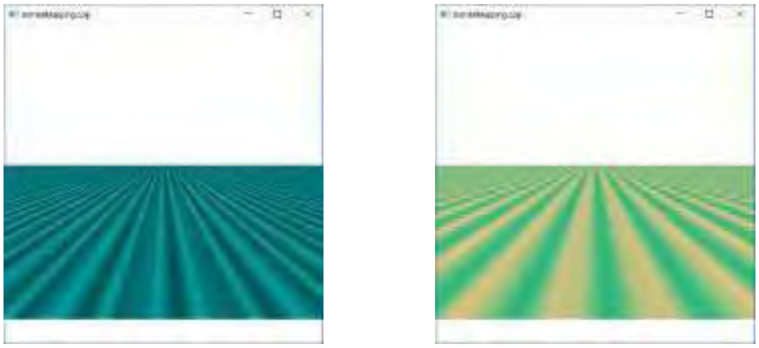

(a) (b)

Figure 15.17: Screenshots of normalMapping.cpp: (a) Normal map applied to a plane (b) Normal map texture as an image.

Experiment 15.11. Run normalMapping.cpp. Press space to toggle between applying a normal map to a plane and displaying the normal map as an image. Figure 15.17 shows both. End

In normalMapping.cpp we must address first a technical issue which arises when trying to create a normal map. We cannot simply store a normal as a texel because a (normalized) normal's (x, y, z) values can each range from -1 to 1, while a texel's RGB values lie each between 0 and 1. However, the simple affine transformations

$$(R, G, B) = (x + 1, y + 1, z + 1)/2 \quad \text{and} \quad (x, y, z) = 2 * (R, G, B) - (1, 1, 1) \qquad (15.1)$$

get us from normals to texels and vice versa.

Next, if you see bumpMappingPerPixelLight.cpp, the bump mapped normal is $(-2\cos(2u), 1, 0)$. Now, instead of trying to normalize this vector, which would create a rather ugly denominator, we simply divide it by 2 to get $(-\cos(2u), 0.5, 0)$, which gives the same normal direction, with each component indeed between -1 and 1, which makes it valid to apply the first transformation of (15.1) to get RGB values

$$(-\cos(2u) + 1, 0.5 + 1, 0 + 1)/2 = ((-\cos(2u) + 1)/2, 0.75, 0.5)$$

That this equation is indeed being used to fill the texel data in the array normalMap can be seen from the part

```
normalMap[i][j][0] = (-cos(2.0*u) + 1.0)/2.0;
normalMap[i][j][1] = 0.75;
normalMap[i][j][2]  =  0.5;
normalMap[i][j][3]  =  1.0;
```

in the loop of the routine createNormalMap() (note that the alpha value is never going to be used). The last block of statements of the initialization routine binds the texel array normalMap as texture unit 0 and links it to the sampler normalMapTex of the fragment shader.

On to normalMapping.cpp's fragment shader next where the reader can check, in the part that draws the plane, that the only difference with bumpMappingPerPixelLight.cpp's fragment shader is that the latter's line

```
normal  =  normalize(normalExport);
```

has been replaced by the former's two lines

```
normal =   2.0 * texture(normalMapTex, texCoordsExport).xyz -
           vec3(1.0, 1.0, 1.0);
normal = normalize(normalMat * normal);
```

So, normalMapping.cpp's fragment shader reads the normal values from the normal map, which resides in the application-program-created texture normalMap, via the sampler normalMapTex, after applying the second transformation of (15.1) on texel values, and then transforms them by the normal matrix and, finally, normalizes them.

Of course, the normal mapped plane of Figure 15.17(a) is identical to the bump mapped plane of Figure 15.7(c) as the normals used in the per-pixel lighting calculations are identical. It's interesting, as well, to view the normal map as a regular image texture as in Figure 15.17(b), though, obviously, a normal map is not supposed to be used as an image texture.

Exercise 15.18. Even though a normal map is not supposed to be interpreted as an image, nevertheless, can you explain Figure 15.17(b), particularly, the alternating green and yellowish-brown stripes?

So, what is the point of normal maps? Analytically calculating the bump mapped normals and storing them in a GPU-side buffer, as in bumpMappingPerPixelLight.cpp, seemed efficient enough. The answer is that normal maps allow for normals to be *imported readymade* – in the form of a texture – from outside, without having to manufacture them mathematically in the program.

In fact, the killer app for normal maps is in allowing the user to read normals from a high-res detailed version of an object and "bake" them onto a low-res one, thereby saving in rendering cost while still providing an illusion of detail.

For example, normalMapping.cpp bakes the normals from the "detailed" surface of Figure 15.18 onto the flat one of Figure 15.19. Supposing, for the moment, that we had, in fact, created the surface of Figure 15.18 as a mesh using some kind of 3D modeling software, e.g., Blender, by moving control points by hand, rather than mathematically, then the only way to retrieve its normals would be to read them from the modeler. This, then, is exactly where normal maps come in – as the means to transport normals from a high-res object to a low-res one. In fact, all the popular modelers, e.g., Blender, have support for normal mapping.

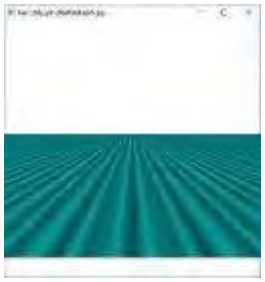

Figure 15.18: Wavy (detailed) plane.

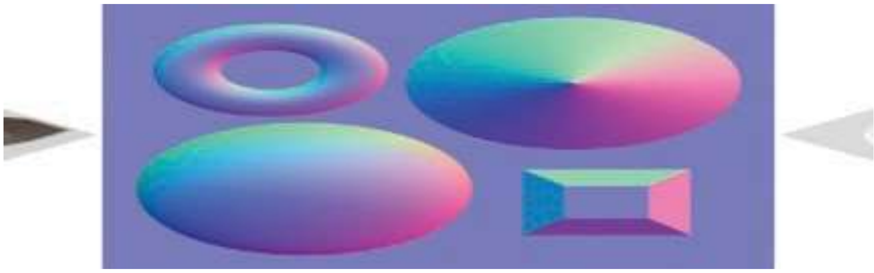

Figure 15.20: Left: detailed scene. Middle: normal map of the scene as an image texture. Right: the normal map baked onto a flat plane. (Thanks Julian Herzog for a Creative Commons license.)

Figure 15.19: Flat plane.

Figure 15.20 shows a more vivid example of normal mapping than our proof-of-concept normalMapping.cpp: in particular, what we see on the right is a perfectly flat plane with only its normals read in from the scene on the left, the normal map texture itself in the middle!

Exercise 15.19. (Programming) Fire up a 3D modeler and bake yourself a normal map.

15.7 Summary, Notes and More Reading

With this chapter began our coverage of the programmable pipeline, particularly OpenGL and GLSL versions 4.3. After learning the basics of GLSL we dissected the 4.3 version of, in fact, our very first OpenGL program from Chapter 2. Then we saw how to do animation, lighting and texturing in 4.3. And, as always, there was plenty of live code along the way, so the student by this point should be fairly comfortable with the new way of doing things. Hopefully, she will agree as well that the pre-shader pipeline we studied so carefully earlier meant much of the programmable-pipeline concepts were already familiar to us, making the learning curve a lot easier.

Particularly exciting for students of shader-based programming might be the fact that, since OpenGL ES (ES for Embedded Systems) version 2.0, shaders have gone mobile with a vengeance: anything that can be done in a shader has been removed from fixed-functionality, and *must be done* in a shader! OpenGL ES – a "lean, mean, shadin' machine" as the OpenGL site calls it – is by far the most common 3D API on mobile devices like smartphones and tablets. The mobile shading language, GLSL ES, itself is very similar to the desktop version. Moreover, OpenGL 4.3 is fully compatible with OpenGL ES 3.0. Therefore, the reader should now be able to begin coding OpenGL for small devices without trouble if she's interested.

There is even more good news. WebGL, the emerging standard for 3D graphics on the web, is based on OpenGL ES 2.0 and, therefore, just a stone's throw in programming methodology from 4.3 (though, not surprisingly as it's for the web, WebGL is written in JavaScript, rather than C++, on the HTML5 canvas element). Currently, WebGL is fully supported on the latest versions of major browsers including Mozilla Firefox, Google Chrome, Safari and Opera. We full expect WebGL to see in the next few years the exponential growth in application development that mobile 3D has already experienced. Oh, and the in-development WebGL 2 is based on OpenGL ES 3.0!

So, the 4.3 programmer has broadly-employable skills which should be in demand for the foreseeable future. Don't go away though. This chapter got us off the ground. There's much more to come.

CHAPTER 16

OpenGL 4.3, Shaders and the Programmable Pipeline: Escape Velocity

We'll now pick up where we left off end of the last chapter. There we set the foundations of OpenGL 4.3. Now we'll study more advanced features, as well as the two optional shader stages, namely, tessellation and geometry.

We begin in Section 16.1 by trying to reconstitute the pre-shader toolbox of Chapter 3. In the process we'll find that even though a few of the older gadgets have been discarded from 4.3, new ones have been added and, in fact, the programmable pipeline often affords a more efficient way to do things than pre-shader.

Section 16.2 introduces two methods to control run-time program flow in a shader more sophisticated than simply branching on if-clauses, namely, shader subroutines and multiple program objects. Just as we try to make ourselves a new toolbox in the first section, in Section 16.3 we revisit Chapter 13 on special visual techniques to see how these can be implemented in 4.3.

In Section 16.4 we'll learn two powerful new techniques related to animation. The first is for picking an object on the screen, familiar from Chapter 4, but done entirely differently via the fragment shader in 4.3. The second is that of transform feedback, which is a way to look ahead in an animation sequence.

Finally, tessellation and geometry shaders are the topics of Sections 16.5 and 16.6, respectively, and we conclude the chapter in Section 16.7.

16.1 Toolbox

What would be a nice collection of gadgets to keep handy while coding 4.3? Let's start by opening again the pre-shader toolbox of Chapter 3 to see if the items still work in 4.3, or if we might not add a few new ones. In fact, we are going to look at all the gadgets from that earlier chapter, though not necessarily in the same order.

16.1.1 VAOs and Instanced Rendering Instead of Display Lists

Vertex arrays, VBOs and VAOs, the topics, respectively, of Sections 3.1-3.3, obviously need little further comment in GL 4.3.

Display lists, on the other hand, so convenient as we saw in Section 3.4 to encapsulate objects and transformations, sadly, are no more in 4.3: glNewList(), glEndList() and glCallList() are all gone. Now, VAOs themselves can take up some of the slack, as VAOs and display lists do share the same purpose of encapsulating objects server-side, though, of course, they go about things rather differently: VAOs package storage states while display lists package a set of commands.

Interestingly, 4.3 has a new gadget, namely, *instanced rendering* , to address a weakness of both VAOs and display lists, that neither can be parametrized at run-time. Instanced rendering allows the same drawing command to be repeated multiple times with certain attributes changing per instance based on the value of a so-called instance counter. There are actually two different ways to do instanced rendering – by setting *instanced vertex attributes* and by using the *instance counter in the shader* . We'll describe both by shaderizing helixList.cpp of Section 3.4 in the two ways.

Instanced Vertex Attributes

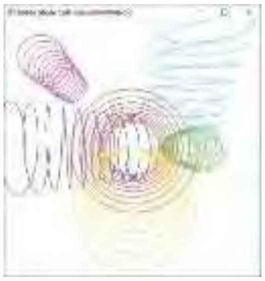

Figure 16.1: Screenshot of helixListShaderized-InstancedVertAttrib.cpp.

Experiment 16.1. Run helixListShaderizedInstancedVertAttrib.cpp. The output of six different helixes is exactly the same as that of helixList.cpp. See Figure 16.1. **End**

The helix itself is created, of course, in the obligatory separate source helix.cpp included in the application program via helix.h. Now, first see the instanced drawing call in the drawing routine:

```
glDrawArraysInstanced(GL_LINE_STRIP, 0, HEL_SEGS, 6);
```

What it does is simply execute the statement glDrawArrays(GL_ LINE STRIP, 0, HEL_ SEGS) successively six times, incrementing the *instance counter* gl_ InstanceID, a built-in shader variable, after each instance (starting from 0). Generally,

glDrawArraysInstanced(*primitive*, *first*, *countVertices*, *countPrimitives*)

executes glDrawArrays(*primitive*, *first*, *countVertices*) successively *countPrimitives* times, incrementing gl_InstanceID after each instance, starting from 0.

Next, note the code in setup() associating the helix color data, copied over from helixList.cpp in the array helColors[6], with the vertex shader:

```
glBindBuffer(GL_ARRAY_BUFFER, buffer[HEL_COLORS]);
glBufferData(GL_ARRAY_BUFFER, sizeof(helColors),
             helColors, GL_STATIC_DRAW);
glVertexAttribPointer(1, 4, GL_FLOAT, GL_FALSE, sizeof(vec4), 0);
glEnableVertexAttribArray(1);
glVertexAttribDivisor(1, 1);
```

It's all routine except for the last statement which makes the color attribute instanced. Generally glVertexAttribDivisor(*location*, *divisor*) declares that successive values of the vertex attribute at *location* of the vertex shader are read every *divisor* instances of the instanced drawing statement. So, the statement glVertexAttribDivisor(1, 1) above, together with the vertex shader line

```
layout(location=1) in vec4 helColors;
```

means that color values for the shader attribute helColors will be read once for each of the six instances a helix is drawn by glDrawArraysInstanced(GL_ LINE STRIP, 0, HEL_ SEGS, 6). If the statement glVertexAttribDivisor(1, 1) had not been there, then color values would have been read once per vertex, rather than once per instance.

In fact,

```
glBindVertexArray(vao[HELIX]);
---
glEnableVertexAttribArray(0);
```

the previous block in setup(), which associates buffer[HEL VERTICES] with the attribute helCoords, has no glVertexAttribDivisor() command, meaning helCoords is uninstanced and will be read once per vertex as, of course, one wants.

Finally, the block

```
glBindBuffer(GL_ARRAY_BUFFER, buffer[HEL_TRANSFORM_MATS]);
glBufferData(GL_ARRAY_BUFFER, sizeof(helTransformMats),
             helTransformMats, GL_STATIC_DRAW);
for (int i = 0; i < 4; i++)
{
   glVertexAttribPointer(2 + i, 4, GL_FLOAT, GL_FALSE,
                         sizeof(mat4), (void*)(sizeof(vec4) * i));
   glEnableVertexAttribArray(2 + i);
   glVertexAttribDivisor(2 + i, 1); // Set attribute instancing.
}
```

in setup() instances the shader vertex attribute helTransformMats, the transforming matrices (again, copied over from helixList.cpp), so that successive ones are applied to successive instances of the helix. The thing to note is that since helTransformMats is of type mat4, the declaration

```
layout(location=2) in mat4 helTransformMats;
```

in the vertex shader causes it to actually occupy locations 2, 3, 4 and 5 (generally, a $p \times q$ matrix will occupy p successive locations, one for each column vector). The application program block above, accordingly, associates the data in buffer[HEL TRANSFORM MATS] with these locations in its for loop.

Finally, of course, the two statements

```
gl_Position = projMat * helTransformMats * helCoords;
colorsExport = helColors;
```

together of the vertex shader's main generate one matrix transform and one color per helix instance.

Instance Counter in the Shader

The primary difference of this method from the previous is that the instanced data is stored in server-side buffers, rather than vertex attribute arrays.

Experiment 16.2. Run helixListShaderizedShaderCounter.cpp. The output, just like that of helixListShaderizedInstancedVertAttrib.cpp, is the same as that of helixList.cpp. See Figure 16.2. End

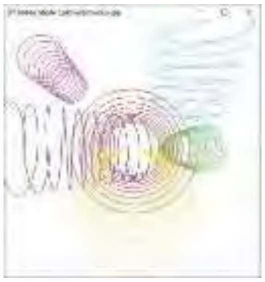

Figure 16.2: Screenshot of helixListShaderized-ShaderCounter.cpp.

Since we want the vertex shader itself to access helix color and transformation matrix values depending on the value of the instance counter gl InstanceID, we need to store these particular colors and matrices somewhat differently. In fact, we'll use *texture buffer objects* (*TBO*s), which are randomly accessible data buffers bound to a texture unit. First, see the block

```
glActiveTexture(GL_TEXTURE0);
glBindTexture(GL_TEXTURE_BUFFER, texture[0]);
glTexBuffer(GL_TEXTURE_BUFFER, GL_RGBA32F, buffer[HEL_COLORS]);
helColorsTexLoc = glGetUniformLocation(programId, "helColorsTex");
glUniform1i(helColorsTexLoc, 0);
```

in the initialization routine binding the color data. The first statement activates texture unit GL_TEXTURE0, the second binds the texture buffer texture[0] to this unit, creating a TBO, while the third specifies buffer[HEL COLORS] as the data source for the TBO kept in the 4-component floating point internal format GL_RGBA32F. The fourth statement reads the location of helColorsTex, a uniform of type samplerBuffer, in the vertex shader; the last statement links helColorsTex to texture unit GL_TEXTURE0.

The next block

```
glActiveTexture(GL_TEXTURE1);
glBindTexture(GL_TEXTURE_BUFFER, texture[1]);
glTexBuffer(GL_TEXTURE_BUFFER, GL_RGBA32F,
            buffer[HEL_TRANSFORM_MATS]);
helTransformMatsTexLoc = glGetUniformLocation(programId,
                         "helTransformMatsTex");
glUniform1i(helTransformMatsTexLoc, 1);
```

creates, likewise, a TBO containing transformation matrix values, which is referenced by the samplerBuffer uniform helTransformMatsTex in the vertex shader. The rest of the application program is routine and, mostly, copied over from helixListShaderizedInstancedVertAttrib.cpp.

So, let's turn next to the vertex shader where the instance counter is actually used. The first statement

```
helColors = texelFetch(helColorsTex, gl_InstanceID);
```

in its main routine returns in helColors the value at location gl InstanceID of the TBO referenced by helColorsTex. Generally, texelFetch(*samplerBuffer*, *intCoord*) returns the value at integer location *intCoord* of the TBO referenced by *samplerBuffer*.

Note: One can, therefore, think of a TBO as a randomly accessible one-dimensional data-containing texture with texels, i.e., data values, located at integer coordinates, or, effectively, a linear array.

Likewise, the block

```
col0 = texelFetch(helTransformMatsTex, gl_InstanceID * 4);
col1 = texelFetch(helTransformMatsTex, gl_InstanceID * 4 + 1);
col2 = texelFetch(helTransformMatsTex, gl_InstanceID * 4 + 2);
col3 = texelFetch(helTransformMatsTex, gl_InstanceID * 4 + 3);
helTransformMats = mat4(col0, col1, col2, col3);
```

in main accesses the TBO referenced by helTransformMatsTex to retrieve four column vectors at a time, subsequently assembling them into a mat4 transformation matrix.

Finally,

```
gl_Position = projMat * helTransformMats * helCoords;
colorsExport = helColors;
```

together generate one matrix transform and one color per helix instance.

Exercise 16.1. (Programming) Apply instanced rendering to create a starry night sky.

Remark 16.1. Comparing the display lists of old to instanced rendering, both with instanced vertex attributes and instance counter, the reader will notice how the latter is more to the spirit of modern OpenGL: display lists require multiple drawing calls, particularly, one per instance, with CPU-to-GPU data shipment each instance, while instanced rendering sends data to the GPU in a single transfer and then creates all instances with one call.

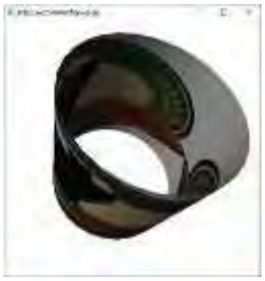

Figure 16.3: Screenshot of litTexturedCylinderClipped.cpp with clipping on.

16.1.2 Clipping Planes

Setting up user-defined clipping planes, in addition to the six automatic ones bounding the viewing volume, was discussed in Section 3.11. We can set up clipping planes in 4.3 as well, though the process, mostly conducted in the vertex shader, is different. Let's get straight to code, particularly, a program made from a quick modification of (the per-pixel lit part of) LitTexturedCylinderShaderized.cpp.

Experiment 16.3. Run litTexturedCylinderClipped.cpp. Pressing 'x'-'Z' turns the can while space toggles between enabling and disabling a clipping plane which slices off the can top. Figure 16.3 is a screenshot with the top gone. End

The two statements

```
clipPlaneLoc = glGetUniformLocation(programId, "clipPlane");
glUniform4fv(clipPlaneLoc, 1, &clipPlane[0]);
```

at the bottom of litTexturedCylinderClipped.cpp's setup() routine pass the value of the global clipPlane, which is the vec4 (0.0, 0.0, −1.0, 0.99), to the vertex shader's corresponding uniform clipPlane. Of course, generally, the clipPlane uniform is meant to hold the coefficient vector (A, B, C, D) of the clipping plane $Ax + By + Cz + D = 0$, so our (0.0, 0.0, −1.0, 0.99) represents the plane $-z + 0.99 = 0$.

To the vertex shader next where

```
float gl_ClipDistance[1];
```

initializes the built-in vertex shader array gl ClipDistance in order to implement a single clip plane. The statement

```
gl_ClipDistance[0] = dot(clipPlane, coords);
```

at the bottom of the shader's main then sets the value of gl ClipDistance[0] to the dot product

$$(A, B, C, D) \cdot (x, y, z, 1) = Ax + By + Cz + D$$

where (A, B, C, D) is the clipping plane's coefficient vector and $(x, y, z, 1)$ are the vertex's pre-transformation world coordinates. It's not hard to see that this dot product is zero on the plane $Ax + By + Cz + D = 0$, negative in one half-plane and positive in the other. The per-vertex values of gl ClipDistance[0] are then interpolated across the primitive, and fragments with value less than 0 are culled.

In other words, fragments whose interpolated value of $Ax + By + Cz + D$ is less than 0 will be culled, which is exactly how clip planes in the fixed-function pipeline worked. In our case above, then, fragments with $-z + 0.99 < 0$, or, equivalently, $z > 0.99$, are culled, which takes off the top of the can because its axis runs from $z = -1$ to $z = 1$.

We define only one clip plane in litTexturedCylinderClipped.cpp, so our array gl_ClipDistance is initialized to size 1. Generally, it can be initialized to any size n (subject to a system-dependent maximum) by

```
float gl_ClipDistance[n];
```

in which case OpenGL culls those fragments with at least one interpolated gl_ClipDistance[i] value, from $0 \leq i \leq n - 1$, being negative. Keep in mind that it's up to the user to set per-vertex values for each gl ClipDistance[i], just as we did above with the statement gl_ClipDistance[0] = dot(...).

Finally, note that glEnable(GL_CLIP_PLANE0) and glDisable(GL_CLIP_PLANE0) near the top of litTexturedCylinderClipped.cpp's drawing routine enable and disable, respectively, GL_CLIP_PLANE0.

Exercise 16.2. (Programming) Currently, litTexturedCylinderClipped.cpp's clipping plane seems to move with the can, always keeping the can's top in the clipped half. Modify the vertex shader to keep it fixed so that the top can be clipped only in certain positions.

16.1.3 Rest of the Toolbox

Text

The GLUT text drawing calls of Section 3.5, both glutBitmap*() and glutStroke*(), are gone from 4.3 because of their immediate mode of operation. We are unaware of a text-drawing library to use with 4.3, and the only practical recourse at this time seems to be to create text oneself in textures. We actually did just this in specularMapping.cpp of the last chapter so we ask the reader to fire it up once again.

Experiment 16.4. Run specularMapping.cpp. Pressing space toggles between specular mapping off and on, the label at the top left indicating the current status. Figure 16.4 is a screenshot with specular mapping on.

We'll leave the reader to check that we have created (using a drawing program) two textures, one saying "Specular mapping on!" and the other "Specular mapping off!", and paste one or the other onto a long thin rectangle in the scene. A tedious process this certainly but, then, OpenGL was never really meant to provide a text-drawing service. End

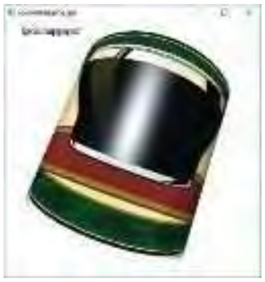

Figure 16.4: Screenshot of specularMapping.cpp.

Mouse Functions

Programming the mouse in 4.3 stays exactly as first discussed in Section 3.6: the commands glutMouseFunc(), glutMotionFunc(), and glutMouseWheelFunc() to register callbacks for mouse clicks, mouse motion and wheel rotation, respectively, can be used as before.

Non-ASCII Keys

We have already used glutSpecialFunc() in several 4.3 programs to register the handler for non-ASCII key presses, in exactly the same manner as discussed earlier in Section 3.7.

Menus

Pop-up menus, too, can be attached to a 4.3 program as described in Section 3.8; specifically, by invoking glutCreateMenu(), glutAddMenuEntry(), glutAddSubMenu() and glutAttachMenu().

Line Stipples

Unfortunately, we cannot stipple lines in 4.3 in the pre-shader way of Section 3.9: glEnable() no longer accepts the parameter GL_LINE_STIPPLE and there is no glLineStipple() in 4.3.

However, there is a fairly straightforward workaround by way of the fragment shader. In particular, we need the help of the built-in input variable gl_FragCoord of type vec4, which is accessible to the fragment shader; its (x, y)-values are the coordinates of the fragment in the windows system, z-value is the depth of the fragment and w-value is $1/W$, the so-called perspective division factor which we do not need at this time. We ask the reader to apply these in the next exercise.

Exercise 16.3. (Programming) Stipple a line so that groups of four pixels are successively off and on by writing a statement of the form

```
if ( mod(gl_FragCoord.x, 8.0) < 4.0 ) discard;
```

in the fragment shader.

FreeGLUT Objects

We have already been doing without the FreeGLUT object calls of Section 3.10, unavailable in 4.3 because of their immediate mode of operation, instead creating objects - e.g., spheres and tori – ourselves in small ancillary source programs, which has proved not too hard. Hopefully, though, someone will figure out soon a benign way to import readymade objects into shader programs.

gluPerspective()

The GLU call gluPerspective(), explained in Section 3.12, is gone from 4.3 for obvious reasons: the projection matrix must be managed by the user in the shader. In fact, GLU itself is deprecated so we had best steer away from all glu*() calls.

However, we have already seen a workaround for gluPerspective(). In fact, litCylinderShaderized.cpp of the last chapter invoked in its drawing routine the GLM command perspective(*fovy*, *aspect*, *near*, *far*), which returns the projection matrix corresponding to gluPerspective(*fovy*, *aspect*, *near*, *far*).

Viewports and Multiple Windows

Finally, creating viewports and top-level windows, topics of Sections 3.13 and 3.14, respectively, remains identical in 4.3 to what it was pre-shader.

16.2 Shader Control Flow

To dynamically choose between alternate threads of control in a shader at run-time, what we've been doing so far is very simple: we've branched on if-clauses conditioned on a uniform, as exemplified in the following extract from the vertex shader of the program ballAndTorusShaderized.cpp of the previous chapter:

```
uniform uint object;
...
    if (object == SPHERE) coords = sphCoords;
    if (object == TORUS) coords = torCoords;
...
```

We'll see next two very different ways of controlling flow in a shader, viz., using so-called shader subroutines and by creating multiple program objects.

16.2.1 Shader Subroutines

Shader subroutines offer an elegant alternative to ifs conditioned on a uniform, allowing the user to dynamically select a subroutine, albeit at a higher set-up cost. In short, what the user does is specify a subroutine type, then a bunch of subroutines of that type, and, finally, a subroutine uniform variable whose value decides the subroutine to execute. The conceptual forebear of shader subroutines is the C function pointer.

Let's get to work. We'll rewrite ballAndTorusShaderized.cpp to use shader subroutines instead of if-clauses.

Experiment 16.5. Run ballAndTorusShaderSubroutines.cpp. The controls are exactly as for ballAndTorusShaderized.cpp: space to toggle animation on and off, up/down arrows to change its speed, and 'x'-'Z' to rotate the scene. Figure 16.5 is a screenshot. End

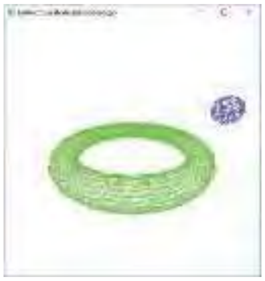

Figure 16.5: Screenshot of ballAndTorusShaderSubroutines.cpp.

The subroutines are in the vertex shader. First, see the two statements

```
subroutine void objectAction(void);
subroutine uniform objectAction object;
```

The first statement declares a *subroutine type* named objectAction with both void parameter list and return type. The general form of this declaration is

subroutine *returnType* *subroutineTypeName*(type *parameter*, type *parameter*, ...)

The second statement declares the *subroutine uniform* variable object corresponding to the just-declared subroutine type objectAction. The general form is

subroutine uniform *subroutineTypeName* *subroutineUniformName*

Next, two simple subroutines, named sphere and torus, respectively, of type objectAction are defined by

```
subroutine (objectAction) void sphere(void)
{
    coords = sphCoords;
    colorsExport = sphColor;
}

subroutine (objectAction) void torus(void)
{
    coords = torCoords;
    colorsExport = torColor;
}
```

Their function evidently is to set the coordinates and the color values to export for the sphere and torus, respectively. Observe that both subroutines have return type and parameter list matching the subroutine type, namely objectAction, to which they belong.

Now, to the initialization routine of ballAndTorusShaderSubroutines.cpp, where the statements

```
sphSubroutineIndex = glGetSubroutineIndex(programId,
                              GL_VERTEX_SHADER, "sphere");
torSubroutineIndex = glGetSubroutineIndex(programId,
                              GL_VERTEX_SHADER, "torus");
```

obtain the indices of the subroutines sphere and torus, respectively.

Finally, back again to the vertex shader where the first line of

```
void main(void)
{
    object();
    gl_Position = projMat * modelViewMat * coords;
}
```

invokes the subroutine whose index is chosen in ballAndTorusShaderSubroutines.cpp's drawing routine by statements of the form

```
glUniformSubroutinesuiv(GL_VERTEX_SHADER, 1, &XSubroutineIndex);
```

where X is either sph or tor. Such statements replace corresponding ones of the form

```
glUniform1ui(objectLoc, X);
```

of the earlier ballAndTorusShaderized.cpp, which used if-based shader control, where X was either SPHERE or TORUS.

16.2.2 Multiple Program Objects

A more drastic solution to controlling flow in shaders, in fact, is a radical surgery: make separate shaders containing the different control threads, attach them to separate program objects, and, then, switch between program objects at run-time. The implementation of this method, as we'll see next in rewrite a ballAndTorusShaderized.cpp, is straightforward.

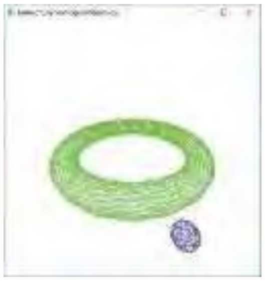

Figure 16.6: Screenshot of ballAndTorusTwoProgramObjects.cpp.

Experiment 16.6. Run ballAndTorusTwoProgramObjects.cpp. The controls are same as for ballAndTorusShaderized.cpp: space to toggle animation on and off, up/down arrows to change its speed, and 'x'-'Z' to rotate the scene. Figure 16.6 is a screenshot.
End

The two statement blocks

```
vertexShaderId[SPHERE] = setShader("vertex",
                                   "vertexShaderSphere.glsl");
fragmentShaderId[SPHERE] = setShader("fragment",
                                     "fragmentShaderSphere.glsl");
...
glLinkProgram(programId[SPHERE]);
```

and

```
vertexShaderId[TORUS] = setShader("vertex",
                                  "vertexShaderTorus.glsl");
fragmentShaderId[TORUS] = setShader("fragment",
                                    "fragmentShaderTorus.glsl");
...
glLinkProgram(programId[TORUS]);
```

in the initialization routine of ballAndTorusTwoProgramObjects.cpp create program objects to draw the sphere and torus, respectively. The shaders for the sphere-drawing program object are modified from the corresponding shaders of ballAndTorusShaderized.cpp by keeping only the thread of control if (object == SPHERE) in the latter program; likewise, for the torus-drawing program object. Further down the initialization routine, the blocks

```
glUseProgram(programId[SPHERE]);
projMatLoc = glGetUniformLocation(programId[SPHERE],"projMat");
..
modelViewMatLoc = glGetUniformLocation(programId[SPHERE],
                                       "modelViewMat");
```

and

```
glUseProgram(programId[TORUS]);
projMatLoc = glGetUniformLocation(programId[TORUS],
                                  "projMat");
...
modelViewMatLoc = glGetUniformLocation(programId[TORUS],
                                       "modelViewMat");
```

set the projection matrix, modelview matrix and color values uniforms for the sphere and torus drawing program objects, respectively, activating either first with the appropriate glUseProgram() call.

Finally, as expected, statements of the form

```
glUseProgram(programId[X])
```

in ballAndTorusTwoProgramObjects.cpp's drawing routine replace corresponding ones of the form

```
glUniform1ui(objectLoc, X);
```

in ballAndTorusShaderized.cpp's drawing routine, where X is either SPHERE or TORUS.

Remark 16.2. We have mostly used if-based shader control for simplicity's sake. In fact, for relatively small programs like ours it's unlikely there is a perceptible difference in performance amongst if-based control, shader subroutines and multiple program objects. However, for large programs the user might want to consider:

(a) Subroutines are most easily optimized by the compiler for better run-time performance, while separate program objects lend themselves little to optimization.

(b) Subroutines and if-based control are the most convenient in order to follow the program logic.

Generally, follow the programming style you are most comfortable with and if you suspect this is somehow hurting run-time, then test to make sure. And, only change the way you like to code for very good reason.

16.3 Special Visual Techniques

We already saw in the form of procedural texturing, specular mapping and normal mapping, at the end of the preceding chapter, some of the effects one can code up in GL 4.3. It's reasonable, then, to revisit the pre-shader Chapter 13 on special visual techniques. What we'll find is that all items there are disposed of easily. In fact, we'll see particularly the power of 4.3 in the case of blending and point sprites, so we'll discuss these two first.

16.3.1 Blending

The fragment shader not only puts the programmer in full charge of blending but makes it easy. Let's get straight to blending textures – we'll shaderize fieldAndSkyTexturesBlended.cpp.

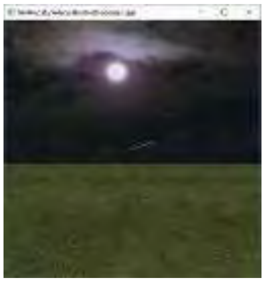

Figure 16.7: Screenshot of fieldAndSkyTexturesBlendedShaderized.cpp early morning.

Experiment 16.7. Run fieldAndSkyTexturesBlendedShaderized.cpp. As in fieldAndSkyTexturesBlended.cpp press the arrow keys to change the direction of the sun, the transition between day and night happening from a blending of day and night textures. See Figure 16.7 for a screenshot. End

All the code of fieldAndSkyTexturesBlendedShaderized.cpp should be routine for the reader at this point except for where the texture blending actually takes place: the line

```
if (object == SKY) colorsOut = mix(nightSkyTexColor,
                                   skyTexColor, alpha);
```

in the main routine of the fragment shader. Now, the built-in GLSL function mix(x, y, a) returns the linear combination $(1 - a)x + ay$ of x and y, so the line above obtains the exact same blending of the night and day sky textures as in fieldAndSkyTexturesBlended.cpp.

Evidently, the user has full pixel-level control of blending in 4.3 through the fragment shader. However, oddly enough, blending can still be enabled in the application program with glEnable(GL_BLEND) and glBlendFunc(), as well as a host of other glBlend*() commands, all still there in fixed-function. We'll see soon a reason for this when we discuss antialiasing.

The reader likely will agree that multitexturing, which is really blending in disguise, should be straightforward to implement in the fragment shader. We first saw multitexturing implemented in Section 12.8 in the program multitexture.cpp with the use of a fairly complex bunch of glTexEnvi() and glMultiTexCoord2f() calls. So, let's revisit an old exercise from that section.

Exercise 16.4. (Programming) Redo Exercise 12.19, now modulating the mountain texture with the fog texture in the fragment shader.

Motion Blur in Screen Space

Pixel-level control of blending makes possible motion blurring in screen space, which can be much more efficient than in world space. We motion blurred the ball in the program ballAndTorusMotionBlurred.cpp in Section 13.1.6 by blending multiple copies of the ball in world space. Let's do something a little different now.

Experiment 16.8. Run launchCameraBlurredcpp.cpp to see an image of a shuttle launch. Press space to blur the image as though the camera jolted rightward and space again to unblur it. Figure 16.8 has screenshots. End

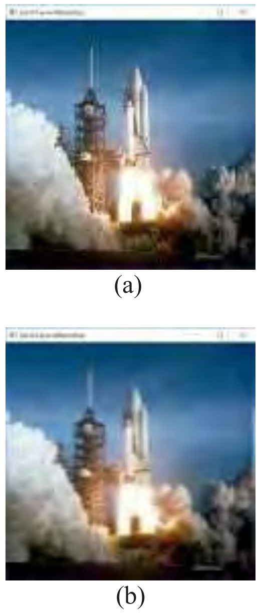

Figure 16.8: Screenshots of launchCameraBlurred.cpp: (a) Not blurred (b) Blurred.

The statement

```
launchTexColor =
    0.4 * texture(launchTex, texCoordsExport) +
    0.3 * texture(launchTex, texCoordsExport + vec2(0.005, 0.0)) +
    0.2 * texture(launchTex, texCoordsExport + vec2(0.01, 0.0)) +
    0.1 * texture(launchTex, texCoordsExport + vec2(0.015, 0.0));
```

in the fragment shader of launchCameraBlurred.cpp does all the work. The camera jolting rightward imparts a leftward "velocity" to the image, in particular, to every fragment. The above statement simulates this movement of the image by blending each fragment with three more successively further to its right with the decreasing alpha values 0.4, 0.3, 0.2 and 0.1, respectively.

Though blurring in screen space is more efficient than in world space because we don't pass redundant objects down the pipeline, it can sometimes be tricky to implement. We'll ask the reader to ponder this next.

Exercise 16.5. (Programming) Shaderize ballAndTorusMotionBlurred.cpp. The difficulty here, compared with camera blur of launchCameraBlurred.cpp, is that fragments have different velocities in screen space depending on the object to which they belong (e.g., torus fragments are still, while ball fragments move).

16.3.2 Points and Sprites

Points are a whole different ball game. In fact, GLSL 4.3 has a rich set of controls allowing the programmer to do pretty much as she pleases with points. You might now want to quickly review the discussion about how points are rendered at the end of Section 13.4.1 and also point sprites in Section 13.5. Good, let's get to code.

Experiment 16.9. Run points.cpp. Drawn are three large points. Press the right and left arrow keys to cycle between four different point renderings and the up and down arrow keys to move the points parallel to the z-axis. Figure 16.9(a) is a screenshot of what is seen at first, while Figures 16.9(b)-(d) show the other three cases. End

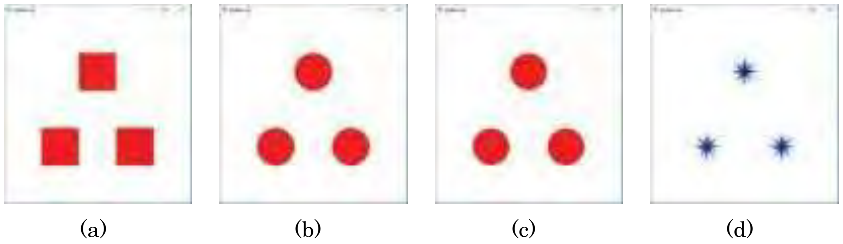

Figure 16.9: Screenshots of points.cpp: (a) Case 0, initial (b) Case 1 (c) Case 2 (d) Case 3.

The four different renderings correspond to the four cases, respectively, of the switch statement in the fragment shader's main. The first,

```
case 0:
    colorsOut = pointColor;
```

simply draws the points unedited in the fragment shader. However, as the up or down arrow keys are pressed to move the points away or near, their size, respectively, decreases or increases. This change is effected by the statement

```
gl_PointSize = 100.0 - zTrans * 10.0;
```

in the vertex shader's main which sets a simple linear ramp on this shader's built-in variable gl_PointSize. Note, of course, that, if the program didn't change the point size, then all three points would be rendered a fixed size, no matter how they were moved (validate this by changing the statement above to fix gl PointSize = 100.0; the reason is explained in the part about rendering points at the end of Section 13.4.1).

Note, as well, that

```
glEnable(GL_PROGRAM_POINT_SIZE);
```

in the application program's initialization routine allows the vertex shader to set the point size in the first place.

In the fragment shader's next switch case

```
case 1:
    coordWRTcenter = gl_PointCoord - vec2(0.5);
    distFromCenter = sqrt(dot(coordWRTcenter, coordWRTcenter));
    if (distFromCenter > 0.5) discard;
    colorsOut = pointColor;
```

is our first use of a point's built-in texture coordinate system, a powerful feature of the newer OpenGL which exposes its internal geometry. Both variables s and t of this coordinate system run from 0 to 1, while a fragment's particular coordinate values are accessed through the built-in variable gl PointCoord.

The first statement above, then, computes the fragment's coordinates w.r.t. the center of the point. Next, the distance of the fragment from the point center is determined and the fragment discarded if it is greater than 0.5. Accordingly, case 1 outputs rounded points. However, note the jaggies along their boundaries.

We try to eliminate these in

```
case 2:
    coordWRTcenter = gl_PointCoord - vec2(0.5);
    distFromCenter = sqrt(dot(coordWRTcenter, coordWRTcenter));
    if (distFromCenter > 0.5) discard;
    alpha = clamp( (distFromCenter - startBlend)/
                   (0.5 - startBlend), 0.0, 1.0 );
    colorsOut = mix(pointColor, backgroundColor, alpha);
```

which is similar to the preceding case, except that a final linear color ramp blends the color of the points with the background color, starting from a distance of startBlend, currently 0.475, from the point's center and ending at its border. Note that the GLSL function clamp(x, a, b) returns x if $a \le x \le b$, a if $x < a$, and b if $x > b$.

Point Sprites

Finally,

```
case 3:
    colorsOut = texture(starTex, gl_PointCoord);
```

very simply implements point sprites – the topic of the pre-shader Section 13.5 – based, obviously, on the point's built-in texture coordinate system. Note that the statements

```
glPointParameteri(GL_POINT_SPRITE_COORD_ORIGIN, GL_LOWER_LEFT);
glEnable(GL_POINT_SPRITE);
```

in setup() of the application program cause the texture t-coordinate to increase from 0 to 1 from bottom to top of the sprite (s is always from left to right) and enable point sprites.

Exercise 16.6. (Programming) Experiment with antialiasing the rounded point by changing the value of startBlend in case 2 of the points.cpp's fragment shader's switch statement.

Try, as well, to use the built-in GLSL function smoothstep (look up the GLSL docs) for a smoother transition from 0 to 1 of the value of the blending parameter alpha (the linear ramp of case 2 may not be smooth where it reaches 0 at the bottom or 1 at the top).

16.3.3 Remaining Effects

Fog

Fog is gone from 4.3. There is no support for fog in the fixed-function part of 4.3 – glFog*() commands are all now obsolete. The reason is simple: as is clear from the discussion in Section 13.2 of the mechanics of fog, to fog is to blend. Ergo, the reader can code fog herself, as we ask her to do next.

Exercise 16.7. (Programming) Shaderize ballAndTorusFogged.cpp from Section 13.2. Obviously, the blending factor in combining an object with the gray fog color will vary with the former's distance from the eye.

Billboarding

Billboarding, discussed earlier in Section 13.3, is simply the clever placement of a textured rectangle to give the illusion of a 3D object. Obviously, this principle does not change whatever OpenGL version we use.

Exercise 16.8. (Programming) Shaderize billboard.cpp.

Antialiasing and Multisampling

We can antialias lines based on the coverage value of their fragments just as in pre-shader OpenGL – see the discussion in Section 13.4.1 – and using the very same commands. We ask the reader to verify this next.

Exercise 16.9. (Programming) Antialias a line in 4.3 with the commands

```
glEnable(GL_BLEND);
glBlendFunc(GL_SRC_ALPHA, GL_ONE_MINUS_SRC_ALPHA);
glEnable(GL_LINE_SMOOTH);
```

in the initialization routine.

Now we see a reason for keeping blending in the fixed-function part of OpenGL 4.3; it would be asking a bit much of the programmer to calculate coverage value per fragment for a line segment and blend accordingly into the color buffer.

Multisampling is enabled in 4.3 via the command glEnable(GL MULTISAMPLE), just as in pre-shader OpenGL. Remember, though, to first create an OpenGL window which supports multisampling by passing GLUT _MULTISAMPLE as a parameter to glutInitDisplayMode().

Sphere Mapping and Cube Mapping

Sphere mapping of Section 13.6, particularly, can be a chore in 4.3. The reason is that neither glTexGeni() nor glEnable(GL TEXTURE GEN _?) is available in 4.3. However, if you followed the math of texture generation – see the footnote on page 424 – then you can probably implement sphere mapping on your own.

The good news is that cube mapping of skyboxes, probably the most popular environment application nowadays, is fully supported in 4.3 with glBindTexture(GL -TEXTURE -CUBE- MAP, ...), glTexParameteri(GL- TEXTURE CUBE MAP, ...) and such all still there to use. Give it a whirl.

Exercise 16.10. (Programming) Shaderize skybox.cpp.

Stencils and Scissors

Thankfully, both the stencil and scissor tests remain very much alive in the fixed-function part of the OpenGL 4.3 pipeline, and in exactly the same manner as discussed in Section 13.7, as we ask the reader to investigate next.

Exercise 16.11. (Programming) Shaderize ballAndTorusStenciled.cpp.

Image Manipulation

One can manipulate images with the help of FBOs just as we saw in Section 13.8, so we ask the reader to do the following.

Exercise 16.12. (Programming) Shaderize imageManipulation.cpp.

Bump Mapping

Of course, the pre-shader bump mapping of Section 13.9 was what we fully redid in the programmable pipeline when discussing 4.3 lighting in Section 15.5 of the last chapter.

Shadow Mapping

The particularly authentic technique of shadow mapping described in Section 13.10 can be implemented in 4.3 as we ask the reader to explore next.

Exercise 16.13. (Programming) Shaderize ballAndTorusShadowMapped.cpp. Some parts will have to be done differently, of course. E.g., in that earlier program we inverted a matrix in a rather roundabout way via the automatic texture coordinate generation sequence

```
glEnable(GL_TEXTURE_GEN_X);
glTexGeni(GL_X, GL_TEXTURE_GEN_MODE, GL_EYE_LINEAR);
glTexGenfv(GL_X, GL_EYE_PLANE, eyePlaneParams);
```

but, now, we have an inverse operation for matrices in the GLSL itself.

16.4 More Animation

We'll add next to our animation repertoire two powerful practical techniques. The first, that of picking an object on the screen, is actually familiar from Chapter 4, but we'll do it entirely differently in 4.3. The second, so-called transform feedback, was introduced in OpenGL 3.0 to allow vertices to be intercepted and their attributes recorded, right after they have been transformed by the vertex, tessellation and geometry shaders (of course, in the case of the latter two, only if they are present). These recorded values may then be used by the program, for example, to modify subsequent passes through the pipeline.

16.4.1 Picking

Figure 16.10: Screenshot of ballAndTorusPicking-Shaderized.cpp moments after the ball has been picked.

Essential to interaction with animated programs is for the user to be able to pick an object on the screen. Section 4.8 from our pre-shader days showed how to do this by entering selection mode via glRenderMode(GL_SELECT) and then setting a pick matrix with gluPickMatrix().

Sadly, glRenderMode() is gone from 4.3, as is gluPickMatrix() and, in fact, the rest of the GLU utility library. Nevertheless, the fragment shader rides to our rescue. In fact, the fragment shader's power affords a much more direct approach to picking than our earlier rather roundabout method via checking for object intersection with a pretend selection volume. Let's see this by shaderizing ballAndTorusPicking.cpp.

Experiment 16.10. Run ballAndTorusPickingShaderized.cpp. The controls are exactly as for ballAndTorusPicking.cpp: space to toggle animation on and off, up/down arrows to change its speed, 'x'-'Z' to rotate the scene, and, most importantly, left mouse click to pick either ball or torus and make it blush. See Figure 16.10 for a screenshot. End

We saw already when discussing line stippling in Section 16.1.3 that the fragment shader has access to the input built-in gl_FragCoord of type vec4, whose (x, y)-values are the coordinates of the fragment in the windows system and z-value is the depth of the fragment. So here's the plan for ballAndTorusPickingShaderized.cpp: obtain mouse click coordinates from the application program and, then, match these in the fragment shader with fragment coordinates; then, pick the object which has a matching fragment of least depth.

What could be simpler? There's a technicality to navigate though. When running the "depth competition" to find the fragment nearest the viewer, we'll evidently need storage which can be shared amongst fragment shader invocations.

The solution is to use variables of the shareable buffer storage type (see the storage qualifiers listed in Table 15.1). Buffer variables must be placed in so-called *interface blocks*, which are blocks of variables declared with a struct-like syntax. Here's the definition of the interface block, named shaderStorage, in ballAndTorusPickingShaderized.cpp's fragment shader:

```
layout(std430, binding=0) buffer shaderStorage
{
    ivec2 clickedCoords;
    uint clickedObj;
    float minClickedDepth;
};
```

The qualifier buffer defines the storage type of the member variables, while the layout directive specifies that member variables will be stored in memory following the particular std430 rules – which will tell us what offsets to use to access these variables from the application program – and that the binding index of the block is 0.

As for the member variables themselves, it's fairly evident what they are intended to hold: the mouse click coordinates place in clickedCoords, while minClickedDepth will hold the smallest depth of a fragment matching the clicked coordinates seen so far, and clickedObj the name of the object to which it belongs.

Note, as well, the redeclaration of gl_FragCoord in the fragment shader

```
layout(origin_upper_left, pixel_center_integer) in  vec4 gl_FragCoord;
```

which moves its origin of pixel coordinates to the upper-left-most pixel (from the default of the lower-left-most) and makes the pixel coordinate values, both gl_FragCoord.x and gl_FragCoord.y, the integral 0.0*,* 1.0*, . . .* (rather than the default of 0.5*,* 1.5*, . . .*). The purpose of this redeclaration is so the coordinate system of the fragment shader matches exactly that of the OpenGL window which, of course, the application's mouse control uses.

To the application program next, where the first three of the statements

```
glBindBuffer(GL_SHADER_STORAGE_BUFFER, buffer[SHADER_STORAGE]);
glBufferData(GL_SHADER_STORAGE_BUFFER, 16, NULL,
             GL_DYNAMIC_COPY);
glBindBufferBase(GL_SHADER_STORAGE_BUFFER, 0,
                 buffer[SHADER_STORAGE]);

storageBufferPtrInt = (int*)glMapBuffer(GL_SHADER_STORAGE_BUFFER,
                                        GL_READ_WRITE);
storageBufferPtrFloat = (float*)&storageBufferPtrInt[0];
```

in the initialization routine set up a shader storage buffer in GPU memory to hold the buffer variables declared in the interface block shaderStorage – in particular, note that the second parameter of glBindBufferBase(), being 0, specifies the binding index of the associated interface block. The final two statements map pointers to the buffer data, the integer pointer also cast as a float pointer in the last statement because we'll need to access both kinds of data in the buffer.

Moreover, the std430 layout rules (see the red book for detailed specs) mean that the variables of the fragment shader's interface block shaderStorage are packed into 128 bits: two successive 32-bit ints for clickedCoords, followed by one 32-bit uint for clickedObj, and then one 32-bit float for minClickedDepth.

Now that we have all the data structures in place, the logic of the program is simple to understand. On a left click, the mouseControl() function executes the following:

```
storageBufferPtrInt[0] = x;
storageBufferPtrInt[1] = y;
storageBufferPtrInt[2] = NONE;
storageBufferPtrFloat[3] = 1.0;

isSelecting = 1;
glUniform1i(isSelectingLoc, isSelecting);

glutPostRedisplay();
```

These statements first of all put the click coordinates into clickedCoords, the value NONE in clickedObj, and 1 in minClickedDepth (note that the fragment depth in gl_FragCoord.z is normalized from 0 to 1, 0 being nearest the eye and 1 farthest away, so a minClickedDepth value of 1 means, effectively, infinite depth or that no object has been selected).

Next, "selection mode" (our own and nothing to do with the OpenGL environment as in using pre-shader glRenderMode()) is entered by setting isSelecting to 1, and the drawing routine called, which means, of course, that the fragment shader will run for each fragment generated. Accordingly, see the following block in the fragment shader's main which runs the "depth competition" for fragments matching the click:

```
if (isSelecting == 1)
if (      (abs(gl_FragCoord.x - clickedCoords.x) <= 1)
       && (abs(gl_FragCoord.y - clickedCoords.y) <= 1)
       && (gl_FragCoord.z < minClickedDepth)
   )
{
   minClickedDepth = gl_FragCoord.z;
   clickedObj = object;
}
```

As you see, we allow a tolerance of one pixel in both the x and y directions for a fragment to match the click; if a fragment does match and it is closer to the eye than the currently closest fragment, then we update minClickedDepth to the depth of the current fragment and clickedObj to the object to which this fragment belongs. The remaining statements

```
if (object == SPHERE)
---
if (object == TORUS)
---
```

in the fragment shader's main either highlight the picked object in red if indeed either ball or torus is picked, or draw both in their respective default colors.

Finally, returning to the application program, the statements

```
if (isSelecting == 1)
{
   highlightFrames = 10;
   glUniform1i(highlightFramesLoc, highlightFrames);

   isSelecting = 0;
   glUniform1i(isSelectingLoc, isSelecting);
}
```

at the end of the drawing routine set the number of frames to highlight the picked object and restore non-selection mode.

Exercise 16.14. (Programming) Redo Exercise 4.83 from Section 4.8, now in 4.3.

Picking by Color Coding

Yet another popular method to pick objects is by means of so-called *color coding*. . Here's how it works. When the user picks a pixel, the program enters a picking phase in which the entire scene is redrawn, but with objects of interest drawn in different colors, in other words, objects are color coded (see Figure 16.11). Next, data from the picked pixel is read with the help of glReadPixels() and its color decoded to determine the picked object. Obviously, one would want to disable actual drawing to the screen in the picking phase, which can be done by enclosing it in a glEnable(GL RASTERIZER DISCARD)-glDisable(GL RASTERIZER DISCARD) block.

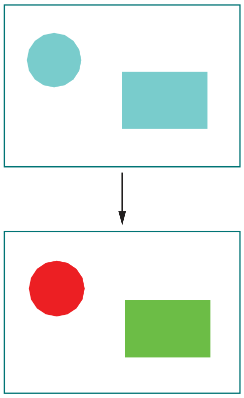

Figure 16.11: Color coding.

Exercise 16.15. (Programming) Rewrite ballAndTorusPickingShaderized.cpp to use color coding instead.

Exercise 16.16. Compare the two methods of picking. Which one is more efficient?

16.4.2 Transform Feedback

Transform feedback is an operation which may be used to tremendous effect, particularly in animated programs. What it does is record into a buffer selected attributes of vertices after they have been transformed by the vertex, tessellation and geometry shaders (or, more precisely, the attributes are recorded after the last of these three shader stages, depending on which are present). The contents of this recording buffer may then serve as a look-ahead. See Figure 16.12. The particular run-time efficiency of this look-ahead process is that it does not involve any CPU-GPU data transfer, all operations happening withing the GPU itself.

For example, one might run a transformation step of an animation without drawing the results to the frame buffer, but using transform feedback to capture, say, the world coordinates of objects post-transformation. These coordinates may then be used to rearrange the animation, e.g., if a collision is detected. In fact, we have a program exactly along these lines.

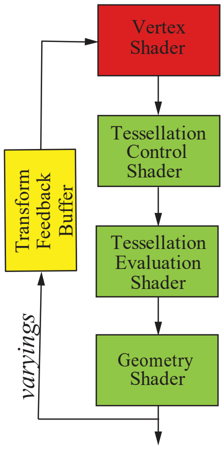
Vertex Shader
Tessellation Control Shader
Tessellation Evaluation Shader
Geometry Shader
Transform Feedback Buffer
varyings

Figure 16.12: Transform feedback data flow. Captured variables are *varyings*.

Experiment 16.11. Run ballsAndTorusTransformFeedback.cpp. The controls are exactly as for ballAndTorusShaderized.cpp: space to toggle animation on and off, up/down arrows to change its speed, and 'x'-'Z' to rotate the scene.

However, instead of one ball, now there are two, initially coincident, which travel in opposite directions around the torus. When the balls intersect they are red, when they are close (closer than a particular threshold distance) they turn orange, and beyond that they are blue. Figure 16.13 is a screenshot when the balls are close. End

Figure 16.13: Screenshot of ballAndTorusTransformFeedback.cpp when the balls are close.

Here's the plan how to use transform feedback in the program. Firstly, observe that since the balls are of radius 2 each, they intersect when the distance between their centers is at most 4 units. So, we'll use transform feedback to record the world coordinates of the two centers in order to determine how far apart they are: if they are at most 4 apart, implying that the balls intersect, we draw them red; if they are at most 8 (an arbitrarily chosen value) apart then orange; otherwise, they are drawn blue. To track the ball centers, then, we create a CENTER object, in addition to SPHERE and TORUS, simply to hold a center's (x, y, z, w) homogeneous world coordinates, particularly in the Vertex variable centerVertex, initialized to $[0, 0, 0, 1]^T$ because sphere.cpp creates balls centered at the origin.

Now, let's see how transform feedback is set up in the initialization routine. The statement

```
glTransformFeedbackVaryings(programId, 1, varyings,
                                            GL_INTERLEAVED_ATTRIBS);
```

specifies the shader outputs, aka *varyings*, to be recorded through transform feedback. Specifically, the third parameter varyings is the array of names of the varyings (only the one name centerWorldCoords in our case defined in the global array varyings[]). The second parameter is the number of names, while the first parameter identifies the program, and the last specifies the mode in which to record the varyings. The options for this last are GL_INTERLEAVED_ATTRIBS, when all the varyings are recorded one after another in one buffer, and GL_SEPARATE_ATTRIBS, when each varying is recorded in its own buffer. Since we have a single varying centerWorldCoords, both options are effectively identical for us.

The program must be linked *after* the transform feedback varyings are defined which explains the location of the glTransformFeedbackVaryings() statement in the code.

Now, if you see the vertex shader, then you find the one varying centerWorldCoords, in fact, set by

```
layout(location=2) in vec4 centerCoords;
---
out vec4 centerWorldCoords;
vec4 coords;
---
    if (object == CENTER)
    {
        coords = centerCoords;
        centerWorldCoords = modelViewMat * coords;
    }
```

In other words, centerWorldCoords are the world coordinates of the current ball's center after modelview transformation.

Returning to the application program's initialization, a *transform feedback object* is created and bound by the statement pair

```
glGenTransformFeedbacks(1, transformFeedback);
glBindTransformFeedback(GL_TRANSFORM_FEEDBACK, transformFeedback[0]);
```

similarly to how VAO and VBOs are created and bound, the id of the object, obviously, stored in transformFeedback[0].

Next, the statement block

```
glBindBuffer(GL_TRANSFORM_FEEDBACK_BUFFER,
                       buffer[TRANSFORM_FEEDBACK]);
glBufferData(GL_TRANSFORM_FEEDBACK_BUFFER, 2*sizeof(centerVertices),
                       NULL, GL_DYNAMIC_COPY);
glBindBufferBase(GL_TRANSFORM_FEEDBACK_BUFFER, 0,
                             buffer[TRANSFORM_FEEDBACK]);
```

sets up a *transform feedback buffer* in a manner exactly similar to how we set up a shader storage buffer in the previous section on picking, in particular, binding the buffer[TRANSFORM_FEEDBACK] as a transform feedback buffer, reserving space for it, and specifying the binding index. Note that the space 2*sizeof(centerVertices) reserved is for the (x, y, z, w)-coordinates of two ball centers, because one draw call draws two balls.

Next,

```
glGenTextures(1, texture);
glActiveTexture(GL_TEXTURE0);
glBindTexture(GL_TEXTURE_BUFFER,    texture[0]);
glTexBuffer(GL_TEXTURE_BUFFER,    GL_RGBA32F,
                     buffer[TRANSFORM_FEEDBACK]);
```

```
tfBufferLoc = glGetUniformLocation(programId,
                                   "transformFeedbackTex");
glUniform1i(tfBufferLoc, 0);
```

creates a TBO – see the discussion of helixListShaderizedInstanceCounter.cpp in Section 16.1 where we first used texture buffer objects – which is referenced by the uniform transformFeedbackTex in the fragment shader and whose data source is the transform feedback buffer set up earlier. The reason to bind a TBO to the transform feedback buffer is for the fragment shader to be able to access its values.

Finally, the application program's drawing routine, as indicated by comments there, is two phase: first, a simulation phase to do transform feedback with nothing drawn to the screen, then a rendering phase where actual drawing happens. The first of the beginning two statements

```
glBeginTransformFeedback(GL_POINTS);
glEnable(GL_RASTERIZER_DISCARD);
```

of the simulation phase starts transform feedback, specifying that the type of primitive to be recorded is points. The second statement cuts the pipeline off just before rasterization, so that drawing and recording takes place in this pass with nothing actually reaching the screen. As expected, the rendering phase begins with the inverse pair

```
glDisable(GL_RASTERIZER_DISCARD);
glEndTransformFeedback();
```

to begin drawing to the screen without recording. Let's now see what exactly is drawn in the two phases. It's best to examine the rendering phase first, where the drawing commands are exactly as in ballAndTorusShaderized.cpp, except that there is an additional ball revolving in a direction opposite to the first, the command

```
modelViewMat = rotate(modelViewMat, longAngle,
                      vec3(0.0, 0.0, 1.0));
```

in the transformation block preceding the first ball vs. the corresponding one

```
modelViewMat = rotate(modelViewMat, -1.0f*longAngle,
                      vec3(0.0, 0.0, 1.0));
```

in the block preceding the second doing the needful.

Now, if you compare, the preceding simulation phase is identical in its transformation commands to the rendering phase; however, the torus is not drawn and, instead of the spheres, their respective centers are drawn because its their world coordinates that we care for. So, at the end of a simulation trip down the pipeline the (transformed) (x, y, z, w)-coordinates of the two ball centers are captured one after another in the TBO transformFeedbackTex.

The rest of the program logic now falls in place from a reading of the fragment shader. Here is the latter's main:

```
void main(void)
{
   center0 = texelFetch(transformFeedbackTex, 0).xyz;
   center1 = texelFetch(transformFeedbackTex, 1).xyz;
   distBetweenCenters = distance(center0 , center1);

   if (object == SPHERE)
   {
      colorsOut = hemColor;
      if (distBetweenCenters <= 8.0) colorsOut = orangeColor;
      if (distBetweenCenters <= 4.0) colorsOut = redColor;
   }
   if (object == TORUS) colorsOut = torColor;
}
```

The two ball center *xyz*-coordinates, as recorded in the simulation pass of the drawing routine, are fetched from the TBO transformFeedbackTex, their distance calculated, and ball colors set accordingly.

The reader thinking "So what's the big deal about calculating the distance between two ball centers?" should consider the difficulty of determining the world coordinates of the ball centers, or any vertex, *after* they have been transformed by animation. In fact, in the pre-shader world the only way to do this would be to parallely do the matrix-vector multiplications happening inside the pipeline on our own in the application program, in order to determine a ball center's current coordinates.

Now, with transform feedback we can simply sneak into the pipeline after the shader stages have worked their magic and "steal" whatever vertex values we want! Transform feedback is a tremendous resource indeed.

Exercise 16.17. (Programming) Exercise 4.46 from Chapter 4 was to animate a single cue ball rolling on a pool table. Use transform feedback to detect and react to collisions in that scenario. Can you add a second ball?

A killer app, so to speak, for transform feedback is particle systems, e.g., to simulate sparks, water spray, smoke, and such. In fact, managing particle systems was a prime motivation for inventing transform feedback in the first place. We have a particle system example ourselves but postpone it till the section on geometry shaders because it needs one.

16.5 Tessellation Shaders

Vertex shaders, while they can accomplish much as we have seen, have two major limitations: (a) they can only update attributes per vertex without access to data from other, say, neighboring, vertices, and (b) cannot generate additional geometry, e.g., new vertices. We'll run into these limitations, for example, in the common game scenario of multiple objects on screen, some moving in close to the viewer, some away. In such a situation, we often want to adaptively refine an object's representation depending on its closeness to the camera – progressively generating more geometry, in other words, detail, as it comes in to occupy greater screen space, and reversing the process as it moves off, neither of which the vertex shader is capable of doing. In fact, it was to solve precisely this kind of problem *within the GPU* – one can always create new meshes for an object in the application program, but then comes the cost of communication over the PCI bus – that the tessellation shader was conceived (and, in fact, got its name).

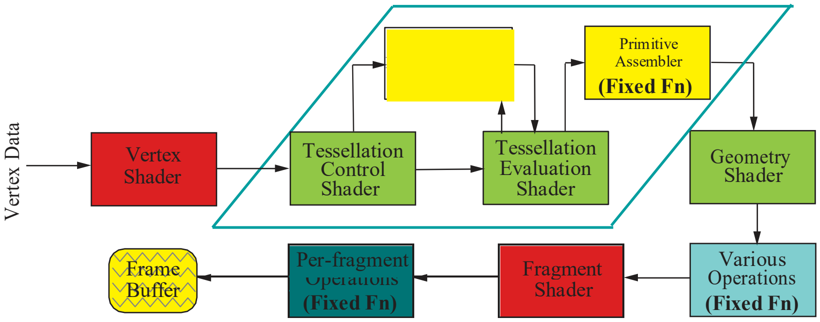
Vertex Data
Vertex Shader
Tessellation Control Shader
Primitive Assembler (Fixed Fn)
Tessellation Evaluation Shader
Geometry Shader
Various Operations (Fixed Fn)
Fragment Shader
Per-fragment Operations (Fixed Fn)
Frame Buffer

Figure 16.14: OpenGL programmable pipeline showing tessellation details in the green parallelogram (modified from Figure 15.1(b)).

The tessellation shader is a fairly complex *optional* component of the programmable pipeline consisting of four modules – the tessellation control shader (TCS), tessellation primitive generator (TPG), tessellation evaluation shader (TES) and a primitive assembler (PA) – the bulk of the workflow going in that order. See Figure 16.14 which shows all possible data paths in the tessellation process. Of the four modules, the TCS and TES are programmable, while the TPG and PA are fixed function, So, the tessellation shader is actually two-shaders-in-one, plus fixed function support. To be more precise, even the TCS is optional; of the two tessellation shaders, only the TES is mandatory if one wants tessellation.

We begin with a simple scenario showing how the four modules combine. Let's say we want to tessellate a cubic Bézier cuve C specified by 4 control points Q_i $0 \leq i \leq 3$, as a line strip (in other words, approximate C with a line strip). See Figure 16.15. Say the parametric functions defining C are

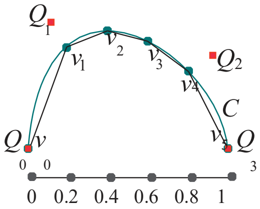

Figure 16.15: Cubic Bézier cuve with control points Q_i tessellated as a 5-segment line strip whose vertices v_i are images of a sample grid on $[0, 1]$.

$$x = f(t), \; y = g(t), \; z = h(t) \tag{16.1}$$

for t in the parameter domain $[0, 1]$. It does not matter here what these functions are actually; just that they exist and depend, obviously, on the control points Q_i.

We plan to draw C following the principles of Section 10.1.3, first splitting $[0, 1]$ into a sample grid of 5 equal intervals – the 6 sample points being $0, 0.2, 0.4, 0.6, 0.8$ and 1 – then computing the mapped samples $v_i = (f(t_i), g(t_i), h(t_i))$, $0 \leq i \leq 5$, on C, where $t_i = 0.2i$. Finally, we want the v_i joined as the vertices of a line strip.

Here, then, is how this plan would execute with tessellation shaders. The TPG, given the tessellation level of 5, would compute the sample sequence $t_i = 0.2i$, $0 \leq i \leq 5$, and send it to the TES. The TES would also be input the control points Q_i. The TES then would use the equations in (16.1) to compute the mapped samples v_i, $0 \leq i \leq 5$, on C, and send them to the PA, which would then make the line strip $v_0v_1v_2v_3v_4v_5$, passing it on down the pipeline.

Think of it this way: the TPG makes the "abstract" tessellation $t_0t_1t_2t_3t_4t_5$ (a straight line strip) of the parameter domain $[0, 1]$, which the TES and PA then turn into the "real" tessellation $v_0v_1v_2v_3v_4v_5$ of C. The TES does the heavy lifting of computing the v_i from the t_i; the PA simply uses the v_i to sequence the final line strip.

Remark 16.3. On a first encounter with tessellations shaders, the TPG is often most confusing. First of all, it's a bit of a misfit in the OpenGL pipeline – it is entirely *oblivious* of application data, e.g., vertex coordinates. The TPG is more of a refugee module from a math app like MATLAB. Given a level specification, which was 5 in our example above, the TPG simply computes a tessellation at that level of an abstract parameter domain, $[0, 1]$ in our example.

What about the TCS? Well, it is optional and the story could very well end just as above with no mention of a TCS. However, if we do have a TCS, then it is right at the front of the tessellation process, receiving input vertices from the vertex shader. The TCS can then use its input set (called, typically, input patch) to produce an output set (output patch) to send on to the TES in pretty much whatever manner it chooses. Moreover, the TCS, if present, must tell the TPG the tessellation levels to use. We'll add a slight twist to the earlier scenario in order to involve a TCS.

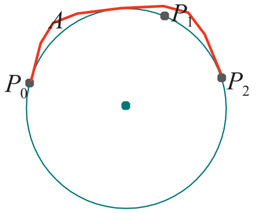

Figure 16.16: Arc A of a circle joining three vertices.

Suppose that we want to tessellate the arc A of a circle which goes through the 3 input vertices P_0, P_1, P_2 in that order. See Figure 16.16 (assuming that the 3 vertices are not collinear, then indeed there is a unique such arc A). So, the TCS's input patch which it receives from the vertex shader, after the latter has transformed the vertices as it sees fit, consists of P_0, P_1, P_2. Now, suppose that we have already made a design decision, for whatever odd reason, that the only curves to be drawn are cubic Bézier curves.

Therefore, we must approximate A with a cubic Bézier curve, in other words, come up with 4 control points Q_i, $0 \leq i \leq 3$. Let's say we do this in the following simple-minded manner:

$$Q_0 = P_0, \; Q_1 = (P_0 + P_1)/2, \; Q_2 = (P_1 + P_2)/2, \; Q_3 = P_2 \tag{16.2}$$

These equations are then implemented in the TCS to produce the output patch Q_i, $0 \leq i \leq 3$, which it then ships to the TES, while simultaneously supplying the TPG with the tessellation level value of 5, at which point we are back to the start of the earlier scenario.

Time now to get technical. We're going to explore, successively, in fair detail the TCS, TES and TPG, which are tessellation-specific modules. The PA, however, is a generic module which assembles real-world primitives given their vertex coordinates and asked geometry (e.g., a line strip or triangle strip from a sequence of vertices). As it is not specific to tessellation, we won't discuss it further here. And, of course, we're going to reference live code all the way. In fact, we have programmed the example scenario above in tessellatedCurve.cpp.

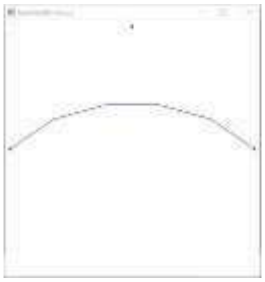

Figure 16.17: Screenshot of tessellatedCurve.cpp initially.

Experiment 16.12. Run tessellatedCurve.cpp. You see the three input vertices and an initially 5-segment Bézier curve polyline. Press the up/down arrow keys to increase/decrease the number of segments. Figure 16.17 is a screenshot with the initial five segments.

The Bézier curve is evidently a poor approximation to the circular arc (not drawn) through the three input vertices because of the rather naive setting of control points in (16.2), but this is irrelevant to our understanding of the code which is discussed through the next few sections.

Incidentally, it's interesting of itself to see how the program goes about drawing the three input vertices and the Bézier curve together. Its initialization routine actually attaches only the vertex and fragment shaders. The drawing routine, then, first attaches the TCS and TES to draw the Bézier polyline, and, next, detaches both to draw the points – of course, one does not want any tessellation happening when drawing just points. End

16.5.1 TCS (Tessellation Control Shader)

The input to the TCS is a new OpenGL primitive, namely *patch* – the symbol being GL_PATCHES – which is just an ordered list of vertices of the size *inputPatchSize* set by a statement of the form

```
glPatchParameteri(GL_PATCH_VERTICES, inputPatchSize)
```

in the application program. The last line

```
glPatchParameteri(GL_PATCH_VERTICES, 3);
```

of tessellatedCurve.cpp's initialization routine sets *inputPatchSize* to 3.

Of course, as is evident from the layout of the OpenGL pipeline (Figure 16.14), each vertex entering into a patch is first processed by the vertex shader. In tessellatedCurve.cpp, though, the vertex shader is particularly hands-off. It simply reads each input vertex's coordinates into the per-vertex built-in variable gl Position, transforming them no further.

Patches themselves are generated using GL_PATCHES in a drawing command – one being created every *inputPatchSize* vertices. Therefore, given that tessellatedCurve.cpp's *inputPatchSize* is 3, the command

```
glDrawArrays(GL_PATCHES, 0, 3);
```

in its drawing routine means that its TCS gets exactly one patch.

Generally, the pair of statements

```
glPatchParameteri(GL_PATCH_VERTICES, inputPatchSize);
...
glDrawArrays(GL_PATCHES, first, countVertices);
```

in the application program would cause the TCS to read *countVertices*/*inputPatchSize* patches from the vertex shader.

The TCS has access to all per-vertex built-in attributes, set by the vertex shader, for every vertex in each input patch. Accordingly, the data for each input patch, as read by the TCS, is in a built-in variable gl_in, which is an array of structures of the size of the patch, the three fields of the structure corresponding to the three built-in vertex attributes. Here is its declaration:

```
in gl_PerVertex
{
    vec4 gl_Position;
    float gl_PointSize;
    float gl_ClipDistance[];
}  gl_in[gl_PatchVerticesIn];
```

The declaration is implicit as gl_in is built-in, so the programmer can access it without making any declarations of her own. The size of the above array is recorded in the built-in gl_PatchVerticesIn, which is accessible by the TCS – it is, of course, equal to *inputPatchSize*, the size of an input patch. The TCS may, additionally, be supplied user-defined per-vertex attribute values, beyond the three built-ins, by the vertex shader (tessellatedCurve.cpp's vertex shader does not do this).

Now, the TCS must produce an output patch for each input patch to send the TES. As well, it has to set the tessellation levels per output patch to control the operation of the TPG.

The number of vertices per output patch is set by a statement of the form

```
layout(vertices = outputPatchSize) out;
```

in the TCS. This number is accessible to the TCS in the built-in gl_PatchVerticesOut. The TCS of tessellatedCurve.cpp sets *outputPatchSize* to 4 with the statement

```
layout(vertices = 4) out;
```

The TCS executes once per output patch vertex. The sequence number of the currently processing output patch vertex within the current patch is the value of the built-in variable gl_InvocationID. Moreover, the sequence number of the current patch in the current drawing statement is contained in the built-in variable gl_PrimitiveID. The per-patch output is a built-in of the same form as the input, viz.,

```
out gl_PerVertex
{
    vec4 gl_Position;
    float gl_PointSize;
    float gl_ClipDistance[];
} gl_out[gl_PatchVerticesOut];
```

the size of the array being that of an output patch.

The switch statement below in the main routine of tessControlShader.glsl creates the four vertices of the output patch, to be used as the control points of a cubic Bézier curve in the TES, from the three input vertices, following the equations (16.2).

```
switch(gl_InvocationID)
{
     case 0:  gl_out[ gl_InvocationID ].gl_Position =
                  gl_in[0].gl_Position; break;
    case 1:  gl_out[ gl_InvocationID ].gl_Position =
                  (gl_in[0].gl_Position + gl_in[1].gl_Position)/2.0; break;
    case 2:  gl_out[ gl_InvocationID ].gl_Position =
                  (gl_in[1].gl_Position + gl_in[2].gl_Position)/2.0; break;
    case 3: gl_out[ gl_InvocationID ].gl_Position =
              gl_in[2].gl_Position; break;
    default: break;
}
```

It is important to note at this time a quantum leap in capability of the TCS over the vertex shader. The vertex shader is invoked once per vertex with access to only the current vertex's data; the TCS, on the other hand, is invoked once per output patch vertex with access to the *entire* gl_ in and gl_ out arrays. The vertex shader is effectively "blind" to its current vertex's neighbors. Not so the TCS, which has a global view, seeing *all* the vertices in its current input and output patches. In fact, we see from the switch statement above how tessellatedCurve.cpp's TCS uses the position of more than one input vertex, as well as the sequence number of the current output vertex, to calculate the latter's position.

At this time, tessellatedCurve.cpp's TCS has discharged its first responsibility of specifying its one output patch. It discharges the second of setting the tessellation levels for this output patch for the benefit of the TPG with the statement pair

```
gl_TessLevelOuter[0] = 1.0;
gl_TessLevelOuter[1] = tessLevelOuter1;
```

Now, the so-called inner and outer tessellation levels are contained in the following built-in per-patch arrays, respectively:

```
patch out float gl_TessLevelInner[2];
patch out float gl_TessLevelOuter[4];
```

So, tessControlShader.glsl sets gl TessLevelOuter[0] to 1.0 and gl TessLevelOuter[1] to the value of the application-provided uniform tessLevelOuter1 (initially, 5.0). It does not set the two inner tessellation levels or the other two outer levels because they are never used in this particular program. We'll see exactly what all these tessellation levels mean to the TPG when we come to the working of the latter.

The TCS may additionally set user-defined per-vertex and per-patch output variables (tessControlShader.glsl does not).

Remark 16.4. As noted earlier, the TCS is not a mandatory part of the tessellation shader. In fact, if there is no need to transform the input patches, simply copying them over as output patches being enough, then one can omit the TCS altogether, leaving the application program to set the tessellation levels via calls

```
glPatchParameterfv(GL_PATCH_DEFAULT_INNER_LEVEL, *pointerToArray)
```

and

```
glPatchParameterfv(GL_PATCH_DEFAULT_OUTER_LEVEL, *pointerToArray)
```

where the pointers are to arrays of inner and outer tessellation levels, respectively.

16.5.2 TES (Tessellation Evaluation Shader)

The input to the TES includes all the built-in attributes for each vertex in the patch output by the TCS, in particular, the array

```
in gl_PerVertex
{
    vec4 gl_Position;
    float gl_PointSize;
    float gl_ClipDistance[]
} gl_in[gl_PatchVerticesIn];
```

which means, just as the TCS, the TES has a global view, seeing *all* the vertices in its own input patch. The size of the above array is the value of the built-in gl PatchVerticesIn accessible by the TES – it is the size of a patch input to the TES, the same, of course, as the size of a patch output from the TCS.

The TES can also read the input per-patch built-in arrays gl TessLevelInner[2] and gl_TessLevelOuter[4] specifying tessellation levels for the TPG.

The TES has two functions. Firstly, it must produce a world space vertex for each *patch domain vertex* – these are the vertices produced by the TPG from tessellating its assigned parameter domain (typically called patch domain in the tessellation shading context). Secondly, the TES has to configure the TPG by assigning values to a particular set of parameters as we'll see.

The TES executes once for each patch domain vertex emitted by the TPG, computing and outputting to the PA the corresponding world space vertex, in particular, setting values for the built-in member variables below:

```
out gl_PerVertex
{
    vec4 gl_Position;
    float gl_PointSize;
    float gl_ClipDistance[];
}
```

For this purpose, it has access to the coordinates of the current patch domain vertex in the built-in 3-vector gl_TessCoord. Keep in mind that the patch domain vertices lie in the abstract patch domain – e.g., [0, 1] in our example scenario – and not world space. Typically, the TES uses these coordinates, as well as its input patch vertex values, to compute the current world space vertex. The sequence number of the current patch in the current rendering statement may be read, too, by the TES in the built-in gl_PrimitiveID.

In the case of tessellatedCurve.cpp, here is the main routine of its TES tessEvaluationShader.glsl:

```
void main( )
{
    q0  =  gl_in[0].gl_Position;
    q1  =  gl_in[1].gl_Position;
    q2  =  gl_in[2].gl_Position;
    q3 = gl_in[3].gl_Position;

    u  =  gl_TessCoord.x;

    c0  = (1.0-u)  *  (1.0-u)  *  (1.0-u);
    c1  =  3.0  *  u  *  (1.0-u)  *  (1.0-u);
    c2 = 3.0 * u  * u  * (1.0-u);
    c3 =  u *  u *  u;

    gl_Position = c0*q0  +  c1*q1  +  c2*q2  +  c3*q3;
}
```

The 4 control points q0, . . ., q3 of the cubic Bézier curve to be drawn are the TES's input patch vertices, as the first four statements indicate. The last five statements show the TES applying the parametric equations for a cubic Bézier curve to calculate the world position of the output vertex. From the middle statement, the curve parameter u is the *x*-value gl_TessCoord.x of the patch domain, the latter being 1-dimensional in this case. The sequence of TES output vertices (initially, numbering 6 for tessellatedCurve.cpp) is sent to the PA to be linked into a line strip, which is finally rendered.

The TES, additionally, configures the TPG with a command of the form

```
layout(primitive, tessellationSpacing, orientation, pointMode) in
```

where *primitive* is one of quads, isolines and triangles, which specifies both the kind of primitive output by the TPG and the kind of patch domain tessellated by the TPG to produce the output primitives; *tessellationSpacing* is one of equal spacing, fractional even _spacing and fractional odd _ spacing; *orientation*, required only if output is 2D, is one of cw and ccw; and, *pointMode* is an optional parameter which may be points. We'll have more to say about these in the next section on the TPG.

The command configuring the TPG in tessEvaluationShader.glsl is

```
layout(isolines, equal_spacing) in;
```

whose meaning will be clear once we understand the TPG.

Remark 16.5. The TCS we know is not mandatory. As we saw in Remark 16.4 at the end of the last section, we can simply copy over the its input patches to the TES and set the tessellation levels in the application program. We said then to do this only if there is no need to transform the input patches.

Well, why can't we do this always, even if the input patches must be transformed, asking the TES to take on the task? In other words, is it that the TCS is not just not mandatory, but, in fact, redundant?

Yes, we can eliminate the TCS if we want to and, no, we don't because the separation of the TCS computing on the input to the TES, while the TES computes its own output, allows for these two operations to be *parallelized* separately. Remember that modern GPUs are really monster parallel computers.

Precisely, the computation of the patch vertices output to the TES can be parallelized in the TCS, while the TES can parallelize the computation of the world space vertices it emits to the PA. Moreover, it might be possible as well to run parallel pipelines for multiple patches.

16.5.3 TPG (Tessellation Primitive Generator)

The math gadget, the TPG, lives in fixed-function – there is no corresponding shader to program. However, the TPG is *configured* by the TCS and TES, specifically, by

(a) the floating point tessellation level arrays gl TessLevelInner[2] and gl TessLevelOuter[4] set by the TCS, and,

(b) the TES command layout(*primitive*, *tessellationSpacing*, *orientation*, *pointMode*) in.

We'll be seeing details shortly, but first an overview beginning actually with the TES-related item (b). The value of *primitive*, which is one of quads, isolines and triangles, specifies the type of the TPG's output primitives – i.e., the result of its tessellation – being actually triangles for quads and the namesake primitives for the latter two. The patch domain itself, the base primitive tessellated by the TPG, is a square if the tessellation primitive is quads or isolines, while it is a triangle if the tessellation primitive is triangles.

The value of *tessellationSpacing* may be one of equal_ spacing, fractional _even_ spacing and fractional odd _spacing, which determines how the TPG tessellates an edge. The parameter *orientation*, either cw or ccw, causes the TPG to output vertices in such an order that 2D primitives produced (if any) are accordingly oriented. If the optional parameter *pointMode* is points, then only vertex values are output by the TPG and no adjacency data, i.e., the geometry is suppressed.

As for the TCS-related item (a), the inner and outer tessellation levels contained in the arrays gl_TessLevelInner[2] and gl TessLevelOuter[4] determine the fineness of the subdivision of the interior and perimeter of the patch domain, respectively.

It is the tessellation primitive and the value of *tessellationSpacing* , both set by the TES which, together with the tessellation levels set by the TCS, determine exactly the tessellation. Henceforth, we are going to make the assumptions, reasonable for most applications, that the value of *tessellationSpacing* is equal spacing and that tessellation levels are all integer-valued.

Now, not all tessellation level values may actually be used: which are used depends on the tessellation primitive. Depending on the tessellation primitive as well is the number of coordinates, which is either 2 or 3, produced per output vertex by the TPG. We saw earlier that the patch domain itself, as well as the output primitive type, depend on the tessellation primitive, too. The following table summarizes these dependencies.

Tessellation Primitive	Patch Domain	gl TessLevel... Values Used	Output Primitive Type	Tessellation Coordinates per Vertex
quads	square	Inner[0]-[1], Outer[0]-[3]	triangle	u, v
isolines	square	Outer[0]-[1]	isoline	u, v
triangles	triangle	Inner[0], Outer[0]-[2]	triangle	u, v, w

Table 16.1: Dependencies on the tessellation primitive.

Next, we'll discuss in detail the working of the TPG for each possible tessellation primitive.

quads

Let's work an example, simultaneously explaining the general quads tessellation procedure. We choose arbitrarily the following tessellation level values.

$$
\begin{aligned}
\text{gl\_TessLevelInner[0]} &= 5.0;\\
\text{gl\_TessLevelInner[1]} &= 4.0;\\
\text{gl\_TessLevelOuter[0]} &= 1.0;\\
\text{gl\_TessLevelOuter[1]} &= 2.0;\\
\text{gl\_TessLevelOuter[2]} &= 3.0;\\
\text{gl\_TessLevelOuter[3]} &= 6.0;
\end{aligned}
$$

The patch domain for a quads is the unit square $[0, 1]\times[0, 1]$ on the uv-plane. The tessellation steps are shown from left to right in Figure 16.18.

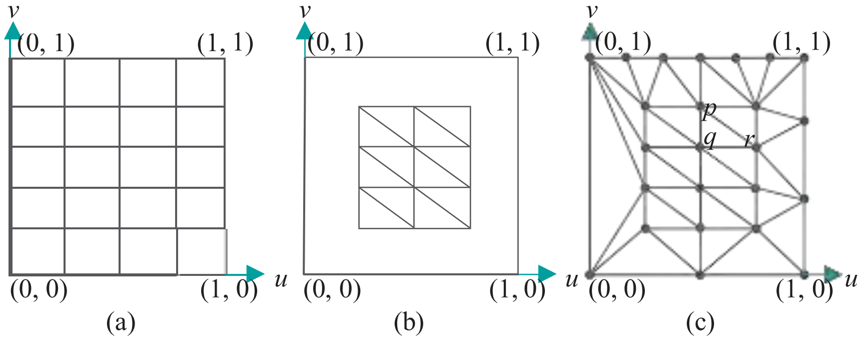

Figure 16.18: Tessellating quads.

Figure 16.18(a): Using the inner tessellation values, first subdivide equally the patch domain into a$\times$4 5 mesh of rectangles, so that there are gl TessLevelInner[0] subdivisions in the v direction, gl TessLevelInner[1] subdivisions in the u direction.

Figure 16.18(b): Next, triangulate each rectangle, except those along the square's perimeter, into two triangles each; erase all rectangles along the perimeter.

Figure 16.18(c): Finally, use the outer values to equally subdivide the four perimeter edges – gl_TessLevelOuter[0] subdivisions of the edge from $(0, 1)$ to

(0, 0), gl_TessLevelOuter[1] subdivisions of the edge from (0, 0) to (1, 0), and so on counter-clockwise. Further, triangulate the annular region along the perimeter using edges connecting the subdivision vertices on the outer perimeter with the outermost vertices of the inner mesh.

Note: Particular triangulations used above are actually left to the OpenGL implementation.

The vertices of the tessellation, shown as solid points in Figure 16.18(c), are sent to the TES, which uses their (u, v) coordinates to compute for each the corresponding world space vertex. The latter are sent next to the PA, which assembles them into the final object following the geometry of the tessellated quad, e.g., the world vertices corresponding to vertices p, q and r of Figure 16.18(c) will define the vertices of one triangle.

Note: The reason for separate tessellation levels for the interior and perimeter is for the user to be able to independently refine the two. In particular, the tessellation of the perimeter of adjoining patches should match.

Isolines

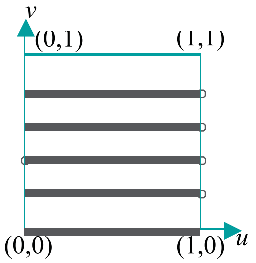

Figure 16.19: Tessellating isolines.

Again, let's do a running example. Only the first two outer tessellation levels are used for isolines. We'll set them to be

```
gl_TessLevelOuter[0] = 5.0;
gl_TessLevelOuter[1] = 4.0;
```

Refer to Figure 16.19 as you read on. As for quads, the patch domain for isolines is the unit square [0, 1]×[0, 1] on the uv-plane. However, instead of triangles, the primitives output are parallel line strips, isolines being the fancy name. In particular, gl _TessLevelOuter[0] horizontal line strips are output, starting with the bottom one on the u-axis (v = 0), splitting the [0, 1] interval of v into gl TessLevelOuter[0] equal subintervals. Note that this means that there is no line strip along v = 1, for, otherwise, the [0, 1] interval would be split into only gl TessLevelOuter[0] _ 1 subintervals. The reason for wanting this asymmetric arrangement, with a line strip on v = 0 but not on v = 1, is to avoid overlap between isolines of adjacent patches. Further, each horizontal line strip consists of gl TessLevelOuter[1] equal line segments.

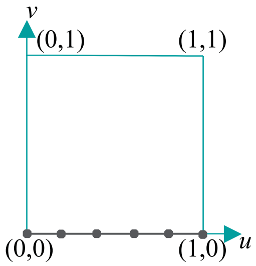

Figure 16.20: tessellatedCurve.cpp's tessellated patch domain.

The final tessellated patch domain output for our example tessellation levels above consists then of the black lines and vertices in Figure 16.19. Again, as for quads, it's the vertices which are delivered to the TES, which uses the (u, v) coordinates of each input vertex to produce the corresponding world space vertex.

Let's revisit tessellatedCurve.cpp. The statement

```
layout(isolines, equal_spacing) in;
```

in tessellatedCurve.cpp's TES and the two

```
gl_TessLevelOuter[0] = 1.0;
gl_TessLevelOuter[1] = tessLevelOuter1;
```

in its TCS mean that the tessellated patch domain output is initially as in Figure 16.20, when tessLevelOuter1 is 5.0 – a single isoline containing 6 vertices dividing it equally into 5 parts – which is why the TES uses only the u-coordinate of patch domain vertices (actually, gl_TessCoord.x in the code) to compute the corresponding world vertex.

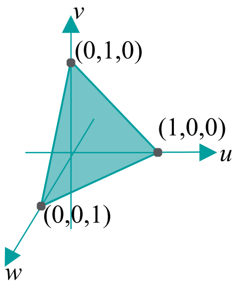

Figure 16.21: Patch domain for triangles.

Triangles

The patch domain for triangles is a triangle situated in uvw 3-space with corners a unit distance along each axis, as in Figure 16.21. The reason for this, rather than a flat triangle on the uv-plane, is the convenience of barycentric coordinates (see Section 7.2). In fact, this patch domain triangle consists exactly of the points (u, v, w) such that $u + v + w = 1$ and $u, v, w \geq 0$, where (u, v, w) serve as barycentric coordinates as well (because $(u, v, w) = u(1, 0, 0) + v(0, 1, 0) + w(0, 0, 1)$). Evidently, the triangle is equilateral. Only the first inner tessellation level and the first three outer levels are used for triangles. So, let's do a running example with the following:

```
gl_TessLevelInner[0]  =  4.0;
gl_TessLevelOuter[0]  =  1.0;
gl_TessLevelOuter[1]  =  2.0;
gl_TessLevelOuter[2]  =  3.0;
```

First, subdivide each triangle edge into gl_TessLevelInner[0] equal segments. From each subdivision vertex drop the perpendicular into the triangle to make a nested inner triangle with each edge subdivided into gl_TessLevelInner[0] −2 equal segments. See Figure 16.22(a) for our example value gl_TessLevelInner[0] = 4.0. Note how the corners of the inner triangle are determined by the perpendiculars dropping from vertices adjacent to the corners of the outer one, e.g., the perpendiculars from p and q meet at the inner corner r.

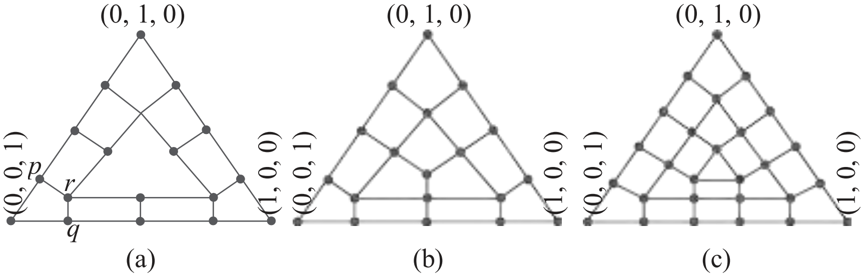

Figure 16.22: Tessellating triangles: (a) & (b) gl_TessLevelInner[0] = 4.0 (c) gl_TessLevelInner[0] = 5.0.

Continue the process of generating nested triangles until one reaches either a single point (which happens when gl_TessLevelInner[0] is even) or an innermost triangle with no subdivided edge (when gl_TessLevelInner[0] is odd). Figure 16.22(b) shows the end figure of this process for our example, where gl_TessLevelInner[0] = 4.0, while Figure 16.22(c) shows it for gl_TessLevelInner[0] = 5.0, an odd number.

Finally, we'll replicate very nearly the final steps for quads: triangulate each quad inside the triangle, except those on the perimeter, into two triangles; erase quads adjacent to the perimeter; use the outer values to equally subdivide the three perimeter edges – gl_TessLevelOuter[0] subdivisions of the edge from (0, 1, 0) to (0, 0, 1), gl_TessLevelOuter[1] subdivisions of the edge from (0, 0, 1) to (1, 0, 0), and gl_TessLevelOuter[2] subdivisions of the edge from (1, 0, 0) to (0, 1, 0); triangulate the annular region along the perimeter using edges connecting the subdivision vertices on the perimeter with the outermost vertices of the inner mesh (as for quads, the triangulations themselves are left to the implementation). Figure 16.23 shows the final tessellation for our example above.

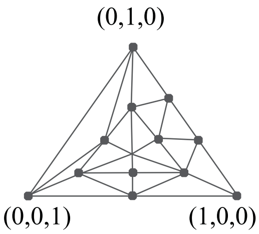

Figure 16.23: Final tessellated triangle for the example tessellation levels.

Remark 16.6. As noted at the start, we have assumed throughout our discussion of the TPG's operation that the value of *tessellationSpacing* is equal_spacing and that tessellation levels are all integer-valued. The variations when this is not true are not difficult and we'll leave the interested reader to consult the red book.

Before we leave tessellation shaders here's a program which tessellates a surface, rather than a curve.

Experiment 16.13. Run tessellatedSphere.cpp. Press space to toggle between filled and wireframe and the up and down arrow keys to move the sphere. The

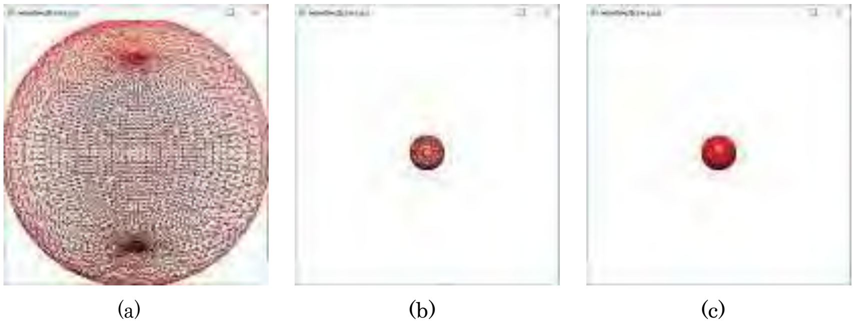

Figure 16.24: Screenshots of tessellatedSphere.cpp all wireframe: (a) Close to the eye (b) Far away (tessellation reduced according to distance) (c) Far away (maximum tessellation).

tessellation primitive is quads and the tessellation levels – all six including the two inner and four outer – are always equal, starting at 50 and decreasing down a staircase function to a minimum of 10 as the sphere moves away. However, pressing 'm' makes all the tessellation levels equal to 50, regardless of how far the sphere has moved; pressing 'm' again restores distance-based tessellation.

Figure 16.24 shows screenshots, all wireframe. The one on the left is a wireframe of the sphere close to the eye; the other two are of the sphere moved the same distance away, the one in the middle being tessellated according to the distance, while the one on the right is maximally tessellated, all levels equal to 50.

The rightmost one is clearly over-tessellated, looking filled rather than wireframe. In fact, the reader can view the filled version of the middle sphere by pressing space to see that it is perfectly smooth, proving that its sparser tessellation is adequate. Excess tessellation is inefficient because it sends redundant triangles down the pipeline and, moreover, tends to introduce aliasing artifacts when the object is moved. End

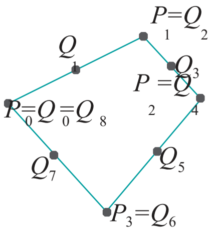

Figure 16.25: The corners of a quad are P_i, control points of a Bézier loop are Q_i.

Exercise 16.18. (Programming) Here's another artificial scenario, much like that for tessellatedCurve.cpp. The four vertices are given of a quad which is to be "approximated" by a 9-control-points Bézier loop, itself drawn as a line loop. See Figure 16.25: the first and last control points are equal and there are control points at the corners of the quad and the middle of its edges.

Write a program for this scenario similar to tessellatedCurve.cpp. Hand-code in the quad's vertex coordinates.

Exercise 16.19. The vertex shader of tessellatedSphere.cpp is, well, empty, yet we have a vertex-rich sphere being drawn. How does this work? How is the sphere's mesh being specfied? In this connection, explain how the command glDrawArrays(GL PATCHES, 0, 1) in the drawing routine instigates the drawing of the sphere.

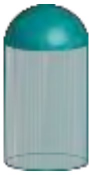

Figure 16.26: Hemisphere on top of a cylinder.

Exercise 16.20. (Programming) Place a tessellated hemisphere on top of a tessellated cylinder, as in Figure 16.26, making sure that the tessellations agree on the shared circular boundary.

The tessellation shader can make good use of transform feedback as we ask the reader to explore next.

Exercise 16.21. (Programming) The tessellation levels in tessellatedSphere.cpp are currently all set in the application program based on the translation parameter zTrans. Do this differently using transform feedback to capture the post-translation coordinates of the sphere's center, in particular, its z-value, and setting tessellation levels accordingly on the server-side at run-time and not in the application program. Of course, you'll need to code a TCS for this, currently there being none.

16.6 Geometry Shaders

Geometry shaders are an optional component of the programmable pipeline meant, just as tessellation shaders, to shift geometry processing from the application program to the GPU. However, geometry shaders are structured quite differently from their tessellation sisters and, in fact, far less complex. A vital commonality, though, is that both derive their computational power from having a global view of input primitives (vs. the one-vertex-at-a-time vertex shader).

Here's an overview of how a geometry shader works: it takes input primitives of a particular specified type (from one of the familiar points, lines and triangles, plus a couple of new so-called ”adjacency” types, namely, lines_adjacency and triangles_adjacency), and produces output primitives of a particular type (precisely, one of points, line strips and triangle strips). Importantly, there is no *a priori* relationship between the input and output types, so, e.g., points may generate line strips, triangles points, and so on. Moreover, one input primitive may generate zero, one or more output primitives. That's it barring gory details (coming up)! Not too bad, huh?

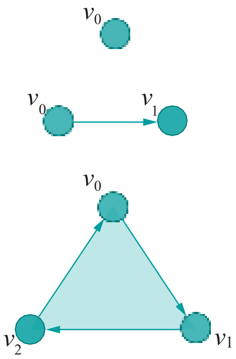

Figure 16.27: Atomic input primitives of type: points, lines, triangles.

The input to a geometry shader arrives from the vertex shader if there is no tessellation, and from the tessellation evaluation shader if there is. So, let's see what sort of input primitive it accepts. The declaration

layout(*inputPrimitive*) in;

in the geometry shader sets *inputPrimitive* to the type accepted, where its value is one of the five on the left of Table 16.2. The corresponding drawing command modes which may be actually used to draw primitives in the application program are in the last column. Whatever drawing command is used, though, its primitives are each split into a sequence of atomic primitives of the input type, whose sizes are in the middle column. The first three input types, points, lines and triangles, whose atomic primitives can be seen in Figure 16.27, are familiar. We'll be explaining the two adjacency input types lines adjacency and triangles adjacency momentarily.

Input Primitive	Atomic Primitive Size	Drawing Command Modes
points	1	GL_POINTS, GL_PATCHES
lines	2	GL_LINES, GL_LINE_STRIP, GL_LINE_LOOP, GL_PATCHES
triangles	3	GL_TRIANGLES, GL_TRIANGLE_STRIP, GL_TRIANGLE_FAN, GL_PATCHES
lines_adjacency	4	GL_LINES_ADJACENCY, GL_LINE_STRIP_ADJACENCY
triangles_adjacency	6	GL_TRIANGLES_ADJACENCY, GL_TRIANGLE_STRIP_ADJACENCY

Table 16.2: Dependencies on the input primitive.

For example, the declaration

```
layout(triangles) in
```

is consistent with the drawing command

```
glDrawElements(GL_TRIANGLE_STRIP, ...)
```

each triangle strip, then, being split into a sequence of (atomic) triangles which are read successively by the geometry shader.

Note: The tessellation shader, if there is one, converts patches into points, lines or triangles before shipping to the geometry shader.

Remark 16.7. The reader may be wondering why we aren't narrating along with live example code as we did for tessellation. We certainly have example programs to show off the geometry shader but thought the technical presentation for this particular topic would go better if we deferred the programs till after.

Output from a geometry shader goes to the fragment shader for rendering. The output type is set to *outputPrimitiveType* by the declaration

```
layout(outputPrimitiveType, maxVertices = maxVerticesVal) out;
```

in the geometry shader, where the value of *outputPrimitiveType* may be one of points, line strip and triangle strip, while *maxVerticesVal* is the maximum number of vertices a single output primitive may have. Observe that 1D and 2D output types are both strips. So, for example, to declare single triangles as output, the appropriate statement would be

```
layout(triangle_strip, max_vertices = 3) out;
```

Note, further, that output primitives are produced one per atomic input primitive. So, if the preceding layout() command is paired with the drawing command

```
glDrawElements(GL_TRIANGLE_STRIP, ...)
```

then one triangle will be output for each one into which the input strip is split.

Adjacency Primitive Types

The purpose of the input adjacency primitive types is to provide the geometry shader with data about the *neighborhood* of a primitive in the object of which it is part. While there are two atomic adjacency primitives types lines_adjacency and triangles_adjacency, there are four drawing command modes whose atomic primitives are one of these two.

The GL_LINES_ADJACENCY drawing mode reads a sequence of individual atomic lines adjacency primitives (just as the GL LINES mode reads a sequence of individual line segments). The GL LINE STRIP_ADJACENCY mode reads a lines_adjacency strip, a drawing primitive which relates to lines_adjacency primitives in the same way a line strip relates to line segments. The GL TRIANGLES ADJACENCY mode reads a sequence of individual atomic triangles adjacency primitives (again as GL_TRIANGLES reads a sequence of triangles). Finally, the GL TRIANGLES_ADJACENCY mode reads a triangles adjacency strip, which relates to triangles _ adjacency in the same way a triangle strip relates to triangles.

Let's discuss next lines_adjacency and triangles adjacency and their strip counterparts.

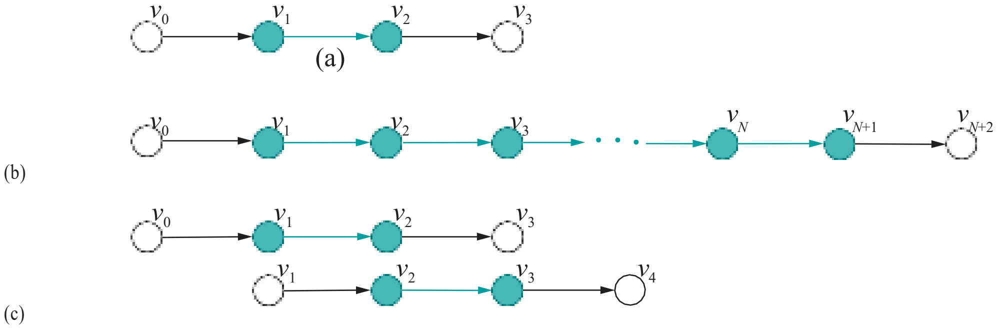

Figure 16.28: (a) Atomic lines adjacency primitive (b) lines adjacency strip primitive (c) First two lines adjacency primitives into which (b) is split. (Arrows indicate line orientation. Hollow black points and black arrows represent adjacency information.)

lines_adjacency: An atomic lines_adjacency primitive is an atomic lines primitive enhanced with adjacency (i.e., neighborhood) information as in Figure 16.28(a); particularly, the middle vertices v_1 and v_2 represent the start and end vertices of a line segment, respectively, while v_0 and v_3 represent v_1's predecessor and v_2's successor, respectively. It is v_0 and v_3 which *represent* the adjacency information for the line segment v_1v_2.

lines_adjacency strip: A lines_adjacency strip primitive consisting of a sequence of $N + 3$ vertices is shown in Figure 16.28(b). The base line strip itself consists of N segments running from vertex v_1 to v_{N+1}, while the predecessor of v_1 is v_0 and the successor of v_{N+1} is v_{N+2}, these representing adjacency.

Now, the atomic primitive corresponding to a lines_adjacency strip is lines_ - adjacency. So, for example, the lines_adjacency strip of Figure 16.28(b), as read in GL_LINE_STRIP_ ADJACENCY drawing mode, in fact, is a sequence of N separate lines_adjacency primitives that is sent to the geometry shader: the first one consists of v_0, v_1, v_2, v_3, the next v_1, v_2, v_3, v_4, and so on, till, finally, v_{N-1}, v_N, v_{N+1}, v_{N+2} (the first two are drawn in Figure 16.28(c)).

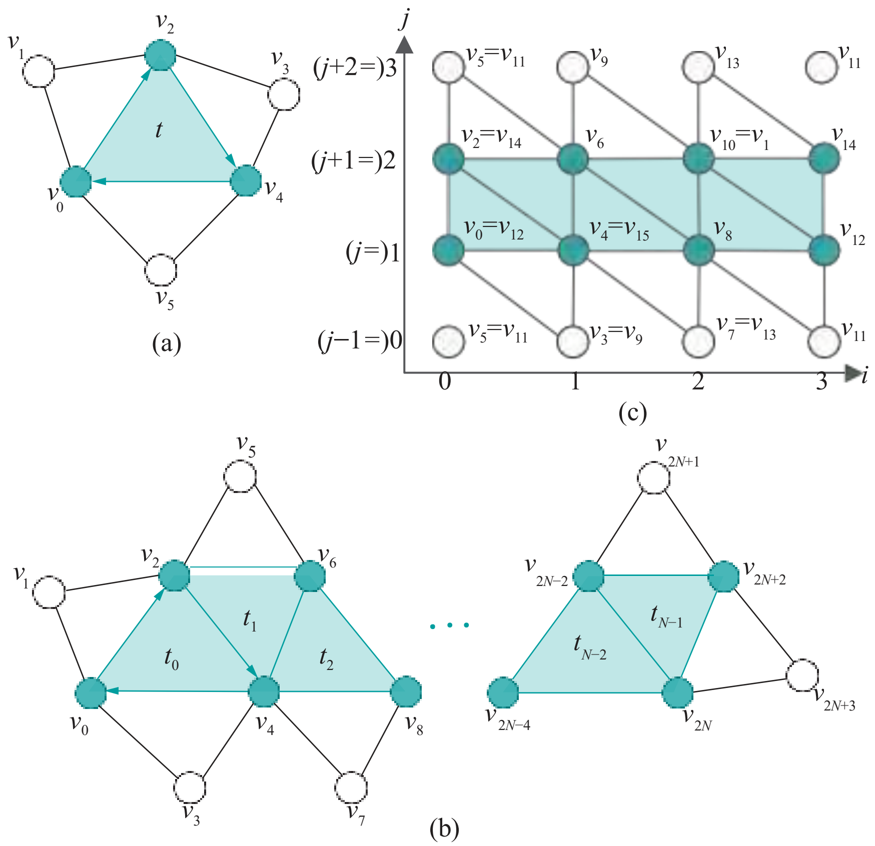

Figure 16.29: (a) Atomic tiangles_adjacency primitive (b) tiangles_adjacency strip primitive. Arrows indicate triangle orientation, e.g., the shaded strip of triangles is consistently oriented beginning with $v_0v_2v_4$. Hollow points and black lines represent adjacency information. (c) Torus mesh with one tiangles_adjacency strip labeled (lower row vertices identified with upper row, left column vertices identified with right column.

triangles_adjacency: An atomic triangles_adjacency primitive is an atomic triangles primitive enhanced with adjacency information. It consists of 6 vertices as in Figure 16.29(a). Specifically, the vertices v_0, v_2 and v_4 are those of a triangle t, while v_1, v_3 and v_5 each is the vertex, not belonging to t, of one of the three triangles abutting t. Obviously, v_1, v_3 and v_5 represent adjacency information.

triangles_adjacency strip: A triangles_adjacency strip primitive consisting of a sequence of $2N + 4$ vertices with a base strip of N (shaded) triangles is shown in Figure 16.29(b) (N is assumed even for this particular configuration; if N is odd, then the last triangle t_{N-1} will look like t_0, rather than t_1). For each triangle of the base strip, we see as well vertices defining each of its three abutting triangles which do not already belong to the base strip, i.e., adjacency information.

The atomic primitive corresponding to a triangles_adjacency strip primitive is triangles_adjacency. So, for example, the triangles_adjacency strip of Figure 16.29(b), as read in GL_TRIANGLE_STRIP_ADJACENCY drawing mode, is a sequence of N triangles_adjacency primitives sent to the geometry shader: the first one consists of triangle t_0's vertices v_0, v_2 and v_4 and its neighboring vertices v_1, v_3 and v_6, the next consists of triangle t_1's vertices v_2, v_4 and v_6 and its neighboring vertices v_0, v_5 and v_8, and so on, till, finally, triangle t_{N-1}'s vertices v_{2N-2}, v_{2N} and v_{2N+2} and its neighboring vertices v_{2N-4}, v_{2N+1} and v_{2N+3}.

Operation of the Geometry Shader

The geometry shader executes once per input atomic primitive and has access to all the per-vertex built-in attributes for every vertex in each input atomic primitive. This global view is precisely the source of the geometry shader's computational power. The data for each such input primitive, as read by the geometry shader, is a built-in variable gl_in, which is an array of structures – the three fields corresponding to the three built-in vertex attributes – of the size of the input primitive (see the middle column of Table 16.2). Here is its definition:

```
in gl_PerVertex
{
    vec4 gl_Position;
    float gl_PointSize;
    float gl_ClipDistance[];
} gl_in[];
```

(Note the similarity with the built-in gl_in defined for the tessellation control shader.) So, for example, the size of gl_in[] is 4 if the input primitive type is lines_adjacency. The geometry shader may additionally be supplied user-defined per-vertex attribute values, beyond the three built-ins. The sequence number of the current atomic primitive in the current drawing statement is contained in the geometry shader's built-in gl_PrimitiveIDIn.

The output data structure of the geometry shader, which goes to the primitive assembler and then on to the fragment shader, is of the same form per vertex as the input, namely,

```
out gl_PerVertex
{
    vec4 gl_Position;
    float gl_PointSize;
    float gl_ClipDistance[];
};
```

Unlike input, though, there is no built-in array to hold multiple gl_PerVertex values to be output. Rather, the geometry shader calls the function EmitVertex() to produce a single vertex using the current values in gl_PerVertex, and, then, the function EndPrimitive() to assemble all the vertices produced since the last EndPrimitive() call (or the beginning of the draw command) into an output primitive of the type specified in the layout(...) out declaration.

Time now to bring the preceding discussion to life with code. We have programmed first a silhouette-extraction algorithm, a popular application for geometry shaders.

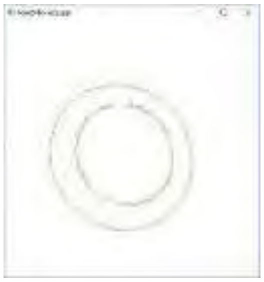

Figure 16.30: Screenshot of torusSilhouette.cpp in silhouette mode.

Experiment 16.14. Run torusSilhouette.cpp. Press the space bar to toggle between the silhouette and mesh of a torus. Press 'x'-'Z' to turn the torus. Figure 16.30

is a screenshot of the torus in silhouette. Note the imperfections in the silhouette at certain alignments arising owing to aliasing, as well as floating point round-off errors, which can be fixed with added effort, but this is not our concern here. End

Let's first understand the simple geometric principle underlying torusSilhouette.cpp. Given a consistent orientation of an object's mesh, an edge is part of its silhouette if it's shared by a front-facing triangle and a back-facing triangle (see Figure 16.31(a)); an edge shared by two front-facing triangles (Figure 16.31(b)) or two back-facing ones is not on the silhouette. Accordingly, our plan is to run through the edges of the torus mesh, comparing the orientation of the triangles on either side, and outputting edges adjacent to differently-oriented triangles.

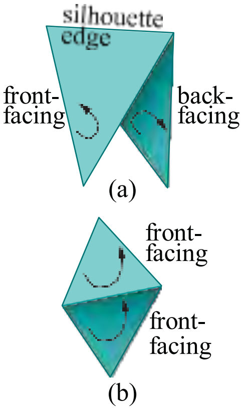

Figure 16.31: Finding a silhouette edge.

Since our plan obviously calls for adjacency information in order to implement, we draw the torus with use of adjacency primitives, precisely,

```
glMultiDrawElements(GL_TRIANGLE_STRIP_ADJACENCY, torCounts,
                    GL_UNSIGNED_INT, (const void **)torOffsets,
                    TOR_LATS);
```

in the drawing routine. For this call to work correctly, the associated source torus.cpp is changed from the version associated earlier with programs such as ballAndTorusShaderized.cpp. The main change is in the function to create the array of index arrays:

```
void fillTorIndices(unsigned int
                    torIndices[TOR_LATS][4*(TOR_LONGS+1)])
{
   int i, j;
   for(j = 0; j < TOR_LATS; j++)
   {
      for (i = 0; i <= TOR_LONGS; i++)
      {
         torIndices[j][4*i] = j * (TOR_LONGS+1) + i;
         torIndices[j][4*i+2] = (j+1) * (TOR_LONGS+1) + i;
      }
      for (i = 0; i < TOR_LONGS; i++)
      {
         torIndices[j][4*i+3] = (j > 0 ? j-1 : TOR_LATS) *
                                (TOR_LONGS+1) + i + 1;
         torIndices[j][4*i+5] = ((j+2) % (TOR_LATS+1)) *
                                (TOR_LONGS+1) + i;
      }
      torIndices[j][1] = (j+1) * (TOR_LONGS + 1) + TOR_LONGS - 1;
      torIndices[j][4*TOR_LONGS+3] = j * (TOR_LONGS + 1) + 1;
   }
}
```

In each of the TOR_LATS iterations of the outer loop, this function computes the 4*TOR_LONGS + 4 (= 2(2*TOR_LONGS) + 4) vertex indices of a triangles adjacency strip primitive containing 2*TOR_LONGS triangles. The best way to understand the computation is from a small concrete example. In fact, see Figure 16.29(c), which shows a torus mesh with both TOR_LATS and TOR_LONGS equal to 3 (note that since this is a torus, the four vertices along the top row are identified with the corresponding vertices along the bottom, and, likewise, for the leftmost and rightmost vertex columns).

Assume that the current value of the outer loop variable j is 1, as indicated by expressions in parentheses to the left of the j-axis. The corresponding triangles adjacency strip, whose base strip is shaded in Figure 16.29(c), is a case of the general such primitive shown in Figure 16.29(b) with the number of triangles N = 2*TOR_LONGS = 6. Match Figures 16.29(b) and (c) to see that the 16 vertices $v_0, \ldots, v_{15}$ of the latter are indeed correctly labeled.

That the four vertices v_0, v_4, v_8 and v_{12}, with indices a multiple of 4, lie successively on row j of the mesh explains the line

```
torIndices[j][4*i] = j * (TOR_LONGS+1) + i;
```

in the function above. Similarly, that the four vertices v_2, v_6, v_{10} and v_{14} lie successively on row $j+1$ of the mesh explains the line

```
torIndices[j][4*i+2] = (j+1) * (TOR_LONGS+1) + i;
```

We'll leave the reader to parse the rest of the function.

The geometry shader takes the stage next. It receives for each of the TOR_LATS number of triangles_adjacency strip primitives produced by the

```
glMultiDrawElements(GL_TRIANGLE_STRIP_ADJACENCY, ...)
```

drawing command, a sequence of $2*$ TOR_LONGS of its corresponding atomic triangles_-adjacency primitive.

Based on the geometric principle stated earlier, the geometry shader must check for each input triangles _ adjacency primitive and each of its edges v_0v_2, v_2v_4 and v_4v_0 – refer to Figure 16.29(a) – if the triangles on either side of the edge are front- or back-facing. If the triangle on one side is front-facing and the other back-facing, then the edge is to be output as a silhouette edge.

To determine if a triangle is front- or back-facing to a viewer located at the origin we have to determine its orientation as perceived by this viewer (by default, CCW is front-facing, CW back-facing). Now, Exercise 9.5 of Chapter 9 tells us that a triangle with vertices (x_1, y_1, z_1), $(x_2, y_2 z_2)$ and (x_3, y_3, z_3), in that order, is perceived by a viewer at the origin to be oriented CW, CCW or as seen edge-on according as the determinant

$$\begin{matrix} x_1 & x_2 & x_3 \\ y_1 & y_2 & y_3 \\ z_1 & z_2 & z_3 \end{matrix}$$

is greater than, less than or equal to zero. Accordingly, the block

```
float orient024 = determinant(mat3(gl_in[0].gl_Position.xyz,
                                   gl_in[2].gl_Position.xyz,
                                   gl_in[4].gl_Position.xyz));
```

in the geometry shader's main calculates the corresponding determinant for triangle $v_0v_2v_4$. Similar blocks compute the determinant for triangles $v_1v_2v_0$, $v_2v_3v_4$ and $v_0v_4v_5$.

Subsequently, in silhouette-drawing mode, edge v_0v_2 is output if the triangles on either side of it, particularly, $v_0v_2v_4$ and $v_1v_2v_0$, are oppositely oriented, in which case their determinant product is negative, the implementing code block being

```
if ( orient024 * orient120 <= 0.0 )
{
   gl_Position = gl_in[0].gl_Position;
   EmitVertex( );
   gl_Position = gl_in[2].gl_Position;
   EmitVertex( );
   EndPrimitive( );
}
```

(observe that we output the edge to silhouette, as well, if one of the triangles is seen edge-on, when its determinant is zero). Similar blocks decide if to output edges v_2v_4 and v_4v_0. In mesh-drawing mode, of course, all three edges v_0v_2, v_2v_4 and v_4v_0 are always output.

Exercise 16.22. (Programming) Comment out the line

```
glAttachShader(programId, geometryShaderId);
```

of torusSilhouette.cpp. What this shows is that, even if there is no geometry shader active, a drawing primitive of adjacency type is still rendered, though, not surprisingly, without use of the adjacency data.

16.6.1 Particle System with Transform Feedback

As we said at the end of Section 16.4.2 on transform feedback, particle systems, in particular, can make powerful use of transform feedback. Following is a program to illustrate just this. We could not include this program in that earlier section because it invokes a geometry shader to create new particles; the reader should certainly review that section though before reading on.

Experiment 16.15. Run particleSystem.cpp. Press space to step through the animation of a decidedly bland particle system. Figure 16.32 is a screenshot a few steps into the animation. We explain below how the program works. End

Figure 16.32: Screenshot of particleSystem.cpp.

To begin with, observe first that we have two program objects, one for the particle system and the other simply to draw the bounding square. We'll pay no more attention, then, to vao[SQUARE] or the programId[SQUARE_PROG] (see Section 16.2.2 if you need to be reminded about control flow using multiple program objects).

On to the particle system itself. Note first of all that we have a struct for particles, defined in particle.h, containing coordinates and velocity.

Now, what our particle system is seen to do is simple. Initially, a single particle starts from the middle of the enclosing square and travels north – a direction arbitrarily set in the velocity of the seed particle initParticle at the top of the application program – in a straight line until it hits a side (the top, of course). Upon collision with the side the particle is destroyed and two new ones created at the point of collision, both traveling back into the square, one in a direction at 45° to the side and the other at $\tan^{-1} 0.5$, approximately 26.57°, to the side. This prescription is repeated for every particle: (a) travel straight until a side of the square is struck, (b) spawn two new particles at that point, one traveling back in at 45° to the side and the other at 26.57°, and (c) die.

To implement this process, we're first going to set up two buffers which are alternately read and updated in successive passes down the pipeline – ping-pong buffering, in other words. The buffer being read will contain the data, both coordinates and velocity, for all the particles in the current configuration of the system. The system will be drawn using this buffer's data, while, in the same pass, the other buffer is updated for the next configuration. Accordingly, the particle system will be drawn reading data alternately from either buffer.

To this end, the following blocks in the initialization routine of particleSystem.cpp bind buffer[TRANSFORM_FEEDBACK_A] to vao[PARTICLES_A] with data initialized to the single initParticle at the top of the code, and likewise bind buffer[TRANSFORM_FEEDBACK_B] to vao[PARTICLES_B], though with empty initial data. The size of both buffers is set to hold data for a maximum of 128 particles.

```
glBindVertexArray(vao[PARTICLES_A]);
glBindBuffer(GL_ARRAY_BUFFER, buffer[TRANSFORM_FEEDBACK_A]);
glBufferData(GL_ARRAY_BUFFER, 128*sizeof(initParticle),
             &initParticle, GL_DYNAMIC_COPY);
glVertexAttribPointer(0, 4, GL_FLOAT, GL_FALSE,
                      sizeof(Particle), 0);
glEnableVertexAttribArray(0);
glVertexAttribPointer(1, 3, GL_FLOAT, GL_FALSE,
   sizeof(Particle), (void*)offsetof(Particle, vel));
glEnableVertexAttribArray(1);

glBindVertexArray(vao[PARTICLES_B]);
glBindBuffer(GL_ARRAY_BUFFER, buffer[TRANSFORM_FEEDBACK_B]);
glBufferData(GL_ARRAY_BUFFER, 128*sizeof(initParticle),
             NULL, GL_DYNAMIC_COPY);
glVertexAttribPointer(0, 4, GL_FLOAT, GL_FALSE,
                      sizeof(Particle), 0);
glEnableVertexAttribArray(0);
```

```
glVertexAttribPointer(1, 3, GL_FLOAT, GL_FALSE,
    sizeof(Particle), (void*)offsetof(Particle, vel));
glEnableVertexAttribArray(1);
```

Note, however, that both buffers are linked to the same vertex shader location indexes – 0 for particleCoords, 1 for particleVel – because we'll use these variables to access data in either buffer depending on the currently active VAO.

Let's go next to the transform feedback activity. Declared in setup() are the varyings updatedCoords and updatedVel, to hold a particle's coordinates and velocity for the next step, as also two transform feedback objects. Now, the global frameParity, which flips between 0 and 1 each drawing pass, says which side of the ping-pong process we are currently on. See the following block from the drawing routine for what happens if frameParity is 0.

```
if (frameParity == 0)
{
    glBindVertexArray(vao[PARTICLES_A]);
    glUniform1ui(objectLoc, PARTICLES_A);
    glBindTransformFeedback(GL_TRANSFORM_FEEDBACK,
       transformFeedback[TRANSFORM_FEEDBACK_A]);
    glBindBuffer(GL_TRANSFORM_FEEDBACK_BUFFER,
                     buffer[TRANSFORM_FEEDBACK_B]);
    glBindBufferBase(GL_TRANSFORM_FEEDBACK_BUFFER, 0,
                         buffer[TRANSFORM_FEEDBACK_B]);
    glBeginTransformFeedback(GL_POINTS);
    if (firstFrame == 1)
    {
        glDrawArrays(GL_POINTS, 0, 1);
        firstFrame = 0;
    }
    else
        glDrawTransformFeedback(GL_POINTS,
           transformFeedback[TRANSFORM_FEEDBACK_B]);
    glEndTransformFeedback();
}
```

Firstly, vao[PARTICLES_A] is activated, the vertex shader accordingly notified, the transform feeback object transformFeedback[TRANSFORM FEEDBACK_A] bound, and buffer[TRANSFORM_ FEEDBACK B] bound as the transform feedback buffer. Next, transform feedback recording is started and drawing is done in one of two ways: for the first frame

```
glDrawArrays(GL_POINTS, 0, 1)
```

draws the initial particle, while for the remaining frames the drawing call is

```
glDrawTransformFeedback(GL_POINTS,
   transformFeedback[TRANSFORM_FEEDBACK_B]);
```

where glDrawTrasformFeedback(*primitive*, *tfID*) is equivalent to glDrawArrays(*primitive*, *0*, *countVertices*), the value of *countVertices* being the number of vertices whose data was recorded the last time transform feedback object *tfID* was active (without glDrawTrasformFeedback() we would be forced to separately query this object). That buffer[TRANSFORM FEEDBACK A], which is the data buffer bound to vao[PARTICLES_A], was updated in the previous pass (if there was one) by the object transformFeedback[TRANSFORM FEEDBACK_B] explains the second parameter of the glDrawTrasformFeedback() call above. Obviously, the first frame has no transform feedback buffer to read from, so is drawn directly.

We'll leave the reader to parse the very similar else block when frameParity is 1.

On to the shaders next. The vertex and fragment shader have little going on in them. It's the geometry shader which does all the heavy lifting, but it's still easy to understand. See the first if clause in the geometry shader's main, which kicks in if a particle crosses the right side of the enclosing square:

```
if (coords[0].x > 95.0)
{
    updatedCoords = coords[0] - vec4(vel[0], 0.0);
    updatedVel = vec3(-1.0, 1.0, 0.0);
    gl_Position = projMat * modelViewMat * updatedCoords;
    EmitVertex( );
    EndPrimitive( );

    updatedCoords = coords[0] - vec4(vel[0], 0.0);
    updatedVel = vec3(-1.0, -2.0, 0.0);
    gl_Position = projMat * modelViewMat * updatedCoords;
    EmitVertex( );
    EndPrimitive( );
}
```

The two statements blocks each create a new particle with initial position equal to that of the current particle the step before (when it was last inside the square) and velocity sending one at $\tan^{-1} 1$ and the other at $\tan^{-1} 0.5$ to the right side, both heading back into the square; the current particle is not emitted again, implying that it is killed.

The next three else-if clauses similarly handle the cases when the particle crosses the other sides. Finally, if the current particle is inside the square, then

```
else
{
    updatedCoords = coords[0] + vec4(vel[0], 0.0);
    updatedVel = vel[0];
    gl_Position = projMat * modelViewMat * coords[0];
    EmitVertex( );
    EndPrimitive( );
}
```

updates its coordinates using its velocity vector, the latter itself kept unchanged.

We have demonstrated a rather tame particle system, but one which ticks all the boxes as far as using transform feedback is concerned. Obviously, particleSystem.cpp can be enhanced in many ways, as we ask you to explore next.

Exercise 16.23. (Programming) Starting from particleSystem.cpp:

(1) Automate the animation so that pressing space toggles between animation on and off. The current size of both particle data buffers is for 128 particles. Increase their size and react when they are nearly full by killing off particles (see (3) below) so that the animation can go on indefinitely.

(2) If you step through the animation far enough, particleSystem.cpp starts to show singular behavior when particles start emanating from one corner in apparently a single-line stream. Fix this.

(3) Add age as an attribute of a particle – measured from counting frames or the system clock – with a particle's behavior depending on its age. Given age, define lifetime as an attribute as well, at the end of which a particle is destroyed. Add a Malthusian element whereby particles begin to die more rapidly as their population grows (particularly, as their data buffers begin to fill up).

(4) Apply randomization, e.g., in setting the initial direction of a newborn particle or its lifetime. Unfortunately, the GLSL has nothing equivalent to the C++

rand() function to generate random numbers. A neat workaround is to populate a texture buffer object (TBO) with random floats at initialization. This can then be accessed with texelFetch()s to generate random numbers server-side at run-time.

(5) Make more than one type of a particle, type being determined at birth, with different behavior. E.g., particles which explode at the end of their life into multiple new particles could be a type.

(6) Implement real-world physics, e.g., the action of gravity on (heavy) particles to make them move in a parabolic path rather than straight, or simulate particles in the air blown by wind or in flowing water.

(7) Use transform feedback to detect proximity between particles, and react in a visually expressive manner when particles come close or collide. In this connection, mind that the computational cost of deciding particle-particle interaction can become prohibitive if there is a large number of moving particles, especially if one is not doing much more than a coordinates comparison between every pair.

(8) Implement the particles as point sprites for richer visuals.

(9) Go 3D by placing the particles in a transparent box.

Figure 16.33: Andromeda galaxy (thanks Adam Evans for a Creative Commons license).

Figure 16.34: Sparkler (thanks Fluzwup for releasing into the public domain).

Particle systems are *de rigueur* in replicating phenomena such as smoke, fire, water spray, sparks, dust, sparklers and galaxies, e.g., Figures 16.33 and 16.34. The reader will find numerous examples of particle systems, some with code, on the web.

16.7 Summary, Notes and More Reading

Following up on the previous chapter, in this we dove deep into OpenGL 4.3, learning an assortment of fairly advanced features, including instanced rendering, shader subroutines and transform feedback amongst others, and learned as well of a bunch of new ways to do old things in the programmable pipeline. And, of course, we examined two new shader stages, tessellation and geometry, thus completing our end-to-end study of the programmable pipeline.

The canonical source for all things OpenGL, including the GLSL is, of course, the OpenGL site [106]. Interestingly, just as there is the red book (programming guide) and the blue book (reference manual), there, too, is the so-called orange book by Rost & Licea-Kane [122] on the OpenGL shading language. However, it is somewhat dated and, in fact, the newest edition of the red book subsumes most of the shader material. A couple of more recent textbooks devoted to the OpenGL shading language are Bailey & Cunningham [6] and Wolff [154].

What next? Well, the reader should now be ready to take on fairly complex 3D projects, and not only on a desktop. As we pointed out at the end of the last chapter, grasp of 4.3 means that one is ready as well to code OpenGL ES for mobile devices and WebGL for browsers.

As they say, all good things must come to an end. This chapter concludes our coverage of the programmable pipeline and (pretty much, except for B-splines and NURBS) all there is to do with *programming* OpenGL in this book. There's still a lot of CG theory left in the next few chapters, in fact, underlying many of the OpenGL gadgets we have learned, which the reader should not ignore.

Part IX

Anatomy of Curves and Surfaces

Chapter 17

Bézier

The goal for this chapter is an understanding of the theory underlying Bézier primitives. We are already familiar with many of their practical aspects. In Section 10.3 of the chapter on drawing we saw how to specify Bézier curves and surfaces and incorporate them into our designs. This was possible then – even before theory – as an intuitive understanding of control points and their role as attractors in shaping Bézier primitives is sufficient to grasp the OpenGL syntax. We went even further in Sections 11.11.4 and 12.5.2, learning how to light and texture Bézier surfaces.

We'll restrict ourselves in this chapter to the theory of *polynomial* Bézier primitives. The more general form is *rational* – a rational function being the ratio of two polynomials. We'll postpone the discussion of the rational primitives to Chapter 20, as an application of projective spaces, which are the natural setting for these primitives.

Several 3D modeling systems support rational Bézier primitives – in fact, often, the even more general class of NURBS (Non-Uniform Rational B-Spline) primitives – in a WYSIWYG environment where users create primitives interactively by manipulating control points. Of course, a system supporting rational primitives supports as well its polynomial subclass. OpenGL is often the front-end of such modelers, itself offering both rational Bézier and NURBS primitives in a low-level "code-it-yourself" manner.

There is a bit of math in the development of Bézier theory, but behind it always is the fairly intuitive "mechanics" of Bézier primitives, which we'll try to make as apparent as possible. Illustrative code is interspersed throughout this chapter as well.

We begin with Bézier curves in Section 17.1. First, de Casteljau's procedural approach to defining linear and quadratic Bézier curves is explained in Sections 17.1.1-17.1.2. The reader is asked to do most of the work for cubic Bézier curves in 17.1.3. Section 17.1.4 generalizes the development to Bézier curves of arbitrary order and we see as well a host of properties that make Bézier curves so useful in design. From Bézier curves to Bézier surfaces in Section 17.2 is fairly intuitive. Section 17.3 concludes the chapter.

17.1 Bézier Curves

Suppose a programmer specifies a sequence $P_0, P_1, \dots, P_n$ of $n + 1$ *control points*, asking for a curve not necessarily passing through them, but, rather, whose shape is molded by the control points. In other words, the control points are expected to act as "attractors", each exerting a pull on the curve. The generated curve is said to *approximate* the control points. Figure 17.1 is illustrative of the situation.

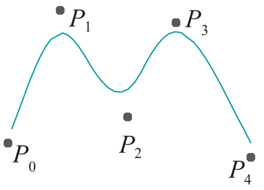

Figure 17.1: A curve approximating five control points.

Circa 1960, two French automotive designers, Bézier [12, 13] and de Casteljau [34, 35], independently invented a particular method to approximate a sequence of control points. It bears the name of Bézier because his publications had earlier circulation in the design community. However, de Casteljau's approach to Bézier curves is actually the more intuitive and it is what we'll first describe.

Linear Bézier Curves

Let's start with the simplest case, where there are only two control points P_0 and P_1. The Bézier curve c approximating P_0 and P_1 is, simply, the straight line segment joining the two. We write the parametric equation of c as follows:

$$c(u) = (1 - u)P_0 + uP_1 \qquad (0 \le u \le 1) \tag{17.1}$$

See Figure 17.2(a). This Bézier curve is said to be *linear*, or of *degree one*, or of *second order*, order being the number of control points.

If the ambient space is R², and $P_0 = [x_0\ y_0]^T$ and $P_1 = [x_1\ y_1]^T$, we can write (17.1) as

$$c(u) = [(1 - u)\,x_0 + u\,x_1 \quad (1 - u)\,y_0 + u\,y_1]^T \qquad (0 \le u \le 1) \tag{17.2}$$

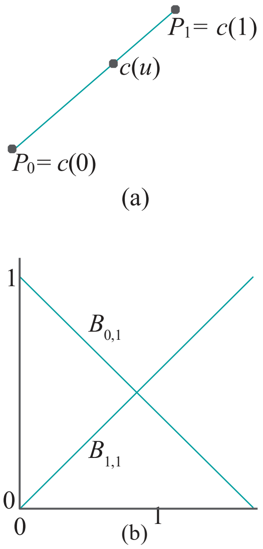

Figure 17.2: (a) Bézier curve of degree 1 (b) Bernstein polynomials of degree 1: $B_{0,1}(u) = 1 - u$, $B_{1,1}(u) = u$.

17.1.1

Example 17.1. What is the equation of the linear Bézier curve c with control points $[5\ 1]^T$ and $[-1\ 0]^T$? What are the points on c corresponding to the values 0, 0.3 and 1 of the parameter u?

Answer: The equation of c is

$$c(u) = (1 - u)[5\ 1]^T + u[-1\ 0]^T = [5 - 6u \quad 1 - u]^T \qquad (0 \le u \le 1)$$

The point corresponding to $u = 0$ is $[5\ 1]^T$, the first control point.
The point corresponding to $u = 0.3$ is $[3.2\ 0.7]^T$.
The point corresponding to $u = 1$ is $[-1\ 0]^T$, the second control point.

Remark 17.1. As far as the theory goes, the control points can belong to a real space of arbitrary dimension, but practical applications are in R² or R³.

Remark 17.2. It is evident from either (17.1) or (17.2) that a linear Bézier curve linearly interpolates between its two control points (recall linear interpolation from Section 7.2).

Exercise 17.1. Write an equation analogous to (17.2) if the ambient space is R³.

Exercise 17.2. What is the equation of the linear Bézier curve c with control points $[0\ 2 - 4]^T$ and $[3\ 8\ 0]^T$? What are the points on c corresponding to the values 0, 0.3 and 1 of the parameter u?

We make the following observations, all straightforward, for a linear Bézier curve c:

1. The parametric equation (17.1) for c is linear in u, which, of course, is why it's called a linear Bézier curve.

2. The *point* $c(u)$ of the curve c is a weighted sum of the control points P_0 and P_1, the weights of P_0 and P_1 being the *values* of $1 - u$ and u, respectively. Accordingly, the *curve* c can be thought of as a weighted sum of P_0 and P_1, where the weights of P_0 and P_1 are the *functions* $1 - u$ and u, respectively. These functions are called the *blending functions* of the respective control points (the term *basis function* is used as well).

   The blending functions $1 - u$ (of the first control point) and u (of the second control point) are known as the *Bernstein polynomials* of degree 1. They are denoted $B_{0,1}(u)$ and $B_{1,1}(u)$, respectively. Figure 17.2(b) shows their graphs. Accordingly, Equation (17.1) can be written as

$$c(u) = B_{0,1}(u)P_0 + B_{1,1}(u)P_1 \qquad (0 \le u \le 1) \tag{17.3}$$

The blending function $B_{0,1}(u)$ of the first control point decreases from 1 to 0 as u goes from 0 to 1, while exactly the opposite is true of that of the second control point.

3. Because

   (a) $B_{0,1}(u)$ and $B_{1,1}(u)$ both lie between 0 and 1, and

   (b) $B_{0,1}(u) + B_{1,1}(u) = 1$,

   for each u in $0 \leq u \leq 1$, every point of c is a convex combination (recall Definition 7.3) of the control points P_0 and P_1 and, therefore, lies in their convex hull, which is actually pretty obvious in this simple case of a linear Bézier curve.

4. c starts at the first control point P_0, when $u = 0$, and ends at the second one P_1, when $u = 1$.

   If an approximating curve passes through a control point, then it is said to *interpolate* it (mind this usage has nothing to do with linear interpolation). So a linear Bézier curve interpolates both its control points.

17.1.2 Quadratic Bézier Curves

Consider next three control points P_0, P_1 and P_2. We want to construct the Bézier curve approximating these control points by means of a process of linear interpolation as in the preceding case of two control points. Is there, though, an evident way to linearly interpolate a curve between three control points "simultaneously"? What does this even mean?

A possibility, of course, is to linearly interpolate between P_0 and P_1 and then between P_1 and P_2, to get the two-segment polyline $P_0P_1P_2$, which is piecewise linear at least (see Figure 17.3(a)). However, the corner at P_1 makes this approximation to P_0, P_1 and P_2 rather unsatisfactory. De Casteljau, however, resolves the problem by adding a third interpolation step to "amalgamate" the two segments P_0P_1 and P_1P_2, smoothening thereby the corner. Here's how it works. Given a u, 0 $\leq u$ 1 $\leq$ (see Figure 17.3(b)):

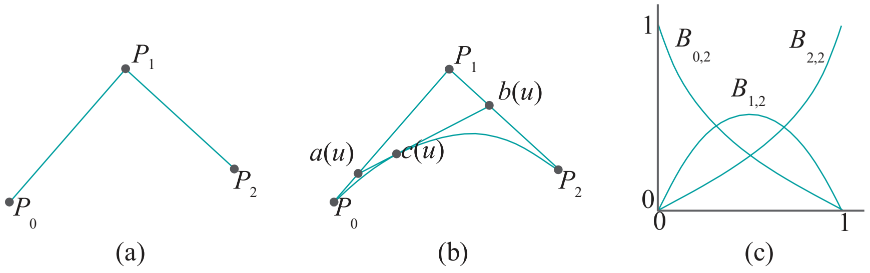

Figure 17.3: (a) An "unhappy" way of approximating three control points (b) $c(u)$ describes a Bézier curve of degree 2 interpolating P_0, P_1 and P_2 after a "triple" interpolation (c) Bernstein polynomials of degree 2: $B_{0,2}(u) = (1-u)^2$, $B_{1,2}(u) = 2(1-u)u$, $B_{2,2}(u) = u^2$.

1. First interpolate between P_0 and P_1 to find the point

$$a(u) = (1-u)P_0 + uP_1$$

2. Next interpolate between P_1 and P_2 to find the point

$$b(u) = (1-u)P_1 + uP_2$$

3. Finally, interpolate between $a(u)$ and $b(u)$ to determine the point

$$c(u) = (1-u)a(u) + u\,b(u)$$

Substituting the expressions for $a(u)$ and $b(u)$ into that for $c(u)$, one obtains the parametric equation for the curve c:

$$c(u) = (1-u)^2 P_0 + 2(1-u)uP_1 + u^2 P_2 \qquad (0 \le u \le 1) \qquad (17.4)$$

As u varies from 0 to 1, $c(u)$ describes the *quadratic*, or *degree two*, or *third-order* , Bézier curve approximating three control points P_0, P_1 and P_2, which is indeed smooth.

Note: Curves drawn in this chapter are fairly accurate sketches, but not necessarily exact plots of their equations.

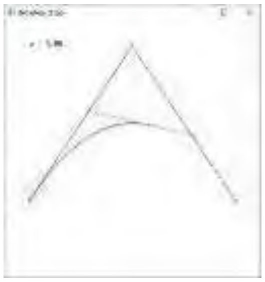

Figure 17.4: Screenshot of deCasteljau3.cpp.

Experiment 17.1. Run deCasteljau3.cpp, which shows an animation of de Casteljau's method for three control points. Press the left or right arrow keys to decrease or increase the curve parameter u. The interpolating points $a(u)$, $b(u)$ and $c(u)$ are colored red, green and blue, respectively. Figure 17.4 is a screenshot. End

Note: As in the above program, we shall often revert to fixed-function OpenGL in order to be able to code text on-screen easily and to be able to use handy object-drawing calls like glMap1(), glMap2(), glu*(), etc. We allow ourselves this latitude as our objective is to illustrate concepts not to do with 4.x per se in the most efficient manner possible. In fact, as we've noted before, fixed-function OpenGL is a perfectly good (if somewhat limited) API itself. It's simply a matter of knowing which API is suited to a particular application.

If the ambient space is R^2, and $P_0 = [x_0\ y_0]^T$, $P_1 = [x_1\ y_1]^T$ and $P_2 = [x_2\ y_2]^T$, one can write (17.4) as

$$\begin{aligned} c(u) \;=\; & [(1-u)^2 x_0 + 2(1-u)ux_1 + u^2 x_2 \\ & \quad (1-u)^2 y_0 + 2(1-u)uy_1 + u^2 y_2]^T \quad (0 \le u \le 1) \qquad (17.5) \end{aligned}$$

Example 17.2. What is the equation of the third-order Bézier curve c with control points $[0\ -1]^T$, $[1\ 2]^T$ and $[5\ -1]^T$?

Answer: The equation of c is

$$\begin{aligned} c(u) &= (1-u)^2[0\ \ -1]^T + 2(1-u)u[1\ 2]^T + u^2[5\ \ -1]^T \\ &= [2u + 3u^2 \quad -1 + 6u - 6u^2]^T \qquad (0 \le u \le 1) \end{aligned}$$

Exercise 17.3. What is the equation of the third-order Bézier curve c with control points $[-2\ 2\ 2]^T$, $[0\ 3\ 5]^T$ and $[-6\ 0\ 2]^T$? What are the points on c corresponding to the values 0, 0.5 and 1 of the parameter u?

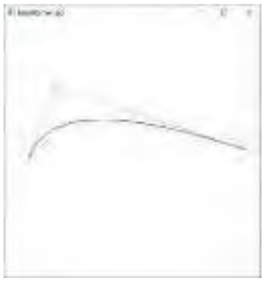

Figure 17.5: Screenshot of bezierCurves.cpp with three control points, showing both the Bézier curve and its control polygon.

Experiment 17.2. Run bezierCurves.cpp of Chapter 10, which allows the user to choose a Bézier curve of order 2-6 and move each control point.

You can choose an order in the first screen by pressing the up and down arrow keys. Select 3. Press enter to go to the next screen to find the control points initially on a straight line. Press space to select a control point – the selected one is red – and then arrow keys to move it. Delete resets to the first screen. Figure 17.5 is a screenshot.

The polygonal line joining the control points, called the *control polygon* of the curve, is drawn in light gray. Evidently, the Bézier curve "mimics" its control polygon, but smoothly, avoiding a corner. End

Compare the following observations for a third-order Bézier curve c with the corresponding ones, made earlier, for a second-order curve:

1. c is quadratic in u.

2. c is a weighted sum of the control points P_0, P_1 and P_2, where the weights of P_0, P_1 and P_2 are the blending functions $(1 - u)^2$, $2(1-u)u$ and u^2, respectively. These blending functions are called the Bernstein polynomials of degree 2, and denoted $B_{0,2}(u)$, $B_{1,2}(u)$ and $B_{2,2}(u)$, respectively. Figure 17.3(c) shows their graphs. Accordingly, Equation (17.4) can be written as

$$c(u) = B_{0,2}(u)P_0 + B_{1,2}(u)P_1 + B_{2,2}(u)P_2 \qquad (0 \le u \le 1) \tag{17.6}$$

   It's useful to think of the value of a control point's blending function at $c(u)$ as the amount of its "attraction" (or "pull", or "weight") on that point of the Bézier curve and of u as a dial propelling $c(u)$ along the curve by altering these attractions.

   The blending function $B_{0,2}(u)$ of the first control point P_0 decreases from 1 to 0 as u goes from 0 to 1; the blending function $B_{1,2}(u)$ of the middle control point P_0 starts and ends at 0, reaching a maximum value of $\frac{1}{2}$ at $u = \frac{1}{2}$; finally, the blending function $B_{2,2}(u)$ of the last control point P_0 increases from 0 to 1. So, e.g., the attraction of the middle control point is greatest on the point of the curve corresponding to $u = \frac{1}{2}$.

3. Every point of c is a convex combination of the control points P_0, P_1 and P_2, because

   (a) $B_{0,2}(u)$, $B_{1,2}(u)$ and $B_{2,2}(u)$ all lie between 0 and 1, and

   (b) $B_{0,2}(u) + B_{1,2}(u) + B_{2,2}(u) = (1 - u)^2 + 2(1 - u)u + u^2 = 1$,

   for each u in $0 \le u \le 1$. It follows that the entire curve c is contained in the convex hull of P_0, P_1 and P_2.

   Colloquially, (a) and (b) say that the attraction of each control point is between 0 and 1 and that the total attraction of all three is always 1.

4. c interpolates (i.e., passes through) the first and last control points, but not necessarily the middle one.

Exercise 17.4. What is the attraction of each of the control points P_0, P_1 and P_2 on $c(0.2)$?

Exercise 17.5. Verify that Equation (17.4) can be written in the matrix form:

$$c(u) = [P_0\ P_1\ P_2] \begin{bmatrix} 1 & -2 & 1 \\ -2 & 2 & 0 \\ 1 & 0 & 0 \end{bmatrix} [u^2\ u\ 1]^T \tag{17.7}$$

17.1.3 Cubic Bézier Curves

Consider, now, four control points P_0, P_1, P_2 and P_3. We're going to ask the reader to do most of the work. Perform step-by-step interpolation, similarly to the case of three control points, as follows.

Given a u in $0 \le u \le 1$ (see Figure 17.6(a)):

1. $a(u)$ interpolates between P_0 and P_1.
2. $b(u)$ between P_1 and P_2.
3. $d(u)$ between P_2 and P_3.
4. $e(u)$ between $a(u)$ and $b(u)$.
5. $f(u)$ between $b(u)$ and $d(u)$.
6. Finally, $c(u)$ between $e(u)$ and $f(u)$.

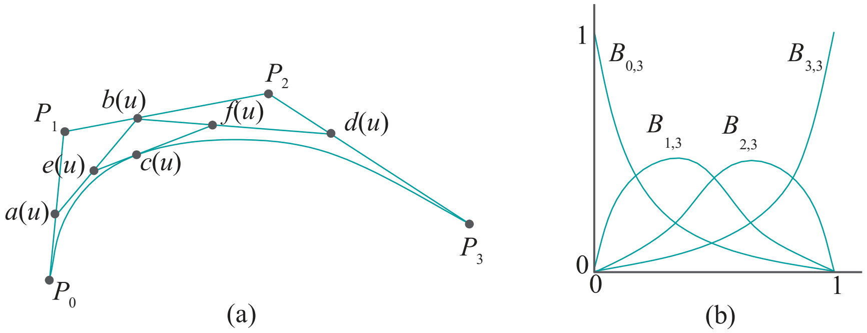

Figure 17.6: (a) Bézier curve of degree 3 (b) Bernstein polynomials of degree 3: $B_{0,3}(u) = (1 - u)^3$, $B_{1,3}(u) = 3(1 - u)^2u$, $B_{2,3}(u) = 3(1 - u)u^2$, $B_{3,3}(u) = u^3$.

As u varies from 0 to 1, $c(u)$ describes the *cubic*, or *degree three*, or *fourth-order* , Bézier curve approximating the four control points P_0, P_1, P_2 and P_3.

Exercise 17.6. Prove that the parametric equation of the Bézier curve c approximating the four control points P_0, P_1, P_2 and P_3 is

$$c(u) = B_{0,3}(u)P_0 + B_{1,3}(u)P_1 + B_{2,3}(u)P_2 + B_{3,3}(u)P_3 \qquad (0 \leq u \leq 1) \qquad (17.8)$$

where the Bernstein polynomials are

$$B_{0,3}(u) = (1 - u)^3, \quad B_{1,3}(u) = 3(1 - u)^2u, \quad B_{2,3}(u) = 3(1 - u)u^2, \quad B_{3,3}(u) = u^3$$

Figure 17.6(b) shows their graphs.

Exercise 17.7. Show that the steps 1-6 above are equivalent to the three:

1. Draw the quadratic Bézier curve $c_0(u)$, $0 \leq u \leq 1$, approximating the three control points P_0, P_1 and P_2.

2. Draw the quadratic Bézier curve $c_1(u)$, $0 \leq u \leq 1$, approximating the three control points P_1, P_2 and P_3.

3. Interpolate along the straight line joining $c_0(u)$ and $c_1(u)$, as u varies from 0 to 1.

Exercise 17.8. How about the following 3-step drawing process? Is it equivalent to steps 1-6 above?

1. Draw the quadratic Bézier curve $c_0(u)$, $0 \leq u \leq 1$, approximating the three control points P_0, P_1 and P_2.

2. Draw the linear Bézier curve $c_1(u)$, $0 \leq u \leq 1$, approximating the two control points P_2 and P_3.

3. Interpolate along the straight line joining $c_0(u)$ and $c_1(u)$, as u varies from 0 to 1.

Exercise 17.9. If the ambient space is R^2 write an equation analogous to (17.5) for the cubic Bézier curve.

Exercise 17.10. What is the equation of the cubic Bézier curve c with control points $[-\ 2\ 2]^T$, $[0\ -\ 3]^T$, $[3\ 4]^T$ and $[7\ 0]^T$? What are the points on c corresponding to the values 0, 0.5 and 1 of the parameter u?

Exercise 17.11. Make four observations for a fourth-order Bézier curve c, corresponding to the four made for Bézier curves of orders 2 and 3 at the end of the last two sections, respectively..

Exercise 17.12. What is the attraction of each of the control points P_0, P_1, P_2 and P_3 at $c(0.2)$, where c is their approximating Bézier curve?

Exercise 17.13. Write Equation (17.8) in a matrix form similar to (17.7).

Exercise 17.14. (Programming) Write a program deCasteljau4.cpp, in the style of deCasteljau3.cpp, to illustrate de Casteljau's method for four control points.

Remark 17.3. Cubic Bézier curves are the ones most commonly used in design applications as three is a sort of "Goldilocks" degree, high enough to allow the curve good flexibility, yet not too high as to be computationally cumbersome.

Here's an exercise to get you warmed up for the general case coming next.

Exercise 17.15. From only the cases $n = 1$, 2 and 3, that we have seen, it's clear how the *variable part* of the Bernstein polynomial will change from $B_{0,n}(u)$ to $B_{1,n}(u)$, . . ., finally, to $B_{n,n}(u)$, for a general n.

In fact, the variable part of $B_{0,n}(u)$ is $(1 - u)^n u^0$. (Of course, $u^0 = 1$.) Next, for $B_{1,n}(u)$, the power of $1 - u$ decreases by one and that of u increases by one, so its variable part is $(1 - u)^{n-1}u^1$. And, so it continues, until the variable part of $B_{n,n}(u)$ is $(1 - u)^0 u^n$.

How about the *constant coefficients* though? Let's see what they are.

For Bernstein polynomials of degree 1: 1 1
For Bernstein polynomials of degree 2: 1 2 1
For Bernstein polynomials of degree 3: 1 3 3 1

Do you see a pattern? (*Hints*: Pascal's triangle, binomial coefficients.) Can you write down now the parametric equation for a fifth-order Bézier curve, without going through a de Casteljau process?

17.1.4 General Bézier Curves

It should now be fairly clear how to generalize de Casteljau's method to construct the Bézier curve approximating an arbitrary number of control points. We'll show that the parametric equation for the Bézier curve c approximating $n + 1$ control points $P_0, P_1, \ldots, P_n$ is

$$c(u) = \sum_{i=0}^{n} B_{i,n}(u)P_i \qquad (0 \le u \le 1) \tag{17.9}$$

where $B_{i,n}(u)$, $0 \le i \le n$, called the ith Bernstein polynomial of degree n, is given by

$$B_{i,n}(u) = \binom{n}{i}(1 - u)^{n-i}u^i \tag{17.10}$$

where $\binom{n}{i} = \frac{n!}{(n-i)!i!}$ is a binomial coefficient. The curve c is called a Bézier curve of *degree n*, or *order n* + 1.

We'll verify Equation (17.9) by induction based on the following recursive specification of de Casteljau's method.

Recursive de Casteljau

We'll start the recursive definition by specifying (again) that the Bézier curve approximating two control points P_0 and P_1 is the straight segment joining them, given by (repeating (17.3)):

$$c(u) = B_{0,1}(u)P_0 + B_{1,1}(u)P_1 \qquad (0 \le u \le 1) \tag{17.11}$$

Assume, then, that we can specify the Bézier curve approximating any n control points, for some given $n \ge 2$, and that, next, we are given $n + 1$ control points

$P_0, P_1, \dots P_n$. Say the Bézier curve $c_0(u)$, $0 \le u \le 1$, approximates the first n of these $P_0, P_1, \dots P_{n-1}$, and that $c_1(u)$, $0 \le u \le 1$, approximates the last n $P_1, P_2, \dots P_n$.

Recursive de Casteljau says, then, that the Bézier curve approximating all $n+1$ control points $P_0, P_1, \dots P_n$ is

$$c(u) = (1-u)c_0(u) + uc_1(u) \qquad (0 \le u \le 1) \qquad (17.12)$$

which is an “interpolation” between $c_0(u)$ and $c_1(u)$. The scheme is indicated in Figure 17.7.

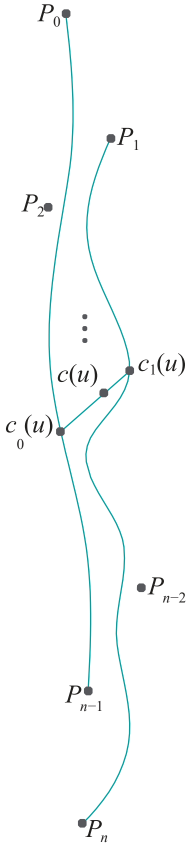

Figure 17.7: Recursive de Casteljau scheme: $c_0(u)$ approximates $P_0, P_1, \dots, P_{n-1}$; $c_1(u)$ approximates $P_1, P_2, \dots, P_n$; $c(u)$ interpolates between $c_0(u)$ and $c_1(u)$ to approximate $P_0, P_1, \dots, P_n$.

Observe that in the case of three control points the earlier construction of a quadratic Bézier curve in Section 17.1.2 matches exactly the recursive one above, while, in the case of four, Exercise 17.7 says that the construction of a cubic Bézier curve in Section 17.1.3 is equivalent to it.

Let’s turn now to proving the general formula (17.9) by induction. Starting the induction is simply a matter of noting that (17.9) is identical to (17.11) when $n = 1$.

Suppose, inductively, that (17.9) is true with $n-1$ in place of n, i.e., it is true for n control points. We’ll prove it next for $n+1$ control points $P_0, P_1, \dots P_n$. By the inductive hypothesis, the Bézier curve approximating the first n of these, $P_0, P_1, \dots P_{n-1}$, is given by

$$c_0(u) = \sum_{i=0}^{n-1} B_{i,n-1}(u)P_i \qquad (0 \le u \le 1)$$

and that approximating the last n points, $P_1, P_2, \dots P_n$, by

$$c_1(u) = \sum_{i=0}^{n-1} B_{i,n-1}(u)P_{i+1} \qquad (0 \le u \le 1)$$

The Bézier curve approximating all $n+1$ control points $P_0, P_1, \dots P_n$ by the recursive formula (17.12), therefore, is

$$\begin{aligned}
c(u) &= (1-u)c_0(u) + uc_1(u) \\
&= (1-u)\sum_{i=0}^{n-1} B_{i,n-1}(u)\, P_i + u \sum_{i=0}^{n-1} B_{i,n-1}(u) \quad P_{i+1} \\
&= (1-u)\sum_{i=0}^{n-1} \binom{n-1}{i} (1-u)^{n-i-1}\, u^i\, P_i + \\
&\qquad u \sum_{i=0}^{n-1} \binom{n-1}{i} (1-u)^{n-i-1}\, u^i\, P_{i+1}
\end{aligned}$$

(applying formula (17.10) for Bernstein polynomials of degree $n-1$)

$$\begin{aligned}
&= (1-u)\sum_{i=0}^{n-1} \binom{n-1}{i} (1-u)^{n-i-1}\, u^i\, P_i + \\
&\qquad u \sum_{i=1}^{n} \binom{n-1}{i-} (1-u)^{n-i}\, u^{i-1}\, P
\end{aligned}$$

(changing the limits on the second summation by replacing i by $i-1$)

$$\begin{aligned}
&= (1-u)^n P_0 + \sum_{i=1}^{n-1} \left(\binom{n-1}{i} (1-u)^{n-i} u^i + \binom{n-1}{i-1} (1-u)^{n-i} u^i \quad P_i \right. + \\
&\qquad u^n P_n
\end{aligned}$$

(bringing together terms for $i = 1, \dots, n-1$ from the two summations)

$$= (1-u)^n P_0 + \sum_{i=1}^{n-1} \binom{n}{i} (1-u)^{n-i} u^i P_i + u^n P_n$$

(using the property of binomial coefficients that $\binom{n-1}{i} + \binom{n-1}{i-1} = \binom{n}{i}$)

$$= \sum_{i=0}^{n} B_{i,n}(u)\, P_i$$

This completes the inductive verification of Equation (17.9).

If the control points are $P_i = [x_i\ y_i\ z_i]^T$, $0 \le i \le n$, in real-world 3-space, then (17.9) can be written as

$$c(u) = \left[\sum_{i=0}^{n} B_{i,n}(u) x_i \quad \sum_{i=0}^{n} B_{i,n}(u) y_i \quad \sum_{i=0}^{n} B_{i,n}(u) z_i \right]^T \qquad (0 \le u \le 1) \qquad (17.13)$$

We collect facts about general Bézier curves in the following:

Proposition 17.1. *If c is the Bézier curve approximating the sequence of $n+1$ control points $P_0, P_1, \ldots, P_n$ – called a Bézier curve of order $n+1$, or degree n – then the following hold:*

- *(a) c is polynomial of degree n in the parameter u. In particular, each coordinate value of c is polynomial of degree n in u.*
- *(b) c is a weighted sum of the control points $P_0, P_1, \ldots, P_n$, where the weight of P_i, for $0 \le i \le n$, is its blending function $B_{i,n}(u)$.*
- *(c) The blending functions $B_{i,n}(u)$, $0 \le i \le n$, form a* partition of unity *over the parameter space* $[0, 1]$ *(a set of functions is said to a form a* partition of unity *over some domain if they are each non-negative and add up to 1 everywhere in that domain).*
- *(d) Every point of c is a convex combination of the control points $P_0, P_1, \ldots, P_n$; therefore, c lies inside the convex hull of $P_0, P_1, \ldots, P_n$.*
- *(e) c interpolates the first and last control points, but not necessarily intermediate ones.*
- *(f) (Affine Invariance) If the control points $P_0, P_1, \ldots, P_n$ belong to* $\mathbb{R}^3$ *and* $g : \mathbb{R}^3 \to \mathbb{R}^3$ *is an affine transformation, then the image curve $g(c)$ is the Bézier curve approximating the images $g(P_0), g(P_1), \ldots, g(P_n)$ of the control points.*

  In other words, the transformed curve approximates the transformed control points.
- *(g) (End Tangents) The tangent to c at P_0 lies along the straight line from P_0 to P_1 and the tangent to c at P_n lies along the straight line from P_{n-1} to P_n.*

Note: Further discussions of affine invariance and end tangents follow the proof.

Proof. Items (a) and (b) follow straightforwardly from Equation (17.9).

It's easily seen that Bernstein polynomials $B_{i,n}(u) = \binom{n}{i}(1-u)^{n-i}u^i$ all lie between 0 and 1, for each u in $0 \le u \le 1$. Further, for any such u,

$$\sum_{i=0}^{n} B_{i,n}(u) = \sum_{i=0}^{n} \binom{n}{i} (1-u)^{n-i} u^i = \left((1-u) + u \right)^n = 1 \qquad (17.14)$$

by the Binomial Theorem. This proves that the blending functions form a partition of unity over the parameter space $[0, 1]$, establishing (c). It follows, as well, that the point $c(u) = \sum_{i=0}^{n} B_{i,n}(u) P_i$, for $0 \le u \le 1$, is indeed a convex combination of the points $P_0, P_1, \ldots, P_n$, proving (d).

Item (e) is verified by checking that $c(0) = P_0$ and $c(1) = P_n$.

The proof of (f) exploits the fact that the blending functions form a partition of unity over the parameter space. Let the affine transformation $g : \mathrm{R}^3 \to \mathrm{R}^3$ be given by $g(P) = MP + D$, where M is a non-singular 3×3 matrix and D a 3-vector (the translational component). For any u in $0 \leq u \leq 1$, we then have

$$\begin{aligned}
g(c(u)) &= Mc(u) + D \\
&= M\left(\sum_{i=0}^{n} B_{i,n}(u)P_i\right) + D \\
&= \sum_{i=0}^{n} B_{i,n}(u)(MP_i) + \left(\sum_{i=0}^{n} B_{i,n}(u)\right) D \\
&\qquad \text{(invoking the partition-of-unity property } \textstyle\sum_{i=0}^{n} B_{i,n}(u) = 1) \\
&= \sum_{i=0}^{n} B_{i,n}(u)(MP_i + D) \\
&= \sum_{i=0}^{n} B_{i,n}(u)g(P_i)
\end{aligned}$$

proving (e).

For (g), observe that the derivative

$$\begin{aligned}
c^1(u) &= \frac{\mathrm{d}}{\mathrm{d}u}\left((1-u)^n P_0 + n(1-u)^{n-1}uP_1 + \ldots\right) \\
&= -n(1-u)^{n-1}P_0 + n(1-u)^{n-1}P_1 + \textit{ terms that} \\
&\qquad \textit{each contain the factor } u
\end{aligned} \tag{17.15}$$

Therefore, the tangent vector at P_0, when $u = 0$, is

$$c^1(0) = -nP_0 + nP_1 = n(P_1 - P_0)$$

as terms after the second of (17.15) all vanish. Evidently, then, the tangent at P_0 is in the direction toward P_1, proving the first part of (g). The second part follows symmetrically.

Remark 17.4. From (a) it follows that a Bézier curve is C^∞, or smooth (recall definitions from Section 10.1.6).

Affine Invariance of Bézier Curves

The affine invariance of Bézier curves given by Proposition 17.1(f) is extremely useful. Here's a simple example of what it means practically. Suppose a cubic Bézier curve c approximating the four control points

$$P_0 = [5\ 5]^T \qquad P_1 = [7\ 8]^T \qquad P_2 = [8\ 4]^T \qquad P_3 = [11\ 5]^T$$

is drawn as a 10-segment polyline l – keeping in mind that OpenGL curves are always drawn as polylines. See Figure 17.8(a), where l is drawn at an offset to c.

Next, suppose we want to magnify c twofold by scaling it a factor of 2 in each coordinate direction. For the purpose of drawing, if the scaling transformation, call it g, is applied simply to the polyline l, then the result $g(l)$ (Figure 17.8(b)) is likely too coarse an approximation of the magnified curve $g(c)$.

Affine invariance, however, says that $g(c)$ is the same as the cubic Bézier curve c^- approximating the four control points

$$g(P_0) = [10\ 10]^T \qquad g(P_1) = [14\ 16]^T \qquad g(P_2) = [16\ 8]^T \qquad g(P_3) = [22\ 10]^T$$

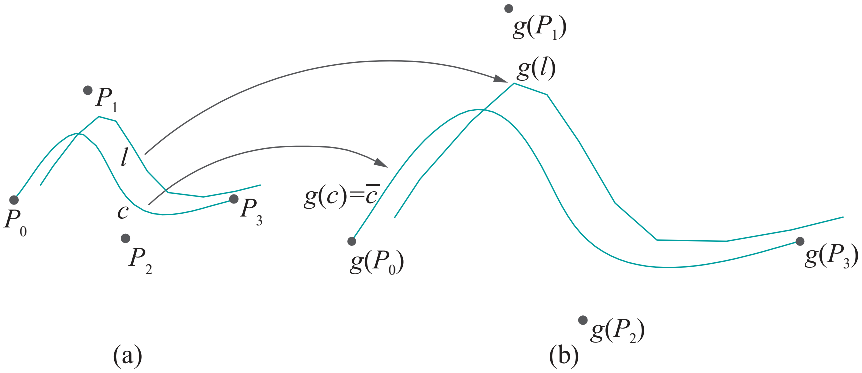

Figure 17.8: (a) A 10-segment fairly smooth-looking polyline l approximation (drawn at an offset) of the Bézier curve c with control points P_0, P_1, P_2 and P_3 (b) The magnification $g(l)$ (also at an offset) is not a good approximation of $g(c)$.

Therefore, one can "forget" the original polyline and, instead, approximate $\overline{c}$ at a resolution of one's choosing (e.g., with a 20-segment polyline).

Bottom line: Affine invariance means that if a Bézier curve is affinely transformed to a new one, then the original control points transform to the new. Therefore, the only "data" required to generate the transformed Bézier curve are the transformed control points.

Exercise 17.16. The transformations

```
glScalef(1.0, 2.0, 2.0);
glTranslatef(2.0, 3.0, 0.0);
```

are applied to the cubic Bézier curve with control points

$$[2\ 1\ 1]^T \qquad [3\ 3\ 2]^T \qquad [-2\ 7\ -1]^T \qquad [0\ 0\ 4]^T$$

Describe the resulting curve.

End Tangents and Joining Bézier Curves

Proposition 17.1(g) enables the user to C^1-*continuously* (see Section 10.1.6) join two Bézier curves c_0 (approximating control points $P_0, P_1, \dots, P_n$) and c_1 (approximating control points $Q_0, Q_1, \dots, Q_m$) by, for instance, making P_n coincide with Q_0 and arranging the three points P_{n-1}, $P_n(= Q_0)$ and Q_1 in that order on one straight line. Compares Figures 17.9(a) and 17.9(b). Another way to say this is that two Bézier curves meet "smoothly" (C^1-continuity is often acceptably smooth visually, though, of course we have a different formal definition of smoothness in Section 10.1.6) if their control polygons meet smoothly.

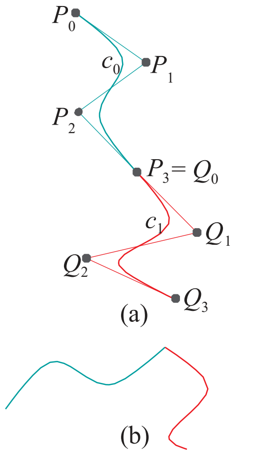

Figure 17.9: (a) Two cubic Bézier curves meet smoothly (actually, C^1-continuously) at an endpoint (b) Two curves meet non-C^1-continuously, making a corner.

Experiment 17.3. Run bezierCurveTangent.cpp of Chapter 10 which shows two cubic Bézier curves. The second curve may be shaped by selecting a control point with the space bar and moving it with the arrow keys. Visually verify Proposition 17.1(g) – the configuration of the screenshot of Figure 17.10, in fact, does this. End

Figure 17.10: Screenshot of bezierCurveTangent.cpp.

Exercise 17.17. (Programming) Show how to use Proposition 17.1(g) to arrange a sequence of control points, so that the approximating Bézier curve is a visually smooth closed loop. Illustrate with the help of bezierCurves.cpp.

Exercise 17.18. A Bézier loop is drawn approximating the six control points

$$[0\ 0\ 0]^T \qquad [4\ 0\ 0]^T \qquad [8\ -5\ 3]^T \qquad [-1\ -5\ -3]^T \qquad [x\ y\ z]^T \qquad [0\ 0\ 0]^T$$

Suggest values for x, y and z for the second to last control point to make the loop look smooth at $[0\ 0\ 0]^T$.

A curve made by joining Bézier curves end to end is called *piecewise Bézier*. E.g., in Figure 17.9, c_0 and c_1 together form a piecewise Bézier curve. Keep in mind though that the joints between the Bézier pieces do not have to be C^1-continuous as in Figure 17.9(a) – there can be a corner as in Figure 17.9(b).

Exercise 17.19. Can a piecewise Bézier curve be Bézier? For example, in Figure 17.9(a) one may ask if the union of c_0 and c_1 is merely the seventh-order Bézier curve with control points $P_0, P_1, P_2, P_3 = Q_0, Q_1, Q_2, Q_3$.

Exercise 17.20. The sequence $P_0, P_1, \ldots, P_n$ of the control points of a Bézier curve is obviously important. Jumbling them up will not give the same curve. How about if the sequence is reversed to $P_n, P_{n-1}, \ldots, P_0$?

Exercise 17.21. There is nothing special about the parameter space $[0, 1]$. Show how to change the parameter space of the Bézier curve, given by Equation (17.9), to $[u_1, u_2]$, where $u_1 < u_2$ may be arbitrary, without changing the curve's shape.

Exercise 17.22. Show that the blending function $B_{i,n}(u)$ of the ith control point P_i reaches its maximum at $u = \frac{i}{n}$, and at this point the value of $B_{i,n}(u)$ exceeds that of all the other blending functions. This means that the attraction of P_i is greatest on the point $c(\frac{i}{n})$ of the curve.

Polynomial Curves and Bézier Curves

As noted in Proposition 17.1(a), each coordinate value of a degree n Bézier curve is a polynomial of degree n in the parameter u. Recall from Section 10.1.4 that a polynomial curve (in $\mathbb{R}^3$) is of the form

$$b(u) = [f(u) \;\; g(u) \;\; h(u)]^T$$

where each coordinate value $f(u)$, $g(u)$ and $h(u)$ is polynomial in u. Bézier curves are, therefore, polynomial. How about the other way around? Are polynomial curves Bézier? Yes, as we see next.

Proposition 17.2. *If*

$$b(u) = [f(u) \;\; g(u) \;\; h(u)]^T \qquad (0 \le u \le 1)$$

is a polynomial curve, each coordinate value being a polynomial of degree at most n, then one can find $n + 1$ *control points* $P_0, P_1, \ldots P_n$*, such that* $b(u) = c(u)$*, where* c *is the Bézier approximation of the* P_i*,* $0 \le i \le n$*. In other words, the Bézier approximation of these control points is the given polynomial curve.*

Proof. The proof is beyond our scope here and the interested reader is referred to the text by Buss [21].

Remark 17.5. It's certainly gratifying that, despite their arising from the very special de Casteljau construction, the proposition assures us that the class of Bézier curves is just as general as the class of polynomial curves.

At this point let's pause a moment to appreciate the power and utility of Bézier curves, particularly in light of the preceding proposition. Suppose that a developers' group set out to design 1D primitives for a modeler. They might quite reasonably decide to support, in addition to straight lines and polylines, cubic polynomial curves, namely, those of the form

$$p(u) \;=\; [f_0 + f_1u + f_2u^2 + f_3u^3 \qquad g_0 + g_1u + g_2u^2 + g_3u^3 \qquad h_0 + h_1u + h_2u^2 + h_3u^3]^T$$

for $0 \le u \le 1$, in order to allow the user to go beyond straight segments and be able to draw simple curves. Then, that's 12 scalar coefficients $f_0, f_2, \ldots, h_3$ required to specify such a curve and a (very simple-minded) design decision might be to allow the user to edit the curve by changing each.

Contrast this with representing a cubic polynomial curve as a cubic Bézier curve specified by four control points. The size of the representation is still 12 scalars – three coordinates per control point – and the preceding proposition says that we still get all cubic polynomial curves. Consider, though, how much more convenient it is to mold the curve by manipulating control points rather than coefficients!

In fact, is there at all an easy-to-understand relationship between the coefficients $f_0, f_2, \ldots, h_3$ and the shape of $p(u)$ as given above? Even for the simple plane paper graph of a curve, say, $y = 3x^3 - x^2 + 5x + 7$, do the four coefficients $3, -1, 5$ and 7 themselves convey anything immediately meaningful about its shape?

17.2 Bézier Surfaces

From an understanding of Bézier curves it's a fairly intuitive next step to defining Bézier surfaces. Suppose we have an $(n+1) \times (m+1)$ *array* of control points

$$P_{i,j}\ , \text{ for } 0 \le i \le n,\ 0 \le j \le m$$

and wish to approximate these with a surface s. A construction of s via Bézier curves is as follows:

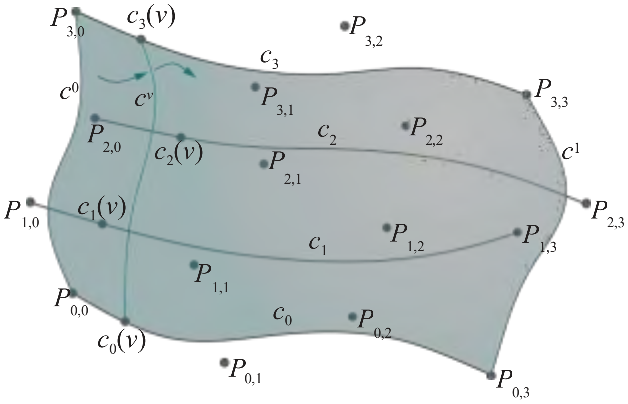

Figure 17.11: Constructing the Bézier surface approximating a 4×4 array of control points by sweeping a Bézier curve of order 4.

Think of the $(n+1) \times (m+1)$ array $P_{i,j}$ as $n+1$ different *sequences*, each of $m+1$ control points. In particular, the ith sequence, for $0 \le i \le n$, consists of $P_{i,0}, P_{i,0}, \ldots, P_{i,m}$, these being the points along the ith row of the control points array. Construct the Bézier curve approximating each of these $n+1$ sequences to obtain $n+1$ different Bézier curves, each of order $m+1$. Say the Bézier curve approximating the ith sequence is c_i, $0 \le i \le n$. See Figure 17.11, where both n and m are 3.

For each v in $0 \le v \le 1$, there are $n+1$ points, one on each curve c_i, corresponding to the parameter value v, namely, the sequence $c_0(v), c_1(v), \ldots, c_n(v)$. Say the Bézier curve c^v of order $n+1$ approximates these points. One such c^v is shown in the figure.

The union of all the Bézier curves c^v, for $0 \le v \le 1$, is the Bézier surface s approximating the control points array $P_{i,j}$, $0 \le i \le n$, $0 \le j \le m$. One can, as well, think of s as being *swept* by c^v, as v changes from 0 to 1.

The polyhedral surface composed of the quadrilateral faces $P_{i,j}P_{i+1,j}P_{i+1,j+1}P_{i,j+1}$, $0 \le i \le n-1$, $0 \le j \le m-1$, is called the *control polyhedron* of the Bézier surface specified by the control points $P_{i,j}$, $0 \le i \le n$, $0 \le j \le m$. As a Bézier curve mimics its control polygon, so a Bézier surface mimics its control polyhedron. See Figure 17.12.

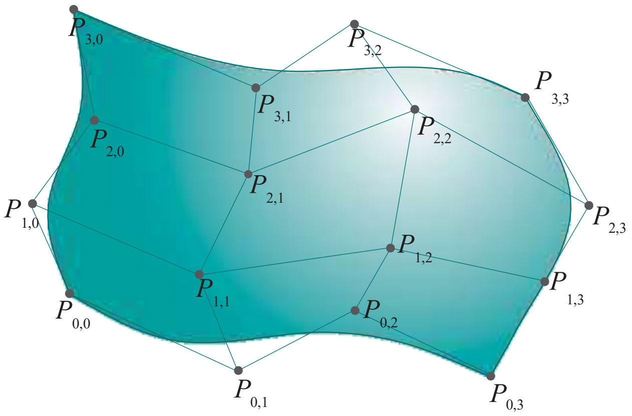

Figure 17.12: The Bézier surface approximating a 4 × 4 array of control points and its control polyhedron.

Figure 17.13: Screenshot of sweepBezierSurface.cpp.

Experiment 17.4. Run sweepBezierSurface.cpp to see an animation of the procedure. Press the left/right (or up/down) arrow keys to move the sweeping curve and the space bar to toggle between the two possible sweep directions. Figure 17.13 is a screenshot.

The 4 × 4 array of the Bézier surface's control points (drawn as small squares) consists of a blue, red, green and yellow row of four control points each. The four fixed Bézier curves of order 4 are drawn blue, red, green and yellow, respectively (the curves are in 3-space, which is a bit hard to make out because of the projection). The sweeping Bézier curve is black and its (moving) control points are drawn as larger squares. The currently swept part of the Bézier surface is the dark mesh. The current parameter value is shown at the top left. End

Determining the parametric equation of the Bézier surface s constructed as above is not difficult. The equation of c_i, the Bézier curve along the ith row of control points, is

$$c_i(v) = \sum_{j=0}^{m} B_{j,m}(v)P_{i,j} \qquad (0 \le v \le 1)$$

for $0 \le i \le n$. Therefore, the equation of the Bézier curve c^v approximating the "column" control sequence $c_0(v), c_1(v), \ldots, c_n(v)$ is

$$\begin{aligned} c^v(u) &= \sum_{i=0}^{n} B_{i,n}(u)c_i(v) \\ &= \sum_{i=0}^{n} B_{i,n}(u)\left[\sum_{j=0}^{m} B_{j,m}(v)P_{i,j}\right] \\ &= \sum_{i=0}^{n}\sum_{j=0}^{m} B_{i,n}(u)B_{j,m}(v)P_{i,j} \qquad (0 \le u \le 1) \end{aligned}$$

Letting both u and v vary one obtains the following parametric equation for the Bézier surface s approximating the control points array $P_{i,j}$, $0 \le i \le n$, $0 \le j \le m$:

$$s(u, v) = \sum_{i=0}^{n}\sum_{j=0}^{m} B_{i,n}(u)B_{j,m}(v)P_{i,j} \qquad (0 \le u \le 1,\ 0 \le v \le 1) \qquad (17.16)$$

Exercise 17.23. If the control points of a Bézier surface are $P_{i,j} = [x_{i,j}\ \ y_{i,j}\ \ z_{i,j}]^T$, $0 \le i \le n$, $0 \le j \le m$, write a parametric equation for its x-, y- and z-values, analogous to (17.13) for Bézier curves. There will now, of course, be two parameter variables instead of the one for curves.

Exercise 17.24. If the procedure to construct the Bézier surface s via Bézier curves is “inverted” to first (a) construct $m + 1$ different Bézier curves, each of order $n + 1$, approximating a *column* of control points, and then (b) sweep the Bézier curve approximating the points corresponding to the same parameter value on each of these $m + 1$ curves, prove that the same surface s is obtained. In particular, derive the parametric form of the surface resulting from the inverted process and show it to be identical to Equation (17.16).

The program sweepBezierSurface.cpp of Experiment 17.4, in fact, allows the user to toggle between either process by pressing the space bar.

Experiment 17.5. Run bezierSurface.cpp from Chapter 10, which allows the user to shape a Bézier surface by selecting and moving control points. Press the space and tab keys to select a control point. Use the left/right arrow keys to move the control point parallel to the x-axis, the up/down arrow keys to move it parallel to the y-axis, and the page up/down keys to move it parallel to the z-axis.

Press ‘x/X’, ‘y/Y’ and ‘z/Z’ to turn the viewpoint. Figure 17.14 is a screenshot.
End

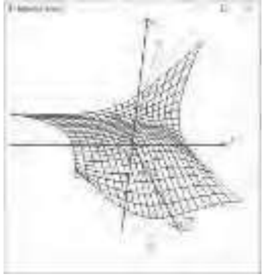

Figure 17.14: Screenshot of bezierSurace.cpp.

The following proposition is similar to Proposition 17.1 for Bézier curves:

Proposition 17.3. *If s is the Bézier surface approximating an $(n + 1) \times (m + 1)$ array of control points $P_{i,j}$, $0 \le i \le n$, $0 \le j \le m$, then the following hold:*

(a) *s is polynomial of degree n in one parameter variable u and polynomial of degree m in the other parameter variable v.*

(b) *s is a weighted sum of the control points $P_{i,j}$, $0 \le i \le n$, $0 \le j \le m$, where the weight of $P_{i,j}$ is the blending function $B_{i,n}(u)B_{j,m}(v)$ (i.e., a product of Bézier curve blending functions).*

(c) *The blending functions $B_{i,n}(u)B_{j,m}(v)$, $0 \le i \le n$, $0 \le j \le m$, form a partition of unity over the parameter space $[0, 1] \times [0, 1]$.*

(d) *Every point of s is a convex combination of the control points $P_{i,j}$, $0 \le i \le n$, $0 \le j \le m$, and, therefore, s lies inside the convex hull of the $P_{i,j}$.*

(e) *s interpolates the four corner control points $P_{0,0}$, $P_{n,0}$, $P_{0,m}$ and $P_{n,m}$, but not necessarily the others.*

(f) *(Affine Invariance) If the control points $P_{i,j}$, $0 \le i \le n$, $0 \le j \le m$, belong to $\mathbb{R}^3$ and $g : \mathbb{R}^3 \to \mathbb{R}^3$ is an affine transformation, then the image surface $g(s)$ is the Bézier surface approximating the images $g(P_{i,j})$, $0 \le i \le n$, $0 \le j \le m$, of the control points.*

In other words, the transformed surface approximates the transformed control points.

Proof. We begin by observing that the blending functions $B_{i,n}(u)B_{j,m}(v)$, $0 \le i \le n$, $0 \le j \le m$, form a partition of unity over the parameter space $[0, 1] \times [0, 1]$ because

$$\sum_{i=0}^{n}\sum_{j=0}^{m} B_{i,n}(u)B_{j,m}(v) = \sum_{i=0}^{n} B_{i,n}(u) \sum_{j=0}^{m} B_{j,m}(v) = 1 * 1 = 1$$

proving (c). We leave the rest of the proof, which is similar to that of Proposition 17.1, to the reader.

Exercise 17.25. What kinds of curves are the u- and v-*parameter curves* – recall these from Section 10.2.4 – on the Bézier surface

$$s(u, v) = \sum_{i=0}^{n}\sum_{j=0}^{m} B_{i,n}(u)B_{j,m}(v)P_{i,j} \ ?$$

Exercise 17.26. Recall Equation (10.20)

$$s(u, v) = (1 - u)(1 - v)\, p_1 + u(1 - v)\, q_1 + (1 - u)v\, p_2 + uv\, q_2, \qquad u, v \in [0, 1]$$

of a bilinear patch from Section 10.2.8. It's again a weighted sum of the "control" points p_1, p_2, q_1 and q_2. Do the blending functions form a partition of unity? Is a bilinear patch a Bézier surface?

Remark 17.6. The discussion of how to "smoothly" join Bézier surfaces in Section 10.3.2 is worth reviewing at this time.

Remark 17.7. Rational Bézier curves and surface, coming up in Chapter 20, are even more powerful design primitives than their polynomial versions which we studied this chapter. This is particularly so because, in addition to its location, each control point of a rational primitive has a scalar *weight*, increasing which increases its "attraction" on the primitive. So, for instance, to draw a polynomial Bézier primitive's shape toward a control point we need to move the latter away from the primitive, while, in the case of a rational primitive, we can simply raise the control point's weight, leaving it stationary, leading to a more elegant design process.

17.3 Summary, Notes and More Reading

This chapter was a fairly thorough introduction to the theory of the Bézier primitives. Our exploration was restricted, however, to the polynomial version, which itself is popularly used in design and, moreover, sets the stage for the rational primitives in a forthcoming chapter. Theory too has now caught up with practice: we learned to code polynomial Bézier curves and surfaces much earlier in Chapter 10.

There are a number of excellent books – Farin [45], Mortenson [97, 99], Rogers & Adams [120] and Vince [149] to name a few – which both complement the material here and take the reader beyond it. It is interesting to read in the first chapter of Farin's book an account by Bézier himself of the invention of the UNISURF CAD system that uses his primitives. In addition to those just mentioned, which are mostly math and modeling books, any CG book itself will likely have a section or two on Bézier theory and practice. The reader should have no trouble now following discussions of Bézier primitives in even advanced CG texts, such as Akenine-Möller, Haines & Hoffman [1], Buss [21], Slater et al. [137] and Watt [150].

CHAPTER 18

B-Spline

Our aim this chapter is to master the theory underpinning B-spline primitives, the dominant class of primitives used in freeform design nowadays. As in the preceding chapter on Bézier theory, we'll restrict ourselves here to the polynomial version, reserving the more general rational class of NURBS (Non-Uniform Rational B-Spline) primitives for Chapter 20, as an application of projective spaces, which are the natural setting for these primitives.

Almost all 3D modelers support NURBS primitives – and so, of course, their polynomial subclass as well – in a WYSIWYG design environment. In such a setting, the user can get by merely pushing control points around, with little understanding of theory. OpenGL, on the other hand, provides an interface at a much lower level. In fact, there is almost a one-to-one correspondence between NURBS theory and OpenGL syntax. Consequently, some knowledge at least of the former is required in order to use the latter.

Unfortunately, as NURBS theory is more complex than Bézier, there really is no use-now-learn-later approach. This is the reason we did not introduce NURBS, or even its polynomial subclass, in the earlier chapter on drawing, as we did polynomial Bézier primitives. True, the lack of shortcuts and a fancy interface will be seen as drawbacks by those who care only about design and not so much about what is under the hood. On the other hand, OpenGL's minimalist setting is ideal for the purpose of grasping the underlying theory.

Our account of B-spline theory begins in Section 18.1 with an analysis of the weakness of Bézier primitives, motivating the progression to B-splines as a search, in fact, for better blending functions. The investigation of the B-spline primitives themselves begins with curves in Section 18.2, setting the stage with so-called knot vectors in anticipation of new blending functions that are polynomial in knot intervals. In subsections 18.2.1-18.2.3, we go from (uniform) first-order to quadratic B-spline curves, applying an intuitive "break-and-make" procedure to increase the degree of the spline functions. The reader is asked to apply this procedure herself in 18.2.4 to fill in the details for cubic B-splines. A significant generalization is made in 18.2.5, not only by extending the theory to B-splines of arbitrary order, but by allowing the knot vector to be non-uniform as well. We'll see the utility of non-uniform knot vectors, particularly of repeated knots which empower the designer with the best of both worlds, Bézier and B-spline. From B-spline curves to surfaces in Section 18.3 is exactly the same process as from Bézier curves to surfaces.

Finally, we come to code in Section 18.4, particularly, the syntax of OpenGL NURBS drawing primitives, though in this chapter we go only as far as their polynomial functionality. Subsections 18.4.1 and 18.4.2 discuss drawing B-spline curves and surfaces, respectively. We describe how to light and texture a B-spline surface in 18.4.3. The useful technique of trimming a B-spline surface is described in 18.4.4.

Section 18.5, with notes and suggestions for future reading, concludes the chapter.

18.1 Problems with Bézier Primitives: Motivating B-Splines

Bézier curves and surfaces, the topics of the previous chapter, are easy to use and powerful enough to create complex designs. However, they suffer from two weaknesses:

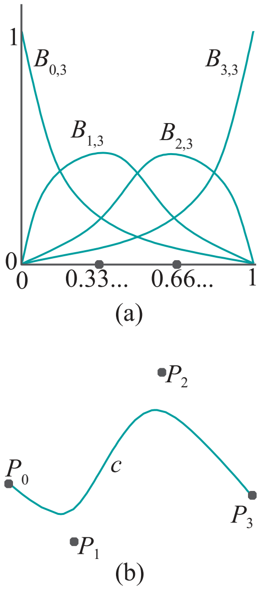

Figure 18.1: (a) Bernstein polynomials of degree 3: $B_{0,3}(u) = (1 - u)^3$, $B_{1,3}(u) = 3(1 - u)^2 u$, $B_{2,3}(u) = 3(1 - u)u^2$, $B_{3,3}(u) = u^3$ (b) A cubic Bézier curve.

1. *Lack of local control.*

   Observe that the blending function of every control point of a Bézier curve is non-zero over the entire open parameter interval $(0, 1)$; in other words, every control point has non-zero weight (or attraction, or pull) at every point of the curve, except, possibly, the endpoints. For example, Figure 18.1(a) shows the blending functions of a cubic Bézier curve, which are, of course, the Bernstein polynomials of degree three.

   This makes modifying a Bézier curve difficult: moving any one control point alters the *entire* curve, not just near the control point. Albeit points on the curve far from the relocated control point move little because its weight is small at distant points, nevertheless, there is change. Moving control point P_1 in Figure 18.1(b), for example, from a reading of its blending function $B_{1,3}(u)$ in Figure 18.1(a) maximally affects the curve in the vicinity of $c(0.33)$, but all points on the curve, except for the endpoints, are altered to some extent. E.g., moving P_1 would cause the curve to twitch even near P_3, which is far from P_1.

   The situation for Bézier surfaces is similar, as each control point has non-zero weight at every point of the surface, except, possibly, the corners.

   Typically, in designing a complex object with numerous control points a designer would prefer to be able to modify parts of the object independently, in other words, have local control, which in turn would necessitate restricting each control point to its own limited "region of influence". For example, in arranging Boris's smirk – see Figure 18.2 – the designer may want to leave his nose and eyes exactly as they are.

Figure 18.2: Mesh of Boris's head (courtesy of Sateesh Malla at www.sateeshmalla.com).

2. *The degree increases with the number of control points.*

   The Bézier curve $c(u)$ approximating $n + 1$ control points is polynomial of degree n in u. Evaluating a high-degree polynomial is expensive and repeated products lead to numerical instability. Complex curves, therefore, with multiple control points present a computational problem. And ditto for surfaces.

What to do about these problems? First, let's step back a bit to take the following abstract view of Bézier curves: a Bézier curve is the sum

$$c(u) = f_0(u)P_0 + f_1(u)P_1 + \ldots + f_n(u)P_n \qquad (0 \le u \le 1) \qquad (18.1)$$

of its control points P_i weighted by blending functions f_i which *happen to be* Bernstein polynomials. There's no reason they *have to be* Bernstein polynomials, provided that the resulting curve c – maybe no longer Bézier – does a satisfactory job of approximating the control points. The plan then is to try and invent new blending functions which, hopefully, alleviate the Bézier difficulties.

Before proceeding, here's a bit of useful terminology: if a function f, defined on the interval domain $[a, b]$, is non-zero everywhere inside the subinterval $[a^1, b^1]$, excepting possibly its endpoints a^1 and b^1, and zero on the rest of $[a, b]$, then it is said to have *support* in $[a^1, b^1]$. Figure 18.3(a) depicts a function $f_i(u)$ defined on $[0, 1]$ with support in the subinterval $[a^1, b^1]$.

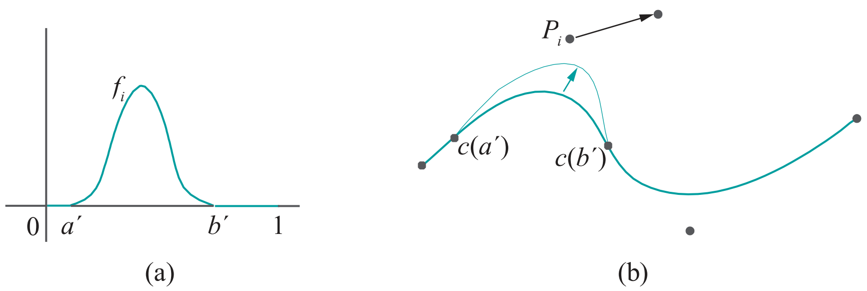

Figure 18.3: (a) Function f_i defined on [0, 1] has support in $[a', b']$ (b) Moving P_i, with associated blending function f_i, changes c only between $c(a')$ and $c(b')$.

Exercise 18.1. If the blending function f_i of control point P_i in expression (18.1) has support in the proper subinterval $[a^1, b^1]$ of the parameter interval [0, 1], then show that moving P_i changes the arc of the approximating curve c only between $c(a^1)$ and $c(b^1)$. See Figure 18.3(b).

Exercise 18.2. Prove that the ith Bernstein polynomial of degree n for every i, $0 \leq i \leq n$, has support in the entire parameter interval [0, 1] (keep in mind that the behavior of the polynomial outside of [0, 1] is of no interest).

From the preceding two exercises, it seems, then, that the first problem with Bézier curves mentioned above arises because the blending function of every control point has support in the entire parameter interval [0, 1]. A solution, therefore, would be to find blending functions each having support in only part of that interval.

Moreover, the second problem would be solved if the degree of the blending functions could be *decoupled* from the number of control points, so that increasing the latter did not necessarily raise the former.

So, now that we have an idea of what we want, let's see what we can find. Suppose, to begin with, that we ask for blending functions all quadratic, *no matter* the number of control points. Further, to obtain local control, then, we seek quadratics with limited support – whose graphs resemble that of f_i in Figure 18.3(a). Sadly, this is a hopeless task because a quadratic is zero only at its at most two roots, not on any interval stretch like that between 0 and a^1, or b^1 and 1. But, look again at f_i. Except for the two straight zero parts at either end, the graph of f_i does resemble somewhat an upside-down parabola – see the graph of the parabola $f(u) = u^2$ in Figure 18.4(a).

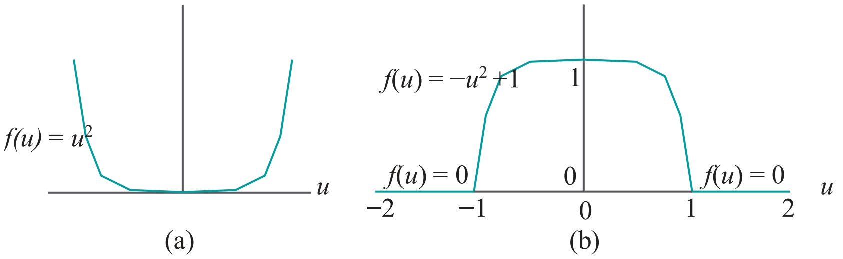

Figure 18.4: (a) Parabola (b) Three-part function: one upside-down parabola and two straight.

Note: Curves drawn in this chapter are fairly accurate sketches, but not necessarily exact plots of their equations.

Here, then, is a drastic solution. Let's make a blending function f like f_i by assembling it from three parts – one quadratic (an upside-down parabola) and two straight zero – as follows:

$$f(u) = \begin{cases} 0, & -2 \leq u \leq -1 \\ -u^2 + 1, & -1 \leq u \leq 1 \\ 0, & 1 \leq u \leq 2 \end{cases}$$

There's no law that says that a formula has to be one line! So the specification of f is fine. Figure 18.4(b) shows its graph. We seem to be headed in the right direction. We have a blending function which is at most quadratic and which has support in $[-1, 1]$, just half of its whole domain $[-2, 2]$.

Note: If the reader is wondering about the new parameter interval $[-2, 2]$, keep in mind that there's nothing special about the parameter interval $[0, 1]$ we use most often, other than that it's convenient to write. Parameter intervals can be any $[a, b]$, with $a < b$. In the case above, $[-2, 2]$ helps avoid fractions in the formula for f.

The corners (C^1-discontinuities, to be precise) at $u = \pm 1$, where the straight parts of f meet the parabolic, are undesirable though, because discontinuities in the blending function will carry over to discontinuities in the approximating curve employing such a function. It'll be nice to be rid of them. How do we get a parabolic part to join a straight part without making a corner? Oddly enough, the parabola $f(u) = u^2$ in Figure 18.4(a) itself suggests a solution. Consider the part of this parabola to the *right* of the y-axis and the (straight) part of the x-axis to the *left* of the y-axis: they meet smoothly at the origin! See Figure 18.5.

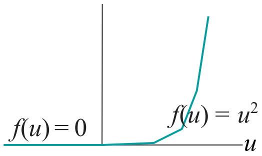

Figure 18.5: The right wing of the parabola $f(u) = u^2$ meeting the straight left half of the x-axis smoothly at the origin.

So here's the next draft. For $u \leq 0$ and $u \geq 4$, define $f(u)$ to be 0, giving two long straight parts; define $f(u) = u^2$ between 0 and 1; and, $f(u) = (u - 4)^2$ between 3 and 4. See the green curves in Figure 18.6. Particularly, $f(u) = u^2$ in $[0, 1]$ is part of the right wing of the parabola of Figure 18.4(a), while $f(u) = (u - 4)^2$ in $[3, 4]$ from the left wing of the same parabola (but shifted 4 units to the right). The two quadratics meet the straight parts smoothly, so that's taken care of, but there's a piece missing in between (pretend you don't see the black curve!). Now, if we could only find a quadratic to sit smoothly atop the two side quadratics and cap the gap.

It turns out that a fairly intuitive choice works: drag $f(u) = u^2$ two units to the right, flip it upside down and then raise it two units. The equation is $f(u) = -(u - 2)^2 + 2$, which in $[1, 3]$ gives the black curve in Figure 18.6. We leave verification to the reader in the next two exercises.

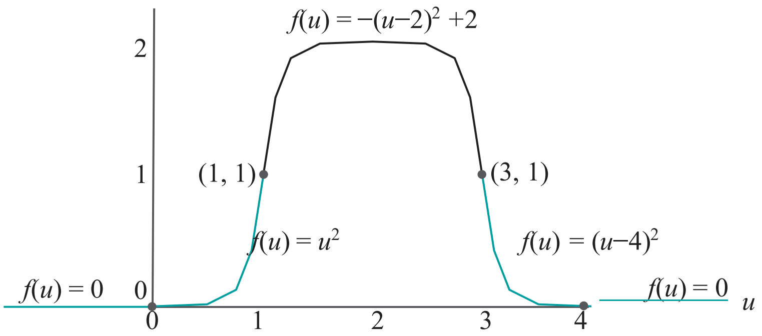

Figure 18.6: Five-part function: three parabolic and two straight parts. Joints are black points.

Exercise 18.3. Show that the curve $f(u) = -(u - 2)^2 + 2$ indeed meets $f(u) = u^2$ at $(1, 1)$ and $f(u) = (u - 4)^2$ at $(3, 1)$.

Exercise 18.4. Show that at each of the four *joints* $(0, 0)$, $(1, 1)$, $(3, 1)$ and $(4, 0)$ of the five-part function depicted in Figure 18.6 the tangent lines of the curves on either side are equal. Therefore, there is no C^1-discontinuity at a joint and the function is C^1-continuous everywhere.

Part answer : At $(1, 1)$, where $u = 1$, the tangent on the left is from $f(u) = u^2$ and on the right from $f(u) = -(u - 2)^2 + 2$. Now, $\frac{d}{du} u^2 = 2u$, which is 2 at $u = 1$, and $\frac{d}{du}(-(u - 2)^2 + 2) = -2(u - 2)$, which is also 2 at $u = 1$, so, indeed, the tangent lines on either side of the joint $(1, 1)$ are equal.

For the record, here's the 5-line formula specifying f:

$$f(u) = \begin{cases} 0, & u \le 0 \\ u^2, & 0 \le u \le 1 \\ -(u-2)^2 + 2, & 1 \le u \le 3 \\ (u-4)^2, & 3 \le u \le 4 \\ 0, & 4 \le u \end{cases} \tag{18.2}$$

f has support in $[0, 4]$ and, from the preceding exercise, is C^1-continuous throughout. Moreover, if its parameter interval is chosen to be an interval larger than $[0, 4]$, e.g., $[-2, 6]$, then we have indeed a C^1-continuous blending function with limited support.

The moral then is to look for blending functions among the class of piecewise polynomial functions – a function is *piecewise polynomial* if its domain can be split into subintervals in each of which it's polynomial. For example, f above is composed of five polynomial pieces. From a computational point of view, evaluating a piecewise polynomial is not much harder than evaluating a polynomial. If one thinks in terms of C or C++ code, then there is simply an extra if-else ladder to determine the appropriate subinterval and corresponding polynomial.

The piecewise polynomials to be used as blending functions must be chosen carefully though. For example, looking back at Propositions 17.1 and 17.3 of the last chapter, it's desirable for the set of blending functions to form a partition of unity over the parameter space. Good things happen then: (a) points on the curve (or surface) are convex combinations of its control points, so the whole lies in the convex hull of its control points and (b) affine invariance.

Writing down all the properties we want, then, we put together a Wish List for blending functions. We ask that they

(a) be at least a C^1-continuous piecewise polynomial,

(b) be of a low degree independent of the number of control points,

(c) each have support in only part of the parameter space, and,

(d) together form a partition of unity over the parameter space.

We're led to B-splines.

18.2 B-Spline Curves

Let's set the stage for the *B-spline blending functions* (or, as they are also called, *B-spline functions*, or *B-splines*, or *spline functions*) that we are going to define. Each will be piecewise polynomial, in other words, polynomial on subintervals. In anticipation, then, let's fix a particular parameter space and chop it up into subintervals. For convenience now, we choose $[0, r]$, where r is some positive integer, and its r subintervals to be the equally sized

$$[0,1],\ [1,2],\ \ldots,\ [r-1,r]$$

See Figure 18.7. The sequence

$$\{0, 1, \ldots, r\}$$

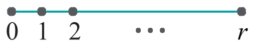

Figure 18.7: Parameter space $[0, r]$ with uniformly-spaced knots.

of successive interval endpoints is called the *knot vector* and the endpoints $0, 1, \ldots, r$ themselves, *knots*. Each subinterval $[i, i+1]$, for $0 \le i \le r-1$, is a *knot interval* . We expect to define blending functions which are polynomial in each knot interval with (hopefully, well-behaved) joints at knot values.

Remark 18.1. A knot vector as above with equally spaced knots is called a *uniform* knot vector. Later in this chapter we'll see non-uniform knot vectors as well.

Remark 18.2. The "B" in B-splines, the name given these functions by Schoenberg [129], a pioneer in their use, comes from "basis".

18.2.1 First-Order B-Splines

We'll start at the lowest level possible and define the *B-splines of degree 0* by means of constant functions. There are r B-splines of degree 0, each equal to 1 on one knot interval and 0 outside it. Precisely, the ith B-spline of degree 0, for $0 \leq i \leq r - 1$, denoted $N_{i,1}$, is defined as follows.

When $i = 0$:

$$N_{0,1}(u) = \begin{cases} 1, & 0 \leq u \leq 1 \\ 0, & \text{otherwise} \end{cases} \tag{18.3}$$

When $1 \leq i \leq r - 1$:

$$N_{i,1}(u) = \begin{cases} 1, & i < u \leq i + 1 \\ 0, & \text{otherwise} \end{cases} \tag{18.4}$$

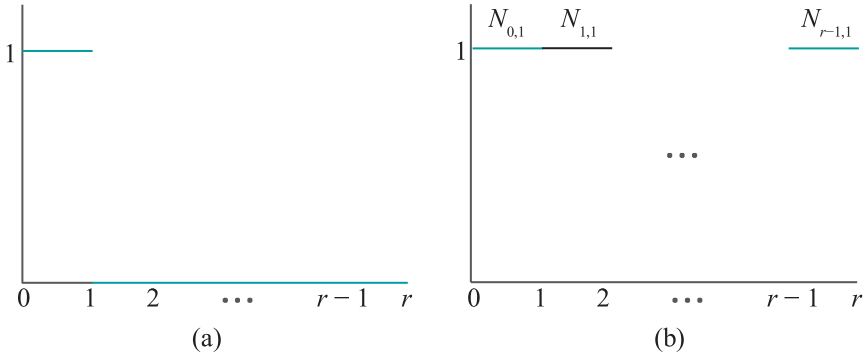

Figure 18.8: First-order B-splines: (a) $N_{0,1}$ (b) Non-zero parts of $N_{i,1}$, $0 \leq i \leq r - 1$, distinguished by alternate green and black colors.

In other words, each $N_{i,1}$ is 1 on the knot interval $[i, i + 1]$, except, possibly, at the endpoints, and 0 outside it; so, $N_{i,1}$ has support in $[i, i + 1]$. Figure 18.8(a) shows the graph of $N_{0,1}$ over the entire parameter space $[0, r]$, while Figure 18.8(b) only the non-zero parts of the graphs of $N_{i,1}$, for $0 \leq i \leq r - 1$. The niggling technicality – see the first line of the two equations above – of having to define $N_{0,1}$ to be 1 on a closed interval, while the other $N_{i,1}$ are equal to 1 on a half-open interval, is unavoidable. For, we want the r B-splines of degree 0 to form together a partition of unity over $[0, r]$, so no two are allowed to be 1 at the same point.

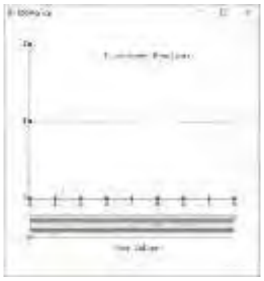

Figure 18.9: Screenshot of bSplines.cpp at first order.

Experiment 18.1. Run bSplines.cpp, which shows the non-zero parts of the spline functions from first order to cubic over the uniformly spaced knot vector

$$[0, 1, 2, 3, 4, 5, 6, 7, 8]$$

Press the up/down arrow keys to choose the order. Figure 18.9 is a screenshot of the first order. The knot values can be changed as well, but there's no need to now. End

B-splines of degree 0 are commonly called *first-order B-splines*. If the knot vector is uniform, as above, they are called *uniform first-order B-splines*.

Interestingly, as the reader may easily verify, all items on the Wish List at the end of Section 18.1 are fulfilled by the first-order B-splines, except for C^1-continuity, where, obviously, they fail badly because the $N_{i,1}$ are not even continuous (i.e., not even C^0-continuous). As we see next, expectedly this deficiency carries over to approximating curves made from first-order B-splines as well.

First-Order B-Spline Curves

A *first-order B-spline approximation* of r control points $P_0, P_1, \dots, P_{r-1}$ is called a first order B-spline curve. This is the curve c obtained from applying the first-order B-splines as blending functions to these control points, namely,

$$c(u) = \sum_{i=0}^{r-1} N_{i,1}(u) P_i \qquad (0 \leq u \leq r) \tag{18.5}$$

What sort of a curve is c? Well, one would be hard pressed to call c a curve in the first place! Applying the definitions of $N_{i,1}$ from Equations (18.3)-(18.4) to Equation (18.5) above, one sees that c is *stationary* at P_0 for u from 0 to 1. When u crosses 1, c *jumps* to P_1, staying stationary again till u crosses 2, when c jumps to P_2, and so on. The graph of c is then just the collection of its own control points! See Figure 18.10. Obviously, if there are even two distinct control points then c is not C^0. Clearly, we'll have to move to higher orders of B-splines for satisfaction.

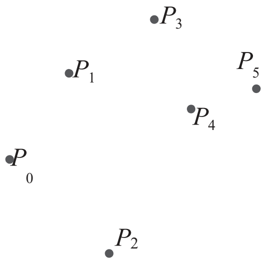

Figure 18.10: First-order B-spline approximation – the "curve" consists of its control points.

First-order B-Spline Properties

However, before leaving the first order, here are a few of their properties for future reference:

1. Each $N_{i,1}$ is piecewise polynomial, consisting of at most three pieces, each of which is constant.
2. $N_{i,1}$ has support in the single knot interval $[i, i+1]$.
3. Each $N_{i,1}$ is not C^0 only at the endpoints of its supporting interval; elsewhere, it's C^∞. In other words, it's smooth – remember from Definition 10.7 that C^∞ is also called smooth – apart from its joints.
4. Together, the $N_{i,1}$ form a partition of unity over the parameter space $[0, r]$.
5. Except for $N_{0,1}$, the $N_{i,1}$ are translates of one another, i.e., the graph of one is a translate of that of another. This is a consequence of the knots being uniformly spaced.
6. A first-order B-spline approximation is, generally, not even C^0.

18.2.2 Linear B-Splines

The clear problem with first-order B-splines is that their polynomial degree 0 is too low, allowing little flexibility in shape. Straight and horizontal is all that they can be. Let's go one higher to degree 1. We'll do this in a particular way which will be easy to generalize down the road.

The trivial formula

$$1 = u + (-u + 1) \tag{18.6}$$

allows one to "break" each B-spline $N_{i,1}$, of degree 0, into two functions $N^0_{i,1}$ and $N^1_{i,1}$ of degree 1. For example, $N_{0,1}$ breaks into $N^0_{0,1}$ and $N^1_{0,1}$, where

$$N^0_{0,1}(u) = \begin{cases} u, & 0 \leq u \leq 1 \\ 0, & \text{otherwise} \end{cases} \tag{18.7}$$

and

$$N^1_{0,1}(u) = \begin{cases} -u + 1, & 0 \leq u \leq 1 \\ 0, & \text{otherwise} \end{cases} \tag{18.8}$$

the two obviously adding to give back $N_{0,1}$, viz.,

$$N_{0,1}(u) = N^0_{0,1}(u) + N^1_{0,1}(u) \tag{18.9}$$

$N_{i,1}$, when $i > 0$, can likewise be broken into $N^0_{i,1}$ and $N^1_{i,1}$, where

$$N^0_{i,1}(u) = \begin{cases} u-i, & i < u \le i+1 \\ 0, & \text{otherwise} \end{cases} \tag{18.10}$$

and

$$N^1_{i,1}(u) = \begin{cases} -u+i+1, & i < u \le i+1 \\ 0, & \text{otherwise} \end{cases} \tag{18.11}$$

which actually invokes an i-shift of (18.6), namely, $1 = (u - i) + (-u + i + 1)$. And, again

$$N_{i,1}(u) = N^0_{i,1}(u) + N^1_{i,1}(u) \tag{18.12}$$

Figure 18.11 shows the (non-zero pieces of the) two parts of each first-order B-spline. For obvious reasons, we call the $N^0_{i,1}$s "up" and the $N^1_{i,1}$s "down". The up parts are all left or right translates of one another, as are the down parts, except that the technicality that their values at the left end of the knot interval $[0, 1]$ are different from those at the left end of other knot intervals persists from first-order.

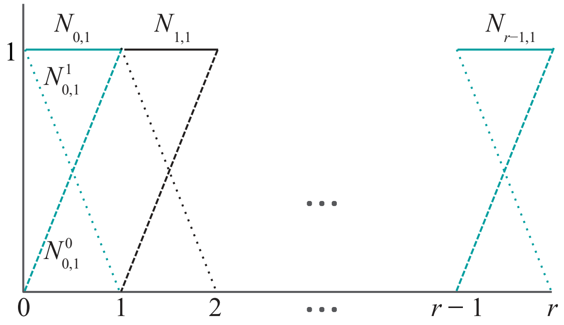

Figure 18.11: First-order B-splines each broken into an up part (dashed) $N^0_{i,1}$ and a down part (dotted) $N^1_{i,1}$. Successive $N_{i,1}$'s are distinguished by color.

Remark 18.3. This is important! For future reference, think of what we have just done as the following: each $N_{i,1}$ is broken into two new functions over its support, one obtained from multiplying $N_{i,1}$ by a *straight-line function increasing from 0 to 1* from the left end of its support to the right (namely, $u - i$), while the other from multiplying it by a *straight-line function decreasing from 1 to 0* over the same interval (namely, $-u + i + 1$). Because $(u - i) + (-u + i + 1) = 1$, the two new functions add to give back the one that was broken. And, of course, multiplication by such degree-1 functions causes the degree of the new functions to rise by 1 (in this case, from the degree 0 of $N_{i,1}$ to degree 1 of $N^0_{i,1}$ and $N^1_{i,1}$).

Equations (18.9) and (18.12) evidently guarantee that $N^0_{i,1}$ and $N^1_{i,1}$ for $0 \le i \le r-1$, together form a partition of unity, because the $N_{i,1}$, $0 \le i \le r-1$, do. However, there are $2r$ of the former, which is twice as many as we need to blend r control points. What to do? Figure 18.11, in fact, suggests a way to pair them up nicely – join each up part to the following down part! Accordingly, define the *second-order B-splines* (or *linear B-splines*), for $0 \le i \le r-2$, as follows:

$$N_{i,2}(u) = N^0_{i,1}(u) + N^1_{i+1,1}(u) = \begin{cases} 0, & u \le i \\ u-i, & i \le u \le i+1 \\ -u+i+2, & i+1 \le u \le i+2 \\ 0, & i+2 \le u \end{cases} \tag{18.13}$$

Figure 18.12 shows the non-zero parts of the linear B-splines $N_{i,2}$, $0 \le i \le r-2$, on the domain $[0, r]$. *See the magic*: pairing has removed all C^0-discontinuities because each linear B-splines drops to zero at the ends of its support, so is continuous everywhere.

Exercise 18.5. Verify that the multi-part formula above for $N_{i,2}(u)$ indeed follows from joining up and down parts (using the equations for $N^0_{i,1}$ and $N^1_{i,1}$ given earlier).

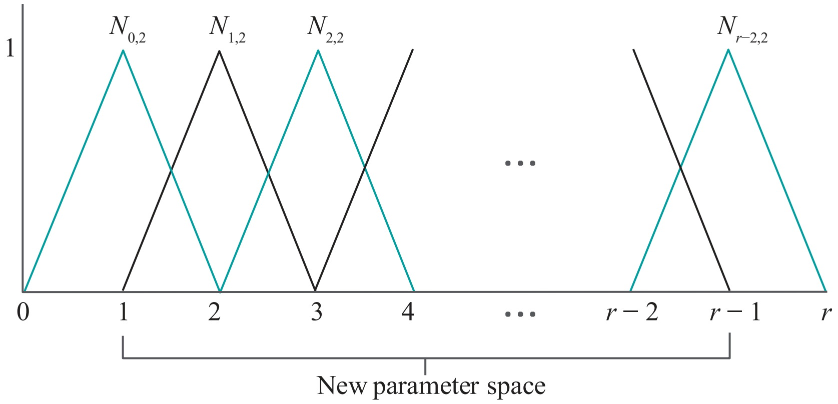

Figure 18.12: Non-zero parts of linear B-splines. Each is an inverted V. Successive ones are distinguished by color. The down part in the first knot interval and the up part in the last are discarded. The new (truncated) parameter space is $[1, r-1]$.

Experiment 18.2. Run again bSplines.cpp and select the linear B-splines over the knot vector

$$[0, 1, 2, 3, 4, 5, 6, 7, 8]$$

Figure 18.13 is a screenshot. End

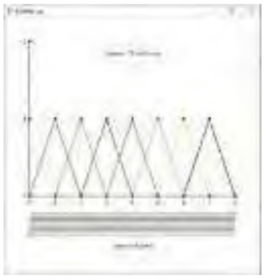

Figure 18.13: Screenshot of bSplines.cpp at second-order.

Remark 18.4. The technicality of the $N_{i,1}$ not being all of the same value at the left endpoint of a supporting interval is now gone. The definition of $N_{i,2}$ is the same for all i in $0 \le i \le r-2$.

Remark 18.5. Second-order B-splines as defined above are often called *uniform linear B-splines* to emphasize the use of a uniform knot vector.

Note that the down part $N^1_{0,1}$ of $N_{0,1}$ and the up part $N^0_{r-1,1}$ of $N_{r-1,1}$ have no partners, so have been discarded, which is why we have $r-1$ linear B-splines $N_{i,2}$, for $i = 0$ to $r-2$, versus the r first-order B-splines we started with. It's clear from Figure 18.12 that the parameter space must be truncated from $[0, r]$ to $[1, r-1]$ as well, for, otherwise, there's a problem with the partition-of-unity property in the two end knot intervals $[0, 1]$ and $[r-1, r]$. Once this is done, though, we're in good shape, or at least in significantly better shape than the first-order B-splines. All items in the Wish List at the end of Section 18.1 are now fulfilled except for C^1-continuity, but now the functions are at least C^0, if not quite C^1 (because of corners at the joints).

Linear B-Spline Curves

What sort of curve is the linear B-spline approximation c of $r-1$ control points $P_0, P_1, \ldots, P_{r-2}$, which uses the linear B-splines as blending functions? It's defined by

$$c(u) = \sum_{i=0}^{r-2} N_{i,2}(u) P_i \qquad (1 \le u \le r-1) \tag{18.14}$$

and we'll ask the reader next to see what this gives.

Exercise 18.6. Verify that the linear B-spline approximation c given by Equation (18.14) is the polygonal line through the control points in the sequence they are given. See Figure 18.14, where $r = 7$. This is certainly more respectable a curve than the first-order approximation.

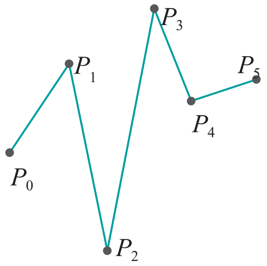

Figure 18.14: Linear B-spline approximation – the curve is a polyline.

Terminology : A B-spline approximation of a sequence of control points is often called a *B-spline curve*, a *spline curve* or, simply, a *spline*. There is ambiguity sometimes, therefore, with the terminology for B-spline blending functions, but it'll be clear from the context if the term refers to a blending function or an approximating curve.

Linear B-Spline Properties

Here's a list of properties of linear B-splines similar to the one made earlier for first-order B-splines:

1. Each $N_{i,2}$ is piecewise polynomial, consisting of at most four pieces, each of which is linear, except for zero end pieces.

2. $N_{i,2}$ has support in $[i, i+2]$, the union of two consecutive knot intervals.

3. Each $N_{i,2}$ is C^0, but not C^1, at its joints. Apart from its joints it's smooth everywhere.

4. Together, the $N_{i,2}$ form a partition of unity over the parameter space $[1, r-1]$.
5. The $N_{i,2}$ are translates of one another.

6. A linear B-spline approximation is C^0, but, generally, not C^1.

18.2.3 Quadratic B-Splines

Linear B-splines are certainly preferable to first-order ones, but we're still shy of C^1-continuity. If we could raise the degree of the polynomial pieces yet again, from 1 to 2, we might do better.

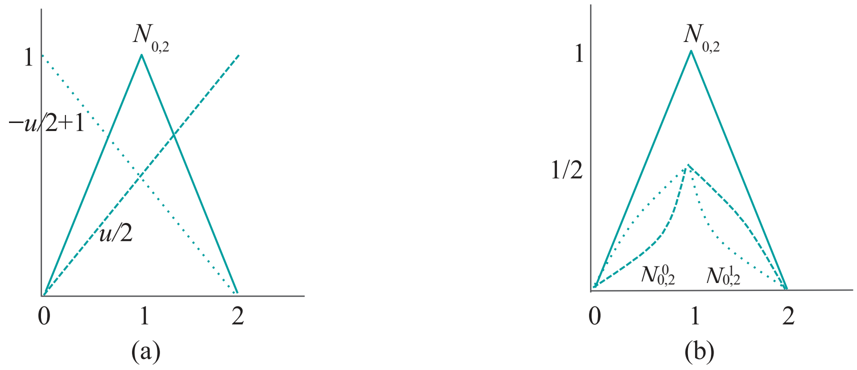

Figure 18.15: (a) The graphs of the two straight-line multiplying functions for $N_{0,2}$, one dashed and one dotted (b) The result of the multiplication: the up part $N^0_{0,2}$ (dashed) and the down part $N^1_{0,2}$ (dotted).

It turns out that the approach introduced in the last section of breaking first-order B-splines into up and down parts of one higher degree, and then pairing them up to make linear B-splines, generalizes. Consider first $N_{0,2}$, whose non-zero part is graphed in Figure 18.15(a). Recalling Remark 18.3, to break $N_{0,2}$ into two we'll multiply it by a straight-line function increasing from 0 at the left end of its support to 1 at the right, as well as by the complementary function decreasing from 1 to 0. Since the supporting interval of $N_{0,2}$ is $[0, 2]$, the two straight-line functions called for are $u/2$ and $-u/2+1$, respectively, which are shown in Figure 18.15(a) as well.

Accordingly, break $N_{0,2}$ as follows:

$$N_{0,2} = \frac{u}{2} N_{0,2} + \left(-\frac{u}{2} + 1\right) N_{0,2} \tag{18.15}$$

where the "up part" – it's not really increasing throughout any more but we'll stick with the term – is

$$N^0_{0,2}(u) = \frac{u}{2} N_{0,2} = \begin{cases} 0, & u \leq 0 \\ \frac{1}{2}u^2, & 0 \leq u \leq 1 \\ -\frac{1}{2}u^2 + u, & 1 \leq u \leq 2 \\ 0, & 2 \leq u \end{cases} \tag{18.16}$$

and the down part is

$$N^1_{0,2}(u) = (-\frac{u}{2} + 1)\, N_{0,2} = \begin{cases} 0, & u \le 0 \\ -\frac{1}{2}u^2 + u, & 0 \le u \le 1 \\ \frac{1}{2}u^2 - 2u + 2, & 1 \le u \le 2 \\ 0, & 2 \le u \end{cases} \qquad (18.17)$$

The graphs of the two parts, resembling opposing shark fins, are shown in Figure 18.15(b).

Exercise 18.7. Verify the formulae for $N^0_{0,2}$ and $N^1_{0,2}$ by multiplying that for $N_{0,2}$ by $u/2$ and $-u/2 + 1$, respectively.

The other linear B-splines $N_{i,2}$, for $1 \le i \le r - 2$, can similarly be broken. Figure 18.16 shows the graphs of the up and down parts.

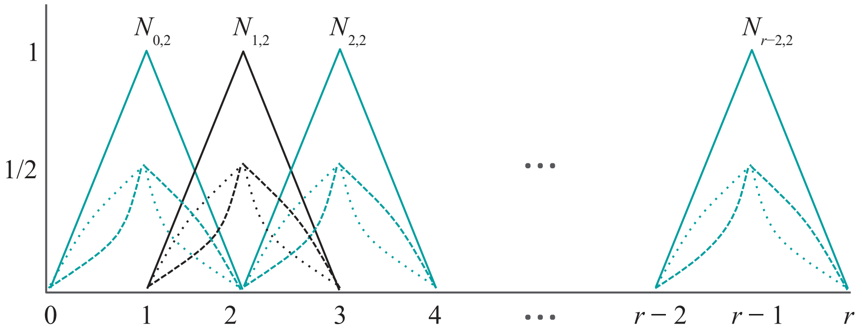

Figure 18.16: Linear B-splines each broken into an up (dashed) part $N^0_{i,2}$ and down (dotted) part $N^1_{i,2}$. Successive ones are distinguished by color.

Next, as in the first-order case, pair them up, adding each up part to the down part of the following linear B-spline. Non-zero pieces of paired up and down parts overlapped only at a point in the first-order case, so adding meant simply splicing graphs end to end. Now, we do actually have to add on interval overlaps.

And again magic! Two adjacent and opposing shark fins, one dashed and the other dotted, both with a sharp corner in the middle, add up to a smooth-looking floppy hat! See Figure 18.17. Precisely, the up part of one linear B-spline adds to the down part of the following one to make a *quadratic B-spline* (or, *third order B-spline*).

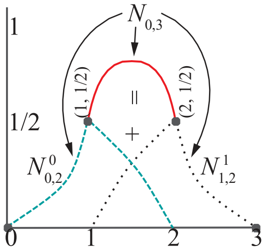

Figure 18.17: Adding $N^0_{0,2}$ and $N^1_{1,2}$ to make $N_{0,3}$. $N_{0,3}$ consists of three parts: on [0, 1], it's just $N^0_{0,2}$, on [2, 3] it's $N^1_{1,2}$, while in the middle, on [1, 2] it is the sum of $N^0_{0,2}$ and $N^1_{1,2}$. Joints are indicated.

Figure 18.17 explains exactly what's happening. The graph of $N^0_{0,2}$ is green dashed, while that of $N^1_{1,2}$ black dotted. The graph $N_{0,3}$ of their sum consists of the outer green dashed arc on [0, 1], the outer black dotted arc on [2, 3] and the unbroken red arc on [1, 2] in the middle, the latter being the sum of the inner green dashed and the inner black dotted. So it's in the middle interval [1, 2] that actual summing takes place. We'll see the summed equation itself momentarily.

Experiment 18.3. Run again bSplines.cpp and select the quadratic B-splines over the knot vector

$$[0, 1, 2, 3, 4, 5, 6, 7, 8]$$

Figure 18.18 is a screenshot. Note the joints indicated as black points. **End**

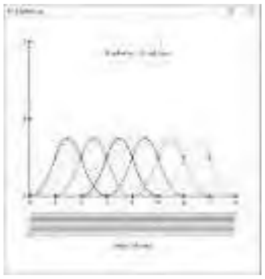

Figure 18.18: Screenshot of bSplines.cpp at third order.

$N_{0,3}$ is the first quadratic B-spline. Figure 18.19 depicts the sequence of quadratic B-splines $N_{i,3}$, $0 \le i \le r - 3$, on the domain $[0, r]$. Now, for their equations. As they are evidently translates of one another, it's sufficient to write only that of the first one:

$$N_{0,3}(u) = N^0_{0,2}(u) + N^1_{1,2}(u) = \begin{cases} 0, & u \le 0 \\ \frac{1}{2}u^2, & 0 \le u \le 1 \\ \frac{3}{4} - (u - \frac{3}{2})^2, & 1 \le u \le 2 \\ \frac{1}{2}(-u + 3)^2, & 2 \le u \le 3 \\ 0, & 3 \le u \end{cases} \qquad (18.18)$$

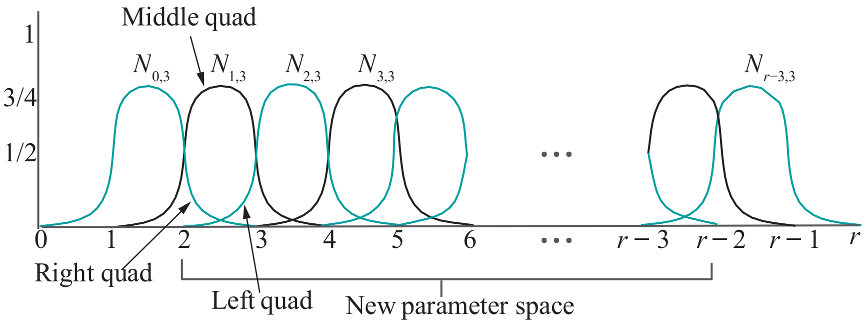

Figure 18.19: Non-zero parts of the quadratic B-splines. Successive splines are distinguished by color. The pieces adding up to 1 on $[2, 3]$ are indicated.

Exercise 18.8. Verify the preceding formula with the help of (18.16) and (18.17). Don't forget to shift the second equation to the right for the formula for $N^1_{1,2}$

Exercise 18.9. Use Equation (18.18) to determine the equation of $N_{1,3}(u)$ and, generally, $N_{i,3}(u)$.

Exercise 18.10. Verify that the first quadratic B-spline $N_{0,3}$ is C^1 *everywhere* by differentiating the functions on the RHS of (18.18) and comparing the tangents on either side at each joint (which is only where discontinuity might occur). The four joints of $N_{0,3}$, with x-values 0, 1, 2 and 3, are indicated in Figure 18.17.

Differentiating again, verify that $N_{0,3}$ is *not* C^2 at its joints.

As the quadratic B-splines are translates one of one another, it follows from the preceding exercise that they are all C^1 everywhere, though not C^2 at their joints.

Remark 18.6. Compare the 5-line formulas (18.2) and (18.18) to see that we've come now full circle back to almost the same piecewise quadratic blending function which we used to motivate B-splines in the first place!

As in the linear case, the parameter space must be truncated, this time to $[2, r-2]$, to ensure that the partition-of-unity property holds. The key to keep in mind is that partition-of-unity holds in those knot intervals on which there is defined a left, a middle and a right quadratic arc – from successive quadratic B-splines (Figure 18.19 shows these three pieces over the interval $[2, 3]$).

Pop the champagne: we now officially have every item on the Wish List!

Quadratic B-Spline Curves

So what sort of curve is the quadratic B-spline approximation c of $r-2$ control points $P_0, P_1, \ldots, P_{r-3}$, defined by

$$c(u) = \sum_{i=0}^{r-3} N_{i,3}(u)P_i \qquad (2 \le u \le r-2) \tag{18.19}$$

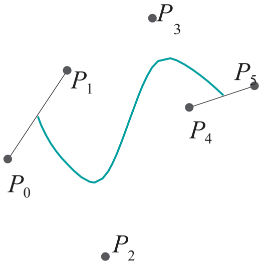

Figure 18.20: Quadratic B-spline approximation.

where the quadratic B-splines are used as blending functions?

First, and importantly, since the quadratic B-splines are all C^1, so is a quadratic B-spline approximation. We've gained at least respectable continuity then. However, as we ask the reader to show next, the property of interpolating the first and last control points has been lost (though not on our Wish List, this, nevertheless, is desirable).

Exercise 18.11. Prove that the quadratic spline curve c defined by Equation (18.19) begins at the midpoint of P_0P_1, ends at the midpoint of $P_{r-4}P_{r-3}$, and doesn't necessarily interpolate *any* of its control points. See Figure 18.20.

Darn, just when we thought things were going our way, a potentially nasty bug rears its ugly head. Not to worry, as soon as we are able to loosen up the knot vector from being uniform, we'll be happily interpolating first and last control points.

Experiment 18.4. Run quadraticSplineCurve.cpp, which shows the quadratic spline approximation of nine control points in 2D space over a uniformly spaced vector of 12 knots. Figure 18.21 is a screenshot.

The control points are green. Press the space bar to select a control point – the selected one turns red – and the arrow keys to move it. The knots are the green points on the black bars at the bottom. At this stage there is no need to change their values. The blue points are the joints of the curve, i.e., images of the knots. Also drawn in light gray is the control polygon.

Ignore the code itself for now. We'll be seeing how to draw spline curves and surfaces using OpenGL soon. End

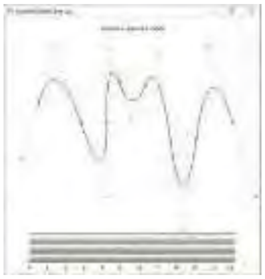

Figure 18.21: Screenshot of quadraticSplineCurve.cpp.

Exercise 18.12. What part of the quadratic spline curve c approximating the control points $P_0, P_1, \ldots, P_{r-3}$ is altered by moving only P_i? Your answer should be in terms of an arc of c between a particular pair of its joints. Verify using quadraticSplineCurve.cpp.

Quadratic B-Spline Properties

A list of properties for quadratic B-splines:

1. Each $N_{i,3}$ is piecewise polynomial, consisting of at most five pieces, each of which is quadratic, except for zero end pieces.
2. $N_{i,3}$ has support in $[i, i+3]$, the union of three consecutive knot intervals.
3. Each $N_{i,3}$ is C^1, but not C^2, at its joints. Apart from its joints it's smooth everywhere.
4. Together, the $N_{i,3}$ form a partition of unity over the parameter space $[2, r-2]$.
5. The $N_{i,3}$ are translates of one another.
6. A quadratic B-spline approximation is C^1, but, generally, not C^2.

When placing it on our Wish List, we expected to be rewarded for the partition-of-unity property by felicitous behavior of the B-spline approximating curves. The reader is asked to show next that indeed we are.

Exercise 18.13.

(a) Prove that the quadratic spline curve approximating a sequence of control points lies in the convex hull of the latter.

(b) Affine invariance: prove that an affine transformation of a quadratic spline curve is the same as the quadratic spline curve approximating the transformed control points.

18.2.4 Cubic B-Splines

We're going to ask you to do most of the lifting in this section.

To start with, break the first quadratic B-spline $N_{0,3}$ into two parts: an "up" part obtained from multiplying it by a straight-line function increasing from 0 at the left end of its support to 1 at the right end and a "down" part from multiplying it by the complementary function decreasing from 1 to 0 over its support. Here's the equation showing the split:

$$N_{0,3} = \frac{u}{3} N_{0,3} + (-\frac{u}{3} + 1)\, N_{0,3} \qquad (18.20)$$

Exercise 18.14. Write equations for the up part

$$N^0_{0,3}(u) = \frac{u}{3} N_{0,3}$$

and the down part

$$N^1_{0,3}(u) = (-\frac{u}{3} + 1) N_{0,3}$$

in a manner analogous to Equations (18.16) and (18.17) for the quadratic B-splines. Both up and down parts are piecewise cubic.

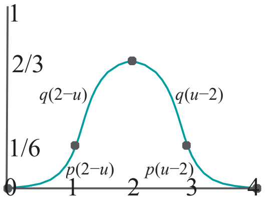

Figure 18.22: The first cubic B-spline function $N_{0,4}$. Joints are indicated.

Exercise 18.15. Verify by adding $N^0_{0,3}(u)$ and $N^1_{1,3}(u)$ that the equation of the first cubic B-spline is:

$$N_{0,4}(u) = \begin{cases} 0, & u \leq 0 \\ p(2-u), & 0 \leq u \leq 1 \\ q(2-u), & 1 \leq u \leq 2 \\ q(u-2), & 2 \leq u \leq 3 \\ p(u-2), & 3 \leq u \leq 4 \\ 0, & 4 \leq u \end{cases} \qquad (18.21)$$

where the functions p and q are given by:

$$p(u) = \frac{1}{6}(2 - u)^3$$

and

$$q(u) = \frac{1}{6}(3u^3 - 6u^2 + 4)$$

See Figure 18.22.

Exercise 18.16. Verify that cubic B-splines are C^2, but not C^3, at their joints.

Exercise 18.17. Sketch the sequence of cubic B-splines $N_{i,4}$, for $0 \leq i \leq r - 4$, over $[0, r]$ similarly to Figure 18.19 for quadratic B-splines. What should be the new parameter range?

Experiment 18.5. Run bSplines.cpp and change the order to see a sequence of cubic B-splines. End

Cubic B-Spline Curves

The cubic spline curve c approximating $r-3$ control points $P_0, P_1, \ldots, P_{r-4}$ is obtained as

$$c(u) = \sum_{i=0}^{r-4} N_{i,4}(u)P_i \qquad (3 \leq u \leq r-3) \qquad (18.22)$$

Figure 18.23: Screenshot of cubicSplineCurve1.cpp.

Experiment 18.6. Run cubicSplineCurve1.cpp, which shows the cubic spline approximation of nine control points in 2D space over a uniformly-spaced vector of 13 knots. The program's functionality is similar to that of quadraticSplineCurve.cpp. See Figure 18.23 for a screenshot.

The control points are green. Press the space bar to select a control point – the selected one is colored red – then the arrow keys to move it. The knots are the green points on the black bars at the bottom. The blue points are the joints of the curve. The control polygon is a light gray. End

Exercise 18.18. Prove that a cubic spline curve doesn't necessarily interpolate any of its control points. See again Exercise 18.11 and say now where a cubic spline curve starts w.r.t. its control points and where it ends.

Cubic B-Spline Properties

A list of properties for cubic B-splines:

1. Each $N_{i,4}$ is piecewise polynomial, consisting of at most six pieces, each of which is cubic, except for zero end pieces.
2. $N_{i,4}$ has support in $[i, i+4]$, the union of four consecutive knot intervals.
3. Each $N_{i,4}$ is C^2, but not C^3, at its joints. Apart from its joints it's smooth everywhere.
4. Together, the $N_{i,4}$ form a partition of unity over the parameter space $[3, r-3]$.
5. The $N_{i,4}$ are translates of one another.
6. A cubic B-spline approximation is C^2, but, generally, not C^3.

Remark 18.7. Cubic B-splines are the most commonly used in design applications, because they offer the best trade-off between continuity and computational efficiency.

18.2.5 General B-Splines and Non-uniform Knot Vectors

It's probably evident now how to manufacture B-splines of arbitrary order over the uniform knot vector $\{0, 1, \ldots, r\}$ One would apply the *break-and-make* procedure to B-splines of each order to derive ones of one higher order. We formalize the derivation of B-splines of arbitrary order over $\{0, 1, \ldots, r\}$ recursively as follows:

Definition 18.1. The first-order B-splines $N_{i,1}$, $0 \le i \le r-1$, are as defined in Section 18.2.1:

$$N_{01}(u) = \begin{cases} 1, & 0 \le u \le 1 \\ 0, & \text{otherwise} \end{cases} \tag{18.23}$$

and for $1 \le i \le r-1$

$$N_{i1}(u) = \begin{cases} 1, & i < u \le i+1 \\ 0, & \text{otherwise} \end{cases} \tag{18.24}$$

Suppose, recursively, that the B-splines $N_{i,m-1}$, for $0 \le i \le r-m+1$, have been defined for some order $m-1 \ge 1$. Then define the ith B-spline $N_{i,m}$ of order m, for $0 \le i \le r-m$, by the equation:

$$N_{i,m}(u) = \left(\frac{u-i}{m-1}\right) N_{i,m-1}(u) + \left(\frac{i+m-u}{m-1}\right) N_{i+1,m-1}(u) \tag{18.25}$$

It's not hard to see that the inductive formula (18.25) comes from a straightforward application of break-and-make. The summand

$$\left(\frac{u-i}{m-1}\right) N_{i,m-1}(u)$$

is the up part of $N_{i,m-1}(u)$ obtained from multiplying it by the straight-line function $(u-i)/(m-1)$ increasing from 0 at i, the left end of its support, to 1 at $i+m-1$, the right end.

Likewise, the summand

$$\left(\frac{i+m-u}{m-1}\right) N_{i+1,m-1}(u)$$

is the down part of $N_{i+1,m-1}(u)$ obtained from multiplying it by the straight-line function $(i+m-u)/(m-1)$ decreasing from 1 to 0 from the left end $i+1$ to the right $i+m$ of its support.

Terminology: The reader will have noted the convention that the *degree* of a B-spline is that of its polynomial pieces, while its *order* is its degree plus one.

Exercise 18.19. A tacit assumption in the discussion above was that the support of $N_{i,m-1}$ is in the interval $[i, i+m-1]$. Prove this is true by induction.

Exercise 18.20. Make a six-point list of properties for uniform B-splines of the mth order like the ones earlier for uniform lower-order splines.

Before proceeding further, though, we are going to loosen restrictions on the knot vector, which till now had been the uniform sequence

$$\{0, 1, \ldots, r\}$$

Keep in mind that the operative word is *uniform*, in particular, that knots are equally spaced; it does not matter that they are integers. For instance, if a knot vector were of the form

$$\{a, a+\delta, a+2\delta, \ldots, a+r\delta\}$$

for some a, and some $\delta > 0$, e.g.,

$$\{1.3, 2.8, 4.3, \ldots, 1.3+1.5r\}$$

all calculations made so far would clearly go through again, though with different (and awkward) number values, and all properties of B-splines deduced previously would hold, too.

The restriction of uniformity is removed by allowing the knot vector to be any sequence of knots of the form

$$T = \{t_0, t_1, \ldots, t_r\}$$

where the t_i are *non-decreasing*, i.e.,

$$t_0 \leq t_1 \leq \ldots \leq t_r \tag{18.26}$$

Such knot vectors are called *non-uniform*. Yes, successive knots can even be equal and such so-called multiple knots have important applications, as we'll see.

Remark 18.8. The term non-uniform knot vector is a little unfortunate in that it actually means *not necessarily* uniform, because a uniform knot vector evidently satisfies (18.26) as well.

Hmm, do we start afresh working our way up from first-order splines, this time around over non-uniform knot vectors? Not at all. Pretty much all our earlier discussions go through again, including break-and-make. Without further ado then, here's the recursive definition of B-splines over non-uniform knot vectors.

Definition 18.2. Let

$$T = \{t_0, t_1, \ldots, t_r\} \tag{18.27}$$

be a non-uniform knot vector, where $r \geq 1$.

The (non-uniform) first-order B-spline functions $N_{i,1}$, for $0 \leq i \leq r-1$, are defined as follows:

$$N_{0,1}(u) = \begin{cases} 1, & t_0 \leq u \leq t_1 \\ 0, & \text{otherwise} \end{cases} \tag{18.28}$$

and for $1 \leq i \leq r-1$

$$N_{i,1}(u) = \begin{cases} 1, & t_i < u \leq t_{i+1} \\ 0, & \text{otherwise} \end{cases} \tag{18.29}$$

The (non-uniform) mth order B-spline functions $N_{i,m}$, where the order m lies within $1 < m \leq r$, and the index i in $0 \leq i \leq r-m$, are recursively defined by:

$$N_{i,m}(u) = \left(\frac{u-t_i}{t_{i+m-1}-t_i}\right) N_{i,m-1}(u) + \left(\frac{t_{i+m}-u}{t_{i+m}-t_{i+1}}\right) N_{i+1,m-1}(u) \tag{18.30}$$

Note: The convention to follow in case the denominator of either of the two fractional terms is 0 – which may occur if there are equal knots – is the following: if the term is of the form $\frac{0}{0}$ then declare its value to be 1; if it is of the form $\frac{a}{0}$, where a is not 0, then declare its value to be 0.

This recursive formula (18.30), discovered by Cox, de Boor and Mansfield independently in 1972, known accordingly as the Cox-de Boor-Mansfield (CdM) formula or recurrence, was an important milestone in B-spline theory. However, it's really straightforward for us to understand now, given our development of the topic so far.

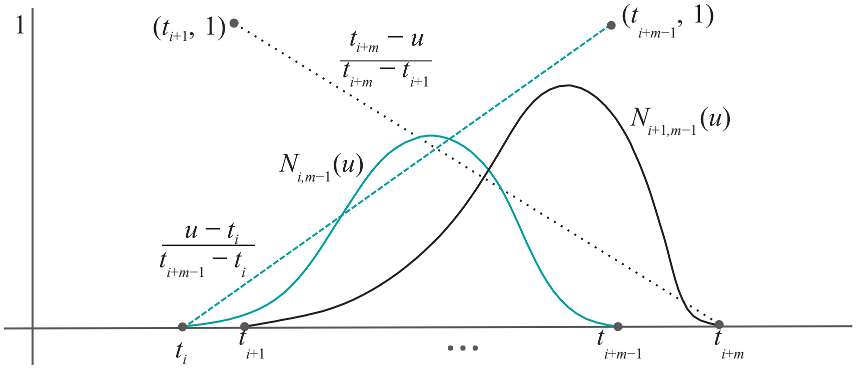

Figure 18.24: Graphs of the functions on the RHS of Equation (18.30): $N_{i,m-1}$ and $N_{i+1,m-1}$ and their respective linear multipliers $\frac{u-t_i}{t_{i+m-1}-t_i}$ and $\frac{t_{i+m}-u}{t_{i+m}-t_{i+1}}$.

Equations (18.28) and (18.29), respectively, replicate, with obvious changes, (18.23) and (18.24) for first-order B-splines over a uniform knot vector. Equation (18.30) imitates (18.25). It formalizes break-and-make – the summands are the up and down parts, respectively, of two successive spline functions of one lower order. Figure 18.24 shows graphs of all four functions on the RHS of Equation (18.30).

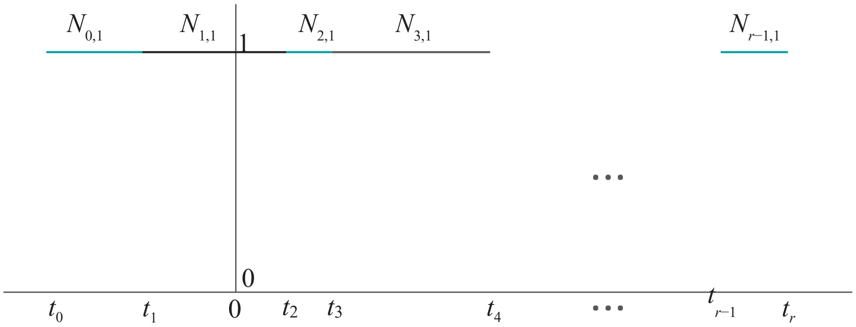

Figure 18.25: Non-zero parts of the first-order B-splines over a non-uniform knot vector.

Figure 18.25 shows the graphs of the first-order B-splines over a non-uniform knot vector, while Figure 18.26 those of linear B-splines over the same knot vector.

The equations of the spline functions themselves are a little more complicated than in the case of integer knots for the simple reason that they now involve variables for knot values. For example, here's the equation, analogous to (18.18), for the first quadratic B-spline over a non-uniform knot vector:

$$N_{0,3}(u) = \begin{cases} 0, & u \le t_0 \\ \frac{u-t_0}{t_2-t_0}\frac{u-t_0}{t_1-t_0}, & t_0 \le u \le t_1 \\ \frac{u-t_0}{t_2-t_0}\frac{t_2-u}{t_2-t_1} + \frac{t_3-u}{t_3-t_1}\frac{u-t_1}{t_2-t_1}, & t_1 \le u \le t_2 \\ \frac{t_3-u}{t_3-t_1}\frac{t_3-u}{t_3-t_2}, & t_2 \le u \le t_3 \\ 0, & t_3 \le u \end{cases} \tag{18.31}$$

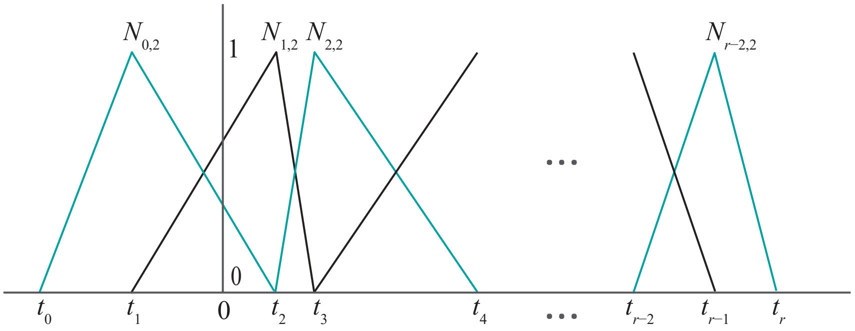

Figure 18.26: Non-zero parts of the linear B-splines over a non-uniform knot vector.

Not pretty, but B-spline computations are almost invariably done recursively in code, so a formula like this rarely needs to be written explicitly.

Experiment 18.7. Run again bSplines.cpp. Change the knot values by selecting one with the space bar and then pressing the left/right arrow keys. Press delete to reset knot values. Note that the routine Bspline() implements the CdM formula (and its convention for 0 denominators).

In particular, observe the quadratic and cubic spline functions. Note how they lose their symmetry about a vertical axis through the center, and that no longer are they translates of one another.

Play around with making knot values equal – we'll soon be discussing the utility of multiple knots. Figures 18.27(a) and (b) are screenshots of the quadratic and cubic functions, respectively, both over the same non-uniform knot vector with a triple knot at the right end. End

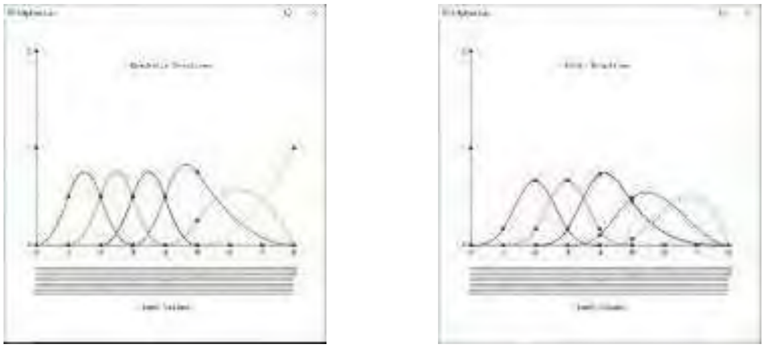

(a)

(b)

Figure 18.27: Screenshots of bSplines.cpp over a non-uniform knot vector with a triple knot at the right end: (a) Quadratic (b) Cubic.

Example 18.1. Find the values of (a) $N_{3,3}(5)$ and (b) $N_{4,3}(5)$, if the knot vector is $\{0, 1, 2, 3, 4, 5, 5, 5, 6, 7, \dots\}$, the non-negative integers, except that 5 has multiplicity three.

Answer: The successive knot values are

$$t_0 = 0,\ t_1 = 1,\ t_2 = 2,\ t_3 = 3,\ t_4 = 4,\ t_5 = 5,\ t_6 = 5,\ t_7 = 5,\ t_8 = 6,\ t_9 = 7,\ \dots$$

(a) Instantiating the CdM formula (18.30):

$$N_{3,3}(u) = \frac{u - t_3}{t_5 - t_3} N_{3,2}(u) + \frac{t_6 - u}{t_6 - t_4} N_{4,2}(u)$$

Plugging in $u = 5$ and the given knot values:

$$N_{3,3}(5) = \frac{5-3}{5-3} N_{3,2}(5) + \frac{5-5}{5-4} N_{4,2}(5) = N_{3,2}(5) \qquad (18.32)$$

Using CdM again,

$$N_{3,2}(u) = \frac{u-t_3}{t_4-t_3} N_{3,1}(u) + \frac{t_5-u}{t_5-t_4} N_{4,1}(u)$$

so that

$$\begin{aligned} N_{3,2}(5) &= \frac{5-3}{4-3} N_{3,1}(5) + \frac{5-5}{5-4} N_{4,1}(5) \\ &= 2*0 + 0*1 \quad \text{(from Equations (18.28) and (18.29))} \\ &= 0 \end{aligned}$$

Taking the above back to (18.32) we have

$$N_{3,3}(5) = 0$$

(b)

$$N_{4,3}(u) = \frac{u-t_4}{t_6-t_4} N_{4,2}(u) + \frac{t_7-u}{t_7-t_5} N_{5,2}(u)$$

giving

$$\begin{aligned} N_{4,3}(5) &= \frac{5-4}{5-4} N_{4,2}(5) + \frac{5-5}{5-5} N_{5,2}(5) \\ &= N_{4,2}(5) + \frac{0}{0} N_{5,2}(5) \\ &= N_{4,2}(5) + N_{5,2}(5) \quad \text{(using convention } \tfrac{0}{0} = 1\text{)} \qquad (18.33) \end{aligned}$$

Using CdM again,

$$N_{4,2}(u) = \frac{u-t_4}{t_5-t_4} N_{4,1}(u) + \frac{t_6-u}{t_6-t_5} N_{5,1}(u)$$

so that

$$\begin{aligned} N_{4,2}(5) &= \frac{5-4}{5-4} N_{4,1}(5) + \frac{5-5}{5-5} N_{5,1}(5) \\ &= 1*1 + 1*0 \quad \text{(note by (18.29) that } N_{5,1} \text{ is zero everywhere)} \\ &= 1 \qquad (18.34) \end{aligned}$$

CdM again gives

$$N_{5,2}(u) = \frac{u-t_5}{t_6-t_5} N_{5,1}(u) + \frac{t_7-u}{t_7-t_6} N_{6,1}(u)$$

implying

$$\begin{aligned} N_{5,2}(5) &= \frac{5-5}{5-5} N_{5,1}(5) + \frac{5-5}{5-5} N_{6,1}(5) \\ &= 1*0 + 1*0 \\ &= 0 \qquad (18.35) \end{aligned}$$

Using (18.34) and (18.35) in (18.33) we have

$$N_{4,3}(5) = 1$$

Exercise 18.21. Find the values of $N_{5,3}(5)$ and $N_{6,3}(5)$ for the same knot vector as in the preceding example.

Exercise 18.22. Compute $N_{4,3}(7)$ again over the knot vector of the preceding example. You will have to invoke the convention that $\frac{a}{0} = 0$, if a is not 0.

General B-Spline Curves

The mth order B-spline approximation c of $r - m + 1$ control points $P_0, P_1, \ldots, P_{r-m}$ is the curve obtained by applying the mth order B-splines as blending functions. Its equation is:

$$c(u) = \sum_{i=0}^{r-m} N_{i,m}(u)P_i \qquad (t_{m-1} \leq u \leq t_{r-m+1}) \tag{18.36}$$

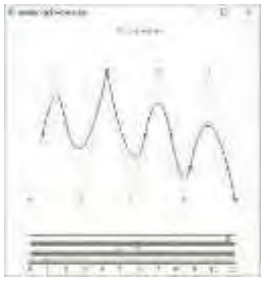

Figure 18.28: Screenshot of quadraticSplineCurve.cpp with a double knot at 5 and a triple knot at 11.

Experiment 18.8. Run again quadraticSplineCurve.cpp. Press 'k' to enter knots mode and alter knot values using the left/right arrow keys and 'c' to return to control points mode. Press delete in either mode to reset.

Try to understand what happens if knots are repeated. Do you notice a loss of C^1-continuity when knots in the interior of the knot vector coincide? What if knots at the ends coincide? Figure 18.28 is a screenshot of quadraticSplineCurve.cpp with a double knot at 5 and a triple at the end at 11. End

Exercise 18.23. Can you find an arrangement of the knots for the quadratic spline curve to interpolate its first and last control points?

Exercise 18.24. Why does changing the value of only the first, or only the last knot, not affect the quadratic spline curve?

Exercise 18.25. (Programming) Run again cubicSplineCurve1.cpp. Press 'k' to enter knots mode and alter knot values using the left/right arrow keys and 'c' to return to control points mode. Press delete in either mode to reset.

Can you find an arrangement of the knots so that the cubic spline curve interpolates its first and last control points?

Exercise 18.26. What part of the mth order spline curve c approximating the control points $P_0, P_1, \ldots, P_{r-m}$ is altered by moving only P_i? Your answer should be in terms of an arc of c between a particular pair of its joints.

We collect information about mth order B-spline functions and their corresponding approximating spline curves in the following proposition.

Proposition 18.1. *Let*

$$T = \{t_0, t_1, \ldots, t_r\}$$

be a non-uniform knot vector, where $r \geq 1$.

The mth order B-spline functions $N_{i,m}$, for some order m lying within $1 \leq m \leq r$, and, where $0 \leq i \leq r - m$, satisfy the following properties:

(a) Each $N_{i,m}$ is piecewise polynomial, consisting of at most $m + 2$ pieces, each of which is a degree $m - 1$ polynomial, except possibly for zero end pieces.

(b) $N_{i,m}$ has support in $[t_i, t_{i+m}]$, the union of m consecutive knot intervals.

(c) If the knots in T are distinct, each $N_{i,m}$ is C^{m-2}, but not C^{m-1}, at its joints. In this case, apart from its joints, each $N_{i,m}$ is smooth everywhere.

(d) The $N_{i,m}$ together form a partition of unity over the parameter space $[t_{m-1}, t_{r-m+1}]$.

(e) Every point of the mth order B-spline approximation c of $r - m + 1$ control points $P_0, P_1, \ldots, P_{r-m}$, defined by Equation (18.36), over the parameter space $[t_{m-1}, t_{r-m+1}]$, is a convex combination of the control points and lies inside their convex hull.

(f) (Affine Invariance) If $g : \mathbb{R}^3 \rightarrow \mathbb{R}^3$ is an affine transformation, and c is the mth order B-spline approximation of $r - m + 1$ control points $P_0, P_1, \ldots, P_{r-m}$ in $\mathbb{R}^3$, then the image curve $g(c)$ is the mth order B-spline approximation of the images $g(P_0), g(P_1), \ldots, g(P_{r-m})$ of the control points.

(g) *If the knots in T are distinct, the mth order B-spline approximation c of $r - m + 1$ control points $P_0, P_1, \ldots, P_{r-m}$ defined by Equation (18.36) is C^{m-2}, but, generally, not C^{m-1}.*

Proof. The proofs are a straightforward technical slog and we'll not write them out.

The following relation for a B-spline curve is useful to remember:

$$\textit{number of knots} = \textit{number of control points} + \textit{order} \qquad (18.37)$$

Exercise 18.27. Deduce (18.37).
Hint: Count the number of knots and control points in (18.36).

Non-uniform Knot Vectors

So, of what use are non-uniform knot vectors?

One is to be able to control the influence that a control point has over an approximating curve. For example, consider the cubic spline curve c approximating control points $P_0, P_1, \ldots$ over the knot vector $\{t_0, t_1, \ldots\}$, as in Figure 18.29(a), which shows a few intermediate control points. Moving control point, say, P_5 alters only the arc of c between $a = c(t_5)$ and $b = c(t_9)$, as $N_{5,4}$ has support in $[t_5, t_9]$. Consequently, the closer or farther apart are the knots from t_5 to t_9, the more concentrated or diffuse the influence of P_5. This generalizes, of course, to all P_i, allowing the designer to vary the domain of influence of control points by rearranging knots.

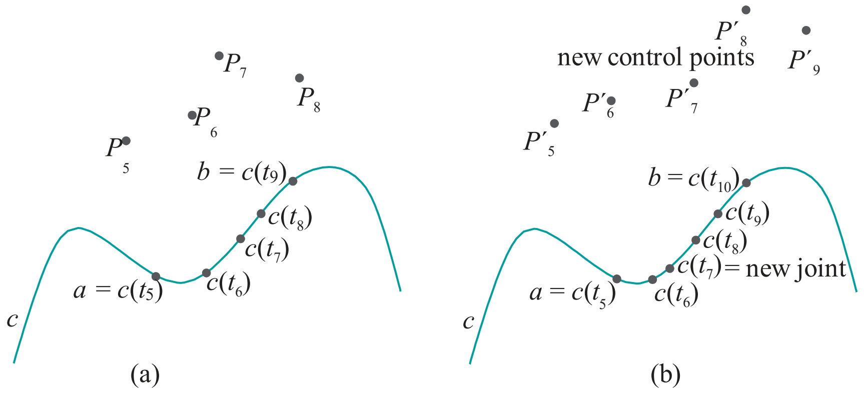

Figure 18.29: (a) Part of a cubic spline curve (b) With a new knot inserted.

Another practical consequence of non-uniform knot vectors is the technique of *knot insertion*, implemented in many commercial modelers, to allow the designer increasingly fine control over part of a spline curve. Clearly, the more knot images (joints, that is) there are in an arc of a curve, the more control points have influence over it and, therefore, the more finely it can be edited. Refer again to Figure 18.29(a). Currently, the shape of the arc between a and b is determined by the four control points P_5, P_6, P_7 and P_8. If one could insert a new knot, say, between t_6 and t_7 *without* changing the shape of the curve, there would then be five control points, instead of four, acting upon the same arc, affording the designer an added level of control.

Knots can, in fact, be inserted without changing either the shape of a spline curve or its degree, though, with a newly computed set of control points. See Figure 18.29(b), where a new knot has been inserted between t_6 and t_7, giving rise to a corresponding new joint. The joints have been re-labeled in sequence and a (hypothetical) new set of control points shown; now, in fact, the arc of the spline curve between a and b is shaped by the five control points $P^1_5, P^1_6, \ldots, P^1_9$, not four as before. We'll not go into the theory of knot insertion ourselves, referring the reader instead to more mathematical texts such as Buss [21], Farin [45] and Piegl & Tiller [113].

Multiple Knots

Coincident knots – *multiple knots* and *repeated knots* are the terms most commonly used – have a particularly useful application.

We'll motivate our discussion with a running example using the knot vector

$$T = \{t_0 = 0,\ t_1 = 1,\ t_2 = 2,\ t_3 = 3,\ t_4 = 3,\ t_5 = 4,\ t_6 = 5,\ t_7 = 6,\ \ldots\}$$

which has a double knot at $t_3 = t_4 = 3$. Generally, the *multiplicity* of a knot is the number of times it repeats.

The graphs of some of the B-spline functions over T are shown in Figure 18.30.

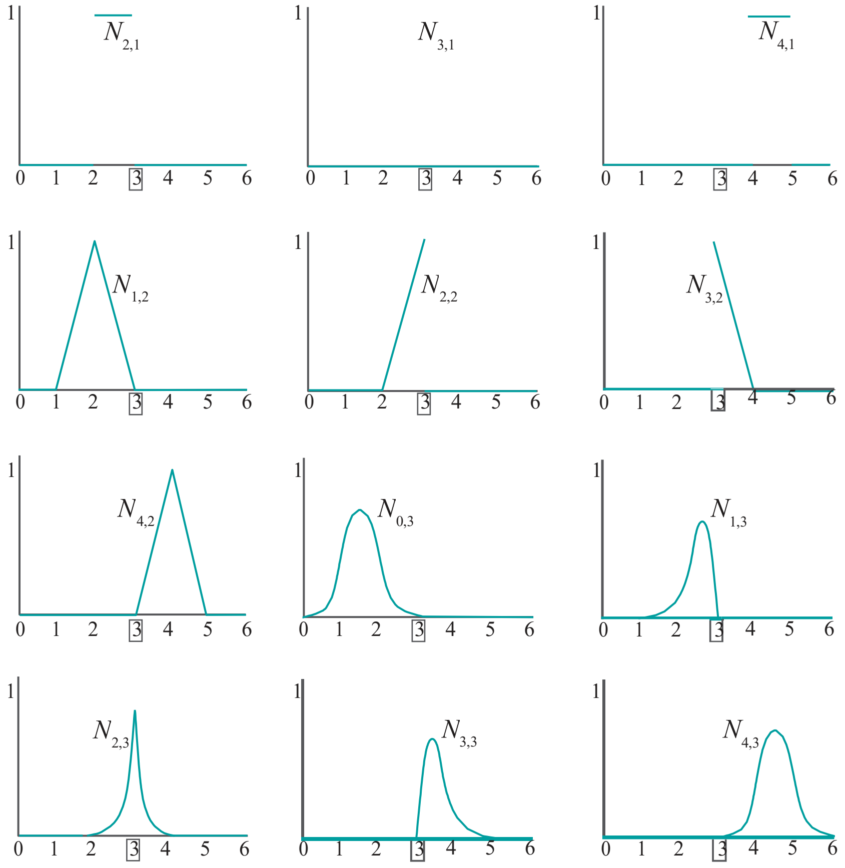

Figure 18.30: B-spline functions over the knot vector $T = \{0, 1, 2, 3, 3, 4, 5, \ldots\}$ with a double knot at 3 (distinguished inside a box).

Exercise 18.28. Verify that the graphs of the first-order B-splines over T are correctly depicted in the top row of Figure 18.30 by applying the defining Equations (18.28) and (18.29). In particular, the first-order B-splines are all 1 on their supporting intervals, excluding possibly endpoints, and 0 elsewhere, *except* for $N_{3,1}$, which is 0 throughout.

Exercise 18.29. Derive the equations of the linear B-splines from the first-order ones – by plugging $m = 2$ into the recursive Equation (18.30) – to verify their graphs in the second row of Figure 18.30, as well as at the leftmost in the third. In particular, the linear B-splines over T are all C^0 and translates of one another, *except* for $N_{2,2}$ and $N_{3,2}$, neither of which is C^0.

Unfortunately, the artifact of vertical edges in the display when knots coincide makes it tricky to use bSplines.cpp to visually verify the linear B-spline graphs in

Figure 18.30. However, there is no such issue with quadratic B-splines, so we ask the reader to do the following.

Exercise 18.30. (**Programming**) Arrange the knots of bSplines.cpp to make their nine successive values 0, 1, 2, 3, 3, 4, 5, 6 and 7, which are the first few knots of T. Then verify visually the graphs of the five quadratic B-splines in Figure 18.30. In fact, all the quadratic B-splines over T are C^1 and translates of one another, *except* for $N_{1,3}$, $N_{2,3}$ and $N_{3,3}$, which are C^0 but not C^1.

Next, we investigate the behavior of the approximating B-spline curve in the presence of repeated knot values.

Exercise 18.31. Use Equation (18.36) and the graphs already drawn of the first-order and linear spline functions over T to verify that the first-order and linear spline curves approximating nine control points – arranged, alternately, in two horizontal rows – are correctly drawn in Figures 18.31(a) and (b), respectively.

In particular, the first-order approximation loses the control point P_3 (drawn hollow) altogether, while the linear approximation loses the segment P_2P_3 and, therefore, is no longer C^0.

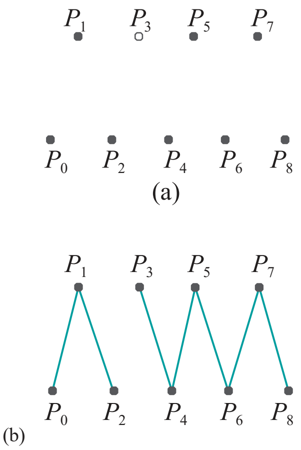

Figure 18.31: (a) First-order and (b) linear spline curves over the knot vector T = 0{, 1, 2, 3, 3, 4, 5, 6, 7, . . .}, approximating nine control points arranged alternately in two horizontal rows. The (hollow) control point P_3 is the only one missing from the first-order "curve", which consists of the remaining eight points. The second-order curve is the polyline $P_0P_1 \ldots P_8$ *minus* P_2P_3.

Experiment 18.9. Use the programs quadraticSplineCurve.cpp and cubicSplineCurve1.cpp to make the quadratic and cubic B-spline approximations over the knot vector T = 0,{1, 2, 3, 3, 4, 5, 6, 7, . .}. of nine control points placed as in Figure 18.31(a) (or (b)). See Figure 18.32(a) and (b) for screenshots of the quadratic and cubic curves, respectively.

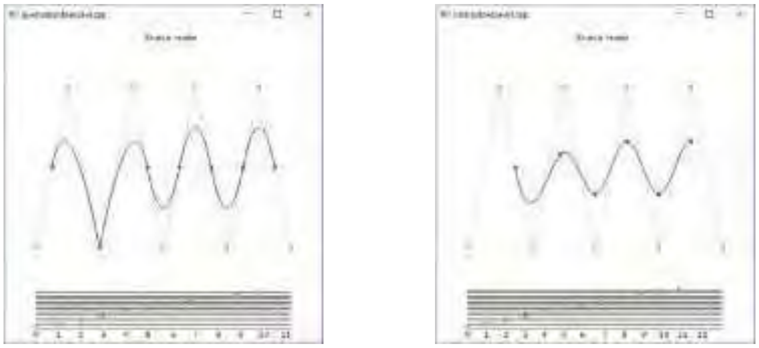
(a)

(b)

Figure 18.32: Screenshots of (a) quadraticSplineCurve.cpp and (b) cubicSplineCurve1.cpp over the knot vector T = 0{, 1, 2, 3, 3, 4, 5, 6, 7, . . . }and approximating nine control points arranged in two horizontal rows.

The quadratic approximation loses C^1-continuity precisely at the control point P_2, which it now *interpolates* as the curve point $c(3)$. It's still C^0 everywhere.

It's not easy to discern visually, but the cubic spline drops from C^2 to C^1-continuous at $c(3)$. End

Let's see next what happens with even higher multiplicity.

Experiment 18.10. Continuing with cubicSplineCurve1.cpp with control points as in the preceding experiment, press delete to reset and then make equal t_4, t_5 and t_6, creating a triple knot at 4. Figure 18.33 is a screenshot of this configuration. Evidently, the control point P_3 is now interpolated at the cost of a drop in continuity there to mere C^0. Elsewhere, the curve is still C^2. End

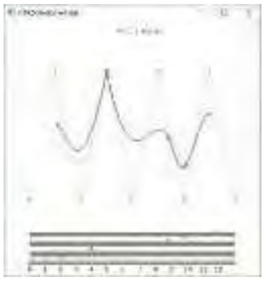

Figure 18.33: Screenshot of cubicSplineCurve1.cpp with a triple knot at 4.

It seems, generally, that repeating a knot increases the influence of a particular control point, to the extent that if the repetition is sufficient then that control point itself is interpolated, though at the cost of continuity at the control point itself. This does not appear to be a particularly appealing trade-off unless a low-continuity artifact, e.g., a corner, is itself a design goal.

Let's examine more closely how the loss arises – evidently, because of the difference in the value of the derivative (of some order) of c *on either side* of a control point P. For example, the tangents to the arcs on either side of the interpolated control point P_2 of the quadratic spline curve in Figure 18.32(a) are different.

Consider now if P were an *endpoint* of c. Then continuity cannot be lost by derivatives differing on the two sides of P, for the simple reason that the curve is only to one side! And, yet, there is no reason why the influence of P cannot still be increased by repeating knots. We are on our way to recovering the property of interpolating end control points that was lost at first by quadratic spline curves.

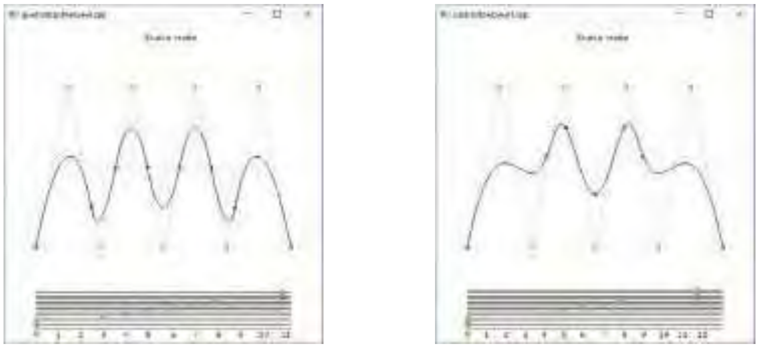

(a) (b)

Figure 18.34: Screenshots of (a) quadraticSplineCurve.cpp and (b) cubicSplineCurve1.cpp, both with knots repeated at the end to interpolate the first and last control points.

Experiment 18.11. Make the first three and last three knots separately equal in quadraticSplineCurve.cpp (Figure 18.34(a)). Make the first four and last four knots separately equal in cubicSplineCurve1.cpp (Figure 18.34(b)). Are the first and last control points interpolated in both. *Yes*. Do you notice any impairment in continuity? *No*. End

Generally, if the first m and last m knots of an mth order spline curve are coincident, and there are no other multiple knots, then the curve interpolates its first and last control points without losing C^{m-2}-continuity anywhere. In fact, a knot vector which starts and ends with a multiplicity of m and whose intermediate knots are uniformly spaced is called a *standard knot vector*. From formula (18.37), the size of a standard knot vector is the sum of the number of control points and the order of the spline curve. E.g., a standard knot vector for a quadratic spline with nine control points is

$$\{0, 0, 0, 1, 2, 3, 4, 5, 6, 7, 7, 7\}$$

Exercise 18.32. Jot down a standard knot vector for a quadratic spline over 10 control points and for a cubic spline over 9 control points.

Exercise 18.33. Use the CdM formula to show that $N_{0,3}(t_2) = 1$ over the standard knot vector

$$T = \{0,\ 0,\ 0,\ 1,\ 2,\ \ldots,\ r-6,\ r-5,\ r-5,\ r-5\}$$

of size r for a quadratic spline. Use this to prove that the quadratic spline

$$c(u) = \sum_{i=0}^{r-3} N_{i,3}(u)P_i \qquad (t_2 = 0 \le u \le r-5 = t_{r-2})$$

approximating the $r-m+1$ control points P_i, $0 \le i \le r-m$, over T indeed interpolates the first one, in particular, $c(t_2) = P_0$.

For the record here's a proposition:

Proposition 18.2. *A spline curve over a standard knot vector interpolates its first and last control points.*

Proof. The proof is a generalization of the preceding exercise to establish that the first control point is always interpolated. We'll leave the reader to do this by an induction. That the last control point is interpolated as well follows by symmetry.

The use of a standard knot vector for splines bequeaths yet another Bézier-like property – recall Proposition 17.1(f) – in addition to the interpolation of the end control points:

Proposition 18.3. *The tangent lines at the endpoints of a spline curve over a standard knot vector each pass through the adjacent control point.*

Proof. We'll prove this for quadratic splines in the next example. The general proof is not difficult but tedious, and we'll leave it to the motivated reader to do on her own.

Example 18.2. Prove that the tangent lines at the endpoints of a quadratic spline curve over a standard knot vector each pass through the adjacent control point.

Answer : We'll show that the tangent vector at the first control point passes through the second. The result at the other end follows by symmetry.

For quadratic splines, the standard knot vector is

$$T = \{0, 0, 0, 1, 2, \ldots\}$$

The quadratic spline curve approximating the control points $P_0, P_1, P_2, \ldots$ is

$$c(u) = N_{0,3}(u)P_0 + N_{1,3}(u)P_1 + N_{2,3}(u)P_2 + N_{3,3}(u)P_3 + \ldots$$

Now, the blending functions $N_{i,3}$, for $i \geq 3$, all vanish in $[t_2, t_3] = [0, 1]$. Consequently, in $[0, 1]$:

$$c(u) = N_{0,3}(u)P_0 + N_{1,3}(u)P_1 + N_{2,3}(u)P_2$$

Plugging the standard knot vector values into formula (18.31) for $N_{0,3}$ we get

$$N_{0,3}(u) = 1 - 2u + u^2, \quad u \in [0, 1]$$

One can use (18.31) to determine $N_{1,3}(u)$ as well by incrementing the subscripts on its RHS by 1. This gives

$$N_{1,3}(u) = 2u - \frac{3}{2}u^2, \quad u \in [0, 1]$$

Likewise, it's found that

$$N_{2,3}(u) = \frac{1}{2}u^2, \quad u \in [0, 1]$$

Therefore,

$$c(u) = (1 - 2u + u^2) P_0 + (2u - \frac{3}{2}u^2) P_1 + (\frac{1}{2}u^2) P_2, \quad u \in [0, 1]$$

Differentiating,

$$c^1(u) = (-2 + 2u) P_0 + (2 - 3u) P_1 + u P_2, \quad u \in [0, 1]$$

Plugging in $u = 0$, one sees that

$$c^1(0) = 2(P_1 - P_0)$$

which is indeed in the direction from P_0 to P_1.

We see it's for good reason, therefore, that standard knot vectors are most often used in B-spline design.

Exercise 18.34. Proposition 18.1(e) says that a spline curve is contained in the convex hull of (all) its control points. Prove the stronger statement that a spline curve of order m can be divided into successive stretches that each lie in the convex hull of only some m of its control points.

Bézier Curves and Spline Curves

It turns out that Bézier curves are special cases of spline curves:

Proposition 18.4. *The* $(n + 1)$*th order Bézier curve approximating the* $n + 1$ *control points*

$$P_0, P_1, \dots, P_n$$

coincides with the $(n + 1)$*th order spline curve approximating the same control points over the particular standard knot vector*

$$\{0, 0, \dots, 0, 1, 1, \dots, 1\}$$

consisting of $n + 1$ *0's followed by* $n + 1$ *1's.*

Proof. In the following example we'll restrict ourselves to establishing the quadratic case, leaving the general proof by induction to the mathematically inclined reader.

Example 18.3. Show that the quadratic Bêzier curve approximating the three control points P_0, P_1 and P_2 coincides with the quadratic spline curve approximating the same control points over the particular standard knot vector $\{0, 0, 0, 1, 1, 1\}$.

Answer: Recall from the previous chapter that the Bézier curve approximating P_0, P_1 and P_2 is

$$c_B(u) = (1 - u)^2 P_0 + 2(1 - u)uP_1 + u^2 P_2, \qquad u \in [0, 1]$$

The quadratic spline approximating the same three points over the knot vector $T = \{t_0 = 0,\ t_1 = 0,\ t_2 = 0,\ t_3 = 1,\ t_4 = 1,\ t_5 = 1\}$ is

$$c_S(u) = N_{0,3}(u)P_0 + N_{1,3}(u)P_1 + N_{2,3}(u)P_2, \qquad u \in [t_2, t_3] = [0, 1]$$

Therefore, we must show that spline blending functions of the preceding equation match the Bernstein polynomial blending functions of the one before it, over the knot interval $[0, 1]$. Refer to formula (18.31) for $N_{0,3}$. The fourth line on the RHS gives

$$\begin{aligned} N_{0,3}(u) &= \frac{t_3 - u}{t_3 - t_1}\,\frac{t_3 - u}{t_3 - t_2} \\ &= (1 - u)^2 \end{aligned}$$

after plugging in the knot values $t_0 = t_1 = t_2 = 0$ and $t_3 = 1$ in the interval $t_2 = 0 \le u \le 1 = t_3$, confirming a match with the first Bernstein polynomial.

We can use (18.31) for $N_{1,3}$ as well, making sure to increment the subscripts on the RHS by 1. This gives

$$N_{1,3}(u) = \frac{u - t_1}{t_3 - t_1}\,\frac{t_3 - u}{t_3 - t_2} + \frac{t_4 - u}{t_4 - t_2}\,\frac{u - t_2}{t_3 - t_2}$$

in $u \in [0, 1]$, using $t_1 = t_2 = 0$ and $t_3 = t_4 = 1$, so matching the second Bernstein polynomial. We'll leave the reader to verify that $N_{2,3}(u) = u^2$, $u \in [0, 1]$, completing the proof.

In the opposite direction, the following is true because spline curves are piecewise polynomial (from the way they are constructed) and polynomial curves are Bézier (from Proposition 17.2).

Proposition 18.5. *A spline curve is piecewise Bézier.*

Exercise 18.35. Why is it not possible that the preceding proposition can somehow be strengthened to say that spline curves are, in fact, Bezier´ entirely, not just piecewise?

Hint: Bézier curves are smooth throughout.

18.3 B-Spline Surfaces

The construction of B-spline surfaces as a continuum of B-spline curves parallels exactly the construction of Bézier surfaces from Bézier curves described in Section 17.2. See Figure 18.35 for the following.

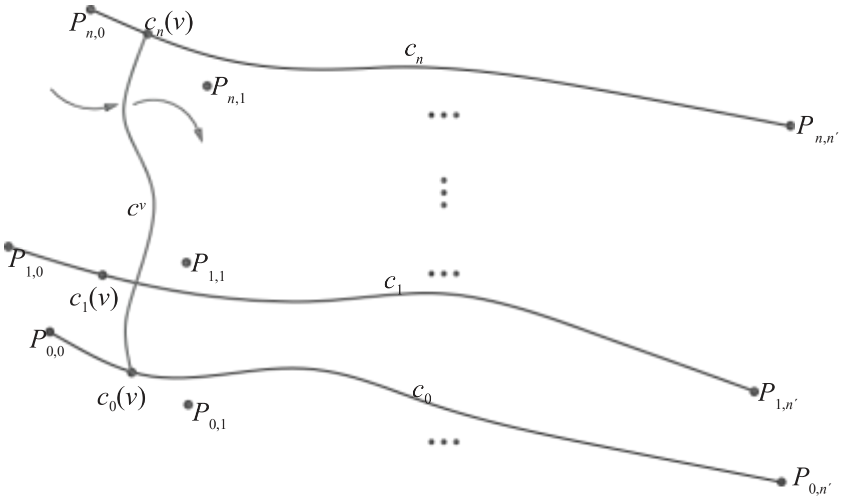

Figure 18.35: Constructing the B-spline surface approximating an array of control points by sweeping a B-spline curve. The B-spline curves depicted all interpolate both end control points, which need not always be the case in practice.

Suppose that we are given an $(n+1) \times (n^1+1)$ array of control points

$$P_{i,j}, \text{ for } 0 \le i \le n,\ 0 \le j \le n^1$$

and two spline orders m and m^1, and a knot vector

$$T = \{t_0, t_1, \ldots, t_r\}, \text{ whose size satisfies } |T| = r+1 = n+1+m$$

(to ensure that *number of knots* = *number of control points* + *order*) and another knot vector

$$T^1 = \{t_0, t_1, \ldots, t_{r^1}\}, \text{ whose size satisfies } |T^1| = r^1+1 = n^1+1+m^1$$

Think of the control points array as $n+1$ different sequences, each of n^1+1 control points. In particular, the ith sequence, for $0 \le i \le n$, consists of $P_{i,0}, P_{i,1}, \ldots, P_{i,n'}$, lying along the ith row of the control points array. Construct the m^1th order B-spline curve c_i, for $0 \le i \le n$, approximating the control points sequence $P_{i,0}, P_{i,1}, \ldots, P_{i,n'}$, each using the knot vector T^1 over the parameter space $[t_{m'-1}, t_{r'-m'+1}]$.

For each v in $t_{m'-1} \le v \le t_{r'-m'+1}$, generate the mth order B-spline curve c^v approximating the control points sequence $c_0(v), c_1(v), \ldots, c_n(v)$, using the knot vector T over the parameter space $[t_{m-1}, t_{r-m+1}]$. The union of all these B-spline curves c^v, for $t_{m'-1} \le v \le t_{r'-m'+1}$, then, is the B-spline surface s approximating the control points array $P_{i,j}$, $0 \le i \le n$, $0 \le j \le n^1$. One may imagine s as being swept by c^v, as v varies from $t_{m'-1}$ to $t_{r'-m'+1}$.

Exercise 18.36. Prove that the parametric equation of the B-spline surface s constructed as above is

$$s(u,v) = \sum_{i=0}^{n}\sum_{j=0}^{n'} N_{i,m}^{T}(u)\, N_{j,m'}^{T'}(v)\, P_{i,j} \qquad (18.38)$$

for $t_{m-1} \le u \le t_{r-m+1}$ and $t_{m'-1} \le v \le t_{r'-m'+1}$, and where $N^T_{i,m}$ (respectively, $N^{T'}_{j,m'}$) denotes the B-spline function $N_{i,m}$ over the knot vector T (respectively, $N_{j,m'}$ over T^1).

In other words, the surface is obtained from applying the blending function $N^T_{i,m}$(u) $N^{T'}_{j,m'}(v)$ to the control point $P_{i,j}$, over the parameter domain $t_{m-1} \le u \le t_{r-m+1}$, $t_{m'-1} \le v \le t_{r'-m'+1}$.

Hint: Mimic the proof of (17.16) for a Bézier surface.

Exercise 18.37. Formulate an analogue for B-spline surfaces of Proposition 18.1 for curves.

We've given thus far an account of NURBS (non-uniform rational B-spline) theory, *except* for the 'R', or rational, part. Instead of generally rational, being a ratio of two polynomials, our functions have been all just polynomial. You could say that we have covered NUPBS, or simply NUBS, as the default for B-splines is polynomial. We'll put the 'R' into NURBS in Chapter 20 with the help of projective spaces.

18.4 Drawing B-Spline Curves and Surfaces

NURBS – the full-blown rational version of B-splines – curves and surfaces are implemented in the GLU library of OpenGL. Now that we have a fair amount of the theory, the GLU NURBS interface will turn out to be simple to use, as the mapping between theory and syntax is almost one-to-one. We'll, of course, restrict ourselves to polynomial B-spline primitives for now, leaving the rational ones to a later chapter.

18.4.1 B-Spline Curves

We had already used OpenGL to draw polynomial B-spline curves in the programs quadraticSplineCurve.cpp and cubicSplineCurve1.cpp earlier this chapter, without caring then about the drawing syntax itself. Let's look at this now.

The command

gluNurbsCurve(**nurbsObject, knotCount, *knots, stride, *controlPoints, order, type*)

defines a B-spline curve which is pointed by *nurbsObject* . The parameter *knotCount* is the number of knots in the knot vector – a one-dimensional array – pointed by *knots*. The parameter *order* is the order of the spline curve, *controlPoints* points to the one-dimensional array of control points, and *stride* is the number of floating point values between the start of the data set for one control point and that of the next in the control points array. The number of control points is not explicitly specified, but computed by OpenGL with the help of (18.37):

$$\textit{number of control points} = \textit{number of knots} - \textit{order}$$

The parameter *type* is GL_MAP1_VERTEX_3 or GL_MAP1_VERTEX_4, according as the spline curve is polynomial or rational.

A gluNurbsCurve() command must be bracketed between a gluBeginCurve()-gluEndCurve() pair of statements. The following statements from the drawing routine of quadraticSplineCurve.cpp, defining a quadratic B-spline curve approximating nine control points, should now be clear:

```
gluBeginCurve(nurbsObject);
gluNurbsCurve(nurbsObject, 12, knots, 3, ctrlpoints[0], 3,
              GL_MAP1_VERTEX_3);
gluEndCurve(nurbsObject);
```

Exercise 18.38. Refer to Section 10.3.1 for the syntax of the call glMap1f() defining a Bézier curve and compare it with that of gluNurbsCurve().

There are certain initialization steps to be completed prior to a gluNurbsCurve() call. First, gluNewNurbsRenderer() returns the pointer to a NURBS object, which is passed to the subsequent gluNurbsCurve() call. Then optional gluNurbsProperty() calls control the quality of the rendering, as well as other related attributes of the curve. We refer the reader to the red book for a complete listing of possible parameter values for gluNurbsProperty(). Our own usage is kept to a simple minimum – the relevant statements from the setup() routine of quadraticSplineCurve.cpp are the following:

```
nurbsObject = gluNewNurbsRenderer();
gluNurbsProperty(nurbsObject, GLU_SAMPLING_METHOD, GLU_PATH_LENGTH);
gluNurbsProperty(nurbsObject, GLU_SAMPLING_TOLERANCE, 10.0);
```

The last two statements specify that the longest length of a line segment in a strip approximating a NURBS curve (or that of a quad edge, in the case of a mesh approximating a NURBS surface) is at most 10.0 pixels.

Experiment 18.12. Change the last parameter of the statement

```
gluNurbsProperty(nurbsObject, GLU_SAMPLING_TOLERANCE, 10.0);
```

in the initialization routine of quadraticSplineCurve.cpp from 10.0 to 100.0. The fall in resolution is noticeable as one sees in Figure 18.36. End

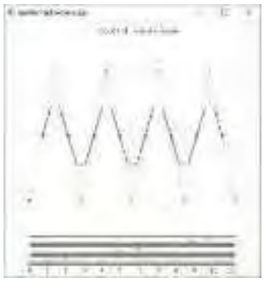

Figure 18.36: Screenshot of quadraticSplineCurve.cpp with sampling tolerance increased to 100.

If you are wondering whether a B-spline curve can be drawn in a manner similar to that using glMapGrid1f() followed by glEvalMesh1() for a Bézier curve – sampling the curve uniformly through the parameter domain – the answer is yes. Though we shall not use them ourselves the two requisite calls for this purpose are gluNurbsProperty(*nurbsObject, GLU_SAMPLING_METHOD, GLU_DOMAIN_DISTANCE) and gluNurbsProperty(*nurbsObject, GLU_U_STEP, *value*). The reader is referred to the red book for implementation details.

Experiment 18.13. Run cubicSplineCurve2.cpp, which draws the cubic spline approximation of 30 movable control points, initially laid out on a circle, over a fixed standard knot vector. Press space and backspace to cycle through the control points and the arrow keys to move the selected control point. The delete key resets the control points. Figure 18.37 is a screenshot of the initial configuration. The number of control points being much larger than the order, the user has good local control.

Incidentally, note how managing large numbers of control points has been made efficient with B-splines. Together 30 control points would have led to a 29th degree polynomial Bézier curve, a computational nightmare; alternatively we could split the control points into smaller sets, e.g., of size 4 for cubic curves, but then would come the issue of smoothly joining the successive sub-curves. End

Figure 18.37: Screenshot of cubicSplineCurve2.cpp.

Exercise 18.39. (Programming) Use cubicSplineCurve2.cpp to draw a closed loop like the one in Figure 18.38.

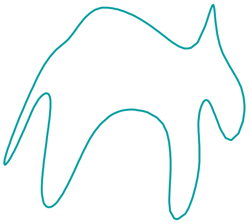

Figure 18.38: A cat or whatever.

18.4.2 B-Spline Surfaces

The OpenGL syntax for a B-spline surface is a straightforward extension of that for a B-spline curve. The gluNurbsSurface() command, which must be bracketed between a gluBeginSurface()-gluEndSurface() pair of statements, has the following form:

```
gluNurbsSurface(*nurbsObject, uknotCount, *uknots, vknotCount, *vknots,
                ustride, vstride, *controlPoints, uorder, vorder, type)
```

vknots points to the knot vector used with the control point row, in other words, to make the parameter curves c_i in the discussion in Section 18.3 of a B-spline curve sweeping a surface; *uknots points to the knot vector used with the control point columns, i.e., to make the curves c^v in that discussion.

The parameter *vknotCount* is the number of knots in the vector pointed by **vknots*, *vorder* is the order of the B-spline curves c_i and *vstride* is the number of floating point values between the data set for one control point and the next in a row of the control points array. The parameters *uknotCount* , *uorder* and *ustride* represent similar values for the control point columns.

The parameter *type* is GL MAP2 VERTEX 3 or GL_MAP2 VERTEX 4 for polynomial or rational surfaces, respectively; it can have other values as well to specify surface normals and texture coordinates.

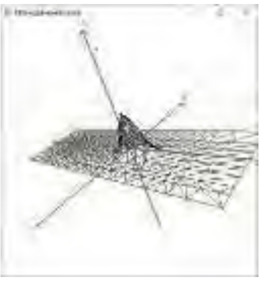

Figure 18.39: Screenshot of bicubicSplineSurface.cpp.

Experiment 18.14. Run bicubicSplineSurface.cpp, which draws a spline surface approximation to a 15×10 array of control points, each of which the user can move in 3-space. The spline is cubic in both parameter directions and a standard knot vector is specified in each as well.

Press the space, backspace, tab and enter keys to select a control point. Move the selected control point using the arrow and page up and down keys. The delete key resets the control points. Press 'x/X', 'y/Y' and 'z/Z' to turn the surface. Figure 18.39 is a screenshot. End

Exercise 18.40. (Programming) Use bicubicSplineSurface.cpp to draw separately a hilly terrain and a boat.

18.4.3 Lighting and Texturing a B-Spline Surface

Lighting and texturing a B-spline surface is similar to doing likewise for a Bézier surface. Normals are required for lighting and the quickest way to create normals for a B-spline surface is to generate them automatically with a call, as for Bézier surfaces, to glEnable(GL AUTO NORMAL).

And, again as for Bézier surfaces, determining texture coordinates for a B-spline surface requires, first, the creation of a "fake" B-spline surface in texture space on the same parameter rectangle as the real one – the reader should review if need be the discussion in Section 12.5 on specifying texture coordinates for a Bézier surfaces. OpenGL, subsequently, assigns as texture coordinates to the image on the real surface of a particular parameter point the image of that same point on the fake surface in texture space. Code will clarify.

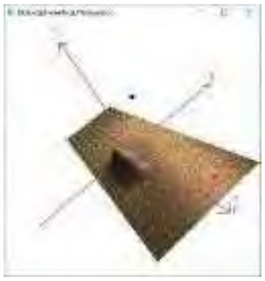

Figure 18.40: Screenshot of bicubicSplineSurface-LitTextured.cpp.

Experiment 18.15. Run bicubicSplineSurfaceLitTextured.cpp, which sugar-coats the spline surface of bicubicSplineSurface.cpp. Figure 18.40 is a screenshot. The surface is illuminated by a single positional light source whose location is indicated by a large black point. User interaction remains as in bicubicSplineSurface.cpp. Note that pressing the 'x'-'Z' keys turns only the surface, not the light source.

The bicubic B-spline surface, as well as the fake bilinear one in texture space, are created by the following statements in the drawing routine:

```
gluBeginSurface(nurbsObject);
gluNurbsSurface(nurbsObject, 19, uknots, 14, vknots,
        30, 3, controlPoints[0][0], 4, 4, GL_MAP2_VERTEX_3);
gluNurbsSurface(nurbsObject, 4, uTextureknots, 4, vTextureknots,
        4, 2, texturePoints[0][0], 2, 2, GL_MAP2_TEXTURE_COORD_2);
gluEndSurface(nurbsObject);
```

We'll leave the reader to parse in particular the third statement and verify that it creates a "pseudo-surface" – a 10 × 10 rectangle – in texture space on the same parameter domain [0, 12] × [0, 7] as the real one. End

Exercise 18.41. (Programming) Light and texture the B-spline surfaces you created for Exercise 18.40.

18.4.4 Trimmed B-Spline Surface

A powerful design tool is to *trim* (i.e., excise or remove) part of a B-spline surface. Here, first, is what happens theoretically.

Say the parametric specification of a surface s is given to be

$$x = f(u, v),\ \ y = g(u, v),\ \ z = h(u, v),\quad \text{where}\quad (u, v) \in W = [u_1, u_2] \times [v_1, v_2]$$

The parametric equations map the rectangle W from uv-space onto the surface s in xyz-space. Moreover, a loop (closed curve) c on W maps to a loop c^1 on s. See Figure 18.41.

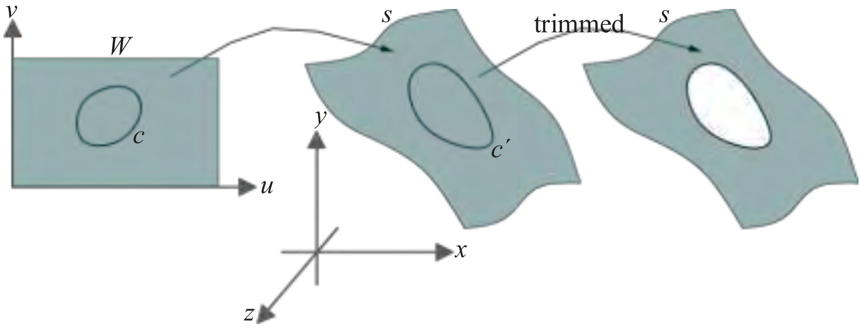

Figure 18.41: The loop c on the parameter space W is mapped to the loop c^1 on the surface s by the parametric equations for s. Then s is trimmed by c.

If the part of s inside, or outside, the loop c^1 is excised, then s is said to be trimmed by the loop c (probably, more accurate would be to say that it is trimmed by c^1, but the given usage is common). Figure 18.41 shows the inside trimmed. Loop c itself is called the *trimming loop*.

OpenGL allows B-spline surfaces to be trimmed. We use the program bicubicBsplineSurfaceTrimmed.cpp, as a running example to explain OpenGL syntax for trimming.

Experiment 18.16. Run bicubicBsplineSurfaceTrimmed.cpp, which shows the surface of bicubicBsplineSurface.cpp trimmed by multiple loops. The code is modified from the latter program, functionality remaining same. Figure 18.42(a) is a screenshot. End

All the code relevant to trimming is in the drawing routine:

```
gluBeginSurface(nurbsObject);
gluNurbsSurface(nurbsObject, 19, uknots, 14, vknots,
          30, 3, controlPoints[0][0], 4, 4, GL_MAP2_VERTEX_3);

gluBeginTrim(nurbsObject);
   gluPwlCurve(nurbsObject, 5, boundaryPoints[0], 2,
               GLU_MAP1_TRIM_2);
gluEndTrim(nurbsObject);

gluBeginTrim(nurbsObject);
   gluPwlCurve(nurbsObject, 11, circlePoints[0], 2,
               GLU_MAP1_TRIM_2);
gluEndTrim(nurbsObject);

gluBeginTrim(nurbsObject);
   gluNurbsCurve(nurbsObject, 10, curveKnots, 2, curvePoints[0], 4,
                  GLU_MAP1_TRIM_2);
gluEndTrim(nurbsObject);

gluEndSurface(nurbsObject);
```

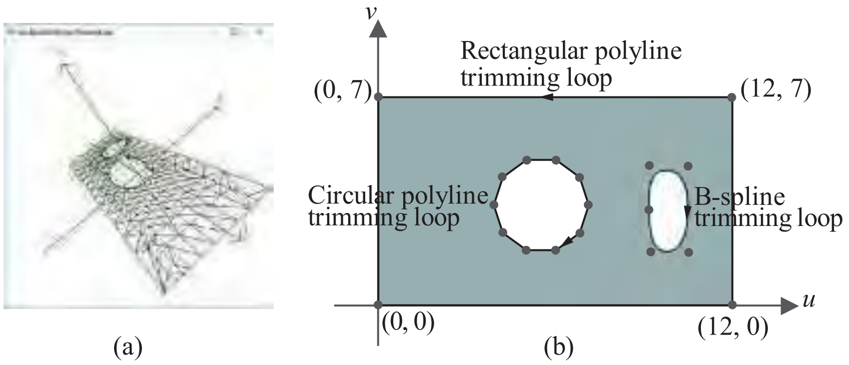
v
Rectangular polyline trimming loop
(0, 7)
(12, 7)
Circular polyline trimming loop
B-spline trimming loop
u
(0, 0)
(12, 0)
(a)
(b)

Figure 18.42: (a) Screenshot of bicubicBsplineSurfaceTrimmed.cpp (b) The three trimming loops – two polygonal and one B-spline.

Points to note:

1. Each trimming loop is defined within gluBeginTrim()-gluEndTrim() pair of statements, which itself must lie within the gluBeginSurface()-gluEndSurface() pair. The trimming loop definitions are located after the gluNurbsSurface() definition.

2. Each trimming loop must be a closed curve in the parameter space.

3. There are two ways to define a trimming loop:

   (a) As a polygonal line loop defined by a

   glPwlCurve(*nurbsObject, pointsCount, *pointsArray,
   stride, type)

   statement, where *pointsCount* is the number of vertices in an array of the form $\{v_0, v_1, \ldots, v_n\}$ pointed by *pointsArray* (it is required that $v_0 = v_n$). There are two such polyline trimming loops in the program (see Figure 18.42(b)):

   (i) The five vertices (first and last equal) of one are in the array boundaryPoints, describing the rectangular boundary of the parameter space itself, oriented *counter-clockwise*. We'll soon see why this particular bounding trimming loop is required.

   (ii) The eleven vertices (again, first and last equal) of the other are in the array circlePoints, equally spaced along a circle, oriented *clockwise*.

   (b) As a B-spline loop defined by

   gluNurbsCurve(nurbsObject, knotCount, *knots, stride,
   *controlPoints, order, type)

   In the program there is a single such B-spline trimming loop, whose six control points (first and last equal) are in the array curvePoints oriented *clockwise* (Figure 18.42(b)).

4. The part outside a trimming loop oriented counter-clockwise is trimmed, while that inside a trimming loop oriented clockwise is trimmed.

   Accordingly, the first trimming polyline loop of the program, which bounds the parameter space going counter-clockwise, trims off the *exterior* of the drawn surface, not trimming the surface itself per se. The other two trimming loops actually create holes in the surface.

Exercise 18.42. (Programming) Draw the forbidding terrain of an uninhabited planet with volcanoes, craters, lakes of lava, and such.

18.5 Summary, Notes and More Reading

We have learned a fair amount of the theory underlying the widely-used class of 3D design primitives – B-splines, both curves and surfaces. Emphasis was on motivating each new concept. We did *not* want to pull stuff out of a hat. A test if we were successful is for the reader to deduce some formula, e.g., (18.18) for the first quadratic B-spline $N_{0,3}$ over a uniform knot vector or the Cox-de Boor-Mansfield recurrence (18.30), using just pencil and paper, and not referring again to the text. This chapter prepares the reader, as well, for the rational version of the theory – NURBS – coming up in Chapter 20.

As for OpenGL, we learned not only how to draw B-spline curves and surfaces, but to illuminate, texture and trim the latter as well.

While B-spline theory is extensive, material we covered in this chapter of the polynomial B-spline primitives, together with what is covered in Chapter 20 of NURBS, is ample for an applications programmer to function knowledgeably. However, the reader is well-advised to expand her knowledge, particularly, of such practical topics as "knot insertion", "degree elevation", etc. It's easy enough given the number of excellent books available – Bartels et al. [9], Farin [45], Mortenson [97], Piegl & Tiller [113] and Rogers & Adams [120] are a few that come to mind. The mathematically inclined reader, in particular, will find much to fascinate her in the more specialized nooks and crannies. Advanced 3D CG books, e.g., Akenine-Möller, Haines & Hoffman [1], Buss [21], Slater et al. [137] and Watt [150], each have a presentation of B-spline theory as well.

B-spline functions were first studied in the 1800s by the Russian mathematician Nicolai Lobachevsky. However, the modern theory began with Schoenberg's [128] application of spline functions to data smoothing and received particular impetus with the discovery in 1972 of the recursive formula (18.30) for B-spline functions by Cox [29], de Boor [33] and Mansfield. It has since seen explosive growth and B-spline (and NURBS) primitives are *de rigueur* in modern-day CG design.

Chapter 19

Hermite

Our objective in this chapter is to learn a method of interpolating a set of control points, in other words, finding a curve (or surface) that passes through each. Bézier curves, as we know, mandatorily interpolate only their first and last control points, while Bézier surfaces only the four corner control points. B-spline curves and surfaces of quadratic and higher degree do not necessarily interpolate any of their control points. Nevertheless, we learned in Section 18.2.5 how to force a B-spline curve to interpolate a control point by raising the multiplicity of a knot. In fact, the so-called standard knot vector, with repeated end knots, is often used to ensure the interpolation of end control points.

However, if a designer wishes to draw a curve or surface interpolating *all* its control points, then it's best to apply an intrinsically interpolating technique, rather than try to coax an approximating one like Bézier or B-spline into interpolating. A popular class of interpolating curves is that of the Hermite splines and this short chapter introduces this class, together with two special subclasses, that of the natural cubic splines and the cardinal splines. We discuss Hermite surface patches, as well, to interpolate 2D arrays of control points.

We begin with a discussion of general Hermite splines in Section 19.1. These curves, unfortunately, are guaranteed only to be piecewise smooth – they can have corners at control points. Moreover, the user is required to specify tangent vectors at all the control points. The subclass of natural cubic splines, the topic of Section 19.2, automatically determines these tangent vectors by imposing an additional C^2-continuity requirement. Cardinal splines, in Section 19.3, are based upon yet another scheme to automatically specify tangent vectors at control points.

We make a brief presentation of Hermite surfaces in Section 19.4 and conclude in Section 19.5.

19.1 Hermite Splines

A *Hermite spline*, also called a *cubic spline*, interpolating a sequence $P_0, P_1, \ldots, P_n$ of $n + 1$ control points, is a *piecewise cubic* curve c passing through the control points. Each cubic arc of c joins successive pairs of control points, so that the entire spline comprises n cubic arcs joined end to end. Figure 19.1 shows a Hermite spline through four control points on a plane. There are corners at the middle two because the tangents of the cubics on either side don't agree.

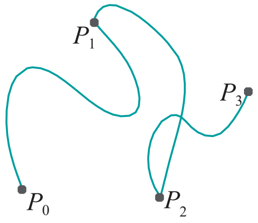

Figure 19.1: A (non-smooth) Hermite spline through four control points, composed of three cubic arcs.

Terminology: A *cubic arc* is a part of a cubic curve; e.g., an arc of the graph of $y = x^3$ is a cubic arc on the plane. Sometimes we'll loosen cubic to mean a polynomial of degree at most three, rather than exactly three.

Remark 19.1. Hermite splines are named after the nineteenth-century French mathematician Charles Hermite.

Remark 19.2. Curves of degree higher than three could be used to interpolate, or even lower, e.g., quadratic. However, three is a “Goldilocks” degree, high enough to assure flexibility, yet low enough to be computationally efficient.

Hermite interpolation for evident reasons is often called *cubic interpolation*.

We’ll soon find a way to eliminate the corners in the interior and create a smooth Hermite spline through a given sequence of control points, but let’s see first how to make a single cubic arc joining two arbitrary points P and Q.

Write the parametric equation of a general cubic curve c as

$$c(u) = A_3u^3 + A_2u^2 + A_1u + A_0 \qquad (0 \le u \le 1) \tag{19.1}$$

where each A_i, $0 \le i \le 3$ is a point – precisely, its vector of coordinates – in the ambient space. If you are wondering about polynomial coefficients which are vectors rather than scalars, then consider the following example.

Example 19.1. Suppose that we are interested in Hermite splines in the real world so that our ambient space is $\mathbb{R}^3$. Then the equation of a cubic curve is claimed to be

$$c(u) = A_3u^3 + A_2u^2 + A_1u + A_0 \qquad (0 \le u \le 1)$$

where each A_i, $0 \le i \le 3$, is a point in 3-space.

To illustrate, say,

$$A_3 = [-1\ 2\ 0]^T, \quad A_2 = [3\ 0\ -2]^T, \quad A_1 = [4\ 3\ 4]^T, \quad \text{and} \quad A_0 = [0\ 8\ 7]^T$$

Then,

$$\begin{aligned} c(u) &= [-1\ 2\ 0]^T u^3 + [3\ 0\ -2]^T u^2 + [4\ 3\ 4]^T u + [0\ 8\ 7]^T \\ &= [-u^3 + 3u^2 + 4u \quad 2u^3 + 3u + 8 \quad -2u^2 + 4u + 7]^T \end{aligned}$$

over the interval $[0, 1]$. As one would expect, the cubic c in $\mathbb{R}^3$ is simply a scalar cubic in *each* of its three coordinates.

Example 19.2. Express in the form (19.1) the twisted cubic given parametrically by

$$x = t, \ y = t^2, \ z = t^3$$

Answer:

$$c(t) = [t\ t^2\ t^3]^T = [0\ 0\ 1]^T t^3 + [0\ 1\ 0]^T t^2 + [1\ 0\ 0]^T t$$

Returning to the general form (19.1) of the cubic, rewrite it as a matrix equation:

$$c(u) = [u^3\ u\ \ u\ 1] \begin{bmatrix} A_3 \\ A_2 \\ A_1 \\ A_0 \end{bmatrix} \qquad (0 \le u \le 1) \tag{19.2}$$

Note: The RHS is a product of a 1 × 4 matrix of scalars with a 4 × 1 matrix of vectors, but this is not a problem if we appropriately multiply a vector by a scalar while following the usual rules of matrix multiplication.

Differentiating (19.2) one obtains the derivative of c as

$$c^1(u) = [3u^2\ \ 2u\ \ 1\ \ 0] \begin{bmatrix} A_3 \\ A_2 \\ A_1 \\ A_0 \end{bmatrix} \qquad (0 \le u \le 1) \tag{19.3}$$

Substitute 0 and 1 for u in Equations (19.2) and (19.3) to find that

$$c(0) = A_0, \quad c(1) = A_3 + A_2 + A_1 + A_0, \quad c^1(0) = A_1, \quad c^1(1) = 3A_3 + 2A_2 + A_1 \tag{19.4}$$

It seems that if one could specify $c(0)$, $c(1)$, $c^1(0)$ and $c^1(1)$, then one would have four equations in the four unknowns A_0, A_1, A_2 and A_3, which should solve to find these coefficients and specify c (*alert* : that's four vector equations in four *vector* unknowns, so, e.g., if we are in 3-space, we'll have actually twelve equations in twelve *scalar* unknowns).

Since we're looking for a cubic arc c from P to Q, we know at least that $c(0) = P$ and $c(1) = Q$; as for the tangent vectors $c^1(0)$ and $c^1(1)$, we have freedom to specify them as we please. Let's choose them to be two vectors denoted P^1 and Q^1, respectively. See Figure 19.2.

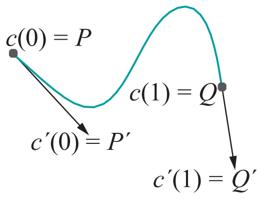

Figure 19.2: Four boundary constraints on a cubic curve c.

Accordingly, write (19.4) as

$$P = A_0, \qquad Q = A_3 + A_2 + A_1 + A_0, \qquad P^1 = A_1, \qquad Q^1 = 3A_3 + 2A_2 + A_1 \tag{19.5}$$

which in matrix form is the equation

$$\begin{bmatrix} P \\ Q \\ P^1 \\ Q^1 \end{bmatrix} = \begin{bmatrix} 0 & 0 & 0 & 1 \\ 1 & 1 & 1 & 1 \\ 0 & 0 & 1 & 0 \\ 3 & 2 & 1 & 0 \end{bmatrix} \begin{bmatrix} A_3 \\ A_2 \\ A_1 \\ A_0 \end{bmatrix} \tag{19.6}$$

Solve this equation by inverting the coefficient matrix as follows

$$\begin{aligned} \begin{bmatrix} A_3 \\ A_2 \\ A_1 \\ A_0 \end{bmatrix} &= \begin{bmatrix} 0 & 0 & 0 & 1 \\ 1 & 1 & 1 & 1 \\ 0 & 0 & 1 & 0 \\ 3 & 2 & 1 & 0 \end{bmatrix}^{-1} \begin{bmatrix} P \\ Q \\ P^1 \\ Q^1 \end{bmatrix} \\ &= \begin{bmatrix} 2 & -2 & 1 & 1 \\ -3 & 3 & -2 & -1 \\ 0 & 0 & 1 & 0 \\ 1 & 0 & 0 & 0 \end{bmatrix} \begin{bmatrix} P \\ Q \\ P^1 \\ Q^1 \end{bmatrix} \end{aligned} \tag{19.7}$$

to see that the four coefficients A_0, A_1, A_2 and A_3 can indeed be derived from the four boundary constraints P, Q, P^1 and Q^1. The 4×4 matrix in the second line of the equation is called the *Hermite matrix* and denoted M_H, so (19.7) is written concisely as

$$[A_3\ A_2\ A_1\ A_0]^T = M_H\,[P\ Q\ P^1\ Q^1]^T \tag{19.8}$$

Finally, let's use (19.2) to write c's equation in terms of its boundary constraints:

$$\begin{aligned} c(u) &= [u^3\ u^2\ u\ 1]\,[A_3\ A_2\ A_1\ A_0]^T \\ &= [u^3\ u^2\ u\ 1]\,M_H\,[P\ Q\ P^1\ Q^1]^T \\ &= (2u^3 - 3u^2 + 1)\,P + (-2u^3 + 3u^2)\,Q + \\ &\qquad (u^3 - 2u^2 + u)\,P^1 + (u^3 - u^2)\,Q^1 \end{aligned} \tag{19.9}$$

in $0 \le u \le 1$, after performing the matrix multiplications in the second line.

Therefore,

$$c(u) = H_0(u)\,P + H_1(u)\,Q + H_2(u)\,P^1 + H_3(u)\,Q^1 \qquad (0 \le u \le 1) \tag{19.10}$$

where the polynomials

$$\begin{aligned} H_0(u) &= 2u^3 - 3u^2 + 1, \qquad & H_1(u) &= -2u^3 + 3u^2, \\ H_2(u) &= u^3 - 2u^2 + u, \qquad & H_3(u) &= u^3 - u^2 \end{aligned}$$

are called *Hermite blending polynomials* , which, of course, are blending functions, but very different clearly from those used earlier in Bézier and B-spline theory; moreover, they blend not just control points, but tangent vectors as well, as one sees in (19.10). Their graphs are sketched in Figure 19.3. Certain symmetries are evident. Observe, as well, that $H_3(u)$ is non-positive in $0 \le u \le 1$, reaching a minimum value of nearly -0.15.

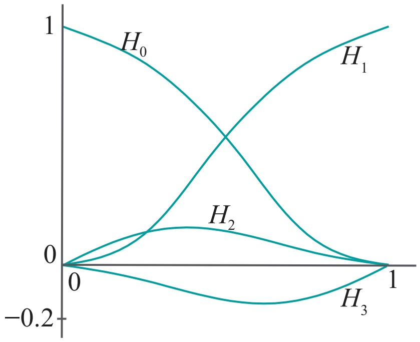

Figure 19.3: Hermite blending polynomials (not exact plots).

The curve $c(u)$ itself is called a *Hermite cubic*. Equation (19.10) is called the *geometric* form of the cubic because its expression is in terms of *c*'s boundary constraints, while (19.1) is its *algebraic* form.

Remark 19.3. Readers familiar with the popular Adobe Illustrator drawing package will recognize that its pen tool, in fact, is used to draw Hermite cubics by specifying endpoints and editing tangents there.

Exercise 19.1. Use calculus to determine the maximum value of $H_2(u)$ and the minimum value of $H_3(u)$ in the interval $[0, 1]$.

Exercise 19.2. Determine the symmetries among the Hermite blending polynomials. For example, that $H_0(u)$ and $H_1(u)$ are mirror images across the vertical line $u = \frac{1}{2}$ down the middle of the parameter interval [0, 1] can be seen by substituting $(1 - u)$ for u in the equation of one to obtain that of the other.

How about the relationship between $H_2(u)$ and $H_3(u)$? Do you see any symmetries?

Exercise 19.3. Prove the affine invariance of the cubic curve c given by Equation (19.10).

Note: Keeping in mind that an affine transformation is a linear transformation followed by a translation, we'll want its linear transformation part applied to all four boundary constraints P , Q, P^1 and Q^1, while the translation should apply only to P and Q.

Figure 19.4: Screenshot of hermiteCubic.cpp.

Experiment 19.1. Run hermiteCubic.cpp, which implements Equation (19.10) to draw a Hermite cubic on a plane. Press space to select either a control point or tangent vector and the arrow keys to change it. Figure 19.4 is a screenshot. The actual cubic is simple to draw, but as you can see in the program we invested many lines of code to get the arrow heads right! End

Exercise 19.4. What sort of curve is c if the two boundary constraints P^1 and Q^1 are both zero (i.e., if the two end velocities vanish)? Determine this from the geometric form of the Hermite cubic and verify it in the preceding program.

It's interesting to contrast (19.10) with the equation of the cubic Bézier curve (Equation (17.8)):

$$c(u) = B_{0,3}(u)P_0 + B_{1,3}(u)P_1 + B_{2,3}(u)P_2 + B_{3,3}(u)P_3 \qquad (0 \le u \le 1)$$

In the case of the Bézier curve, the control points are blended with weights equal to the Bernstein polynomials of degree 3; in the case of the Hermite cubic, the two end control points and their respective tangents are blended with weights equal to the Hermite blending polynomials, which are of degree 3 as well.

Remark 19.4. Since a Hermite cubic interpolates not only its two specified control points, but also the specified tangents there, it's said to make a first-order interpolation (versus a zeroth-order one which would interpolate merely control points).

Let's return to the original problem of joining successive pairs of the $n+1$ control points $P_0, P_1, \dots, P_n$ by means of cubic arcs so that the resulting Hermite spline is smooth. A strategy that comes to mind from the discussion above is to ask the designer to specify, in addition to the $n+1$ control points, the tangent vectors $P'_0, P'_1, \dots, P'_n$ at each, as indicated in Figure 19.5.

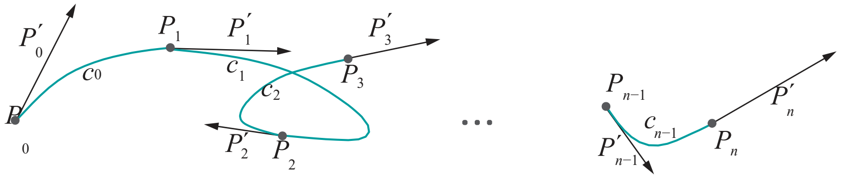

Figure 19.5: Specifying a Hermite spline by specifying the tangent vector at each control point.

Then, using (19.10) to manufacture each of the n successive Hermite cubic arcs c_i, $0 \le i \le n$, subject to the respective boundary constraints P_i, P_{i+1}, P'_i and P'_{i+1} yields a C^1-continuous Hermite spline, as the derivatives on either side of each internal control point agree.

However, asking the designer for $n+1$ tangent values, in addition to the control points themselves, may be a bit much. It would be nice to have an *automatic* way to deduce these tangent values from other constraints, *transparently* to the user. In fact, there is and we'll discuss next two popular types of Hermite splines arising from particular sets of constraints. These are the natural cubic and cardinal splines.

19.2 Natural Cubic Splines

A *natural cubic spline* is a Hermite spline with two constraints: (a) it is C^2-continuous, i.e., its second derivative is continuous, and (b) its second derivative vanishes at its two end control points. It turns out, as we'll see, that these two constraints are enough to uniquely determine the spline.

Assume that the $n+1$ control points through which a natural cubic spline passes are $P_0, P_1, \dots, P_n$. Because of C^1-continuity – mind that C^2-continuity implies C^1-continuity – one assumes that the tangents at the control points are well-defined, in particular, that there are no corners and the value of the tangent is the same on either side of a control point. Say the tangent values at $P_0, P_1, \dots, P_n$ are $P'_0, P'_1, \dots, P'_n$, respectively. We'll compute these values from the constraints given.

Rewrite (19.9) as the equation of the cubic arc c_i from P_i to P_{i+1}:

$$\begin{aligned} c_i(u) \;=\; & (2u^3 - 3u^2 + 1)\, P_i + (-2u^3 + 3u^2)\, P_{i+1} \;+ \\ & (u^3 - 2u^2 + u)\, P'_i + (u^3 - u^2)\, P'_{i+1} \quad (0 \le u \le 1) \end{aligned}$$

Differentiating twice one finds the second derivative

$$c''_i(u) = (12u-6)\, P_i + (-12u+6)\, P_{i+1} + (6u-4)\, P'_i + (6u-2)\, P'_{i+1} \quad (0 \le u \le 1) \quad (19.11)$$

Observe now that the constraints on a natural cubic spline through $P_0, P_1, \dots, P_n$ can be written as the $n+1$ equations:

$$c''_0(0) = 0, \qquad c''_{i-1}(1) = c''_i(0), \quad \text{for } 1 \le i \le n-1, \qquad c''_{n-1}(1) = 0$$

the middle equations saying that the values of the second derivative on either side of each internal control point are equal, assuring C^2-continuity. Expand the constraint equations using (19.11):

$$\begin{aligned}
-6P_0 + 6P_1 - 4P^1_0 - 2P^1_1 &= 0\\
6P_{i-1} - 6P_i + 2P^1_{i-1} + 4P^1_i &= -6P_i + 6P_{i+1} - 4P^1_i - 2P^1_{i+1}, \quad 1 \le i \le n-1\\
6P_{n-1} - 6P_n + 2P^1_{n-1} + 4P^1_n &= 0
\end{aligned}$$

Simplifying and rearranging, we have the system

$$\begin{aligned}
2P^1_0 + P^1_1 &= -3P_0 + 3P_1\\
P^1_{i-1} + 4P_i + P_{i+1} &= -3P_{i-1} + 3P_{i+1}, \quad 1 \le i \le n-1\\
P^1_{n-1} + 2P^1_n &= -3P_{n-1} + 3P_n
\end{aligned} \tag{19.12}$$

of $n+1$ equations in $n+1$ unknowns, which can be solved for the P^1_i in terms of the P_i. In fact, writing out the system (19.12) in matrix form one obtains

$$\begin{bmatrix}
2 & 1 & 0 & 0 & 0 & 0 & \dots & 0 & 0 & 0 & 0\\
1 & 4 & 1 & 0 & 0 & 0 & \dots & 0 & 0 & 0 & 0\\
0 & 1 & 4 & 1 & 0 & 0 & \dots & 0 & 0 & 0 & 0\\
0 & 0 & 1 & 4 & 1 & 0 & \dots & 0 & 0 & 0 & 0\\
\dots & & & \dots & & & \dots & & & & \dots\\
0 & 0 & 0 & 0 & 0 & 0 & \dots & 0 & 1 & 4 & 1\\
0 & 0 & 0 & 0 & 0 & 0 & \dots & 0 & 0 & 1 & 2
\end{bmatrix}
\begin{bmatrix}
P^1_0\\ P^1_1\\ P^1_2\\ P^1_3\\ \dots\\ P^1_{n-1}\\ P^1_n
\end{bmatrix}
=
\begin{bmatrix}
-3P_0 + 3P_1\\ -3P_0 + 3P_2\\ -3P_1 + 3P_3\\ -3P_2 + 3P_4\\ \dots\\ -3P_{n-2} + 3P_n\\ -3P_{n-1} + 3P_n
\end{bmatrix} \tag{19.13}$$

where the coefficient matrix is *tridiagonal* because it has non-zero entries only along the principal diagonal and its two neighboring diagonals. Tridiagonal matrices are particularly efficient to invert [116]; accordingly, equation systems with a tridiagonal coefficient matrix are efficiently solvable .

Consequently, using the solved values $P^1_0, P^1_1, \dots, P^1_n$ from (19.13) and the geometric form (19.10) of the Hermite cubic, one determines the n Hermite cubic arcs between successive pairs from $P_0, P_1, \dots, P_n$. These arcs then join end to end to give the natural cubic spline through these $n+1$ control points.

Exercise 19.5. (Programming) Solve (19.13) by hand for only three control points P_0, P_1 and P_2. Write a program to draw a natural cubic spline through three control points, each of which can be moved on a plane.

Exercise 19.6. Investigate the local control (or lack thereof) of natural cubic splines. In particular, which of the cubic arcs of a natural cubic spline are affected by moving only one control point?
Hint: Playing with a natural cubic spline applet (there are many on the web) should suggest an answer.

19.3 Cardinal Splines

A *cardinal spline* is a C^1 Hermite spline whose tangent vector at each internal control point is determined by the location of its two adjacent control points in the following simple manner. Say the control points through which a cardinal spline passes are $P_0, P_1, \dots, P_n$. The tangent vector P^1_i at P_i, $1 \le i \le n-1$, then is specified to be *parallel* to the vector from P_{i-1} to P_{i+1} by the equation

$$P^1_i = \frac{1}{2}(1 - t_i)(P_{i+1} - P_{i-1}) \tag{19.14}$$

See Figure 19.6.

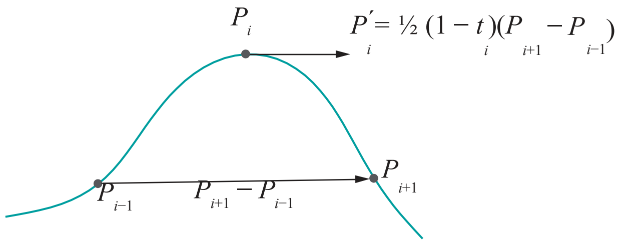

Figure 19.6: The tangent vector at an internal control point of a cardinal spline is parallel to the vector joining the adjacent control points – the tension parameter t_i is user-specified.

The constant of proportionality $\frac{1}{2}(1 - t_i)$ in (19.14) involves a designer-specified parameter t_i, called the *tension parameter* . The tension parameter is usually set between -1 and 1 at each internal control point, in turn setting $\frac{1}{2}(1 - t_i)$ between 1 and 0. If the tension parameter is set to 0 at *every* internal control point, one gets a popularly used special kind of cardinal spline called a *Catmull-Rom* spline. Specifically, the tangent vector at the internal control point P_i of a Catmull-Rom spline is

$$P_i^1 = \frac{1}{2}(P_{i+1} - P_{i-1}) \tag{19.15}$$

Now, from (19.14), $1 \leq i \leq n - 1$, one has only $n - 1$ equations in the $n + 1$ unknowns P_i^1, $0 \leq i \leq n$. Therefore, two more are required to uniquely solve for these unknowns and determine the cardinal spline through P_i, $0 \leq i \leq n$. Typically, as in the case of a natural cubic spline, these are obtained from requiring the second derivatives to vanish at the two end control points.

Exercise 19.7. Write a matrix equation analogous to (19.13) relating P_i^1 to P_i for a cardinal spline, assuming the additional constraints that the second derivatives vanish at the terminal control points. Is the coefficient matrix tridiagonal?

Exercise 19.8. What can you say of local control in cardinal splines? In other words, which of the cubic arcs of a cardinal spline are affected by moving a specific control point?

Exercise 19.9. Natural cubic splines are C^2 by definition. How about cardinal splines – are they C^2?
Hint : The answer is no in general and we ask the reader to try and come up with a counter-example. A Catmull-Rom spline through three control points which loses C^2-continuity in the middle is probably easiest.

19.4 Hermite Surface Patches

We'll give a brief introduction to the 2D version of Hermite curves, namely, Hermite surfaces. Analogously to (19.1), one can write the parametric equation of a *Hermite surface patch* (or *bicubic surface patch*) in algebraic form as

$$\begin{aligned} s(u, v) &= \sum_{i=0}^{3}\sum_{j=0}^{3} A_{i,j}u^i v^j \\ &= A_{3,3}\,u^3v^3 + A_{3,2}\,u^3v^2 + A_{3,1}\,u^3v + A_{3,0}\,u^3 \\ &\quad + A_{2,3}\,u^2v^3 + A_{2,2}\,u^2v^2 + A_{2,1}\,u^2v + A_{2,0}\,u^2 \\ &\quad + A_{1,3}\,uv^3 + A_{1,2}\,uv^2 + A_{1,1}\,uv + A_{1,0}\,u \\ &\quad + A_{0,3}\,v^3 + A_{0,2}\,v^2 + A_{0,1}\,v + A_{0,0} \end{aligned} \tag{19.16}$$

for $0 \leq u, v \leq 1$. The expression after the second equality consists of 16 monomial summands, where A_{ij}, $0 \leq i \leq 3$, $0 \leq j \leq 3$, are points in the ambient space.

Going back to curves for a moment, observe that the geometric form (19.10), viz.,

$$c(u) = H_0(u)\,P + H_1(u)\,Q + H_2(u)\,P^1 + H_3(u)\,Q^1$$

of the equation of a Hermite cubic is more useful than the algebraic (19.1), viz.,

$$c(u) = A_3u^3 + A_2u^2 + A_1u + A_0$$

because it gives an equation in terms of *perceptible* boundary constraints, in particular, the endpoints P and Q and the tangent vectors P^1 and Q^1 there. Moreover, we were able to derive the algebraic form from the geometric because these four boundary constraints were sufficient to uniquely recover the four coefficients A_i, $0 \le i \le 3$, of the algebraic form.

So what would be a suitable set of boundary constraints for a geometric form of the equation of a Hermite patch? Clearly, one would want sixteen constraints leading to a unique determination of the sixteen coefficients A_{ij}, $0 \le i \le 3$, $0 \le j \le 3$, on the RHS of (19.16).

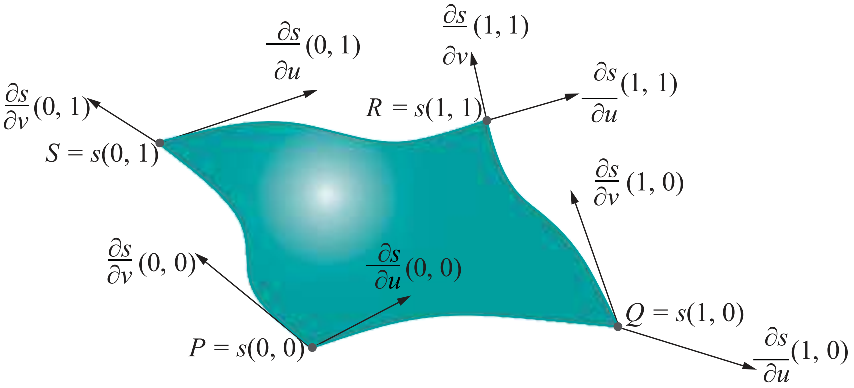
$\frac{\partial s}{\partial u}(0, 1)$
$\frac{\partial s}{\partial v}(1, 1)$
$\frac{\partial s}{\partial v}(0, 1)$
$R = s(1, 1)$
$\frac{\partial s}{\partial u}(1, 1)$
$S = s(0, 1)$
$\frac{\partial s}{\partial v}(1, 0)$
$\frac{\partial s}{\partial v}(0, 0)$
$\frac{\partial s}{\partial u}(0, 0)$
$Q = s(1, 0)$
$P = s(0, 0)$
$\frac{\partial s}{\partial u}(1, 0)$

Figure 19.7: Twelve boundary constraints on a bicubic patch.

Twelve choices are fairly clear. See Figure 19.7. Firstly, the four corners $s(0, 0)$, $s(1, 0)$, $s(1, 1)$, $s(0, 1)$ of the patch s evidently evidently coincide with user-specified control points P, Q, R and S, respectively. Next, analogous to asking for end tangent vectors in the case of a curve, the values of the partial derivatives with respect to u and v at each corner provide eight more constraints. Observe that the two partial derivatives at each corner are nothing but the tangent vectors to the two boundary curves meeting there. Four remaining boundary constraints are up to the designer, but are usually taken to be values of the second-order mixed partial derivatives at the corners, namely,

$$\frac{\partial^2 s}{\partial u \partial v}(0,0), \qquad \frac{\partial^2 s}{\partial u \partial v}(1,0), \qquad \frac{\partial^2 s}{\partial u \partial v}(0,1), \qquad \frac{\partial^2 s}{\partial u \partial v}(1,1)$$

These four are called *twist vectors* and have geometric significance too – though not as straightforwardly as the first twelve – which we'll not go into here.

We'll conclude our discussion by saying that it turns out that, indeed, the four corner position vectors, the eight tangent vectors at the corners and the four twist vectors together provide sixteen boundary constraints which are sufficient to uniquely specify a Hermite patch. We'll not go further into the derivation ourselves, but refer the interested reader to the chapter on Hermite surfaces in the book by Mortenson [97].

Lagrange Interpolation

At the conclusion of this chapter, we'll briefly describe a method of polynomial (in fact, *entirely* polynomial, not piecewise like Hermite) interpolation, called *Lagrange interpolation*, actually of more theoretical interest than practical value in design.

The *Lagrange polynomial* $f_{i,n}$, where n is a positive integer and i is an integer between 0 and n, is defined by the equation

$$f_{i,n}(u) = \prod_{0 \leq j \leq n,\ j \neq i} \frac{u-j}{i-j}$$

For example,

$$\begin{aligned} f_{2,4}(u) &= \frac{(u-0)(u-1)(u-3)(u-4)}{(2-0)(2-1)(2-3)(2-4)} \\ &= \frac{1}{4}\, u(u-1)(u-3)(u-4) \end{aligned}$$

Lagrange polynomials have the easily verified property that

$$f_{i,n}(u) = \begin{cases} 1, & u = i \\ 0, & u \in \{0, 1, \ldots, n\},\ u \neq i \end{cases}$$

In other words, on the particular set of integers $\{0, 1, \ldots, n\}$, the Lagrange polynomial $f_{i,n}$ is 1 at exactly one point, namely i, and 0, elsewhere.

Exercise 19.10. Write the formula for $f_{0,4}(u)$ and check it for the above-mentioned property.

If, now, one uses the Lagrange polynomials as blending functions for $n+1$ control points P_i, $0 \leq i \leq n$, obtaining the curve

$$c(u) = f_{0,n}(u)P_0 + f_{1,n}(u)P_1 + \ldots + f_{n,n}(u)P_n \qquad (0 \leq u \leq n)$$

then c, called a *Lagrange curve*, is a polynomial curve of degree n. It's seen easily from its definition that c interpolates all its control points; in particular, c is equal to P_i at the point i of the parameter domain $[0, n]$, for $0 \leq i \leq n$.

Exercise 19.11. Write the formula for the Lagrange curve interpolating the four control points

$$[0\ \ -1\ \ 3]^T \qquad [1\ \ 2\ \ -3]^T \qquad [5\ \ -1\ \ 4]^T \qquad [2\ \ 0\ \ 8]^T$$

Remark 19.5. Lagrange interpolation is rarely used in practice because it suffers from the Bézier-like problem that the degree of the interpolating curve grows with its number of control points. It lacks local control as well.

19.5 Summary, Notes and More Reading

After a couple of chapters on Bézier and B-spline approximation of control points, we learned in this chapter practical methods to interpolate. These will come in handy in design applications that do require interpolation and most 3D modelers, in fact, offer at least a flavor or two of Hermite interpolation, such as natural cubic and Catmull-Rom splines. It's true, though, in the majority of real-life applications that the only known hard constraints on a curve or surface are at its boundary, e.g., by the way a surface patch meets its neighbors, so the designer typically prefers using internal control points as attractors *a la* Bézier or B-spline, rather than having them tightly latched to an interpolating curve or surface.

For more about Hermite interpolation the reader should consult Farin [45] and Mortenson [97].

Part X

Well Projected

CHAPTER 20

Applications of Projective Spaces: Projection Transformations and Rational Curves

Projective spaces and transformations play an important role in computer graphics and our goal in this chapter is to study two critical applications. The first is in the “shoot” part of shoot-and-print in the OpenGL pipeline, which comes down to devising a so-called projection transformation. The second application is in developing rational versions of Bézier and B-spline theory.

It’s best to come to this chapter with some familiarity with projective spaces. If you have this already, maybe from a college math course or from books on projective geometry such as Henle [73], Jennings [78] and Pedoe [111], you are set; if not, Appendix A, which is an introduction to projective spaces and transformations, has all you need. Appendix A has been written particularly for a CG audience, with connections constantly drawn to familiar CG settings. In fact, you are strongly urged to flip through this appendix even if already acquainted with projective geometry.

However, we do realize there might be a significant readership as yet unfamiliar with projective spaces who, nevertheless, would like a view of their applications without necessarily going through all the math first. This chapter has been arranged to be accessible to them as far as possible. Before each part that invokes projective theory, the reader is alerted with a note containing the minimum information needed to make sense of it. Of course, understanding will not be 100% but, hopefully, good enough for a first light on the applications. Familiarity at least with Section 5.2 on affine transformations, though, particularly the use of homogeneous coordinates, is assumed on everyone’s part.

The first application of projective transformations in Section 20.1 is to accomplish the so-called projection transformation step in the synthetic-camera graphics pipeline – mapping the viewing volume to a box. This leads to a derivation of OpenGL’s 4×4 projection matrices, as well as an understanding of how these matrices compose in the graphics pipeline with modelview matrices.

The second application is in Section 20.2 where we learn the rational versions of both Bézier and B-spline theory. This lengthy section begins with an extensive discussion of rational Bézier curves which, once assimilated, lends itself to fairly straightforward generalization first to rational Bézier surfaces and then rational B-spline, or NURBS, primitives. Section 20.3 concludes the chapter.

20.1 OpenGL Projection Transformations

Way back in Section 2.2 we described OpenGL's rendering as conceptually a two-step process, shoot-and-print. Shooting consists of projecting – parallely in the case of a viewing box and perspectively in that of a viewing frustum – the scene onto the viewing face. Printing consists of scaling the viewing face to fit the OpenGL window. This account, though simplified, is not far from the actual implementation in the OpenGL graphics pipeline.

The second step of printing, aka scaling, is evidently straightforward, but the first of projection is more difficult. Projection itself is performed in two stages.

In the first stage, OpenGL transforms the viewing volume – a box defined by glOrtho(), or a frustum by glFrustum() and gluPerspective(), in classical OpenGL – into a *canonical viewing box* . The canonical viewing box is an axis-aligned cubical box centered at the origin with side lengths two. Figure 20.1 shows the canonical viewing box, as well as a generic viewing box and a generic viewing frustum. Now, the transformation taking a viewing volume to the canonical box, called a *projection transformation*, is really a transformation of $\mathbb{R}^3$ defined by a 4 × 4 matrix, just like glTranslatef() et al. – the image by this transformation of the viewing volume being the canonical box.

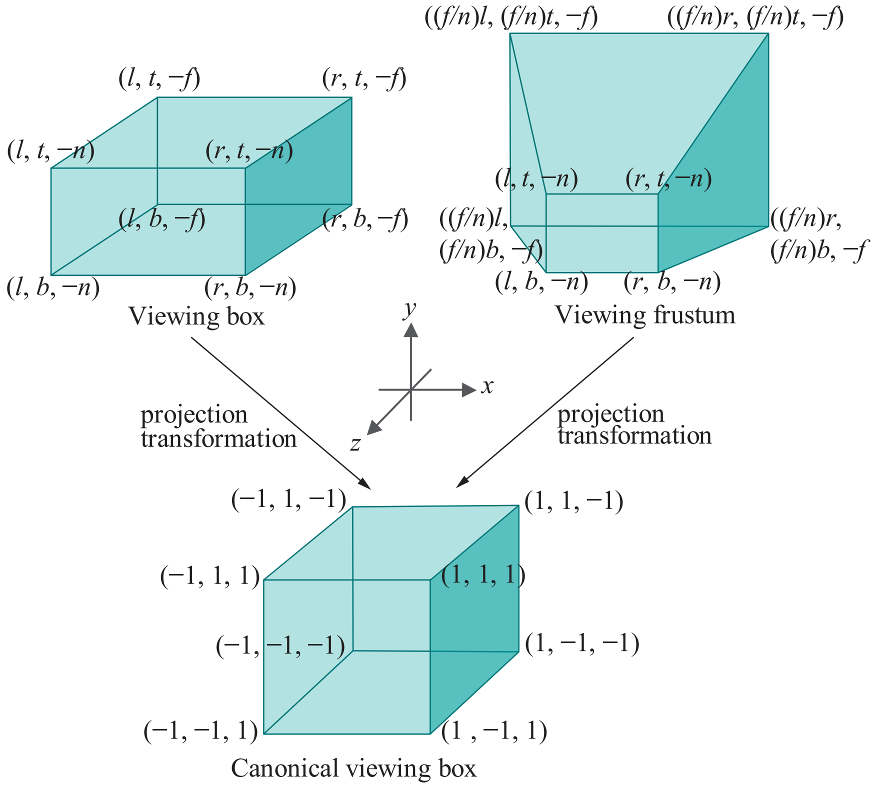

Figure 20.1: As part of the OpenGL rendering pipeline a glOrtho(*l*, *r*, *b*, *t*, *n*, *f*)-defined viewing box or glFrustum(*l*, *r*, *b*, *t*, *n*, *f*)-defined viewing frustum is transformed into the canonical viewing box by a projection transformation.

The crux of what a projection transformation does geometrically is to take lines of sight to lines of sight, "straightening" them out in the process in the case of a frustum. See Figure 20.2 for a sectional view along the *xz*-plane. For example, the lines of sight l_1 and l_2, both in the box and frustum, are mapped by the projection transformation to the corresponding lines of sight l_1^1 and l_2^1 in the canonical viewing box. Note the little quirk that orientation of the lines of sight is reversed by the transformation – we'll see momentarily why. The points *p*, *q* and *r* on both lines of sight l_1 are mapped to p^1, q^1 and r^1, respectively, on the line of sight l^1_1 Rectangle Xin the box and rectangle Y in the frustum are transformed to rectangle X^1 and the trapezoid Y^1, respectively, bold edge going to bold edge. The distortion from Y to Y^1 is precisely the foreshortening one would expect from a perspective view.

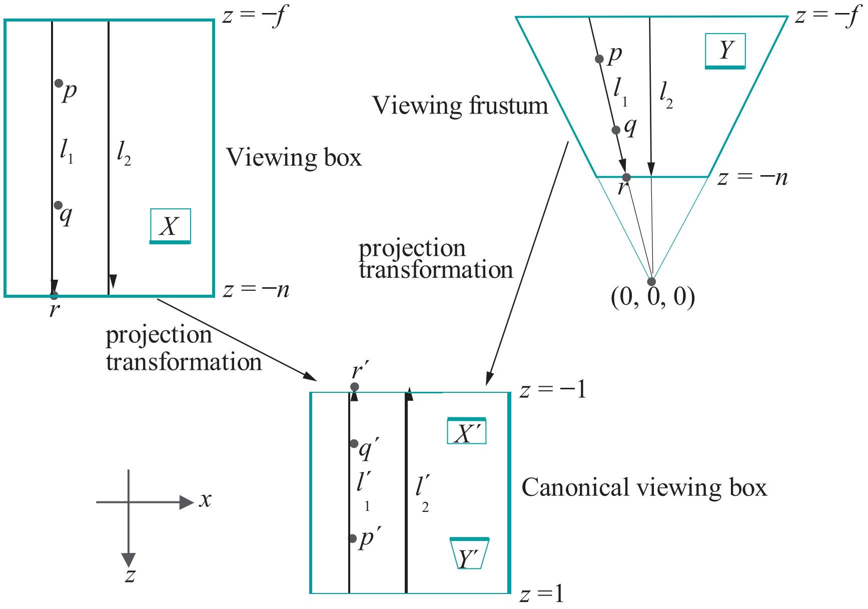

Figure 20.2: Sectional view along the xz-plane of the viewing volumes from Figure 20.1. Black arrows inside the viewing volumes are lines of sight: they are directed toward the $+z$ direction in the viewing box and frustum and toward the $-z$ direction in the canonical viewing box.

In the second stage of the two-stage projection process, OpenGL projects primitives in the canonical viewing box parallely onto its back face, the one lying on $z = -1$. It's because of this reversal of the direction of projection that the orientation of the lines of sight is reversed. The reason for projecting toward $z = -1$, rather than $z = 1$, which would have been as valid, will be apparent soon when we discuss depth testing.

Observe, now, that projection in the canonical viewing box to its back face is *exactly equivalent* to that in the original viewing volume to its viewing face, precisely because the projection transformation preserves lines of sight. In Figure 20.2, for example, the point p, in both box and frustum, projects to the point r on the respective viewing face, while p^1 (the image of p by the projection transformation) projects to r^1 (the image of r by the projection transformation) in the canonical viewing box.

Of the two stages of the projection process, the second one of back-face projection is certainly computationally simpler, as it's a matter simply of tossing the z-values *after* they've been used in depth testing if need be.

If depth testing is enabled, then z-values in the canonical box are used for this purpose, rather than the original ones from world space. It's valid to do so because if, say, point q obscures point p in the viewing volume prior to transformation, as in Figure 20.2, then transformed point q^1 obscures transformed point p^1 as well, again because lines of sight are preserved. Of course, given the direction of the lines of sight in the canonical box, lower z-values win the depth competition, which explains the reason for projecting toward $z = -1$, rather than toward $z = 1$, when higher z-values would win – it's more intuitive for lower z-values to win if z represents depth, lesser depth meaning closer to the eye.

OpenGL accomplishes the projection transformation, from programmer-specified viewing volume to canonical viewing box, by means of a 4 4× *projection matrix* whose nature depends on whether it is a box or frustum to be transformed into the canonical box. Our next objective is to derive the projection matrix in both cases.

Remark 20.1. To be fastidious we should now rephrase our earlier description of the print part of shoot-and-print to say that it scales the back face of the canonical box, rather than the front face of the viewing volume, to fit the OpenGL window.

Remark 20.2. In the fixed-function pipeline of classical OpenGL, the projection matrix is computed opaquely by OpenGL from the programmer-specified projection transformation, e.g., glFrustum(). In the programmable pipeline, as we saw in Chapter 15, the programmer is responsible for specifying the projection matrix herself, projection transformation calls, such as glFrustum(), having been discarded.

20.1.1 Viewing Box to Canonical Viewing Box

The strategy to transform a glOrtho()-defined viewing box into the canonical box is straightforward: translate the viewing box so that its center coincides with that of the canonical one, then scale its sides so that they match those of the canonical box.

The center of the viewing box defined by glOrtho(l, r, b, t, n, f) is at $[(r+l)/2 \;\; (t+b)/2 \;\; -(f+n)/2]^T$, while the center of the canonical box is at the origin $[0 \;\; 0 \;\; 0]^T$. Therefore, the displacement vector translating the first to the second is $[-(r+l)/2 \;\; -(t+b)/2 \;\; (f+n)/2]^T$. The corresponding 4 × 4 translation matrix is

$$T(\,-(r+l)/2,\; -(t+b)/2,\; (f+n)/2\,)$$

(see Section 5.4 for a listing of affine transformation matrices in homogeneous form).

Since the viewing box is of size $(r-l)\times(t-b)\times(f-n)$, while the canonical box is of size $2\times 2\times 2$, the scaling transformation matching the sides of the former with those of the latter has the matrix

$$S(\,2/(r-l),\, 2/(t-b),\; 2/(f-n)\,)$$

Finally, to account for the reversal in direction of the lines of sight, the needed transformation is $(x, y, z) \mapsto (x, y, -z)$, whose matrix is

$$S(1, 1, -1)$$

Composing the preceding three transformations, one obtains the projection transformation, denoted P(glOrtho(l, r, b, t, n, f)), mapping the viewing box of glOrtho(l, r, b, t, n, f) to the canonical viewing box. So, the projection matrix corresponding to P(glOrtho(l, r, b, t, n, f)), using eponymous notation, is

$$\begin{aligned}
& P(\text{glOrtho}(l, r, b, t, n, f)) \\
={}& S(1,1,-1)\;\; S(\,2/(r-l),\; 2/(t-b),\; 2/(f-n)\,) \\
& T(\,-(l+r)/2,\; -(b+t)/2,\; (n+f)/2\,) \\
={}& \begin{bmatrix} 1 & 0 & 0 & 0 \\ 0 & 1 & 0 & 0 \\ 0 & 0 & -1 & 0 \\ 0 & 0 & 0 & 1 \end{bmatrix}
\begin{bmatrix} \frac{2}{r-l} & 0 & 0 & 0 \\ 0 & \frac{2}{t-b} & 0 & 0 \\ 0 & 0 & \frac{2}{f-n} & 0 \\ 0 & 0 & 0 & 1 \end{bmatrix}
\begin{bmatrix} 1 & 0 & 0 & -\frac{r+l}{2} \\ 0 & 1 & 0 & -\frac{t+b}{2} \\ 0 & 0 & 1 & \frac{f+n}{2} \\ 0 & 0 & 0 & 1 \end{bmatrix} \\
={}& \begin{bmatrix} \frac{2}{r-l} & 0 & 0 & -\frac{r+l}{r-l} \\ 0 & \frac{2}{t-b} & 0 & -\frac{t+b}{t-b} \\ 0 & 0 & -\frac{2}{f-n} & -\frac{f+n}{f-n} \\ 0 & 0 & 0 & 1 \end{bmatrix}
\end{aligned} \tag{20.1}$$

As it is a composition of a translation and scalings, P(glOrtho(l, r, b, t, n, f)) is an affine transformation of $\mathbb{R}^3$.

Example 20.1. Determine how the point $[20 \; 80 \; 0]^T$ is transformed by the projection transformation corresponding to glOrtho(0, 100, 0, 100, -1, 1).

Answer: Now

$$P(\mathrm{glOrtho}(0,100,0,100,-1,1)) = \begin{bmatrix} \frac{2}{100} & 0 & 0 & -\frac{100}{100} \\ 0 & \frac{2}{100} & 0 & -\frac{100}{100} \\ 0 & 0 & -\frac{2}{2} & \frac{0}{2} \\ 0 & 0 & 0 & 1 \end{bmatrix}$$

$$= \begin{bmatrix} 0.02 & 0 & 0 & -1 \\ 0 & 0.02 & 0 & -1 \\ 0 & 0 & -1 & 0 \\ 0 & 0 & 0 & 1 \end{bmatrix} \qquad (20.2)$$

Writing $[20\ 80\ 0]^T$ in homogeneous coordinates as $[20\ 80\ 0\ 1]^T$, one sees that it's transformed to the point

$$\begin{bmatrix} 0.02 & 0 & 0 & -1 \\ 0 & 0.02 & 0 & -1 \\ 0 & 0 & -1 & 0 \\ 0 & 0 & 0 & 1 \end{bmatrix} \begin{bmatrix} 20 \\ 80 \\ 0 \\ 1 \end{bmatrix} = \begin{bmatrix} -0.6 \\ 0.6 \\ 0 \\ 1 \end{bmatrix}$$

which is $[-0.6\ 0.6\ 0]^T$ in Cartesian coordinates.

Exercise 20.1. Determine how the following points are transformed by the projection transformation corresponding to glOrtho(-20, 20, 0, 50, -1, 1): (a) $[0\ 40\ 0]^T$ (b) $[50\ 20\ 0.5]^T$ (see the following remark)

Remark 20.3. Just as points inside the viewing box are transformed to points inside the canonical box, those outside, e.g., (b) of the preceding exercise, are transformed to points outside the canonical box. The latter are clipped subsequently in the pipeline prior to rendering; in other words, operationally, clipping is done against the canonical box.

20.1.2 Viewing Frustum to Canonical Viewing Box

No affine transformation can map the viewing frustum defined by the call glFrustum(l, r, b, t, n, f) to the canonical viewing box, for the simple reason that this requires mapping intersecting lines (along edges of the frustum) to parallel ones (along edges of the box), while we know (see Proposition 5.1) that an affine transformation of $\mathbb{R}^3$ takes parallel straight lines to parallel straight lines and intersecting ones again to intersecting ones. We've run into a brick wall as far as affine transformations go. It's time to appeal to the projective.

Note to Readers Unfamiliar with Projective Geometry : Here's what you need to know for the rest of this particular section. Projective 3-space $\mathbb{P}^3$ consists of 4-tuples of the form $[x\ y\ z\ w]^T$, where these so-called homogeneous coordinates cannot all be zero. Two tuples represent the same point if one's a scalar multiple of the other, e.g., $[2\ 4\ 1\ -3]^T$, $[4\ 8\ 2\ -6]^T$ and $[-3\ -6\ -1.5\ 4.5]^T$ all represent the same point. Real 3-space $\mathbb{R}^3$ is embedded in $\mathbb{P}^3$ by mapping the point $[x\ y\ z]^T$ of $\mathbb{R}^3$ to $[x\ y\ z\ 1]^T$ of $\mathbb{P}^3$, e.g., $[2\ 4\ 1]^T$ maps to $[2\ 4\ 1\ 1]^T$.

Yet another thing to keep in mind is that, in addition to the points of $\mathbb{R}^3$ embedded into it as above, $\mathbb{P}^3$ has points corresponding to "directions" in $\mathbb{R}^3$. These points, which are called points at infinity, have a w-value of 0. E.g., $[3\ -1\ 2\ 0]^T$ is the point at infinity corresponding to the direction from the origin toward $[3\ -1\ 2]^T$, as also the direction from $[3\ -1\ 2]^T$ toward the origin, a direction in $\mathbb{R}^3$ and its reversal corresponding to the same point at infinity. Points with non-zero w-values are called regular points because they are each equal to a point of $\mathbb{R}^3$ embedded in $\mathbb{P}^3$ as above.

Finally, a projective transformation of $\mathbb{P}^3$ is defined by a non-singular 4×4 matrix and acts on tuples of $\mathbb{P}^3$ by multiplication from the left (similarly to how linear transformations of $\mathbb{R}^3$ act on 3-tuples).

You should jump now to the paragraph below containing Equation (20.3).

(Resuming from just before the note.......) However, our experience with projective transformations – Example A.16 which illustrates a projective transformation of $\mathbf{P}^3$ mapping a trapezoid to a rectangle is particularly motivating – suggests applying one.

Projectively transforming $\mathbf{R}^3$, in fact, is analogous to projectively transforming $\mathbf{R}^2$. For the latter, we identified $\mathbf{R}^2$ with a "film" in $\mathbf{R}^3$, almost always the plane $z = 1$, to capture the transformation of 2D objects lifted to $\mathbf{P}^2$ (note that the allusion to films is developed in Appendix A). Likewise, to projectively transform $\mathbf{R}^3$, we'll identify it with the hyperplane $w = 1$ in four-dimensional $xyzw$-space $\mathbf{R}^4$ in order to capture the transformation of 3D objects lifted to $\mathbf{P}^3$.

In particular, for the current application, we seek a projective transformation h^M of $\mathbf{P}^3$ which is captured on $\mathbf{R}^3$ as taking the viewing frustum specified by glFrustum(l, r, b, t, n, f) to the canonical box – as indicated on the right of both Figures 20.1 and 20.2. Suppose its defining matrix is

$$M = \begin{bmatrix} a_{11} & a_{12} & a_{13} & a_{14} \\ a_{21} & a_{22} & a_{23} & a_{24} \\ a_{31} & a_{32} & a_{33} & a_{34} \\ a_{41} & a_{42} & a_{43} & a_{44} \end{bmatrix} \qquad (20.3)$$

so that it maps the point $[x\ y\ z\ w]^T$ of $\mathbf{P}^3$ to $M[x\ y\ z\ w]^T$.

The four lines along the four sides of the frustum which meet at its apex $[0\ 0\ 0]^T$ in $\mathbf{R}^3$, corresponding to the regular point $[0\ 0\ 0\ 1]^T$ in $\mathbf{P}^3$, are mapped, respectively, to four lines along edges of the canonical box all parallel to the z-axis, meeting, therefore, at the point at infinity $[0\ 0\ 1\ 0]^T$. Accordingly, we ask that

$$h^M([0\ 0\ 0\ 1]^T) = [0\ 0\ 1\ 0]^T$$

giving the matrix equation

$$\begin{bmatrix} a_{11} & a_{12} & a_{13} & a_{14} \\ a_{21} & a_{22} & a_{23} & a_{24} \\ a_{31} & a_{32} & a_{33} & a_{34} \\ a_{41} & a_{42} & a_{43} & a_{44} \end{bmatrix} \begin{bmatrix} 0 \\ 0 \\ 0 \\ 1 \end{bmatrix} = \begin{bmatrix} 0 \\ 0 \\ d \\ 0 \end{bmatrix}$$

where d can be any non-zero scalar because homogeneous coordinates $[0\ 0\ 1\ 0]^T$ and $[0\ 0\ d\ 0]^T$ represent the same point. This equation implies that

$$a_{14} = 0, \quad a_{24} = 0, \quad a_{34} = d, \quad a_{44} = 0$$

It turns out that choosing $d = -\frac{2fn}{f-n}$ simplifies manipulations down the road so we'll write

$$M = \begin{bmatrix} a_{11} & a_{12} & a_{13} & 0 \\ a_{21} & a_{22} & a_{23} & 0 \\ a_{31} & a_{32} & a_{33} & -\frac{2fn}{f-n} \\ a_{41} & a_{42} & a_{43} & 0 \end{bmatrix}$$

The mappings

$$\begin{aligned} h^M([l\ b\ -n\ 1]^T) &= [-1\ -1\ -1\ 1]^T \\ h^M([r\ b\ -n\ 1]^T) &= [1\ -1\ -1\ 1]^T \\ h^M([l\ t\ -n\ 1]^T) &= [-1\ 1\ -1\ 1]^T \\ h^M([r\ t\ -n\ 1]^T) &= [1\ 1\ -1\ 1]^T \end{aligned}$$

from the mapping of the four vertices at the front of the frustum to the corresponding ones at the back of the canonical box give the four matrix equations

$$\begin{bmatrix} a_{11} & a_{12} & a_{13} & 0 \\ a_{21} & a_{22} & a_{23} & 0 \\ a_{31} & a_{32} & a_{33} & -\frac{2fn}{f-n} \\ a_{41} & a_{42} & a_{43} & 0 \end{bmatrix} \begin{bmatrix} l \\ b \\ -n \\ 1 \end{bmatrix} = \begin{bmatrix} -c_1 \\ -c_1 \\ -c_1 \\ c_1 \end{bmatrix}$$

$$\begin{bmatrix} a_{11} & a_{12} & a_{13} & 0 \\ a_{21} & a_{22} & a_{23} & 0 \\ a_{31} & a_{32} & a_{33} & -\frac{2fn}{f-n} \\ a_{41} & a_{42} & a_{43} & 0 \end{bmatrix} \begin{bmatrix} r \\ b \\ -n \\ 1 \end{bmatrix} = \begin{bmatrix} c_2 \\ -c_2 \\ -c_2 \\ c_2 \end{bmatrix}$$

$$\begin{bmatrix} a_{11} & a_{12} & a_{13} & 0 \\ a_{21} & a_{22} & a_{23} & 0 \\ a_{31} & a_{32} & a_{33} & -\frac{2fn}{f-n} \\ a_{41} & a_{42} & a_{43} & 0 \end{bmatrix} \begin{bmatrix} l \\ t \\ -n \\ 1 \end{bmatrix} = \begin{bmatrix} -c_3 \\ c_3 \\ -c_3 \\ c_3 \end{bmatrix}$$

$$\begin{bmatrix} a_{11} & a_{12} & a_{13} & 0 \\ a_{21} & a_{22} & a_{23} & 0 \\ a_{31} & a_{32} & a_{33} & -\frac{2fn}{f-n} \\ a_{41} & a_{42} & a_{43} & 0 \end{bmatrix} \begin{bmatrix} r \\ t \\ -n \\ 1 \end{bmatrix} = \begin{bmatrix} c_4 \\ c_4 \\ -c_4 \\ c_4 \end{bmatrix}$$

(c_i, $1 \le i \le 4$, are non-zero scalars) leading to 16 equations simultaneously in 16 unknowns:

$$\begin{aligned} l a_{11} + b a_{12} - n a_{13} &= -c_1 \\ l a_{21} + b a_{22} - n a_{23} &= -c_1 \\ l a_{31} + b a_{32} - n a_{33} - \frac{2fn}{f-n} &= -c_1 \\ l a_{41} + b a_{42} - n a_{23} &= c_1 \\ \ldots &= \ldots \\ r a_{41} + t a_{42} - n a_{43} &= c_4 \end{aligned}$$

These can be solved – not difficult, but tedious – to find

$$a_{11} = \frac{2n}{r-l}, \quad a_{12} = 0, \quad a_{13} = \frac{r+l}{r-l}, \quad a_{21} = 0, \quad a_{22} = \frac{2n}{t-b},$$
$$a_{23} = \frac{t+b}{t-b}, \quad a_{31} = 0, \quad a_{32} = 0, \quad a_{33} = -\frac{f+n}{f-n}, \quad a_{41} = 0,$$
$$a_{42} = 0, \quad a_{43} = -1, \quad c_1 = n, \quad c_2 = n, \quad c_3 = n, \quad c_4 = n$$

It follows that the projection transformation mapping the viewing frustum of the call glFrustum(l, r, b, t, n, f) to the canonical viewing box is given by the matrix

$$P(\text{glFrustum}(l, r, b, t, n, f)) = \begin{bmatrix} \frac{2n}{r-l} & 0 & \frac{r+l}{r-l} & 0 \\ 0 & \frac{2n}{t-b} & \frac{t+b}{t-b} & 0 \\ 0 & 0 & -\frac{f+n}{f-n} & -\frac{2fn}{f-n} \\ 0 & 0 & -1 & 0 \end{bmatrix} \qquad (20.4)$$

That $a_{43} \neq 0$ confirms that P(glFrustum(l, r, b, t, n, f)) is not affine, as a 4 × 4 projective transformation matrix is affine if and only if its last row is all 0 except for the last element.

Exercise 20.2. Characterize those regular points that P(glFrustum(l, r, b, t, n, f)) maps to points at infinity.

At this time we ask the reader to open the red book (9th edition) to Appendix E, where OpenGL's 4 × 4 projection matrices are given and compare their values to those in Equations (20.1) and (20.4) above (they are same). Seeing these together with its 4 × 4 matrices for translation, rotation and scaling, listed in Appendix E as well, and derived by us in Section 5.4, the reader may tend to agree that OpenGL "lives" in projective 3-space.

Example 20.2. Determine how the point $[0\ 0\ -10]^T$ is transformed by the projection transformation corresponding to glFrustum(-5, 5, -5, 5, 5, 100), which we have used frequently in our programs.

Answer:

$$P(\text{glFrustum}(-5,5,-5,5,5,25)) = \begin{bmatrix} \frac{10}{10} & 0 & \frac{0}{10} & 0 \\ 0 & \frac{10}{10} & \frac{0}{10} & 0 \\ 0 & 0 & -\frac{105}{95} & -\frac{1000}{95} \\ 0 & 0 & -1 & 0 \end{bmatrix} = \begin{bmatrix} 1 & 0 & 0 & 0 \\ 0 & 1 & 0 & 0 \\ 0 & 0 & -1.105 & -10.526 \\ 0 & 0 & -1 & 0 \end{bmatrix}$$

Writing $[0\ 0\ -10]^T$ in homogeneous coordinates as $[0\ 0\ -10\ 1]^T$, one sees that it's transformed to the point

$$\begin{bmatrix} 1 & 0 & 0 & 0 \\ 0 & 1 & 0 & 0 \\ 0 & 0 & -1.105 & -10.526 \\ 0 & 0 & -1 & 0 \end{bmatrix} \begin{bmatrix} 0 \\ 0 \\ -10 \\ 1 \end{bmatrix} = \begin{bmatrix} 0 \\ 0 \\ 0.524 \\ 10 \end{bmatrix}$$

which is $[0\ 0\ 0.0524]^T$ in Cartesian coordinates.

The last step, where the homogeneous coordinates are divided by the w-value – in this case $[0\ 0\ 0.524\ 10]^T$ by 10 – to map the transformed point back into xyz-space ($w = 1$) is often called *perspective division*, especially when performed as a part of the graphics pipeline.

Exercise 20.3. Determine how the following points are transformed by the projection transformation corresponding to glFrustum(-10, 10, -10, 10, 1, 10): (a) $[1\ 1\ -2]^T$ (b) $[10\ 20\ -1]^T$ (c) $[5\ 5\ 0]^T$.

If any of them is mapped to a point at infinity – whose w-value is 0 – simply identify it as such. Obviously, you'll not be able to complete the projection transformation for such points, as they will not pass perspective division. We'll discuss in Section 21.1 of the next chapter how they are, in fact, handled in the pipeline.

Remark 20.4. Do keep in mind the terminological distinction that a *projective transformation* is one of projective space, while a *projection transformation* is a particular transformation in the graphics pipeline, which is implemented *by means of* a projective transformation, *if* the viewing volume is a frustum.

Projection Matrix of gluPerspective()

We are going to leave the reader to solve the following:

Exercise 20.4. Write an equation similar to (20.4) for the projection matrix corresponding to the GLU call gluPerspective(*fovy*, *aspect*, *n*, *f*).

20.1.3 Projection Matrix in the Pipeline

Consider the fixed-function pipeline first. We know now how the projection matrix corresponding to a programmer-specified projection command – glOrtho(), glFrustum() or gluPerspective() – is computed by OpenGL. How, then, is this matrix stored? And how is it applied in the graphics pipeline?

The answer to the first question is in a manner exactly similar to modelview matrices. As the current modelview matrix is at the top of the modelview matrix stack, so the *current projection matrix* is the topmost of the *projection matrix stack* . Again, as for modelview statements, a projection statement is applied by multiplying the current projection matrix on the right by the matrix corresponding to that statement. Moreover, the projection matrix stack can be pushed and popped, and the current projection matrix accessed and manipulated, just as the modelview matrix stack. Refer to Section 5.4.6 for commands to access the current modelview matrix.

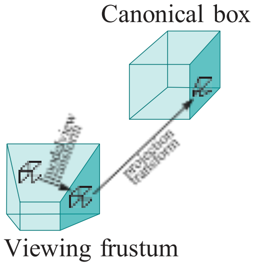

Figure 20.3: Combining modelview and projection transformations. The projection transform skews the rectangular box.

The reader can probably guess the answer to the second question: if the current modelview and projection matrices are M and P , respectively, then the vertex $V = [x\ y\ z\ 1]^T$, using homogeneous coordinates, in world space is transformed to the vertex V^1 given by

$$V^1 = PMV \qquad (20.5)$$

In fact, Figure 20.3 illustrates what is actually the first part of the graphics pipeline – observe that the rectangular box is skewed by the non-affine projection transformation.

Experiment 20.1. Run manipulateProjectionMatrix.cpp, a simple modification of manipulateModelviewMatrix.cpp of Chapter 5. Figure 20.4 is a screenshot, though the output to the OpenGL window is of little interest. Of interest, though, are the new statements in the resize() routine that output the current projection matrix just before and after the call glFrustum(-5.0, 5.0, -5.0, 5.0, 5.0, 100.0).

Compare the second matrix output to the command window by the program with P(glFrustum(-5.0, 5.0, -5.0, 5.0, 5.0, 100.0)) as computed with the help of Equation (20.4). End

Figure 20.4: Screenshot of manipulateProjectionMatrix.cpp.

Exercise 20.5. (Programming) Continue with the preceding experiment by replacing the projection statement with glOrtho(-10.0, 10.0, -10.0, 10.0, 0.0, 20.0). Compare the second matrix output to the command window with P(glOrtho(-10.0, 10.0, -10.0, 10.0, 0.0, 20.0)) as computed using Equation (20.4).

Remark 20.5. It's unlikely that you'll ever need to access the projection matrix stack in an ordinary classical OpenGL program, other than in the mandatory definition of the viewing volume – being one of glOrtho() or glFrustum() or gluPerspective() – in a resize() routine.

Moving on to the programmable pipeline, we know already that we are on our own as far as modelview and projection transformations are concerned. It's our responsibility to explicitly write the corresponding matrices in the vertex shader, typically, in a statement like

```
gl_Position = projMat * modelViewMat * squareCoords
```

which is from Chapter 15's squareShaderized.cpp's vertex shader. So, we have two choices. We can either compute the modelview and projection matrices ourselves using what we learned in Chapter 5 and here, or (more sensibly) import a helper library like GLM to do the work for us. We used the first approach only in squareShaderized.cpp, after which we consistently imported the GLM in our 4.x programs.

And, of course, the programmable pipeline has no stack manipulation commands, either modelview or projection, because, well, there aren't any such program-managed stacks. If we want stacks we have to make them ourselves.

20.2 Rational Bézier and NURBS Curves and Surfaces

Our second application of projective geometry is to set the stage for rational Bézier primitives, as well as to put the 'R' – 'R' stands for rational, of course – into NURBS. In Chapters 17 and 18 we investigated the polynomial versions of Bézier and NURBS theory, respectively.

We'll begin with rational Bézier curves, as conceptually they are the simplest and notationally least cumbersome. Once we have rational Bézier curves under our belts, extending our understanding to rational Bézier surfaces and then to NURBS curves and surfaces will not be difficult.

20.2.1 Rational Bézier Curves Basics

Recall Equation (17.13) of a Bézier curve in $\mathbb{R}^3$ specified by $n+1$ control points $P_i = [x_i\ y_i\ z_i]^T$, $0 \le i \le n$:

$$C(u) = \left[\sum_{i=0}^{n} B_{i,n}(u) x_i \quad \sum_{i=0}^{n} B_{i,n}(u) y_i \quad \sum_{i=0}^{n} B_{i,n}(u) z_i \right]^T \qquad (0 \le u \le 1) \qquad (20.6)$$

Note to Readers Unfamiliar with Projective Geometry : Here's what you need to know for most of this particular section. Projective 2-space $\mathbb{P}^2$ consists of 3-tuples of the form $[x\ y\ z]^T$, where these so-called homogeneous coordinates cannot all be zero. Two tuples represent the same point if one's a scalar multiple of the other, e.g., $[0\ 1\ 2]^T$ and $[0\ 4\ 8]^T$.

Real 2-space $\mathbb{R}^2$ is embedded in $\mathbb{P}^2$ by mapping the point $[x\ y]^T$ of $\mathbb{R}^2$ to $[x\ y\ 1]^T$ of $\mathbb{P}^2$, e.g., $[2\ 4]^T$ maps to $[2\ 4\ 1]^T$. Conversely, a point $[x\ y\ z]^T$ of $\mathbb{P}^2$, with $z = 0$, is an image by this embedding of the point $[x/z\ y/z]^T$ of $\mathbb{R}^2$.

Getting back to (20.6) above, what if none of the controls P_i has coordinates all zero, so that one can imagine each to be a projective point with homogeneous coordinates $[x_i\ y_i\ z_i]^T$, rather than the real point $[x_i\ y_i\ z_i]^T$? Certainly, then, (20.6) defines a point $C(u)$ in $\mathbb{P}^2$ for every u in $0 \le u \le 1$, as long as all its three components are not simultaneously zero either. In this case, one could call C *the* projective Bézier curve over the projective control points P_i, $0 \le i \le n$, *provided* that it doesn't depend on the choice of the P_i's homogeneous coordinates, for, otherwise, (20.6) would give different curves $C(u)$ for different choices and not be a proper definition at all.

Let's see first if C, in fact, is independent of the choice of homogeneous coordinates for its control points. Accordingly, write $P_i = [w_i x_i\ \ w_i y_i\ \ w_i z_i]^T$, where $w_i \neq 0$, for $0 \le i \le n$, and plug into (20.6):

$$D(u) = \left[\sum_{i=0}^{n} B_{i,n}(u) w_i x_i \quad \sum_{i=0}^{n} B_{i,n}(u) w_i y_i \quad \sum_{i=0}^{n} B_{i,n}(u) w_1 z_i \right]^T \qquad (0 \le u \le 1) \ (20.7)$$

Is $D(u) = C(u)$? Not necessarily: playing a bit with the equation it's clear that there's no way to "pull the w_i's out of the square brackets" and write

$$\begin{aligned} &\left[\sum_{i=0}^{n} B_{i,n}(u) w_i x_i \quad \sum_{i=0}^{n} B_{i,n}(u) w_i y_i \quad \sum_{i=0}^{n} B_{i,n}(u) w_i z_i \right]^T \\ = \ & w \left[\sum_{i=0}^{n} B_{i,n}(u) x_i \quad \sum_{i=0}^{n} B_{i,n}(u) y_i \quad \sum_{i=0}^{n} B_{i,n}(u) z_i \right]^T \end{aligned}$$

for some one scalar w, unless all the w_i's happen to be equal to w.

Ouch, but there's a positive way to look at this seeming roadblock. Might not different projective Bézier curves for different sets of homogeneous coordinates mean more choice for the designer?! To explore this angle, let's start with control point all in $\mathbb{R}^2$, not $\mathbb{P}^2$, as at the end of the day we'll be modeling in real space, not projective. However, first, identify $\mathbb{R}^2$ with the plane $z = 1$ in $\mathbb{R}^3$, i.e., $[x\ y]^T \in \mathbb{R}^2$ with $[x\ y\ 1]^T \in \mathbb{R}^3$, so that we can duck back into $\mathbb{P}^2$ as need be.

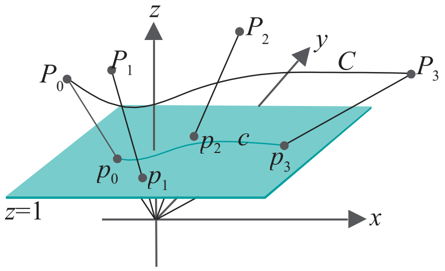

Figure 20.5: Four real control points $p_i = [x_i\ y_i\ 1]^T$, with weights w_i, are lifted to the projective control points $P_i = [w_i x_i\ \ w_i y_i\ \ w_i]^T$, $0 \le i \le 3$. The (black) polynomial projective Bézier curve C projects to the (green) rational real Bézier curve c.

Choose $n+1$ control points $p_i = [x_i\ y_i\ 1]^T$, $0 \le i \le n$, in $\mathbb{R}^2$, as well as $n+1$ non-zero scalars w_i, $0 \le i \le n$. Lift each p_i to the projective point $P_i = [w_i x_i\ \ w_i y_i\ \ w_i]^T$ in $\mathbb{P}^2$, expressed using *these particular* homogeneous coordinates. See Figure 20.5. The scalar w_i is called the *weight* of the control point p_i. The projective *polynomial* Bézier curve C specified by the control points $P_i = [w_i x_i\ \ w_i y_i\ \ w_i]^T$ is

$$C(u) = \left[\sum_{i=0}^{n} B_{i,n}(u) w_i x_i \quad \sum_{i=0}^{n} B_{i,n}(u) w_i y_i \quad \sum_{i=0}^{n} B_{i,n}(u) w_i\right]^T \quad (0 \le u \le 1) \quad (20.8)$$

To return to $\mathbb{R}^2$, divide C throughout by its z-coordinate to get the plane curve

$$c(u) = \left[\frac{\sum_{i=0}^{n} B_{i,n}(u) w_i x_i}{\sum_{i=0}^{n} B_{i,n}(u) w_i} \quad \frac{\sum_{i=0}^{n} B_{i,n}(u) w_i y_i}{\sum_{i=0}^{n} B_{i,n}(u) w_i} \quad 1\right]^T \quad (0 \le u \le 1) \qquad (20.9)$$

assuming that $\sum_{i=0}^{n} B_{i,n}(u) w_i \neq 0$ in $0 \le u \le 1$, so there's never division by zero. Rewriting (20.9) as a proper equation in $\mathbb{R}^2$ by dropping the z-value 1, we have

$$c(u) = \left[\frac{\sum_{i=0}^{n} B_{i,n}(u) w_i x_i}{\sum_{i=0}^{n} B_{i,n}(u) w_i} \quad \frac{\sum_{i=0}^{n} B_{i,n}(u) w_i y_i}{\sum_{i=0}^{n} B_{i,n}(u) w_i}\right]^T \quad (0 \le u \le 1) \qquad (20.10)$$

which is said to be the *rational Bézier curve* in $\mathbb{R}^2$ approximating the control points $p_i = [x_i\ y_i]^T$, with respective weights w_i, $0 \le i \le n$.

If the weights w_i, $0 \le i \le n$, are all positive, then it's easy to see that the denominator $\sum_{i=0}^{n} B_{i,n}(u) w_i$ in (20.10) is positive as well, and so non-zero, in $0 \le u \le 1$. Consequently, this condition on the weights is, typically, assumed as a design constraint. *We'll make a tacit assumption ourselves of positive weights henceforth.*

It's a bit hard to make out from (20.10) exactly what's going on. Let's consider a particular case with few control points, say three, so $n = 2$. Write out the Bernstein polynomials in (20.10) to obtain the following equation for the quadratic rational Bézier curve on three control points $[x_0\ y_0]^T$, $[x_1\ y_1]^T$ and $[x_2\ y_2]^T$, with weights w_0, w_1 and w_2, respectively:

$$c(u) = \left[\frac{w_0 x_0 (1-u)^2 + 2 w_1 x_1 (1-u) u + w_2 x_2 u^2}{w_0 (1-u)^2 + 2 w_1 (1-u) u + w_2 u^2} \quad \frac{w_0 y_0 (1-u)^2 + 2 w_1 y_1 (1-u) u + w_2 y_2 u^2}{w_0 (1-u)^2 + 2 w_1 (1-u) u + w_2 u^2}\right]^T \qquad (20.11)$$

in $0 \le u \le 1$.

Compare with (17.5), which is

$$c(u) = [x_0(1-u)^2 + 2x_1(1-u)u + x_2u^2 \qquad y_0(1-u)^2 + 2y_1(1-u)u + y_2u^2]^T$$

in $0 \leq u \leq 1$, the equation of the quadratic polynomial Bézier curve on the same three control points. Observe, first, that both the x- and y-values on the RHS of (20.11) are rational functions, i.e., *ratios* of two polynomials, particularly of two quadratics in this case. The values on the RHS of the equation for the polynomial curve, on the other hand, are simply quadratic polynomials. The following three exercises shed further light on the quadratic rational Bézier curve.

Exercise 20.6. Putting $u = 0$ and 1 in Equation (20.11), show that, whatever the assignment of weights, a quadratic rational Bézier curve always interpolates both its first and last control points.

Exercise 20.7. Show that if the weights of its three control points are equal, then a quadratic rational Bézier curve coincides with the quadratic polynomial Bézier curve specified by the same control points.

Evidently, then, at least for three control points, a polynomial Bézier curve is simply a special case of a rational one.

Exercise 20.8. The quadratic polynomial Bézier curve we know is a weighted sum of its control points. In fact, one can rewrite (17.5) as follows to see this.

$$\begin{aligned} &c(u) \\ &\quad = [x_0(1-u)^2 + 2x_1(1-u)u + x_2u^2 \quad y_0(1-u)^2 + 2y_1(1-u)u + y_2u^2]^T \\ &\quad = (1-u)^2[x_0 \;\; y_0]^T \; + \; 2(1-u)u\,[x_1 \;\; y_1]^T \; + \; u^2[x_2 \;\; y_2]^T \end{aligned}$$

in $0 \leq u \leq 1$, where the weights in the second line, namely, $(1-u)^2$, $2(1-u)u$ and u^2, are the so-called blending functions of the control points. As we know too, these particular blending functions, called degree-2 Bernstein polynomials, form a partition of unity.

How about the quadratic rational Bézier curve of (20.11)? Write it similarly as a sum

$$c(u) = (\ldots)\,[x_0 \;\; y_0]^T + (\ldots)\,[x_1 \;\; y_1]^T + (\ldots)\,[x_2 \;\; y_2]^T$$

weights being rational blending functions, rather than polynomial. Do these new blending functions still form a partition of unity? (*Yes*.)

Going from quadratic rational to cubic rational with four weighted control points is straightforward, as we ask the reader to show next.

Exercise 20.9. Write an equation analogous to (20.11) for a cubic rational Bézier curve.

Figure 20.6: Screenshot of rationalBezierCurve1.cpp.

So, do the weights w_i of the rational Bézier curve of (20.10) influence its shape in a meaningful manner as we hoped before beginning our project of lifting real control points to projective? The next experiment should shed light on this question.

Experiment 20.2. Run rationalBezierCurve1.cpp, which draws the cubic rational Bézier curve specified by four control points on the plane at *fixed* locations, but with *changeable* weights.

The control points on the plane (light gray triangular mesh) are all red, except for the currently selected one, which is black. Press space to cycle through the control points. The control point weights are shown at the upper-left, that of the currently selected one being changed by pressing the up/down arrow keys. The rational Bézier curve on the plane is red as well. Figure 20.6 is a screenshot.

Drawn in green are all the lifted control points, except for that of the currently selected control point, which is black. The projective polynomial Bézier curve approximating the lifted control points is green too. The lifted control points are a larger size as well.

Note: The lifted control points and the projective Bézier curve are primitives in $\mathbf{P}^2$, of course, but represented in $\mathbf{R}^3$ using their homogeneous coordinates.

Also drawn is a cone of several gray lines through the projective Bézier curve which intersects the plane in its projection, the rational Bézier curve.

Observe that increasing the weight of a control point pulls the (red rational Bézier) curve toward it, while reducing it has the opposite effect. Moreover, the end control points are always interpolated regardless of assigned weights. It's sometimes hard to discern the very gradual change in the shape of the curve as one varies the weights. A trick is to press delete for the curve to spring back to its original configuration, at which moment the difference should be clear. It seems, then, that control point weights are indeed an additional set of "dials" at the designer's disposal to fine-tune a rational Bézier curve.

The code of rationalBezierCurve1.cpp is instructive as well, as we'll see in the next section on drawing. End

Remark 20.6. It's interesting that, though we made a detour through $\mathbf{P}^2$ to draw rational Bézier curves in $\mathbf{R}^2$, a designer living in $\mathbf{P}^2$ itself seemingly does not have Bézier curves for her own use at all. The reason is that all liftings of a point in $\mathbf{R}^2$ to $\mathbf{P}^2$ are for her the same, particularly $[w_i x_i \ \ w_i y_i \ \ w_i z_i]^T$, for all $w_i = 0$, are for her the same projective point, which means that she will have to choose *one* of the continuum of curves $D(u)$ of (20.7) as *the* Bézier curve of control points $[x_i \ y_i \ z_i]^T$, $0 \le i \le n$, in $\mathbf{P}^2$, which does not seem uniquely (i.e., algorithmically) possible.

To put it another way, even though we imagined lifting control points from $\mathbf{R}^2$ to $\mathbf{P}^2$, we *effectively* were lifting from $\mathbf{R}^2$ to $\mathbf{R}^3$ for the simple reason that we were forced at the end to make a distinction between the points $[w_i x_i \ \ w_i y_i \ \ w_i z_i]^T$ for different w_i, which cannot be the case in $\mathbf{P}^2$.

We've been studying rational Bézier curves on the plane for really no other reason than that, though we started with the 3D equation (20.6), we ended up projecting it down to 2D. In fact, deriving the equation for a rational Bézier curve in 3-space is not hard and almost a repeat of the 2D process, as we ask the reader to show next.

Exercise 20.10. Identify $\mathbf{R}^3$ with the hyperplane $w = 1$ in $xyzw$-space $\mathbf{R}^4$, just as we identify $\mathbf{R}^2$ with the plane $z = 1$ in xyz-space $\mathbf{R}^3$. Suppose $p_i = [x_i \ y_i \ z_i \ 1]^T$, $0 \le i \le n$, are $n+1$ control points in $\mathbf{R}^3$ with assigned weights w_i, $0 \le i \le n$.

Lift each p_i to the projective point $P_i = [w_i x_i \ \ w_i y_i \ \ w_i z_i \ \ w_i]^T$ in $\mathbf{P}^3$, expressed using those particular homogeneous coordinates. Reasoning as earlier in the 2D case, show that the equation of the rational Bézier curve in $\mathbf{R}^3$ approximating the control points $p_i = [x_i \ y_i \ z_i]^T$, with respective weights w_i, $0 \le i \le n$, is

$$c(u) = \left[\frac{\sum_{i=0}^{n} B_{i,n}(u) w_i x_i}{\sum_{i=0}^{n} B_{i,n}(u) w_i} \quad \frac{\sum_{i=0}^{n} B_{i,n}(u) w_i y_i}{\sum_{i=0}^{n} B_{i,n}(u) w_i} \quad \frac{\sum_{i=0}^{n} B_{i,n}(u) w_i z_i}{\sum_{i=0}^{n} B_{i,n}(u) w_i} \right]^T \qquad (20.12)$$

for $0 \le u \le 1$, which, of course, is the analogue of the 2D equation (20.10) that we have already derived.

20.2.2 Drawing Rational Bézier Curves

OpenGL can draw rational Bézier curves in 3-space. To draw the curve with control points $p_i = [x_i \ y_i \ z_i]^T$ and weights w_i, $0 \le i \le n$, the command is

```
glMap1f(GL_MAP1_VERTEX_4, t1, t2, stride, order, *controlPoints)
```

where *controlPoints* points to the $(n+1) \times 4$ array

$$\{\{w_0x_0 \ \ w_0y_0 \ \ w_0z_0 \ \ w_0\}, \{w_1x_1 \ \ w_1y_1 \ \ w_1z_1 \ \ w_1\}, \ldots, \{w_nx_n \ \ w_ny_n \ \ w_nz_n \ \ w_n\}\} \qquad (20.13)$$

and other parameters have the same meaning as for the command

```
glMap1f(GL_MAP1_VERTEX_3, t1, t2, stride, order, *controlPoints)
```

with which we are familiar from drawing polynomial Bézier curves in Section 10.3.1.

Returning to rationalBezierCurve1.cpp, let's see if OpenGL's commands to draw a rational Bézier curve in 3-space have been correctly invoked. Say the four planar control points of the program are $[x_i\ y_i]^T$, $0 \leq i \leq 3$, represented in homogeneous coordinates by $[x_i\ y_i\ 1]^T$, the values of the latter being stored in the array controlPoints. Their respective weights w_i are stored in the array weights.

Note: We are using variable names for convenience, of course. The actual values in the program, as you can see, are $[7.0\ 2.0]^T$ for $[x_1\ y_1]^T$, 1.5 for w_1, and so on.

The array ControlPointsLifted is filled by the routine computeControlPointsLifted() with the lifted coordinate values $[w_ix_i\ \ w_iy_i\ \ w_i]^T$, $0 \leq i \leq 3$. The green Bézier curve is the 3D polynomial Bézier approximation of the lifted points drawn using glMap1f(GL_MAP1_VERTEX_3, . . .).

The array controlPointsHomogeneous is filled by computeControlPointsHomogeneous() with the values $[w_ix_i\ \ w_iy_i\ \ w_i\ \ w_i]^T$. From our understanding of the syntax of glMap1f(GL_MAP1_VERTEX_4, ...) – compare, in particular, array controlPointsHomogeneous with array (20.13) above – the red rational Bézier curve approximates the control points $[x_i\ y_i\ 1]^T$ in $\mathbb{R}^3$ with weights w_i, $0 \leq i \leq 3$. By (20.12) the equation of the latter is seen to be

$$c(u) = \left[\frac{\sum_{i=0}^{n} B_{i,n}(u)w_ix_i}{\sum_{i=0}^{n} B_{i,n}(u)w_i} \quad \frac{\sum_{i=0}^{n} B_{i,n}(u)w_iy_i}{\sum_{i=0}^{n} B_{i,n}(u)w_i} \quad 1 \right]^T \qquad (0 \leq u \leq 1)$$

which is precisely the 2D rational Bézier approximation of the control points $[x_i\ y_i]^T$, $0 \leq i \leq 3$, drawn on the plane $z = 1$.

We have verified, therefore, that the green and red curves of rationalBezierCurve1.cpp are indeed the particular Bézier approximations claimed in Experiment 20.2.

So what do rational Bézier curves have that the polynomial curves do not? Let's see . . . .

20.2.3 Rational Bézier Curves and Conic Sections

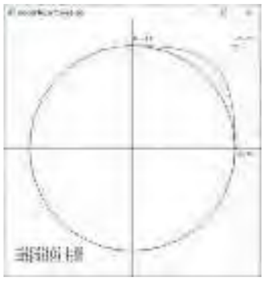

Figure 20.7: Screenshot of rationalBezierCurve2.cpp with the weight of the middle control point 1.13.

Experiment 20.3. Run rationalBezierCurve2.cpp, which draws a red quadratic rational Bézier curve on the plane specified by the three control points $[1, 0]^T$, $[1, 1]^T$ and $[0, 1]^T$. See Figure 20.7. Also drawn is the unit circle centered at the origin. Press the up/down arrow keys to change the weight of the middle control point $[1, 1]^T$. The weights of the two end control points are fixed at 1.

Decrease the weight of the control point $[1, 1]^T$ from its initial value of 1.5. It seems that at some value between 0.70 and 0.71 the curve lies exactly along a quarter of the circle (the screenshot of Figure 20.7 is at 1.13). This is no accident, as the following exercise shows. End

Exercise 20.11. Plug the values

$$[x_0\ y_0]^T = [1, 0]^T, \qquad [x_1\ y_1]^T = [1, 1]^T, \qquad [x_2\ y_2]^T = [0, 1]^T$$

of the control points of the preceding experiment, together with the weights

$$w_0 = 1, \qquad w_1 = 1/\sqrt{2}, \qquad w_2 = 1$$

into Equation (20.11). Show, then, that $c(u) = [x(u), y(u)]^T$, where the rational functions $x(u)$ and $y(u)$ satisfy $x(u)^2 + y(u)^2 = 1$.

One sees from the preceding exercise that the quadratic rational Bézier curve specified by the control points $[1, 0]^T$ with weight 1, $[1, 1]^T$ with weight $1/\sqrt{2}$ (':: 0.7071) and $[0, 1]^T$ with weight 1 is indeed a quarter of a circle. It follows that any whole circle can be obtained by joining end to end at most four quadratic rational Bézier curves. In fact, this generalizes to a very close relationship between quadratic rational Bézier curves and conic sections:

Proposition 20.1. *Any bounded arc of a conic section can be obtained by joining end to end a finite number of quadratic rational Bézier curves.*

In the other direction, any quadratic rational Bézier curve is an arc of a conic section.

The proof is beyond our scope here. We refer the interested reader to the text by Buss [21].

Remark 20.7. The qualifier "bounded" in the proposition is necessary simply because a rational Bézier curve is bounded by definition, so that no unbounded arc of a conic section (e.g., an entire parabola or wing of a hyperbola) can be assembled from a finite number of rational Bézier curves.

Remark 20.8. If the reader is wondering how a quadratic rational Bézier curve which happens to be a straight line segment, e.g., if its three control points are collinear, can be an arc of a conic section, keep in mind that straight lines are, in fact, degenerate conic sections (refer to Exercise 10.22).

Proposition 20.1 says, then, that using rational Bézier curves one can draw any finite piece of any conic section, including circles, ellipses, parabolas and hyperbolas, all curves which arise naturally in diverse applications; however, not even a circle, the simplest of conic sections, can be constructed from polynomial Bézier curves, because no non-trivial arc of a circle has a polynomial parametrization, as we saw in Example 10.8. *Score one for the rationals*!

Remark 20.9. The original Utah Teapot, discussed toward the end of Section 10.3.2, composed of bicubic polynomial Bézier patches, is not – and can never be – perfectly round! To make it so, it has to be redesigned with the help of rational patches.

20.2.4 Properties of Rational Bézier Curves

We ask the reader to establish some properties of rational Bézier curves in general. We'll work on the plane $\mathbb{R}^2$ first. Observe that the x and y components of the rational Bézier curve c given by Equation (20.10), written below again,

$$c(u) = \left[\frac{\sum_{i=0}^{n} B_{i,n}(u) w_i x_i}{\sum_{i=0}^{n} B_{i,n}(u) w_i} \quad \frac{\sum_{i=0}^{n} B_{i,n}(u) w_i y_i}{\sum_{i=0}^{n} B_{i,n}(u) w_i} \right]^T \qquad (0 \le u \le 1)$$

are both ratios of polynomials of degree n in u. Accordingly, c is said to be the rational Bézier curve of *degree* n, or *order* $n+1$, the latter being the number of control points.

The earlier Exercises 20.6 and 20.7 both generalize to rational Bézier curves of arbitrary order, as we see next.

Exercise 20.12. Prove that any rational Bézier curve always interpolates both its first and last control points, no matter what the assignment of weights.

Exercise 20.13. Prove that any rational Bézier curve whose control points have all equal weights coincides with the polynomial Bézier curve specified by the same control points.

Therefore, generally, a polynomial Bézier curve is simply a special case of a rational one.

Let's massage (20.10) into a form which will afford us a familiar way of understanding rational Bézier curves:

$$c(u) = \begin{bmatrix} \frac{\sum_{i=0}^{n} B_{i,n}(u)w_i x_i}{\sum_{i=0}^{n} B_{i,n}(u)w_i} & \frac{\sum_{i=0}^{n} B_{i,n}(u)w_i y_i}{\sum_{i=0}^{n} B_{i,n}(u)w_i} \end{bmatrix}^T$$

$$= \begin{bmatrix} \sum_{i=0}^{n} \frac{B_{i,n}(u)w_i}{\sum_{i=0}^{n} B_{i,n}(u)w_i} x_i & \sum_{i=0}^{n} \frac{B_{i,n}(u)w_i}{\sum_{i=0}^{n} B_{i,n}(u)w_i} y_i \end{bmatrix}^T$$

$$= \sum_{i=0}^{n} \frac{B_{i,n}(u)w_i}{\sum_{i=0}^{n} B_{i,n}(u)w_i} p_i \qquad (20.14)$$

in $0 \leq u \leq 1$, where the control point $p_i = [x_i \; y_i]^T$, $0 \leq i \leq n$.

One sees from Equation (20.14) that a rational Bézier curve is a weighted sum of its control points, as is a polynomial Bézier curve, but using a different set of blending functions as weights: instead of the Bernstein polynomial $B_{i,n}(u)$, the rational function

$$\frac{B_{i,n}(u)w_i}{\sum_{i=0}^{n} B_{i,n}(u)w_i}$$

blends control point p_i.

Exercise 20.14. Verify that the blending functions of a rational Bézier curve form a partition of unity. Therefore, a rational Bézier curve is (a) constrained to lie in the convex hull of its control points, and (b) affinely invariant.
Hint: See the proof of Proposition 17.1.

Exercise 20.15. Prove that if the weight w_i of one particular control point p_i is increased in Equation (20.14), then the value

$$\frac{B_{i,n}(u)w_i}{\sum_{i=0}^{n} B_{i,n}(u)w_i}$$

of its blending function increases everywhere in the open interval $0 < u < 1$, while that of every other control point decreases.

The preceding exercise explains the phenomenon observed in Experiment 20.2, that increasing a control point's weight attracts the curve to it. Contrast this with the situation of a polynomial Bézier curve which can be pulled toward a particular control point only by moving that control point in a direction away from the curve; given a rational curve, on the other hand, the designer has simply to ratchet up a control point's weight, otherwise leaving it stationary, a far more efficient method. *Score two for rationals*! Here's another program to show off weighted control points.

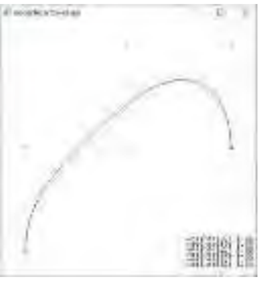

Figure 20.8: Screenshot of rationalBezierCurve3.cpp.

Experiment 20.4. Run rationalBezierCurve3.cpp, which shows a rational Bézier curve on the plane specified by six control points. See Figure 20.8 for a screenshot. A control point is selected by pressing the space key, moved with the arrow keys and its weight changed by the page up/down keys. Pressing delete resets. End

20.2.5 Rational Bézier Curves and Projective Invariance

Note to Readers Unfamiliar with Projective Geometry : This section investigates how a projective transformation transforms a Bézier curve. It begins, though, with the effect of so-called snapshot transformations, a subclass of the projective, defined in Appendix A. Informally, a snapshot transformation is the change induced in how an object is seen by altering the alignment of a point camera. Unfortunately, just this much may not be enough to follow the entire discussion and to go farther it seems referring to Appendix A is unavoidable. Our suggestion, therefore, to the reader not inclined to peruse that appendix is to simply read once Proposition 20.2, which describes how a rational Bézier curve changes through projective transformation, and take it for granted.

What happens when a snapshot transformation (snapshot transformations, a special subclass of the projective, are introduced in Section A.5 of Appendix A) is applied to a Bézier curve, either polynomial or rational? Let's try and repeat Experiment A.1, where we run the program turnFilm.cpp to compare snapshots of parallel power lines taken with the film along the $z = 1$ and $x = 1$ plane, respectively, but, with power lines now replaced by a polynomial Bézier curve drawn on the $z = 1$ plane.

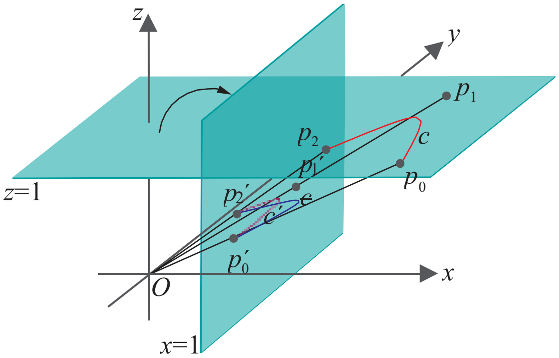

Figure 20.9: The (red) quadratic polynomial Bézier curve c on the $z = 1$ plane is specified by the control points p_0, p_1 and p_2. The points p_0, p_1 and p_2 and the curve c project to the points p'_0, p'_1 and p'_2 and the (magenta) curve c', respectively, on the plane $x = 1$. The (blue) curve $\bar{c}$ is the polynomial Bézier approximation of p'_0, p'_1 and p'_2.

See Figure 20.9, where the control points p_0, p_1 and p_2 lie on the $z = 1$ plane, and the (red) quadratic polynomial Bézier curve c approximates them. The points p_0, p_1 and p_2 and the curve c are projected along lines toward the origin to the points $p^1{}_0$, $p^1{}_1$ and $p^1{}_3$ and the (magenta) curve c^1, respectively, on the plane $x = 1$. Therefore, c^1 is the snapshot transformation of c.

Is c^1 the polynomial Bézier curve approximating p^1_0, p^1_1 and p^1_3? No! That happens to be the different (blue) curve $\bar{c}$. Coding is believing . . ..

Experiment 20.5. Run turnFilmBezier.cpp, which animates the snapshot transformation of a polynomial Bézier curve described above. Three control points and their magenta approximating polynomial Bézier curve are initially drawn on the $z = 1$ plane. The locations of the control points, and so of their approximating curve as well, are *fixed* in world space and never change through the program.

Initially, the film lies along the $z = 1$ plane. Pressing the right arrow key rotates it toward the $x = 1$ plane, while pressing the left arrow key rotates it back. The film itself, of course, is never seen. As the film turns, the control points and the magenta curve *appear* to move because what is drawn actually is their *projection* (snapshot transformations, particularly) onto the film at its current position. Also drawn on the film is a blue curve, which is the polynomial Bézier curve approximating the current projections of the control points.

Note: The control points and their approximating curve, all fixed on the $z = 1$ plane, corresponding to p_0, p_1 and p_2 and the red curve in Figure 20.9, are *not* drawn by the program – only their snapshot transformations on the turning film.

Initially, when the plane of the film coincides with that on which the control points are drawn, viz., $z = 1$, the projection onto the film of the polynomial Bézier curve approximating the control points (the magenta curve) coincides with the polynomial Bézier curve approximating the projected control points (the blue curve). This is to be expected because the control points coincide with their projections. See Figure 20.10(a) for the initial configuration where the blue curve actually overwrites the magenta one as it comes later in code.

However, as the film turns away from the $z = 1$ plane, the magenta and blue curves begin to separate. Their final configuration, when the film lies along $x = 1$, is shown in Figure 20.10(b). There is more functionality to the program that we'll discuss momentarily.
End

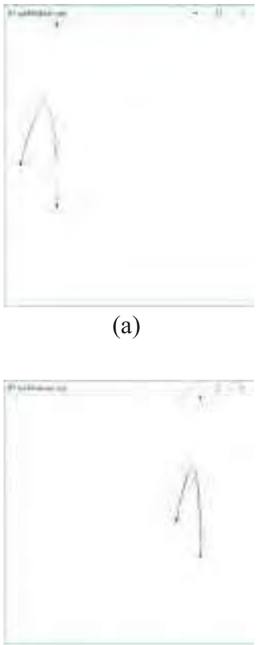
(a)

(b)

Figure 20.10: Screenshots of turnFilmBezier.cpp: (a) Initial configuration (b) Final configuration.

So, if the snapshot transformation c' of the approximating polynomial Bézier curve (the magenta curve of turnFilmBezier.cpp) is not the polynomial Bézier curve $\overline{c}$ approximating the transformed control points (the blue curve), then what is it?

It's not hard to deduce the answer by comparing the earlier Figure 20.5 with Figure 20.9. Imagine the plane $z = 1$ of the former figure replaced by $x = 1$ of the latter. Accordingly, points p_0, p_1 and p_2 of Figure 20.9 are liftings of their respective projections p'_0, p'_1 and p'_2 on $x = 1$, the weights associated with the latter three being the respective *x-values* of the first three.

Conclusion: the snapshot transformation of the polynomial Bézier curve on the control points p_0, p_1 and p_2, from the plane $z = 1$ to $x = 1$, is not the polynomial Bézier curve approximating the projected control points p'_0, p'_1 and p'_2, but, rather, the rational Bézier curve approximating them, with the weight of p'_i equal to the x-value of p_i, $0 \le i \le 2$.

What about snapshot transforming an arbitrary rational Bézier curve, rather than a polynomial one? Exactly the same principle applies. The result is a rational Bézier curve approximating the transformed control points, with *new* weights.

Figure 20.11 explains how the new weights are calculated in the simple case of transforming from $z = 1$ to $x = 1$. If the control point p on the $z = 1$ plane is $[x\ y\ 1]^T$ with weight w, then its lifted control point P in $\mathbb{R}^3$ is $[wx\ wy\ w]^T$. The projection of p, as that of P, on $x = 1$ is the point $p' = [1\ y/x\ 1/x]^T$. Therefore, the weight of p' so that its lifting coincides with P is wx.

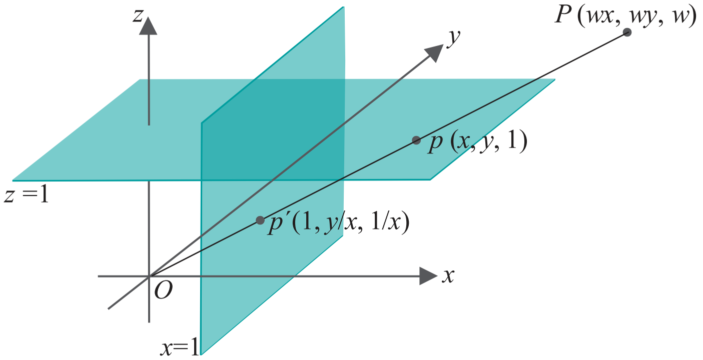

Figure 20.11: Both the control point p on $z = 1$, with weight w, and its lifting P project to the point p' on $x = 1$.

Suppose, now, that c is the rational Bézier curve approximating $n + 1$ control points $[x_i\ y_i\ 1]^T$ on the plane $z = 1$, with weights w_i, $0 \le i \le n$. It follows that the snapshot transformation of c from $z = 1$ to $x = 1$ is the rational Bézier curve on the transformed control points $p'_i = [1\ y_i/x_i\ 1/x_i]^T$, with weights $w_i x_i$, $0 \le i \le n$.

Example 20.3. Compute the snapshot transformation onto the $x = 1$ plane of the rational Bézier curve c on the $z = 1$ plane with control points $[1\ -1\ 1]^T$, $[2\ 1\ 1]^T$ and $[4\ 3\ 1]^T$, and respective weights 0.5, 2.0 and 1.0.

Answer: From the preceding discussion the transformation of c onto the $x = 1$ plane is the rational Bezier´curve with control points $[1\ -1\ 1]^T$, $[1\ 0.5\ 0.5]^T$ and $[1\ 0.75\ 0.25]^T$, and respective weights 0.5, 4 and 4.

Example 20.4. A polynomial Bézier curve c is drawn in 3-space with control points at $[2\ 2\ 5]^T$, $[3\ 1\ 4]^T$ and $[0\ 4\ 2]^T$. What is its projection on the $z = 1$ plane?

Answer: The projection of c on $z = 1$ is the rational Bézier curve with control points at $[0.4\ 0.4\ 1]^T$, $[0.75\ 0.25\ 1]^T$ and $[0\ 2\ 1]^T$, and respective weights 5, 4 and 2.

Exercise 20.16. Compute the snapshot transformation onto the $y = 1$ plane of the rational Bézier curve c on the $z = 1$ plane with control points at $[2\ 2\ 1]^T$, $[1\ 4\ 1]^T$ and $[5\ 1\ 1]^T$, and respective weights 1.0, 4.0 and 0.5.

Exercise 20.17. A polynomial Bézier curve c is drawn in 3-space with control points at $[4\ 1\ 5]^T$, $[2\ 2\ 3]^T$ and $[1\ 2\ 2]^T$. What is its projection on the $z = 1$ plane?

Experiment 20.6. Fire up turnFilmBezier.cpp once again. Pressing space at any time draws, instead of the blue curve, the green *rational* Bézier curve approximating the projected control points on the current plane of the film. The control point weights of the green curve are computed according to the strategy just described.

And, one sees: the green rational curve and the magenta projected curve are inseparable, though only the green one is visible because it overwrites the magenta. End

Exercise 20.18. (Programming) Verify that turnFilmBezier.cpp does as just claimed. In particular, check that the weights of the projected control points used to draw the green curve are correctly calculated as the new weights following a snapshot transformation.

Hint: The code is a little tricky as the projection of the control points on the turning film are computed "by hand", via the routine computeProjectedControlPoints(). What this routine does, in fact, is simulate the rotation of the film clockwise about the y-axis by computing the projection of the control points on the plane $z = 1$, after rotating the control points *counter-clockwise* about the y-axis (but leaving the film fixed). For this reason, the first viewing transformation, which is used to turn the film, is not applied to the projected control points, but rather a second one keeping the camera pointed at the $z = 1$ plane.

The routine computeWeightedProjectedControlPoints() assigns the new weights to the projected control points that then are used to draw the green curve.

Let's pause a moment to take stock. A snapshot transformation of a polynomial Bézier curve may not even be a polynomial Bézier curve. However, that of a rational Bézier curve is not only a rational Bézier curve, but the control points of the transformed curve are transformations of the original control points. Moreover, their new weights can be computed from values of the original weights and original control points. We call this property the *snapshot invariance* of rational Bézier curves.

In fact, rational Bézier curves are *projectively invariant*:

Proposition 20.2. *Applying a projective transformation of* $\mathbb{P}^2$ *to a rational Bézier curve in* $\mathbb{R}^2$ *gives another rational Bézier curve in* $\mathbb{R}^2$ *whose control points are the transformations of the original control points, with altered weights which can be computed from the values of the original weights and original control points.*

Proof. Again, do keep in mind that a projective transformation acts on a curve in $\mathbb{R}^2$ by transforming its lifting (which belongs to $\mathbb{P}^2$). The proof of the proposition, though not difficult, involves a fair amount of algebraic manipulation which we'll not get into. The mathematically inclined reader should try to prove it for herself. Otherwise, refer to Piegl and Tiller [113].

Projective invariance versus only affine: *make that 3-0 in favor of the rationals then*!

In Exercise 20.14 we deduced the affine invariance of rational Bézier curves as a consequence of the partition-of-unity property of their blending functions. It's also a consequence of the preceding proposition because affine transformations are a subclass of the projective.

Exercise 20.19. Prove that an affine transformation of a rational Bézier curve in $\mathbb{R}^2$ does not alter its weights.

Exercise 20.20. Find the flaw in the following argument: "Rational Bézier curves are projectively invariant. Polynomial Bézier curves are special cases of rational Bézier curves with weights all equal. Therefore, polynomial Bézier curves are projectively invariant as well."

Recall that a projective transformation can map a regular point to a point at infinity (and vice versa). In fact, one may even contemplate control points of a Bézier curve at infinity! Here's an interesting application to obtain a very familiar curve as a rational Bézier curve with one control point indeed at infinity:

Exercise 20.21. Embed $\mathbb{R}^2$ in $\mathbb{P}^2$ as the plane $z = 1$. Prove that the polynomial Bézier curve in $\mathbb{P}^2$ with control points $[1\ 0\ 1]^T$, $[0\ 1\ 0]^T$ and $[-1\ 0\ 1]^T$ projects to the upper-half of the unit circle centered at the origin of $\mathbb{R}^2$. Observe that the middle control point is at infinity with respect to $z = 1$. (To be fair though, as explained in Remark 20.6, we're effectively projecting from $\mathbb{R}^3$ to $\mathbb{R}^2$.)

20.2.6 Rational Bézier Curves in the Real World

Except for Exercise 20.10, our discussion thus far in this section has been exclusively of rational Bézier curves on the plane. Extension to curves in 3-space, however, is straightforward. For example, Equation (20.12)

$$c(u) = \left[\frac{\sum_{i=0}^{n} B_{i,n}(u) w_i x_i}{\sum_{i=0}^{n} B_{i,n}(u) w_i} \quad \frac{\sum_{i=0}^{n} B_{i,n}(u) w_i y_i}{\sum_{i=0}^{n} B_{i,n}(u) w_i} \quad \frac{\sum_{i=0}^{n} B_{i,n}(u) w_i z_i}{\sum_{i=0}^{n} B_{i,n}(u) w_i} \right]^T$$

$0 \le u \le 1$, of a rational Bézier curve in $\mathbb{R}^3$ approximating the control points $[x_i\ y_i\ z_i]^T$, with respective weights w_i, $0 \le i \le n$, which the reader was asked to deduce in Exercise 20.10, adds the expected z-component to its 2D counterpart (20.10)

$$c(u) = \left[\frac{\sum_{i=0}^{n} B_{i,n}(u) w_i x_i}{\sum_{i=0}^{n} B_{i,n}(u) w_i} \quad \frac{\sum_{i=0}^{n} B_{i,n}(u) w_i y_i}{\sum_{i=0}^{n} B_{i,n}(u) w_i} \right]^T \qquad (0 \le u \le 1)$$

Exercise 20.22. Show that the projection of a rational 3D Bézier curve on any plane is a rational 2D Bézier curve.

Exercise 20.23. (Programming) Write a 3D version of rationalBezierCurve3.cpp of Experiment 20.4 with control points which can be moved in 3-space, and with changeable weights. Add functionality to rotate the viewpoint.

20.2.7 Rational Bézier Surfaces

With the spadework for rationalization mostly done, the step up from curves to rational Bézier surfaces is not going to be much more than a matter of jotting down successive equations with an eye still on curves.

Recall from Section 17.2 the equation

$$s(u, v) = \sum_{i=0}^{n} \sum_{j=0}^{m} B_{i,n}(u) B_{j,m}(v) p_{i,j} \qquad (0 \le u \le 1,\ 0 \le v \le 1) \tag{20.15}$$

of a polynomial Bézier surface in 3-space with control points $p_{i,j}$, for $0 \le i \le n$ and $0 \le j \le m$, and the process of "sweeping by a Bézier curve" by which it was derived.

Following a similar process, one can write the equation of a *rational Bézier surface* specified by control points $p_{i,j}$ with respective weights $w_{i,j}$, $0 \le i \le n$ and $0 \le j \le m$:

$$s(u, v) = \sum_{i=0}^{n} \sum_{j=0}^{m} \frac{B_{i,n}(u) B_{j,m}(v)\, w_i}{\sum_{i=0}^{n} \sum_{j=0}^{m} B_{i,n}(u) B_{j,m}(v)\, w_i}\, p_{i,j} \quad (0 \le u \le 1,\ 0 \le v \le 1) \tag{20.16}$$

From (20.15) to (20.16) the change is simply in the blending functions, now rational, rather than polynomial. We ask the reader next to determine equations for a rational Bézier surface in forms analogous to those that we have already deduced for curves.

Exercise 20.24. Find equations for rational Bézier surfaces in $\mathbb{R}^3$ analogous to Equations (20.6)-(20.11) for rational Bézier curves.

Exercise 20.25. State and solve analogues of Exercises 20.12-20.15 for surfaces.

It should come as no surprise to the reader that rational Bézier surfaces are projectively invariant and, therefore, affine and snapshot invariant as well. Moreover, they can represent exactly parts of paraboloids, ellipsoids and hyperboloids, and other quadric surfaces. From a designer's perspective, a control point's weight, similarly to the case of a rational Bézier curve, is an additional dial to turn up or down its attractive pull on the surface without having to move it.

All the advantages of rational Bézier curves over polynomial propagate, therefore, to rational Bézier surfaces.

Drawing Rational Bézier Surfaces

As expected, the main change in drawing polynomial versus rational Bézier surfaces, as we saw in Section 20.2.2 going from polynomial to rational Bézier curves, is replacing "VERTEX_3" with "VERTEX_4" to include the extra weight parameter w, in addition to x, y and z, per control point.

Experiment 20.7. Run rationalBezierSurface.cpp, based on bezierSurface.cpp, which draws a rational Bézier surface with the functionality that the location and weight of each control point can be changed. Press the space and tab keys to select a control point. Use the arrow and page up/down keys to translate the selected control point. Press '</>' to change its weight. Press delete to reset. The 'x/X', 'y/Y' and 'z/Z' keys turn the viewpoint. Figure 20.12 is a screenshot.

Mark the use of glMap2f(GL_MAP2_VERTEX_4, . . .), as also of glEnable(GL_MAP2_VERTEX_4). The 2's in the syntax are for a surface. End

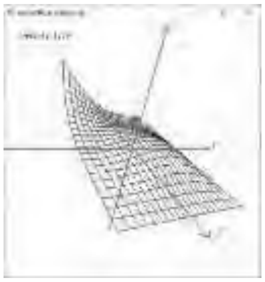

Figure 20.12: Screenshot of rationalBezierSurface.cpp.

20.2.8 The 'R' in NURBS

With all the groundwork laid in rational Bézier theory, putting the 'R' now into NURBS (Non-Uniform Rational B-Splines) is going to be rather anti-climactic.

Recall Equation (18.36) of the mth order B-spline curve c approximating $r-m+1$ control points $p_0, p_1, \ldots, p_{r-m}$ over the knot vector $\{t_0, t_1, \ldots, t_r\}$:

$$c(u) = \sum_{i=0}^{r-m} N_{i,m}(u)p_i \qquad (t_{m-1} \le u \le t_{r-m+1}) \tag{20.17}$$

where the blending function of the ith control point is the mth order B-spline function $N_{i,m}$, $0 \le i \le r-m$.

Following a development *exactly parallel* to that for rational Bézier curves, one can write for a NURBS curve an equation analogous to (20.14), which expresses a rational Bézier curve as a weighted sum of its control points, the weights being rational blending functions. In fact, the equation for a NURBS curve approximating $r-m+1$ control points p_i, with weights w_i, $0 \le i \le r-m$, over the knot vector $\{t_0, t_1, \ldots, t_r\}$, is

$$c(u) = \sum_{i=0}^{r-m} \frac{N_{i,m}(u)w_i}{\sum_{i=0}^{r-m} N_{i,m}(u)w_i} p_i \qquad (t_{m-1} \le u \le t_{r-m+1}) \tag{20.18}$$

where, of course, the blending functions are now ratios of terms composed of B-splines.

We'll leave finding the equation of a NURBS surface to the reader in the following exercise.

Exercise 20.26. Recall Equation (18.38) of a B-spline surface approximating an $(n + 1) \times (n^1 + 1)$ array of control points over a pair of non-uniform knot vectors. Rewrite it for a NURBS surface, taking into account control point weights. What is the blending function of the control point $p_{i,j}$, $0 \leq i \leq n$, $0 \leq j \leq n^1$?

Exercise 20.27. Prove that NURBS curves and surfaces are affinely invariant. (In fact, they are projectively invariant.)
Hint: Think partition of unity.

Drawing NURBS Curves and Surfaces

The reader may wish to review Section 18.4 where the GLU NURBS interface is explained and used to draw polynomial B-spline curves and surfaces. With the practicalities of the transition from drawing polynomial Bézier primitives to rational ones already learned from earlier in this chapter, those for drawing rational NURBS primitives are straightforward and left to the reader. The following two exercises ask her to apply the NURBS interface to draw a rational curve and a rational surface, respectively.

Exercise 20.28. (Programming) Modify cubicSplineCurve1.cpp of Experiment 18.6 to draw a cubic NURBS curve so that the weight of the selected control point can be changed, in addition to all the original functionality. You must use the call gluNurbsCurve(GL MAP1 VERTEX 4, . . .).

Exercise 20.29. (Programming) Modify bicubicSplineSurface.cpp of Experiment 18.14 to draw a NURBS surface.

20.3 Summary, Notes and More Reading

In this chapter we studied two extremely important applications of projective spaces to CG: (a) the projection transformation to convert a viewing volume into the canonical box in the synthetic-camera pipeline, and (b) rational Bézier and B-spline theory. The first demonstrates the practical importance of projective geometry in the CG rendering pipeline. The second application is important for a deeper understanding of design because rational primitives, in particular NURBS, are the de facto standard in CAD.

There are several excellent sources for the reader to follow up on both rational Bézier and NURBS primitives. A few are the books by Buss [21], Farin [45, 46], Mortenson [97], Piegl & Tiller [113] and Rogers [118].

Part XI

Time for a Pipe

Chapter 21

Pipeline Operation

At the end of Chapter 4 about moving and shaping objects and manipulating the OpenGL camera, we said that it was like having gotten our animator's driver's license. It's time now to look under the hood to understand the whole process, from ignition to motion. So, this chapter is about graphics rendering pipelines – processes that transform a user-defined scene into an image on a raster display.

To avoid inessential complexity, we limit ourselves here to fixed-function pipelines where, once the programmer has specified the scene, she has little further say in the rendering process. OpenGL's synthetic-camera pipeline in its pre-shader (i.e., pre-programmable) form falls in this category. The basic ray tracing pipeline, based on a global illumination model – versus a local one in the case of the synthetic camera – is fixed-function as well, as is radiosity, another global illumination model often implemented in tandem with ray tracing.

We begin in Section 21.1 with the fixed-function synthetic-camera pipeline. Our description of this particular pipeline began, in fact, with the shoot-and-print analogy of Chapter 2. We'll put all the pieces together now to get a fairly complete idea of its implementation.

Section 21.2 introduces ray tracing, the most popular global illumination model and its rendering pipeline. As its name suggests, ray tracing is based upon following individual light rays through a scene. It is a near photorealistic way of rendering, but computationally so expensive as to be almost never used in real-time applications such as games. For off-line applications, though, e.g., movies, where computational resources and time are not major constraints, ray tracing is far more authentic an alternative to synthetic-camera-based rendering.

Radiosity, another global lighting model and the topic of Section 21.3, is frequently implemented together with ray tracing, as the two have complementary models of light transport. We conclude in Section 21.4.

21.1 Synthetic-Camera Pipeline

Happily, we're in a position at this time to put together, with pieces learned so far in this book, a fairly complete synthetic-camera rendering pipeline. Let's see.

As the program executes modelview transformations are applied first to objects in the scene. Chapters 4 and 5 explained the process, modelview transformations, represented each by a 4×4 matrix, being composed by multiplication and, finally, transforming a vertex, represented in $xyzw$-coordinates by a 4×1 column matrix, by multiplying it from the left. Next, the scene is "captured on film" by applying the shoot-and-print paradigm described in the first part of Chapter 2, where primitives are projected to the front face of the viewing box or frustum (shoot) and then scaled to fit the OpenGL window (print).

In Section 20.1 we saw that the shoot process itself is implemented in two stages. First comes a projection transformation mapping the viewing volume to the canonical viewing box, this transformation consisting of multiplying the vertices in homogeneous $xyzw$-coordinates by the projection matrix, followed, possibly, by a perspective division step to divide out the w-value. The next stage is a parallel projection to the canonical box's back plane of the parts of primitives *inside* it, because only these are rendered to the screen.

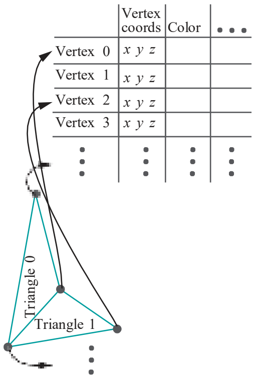

Figure 21.1: Logical representation of data using vertex arrays (adapted from Figure 3.5).

Implicit between the first and second stages, then, is a *primitive assembly* step where the program's points, lines and triangles, particularly the vertices of each, are defined from its code. E.g., a glDrawElements(GL TRIANGLES, . . .) statement defines a sequence of triangles in terms of their vertices in a manner logically represented by Figure 21.1.

Implicit in the second stage is the clipping of primitives to within the canonical box. This can be accomplished for 1D and 2D primitives, respectively, with use of the Cohen-Sutherland line clipper from Section 14.1 (particularly its extension to 3-space suggested in Exercise 14.5) and the Sutherland-Hodgman polygon clipper from Section 14.2 (Exercise 14.11 suggests the 3-space version). Note that clipping 0D primitives, i.e., points, is a trivial matter of tossing those whose coordinates place them outside the canonical box.

The last print step, where the back face of the canonical box is rendered to (or, "scaled to fit") the OpenGL window, involves choosing and coloring a set of pixels in the latter for each primitive on the former, which, of course, is the process of rasterization. Again, 0D primitives, or points, are easily rasterized, though one must keep in mind the discussion in Section 13.4 of why their shape on the screen is unaffected by translation and rotation; further, 1D and 2D primitives can be processed with the use, respectively, of the line and polygon rasterizers from Sections 14.3 and 14.4 (enhanced – we'll see how – to compute the color of chosen pixels). Just prior to rasterization, depth testing may be invoked to decide which part, if any, of a primitive is obscured by others, in which case this part is not allowed to colorize its corresponding pixels.

That's it. This is enough to give us a skeletal code-to-image pipeline. Texture, lighting and other features can come in later. Let's keep it simple to start with.

21.1.1 Pipeline: Preliminary Version

Time now for specifics. Let's follow a vertex – obviously part of the definition of a geometric primitive – given in homogeneous coordinates, down a simple pipeline which follows the strategy outlined above (a description of each stage is in italics just below it; see also the notes after the pipeline):

Synthetic-camera Rendering Pipeline (Preliminary Version)

1. $[x\ y\ z\ 1]^T$ $\dashrightarrow$ $[x^M\ \ y^M\ \ z^M\ \ 1]^T$
Modelview transformation = multiplication by the modelview matrix.

2. $\dashrightarrow$ $[x^{PM}\ \ y^{PM}\ \ z^{PM}\ \ w^{PM}]^T$
Multiplication by the projection matrix.

3. $\dashrightarrow$ $\left[\frac{x^{PM}}{w^{PM}}\ \ \frac{y^{PM}}{w^{PM}}\ \ \frac{z^{PM}}{w^{PM}}\right]^T$
Perspective division.

4. $\dashrightarrow$ Primitive Assembly
Defining points, lines and triangles.

5. $\longrightarrow$ $\begin{bmatrix}\frac{x^{PM}}{w^{PM}} & \frac{y^{PM}}{w^{PM}} & \frac{z^{PM}}{w^{PM}}\end{bmatrix}^T$
Clipping to the canonical box.

6. $\longrightarrow$ $\begin{bmatrix}\frac{x^{PM}}{w^{PM}} & \frac{y^{PM}}{w^{PM}}\end{bmatrix}^T$
Projection to the back of the canonical box
(z-values possibly retained for depth testing).

7. $\longrightarrow$ $[i\ j]^T$
Rasterization.

Notes:

(i) Superscripts indicate the transforming matrix, e.g., $[x^M\ y^M\ z^M\ 1]^T = M[x\ y\ z\ 1]^T$. Notation: M = modelview and P = projection.

(ii) Multiplication by the projection matrix P (Stage 2) followed by perspective division (Stage 3) equals the projection transformation of Section 20.1, which transforms the viewing volume into the canonical viewing box.

(iii) Perspective division (Stage 3) is a non-operation in the case of a glOrtho()-defined viewing box, as w^{PM} are all 1.

(iv) All the x-, y-, z- and w-values, with or without superscripts, are floating points up to and including Stage 6. It's only at the final Stage 7 that the vertex "jumps" from $\mathbb{R}^2$ (precisely, the subset $[-1, 1] \times [-1, 1]$ on the back face of the canonical box) plus a depth z-value to a discrete $m \times n$ raster (in the frame buffer) plus the same z-value. In other words, save for the floating point z-value, it's at Stage 7 that a vertex goes from being an $[x\ y]^T$ *floating point* tuple to an $[i\ j]^T$ *integer* tuple.

(v) Color data, not shown, is transported with each vertex down the pipeline and used finally in rasterization (Stage 7).

Figure 21.2 is a pictorial view of the passage of a rectangular box through the pipeline. This barebones pipeline is *almost* good enough to render a simple colored image – there are two significant technicalities, though, still to deal with in order to ensure its correct operation. First is the problem of handling zero w-values in the perspective division of Stage 3; the next is the issue of so-called perspective correction needed to be taken into account when colorizing a raster primitive in Stage 7. The next two subsections discuss these two technicalities, respectively. *Both are fairly mathematical, so if you are not so inclined skip to Section 21.1.4, taking the revised pipeline there for granted.*

21.1.2 Perspective Division by Zero

You may need to review Section 20.1 as our discussion here is a follow-on of the account in that section of the projection transformation.

Perspective division in Stage 3 of the pipeline could involve division by zero. Prima facie, however, this appears to be not much of a problem because the canonical box, into which the viewing volume is transformed by multiplication by the projection matrix, consists only of regular points (with respect to $w = 1$). Therefore, a point that's mapped to a point at infinity – with w-value 0 and, hence, outside the canonical box – never belonged to the viewing volume in the first place. So it seems all we have to do is add a filter before the perspective division stage to simply eject points with w-value equal to 0. Unfortunately, the problem is a bit more complicated, as the following experiment indicates.

Experiment 21.1. Replace the box glutWireCube(5.0) of box.cpp of Chapter 4 with the line segment

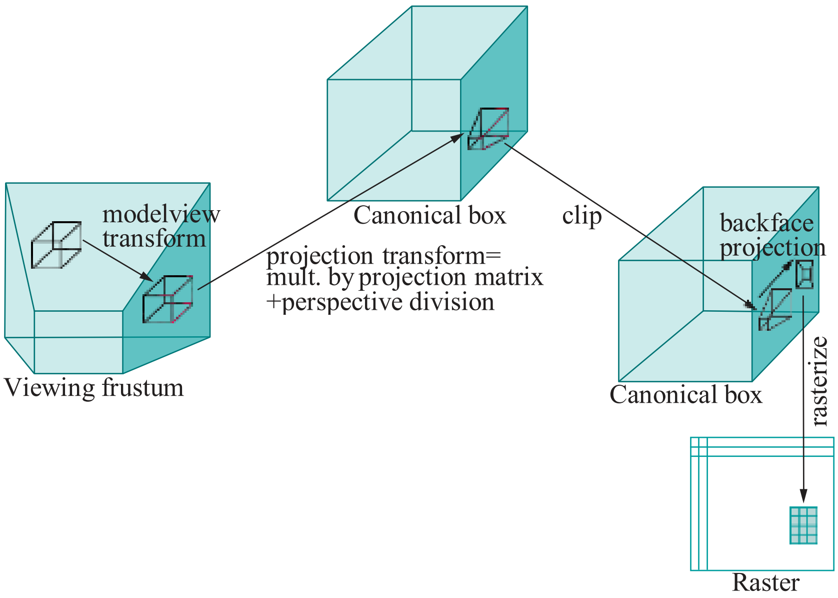

Figure 21.2: Rectangular box passing through a synthetic-camera rendering pipeline: the red part of the box is outside the viewing frustum; the corresponding transformed part is outside the canonical box, so clipped; the box is skewed by the projection transform.

Figure 21.3: Screenshot of Experiment 21.1.

```
glBegin(GL_LINES);
   glVertex3f(1.0, 0.0, -10.0);
   glVertex3f(1.0, 0.0, 0.0);
glEnd();
```

and delete the glTranslatef(0.0, 0.0, -15.0) statement.

You see a short segment, the clipped part of the defined line segment, whose first endpoint $[1\ 0\ -10]^T$ is inside the viewing frustum defined by the program's projection statement glFrustum(-5.0, 5.0, -5.0, 5.0, 5.0, 100.0), while the second $[1\ 0\ 0]^T$ is outside (as is easily checked). Figure 21.3 is a screenshot. End

Here's what's interesting though about the experiment – the second endpoint of the drawn segment is mapped to a point at infinity by multiplication by OpenGL's projection matrix! This is easy to verify. Simply take the dot product of $[0\ 0\ -1\ 0]$, which is the last row of the projection matrix corresponding to glFrustum(-5.0, 5.0, -5.0, 5.0, 5.0, 100.0) as given by Equation (20.4), and $[1\ 0\ 0\ 1]$, the homogeneous coordinates of the second endpoint, to find that the endpoint's transformed w-value is 0 (the other coordinate values are irrelevant).

The conclusion from this experiment is that even though vertices that map to infinity don't belong in the viewing volume, they may be corners of primitives which partially do. So we just can't toss them – we'll have to make sure that the primitives they belong to are handed off correctly to the next stage of the pipeline. This requires a little care.

It's convenient at this time to climb a dimension down to 2D to visualize the right strategy, so we'll operate on a plane for the rest of the section.

Note: If you have not yet read Appendix A on projective spaces and transformations, then simply take the following transformation for granted.

Example A.16 of Appendix A shows that the projective transformation h^M of $\mathbf{P}^2$ given by

$$M = \begin{bmatrix} -1/2 & 0 & 0 \\ 0 & -3/2 & 1 \\ 0 & -1/2 & 0 \end{bmatrix}$$

transforms the trapezoid q on the plane $z = 1$, aka R^2, with vertices at

$$[-1\ 1]^T,\ [1\ 1]^T,\ [2\ 2]^T \text{ and } [-2\ 2]^T$$

to the rectangle q^1 with vertices at

$$[-1\ 1]^T,\ [1\ 1]^T,\ [1\ 2]^T \text{ and } [-1\ 2]^T$$

this being precisely the 2D analogue of transforming a frustum to a box – instead of a frustum we now have a trapezoid and instead of a box a rectangle. See Figure 21.4.

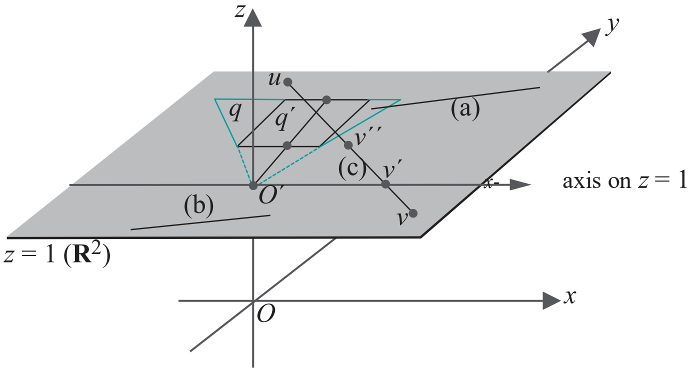

Figure 21.4: The synthetic camera in Flatland: the point camera is at O^1, the "viewing trapezoid" is q, the "canonical rectangle" q^1.

Note: Keep in mind that h^M maps the plane point $[x\ y]^T$ to the one on the plane $z = 1$ with homogeneous coordinates $M\ [x\ y\ 1]^T$. For example, to determine $h^M([-1\ 1]^T)$, we compute $M\ [-1\ 1\ 1]^T = [1/2\ -\ 1/2\ -\ 1/2]^T$. Dividing the latter through by its z-value, and then dropping the z-value, we see that $h^M([-1\ 1]^T) = [-1\ 1]^T$.

Let's see how to deal with a line segment primitive, say uv, on R^2, subject to transformation by h^M, and subsequent clipping to the "canonical" rectangle q^1. Exercise A.29 of Appendix A tells us the nature of $h^M(uv)$. It is either a segment (if no point of uv maps to a point at infinity) or two semi-infinite segments (if an interior point maps to infinity) or one semi-infinite segment (if one endpoint maps to infinity) or empty (if both endpoints map to infinity).

It's checked easily that points of the plane mapped by h^M to points at infinity are precisely those on the x-axis. Here, then, is how to clip $h^M(uv)$ to the canonical rectangle – assumed available is a Cohen-Sutherland line clipper for this rectangle with the additional ability to clip semi-infinite segments *a la* Exercise 14.4. The three cases that may arise are listed below, for each an example segment correspondingly labeled drawn in Figure 21.4.

(a) Both u and v are above the x-axis (i.e., with positive y-values):

Pass the transformed segment $h^M(u)h^M(v)$ to the clipper. Note that the transformed segment itself is not drawn in the figure.

(b) Both u and v are below or on the x-axis:

Pre-clip uv altogether as it doesn't intersect the viewing trapezoid.

(c) One endpoint, say u, is above the x-axis and the other endpoint v is on or below:

Determine the point v^1 of intersection of uv with the x-axis. Pass the image $h^M(uv^1)$, which is a semi-infinite segment, to the clipper (even if v is below the x-axis, the image of v^1v, another semi-infinite segment, cannot intersect the trapezoid and need not be transmitted).

Note: If the clipper has been extended to handle semi-infinite segments in the manner suggested in Exercise 14.4, then it will need as input the finite endpoint of $h^M(uv^1)$, as well as the direction in which it is infinite. The finite endpoint is, of course, $h^M(u)$, while the direction it is infinite is toward $h^M(v^{11})$, where v^{11} is any point between u and v^1, e.g., the midpoint. Mind that the enhanced clipper of Exercise 14.4 asks for a finite point in the direction of which $h^M(uv^1)$ is infinite, so cannot be given $h^M(v^1)$ as input.

Exercise 21.1. Determine what is transmitted to the extended clipper in the 2D scenario above in the following cases.

(1) $u = [0\ 2]^T$ and $v = [3\ \ 1]^T$

(2) $u = [0\ -\ 2]^T$and $v = [3\ 0]^T$

(3) $u = [0\ 2]^T$ and $v = [3\ -\ 1]^T$

Part answer:

(3) Here, u is above and v below the x-axis, so we are in case (c) above. The point where uv intersects the x-axis is $v^1 = [2\ 0]^T$. Take v^{11} to be the midpoint $[1\ 1]^T$ of uv^1.

Therefore, passed to the extended clipper is a semi-infinite segment which has a finite end at the point on $z = 1$ with homogeneous coordinates

$$h^M(u) = \begin{bmatrix} -1/2 & 0 & 0 \\ 0 & -3/2 & 1 \\ 0 & -1/2 & 0 \end{bmatrix} [0\ 2\ 1]^T = [0\ \ -2\ \ -2]^T$$

and is infinite toward the point on $z = 1$ with homogeneous coordinates

$$h^M(v^{11}) = \begin{bmatrix} -1/2 & 0 & 0 \\ 0 & -3/2 & 1 \\ 0 & -1/2 & 0 \end{bmatrix} [1\ 1\ 1]^T = [-\frac{1}{2}\ \ -\frac{1}{2}\ \ -\frac{1}{2}]^T$$

One sees, therefore, that the segment passed to the clipper has a finite end at $[0\ 1]^T$ and is infinite toward $[1\ 1]^T$.

We're going to leave it at this, hoping the reader is convinced that the technique just described to handle vertices, which otherwise lead to perspective division by zero, can be implemented, even in 3D, by appropriately enhancing Stage 3 of the seven-stage synthetic-camera rendering pipeline. A point to note is that, as our application of the technique to line segments in 2D showed, its output is a clipped primitive which, in fact, can be handed off to Stage 6. The reason is that, even though we describe the technique as an enhancement of Stage 3, it needs and implicitly reads the geometric data for primitive assembly (Stage 4), and, of course, it clips (Stage 5) as well.

21.1.3 Rasterization with Perspectively Correct Interpolation

Rasterization is more than a matter of plugging in Bresenham's rasterizer for lines and the scan-based rasterizer for polygons (Sections 14.3 and 14.4, respectively). The reason is that both these rasterizing algorithms choose the pixels comprising a primitive but say nothing about how to color them.

However, coloring the pixels of a rasterized primitive seems merely a question of linearly interpolating the values specified at its vertices through its interior. It really ought to be since we made such a fuss in Chapter 7 about how nice are points, line segments and triangles – the fundamental primitives of OpenGL – because values at their vertices can, in fact, be unambiguously interpolated through their interiors. Well, it is, pretty much, *except* . . .

Experiment 21.2. Run perspectiveCorrection.cpp. You see a thick straight line segment which starts at a red vertex at its left and ends at a green one at its right. Also seen is a big point just above the line, which can be slid along it by pressing the left/right arrow keys. The point's color can be changed, as well, between red and green by pressing the up/down arrow keys. Figure 21.5 is a screenshot.

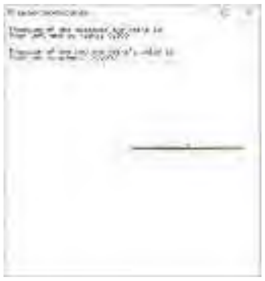

Figure 21.5: Screenshot of perspective-Correction.cpp.

The color-tuple of the segment's left vertex, as you can verify in the code, is $(1.0, 0.0, 0.0)$, a pure red, while that of the right is $(0.0, 1.0, 0.0)$, a pure green. As expected by interpolation, therefore, there is a color transition from red at the left end of the segment to green at its right.

The number at the topmost right of the display indicates the fraction of the way the big movable point is from the left vertex of the segment to the right. The number below it indicates the fraction of the "way" its color is from red to green – precisely, if the value is u then the color of the point is $(1-u, u, 0)$.

Initially, the point is at the left and a pure red; in other words, it is 0 distance from the left end, and its color 0 distance from red. Change both values to 0.5 – the color of the point does *not* match that of the segment below it any more. It seems, therefore, that the midpoint of the line is not colored $(0.5, 0.5, 0.0)$, which is the color of the point. Shouldn't it be so, though, by linear interpolation, as it is half-way between two end vertices colored $(1.0, 0.0, 0.0)$ and $(0.0, 1.0, 0.0)$, respectively? End

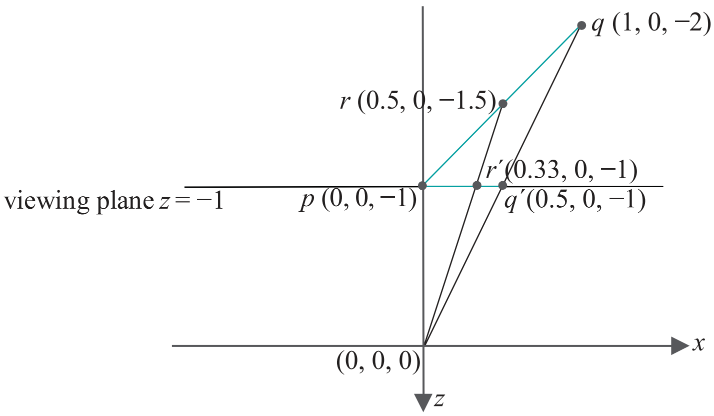

Figure 21.6: The line segment drawn in perspectiveCorrection.cpp is pq and its projection on the viewing face pq^1.

The apparent conundrum of the preceding experiment is not hard to resolve. Figure 21.6, an xz-section of world space, shows what's happening. The line segment drawn in perspectiveCorrection.cpp is from $p = [0\ 0\ -1]^T$ to $q = [1\ 0\ -2]^T$, as specified in the drawScene() routine. The midpoint of pq is $r = [0.5\ 0 -1.5]^T$. Moreover, the perspective projections – note that the viewing volume specified in resize() is a frustum – of p, q and r on the viewing plane $z = -1$ are p itself, q^1 and r^1, respectively. The coordinates shown in the figure of q^1 and r^1 can be easily verified by properties of similar triangles.

One sees, then, that r^1, the projection of the midpoint of the segment pq, is *not* the midpoint of the projected segment pq^1, but rather approximately 0.66 (= 0.33/0.5) of the way from its left end p. With this in mind, return to the program to set the color fraction of the movable point to 0.5 and its distance fraction to 0.66 – now you see a color match with the point of the segment below it. If perspective projections preserved convex combinations, like linear transformations do, then midpoints would map to midpoints, but, unfortunately, as we have just found out, they do not.

The conclusion, then, is that the colors at its endpoints *are* linearly interpolated along the user-specified line segment, which is a virtual object in world space; however, as perspective projection does not preserve convex combination, colors of the projected endpoints *are not* linearly interpolated through the segment drawn on screen.

We understand the issue now, so let's square it with our rasterization procedure by incorporating an additional *perspective correction* factor.

A point $p = [p_x \; p_y \; p_z]^T$ in a given viewing frustum is mapped by projection transformation to the point $p^1 = [p^1_x \; p^1_y p^1_z]^T$ in the canonical viewing box; parallel projection to the back face of the box then maps p^1 to $p = [p^1{}_x \, p^1{}_y]^T$. See Figure 21.7(a).

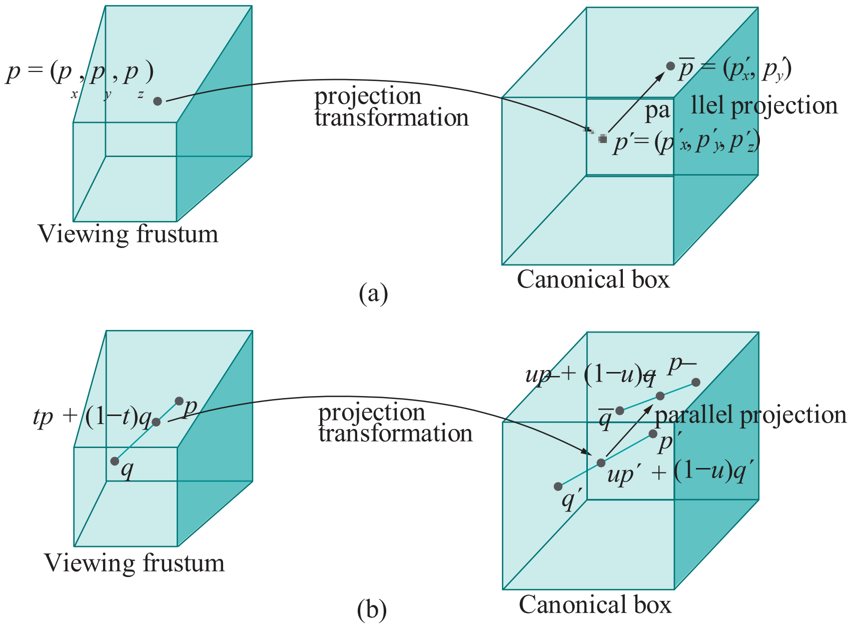

Figure 21.7: (a) A point is mapped by the projection transformation from a viewing frustum to the canonical viewing box, followed by parallel projection to the latter's back face. (b) Likewise for a line segment: the projection transformation does not preserve convex combinations, but parallel projection does.

Moreover, a point $tp + (1-t)q$ on the segment joining two points p and q in the frustum maps to a point $up^1 + (1-u)q^1$ on the segment joining their respective images p^1 and q^1 in the box, though, as we understand now, not necessarily does $u = t$. See Figure 21.7(b).

We want to find the function $u \rightarrow t$ giving the pre-image $tp + (1-t)q$ of $up^1 + (1 - u)q^1$. This will serve our purpose of perspective correction, for we'll color the point $u\overline{p} + (1-u)\overline{q}$ – identifying the box's back face with the raster – with the color values $tC(\overline{p}) + (1-t)C(\overline{q})$, instead of $uC(\overline{p}) + (1-u)C(\overline{q})$ as in the case of uncorrected interpolation. $C(\overline{p}) = C(p)$ and $C(\overline{q}) = C(q)$ are, of course, the programmer-specified colors at p and q, respectively. Observe that correction is required only for the projection transformation, not the parallel projection to the back face of the canonical box, as the latter is a linear map preserving convex combinations.

Finding the function $u \rightarrow t$ is a matter of some calculation. Write $p = [p_x \; p_y \; p_z]^T$ in homogeneous coordinates as $[p \; 1]^T = [p_x \; p_y \; p_z \; 1]^T$ and q as $[q \; 1]^T = [q_x \; q_y \; q_z \; 1]^T$. Let P be the projection matrix. Denote the results of multiplying $[p \; 1]^T$ and $[q \; 1]^T$ by P as follows:

$$P[p \; 1]^T = [p^*_x \; p^*_y \; p^*_z \; -p_z]^T \qquad \text{and} \qquad P[q \; 1]^T = [q^*_x \; q^*_y \; q^*_z \; -q_z]^T \tag{21.1}$$

where the starred symbols are variables to be determined, while the two w-values on the RHS's follow because the last row of the projection matrix P is always $[0 \; 0 \; -1 \; 0]$ (see Equation (20.4)). Applying perspective division, denoted D, next, we have

$$DP[p \; 1]^T = [-\frac{p^*_x}{p_z} \quad -\frac{p^*_y}{p_z} \quad -\frac{p^*_z}{p_z} \quad 1]^T = [p^1{}_x \; p^1{}_y \; p^1{}_z \; 1]^T = [p^1 \; 1]^T$$

and

$$DP[q\ 1]^T = [-\frac{q^*_x}{q_z}\quad -\frac{q^*_y}{q_z}\quad -\frac{q^*_z}{q_z}\quad 1]^T = [q^1_x\ q^1_y\ q^1_z\ 1]^T = [q^1\ 1]^T$$

where the second equality in both equations above follows because DP, in fact, is the projection transformation mapping p to p^1 and q to q^1. The preceding two equations imply that

$$p^*_x = -p_z p^1_x,\ p^*_y = -p_z p^1_y,\ p^*_z = -p_z p^1_z,\ q^*_x = -q_z q^1_x,\ q^*_y = -q_z q^1_y,\ q^*_z = -q_z q^1_z \qquad (21.2)$$

Consider, next, an interpolated point $tp + (1 - t)q$ between p and q. Multiplying it by P:

$$\begin{aligned}
& P\,[tp + (1-t)q \quad 1]^T \\
&= P\,(\,t[p\ 1]^T + (1-t)\,[q\ 1]^T\,) \\
&= t(P\,[p\ 1]^T) + (1-t)\,(P\,[q\ 1]^T) \\
&= t[p^*_x\ p^*_y\ p^*_z\ \ -p_z]^T + (1-t)[q^*_x\ q^*_y\ q^*_z\ \ -q_z]^T \quad \text{(applying (21.1))} \\
&= [tp^*_x + (1-t)q^*_x\ \ tp^*_y + (1-t)q^*_y\ \ tp^*_z + (1-t)q^*_z\ \ -tp_z - (1-t)q_z]^T
\end{aligned}$$

Applying D by dividing through by the w-value:

$$\begin{aligned}
& DP\,[tp + (1-t)q \quad 1]^T \\
&= \left[-\frac{tp^*_x + (1-t)q^*_x}{tp_z + (1-t)q_z}\quad -\frac{tp^*_y + (1-t)q^*_y}{tp_z + (1-t)q_z}\quad -\frac{tp^*_z + (1-t)q^*_z}{tp_z + (1-t)q_z}\quad 1\right]^T \\
&= \left[\frac{tp_z p^1_x + (1-t)q_z q^1_x}{tp_z + (1-t)q_z}\quad \frac{tp_z p^1_y + (1-t)q_z q^1_y}{tp_z + (1-t)q_z}\quad \frac{tp_z p^1_z + (1-t)q_z q^1_z}{tp_z + (1-t)q_z}\quad 1\right]^T \\
& \quad \text{(using (21.2))} \\
&= \frac{tp_z}{tp_z + (1-t)q_z}[p^1_x\ p^1_y\ p^1_z\ 1]^T + \frac{(1-t)q_z}{tp_z + (1-t)q_z}[q^1_x\ q^1_y\ q^1_z\ 1]^T \\
&= \frac{tp_z}{tp_z + (1-t)q_z}[p^1\ 1]^T + \frac{(1-t)q_z}{tp_z + (1-t)q_z}[q^1\ 1]^T \\
&= u\,[p^1\ 1]^T + (1-u)\,[q^1\ 1]^T
\end{aligned}$$

where

$$u = \frac{tp_z}{tp_z + (1-t)q_z}$$

Inverting the preceding relationship gives the desired function $u \to t$:

$$\begin{aligned}
t &= \frac{uq_z}{(1-u)p_z + uq_z} \\
&= \frac{q_z}{(\frac{1}{u} - 1)p_z + q_z},\ \text{if } u > 0\,; \qquad 0,\ \text{if } u = 0
\end{aligned} \qquad (21.3)$$

Whew! But now we know exactly what to do: Referring back to Figure 21.7(b), we'll color the point $u\overline{p} + (1- u)\overline{q}$ with the color values $tC(\overline{p}) + (1- t)C(\overline{q})$, instead of $uC(\overline{p}) + (1 - u)C(\overline{q})$ as in the case of uncorrected interpolation, where t is given by the formula 21.3. This process is called *perspectively correct interpolation* or *linear interpolation with perspective correction*.

Here, then, is how to apply perspectively correct interpolation in coloring pixels along a line segment. Suppose the rasterization $R(S)$ – say by Bresenham's algorithm of Section 14.3 – of the line segment S joining the points $p = [p_x\ p_y\ p_z]^T$ and $q = [q_x\ q_y\ q_z]^T$ in the viewing frustum consists of $N + 1$ pixels in the raster, as depicted in Figure 21.8.

The end pixel of $R(S)$ corresponding to p is (i_1, j_1) and that to q is (i_2, j_2). Precisely, (i_1, j_1) is obtained from mapping p to $\overline{p}$ on the back face of the canonical

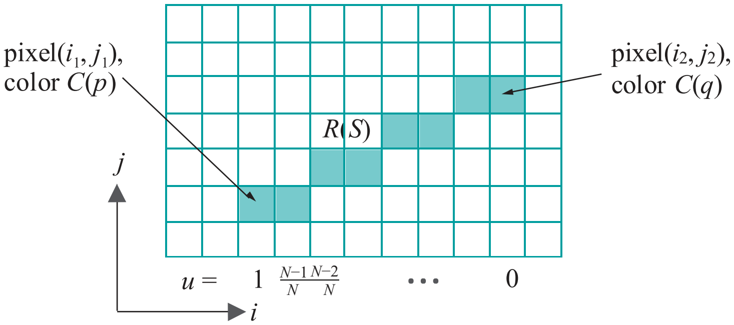

Figure 21.8: The rasterization $R(S)$ of a line segment S consists of $N + 1$ pixels, each corresponding to a particular u-value (a few u-values are shown vertically below the corresponding pixel).

box by projection transformation and parallel projection, followed by mapping $\bar{p}$ to a point on the raster by the scaling transformation matching the back face of the canonical box to the raster and, finally, a rounding to integer coordinates. Likewise, (i_2, j_2) is obtained from $\bar{q}$. Suppose, as well, that $R(S)$ makes an angle of at most 45° with the positive i-axis – other dispositions of $R(S)$ can be handled by symmetry – which means that each successive pixel of $R(S)$ picked by Bresenham going from left to right will have one higher i-value, so that, clearly, $i_2 = i_1 + N$.

Each of the $N + 1$ pixels of $R(S)$, counting from the left, corresponds successively to a point $u\bar{p} + (1 - u)\bar{q}$ of $\overline{pq}$, where $u = 1, \frac{N-1}{N}, \frac{N-2}{N}, \ldots, 0$. The first few u-values are indicated at the bottom of a pixel's column in the figure.

The color tuples $C(p)$ and $C(q)$ of the two end pixels are, of course, the programmer-specified colors of the corresponding end vertices. It remains to color the in-between pixels. The pixel next to the leftmost corresponds to $u = \frac{N-1}{N}$, therefore, in turn, by Equation (21.3), to the perspectively correct

$$t = \frac{q_z}{(\frac{N-1}{N}^{-1} - 1)p_z + q_z} = \frac{q_z}{\frac{p_z}{N-1} + q_z}$$

In other words, that pixel corresponds to the point $tp + (1 - t)q$ of S, where t is given by the preceding equation. Consequently, the color to apply is $tC(p) + (1 - t)C(q)$. Likewise, the color to apply to the next pixel is $tC(p) + (1 - t)C(q)$, after updating t to

$$t = \frac{q_z}{\frac{2p_z}{N-2} + q_z}$$

by setting $u = \frac{N-2}{N}$ in (21.3). The procedure of decrementing u by $\frac{1}{N}$, updating t and applying the interpolated colors $tC(p) + (1 - t)C(q)$ to the next pixel is repeated until the pixel just before the rightmost is colored, which, of course, completes the coloring of $R(S)$. This procedure can be integrated into Bresenham's line rasterizer: simultaneously picking the pixels along a line segment *and* coloring them with perspective correction.

We'll leave the reader to convince herself that, going from 1D objects to 2D, a similar perspective correction can be incorporated into triangle rasterization.

Remark 21.1. Not only color values, but other numerical data defined per vertex, e.g., normals, can be linearly interpolated with perspective correction as well.

Remark 21.2. Perspective correction is a non-issue obviously in case of orthographic projection.

21.1.4 Revised Pipeline

Below is the preliminary synthetic-camera rendering pipeline of Section 21.1.1 now enhanced to handle perspective division by zero in Stage 3 (following Section 21.1.2) and to incorporate perspective correction into rasterization in Stage 7 (Section 21.1.3). Additions to the preliminary version are shown in bold. Figure 21.9 is a flow diagram. This is a complete synthetic-camera pipeline in that it will transform a user-specified scene correctly into a picture on the monitor. However, it is still skeletal. The OpenGL pipeline, as we'll see next, adds several features.

Synthetic-camera Rendering Pipeline (Revised)

1. $[x\, y\, z\, 1]^T$ $\longrightarrow$ $[x^M \;\; y^M \;\; z^M \;\; 1]^T$
Modelview transformation =
multiplication by the modelview matrix.

2. $\longrightarrow$ $[x^{PM} \;\; y^{PM} \;\; z^{PM} \;\; w^{PM}]^T$
Multiplication by the projection matrix.

3. $\longrightarrow$ $\frac{x^{PM}}{w^{PM}} \;\; \frac{y^{PM}}{w^{PM}} \;\; \frac{z^{PM}}{w^{PM}} \;\; {}^T$
Perspective division with rules to handle zero w-values.

4. $\longrightarrow$ Primitive Assembly
Defining points, lines and triangles.

5. $\longrightarrow$ $\frac{x^{PM}}{w^{PM}} \;\; \frac{y^{PM}}{w^{PM}} \;\; \frac{z^{PM}}{w^{PM}} \;\; {}^T$
Clipping to the canonical box.

6. $\longrightarrow$ $\frac{x^{PM}}{w^{PM}} \;\; \frac{y^{PM}}{w^{PM}} \;\; {}^T$
Projection to the back of the canonical box
(*z-values possibly retained for depth testing*).

7. $\longrightarrow$ $[i\, j]^T$
Rasterization with perspective correction.

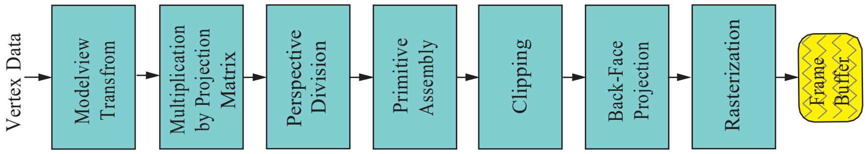

Figure 21.9: Complete minimal synthetic-camera rendering pipeline.

21.1.5 OpenGL Fixed-function Pipeline

The first-generation OpenGL fixed-function rendering pipeline, while keeping the gist of the synthetic-camera pipeline as described above, augments it necessarily with additional practical capabilities – remember we ignored texture, lighting and such in creating that earlier pipeline. The major additions are indicated in a darker shade in Figure 21.10.

The first addition is texturing, where vertex data (vertex and texture coordinates, particularly) and a set of controlling parameters (filters, environment settings, etc.) are used to combine the texture images into the raster. We learned the fundamentals of texturing ourselves in Chapter 12.

Next, instead of simply copying the raster into the frame buffer, the user can define *per-fragment* operations – a raster pixel with color data and z-value is called a fragment. The per-fragment operations allowed in OpenGL consist of the four tests

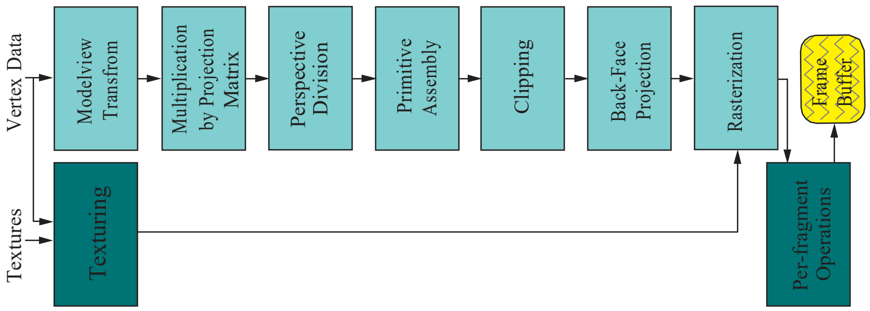

Figure 21.10: OpenGL fixed-function pipeline. Additions to the minimal synthetic-camera pipeline are darkly shaded.

1. Scissor test
2. Alpha test
3. Stencil test
4. Depth test

in that order, followed by

5. Blending

If a fragment fails an early test then it is eliminated immediately and does not proceed to subsequent tests. A fragment which survives all tests graduates into a pixel.

We are already familiar with the stencil test from Section 13.7, where there was a brief discussion of the scissor test as well, and the depth test from as far back as Section 2.8. The alpha test allows the user to accept or reject a fragment depending upon its alpha value (it has been discarded since OpenGL 3.1 because its functionality can be executed in a fragment shader, part of the programmable pipeline).

If the reader is wondering why lighting is missing from the pipeline of Figure 21.10, then note that lighting computations, in fact, are done along the top path, starting from vertex data, which includes normal values as well. Specific lighting calculation stages have been omitted, as have some other processing stages, such as fogging and antialiasing, simply to avoid clutter in the figure.

A point of final note: as the reader knows from Chapters 15-16, shaders written in GLSL transform the pipeline of Figure 21.10 by allowing the user herself to program substantial sections currently of fixed functionality.

21.1.6 1D Primitive Example

Let's chase a 1D primitive down the synthetic-camera rendering pipeline of Section 21.1.4, which is the first-generation OpenGL pipeline minus bells and whistles.

Example 21.1. The projection statement in the reshape routine of a program is

```
glFrustum(-5, 5, -5, 5, 5, 25)
```

The only primitive definition and the only modelview transformation in the drawing routine are

```
glTranslatef(0, 5, 0);
glBegin(GL_LINES);
    glColor3f(1, 0, 0); glVertex3f(0, 0, -10);
    glColor3f(0, 1, 0); glVertex3f(25, 5, -20);
glEnd();
```

All other statements in the program are routine. Determine what is rendered in a 100 × 100 raster after the program passes through a synthetic-camera pipeline.

Answer: The program draws a single line segment whose endpoints in homogeneous coordinates are

$$p = [0\ 0\ \ -10\ 1]^T \quad \text{and} \quad q = [25\ 5\ -20\ 1]^T$$

The matrix corresponding to the translation is (from Equation (5.22))

$$M = \begin{bmatrix} 1 & 0 & 0 & 0 \\ 0 & 1 & 0 & 5 \\ 0 & 0 & 1 & 0 \\ 0 & 0 & 0 & 1 \end{bmatrix}$$

The matrix corresponding to the projection statement is (from Equation (20.4))

$$P = \begin{bmatrix} 1 & 0 & 0 & 0 \\ 0 & 1 & 0 & 0 \\ 0 & 0 & -1.5 & -12.5 \\ 0 & 0 & -1 & 0 \end{bmatrix}$$

Apply the modelview transformation first, multiplying both endpoints by M:

$$Mp = [0\ 5\ \ -10\ 1]^T \quad \text{and} \quad Mq = [25\ 10\ -20\ 1]^T$$

At this point we note that both z-values are negative, so we are in a situation analogous to case (a) at the end of the discussion in Section 21.1.2 and can proceed down the pipeline without worrying about invoking enhancements to handle zero w-values in Stage 3. Accordingly, multiplying by P next:

$$PMp = P[0\ 5\ -10\ 1]^T = [0\ 5\ 2.5\ 10]^T$$

and

$$PMq = P[25\ 10\ -20\ 1]^T = [25\ 10\ 17.5\ 20]^T$$

Perspective division, then, gives the Cartesian coordinates of the transformed endpoints as follows:

$$[0/10\ 5/10\ 2.5/10]^T = [0\ 0.5\ 0.25]^T$$

and

$$[25/20\ 10/20\ 17.5/20]^T = [1.25\ 0.5\ 0.875]^T$$

As the first point lies in the canonical box, while the second outside of only the $x = 1$ plane, clipping involves a single intersection computation – that of the transformed segment with the $x = 1$ plane. We'll leave the reader to verify by means of elementary geometry that the intersection, in fact, is $[1\ 0.5\ 0.75]^T$, so that the endpoints of the clipped segment are

$$[0\ 0.5\ 0.25]^T \text{ and } [1\ 0.5\ 0.75]^T$$

We must determine the color tuple to assign the new second endpoint. It's checked that the new endpoint as a convex combination of the old ones is:

$$[1\ 0.5\ 0.75]^T = u[0\ 0.5\ 0.25]^T + (1-u)[1.25\ 0.5\ 0.875]^T$$

where $u = 0.2$. Therefore, by Equation (21.3), it corresponds to the point $tp + (1-t)q$ on pq, where

$$t = \frac{0.875}{(\frac{1}{0.2} - 1)0.25 + 0.875} = 0.467$$

Accordingly, the color tuple assigned the new endpoint is

$$0.467(1, 0, 0) + 0.533(0, 1, 0) = (0.467, 0.533, 0)$$

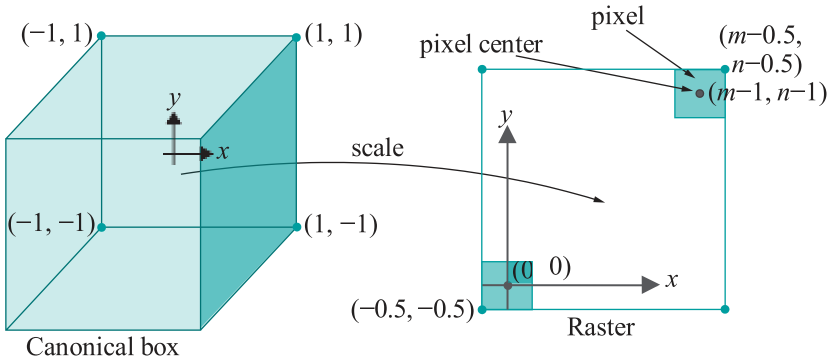

Figure 21.11: Scaling from the 2 × 2 back face of the canonical box, located on an xy-plane, to the $m \times n$ area of the raster.

Projecting the first endpoint of the clipped segment to the back face of the canonical box gives then the point $[0\ 0.5]^T$, with color value (1, 0, 0) and z-value 0.25 (retained for perspective correction calculations and, possibly, depth testing). Likewise, the second endpoint projects to $[1\ 0.5]^T$ with color value (0.467, 0.533, 0) and z-value 0.75. Time to leap from world space to screen space!

Generally, if the raster is $m \times n$ and pixel centers have integer coordinates (i, j), where $0 \leq i \leq m - 1$ and $0 \leq j \leq n - 1$, then the area of the raster is an axis-aligned rectangle, whose lower-left corner is $(-0.5, -0.5)$ and upper-right $(m - 0.5, n - 0.5)$. See Figure 21.11. The back face of the canonical box, on the other hand, can be imagined as a 2×2 square with corner coordinates $x = \pm 1$ and $y = \pm 1$ on the xy-plane. Accordingly, functions that scale the back face onto the raster – we're doing the print part of shoot-and-print now – are:

$$x \rightarrow \frac{x+1}{2} m - 0.5 \quad \text{and} \quad y \rightarrow \frac{y+1}{2} n - 0.5$$

Applying these functions to the projected endpoints on the back face of the canonical box, with $m = n = 100$, we get:

$$[0\ 0.5]^T \rightarrow [49.5\ 74.5]^T \quad \text{and} \quad [1\ 0.5]^T \rightarrow [99.5\ 74.5]^T$$

Rounding, one has the endpoint pixels on the raster as (49, 74) and (99, 74), respectively. Data associated with these pixels are the color values (1, 0, 0) and (0.467, 0.533, 0) and z-values 0.25 and 0.75, respectively.

As the rasterized segment is horizontal, choosing pixels along it is trivial – (49, 74), (50, 74), . . . , (99, 74) – obtaining a raster line segment of length $N = 50$ (containing 51 pixels).

It remains to color the in-between pixels using perspective correction, as well as assign their z-values. The u-value corresponding to pixel (50, 74), second from left, is $1 - \frac{1}{50} = 0.98$, and t-value, therefore (applying (21.3)):

$$\frac{0.75}{(\frac{1}{0.98} - 1)0.25 + 0.75} = 0.993$$

Accordingly, its color tuple is

$$0.993(1, 0, 0) + 0.007(0.467, 0.533, 0) = (0.996, 0.004, 0)$$

and z-value

$$0.98 * 0.25 + 0.02 * 0.75 = 0.26$$

using u itself, rather than t, to interpolate.

Note: z-values *need not* be perspectively corrected as their values in the canonical box, following projection transformation, are valid.

We'll leave the reader to calculate the color and z-values of a few more pixels or, better still, write a routine to generate them all.

21.1.7 Exercising the Pipeline

Exercise 21.2. Redo the preceding example with only the part in the drawing routine changed to

```
glRotatef(45, 0, 0, 1);
glBegin(GL_LINES);
   glColor3f(1, 1, 1); glVertex3f(5, 0, -10);
   glColor3f(0, 0, 0); glVertex3f(10, 10, -5);
glEnd();
```

Exercise 21.3. Repeat the previous exercise with the drawing routine changed again to

```
glRotatef(90, 0, 1, 0);
glBegin(GL_LINES);
   glColor3f(1, 0, 0); glVertex3f(1, 0, -1);
   glColor3f(1, 0, 0); glVertex3f(-4, 4, 0);
glEnd();
```

and the projection statement, as well, to

```
glOrtho(-5, 5, -5, 5, 5, -5)
```

Exercise 21.4. Repeat the previous exercise with the drawing routine changed once more to

```
glTranslatef(1, 1, 1);
glBegin(GL_LINES);
   glColor3f(1, 1, 1); glVertex3f(5, 0, -10);
   glColor3f(0, 0, 0); glVertex3f(10, 10, 5);
glEnd();
```

and the projection statement back to

```
glFrustum(-5, 5, -5, 5, 5, 25)
```

Note: You can roughly check your result for each of the preceding exercises by comparing it with the output of a minimal OpenGL program containing the given statements.

Exercise 21.5. (Programming) This is a substantial programming project: implement the synthetic-camera pipeline to render (only) 0D and 1D primitives (drawn in 3-space, of course). Use the OpenGL window to simulate the raster as in the program DDA.cpp of Chapter 14.

21.2 Ray Tracing Pipeline

The ray tracing pipeline is an “alternate” to the synthetic-camera graphics pipeline. The reason for the quotes is that the ray tracing approach is entirely different from that of the synthetic-camera-based one and rarely does a programmer have the option of simply exchanging one for the other. Why this is the case will be apparent once we understand how ray tracing works.

The idea behind ray tracing is straightforward: to follow light rays from each source as they interact with the scene – reflecting off opaque objects one to another, and both reflecting off and refracting through translucent ones, in the process casting shadows and creating reflections – till they finally reach the eye. However, implementing this idea as just stated is not a particularly well-advised endeavor, as (a) there is an infinite continuum of light rays emanating from each source, and (b) even after somehow discretizing them to a finite number, only a fraction thereof reach the viewer. See Figure 21.12 for an idea of the situation.

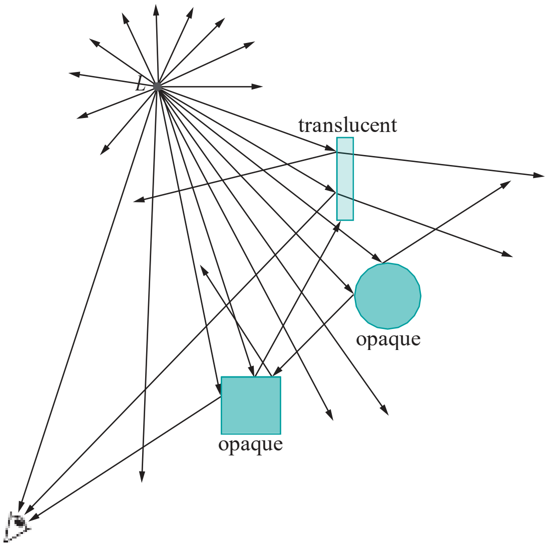

Figure 21.12: Tracing rays *from* a light source L – only few reach the eye.

Ray tracing, instead, implements the plan "backwards". Rays are traced *from* the eye, treated obviously as a point, one through each pixel, so that no computation is expended on rays which are surely invisible. Each ray is followed through the pixel and into and around the scene, possibly bouncing off opaque objects and passing through translucent ones, till a determination is made of its color. Of course, an implementation has to "cut off" each ray after a finite number of steps and determine the color it has picked up through interactions with objects up to that point, or the ray tracing process will continue indefinitely.

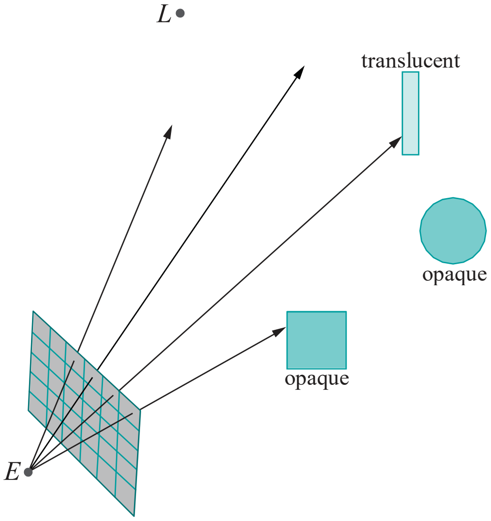

Figure 21.13: Tracing rays *from* the eye E, one through each pixel. Rays are "stopped" when they strike an object. LIght source is L.

See Figure 21.13 for a very simple scene. The screen is virtual – akin to the front face of an OpenGL viewing box or frustum. In this particular figure, rays either go off to infinity (there are two such drawn) or stop upon hitting the surface of an object (there are two such as well). We don't, as yet, follow rays beyond their first encounter with an object.

This, in fact, suggests a simple first implementation of ray tracing: color pixels, rays through which go off to infinity without collision, with the background color; assign every other pixel the color of the first point of intersection of the ray through it with an object's surface. This particular color is determined from Phong's lighting model – see Chapter 11, in particular the lighting equation (11.13).

Here's pseudo-code:

Ray Tracer Version 1: Non-recursive local

```
void topLevelRoutineCallsTheRayTracer()
{
    positionEye = position of eye in world space;
    for (each pixel P of the virtual screen)
    {
        d = unit vector from positionEye toward the center point of P;
        color of P = rayTracer(positionEye, d);
    }
}

Color rayTracer(Point p, Direction d)
{
    if (ray from p along d does not intersect the suface
         of any object) return backgroundColor;
    else
    {
        q = first point of intersection with an object's surface;
        computedColor = color computed at q using Phong's lighting model;
        return computedColor;
    }
}
```

Notes:

1. The *base* case of Version 1, when the ray is stopped at an intersection with an object, uses Phong for color calculation. It is typical, in fact, of ray tracers to invoke a local lighting model at the base case.

2. Intersection detection, implicit in the code, is the most computationally intensive part of the ray tracer. We'll not go into intersection computation in our account of ray tracing, but focus instead on color calculations.

Interestingly, the ray tracer version above renders the same image as a synthetic-camera pipeline – *a la* OpenGL – implementing Phong's lighting model with depth testing. The only difference is that depth testing via the z-buffer has been replaced by ray tracing to determine visible surfaces (one surface obscuring another if it blocks rays from reaching the other).

21.2.1 Going Global: Shadows

The next step up is shadow computation. This is simple to do. If a ray through a pixel intersects a surface, then send a *feeler ray* from the point of intersection toward each light source. If the feeler ray hits an object before reaching a light source, then the point of intersection is in the shadow of the struck object and not illuminated directly by that source. Recall in this connection that, according to Phong's model, only the diffuse and specular components of light reflected off a surface depend upon direct, i.e., straight-line, illumination from the light source, while the ambient does not.

See Figure 21.14. For example, point p_1 on ball S_2 is in the shadow of the ball S_1 cast by light from L_1 – because the feeler ray from it toward L_1 is cut off by S_1 – so it reflects only the ambient component of light from that particular source; on the other hand, p_1 is directly illuminated by L_2, so reflects all components of light from that source; p_2 is in the shadows of S_1, of which it is a point itself, cast both by L_1 and L_2; p_3 is illuminated directly by both sources.

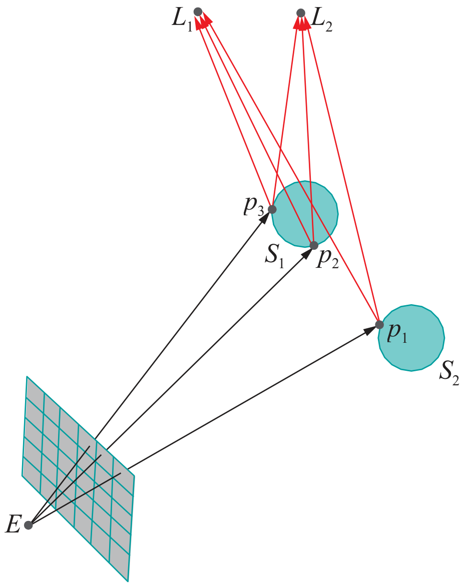

Figure 21.14: Shadow computation: feeler rays are red.

Here's pseudo-code for a shadow-computing ray tracer (a top-level routine the same as that of the first version is not repeated):

Ray Tracer Version 2: Non-recursive global, with shadows

```
void topLevelRoutineCallsTheRayTracer(); // See Version 1.

Color rayTracer(Point p, Direction d)
{
    if (ray from p along d does not intersect the suface
         of any object) return backgroundColor;
    else
    {
        q = first point of intersection;
        computedColor = black; // Color values all set to zero.
        for (each light source L)
        {
            // Object not shadowed.
            if (feeler ray from q toward L does not intersect the
                 surface of any object before reaching L)
                 computedColor  += color computed at q, due to light from
                                   L, using Phong's lighting model;

            // Object shadowed.
            else computedColor += ambient component of color computed at
                                   q, due to light from L, using Phong's
                                   lighting model;
        }
        return computedColor;
    }
}
```

A hugely significant development in Version 2 is that the lighting model has now gone *global* : object-object light interaction comes into play in computing shadows. A local lighting model, like pre-shader OpenGL's default Phong, on the other hand, does not take into account other objects when coloring a particular one. Recollect, in fact, how we computed shadows ourselves in the programs ballAndTorusLitOrthoShadowed.cpp and ballAndTorusShadowMapped.cpp. Now, this global version of ray tracing not only gives us shadows automatically, but ones as authentic as those drawn by Mother Nature, in particular, the laws of light.

21.2.2 Going Even More Global: Recursive Reflection and Transmission

We are ready now for the full blast of ray tracing power. So far, we've stopped at the first intersection of a ray from the eye with a surface. In reality, rays from a light source can bounce from object to object, or even pass through them, several times before reaching the viewer, giving rise to such phenomena as reflection and translucence. To model this in keeping with ray tracing's backward approach of following rays from the eye into the scene, one must allow a ray to continue even after it hits an object. The physics of light suggests that a ray striking an object is partially reflected off its surface and partially transmitted through it, depending on the characteristics of the material, as well as the color of the light. For example, an opaque object transmits almost zero light and reflects the remainder according to its surface finish and color, while a translucent one transmits most.

Accordingly, we'll enhance Ray Tracer Version 2 such that each ray from the eye that strikes a surface spawns two additional rays: a *reflected ray* in the direction of perfect reflection and a *transmitted ray* passing through the surface, possibly with its direction altered by refraction. The two spawned rays are treated *exactly* as an incoming ray and may each spawn additional rays themselves upon subsequent intersection with a surface. If you are thinking recursion, then that's exactly where we're headed.

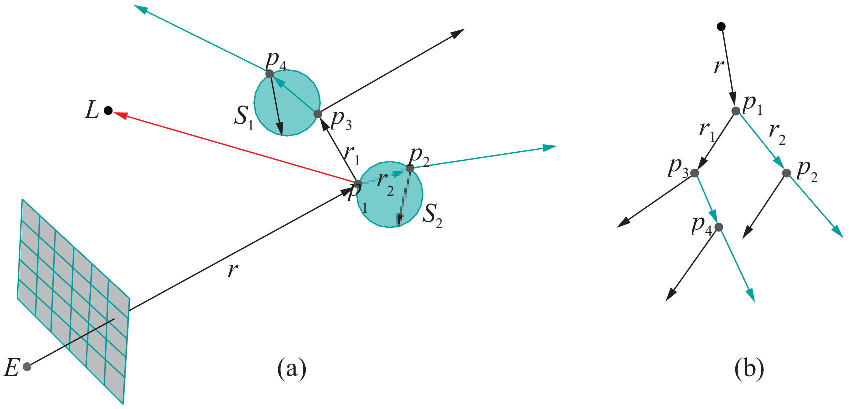

Figure 21.15: (a) Reflection and transmission: reflected rays are black, transmitted green. One red feeler ray is drawn. (b) Ray tree (not all edges are labeled).

As an example, Figure 21.15(a) follows a single ray r from the eye through a few intersections with two translucent balls. The resulting binary *ray tree* data structure is shown in Figure 21.15(b). Observe that the transmitted rays are refracted by the material of the balls, instead of passing straight through. The color computed at a point now has three components – one computed locally, one returned by the reflected ray, and one by the transmitted ray – as given by the following equation:

$$computedColor = color_{local} + coef_{refl}\, color_{refl} + coef_{tran}\, color_{tran}$$

For example, at point p_1 of the figure, $color_{local}$ is computed using Phong (exactly as in Version 2, with the help of feeler rays to find "visible" light sources – the feeler ray from p_1 to L is shown in the figure); $color_{refl}$ is the value returned recursively by the reflected ray r_1, attenuated by a material-dependent multiplicative factor $coef_{refl}$, which specifies the fraction of the incoming ray r that is reflected; $color_{tran}$ is likewise returned recursively by the transmitted ray r_2 and attenuated by $coef_{tran}$.

Pseudo-code is below. The new top-level routine passes a user-set non-negative integer depth parameter maxDepth to the ray tracer to cut off recursion after a finite number of levels.

Ray Tracer Version 3: Recursive global, with shadows, reflection and transmission

```
void topLevelRoutineCallsTheRayTracer()
{
    positionEye = position of eye in world space;
    for (each pixel P of the virtual screen)
    {
        d = unit vector from positionEye toward the center point of P;
        color of P = rayTracer(positionEye, d, maxDepth);
    }
}

Color rayTracer(Point p, Direction d, int depth)
{
    if (ray from p along d does not intersect the surface
         of any object) return backgroundColor;
    else
    {
        q = first point of intersection;
        computedColor = black; // Color values all set to zero.

      // Local component, copy of Version 2 calculations.
        for (each light source L)
        {
            // Object not shadowed.
            if (feeler ray from q toward L does not intersect the
                   surface of any object before reaching L)
                  computedColor  += color computed at q, due to light from
                                     L, using Phong's lighting model;

            // Object shadowed.
            else computedColor += ambient component of color computed at
                                     q, due to light from L, using Phong's
                                     lighting model;
        }

        // Global component.
        if (depth > 0)
        {
            d1 = unit vector from q in direction of perfect reflection;
            d2 = unit vector from q in direction of transmission;

            // Reflected component added in recursively.
            computedColor += coefRefl * rayTracer(q, d1, depth-1)

            // Transmitted component added in recursively.
            computedColor += coefTran * rayTracer(q, d2, depth-1)
        }
        return computedColor;
    }
}
```

Note:

1. Determining where an incident ray strikes an object and spawns a reflected and a transmitted ray obviously requires intersection computation. Subsequent

calculation of the direction of the reflected and transmitted rays requires computation of the normal to the surface at the point of incidence as well:

(a) The direction of the reflected ray is given by the laws of reflection, which say that both the incident and reflected rays make the same angle with the normal to the surface, and that all three lie on the same plane. See Figure 21.16, where the equation for reflection is $A = B$.

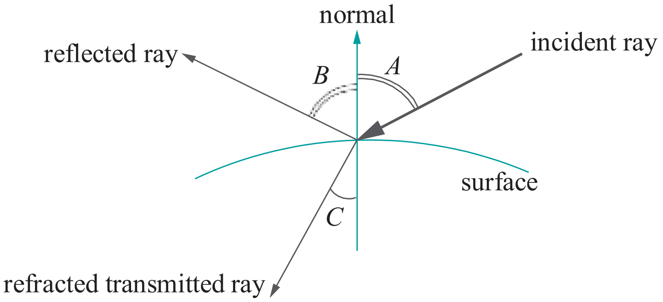

Figure 21.16: Calculating the direction of the reflected and transmitted rays: A = angle of incidence, B = angle of reflection, C = angle of refraction.

(b) Routines to compute the direction of transmission can be simple or as fancy as the need for realism dictates.

For instance, refraction is often taken into account with the help of Snell's law, which says that the ratio of the sine of the angle of incidence to the sine of the angle of refraction is equal to the ratio of the speed of light in the medium of the incident ray to that in the medium of the refracted ray; moreover, the incident ray, refracted ray and normal to the surface all lie on the same plane.

The ratio of the speed of light in two different media is the inverse ratio of the refractive indices of the media. Therefore, in Figure 21.16, one can write the equation for refraction as $\frac{\sin A}{\sin C} = \frac{\eta_2}{\eta_1}$, where η_1 is the refractive index of the medium on the side of the incident ray and η_2 that on the side of the refracted ray.

Exercise 21.6. Neither version 2 nor 3 of our ray tracer seems to take into account global ambient light in their Phong base case. Revise both to do so.

Remark 21.3. It's interesting to observe that a ray tracer does not ask for a small set of simple drawing primitives, e.g., points, line segments and triangles, as needed for efficient implementation of the synthetic-camera model. As long as their intersection with a given ray can be computed and the normal at a given point determined, arbitrary curved surfaces may be rendered directly without first approximating them with simpler primitives.

Remark 21.4. Ray Tracer Version 3 above takes the direction of the reflected ray to be that of perfect mirror-like reflection. This models well the transport of specular light but not that of diffuse. For the latter is needed *multiple* reflected rays – remember that diffuse light is scattered in all directions by the lit object – which would make the ray tracing process computationally overwhelming.

This inability of ray tracing to realistically model diffuse illumination is a weakness often overcome by combining it with radiosity, another global lighting model which is specially designed to track the dispersion of diffuse light. We'll discuss radiosity in the next section.

Implementing Ray Tracing

We're going to implement ray tracing with the help of POV-Ray (Persistence of Vision Ray Tracer, our version 3.7.0), a freely downloadable ray tracer from povray.org [115]. Here's POV-Ray code to show off how realistic ray traced rendering can be.

Experiment 21.3. If you have successfully installed POV-Ray, then open sphereInBoxPOV.pov using that application and press the Run button at the top; if not, use any editor to at least view the code. Figure 21.17(a) is the output. Impressive, is it not, especially if you compare with the output in Figure 21.17(b) of sphereInBox1.cpp of Chapter 11, which, of course, is almost the exact scene captured with OpenGL's synthetic camera? The inside of the box, with the interplay of light evident in shadows and reflections, is far more realistic in the ray-traced picture (the front of the ray-traced box could do with an additional light source, though, but we wanted to keep the OpenGL and POV-Ray versions as similar as possible). End

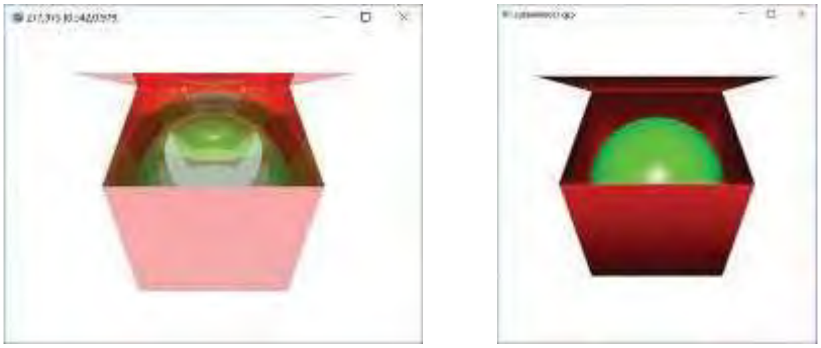
(a) (b)

Figure 21.17: Ray tracing versus OpenGL: screenshot of (a) sphereInBoxPOV.pov (b) sphereInBox1.cpp.

The code itself is fairly self-explanatory. It's written in POV-Ray's scene description language (SDL), which, unlike OpenGL, is *not* a library meant to be called from a C++ program – the SDL is stand-alone. We've obviously tried to follow the settings in our OpenGL program sphereInBox1.cpp as far as possible. The camera and a white light source are placed identically as in sphereInBox1.cpp. The red box, as in sphereInBox1.cpp, is an axis-aligned cube of side lengths two centered at the origin. It comprises six polygonal faces, each originally drawn as a square with vertices at $(-1, -1)$, $(1, -1)$, $(1, 1)$ and $(-1, 1)$ on the xy-plane, and then appropriately rotated and translated. The top face is opened to an angle of 60°. Finally drawn is a green sphere of radius one. The material finishes are minimally complex, just enough to obtain reflection and a specular highlight on the sphere.

So what gives? If ray tracing is so much more realistic than the synthetic-camera-based OpenGL pipeline, then why bother with the latter, or, for that matter, write fat books about it?! You will have your answer if you compare the CPU time used on your platform (see the POV-Ray docs for how to benchmark) to render the output of sphereInBoxPOV.pov vs. that for sphereInBox1.cpp: ray tracing is orders of magnitude slower than OpenGL's synthetic-camera model. It is computationally *very very* intensive because intersection computations don't come cheap and they have to be done for every ray at every level in every ray tree generated, and there's one ray tree for each of maybe a million pixels. To even open the lid of the simple box of sphereInBoxPOV.pov in *real-time*, in the manner of sphereInBox1.cpp, is beyond the power of any modern-day desktop. Interactive animation, therefore, of remotely complex scenes (read games) is likely to remain beyond the reach of ray traced rendering for a while now.

On the other hand, still-life and movies, where there is either no animation or the animation is pre-created off-line, are perfect applications for ray tracing. Computer animation in Hollywood is almost exclusively ray traced, individual frames of complex and highly realistic animated sequences sometimes taking hours each to render on special-purpose hardware (which often are clusters of computers called *render farms*). Incidentally, POV-Ray, too, has the capability to sequence an animation from individually generated frames – refer to their tutorial.

Remark 21.5. The holy grail of ray tracing research is, in fact, real-time ray-traced rendering.

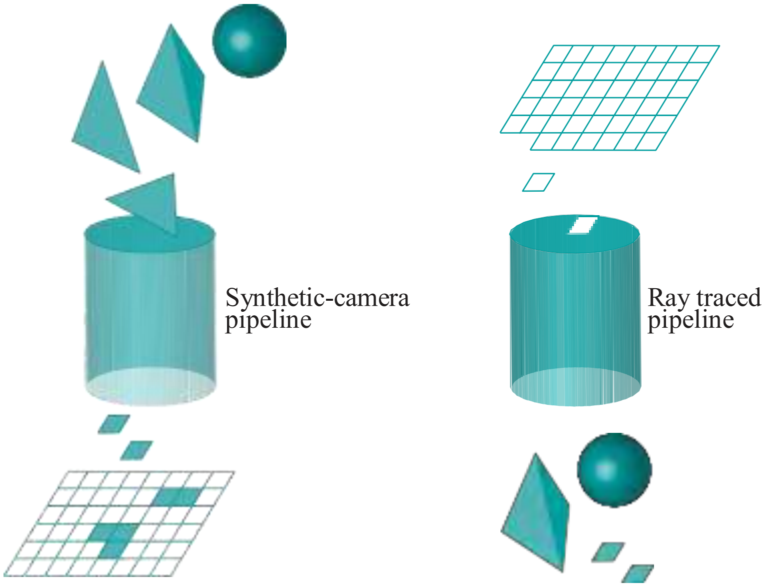

Figure 21.18: The (object-oriented) synthetic-camera pipeline versus the (screen-oriented) ray traced pipeline.

A somewhat amusing, though fairly authentic, comparison of the synthetic-camera pipeline with ray tracing is to say that the former is “object-oriented”, while the latter “screen-oriented”. See Figure 21.18: on the left, objects (primitives) are dropped into the synthetic-camera pipeline to emerge rasterized, while it’s upside down on the right, pixels being dropped into the ray tracing pipeline to emerge colorized.

In case you enjoyed the little of POV-Ray that we showed and want to try your own hand at ray tracing, here are a couple of exercises.

Exercise 21.7. (Programming) Use POV-Ray to generate a ray traced ball and torus with both shadows and reflections. Start with rendering a single still shot and then, if you are brave, animate.

Exercise 21.8. (Programming) Animate the opening of the lid of the box of sphereInBoxPOV.pov by generating a sequence of stills – one for every degree the lid turns would mimic sphereInBox1.cpp.

21.3 Radiosity

21.3.1 Introduction

Radiosity is a global lighting model which uses principles of heat transfer to track the dispersion of diffuse light around a scene.

It is quite often that a significant component of the light illuminating a scene is, in fact, multiply reflected diffuse light. For an example, consider a living room like the one depicted in Figure 21.19, populated with non-shiny furniture and lit by early morning rays. In such a setting there is little specular transport of light (i.e., by mirror-like reflection). Instead, in addition to the ambient component, which is fairly constant throughout, is mostly diffuse activity. For example, light from the floor and walls reflect diffusely onto the shelves and furniture fabric. Even parts of the environment obscured from direct lighting, such as the floor between the sofas, are not in a well-defined shadow, but mildly illuminated by light reflecting off adjacent objects.

Figure 21.19: Living room lit mostly with diffuse light (courtesy www.freshome.com).

Diffuse reflection is difficult to model with ray tracing. In fact, if you see again the Ray Tracer Version 3 algorithm in the previous section, a ray upon intersecting an object spawns a single ray in the direction of transmission and another in the direction of perfect reflection. However, as noted in Remark 21.4, modeling diffuse reflection would require each incident ray to spawn multiple reflected rays, leading to a blow-up in complexity.

Radiosity complements ray tracing by modeling diffuse illumination at acceptable cost. Together, they can deliver highly realistic rendering – in practical terms, ray tracing emphasizing the shadows and highlights and radiosity recording the softer lights.

21.3.2 Basic Theory

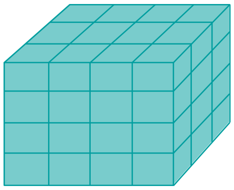

Figure 21.20: Patchified box.

The radiosity algorithm that we'll describe begins by dividing the scene into some number n of small flat, typically polygonal, *patches*, P_i, $1 \leq i \leq n$, e.g., see Figure 21.20. A triangulated scene is, of course, automatically patchified. However, even then, one may want to refine certain triangles, or combine others to coarsen the given triangulation in response to two opposing forces in patchification: the smaller and more numerous the patches the more authentic is the lighting calculation; on the other hand, the time complexity of the radiosity algorithm, which is $O(n^2)$, increases rapidly with the number of patches. The best strategy is an adaptive one where a region over which light intensities are expected to vary rapidly is finely patchified, while one of steadier light levels more coarsely.

The *brightness* or *radiosity* of a patch is the light energy per unit time per unit area leaving the patch, measured, typically, in a unit such as *joules*/(*second*× *meter*^{2}) (equivalent to *watts*/*meter*^{2}). The brightness varies with the frequency of the light in a manner that determines the perceived color of the patch; e.g., a red patch emits the greatest intensity at the red end of the visible spectrum. However, for simplicity's sake, we'll develop the theory assuming the brightness of a patch P_i as a single scalar value B_i, while a practical implementation would have three different scalar values corresponding to the RGB brightnesses.

Our starting point is the following equation which, in fact, holds for each i, $1 \leq i \leq n$,

$$A_iB_i = A_iE_i + R_i \sum_{j=1}^{n} F_{ji}A_jB_j \qquad (21.4)$$

given n patches, where A_i is the area of patch P_i, B_i its brightness, E_i its emission rate, R_i the reflective scaling factor and, finally, F_{ji}, the so-called *form factor* between patches P_j and P_i.

The equation simply states that the amount of light energy leaving a patch P_i, which is the *area*×*brightness* term on the LHS, is equal to (a) the amount it emits as a source *plus* (b) the amount it reflects of incoming light, the two additive terms, respectively, on the RHS.

The value of (a) as the product of the patch's area and emission rate is clear. For (b), note first that the form factor F_{ji} denotes the fraction of the total light energy leaving patch P_j that reaches P_i. Therefore, $F_{ji}(A_jB_j)$ is, in fact, the amount of light leaving P_j for P_i; moreover, multiplied by P_i's reflective scaling factor R_i, this gives the amount of light from P_j actually reflected from P_i. Accordingly, the value of (b) is the summation of $R_iF_{ji}(A_jB_j)$ over all patches P_j, which is precisely the second term on the RHS of the equation above.

Shortly, we'll be computing form factors mathematically but it's easy to understand intuitively that F_{ji} depends on the orientation of P_j and P_i relative to each other, their distance and, further, if there is occlusion by intermediate patches between the two. For example, in Figure 21.21, the form factor between patches P_1 and P_2 and between P_2 and P_3 is high, because the two pairs are side by side and parallel, while that between P_1 and P_3 low because P_2 is between them. The form factor between P_4 and any one of P_1, P_2 and P_3 is low because of unfavorable orientation. The form factor between P_5 and any one of P_1, P_2 and P_3 is low as well because of distance.

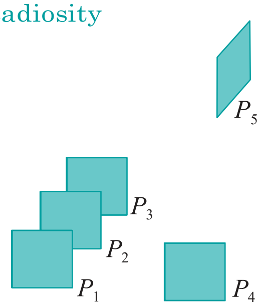

Figure 21.21: Form factor between patches depends on their respective orientation, the distance between them and if there is occlusion by other patches.

Form factors will be seen soon to satisfy the *reciprocity equation*:

$$F_{ij}A_i = F_{ji}A_j \tag{21.5}$$

Assuming this reciprocity for now, rewrite Equation (21.4) as

$$A_iB_i = A_iE_i + R_i \sum_{j=1}^{n} F_{ij}A_iB_j \tag{21.6}$$

Dividing out A_i, one gets the *radiosity equations*:

$$B_i = E_i + R_i \sum_{j=1}^{n} F_{ij}B_j, \quad 1 \le i \le n \tag{21.7}$$

which is a set of simultaneous linear equations in the brightnesses B_i, the latter being the only unknowns, provided we already have at hand the emissivities E_i and reflectivities R_i from a knowledge of material properties, and provided we can compute, as well, the form factors F_{ij} from the patch geometry.

Rearranging the radiosity equations as

$$(1 - R_iF_{ii})B_i - \sum_{1\le j\le n,\ j\ \ i} R_iF_{ij}B_j = E_i, \quad 1 \le i \le n$$

one can write them in the matrix form

$$\begin{pmatrix} 1 - R_1F_{11} & -R_1F_{12} & \ldots & -R_1F_{1n} \\ -R_2F_{21} & 1 - R_2F_{22} & \ldots & -R_2F_{2n} \\ . & . & \ldots & . \\ -R_nF_{n1} & -R_nF_{n2} & \ldots & 1 - R_nF_{nn} \end{pmatrix} \begin{pmatrix} B_1 \\ B_2 \\ . \\ B_n \end{pmatrix} = \begin{pmatrix} E_1 \\ E_2 \\ . \\ E_n \end{pmatrix} \tag{21.8}$$

Denoting

$$\mathrm{B} = \begin{pmatrix} B_1 \\ B_2 \\ . \\ B_n \end{pmatrix}, \quad \mathrm{E} = \begin{pmatrix} E_1 \\ E_2 \\ . \\ E_n \end{pmatrix}, \quad \text{and } Q = \begin{pmatrix} R_1F_{11} & R_1F_{12} & \ldots & R_1F_{1n} \\ R_2F_{21} & R_2F_{22} & \ldots & R_2F_{2n} \\ . & . & \ldots & . \\ R_nF_{n1} & R_nF_{n2} & \ldots & R_nF_{nn} \end{pmatrix}$$

a succinct matrix form of the radiosity equations is obtained from (21.8):

$$(I_n - Q)\mathrm{B} = \mathrm{E} \tag{21.9}$$

where, of course, I_n is the $n \times n$ identity matrix.

Therefore, once we know how to do the following two tasks efficiently, we'll be in a position to practically implement the theory developed thus far:

(a) Compute form factors.

(b) Solve the radiosity equation (21.9) to determine patch brightnesses.

We discuss the two in the next sections.

Remark 21.6. Patchifying to compute radiosity is a *finite element* method because patches represent a discretization (into finite elements) of the problem of determining the diffuse lighting over the whole domain, each patch leading to one of the radiosity equations (21.7), which then have to be solved together to resolve the original problem.

21.3.3 Computing Form Factors

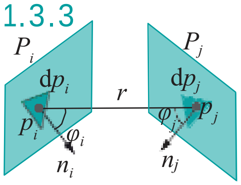

Figure 21.22: Computing form factors.

Consider two patches P_i and P_j. Even though the respective normal directions, n_i and n_j, remain constant over the patches, assumed flat, the amount of light from a point on P_i reaching a point on P_j, e.g., p_i and p_j in Figure 21.22, varies as the points vary, depending on the distance between them and the angle the line joining them makes with n_i and n_j, respectively. Therefore, one must integrate over the two patches – points being represented by infinitesimal areas – in order to determine the total light reaching P_j from P_i. In the figure, small triangles indicate the infinitesimal areas $\mathrm{d}p_i$ and $\mathrm{d}p_j$ at p_i and p_j, respectively.

In fact, if patches are presumed to be Lambertian, i.e., they reflect light uniformly in all directions from every surface point, then it can be proved that the form factor F_{ij}, the fraction of the total light emanating from F_i that reaches F_j, is given by:

$$F_{ij} = \frac{1}{A_i} \int_{p_i \in P_i} \int_{p_j \in P_j} v_{ij} \frac{\cos \varphi_i \cos \varphi_j}{\pi r^2} \, \mathrm{d}p_j \, \mathrm{d}p_i \qquad (21.10)$$

where A_i is the area of P_i, φ_i and φ_j are the angles between the segment $p_i p_j$ and the normals n_i and n_j, respectively, r is the length of $p_i p_j$, and v_{ij} is a Boolean which is 1 if p_j is visible from p_i and 0 otherwise.

Exercise 21.9. Deduce the reciprocity equation (21.5) from the formula (21.10) for a form factor.

Except for the simplest cases, the double integral in Formula (21.10) is impossible to compute exactly. The *hemicube method* , however, is a clever approximation algorithm developed by Cohen and Greenberg [24], which takes advantage of fast hardware-based z-buffers.

Write formula (21.10) as

$$F_{ij} = \frac{1}{A_i} \int_{p_i \in P_i} \left[\int_{p_j \in P_j} v_{ij} \frac{\cos \varphi_i \cos \varphi_j}{\pi r^2} \, \mathrm{d}p_j \right] \mathrm{d}p_i \qquad (21.11)$$

The inner integral can be imagined to be the form factor between p_i – or, more precisely, an infinitesimal patch $\mathrm{d}p_i$ containing p_i as in Figure 21.22 – and P_j, while F_{ij} itself is the average of these form factors over points of P_i.

The first assumption of the hemicube method is that the form factor between p_i and P_j does not vary significantly as p_i varies over P_i, which is justified if the distance between P_i and P_j is large in comparison to their respective sizes. In such a case, the average F_{ij} can be approximated by a single value, say that of the form factor at a fixed point p_i located centrally in P_i; precisely,

$$F_{ij} = \int_{p_j \in P_j} v_{ij} \frac{\cos \varphi_i \cos \varphi_j}{\pi r^2} \, \mathrm{d}p_j \qquad (21.12)$$

obtained from assuming the inner integral of (21.11) to be constant over P_i.

The next assumption is that this p_i-P_j form factor itself can be approximated by replacing P_j with its projection P'_j on an (imaginary) hemicube – half a cube – with its base lying on the plane of P_i and centered at p_i. Figure 21.23(a) shows such a hemicube, being half of a cube of side lengths 2. The justification for this assumption is as follows.

As P_i is Lambertian, light from each of its points emanates uniformly in all directions, which means that the light from p_i uniformly illuminates a hemisphere with its base along P_i and center at p_i. So the projection of P_j onto such a hemisphere would be an "ideal" replacement for P_j. However, for the sake of computational advantages, which will be perceived momentarily, the hemi*sphere* is replaced with

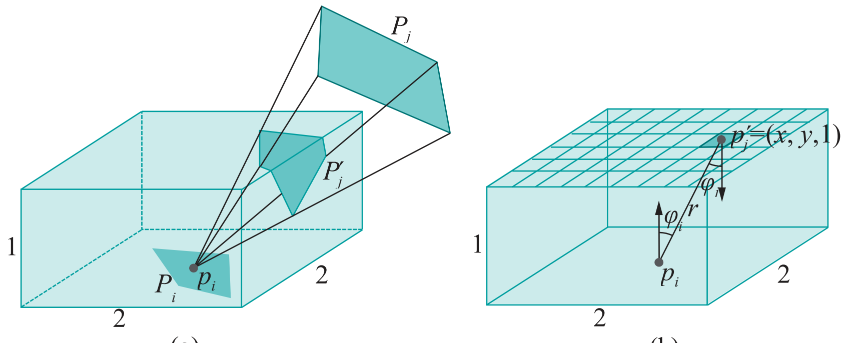

(a) (b)

Figure 21.23: (a) Projecting a patch onto a hemicube (b) Computing the delta form factor.

a hemi*cube* centered at p_i. So we get the following approximation from (21.12) by replacing the patch P_j with its projection P'_j on the replacement hemicube:

$$F_{ij} = \int_{p'_j \in P'_j} v_{ij} \frac{\cos \varphi_i \cos \varphi_j}{\pi r^2} \, dp'_j \qquad (21.13)$$

The hemicube algorithm, next, discretizes the computation of the preceding integral by dividing the hemicube into a grid of squares, called (suggestively, as we shall see) pixels, and treating each as an infinitesimal area dp'_j. Figure 21.23(b) shows a division into pixels of the top face. This process effectively replaces the integral with a finite sum.

It's in the evaluation of this sum that the beauty of the hemicube method lies. Here's what it asks: for each of the five faces of the hemicube – top and four sides – render the scene with the eye at p_i and the front face of the viewing frustum coinciding with that hemicube face. Presto! Screen pixels now correspond to pixels on the hemicube face so that occlusion – the pesky v_{ij} in the integral (21.13) – is automatically taken care of by means of the z-buffer.

To determine all v_{ij}, then, color code each patch – with, typically, 2^{24} colors to choose from, there should be plenty to assign a unique one to each patch – and render the scene with depth testing to find the screen pixels of a given color, which, in turn, determines the projection of the patch of that color on a hemicube face. For example, the projection P'_j of patch P_j in Figure 21.23(a) has a part on the top and one on the side of the hemicube. If P_j were coded, say, red, then the red pixels, when the scene is rendered with the hemicube top as the viewing face, comprise the part of the top not occluded (in the figure there happens to be no occlusion of P_j at all).

Consider, next, a single pixel belonging to patch P'_j lying on the top face and centered at the point $p'_j = (x, y, 1)$, e.g., the darker one in Figure 21.23(b). We have $r = \sqrt{x^2 + y^2 + 1}$, $\varphi_i = \varphi_j$ and $\cos \varphi_i = \cos \varphi_j = 1/r$. Moreover, the area of the pixel is $\frac{4}{wh}$, where the screen size is w pixels $\times$ h pixels. Therefore, the contribution of the top face of the hemicube to the integral (21.13) is approximated by the sum

$$\sum_{\substack{\text{pixel on top face}\\ \text{with color of } P_j}} \frac{(1/r)(1/r)}{\pi r^2} \frac{4}{wh} = \frac{4}{\pi w h} \sum_{\substack{\text{pixel on top face}\\ \text{with color of } P_j}} \frac{1}{(x^2 + y^2 + 1)^2} \qquad (21.14)$$

Exercise 21.10. Write sums analogous to (21.14) for the contributions of each of the four side faces of the hemicube to the integral (21.13).

The implementation of the hemicube algorithm should now be clear. First, color code patches. Next, for each patch, and for each of the five faces of the hemicube centered at the middle of the patch, render the scene using that particular face as the viewing face and then process the resulting screen by tallying the contribution of each pixel according to its color. The contribution of a pixel to the form factor between p_i and the patch of the pixel's color, e.g.,

$$\frac{4}{\pi(x^2 + y^2 + 1)^2 wh}$$

for a pixel on top of the hemicube, is called a *delta form factor* . Accordingly, the computation of each form factor is reduced to the process of incrementing it from zero, by a delta form factor at each step, as the screen is swept row by row, pixel by pixel, for each of the five renderings.

21.3.4 Solving the Radiosity Equation to Determine Patch Brightnesses

The second and final piece before we can practically implement the radiosity method is an efficient algorithm to solve the radiosity equation (copied from (21.9))

$$(I_n - Q)\mathrm{B} = \mathrm{E}$$

to determine the *patch brightness vector* B, where the matrix

$$I_n - Q = \begin{bmatrix} 1 - R_1 F_{11} & R_1 F_{12} & \dots & R_1 F_{1n} \\ R_2 F_{21} & 1 - R_2 F_{22} & \dots & R_2 F_{2n} \\ . & . & \dots & . \\ R_n F_{n1} & R_n F_{n2} & \dots & 1 - R_n F_{nn} \end{bmatrix}$$

Trying to solve the preceding equation by writing $\mathrm{B} = (I_n - Q)^{-1}\mathrm{E}$ and straightforwardly inverting $I_n - Q$ would be prohibitively expensive as the computation involved is $O(n^3)$, where the number n of patches is typically in the thousands. However, certain properties of the matrix $I_n - Q$, derived from properties of the form factors, lead to an efficient method to approximate its inverse.

First,

$$F_{ii} = 0, \quad 1 \le i \le n$$

because patches, being flat, cannot self-reflect. Moreover, we can assume as well that

$$\sum_{j=1}^{n} F_{ij} = 1, \quad 1 \le i \le n$$

which means all light leaving any given patch strikes other patches, by closing off the environment with black (i.e., non-reflective) patches. These properties of the form factors, together with that each reflectivity R_i is at most 1, imply that the principal diagonal of $I_n - Q$ consists of all 1's and that the sum of non-diagonal entries in any row of $I_n - Q$ is at most 1. One can then prove that

$$(I_n - Q)^{-1} = I_n + Q + Q^2 + \dots$$

where the series on the right converges (which might remind the reader of the power series expansion $(1 - x)^{-1} = 1 + x + x^2 + \dots$, which converges if $|x| < 1$). Therefore,

$$\mathrm{B} = (I_n - Q)^{-1}\mathrm{E} = \mathrm{E} + Q\mathrm{E} + Q^2\mathrm{E} + \dots$$

allowing the patch brightness vector B to be approximated to arbitrary accuracy by adding sufficiently many terms of the series on the right. Care needs still to be taken, as a simple-minded computation of the term $Q^k\mathrm{E}$ by repeatedly multiplying by Q is nearly $O(n^3)$ again. A simple observation, however, helps cut the cost.

Denote successive partial sums of the series $\mathrm{E} + Q\mathrm{E} + Q^2\mathrm{E} + \dots$ by $\mathrm{B}_0, \mathrm{B}_1, \dots$. In other words, $\mathrm{B}_0 = \mathrm{E}$, $\mathrm{B}_1 = \mathrm{E} + Q\mathrm{E}$, $\mathrm{B}_2 = \mathrm{E} + Q\mathrm{E} + Q^2\mathrm{E}$ and so on. Then we have the recurrence

$$\mathrm{B}_{k+1} = \mathrm{E} + Q\mathrm{B}_k, \quad k \ge 0$$

so that each successive term of the sequence $B_0, B_1, B_2, \ldots$ of partial sums converging to B can be computed from the previous by a matrix-vector product and a vector-vector addition, the two operations together being of $O(n^2)$ complexity. In fact, if the matrix Q is sparse, likely if the form factor between patches at a distance greater than some threshold value are set to 0, then the complexity may be closer to linear.

Exercise 21.11. Consider the operator Ψ that acts on n-vectors by

$$\Psi(X) = E + QX$$

Prove that the solution B of the radiosity equation is a *fixed point* of Ψ, i.e., a vector X such that $\Psi(X) = X$.

The preceding exercise leads to *Jacobi's iterative method* to approximate the fixed point B of Ψ as follows. Choose arbitrarily a start vector X^1. Then repeatedly apply Ψ to X^1 to obtain a sequence $X^1, \Psi(X^1), \Psi(\Psi(X^1)),$ Properties of the radiosity equations guarantee that this sequence converges to the unique fixed point of the operator Ψ. We'll not discuss the theory underlying Jacobi's method any further ourselves, but the interested reader is referred to Hageman & Young [68].

Exercise 21.12. Prove that Jacobi's iterative method to approximately determine the solution B of the radiosity equation, using a *zero* start vector, is precisely equivalent to the power series method of approximating B.

A useful physical insight into the sequence $B_0, B_1, B_2,$ of partial sums converging to B is that the first term represents only emitted light, the second emitted light together with diffuse light coming to the eye after a single reflection, the third emitted light together with diffuse light after at most two reflections and so on.

In practical terms, this means that using the sequence $B_0, B_1, B_2,$ as brightness vectors illuminates the scene in an increasingly authentic manner, which leads to the cost-saving technique of executing each iteration to compute B_i only on demand, called *progressive refinement*.

21.3.5 Implementing Radiosity

Figure 21.24 shows the four steps of the radiosity algorithm. The first three are *view-independent* and may be pre-computed for a scene whose geometry does not change. The last rendering step, of course, depends on the location of the viewer. To reduce aliasing artifacts at patch borders, instead of rendering each patch with its computed brightness, each *vertex* is assigned a brightness computed from its adjacent patches, e.g., a weighted average. Subsequently, vertex colors are interpolated through each patch via Gouraud shading.

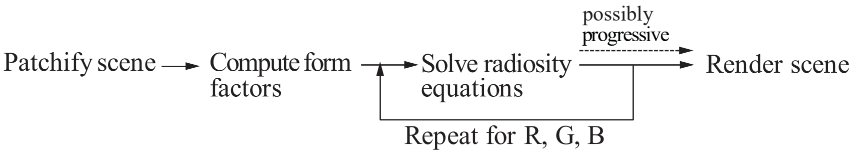

Figure 21.24: The radiosity algorithm.

Remark 21.7. As the first three steps of the radiosity algorithm are view-independent, while the last, even though dependent on the viewer's location, is not particularly computationally intensive, radiosity can be efficiently incorporated into a real-time walk-through of a static scene, e.g., a building interior.

Experiment 21.4. Run again sphereInBoxPOV.pov. Then run again after uncommenting the line

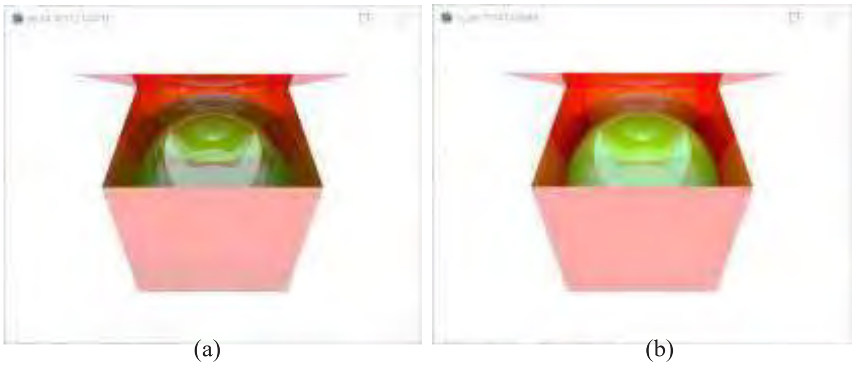

(a) (b)

Figure 21.25: Without and with radiosity: screenshot of sphereInBoxPOV.pov with (a) radiosity disabled (b) radiosity enabled.

```
global_settings{radiosity{}}
```

at the top to enable radiosity computation with default settings. The difference is significant, is it not? Figure 21.25(a) is the ray-traced output without radiosity, while Figure 21.25(b) is the output with radiosity. There clearly is much more light going around inside the box in the latter rendering. End

Exercise 21.13. If the lighting in a scene changes, then which steps of the radiosity algorithm need to be redone? How about if the geometry changes, e.g., with a ball looping in and out of a torus?

21.4 Summary, Notes and More Reading

In this chapter we went into particularly gory detail about the synthetic-camera pipeline that OpenGL implements, the fixed-function variant in particular. The reader should now be in a position to even implement a barebones version of her own. The synthetic-camera pipeline is based on a local illumination model. We were introduced as well to two global models, those of ray tracing and radiosity, and saw how much more realism they afford than the synthetic camera, though at hugely more computation cost.

The book by Jim Blinn [16], a CG pioneer, has several insightful articles, written in his particularly entertaining style, on various pipeline-related topics. Segal-Akeley [130] is a must-read high-level overview of the OpenGL pipeline written by two members of the original design team and, of course, the red book itself is a canonical source.

The seminal work on ray tracing was by Appel [3] and Whitted [151], and on radiosity by Goral [60]. A classic introduction to ray tracing is by Glassner [56]. For more advanced reading about ray tracing and radiosity, some useful textbooks are Akenine-Möller, Haines & Hoffman [1], Buss [21] and Watt [150]. Cohen & Wallace [25] and Sillion & Puech [134] are especially about radiosity.

APPENDIX A

Projective Spaces and Transformations

Projective geometry is at the heart of computer graphics whichever view you take of it, practical or theoretical. The various transformations of real 3-space we learned to use for the purpose of animation in Chapter 4 and studied mathematically in Chapter 5 are, in fact, most naturally viewed as transformations of projective 3-space, following a so-called lifting of the scene from real to projective space. A consequence is that representing these transformations as projective is more efficient from a computational point of view, a fact that OpenGL takes constant advantage of in its design. Capturing the scene after a perspective projection on film – "shooting" as we imagine the OpenGL point camera to do – involves a projective transformation as well.

In fact, it's not an exaggeration to say that projective geometry is the mathematical foundation of modern-day CG, and that API's such as OpenGL "live" in projective 3-space. Unfortunately, though, because projective geometry works its magic deep inside the graphics pipeline, its importance often is not realized.

There are several books out there which discuss projective geometry – Coxeter [30], Henle [73], Jennings [78], Pedoe [111] and Samuel [124] come to mind – from mainly a geometer's point of view, as well as a few, such as Baer [5] and Kadison & Kromann [79], which take an algebraic standpoint. All these books, however, seem written primarily for a student of mathematics. There seems none yet dedicated to answering the computer scientist's (almost certainly a CG person) question of projective geometry, "What can you do for me?"

This appendix is a small attempt to fill this gap in the literature and introduce projective spaces and transformations from a CG point of view.

Projective spaces generalize real space. They are not difficult to understand, but geometric primitives, such as lines and planes, behave somewhat differently in a projective space than a real one. By applying a camera-view analogy from the outset, we try to convey a physical-based intuition for basic concepts, establishing at the same time connection with CG.

This appendix is long and the mathematics often admittedly abstract, but the payback for persevering through it comes in the form of a wealth of applications, including the projection transformation in the graphics pipeline, as well as the rational Bézier and all-important NURBS primitives, which are all topics of Chapter 20 on applications of projective spaces.

Logically, this appendix could as well have been a chapter of the book, just prior to Chapter 20. However, we decided against upsetting the fairly easy gradient of the book from the first chapter to the last with the insertion of a mathematical "hill".

In fact, Chapter 20 on applications has been written so that the reader reluctant to take on the venture into projective theory can still make her way through it with minimal loss. This is not in any way to diminish the importance of the material in this appendix, but merely recognition of the reality that there are numbers of people out there who would make fine CG professionals, but care little for abstract mathematics.

We begin in Section A.1 by invoking a camera's point of view to motivate the definition of the projective plane. The geometry of this plane, including its surprising point-line duality and coordinatization by means of the homogeneous coordinate system, is the topic of Sections A.2 and A.3. In Section A.4 we study the structure of the projective plane and learn that the real plane can be embedded in the projective, which in turn yields a classification of projective points into regular ones and those at infinity.

A particularly intuitive kind of projective transformation, the so-called snapshot transformation, comes next in Section A.5. Section A.6 covers a few applications of homogeneous polynomial equations, including an algebraic insight into the projective plane's point-line duality, and an algebraic method to compute the outcome of a snapshot transformation. Following a brief discussion of projective spaces of arbitrary dimension in Section A.7, we move on to projective transformations.

Projective transformations are first defined algebraically in Section A.8 and then understood geometrically in A.9. In Section A.10 we relate projective, snapshot and affine transformations, and see that projective transformations are more powerful than either of the other two. The process of determining the projective transformation to accomplish some particular mapping – often beyond the reach of an affine transformation – is the topic of Section A.11.

A.1 Motivation and Definition of the Projective Plane

Consider a viewer taking pictures with a point camera with a film in front of it. Light rays from objects in the scene travel toward the camera and their intersections with the film render the scene. See Figure A.1. Captured on film is the (perspective) projection of the objects. In the case of OpenGL, this is precisely the situation when the user defines a viewing frustum: the point camera is at the apex of the frustum, while the film lies along its front face.

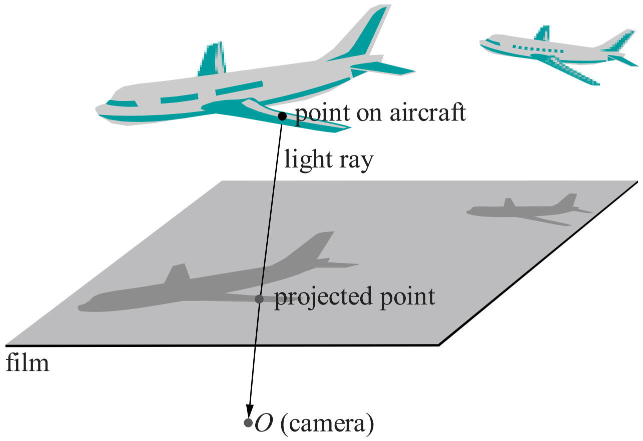

Figure A.1: Perceiving objects with a point camera and a plane film.

Clearly, points in the scene that lie on the same (straight) line through the camera cannot be distinguished by the viewer. In fact, all objects, e.g., points and line segments, lying on one line l through the camera cannot be distinguished by the viewer. They all project to and are perceived as a single point on the film. See Figure A.2(a). Assume for the moment that the film is two-sided and that objects behind project onto it as well (depicted is one such point). For now, ignore as well that lines through the camera parallel to the film, e.g., l^1, do not intersect the latter at all. This is owing to the alignment of the film, which can always be changed.

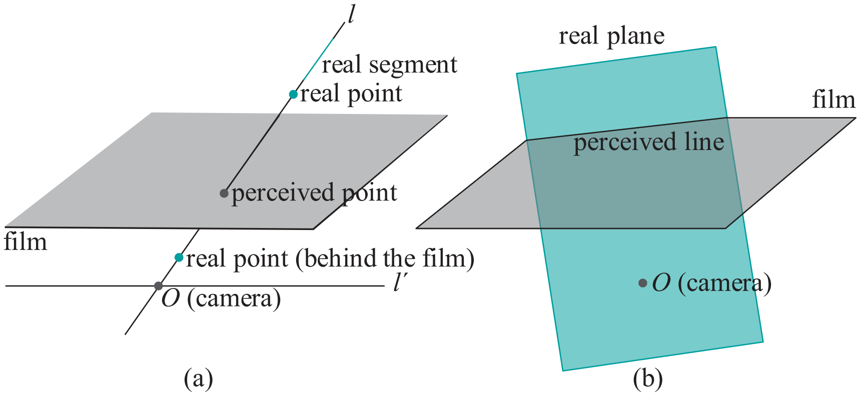

Figure A.2: Perceiving points, lines and planes by projection.

So, one can say that the viewer perceives *every* line through the camera as a point. What then does he perceive as a line? The likely answer is a plane. Indeed, any plane through the camera intersects the film in a line, though, again, the film may have to be re-aligned so as not to be parallel to the plane. See Figure A.2(b).

Lines are points, planes are lines, Let's take a moment to formalize, as a new space, the world as it is perceived through a point camera at the origin. Recall that a *radial* primitive is one which passes through the origin.

Definition A.1. A radial line in 3-space $\mathbb{R}^3$ is called a *projective point* . The set of all projective points lying on any one radial plane in $\mathbb{R}^3$ is called a *projective line*. (See Figure A.3.)

The set of all projective points is called 2-dimensional *projective space* and denoted $\mathbb{P}^2$. $\mathbb{P}^2$ is also called the *projective plane*.

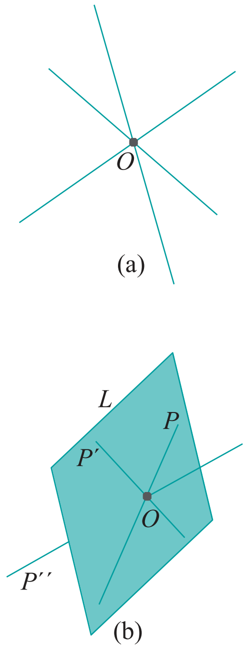

Figure A.3: (a) Projective points are radial lines (b) A projective line consists of all projective points on a radial plane: projective points P and $P^!$ belong to the projective line L, while $P^{!!}$ does not.

Remark A.1. We are taking a significant step up in abstraction in leaving $\mathbb{R}^2$ for $\mathbb{P}^2$. The real plane $\mathbb{R}^2$ is easy to visualize as, well, a real plane, e.g., a table top or a sheet of paper. Not so the projective plane. There is no real object to which it corresponds nicely.

Things such as a line, which is a set of points in one space, being just a point of another may seem a bit strange as well. It's mostly a matter of getting used to it though – like learning a foreign language. As with a new language, some words translate literally, but some don't simply because the concept isn't familiar (what's sandstorm in Eskimoan?).

It's recommended that the reader stick close to the real-based definitions at first. A thought process like "Hmm, the projective point P belongs to the projective line L. Well, then, this means that the real line which is P sits inside the real plane which is L" may seem cumbersome at first, but projective primitives will seem less and less strange as we go along.

The term "projective" arose because objects on the projective plane are perceived by projection onto a real one, which for us is the film. Observe that in Figure A.3(b) we denote by L both a radial plane (a primitive in $\mathbb{R}^3$), as well as the projective line (a primitive in $\mathbb{P}^2$) consisting of projective points that lie on that plane. There should be no cause for ambiguity as it'll be clear from the context which we mean.

Terminology: We'll generally use lower case letters to denote primitives in $\mathbb{R}^2$ and upper case for those in $\mathbb{P}^2$.

Remark A.2. The dimension of P² is two (as indicated by the superscript). This is because, while points in R³ have three "degrees of freedom", radial lines in R³ have only two. We'll elaborate on the dimension of the projective plane in Section A.7.

A.2 Geometry on the Projective Plane and Point-Line Duality

We have, then, on the projective plane P² projective points and projective lines, just as on the real plane R² we have real points and lines. It's interesting to compare the relationship between points and lines in the two spaces.

Recall the following two facts from Euclidean geometry (geometry in real space is called Euclidean):

(a) There is a unique line containing two distinct points in R².

(b) Two distinct lines in R² intersect in a unique point, *except* if they are parallel, in which case they do not intersect at all.

What is the situation in projective geometry?

Two distinct projective points P and P^1 correspond to two distinct radial lines in R³, and, in fact, there is a unique radial plane L in R³ containing the latter two. See Figure A.4(a).

It follows that:

(A) There is a unique projective line containing two distinct projective points in P².

How about two distinct projective lines? Observe that the corresponding two distinct radial planes, say, L and L^1 in R³, intersect in a unique radial line corresponding, in fact, to some projective point P. See Figure A.4(b). We have:

(B) Two distinct projective lines in P² intersect in a unique projective point.

No exceptions! There's no such thing as parallelism in P²! Any two different lines always intersect in a point. Two points–one line, two lines–one point, *always*: P² has better so-called *point-line duality* than R². We'll have more to say about the point-line duality of P² as we go along.

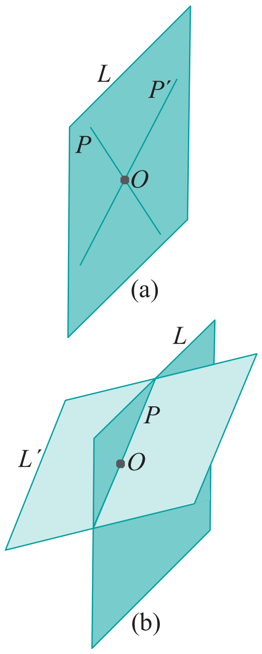

Figure A.4: (a) Radial lines corresponding to projective points P and $P^!$ are contained in a unique radial plane corresponding to the projective line L
(b) Radial planes corresponding to projective lines L and $L^!$ intersect in a unique radial line corresponding to the projective point P.

Exercise A.1. Consider three distinct projective lines L, L^1 and L^{11}. We know that their pairwise intersections are three projective points, say, P, P^1 and P^{11}. Give examples where (a) all three points are identical and (b) all three are distinct. Can only two of them be distinct? If all three are distinct can they be collinear, i.e., lie on one projective line?

A.3 Homogeneous Coordinates

We want to *coordinatize* P², if possible, in a manner similar to that of R² by Cartesian coordinates. This is important for the purpose of geometric calculations. For example, Cartesian coordinates on the real plane allow us to make a statement such as "The equation of the line through the $[-2 - 5]^T$ and $[1\ 1]^T$ is $y - 2x + 1 = 0$, which is satisfied as well by $[0\ -1]^T$, so that all three points are collinear."

So how does one coordinatize P²? As follows:

Definition A.2. The *homogeneous coordinates* of a projective point are the Cartesian coordinates of any real point on it, *other than* the origin. (No, homogeneous coordinates are not unique, a projective point having many different homogeneous coordinates. This may seem strange at first but read on)

Example A.1. The projective point P corresponding to the radial line through $[1\ 3\ -\ 2]^T$ has, as shown in Figure A.5, among others, homogeneous coordinates $[1\ 3\ -\ 2]^T$, $[2\ 6\ -\ 4]^T$, $[-1\ -\ 3\ 2]^T$ and $[1.7\ 5.1\ -\ 3.4]^T$. In fact, any tuple of the form $[c\ 3c\ -\ 2c]^T$, where c /= 0, can serve as homogeneous coordinates for P.

Terminology : To avoid clutter in diagrams, we'll often write homogeneous coordinates $[x\ y\ z]^T$ as (x, y, z).

That a projective point has infinitely many different homogeneous coordinates may seem odd, but it's not really a problem because two distinct projective points cannot share the same homogeneous coordinates. This is because two distinct radial lines do not share any point other than the origin. In other words, even though projective points have non-unique homogeneous coordinates, there is no risk of ambiguity. As an analogy, think of a roomful of people, each having multiple nicknames, but no two having a nickname in common – there is no danger of confusion then. As a non-zero tuple $[x\ y\ z]^T$ gives homogeneous coordinates of a unique projective point, we'll often refer to *the* projective point $[x\ y\ z]^T$ or write, say, the projective point $P = [x\ y\ z]^T$.

If you are wondering if P^2 can at all be coordinatized in a unique manner, as is R^2 by Cartesian coordinates, the answer is that there is no "natural" way to do this. Don't take our word for it, but give the question a bit of thought and you'll see the pitfalls. For example, a likely approach is to choose the coordinates of *one* real point from the radial line corresponding to each projective point. But then one has to come up with a *well-defined* way of choosing such a point; in other words, an *algorithm* that, given input a radial line, uniquely outputs a point from it. Try and devise such an algorithm! (The point on the line a unit distance from the origin? There are two such! The one in the positive direction? Be careful now: exactly which direction is this?)

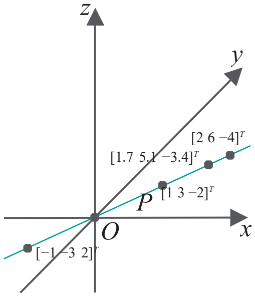

Figure A.5: The coordinates of any point on P , except the origin, can be used as its homogeneous coordinates – four possibilities are shown.

Remark A.3. An important difference between the Cartesian and homogeneous coordinate systems is the lack of an origin in the latter. No matter how one sets up a Cartesian coordinate system in R^3, i.e., no matter how one sets up the coordinate axes, the origin $(0, 0, \dots, 0)$ is always distinguished as a special point. This is not the case for the homogeneous coordinate system in P^2 – no projective point is special. It is truly homogeneous!

Example A.2. Find homogeneous coordinates of the projective point P of intersection of the projective lines L and L^1, corresponding, respectively, to the radial planes $2x + 2y - z = 0$ and $x - y + z = 0$.

Answer: Solving the simultaneous equations

$$\begin{aligned} 2x + 2y - z &= 0 \\ x - y + z &= 0 \end{aligned}$$

one finds that points on their intersecting line are of the form

$$y = -3x, \quad z = -4x$$

Therefore, homogeneous coordinates of P are (arbitrarily choosing $x = 1$)

$$[1\ -\ 3\ -\ 4]^T$$

Exercise A.2. Find homogeneous coordinates of the projective point P of intersection of the projective lines L and L^1 corresponding, respectively, to the radial planes $-x - y + z = 0$ and $3x + 2y = 0$.

Exercise A.3. Find the equation of the radial plane in R^3 corresponding to the projective line L which intersects the two projective points $P = [1\ 2\ 3]^T$ and $P^1 = [2\ \ -1\ 0]^T$.

A.4 Structure of the Projective Plane

We're going to try and understand the structure of P^2 by relating it to that of R^2. In fact, we'll start off by using the homogeneous coordinate system of P^2 to *embed* R^2 inside P^2.

A.4.1 Embedding the Real Plane in the Projective Plane

Associate a point $p = [x\ y]^T$ of R^2 with the projective point $\varphi(p) = [x\ y\ 1]^T$. The easiest way to picture this association is to first identify R^2 with the plane $z = 1$; particularly, $[x\ y]^T$ of R^2 is identified with $[x\ y\ 1]^T$ of $z = 1$. See Figure A.6. Following this, the association $p\rceil \rightarrow \varphi(p)$ is simply each real point with the radial line through it, in particular, the real point $[x\ y\ 1]^T$ (Cartesian coordinates) with the projective point $[x\ y\ 1]^T$ (homogeneous coordinates).

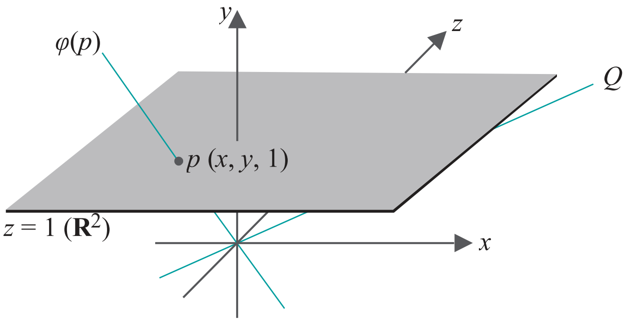

Figure A.6: Real point p on the plane $z = 1$ is associated with the projective point $\varphi(p)$. Projective point Q, lying on the plane $z = 0$, is not associated with any real point.

The association $p\rceil \rightarrow\ \varphi(p)$ is clearly one-to-one as distinct points of $z = 1$ give rise to distinct radial lines through them. It's not onto as points of P^2 that lie *on* the plane $z = 0$ or, equivalently, are parallel to $z = 1$, do not intersect $z = 1$ and, therefore, are not associated with any point of R^2 (e.g., Q in the figure). Precisely, points of P^2 with homogeneous coordinates of the form $[x\ y\ 0]^T$ are not associated with any point of R^2.

R^2, therefore, is embedded by φ as the *proper* subset of P^2 consisting of radial lines intersecting $z = 1$. We're at the point now where we can try to understand how we ended up trading parallelism in R^2 for perfect point-line duality in P^2.

A.4.2 A Thought Experiment

Here's a thought experiment. Two parallel lines l and l^1 lie on R^2, aka the plane $z = 1$ in R^3, a distance of d apart. Points p and p^1 on l and l^1, respectively, start a distance d apart and begin to travel at the same speed and in the same direction on their individual lines. See Figure A.7. Evidently, they remain d apart no matter how far they go. Well, of course, as l and l^1 are parallel!

Consider next what happens to the projective points $\varphi(p)$ and $\varphi(p^1)$ associated with p and p^1, respectively. See again Figure A.7 to convince yourself that both $\varphi(p)$ and $\varphi(p^1)$ draw closer and closer to that particular radial line l^{11} on the plane $z = 0$ which is parallel to l and l^1. As it lies on $z = 0$, l^{11} corresponds to a projective point P^{11} not associated with any real; in fact, P^{11}'s homogeneous coordinates are of the form $[x\ y\ 0]^T$.

Observe that the projective point $\varphi(p)$ itself travels along a projective line L – the one whose radial plane contains l. We'll call L the projective line corresponding to l. Likewise, the projective point $\varphi(p^1)$ travels along the projective line L^1 corresponding to l^1. Moreover, L and L^1 intersect in P^{11}. See Figure A.8.

Let's take stock of the situation so far. The parallel lines l and l^1 on the real plane never meet, but the projective lines L and L^1 corresponding to them in P^2 meet in P^{11}.

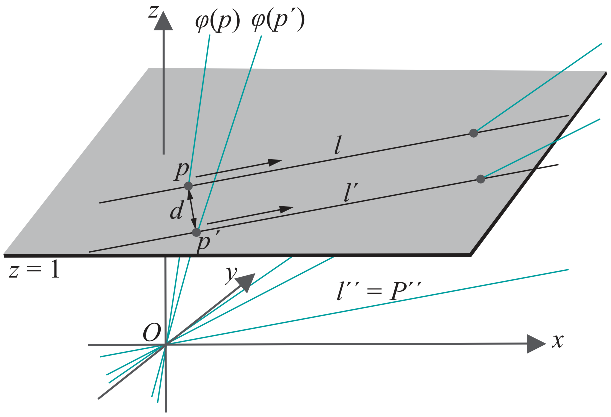

Figure A.7: The real points p and $p^{!}$ travel along parallel lines l and $l^{!}$. Associated projective points $\varphi(p)$ and $\varphi(p^{!})$ travel with p and $p^{!}$.

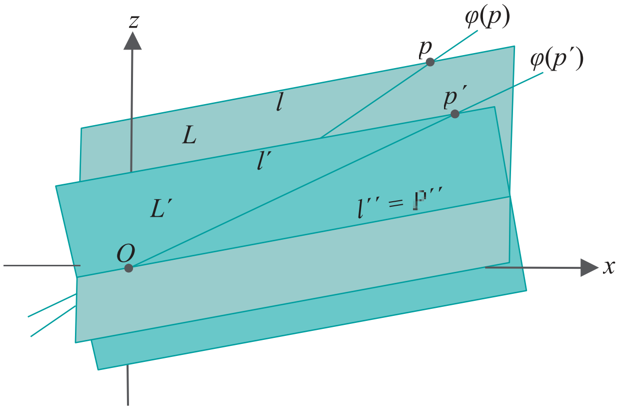

Figure A.8: $\varphi(p)$ travels along L and $\varphi(p^{!})$ along $L^{!}$. L and $L^{!}$ meet at $P^{!!}$.

Moreover, every point of L or L^1, *except* for P^{11}, is associated by φ to a point of l or l^1, respectively. We can say then that the projective line L equals its real counterpart l *plus* the extra point P^{11}; L^1, likewise, is its real counterpart l^1 *plus* P^{11}. And, it's at this point P^{11}, beyond the reals, that the two projective lines meet, while their real counterparts never do.

Example A.3. What if both points p and p^1, and together with them $\varphi(p)$ and $\varphi(p^1)$, travel along their respective lines in directions opposite to those indicated in Figure A.7? What if only one reversed its direction?

Answer : If both p and p^1 reversed directions, then again they would travel forever exactly d apart. If only one of the two reversed its direction, then, of course, the distance between them would continuously increase.

However, in either case, $\varphi(p)$ and $\varphi(p^1)$ draw closer, again both to P^{11}. It seems that, whatever the sense of travel is of $\varphi(p)$ and $\varphi(p^1)$ along their respective projective lines L and L^1, they approach that one point of intersection of these two lines. Two points traveling in opposite directions along a real line ultimately grow farther and farther apart. A projective line, on the other hand, apparently behaves more like a circle.

A.4.3 Regular Points and Points at Infinity

Recall *equivalence relations* and *equivalence classes* from undergrad discrete math. In particular, recall that the lines of R^2 can be split into equivalence classes by the equivalence relation of being parallel. Consider any equivalence class l of parallel lines of R^2, the latter being identified with the plane z = 1 in R^3 as before. There is a unique radial line l on the plane z = 0 parallel to the members of l. See Figure A.9.

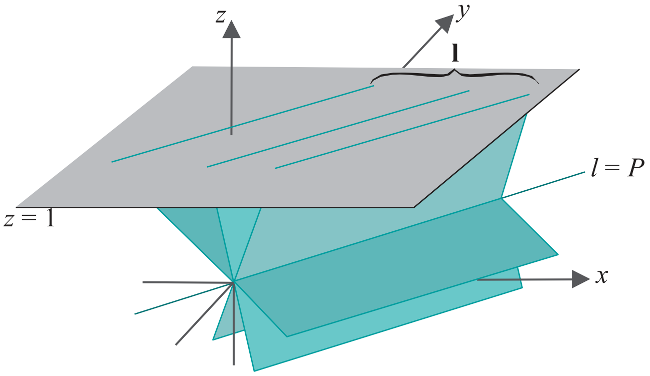

Figure A.9: The line l (= projective point P) is parallel to lines in l. P is said to be the point at infinity along the equivalence class l of parallel lines.

Denote the projective point corresponding to l by P . Projective lines corresponding to lines in l all meet at P , because their radial planes each contain l. The point P , which is not associated with any real point by φ as it lies on z = 0, is called the *point at infinity* along l or, simply, the point at infinity along any one of the lines in l. Conversely, any radial line l on the plane z = 0 is the point at infinity along the equivalence class of lines in R^2 parallel to it. In other words, the correspondences

$$\text{equivalence class of parallel lines in R}^2 \longleftrightarrow \text{radial line on } z = 0$$
$$\longleftrightarrow \text{point at infinity of P}^2$$

are both one-to-one. Note that points at infinity of P^2 are precisely those with homogeneous coordinates of the form $[x\ y\ 0]^T$.

Returning to the thought experiment of Section A.4.2, one can imagine points at infinity plugging the "holes" along the "border" of R^2 through which parallel lines "run off" without meeting, which explains why every pair of lines on the projective plane meets.

Projective points which are not points at infinity are called *regular points*. Regular points have homogeneous coordinates of the form $[x\ y\ z]^T$, where z is *not* zero. Moreover, regular points intersect z = 1, so are associated each by φ^{-1} with a point of R^2 (remember φ takes a real point of R^2, represented by the plane z = 1, to the projective point whose corresponding radial line passes through that point). Accordingly, one can write:

$$\text{P}^2 = \text{R}^2 \cup \{\text{points at infinity}\} = \{\text{regular points}\} \cup \{\text{points at infinity}\}$$

The union of all points at infinity, called the *line at infinity*, is the projective line whose radial plane is z = 0. Therefore, one can as well write:

$$\text{P}^2 = \text{R}^2 \cup \text{line at infinity} = \{\text{regular points}\} \cup \text{line at infinity}$$

Our embedding φ of R^2 as a subset of P^2 depends on the plane z = 1, particularly because we identify z = 1 with R^2 and subsequently associate each point of R^2 with the radial line in R^3 through it. Is there anything special about the plane z = 1? Not at all. It just seemed convenient. In fact, we could have used any *any* non-radial plane p.

Exercise A.4. Why does p have to be non-radial?

Example A.4. Instead of z = 1, identify R^2 with the plane x = 2 in R^3. Accordingly, embed R^2 into P^2 by associating $[x\ y]^T$ with the radial line through $[2\ x\ y]^T$. Which now are the regular points and which are the points at infinity of P^2?

Answer : The regular points of P^2 are the radial lines in R^3 which intersect the plane $x = 2$. These are precisely the radial lines which do not lie on the plane $x = 0$. The points at infinity are the radial lines which do lie on the plane $x = 0$. Equivalently, regular points have homogeneous coordinates of the form $[x\ y\ z]^T$, where $x = 0$, while points at infinity have homogeneous coordinates of the form $[0\ y\ z]^T$.

Exercise A.5. Identify R^2 with the plane $x + y + z = 1$ in R^3, embedding it into P^2 by associating $[x\ y]^T$ with the radial line through $[x\ y\ \ 1\ -x\ -y]^T$. Which now are the regular points and which the points at infinity of P^2?

It may seem strange at first that the separation of P^2 into regular points and points at infinity depends on the particular embedding of R^2 in P^2. However, this situation becomes clearer after a bit of thought. It's related, as a matter of fact, to the discussion at the beginning of the chapter, where we motivated projective spaces by observing that lines through a point camera are perceived as points on the plane film. Even though all lines through the camera do not intersect the film, we argued this to be merely an artifact of the alignment of the film, the latter being changeable. Therefore, we concluded that all radial lines should be taken as points in projective space.

We now come full circle back to this initially motivating scenario. Embedding R^2 in P^2 corresponds exactly to choosing an alignment of the film – the film is a copy of R^2 and each point on it associated with the light ray (= radial line in R^3 = point of P^2) through that point to the camera. Light rays toward the camera which intersect the film are regular points of P^2 and visible, while those which do not are points at infinity and invisible. Moreover, the line at infinity corresponds to the plane through the camera parallel to the film. And, of course, we are at perfect liberty to align the film, i.e., embed R^2 in P^2, as we like, different choices leading to different sets of visible and invisible light rays.

A.5 Snapshot Transformations

Here's another interesting thought experiment.

Example A.5. A point camera is at the origin with two power lines passing over it, both parallel to the x-axis. One lies along the line $y = 2,\ z = 2$ (i.e., the intersection of the planes $y = 2$ and $z = 2$) and the other along the line $y = -2, z = 2$.

Take "snapshots" of the power lines with the film aligned along (a) the plane $z = 1$ and (b) the plane $x = 1$. Sketch and compare the two snapshots.

Answer: This is one you might want to try yourself before reading on!

See Figure A.10. Figure A.10(a) shows the snapshot (or, projection) of the power lines (thin black lines) on the plane $z = 1$. These projections are the two *parallel* lines $y = 1$ and $y = -1$ (green). This is not hard to understand: by simple geometry, the line $y = 2,\ z = 2$ projects toward the origin (the camera) to the line $y = 1$ on the plane $z = 1$; likewise, $y = -2, z = 2$ projects to $y = -1$ on $z = 1$.

Figure A.10(b) shows the snapshot on the plane $x = 1$. It is the two *intersecting* lines $z = y$ and $z = -y$ making an X-shape. This requires explanation. The top of the X, above its center $[1\ 0\ 0]^T$, is formed from intersections with the film of light rays through points on the power lines with x-value greater than zero, while the bottom from rays through points with x-value less than zero. The rays from the points on either power line with x-value equal to zero do not strike the film.

The point $[1\ 0\ 0]^T$ at the center of the X is included in the snapshot, though no ray from either power line passes through it, because it's the intersection with the film of the "limit" of the rays from points on either power line as they run off to infinity. It's convenient to imagine the limits of visible rays as being visible as well and we ask the reader to accept this. In geometric drawing parlance $[1\ 0\ 0]^T$ is the *vanishing point* of the power lines – it's where they *seem* to meet on the film $x = 1$.

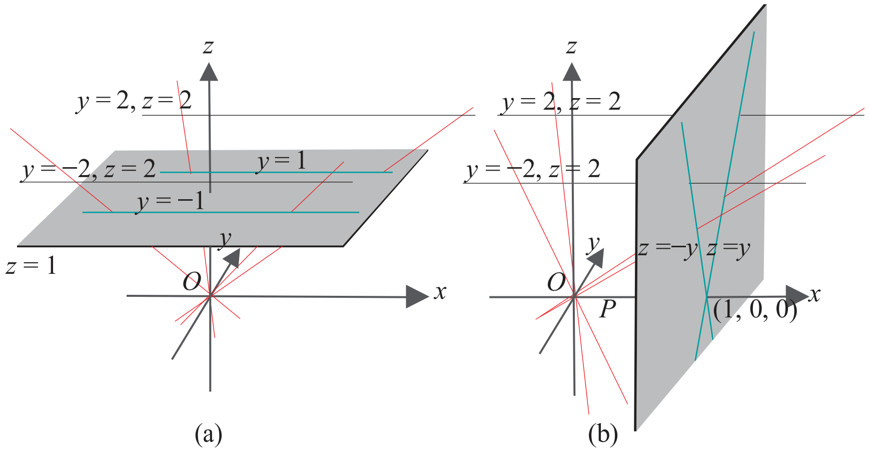

Figure A.10: Thin black power lines $y = \pm 2, z = 2$ projected onto the planes (a) $z = 1$ and (b) $x = 1$ as green lines. Red lines depict light rays. The x-axis corresponds to the projective point P.

Contemplate the situation from the point of view of projective geometry. The projective lines corresponding to the two power lines meet at the projective point P corresponding to the x-axis, as the radial planes through the power lines intersect in the x-axis. Now, P is a point at infinity with respect to the plane $z = 1$ (because the x-axis doesn't intersect this plane), while it's a regular point with respect to the plane $x = 1$ (because the x-axis intersects this plane at $[1\ 0\ 0]^T$). In terms of shooting pictures, then, the camera with its film along $z = 1$ cannot see where the two power lines meet, so they appear parallel. However, with its film along $x = 1$ the camera sees them meet at $[1\ 0\ 0]^T$.

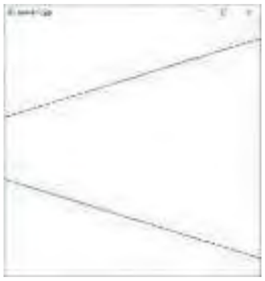

Figure A.11: Screenshot of turnFilm.cpp.

Experiment A.1. Run turnFilm.cpp, which animates the setting of the preceding exercise by means of a viewing transformation. Initially, the film lies along the $z = 1$ plane. Pressing the right arrow key rotates it toward the $x = 1$ plane, while pressing the left one reverses the rotation. Figure A.11 is a screenshot midway. You cannot, of course, see the film, only the view of the lines as captured on it.

The reason that the lower part of the X-shaped image of the power lines cannot be seen is that OpenGL film doesn't capture rays hitting it from behind, as the viewing plane is a clipping plane too. Moreover, if the lines seem to actually meet to make a V after the film turns a certain finite amount, that's because they are very long and your monitor has limited resolution!

This program itself is simple with the one statement of interest being gluLookAt(), which we ask the reader to examine next. End

Exercise A.6. (Programming) Verify that the gluLookAt() statement of turnFilm.cpp indeed simulates the film's rotation as claimed between the $z = 1$ and $x = 1$ planes.

Example A.6. Refer to Figure A.10(b). Suppose two power lines *actually* lie along the two intersecting lines $z = y$ and $z = -y$ on the plane $x = 1$, which is the snapshoton the plane $x = 1$ of the power lines of the preceding example. What would *their* snapshot look like on the films $z = 1$ and $x = 1$?

Answer : Exactly as in the preceding Example A.5, as depicted in Figures A.10(a) and (b)! It's not possible to distinguish between these two pairs of power lines – the pair in Example A.5 being "really" parallel and the current one "really" intersecting – with a point camera at the origin.

A somewhat whimsical take on all this is to imagine a Matrix-like world where one can never know reality. Perception is limited to whatever is captured on film. Therefore, one agent's intersecting power lines are just as real as the other's parallel ones!

It's useful to think of one snapshot of Example A.5 or A.6 as a *transformation* of the other. Keep in mind that if a snapshot appears as the two parallel lines $y = \pm 1$ on the film $z = 1$, then it always appears as the two intersecting lines $z = \pm y$ on the film $x = 1$, *regardless* of what the "real" objects are.

Convince yourself of this by mentally tilting one of the power lines in Figure A.10(a) on the radial plane (not drawn) through it, so that its projection on the $z = 1$ plane does not change. The power line's projection on the $x = 1$ plane remains unchanged, as well, because the set of light rays from it through the camera doesn't change. For this reason, it makes sense to talk of transforming one snapshot to another, without any reference to the real scene. We'll informally call such transformations *snapshot transformations*.

Remark A.4. Snapshot transformations as described are not really transformations in the mathematical sense, as they don't map some space to itself but, rather, one plane (film) to another. A rigorous formulation is possible, though likely not worth the effort, as we'll see soon that snapshot transformations are subsumed within the class of projective transformations, which we'll be studying in depth. Nevertheless, the notion of a snapshot transformation is geometrically intuitive and useful.

Here are more for you to ponder.

Exercise A.7. In each case below you are told what the snapshot looks like on the film $z = 1$, aka R^2, and asked what is captured on the film $x = 1$. The $z = 1$ shots are drawn in Figure A.12, each labeled the same as the item to which it corresponds. You don't have to find equations for your answer for $x = 1$. Just a sketch or a verbal description is enough.

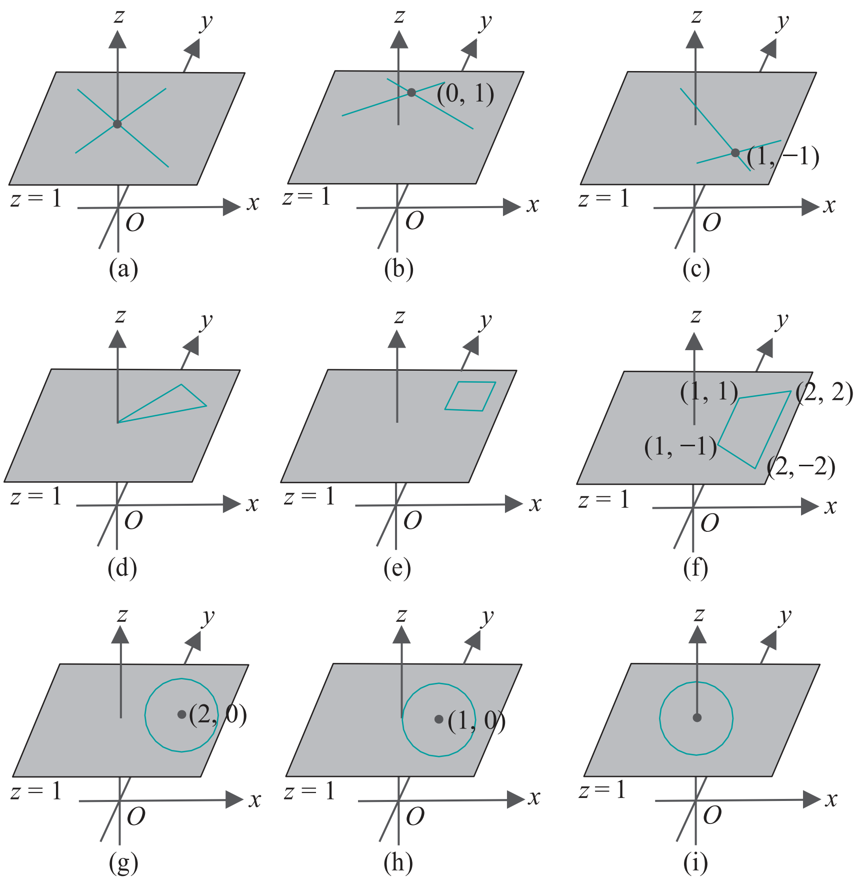

Figure A.12: Transform these snapshots on the plane $z = 1$ to the plane $x = 1$. Some points on the plane $z = 1$ are shown with their xy coordinates. Labels correspond to items of Exercise A.7.

Answers are in italics. Figure A.13 justifies the answer to (h).

(a) Two lines that intersect at the origin, neither being the y-axis (on $\mathbb{R}^2$).
Two parallel lines. Why the caveat? What happens if one is the y-axis?

(b) Two lines that intersect at the point $[0\ 1]^T$, neither being the y-axis.
Two parallel lines.

(c) Two lines that intersect at the point $[1\ -1]^T$.
Two intersecting lines.

(d) A triangle in the upper-right quadrant with one vertex at the origin but, otherwise, not touching the axes.
An infinitely long U-shape with straight sides.

(e) A square in the upper-right quadrant not touching any of the axes.
A quadrilateral with no two parallel sides.

(f) A trapezoid symmetric about the x-axis with vertices at $[1\ 1]^T$, $[1\ -1]^T$, $[2\ -2]^T$ and $[2\ 2]^T$.
A rectangle.

(g) A unit radius circle centered at $[2\ 0]^T$.
An ellipse.

(h) A unit radius circle centered at $[1\ 0]^T$.
A parabola – see Figure A.13.

(i) A unit radius circle centered at the origin.
A hyperbola.

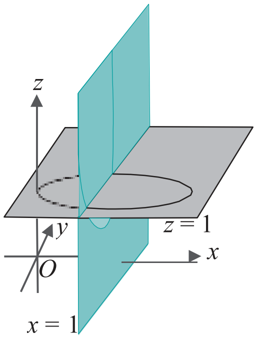

Figure A.13: Answer to Exercise A.7(h).

Remark A.5. Exercise A.7(f) seems innocuous enough, but it is very important. Its generalization to 3D will help convert viewing frustums to rectangular boxes in the graphics pipeline.

Exercise A.8. Refer to the geometric construction of conic sections in Section 10.1.5 as plane sections of a double cone, and show that any non-degenerate conic section can be snapshot transformed to another such.

Exercise A.9. (Programming) Write code similar to turnFilm.cpp to animate the snapshot transformation of Exercise A.7(h). Again, you'll see only part of the parabola because OpenGL cannot see behind its film.

It's not hard to see that none of the snapshot transformations of Exercise A.7, except for (c) and (g), can be accomplished using OpenGL modeling transformations. This is because they are not affine – recall from Section 5.4.5 that OpenGL implements only affine transformations.

Remark A.6. We just said that most of the snapshot transformations of Exercise A.7 are not affine and yet seem to be suggesting with the preceding Exercise A.9 that they may be implemented by means of an OpenGL viewing transformation. We know, however, that the latter is equivalent to a sequence of modeling transformations and, therefore, affine.

The apparent conundrum is not hard to resolve. The result of the viewing transformation of, e.g., turnFilm.cpp, is indeed a snapshot transformation in terms of what is *seen on the screen*. In other words, the transformation from the OpenGL window prior to applying the viewing transformation to that after is a snapshot transformation. However, the viewing transformation serves only to change the scene to one which OpenGL *projects* onto the window as the new one. A snapshot transformation, therefore, is more than a viewing transformation – it's a viewing transformation *plus* a projection.

Exercise A.10. By considering how to turn the film, i.e., viewing plane, show that implementing a snapshot transformation in OpenGL is equivalent to:

(a) setting the *centerx* , *centery* , *centerz* , *upx* , *upy* and *upz* parameters of the viewing transformation

gluLookAt(0, 0, 0, *centerx*, *centery*, *centerz*, *upx*, *upy*, *upz*)

and

(b) setting the *near* parameter of the perspective projection call

glFrustum(*left*, *right*, *bottom*, *top*, *near*, *far*)

where the other five parameters can be kept fixed at some initially chosen values.

A.6 Homogeneous Polynomial Equations

The only application we've made so far of homogeneous coordinates is to embed $\mathbb{R}^2$ in $\mathbb{P}^2$. We haven't used them yet to write equations of curves on the projective plane. Let's try now to do this.

We'll start with the simplest curve on the projective plane, in fact, a projective line. We want an equation – as for straight lines in real geometry – that will say if a projective point belongs to a projective line. For example, an equation such as $2x + y - 1 = 0$ for a straight line on the real plane gives the condition for a real point $[x\ y]^T$ to lie on that line.

Now, a projective point is a radial line and a projective line a radial plane. Moreover, a radial line lies on a radial plane if and only if any point of it, other than the origin, lies on that plane (the origin always does). See Figure A.14.

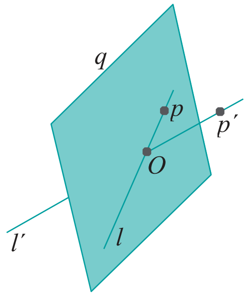

Figure A.14: Point p of radial line l lies on radial plane q, implying that l lies on q; point p' of l' doesn't lie on q, implying that no point of l', other than the origin, lies on q.

Therefore, a projective point $P = [x\ y\ z]^T$ belongs to a projective line L, whose radial plane has the equation $ax + by + cz = 0$, if and only if the real point $[x\ y\ z]^T$ lies on the real plane $ax + by + cz = 0$. It follows that the equation of L is identical to that of its radial plane:

$$ax + by + cz = 0 \tag{A.1}$$

Accordingly, a projective point $P = [x\ y\ z]^T$ belongs to L if it satisfies (A.1). Does it matter if we choose some other homogeneous coordinates for P? No, because

$$a(kx) + b(ky) + c(kz) = k(ax + by + cz) = 0$$

so any homogeneous coordinates $[kx\ ky\ kz]^T$ for P satisfy Equation (A.1).

Exercise A.11. Prove that if the projective line L is specified by the equation

$$ax + by + cz = 0$$

then it is specified by any equation of the form

$$(ma)x + (mb)y + (mc)z = 0$$

where m 0, as well.

Exercise A.12. What is the equation of the projective line through the projective points $[2\ 1\ -1]^T$ and $[3\ 4\ 2]^T$?

Answer: Suppose that the line is L with equation

$$ax + by + cz = 0$$

Since $[2\ 1\ \ -1]^T$ and $[3\ 4\ 2]^T$ lie on L they must satisfy its equation, giving

$$\begin{aligned} 2a + b - c &= 0 \\ 3a + 4b + 2c &= 0 \end{aligned}$$

Any solution to these simultaneous equations, not all zero, then determines L. As there are more variables then equations, let's set one of them, say c, arbitrarily to 1, to get the equations

$$\begin{aligned} 2a + b - 1 &= 0 \\ 3a + 4b + 2 &= 0 \end{aligned}$$

These solve to give $a = 1.2$ and $b = -1.4$. The equation of the projective line L is, therefore,

$$1.2x - 1.4y + z = 0$$

(or, equivalently, $6x - 7y + 5z = 0$, from Exercise A.11.)

Exercise A.13. What is the projective point of intersection of the projective lines $3x + 2y - 4z = 0$ and $x - y + z = 0$?

Exercise A.14. When are three projective points $[x\ y\ z]^T$, $[x^1\ y^1\ z^1]^T$ and $[x^{11}\ y^{11}\ z^{11}]^T$ collinear, i.e., when do they belong to the same projective line? Find a simple condition involving a determinant.

A.6.1 More About Point-Line Duality

In Section A.4.2 we tried to understand the point-line duality of the projective plane from a geometric point of view. We'll examine the phenomenon now from an algebraic standpoint.

The correspondence from the set of projective points to the set of projective lines given by

$$\text{projective point } [a\ b\ c]^T \quad 1\!\rightarrow \quad \text{projective line } \ ax + by + cz = 0 \qquad \text{(A.2)}$$

is well-defined as, whatever homogeneous coordinates we choose for a projective point, the image is the same projective line (by Exercise A.11). Moreover, the correspondence is easily seen to be one-to-one and onto.

Definition A.3. The projective line $ax + by + cz = 0$ is said to be the *dual* of the projective point $[a\ b\ c]^T$ and vice versa.

Exercise A.15. Prove that a projective point P belongs to a projective line L if and only if the dual of L belongs to the dual of P.

The preceding exercise implies that if some statement about the incidence of projective points and lines is true, then so is the dual statement, obtained by replacing "point" with "line" and "line" with "point".

Exercise A.16. What is the dual of the following statement? "There is a unique projective line incident to two distinct projective points."

From this last exercise one sees, then, the point-line duality of the projective plane as a consequence of the one-to-one correspondence (A.2) between projective points and lines. We ask the reader to contemplate if there exists a similar correspondence between real points and lines.

A.6.2 Lifting an Algebraic Curve from the Real to the Projective Plane

Let's see next projective curves more complex than a line. Consider, then, the curve Q^1 in P^2 consisting of the projective points intersecting the parabola q

$$y - x^2 = 0 \tag{A.3}$$

on R^2 (the plane $z = 1$). See Figure A.15.

The intersection of the projective point $P = [x\ y\ z]^T$ with the plane $z = 1$ is the real point $[x/z\ y/z\ 1]^T$, assuming $z \neq 0$, for, otherwise, there is no intersection. Now, $[x/z\ \ y/z\ 1]^T$ satisfies the equation of the parabola q if

$$y/z - (x/z)^2 = 0 \quad \Longrightarrow \quad yz - x^2 = 0$$

Accordingly, the curve consisting of projective points $[x\,y\,z]^T$ which satisfy

$$yz - x^2 = 0 \tag{A.4}$$

is called the *lifting* Q of q from the real to the projective plane. Q is sometimes simply called the lifting of q and also the *projectivization* of q. In this particular case, as a lifting of a parabola, Q is a *parabolic projective curve*.

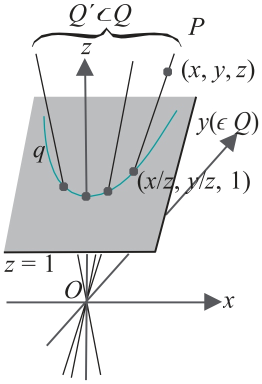

Figure A.15: Lifting a parabola drawn on the real plane $z = 1$ to the projective plane.

The camera analogy is that Q is the set of rays seen, by intersection with the film $z = 1$, as q. However, Q is actually one point *bigger* than Q^1, the set of projective points intersecting the parabola q on R^2, as it includes the projective point $[0\ 1\ 0]^T$, the y-axis of 3-space, which satisfies (A.4), but does not intersect q. So, $Q = Q^1 \cup \{[0\,1\,0]^T\}$. We can justify the inclusion of this extra point, with the help of the proviso from Section A.5 that a limit of visible rays is visible, as follows.

From its equation $y - x^2 = 0$, a point of q is of the form $[x\ x^2\ 1]^T$, for any x. Therefore, the homogeneous coordinates of a projective point intersecting q are $[x\ x^2\, 1]^T$, for any x, as well. Rewriting these coordinates as $[\frac{1}{x}\ 1\ \frac{1}{x^2}]^T$ we see that its limit as $x \to \infty$ is indeed $[0\ 1\ 0]^T$. More intuitively, *a la* the thought experiment of Section A.4.2, as a point p travels off along either wing of the parabola, the projective point $\varphi(p)$, corresponding to the line through p, approaches $[0\ 1\ 0]^T$, the projective point corresponding to the y-axis.

Definition A.4. A *homogeneous polynomial* is one whose terms each have the same degree, the degree of a term being the sum of the powers of the variables in the term. This common degree is called the degree of the homogeneous polynomial.

An equation with a homogeneous polynomial on the left and 0 on the right is called a homogeneous polynomial equation.

The equations $ax + by + cz = 0$ of a projective line and $yz - x^2 = 0$ of a parabolic projective curve are homogeneous polynomial equations of degree one and two, respectively. That they are both homogeneous is no accident, as we'll soon see.

Exercise A.17. Suppose that $p(x_1, x_2, \ldots, x_n)$ is a homogeneous polynomial in n variables. Then, if $[x_1\ x_2 \ldots x_n]^T$ satisfies the equation $p(x_1, x_2, \ldots, x_n) = 0$, so does $[cx_1\ cx_2\ \ldots\ cx_n]^T$, for any scalar c.
Hint: Show, first, that, if $p(x_1, x_2, \ldots, x_n)$ is homogeneous of degree r, then

$$p(cx_1, cx_2, \ldots, cx_n) = c^r p(x_1, x_2, \ldots, x_n)$$

For example, for the homogeneous polynomial $yz - x^2$ of degree 2,

$$(cy)(cz) - (cx)^2 = c^2(yz - x^2)$$

So, in this case, if (x, y, z) satisfies $yz - x^2 = 0$, then so does (cx, cy, cz), because $(cy)(cz) - (cx)^2 = 0$ as well, by the equation just above.

The preceding exercise implies that a homogeneous polynomial equation of the form $p(x, y, z) = 0$ is legitimately an equation in P^2, because a point of P^2 can be tested if it satisfies $p(x, y, z) = 0$, independently of the homogeneous coordinates used to represent the point. Here are some definitions.

Definition A.5. An *algebraic curve* on the real plane consists of points satisfying an equation of the form

$$p(x, y) = 0$$

where p is a polynomial in the two variables x and y. The degree of the curve is the highest degree of a term belonging to $p(x, y)$.

Familiar algebraic curves of degree one include straight lines, e.g., $2x + y - 3 = 0$, while conic sections, e.g., the hyperbola $xy - 1 = 0$, are of degree two.

Definition A.6. A *projective algebraic curve* on the projective plane consists of points satisfying an equation of the form

$$p(x, y, z) = 0$$

where p is a homogeneous polynomial in the three variables x, y and z. The degree of the curve is the degree of $p(x, y, z)$.

Projective algebraic curves that we have already seen are the projective line $ax + by + cz = 0$ of degree one and the projective parabola $yz - x^2 = 0$ of degree two. Let's get a few more via lifting.

Example A.7. Lift the algebraic curve of degree 3

$$x^3 + 3x^2y + y^2 + x + 2 = 0$$

drawn on the plane $z = 1$, to P^2.

Answer : The projective point $[x\ y\ z]^T$ intersects the plane $z = 1$ at the real point $[x/z\ y/z\ 1]^T$ (assuming $z = 0$). Accordingly, replace x by x/z and y by y/z in the given polynomial equation:

$$\begin{aligned} & (x/z)^3 + 3(x/z)^2(y/z) + (y/z)^2 + x/z + 2 = 0 \\ \Longrightarrow\quad & x^3/z^3 + 3x^2y/z^3 + y^2/z^2 + x/z + 2 = 0 \\ \Longrightarrow\quad & x^3 + 3x^2y + y^2 z + xz^2 + 2z^3 = 0 \end{aligned}$$

defining the lifted curve, a projective algebraic curve of degree 3.

Exercise A.18. Lift the algebraic curve of degree 5

$$xy^4 - 2x^2y^2 + 3xy^2 + y^3 - xy + 2 = 0$$

drawn on the plane $z = 1$, to P^2.

Exercise A.19. Show that the lifting of the straight line

$$ax + by + c = 0$$

drawn on the plane $z = 1$, to P^2, in fact, is the projective line corresponding to it, as defined in Section A.4.2. Moreover, this line is a projective algebraic curve of degree 1.

It should be fairly clear at this point that the lifting of an algebraic curve $p(x, y) = 0$ is a projective algebraic curve $\bar{p}(x, y, z) = 0$ of the same degree. We leave a formal proof to the reader in the following exercise.

Exercise A.20. Show that the lifting of an algebraic curve $p(x, y) = 0$ of degree r is a projective algebraic curve $\bar{p}(x, y, z) = 0$ of degree r.

Definition A.7. The process of going from the equation of an algebraic curve on the real plane to the homogeneous polynomial equation of its lifting is called *homogenization*.

It's worth keeping mind that the process of homogenization depends on the particular plane on which the algebraic equation holds. E.g., in Example A.7 and Exercises A.18-A.19 the plane was $z = 1$. This need not always be the case as we see next.

Example A.8. Homogenize the polynomial equation

$$y^2 + z^2 + z = 0$$

drawn on the plane $x = 2$. (So, $x = 2$ is treated as a copy of the yz-plane.)

Answer : The projective point $[x\ y\ z]^T$ intersects the plane $x = 2$ at the real point$[2\ \ 2y/x\ \ 2z/x]^T$ (assuming $x = 0$, and multiplying $[x\ y\ z]^T$ by $2/x$). Accordingly, replace y by $2y/x$ and z by $2z/x$ in the given polynomial equation:

$$(2y/x)^2 + (2z/x)^2 + 2z/x = 0 \quad \Longrightarrow \quad 4y^2/x^2 + 4z^2/x^2 + 2z/x = 0$$

Multiplying throughout by x^2 one gets the homogenized polynomial equation

$$4y^2 + 4z^2 + 2xz = 0$$

Not surprisingly, giving the algebraic equation on different real planes corresponds, simply, to specifying the algebraic curve as seen by the viewer on differently aligned films. The lifting itself, of course, is the set of rays intersecting the film in the given curve, which does not change.

Exercise A.21. Homogenize the polynomial equation

$$3x^4 + 2x^2y + 2y^3 + 2x^2 + xy + x = 0$$

drawn on the plane $z = 4$.

Exercise A.22. Homogenize the polynomial equation

$$x^3 + 2xz - z^4$$

drawn on the plane $y = 2$.

Remark A.7. It's possible to define the homogenization of a polynomial in an abstract manner independent of reference to a particular plane. See Jennings [78].

One sees, then, that the algebraic analogue of lifting an algebraic curve from the real to the projective plane is homogenization. The reverse process of projecting a (projective algebraic) curve onto a real plane consists of taking the section of the projective points composing the curve with the given plane. Algebraically, this means simultaneously solving the equation of the curve and that of the plane – a process not surprisingly called *de-homogenization*.

Example A.9. Project the curve

$$yz - x^2 = 0$$

in P^2 onto the real plane $z = 1$.

Answer: De-homogenize the equation of the curve by simultaneously solving

$$\begin{aligned} yz - x^2 &= 0 \\ z &= 1 \end{aligned}$$

to get

$$y - x^2 = 0$$

which is the equation of a parabola.

Exercise A.23. Project the curve of the preceding example onto the real plane $x = 1$.

Exercise A.24. Project the curve

$$4y^2 + 4z^2 + 2xz = 0$$

in P^2 onto the real plane $y = -2$.

A.6.3 Snapshot Transformations Algebraically

It should make sense now that the snapshot transformation of an algebraic curve c from one real plane p to another p^1 can be determined by (a) first homogenizing the equation of c to lift it to the projective plane, and, then (b) de-homogenizing to project it back onto p^1.

Example A.10. Let's solve the snapshot transformation problem of Exercise A.7(h) algebraically. The equation of the unit circle, centered at $[1\ 0]^T$ on the $z = 1$ plane, is

$$x^2 + y^2 - 2x = 0$$

Homogenizing, one gets

$$x^2 + y^2 - 2xz = 0$$

To project onto the plane $x = 1$, de-homogenize by simultaneously solving

$$\begin{aligned} x^2 + y^2 - 2xz &= 0 \\ x &= 1 \end{aligned}$$

to get

$$y^2 - 2z + 1 = 0 \quad \Longrightarrow \quad z = \frac{1}{2}y^2 + \frac{1}{2}$$

which indeed agrees with the sketch of a parabola in Figure A.13.

Exercise A.25. Solve Exercises A.7(g) and (i) algebraically.

A.7 The Dimension of the Projective Plane and Its Generalization to Higher Dimensions

Note: The next few paragraphs about P^2 as a surface require recollecting some of the material from Section 10.2.12 on surface theory. If the reader is not inclined to do so, then she can safely skip ahead to Definition A.8. It won't affect her understanding of anything that follows.

Why do we say that the projective plane is a projective space of dimension 2? Because, as we'll see momentarily, P^2 is a surface. In fact, it's a regular C^∞ surface, *except* that it is not a subset of R^3: it's not possible to embed P^2 in R^3. One must go at least one dimension higher to R^4.

Ignoring for now the question of the space in which it's embedded, it's not hard to find a coordinate patch containing any given point $P \in \mathbb{P}^2$. Suppose, for the moment, that P intersects the point p on the plane $z = 1$ (our favorite copy of $\mathbb{R}^2$). See Figure A.16. Let W be a closed rectangle containing p and B be the set of projective points intersecting W. The function

$$\text{point} \mapsto \text{the radial line through it}$$

from W to B is a one-to-one correspondence that makes B a coordinate patch.

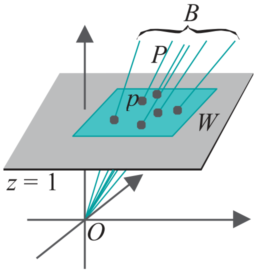

Figure A.16: The coordinate patch B containing P in $\mathbb{P}^2$ is in one-to-one correspondence with the rectangle W containing p in $\mathbb{R}^2$ (a few points in W and their corresponding projective points are shown).

And what if P doesn't intersect $z = 1$, i.e., if P is a point at infinity with respect to $z = 1$? Remember, there's nothing special about $z = 1$ – simply choose another non-radial plane with respect to which P is regular.

The reader has guessed by now that there exist projective spaces of various dimensions. True.

Definition A.8. A radial line in $\mathbb{R}^{n+1}$ is said to be an *n-dimensional projective point* . The set of all n-dimensional projective points is *n-dimensional projective space*, denoted $\mathbb{P}^n$.

$\mathbb{P}^0$, not very interestingly, is a one-point space as there is only one line, radial or otherwise, in $\mathbb{R}^1$. We'll try to convince the reader next, without being mathematically precise, that $\mathbb{P}^1$ is a circle.

Let U be the upper-half of a circle centered at the origin of $\mathbb{R}^2$. Associate with each radial line in $\mathbb{R}^2$ its intersection(s) with U . See Figure A.17, where, e.g., the radial line P is associated with the point p. Each radial line in $\mathbb{R}^2$ is then associated with a unique point of U, except for the x-axis, which we denote Q; Q intersects U in two points q_1 and q_2. And, the other way around, every point of U is associated with a unique radial line, except only for q_1 and q_2, which are associated with the same one Q. It follows, then, that the set $\mathbb{P}^1$ of all radial lines in $\mathbb{R}^2$ is in one-to-one correspondence with the space obtained by "identifying" the two endpoints q_1 and q_2 of U as one. But this latter space is clearly a circle (imagine U as a length of string whose ends are brought together).

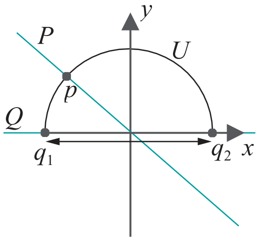

Figure A.17: Identifying $\mathbb{P}^1$ with a circle.

One can set up homogeneous coordinates for an arbitrary $\mathbb{P}^n$ in a manner similar to what we did for $\mathbb{P}^2$. For example, the homogeneous coordinates of a point $P \in \mathbb{P}^3$ are the coordinates of any point, other than the origin, on the radial line in $\mathbb{R}^4$ to which it corresponds. So the homogeneous coordinates of the point in $\mathbb{P}^3$ corresponding to the radial line through $[x\ y\ z\ w]^T$, where x, y, z and w are not all zero, is any tuple of the form $[cx\ cy\ cz\ cw]^T$, where $c = 0$.

It's hard to visualize $\mathbb{P}^3$ and higher-dimensional projective spaces for the same reason that it's hard to visualize $\mathbb{R}^4$ and higher-dimensional real spaces. The trick is to develop one's intuition in $\mathbb{P}^2$, as many of its properties do generalize.

A.8 Projective Transformations Defined

That the homogeneous coordinates of a point $P \in \mathbb{P}^2$ are of the form $[x\ y\ z]^T$ suggests defining transformations of $\mathbb{P}^2$ by mimicking the definition of a linear transformation of real 3-space. In particular, if

$$M = \begin{bmatrix} a_{11} & a_{12} & a_{13} \\ a_{21} & a_{22} & a_{23} \\ a_{31} & a_{32} & a_{33} \end{bmatrix}$$

is a 3×3 matrix, then tentatively define a transformation of $\mathbb{P}^2$ by

$$[x\ y\ z]^T \mapsto M[x\ y\ z]^T \tag{A.5}$$

This definition has the virtue at least of being unambiguous because

$$[cx\ cy\ cz]^T \mapsto M[cx\ cy\ cz]^T = c(M[x\ y\ z]^T)$$

which represents the same point as $M\ [x\ y\ z]^T$, implying that the choice of any homogeneous coordinates for P gives the same image by the transformation.

The potential glitch to consider before putting (A.5) into production is if it maps a non-zero tuple to a zero tuple, for then it would map the homogeneous coordinates of a point $P \in$ P^2 to a value not even belonging to P^2. However, we know from basic linear algebra that there is a non-zero tuple $[x\ y\ z]^T$ such that

$$M[x\ y\ z]^T = [0\ \ 0\ \ 0]^T$$

if and only if M is a singular matrix; otherwise, M maps non-zero tuples to non-zero tuples. We conclude that defining a transformation of P^2 by (A.5) is indeed valid provided M is non-singular. Ergo:

Definition A.9. If M is a non-singular 3×3 matrix, then the transformation

$$[x\ y\ z]^T \ 1\!\rightarrow\ M[x\ y\ z]^T$$

denoted h^M, is called a *projective transformation* of the projective plane. The transformation f^M of R^3 – the linear transformation defined by M – is called a *related* linear transformation.

A simple relation between h^M and f^M is the following: if the radial line corresponding to a point P of P^2 is l, then that corresponding to $h^M(P)$ is $f^M(l)$, the image of l by f^M.

Exercise A.26. Prove that if M is a non-singular 3×3 matrix and c is a scalar such that $c = 0$, then M and cM define the same projective transformation of P^2, i.e., $h^M = h^{cM}$.

Remark A.8. The preceding exercise implies that actually there is not a unique linear transformation related to a projective transformation h^M, because f^{cM} is related to $h^{cM} = h^M$, for any non-zero c. However, when we do have a specific M that we are using to define h^M, then we'll often speak of *the* related linear transformation f^M.

Exercise A.27. Prove that a projective transformation h^M of P^2 takes projective lines to projective lines.
Hint: The related (non-singular) linear transformation f^M takes radial planes in R^3 to radial planes in R^3.

Exercise A.28. Prove that the composition $h^M \circ h^N$ of two projective transformations of P^2 is equal to the projective transformation h^{MN}.

A.9 Projective Transformations Geometrically

Our definition of projective transformations was purely algebraic. We would like to picture, if possible, how they transform primitives in P^2. Now, projective primitives are "seen" by projection onto the real plane – by capture on a point camera's film as we've been putting it. Let's find out, then, what a projective transformation looks like through a point camera.

Here's what we plan to do. Start with a primitive s, on the plane $z = 1$, our favorite copy of R^2, as the designated film. Suppose that the given projective transformation is h^M. Then we'll transform the lifting S of s by h^M to $h^M(S)$. Finally, we'll project $h^M(S)$ back to $z = 1$ to obtain a new primitive s^1. It's precisely the change from s to s^1 which is seen as the transformation h^M by a point camera at the origin. For example, in Figure A.18, a boxy car is changed (fancifully) into a sleek convertible.

Back to reality, let's begin with a simple example. Consider a straight segment s joining two points p and q on $z = 1$. Given a projective transformation h^M, we want to determine s^1. The lifting S of s, which is the set of all radial lines intersecting s, is

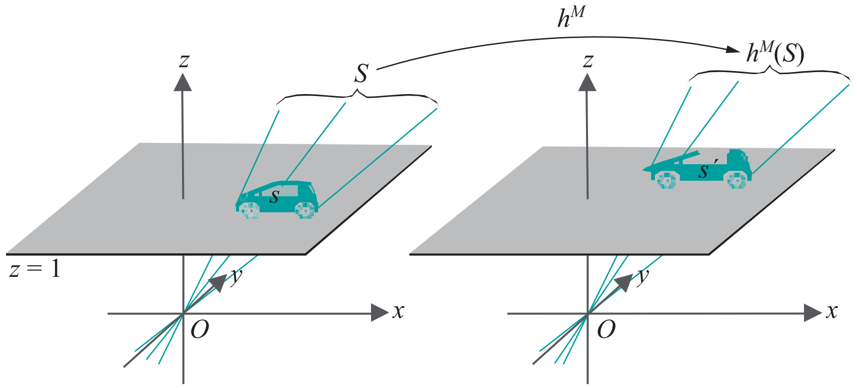

Figure A.18: Projective transformation of a car (purely conceptual!).

not hard to visualize: it forms an “infinite double triangle” which lies on the radial plane containing s and the origin. See Figure A.19(a). The radial lines through p and q are denoted P and Q, respectively.

The related linear transformation f^M transforms s to a segment $\bar{s} = \bar{p}\,\bar{q}$, where $f^M(p) = \bar{p}$ and $f^M(q) = \bar{q}$. See Figure A.19(b). Note that $\bar{s}$ can be anywhere in 3-space, depending on f^M, unlike s and s^1, which are both on $z = 1$.

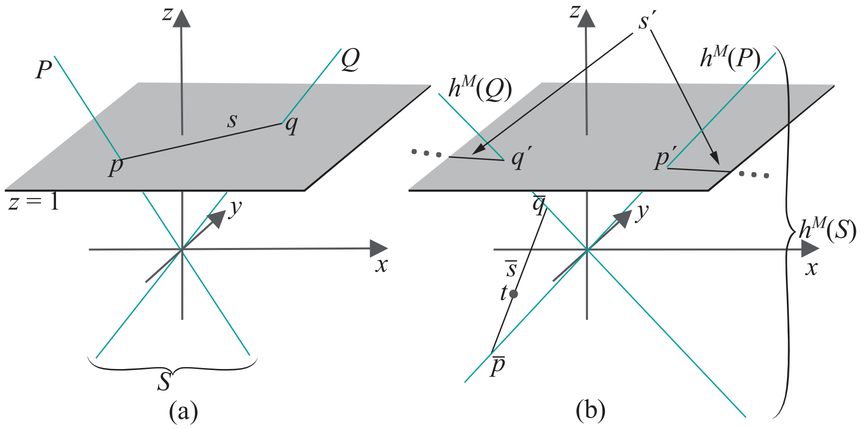

Figure A.19: (a) A segment s on R^2 and its lifting S (b) f^M transforms s to $\bar{s}$ and S to $h^M(S)$, while s^1 is the intersection of $h^M(S)$ with $z = 1$.

Moreover, each radial line in S, the lifting of s, is transformed by f^M to a radial line in $h^M(S)$. Each radial line in $h^M(S)$, of course, intersects $\bar{s}$. A diagram depicting a particular disposition of $\bar{s}$, where it intersects the xy-plane in a single point t, is shown in Figure A.19(b).

The transformed primitive s^1 is the intersection of the radial lines in $h^M(S)$ with $z = 1$. At this time we ask the reader to complete the following exercise to find out for herself what it looks like, depending on the situation of $\bar{s}$.

Exercise A.29. Show that exactly one of (a)-(c) is true:

(a) $\bar{s}$ does not intersect the xy-plane, equivalently, every radial line in $h^M(S)$ is a regular point with respect to $z = 1$.

In this case, s^1 is the segment between the points p^1 and q^1 where $h^M(P)$ and $h^M(Q)$, respectively, intersect $z = 1$ (remember that P and Q are the radial lines through p and q, the endpoints of s, respectively). Sketch this case.

(b) $\bar{s}$ intersects the xy-plane at one point, equivalently, exactly one radial line in $h^M(S)$ is a point at infinity with respect to $z = 1$. Now, there are two subcases:

(b1) If the intersection point, call it t, is in the interior of $\bar{s}$, then s^1 consists of the *entire* infinite straight line through p^1 and q^1, where $h^M(P)$ and $h^M(Q)$, respectively, intersect $z = 1$, *minus* the finite open segment between p^1 and q^1. This situation is sketched in Figure A.19(b).

(b2) If the intersection is an endpoint of $\bar{s}$, say $\bar{p}$, then s^1 is a straight line infinite in one direction and with an endpoint at q^1, where $h^M(Q)$ intersects $z = 1$, in the other. Sketch this case.

(c) $\bar{s}$ lies on the xy-plane, equivalently, every radial line in $h^M(S)$ is a point at infinity with respect to $z = 1$.

In this case, s^1 is empty.

The answer to the preceding exercise is not tidy, but in most practical situations it will be case (a), the most benign of the three, which applies.

So we know now what we set out to find: how the projective transformation of the lifting of a segment looks like on film. Generally, for any primitive s on the plane, if s^1 is the “film-capture” of the transformation by h^M of the lifting of s, we'll call s^1 the *projective transformation* of s by h^M, and denote it $h^M(s)$ – giving thus a geometric counterpart of the algebraic definition of a projective transformation in Section A.8. Although h^M is well-defined, it is not a transformation of R^2 in general because $h^M(p)$ may not even exist for a point $p \in$ R^2, particularly if p's corresponding projective point is taken by h^M to a point at infinity (which has no film-capture).

In our usage, therefore, h^M can represent either a transformation of projective space (as defined in Section A.8) or a transformation of real primitives (as just defined above). There is no danger of ambiguity as the nature of the argument in $h^M(*)$ will make clear how it's being used.

Example A.11. The segment s joins $p = [1\ -\ 1]^T$ and $q = [-2\ -\ 2]^T$ on the plane $z = 1$, the latter identified with R^2. The projective transformation h^M : P^2 → P^2 is specified by

$$M = \begin{pmatrix} 0 & 0 & -1 \\ 0 & 1 & 0 \\ 1 & 0 & 0 \end{pmatrix}$$

which is the matrix corresponding to a rotation f^M of R^3 by 90° about the y-axis, clockwise when seen from the positive side of the y-axis. Determine $h^M(s)$.

Answer: f^M transforms s to the segment $\bar{s} = \bar{p}\,\bar{q}$, where $\bar{p}$ and $\bar{q}$ are the images by f^M of p and q, respectively. Multiplying p and q, written as points of $z = 1$, on the left by M we get:

$$\bar{p} = M[1\ \ -1\ 1]^T = [-1\ \ -1\ 1]^T$$

and

$$\bar{q} = M[-2\ -\ 2\ 1]^T = [-1\ \ -\ 2\ \ -\ 2]^T$$

As the z-values of $\bar{p}$ and $\bar{q}$ are of different signs, an interior point of $\bar{s}$ lies on the xy-plane. Therefore, we are in case (b1) of Exercise A.29 above.

Let P and Q denote the radial lines through p and q, respectively. The radial line $h^M(P)$ through $\bar{p}$ meets $z = 1$ at $h^M(p) = [-1\ -1\ 1]^T$, which is $\bar{p}$ itself. The radial line $h^M(Q)$ through $\bar{q}$ meets $z = 1$ at $h^M(q) = [\frac{1}{2}\ 1\ 1]^T$ (multiplying the coordinate tuple of $\bar{q}$ by $-\frac{1}{2}$ to make its z-value equal to 1).

Applying Exercise A.29 case (b1), $h^M(s)$ is the entire straight line through the points $[-1\ -\ 1]^T$ and $[\frac{1}{2}\ 1]^T$ minus the finite open segment joining $[-1\ -\ 1]^T$ to $[\frac{1}{2}\ 1]^T$.

Example A.12. The rectangle r lies on the plane $z = 1$, the latter identified with R^2. Its vertices are $p_1 = [0.5\ 1]^T$, $p_2 = [0.5 -\ 1]^T$, $p_3 = [1\ -1]^T$ and $p_4 = [1\ 1]^T$. See Figure A.20. Determine $h^M(r)$, where h^M is the same projective transformation as in the preceding example.

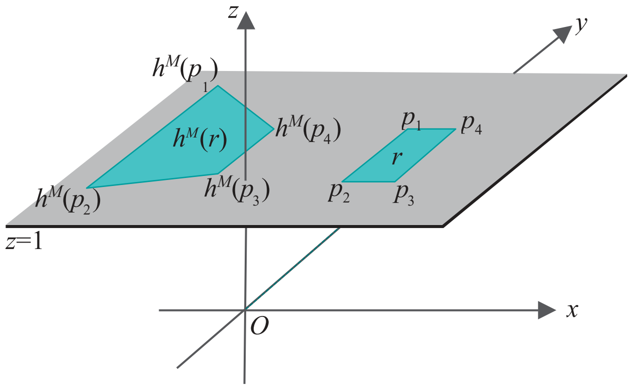

Figure A.20: Rectangle r is transformed to the trapezoid $h^M(r)$.

Answer : f^M transforms r to the rectangle $\overline{r}$ with vertices $\overline{p_i} = f^M(p_i)$, $1 \leq i \leq 4$. Multiplying each p_i, written as points of $z = 1$, on the left by M we get:

$$\begin{aligned}
\overline{p_1} &= M[0.5\ 1\ 1]^T = [-1\ 1\ 0.5]^T \\
\overline{p_2} &= M[0.5\ -1\ 1]^T = [-1\ -1\ 0.5]^T \\
\overline{p_3} &= M[1\ -1\ 1]^T = [-1\ -1\ 1]^T \\
\overline{p_4} &= M[1\ 1\ 1]^T = [-1\ 1\ 1]^T
\end{aligned}$$

As the z-value of every $\overline{p_i}$, $1 \leq i \leq 4$, is greater than 0, none of the edges of $\overline{r}$ intersects the xy-plane. According to case (a) of Exercise A.29 then, $h^M(r)$ is the quadrilateral with vertices at the points $h^M(p_i)$, where the radial lines through $\overline{p_i}$, $1 \leq i \leq 4$, intersect $z = 1$. See Figure A.20. Multiply the coordinate tuple of each $\overline{p_i}$ by a scalar to make its z-value equal to 1, to find that

$$\begin{aligned}
h^M(p_1) &= [-2\ \ 2\ \ 1]^T \\
h^M(p_2) &= [-2\ -2\ \ 1]^T \\
h^M(p_3) &= [-1\ -1\ \ 1]^T \\
h^M(p_4) &= [-1\ 1\ 1]^T
\end{aligned}$$

One sees, therefore, that $h^M(r)$ has vertices at $[-2\ 2]^T$, $[-2\ -2]^T$, $[-1\ -1]^T$ and $[-1\ 1]^T$, which makes it a trapezoid.

It's interesting to note that no affine transformation of R^2 can map a rectangle to a trapezoid: as affine transformations preserve parallelism (see Proposition 5.1), at most they can transform a rectangle to a parallelogram.

Exercise A.30. Exercise A.7(f), where we snapshot transformed a trapezoid to a rectangle, evidently is related to the preceding example. Say how.

Clearly, with the help of Exercise A.29 we can determine the projective transformation of any shape specified by straight edges. More general shapes are curved and curves specified by equations. Let's see, for example, how a parabola is projectively transformed.

Example A.13. Determine how the parabola $y - x^2 = 0$ on $z = 1$, the latter identified with R^2, is mapped by the same projective transformation h^M as in the previous example.

Answer : The point $[x\ y]^T$ on $z = 1$, which has coordinates $[x\ y\ 1]^T$ in R^3, is transformed by f^M to the point $[\overline{x}\ \overline{y}\ \overline{z}]^T$, where

$$\begin{bmatrix} \overline{x} \\ \overline{y} \\ \overline{z} \end{bmatrix} = \begin{bmatrix} 0 & 0 & -1 \\ 0 & 1 & 0 \\ 1 & 0 & 0 \end{bmatrix} \begin{bmatrix} x \\ y \\ 1 \end{bmatrix} = \begin{bmatrix} -1 \\ y \\ x \end{bmatrix}$$

which gives

$$\overline{x} = -1, \qquad \overline{y} = y, \qquad \overline{z} = x$$

The image $[x^1\ y^1]^T$ of $[x\ y]^T$ by h^M, then, is the point $[\overline{x}/\overline{z}\ \ \overline{y}/\overline{z}]^T$, where the radial line through $[\overline{x}\ \overline{y}\ \overline{z}]^T$ intersects $z = 1$. Therefore:

$$x^1 = \overline{x}/\overline{z} = -1/x \quad \Longrightarrow \quad x = -1/x^1$$

and

$$y^1 = \overline{y}/\overline{z} = y/x \quad \Longrightarrow \quad y = y^1 x = -y^1/x^1 \text{ (using } x = -1/x^1 \text{ from above)}$$

Plugging these expressions for x and y into the equation of the parabola $y - x^2 = 0$, we have the equation

$$-y^1/x^1 - 1/x^{12} = 0, \text{ equivalently,} \quad x^1 y^1 + 1 = 0$$

of the transformed curve, which describes a hyperbola.

Here's another rather interesting example.

Example A.14. Determine how points of $\mathbb{R}^2$, identified with $z = 1$, are transformed by the projective transformation h^M of $\mathbb{P}^2$ specified by

$$M = \begin{bmatrix} 1 & 0 & 7 \\ 0 & 1 & 0 \\ 0 & 0 & 1 \end{bmatrix}$$

Answer: The point $[x\ y]^T$ on $z = 1$, which has coordinates $[x\ y\ 1]^T$ in $\mathbb{R}^3$, is transformed by f^M to the point $[\overline{x}\ \overline{y}\ \overline{z}]^T$, where

$$\begin{bmatrix} \overline{x} \\ \overline{y} \\ \overline{z} \end{bmatrix} = \begin{bmatrix} 1 & 0 & 7 \\ 0 & 1 & 0 \\ 0 & 0 & 1 \end{bmatrix} \begin{bmatrix} x \\ y \\ 1 \end{bmatrix} = \begin{bmatrix} x+7 \\ y \\ 1 \end{bmatrix}$$

giving

$$\overline{x} = x + 7, \qquad \overline{y} = y, \qquad \overline{z} = 1$$

The image $[x^1\ y^1]^T$ of $[x\ y]^T$ by h^M, then, is the point $[\overline{x}/\overline{z}\ \ \overline{y}/\overline{z}\ \ 1]^T$, where the radial line through $[\overline{x}\ \overline{y}\ \overline{z}]^T$ intersects $z = 1$. Therefore,

$$x^1 = \overline{x}/\overline{z} = x + 7 \quad \text{and} \quad y^1 = \overline{y}/\overline{z} = y$$

which is nothing but a *translation* by 7 units in the x-direction.

Incidentally, we did not pull the matrix M above out of a hat: it is the transformation matrix of a 3D shear whose plane is the xy-plane and line the x-axis (recall 3D shears from Section 5.4).

A projection transformation has just done something beyond the reach of linear transformations, for a linear transformation cannot translate. Translations, as we learned in Chapter 5, are in the domain of affine transformations. Further, in Example A.12, we saw a projective transformation convert a rectangle into a trapezoid, something beyond even affine transformations. For transformations inspired by and defined by matrix-vector multiplication, just like linear transformations, projective transformations certainly seem to carry plenty of additional firepower. It turns out that this makes them particularly worthy allies in the advancement of computer graphics.

Exercise A.31. Find a projective transformation to translate points of $\mathbb{R}^2$ 3 units in the x-direction and 2 in the y-direction, i.e., whose displacement vector is $[3\ 2]^T$. *Hint*: Think another shear.

Exercise A.32. Determine how the segment s on $\mathbb{R}^2$, the latter identified with the plane $z = 1$, joining $p = [2\ -2]^T$ and $q = [-2\ 1]^T$, is mapped by the projective transformation h^M of $\mathbb{P}^2$ specified by

$$M = \begin{bmatrix} 0 & 1 & 1 \\ 1 & 0 & 1 \\ 1 & 1 & 0 \end{bmatrix}$$

Exercise A.33. Determine how the hyperbola $xy = 1$ on $z = 1$, the latter identified with $\mathbb{R}^2$, is mapped by the same projective transformation h^M as in the previous exercise.

Part answer: The problem is not hard but there is a fair amount of manipulation.

The point $[x\ y]^T$ on $z = 1$, which has coordinates $[x\ y\ 1]^T$ in $\mathbb{R}^3$, is transformed by f^M to the point $[\bar{x}\ \bar{y}\ \bar{z}]^T$, where

$$\begin{bmatrix} \bar{x} \\ \bar{y} \\ \bar{z} \end{bmatrix} = \begin{bmatrix} 0 & 1 & 1 \\ 1 & 0 & 1 \\ 1 & 1 & 0 \end{bmatrix} \begin{bmatrix} x \\ y \\ 1 \end{bmatrix}$$

Let's flip this equation over with the help of an inverse matrix:

$$\begin{bmatrix} x \\ y \\ 1 \end{bmatrix} = \begin{bmatrix} 0 & 1 & 1 \\ 1 & 0 & 1 \\ 1 & 1 & 0 \end{bmatrix}^{-1} \begin{bmatrix} \bar{x} \\ \bar{y} \\ \bar{z} \end{bmatrix} = \frac{1}{2}\begin{bmatrix} -1 & 1 & 1 \\ 1 & -1 & 1 \\ 1 & 1 & -1 \end{bmatrix} \begin{bmatrix} \bar{x} \\ \bar{y} \\ \bar{z} \end{bmatrix}$$

which gives

$$x = \frac{1}{2}(-\bar{x} + \bar{y} + \bar{z}) \qquad y = \frac{1}{2}(\bar{x} - \bar{y} + \bar{z}) \qquad 1 = \frac{1}{2}(\bar{x} + \bar{y} - \bar{z})$$

Plugging these expressions into the equation of the hyperbola $xy = 1 = 1^2$ we get:

$$\frac{1}{4}(-\bar{x} + \bar{y} + \bar{z})(\bar{x} - \bar{y} + \bar{z}) = \frac{1}{4}(\bar{x} + \bar{y} - \bar{z})^2$$

Now, the image $[x^1\ y^1]^T$ of $[x\ y]^T$ by h^M is the point $[\bar{x}/\bar{z}\ \bar{y}/\bar{z}]^T$, where the radial line through $[\bar{x}\ \bar{y}\ \bar{z}]^T$ intersects $z = 1$. We ask the reader to complete the exercise by dividing the preceding equation by $\bar{z}^2$ throughout to obtain an equation relating x^1 and y^1, and identifying the corresponding curve.

Exercise A.34. Determine how the straight line $x + y + 1 = 0$ on $z = 1$ is mapped by the same projective transformation h^M as in the previous exercise.

Exercise A.35. We saw in Example 5.4 that affine transformations preserve convex combinations and barycentric coordinates. Show that projective transformations in general do not.

Remark **A.9.** Projective transformations of $\mathbb{P}^2$ can be thought of as a powerful class of *pseudo-transformations* of $\mathbb{R}^2$ – pseudo because a projective transformation may map a regular point to a point at infinity, in which case the corresponding point of $\mathbb{R}^2$ has no valid image. If one is careful, however, to restrict its domain to a region of $\mathbb{R}^2$ where it *is* valid throughout, one may be able to exploit the ability of a projective transformation to do more than an affine one.

A.10 Relating Projective, Snapshot and Affine Transformations

We'll explore in this section the inter-relationships between projective, snapshot and affine transformations.

A.10.1 Snapshot Transformations via Projective Transformations

Snapshot transformations, being transformations of an object seen through a point camera as the film changes alignment, are geometrically intuitive. They are, in fact, a kind of projective transformation, as we'll now see.

Consider again Example A.12 for motivation. We saw that the rectangle r on the plane $z = 1$ (aka R^2) with vertices at $p_1 = [0.5\ 1]^T$, $p_2 = [0.5\ \ -1]^T$, $p_3 = [1\ \ -\ \ 1]^T$ and $p_4 = [1\ 1]^T$ is mapped to the trapezoid $r^1 = h^M(r)$ with vertices at $p^1{}_1 = [-2\ 2]^T$, $p^1{}_2 = [-\ 2\ -\ \ 2]^T$, $p^1{}_3 = -[\ \ 1-\ \ \ 1]^T$ and $p^1{}_4 = -[\ 1\ 1]^T$, by the projective transformation h^M specified by

$$M = \begin{bmatrix} 0 & 0 & -1 \\ 0 & 1 & 0 \\ 1 & 0 & 0 \end{bmatrix}$$

See Figure A.21(a).

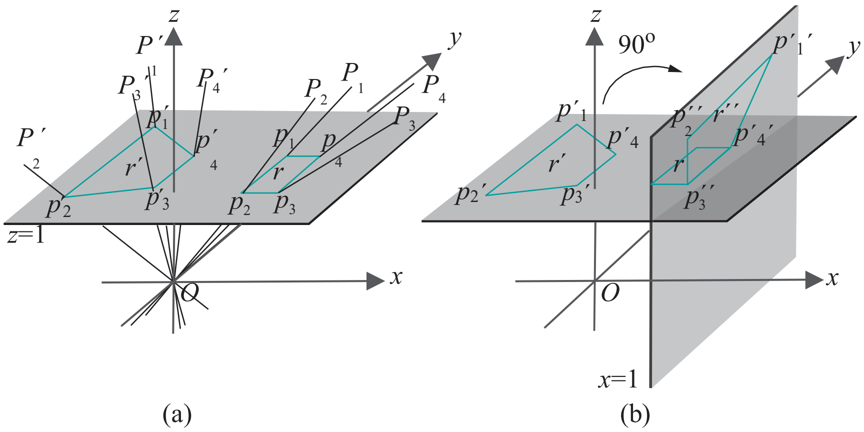

Figure A.21: (a) Projective transformation h^M maps rectangle r to trapezoid $r^1 = h^M(r)$ (b) r^1 is the "same" as r^{11}, the picture of r captured on a film along $x = 1$.

We observed, as well, that the related linear transformation f^M is a rotation of R^3 by 90° about the y-axis, which is clockwise when seen from the positive side of the y-axis.

Denote the radial line through p_i by P_i, $1 \le i \le 4$, and their respective images $h^M(P_i)$ by P^1_i. Now rotate the radial lines P^1_i, *as well as* the plane $z = 1$, an angle of 90° about the y-axis, this time counter-clockwise when seen from the positive side of the y-axis, in order to undo the effect of f^M; in other words, apply $f^{M^{-1}}$. We see the following:

(a) The radial line P^1_i, of course, rotates back onto (its pre-image) the radial line P_i, $1 \le i \le 4$.

(b) The plane $z = 1$ is taken by the rotation onto the plane $x = 1$.

(c) The trapezoid r^1, as a consequence of (a) and (b), rotates onto a trapezoid r^{11} with vertices at the intersections p^{11}_i of P_i with $x = 1$, for $1 \le\ i \le\ 4$. See Figure A.21(b) (note that the edge of r that happens to lie on the intersection of the planes $z = 1$ and $x = 1$ is shared with r^{11}).

But r^{11} is precisely the snapshot transformation of r from the film along $z = 1$ to the one along $x = 1$! Here's what is happening. The image r^1 is obtained by applying the rotation f^M to the radials P_i and intersecting them with the plane $z = 1$, while r^{11} is obtained from r^1 by applying the reverse rotation $f^{M^{-1}}$, which takes the radials back to the where they were, and, at the same time, changes the intersecting plane from $z = 1$ to $x = 1$. Therefore, the transformation from r to r^{11} comes from a change in the plane (= film) intersecting the radials, which is precisely a snapshot transformation.

One sees, therefore, that, generally, a snapshot transformation in which the film is re-aligned by a rotation f about a radial axis is equivalent to a projective transformation whose related linear transformation is f^{-1}, in that the images are identical, though situated differently in space (precisely, the two images differ by a rigid transformation of $\mathbb{R}^3$). But, how about snapshot transformations where the new alignment of the film cannot be obtained from the original by mere rotation? To answer this question, we ask the reader, first, to prove the following, which says that an arbitrary snapshot transformation can be composed from two very simple ones.

Exercise A.36. Prove that any plane p in $\mathbb{R}^3$ can be aligned with any other p^1 by a translation parallel to itself followed by a rotation about a radial axis.

Therefore, any snapshot transformation is the composition of two: first, a snapshot transformation from one film to a parallely translated one and then another, where one film is obtained from the other by a rotation about a radial axis.
Hint: See Figure A.22.

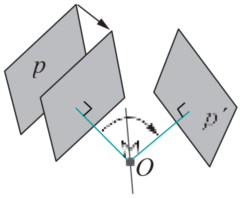

Figure A.22: Aligning plane p with p^1 by a parallel displacement, so that their respective distances from the origin are equal, followed by a rotation.

We have already seen how a snapshot transformation from one film to a rotated one is equivalent to a projective transformation. A snapshot transformation to a parallely translated one is also equivalent to a projective transformation, as the next exercise asks the reader to show.

Exercise A.37. Suppose that two parallel non-radial planes p and p^1 in $\mathbb{R}^3$ are at a distance of c and c^1 from the origin, respectively. Then the snapshot transformation from p to p^1 is equivalent to the projective transformation h^M, where

$$M = \begin{pmatrix} \frac{c'}{c} & 0 & 0 \\ 0 & \frac{c'}{c} & 0 \\ 0 & 0 & \frac{c'}{c} \end{pmatrix} = \frac{c^1}{c} I$$

(i.e., a projective transformation whose related linear transformation is a *uniform* scaling of $\mathbb{R}^3$ by a factor of $\frac{c'}{c}$ in all directions).

Hint: See Figure A.23.

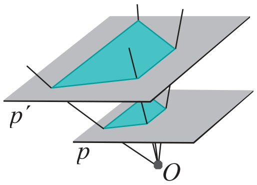

Figure A.23: A snapshot transformation to a parallel plane is equivalent to a scaling by a constant factor in all directions.

Putting the pieces together we have the following proposition:

Proposition A.1. *A snapshot transformation k from a non-radial plane p in* $\mathbb{R}^3$ *to another* p^1 *is equivalent to a projective transformation* h^M *of* $\mathbb{P}^2$*, in the sense that the images of primitives by k and* h^M *are identical modulo a rigid transformation of* $\mathbb{R}^3$*. In particular, k is equivalent to the projective transformation* h^M *which is the composition of a projective transformation* h^{dI}*, whose related linear transformation is a uniform scaling, with a projective transformation* h^N*, whose related linear transformation is a rotation of* $\mathbb{R}^3$ *about a radial axis.*

In other words, k is equivalent to h^{dN}*, where d is a scalar and N is the matrix of a rotation of* $\mathbb{R}^3$ *about a radial axis.*

Exercise A.38. Determine the projective transformation equivalent to the snapshot transformation from the plane $z = 1$ to the plane $x = 2$.

A.10.2 Affine Transformations via Projective Transformations

We begin by asking if there exist projective transformations of $\mathbb{P}^2$ that respect regular points, i.e., map regular points to regular points. Such a transformation could then be *entirely* captured on film because it takes no point of the film out of it, as would happen, say, if a regular point were mapped to one at infinity. Looking back at

Remark A.9, one could then say that such a projective transformation is no longer "pseudo", but a true transformation of $\mathbb{R}^2$.

So suppose the film lies along the plane (surprise) $z = 1$. What condition must a projective transformation h^M, where

$$M = \begin{bmatrix} a_{11} & a_{12} & a_{13} \\ a_{21} & a_{22} & a_{23} \\ a_{31} & a_{32} & a_{33} \end{bmatrix}$$

satisfy in order to transform each point regular with respect to $z = 1$ to another such? Homogeneous coordinates of regular points are of the form $[x\ y\ 1]^T$. Now,

$$h^M([x\ y\ 1]^T) = M[x\ y\ 1]^T = \begin{bmatrix} a_{11}x + a_{12}y + a_{13} \\ a_{21}x + a_{22}y + a_{23} \\ a_{31}x + a_{32}y + a_{33} \end{bmatrix}$$

For this image point to be regular we must have

$$a_{31}x + a_{32}y + a_{33} \neq 0$$

However, if either one of a_{31} and a_{32} is non-zero, or if a_{33} is zero, then it's possible to find values of x and y such that $a_{31}x + a_{32}y + a_{33} = 0$. The conclusion then is that for h^M to transform all regular points to regular points, one must have both a_{31} and a_{32} equal to zero and a_{33} non-zero. Therefore, M must be of the form

$$\begin{bmatrix} a_{11} & a_{12} & a_{13} \\ a_{21} & a_{22} & a_{23} \\ 0 & 0 & a_{33} \end{bmatrix}$$

with $a_{33} \neq 0$. By Exercise A.26, M can be multiplied by $1/a_{33}$ to still represent the same projective transformation, so one can assume $a_{33} = 1$, implying that the form of M is

$$\begin{bmatrix} a_{11} & a_{12} & a_{13} \\ a_{21} & a_{22} & a_{23} \\ 0 & 0 & 1 \end{bmatrix}$$

In this case, h^M transforms $[x\ y\ 1]^T$ to

$$\begin{bmatrix} a_{11} & a_{12} & a_{13} \\ a_{21} & a_{22} & a_{23} \\ 0 & 0 & 1 \end{bmatrix} \begin{bmatrix} x \\ y \\ 1 \end{bmatrix} = \begin{bmatrix} a_{11}x + a_{12}y + a_{13} \\ a_{21}x + a_{22}y + a_{23} \\ 1 \end{bmatrix}$$

Tossing the last coordinate, it transforms $[x\ y]^T \in \mathbb{R}^2$ to

$$\begin{bmatrix} a_{11}x + a_{12}y + a_{13} \\ a_{21}x + a_{22}y + a_{23} \end{bmatrix} = \begin{bmatrix} a_{11} & a_{12} \\ a_{21} & a_{22} \end{bmatrix} \begin{bmatrix} x \\ y \end{bmatrix} + \begin{bmatrix} a_{13} \\ a_{23} \end{bmatrix}$$

which is precisely an affine transformation!

We conclude that a projective transformation of $\mathbb{P}^2$ that respects regular points gives nothing but an affine transformation of $\mathbb{R}^2$. Conversely, it's not hard to see that any affine transformation of $\mathbb{R}^2$ can be obtained as a projective transformation preserving regular points. We record these facts in the following proposition.

Proposition A.2. *An affine transformation of* $\mathbb{R}^2$ *is equivalent to a projective transformation of* $\mathbb{P}^2$*, in particular, one that respects regular points.*

Conversely, a projective transformation of $\mathbb{P}^2$ *that respects regular points is equivalent to an affine transformation of* $\mathbb{R}^2$*.*

Evidently, the constraint to respect regular points is a burden on projective transformations. It dumbs them down to affine and all the excitement of parallel lines turning into intersecting ones, rectangles into trapezoids, and circles into hyperbolas is lost!

However, one does see now a good reason for the use of homogeneous coordinates of real points in computing affine transformations. When first we did this in Section 5.2.3, it seemed merely a neat maneuver to obtain an affine transformation as a single matrix-vector multiplication. The bigger picture is that affine transformations are a subclass of the projective. Therefore, as the latter are obtained (by definition) from matrix-vector multiplication, so can the former, provided we relocate to projective space, in other words, use homogeneous coordinates.

A Roundup of the Three Kinds of Transformations

Snapshot and affine transformations are subclasses of the projective, as we have just seen. How about the relationship between these two subclasses themselves? Are snapshot transformations affine or affine transformations snapshot?

At the start of Section A.10.1 we saw a projective transformation, equivalent, in fact, to a snapshot transformation, map a rectangle to a trapezoid. This is not possible for an affine transformation to do, as it is obliged to preserve parallelism (Proposition 5.1). Therefore, snapshot transformations are certainly not all affine.

A shear on the plane, an affine transformation, can map a rectangle to a non-rectangular parallelogram. We leave the reader to convince herself that this is not possible for a snapshot transformation. So not all affine transformations are snapshot.

We see then that neither of the two subclasses, snapshot and affine, of projective transformations contains the other. However, what transformations, if any, do they have in common? We ask the reader herself to characterize the transformations at the intersection of affine and snapshot in the next exercise.

Exercise A.39. Prove that projective transformations which are both affine and snapshot are precisely those whose related linear transformation is a uniform scaling.

The final important question on the relationship between the three classes is if the union of snapshot and affine covers projective transformations or if the latter is strictly bigger. In Exercise A.42 in the next section we'll see an example of a projective transformation neither snapshot nor affine. Therefore, indeed, the class of projective transformations is strictly bigger than the union of snapshot and affine. Figure A.24 summarizes the relationship between the three classes.

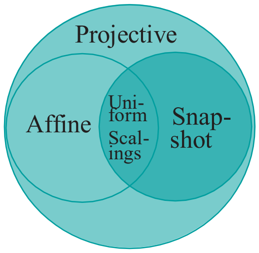

Figure A.24: Venn diagram of transformation classes of $\mathbb{R}^2$.

A.11 Designer Projective Transformations

We know from elementary linear algebra that a linear transformation is uniquely specified by defining its values on a basis. Here's a like-minded claim for projective transformations of $\mathbb{P}^2$.

Proposition A.3. *If two sets $\{P_1, P_2, P_3, P_4\}$ and $\{Q_1, Q_2, Q_3, Q_4\}$ of four points each from $\mathbb{P}^2$ are such that no three in any one set are collinear, then there is a unique projective transformation of $\mathbb{P}^2$ that maps P_i to Q_i, for $1 \le i \le 4$.*

Proof. Choose non-zero vectors p_1, p_2, p_3 and p_4 from $\mathbb{R}^3$ lying on P_1, P_2, P_3 and P_4, respectively, and non-zero vectors q_1, q_2, q_3 and q_4 lying on Q_1, Q_2, Q_3 and Q_4, respectively.

Since P_1, P_2 and P_3 do not lie on one projective line, p_1, p_2 and p_3 do not lie on one radial plane. The latter three form, therefore, a basis of $\mathbb{R}^3$. Likewise, q_1, q_2 and q_3 form a basis of $\mathbb{R}^3$ as well.

Let c_1, c_2 and c_3 be arbitrary scalars, all three non-zero, whose values will be determined. As q_1, q_2 and q_3 form a basis of $\mathbb{R}^3$, so do c_1q_1, c_2q_2 and c_3q_3. Therefore, there is a unique non-singular linear transformation f^M : R^3 → R^3 such that

$$f^M(p_i) = c_i q_i, \text{ for } 1 \le i \le 3$$

which, then, is related to a projective transformation h^M : P^2 → P^2, such that

$$h^M(P_i) = Q_i, \text{ for } 1 \le i \le 3$$

It remains to make $h^M(P_4) = Q_4$.

As p_1, p_2 and p_3 form a basis of R^3, there exist unique scalars a, β and γ such that

$$p_4 = a p_1 + \beta p_2 + \gamma p_3$$

Now, a, β and γ are all three non-zero, for, otherwise, p_4 lies on the same radial plane as two of p_1, p_2 and p_3, which implies that P_4 lies on the same projective line as two of P_1, P_2 and P_3, contradicting an initial hypothesis. Likewise, there exist unique non-zero scalars, λ, μ and ν such that

$$q_4 = \lambda q_1 + \mu q_2 + \nu q_3$$

For

$$h^M(P_4) = Q_4$$

to hold, then, one requires a scalar c_4 0 such that

$$\begin{aligned} f^M(p_4) &= c_4 q_4 \\ &= c_4(\lambda q_1 + \mu q_2 + \nu q_3) \\ &= \lambda c_4 q_1 + \mu c_4 q_2 + \nu c_4 q_3 \end{aligned} \tag{A.6}$$

However,

$$\begin{aligned} f^M(p_4) &= f^M(a p_1 + \beta p_2 + \gamma p_3) \\ &= a f^M(p_1) + \beta f^M(p_2) + \gamma f^M(p_3) \\ &= a c_1 q_1 + \beta c_2 q_2 + \gamma c_3 q_3 \end{aligned} \tag{A.7}$$

Combining (A.6) and (A.7) one has

$$a c_1 q_1 + \beta c_2 q_2 + \gamma c_3 q_3 = \lambda c_4 q_1 + \mu c_4 q_2 + \nu c_4 q_3$$

As q_1, q_2 and q_3 is a basis of R^3, it follows that

$$a c_1 = \lambda c_4, \quad \beta c_2 = \mu c_4, \quad \gamma c_3 = \nu c_4$$

giving

$$c_1 = (\lambda/a) c_4, \quad c_2 = (\mu/\beta) c_4, \quad c_3 = (\nu/\gamma) c_4$$

determining c_1, c_2, c_3 and c_4 uniquely, up to a constant of proportionality, so completing the proof.

The following corollary, which is a straightforward application of the proposition, is particularly important.

Corollary A.1. *Any non-degenerate quadrilateral, i.e., one with no three collinear vertices, in* R^2 *can be projectively transformed to any other such.*

More than just theoretically, the proposition is important in that it suggests how to go about finding projective transformations specified at only a few points.

Example A.15. Determine the projective transformation h^M of P^2 mapping the projective points

$$P_1 = [1\ 0\ 0]^T, \ P_2 = [0\ 1\ 0]^T, \ P_3 = [0\ 0\ 1]^T \text{ and } P_4 = [1\ 1\ 1]^T$$

to the respective images

$$Q_1 = [2\ 1\ 3]^T, \ Q_2 = [-1\ -1\ 1]^T, \ Q_3 = [0\ 1\ 1]^T \text{ and } Q_4 = [0\ 0\ 6]^T$$

Answer: Choose (not particularly imaginatively)

$$p_1 = [1\ 0\ 0]^T,\ p_2 = [0\ 1\ 0]^T,\ p_3 = [0\ 0\ 1]^T \text{ and } p_4 = [1\ 1\ 1]^T$$

in $\mathbb{R}^3$ lying on P_i, $1 \leq i \leq 4$, and

$$q_1 = [2\ 1\ 3]^T,\ q_2 = [-1\ -1\ 1]^T,\ q_3 = [0\ 1\ 1]^T \text{ and } q_4 = [0\ 0\ 6]^T$$

lying on Q_i, $1 \leq i \leq 4$.

The linear transformation $f^M : \mathbb{R}^3 \to \mathbb{R}^3$ such that $f^M(p_i) = c_i q_i$, for $1 \leq i \leq 3$, where c_1, c_2 and c_3 are non-zero scalars, is easily verified to be given by

$$M = \begin{bmatrix} 2c_1 & -c_2 & 0 \\ c_1 & -c_2 & c_3 \\ 3c_1 & c_2 & c_3 \end{bmatrix}$$

One can verify as well that

$$p_4 = p_1 + p_2 + p_3$$

and

$$q_4 = q_1 + 2q_2 + q_3$$

Therefore,

$$f^M(p_4) = f^M(p_1 + p_2 + p_3) = f^M(p_1) + f^M(p_2) + f^M(p_3) = c_1q_1 + c_2q_2 + c_3q_3$$

Accordingly, if $f^M(p_4) = c_4q_4$, for some $c_4 \neq 0$, then

$$c_1q_1 + c_2q_2 + c_3q_3 = c_4(q_1 + 2q_2 + q_3) = c_4q_1 + 2c_4q_2 + c_4q_3$$

which implies that

$$c_1 = c_4, \quad c_2 = 2c_4, \quad c_3 = c_4$$

Setting $c_4 = 1$, one has: $c_1 = 1$, $c_2 = 2$, $c_3 = 1$, $c_4 = 1$. One concludes that the required projective transformation h^M is given by

$$M = \begin{bmatrix} 2 & -2 & 0 \\ 1 & -2 & 1 \\ 3 & 2 & 1 \end{bmatrix}$$

The following example will help in an application of projective transformations in the graphics pipeline.

Example A.16. Determine the projective transformation h^M of $\mathbb{P}^2$ that transforms the trapezoid q on the plane $z = 1$ (aka $\mathbb{R}^2$) with vertices at

$$p_1 = [-1\ 1]^T,\ p_2 = [1\ 1]^T,\ p_3 = [2\ 2]^T \text{ and } p_4 = [-2\ 2]^T$$

to the rectangle q' on the same plane with vertices at

$$p'_1 = [-1\ 1]^T,\ p'_2 = [1\ 1]^T,\ p'_3 = [1\ 2]^T \text{ and } p'_4 = [-1\ 2]^T$$

See Figure A.25.

Answer: Suppose that the required projective transformation h^M is defined by the matrix

$$M = \begin{bmatrix} a_{11} & a_{12} & a_{13} \\ a_{21} & a_{22} & a_{23} \\ a_{31} & a_{32} & a_{33} \end{bmatrix}$$

We have to determine the a_{ij} up to a non-zero multiplicative constant.

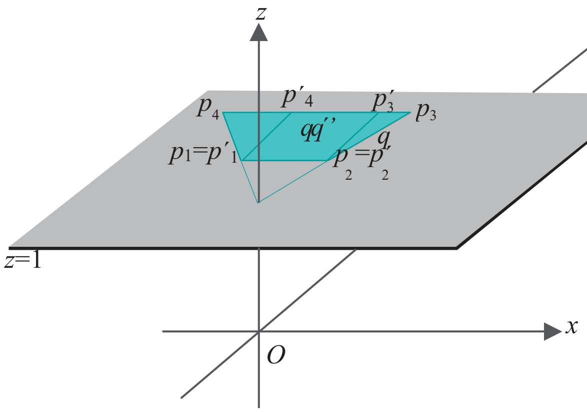

Figure A.25: Transforming the trapezoid q on $z = 1$ to the rectangle (bold) q^1.

The two sides p_1p_4 and p_2p_3 of the trapezoid q meet at the regular point (with respect to $z = 1$) $[0\ 0\ 1]^T$, while the corresponding sides $p^1{}_1p^1{}_4$ and $p^1{}_2p^1{}_3$ of the rectangle q^1 are parallel and meet at the point at infinity $[0\ 1\ 0]^T$. The transformation must, therefore, map $[0\ 0\ 1]^T$ to $[0\ 1\ 0]^T$, yielding our first equation

$$h^M([0\ 0\ 1]^T) = [0\ 1\ 0]^T$$

(the RHS could be $c[0\ 1\ 0]^T$ for any non-zero scalar c, but there's no loss in assuming that $c = 1$) which translates to the matrix equation

$$\begin{bmatrix} a_{11} & a_{12} & a_{13} \\ a_{21} & a_{22} & a_{23} \\ a_{31} & a_{32} & a_{33} \end{bmatrix} \begin{bmatrix} 0 \\ 0 \\ 1 \end{bmatrix} = \begin{bmatrix} 0 \\ 1 \\ 0 \end{bmatrix}$$

giving

$$a_{13} = 0, \quad a_{23} = 1, \quad a_{33} = 0$$

So we write

$$M = \begin{bmatrix} a_{11} & a_{12} & 0 \\ a_{21} & a_{22} & 1 \\ a_{31} & a_{32} & 0 \end{bmatrix}$$

That we have $h^M(p_1) = p^1{}_1$ and $h^M(p_2) = p^1{}_2$ gives two more matrix equations

$$\begin{bmatrix} a_{11} & a_{12} & 0 \\ a_{21} & a_{22} & 1 \\ a_{31} & a_{32} & 0 \end{bmatrix} \begin{bmatrix} -1 \\ 1 \\ 1 \end{bmatrix} = \begin{bmatrix} -c \\ c \\ c \end{bmatrix} \text{ and } \begin{bmatrix} a_{11} & a_{12} & 0 \\ a_{21} & a_{22} & 1 \\ a_{31} & a_{32} & 0 \end{bmatrix} \begin{bmatrix} 1 \\ 1 \\ 1 \end{bmatrix} = \begin{bmatrix} d \\ d \\ d \end{bmatrix}$$

where c and d are arbitrary non-zero scalars, yielding the six equations

$$\begin{aligned} -a_{11} + a_{12} &= -c \\ -a_{21} + a_{22} + 1 &= c \\ -a_{31} + a_{32} &= c \\ a_{11} + a_{12} &= d \\ a_{21} + a_{22} + 1 &= d \\ a_{31} + a_{32} &= d \end{aligned} \tag{A.8}$$

Subtracting the first equation from the fourth, adding the second and fifth, and adding the third and sixth, one gets

$$a_{11} = \frac{c+d}{2}, \quad a_{22} = \frac{c+d}{2} - 1, \quad a_{32} = \frac{c+d}{2}$$

implying that

$$a_{22} = a_{11} - 1 \quad \text{and} \quad a_{32} = a_{11}$$

Likewise, adding the first and fourth equations, subtracting the second from the fifth, and subtracting the third from the sixth, one gets

$$a_{12} = a_{21} = a_{31}$$

We can now write

$$M = \begin{bmatrix} a_{11} & a_{12} & 0 \\ a_{12} & a_{11} - 1 & 1 \\ a_{12} & a_{11} & 0 \end{bmatrix}$$

That $h^M(p_3) = p^1{}_3$ and $h_M(p_4) = p^1{}_4$ give another two matrix equations

$$\begin{bmatrix} a_{11} & a_{12} & 0 \\ a_{12} & a_{11} - 1 & 1 \\ a_{12} & a_{11} & 0 \end{bmatrix} \begin{bmatrix} 2 \\ 2 \\ 1 \end{bmatrix} = \begin{bmatrix} e \\ 2e \\ e \end{bmatrix} \quad \text{and}$$

$$\begin{bmatrix} a_{11} & a_{12} & 0 \\ a_{12} & a_{11} - 1 & 1 \\ a_{12} & a_{11} & 0 \end{bmatrix} \begin{bmatrix} -2 \\ 2 \\ 1 \end{bmatrix} = \begin{bmatrix} -f \\ 2f \\ f \end{bmatrix}$$

where e and f are arbitrary non-zero scalars. Again one obtains six equations, as in (A.8), which can be solved to find that

$$a_{11} = -1/2 \quad \text{and} \quad a_{12} = 0$$

We have, finally, that

$$M = \begin{bmatrix} -1/2 & 0 & 0 \\ 0 & -3/2 & 1 \\ 0 & -1/2 & 0 \end{bmatrix}$$

(or, a non-zero scalar multiple of the matrix on the RHS).

Exercise A.40. The projective transformation h^M of the preceding example mapped, by design, the regular point $[0\ 0\ 1]^T$ to the point at infinity $[0\ 1\ 0]^T$. What other regular points, if any, does it map to a point at infinity?

Exercise A.41. Determine the projective transformation h^M of $\mathbb{P}^2$ that transforms the rectangle q on the plane $z = 1$ with vertices at

$$p_1 = [0.5\ 1]^T,\ p_2 = [0.5\ -1]^T,\ p_3 = [1\ \ -1]^T \text{ and } p_4 = [1\ 1]^T$$

to the trapezoid q^1 on $z = 1$ with vertices at

$$p^1{}_1 = [-2\ 2]^T,\ p^1{}_2 = [-2\ -2]^T,\ p^1{}_3 = [-1\ \ -1]^T \text{ and } p^1{}_4 = [-1\ 1]^T$$

(see Example A.12 earlier for the solution).

Exercise A.42. Prove that there exist projective transformations which are neither affine nor snapshot.

Suggested approach: Corollary A.1 implies that a square can be projectively transformed to any non-degenerate quadrilateral. Non-degenerate quadrilaterals q^1 that can be obtained from a square q by a snapshot transformation are the intersections of a non-radial plane with the "cone" C through q (see Figure A.26). Those that can be obtained by an affine transformation, on the other hand, are parallelograms.

Therefore, if one can find a non-degenerate quadrilateral q^{11} which is neither a parallelogram nor the intersection of C with a plane, then one shows that there exists a projective transformation neither affine nor snapshot.

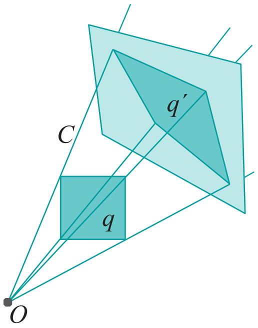

Figure A.26: The square q is mapped to the quadrilateral q' by a snapshot transformation.

Taylor & Francis
Taylor & Francis Group
http://taylorandfrancis.com

APPENDIX B

Math Self-Test

This self-test is designed to help you assess your math readiness. The essentials in order to study computer graphics are coordinate geometry, trigonometry, linear algebra and calculus, all at elementary level.

Try to answer all 30 questions. Time is not an issue. And feel free to dust off old math books you may have stashed away in some corner, stroll over to the school or public library, or, even, check into the internet. The principle, of course, is that each and every one of these activities will be allowed throughout your career as a student and practitioner of CG (except, maybe, when you are actually in an exam). Having just the right formula or solution method pop off the top of your head is fantastic, but it's fine as well, given a problem, that you know how to *go about* solving it.

Give yourself 4 points for each correct answer (solutions follow in the next section). If you score at least 100, come on in, the water's fine.* If you're between 80 and 100 then the questions you missed tell where the rust is and, as long as you are willing to put in the extra work, you should be okay. If less than 80 then you need to sit down with yourself and be perfectly honest: is it simply rust that will come off or things that I've just never had in school but trust myself to be able to pick up or is this the kind of stuff that makes me want to curl into a fetal position?

A word about math and CG, especially to those who did not fare well in the test. If you are motivated to study CG then picking up the math on the way isn't just possible, it can be a lot of fun. Its application to CG will bring to life stuff that caused your eyes to roll in high school. "The middle of the spacecraft is light because of the interpolated color values from the ends of the long triangle" or "This matrix will skew the evil character's head" are a lot different from "Groan, that's 12 different theorems and a chapter-load of trig formulas I have to cram for the mid-term."

If you are interested, there are several books out there dedicated to teaching the math needed for CG. A few that come to mind are Dunn [37], Lengyel [87], Mortenson [99] and Vince [149].

*There's more math you'll learn while studying CG (some from this book itself) than is covered in the test. Doing well here simply means you're unlikely to have serious problems.

Use the following if you need to (some are approximations): $\sin 30^\circ = \cos 60^\circ = 0.5$, $\sin 45^\circ = \cos 45^\circ = 0.707$, $\sin 60^\circ = \cos 30^\circ = 0.866$, $\pi = 3.141$, $\sqrt{2} = 1.414$, $3 = 1.732$.

The first seven questions refer to Figure B.1.

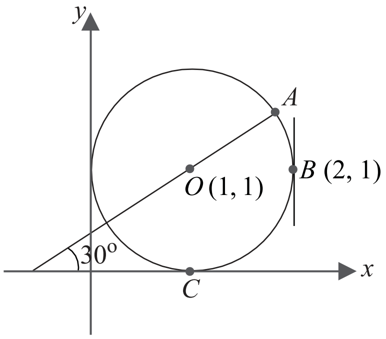

Figure B.1: Circle of unit radius.

1. What is the equation of the circle?

2. What are the coordinates of point C?

3. What is the equation of the tangent to the circle at B?

4. What is the length of the short arc of the circle from A to B?

5. What are the coordinates of point A?

6. If the circle is moved (without turning) so that its center lies at $(-3, -4)$, where then does point B lie?

7. Suppose another circle is drawn with center at A and passing through O. The two circles intersect in two points. What angles do their tangents make at these points (which, of course, is the same as the angles the circles make with each other)?

8. If a straight line on a plane passes through the points $(3, 1)$ and $(5, 2)$, which, if any, of the following two points does it pass through as well: $(9, 4)$ and $(12, 6)$?

9. What are the coordinates of the midpoint of the straight line segment joining the points $(3, 5)$ and $(4, 7)$?

10. At what point do the straight lines $3x+4y-6=0$ and $4x+7y-8=0$ intersect?

11. What is the equation of the straight line through the point (3, 0) that is parallel to the straight line $3x-4y-6=0$?

12. What is the equation of the straight line through the point (3, 0) that is perpendicular to the straight line $3x-4y-6=0$?

13. What are the coordinates of the point that is the reflection across the line $y=x$ of the point $(3,1)$?

14. What is the length of the straight line segment on the plane joining the origin (0, 0) to the point (3, 4)? In 3-space (xyz-space) what is the length of the straight line segment joining the points $(1,2,3)$ and $(4,6,8)$?

15. Determine the value of sin 75° using only the trigonometric values given at the top of the test (in other words, don't use your calculator to do anything other than arithmetic operations).

16. What is the dot product (or, scalar product, same thing) of the two vectors u and v in 3-space, where u starts at the origin and ends at $(\frac{1}{\sqrt{2}}, \frac{1}{\sqrt{2}}, 0)$ and v starts at the origin and ends at $(\frac{1}{\sqrt{2}}, \frac{1}{\sqrt{2}}, \sqrt{3})$, i.e., $u = \frac{1}{\sqrt{2}}\mathrm{i} + \frac{1}{\sqrt{2}}\mathrm{j}$ and $v = \frac{1}{\sqrt{2}}\mathrm{i} + \frac{1}{\sqrt{2}}\mathrm{j} + \sqrt{3}\mathrm{k}$. Use the dot product to calculate the angle between u and v.

17. Determine a vector that is perpendicular to *both* the vectors u and v of the preceding question.

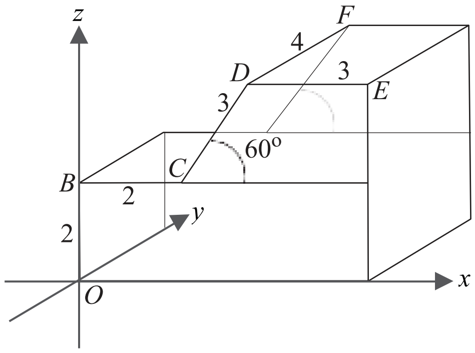

Figure B.2: Solid block (some edges are labeled with their length).

18. For the block in Figure B.2, what are the coordinates of the corner point F?

19. For the block again, what is the angle *CDE*?

20. For the unit sphere (i.e., of radius 1) centered at the origin, depicted in Figure B.3, the equator (0° latitude) is the great circle cut by the xy-plane, while 0° longitude is that half of the great circle cut by the xz-plane where x-values are non-negative.

What are the xyz coordinates of the point P whose latitude and longitude are both 45° ?

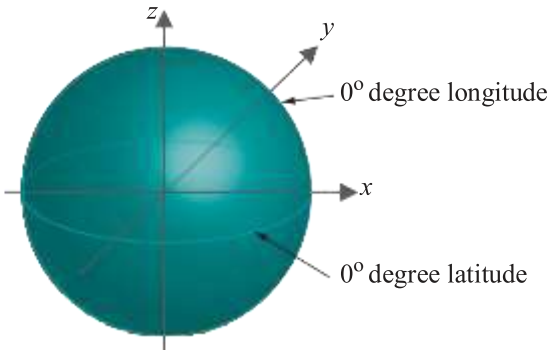

Figure B.3: Unit sphere.

21. Multiply two matrices:

$$\begin{bmatrix} 2 & 4 \\ 3 & 1 \end{bmatrix} \times \begin{bmatrix} 1 & 1 & 0 \\ 2 & 1 & -1 \end{bmatrix}$$

22. Calculate the value of the following two determinants:

$$\begin{vmatrix} 2 & 4 \\ 3 & 1 \end{vmatrix} \quad \text{and} \quad \begin{vmatrix} -1 & 2 & -3 \\ 0 & 5 & -2 \\ 0 & 3 & 3 \end{vmatrix}$$

23. Calculate the inverse of the following matrix:

$$\begin{bmatrix} 4 & 7 \\ 2 & 4 \end{bmatrix}$$

24. If the Dow Jones Industrial Average were a straight-line (or, linear, same thing) function of time and if its value on January 1, 2007 is 12,000 and on January 1, 2009 it's 13,500, what is the value on January 1, 2010?

25. Are the following vectors linearly independent?

$$[2\ 3\ 0]^T \quad [3\ 7\ -1]^T \quad [1\ -6\ 3]^T$$

26. Determine the linear transformation of R^3 that maps the standard basis vectors

$$[1\ 0\ 0]^T \qquad [0\ 1\ 0]^T \qquad [0\ 0\ 1]^T$$

to the respective vectors

$$[-1\ \ -1\ 1]^T \qquad [-2\ 3\ 2]^T \qquad [-3\ 1\ -2]^T$$

27. What is the equation of the normal to the parabola

$$y = 2x^2 + 3$$

at the point $(2, 11)$?

28. If x and y are related by the equation

$$xy + x + y = 1$$

find a formula for $\frac{\mathrm{d}y}{\mathrm{d}x}$.

29. The formula for the height at time t of a projectile shot vertically upward from the ground with initial velocity u is

$$h = ut - \frac{1}{2}gt^2$$

assuming only the action of gravitational acceleration g (ignoring wind resistance and other factors). What is the velocity of the projectile at time t? What is the maximum height reached by the projectile?

30. At what points do the curves $y = \sin x$ and $y = \cos x$ meet for values of x between 0 and 2π? What angles do the curves make with each other at these points?

APPENDIX C

Math Self-Test Solutions

The test is in the preceding appendix. Score 4 points for each correct answer. For an assessment of your total, read the part before the start of the test.

Use the following if you need to (some are approximations): $\sin 30^\circ = \cos 60^\circ = 0.5$, $\sin 45^\circ = \cos 45^\circ = 0.707$, $\sin 60^\circ = \cos 30^\circ = 0.866$, $\pi = 3.141$, $\sqrt{2} = 1.414$, $\sqrt{3} = 1.732$.

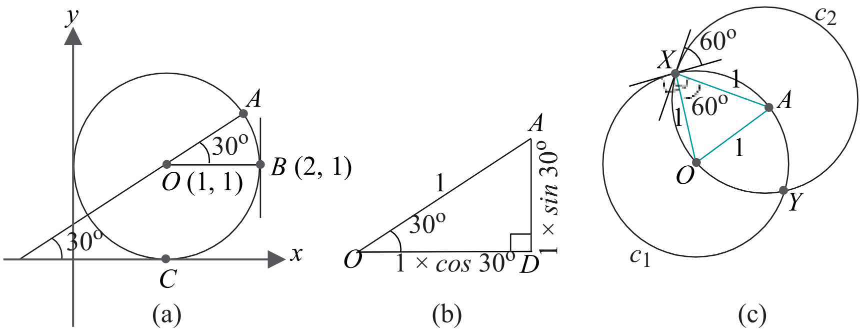

Figure C.1: (a) Circle of unit radius (b) Right-angled triangle (c) Two circles of unit radius.

The first seven questions refer to Figure C.1(a).

1. What is the equation of the circle?

   Answer: Generally, the equation of a circle on the xy-plane centered at (a, b) and of radius r is

   $$(x - a)^2 + (y - b)^2 = r^2$$

   So the equation of the drawn circle is

   $$(x - 1)^2 + (y - 1)^2 = 1^2 \text{ which evaluates to } x^2 + y^2 - 2x - 2y + 1 = 0$$

2. What are the coordinates of point C?

   Answer: $(1, 0)$.

3. What is the equation of the tangent to the circle at B?

   Answer: $x = 2$.

4. What is the length of the short arc of the circle from A to B?

Answer: The angle subtended at the center by this arc is $\angle AOB = 30^\circ$ (Figure C.1(a)).
Therefore, the length of the arc is $\frac{30}{360}$ of the circumference $= \frac{30}{360} \times 2\pi \times 1 = \frac{\pi}{6} = 3.141/6 = 0.5235$.

5. What are the coordinates of point A?

   Answer : Suppose the horizontal line through O and the vertical line through A intersect at D (Figure C.1(b)). The hypotenuse OA of the right-angled triangle ODA is of length 1 (= radius of the circle). Therefore, the length of $OD = 1 \times \cos 30^\circ = 0.866$ and the length of $AD = 1 \times \sin 30^\circ = 0.5$.
   These lengths are the displacements of A in the x- and y-direction, respectively, from O. Therefore, the coordinates of A are $(1, 1) + (0.866, 0.5) = (1.866, 1.5)$.

6. If the circle is moved (without turning) so that its center lies at $(-3, -4)$, where then does point B lie?

   Answer : Since the center is originally at $(1, 1)$ the translation that moves it to $(-3, -4)$ consists of a displacement of -4 in the x-direction and -5 in the y direction. The same translation applies to B, so B moves $(2, 1) + (-4, -5) = (-2, -4)$.

7. Suppose another circle is drawn with center at A and passing through O. The two circles intersect in two points. What angles do their tangents make at these points (which, of course, is the same as the angles the circles make with each other)?

   Answer : The two circles c_1 and c_2 intersect at points X and Y (Figure C.1(c)). The triangle OAX is equilateral as all its sides are of length 1, the radius of either circle. All its angles, therefore, are 60°.

   Now, the tangents to c_1 and c_2 at X are perpendicular, respectively, to OX and AX. Therefore, the angle between them is the same as that between OX and AX, which is 60°.

   Symmetrically, the tangents to the two circles at Y intersect at 60° as well.

8. If a straight line on a plane passes through the points $(3, 1)$ and $(5, 2)$, which, if any, of the following two points does it pass through as well: $(9, 4)$ and $(12, 6)$?

   Answer : Suppose the equation of the straight line is $y = mx+c$ (any non-vertical straight line has an equation of this form, called the slope-intercept form). Since it passes through $(3, 1)$ and $(5, 2)$, we have the two equations

$$\begin{aligned} 1 &= 3m + c \\ 2 &= 5m + c \end{aligned}$$

   Solving simultaneously, we get $m = \frac{1}{2}$ and $c = -\frac{1}{2}$, yielding the equation $y = \frac{1}{2}x - \frac{1}{2}$ for the line. Of the two points $(9, 4)$ and $(12, 6)$, only $(9, 4)$ satisfies this equation and so lies on it.

9. What are the coordinates of the midpoint of the straight line segment joining the points $(3, 5)$ and $(4, 7)$?
   Answer: The coordinates of the midpoint are $(\frac{3+4}{2}, \frac{5+7}{2}) = (3.5, 6)$.

10. At what point do the straight lines $3x + 4y - 6 = 0$ and $4x + 7y - 8 = 0$ intersect?
    Answer : Simultaneously solving the two equations we get the intersection as $(2, 0)$.

11. What is the equation of the straight line through the point $(3, 0)$ that is parallel to the straight line $3x - 4y - 6 = 0$?

Answer : Any line parallel to $3x - 4y - 6 = 0$ may be written as $3x - 4y - c = 0$, where c can be an arbitrary number. If such a line passes through $(3, 0)$ then this point's coordinates must satisfy $3x - 4y - c = 0$.

In other words, $3 \times 3 - 4 \times 0 - c = 0 \Longrightarrow c = 9$.

Therefore, the required equation is $3x - 4y - 9 = 0$.

12. What is the equation of the straight line through the point $(3, 0)$ that is perpendicular to the straight line $3x - 4y - 6 = 0$?

Answer: Rewrite the given straight line's equation in slope-intercept form: $y = \frac{3}{4}x - \frac{3}{2}$. Its gradient, therefore, is $\frac{3}{4}$. Now the gradient of a straight line that is perpendicular to one of gradient m is $-\frac{1}{m}$.

Therefore, the gradient of the straight line perpendicular to the given one is $-\frac{4}{3}$ and its equation is of the form $y = -\frac{4}{3}x + c$. Since it passes through $(3, 0)$ we have $0 = -\frac{4}{3} \times 3 + c \Longrightarrow c = 4$.

Therefore, the required equation is $y = -\frac{4}{3}x + 4$ or $3y + 4x - 12 = 0$.

13. What are the coordinates of the point that is the reflection across the line $y = x$ of the point $(3, 1)$?

Answer: Reflecting a point across the line $y = x$ interchanges its x and y coordinates. So the reflection of $(3, 1)$ is $(1, 3)$.

14. What is the length of the straight line segment on the plane joining the origin $(0, 0)$ to the point $(3, 4)$? In 3-space (xyz-space) what is the length of the straight line segment joining the points $(1, 2, 3)$ and $(4, 6, 8)$?

Answer : The (Euclidean) distance between two points (x_1, y_1) and (x_2, y_2) on the plane is $\sqrt{(x_2 - x_1)^2 + (y_2 - y_1)^2}$, while that between two points (x_1, y_1, z_1) and (x_2, y_2, z_2) in 3-space is (similarly) $\sqrt{(x_2 - x_1)^2 + (y_2 - y_1)^2 + (z_2 - z_1)^2}$.

Therefore, the length of the straight line segment joining $(0, 0)$ and $(3, 4)$ is $\sqrt{(3 - 0)^2 + (4 - 0)^2} = \sqrt{25} = 5$ and that joining $(1, 2, 3)$ and $(4, 6, 8)$ is

$$\sqrt{(4 - 1)^2 + (6 - 2)^2 + (8 - 3)^2} = \sqrt{50} = \sqrt{25 \times 2} = \sqrt{25} \times \sqrt{2} = 5 \times 1.414 = 7.07$$

using only the value of $\sqrt{2}$ given above.

15. Determine the value of sin 75° using only the trigonometric values given at the top of the test (in other words, don't use your calculator to do anything other than arithmetic operations).

Answer: Use the formula

$$\sin(A + B) = \sin A \cos B + \cos A \sin B$$

to write

$$\begin{aligned} \sin 75^\circ &= \sin(45^\circ + 30^\circ) \\ &= \sin 45^\circ \cos 30^\circ + \cos 45^\circ \sin 30^\circ \\ &= 0.707 \times 0.866 + 0.707 \times 0.5 \\ &= 0.966 \end{aligned}$$

16. What is the dot product (or, scalar product, same thing) of the two vectors u and v in 3-space, where u starts at the origin and ends at $(\frac{1}{\sqrt{2}}, \frac{1}{\sqrt{2}}, 0)$ and v starts at the origin and ends at $(\frac{1}{\sqrt{2}}, \frac{1}{\sqrt{2}}, \sqrt{3})$, i.e., $u = \frac{1}{\sqrt{2}}\mathrm{i} + \frac{1}{\sqrt{2}}\mathrm{j}$ and $v = \frac{1}{\sqrt{2}}\mathrm{i} + \frac{1}{\sqrt{2}}\mathrm{j} + \sqrt{3}\mathrm{k}$.

Use the dot product to calculate the angle between u and v.

Answer:
$u \cdot v = (\frac{1}{\sqrt{2}}, \frac{1}{\sqrt{2}}, 0) \cdot (\frac{1}{\sqrt{2}}, \frac{1}{\sqrt{2}}, \sqrt{3}) = \frac{1}{\sqrt{2}} \times \frac{1}{\sqrt{2}} + \frac{1}{\sqrt{2}} \times \frac{1}{\sqrt{2}} + 0 \times \sqrt{3} = 1$

Moreover,

$|u| = \sqrt{(\frac{1}{\sqrt{2}})^2 + (\frac{1}{\sqrt{2}})^2 + 0^2} = 1$ and $|v| = \sqrt{(\frac{1}{\sqrt{2}})^2 + (\frac{1}{\sqrt{2}})^2 + (\sqrt{3})^2} = 2.$

Now, $u \cdot v = |u||v| \cos\theta$, where θ is the angle between u and v. Therefore, $\cos\theta = \frac{u \cdot v}{|u||v|} = \frac{1}{1 \times 2} = \frac{1}{2}$, which means $\theta = 60^\circ$.

17. Determine a vector that is perpendicular to *both* the vectors u and v of the preceding question.

Answer: The cross-product of two (non-zero and non-collinear) vectors is perpendicular to both of them. Now, $u \times v = (\frac{1}{\sqrt{2}}\mathrm{i} + \frac{1}{\sqrt{2}}\mathrm{j}) \times (\frac{1}{\sqrt{2}}\mathrm{i} + \frac{1}{\sqrt{2}}\mathrm{j} + \sqrt{3}\mathrm{k})$ =

$$\begin{vmatrix} \mathrm{i} & \frac{1}{\sqrt{2}} & \frac{1}{\sqrt{2}} \\ \mathrm{j} & \frac{1}{\sqrt{2}} & \frac{1}{\sqrt{2}} \\ \mathrm{k} & 0 & \sqrt{3} \end{vmatrix} = \frac{\sqrt{3}}{\sqrt{2}}\mathrm{i} - \frac{\sqrt{3}}{\sqrt{2}}\mathrm{j}$$

Therefore, the vector that starts at the origin and ends at $(\frac{\sqrt{3}}{\sqrt{2}}, -\frac{\sqrt{3}}{\sqrt{2}}, 0)$ is perpendicular to both u and v (the answer is not unique).

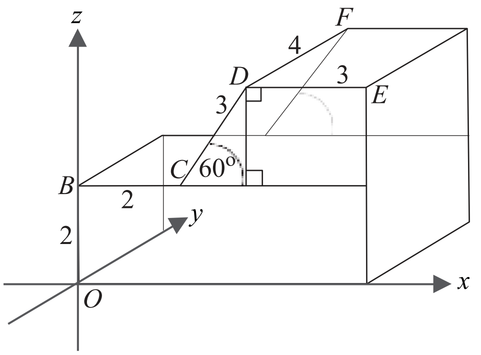

Figure C.2: Solid block (some edges are labeled with their length).

18. For the block in Figure C.2, what are the coordinates of the corner point F?

Answer: Drop the perpendicular DG from D to the straight line through B and C (Figure C.2).

The x-coordinate of F is $|BC| + |CG| = 2 + 3\cos 60^\circ = 2 + 3 \times 0.5 = 3.5$.

The y-coordinate of F is $|DF| = 4$.

The z-coordinate of F is $|OB| + |GD| = 2 + 3\sin 60^\circ = 2 + 3 \times 0.866 = 4.598$. Therefore, $F = (3.5, 4, 4.598)$.

19. For the block again, what is the angle CDE?

Answer: $\angle CDE = \angle CDG + \angle GDE = 30^\circ + 90^\circ = 120^\circ$.

20. For the unit sphere (i.e., of radius 1) centered at the origin, depicted in Figure C.3, the equator (0° latitude) is the great circle cut by the xy-plane, while 0° longitude is that half of the great circle cut by the xz-plane where x-values are non-negative.

What are the xyz coordinates of the point P whose latitude and longitude are both 45°?

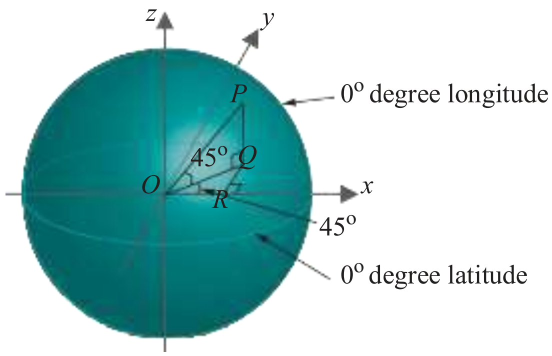

Figure C.3: Unit sphere.

Answer: Drop the perpendicular from P to Q on the xy-plane and then the perpendicular from Q to R on the x-axis (Figure C.3).

Now, $|OP| = 1$, so that $|PQ| = 1 \times \sin 45^\circ = \frac{1}{\sqrt{2}}$ and $|OQ| = 1 \times \cos 45^\circ = \frac{1}{\sqrt{2}}$ Moreover, $QR = |OQ| \sin 45^\circ = \frac{1}{\sqrt{2}} \times \frac{1}{\sqrt{2}} = \frac{1}{2}$ and $OR = |OQ| \cos 45^\circ = \frac{1}{\sqrt{2}} \times \frac{1}{\sqrt{2}} = \frac{1}{2}$.

Now, the x, y and z coordinates of P are $|OR|$, $|QR|$ and $|PQ|$, respectively. Therefore, $P = (\frac{1}{2}, \frac{1}{2}, \frac{1}{\sqrt{2}})$.

21. Multiply two matrices:

$$\begin{bmatrix} 2 & 4 \\ 3 & 1 \end{bmatrix} \times \begin{bmatrix} 1 & 1 & 0 \\ 2 & 1 & -1 \end{bmatrix}$$

Answer:

$$\begin{bmatrix} 2 & 4 \\ 3 & 1 \end{bmatrix} \times \begin{bmatrix} 1 & 1 & 0 \\ 2 & 1 & -1 \end{bmatrix} = \begin{bmatrix} 10 & 6 & -4 \\ 5 & 4 & -1 \end{bmatrix}.$$

22. Calculate the value of the following two determinants:

$$\begin{vmatrix} 2 & 4 \\ 3 & 1 \end{vmatrix} \quad \text{and} \quad \begin{vmatrix} -1 & 2 & -3 \\ 0 & 5 & -2 \\ 0 & 3 & 3 \end{vmatrix}$$

Answer:

$$\begin{vmatrix} 2 & 4 \\ 3 & 1 \end{vmatrix} = 2 \times 1 - 4 \times 3 = -10$$

$$\begin{vmatrix} -1 & 2 & -3 \\ 0 & 5 & -2 \\ 0 & 3 & 3 \end{vmatrix} = -1 \times \begin{vmatrix} 5 & -2 \\ 3 & 3 \end{vmatrix} - 0 \times \begin{vmatrix} 2 & -3 \\ 3 & 3 \end{vmatrix} + 0 \times \begin{vmatrix} 2 & -3 \\ 5 & -2 \end{vmatrix}$$

$$= -(5 \times 3 - (-2) \times 3) = -21$$

23. Calculate the inverse of the following matrix:

$$\begin{bmatrix} 4 & 7 \\ 2 & 4 \end{bmatrix}$$

Answer: To obtain the inverse we have to replace each element by its cofactor, take the transpose and, finally, divide by the determinant of the original matrix.

Replacing each element by its cofactor we get the matrix

$$\begin{bmatrix} 4 & -2 \\ -7 & 4 \end{bmatrix}$$

Taking the transpose next gives

$$\begin{bmatrix} 4 & -7 \\ -2 & 4 \end{bmatrix}$$

Finally, dividing by the determinant $4 \times 4 - 2 \times 7 = 2$ of the original matrix, we have its inverse

$$\begin{bmatrix} 2 & -3.5 \\ -1 & 2 \end{bmatrix}$$

24. If the Dow Jones Industrial Average were a straight-line (or, linear, same thing) function of time and if its value on January 1, 2007 is 12,000 and on January 1, 2009 it's 13,500, what is the value on January 1, 2010?

Answer : As a linear function of time then the DJIA grows 1500 points in two years, or 750 per year, which takes it to 14,250 on January 1, 2010.

25. Are the following vectors linearly independent?

$$[2\ 3\ 0]^T \qquad [3\ 7\ -1]^T \qquad [1\ -6\ 3]^T$$

Answer: The vectors are linearly independent if the only solution to the equation

$$c_1[2\ 3\ 0]^T + c_2[3\ 7\ -1]^T + c_3[1\ -6\ 3]^T = [0\ 0\ 0]^T$$

is $c_1 = c_2 = c_3 = 0$.

The vector equation above is equivalent to the following set of three simultaneous equations – one from each position in the vectors – in c_1, c_2 and c_3:

$$\begin{aligned} 2c_1 + 3c_2 + c_3 &= 0 \\ 3c_1 + 7c_2 - 6c_3 &= 0 \\ -c_2 + 3c_3 &= 0 \end{aligned}$$

Solving we find solutions not all 0, e.g., $c_1 = 5$, $c_2 = -3$ and $c_3 = -1$, proving that the given set of vectors is not linearly independent.

26. Determine the linear transformation of R^3 that maps the standard basis vectors

$$[1\ 0\ 0]^T \qquad [0\ 1\ 0]^T \qquad [0\ 0\ 1]^T$$

to the respective vectors

$$[-1\ -1\ 1]^T \qquad [-2\ 3\ 2]^T \qquad [-3\ 1\ -2]^T$$

Answer : The required linear transformation is defined by the matrix whose columns are, respectively, the images of the successive basis vectors. In particular, then, its matrix is

$$\begin{bmatrix} -1 & -2 & -3 \\ -1 & 3 & 1 \\ 1 & 2 & -2 \end{bmatrix}$$

27. What is the equation of the normal to the parabola

$$y = 2x^2 + 3$$

at the point $(2, 11)$?

Answer: $\frac{dy}{dx} = 4x$, so at the point $(2, 11)$ the gradient of the tangent is $4 \times 2 = 8$. The gradient of the normal, therefore, is $-\frac{1}{8}$. Its equation, accordingly, is

$$\frac{y - 11}{x - 2} = -\frac{1}{8} \quad \text{or} \quad x + 8y - 90 = 0$$

28. If x and y are related by the equation

$$xy + x + y = 1$$

find a formula for $\frac{dy}{dx}$.

Answer: Differentiating the equation throughout with respect to x:

$$(\frac{d}{dx}x)y + x(\frac{d}{dx}y) + \frac{d}{dx}x + \frac{d}{dx}y = \frac{d}{dx}1$$

which simplifies to

$$y + x\frac{dy}{dx} + 1 + \frac{dy}{dx} = 0$$

giving

$$\frac{dy}{dx} = -\frac{y + 1}{x + 1}$$

29. The formula for the height at time t of a projectile shot vertically upward from the ground with initial velocity u is

$$h = ut - \frac{1}{2}gt^2$$

assuming only the action of gravitational acceleration g (ignoring wind resistance and other factors). What is the velocity of the projectile at time t? What is the maximum height reached by the projectile?

Answer: Its velocity at time t is

$$\frac{dh}{dt} = u - gt$$

When the projectile attains maximum height, its velocity is 0. Therefore, $u - gt = 0$, implying that $t = \frac{u}{g}$. Therefore, the maximum height reached by the projectile is obtained by substituting $t = \frac{u}{g}$ in the formula for its height, which gives the maximum height as

$$u\frac{u}{g} - \frac{1}{2}g\left(\frac{u}{g}\right)^2 = \frac{u^2}{g} - \frac{u^2}{2g} = \frac{u^2}{2g}$$

30. At what points do the curves $y = \sin x$ and $y = \cos x$ meet for values of x between 0 and 2π? What angles do they make at these points?

Answer : When the curves (see Figure C.4) meet, their y-values are equal, so $\sin x = \cos x$, giving $\tan x = \frac{\sin x}{\cos x} = 1$. The two values in the interval $[0, 2\pi]$ where $\tan x = 1$ are $\frac{\pi}{4}$ and $\frac{5\pi}{4}$. Therefore, the two points at which the curves meet are $(\frac{\pi}{4}, \frac{1}{\sqrt{2}})$ and $(\frac{5\pi}{4}, -\frac{1}{\sqrt{2}})$ ($\cos\frac{\pi}{4} = \sin\frac{\pi}{4} = \frac{1}{\sqrt{2}}$ and $\cos\frac{5\pi}{4} = \sin\frac{5\pi}{4} = -\frac{1}{\sqrt{2}}$).

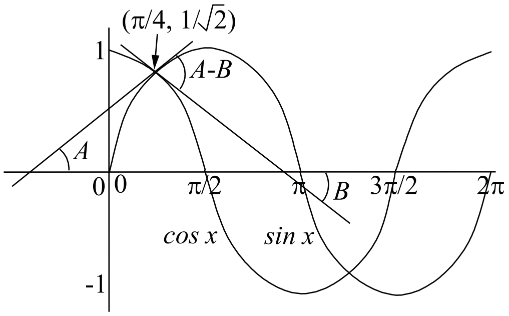

Figure C.4: Graphs of sin x and cos x (*sketch, not exact*).

For the first curve $\frac{dy}{dx} = \cos x$, while for the second $\frac{dy}{dx} = -\sin x$. At the point of intersection $(\frac{\pi}{4}, \frac{1}{\sqrt{2}})$, therefore, the gradients of the two curves are $\cos\frac{\pi}{4} = \frac{1}{\sqrt{2}}$ and $-\sin\frac{\pi}{4} = -\frac{1}{\sqrt{2}}$, respectively.

If the tangent lines at $(\frac{\pi}{4}, \frac{1}{\sqrt{2}})$ make angles A and B, respectively, with the x-axis, then the gradients are precisely the tan of these angles. Therefore, $\tan A = \frac{1}{\sqrt{2}}$ and $\tan B = -\frac{1}{\sqrt{2}}$ (B is a negative angle). The angle between the curves – which by definition is the angle between their tangents – at $(\frac{\pi}{4}, \frac{1}{\sqrt{2}})$ is $A - B$. Now,

$$\tan(A - B) = \frac{\tan A - \tan B}{1 + \tan A \tan B} = \frac{\frac{1}{\sqrt{2}} + \frac{1}{\sqrt{2}}}{1 - \frac{1}{\sqrt{2}}\frac{1}{\sqrt{2}}} = 2\sqrt{2}$$

which means $A - B = \tan^{-1} 2\sqrt{2} = \tan^{-1} 2.828 = 1.231$ radians or 70.526° (approximately). The angle between the curves at the other point of intersection is the same by symmetry.

Bibliography

[1] T. Akenine-Möller, E. Haines, N. Hoffman, *Real-Time Rendering* , 3rd Edn., A K Peters, 2008.

[2] E. Angel, *Interactive Computer Graphics: A Top-Down Approach with WebGL*, 7th Edn., Addison-Wesley, 2014.

[3] A. Appel, Some techniques for the machine rendering of solids, *Proceedings of the Spring Joint Computer Conference*, 1968, 37-45.

[4] F. Ayres, E. Mendelson, *Schaum's Outlines: Calculus*, 6th Edn., McGraw-Hill, 2012.

[5] R. Baer, *Linear Algebra and Projective Geometry* , Kindle Edn., Dover Publications, 2012.

[6] M. Bailey, S. Cunningham, *Graphics Shaders: Theory and Practice*, 2nd Edn., A K Peters, 2012.

[7] T. Banchoff, J. Wermer, *Linear Algebra through Geometry* , 2nd Edn., Springer-Verlag, 1993.

[8] M. F. Barnsley, *Fractals Everywhere*, Kindle Edn., Dover Publications, 2013.

[9] R. H. Bartels, J. C. Beatty, B. A. Barsky, *An Introduction to Splines for Use in Computer Graphics and Geometric Modeling*, Morgan Kaufmann, 1987.

[10] M. de Berg, O. Cheong, M. van Kreveld, M. Overmars, *Computational Geometry: Algorithms and Applications*, 3rd Edn., Springer-Verlag, 2008.

[11] R. S. Berns, *Billmeyer and Saltzman's Principles of Color Technology*, 3rd Edn., Wiley-Interscience, 2000.

[12] P. E. Bézier, How Renault uses numerical control for car body design and tooling, *Society of Automotive Engineers' Congress*, SAE paper 680010, Detroit, 1968.

[13] P. E. Bézier, Mathematical and practical possibilities of UNISURF, in *Computer Aided Geometric Design: Proceedings of a Conference Held at the University of Utah*, R. Barnhill and R. Riesenfeld, editors, Academic Press, 1974, 127-152.

[14] J. F. Blinn, Models of light reflection for computer synthesized pictures, *Computer Graphics (Proceedings SIGGRAPH 1977)* 11 (1977), 192-198.

[15] J. F. Blinn, Simulation of wrinkled surfaces, *Computer Graphics (Proceedings SIGGRAPH 1978)* 12 (1978), 286-292.

[16] J. F. Blinn, *Jim Blinn's Corner: A Trip Down the Graphics Pipeline*, Morgan Kaufmann, 1996.

[17] J. F. Blinn, *Jim Blinn's Corner: Dirty Pixels*, Morgan Kaufmann, 1998.

[18] J. Blinn, M. Newell, Texture and reflection in computer generated images, *Communications of the ACM*, 19 (1976), 456-547.

[19] D. Bourg, B. Bywalec, *Physics for Game Developers: Science, math, and code for realistic effects*, 2nd Edn., O'Reilly, 2013.

[20] J. E. Bresenham, Algorithm for computer control of digital plotter, *IBM Systems Journal* 4 (1965), 25-30.

[21] S. R. Buss, *3-D Computer Graphics: A Mathematical Introduction with OpenGL*, Cambridge University Press, 2003.

[22] E. Catmull, R. Rom, A class of local interpolating splines, in *Computer Aided Geometric Design: Proceedings of a Conference Held at the University of Utah*, R. Barnhill and R. Riesenfeld, editors, Academic Press, 1974, 317-326.

[23] C. Chuon, S. Guha, Volume Cost Based Mesh Simplification, *Proceedings 6th International Conference on Computer Graphics, Imaging and Visualization (CGIV 09)* (2009), 164-169.

[24] M. F. Cohen, D. P. Greenberg, The hemi-cube: a radiosity solution for complex environments, *Computer Graphics (Proceedings SIGGRAPH 1985)* 19 (1985), 31-40.

[25] M. F. Cohen, J. R. Wallace, *Radiosity and Realistic Image Synthesis* , Morgan Kaufmann, 1993.

[26] Comparison of OpenGL and Direct3D (in Wikipedia), https://en.wikipedia.org/wiki/Comparison_of_OpenGL_and_Direct3D.

[27] Computational Geometry Algorithms Library, http://www.cgal.org.

[28] R. L. Cook, K. E. Torrance, A reflectance model for computer graphics, *ACM Transaction on Graphics* 1 (1982), 7-24.

[29] M. G. Cox, The numerical evaluation of B-splines, *Journal of the Institute of Mathematics and Its Applications* 10 (1972), 134-149.

[30] H. S. M. Coxeter, *Projective Geometry*, Springer, 2nd Edn., 2013.

[31] F. C. Crow, The origins of the teapot, *IEEE Computer Graphics and Applications* 7 (1987), 8-19.

[32] F. C. Crow, Shadow algorithms for computer graphics, *Computer Graphics (Proceedings SIGGRAPH 1977)* 11 (1977), 242-248.

[33] C. de Boor, On calculating with B-splines, *Journal of Approximation Theory* 6 (1972), 50-62.

[34] P. de Casteljau, Outillages méthodes calcul, Technical report, A. Citroen, Paris, 1959.

[35] P. de Casteljau, Courbes et surfaces à poles, Technical report, A. Citroen, Paris, 1963.

[36] M. P. Do Carmo, *Differential Geometry of Curves and Surfaces*, Revised Edn., Dover Publications, 2016..

[37] F. Dunn, I. Parberry, *3D Math Primer for Graphics and Game Development* , 2nd Edn., A K Peters, 2011.

[38] D. H. Eberly, *3D Game Engine Design: A Practical Approach to Real-Time Computer Graphics*, 2nd Edn., Morgan Kaufmann, 2006.

[39] D. H. Eberly, *Game Physics*, 2nd Edn., Morgan Kaufmann, 2010.

[40] H. Edelsbrunner, *A Short Course in Computational Geometry and Topology*, Springer, 2014.

[41] H. Edelsbrunner, *Geometry and Topology for Mesh Generation*, Cambridge University Press, 2006.

[42] H. Edelsbrunner, J. L. Harer, *Computational Topology* , American Mathematical Society, 2009.

[43] C. Ericson, *Real-Time Collision Detection*, Morgan Kaufmann, 2005.

[44] K. Falconer, *Fractal Geometry: Mathematical Foundations and Applications*, 3rd Edn., John Wiley & Sons, 2014.

[45] G. Farin, *Curves and Surfaces for CAGD: A Practical Guide*, 5th Edn., Morgan Kaufmann, 2001.

[46] G. Farin, *NURBS: from Projective Geometry to Practical Use*, 2nd Edn., A K Peters, 1999.

[47] J. F. Hughes, A. van Dam, M. McGuire, D. F. Sklar, J. D. Foley, S. K. Feiner, K. Akeley, *Computer Graphics: Principles and Practice*, 3rd Edn., Addison-Wesley, 2013.

[48] J. D. Foley, A. van Dam, S. K. Feiner, J. F. Hughes, R. L. Phillips, *Introduction to Computer Graphics*, Addison-Wesley, 1993.

[49] FreeGLUT, http://freeglut.sourceforge.net.

[50] S. H. Friedberg, A. J. Insel, L. E. Spence, *Linear Algebra*, 4th Edn., Prentice Hall, 2002.

[51] H. Fuchs, Z. M. Kedem, B. F. Naylor, On visible surface generation by a priori tree structures, *Computer Graphics (Proceedings SIGGRAPH 1980)* 14 (1980), 124-133.

[52] D. C. Giancoli, *Physics for Scientists and Engineers with Modern Physics*, 4th Edn., Pearson, 2008.

[53] GIMP, http://www.gimp.org.

[54] A. S. Glassner, *Andrew Glassner's Notebook: Recreational Computer Graphics*, Morgan Kaufmann, 1999.

[55] A. S. Glassner, *Andrew Glassner's Other Notebook: Further Recreations in Computer Graphics*, A K Peters, 2002.

[56] A. S. Glassner, *An Introduction to Ray Tracing*, Academic Press, 1989.

[57] GLFW, http://www.glfw.org.

[58] GLM, https://glm.g-truc.net/0.9.8/index.html.

[59] GLUI, http://www.cs.unc.edu/∼rademach/glui.

[60] C. M. Goral, K. E. Torrance, D. P. Greenberg, B. Battaile, Modeling the interaction of light between diffuse surfaces, *Computer Graphics (Proceedings SIGGRAPH 1984)* 18 (1984), 213-222.

[61] H. Gouraud, Continuous shading of curved surfaces, *IEEE Transactions on Computers* 20 (1971), 623-629.

[62] S. Govil-Pai, *Principles of Computer Graphics: Theory and Practice Using OpenGL and Maya*, Springer, 2005.

[63] W. H. Greub, *Linear Algebra*, 4th Edn., Springer India, 2010.

[64] S. Guha, Joint separation of geometric clusters and the extreme irregularities of regular polyhedra, *International Journal of Computational Geometry and Applications* 15 (2005), 491-510.

[65] A. J. Hanson, *Visualizing Quaternions*, Morgan Kaufmann, 2006.

[66] P. Haeberli, K. Akeley, The accumulation buffer: hardware support for high-quality rendering, *Computer Graphics (Proceedings 17th Annual Conference on Computer Graphics and Interactive Techniques)* 24 (1990), 309-318.

[67] P. Haeberli, M. Segal, Texture mapping as a fundamental drawing primitive, *Proceedings Fourth Eurographics Workshop on Rendering* (1993), 259-266 (on-line version at http://www.sgi.com/misc/grafica/texmap).

[68] L. A. Hageman, D. M. Young, *Applied Iterative Methods*, Kindle Edn., Dover Publications, 2012.

[69] X. D. He, K. E. Torrance, F. X. Sillion, D. P. Greenberg, A comprehensive physical model for light reflection, *Computer Graphics (Proceedings SIGGRAPH 1991)* 25 (1991), 175-186.

[70] X. D. He, P. O. Heynen, R. L. Phillips, K. E. Torrance, D. H. Salesin, D. P. Greenberg, A fast and accurate light reflection model, *Computer Graphics (Proceedings SIGGRAPH 1992)* 26 (1992), 253-254.

[71] D. Hearn, M. P. Baker, W. Carithers, *Computer Graphics with OpenGL*, 4th Edn., Prentice Hall, 2010.

[72] P. S. Heckbert, Survey of texture mapping, *IEEE Computer Graphics and Applications* 6 (1986), 56-67.

[73] M. Henle, *Modern Geometries: Non-Euclidean, Projective, and Discrete Geometry*, 2nd Edn., Prentice Hall, 2001.

[74] F. S. Hill, Jr., S. M. Kelley, *Computer Graphics Using OpenGL*, 3rd Edn., Prentice Hall, 2006.

[75] K. M. Hoffman, R. Kunze, *Linear Algebra*, 2nd Edn., Pearson, 2018.

[76] International Meshing Roundtable, http://www.imr.sandia.gov.

[77] R. Jackson, L. MacDonald, K. Freeman, *Computer Generated Colour: A Practical Guide to Presentation and Display*, John Wiley & Sons, 1994.

[78] G. A. Jennings, *Modern Geometry with Applications*, 2nd Edn., Springer, 1997.

[79] L. Kadison, M. T. Kromann, *Projective Geometry and Modern Algebra*, Birkhäuser, 1996.

[80] M. J. Kilgard, Improving shadows and reflections via the stencil buffer, https://developer.nvidia.com/sites/default/files/akamai/gamedev/docs/stencil.pdf.

[81] Khronos Group OpenGL ES, http://www.opengles.org.

[82] B. Kolman, D. R. Hill, *Introductory Linear Algebra: An Applied First Course*, 8th Edn., Prentice Hall, 2004.

[83] E. Kreyszig, *Differential Geometry*, Kindle Edn., Dover Publications, 2013.

[84] J. B. Kuipers, *Quaternions and Rotation Sequences: A Primer with Applications to Orbits, Aerospace and Virtual Reality* , Princeton University Press, 2002.

[85] A. Kumar, V. Kwatra, B. Singh, S. Kapoor, Dynamic Binary Space Partitioning for Hidden Surface Removal, *Proceedings Indian Conference on Computer Vision, Graphics and Image Processing (ICVGIP 1998)*, 1998.

[86] D. C. Lay, S. R. Lay, J. J. McDonald, *Linear Algebra and Its Applications*, 5th Edn., Pearson, 2015.

[87] E. Lengyel, *Mathematics for 3D Game Programming & Computer Graphics*, 3rd Edn., Cengage Learning, 2011.

[88] Y. Liang, B. Barsky, A new concept and method for line clipping, *ACM Transactions on Graphics* 3 (1984), 1-22.

[89] Lighthouse 3D, http://www.lighthouse3d.com/opengl.

[90] M. M. Lipschutz, *Schaum's Outlines: Differential Geometry* , McGraw-Hill, 1969.

[91] D. Luebke, M. Reddy, J. D. Cohen, A. Varshney, B. Watson, R. Huebner, *Level of Detail for 3D Graphics*, Morgan Kaufmann, 2002.

[92] F. D. Luna, *Introduction to 3D Game Programming with DirectX 11* , Kindle Edn., Mercury Learning and Information, 2012.

[93] B. Mandelbrot, *The Fractal Geometry of Nature*, Times Books, 1982.

[94] S. Marschner, P. Shirley, *Fundamentals of Computer Graphics*, 4rd Edn., A K Peters, 2015.

[95] T. McReynolds, D. Blythe, *Advanced Graphics Programming Using OpenGL*, Morgan Kaufmann, 2005.

[96] Mesa 3D, http://www.mesa3d.org.

[97] M. E. Mortenson, *Geometric Modeling*, 3rd Edn., Industrial Press, 2006.

[98] M. E. Mortenson, *Geometric Transformations for 3D Modeling* , 2nd Edn., Industrial Press, 2007.

[99] M. E. Mortenson, *Mathematics for Computer Graphics Applications*, 2nd Edn., Industrial Press, 1999.

[100] T. K. Mukherjee, *private communication*, 2008.

[101] J. Munkres, *Elements of Algebraic Topology*, Westview Press, 1996.

[102] J. Munkres, *Topology*, New International Edn., Pearson, 2018.

[103] S. K. Nayar, M. Oren, Generalization of the Lambertian model and implications for machine vision, *International Journal of Computer Vision* 14 (1995), 227-251.

[104] Open 3D Model Viewer, http://www.open3mod.com.

[105] Open Asset Import Library, http://assimp.sourceforge.net.

[106] OpenGL, http://www.opengl.org.

[107] OpenGL Architecture Review Board, *OpenGL Programming Guide*, 8th Edn., Addison-Wesley, 2013.

[108] OpenGL Architecture Review Board, *OpenGL Reference Manual* , 4th Edn., Addison-Wesley, 2004.

[109] B. O'Neill, *Elementary Differential Geometry* , 2nd Edn., Academic Press, 2006.

[110] J. O'Rourke, *Computational Geometry in C* , 2nd Edn., Cambridge University Press, 2013.

[111] D. Pedoe, *Geometry: A Comprehensive Course*, Kindle Edn., Dover Publications, 2013.

[112] B. T. Phong, Illumination for computer generated pictures, *Communications of the ACM* 18 (1975), 311-317.

[113] L. Piegl, W. Tiller, *The NURBS Book*, 2nd Edn., Springer, 2012.

[114] P. Poulin, A. Fournier, A model for anisotropic reflection, *Computer Graphics (Proceedings SIGGRAPH 1990)* 24 (1990), 273-282.

[115] POV-Ray, http://www.povray.org.

[116] W. H. Press, S. A. Teukolsky, W. T. Vetterling, B. P. Flannery, *Numerical Recipes: The Art of Scientific Computing* , 3rd Edn., Cambridge University Press, 2007.

[117] A. Pressley, *Elementary Differential Geometry*, 2nd Edn., Springer, 2010.

[118] D. F. Rogers, *An Introduction to NURBS: With Historical Perspective*, Morgan Kaufmann, 2000.

[119] D. F. Rogers, *Procedural Elements for Computer Graphics*, 2nd Edn., McGraw-Hill, 1997.

[120] D. F. Rogers, J. A. Adams, *Mathematical Elements for Computer Graphics*, 2nd Edn., McGraw-Hill, 1989.

[121] S. Roman, *Advanced Linear Algebra*, 3rd Edn., Springer, 2007.

[122] R. J. Rost, B. Licea-Kane, *OpenGL Shading Language*, 3rd Edn., Addison-Wesley, 2009.

[123] H. Samet, *Foundations of Multidimensional and Metric Data Structures*, Morgan Kaufmann, 2006.

[124] P. Samuel, *Projective Geometry*, Springer-Verlag, 1988.

[125] H. M. Schey, *Div, Grad, Curl, and All That: An Informal Text on Vector Calculus*, 4th Edn., W. W. Norton & Co., 2004.

[126] H. Schildt, *STL Programming from the Ground Up*, Osborne/McGraw-Hill, 1998.

[127] C. Schlick, An inexpensive BRDF model for physically-based rendering, *Computer Graphics Forum* 13 (1994), 233-246.

[128] I. Schoenberg, Contributions to the problem of approximation of equidistant data by analytic functions, *Quarterly of Applied Mathematics* 4 (1946), 45-99.

[129] I. Schoenberg, On spline functions, in *Inequalities*, O. Sisha, editor, Academic Press, 1967, 249-274.

[130] M. Segal, K. Akeley, The design of the OpenGL graphics interface, 1994 (on-line version available from http://citeseerx.ist.psu.edu/viewdoc/summary?doi=10.1.1.126.8268).

[131] G. Sellers, J. Kessenich, *Vulkan Programming Guide: The Official Guide to Learning Vulkan (OpenGL)*, Addison-Wesley, 2016.

[132] G. Sellers, R. S. Wright, Jr., N. Haemel, *OpenGL Superbible*, 7th Edn., Addison-Wesley, 2015.

[133] ACM SIGGRAPH, http://www.siggraph.org.

[134] F. X. Sillion, C. Puech, *Radiosity and Global Illumination*, Morgan Kaufmann, 1994.

[135] G. F. Simmons, *Calculus With Analytic Geometry* , 2nd Edn., McGraw-Hill, 1996.

[136] I. M. Singer, J. A. Thorpe, *Lecture Notes on Elementary Topology and Geometry*, Springer-Verlag, 1976.

[137] M. Slater, A. Steed, Y. Chrysanthou, *Computer Graphics and Virtual Environments: From Realism to Real-Time*, Addison-Wesley, 2001.

[138] M. R. Spiegel, *Schaum's Outlines: Vector Analysis and an Introduction to Tensor Analysis*, McGraw-Hill, 1968.

[139] J. Stewart, *Calculus*, 7th Edn., Cengage Learning, 2012.

[140] G. Strang, *Introduction to Linear Algebra*, 5th Edn., Wellesley-Cambridge Press, 2016.

[141] I. E. Sutherland, *Sketchpad: A Man-Machine Graphical Communication System*, MIT Thesis, 1963.

[142] I. E. Sutherland, G. W. Hodgman, Reentrant polygon clipping, *Communications of the ACM* 17 (1974), 32-42.

[143] G. Szauer, *Game Physics Cookbook*, Packt Publishing, 2017.

[144] A. Thorn, *DirectX 9 Graphics: The Definitive Guide to Direct3D*, Jones & Bartlett Publishers, 2005.

[145] Trolltech, http://www.trolltech.com.

[146] UNC GAMMA Research Group, http://www.cs.unc.edu/~geom.

[147] G. van den Bergen, *Collision Detection in Interactive 3D Environments*, CRC Press, 2003.

[148] J. M. van Verth, L. M. Bishop, *Essential Mathematics for Games and Interactive Applications: A Programmer's Guide*, 2nd Edn., Morgan Kaufmann, 2008.

[149] J. Vince, *Mathematics for Computer Graphics*, 5th Edn., Springer, 2017.

[150] A. Watt, *3D Computer Graphics*, 3rd Edn., Addison-Wesley, 1999.

[151] J. T. Whitted, An improved illumination model for shaded display, *Communications of the ACM* 23 (1980), 343-349.

[152] L. Williams, Casting curved shadows on curved surfaces, *Computer Graphics (Proceedings SIGGRAPH 1978)* 12 (1978), 270-274.

[153] L. Williams, Pyramidal parametrics, *Computer Graphics (Proceedings SIGGRAPH 1983)* 17 (1983), 1-11.

[154] D, Wolff, *OpenGL Shading Language Cookbook*, 2nd Edn., Packt Publishing, 2013.

[155] R. C. Wrede, M. Spiegel, *Schaum's Outlines: Advanced Calculus*, 3rd Edn., McGraw-Hill, 2010.

[156] G. Wyszecki, W. S. Stiles, *Color Science: Concepts and Methods, Quantitative Data and Formulae*, 2nd Edn., Wiley-Interscience, 2000.

[157] Z. Xiang, *Computer Graphics: Theory and Practice with OpenGL*, CreateSpace Independent Publishing Platform, 2018.

[158] Z. Xiang, R. Plastock, *Schaum's Outlines: Computer Graphics*, 2nd Edn., McGraw-Hill, 2000.

[159] I. M. Yaglom, *Geometric Transformations I*, Mathematical Association of America, 1962.

[160] I. M. Yaglom, *Geometric Transformations II*, Mathematical Association of America, 1968.

[161] I. M. Yaglom, *Geometric Transformations III*, Mathematical Association of America, 1973.

Taylor & Francis

Taylor & Francis Group

http://taylorandfrancis.com